PROCEEDINGS

OF THE

ROYAL SOCIETY OF LONDON

SERIES A—MATHEMATICAL AND PHYSICAL SCIENCES

VOL. CLIII

LONDON
Printed and published for the Royal Society
By Harrison & Sons, Ltd., 44–47, St. Martin's Lane
Printers in Ordinary to His Majesty

February 1, 1936

LONDON:
HARRISON AND SONS, LTD., PRINTERS IN ORDINARY TO HIS MAJESTY
ST. MARTIN'S LANE

CONTENTS

SERIES A VOL CLIII

No. A 878—December 2, 1935

PAGE

On the Acoustic Radiation Pressure on Circular Discs: Inertia and Diffraction Corrections. By L. V. King, F.R.S. 1

On the Theory of the Inertia and Diffraction Corrections for the Rayleigh Disc. By L. V. King, F.R.S. 17

Stress-Calculation in Frameworks by the Methods of Systematic Relaxation of Constraints -III. By R. V. Southwell, F.R.S. 41

The Sorption of Hydrogen and Deuterium by Copper and Palladium. I—The Behaviour of Copper and Copper Oxides. By H. W. Melville and E. K. Rideal, F.R.S. 77

The Sorption of Hydrogen and Deuterium by Copper and Palladium. II—The Sorption of Palladium and Diffusion through Copper. By H. W. Melville and E. K. Rideal, F.R.S. 89

Pro-Knocks and Hydrocarbon Combustion. By A. R. Ubbelohde, J. W. Drinkwater, and A. Egerton, F.R.S. 103

Reactions in Monolayers of Drying Oils. I—The Oxidation of the Maleic Anhydride Compound of β-Elaeostearin. By G. Gee and E. K. Rideal, F.R.S. 116

Reactions in Monolayers of Drying Oils. II—Polymerization of the Oxidized Forms of the Maleic Anhydride Compound of β-Flaeosterin. By G. Gee. Communicated by E. K. Rideal, F.R.S. 129

Quantitative Spectrographic Analysis of Biological Material. I—A Method for the Determination of Lead in Cerebrospinal Fluid. By J. S. Foster, F.R.S., G. O. Langstroth, and D. R. McRae. (Plate 1) 141

The Oxygen Afterglow. By E. M. Stoddart. Communicated by F. G. Donnan, F.R.S. 152

The Dielectric Loss Characteristics of a Chlorinated Diphenyl By W. Jackson. Communicated by E. V. Appleton, F.R.S. 158

The Crystal Structure of Ice at Low Temperatures. By E. F. Burton, F.R.S.C., and W. F. Oliver. Communicated by Sir John McLennan, F.R.S. (Plate 2) 166

Iron of High Purity. By F. Adcock and C. A. Bristow. Communicated by C. H. Desch, F.R.S. (Plate 3) 172

Isotherms of CO_2 between 0° and 150° and Pressures from 16 to 250 Atm (Amagat Densities 18–206). By A. Michels and C. Michels. Communicated by F. A. Freeth, F.R.S. 201

PAGE

Isotherms of CO_2 between 70 and 3000 Atm (Amagat Densities between 200 and 600) By A. Michels, C. Michels, and H. Wouters. Communicated by F. A. Freeth, F.R.S. 214

The Crystal Structure of Para-Dinitrobenzene. By R. W. James, G. King, and H. Horrocks Communicated by W. L. Bragg, F.R.S. 225

No. A 879--January 1, 1936

Address of the President, Sir Frederick Gowland Hopkins, O.M., at the Anniversary Meeting, November 30, 1935 247

The Distortion of β-Brass and Iron Crystals. By C. F. Elam. Communicated by G. I. Taylor, F.R.S. (Plates 4–7) 273

Breaking up of a Drop of Viscous Liquid Immersed in Another Viscous Fluid which is Extending at a Uniform Rate. By S. Tomotika. Communicated by G. I. Taylor, F.R.S. 302

The Infra-Red Absorption Spectra of Quartz and Fused Silica from 1 to 7·5 μ. I—Experimental Method. By D. G. Drummond. Communicated by W. E. Curtis, F.R.S. 318

The Infra-Red Absorption Spectra of Quartz and Fused Silica from 1 to 7·5 μ. II—Experimental Results By D. G. Drummond. Communicated by W. E. Curtis, F.R.S. 328

On the Theory of Optical Activity. III—A Regular Tetrahedron Twisted through a Small Angle about a Binary Axis. By B. Y. Oke. Communicated by T. M. Lowry, F.R.S. 339

The Scattering of Fast β-Particles by Nitrogen Nuclei. By F. C. Champion. Communicated by E. V. Appleton, F.R.S. 353

The Formation of Mercury Molecules. By F. L. Arnot and J. C. Milligan. Communicated by H. S. Allen, F.R.S. 359

Refractive Dispersion of Organic Compounds. VII—The Refractive Indices of Hexane and the Refractivities of Hydrogen and Carbon. Significance of the Dispersion Constants. By C. B. Allsopp and H. F. Willis. Communicated by T. M. Lowry, F.R.S. 379

Refractive Dispersion of Organic Compounds. VIII—Isomers of the Formula $C_4H_8O_2$: Dioxan, Ethyl Acetate, *iso*-Butyric Acid, and Acetoin. By C. B. Allsopp and H. F. Willis. Communicated by T. M. Lowry, F.R.S. 392

The Band Spectra of the Lead Halides, PbF and PbCl By G. D. Rochester. Communicated by W. E. Curtis, F.R.S. (Plate 8) 407

The Emission of Positive Ions by Platinum when Heated in Oxygen. By T. B. Rymer. Communicated by O. W. Richardson, F.R.S. 422

On the Production of Electron Pairs. By J. C. Jaeger and H. R. Hulme. Communicated by R. H. Fowler, F.R.S. 443

The Oxidation of Aromatic Hydrocarbons at High Pressures. I—Benzene. II—Toluene. III—Ethyl Benzene. By D. M. Newitt and J. H. Burgoyne. Communicated by W. A. Bone, F.R.S. 448

PAGE

The Electrical Resistance of Aluminium at Low Temperatures. By H. A. Boorse and H. Niewodniczański. Communicated by Lord Rutherford, O.M., F.R.S. 463

Neutrons of Thermal Energies. By P. B. Moon and J. R. Tillman. Communicated by G. P. Thomson, F.R.S. 476

No. A 880—February 1, 1936

The Structure of Atomic Nuclei. By H. A. Wilson, F.R.S. 493

The Diffusion of Hydrogen through Copper. By E. O. Braaten and G. F. Clark. Communicated by Sir John McLennan, F.R.S. 504

The Theory of the Surface Photoelectric Effect in Metals—II. By K. Mitchell. Communicated by R. H. Fowler, F.R.S. 513

Ultra-Violet Absorption of Ice. By E. J. Cassel. Communicated by F. A. Lindemann, F.R.S. (Plate 9) 534

Investigations on the Preliminary Stages of Spark Formation in various Gases by the use of the Wilson Chamber. By U. Nakaya and F. Yamasaki. Communicated by C. T. R. Wilson, F.R.S. (Plates 10–17) 542

The Structure of the near Infra-Red Bands of Methane. I—General Survey, and a New Band at 11,050 A. By W. H. J. Childs. Communicated by Sir William Bragg, F.R.S. 555

The Disintegration of Boron. By D. Roaf. Communicated by F. A. Lindemann, F.R.S. (Plate 18) 568

On Condensed Helium at Absolute Zero. By F. London. Communicated by F. A. Lindemann, F.R.S. 576

Studies on Gas-Solid Equilibria. VI—Adsorption from Binary Gas Mixtures by Silica Gel. By B. Lambert and H. S. Heaven. Communicated by F. Soddy, F.R.S. 584

The Rotation of Molecules in Fields of Octahedral Symmetry. By A. F. Devonshire. Communicated by J. E. Lennard-Jones, F.R.S. 601

A Quantum Mechanical Calculation of the Elastic Constants of Monovalent Metals. By K. Fuchs. Communicated by A. M. Tyndall, F.R.S. 622

Some Measurements of the Reflexion Coefficient of the Ionosphere for Wireless Waves. By F. W. G. White and L. W. Brown. Communicated by E. V. Appleton, F.R.S. 639

The Relativistic Theory of the Auger Effect. By H. S. W. Massey and E. H. S. Burhop. Communicated by R. H. Fowler, F.R.S. 661

The Absorption Spectrum of Lead Oxide (PbO). By H. G. Howell. Communicated by W. E. Curtis, F.R.S. 683

The Electrical Conductivity of Transition Metals. By N. F. Mott. Communicated by R. H. Fowler, F.R.S. 699

Index 719

On the Acoustic Radiation Pressure on Circular Discs: Inertia and Diffraction Corrections

By LOUIS V. KING, F.R.S., Macdonald Professor of Physics, McGill University, Montreal

(*Received July* 1, 1935)

1—INTRODUCTION

In supersonic radiation fields the acoustic radiation pressure on a circular disc may be measured by means of a suitably designed torsion balance.* In order to interpret such measurements it is necessary to have available an exact formula for this pressure in various types of radiation fields. It is found that the radiation pressure on a disc, however small compared with the wave-length, depends on the nature of the field as a whole as related to the mode of generation of the sound-waves. In a progressive plane wave the magnitude of the radiation pressure on a small disc is very much less than that in a stationary wave. The disc shares these peculiarities as regards pressure with the sphere, for which exact formulae may be obtained in certain types of radiation fields, including plane progressive and stationary waves.†

For discs, the exact evaluation of the radiation pressure involves the complete solution of the associated diffraction problem. To avoid unduly complex analysis, the problem is here dealt with by means of cylindrical wave functions, although the solution arrived at is limited to discs of circumference considerably less than the wave-length.

To obtain exact solutions valid for all wave-lengths, it is probably necessary to work with wave functions associated with oblate spheroidal co-ordinates. Considerable progress has recently been made along these lines by Kotani‡ and Hanson§.

The discs to which the following analysis refers are assumed to be extremely thin and perfectly rigid. The effect of compressibility in a disc of finite thickness is to allow of possible compressional and flexural waves, which in circumstances of resonance will produce an effect on the radiation pressure whose magnitude may be estimated if necessary.

---

* Boyle and Lehmann, 'Can. J. Res.,' vol. 3, p. 491 (1930).

† L. V. King, 'Proc. Roy. Soc.,' A, vol. 147, p. 212 (1934).

‡ 'Proc. Phys. Math. Soc. Japan,' vol. 15, p. 30 (1933).

§ 'Phil. Trans.,' A, vol. 232, p. 223 (1934).

2—DETERMINATION OF VELOCITY POTENTIAL IN TERMS OF CYLINDRICAL WAVE FUNCTIONS

We denote by ϕ_i the velocity potential of the incident radiation field which we will suppose for simplicity possesses radial symmetry with respect to the z-axis. In such circumstances the first-order pressure-variation integrated over the surface of the disc causes it to oscillate with velocity $\dot{\zeta}$ perpendicular to its plane. Owing to the radial symmetry of the incident field there will be no couples and no angular oscillations of the disc. To satisfy the boundary conditions, the origin is taken at the centre of the disc and has, therefore, the velocity component $\dot{\zeta}$. The radiation field is divided by the plane $z = 0$ into two regions. On the positive side of the disc the velocity potential is denoted by ϕ_p and on the negative, or minus side, by ϕ_m. In terms of the cylindrical co-ordinates (ρ, z) the appropriate expressions for the velocity potentials of the combined incident and secondary fields due to diffraction by the oscillating disc may be written

$$\phi_p = \phi_i + \int_0^\infty e^{-\mu z} J_0(\lambda\rho) f(\lambda)\, d\lambda \tag{1}$$

$$\mu = (\lambda^2 - \kappa^2)^{\frac{1}{2}}$$

$$\phi_m = \phi_i - \int_0^\infty e^{\mu z} J_0(\lambda\rho) f(\lambda)\, d\lambda, \tag{2}$$

the time-factor being, as usual, $e^{i\omega t}$, and $\kappa = \omega/c$.

The function $f(\lambda)$ has been chosen the same in the two equations to make $\partial\phi_p/\partial z = \partial\phi_m/\partial z$ over the plane $z = 0$. In particular, if $\dot{\zeta}$ is the velocity of the disc, the boundary condition is

$$\dot{\zeta} = -(\partial\phi_p/\partial z)_{z=0} = -(\partial\phi_m/\partial z)_{z=0}, \quad (0 < \rho < a), \tag{3}$$

while continuity of pressure over the plane $z = 0$ in the region $a < \rho < \infty$ requires that $\dot{\phi}_p = \dot{\phi}_m$ in this region, or integrating with respect to t,

$$(\phi_p)_{z=0} = (\phi_m)_{z=0}, \quad (a \leqslant \rho < \infty), \tag{4}$$

a condition which also makes $(\partial\phi_p/\partial\rho)_{z=0} = (\partial\phi_m/\partial\rho)_{z=0}$ for $a < \rho < \infty$.

The boundary conditions (3) and (4) give

$$\left.\begin{aligned} &\int_0^\infty \mu f(\lambda) J_0(\lambda\rho)\, d\lambda = \dot{\zeta} + \left(\frac{\partial\phi_i}{\partial z}\right)_{z=0}, && (0 < \rho < a) \\ &\int_0^\infty f(\lambda) J_0(\lambda\rho)\, d\lambda = 0 && (a \leqslant \rho < \infty) \end{aligned}\right\}. \tag{5}$$

The two equations (5) constitute an unusual type of integral equation for the determination of $f(\lambda)$.

3—DYNAMICAL EQUATION FOR THE OSCILLATION OF THE DISCS

If we denote by δp_p and δp_m the pressure variations on the positive and negative faces of the disc, the dynamical equation is, evidently,

$$\int_0^a (\delta p_m - \delta p_p)\, 2\pi\rho d\rho = m_0 \dot{\zeta}, \tag{6}$$

where m_0 is the mass of the disc.

Since $\delta p_m = \rho_0 (\dot{\phi}_m)_{z=0}$ and $\delta p_p = \rho_0 (\dot{\phi}_p)_{z=0}$, where ρ_0 is the density of the medium, we have, on integrating (6) with respect to the time,

$$2\pi\rho_0 \int_0^a (\phi_m - \phi_p)_{z=0}\, \rho\, d\rho = m_0 \dot{\zeta}. \tag{7}$$

Introducing ϕ_m and ϕ_p from (1) and (2), we find

$$-4\pi\rho_0 a \int_0^\infty f(\lambda)\, J_1(\lambda a) \frac{d\lambda}{\lambda} = m_0 \dot{\zeta}. \tag{8}$$

If now we write

$$f(\lambda) = \dot{\zeta} g(\lambda) + G(\lambda), \tag{9}$$

where $g(\lambda)$ and $G(\lambda)$ are determined from the integral equations

$$\int_0^\infty \mu g(\lambda)\, J_0(\lambda\rho)\, d\lambda = 1, \quad (0 < \rho < a):$$

$$\int_0^\infty g(\lambda)\, J_0(\lambda\rho)\, d\lambda = 0, \quad (a \leqslant \rho < \infty) \tag{10}$$

$$\int_0^\infty \mu\, G(\lambda)\, J_0(\lambda\rho)\, d\lambda = \left(\frac{\partial \phi_i}{\partial z}\right)_{z=0}, \quad (0 < \rho < a):$$

$$\int_0^\infty G(\lambda)\, J_0(\lambda\rho)\, d\lambda = 0, \quad (a \leqslant \rho < \infty), \tag{11}$$

and denote

$$m_1 + i m_2 = 4\pi\rho_0 a \int_0^\infty g(\lambda)\, J_1(\lambda a) \frac{d\lambda}{\lambda} \tag{12}$$

$$M_1 + i M_2 = 4\pi\rho_0 a \int_0^\infty G(\lambda)\, J_1(\lambda a) \frac{d\lambda}{\lambda}, \tag{13}$$

we have from equation (8)

$$\dot{\zeta} = -\frac{(M_1 + i M_2)}{m_0 + m_1 + i m_2}. \tag{14}$$

4—CALCULATION OF RADIATION PRESSURE

The pressure variation in a compressible medium in which the pressure is any function of the density may be shown to be given by

$$\delta p = \rho_0 \dot{\phi} - \tfrac{1}{2}\rho_0 q^2 + \tfrac{1}{2}\frac{\rho_0}{c^2}\dot{\phi}^2. \tag{15}^*$$

The velocity potential ϕ is the solution of the usual wave equation with appropriate boundary conditions, which make it necessary in many problems to refer the solution to an origin moving with the boundary. The differentiation with respect to the time implied in (15) refers to an origin at rest. If $D\phi/Dt$ refers to an origin having components of velocity $(\dot{\xi}, \dot{\eta}, \dot{\zeta})$, we have

$$\dot{\phi} = D\phi/Dt + u\dot{\xi} + v\dot{\eta} + w\dot{\zeta}, \tag{16}$$

where, as usual, $(u, v, w) = -\operatorname{grad}\phi$, are the velocity components of the fluid referred to these axes.

The wave equation for ϕ neglects the squares of the velocities in the medium as compared with c^2. The inclusion of these terms in a solution of the exact wave equation introduces into (15) terms in $(\dot{\phi}/c)^3$, q^3, and higher powers, considered as negligible in the present theory.

To second-order terms, the time-average of the acoustic radiation pressure on the disc consists of three terms,

$$\overline{P} = \overline{P}_q + \overline{P}_\phi + \overline{P}_\zeta, \tag{17}$$

where $\overline{P}_q$ and $\overline{P}_\phi$ are contributed by the second and third terms of (15) while $\overline{P}_\zeta$ is contributed by the last three terms of (16) arising from the motion of the origin at the centre of the disc, which performs small oscillations under the influence of the first-order radiation pressure.

We have the following formulae for these contributions when the disc is so thin that the opposite faces are oscillating with the same amplitude and phase, in which circumstances $\zeta = -(\partial\phi_m/\partial z) = (\partial\phi_p/\partial z)$,

$$\left.\begin{aligned}
P_q &= -\tfrac{1}{2}\rho_0\int_0^a \left\{\left(\frac{\partial\phi_m}{\partial\rho}\right)^2 - \left(\frac{\partial\phi_p}{\partial\rho}\right)^2\right\}_{z=0} 2\pi\rho\, d\rho \\
P_\phi &= \tfrac{1}{2}\frac{\rho_0}{c^2}\int_0^a (\dot{\phi}_m^2 - \dot{\phi}_p^2)_{z=0}\, 2\pi\rho\, d\rho \\
P_z &= -\rho_0\,\zeta\int_0^a \left\{\left(\frac{\partial\phi_m}{\partial z}\right) - \left(\frac{\partial\phi_p}{\partial z}\right)\right\}_{z=0} 2\pi\rho\, d\rho = 0
\end{aligned}\right\}. \tag{18}$$

---

* King, 'Proc. Roy. Soc.,' A, vol. 147, p. 215 (1934); *see also* Kotani, 'Proc. Phys. Math. Soc. Japan,' vol. 15, p. 31 (1933).

In these formulae the values of ϕ_v, ϕ_m and their derivatives refer to the plane of the disc, $z = 0$. Before carrying out the integrations and taking time-averages, the velocity potentials must be freed from imaginary quantities.

5—SOLUTION OF NORMAL DIFFRACTION EQUATION BY SUCCESSIVE APPROXIMATIONS

The solution of the integral equations (10) and (11) may be made to depend on that of integral equations of the type

$$\int_0^\infty \lambda g_\nu(\lambda) J_\nu(\lambda\rho)\, d\lambda = F_\nu(\rho), (0 < \rho < a):$$
$$\int_0^\infty g_\nu(\lambda) J_\nu(\lambda\rho)\, d\lambda = 0, (a \leqslant \rho < \infty), \qquad (19)^*$$

of which the solution is

$$g_\nu(\lambda) = \lambda^{\frac{1}{2}} \int_0^a \phi_\nu(x) J_{\nu+\frac{1}{2}}(\lambda x)\, dx, \qquad (20)^*$$

where

$$\phi_\nu(x) = \sqrt{\frac{2}{\pi}}\, x^{3/2} \int_0^{\frac{1}{2}\pi} (\sin\theta)^{\nu+1} F_\nu(x \sin\theta)\, d\theta. \qquad (21)^*$$

In particular it is easily shown by the use of the above theorem that the solution of the equation

$$\int_0^\infty \lambda g_0(\lambda) J_0(\lambda\rho)\, d\lambda = 1, \quad (0 < \rho < a):$$
$$\int_0^\infty g_0(\lambda) J_0(\lambda\rho)\, d\lambda = 0, \quad (a \leqslant \rho < \infty) \qquad (22)$$

is

$$g_0(\lambda) = \sqrt{\frac{2}{\pi}}\, a^2 \frac{J_{3/2}(a\lambda)}{(a\lambda)^{\frac{1}{2}}}, \qquad (23)$$

---

* Equations of the type (19) for $\nu = 0$ seem to have first been considered by Beltrami ('R.C. Accad. Bologna,' vol. 2, p. 461 (1881)). An account of Beltrami's theorems are given in Webster's "Partial Differential Equations of Mathematical Physics," p. 272 (Stechert and Co., New York, 1933). The more general equations (19) involving $J_\nu(\lambda\rho)$ occur in the theory of a perfectly conducting disc in any electrical field of force and have been dealt with by Macdonald ('Proc. Lond. Math. Soc.,' vol. 26, p. 257 (1895)). The explicit form of the theorem contained in equations (20) and (21) is easily derived from H. Bateman's account of Macdonald's results ("Partial Differential Equations," Camb. Univ. Press, 1932, § 10.8, p. 474). An independent proof of a more general class of inversion theorems will be dealt with by the writer in a future paper.

while the solution of the equation

$$\int_0^\infty \lambda\, g_2(\lambda)\, J_0(\lambda\rho)\, d\lambda = \frac{\rho^2}{a^2}, \quad (0 < \rho < a):$$

$$\int_0^\infty g_2(\lambda)\, J_0(\lambda\rho)\, d\lambda = 0, \quad (a \leqslant \rho < \infty) \qquad (24)$$

is

$$g_2(\lambda) = \sqrt{\frac{2}{\pi}}\, a^2\, \tfrac{2}{3} \left\{ \frac{J_{3/2}(a\lambda)}{(a\lambda)^{\frac{1}{2}}} - 2\, \frac{J_{5/2}(a\lambda)}{(a\lambda)^{3/2}} \right\}. \qquad (25)$$

The results (23) and (25) are easily verified by the use of the general formula due to Sonine and Schafheitlin*

$$\int_0^\infty \frac{J_\mu(a\lambda)\, J_\nu(\rho\lambda)\, d\lambda}{\lambda^\beta} = \frac{\rho^\nu\, \Gamma\{\frac{1}{2}(\mu + \nu - \beta + 1)\}}{2^\beta a^{\nu-\beta+1}\, \Gamma(\nu+1)\, \Gamma\{\frac{1}{2}(\mu - \nu + \beta + 1)\}}$$

$$\times\, F\left\{\tfrac{1}{2}(-\mu + \nu - \beta + 1),\ \tfrac{1}{2}(\mu + \nu + \beta + 1);\ \nu + 1,\ \frac{\rho^2}{a^2}\right\}, \qquad (26)$$

valid for $0 < \rho < a$, $\beta > -1$, $\mu + \nu - \beta + 1 > 0$, which we shall again use in the sequel. Gauss's hypergeometric function $F(\alpha, \beta;\ \gamma, z)$, occurring on the right-hand side of (26), is defined by

$$F(\alpha, \beta;\ \gamma, z) = 1 + \frac{\alpha\beta}{1!\ \gamma z} + \frac{\alpha(\alpha+1)\,\beta(\beta+1)}{2!\ \gamma(\gamma+1)}\, z^2 + \ldots \qquad (27)$$

To solve the diffraction equation

$$\int_0^\infty \mu\, g(\lambda)\, J_0(\lambda\rho)\, d\lambda = 1, \quad (0 < \rho < a):$$

$$\int_0^\infty g(\lambda)\, J_0(\lambda\rho)\, d\lambda = 0, \quad (a \leqslant \rho < \infty), \qquad (28)$$

we write

$$g(\lambda) = g_0(\lambda) + g_{01}(\lambda), \qquad (29)$$

where $g_0(\lambda)$ satisfies (22) and is given by (23). Substituting in (28) $g_{01}(\lambda)$ is determined from the equation

$$\left.\begin{aligned} &\int_0^\infty \mu\, g_{01}(\lambda)\, J_0(\lambda\rho)\, d\lambda = 1 - \int_0^\infty \mu\, g_0(\lambda)\, J_0(\lambda\rho)\, d\lambda, && (0 < \rho < \infty) \\ &\int_0^\infty g_{01}(\lambda)\, J_0(\lambda\rho)\, d\lambda = 0, && (a \leqslant \rho < \infty) \end{aligned}\right\}. \qquad (30)$$

---

* Watson's "Theory of Bessel Functions," Camb. Univ. Press, 1922, § 13.4, formula (2). The details of the calculation of this section require the frequent use of § 13.41, formula (1).

Remembering that $\mu = (\lambda^2 - \kappa^2)^{\frac{1}{2}}$, we find on resolving (28) into real and imaginary parts that

$$\int_0^\infty \mu\, g_0(\lambda)\, J_0(\lambda\rho)\, d\lambda = i\kappa^2 \int_0^{\frac{1}{2}\pi} g_0(\kappa \sin\theta)\, J_0(\kappa\rho\sin\theta) \cos^2\theta\, d\theta$$

$$+ \int_0^\infty \frac{g_0\{(\lambda^2+\kappa^2)^{\frac{1}{2}}\}}{(\lambda^2+\kappa^2)^{\frac{1}{2}}} J_0\{\rho(\lambda^2+\kappa^2)^{\frac{1}{2}}\}\, \lambda^2\, d\lambda, \quad (0 < \rho < a). \qquad (31)$$

When $(\kappa a) \ll 1$, and $\rho < a$, we proceed to expand the integrals on the right-hand side of (31) in powers of $(\kappa\rho)$ and (κa).

By Taylor's Theorem, or by the addition-theorems for Bessel's functions, we easily find

$$\frac{J_{3/2}\{a(\lambda^2+\kappa^2)^{\frac{1}{2}}\}}{\{a^2(\lambda^2+\kappa^2)\}^{\frac{3}{4}}} = \frac{J_{3/2}(\lambda a)}{(\lambda a)^{3/2}} - \tfrac{1}{2}(\kappa a)^2 \frac{J_{5/2}(\lambda a)}{(\lambda a)^{5/2}} + \ldots$$

$$J_0\{\rho(\lambda^2+\kappa^2)^{\frac{1}{2}}\} = J_0(\lambda\rho) - \tfrac{1}{2}(\kappa\rho)^2 \frac{J_1(\lambda\rho)}{\lambda\rho} + \ldots$$

If we multiply the two series and perform the integrations by the use of formula (26), we find after a few reductions:

$$\int_0^\infty \frac{g_0\{(\lambda^2+\kappa^2)^{\frac{1}{2}}\}}{(\lambda^2+\kappa^2)^{\frac{1}{2}}} J_0\{\rho(\lambda^2+\kappa^2)^{\frac{1}{2}}\}\, \lambda^2\, d\lambda \sim 1 - \tfrac{1}{4}(\kappa a)^2 + \tfrac{1}{8}(\kappa\rho)^2 + \ldots,$$

and similarly

$$\int_0^{\frac{1}{2}\pi} g_0(\kappa\sin\theta)\, J_0(\kappa\rho\sin\theta)\cos^2\theta\, d\theta \sim \frac{2}{9\pi} a^3\kappa + \ldots$$

It now follows from (30) that the integral equation for $g_{01}(\lambda)$ is

$$\left.\begin{aligned} &\int_0^\infty \mu\, g_{01}(\lambda)\, J_0(\lambda\rho)\, d\lambda = \tfrac{1}{4}(\kappa a)^2 - i\frac{2}{9\pi}(\kappa a)^3 - \tfrac{1}{8}(\kappa\rho)^2 + \ldots, \\ &\qquad\qquad\qquad\qquad\qquad\qquad\qquad\qquad (0 < \rho < a) \\ &\int_0^\infty g_{01}(\lambda)\, J_0(\lambda\rho)\, d\lambda = 0, \qquad\qquad\qquad\qquad (a \leqslant \rho < \infty) \end{aligned}\right\}. \qquad (32)$$

As in (29) we write $g_{01}(\lambda) = g_{00}(\lambda) + g_{02}(\lambda)$, where $g_{00}(\lambda)$ is given by

$$\left.\begin{aligned} &\int_0^\infty \lambda g_{00}(\lambda)\, J_0(\lambda\rho)\, d\lambda = \tfrac{1}{4}(\kappa a)^2 - i\frac{2}{9\pi}(\kappa a)^3 - \tfrac{1}{8}(\kappa\rho)^2 + \ldots, \\ &\qquad\qquad\qquad\qquad\qquad\qquad\qquad\qquad (0 < \rho < a) \\ &\int_0^\infty g_{00}(\lambda)\, J_0(\lambda\rho)\, d\lambda = 0 \end{aligned}\right\}. \qquad (33)$$

According to (22) and (24), the solution of the above equation is

$$g_{00}(\lambda) = \left\{\tfrac{1}{4}(\kappa a)^2 - i\frac{2}{9\pi}(\kappa a)^3\right\} g_0(\lambda) - \tfrac{1}{8}(\kappa a)^2 g_2(\lambda),$$

where $g_2(\lambda)$ is defined by (25).

It is easily seen that the next approximation for $g_{22}(\lambda)$ introduces terms in $(\kappa a)^4$ and higher powers.

Finally we have as the approximate solution of the original diffraction equation (28) correct to the order $(\kappa a)^3$,

$$g(\lambda) = \left\{1 + \tfrac{1}{4}(\kappa a)^2 - i\frac{2}{9\pi}(\kappa a)^3 \,..\right\} g_0(\lambda) - \tfrac{1}{8}(\kappa a)^2 g_2(\lambda). \qquad (34)$$

We note the following asymptotic expression for the radiation field in terms of the polar co-ordinates (γ, θ), $(r \gg \lambda \gg 2\pi a)$,

$$\phi = \int_0^\infty e^{-\mu|z|} J_0(\lambda\rho) f(\lambda) \frac{\lambda}{\mu} d\lambda \sim \frac{e^{-i\kappa r}}{r} f(\kappa \sin\theta), \qquad (35)^*$$

which gives as the asymptotic expression for the normal diffraction field,

$$\chi = \int_0^\infty e^{-\mu|z|} J_0(\lambda\rho)\, g(\lambda)\, d\lambda \sim i\kappa \cos\theta \, \frac{g(\kappa \sin\theta)}{\kappa \sin\theta} \cdot \frac{e^{-i\kappa r}}{r}.$$

Remembering that $\kappa a \sin\theta \leqslant 1$, we find from (23) and (25), since, for small values of x,

$$g_0(x)/x \sim \frac{2}{3\pi} a^2, \qquad g_2(x)/x \sim \frac{4}{15\pi} a^2,$$

the following asymptotic expression for the diffraction field,

$$\chi \sim \frac{2}{3\pi} i\kappa a^3 \left\{1 + \tfrac{1}{5}(\kappa a)^2 - i\frac{2}{9\pi}(\kappa a)^3\right\} \cos\theta \, \frac{e^{-i\kappa r}}{r}. \qquad (36)$$

On making use of (34) to calculate the inertia constants m_1, and m_2 according to equation (12), we easily find, on carrying out successive approximations to include terms in $(\kappa a)^5$,

$$m_1 + im_2 \sim \tfrac{8}{3}\rho_0 a^3 \left[1 + \tfrac{1}{5}(\kappa a)^2 - i\frac{2}{9\pi}(\kappa a)^3 \{1 + \tfrac{1}{4}(\kappa a)^2\}\right]. \qquad (37)\dagger$$

It is evident that the procedure of this section provides a solution of the normal diffraction problem for a circular disc which may be carried

---

* King, ' Can. J. Res.,' vol. 11, p. 140 (1934).

† According to Hanson's theory of diffraction (' Phil. Trans.,' A, vol. 232, p. 267 (1934)), based on the use of ellipsoidal wave functions, I find

$$m_1 + im_2 \sim \tfrac{8}{3}\rho_0 a^3 \left\{1 + \tfrac{1}{5}(\kappa a)^2 - i\frac{8}{35\pi}(\kappa a)^3 \ldots\right\}.$$

It would appear that m_2 for a small disc which is the limit of an oblate spheroid differs slightly (one part in thirty-five) from the corresponding value when the disc is considered to be the limit of a circular lamina of uniform thickness.

out to any required degree of accuracy in powers of (κa), although the computations necessary for powers beyond the third become progressively tedious.

To compare the results of this section with Rayleigh's approximations for the diffraction of plane waves by a fixed circular disc, we write

$$\phi_p = e^{i\kappa z} + \chi_p, \qquad \phi_m = e^{i\kappa z} - \chi_m,$$

with

$$\chi_p = \int_0^\infty g(\lambda)\, e^{-\mu z}\, J_0(\lambda\rho)\, d\lambda, \quad (z > 0):$$

$$\chi_m = \int_0^\infty g(\lambda)\, e^{\mu z}\, J_0(\lambda\rho)\, d\lambda, \quad (z < 0).$$

The boundary conditions,

$$(\partial\phi_p/\partial z)_{z=0} = (\partial\phi_m/\partial z)_{z=0} = 0, \quad (0 < \rho < a):$$

$$(\phi_p)_{z=0} = (\phi_m)_{z=0}, \quad (a \leqslant \rho < \infty),$$

require the solution of the integral equation,

$$\int_0^\infty \mu\, g(\lambda)\, J_0(\lambda\rho)\, d\lambda = i\kappa, \quad (0 < \rho < a):$$

$$\int_0^\infty g(\lambda)\, J_0(\lambda\rho)\, d\lambda = 0, \quad (a \leqslant \rho < \infty).$$

On comparing the above equation with (28) we see that $\chi_p = i\kappa\chi$, so that according to (36)

$$\chi_p = -\frac{2}{3\pi}\kappa^2 a^3 \left\{1 + \tfrac{1}{5}(\kappa a)^2 - i\frac{2}{9\pi}(\kappa a)^3 \ldots\right\} \cos\theta\, \frac{e^{-i\kappa r}}{r},$$

the leading terms of which agree with Rayleigh's solution as quoted by Lamb.*

6—ACOUSTIC RADIATION PRESSURE ON SMALL CIRCULAR DISC IN A PROGRESSIVE PLANE WAVE $(\kappa a \lll 1)$

In a plane wave propagated along the normal to the disc, the velocity potential is independent of ρ, so that $(\partial\phi_i/\partial\rho)_{z=0} = 0$. It follows from equations (1) and (2) that $(\partial\phi_p/\partial\rho)_{z=0} = -(\partial\phi_m/\partial\rho)_{z=0}$, with the result that according to (18) $P_q = 0$. Since we have also $P_\zeta = 0$, we have from (17),

$$P = P_\phi = \tfrac{1}{2}\frac{\rho_0}{c^2}\int_0^a (\dot{\phi}_m^2 - \dot{\phi}_p^2)_{z=0} \,.\, 2\pi\rho\, d\rho.$$

---

* Lamb, "Hydrodynamics," 6th ed., 1932, § 299, p. 517; also Rayleigh, "Scientific Papers," vol. 2, p. 283.

Furthermore, according to (1) and (2), $\frac{1}{2}(\dot{\phi}_m + \dot{\phi}_v) = \dot{\phi}_i$, so that

$$P = \frac{\rho_0}{c^2}\int_0^a \dot{\phi}_i(\dot{\phi}_m - \dot{\phi}_v)_{z=0}\, 2\pi\rho\, d\rho. \tag{38}$$

In the circumstances of the present section $\dot{\phi}_i$ is independent of ρ, and

$$P = \frac{\rho_0 \dot{\phi}_i}{c^2}\int_0^a (\dot{\phi}_m - \dot{\phi}_v)_{z=0}\, 2\pi\rho\, d\rho. \tag{39}$$

In a plane progressive wave, we have

$$\phi_i = |A|\, e^{-i(\kappa z - \omega t)}, \tag{40}$$

and cleared of imaginary quantities,

$$(\dot{\phi}_i)_{z=0} = -\,|A|\,\omega \sin \omega t. \tag{41}$$

Furthermore,

$$\begin{aligned}\rho_0\int_0^a (\dot{\phi}_m - \dot{\phi}_v)\, 2\pi\rho\, d\rho &= i\omega\rho_0\int_0^a (\phi_m - \phi_v)\, 2\pi\rho\, d\rho \\ &= -\,i\omega\,.\,4\pi\rho_0 a\int_0^\infty J_1(\lambda a) f(\lambda)\frac{dt}{\lambda} \\ &= i\omega m_0 \dot{\zeta},\end{aligned}$$

according to equation (8). If we now make use of (14) we have

$$\rho_0\int_0^a (\dot{\phi}_m - \dot{\phi}_v)\, 2\pi\rho\, d\rho = \frac{-\,i\omega m_0(M_1 + iM_2)}{m_0 + m_1 + im_2}. \tag{42}$$

According to (9), (10), (11), and (13),

$$M_1 + iM_2 = (m_1 + im_2)(\partial\phi_i/\partial z)_{z=0} = -\,|A|\, i\kappa\,(m_1 + im_2)\, e^{i\omega t},$$

so that

$$\begin{aligned}\rho_0\int_0^a (\dot{\phi}_m - \dot{\phi}_v)\, 2\pi\rho\, d\rho &= -\,\frac{|A|\,\kappa\omega m_0(m_1 + im_2)}{m_0 + m_1 + im_2}\, e^{i\omega t} \\ &= R_p \cos\omega t + S_p \sin\omega t,\end{aligned}$$

where

$$S_p = \frac{\kappa\omega m_0^2 m_2\,|A|}{(m_0 + m_1)^2 + m_2^2}, \tag{43}$$

the suffix $_p$ denoting that we are dealing with a *progressive wave*.

From (39) we have

$$P = -\,\frac{|A|\,\omega}{c^2}\sin\omega t\,\{R_p\cos\omega t + S_p\sin\omega t\},$$

which gives, on taking the time-average,

$$\overline{\mathrm{P}} = -\tfrac{1}{2}\frac{|\mathrm{A}|\,\omega}{c^2}\,\mathrm{S}_v = -\tfrac{1}{2}\kappa^3\,|\mathrm{A}|^2\,m_2\,\frac{m_0^{\,2}}{(m_0+m_1)^2+m_2^{\,2}}.$$

If we now introduce the approximate values of m_1 and m_2 according to equation (37), we have, neglecting m_2 compared with m_1, for a thin disc of uniform thickness,

$$\overline{\mathrm{P}} \sim \frac{8}{27\pi}\,\rho_0\,|\mathrm{A}|^2\,(\kappa a)^6\left\{\frac{m_0}{m_0+m_1}\right\}^2\{1+\tfrac{1}{4}(\kappa a)^2\}, \qquad (44)^*$$

where m_0 is the mass of the disc, and $m_1 = \frac{8}{3}\,\rho_0\,a^3\,\{1+\frac{1}{5}(\kappa a)^2\}$.

For a thin disc which is considered to be the limit of an oblate spheroid, the numerical factor $8/27\pi$ is replaced by $32/105\pi$.

We notice from (44) that the radiation pressure is in the direction of propagation of the wave, and is extremely small, being proportional to the sixth power of the ratio of the circumference to the wave-length. The term $m_0^{\,2}/(m_0+m_1)^2$ is the "inertia factor" arising from the small oscillations of the disc in the incident wave, a state of affairs which occurs in practice when the acoustic radiation pressure on a freely suspended disc is used to measure the amplitude of a sound-wave. A numerical estimate of $\bar{\mathrm{P}}$ from (37) with an optimum inertia factor $(m_1/m_0 \to 0)$ indicates that in a progressive air wave of even 100 decibels the acoustic radiation pressure is too small to be measured.

Since the mean total energy-density in the wave is $\overline{\mathrm{E}} = \frac{1}{2}\rho_0\kappa^2\,|\mathrm{A}|^2$, we may write (44) in the form

$$\left.\begin{aligned} &\frac{\bar{\mathrm{P}}}{\pi a^2} \sim \frac{16}{27\pi^2}(\kappa a)^4\,\mathrm{F}_v\,(\rho_0/\rho_1)\,\overline{\mathrm{E}},\\ \text{where}\quad &\mathrm{F}_v(\rho_0/\rho_1) = \frac{1+\frac{1}{4}(\kappa a)^2}{\left[1+\dfrac{8}{3\pi}\dfrac{\rho_0}{\rho_1}\dfrac{a}{t_1}\{1+\frac{1}{5}(\kappa a)^2\}\right]^2}, \end{aligned}\right\} \qquad (45)$$

---

[*] For a small sphere of radius a and density ρ_1, the corresponding expression for the acoustic radiation pressure in a progressive plane wave is found to be

$$\overline{\mathrm{P}}_s \sim \tfrac{1}{2}\pi\rho_0\,|\mathrm{A}|^2\,(\kappa a)^6\,\frac{\left\{1+\frac{2}{9}\left(1-\frac{\rho_0}{\rho_1}\right)^2\right\}}{(1+\frac{1}{2}\rho_0/\rho_1)^2},$$

considerably greater than that on a circular disc of the same radius. In fact, comparing the pressures on sphere and disc of the same radius for which $\rho_0/\rho_1 \to 0$, we find $\overline{\mathrm{P}}_s/\overline{\mathrm{P}}_d = \dfrac{33\pi^2}{16} = 20{\cdot}2$.

t_1 being the uniform thickness of the disc and ρ_1 its density. For a thin disc which is the limit of an oblate spheroid of maximum thickness t_1, the numerical factor in the expression for $\overline{\mathrm{P}}$ must be replaced by $64/105\pi^2$, while the denominator of the inertia factor $\mathrm{F}_p(\rho_0/\rho_1)$ becomes

$$\left\{1 + \frac{4}{\pi}\frac{\rho_0}{\rho_1}\frac{a}{t_1}\left(1 + \tfrac{1}{6}(\kappa a)^2\right)\right\}^2.$$

7—ACOUSTIC RADIATION PRESSURE ON A SMALL CIRCULAR DISC IN A STATIONARY PLANE WAVE ($\kappa a \leqslant 1$)

As in § 6, we have $\mathrm{P}_\rho = 0$ and $\mathrm{P}_\zeta = 0$ for an incident velocity potential independent of ρ. For a system of plane stationary waves we take

$$\phi_i = |\mathrm{A}| \cos \kappa (z + h)\, e^{i\omega t}, \tag{46}$$

where the plane of the disc is at a distance h from a fixed plane of reference. We find

$$(\dot{\phi}_i)_{z=0} = -\, |\mathrm{A}|\, \omega \cos \kappa h \sin \omega t, \tag{47}$$

and, according to (10) and (13),

$$\mathrm{M}_1 + i\mathrm{M}_2 = (m_1 + im_2)\,(\partial\phi_i/\partial z)_{z=0} = -\,(m_1 + im_2)\,|\mathrm{A}|\,\kappa \sin \kappa h e^{i\omega t}.$$

Equation (42), which applies to all plane wave systems, now gives

$$\rho_0 \int_0^a (\dot{\phi}_m - \dot{\phi}_p)\, 2\pi\rho\, d\rho = |\mathrm{A}|\, i\omega\kappa m_0 \sin \kappa h \,\frac{m_1 + im_2}{m_0 + m_1 + im_2}\, e^{i\omega t}$$

$$= \mathrm{R}_s \cos \omega t + \mathrm{S}_s \sin \omega t,$$

where

$$\mathrm{S}_s = -\, |\mathrm{A}|\, \omega\kappa \sin \pi h\, m_0 \,\frac{\{m_1(m_0 + m_1) + m_2^2\}}{(m_0 + m_1)^2 + m_2^2}, \tag{48}$$

the suffix s referring to a *stationary wave*.

According to (39) we have, introducing $\dot{\phi}_i$ from (47),

$$\overline{\mathrm{P}} = -\,\frac{|\mathrm{A}|\,\omega}{c^2} \cos \kappa h \sin \omega t\,\{\mathrm{R}_s \cos \omega t + \mathrm{S}_s \sin \omega t\},$$

which gives, on taking the time-average,

$$\overline{\mathrm{P}} = -\tfrac{1}{2}\,|\mathrm{A}|\,(\omega/c^2) \cos \kappa h \mathrm{S}_s = \tfrac{1}{2}\,|\mathrm{A}|^2 k^3 \sin \kappa h \cos \kappa h m_0 \,.\, \frac{m_1(m_0 + m_1) + m_2^2}{(m_0 + m_1)^2 + m_2^2}.$$

Since we may neglect m_2 in comparison with m_1, we finally obtain

$$\overline{\mathrm{P}} \sim \tfrac{2}{3}\rho_0 \, |\mathrm{A}|^2 \, (\kappa a)^3 \sin 2\kappa h \, \frac{m_0}{m_0 + m_1} . \tag{49*}$$

In terms of the total energy-density of the medium, $\overline{\mathrm{E}} = \tfrac{1}{2}\rho_0 \, \kappa^2 \, | \mathrm{A} |^2$, we may write (49) in the form,

$$\left.\begin{aligned} \frac{\overline{\mathrm{P}}}{\pi a^2} &\sim \frac{4}{3\pi} (\kappa a) \sin 2\kappa h \, \mathrm{F}_s (\rho_0/\rho_1) \\ \text{where} \quad \mathrm{F}_s (\rho_0/\rho_1) &= \left\{1 + \frac{8}{3\pi} \frac{\rho_0}{\rho_1} \frac{a}{t_1} (1 + \tfrac{1}{6} (\kappa a)^2)\right\}^{-1} \end{aligned}\right\} . \tag{50}$$

In the case of a thin disc which is the limit of an oblate spheroid of maximum thickness t_1, the numerical factor $4/3\pi$ remains unaltered, but the inertia factor $\mathrm{F}_s (\rho_0/\rho_1)$ becomes

$$\left\{1 + \frac{4}{\pi} \frac{\rho_0}{\rho_1} \frac{a}{t_1} (1 + \tfrac{1}{6} (\kappa a)^2)\right\}^{-1} .$$

It will be noticed on comparing (44) and (49) that the mean radiation pressure on a small, thin disc in a plane stationary radiation field is of a much greater order of magnitude than that exerted on it by progressive waves of the same amplitude.

The inertia factors in (44) and (49) vanish as $m_0/m_1 \to 0$. The disc then sways backwards and forwards in phase with medium itself, generates no secondary radiation field, and, as a result, the radiation pressure vanishes. From a practical point of view the ratio m_0/m_1 should be as large as possible in designing pressure discs for the measurement of supersonics in water.

Since the inertia factor $\mathrm{F} (\rho_0/\rho_1)$ is always positive, it is readily seen that radiation pressure is always such as to urge the disc away from the nodes ($\xi = 0$ at $h = 0, \pm \pi/\kappa, \pm 2\pi/\kappa$, etc.) toward the loops.

It is interesting to notice that (50), as regards its linear dependence on (κa), follows the early trend of observations by Boyle and Lehmann†

---

* For a small sphere of radius a and the mass m_0 the corresponding formula for the radiation pressure in a plane stationary wave is

$$\overline{\mathrm{P}}_s \simeq \frac{5\pi}{6} \rho_0 \, | \mathrm{A} |^2 \, (\kappa a)^3 \sin 2\kappa h \, . \left\{\frac{m_0 - \tfrac{4}{5} m_1}{m_0 + m_1}\right\},$$

where $m_1 = \frac{2\pi}{3} \rho_0 a^3$. Comparing the pressures on sphere and disc for $\rho_0/\rho_1 \to 0$ we see that $\overline{\mathrm{P}}_s/\overline{\mathrm{P}}_d \simeq \frac{5\pi}{4} = 3{\cdot}92$.

† 'Can. J. Res.,' vol. 3, p. 491 (1930).

relating to radiation pressures on circular discs of lead placed in the central beam of a supersonic piezo-electric oscillator. In view of the fact that the radiation pressure on discs is employed to study the characteristics of supersonic radiation fields, a detailed experimental examination of the problem is worthy of consideration. It is evident on comparing (44) and (49) that the radiation pressure on a small, thin disc does not depend only on the local specifications of the field such as the total mean energy-density in the neighbourhood of the disc, but depends, according to theory, on the nature of the incident field as a whole as related to the mode of generation of the sound waves.

When the incident radiation field is symmetrical about the normal through the centre of the disc and varies appreciably with ρ over the radius of the disc, it is necessary to solve the integral equation (11) for $G(\lambda)$ according to the procedure of § 5, and to calculate the inertia coefficients M_1 and M_2 according to (13). In these circumstances it is evident from (18) that P_q will contribute towards the total radiation pressure.

It appears possible, furthermore, to extend the procedure of § 5 to obtain asymptotic solutions of the fundamental integral equations of diffraction, (10) and (11), to the case $(\kappa a) \gg 1$, the detailed consideration of which development must be deferred to a future communication.

8—SUMMARY AND CONCLUSIONS

The calculation of the acoustic radiation pressure on a thin, circular disc of uniform thickness in an axially symmetrical incident field whose velocity potential is ϕ_i requires the solution of the corresponding diffraction problem in such a form that the velocity potentials on the two sides of the disc may be evaluated.

By expressing the velocity potential of the diffracted wave in cylindrical co-ordinates, use is made of the wave function

$$\chi = \int_0^\infty e^{-\mu|z|}\, J_0(\lambda\rho)\, g(\lambda)\, d\lambda, \qquad \text{(i)}$$

where $\mu = (\lambda^2 - \kappa^2)^{\frac{1}{2}}$.

The boundary conditions over the plane $z = 0$ in which the disc is situated lead to an integral equation of the type

$$\int_0^\infty \mu g(\lambda)\, J_0(\lambda\rho)\, d\lambda = F_0(\rho), \quad (0 < \rho < a):$$

$$\int_0^\infty g(\lambda)\, J_0(\lambda\rho)\, d\lambda = 0, \quad (a \leqslant \rho < \infty), \qquad \text{(ii)}$$

in which the "kernel" is discontinuous at the radius $\rho = a$ of the disc, and $F_\nu(\rho)$ is an assigned function of ρ depending on the nature of the incident radiation field.

By making use of the known solution of the corresponding equations in potential theory, $(\kappa = 0)$,

$$\int_0^\infty \lambda g_0(\lambda)\, J_0(\lambda\rho)\, d\lambda = F_0(\rho), \quad (0 < \rho < a):$$
$$\int_0^\infty g_0(\lambda)\, J_0(\lambda\rho)\, d\lambda = 0, \quad (a \leqslant \rho < \infty), \qquad \text{(iii)}$$

it is shown how the solution of the integral equation of diffraction (ii) may be solved to any degree of accuracy by a method of successive approximations.

The pressure variation in a compressible medium in which the pressure is any function of the density is given by

$$\delta p = \rho_0 \dot{\phi} - \tfrac{1}{2}\rho_0 q^2 + \tfrac{1}{2}\frac{\rho_0}{c^2}\dot{\phi}^2. \qquad \text{(iv)}$$

On integrating over the disc the time-average of the acoustic radiation pressure $\overline{P}$ is obtained. For plane waves travelling normally to the disc, the term $\tfrac{1}{2}(\rho_0/c^2)\,\dot{\phi}^2$ alone contributes to the total mean pressure. When the incident potential depends on ρ the term $\tfrac{1}{2}\rho_0 q^2$ also contributes. A possible contribution $\overline{P}_\nu$, arising from the motion of the origin at the centre of the obstacle which performs small oscillations under the influence of the first-order radiation pressure, is always zero for uniformly thin discs, but has to be taken into account in dealing with obstacles of finite thickness along the z-axis.

In a plane progressive wave for which $\phi_i = |A|\, e^{-i\kappa z}$, the radiation pressure $\overline{P}$ is always positive. For a disc of uniform thickness t_1 and density ρ_1, whose circumference is small compared with the wave-length

$$\frac{\overline{P}}{\pi a^2} \sim \frac{16}{27\pi^2}(\kappa a)^4\, F_\nu(\rho_0/\rho_1)\,.\,\overline{E}, \qquad \text{(v)}$$

where $\overline{E}$ is the mean total energy-density in the medium and $F_\nu(\rho_0/\rho_1)$ is the inertia factor corrected for diffraction,

$$F_\nu(\rho_0/\rho_1) = \frac{1 + \frac{1}{4}(\kappa a)^2}{\left\{1 + \frac{8}{3\pi}\frac{\rho_0}{\rho_1}\frac{a}{t_1}\left(1 + \frac{1}{6}(\kappa a)^2\right)\right\}^2}. \qquad \text{(vi)}$$

In a stationary wave-field for which $\phi_i = |A| \cos\kappa(z + h)$, the radiation pressure $\overline{P}$ is periodic, depending on the position of the plane of the disc with respect to the planes of loops and nodes. For discs of small radius

$$\frac{\overline{\mathrm{P}}}{\pi a^2} \sim \frac{4}{3\pi}(\kappa a)\sin 2\kappa h\,\mathrm{F}_s(\rho_0/\rho_1)\,.\,\overline{\mathrm{E}}, \tag{vii}$$

where

$$\mathrm{F}_s(\rho_0/\rho_1) = \left\{1 + \frac{8}{3\pi}\frac{\rho_0}{\rho_1}\frac{a}{t_1}\left(1 + \tfrac{1}{5}(\kappa a)^2\right)\right\}^{-1}. \tag{viii}$$

It is important to note that the radiation pressure on a small disc is of a much higher order of magnitude than in a progressive wave, while the inertia factor is different in the two cases.

As in the problem of radiation pressures on small spheres previously dealt with by the writer, it is important to note that $\overline{\mathrm{P}}$ does not depend only on $\overline{\mathrm{E}}$ in the neighbourhood of the disc but on the nature of the incident field as a whole as related to the mode of generation of the sound waves.

[*Note added in proof, October* 25, 1935—The finite thickness t of the disc may be approximately taken into account by carrying out the integration in the dynamical equation (7) over the faces $z = \pm \frac{1}{2}t$ of the disc. The result of doing so is to replace m_0 in formulae (44) and (49) by $(m_0 - m_w)$, where $m_w = \pi\rho_0 a^2 t$ is the mass of the medium displaced by the disc. The procedure is briefly indicated in the accompanying paper on the theory of the Rayleigh disc. The corresponding changes in the inertia factors $\mathrm{F}_p(\rho_0/\rho_1)$ and $\mathrm{F}_s(\rho_0/\rho_1)$ are easily made.]

On the Theory of the Inertia and Diffraction Corrections for the Rayleigh Disc

By LOUIS V. KING, F.R.S., Macdonald Professor of Physics, McGill University, Montreal

(*Received July* 8, 1935)

1—INTRODUCTION

A thin circular disc suspended by a quartz fibre tends to set itself broadside on to the direction of propagation of incident sound waves, and its use in combination with resonators is well known as a means of measuring relative intensities of acoustic radiation fields.*

In a progressive or stationary wave in which the velocity amplitude is $|\dot{\xi}|$, the average couple on a circular disc of radius a is usually given by the well-known formula

$$\overline{\mathrm{L}} = -\tfrac{4}{3}\rho_0 a^3 |\dot{\xi}|^2 \sin 2\alpha, \tag{1}$$

where ρ_0 is the density of the medium and α is the angle between the direction of propagation of the wave-front and the normal to the disc, while the negative sign indicates that the couple tends to diminish α.

Formula (1), in Rayleigh's original treatment,† depends on the hydrodynamical theory of the couple exerted on an oblate spheroid in a stream of incompressible fluid of uniform velocity,‡ in which the disc is taken to be an extremely thin spheroid.

In a recent paper Kotani§ has calculated the couple $\overline{\mathrm{L}}$ on a *rigidly fixed* disc in a plane progressive sound-wave. His treatment makes use of ellipsoidal co-ordinates to solve the corresponding problem of oblique diffraction, and the following formula is given,

$$\overline{\mathrm{L}} = -\tfrac{4}{3}\rho_0 a^3 |\dot{\xi}|^2 \sin 2\alpha \left\{1 + \tfrac{1}{5}(\kappa a)^2 (1 + \tfrac{1}{3}\cos 2\alpha) + \dots\right\}, \qquad (2)\|$$

---

* [*Added, October* 18, 1935—A brief account of the Rayleigh disc, with references to its practical use in the measurement of sound, is given in a recent paper by Wente, 'J. Acoustical Soc. Amer.,' vol. 7, p. 1 (1935).]

† "Theory of Sound," 2nd ed., 1896, vol. 2, p. 253*b*, p. 43.

‡ 'Wied. Ann.,' vol. 43, p. 51 (1891).

§ 'Proc. Phys. Math. Soc. Japan,' vol. 15, p. 30 (1933).

|| Kotani's formula includes terms to $(\kappa a)^4$. Opportunity is here taken of correcting an obvious numerical slip in Kotani's formulae (1), (43), and (44) in which the numerical factor 3/4 should be written 4/3.

where in the usual notation κa is the ratio of the circumference of the disc to the wave-length. As might be expected, the analysis involving the use of ellipsoidal wave functions is somewhat difficult, and numerical computation tedious when $\kappa a > 1$.

As employed in practice, a Rayleigh disc is *freely suspended*, in which circumstances it performs small oscillations along its normal under the influence of the first-order radiation pressure, as well as angular oscillations about the axis of suspension. The inclusion of the first effect is to introduce a factor $m_1/(m_1 + m_0)$ on the right-hand side of equation (1), m_1 being the mass of the disc, and m_0 its hydrodynamic mass, $m_0 = \frac{8}{3} . \rho_0 a^3$. This will be called the " inertia factor," and its magnitude may differ appreciably from unity in Rayleigh discs of high sensitivity, especially when employed to measure the intensity of sound in liquids. The effect of the angular oscillations is to introduce a factor $I_1/(I_1 + I_0)$ in the terms of order $(\kappa a)^2$, and is of lesser importance in discs of circumference small compared with the wave-length. In this " angular inertia factor," I_1 is the moment of inertia of the disc *in vacuo* and I_0 its hydrodynamic moment of inertia.*

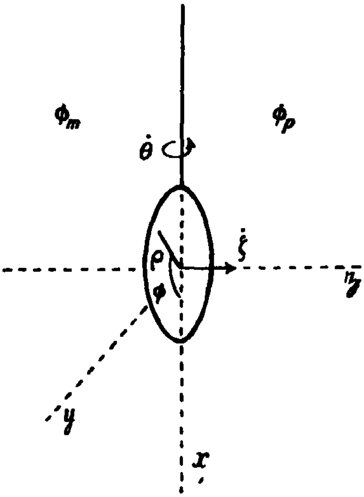

Fig. 1.

The inertia and diffraction corrections to the fundamental formula (1) require the solution of the diffraction of the incident radiation field when the direction of propagation in the neighbourhood of the disc is inclined at an angle α to its normal. In the following sections this problem is dealt with in terms of cylindrical wave functions. The boundary conditions over the plane of the disc lead to a set of integral equations having a discontinuous kernel, the solutions of which may be obtained to any degree of accuracy by a method of successive approximations, while the analysis is confined to the use of well-known formulae in the theory of Bessel's functions.

---

* [*Added, October* 18, 1935—When the finite thickness t_1 of the disc is taken into account it is shown in the first note inserted at the end of this paper that m_1 and I_1 are replaced by $(m_1 - m_w)$ and $(I_1 - I_w)$, where $m_w = \pi a^2 \rho_0 t_1$ is the mass of the medium displaced by the disc, and $I_w = m_w \pi^2$ is the moment of inertia of an equal disc having the density of the medium.]

2—DERIVATION OF THE FUNDAMENTAL INTEGRAL EQUATIONS

The position of the disc with regard to the axes of reference is shown in fig. 1. The axis of z is taken along the normal to the disc, the origin at its centre and the axis of suspension along the axis of x. The position of any point in space is defined by the cylindrical co-ordinates (ρ, z, ϕ), the azimuth ϕ being measured from the x-axis towards that of y. The velocity potential of the incident radiation field is denoted by ϕ_i, that of the diffracted field on the positive side of the plane of the disc by ϕ_p, and that on the negative or minus side by ϕ_m. Each of the ϕ's must satisfy the wave equation expressed in cylindrical co-ordinates

$$\frac{\partial^2\phi}{\partial\rho^2} + \frac{1}{\rho}\frac{\partial\phi}{\partial\rho} + \frac{1}{\rho^2}\frac{\partial^2\phi}{\partial\phi^2} + \frac{\partial^2\phi}{\partial z^2} = \frac{1}{c^2}\frac{\partial^2\phi}{\partial t^2}. \tag{3}$$

We write down as a general type of solution for the velocity potentials on the positive and minus sides of the disc the following expressions

$$\left.\begin{aligned} \phi_p &= \phi_i + \sum_0^\infty \int_0^\infty \{A_s(\lambda)\cos s\phi + B_s(\lambda)\sin s\phi\}\, e^{-\mu z} J_s(\lambda\rho)\, d\lambda \\ \phi_m &= \phi_i - \sum_0^\infty \int_0^\infty \{A(\lambda)\cos s\phi + B_s(\lambda)\sin s\phi\}\, e^{\mu z} J_s(\lambda\rho)\, d\lambda \end{aligned}\right\}. \tag{4}^*$$

where $\mu = (\lambda^2 - \kappa^2)^{1/2}$, and, as usual, the time-factor is $e^{i\omega t}$, while $\kappa = \omega/c$.

Let ζ be the velocity of the disc along the z axis, and $\dot{\theta}$ its angular velocity about the x-axis due to the first-order pressures arising from the incident radiation field. At any point (ρ, ϕ) on the disc the velocity is

$$\zeta + y\theta = \zeta + \dot{\theta}\rho \sin\phi.$$

The boundary conditions over the plane $z = 0$ are therefore

$$\left.\begin{aligned} \zeta + \theta\rho\sin\phi = -(\partial\phi_p/\partial z)_{z=0} &= -(\partial\phi_m/\partial z)_{z=0}, \quad (0 < \rho < a) \\ -(\partial\phi_p/\partial z)_{z=0} &= -(\partial\phi_m/\partial z)_{z=0}, \quad (a < \rho < \infty) \end{aligned}\right\}. \tag{5}$$

We shall suppose that over the plane of the disc, $z = 0$, $(\partial\phi_i/\partial z)_{z=0}$ is expanded in the form

$$(\partial\phi_i/\partial z)_{z=0} = \sum_0^\infty \{A_{is}(\rho)\cos s\phi + B_{is}(\rho)\sin s\phi\}. \tag{6}$$

---

[*] Since $\int_0^\infty (\lambda/\mu)\, e^{-\mu z} J_0(\lambda\rho)\, d\lambda = e^{-i\kappa R}/R$, (Watson, "Theory of Bessel Functions" (1922), § 13.47), it is evident that in general the terms on the right-hand side of (4) also represent divergent waves when associated with the time-factor $e^{i\omega t}$.

Furthermore, equality of pressure in the medium on the two sides of the plane $z = 0$ at, and outside, the boundary of the disc $\rho = a$ necessitates the further boundary condition

$$(\phi_p)_{z=0} = (\phi_m)_{z=0}, \quad (a \leqslant \rho < \infty). \tag{7}$$

Since the boundary conditions (5) and (7) hold for all values of ρ and ϕ, we are led to the following set of integral equations for the determinations of the " kernels " $A_s(\lambda)$ and $B_s(\lambda)$:

$$\begin{array}{l|l}
0 < \rho < a & a \leqslant \rho < \infty \\
\hline
\int_0^\infty \mu A_0(\lambda) J_0(\lambda\rho)\, d\lambda = \dot{\zeta} + A_{i0}(\rho) & \int_0^\infty A_0(\lambda) J_0(\lambda\rho)\, d\lambda = 0 \\
\int_0^\infty \mu B_0(\lambda) J_0(\lambda\rho)\, d\lambda = B_{i0}(\rho) & \int_0^\infty B_0(\lambda) J_0(\lambda\rho)\, d\lambda = 0 \\
\int_0^\infty \mu A_1(\lambda) J_1(\lambda\rho)\, d\lambda = A_{i1}(\rho) & \int_0^\infty A_1(\lambda) J_1(\lambda\rho)\, d\lambda = 0 \\
\int_0^\infty \mu B_1(\lambda) J_1(\lambda\rho)\, d\lambda = \rho\dot{\theta} + B_{i1}(\rho) & \int_0^\infty B_1(\lambda) J_1(\lambda\rho)\, d\lambda = 0 \\
\cdots\cdots\cdots\cdots\cdots\cdots & \cdots\cdots\cdots\cdots\cdots \\
\int_0^\infty \mu A_s(\lambda) J_s(\lambda\rho)\, d\lambda = A_{is}(\rho) & \int_0^\infty A_s(\lambda) J_s(\lambda\rho)\, d\lambda = 0 \\
\int_0^\infty \mu B_s(\lambda) J_s(\lambda\rho)\, d\lambda = B_{is}(\rho) & \int_0^\infty B_s(\lambda) J_s(\lambda\rho)\, d\lambda = 0 \\
\cdots\cdots\cdots\cdots\cdots\cdots & \cdots\cdots\cdots\cdots\cdots
\end{array} \tag{8}$$

The solution of this set of integral equations having discontinuous kernels is essentially the crux of the problem of oblique diffraction of an incident radiation field by a circular disc.

3—THE DYNAMICAL EQUATIONS FOR THE OSCILLATIONS OF THE DISC

The linear and angular velocities $\dot{\zeta}$ and $\dot{\theta}$ which appear in equations (8) are determined from the dynamical equations for the motion of the disc. If δp_m and δp_p are the first-order pressure variations in the medium on the minus and positive sides of the plane $z = 0$,

$$\delta p_m = \rho_0 \dot{\phi}_m \qquad \delta p_0 = \rho_0 \dot{\phi}_p \tag{9}$$

so that if m_1 is the mass of the disc, the dynamical equation is

$$\int_0^{2\pi} d\phi \int_0^a (\delta p_m - \delta p_p)\, \rho d\rho = m_1\ddot{\zeta} \qquad (z = 0),$$

which gives on integration with respect to the time

$$\rho_0 \int_0^{2\pi} d\phi \int_0^a (\phi_m - \phi_p)\, \rho d\rho = m_1\dot{\zeta} \qquad (z = 0).$$

On inserting the values of ϕ_m and ϕ_p from (4) and effecting the integrations, we are left with

$$m_1\dot{\zeta} = -4\pi\rho_0 a \int_0^\infty \mathrm{A}_0(\lambda)\, \mathrm{J}_1(\lambda a) \frac{d\lambda}{\lambda}. \tag{10}$$

Similarly if I_1 is the moment of inertia of the disc about the axis of suspension, moments about the x-axis gives

$$\int_0^{2\pi} d\phi \int_0^a y\,(\delta p_m - \delta p_p)\, \rho d\rho = \mathrm{I}_1\ddot{\theta}.$$

On making use of (9), introducing ϕ_m and ϕ_p from (4), and effecting the integrations, we are left with

$$\mathrm{I}_1\dot{\theta} = -2\pi\rho_0 a^2 \int_0^\infty \mathrm{B}_1(\lambda)\, \mathrm{J}_2(\lambda a) \frac{d\lambda}{\lambda}. \tag{11}$$

4—CALCULATION OF THE MOMENT OF THE ACOUSTIC RADIATION PRESSURE

The pressure variation in a compressible medium in which the pressure is any function of the density is given by

$$\delta p = \rho_0\dot{\phi} - \tfrac{1}{2}\rho_0 q^2 + \tfrac{1}{2}(\rho_0/c^2)\,\dot{\phi}^2, \tag{12}$$ *

in which the differentiation with respect to the time implied in $\dot{\phi}$ refers to an origin at rest. In the present problem the origin at the centre of the disc has a velocity $\dot{\zeta}$, so that if $\mathrm{D}\phi/\mathrm{D}t$ refers to this moving origin,

$$\dot{\phi} = \mathrm{D}\phi/\mathrm{D}t - \dot{\zeta}\,(\partial\phi/\partial z). \tag{13}$$

This correction to $\dot{\phi}$ is of the second order and its introduction into the last two second-order terms of (12) may be neglected. We now have for the pressure difference on the two sides of the disc $z = 0$,

$$\delta p_m - \delta p_p = \rho_0 \frac{\mathrm{D}}{\mathrm{D}t}(\phi_m - \phi_p) - \dot{\zeta}\frac{\partial}{\partial z}(\phi_m - \phi_p) - \tfrac{1}{2}\rho_0\,(q_m^2 - q_p^2) + \tfrac{1}{2}\frac{\rho_0}{c^2}(\dot{\phi}_m^2 - \dot{\phi}_p^2). \tag{14}$$

---

* On the derivation of this equation *see* King, 'Proc. Roy. Soc.,' A, vol. 147, p. 213 (1934).

Since the time-average of the first term vanishes, while the second is zero over the disc in view of the boundary conditions (5), only the last two terms contribute to the time-average of the couple on the disc.

We thus write

$$\left.\begin{aligned} L_q &= -\tfrac{1}{2}\rho_0 \int y\,(q_m^2 - q_p^2)\,dS \\ &\qquad = -\tfrac{1}{2}\rho_0 \int_0^{2\pi} \sin\phi\,d\phi \int_0^a (q_m^2 - q_p^2)\,\rho^2\,d\rho \\ L_\phi &= \tfrac{1}{2}\frac{\rho_0}{c^2} \int y(\dot{\phi}_m^2 - \phi_m^2)\,dS \\ &\qquad = \tfrac{1}{2}\frac{\rho_0}{c^2} \int_0^{2\pi} \sin\phi\,d\phi \int_0^a (\dot{\phi}_m^2 - \dot{\phi}_p^2)\,\rho^2 d\rho \end{aligned}\right\} . \qquad (15)$$

The total couple on the disc at any instant is

$$L = L_q + L_\phi, \qquad (16)$$

and the final result desired is obtained by taking time-averages of the terms $(q_m^2 - q_p^2)$ and $(\dot{\phi}_m^2 - \phi_p^2)$ before carrying out the integrations over the area of the discs.

Since we have for the squared velocity in the medium

$$q^2 = \left(\frac{\partial\phi}{\partial\rho}\right)^2 + \frac{1}{\rho^2}\left(\frac{\partial\phi}{\partial\phi}\right)^2 + \left(\frac{\partial\phi}{\partial z}\right)^2,$$

it follows that we may write

$$\begin{aligned} q_m^2 - q_p^2 = \frac{\partial}{\partial\rho}(\phi_m - \phi_p)\cdot\frac{\partial}{\partial\rho}(\phi_m + \phi_p) + \frac{1}{\rho^2}\frac{\partial}{\partial\phi}(\phi_m - \phi_p) \\ \cdot\frac{\partial}{\partial\phi}(\phi_m + \phi_p) + \frac{\partial}{\partial z}(\phi_m - \phi_p)\cdot\frac{\partial}{\partial z}(\phi_m + \phi_p). \end{aligned} \qquad (17)$$

On account of the boundary conditions (5) over the disc the last term vanishes.

We now denote, on writing $z = 0$ in equation (4),

$$\chi_s = \cos s\phi \int_0^\infty A_s(\lambda)\,J_s(\lambda\rho)\,d\lambda + \sin s\phi \int_0^\infty B_s(\lambda)\,J_s(\lambda\rho)\,d\lambda, \qquad (18)$$

so that $\phi_p = \phi_i + \sum\limits_s \chi_s$ and $\phi_m = \phi_i - \sum\limits_s \chi_s$, while (6) gives, together with (17),

$$q_m^2 - q_p^2 = -4\frac{\partial\phi_i}{\partial\rho}\Sigma\frac{\partial\chi_s}{\partial\rho} - \frac{4}{\rho^2}\frac{\partial\phi_i}{\partial\phi}\Sigma\frac{\partial\chi_s}{\partial\phi}. \qquad (19)$$

On introducing the time-factor $e^{i\omega t}$ we may write

$$\phi_i = (P_i + iQ_i)\, e^{i\omega t} \qquad \chi_s = (P_s + iQ_s)\, e^{i\omega t}. \tag{20}$$

If we take the real part of ϕ_i and χ_s and take the time-average of the product terms in (19) we find, according to (15),

$$\overline{L}_q = \rho_0 \sum_s \int_0^{2\pi} \sin\phi\, d\phi \int_0^a \left\{\rho^2 \left(\frac{\partial P_i}{\partial\rho}\frac{\partial P_s}{\partial\rho} + \frac{\partial Q_i}{\partial\rho}\frac{\partial Q_s}{\partial\rho}\right) + \left(\frac{\partial P_i}{\partial\phi}\frac{\partial P_s}{\partial\phi} + \frac{\partial Q_i}{\partial\phi}\frac{\partial Q_s}{\partial\phi}\right)\right\} d\rho. \tag{21}$$

Similarly we find from the second formula in (15)

$$\overline{L}_\phi = -\kappa^2\rho_0 \sum_s \int_0^{2\pi} \sin\phi\, d\phi \int_0^a (P_iP_s + Q_iQ_s)\, \rho^2\, d\rho. \tag{22}$$

Having solved the integral equations (8) to the required degree of accuracy, we are enabled to determine P_s and Q_s from (18) and (20). Finally the integrations implied in (21) and (22) enable us to determine the required average couple on the disc.

5—RAYLEIGH DISC IN A PROGRESSIVE PLANE WAVE—SOLUTION OF INTEGRAL EQUATIONS BY SUCCESSIVE APPROXIMATIONS FOR SMALL DISCS ($\kappa a \ll 1$)

A plane progressive sound wave making an angle α with the normal to the disc is represented by the velocity-potential

$$\phi_i = Ae^{-i\kappa(y\sin\alpha + z\cos\alpha)} = Ae^{\;i\kappa(my+zn)}, \tag{23}$$

where, for brevity, we write

$$m = \sin\alpha \qquad n = \cos\alpha. \tag{24}$$

Referring to equation (6), we have in cylindrical co-ordinates

$$\begin{aligned}(\partial\phi_i/\partial z)_{z=0} &= -Ai\kappa n e^{-i\kappa m\rho\sin\phi} \\ &= -Ai\kappa n\{J_0(\kappa m\rho) - 2iJ_1(\kappa m\rho)\sin\phi + 2J_2(\kappa m\rho\cos 2\phi) - \ldots\}.\end{aligned}$$

Comparing the above expansion with (6) we have

$$\left.\begin{aligned} A_{i0}(\rho) &= -Ai\kappa nJ_0(\kappa m\rho) & B_{i0}(\rho) &= 0 \\ A_{i1}(\rho) &= 0 & B_{i1}(\rho) &= -2A\kappa nJ_1(\kappa m\rho) \\ A_{i2}(\rho) &= -2Ai\kappa nJ_2(\kappa m\rho) & B_{2i}(\rho) &= 0 \end{aligned}\right\}. \tag{25}$$

Since we are dealing with the case $\kappa a \leqslant 1$, it follows that $\kappa m\rho \leqslant 1$ in the range $0 < \rho < a$, so that retaining second powers of $\kappa m\rho$ in (25), the solution of the oblique diffraction problem to an accuracy $(\kappa a)^2$ requires the solution of three integral equations of the set given in (8),

$$\begin{array}{l|l}
0 < \rho < a & a \leqslant \rho < \infty \\
\hline
\int_0^\infty \mu A_0(\lambda) J_0(\lambda\rho)\, d\lambda = \dot{\zeta} - Ai\kappa n\,(1 - \tfrac{1}{4}\kappa^2 m^2 \rho^2) & \int_0^\infty A_0(\lambda) J_0(\lambda\rho)\, d\lambda = 0 \\
\int_0^\infty \mu B_1(\lambda) J_1(\lambda\rho)\, d\lambda = \rho\,(\dot{\theta} - A\kappa^2 mn) & \int_0^\infty B_1(\lambda) J_1(\lambda\rho)\, d\lambda = 0 \\
\int_0^\infty \mu A_2(\lambda) J_2(\lambda\rho)\, d\lambda = -\tfrac{1}{4} Ai\kappa n\kappa^2 m^2 \rho^2 & \int_0^\infty A_2(\lambda) J_2(\lambda\rho)\, d\lambda = 0
\end{array} \qquad (26)$$

To solve these equations by successive approximations, when $\kappa a \leqslant 1$, we make use of the following theorem. The kernel $g_\nu(\lambda)$ of the integral equation

$$\int_0^\infty \lambda g_\nu(\lambda) J_\nu(\lambda\rho)\, d\lambda = F_\nu(\rho), \quad (0 < \rho < a):$$

$$\int_0^\infty g_\nu(\lambda) J_\nu(\lambda\rho)\, d\lambda = 0, \quad (a \leqslant \rho < \infty), \qquad (27)$$

is given by

$$\left.\begin{array}{l}
g_\nu(\lambda) = \lambda^{1/2} \int_0^a \phi_\nu(x) J_{\nu+\frac{1}{2}}(\lambda x)\, dx \\
\text{where} \\
\phi_\nu(x) = \sqrt{\frac{2}{\pi}}\, x^{3/2} \int_0^{\frac{1}{2}\pi} (\sin\theta)^{\nu+1} F_\nu(x \sin\theta)\, d\theta
\end{array}\right\}. \qquad (28)^*$$

(i) To solve the first of equations (26) we make use of (27) and (28) with $\nu = 0$, which give as the solution of

$$\left.\begin{array}{l}
\int_0^\infty \lambda g_0(\lambda) J_0(\lambda\rho)\, d\lambda = 1, \quad (0 < \rho < a): \\
\qquad \int_0^\infty g_0(\lambda) J_0(\lambda\rho)\, d\lambda = 0, \quad (a \leqslant \rho < \infty) \\
\qquad g_0(\lambda) = \sqrt{\frac{2}{\pi}}\, a^2 \frac{J_{3/2}(a\lambda)}{(a\lambda)^{1/2}}
\end{array}\right\}, \qquad (29)$$

---

* The explicit form of the theorem contained in equations (27) and (28) is easily derived from results due to Macdonald (' Proc. Lond. Math. Soc.,' vol. 26, p. 257 (1895)), quoted in Bateman's " Partial Differential Equations," p. 474 (Camb. Univ. Press, (1932)). Special cases of such theorems due to Beltrami are quoted in Webster's " Partial Differential Equations of Mathematical Physics " (Stechert & Co., New York, 1933), p. 372, equation (187).

and as that of

$$\left.\begin{aligned} &\int_0^\infty \lambda g_2(\lambda)\, J_0(\lambda\rho)\, d\lambda = \frac{\rho^2}{a^2}, \quad (0 < \rho < a): \\ &\qquad\qquad \int_0^\infty g_0(\lambda)\, J_0(\lambda\rho)\, d\lambda = 0, \quad (a \leqslant \rho < \infty) \\ &\qquad g_2(\lambda) = \sqrt{\frac{2}{\pi}} a^2 \cdot \tfrac{2}{3} \left\{ \frac{J_{3/2}(a\lambda)}{(a\lambda)^{1/2}} - 2\frac{J_{5/2}(a\lambda)}{(a\lambda)^{3/2}} \right\} \end{aligned}\right\}. \qquad (30)$$

To solve the integral equation of normal diffraction to $(\kappa a)^2$,

$$\int_0^\infty \mu g(\lambda)\, J_0(\lambda\rho)\, d\lambda = 1, \quad (0 < \rho < a):$$

$$\int_0^\infty g(\lambda)\, J_0(\lambda\rho)\, d\lambda = 0, \quad (a \leqslant \rho < \infty), \qquad (31)$$

we write

$$g(\lambda) = g_0(\lambda) + g_{01}(\lambda). \qquad (32)$$

Substitution in (31) leads to the following equation for $g_{01}(\lambda)$

$$\left.\begin{aligned} &\int_0^\infty \mu\, g_{01}(\lambda)\, J_0(\lambda\rho)\, d\lambda = 1 - \int_0^\infty \mu\, g_0(\lambda)\, J_0(\lambda\rho)\, d\lambda, \quad (0 < \rho < a) \\ &\int_0^\infty g_{01}(\lambda)\, J_0(\lambda\rho)\, d\lambda = 0, \qquad\qquad\qquad\qquad (a \leqslant \rho < \infty) \end{aligned}\right\}, \qquad (33)$$

When $\kappa a \ll 1$, the right-hand side of (33), with $g_0(\lambda)$ given by (29), may be evaluated approximately,* so that the former equation becomes

$$\left.\begin{aligned} &\int_0^\infty \mu\, g_{01}(\lambda)\, J_0(\lambda\rho)\, d\lambda \sim \tfrac{1}{4}(\kappa a)^2 - \frac{2i}{9\pi}(\kappa a)^3 - \tfrac{1}{8}(\kappa\rho)^2 \ldots, \quad (0 < \rho < a) \\ &\int_0^\infty g_{01}(\lambda)\, J_0(\lambda\rho)\, d\lambda = 0, \qquad\qquad\qquad\qquad (a \leqslant \rho < \infty) \end{aligned}\right\}. \qquad (34)$$

As the quantities on the right-hand side of (34) are of the order $(\kappa a)^2$, the approximate value of $g_{01}(\lambda)$ is obtained by replacing μ on the left-hand side of (34) by λ, so that, according to (30),

$$g_{01}(\lambda) \sim \left\{ \tfrac{1}{4}(\kappa a)^2 - \frac{2i}{9\pi}(\kappa a)^3 \right\} g_0(\lambda) - \tfrac{1}{8}(\kappa a)^2 g_2(\lambda). \qquad (35)$$

It now follows that to an accuracy of the order $(\kappa a)^2$, the solution of the first of equations (15) is, in view of (19) and (21), discarding the imaginary term in $(\kappa a)^3$,

$$A_0(\lambda) \sim (\dot{\zeta} - Ai\kappa n)\{(1 + \tfrac{1}{4}(\kappa a)^2)\, g_0(\lambda) - \tfrac{1}{8}(\kappa a)^2 g_2(\lambda)\} \\ + \tfrac{1}{4} Ai\kappa n\, (\kappa am)^2\, g_2(\lambda).$$

---

* Details of the evaluation are given in the previous paper.

We now substitute in the dynamical equation (10). It is easily proved that

$$\int_0^\infty J_1(\lambda a)\, g_0(\lambda)\frac{d\lambda}{\lambda} = \tfrac{2}{3}\frac{a^2}{\pi} \quad \text{and} \quad \int_0^\infty J_1(\lambda a)\, g_2(\lambda)\frac{d\lambda}{\lambda} = \tfrac{1}{15}\frac{a^2}{\pi}. \tag{36*}$$

On writing $m_0 = \frac{8}{3}\rho_0 a^3$, we find

$$\dot{\zeta} - \mathrm{A}i\kappa n = -\mathrm{A}i\kappa n \,.\, \frac{m_1 + \frac{1}{10} m_0 (\kappa a m)^2}{m_1 + m_0 (1 + \frac{1}{5}(\kappa a)^2)}. \tag{37}$$

Finally, denoting

$$\left.\begin{aligned} \alpha_0 &= -\frac{\{m_1 + \frac{1}{10} m_0 (\kappa a m)^2\}\{1 + \frac{1}{4}(\kappa a)^2\}}{m_1 + m_0 (1 + \frac{1}{5}(\kappa a)^2)} \\ \alpha_2 &= \tfrac{1}{8}(\kappa a)^2 \frac{m_1 (1 + 2m^2) + 2 m_0 m^2 (1 + \frac{1}{4}(\kappa a)^2)}{m_1 + m_0 (1 + \frac{1}{5}(\kappa a)^2)} \end{aligned}\right\}, \tag{38}$$

we may write

$$\mathrm{A}_0(\lambda) = (\mathrm{A}i\kappa n)\{\alpha_0 g_0(\lambda) + \alpha_2 g_2(\lambda)\}. \tag{39}$$

(ii) We notice from the preceding work that the first approximation to the solution of integral equations of the type (26) is obtained by suppressing κ on the left-hand side, and making use of (28). In this way we readily obtain the solution of the second of equations (26) in the form

$$\mathrm{B}_1(\lambda) = -\tfrac{2}{3}\frac{\mathrm{I}_1}{\mathrm{I}_1 + \mathrm{I}_0}\mathrm{A}\kappa^2 m n a^3 \sqrt{\frac{2}{\pi}}\frac{\mathrm{J}_{5/2}(a\lambda)}{(a\lambda)^{1/2}}, \tag{40}$$

in which use is made of the dynamical equation (11), and $\mathrm{I}_0 = \frac{16}{45}\rho_0 a^5$ is the hydrodynamic moment of inertia of the disc. It is evident from (40) that a higher approximation for $\mathrm{B}_1(\lambda)$ would introduce terms in $(\kappa a)^3$ which we neglect.

(iii) As before, we obtain as the solution of the third equation in (26),

$$\mathrm{A}_2(\lambda) = -\tfrac{2}{15}(\mathrm{A}i\kappa n)(\kappa m a)^2 \sqrt{\frac{2}{\pi}}\, a^2 \frac{\mathrm{J}_{7/2}(a\lambda)}{(a\lambda)^{1/2}}. \tag{41}$$

Calculation of Moments

We are now in a position to make use of the results of § 4. In a progressive plane wave we have for $z = 0$, according to (23),

$$(\phi_i)_{z=0} = \mathrm{A}e^{-i\kappa m\rho \sin\phi + i\omega t},$$

so that according to (20)

$$\mathrm{P}_i = \mathrm{A}\cos(\kappa m\rho\sin\phi) \qquad \mathrm{Q}_i = -\mathrm{A}\sin(\kappa m\rho\sin\phi). \tag{42}$$

---

* Watson, " Theory of Bessel Functions " (1922), § 13.41 (2).

Three terms of the summations (21) and (22) are required to give the average moment to an order of accuracy $(\kappa a)^2$.

(i) Corresponding to $s = 0$ we obtain from (18) and (39)

$$P_0 = 0, \qquad Q_0 = A\kappa n \int_0^\infty \{\alpha g_0(\lambda) + \alpha_2 g_2(\lambda)\} J_0(\lambda\rho)\, d\lambda. \tag{43}$$

According to (21) we have, in this case, on making use of (42),

$$\begin{aligned}(\bar{L}_q)_0 &= \rho_0 \int_0^{2\pi} \sin\phi\, d\phi \int_0^a \frac{\partial Q_i}{\partial\rho} \cdot \frac{\partial Q_0}{\partial\rho}\, \rho^2\, d\rho \\ &= -A\kappa m\rho_0 \int_0^a \rho^2 \frac{\partial Q_0}{\partial\rho}\, d\rho \int_0^{2\pi} \{1 - \tfrac{1}{2}(\kappa m)^2 \rho^2 \sin^2\phi\} \sin^2\phi\, d\phi \\ &= -A\kappa m\rho_0\pi \int_0^a \{1 - \tfrac{3}{8}(\kappa m)^2 \rho^2\} \frac{\partial Q_0}{\partial\rho}\, \rho^2\, d\rho.\end{aligned}$$

On integrating by parts and noting from (43) that $(Q_0)_{\rho=a} = 0$,* we easily deduce that

$$(\bar{L}_q)_0 = \pi A\kappa m\rho_0 \left\{2\int_0^a Q_0\rho\, d\rho - \tfrac{3}{2}(\kappa m)^2 \int_0^a \rho^3 Q_0\, d\rho\right\}. \tag{44}$$

Similarly, (22) gives

$$(\bar{L}_\phi)_0 = -\kappa^2\rho_0 \int_0^{2\pi} \sin\phi\, d\phi \int_0^a Q_i Q_0 \rho^2\, d\rho.$$

As this contribution to the moment is already of the second order, it suffices to use $Q_i \sim -A\kappa m\rho \sin\phi$, so that on integrating with respect to ϕ,

$$(\bar{L}_\phi)_0 = \pi A\kappa m\rho_0\kappa^2 \int_0^a \rho^3 Q_0\, d\rho. \tag{45}$$

On combining (44) and (45) we have, according to (16),

$$\bar{L}_0 = (\bar{L}_q)_0 + (\bar{L}_\phi)_0,$$

so that

$$\bar{L}_0 = \pi A\kappa m\rho_0 \left\{2\int_0^a Q_0\rho\, d\rho + \kappa^2(1 - \tfrac{3}{2}m^2)\int_0^a Q_0\rho^3\, d\rho\right\}. \tag{46}$$

On introducing Q_0 from (43), we notice, on integrating first with respect to ρ, that

$$\int_0^a J_0(\lambda\rho)\,\rho\, d\rho = \frac{a}{\lambda} J_1(\lambda a),$$

---

* This follows by writing $\rho = a$ in (43) and evaluating the integral by making use of the well-known formula given in Watson's "Bessel Functions," § 13.41 (2). Its physical meaning is that $\phi_p = \phi_m$ at $\rho = a$ for all values of ϕ, *i.e.*, that there is continuity of pressure on both sides of the plane $z = 0$ at the edge of the disc: so in general $P_s = Q_s = 0$ at $\rho = a$, a result easily verified by the use of the above-mentioned formula.

and

$$\int_0^a J_0(\lambda\rho)\,\rho^3\,d\rho = \frac{2(a\lambda)^2 J_2(a\lambda) - (a\lambda)^3 J_3(a\lambda)}{\lambda^4}.$$

To effect the integrations with respect to λ is now a simple matter. We find, after a few reductions,

$$\bar{L}_0 = \tfrac{4}{5}\,|A\kappa|^2\,\rho_0 mna^3\{\alpha_0 + \tfrac{2}{5}\alpha_2 + \tfrac{1}{5}(\kappa a)^2\,\alpha_0\,(1 - \tfrac{3}{2}m^2)\}. \qquad (47)$$

On substituting for α_0 and α_2 from (38), and remembering that according to (24) $m = \sin\alpha$, $n = \cos\alpha$, we find after some reductions, retaining terms to $(\kappa a)^2$,

$$\bar{L}_0 = -\tfrac{2}{3}\,\rho_0 a^3 \sin 2\alpha\,|A\kappa|^2\,\frac{m_1\{1 + \tfrac{2}{5}(\kappa a)^2\cos^2\alpha\}}{m_1 + m_0\{1 + \tfrac{1}{5}(\kappa a)^2\}}. \qquad (48)$$

(ii) Corresponding to $s = 1$ in (21) and (22), we have from (20)

where

$$\left.\begin{aligned} P_1 &= p_1 \sin\phi \qquad Q_1 = 0 \\ p_1 &= \int_0^\infty B_1(\lambda)\,J_1(\lambda\rho)\,d\lambda \end{aligned}\right\}. \qquad (49)$$

According to (21) we have

$$(\bar{L}_q)_1 = \rho_0 \int_0^{2\pi} \sin\phi\,d\phi \int_0^a \left\{\rho^2 \frac{\partial P_i}{\partial\rho}\frac{\partial P_1}{\partial\rho} + \frac{\partial P_i}{\partial\phi}\frac{\partial P_1}{\partial\phi}\right\} d\rho.$$

From (42), $P_i \sim A\{1 - \tfrac{1}{2}(\kappa m\rho)^2 \sin^2\phi + \ldots\}$, so that effecting the integration with respect to ϕ we find

$$(\bar{L}_q)_1 = -A(\kappa m)^2\,\rho_0\,\frac{\pi}{4}\int_0^a \left\{3\rho^3\frac{\partial p_1}{\partial\rho} + p_1\rho^2\right\} d\rho.$$

If we now integrate by parts, it is easily proved from (49), with $\rho = a$, that $(p_1)_{\rho=a} = 0$, and we are left with

$$(\bar{L}_q)_1 = 2\pi A(\kappa m)^2\,\rho_0 \int_0^a p_1\rho^2\,d\rho. \qquad (50)$$

Similarly, we find from (22

$$(\bar{L}_\phi)_1 = -\kappa^2\rho_0 \int_0^{2\pi} \sin\phi\,d\phi \int_0^a P_i P_1 \rho^2\,d\rho,$$

which gives, on integrating with respect to ϕ,

$$(\bar{L}_\phi)_1 = -A\kappa^2\pi\rho_0 \int_0^a p_1\rho^2\,d\rho. \qquad (51)$$

On adding (50) and (51) we have

$$\overline{\mathrm{L}}_1 = \pi\rho_0\mathrm{A}\kappa^2\,(2m^2-1)\int_0^a p_1\rho^2\,d\rho. \tag{52}$$

We now introduce p_1 from (49) and $\mathrm{B}_1(\lambda)$ from (40), and obtain without difficulty

$$\overline{\mathrm{L}}_1 = -\tfrac{8}{45}\,|\mathrm{A}\kappa|^2\,\rho_0\,mn\,a^3\,(\kappa a)^2\,\frac{\mathrm{I}_1}{\mathrm{I}_1+\mathrm{I}_0}\,(2m^2-1),$$

or finally, remembering that $m = \sin\alpha$ and $n = \cos\alpha$,

$$\overline{\mathrm{L}}_1 = \tfrac{2}{3}\,\rho_0\,a^3\sin 2\alpha\,|\mathrm{A}\kappa|^2\,.\,\tfrac{2}{15}\,(\kappa a)^2\cos 2\alpha\,.\,\frac{\mathrm{I}_1}{\mathrm{I}_1+\mathrm{I}_0}\,. \tag{53}$$

(iii) Corresponding to $s = 2$ in (21) and (22), we have from (20)

$$\left.\begin{aligned} &\mathrm{P}_2 = 0 \qquad \mathrm{Q}_2 = q_2\cos 2\phi \\ \text{where}\qquad &q_2 = \int_0^\infty \mathrm{A}_2(\lambda)\,\mathrm{J}_2(\lambda\rho)\,d\lambda \end{aligned}\right\}. \tag{54}$$

According to (21) we have

$$(\overline{\mathrm{L}}_\rho)_2 = \rho_0\int_0^{2\pi}\sin\phi\,d\phi\int_0^a\left\{\rho^2\,\frac{\partial \mathrm{Q}_i}{\partial\rho}\,\frac{\partial \mathrm{Q}_2}{\partial\rho} + \frac{\partial \mathrm{Q}_i}{\partial\phi}\,.\,\frac{\partial \mathrm{Q}_2}{\partial\phi}\right\}d\phi.$$

With $\mathrm{Q}_i \sim \mathrm{A}\kappa m\rho\sin\phi$, we find

$$(\overline{\mathrm{L}}_\rho)_2 = \tfrac{1}{2}\pi\mathrm{A}\kappa m\rho_0\int_0^a\left\{\rho^2\,\frac{\partial q_2}{\partial\rho} + 2\rho q_2\right\}d\rho = \tfrac{1}{2}\pi\mathrm{A}\kappa m\rho_0\,(q_2\rho^2)_{\rho=a}.$$

With the value of $\mathrm{A}_2(\lambda)$ from (41), it is easily proved that $(q_2)_{\rho=a} = 0$, so that to the order $(\kappa a)^2$,

$$(\overline{\mathrm{L}}_\rho)_2 = 0. \tag{55}$$

Similarly we have from (22),

$$\begin{aligned}(\overline{\mathrm{L}}_\phi)_2 &= -\,\kappa^2\rho_0\int_0^{2\pi}\sin\phi\,d\phi\int_0^a \mathrm{Q}_i\mathrm{Q}_1\rho^2 d\rho \\ &= -\,\tfrac{1}{2}\pi\kappa^2\rho_0\mathrm{A}\kappa m\int_0^a q_2\,\rho^3\,d\rho,\end{aligned}$$

and ultimately, on carrying out the integration, we find

$$(\mathrm{L}_\phi)_2 = \tfrac{8}{1575}\,|\mathrm{A}\kappa|^2\,mn\,\rho_0\,a^3\,(\kappa a)^2\,(\kappa ma)^2. \tag{56}$$

This is of the fourth order in κa, and to the order of accuracy with which we are working is negligible, in which circumstances we have, from (55) and (56),

$$\mathrm{L}_2 \sim 0 + \text{terms in } (\kappa a)^4. \tag{57}$$

Final Results

On adding the contributions (44), (53), and (57), we have, correct to $(\kappa a)^2$, the time-average of the torque on the Rayleigh disc corrected for inertia and diffraction, in a *plane progressive wave* of velocity amplitude $|\dot{\xi}| = |A\kappa|$,

$$\bar{L} = -\tfrac{2}{3}\rho_0 a^3 \sin 2\alpha\, |A\kappa|^2 \left[\frac{m_1\{1 + \frac{2}{5}(\kappa a)^2 \cos^2 \alpha\}}{m_1 + m_0\{1 + \frac{1}{5}(\kappa a)^2\}} - \tfrac{2}{15}(\kappa a)^2 \cdot \frac{I_1}{I_1 + I_0} \cos 2\alpha \right], \quad (58)$$

where m_1 is the mass of the disc given by $m_1 = \pi a^2 \rho_1 t_1$, and ρ_1 is its density and t_1 its uniform thickness: m_0 is the hydrodynamic mass given by $m_0 = \frac{8}{3}\rho_0 a^3$. I_1 is the moment of inertia of the disc given by $I_1 = \frac{1}{4} m_1 a^2$, and I_0 the hydrodynamic moment of inertia given by $I_0 = \frac{2}{15} m_0 a^2$.

The particular case of a rigidly fixed disc is obtained by writing $m_0/m_1 = 0$ and $I_0/I_1 = 0$ in the above formula. We easily find

$$\underset{m_0/m_1=0}{\mathrm{Lt}}\ \bar{L} = -\tfrac{2}{3}\rho_0 a^3 \sin 2\alpha\, |A\kappa|^2 \{1 + \tfrac{1}{5}(\kappa a)^2 (1 + \tfrac{1}{3}\cos 2\alpha) + \ldots\}, \quad (59)$$

which agrees as far as $(\kappa a)^2$ with Kotani's formula quoted in § 1 of this paper.

6—COUPLE ON RAYLEIGH DISC IN PLANE STANDING WAVE

With a few changes the results of § 5 may be used to determine the average couple on a small circular disc in a standing wave represented by the velocity potential

$$\phi_t = A \cos\{\kappa(my + nz + h)\}, \quad (60)$$

where as before we have written $m = \sin\alpha$ and $n = \cos\alpha$. The wave is propagated in a direction α to the normal to the disc from a plane of reference at a distance h from the centre of the disc measured along the direction of propagation of the wave.

Since $(\partial\phi_t/\partial z)_{z=0} = -A\kappa n \sin\{\kappa(m\rho \sin\phi + h)\}$, we have, according to (6),

$$A_{t0}(\rho) = -A\kappa n \sin \kappa h\, J_0(\kappa m\rho) \qquad B_{t0}(\rho) = 0$$

$$A_{t1}(\rho) = 0 \qquad B_{t1}(\rho) = -2A\kappa n \cos \kappa h\, J_1(\kappa m\rho)$$

$$A_{t2}(\rho) = -2A\kappa n \sin \kappa h\, J_2(km\rho) \qquad B_{t2}(\rho) = 0.$$

With these changes on the right-hand sides of (26) we have for the approximate solutions of these integral equations,

$$\left.\begin{aligned} &\text{(i)} && A_0(\lambda) = A\kappa n \sin \kappa h \{\alpha_0 g_0(\lambda) + \alpha_2 g_2(\lambda)\} \\ &\text{(ii)} && B_1(\lambda) = -\tfrac{2}{3}\frac{I_1}{I_1 + I_0} A\kappa^2 m n a^3 \cos \kappa h \sqrt{\frac{2}{\pi}}\frac{J_{5/2}(a\lambda)}{(a\lambda)^{\frac{1}{2}}} \\ &\text{(iii)} && A_2(\lambda) = -\tfrac{2}{15} A\kappa n \sin \kappa h\, (\kappa a m)^2 \sqrt{\frac{2}{\pi}}\frac{J_{7/2}(a\lambda)}{(a\lambda)^{\frac{1}{2}}} \end{aligned}\right\}. \qquad (61)$$

The calculation of the moment proceeds as before.

Since $(\phi_i)_{z=0} = A \cos \{\kappa (m\rho \sin \phi + h)\} e^{i\omega t}$, we have, according to (20),

$$P_i = Q_i = A \cos \{\kappa (m\rho \sin \phi + h)\}.$$

The contributions of the terms corresponding to $s = 0, 1, 2$ of equations (21) and (22) are as follows:

(i) $s = 0$.

$$P_0 = A\kappa n \sin \kappa h \int_0^\infty \{\alpha g_0(\lambda) + \alpha_2 g_2(\lambda)\} J_0(\lambda\rho)\, d\lambda, \quad Q_0 = 0. \qquad (62)$$

According to (21) and (22),

$$(\overline{L}_\phi)_0 = \rho_0 \int_0^{2\pi} \sin\phi \int_0^a \frac{\partial P_i}{\partial \rho}\frac{\partial P_0}{\partial \rho}\rho^2\, d\rho : (\overline{L}_\phi)_0 = -\kappa^2\rho_0 \int_0^{2\pi} \sin\phi\, d\phi \int_0^a P_i P_0 \rho^2\, d\rho.$$

We find, on carrying out the integrations with respect to ϕ, that the coefficients of $\cos \kappa h$ vanish, and we are left with

$$\overline{L}_0 = \pi A\kappa m \rho_0 \sin \kappa h \left\{2\int_0^a P_0\rho\, d\rho + \kappa^2(1 - \tfrac{3}{2}m^2)\int_0^a P_0\rho^3\, d\rho\right\}. \qquad (63)$$

On comparing the above expression with (46), and (62) with (43), it follows from (44) that we have in the present circumstances

$$\overline{L}_0 = -\tfrac{2}{3}\rho_0 a^3 \sin 2\alpha\, (A\kappa \sin \kappa h)^2 . \frac{m_1\{1 + \frac{2}{5}(\kappa a)^2 \cos^2\alpha\}}{m_1 + m_0\{1 + \frac{1}{5}(\kappa a)^2\}}. \qquad (64)$$

(ii) $s = 1$.

Since

$$P_1 = p_1 \sin \phi, \quad Q_1 = 0, \qquad \text{where} \quad p_1 = \int_0^\infty B_1(\lambda) J_1(\lambda\rho)\, d\lambda,$$

we find after some reductions

$$\overline{L}_1 = \pi\rho_0 A\kappa^2 \cos^2 \kappa h\, (2m^2 - 1)\int_0^a p_1\rho^2\, d\rho, \qquad (65)$$

and as before

$$\bar{L}_1 = \tfrac{2}{3}\rho_0 a^3 \sin 2\alpha\, (A\kappa \cos \kappa h)^2 \,.\, \tfrac{2}{15}\, (\kappa a)^2 \cos 2\alpha \frac{I_1}{I_1 + I_0}\,. \tag{66}$$

(iii) $s = 2$.

As in the preceding section,

$$\bar{L}_2 \sim 0 + \text{terms in } (\kappa a)^4.$$

We thus have, correct to $(\kappa a)^2$, the following expression for the time-average of the torque on the Rayleigh disc in a *plane standing wave* represented by the velocity potential.

$$\left.\begin{aligned} \phi_i &= A \cos \{\kappa (z \cos \alpha + y \sin \alpha + h)\} \\ \bar{L} &= -\tfrac{2}{3}\rho_0 a^3 \sin 2\alpha\, |A\kappa|^2 \left[\sin^2 \kappa h \,.\, \frac{m_1 \{1 + \frac{2}{5}(\kappa a)^2 \cos^2 \alpha\}}{m_1 + m_0 \{1 + \frac{1}{5}(\kappa a)^2\}}\right. \\ &\qquad\qquad \left. - \tfrac{2}{15} \cos^2 \kappa h\, (\kappa a)^2 \frac{I_1}{I_1 + I_0} \cos 2\alpha \right] \end{aligned}\right\}. \tag{67}$$

At the *loops* of the system of standing waves, $\sin^2 \kappa h = 1$, and so we have

$$(\bar{L})_{\text{loops}} = -\tfrac{2}{3}\rho_0 a^3 \sin 2\alpha\, |A\kappa|^2 \,.\, \frac{m_1 \{1 + \frac{2}{5}(\kappa a)^2 \cos^2 \alpha\}}{m_1 + m_0 \{1 + \frac{1}{5}(\kappa a)^2\}}. \tag{68}$$

In these circumstances there are no angular oscillations of the disc.

At the *nodes* of the standing waves, there are no linear oscillations of the disc, $\cos^2 \kappa h = 1$, and in these circumstances

$$(\bar{L})_{\text{nodes}} = \tfrac{2}{45}\rho_0 a^3 \sin 4\alpha\, (\kappa a)^2 \frac{I_1}{I_1 + I_0}\,. \tag{69}$$

The couple on a small disc for which $(\kappa a) \ll 1$, situated in the nodes is thus of a much smaller order of magnitude than that exerted on it in the loops, and is of opposite sign. The stable positions of the disc in the range $0 < \alpha < \frac{1}{2}\pi$ are those corresponding to $\alpha = \frac{1}{8}\pi$ and $\alpha = \frac{3}{8}\pi$.

In the measurement of the intensity of sound, a Rayleigh disc is mounted in a resonator at the loop of a system of standing waves. Formula (68) is thus of considerable importance in the design of an instrument for the accurate measurement of acoustic intensities in absolute units. It is obvious that to avoid correcting for the influence of the walls of the resonator on the motion of the disc, its diameter must be made as small as possible, and its thickness conform, if possible, to conditions of optimum sensitivity. These we proceed to determine in the following section.

The problem of connecting the velocity amplitude inside the resonator with that of the wave incident on it constitutes a somewhat difficult investigation which the writer hopes to deal with in a future communication.

7—ON RAYLEIGH DISCS OF OPTIMUM SENSITIVITY

It is evident from the formulae (58) and (67) that for a disc, sufficiently small that $(\kappa a)^2$ is negligible, situated in a progressive wave of velocity amplitude $|\xi| = |\kappa A|$, or at the loops of a stationary wave system of the same velocity amplitude, the torque tending to set the disc broadside to the wave-normal is given by

$$\bar{L} \sim -\tfrac{2}{3}\rho_0 a^3 \sin 2\alpha \, |A\kappa|^2 \frac{m_1}{m_1 + m_0}. \tag{70}$$

If the disc is suspended by means of a fibre whose torsional constant is denoted by τ, the angular deviation θ of the disc from its equilibrium position, or the angle θ through which the torsion head must be turned to bring the disc back to its original position, is given by

$$L = -\tau\theta. \tag{71}$$

On introducing $\bar{L}$ from (70) and writing $m_0 = \frac{8}{3}\rho_0 a^3$, the velocity amplitude is given by

$$|A\kappa|^2 = \frac{4}{\sin 2\alpha} \frac{m_1 + m_0}{m_1 m_0} \tau\theta. \tag{72}$$

The torsional constant τ is most easily determined in terms of the time of the free oscillations of the disc in air, determined from the equation of motion,

$$(I_1 + I_0)\,\theta + \tau\theta = 0, \tag{73}$$

where I_1 is the moment of inertia of the disc *in vacuo*, and I_0 the hydrodynamical moment of inertia, comparable in magnitude to I_0 in the case of light, thin discs. Equation (73), which may be corrected for viscosity if desired, represents oscillations of period T given by

$$T = 2\pi\{(I_1 + I_0)/\tau\}^{1/2}. \tag{74}$$

Substituting for τ in (72), we obtain the working formula for the Rayleigh disc in the form

$$|\dot{\xi}|^2 = |A\kappa|^2 = \frac{16\pi^2}{T^2} \frac{1}{\sin 2\alpha} \frac{(I_1 + I_0)(m_1 + m_0)}{m_1 m_0}\,\theta, \tag{75}$$

in which the coefficient of θ consists of measurable or observed quantities.

Conditions of optimum sensitivity require that this factor should be a minimum. We consider first the inertia factor

$$f(m_1, m_0) = (I_1 + I_0)(m_1 + m_0)/(m_1 m_0). \tag{76}$$

We have

$$\left.\begin{array}{lll} I_1 = m_1\kappa_1^2, & m_1 = \pi\rho_1 a^2 t_1, & \kappa_1^2 = \frac{1}{4}a^2 \\ I_0 = m_0\kappa_0^2, & m_0 = \frac{8}{3}\rho_0 a^3, & \kappa_0^2 = \frac{2}{15}a^2 \end{array}\right\}, \tag{77}$$

so that

$$f(m_1, m_0) = \kappa_1^2 + \frac{m_1}{m_0}\kappa_1^2 + \frac{m_0}{m_1}\kappa_0^2 + \kappa_0^2.$$

For a given radius, the inertia factor $f(m_1, m_0)$ is obviously a minimum when

$$m_1\kappa_1 = m_0\kappa_0, \qquad \text{when} \qquad [f(m_1, m_0)]_{\min} = (\kappa_1 + \kappa_0)^2, \tag{78}$$

which gives for the optimum thickness t_1 of the disc the interesting relation

$$\frac{t_1}{a} = \frac{\rho_0}{\rho_1}\frac{16}{3\pi}\left(\tfrac{2}{15}\right)^{\frac{1}{2}} = 0{\cdot}620\frac{\rho_0}{\rho_1}, \tag{79}$$

while (78) gives for the optimum inertia factor

$$[f(m_1, m_0)]_{\min} = a^2\{\tfrac{1}{2} + (\tfrac{2}{15})^{\frac{1}{2}}\}^2 = 0{\cdot}748a^2. \tag{80}$$

Thus, with an optimum inertia factor, and with $\alpha = 45°$, we have in these circumstances

$$|\xi|^2 = |A\kappa|^2 = \frac{16\pi^2}{T^2} \times 0{\cdot}748a^2\theta \qquad \text{(optimum disc).} \tag{81*}$$

NUMERICAL RESULTS

(i) *Optimum Rayleigh Disc in Air*—The angular deflection of the disc is most easily measured by means of a galvanometer lamp and scale. We therefore have $\theta = \frac{1}{2}\delta/D$, where δ is the scale deflexion and D the distance of the scale from the disc. The intensity of the sound in the neighbourhood of the disc is given by

$$I = \tfrac{1}{2}\rho_0 c\,|\xi|^2 = \tfrac{1}{2}\rho_0 c\,|A\kappa|^2. \tag{82}$$

In air at 0° C and 76 cm pressure, $\rho_0 = 0{\cdot}001293$, $c = 332$ metres/sec,

---

*[*Added, October* 18, 1935—When the correction is made for the finite thickness t_1 of the disc, m_1 is replaced by $(m_1 - m_w)$ where m_w is the mass of the medium displaced by the disc, given by $m_w = \pi a^2\rho_0 t_1$. (*See* note (i) inserted at the end of this paper.) The necessary modifications to the conditions of optimum sensitivity are easily worked out.]

and at 20° C we find $\rho_0 c = 41\cdot4$. It is convenient for practical purposes to measure the intensity of sound on a logarithmic scale given by

$$\alpha \text{ decibels} = 10 \log_{10} (\mathrm{I}/\mathrm{I}_0), \tag{83}$$

where α is given in decibels and $\mathrm{I}_0 = 10^{-9}$ ergs/cm²/sec.

Combining (81), (82), and (84) into a convenient practical formula in terms of scale deflexions we find for an *optimum Rayleigh disc in air*,

$$\alpha \text{ decibels} = 91 - 20 \log_{10} \frac{\mathrm{T}\,(\text{sec})}{a\,(\text{cm})} + 10 \log_{10} \frac{\delta\,(\text{mm})}{\mathrm{D}\,(\text{metre})}, \tag{84}$$

the optimum thickness t_1 being given by

$$t_1/a = 0\cdot620\,(\rho_0/\rho_1), \qquad \text{with} \qquad \rho_0 = 0\cdot001293. \tag{85}$$

The first two terms of (84) give the intensity on the decibel scale required to give a deflexion of 1 mm on a scale 1 metre distant. It is evident that for a given time of swing the radius of the disc should be made as small as possible. As in practice it is hardly possible for T to exceed 10 sec and a to be less than 1 mm, it appears from (84) that 51 decibels is about the lowest level of acoustic intensity which it is possible to measure by this means. For this reason it is necessary to magnify $|\dot{\xi}|^2$ by mounting an optimum disc in a suitably designed resonator allowing for a calculable ratio between the amplitude of the incident waves and that of the standing waves within the resonator in the neighbourhood of the disc.

(ii) *Optimum Rayleigh Disc in Water*—The velocity of sound in water is $c = 1\cdot49 \times 10^5$ cm/sec, while $\rho_0 = 1$. In such a medium (85) is replaced by

$$\alpha \text{ decibels} = 126\cdot5 - 20 \log_{10} \frac{\mathrm{T}\,(\text{sec})}{a\,(\text{cm})} + 10 \log_{10} \frac{\delta\,(\text{mm})}{\mathrm{D}\,(\text{metre})}, \tag{86}$$

the optimum thickness of the disc being given by

$$t_1/a = 0\cdot620\,(\rho_0/\rho_1) \quad \text{with } \rho_0 = 1. \tag{87}$$

It is evident that in water with T = 10 sec and a as small as 1 mm, it is hardly possible to measure acoustic levels below 86 decibels.

8—SUMMARY AND CONCLUSIONS

In order to calculate the torque on a freely suspended thin circular disc resulting from the acoustic radiation pressure arising from an incident sound-wave, it is necessary to solve the problem of diffraction of sound when the wave-front makes an angle α with the plane of the disc.

The velocity potential of the diffracted wave is represented by the sum of a number of cylindrical wave-functions of the type

$$\chi_s = \int_0^\infty \{A_s(\lambda) \cos s\phi + B_s(\lambda) \sin s\phi\} e^{-\mu|z|} J_s(\lambda\rho)\, d\lambda, \qquad \text{(i)}$$

where $\mu = (\lambda^2 - \kappa^2)^{\frac{1}{2}}$, and each term represents a diverging wave for $|z| > 0$.

The boundary conditions over the plane $z = 0$ in which the disc is situated lead to a family of integral equations of the type

$$\int_0^\infty \mu g_s(\lambda) J_s(\lambda\rho)\, d\lambda = F_s(\rho), \quad (0 < \rho < a):$$
$$\int_0^\infty g_s(\lambda) J_s(\lambda\rho)\, d\lambda = 0, \quad (a \leqslant \rho < \infty), \qquad \text{(ii)}$$

in which the "kernel" is discontinuous at the radius $\rho = a$ of the disc and $F_s(\rho)$ is an assigned function of ρ depending on the expansion of the incident velocity potential in cylindrical co-ordinates.

By making use of the known solution of the corresponding equations in potential theory, $(\kappa = 0)$,

$$\int_0^\infty \lambda g_s(\lambda) J_s(\lambda\rho)\, d\lambda = F_s(\rho), \quad (0 < \rho < a):$$
$$\int_0^\infty g_s(\lambda) J_s(\lambda\rho)\, d\lambda = 0, \quad (a \leqslant \rho < \infty), \qquad \text{(iii)}$$

the equations (ii) may be solved to any degree of accuracy by a method of successive approximations.

The pressure variation in the medium, in which the pressure is any function of the density, is given by

$$\delta p = \rho_0 \phi - \tfrac{1}{2}\rho_0 q^2 + \tfrac{1}{2}(\rho_0/c^2)\, \dot{\phi}^2. \qquad \text{(iv)}$$

The first term gives rise to small oscillations of the disc along its normal and, in addition, to small angular vibrations about the axis of suspension. These are taken into account by two dynamical equations and these effects lead to important inertia corrections in the final expression for the torque on the disc. Each of the last two terms of (iv), calculated for each side of the disc, contribute to the time-average of the moment arising from the radiation pressures.

In a *plane progressive wave*, for which the velocity potential is given by

$$\phi_i = Ae^{-i\kappa(y \sin \alpha + z \cos \alpha) + i\omega t}, \qquad \text{(v)}$$

the time-average of the torque on the disc is given to terms in $(\kappa a)^2$ by the formula

$$\bar{L} = -\tfrac{2}{3}\rho_0 a^3 \sin 2\alpha\, |A\kappa|^2 \left[\frac{m_1\{1+\tfrac{2}{5}(\kappa a)^2\cos^2\alpha\}}{m_1 + m_0\,\{1+\tfrac{1}{5}(\kappa a)^2\}} - \tfrac{2}{15}(\kappa a)^2 \frac{I_1}{I_1+I_0}\cos 2\alpha\right], \quad \text{(vi)}$$

where m_1 is the mass of the disc, and m_0 its hydrodynamic mass given by $m_0 = \frac{8}{3}\rho_0 a^3$. I_1 is the moment of inertia of the disc and I_0 its hydrodynamic moment of inertia given by $I_0 = \frac{2}{15} m_0 a^2$.

In a *plane stationary wave-field* represented by the velocity potential

$$\phi_t = A\cos\{\kappa(y\sin\alpha + z\cos\alpha + h)\}\,.\cos\omega t,$$

the time-average of the torque is given by the formula

$$\bar{L} = -\tfrac{2}{3}\rho_0 a^3 \sin 2\alpha\, |A\kappa|^2 \left[\sin^2\kappa h \frac{m_1\{1+\tfrac{2}{5}(\kappa a)^2\cos^2\alpha\}}{m_1 + m_0\{1+\tfrac{1}{5}(\kappa a)^2\}} - \tfrac{2}{15}\cos^2\kappa h\,(\kappa a)^2 \frac{I_1}{I_1+I_0}\cos 2\alpha\right], \quad \text{(vii)}$$

and is evidently a maximum at the loops where $\sin^2\kappa h = 1$.

When the circumference of the disc is so small compared with the wavelength that the terms in $(\kappa a)^2$ in the above formulae are negligible, the important correction to Rayleigh's original formula is included in the simple expression

$$\bar{L} \sim -\tfrac{2}{3}\rho_0 a^3 \sin 2\alpha\, |A\kappa|^2 \frac{m_1}{m_1+m_0}\,. \quad \text{(viii)}$$

When very light discs are used in measuring air-waves, and, more especially in water, the torsional constant of the suspending fibre is measured in terms of T, the time of a complete oscillation. In these circumstances it is necessary to take into account the hydrodynamic moment of inertia of the disc. If 0 is the angular deviation of the disc under the influence of incident sound-waves, we have the working formula for the velocity-amplitude $|\xi|$ in the form

$$|\dot{\xi}|^2 = |A\kappa|^2 = \frac{16\pi^2}{T^2}\frac{1}{\sin 2\alpha}\cdot\frac{(I_1+I_0)(m_1+m_0)}{m_1 m_0}\,. \quad \text{(ix)}$$

Optimum sensitivity requires that $\alpha = 45°$, while the inertia factor is a minimum for $m_1\kappa_1 = m_0\kappa_0$, in which circumstances the optimum thickness of the disc is given by $t_1/a = 0{\cdot}620\,(\rho_0/\rho_1)$, and if this condition is satisfied, the working formula for such a disc is

$$|\dot{\xi}|^2 = |A\kappa|^2 = (16\pi^2/T^2) \times 0{\cdot}748\, a^3\theta. \qquad \text{(x)}$$

If the optical arrangements for observing the angular deflection θ are such that a deflection δ mm is obtained on a scale at D metres, the intensities on the decibel scale foı air and water are given by the formulae

$$\text{(Air)} \quad \alpha\,(\text{decibels}) = 91 - 20 \log_{10} \frac{T\,(\text{sec})}{a\,(\text{cm})} + 10 \log_{10} \frac{\delta\,(\text{mm})}{D\,(\text{metre})}: \qquad \text{(xi)}$$

$$\text{(Water)} \quad \alpha\,(\text{decibels}) = 126{\cdot}5 - 20 \log_{10} \frac{T\,(\text{sec})}{a\,(\text{cm})} + 10 \log_{10} \frac{\delta\,(\text{mm})}{D\,(\text{metre})}. \qquad \text{(xii)}$$

Both formulae refer to a disc of optimum thickness, and show at a glance that even with $T = 10$ sec and $a = 1$ mm, it is barely possible to measure sound under a level of 50 decibels in air, and 86 decibels in water.

The corrected formula (viii) indicates that the Rayleigh disc may be used for the absolute measurement of sound-waves in air of sufficiently high intensity, above a level of 50 decibels especially if its thickness approximates to the optimum. The formula (ix) referring to optimum conditions indicates that sensitivity is enhanced by employing as small discs as possible with a suspension giving as long a natural period as is feasible. The diffraction corrections in (vi) and (vii) enable the upper limit of frequency for which the simple formula (viii) is valid within errors of observation to be ascertained. As an absolute instrument for measuring acoustic intensities below a level of 50 decibels, the use of a suitably designed resonator is suggested, of such a type that velocity amplitude in the neighbourhood of the disc may be computed in terms of the intensity of the incident wave.

[*Notes added in proof, October* 18, 1935—

(i) *Correction for Finite Thickness of Disc*—If t_1 be the thickness of the disc the pressure over the faces $z = \pm \frac{1}{2}t_1$ are

$$\delta p_p = \rho_0 (\dot{\phi}_p)_{z=\frac{1}{2}t_1} \qquad \delta p_m = \rho_0 (\dot{\phi}_m)_{z=-\frac{1}{2}t_1}.$$

Since

$$(\dot{\phi})_{z=\pm\frac{1}{2}t_1} = (\dot{\phi})_{z=0} \pm \tfrac{1}{2}t_1 \left(\frac{\partial \dot{\phi}}{\partial z}\right)_{z=0} + \dots$$

it is easily proved that the dynamical equation (10) is replaced by

$$(m_1 - m_w)\,\dot{\zeta} = -4\pi\rho_0 a \int_0^\infty A_0(\lambda)\, J_1(\lambda a)\, \frac{d\lambda}{\lambda},$$

where $m_w = \pi a^2 \rho_0 t_1$ is the mass of the medium displaced by the disc.

Similarly the dynamical equation (11) is replaced by

$$(\mathrm{I}_1 - \mathrm{I}_w)\,\dot{\theta} = -\,2\pi\rho_0 a^2 \int_0^\infty \mathrm{B}_1(\lambda)\,\frac{\mathrm{J}_2(\lambda a)}{\lambda}\,d\lambda,$$

where $\mathrm{I}_w = m_w \kappa^2$ is the moment of inertia of an equal disc having the density of the medium. It thus follows that the finite thickness of the disc may be allowed for in the formulae (58) and (67) by replacing m_1 and I_1 by $(m_1 - m_w)$ and $(\mathrm{I}_1 - \mathrm{I}_w)$, respectively, throughout. The correction for finite thickness is obviously inappreciable for Rayleigh discs in air, but may become noticeable for discs of low density in liquid media. In such circumstances the conditions of optimum sensitivity require slight modifications which may be easily worked out if desired. We notice that as $(m_1 - m_w)/m_0 \to 0$, $\overline{\mathrm{L}} \to 0$, that is, to the order $(\kappa a)^2$ the couple on a rigid disc of the same density as the medium tends to vanish. In these circumstances it is necessary to solve the fundamental integral equations to a higher degree of approximation, so that $\overline{\mathrm{L}}$ for such a disc depends on $(\kappa a)^4$ and higher powers.

(ii) *Comparison of Theory with Observation*—Since this paper was communicated an account of observation on the behaviour of Rayleigh discs in water has been published by Wood.* In one set of experiments cylindrical brass discs of radius 1 cm and varying thicknesses were set up in a constant radiation field of 1000 cycles and the torque measured to maintain the disc at an angle $\alpha = 45°$ with the wave-front. In these circumstances it follows from (70) and (71) that the deflexion θ is given by

$$\theta = \tfrac{2}{3}\rho_0 a^3 \frac{|\mathrm{A}\kappa|^2}{\tau}\,\frac{m'_1}{m'_1 + m_0}$$

where $m_0 = \frac{8}{3}\rho_0 a^3$ and $m_1^1 = m_1 - m_w$ is the mass of the disc corrected for finite thickness as mentioned in the above note. In the following Table I the first two rows refer to observational data taken from fig. 2, *a*, of Wood's paper.

TABLE I

m_1 (grammes)	1·3	2·6	5·2	6·5	9·1
θ (deflexion)	10	17·6	28·2	31·0	33·8
m'_1 (grammes)	1·15	2·30	4·60	5·75	8·05
$m'_1/(m'_1 + m_0)$	0·29	0·46	0·63	0·69	0·75
$\theta\,(m'_1 + m_0)/m'_1$	34·2	40	45	45	45

---

* 'Proc. Phys. Soc. Lond.,' vol. 47, p. 779 (1935).

The third row is calculated from the formula $m_1^1 = m_1(1 - \rho_0/\rho_1)$, taking $\rho_0 = 1$ and the density of brass $\rho_1 = 8{\cdot}0$, while $m_0 = 2{\cdot}67$ gm.

A similar analysis of observations for cylindrical discs of the same dimensions (radius 1 cm, thickness 2 mm) but of different densities, taken from fig. 3, *a*, of Wood's paper, is given in Table II.

TABLE II

ρ_1 (density)	2·70	5·40	8·65	10·55	11·31	21·3
θ (deflexion)	7·65	20·7	30·8	37·0	35·1	46·5
m_1 (grammes)	1·68	3·39	5·31	6·92	7·08	13·88
m'_1 (grammes)	1·06	2·76	4·70	6·20	6·45	13·20
$m'_1/(m'_1 + m_0)$	0·281	0·506	0·690	0·704	0·704	0·833
$\theta\,(m'_1 + m_0)/m'_1$	27·0	40·5	44·5	52·0	50·0	56·0

According to theory, the last row in the above tables should be constant. This is seen to be the case for the thicker and denser discs. It must be remembered that several important factors have not been taken into account in the preceding theory. Among these the elastic bending of the discs under the first-order pressures of the acoustic radiation field and the transmission of elastic waves through the discs are factors likely to affect the thinner and lighter discs in such a medium as water, and may account for the discrepancies referred to in the above analyses of Wood's observations.]

Stress-Calculation in Frameworks by the Method of Systematic Relaxation of Constraints—III

By R. V. SOUTHWELL, F.R.S.

(*Received July* 29, 1935)

INTRODUCTION

An earlier paper bearing this title* dealt in detail (Part I) with the application of relaxation methods to frameworks having frictionless joints, and in general terms (Part II) with their relation to the Moment Distribution Method of Professor Hardy Cross.† Given any framework and a (self-equilibrating) system of applied forces, we may imagine constraints to be provided at every joint whereby the three components of displacement and the three components of rotation can be severally controlled. Then initially, if all constraints are fixed before the forces are applied, extension of members is prevented, and hence the forces (of known magnitude) are taken wholly by the constraints.‡ Subsequently, by permitting a suitable relaxation, we can transfer any component of force or moment from a constraint to the framework, and in so doing we shall store strain-energy in the latter. If the successive relaxations are systematically chosen, we can bring about a continuous approximation§ to the required conditions, in which every constraint is relieved of load and all forces have been transferred to the framework.

When all the joints are frictionless (as in the problems of Part I) the constraints at any one joint have only to control its three component displacements, because no stresses are entailed by joint rotations; but if any joint is rigid it can by rotating transmit couples to adjacent joints through the agency of shearing forces and the consequent bending moments. When the members have uniform flexural rigidity, it can be shown‖ that any one which shares in the rotation of a joint, and which in consequence transfers a couple M away from that joint, transmits it partly as a couple $-\frac{1}{2}M$ applied to its other end joint by bending moment, and partly as a couple $3M/2$ in the form of equal and opposite forces applied as shears to the two end joints. Consequently, when an applied couple is transferred by a joint rotation, only one half is transmitted to adjacent constraints in the form of couples,—the difference appears as changes in the applied forces.

---

* 'Proc. Roy. Soc.,' A, vol. 151, p. 56 (1935).

† "Analysis of Continuous Frames by Distributing Fixed-End Moments," published in 'Trans. Amer. Soc. Civ. Eng.,' vol. 96, pp. 1–10 (1932).

‡ This statement requires qualification if any force is applied otherwise than at a joint (*cf.* § 39): such cases are, for the moment, excluded.

§ *See* note added (October 8, 1935) at the end of this introduction.

‖ *Cf.* Part II, §35–6.

In problems of the kind which Professor Hardy Cross considered in his paper, the effects of these transmitted forces can safely be neglected. On that understanding, since one half of each transferred couple (apparently) goes out of existence forthwith, it is evident without further discussion that the constraints can very quickly be relieved of couples, and no appeal has to be made to arguments concerned with strain-energy. But the forces, at this stage, are still sustained by the constraints, and joint displacements will be required to transfer them to the framework: to end the relaxation process here is justifiable only if we have reason to believe that transference of the forces would involve an addition to the strain-energy negligible in comparison with what has been stored already as a result of joint rotations. In relation to frameworks which derive their stiffness in comparable amounts from joint rigidity and from "diagonal bracing", joint displacements are comparable in importance with joint rotations; and since the former transfer forces *unchanged*, the validity of the relaxation process seems to call for demonstration by arguments such as were employed in Part I.

Professor Cross's paper has brought into existence a very considerable literature concerning what are here termed "relaxation methods", but I know of no paper in which formulae have been derived for use in the general problem,—that is, a three-dimensional framework having some joints rigid and others free, which is also stiffened by diagonal or cross bracing, and to which forces are applied not only at the joints but also at intermediate sections of the constituent members. Since writing my earlier paper on relaxation methods I have realized that such formulae are quite easy to derive and to apply;* accordingly they are given now in additional paragraphs which (to facilitate reference) have been numbered to follow concurrently on those of Parts I and II.†

The scope of the present paper, and the simplifying assumptions which restrict its application, are indicated in the appended summary. Of the latter, (*f*) and (*g*) are not necessary, except to the end that general and quantitative formulae may be obtained, but assumption (*h*) I believe to be necessary to the strict validity of a method which depends (as the relaxation method evidently does) upon the Principle of Superposition, although it appears that a solution for " P . *y* effects " could be obtained without difficulty by a slight modification of the standard procedure. Some remarks on this aspect are given in Appendix C.

---

* They are clearly applicable to other problems,—*e.g.*, to continuous beams.

† The figures and tables have also been numbered concurrently, but the equations of this paper have been numbered afresh from (1).

[*Note added, October* 8, 1935—It has been brought to my notice by Mr. A. N. Black that the process of approximation in the relaxation method will only in special instances be correctly described as " continuous", and that accordingly some of the statements made in § 7 (Part I) are subject to correction. Unless, in the problem presented, every joint is subjected to some external force, it is certain that at some stage in the process of " liquidation " we shall have to relieve a constraint of an action which comes upon it not from outside but as a force exerted by the framework; and in these circumstances work is done *on* the constraint *by* the framework, with a consequent (temporary) *reduction* in the total strain-energy. To restrict the permissible relaxations by the requirement that each one must entail an increase of the strain-energy may mean that the solution cannot be completed.

It thus appears that the idea of continuous approximation (by successive *additions* to the total strain-energy) must be relinquished as impracticable, and it is questionable whether anything is to be learned by the keeping of an " energy account " (§ 16 and fig. 2) which would not be shown equally well by the decay of the " unliquidated " forces in Tables III or VII. The relaxation method is still justified by the argument (§ 8) that if at every stage we liquidate the largest force remaining on any one of the constraints, then since the external forces are self-equilibrating they will tend to meet and cancel; but its approximation may not be so rapid as was suggested by the original (and fallacious) argument from strain-energy. The device of " block relaxation " seems to acquire additional importance.

This error in the initial argument might have been detected but for an unfortunate slip made in relation to fig. 3. The values of U in the stages 3–3*d* should have been given as $\frac{1}{2}P\varepsilon \times (0, 2, 2 - 1, 2 - 1 + \frac{3}{2}, 2 - 1 + \frac{3}{2} - \frac{1}{4})$, the strain-energy being alternately increased and decreased when the forces on the constraints are liquidated in the order indicated by the diagrams.]

SUMMARY

Formulae are derived by which the standard procedure of the relaxation method may be applied to problems in which:

(*a*) the framework is three-dimensional (a " space frame "),

(*b*) its members are connected either rigidly or by frictionless joints at either end,
(*c*) members are so orientated that torsional as well as flexural rigidity comes into play to resist distortion,
(*d*) forces are applied either at joints or to the members at intermediate sections,
(*e*) any degree of rigid constraint is imposed,—*e.g.*, by members " built-in " to rigid walls.

Two simplifying assumptions are made (the first being necessary in order that the resulting formulae may have general application):

(*f*) all members are straight and uniform in cross-section and material,
(*g*) there are no " offset moments ",
(*h*) " P . *y* effects " (*i.e.*, bending-moments due to thrusts operating on a bent central-line) are ignored.

The application of the formulae is illustrated by an example in which all of the features (*a*)–(*e*) are exhibited, except that the framework is two-dimensional (a " plane frame ") and therefore torsional rigidity (*c*) does not operate. No feature of the *method* is lost by this restriction, which shortens the numerical calculations which have to be reproduced, and enables an exact solution to be obtained (for comparison) by orthodox methods. This exact solution is reproduced in Appendix A, and the maximum error in the approximate solution is about 1·7%. At the cost of slightly greater labour, this error could easily be reduced by any required amount.

Appendix B deals with the problem of assessing the order of redundancy in a framework having rigid joints, and some remarks on the problem of " P . *y* effects " are given in Appendix C.

PART III—THE METHOD OF SYSTEMATIC RELAXATION AS APPLIED TO A BRACED FRAMEWORK HAVING RIGID JOINTS

General Outline of the Method

38—The basis of the relaxation method is essentially physical,—it contemplates a series of operations which could (at least, to a close approximation) be actually performed. These operations are most easily explained in relation to a particular example, and in what follows a plane (two-dimensional) framework will be considered for the sake of simplicity; but it should be emphasized that the formulae obtained in the mathematical treatment are three-dimensional, and that no new consideration will arise when they are applied to a " space frame ".

Fig. 11 shows a problem in which all customary features are represented, excepting only " offset moments " and " P . *y* effects ".* Thus,

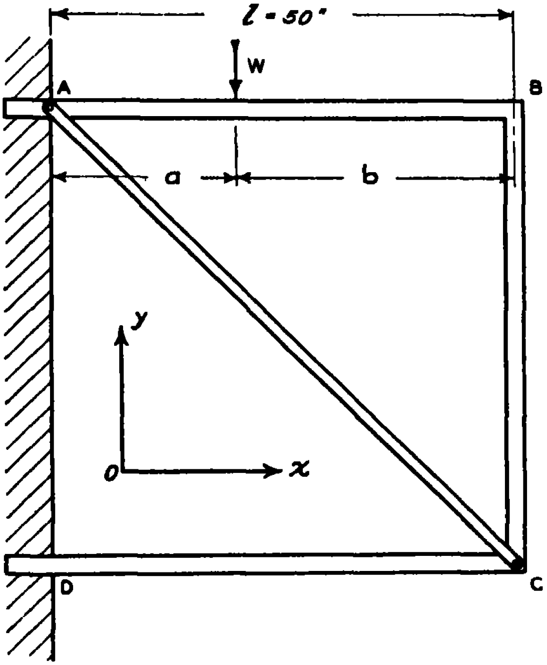

Fig. 11.

(*a*) the constraints at A and D are hyperstatic; (*b*) some, but not all, of the members are rigidly connected at their ends; (*c*) the external force (W) is applied as lateral loading on a member (AB) at a section remote from its ends. The order of redundancy is 4,† so the problem can be solved exactly by conventional methods.‡ Fig. 12 shows the nature of the distortion (to an exaggerated scale), the tensions and thrusts in the members (in tons per ton applied as W, and when $l = 50$ inches) and the flexural moments (in tons-inches per ton applied as W) at the sections where members are attached to rigid joints.§

In applying relaxation methods to this problem, we assume that constraints are provided at the joints B and C whereby the x and y co-ordinates of either joint, and its orientation, can be separately controlled. (At A and D the constraints are specified as permanently rigid.) We assume that these constraints are operative (so as to *fix* B and C) when the load is first applied.

---

* *Cf.* (*g*) and (*h*) of the Summary.

† *Cf.* Appendix B.

‡ *Cf.* Appendix A.

§ *Cf.* § 58.

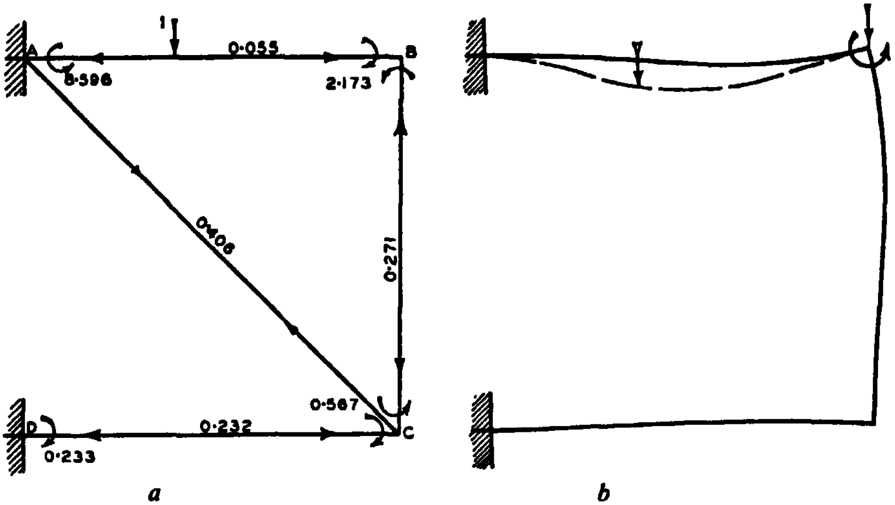

FIG. 12.

THE TREATMENT OF LATERALLY-LOADED MEMBERS

39—In Part I (which related to pin-jointed frameworks) we similarly assumed the operation of constraints, but these were of such a kind as to control only the co-ordinates, not the orientations, of the joints; and the external forces, being applied at the joints, came at first wholly upon the constraints, which accordingly sustained forces but no moments. Here, when W is applied, it is transmitted to the constraints by the member AB, which thus sustains lateral loading from the first. Under this loading AB bends, and so calls for clamping couples at A and B which must (initially) be supplied by the constraints: accordingly these sustain, initially, moments as well as forces.

At the outset we must dispose of forces applied in this way as lateral loading on members. Treating AB as a girder separated from the framework and having both its ends clamped rigidly, we can by ordinary methods determine the values of R_1, R_2, M_1, M_2 in fig. 13.* These actions combined with W constitute a self-equilibrating system which, by the Reciprocal Theorem, will do no work in any displacement or distortion of AB which can occur as the result of actions applied to its ends;* therefore, so far as concerns the rest of the framework, the member AB *with* W, R_1, R_2, M_1, M_2 *operative* behaves exactly as though it were unloaded. Accordingly we imagine these forces to be applied to the member, and forces and moments equal and opposite to R_1, R_2, M_1, M_2 to be applied at the same time to the joints at A and B. Since the new forces cancel identically, we have made no difference to the problem; during the process of relaxation we can neglect the actions on AB; and hence (for the purpose of this process) our problem is reduced to one in which the loads are applied only at the joints.

---

* Their expressions are given in (20), § 54.

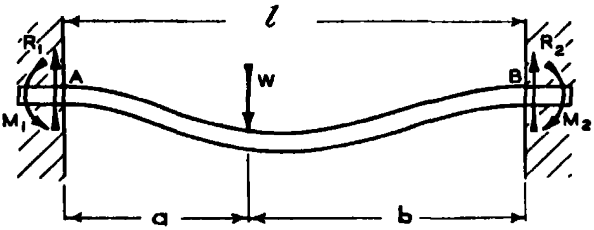

FIG. 13.

40—Initially these loads come wholly upon the constraints, and at A and D (since no movement is permitted) they will remain on the constraints: hence, in the process of relaxation, we have only to "liquidate" (§ 8) the actions imposed on the constraints at B and C. Thus our problem is reduced (for immediate purposes) to what is shown in fig. 14.

In the general (three-dimensional) case a problem involving lateral loads on some or all of the members can be correspondingly simplified. Occasionally the lateral loading on a member will subject it to twist as well as flexure; but the problem corresponding with that of fig. 13 will still be soluble without difficulty, and again we shall be left with actions applied only at the joints.

"STAGES" IN THE PROCESS OF RELAXATION

41—Having reduced our problem to what is exemplified by fig. 14, we may proceed to transmit the applied forces from the constraints to the framework. The process is in essence similar to what was described in Part I; but now (in the general case) the distinct relaxations which can be permitted at any joint comprise not only three independent displacements (u, v, w) but also three independent rotations (p, q, r), and when one end of a rigid member shares in a joint displacement (u, say) we have to imagine that change of orientation is prevented at that end, as well as at the other end which remains fixed during the relaxation.

---

* According to the theorem such work must equal the work done by these terminal actions in the actual displacements of fig. 13; and the latter work is zero, since the distortion of fig. 13 involves no relative movement and no rotation of the terminal sections.

The relaxations are conveniently performed by "stages" in which, alternately, either joint displacements unaccompanied by rotation are permitted, or joint rotations unaccompanied by displacement. In our particular example, M_2 being large in fig. 14, the first stage will preferably consist of operations of the second type: Table VIII (§ 55) gives the whole sequence, which consists of four stages (10 operations in all) and reduces the unliquidated forces and moments, in this example, to 0·4% and 0·05%, respectively, of their initial values. Compared with the exact solution given in Appendix A, our approximate solution (even when stopped after this small number of operations, which have left appreciable forces on the constraints) has given the actions in the constituent members with a maximum error of about 1·7%. Such accuracy is, of course, more than sufficient for practical purposes, and greater accuracy could be attained, if required, at the cost of slightly greater labour.

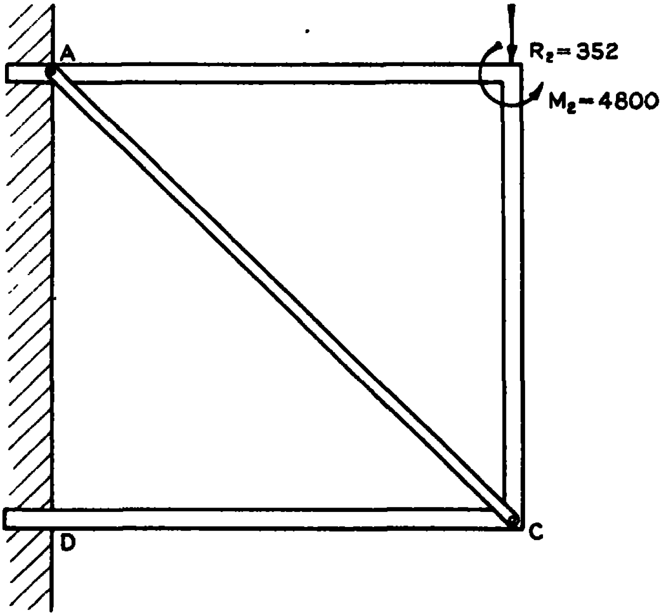

FIG. 14.

THE BASIC FORMULAE

42—We shall obtain all the formulae that are required in the general (three-dimensional) case if we investigate the distortion produced by terminal displacements in a member having any arbitrary orientation. As stated in the Summary,* we assume that the member is straight and uniform both in cross-section and material: regarding A as the end which is moved, we take its central line AB as having (initially) the direction Ox' and the principal axes of inertia of its cross-section as having the directions Oy', Oz' respectively, where x', y', z' are related with the directions x, y, z of our axes of reference by the orthogonal scheme

$$\begin{array}{c|c|c|c|} & x & y & z \\ \hline x' & l & m & n \\ y' & l_1 & m_1 & n_1 \\ z' & l_2 & m_2 & n_2 \end{array} \tag{1}$$

We suppose that the member is compressed, twisted and bent by forces $\mathbf{X}'$, $\mathbf{Y}'$, $\mathbf{Z}'$ and couples $\mathbf{T}$, $\mathbf{M}_1$, $\mathbf{M}_2$ acting on it at the end (A) which moves; the forces have the directions x', y', z' respectively, and the couples are right-handed with respect to axes having these directions. Then at the section distant r from A the axial thrust is $\mathbf{X}'$, the shearing actions are $\mathbf{Y}'$ and $\mathbf{Z}'$, the twisting couple is $\mathbf{T}$, and the bending moments are

$$\left.\begin{aligned} \mathrm{M}_1 &= \mathbf{M}_1 + r\mathbf{Z}', \\ \mathrm{M}_2 &= \mathbf{M}_2 - r\mathbf{Y}', \end{aligned}\right\} \tag{2}$$

about axes parallel to Oy', Oz' respectively.

The strain-energies involved by thrust, twist and bending in the planes of the principal axes are (for a straight member) additive. Accordingly (if, as is customary, we neglect the strain-energy involved by direct shear) the total strain-energy stored in the member is given by

$$\mathrm{U} = \tfrac{1}{2}\int_0^{\mathrm{L}} \left(\frac{\mathbf{X}'^2}{\mathrm{EA}} + \frac{\mathrm{M}_1^2}{\mathrm{B}_1} + \frac{\mathrm{M}_2^2}{\mathrm{B}_2} + \frac{\mathbf{T}^2}{\mathrm{C}}\right) dr, \tag{3}$$

---

* 'Assumption (*f*)'.

where

E is Young's modulus for the material,
L is the length and
A is the cross-sectional area of the member,
B_1 ($= EAk_1^2$) is its flexural rigidity about an axis parallel to Oy',
B_2 ($= EAk_2^2$) is its flexural rigidity about an axis parallel to Oz', and
C is the torsional rigidity of the cross-section. (4)

MEMBER HAVING BOTH ENDS ATTACHED TO RIGID JOINTS

43—The displacement corresponding with $\mathbf{X}'$ is the component displacement of A in the direction Ox',—that is, according to (1), the quantity $(lu_A + mv_A + nw_A)$, where u_A, v_A, w_A are the component displacements of A in the directions Ox, Oy, Oz. Hence, by Castigliano's First Theorem, we have from (3)

$$lu_A + mv_A + nw_A = \frac{\partial U}{\partial \mathbf{X}'} = \int_0^L \frac{\mathbf{X}'}{EA}\,dr = \frac{L}{EA}\mathbf{X}', \ldots$$

and in the same way we obtain

$$\left.\begin{aligned} l_1u_A + m_1v_A + n_1w_A &= \frac{\partial U}{\partial \mathbf{Y}'} = \int_0^L \frac{\mathbf{M}_2}{B_2}\cdot\frac{\partial \mathbf{M}_2}{\partial \mathbf{Y}'}\,dr,\\ &= -\int_0^L \frac{r}{B_2}(\mathbf{M}_2 - r\mathbf{Y}')\,dr,\\ &= \frac{L^2}{B_2}(\tfrac{1}{3}L\mathbf{Y}' - \tfrac{1}{2}\mathbf{M}_2), \ldots\\ l_2u_A + m_2v_A + n_2w_A &= \frac{\partial U}{\partial \mathbf{Z}'} = \frac{L^2}{B_1}(\tfrac{1}{3}L\mathbf{Z}' + \tfrac{1}{2}\mathbf{M}_1). \ldots \end{aligned}\right\} \quad (5)$$

Also if p_A, q_A, r_A are the component rotations of A about axes parallel to Ox, Oy, Oz, we deduce in the same way that

$$\left.\begin{aligned} lp_A + mq_A + nr_A &= \frac{\partial U}{\partial \mathbf{T}} = \frac{L}{C}\mathbf{T}, \ldots\\ l_1p_A + m_1q_A + n_1r_A &= \frac{\partial U}{\partial \mathbf{M}_1} = \int_0^L \frac{\mathbf{M}_1}{B_1}\cdot\frac{\partial \mathbf{M}_1}{\partial \mathbf{M}_1}\,dr,\\ &= \frac{L}{B_1}(\mathbf{M}_1 + \tfrac{1}{2}L\mathbf{Z}'), \ldots\\ l_2p_A + m_2q_A + n_2r_A &= \frac{\partial U}{\partial \mathbf{M}_2} = \frac{L}{B_2}(\mathbf{M}_2 - \tfrac{1}{2}L\mathbf{Y}'). \ldots \end{aligned}\right\} \quad (6)$$

The last two of (5) and the last two of (6) may be replaced by

$$\left.\begin{aligned}
\frac{L^3}{B_2}\mathbf{Y}' &= 12\,(l_1u_A + m_1v_A + n_1w_A) + 6L\,(l_2p_A + m_2q_A + n_2r_A),\\
\frac{L^3}{B_1}\mathbf{Z}' &= 12\,(l_2u_A + m_2v_A + n_2w_A) - 6L\,(l_1p_A + m_1q_A + n_1r_A),\\
\frac{L^2}{B_1}\mathbf{M}_1 &= -\,6\,(l_2u_A + m_2v_A + n_2w_A) + 4L\,(l_1p_A + m_1q_A + n_1r_A),\\
\frac{L^2}{B_2}\mathbf{M}_2 &= 6\,(l_1u_A + m_1v_A + n_1w_A) + 4L\,(l_2p_A + m_2q_A + n_2r_A),
\end{aligned}\right\}\qquad(7)$$

Member having One End Attached to a Rigid Joint, the other End Freely-Jointed

44—Evidently, if the joint at A opposes no resistance to a particular rotation, the corresponding moment at A is zero, and the corresponding equation (6) is not obtained. If p_A, q_A, r_A can all occur freely, then all of $\mathbf{T}$, $\mathbf{M}_1$, $\mathbf{M}_2$ are zero, and all of equations (6) are suppressed: we are left with the relations

$$\left.\begin{aligned}
lu_A + mv_A + nw_A &= \frac{L}{EA}\mathbf{X}',\\
l_1u_A + m_1v_A + n_1w_A &= \tfrac{1}{3}\,\frac{L^3}{B_2}\,\mathbf{Y}',\\
l_2u_A + m_2v_A + n_2w_A &= \tfrac{1}{3}\,\frac{L^3}{B_1}\,\mathbf{Z}',
\end{aligned}\right\}\qquad(5\text{A})$$

which replace (5), while (6) are replaced by

$$\mathbf{T} = \mathbf{M}_1 = \mathbf{M}_2 = 0. \qquad (6\text{A})$$

The circumstances are different if it is at the other end (B) that no resistance is offered to rotation. Then $\mathbf{T}$ must vanish as before, and $M_1 = M_2 = 0$ when $r = L$; so we have in place of (2)

$$\left.\begin{aligned}
M_1 &= (r - L)\,\mathbf{Z}',\\
M_2 &= (L - r)\,\mathbf{Y}',
\end{aligned}\right\}\qquad(2\text{B})$$

and when these substitutions are made in (3) the equations (5) are replaced by

$$\left.\begin{aligned} lu_A + mv_A + nw_A &= \frac{L}{EA}\mathbf{X}' \text{ (as before)}, \ldots \\ l_1u_A + m_1v_A + n_1w_A + L\,(l_2p_A + m_2q_A + n_2r_A) &= \frac{\partial U}{\partial \mathbf{Y}'}, \\ &= \int_0^L (L-r)^2 \frac{\mathbf{Y}'}{B_2}\,dr, \\ &= \tfrac{1}{3}\frac{L^3}{B_2}\mathbf{Y}', \ldots \\ l_2u_A + m_2v_A + n_2w_A - L\,(l_1p_A + m_1q_A + n_1r_A) &= \tfrac{1}{3}\frac{L^3}{B_1}\mathbf{Z}', \ldots \end{aligned}\right\} \quad (5\text{B})$$

These equations determine $\mathbf{X}'$, $\mathbf{Y}'$, $\mathbf{Z}'$, and then the couples at A are given by

$$\mathbf{T} = 0, \quad \mathbf{M}_1 = -L\mathbf{Z}', \quad \mathbf{M}_2 = L\mathbf{Y}'. \qquad (6\text{B})$$

(The first of these equations implies that no resistance is offered to a combined rotation in which $lp_A + mq_A + nr_A = 0$.)

Cases can, of course, occur in which either one, two or three components of rotation are resisted at a particular joint. Part I dealt with members freely jointed at both ends; we have dealt here with a member attached either to two rigid joints or to one rigid and one entirely free joint; and the procedure required in other cases is obvious.

THE INFLUENCE COEFFICIENTS

45—Let X, Y, Z be the forces in the directions of x, y, z, and M_x, M_y, M_z the couples right-handed with respect to axes having these directions, which are statically equivalent to $\mathbf{X}'$, $\mathbf{Y}'$, $\mathbf{Z}'$, $\mathbf{T}$, $\mathbf{M}_1$ $\mathbf{M}_2$. Then we have from (1)

$$\left.\begin{aligned} X &= l\mathbf{X}' + l_1\mathbf{Y}' + l_2\mathbf{Z}', \\ Y &= m\mathbf{X}' + m_1\mathbf{Y}' + m_2\mathbf{Z}', \\ Z &= n\mathbf{X}' + n_1\mathbf{Y}' + n_2\mathbf{Z}', \\ M_x &= l\mathbf{T} + l_1\mathbf{M}_1 + l_2\mathbf{M}_2, \\ M_y &= m\mathbf{T} + m_1\mathbf{M}_1 + m_2\mathbf{M}_2, \\ M_z &= n\mathbf{T} + n_1\mathbf{M}_1 + n_2\mathbf{M}_2, \end{aligned}\right\} \quad (8)$$

and on substituting in these expressions from (5), (6), and (7) we find that

$$\left.\begin{aligned}
\mathrm{X} &= (x, x)\,u_{\mathrm{A}}+(x, y)\,v_{\mathrm{A}}+(x, z)\,w_{\mathrm{A}}+(x, p)\,p_{\mathrm{A}}+(x, q)\,q_{\mathrm{A}}+(x, r)\,r_{\mathrm{A}},\\
\mathrm{Y} &= (y, x)\,u_{\mathrm{A}}+(y, y)\,v_{\mathrm{A}}+(y, z)\,w_{\mathrm{A}}+(y, p)\,p_{\mathrm{A}}+(y, q)\,q_{\mathrm{A}}+(y, r)\,r_{\mathrm{A}},\\
\mathrm{Z} &= (z, x)\,u_{\mathrm{A}}+(z, y)\,v_{\mathrm{A}}+(z, z)\,w_{\mathrm{A}}+(z, p)\,p_{\mathrm{A}}+(z, q)\,q_{\mathrm{A}}+(z, r)\,r_{\mathrm{A}},\\
\mathrm{M}_x &= (p, x)\,u_{\mathrm{A}}+(p, y)\,v_{\mathrm{A}}+(p, z)\,w_{\mathrm{A}}+(p, p)\,p_{\mathrm{A}}+(p, q)\,q_{\mathrm{A}}+(p, r)\,r_{\mathrm{A}},\\
\mathrm{M}_y &= (q, x)\,u_{\mathrm{A}}+(q, y)\,v_{\mathrm{A}}+(q, z)\,w_{\mathrm{A}}+(q, p)\,p_{\mathrm{A}}+(q, q)\,q_{\mathrm{A}}+(q, r)\,r_{\mathrm{A}},\\
\mathrm{M}_z &= (r, x)\,u_{\mathrm{A}}+(r, y)\,v_{\mathrm{A}}+(r, z)\,w_{\mathrm{A}}+(r, p)\,p_{\mathrm{A}}+(r, q)\,q_{\mathrm{A}}+(r, r)\,r_{\mathrm{A}},
\end{aligned}\right\}\quad(9)$$

where

$$\left.\begin{aligned}
(x, x) &= \frac{\mathrm{EA}}{\mathrm{L}}\,l^2 + \frac{12}{\mathrm{L}^3}(\mathrm{B}_2 l_1^{\,2} + \mathrm{B}_1 l_2^{\,2}),\\
(y, y) &= \frac{\mathrm{EA}}{\mathrm{L}}\,m^2 + \frac{12}{\mathrm{L}^3}(\mathrm{B}_2 m_1^{\,2} + \mathrm{B}_1 m_2^{\,2}),\\
(z, z) &= \frac{\mathrm{EA}}{\mathrm{L}}\,n^2 + \frac{12}{\mathrm{L}^3}(\mathrm{B}_2 n_1^{\,2} + \mathrm{B}_2 n_1^{\,2}),\\
(z, y) = (y, z) &= \frac{\mathrm{EA}}{\mathrm{L}}\,mn + \frac{12}{\mathrm{L}^3}(\mathrm{B}_2 m_1 n_1 + \mathrm{B}_1 m_2 n_2),\\
(x, z) = (z, x) &= \frac{\mathrm{EA}}{\mathrm{L}}\,nl + \frac{12}{\mathrm{L}^3}(\mathrm{B}_2 n_1 l_1 + \mathrm{B}_1 n_2 \mathrm{L}_2),\\
(y, x) = (x, y) &= \frac{\mathrm{EA}}{\mathrm{L}}\,lm + \frac{12}{\mathrm{L}^3}(\mathrm{B}_2 l_1 m_1 + \mathrm{B}_1 l_2 m_2),\\
(p, p) &= \frac{\mathrm{C}}{\mathrm{L}}\,l^2 + \frac{4}{\mathrm{L}}(\mathrm{B}_1 l_1^{\,2} + \mathrm{B}_2 l_2^{\,2}),\\
(q, q) &= \frac{\mathrm{C}}{\mathrm{L}}\,m^2 + \frac{4}{\mathrm{L}}(\mathrm{B}_1 m_1^{\,2} + \mathrm{B}_2 m_2^{\,2}),\\
(r, r) &= \frac{\mathrm{C}}{\mathrm{L}}\,n^2 + \frac{4}{\mathrm{L}}(\mathrm{B}_1 n_1^{\,2} + \mathrm{B}_2 n_2^{\,2}),\\
(r, q) = (q, r) &= \frac{\mathrm{C}}{\mathrm{L}}\,mn + \frac{4}{\mathrm{L}}(\mathrm{B}_1 m_1 n_1 + \mathrm{B}_2 m_2 n_2),\\
(p, r) = (r, p) &= \frac{\mathrm{C}}{\mathrm{L}}\,nl + \frac{4}{\mathrm{L}}(\mathrm{B}_1 n_1 l_1 + \mathrm{B}_2 n_2 l_2),\\
(q, p) = (p, q) &= \frac{\mathrm{C}}{\mathrm{L}}\,lm + \frac{4}{\mathrm{L}}(\mathrm{B}_1 l_1 m_1 + \mathrm{B}_2 l_2 m_2),\\
(p, x) = (x, p) &= \frac{6}{\mathrm{L}^3}(\mathrm{B}_2 - \mathrm{B}_1)\,l_1 l_2,
\end{aligned}\right|$$

$$
\left.
\begin{aligned}
(q, x) = (x, q) &= \frac{6}{L^2}(B_2 l_1 m_2 - B_1 l_2 m_1),\\
(r, x) = (x, r) &= \frac{6}{L^2}(B_2 l_1 n_2 - B_1 l_2 n_1),\\
(p, y) = (y, p) &= \frac{6}{L^2}(B_2 m_1 l_2 - B_1 m_2 l_1),\\
(q, y) = (y, q) &= \frac{6}{L^2}(B_2 - B_1)\, m_1 m_2,\\
(r, y) = (y, r) &= \frac{6}{L^2}(B_2 m_1 n_2 - B_1 m_2 n_1),\\
(p, z) = (z, p) &= \frac{6}{L^2}(B_2 n_1 l_2 - B_1 n_2 l_1),\\
(q, z) = (z, q) &= \frac{6}{L^2}(B_2 n_1 m_2 - B_1 n_2 m_1),\\
(r, z) = (z, r) &= \frac{6}{L^2}(B_2 - B_1)\, n_1 n_2.
\end{aligned}
\right\} \quad . \qquad (10)
$$

The quantities (x, x), . ., defined in (10) are " influence coefficients " of the kind employed in Part I,—their number being now increased from 6 to 21 (independent quantities) by reason of the fact that three independent rotations are now involved, as well as three independent displacements.

46—When p_A, q_A, r_A are unresisted (§ 44), only u_A, v_A, w_A appear in (9), and the expressions (10) are replaced by

$$
\left.
\begin{aligned}
(x, x) &= \frac{EA}{L} l^2 + \frac{3}{L^3}(B_2 l_1^2 + B_1 l_2^2)\\
&\qquad \text{and two similar expressions,}\\
(z, y) = (y, z) &= \frac{EA}{L} mn + \frac{3}{L^3}(B_2 m_1 n_1 + B_1 m_2 n_2)\\
&\qquad \text{and two similar expressions.}
\end{aligned}
\right\} \quad (10\text{A})
$$

When p_B, q_B, r_B are unresisted, by substituting in (8) from (5B) and (6B) we obtain the relations (10A) again, with

$$
\begin{aligned}
(p, p) &= \frac{3}{L}(B_1 l_1^2 + B_2 l_2^2) \ldots\\
&\qquad \text{and two similar expressions,}\\
(r, q) = (q, r) &= \frac{3}{L}(B_1 m_1 n_1 + B_2 m_2 n_2) \ldots\\
&\qquad \text{and two similar expressions,}
\end{aligned}
$$

$$\left.\begin{array}{l}
(p, x) = (x, p) = \dfrac{3}{L^2}(B_2 - B_1)\, l_1 l_2, \ldots \\[2ex]
(q, x) = (x, q) = \dfrac{3}{L^2}(B_2 l_1 m_2 - B_1 l_2 m_1), \\[2ex]
(r, x) = (x, r) = \dfrac{3}{L^2}(B_2 l_1 n_2 - B_1 l_2 n_1), \ldots \\[2ex]
\qquad\qquad\text{and six similar expressions.}
\end{array}\right\} \quad (10\text{B})$$

47—The foregoing expressions can be simplified when the member has the same flexural rigidity against bending in all planes, so that $B_1 = B_2 = B$ (say). For since the direction-cosines given in (1) constitute an orthogonal scheme of transformation, we have

$$\left.\begin{array}{l}
l^2 + l_1^2 + l_2^2 = 1, \text{ etc.} \\
lm + l_1 m_1 + l_2 m_2 = 0, \text{ etc.} \\
l_1 m_2 - l_2 m_1 = n, \text{ etc.}^*
\end{array}\right\} \quad (11)$$

Accordingly, in this instance, we may replace the expressions (10) by

$$\left.\begin{array}{lll}
\multicolumn{3}{c}{(x, x), (y, y), (z, z) = 12\dfrac{B}{L^3} + F(l^2, m^2, n^2),} \\[2ex]
(z, y) = (y, z) = Fmn, & (x, z) = (z, x) = Fnl, & (y, x) = (x, y) = Flm, \\[1ex]
\multicolumn{3}{c}{(p, p), (q, q), (r, r) = 4\dfrac{B}{L} + G(l^2, m^2, n^2),} \\[2ex]
(r, q) = (q, r) = Gmn, & (p, r) = (r, p) = Gnl, & (q, p) = (p, q) = Glm, \\
(p, x) = (x, p) & = (q, y) = (y, q) & = (r, z) = (z, r) = 0, \\[1ex]
-(q, z) = -(z, q) & = (r, y) = (y, r) & = 6\dfrac{B}{L^2}\, l, \\[2ex]
-(r, x) = -(x, r) & = (p, z) = (z, p) & = 6\dfrac{B}{L^2}\, m, \\[2ex]
-(p, y) = -(y, p) & = (q, x) = (x, q) & = 6\dfrac{B}{L^2}\, n, \\[1ex]
\text{where} & & \\
\multicolumn{3}{c}{F = \dfrac{EA}{L} - 12\dfrac{B}{L^3}, \qquad G = \dfrac{C - 4B}{L}.}
\end{array}\right\} \quad (12)$$

---

* It is assumed that $\begin{vmatrix} l, & m, & n \\ l_1, & m_1, & n_1 \\ l_2, & m_2, & n_2 \end{vmatrix} = 1.$ This can always be arranged by suitably choosing the directions Oy', Oz' (§ 42).

The formulae (10A) are replaced by

$$\left.\begin{aligned}
&(x,x),(y,y),(z,z) = 3\frac{B}{L^3} + F_A(l^2, m^2, n^2),\\
&(z,y) = (y,z) = F_A mn, \quad (x,z) = (z,x) = F_A nl, \quad (y,x) = (x,y) = F_A lm,
\end{aligned}\right\}$$

where

$$F_A = \frac{EA}{L} - 3\frac{B}{L^3}, \tag{12A}$$

and the formulae (10B) by

$$\left.\begin{aligned}
&(p,p),(q,q),(r,r) = 3\frac{B}{L} - 3\frac{B}{L}(l^2, m^2, n^2),\\
&(r,q) = (q,r) = -3\frac{B}{L}mn, \quad (p,r) = (r,p) = -3\frac{B}{L}nl, \quad (q,p) = (p,q) = -3\frac{B}{L}lm,\\
&(p,x) = (x,p) = (q,y) = (y,q) = (r,z) = (z,r) = 0,\\
&-(q,z) = -(z,q) = (r,y) = (y,r) = 3\frac{B}{L^2}l,\\
&-(r,x) = -(x,r) = (p,z) = (z,p) = 3\frac{B}{L^2}m,\\
&-(p,y) = -(y,p) = (q,x) = (x,q) = 3\frac{B}{L^2}n,
\end{aligned}\right\} \tag{12B}$$

Forces and Moments Imposed upon the Joints

48—The quantities X, Y, Z, M_x, M_y, M_z, in (9), are the forces and moments which come *upon* the member at its end (A) which moves. It is easy to see that the forces and moments which in consequence are exerted *by* the member are as follows:

on the joint which is moved in the relaxation:

$$X_M, Y_M, Z_M, (M_x)_M, (M_y)_M, (M_z)_M = -(X, Y, Z, M_x, M_y, M_z),$$

on the joint which is not moved:

$$\begin{aligned}
X_F, Y_F, Z_F &= X, Y, Z,\\
(M_x)_F &= M_x + L(nY - mZ),\\
(M_y)_F &= M_y + L(lZ - nX),\\
(M_z)_F &= M_z + L(mX - lY),
\end{aligned}$$

as given by (9).

Using these formulae we can calculate directly, from (10), the influence coefficients which must be inserted in (9) to give the forces and moments on the fixed and moving joint. We shall give results only for the special case in which $B_1 = B_2 = B$, so that the expressions (10) may be replaced by (12). On this understanding we obtain

$$\left.\begin{array}{lll}
\multicolumn{3}{c}{(x, x)_F,\ (y, y)_F,\ (z, z)_F = 12\dfrac{B}{L^3} + F\,(l^2, m^2, n^2),} \\
(z, y)_F = (y, z)_F = Fmn, & (x, z)_F = (z, x)_F = Fnl, & (y, x)_F = (x, y)_F = Flm, \\
\multicolumn{3}{c}{(p, p)_F,\ (q, q)_F,\ (r, r)_F = -2\dfrac{B}{L} + H\,(l^2, m^2, n^2),} \\
(r, q)_F = (q, r)_F = Hmn, & (p, r)_F = (r, p)_F = Hnl, & (q, p)_F = (p, q)_F = Hlm, \\
(p, x)_F = (x, p)_F & = (q, y)_F = (y, q)_F & = (r, z)_F = (z, r)_F = 0, \\
(q, z)_F = -(z, q)_F & = -(r, y)_F = (y, r)_F & = 6\dfrac{B}{L^2}\,l, \\
(r, x)_F = -(x, r)_F & = -(p, z)_F = (z, p)_F & = 6\dfrac{B}{L^2}\,m, \\
(p, y)_F = -(y, p)_F & = -(q, x)_F = (x, q)_F & = 6\dfrac{B}{L^2}\,n, \\
\text{where} & & \\
\multicolumn{3}{c}{F = \dfrac{EA}{L} - 12\dfrac{B}{L^3}, \qquad H = \dfrac{C + 2B}{L},}
\end{array}\right\} \tag{13}$$

as the influence coefficients appropriate to the joint which is fixed,* and

$$\begin{array}{lll}
\multicolumn{3}{c}{(x, x)_M,\ (y, y)_M,\ (z, z)_M = -12\dfrac{B}{L^3} - F\,(l^2, m^2, n^2),} \\
(z, y)_M = (y, z)_M = -Fmn, & (x, z)_M = (z, x)_M = -Fnl, & (y, x)_M = (x, y)_M = -Flm, \\
\multicolumn{3}{c}{(p, p)_M,\ (q, q)_M,\ (r, r)_M = -4\dfrac{B}{L} - G\,(l^2, m^2, n^2),} \\
(r, q)_M = (q, r)_M = -Gmn, & (p, r)_M = (r, p)_M = -Gnl, & (q, p)_M = (p, q)_M \\
 & & \quad = -Glm, \\
(p, x)_M = (x, p)_M & = (q, y)_M = (y, q)_M & = (r, z)_M = (z, r)_M = 0, \\
(q, z)_M = (z, q)_M & = -(r, y)_M = -(y, r)_M & = 6\dfrac{B}{L^2}\,l,
\end{array}$$

---

* It should perhaps be remarked that equalities of the type $(q, z) = (z, q)$, which can be deduced from the Reciprocal Theorem in relation to the moving end, are not required by that theorem to hold in relation to the fixed end.

$$\left.\begin{aligned}
(r, x)_M &= (x, r)_M = -(p, z)_M = -(z, p)_M = 6\frac{B}{L^2}m,\\
(p, y)_M &= (y, p)_M = -(q, x)_M = -(x, q)_M = 6\frac{B}{L^2}n,\\
\text{where}\quad F &= \frac{EA}{L} - 12\frac{B}{L^3}, \qquad G = \frac{C-4B}{L},
\end{aligned}\right\} \tag{14}$$

as the influence coefficients appropriate to the end which is moved in the relaxation. Similar calculations are easily made when the member has one joint rigid and the other free,—equations (12) being replaced for this purpose by (12A) and (12B) in turn (so that influence coefficients are available for a relaxation permitted at either of the joints).

It should be emphasized that l, m, n, in these formulae, are the direction-cosines of AB, *the line drawn from the end which is moved to the end which is fixed.* Having regard to this convention, it is easy to show that the expressions for (x, x), (x, y) .. etc., are equivalent, when the terms involving B and C are omitted, to those which were derived by slightly different methods in Part I.

We also observe that since

$$\frac{B}{L^3} = \frac{EAk^2}{L^3} = \frac{k^2}{L^2}\left(\frac{EA}{L}\right),$$

and since k/l is usually small, the value of F will in general be only slightly dependent on the flexural rigidity B.

Using (13) and (14), we can easily calculate the effects of any required joint displacement upon any particular member, and therefore upon all of the members which come to any particular joint; and the device of "Block Relaxations" (Part I, §§ 19–25) will evidently be as applicable when the joints are rigid as when they are free.

SIMPLIFIED FORMULAE FOR PROBLEMS IN TWO DIMENSIONS

49—The application of these results will follow exactly the lines of Part I, § 13, except that three couples, as well as three forces, come on each joint as a consequence of any given displacement, and six distinct types of displacement call for consideration. We shall illustrate the numerical calculations by an example in two dimensions, fig. 11.

Here $n = 0$ for all members, and displacements of the type w, p, q do not occur. Accordingly the influence coefficients which we require are

(x, x), (x, y), (y, y), (r, r), (r, x), (r, y), and these can be obtained from (13) and (14) by making n zero. We have

$$\left.\begin{array}{l}
\textit{for the fixed end:}\\
\quad (x, x)_F,\ (y, y)_F = 12\dfrac{B}{L^3} + F(l^2, m^2), \quad (r, r)_F = -2\dfrac{B}{L},\\
\quad (y, x)_F = (x, y)_F = Flm,\\
\quad (r, x)_F = -(x, r)_F = 6\dfrac{B}{L^2}m, \quad -(r, y)_F - (y, r)_F = 6\dfrac{B}{L^2}l,\\
\textit{for the moving end:}\\
\quad (x, x)_M,\ (y, y)_M = -12\dfrac{B}{L^3} - F(l^2, m^2), \quad (r, r)_M = -4\dfrac{B}{L},\\
\quad (y, x)_M = (x, y)_M = -Flm,\\
\quad (r, x)_M = (x, r)_M = 6\dfrac{B}{L^2}m, \quad -(r, y)_M = -(y, r)_M = 6\dfrac{B}{L^2}l,\\
\text{where} \qquad F = \dfrac{EA}{L} - 12\dfrac{B}{L^3}.
\end{array}\right\} \quad (15)$$

A NUMERICAL EXAMPLE

50—The framework shown in fig. 11 forms three sides of a square ABCD for which

$$AB = BC = CD = 50 \text{ inches},$$
$$AC = 50\sqrt{2} = 70{\cdot}7 \text{ inches}.$$

The material is steel having Young's Modulus 13,000 tons/inch^2, and the members AB, BC, CD have the same cross-sectional area (1 square inch) and moment of inertia ($I = 1{\cdot}25$ inch^4 units). The cross-sectional area of AC (which is freely-jointed at both ends) is 1·5 square inches. Thus "B" for the members AB, BC, CD is 16,250 tons-inch^2 units, and "EA" for the member AC is 19,500 tons.

51—We take axes Ox, Oy in the directions AB, DA, as shown in fig. 11, and we adopt the ton-weight and inch as units of force and length. Then, considering the member AB, and imagining B to be moved, we have as values for insertion in the formulae (15)*

$$\left.\begin{array}{l}
\qquad\qquad l = -1, \quad m = 0, \quad L = 50,\\
B = 16{,}250. \quad B/L = 325, \quad B/L^2 = 6{\cdot}5, \quad 12B/L^3 = 1{\cdot}56,\\
\qquad\qquad F = \dfrac{13{,}000}{50} - 12\dfrac{B}{L^3},\\
\qquad\qquad\ \ = 260 - 1{\cdot}56 = 258{\cdot}44,
\end{array}\right\} \quad (16)$$

---

* Concerning the convention stated in § 48 regarding l and m.

so that we may write (now using a suffix A for the fixed and B for the moving joint)

$$\left.\begin{aligned}
&(x,x)_A = 260, \quad (y,y)_A = 1{\cdot}56, \quad (r,r)_A = -650,\\
&(y,x)_A = (x,y)_A = (r,x)_A = (x,r)_A = 0,\\
&(r,y)_A = -(y,r)_A = 39,\\
&\text{and}\\
&(x,x)_B = -260, \quad (y,y)_B = -1{\cdot}56, \quad (r,r)_B = -1300,\\
&(y,x)_B = (x,y)_B = (r,x)_B = (x,r)_B = 0,\\
&(r,y)_B = (y,r)_B = 39.
\end{aligned}\right\} \quad (17)$$

The other member attached to the joint B is BC, and the calculations for this member are exactly similar, except that $l = 0$, $m = -1$. So, for this member, the values (17) are replaced by

$$\left.\begin{aligned}
&(x,x)_C = 1{\cdot}56, \quad (y,y)_C = 260, \quad (r,r)_C = -650,\\
&(y,x)_C = (x,y)_C = (r,y)_C = (y,r)_C = 0,\\
&-(r,x)_C = (x,r)_C = 39,\\
&\text{and}\\
&(x,x)_B = -1{\cdot}56, \quad (y,y)_B = -260, \quad (r,r)_B = -1300,\\
&(y,x)_B = (x,y)_B = (r,y)_B = (y,r)_B = 0,\\
&(r,x)_B = (x,r)_B = -39.
\end{aligned}\right\} \quad (18)$$

52—These calculations replace (in the problem now under consideration) the simpler calculations (for pin-jointed frameworks) which were summarized in Table I of Part I. Since different magnitudes, as well as different signs, now distinguish the influence coefficients appropriate to the fixed and moving joint of any member, tabulation is no longer worth while.

The calculations of § 13, on the other hand, are almost exactly repeated, and here the results (namely, the actions on the constraints which result from given displacements) may conveniently be tabulated. Thus, if we substitute from (17) and (18) in expressions of the form (9), we find (for example) that a displacement u_B, in a relaxation confined to this particular joint and direction, involves forces and moments as under:

forces in direction Ox

$$u_B \times \left| \begin{array}{r} 260 \text{ on A} \\ 1{\cdot}56 \text{ on C} \\ \hline -261{\cdot}56 \text{ on B} \end{array}\right.$$

forces in direction Oy

$$u_B \times \left| \begin{array}{r} 0 \text{ on A} \\ 0 \text{ on C} \\ \hline 0 \text{ on B} \end{array}\right.$$

moments about Oz

$$u_B \times \left| \begin{array}{r} 0 \text{ on A} \\ -39 \text{ on C} \\ \hline -39 \text{ on B} \end{array}\right.$$

It will be seen that the sum of the *forces* imposed in either direction vanishes as it did in Part I; but the sum of the *moments* does not vanish, being balanced (statically) by the forces ($\pm 1 \cdot 56$) which are imposed on B and C by shearing actions in BC.

53—These results are recorded in the first line of Table VII, which corresponds with Table II of Part I. The second line is derived in the manner described in §14, and the next four lines (relating to the operations numbered 2 and 3 in Table VII) are obtained from (17) and (18) by the methods of § 52.

Operations 4–6 are concerned with relaxations permitted to the joint C and affecting the members CB, CD, CA. For CB and CD the calculations are closely similar to those of § 51.* In dealing with CA (which is pin-jointed at both ends) we must omit from (15) the terms which involve the flexural rigidity B: then we have

$$\begin{aligned} \mathrm{F} &= \frac{\mathrm{EA}}{\mathrm{L}} = \frac{19{,}500}{50\sqrt{2}} \ (cf.\ \S\ 50), \\ &= 195\sqrt{2}, \\ -l &= m = 1/\sqrt{2}, \end{aligned}$$

and we find that all the influence coefficients vanish except

$$\left.\begin{aligned} (x, x)_{\mathrm{A}} &= (y, y)_{\mathrm{A}} = 138, \\ (y, x)_{\mathrm{A}} &= (x, y)_{\mathrm{A}} = -138, \\ \text{and} \qquad (x, x)_{\mathrm{C}} &= (y, y)_{\mathrm{C}} = -138, \\ (y, x)_{\mathrm{C}} &= (x, y)_{\mathrm{C}} = 138. \end{aligned}\right\} \quad (19)$$

Operations 7 and 8, Table VII, are block displacements involving translation of BC as a rigid body; they are combinations respectively of Operations 1 and 4 and of Operations 2 and 5. It will be found convenient later to have them included in Table VII: " block rotations " (in this particular problem) do not call for separate consideration, since the joint displacement u_{C} (Operation 4) gives us what we want.

ELIMINATION OF THE LATERAL LOADING ON AB

54—Having Table VII, we are in a position to deal with the problem depicted in fig. 11. We shall assume that

$$a = 20 \text{ inches}, \quad b = 30 \text{ inches}, \quad \mathrm{W} = 1000 \text{ tons weight.}\dagger$$

---

* For CD we have $l = -1$, $m = 0$; for CB, $l = 0$, $m = 1$.

† Since the stresses and displacements, by Hooke's law, are proportional to W, the value assumed for this load is immaterial. We may conveniently take it as 1000 units, leaving for subsequent investigation the question of what load is actually permissible.

TAB

No.		X_A	Y_A	$(M_z)_A$	X_B	Y_B	$(M_z)_B$
1(a)	$u_B = 1$	*260*	*0*	*0*	*−261·56*	*0*	*−39*
1(*b*)	$= 0·3823$	99·4	0	0	−100	0	−14·9
2(a)	$v_B = 1$	*0*	*1·56*	*39*	*0*	*−261·56*	*39*
2(*b*)	$= 0·3823$	0	0·60	14·9	0	−100	14·9
3(a)	$r_B = 1$	*0*	*−39*	*−650*	*−39*	*39*	*−2600*
3(*b*)	$= 0·3846$	0	−15	−250	−15	15	−1000
4(a)	$u_C = 1$	*138*	*−138*	*0*	*1·56*	*0*	*39*
4(*b*)	$= 0·2503$	34·6	−34·6	0	0·39	0	9·76
5(a)	$v_C = 1$	*−138*	*138*	*0*	*0*	*260*	*0*
5(*b*)	$= 0·2503$	34·6	34·6	0	0	65·1	0
6(a)	$r_C = 1$	*0*	*0*	*0*	*−39*	*0*	*−650*
6(*b*)	$= 0·3846$	0	0	0	−15	0	−250
7(a)	"*Block displacement*" $u_B = u_C = \mathbf{u} = 1$	*398*	*−138*	*0*	*−260*	*0*	*0*
8(a)	"*Block displacement*" $v_B = v_C = \mathbf{v} = 1$	*−138*	*139·56*	*39*	*0*	*−1·56*	*39*

We must begin by calculating, for the laterally loaded member AB, the terminal reactions and moments denoted by R_1, R_2, M_1, M_2 in fig. 13. Referring to that diagram, we easily find that

$$\left.\begin{aligned} R_1 l^3 &= Wb^2(3a+b), & R_2 l^3 &= Wa^2(a+3b), \\ M_1 l^2 &= Wab^2, & M_2 l^2 &= Wa^2 b, \end{aligned}\right\} \quad (20)$$

and hence, in this instance,

$$R_1 = 648 \text{ tons}, \quad R_2 = 352 \text{ tons}, \quad M_1 = 7200 \text{ tons-inches},$$
$$M_2 = 4800 \text{ tons-inches}.$$

In accordance with §§ 39–40, we imagine that these reactions and moments are applied to, and move with, the member AB, and that equal and

LE VII

X_C	Y_C	$(M_z)_C$	X_D	Y_D	$(M_z)_D$	Resultant actions on " Block " BC
1·56	*0*	*−39*	*0*	*0*	*0*	$\mathbf{X} = X_B + X_C = -260$, $\mathbf{Y} = Y_B + Y_C = 0$, $\mathbf{M}_C = (M_z)_B + (M_z)_C - 50X_B = +3000$
0·60	0	−14·9	0	0	0	
0	*260*	*0*	*0*	*0*	*0*	
0	99·4	0	0	0	0	
39	*0*	*−650*	*0*	*0*	*0*	
15	0	−250	0	0	0	
−399·56	*138*	*39*	*260*	*0*	*0*	
−100	34·6	9·76	65·1	0	0	
138	***−399·56***	*39*	*0*	*1·56*	*39*	
34·6	**−100**	9·76	0	0·39	9·76	
39	*39*	***−2600***	*0*	*39*	*−650*	
15	15	**−1000**	0	15	−250	
−398	*138*	*0*	*260*	*0*	*0*	$\mathbf{X} = X_B + X_C = -658$, $\mathbf{Y} = Y_B + Y_C = 138$, $\mathbf{M}_C = +13000$.
138	*−139·56*	*39*	*0*	*1·56*	*39*	$\mathbf{X} = X_B + X_C = +138$, $\mathbf{Y} = Y_B + Y_C = -141·12$, $\mathbf{M}_C = +78$.

opposite actions are applied (initially) to the constraints. In this way we reduce our problem to what is shown in fig. 14: with axes as indicated in fig. 11 we have, initially,

$$\left.\begin{array}{lll} X_A = 0, & Y_A = -648, & (M_z)_A = -7200, \\ X_B = 0, & Y_B = -352, & (M_z)_B = +4800, \end{array}\right\} \quad (21)$$

the constraints at C and D being unloaded; and of the actions (21) only those at B have to be " liquidated," since the problem calls for permanent and rigid constraints at A and D. When we have (to a sufficient approximation) transferred Y_B, $(M_z)_B$ to the framework and to the constraints at A and D, we shall only need to impose the actions Y_A, $(M_z)_A$, from (21), at A, and the system shown in fig. 13 (with values for

TAB

Stage	Operation and multiplier	X_A	Y_A	$(M_z)_A$	X_B	Y_B	$(M_z)_B$
	Initial forces and moments:	—	—	—	0	−352	(4800)
I (i)	3(*b*) × 5·12	0	−76·8	−1280	−76·8	76·8	−5120
		0	−76·8	−1280	−76·8	−275·2	−320
(ii)	6(*b*) × − 1·28	0	0	0	19·2	0	320
		0	−76·8	−1280	−57·6	−275·2	0
II (i)	8(*a*) × − 2·96	408·5	−413	−115·4	0	4·6	−115·4
		408·5	−489·8	−1395·4	−57·6	−270·6	−115·4
(ii)	7(*a*) × − 0·89	−354·2	122·9	0	231·5	0	0
		54·3	−366·9	−1395·4	173·9	−270·6	−115·4
(iii)	1(*a*) × 0·69	179·4	0	0	−180·5	0	−26·9
		233·7	−366·9	−1395·4	−6·6	(−270·6)	−142·3
(iv)	2(*a*) × − 1	0	−1·6	−39	0	261·6	−39
		233·7	−368·5	−1434·4	−6·6	−9	(−181·3)
III (i)	3(*b*) × − 0·16	0	2·4	40	2·4	−2·4	160
		233·7	−366·1	−1394·4	−4·2	−11·4	−21·3
(ii)	6(*b*) × − 0·1	0	0	0	1·5	0	25
		233·7	−366·1	−1394·4	−2·7	(−11·4)	3·7
IV (i)	2(*b*) × − 0·1	0	−0·1	−1·5	0	10	−1·5
		233·7	−366·2	−1395·9	(−2·7)	−1·4	2·2
(ii)	1(*a*) × − 0·01	−2·6	0	0	2·6	0	0·4
	Totals for fig. 4	231·1	−366·2	−1395·9	−0·1	−1·4	2·6
	Added in § 58 ..	0	−648	−7200			
	Totals for fig. 1	231·1	−1014·2	−8595·9			

LE VIII

X_C	Y_C	$(M_z)_C$	X_D	Y_D	$(M_z)_D$	Resultants for "Block" BC
—	—	—	—	—	—	
76·8	0	−1280	0	0	0	
76·8	0	(−1280)	0	0	0	
−19·2	−19·2	1280	0	19·2	320	
57·6	−19·2	0	0	19·2	320	$X = X_B + X_C = 0$ $Y = Y_B + Y_C = -294·4$ $M_C = 2880$
−408·5	413	−115·4	0	4·6	−115·4	
350·9	393·8	−115·4	0	14·6	204·6	
354·2	−122·9	0	−231·5	0	0	
3·3	270·9	−115·4	−231·5	14·6	204·6	
1·1	0	−26·9	0	0	0	
4·4	(270·9)	−142·3	−231·5	14·6	204·6	
0	−260	0	0	0	0	
4·4	10·9	−142·3	−231·5	14·6	204·6	
−2·4	0	40	0	0	0	
2·0	10·9	(−102·3)	−231·5	14·6	204·6	
−1·5	−1·5	100	0	1·5	25	
0·5	9·4	−2·3	−231·5	16·1	229·6	
0	−9·9	0	0	0	0	
0·5	−0·5	−2·3	−231·5	16·1	229·6	
−0·02	0	0·4	0	0	0	
0·5	−0·5	−1·9	−231·5	16·1	229·6	

the actions as found above) upon the member AB, in order to arrive at a complete solution of the problem of fig. 11.

LIQUIDATION OF THE ACTIONS ON THE CONSTRAINTS

55—Accordingly we set out the actions Y_B, $(M_z)_B$ in the first line of Table VIII, and we proceed to " liquidate " them in the manner of Part I, § 15, using Table VII for this purpose. We divide the process into " stages " in which we concentrate attention, alternately, on moments and on forces.

Stage I—Since the procedure works most rapidly as applied to *moments*, we begin by disposing of $(M_z)_B$. On referring to Table VII we see that Operation 3 will dispose of 16 units of $(M_z)_B$ at the cost of introducing a moment $(M_z)_C$ of -4 units; and that Operation 6 will dispose of this latter moment by introducing similarly a moment $(M_z)_B$ of $+1$ unit. The double operation disposes of 15 units of $(M_z)_B$ while leaving $(M_z)_C$ zero: thus we see that to cancel the moment $(M_z)_B = 4800$ we must in Operation (i) of Table VIII introduce a moment at B of magnitude

$$-\frac{16}{15} \times 4800 = -5120$$

leaving a moment of—320 to be cancelled in Operation (ii).

Stage II—We now start to eliminate *forces*, and we begin this process (as in the example of Part I, § 22) with operations involving *block displacements*. Time will be saved if the required displacements are determined at once, and precisely, from the relevant simultaneous equations; and since this procedure will be practicable in the general (three dimensional) case it may fairly be adopted here. We have to *cancel* resultant forces $\mathbf{X} = 0$, $\mathbf{Y} = -294 \cdot 4$ and a moment about C given by $\mathbf{M}_C = 2880$ tons-inches, acting on the " block " BC, by a combination of the block displacements represented by Operations Nos. 1*a*, 7*a*, 8*a*. Let k_1, k_7, k_8 be the required multipliers: then from the figures given in the last column of Table VII we have

$$\begin{aligned} -260\,k_1 - 658\,k_7 + 138\,k_8 &= 0, \\ 138\,k_7 - 141 \cdot 12\,k_8 &= 294 \cdot 4, \\ 13{,}000\,k_1 + 13{,}000\,k_7 + 78\,k_8 &= -2880, \end{aligned}$$

and these equations are approximately satisfied by the values

$$k_1 = 0 \cdot 69, \quad k_7 = -0 \cdot 89, \quad k_8 = -2 \cdot 96. \qquad (22)$$

The multipliers for the first three operations of Stage II are chosen accordingly. When those operations have been applied, the only large *forces* remaining are Y_B, Y_C, and these are reduced simultaneously by an operation of the type 2 (*a*). We end Stage II at this point, and proceed to liquidate the unbalanced moments at B and C.

Stage III—Two operations serve to eliminate the greater part of either moment, and we turn again to the forces.

Stage IV—Two operations reduce the largest unbalanced force from 11·4 to 1·4 tons, and at the same time reduce the larger of the unbalanced moments from 3·7 to 2·6 tons-inches. Comparing these figures with what we had given initially, we see that they represent about 0·4% of the specified force and 0·05% of the specified moment. It is not worth while (although it would be easy) to proceed to a closer approximation.

TABLE IX

Stage	u_B	v_B	r_B	u_C	v_C	r_C
I (i)	—	—	5·12 × 0·3846	—	—	—
I (ii)	—	—	—	—	—	−1·28 × 0·3846
II (i)	—	−2·96	—	—	−2·96	—
II (ii)	−0·89	—	—	−0·89	—	—
II (iii)	0·69	—	—	—	—	—
II (iv)	—	−1·00	—	—	—	—
III (i)	—	—	−0·16 × 0·3846	—	—	—
III (ii)	—	—	—	—	—	−0·1 × 0·3846
IV (i)	—	−0·1 × 0·3823	—	—	—	—
IV (ii)	−0·01	—	—	—	—	—
Totals	−0·210	−3·998	$1{\cdot}907_8$	−0·890	−2·960	$-0{\cdot}530_8$

CALCULATION OF DISPLACEMENTS AND ROTATIONS

56—Having decided that its approximation is sufficient, we may complete the solution by finding the displacements and the stresses which it entails. The former may be deduced as shown in Table IX, where multipliers taken for the second column of Table VIII are combined with displacements taken from the second column of Table VII.

CALCULATION OF THE ACTIONS IMPOSED ON THE MEMBERS

57—The actions which our solution imposes on the constraints at A and D can be read off from the last line of Table VIII. The actions imposed on the constituent members can be deduced from (9), (13), and (14) in the general case,* and in this particular example from (9) combined with the calculations of § 51. Thus we have from (9) and (17), substituting for the displacements,

$$\left.\begin{aligned}
&\text{Tension in AB} = (x,x)_A \times u_B = 260 \times -0\cdot 210 = -54\cdot 6 \text{ tons,}\\
&\text{and we find similarly that}\\
&\text{Tension in BC} = 260 \times (v_B - v_C) = 260 \times -1\cdot 038\\
&\qquad\qquad = -269\cdot 9 \text{ tons,}\\
&\text{Tension in CD} = 260 \times u_C = 260 \times -0\cdot 890 = -231\cdot 4 \text{ tons,}\\
&\text{Tension in AC} = \sqrt{2} \times 138\,(u_C - v_C) = 195 \times 2\cdot 07\\
&\qquad\qquad = 403\cdot 6_5 \text{ tons.}
\end{aligned}\right\}\quad (23)$$

In this simple example we can proceed at once to calculate the shearing actions by Statics, since we know (from Table VIII) the forces on the joints and (from the above figures) how much of each force is imposed by tensions. We find in this way that†

$$\left.\begin{aligned}
&\text{shear in AB (from force on B)} = (352 - 1\cdot 4) - 269\cdot 9 = 80\cdot 7 \text{ tons}\\
&\text{shear in BC (from force on B)} = 54\cdot 6 + 0\cdot 1 = 54\cdot 7 \text{ tons}\\
&\text{shear in CD (from force on C)} = \frac{1}{\sqrt{2}} \times 403\cdot 6_5 - 269\cdot 9\\
&\qquad\qquad + 0\cdot 5 = 16\cdot 0 \text{ tons}
\end{aligned}\right\}\quad (24)$$

the senses of the shearing forces being such as would rotate AB, BC, CD respectively clockwise, clockwise, and counterclockwise. The bending moments at A and B in AB are given by

$$\left.\begin{aligned}
M_A &= (r,y)_A\, v_B + (r,r)_A\, r_B = 39 \times (-3\cdot 998) - 650 \times 1\cdot 907_5,\\
&= -155\cdot 9 - 1240 = -1396 \text{ tons-inches,}\\
M_B &= (r,y)_B\, v_B + (r,r)_B\, r_B = 39 \times (-3\cdot 998) - 1300 \times 1\cdot 907_5,\\
&= -155\cdot 9 - 2480 = -2636 \text{ tons-inches,}
\end{aligned}\right.$$

---

* Alternatively, the tensions and thrusts can be deduced by the methods of Part I, § 17.

† Allowance is made in these expressions for the forces still remaining on the constraints.

and we have similarly, for CD,

$$\left.\begin{aligned} M_D &= 39\,v_C - 650\,r_C = 39 \times (-2\cdot96) + 650 \times 0\cdot530_5 \\ &= -115\cdot4 + 344\cdot6 = 229 \text{ tons-inches}, \\ M_C &= 39\,v_C - 1300\,r_C = 39 \times (-2\cdot96) + 1300 \times 0\cdot530_5 \\ &= -115\cdot4 + 689\cdot2 = 574 \text{ tons-inches.} \end{aligned}\right\} \quad (25)$$

Allowing for the unbalanced couples which our solution has left on the constraints at B and C, we may deduce that the bending moments in BC are

$$\left.\begin{aligned} M_B &= (4800 - 2\cdot6) - 2636 = 2161_5 \text{ tons-inches}, \\ M_C &= 574 + 1\cdot9 \qquad\qquad\quad = 576 \text{ tons-inches.} \end{aligned}\right\} \quad (26)$$

These figures check well with (24) and with the residual actions given in the last line of Table VIII. They may be compared with the " exact " values (entailing no residual actions on the constraints) which are given in Appendix B.*

COMPLETION OF THE SOLUTION

58—Reverting to § 40, we have now completed our solution of the modified problem presented in fig. 14, and it only remains to complete the solution for fig. 11. We have determined the values of R_1, R_2, M_1, M_2 (fig. 13) in § 54, and we have already applied R_2 and M_2 to the framework. If we now apply R_1, M_1 to the constraint at A (as in the supplementary line of Table VIII), we have a solution satisfying all the conditions which are imposed when the framework is loaded by a force of 1000 tons applied to AB in the manner of fig. 11, and we can construct fig. 12 as a diagrammatic summary of results.

It is perhaps worth while to repeat† that a load of 1000 units was imposed for numerical convenience; the value assumed is immaterial in a problem governed by Hooke's law. In fig. 12*a*, values are given for the tensions and thrusts in tons, and for the bending moments in tons-inches, which result from each ton of applied load W, fig. 11. In fig. 12*b*, the full lines show (greatly exaggerated) the distortions produced by the applied force and moment in the simplified problem of fig. 14; the dotted lines show the additional distortion of AB under the actions of fig. 13, and thus give the total distortion of the framework in the problem taken initially (fig. 11).

---

* The expressions (23), (24), (25), and (26) compare respectively with those given in (vi), (vii), and (viii) of that Appendix.

† *Cf.* footnote to § 54.

APPENDIX A

CONVENTIONAL METHODS APPLIED TO THE PROBLEM OF FIG. 14

1—The order of redundancy is 4 (*cf.* Appendix B). We shall take the unknowns to be the tensions in AB and AC (which we denote by T_1 and $T_3\sqrt{2}$), the bending moment (M_1) which is applied to AB at A, and the shear (V_1) in AB. Then the actions in the remaining members can be deduced from statical considerations, and are as indicated in fig. 15

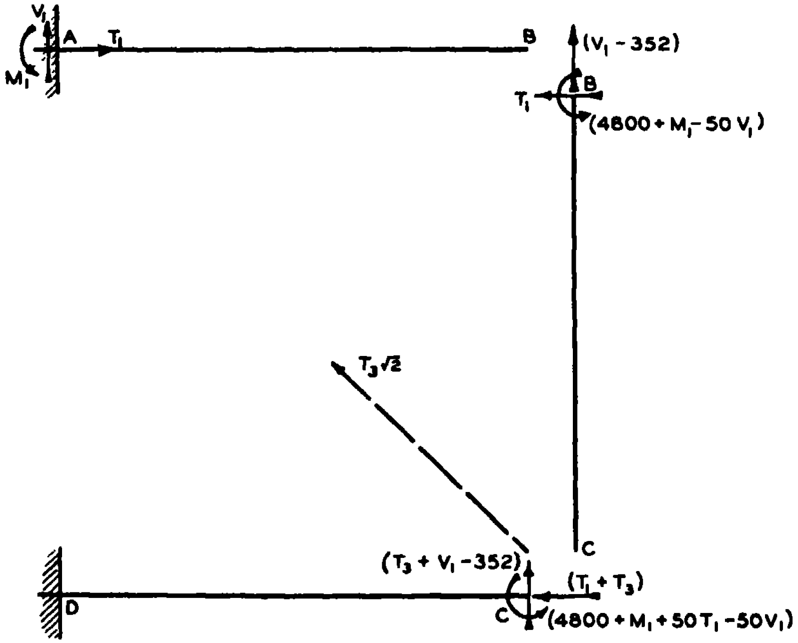

FIG. 15.

In AB, the tension is T_1,

" the bending moment M ranges from M_1 to $(M_1 - 50V_1)$;

in BC, the tension is $(V_1 - 352)$,

M ranges from $(4800 + M_1 - 50V_1)$ to $(4800 + M_1 + 50T_1 - 50V_1)$;

in CD, the thrust is $(T_1 + T_3)$,

M ranges from $(4800 + M_1 + 50T_1 - 50V_1)$ to $(M_1 - 12{,}800 + 50T_1 + 50T_3)$.

2—Now for any member of length l, if the tension is P and if the bending moment ranges from M′ to M″, it is easy to show that

$$\text{strain-energy of direct tension} = \tfrac{1}{2}\frac{P^2 l}{EA},$$

$$\text{strain-energy of flexure} = \tfrac{1}{6}\frac{l}{B}(M'^2 + M'M'' + M''^2).$$

Therefore, since for

$$AB, BC, CD, \ l = 50, \ EA = 13{,}000, \ B = 16{,}250,$$

and for

$$AC, \ l = 50\sqrt{2}, \ EA = 19{,}500, \ B = 0 \text{ (in effect)},$$

the total strain-energy of direct thrust and tension is

$$U_t = \frac{50}{2 \times 13{,}000}\left[T_1^2 + (V_1 - 352)^2 + (T_1 + T_3)^2 + \frac{2\sqrt{2}}{1 \cdot 5}T_3^2\right],$$

and the total strain-energy of flexure is

$$U_f = \frac{50}{97{,}500}[M_1^2 + M_1(M_1 - 50V_1) + (M_1 - 50V_1)^2$$
$$+ \text{(similar terms for BC and CD)}].$$

The total strain-energy $U = U_t + U_f$. Accordingly we have

$$\begin{aligned}\tfrac{3}{5} \times 13{,}000\,U = {} & 15[T_1^2 + (V_1 - 352)^2 + (T_1 + T_3)^2 + 20\sqrt{2}\,T_3^2] + \\ & + 4[M_1^2 + M_1(M_1 - 50V_1) + (M_1 - 50V_1)^2 + \\ & + (4800 + M_1 - 50V_1)^2 + (4800 + M_1 - 50V_1) \times \\ & \times (4800 + M_1 + 50T_1 - 50V_1) + \\ & + 2(4800 + M_1 + 50T_1 - 50V_1)^2 + \\ & + (2M_1 - 8000 + 100T_1 + 50T_3 - 50V_1) \times \\ & \times (M_1 - 12{,}800 + 50T_1 + 50T_3)],\end{aligned}$$

and hence (since U assumes its minimum value in accordance with Castigliano's "Principle of Least Work") we deduce that

$$\frac{\partial U}{\partial T_3} = 0; \text{ therefore } 3M_1 - 50V_1 + 150 \cdot 15T_1 + 100 \cdot 433T_3 = 20{,}800 \quad \text{(i)}$$

$$\frac{\partial U}{\partial T_1} = 0; \text{ therefore } 9M_1 - 300V_1 + 400 \cdot 3T_1 + 150 \cdot 15T_3 = 9{,}600 \quad \text{(ii)}$$

$$\frac{\partial U}{\partial V_1} = 0; \text{ therefore } 12M_1 - 500\cdot15V_1 + 300T_1 + 50T_3 = -25{,}652\cdot8 \tag{iii}$$

$$\frac{\partial U}{\partial M_1} = 0; \text{ therefore } 18M_1 - 600V_1 + 450T_1 + 150T_3 = -4800. \tag{iv}$$

3—Solving these simultaneous equations, we have approximately

$$\left.\begin{aligned} T_1 &= -54\cdot8, & T_3 &= 287\cdot3, \\ V_1 &= 80\cdot7, & M_1 &= 1408, \end{aligned}\right\} \tag{v}$$

and we can deduce the other actions shown in fig. 15. We find that

$$\left.\begin{aligned} &\textit{Tension} \text{ in AB} = T_1 &&= -54\cdot8 \text{ (tons)}, \\ &\textit{Tension} \text{ in BC} = V_1 - 352 &&= -271\cdot3 \text{ (tons)}, \\ &\textit{Tension} \text{ in CD} = -(T_1 + T_3) &&= -232\cdot5 \text{ (tons)}, \\ &\textit{Tension} \text{ in AC} = T_3\sqrt{2} &&= 406\cdot2 \text{ (tons)}, \end{aligned}\right\} \tag{vi}$$

$$\left.\begin{aligned} &\textit{Shear} \text{ in AB} = V_1 &&= 80\cdot7 \text{ tons}, \\ &\textit{Shear} \text{ in BC} = -T_1 &&= 54\cdot8 \text{ tons}, \\ &\textit{Shear} \text{ in CD} = T_3 + V_1 - 352 &&= 16 \text{ tons}, \end{aligned}\right\} \tag{vii}$$

Bending moments—

$$\left.\begin{aligned} &\text{in AB}: M_A = M_1 = 1408; \\ &\qquad\qquad M_B = 50V_1 - M_1 = 2627 \text{ tons-inches} \\ &\text{in BC}: M_B = 4800 + M_1 - 50V_1 = 2173; \\ &\qquad\qquad M_C = M_B + 50T_1 = 567 \text{ tons-inches} \\ &\text{in CD}: M_C = 567;\ M_D = 800 - 567 = 233 \text{ tons-inches}. \end{aligned}\right\} \tag{viii}$$

APPENDIX B

THE ORDER OF REDUNDANCY OF A FRAMEWORK HAVING STIFF JOINTS

1—The number of independent actions which can operate on a given member will depend upon the nature of its end joints. If these are entirely free, only tension (or compression) can be exerted. If one component rotation (of an end relative to its joint) is prevented, an additional action (the constraining couple) can occur. At most we can have six unknown actions on a member—namely, tension, a twisting action, and two bending couples at either end.*

---

* Knowing these, we can deduce the two components of shear force.

The number of equations which can be formulated for any one joint will also depend upon the nature of its attachments to members. We can always formulate 3 force-equations of equilibrium; we may be able, in addition, to formulate 1, 2 or 3 moment-equations.

To fix the framework in space, 6 constraints *must* be imposed. But if in fact the constraints prevent C distinct types of displacement (including rotations), the *unknown* constraining forces number C, where $C \nless 6$.

2—Let

m be the number of the members,

j be the number of the joints,

M be the total number of independent actions (on members) which have to be determined,

J be the total number of equations which can be formulated as conditions of equilibrium for the joints.

Then (for a space frame) we have in all

$M + C - 6$ unknowns to be determined,

J equations for their determination,

and accordingly the order of redundancy

$$N = M + C - J \qquad (C \nless 6), \tag{1}$$

reducing in the case of a pin-jointed framework which is held only against rigid-body movements ($M = m$; $C = 6$; $J = 3j$) to the usual formula

$$N = m - 3j + 6.$$

For a plane frame we have similarly

$$N = M + C - J \qquad (C \nless 3), \tag{2}$$

reducing in the case of a pin-jointed framework ($M = m$; $C = 3$; $J = 2j$) to

$$N = m - 2j + 3.$$

3—In a plane framework, if both ends of a member are fixed, it contributes 3 unknowns to M (the tension, and one bending couple at either end). If both ends are free, it contributes 1 unknown (the tension).

Each pin-joint contributes 2 equations to J, and each rigid (and unconstrained) joint contributes 3 equations (2 force-equations and one moment equation).

In fixing the position of a pin-joint we introduce 2 constraining forces, and in clamping a rigid joint we add 3 to the number C.

4—In the problem of fig. 11 there are 3 members having both ends fixed, and one having both ends pin-jointed. So $M = 3 \times 3 + 1 = 10$.

There are 4 joints for which equations of equilibrium can be formulated, —all rigid. So $J = 4 \times 3 = 12$.

Two stiff joints are rigidly fixed. So $C = 2 \times 3 = 6$.

Accordingly, in this problem, we have from (2)

$$N = 10 + 6 - 12 = 4.$$

APPENDIX C

THE EFFECTS OF BENDING IN COMPRESSION MEMBERS

1—We have assumed in this paper that the actions (bending, twisting, and tension or compression) which come upon a member as a result of distortions in the framework can be combined in accordance with the principle of superposition. Actually, if the thrust in a member is appreciable, and if the member is appreciably bent, the thrust will induce bending moments (by actions described in the Introduction as "P . y effects") additional to those which we have considered; and in any event bending, if appreciable, will alter the distance between the two ends of a member, and hence the tension (or thrust) involved by given joint displacements.

Let Ox be drawn through the end joints of a member in their displaced positions, with the origin O at one end; and let y be the deflexion of a section, due to bending, in a direction perpendicular to this line. Then, if s is measured from O along the bent central-line, the distance between the two ends is

$$\int_0^l \frac{dx}{ds}\,ds = \int_0^l \left[1 - \left(\frac{dy}{ds}\right)^2\right]^{\frac{1}{2}} ds = l - \tfrac{1}{2}\int_0^l \left(\frac{dy}{dx}\right)^2 dx,$$

very nearly, if dy/dx is everywhere small. So the approach of the two ends due to bending is measured by

$$\tfrac{1}{2}\int_0^l \left(\frac{dy}{dx}\right)^2 dx,$$

and to neutralize this approach we should require to apply an additional tension T, where (in the notation of this paper)*

$$T \doteq \tfrac{1}{2}\,\frac{EA}{l}\int_0^l \left(\frac{dy}{dx}\right)^2 dx. \qquad (1)$$

---

* In the body of the paper T was used to denote a twisting couple.

We have not, in this paper, allowed for the effect here considered. The form of (1) shows that it is a second-order effect, and as such it will not fall within the scope of the Principle of Superposition; but if, at the close of a relaxation process, T is calculated from (1) and applied as additional forces on the constraints which control the joint displacements, we can evidently continue the relaxation process so as to "liquidate" these forces, and in this way it should be possible to arrive eventually at a solution in which adequate allowance has been made for "P . y effects".

2—Accordingly we proceed to examine further the form of (1) when, as in this paper, y arises from end thrust P acting on a member which is bent by terminal couples M_1, M_2 and by the accompanying shearing actions.

If M_1, M_2 are taken as positive when their sense is such as would make y positive, the equation governing y is

$$-B\frac{d^2y}{dx^2} = Py + M_t, \tag{2}$$

where B is the flexural rigidity (taken as before to be uniform) and M_t is the bending moment which would exist in the absence of P, so that

$$M_t = M_1 + (M_2 - M_1)\frac{x}{l}. \tag{3}$$

Substituting from (3) in (2), we solve this equation in the form

$$y = \frac{1}{P}\left[\frac{1}{\sin \alpha l}\{M_1 \sin \alpha(l-x) + M_2 \sin \alpha x\} - M_1 - (M_2 - M_1)\frac{x}{l}\right], \tag{4}$$

where

$$\alpha^2 = \frac{P}{B}. \tag{5}$$

This expression makes y zero at either end. Substituting it in (1), we find that

$$T = \frac{1}{2}\frac{EA}{P^2 l^2}\left[(M_1^2 + M_2^2)\left(\frac{\alpha^2 l^2}{2\sin^2 \alpha l} + \frac{1}{2}\alpha l \cot \alpha l - 1\right)\right.$$
$$\left. - 2M_1M_2\left(\frac{\alpha^2 l^2}{2\sin^2 \alpha l}\cos \alpha l + \frac{\alpha l}{2\sin \alpha l} - 1\right)\right]. \tag{6}$$

Observing that $B = EAk^2$, where k is the relevant radius of gyration, and substituting for P from (5), we may write (6) in the form

$$\left.\begin{aligned} T &= \frac{1}{2B}\frac{l^2}{k^2}[(M_1^2 + M_2^2)F_1(\lambda) - 2M_1M_2 . F_2(\lambda)], \\ &\text{where} \\ \lambda &= \alpha l = l\sqrt{(P/B)}, \end{aligned}\right\}$$

$$\left.\begin{aligned} F_1(\lambda) &= \frac{\lambda^2 + \frac{1}{2}\lambda \sin 2\lambda - 1 + \cos 2\lambda}{\lambda^4 (1 - \cos 2\lambda)}, \\ F_2(\lambda) &= \frac{\lambda^2 \cos \lambda + \lambda \sin \lambda - 1 + \cos 2\lambda}{\lambda^4 (1 - \cos 2\lambda)}. \end{aligned}\right\} \qquad (7)$$

3—Equation (7) enables us, given P (and therefore λ), to calculate the amount T by which bending reduces the thrust in a member when its ends are held at a fixed distance apart: for this purpose $F_1(\lambda)$ and $F_2(\lambda)$ may be calculated once for all in the range $(0 < \lambda < \pi)$. We observe that the lowest power of λ in both the numerators and denominator of $F_1(\lambda)$, $F_2(\lambda)$ is λ^6. As $\lambda \to 0$, $F_1(\lambda) \to 1/45$, $F_2(\lambda) \to -7/360$; accordingly

$$T \to \frac{1}{2B}\frac{l^2}{k^2} \cdot \frac{1}{180}[4(M_1^2 + M_2^2) + 7M_1M_2], \qquad (8)$$

and this is also the value obtained for T from (1) when we neglect P, in (2), from the beginning.

Having calculated T, we can impose this as a tension applied externally to the end joints of the member considered, and we can continue the relaxation process. But, of course, as a result, the value of the thrust will in general be altered, and our calculated value of T will no longer apply: accordingly we must in this problem proceed by trial and error, instead of by continuous approximation.

The Sorption of Hydrogen and Deuterium by Copper and Palladium I—The Behaviour of Copper and Copper Oxides

By H. W. MELVILLE and ERIC K. RIDEAL, F.R.S., Laboratory of Colloid Science, Cambridge

(*Received July* 5, 1935)

The investigation of homogeneous reactions of deuterium and of deuterides has shown that the heavy isotopic molecules react in general less readily than the light, owing to the greater energy of activation required in the deuterium reactions. This result is qualitatively in accordance with theoretical expectations, the reason for the difference being mainly due to the larger zero point energy of the hydrogen compounds. Quantitative analysis of reactions whose mechanism is well established has, however, shown that the ratio of the velocities is often considerably less than that expected if all the zero point energy is contributed to the energy pool in the activating collision. The smaller ratio of velocities is due to the fact that the zero point energy of the activated state cannot be neglected, the difference for H and for D reactions often being considerable. For example, in the reaction* $Br + H_2 [D_2] \rightarrow HBr [DBr] + H [D]$ the difference in the energy of activation is 1·50 kg cal, and therefore the difference in zero point energies in the activated state is 0·3 kg cal; similarly for $Cl + H_2 (D_2) \rightarrow HCl (DCl) + H (D)$ the respective figures are 1·23 and 0·55† kg cal, while for the reactions $H + H_2$ (para) = H_2 (ortho) + H and $D + D_2$ (ortho) = D_2 (para) + D, the difference in the activated state is no less than 1·20 kg cal.‡

The position with regard to heterogeneous reactions of hydrogen is much less satisfactory and therefore any further means of obtaining information in this branch of kinetics is of value. Deuterium at first sight promised to be a useful tool in helping to discriminate between various hypotheses. Unfortunately, it is difficult to predict theoretically exactly what will happen in any well-defined instance even with a complete experimental knowledge of the mechanism of the reaction. The state of affairs is analogous to that obtaining with homogeneous reactions, it being necessary to determine experimentally the behaviour of the two isotopes in a variety of heterogeneous processes.

---

* Bach, Bonhoeffer, and Moelwyn-Hughes, 'Z. phys. Chem.,' B, vol. 27, p. 71 (1934).

† Rollefson, 'J. Amer. Chem. Soc.,' vol. 56, p. 144 (1934).

‡ A. and L. Farkas, 'Proc. Roy. Soc.,' A (*in the press*).

A number of investigations has been carried out on the sorption of hydrogen by metals; whilst there is general agreement as to the existence of a chemi-adsorbed layer forming a surface hydride, and under suitable conditions a layer held by van der Waals forces on this original chemi-adsorbed layer, there is in addition a slow process entailing the sorption of hydrogen which is considered to be either a process of activated chemi-adsorption or a process of activated diffusion. In processes of catalytic hydrogenation the view first expressed by Sabatier that hydrogenation was brought about through the intermediary of a hydride is now generally accepted, but it is uncertain whether the energy of activation required for such processes entails the activation of the chemi-adsorbed layer formed at low temperatures and pressures or is connected in any way with the hydrogen which undergoes the process of slow sorption the nature of which is still a matter of controversy. Estimates have been made of the zero point energies of several metallic hydrides,* and therefore by careful control of suitable reactions it may be possible to identify the hydride and to measure the zero point energies in the transitional or activated state which is the first step in the elucidation of the mechanism. That hydrides are really involved and that the differences in the activated state in simple hydrogenation reactions at a nickel surface may be relatively small, has already been demonstrated in a preliminary observation,† for the observed difference in the energy of activation approximates to the value calculated for the normal hydride molecules. In this communication we discuss the reduction of copper oxide by atomic and molecular hydrogen and examine the slow sorption of hydrogen by copper and palladium in relation to the diffusion of the gas through copper, palladium, and nickel.

EXPERIMENTAL

Deuterium was prepared by the decomposition of heavy water on a well outgassed tungsten filament and then diffused through palladium into an evacuated reservoir. The deuterium content of the gas was measured by the thermal conductivity method. Hydrogen was prepared by passing the electrolytic gas over palladized copper, phosphorus pentoxide, and then through a liquid air trap. To ensure that this hydrogen was of sufficient purity, check experiments were made with hydrogen prepared in the apparatus used for heavy hydrogen. The remainder of the experimental details are most conveniently given with the numerical data.

---

* Eyring and Sherman, ' J. Chem. Phys.,' vol. 1, p. 345 (1933).

† Melville, ' J. Chem. Soc.,' p. 797 (1934).

The Reduction of Copper Oxide

In the homogeneous reactions of hydrogen and deuterium atoms, it has been shown* that apart from a $\sqrt{2}$ factor (due to the greater velocity of the hydrogen atom) the probability of reaction with O_2, N_2O, C_2H_4 is identical for H and for D. From the early experiments of Cario and Franck,† it is known that photochemically produced hydrogen atoms react rapidly with copper oxide at room temperature, the reduction requiring little, if any, energy of activation.

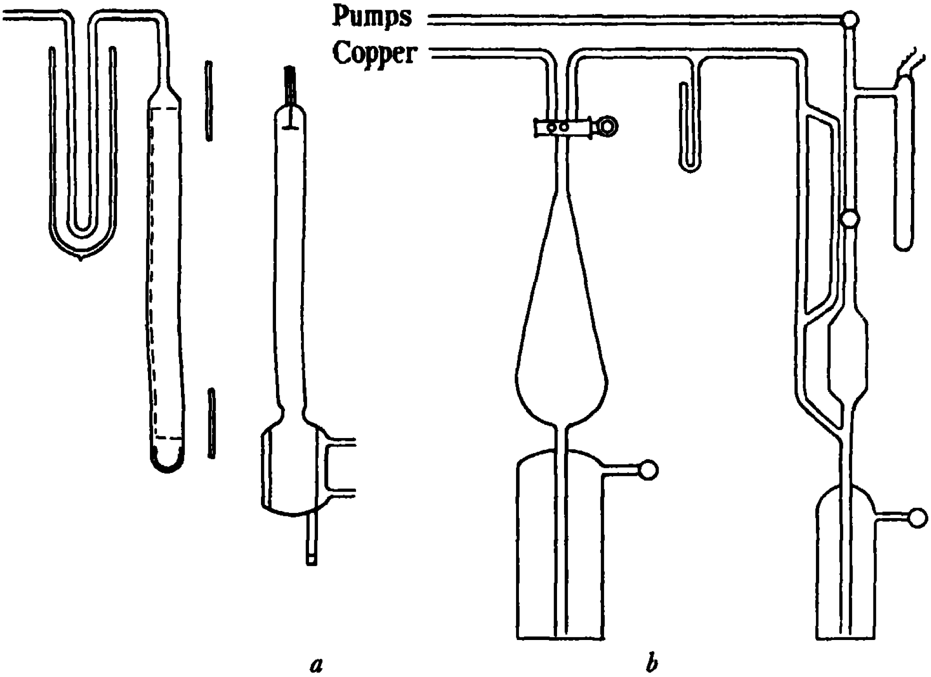

FIG. 1.

A silica tube 1 cm in diameter contained a cylinder of partially oxidized copper foil with a slit running parallel to its axis, the slit facing a mercury lamp with a water cooled cathode, fig. 1, *a*. At the bottom of the tube there was a small cup containing calcium chloride, thoroughly dehydrated by heating in a good vacuum, to absorb the water produced. This was shielded from the lamp to prevent photo dissociation of the chloride. A U-tube containing mercury droplets and immersed in an ice bath supplied mercury vapour at the constant and low pressure of 0·0001 mm.

---

* Melville, 'J. Chem. Soc.,' p. 1243 (1934).

† 'Z. Physik,' vol. 33, p. 871 (1925).

As has been pointed out in a previous paper (*loc. cit.*) on the reactions of H and D atoms, it is necessary to have some competing reaction with which to compare the rate of hydrogenation. This is the reason for using a partially oxidized foil, for we thus ensure the recombination of an appreciable fraction of the atoms on the copper surface and therefore the observed reaction velocity is really the ratio of the rate of reduction to that of recombination. At the low pressures employed in the experiments described below, an appreciable fraction of the mercury atoms excited lose their energy by radiation. Fortunately H_2 and D_2 molecules deactivate excited atoms at the same speed,* and the fraction of atoms radiating is not altered by the substitution of D_2 to H_2.

The following precautions were then taken. Mercury vapour was removed from the insolation tube (containing hydrogen) by a liquid air trap in order to find whether, in consequence of the ejection of electrons from the oxide or a photo surface reaction between oxide and adsorbed hydrogen, reduction of the oxide occurred—none was found. A little oxygen was admitted, but the rate of water formation was less than 0·5% of that when mercury vapour at a pressure of 0·0001 mm was present in addition. At a pressure of 2·38 mm hydrogen and after 5 minutes' exposure, mercury vapour being present, the pressure fell 0·15 mm, 1·11 mm of oxygen were then added and the pressure fell 1·17 mm in 2 minutes, showing that only one-twentieth of the hydrogen atoms formed reduced the oxide. The lamp was placed closer to the reaction vessel and a number of runs made with hydrogen and deuterium, but, as will be seen from fig. 2, curve 2, no difference in velocity is apparent. This means that the ratio of the rates of reduction of copper oxide to that of the combination of H and D atoms on the copper surface is the same, and, if to a first approximation the reasonable assumption is made that the recombination of the atoms goes at the same speed for both isotopes, it follows that the rates of reduction are likewise identical.

The apparatus was altered for experiments with molecular hydrogen. A number of attempts was made to use copper wires and also copper plated nickel wires, but these gave unsatisfactory results in that it was difficult to ensure uniform reduction. Finally, a silica tube was partially filled with granules of copper oxide and placed in a furnace; a small diffusion pump was employed to withdraw the water vapour. The reaction velocity was never allowed to rise to such a value that it was limited by the speed of the pump. Two typical runs are given in fig. 2, curves 1 and 3, and in Table I. The constant k is calculated on the assumption that the reaction is unimolecular and its constancy shows that this is nearly correct.

---

* Evans, 'J. Chem. Phys.,' vol. 2, p. 450 (1934).

The photo-chemical experiments show that the reaction of atomic hydrogen with copper oxide occurs with great ease; indeed, with the partially oxidized surface the question as to whether or not an atom will reduce the oxide probably only depends on its hitting the oxide or the hydrogen-covered metal surface. If the behaviour is similar to that obtaining in the gas reactions, then no difference in reactivity of the isotopes is to be expected. The difference in velocity obtained in the thermal reduction of the oxide must occur either in the dissociation of the hydrogen and its chemi-adsorption as atoms or at some stage in bringing an atom of chemi-adsorbed hydrogen to the oxide and in supplying the necessary energy of activation for the reaction $CuO + CuH = 2Cu + OH_{ads}$ followed by $OH + H = H_2O$ which probably takes place as

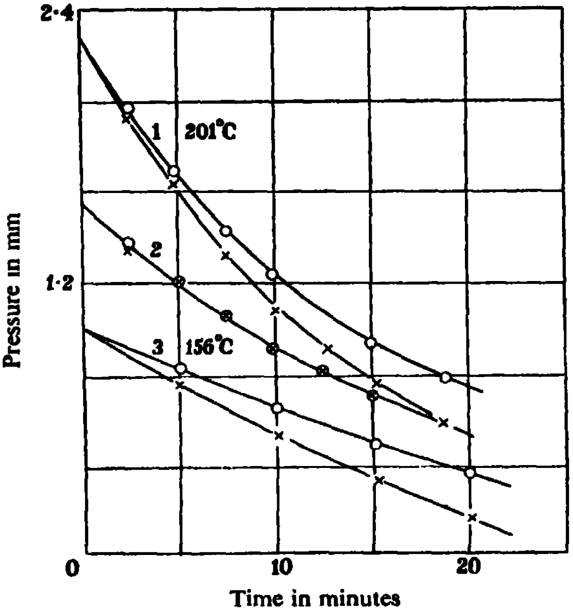

FIG. 2—Reduction of copper oxide by hydrogen. Curves 1 and 3 for molecules, 2 for atoms. × refers to H_2 and O to a 47% D mixture.

rapidly on a copper as on a platinum surface.* The water molecule then evaporates, but it is clear from the experiments with hydrogen atoms at lower temperatures that no inhibition by the accumulation of water vapour, as occurs in some conditions,† when the ratio of the rates of evaporation of light and heavy water (present also in the hydrogen atom reactions) might be sufficiently different to account for the ratios observed.

TABLE I—REDUCTION OF COPPER OXIDE BY MOLECULAR HYDROGEN

	Temperature 201° C				Temperature 156° C		
t min	*p* (H) mm	*k*	*p* (D)*	*t*	*p* (H)	*p* (D)	*p* (H)
0	2·29	—	2·31	0	3·06	2·63	3·06
1	2·12	—	2·10	5	(9) 2·59	2·42	2·80
2	1·96	0·078	1·94	10	2·54	2·26	2·54
3	1·80	0·081	1·73	15	2·09	2·09	2·28
4	1·63	0·085	1·62	20	2·11	1·97	2·05
6	1·33	0·091	1·38	25	1·89	1·81	1·83
8	1·07	0·095	1·20	30	1·69	—	(42) 1·22
10	0·88	0·095	1·02	$t_{1/3}$	22·4	28·0	22·4
15	0·57	0·093	0·74				

* D content 47%.

$t_{1/3}$ time for reaction to 1/3 to completion.

The ratios of the velocities of reduction of copper oxide by hydrogen and deuterium for the 47% mixture can be calculated with each of the above hypotheses and it is found that the second one is most probable. In the following table are given the observed ratios and those calculated on the assumptions that (*a*) the rate determining step is the reaction between CuH and CuO; (*b*) the difference in the zero point energies of CuH and CuD is 0·7 kg cal. (If the first reaction, viz., dissociation and chemiadsorption, governed the reaction velocity, and H_2 and D_2 had been involved, the difference would have been a little less than 1·8 kg cal); and (*c*) the zero point energies in the activated states are identical.

Temperature ° C ..	156	201	269
Ratio of rates	1·26	1·15, 1·20	1·10–1·15
Ratio calculated ..	1·35	1·31	1·28

A comparison of the two sets of values suggests that this is the actual mechanism of the reduction process. Whilst the observed rates are not closely reproducible the calculated rates are definitely a little higher than those observed, suggesting the existence of some zero point energy in the activated state, actual agreement being obtained with a value of $\Delta E = 0 \cdot 4$ kg cal.

---

* Taylor and Lavin, 'J. Amer. Chem. Soc.,' vol. 52, p. 1910 (1930).

† Okajama, 'J. Soc. Chem. Ind. Japan,' vol. 31, p. 399 (1928).

A further conclusion can be drawn from these experiments, for when dealing with comparatively large pieces of oxide consisting of rods 0·5 mm in diameter and 1–2 mm in length the layers of oxide near the surface are soon reduced after orientating experiments, with the result that the hydrogen has to diffuse through or over metallic copper to attack more oxide. The difference in velocities of reduction must be due to a difference in the rates of diffusion of the hydrogen and deuterium atoms or hydrides and deuteride or to a difference in the energies of activation of the hydride and deuteride after it has diffused into the proximity of the oxide. The slow activated diffusion of hydrogen into copper has been carefully studied experimentally by Ward* and theoretically by Lennard Jones.† Whilst the energies of activated diffusion are not very reproducible it was found that a partially oxidized copper on reduction gave a half life of the hydrogen at 156° C of 34·5 minutes and at 201° C 7·4 minutes corresponding to an energy of activation of 14·2 kg cal compared with 14·1 kg cal found by Ward for the diffusion process into copper.

THE ACTIVATED SORPTION OF HYDROGEN AND DEUTERIUM BY COPPER

A sample of copper powder was prepared from copper nitrate by calcining to the oxide, reducing with hydrogen, then oxidizing and reducing at successively lower temperatures until the final reduction was made at 200° C. The copper was now so active that in a few hours it became covered with a superficial layer of oxide on exposure to air at room temperature. It was sealed into a bulb and out-gassed at 200° C until the equilibrium pressure was 10^{-4} mm, the copper being protected from grease and mercury vapour by a liquid air trap. Connected by a tap to the absorption bulb was a pipette of known volume and a glass spring gauge to follow the course of the adsorption. The dead space of the bulb containing the copper was determined by calibration with nitrogen. It amounted to 8·8 cc, the weight of copper being 7·0 gm.

Several experiments were then made to determine the minimum time required for outgassing after an adsorption run by (1) measuring the volume of gas sorbed and the volume desorbed as a function of the time of previous evacuation. These experiments need not be detailed, but several hours' exhaustion at 200° yielded sorption rates and saturation values in good agreement with Ward's results.

---

* 'Proc. Roy. Soc.,' A, vol. 133, p. 506 (1931).

† 'Trans. Faraday Soc.,' vol. 28, p. 333 (1932).

In carrying out a series of runs, the first two were made with hydrogen, the third with deuterium, and finally a check run with hydrogen. This was repeated at a number of different temperatures. Two typical runs are given in detail in Table II; the first at 96° showing that, throughout, the amount of deuterium adsorbed is almost exactly equal to that of the hydrogen, and the second at 170° where the rate of sorption of the heavier isotope is somewhat smaller; two hydrogen runs are given to demonstrate the reproducibility of the rate measurements.

TABLE II

Temp. 96°.	Initial press. 6·83 mm.		Temp. 170°.	Initial press. 7·05 mm.		
t min	Vol. sorbed cc at N.T.P. per 100 gm Cu (total)		*t* min	Vol. sorbed in cc at N.T.P. per 100 gm Cu (total)		
	H	D		H	D	H
0·083	0·28	0·17	0·083	0·44	0·30	0·42
0·16	0·35	0·26	0·16	0·60	0·45	0·56
0·25	0·37	0·31	0·25	0·69	0·55	0·66
0·50	0·45	0·39	0·33	0·72	0·61	0·72
1·0	0·53	0·50	0·42	0·78	0·67	0·74
2·00	0·64	0·61	0·50	0·81	0·70	0·79
3·0	0·73	0·73	0·75	0·84	0·79	0·82
4·0	0·79	0·76	1·00	0·85	0·84	0·85
6·0	0·88	0·86	2·0	0·92	0·93	0·93
10·0	1·02	1·00	6·00	0·97	1·03	0·97
20·0	1·23	1·22				
30·0	1·30	1·32				

The D content of the heavy hydrogen was 70·0%

Some typical results obtained are plotted in fig. 3, the total volume sorbed being plotted against the square root of the time. The following conclusions may be drawn from the curves in fig. 3. (1) The initial portion of the curves is straight, as found by Ward; (2) the extrapolation to zero time yields finite intercepts on the ordinates; (3) the volume sorbed quickly is identical for both isotopes; (4) the volume of hydrogen dissolved is, if any, a little greater than that of deuterium; (5) at low temperatures the rate of sorption of both isotopes is practically the same, but as the temperature, and therefore the velocity, of sorption increases the hydrogen enters the copper more quickly than deuterium, the relative velocities for the 70% D mixture are:

Temperature ° C	72	96	139	153	170
Relative velocities	1·00	1·04	1·24	1·32	1·25

The energy of activation for the sorption of H_2 from these data is 9·7 kg cal H_2.

Even at 96° there is, at the commencement of the run, a tendency for the lighter isotope to be adsorbed more quickly. That the sample of copper must have been in a similar state to that of Ward is also shown by a comparison of the absolute rates of sorption. Interpolating from these results at 72° and 96°, it is found that at 85° the initial slope of the curve is 0·240 for an initial pressure of 6·8 mm. From fig. 2* at 4 mm the slope is 0·180 and at 20 mm 0·300, the value obtained in the present investigation lying between these extremes.

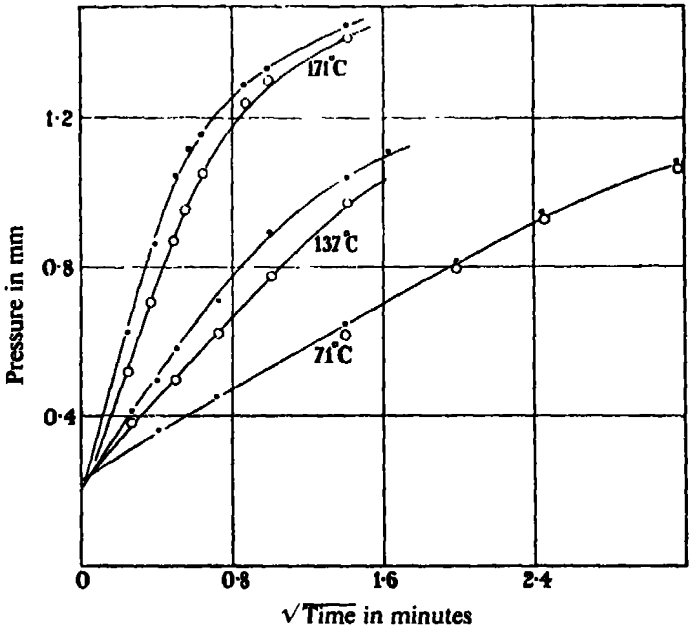

FIG. 3—Sorption on copper. • H_2, O 70% D mixture. Initial pressure 7·0 mm. 1 mm decrease in pressure is equivalent to 0·65 cc of gas at N.T.P. per 100 gm Cu.

To complete the evidence from this specimen of copper the rates of desorption were also measured. The procedure was as follows. After the sorption had been completed, the tube was pumped out for 1 minute, then the tap leading to the pump shut and one leading to a McLeod gauge opened, the gas issuing from the copper being collected in the McLeod system of known volume for 1 minute. The whole system was then connected to the pump. At intervals the rate of degassing was determined in this manner, while between these determinations the pressure of hydrogen was less than 10^{-4} mm. Four runs at 170° are given in fig. 4 corresponding to the sorption runs in Table II, but no significant difference appears in the rate of desorption. In the curve nearer the origin the pressure scale is 10 times smaller and the dotted rectangle shows approximately the volume of gas dissolved. The area under the rate of desorption time curve is nearly equal to that of the rectangle, which means that all the gas sorbed may be recovered.

---

* 'Proc. Roy. Soc.,' A, vol. 133, p. 526 (1931).

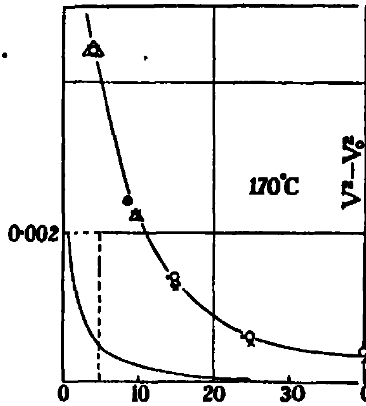

FIG. 4—Desorption from copper at 170°. Order of runs •, ○, ×, Δ. 0·001 mm per min is equivalent to $4 \cdot 3 \times 10^{-4}$ cc. Area of dotted rectangle represents 5×10^{-3} cc. • H; ○ H; × D; Δ H.

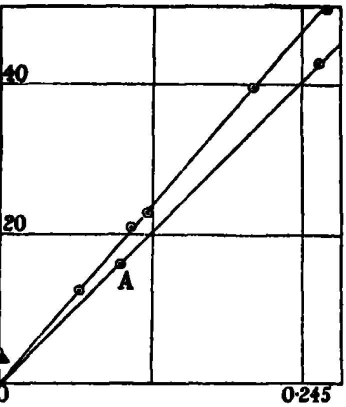

FIG. 5—Pirani calibration curves for H_2 and for 70% D mixture. Voltage scale arbitrary. The upper curve is for H_2 and the lower for 70% D. A is the point obtained after the deuterium had been in contact with the copper.

This equality in the rate of sorption and of desorption (except the higher temperatures) is a most unexpected phenomenon. Equality in sorption rates for H_2 and D_2 on nickel and chromium oxide has also been observed by Pace and Taylor*; Klar,† however, finds that with metal below 100° C, H_2 is sorbed more quickly, but above 200°, on the other hand, D_2 is sorbed faster than H_2. This is a reaction of hydrogen and a metal involving quite a large energy of activation, yet, unlike all hitherto investigated reactions of deuterium, it fails to exhibit the expected difference in velocity for the reaction of the two isotopes. Furthermore, it would appear that a $\sqrt{2}$ factor is also absent. One explanation of the discrepancy might be that the copper, even although baked at the highest temperature compatible with the prevention of sintering, is not properly freed from hydrogen and does indeed contain very much more hydrogen than is actually sorbed. On first admitting deuterium an immediate exchange reaction occurs with hydrogen in the copper, after which the normal activated sorption takes place, the velocity naturally being identical with that for hydrogen. Fortunately all the deuterium which had been in contact with the copper had been pumped off and stored in a bulb and therefore an analysis was carried out in the following way. Hydrogen was first admitted to a small McLeod gauge, its pressure measured; the gas in the closed capillary was then transferred to a small Pirani gauge and the voltage required to balance the Pirani resistance bridge determined, fig. 1, *b*.

---

* 'J. Chem. Phys.,' vol. 578 (1934).

† 'Naturwiss.,' vol. 49, p. 822 (1934).

Similar measurements were made with the deuterium prepared for these experiments and with the gas after having been in contact with the copper. The results are given in fig. 5 where the quantity ($V^2 - V_0^2$) is plotted against pressure (V and V_0 are respectively the voltage required to balance the bridge in presence of gas at a pressure p and *in vacuo*). Owing to the smaller molecular velocity, the line for the deuterium lies below that for hydrogen. On measuring a sample of gas which had been in contact with the copper, the point obtained lies on the D line and therefore the deuterium content of the gas had not been altered by more than 10%; certainly there had been no complete exchange in the interval required for making adsorption runs.

These experiments indicate that this slow process which proceeds with an apparent energy of activation is in reality a composite reaction. Whilst the oxide reduction experiments suggest that the activated migration and diffusion of the atoms or the hydrides does indeed take place and with a ratio of velocities only slightly less than is indicated from the difference in the zero point energies of CuH and CuD, the sorption experiments suggest that at low temperatures this diffusion process does not govern the reaction velocity for the rates of sorption and desorption of the two isotopes is identical. When the temperature is raised, however, the influence of the rate of the activated diffusion process on the velocity becomes more marked and is predominant with this specimen of copper at 150° C. It was therefore necessary to devise some method of actually measuring the velocity of diffusion of hydrogen through copper and to examine the nature of the other reaction which not only controls the speed at low temperatures but is unique in that the rate is uninfluenced either by the mobility or zero point energy differences of the hydrogen isotopes.

SUMMARY

The following heterogeneous reactions of hydrogen and deuterium have been investigated with these results:

Copper oxide is reduced by atomic hydrogen and deuterium at 20° C at the same velocity. This is in agreement with previous experiments showing that free atoms of H and of D react at identical velocities.

Copper oxide is more rapidly reduced by molecular hydrogen than by molecular deuterium at 156–269° C. The difference in energy of activation is 0·4 kg cal. This is also in agreement with the observation that hydrogen reduces simple molecules on a metal (nickel) surface more quickly than deuterium.

H_2 and D_2 are sorbed by and desorbed from copper at the same velocity at temperatures from 71° to 200° C, except that at higher temperatures H_2 is sorbed slightly more quickly.

The Sorption of Hydrogen and Deuterium by Copper and Palladium II—The Sorption by Palladium and Diffusion through Copper

By H. W. MELVILLE and E. K. RIDEAL, F.R.S.

(*Received July* 5, 1935)

In Part I it was shown that the process of activated diffusion of hydrogen into copper was composite including a true activated diffusion; the energy of activation for the hydrogen and deuterium migration differing from one another to an extent which was slightly less than the zero point energy differences of the compounds CuH and CuD. In addition another reaction independent of the nature of the two gases was found to be present and which governed the reaction velocity at low temperatures. In order to discover whether this second reaction was localized at the gas solid interface or not, methods had to be devised for observing the diffusion of hydrogen through thin copper films. Copper films formed by electroplating on stainless steel and stripping off by razor blades proved too fragile to use without support, and finally deposition on palladium as support was adopted. This necessitated a series of investigations on the behaviour of palladium in respect to its permeability for the two isotopes and an examination as to how far a palladium copper interface differed from a gas copper interface in respect to diffusion.

SOLUTION AND DIFFUSION IN PALLADIUM

The palladium was employed in two forms, a thin palladium tube and a palladium disc of approximately the same area and thickness as the tube.

The disc was welded to a platinum ring which in turn was fused into a glass tube. The disc was therefore subjected to a much higher temperature, certainly above 400° C at which the rate of recrystallization is rapid,* than the tube which was gold soldered to a platinum tube sealed to glass. The arrangement of taps is shown in fig. 1.

With this arrangement the volume of gas on both sides of the palladium could be measured during a run in which a pressure ratio of about 10 : 1 was maintained, the ratio of volumes being about 1 : 10; separate experiments showing that, provided the pressure on the low pressure side did not exceed 1/10 of that on the other, the rate of diffusion was not affected. By admission of gas from both sides simultaneously the rate of solution and also the volume dissolved at equilibrium could be estimated. Similarly by sudden expansion the rate of desorption could be measured either by the Bourdon or the McLeod gauge. Calibration of the apparatus was carried out with pure nitrogen.

---

* Smith and Derge, 'J. Amer. Chem. Soc.,' vol. 56, p. 2518 (1934).

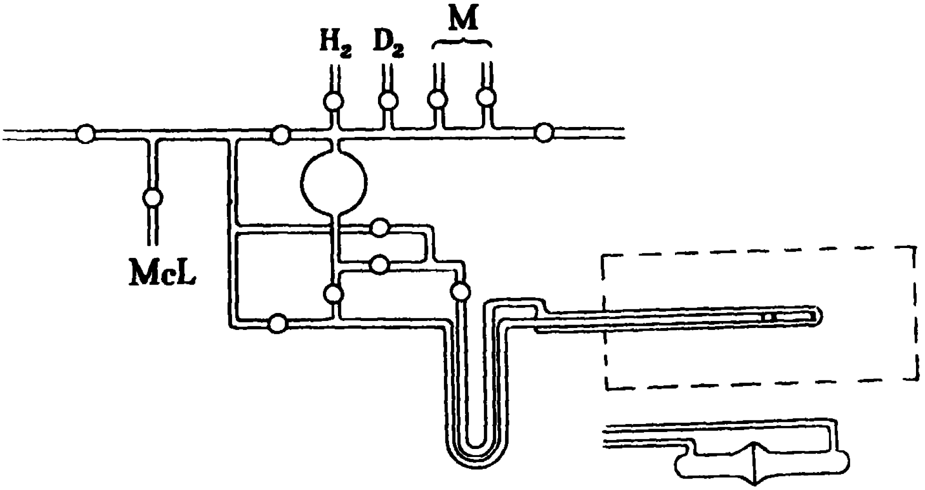

FIG. 1—M = Manometer; McL = McLeod gauge.

In Table I are given data on the equilibria attained for solution.

TABLE I

Volume of Pd $1 \cdot 51 \times 10^{-2}$ cc. Temperature 363° C. Volume of system 37 cc.

Initial pressure mm Hg (H_2)	Final pressure mm	Δp	$\frac{\Delta p}{p^{\frac{1}{2}}} = k^{\frac{1}{2}}$
9·74	8·44	1·30	0·45
3·63	2·88	0·79	0·47
2·44	1·82	0·62	0·46

The variation of k with the temperature gives the heat evolved on solution by means of the equation $\frac{d \log k}{dT} = \frac{\Delta H}{RT_2}$.

The data are given in Table II.

The heat of solution is calculated to be $\Delta H = 2 \cdot 50$ kg cals/mol.

Finally in Table III are given the data for the solubility of hydrogen and of deuterium made at different stages of the work. The gases were admitted at both sides and also at one side, diffusion through being prevented by a thick copper plating on the outside of the tube.

If the difference between the integration constants in the equation $\frac{d \log k}{dT} = \frac{\Delta H}{RT_2}$ be neglected (the differences in the chemical constants and the specific heats at these temperatures being small, *cf.* A. Farkas, "Light and Heavy Hydrogen," p. 168) the value of K_H/D_H for 100% deuterium can be calculated. The mean value is 0·78 kg cal/mol. Since ΔH_H is 2·50 kg cal per mol, ΔH_D is 1·72 kg cal per mol. If the energy of dissociation of H_2 be taken as 101·9 kg cal, that for D_2 as 1·8 kg cal higher, viz., 103·7 kg cal, the energy required to remove one atom of hydrogen from inside the palladium is 52·2 kg cal and for deuterium 52·7 kg cal. The difference—0·50 kg cal—is the zero point energy difference between H and D in the palladium. No calculations have been made for the PdH link but for PtH and PtD, this difference is 0·50 kg cal.*

TABLE II

Temperature ° C	Initial pressure	Final pressure
363	3·63	2·84
301	3·59	2·74
258	3·63	2·62

TABLE III

Gas	Temperature ° C	P initial mm	P final mm	$\frac{K_H}{K_D}$ *	$\Delta H_{H_2} - \Delta H_{D_2}$, kg cal
H	229	2·30	1·90	1·86	0·79
D	229	2·30	2·00		
H	247	3·06	2·27	1·74	0·76*
D	247	3·06	2·44		
H	278	2·85	2·30	1·38	0·65
D	278	2·87	2·42		
H	320	3·50	2·85	1·78	0·75
D	320	3·50	3·00		
H	363	3·55	2·81	1·71	0·87
D	363	3·55	2·97		

* For 70% deuterium.

---

* Sherman and Eyring, 'J. Chem. Phys.,' vol. 1, p. 347 (1933).

The relative velocities of diffusion of the two isotopes through palladium were next measured between the temperatures of 150° C and 300° C, using the disc for the lower temperature and the tube above 200° C. Two experiments are depicted in fig. 2 where the volume and pressure of the gases on both sides of the tube or disc are given as a function of the time (curves 2 and 3), whilst curve 1 is the sum of 2 and 3 and consequently indicates the volume of gas dissolved in the palladium. The velocity of diffusion increases about 10-fold for a rise in temperature of 93° C, but the volume of gas dissolved does not change much and a stationary state is established not long after diffusion has begun. Denoting by $t_{0\cdot25}$, $t_{0\cdot5}$, and $t_{0\cdot75}$ for the times for 0·25, 0·5, and 0·75 of the hydrogen to diffuse through the data given in Table IV.

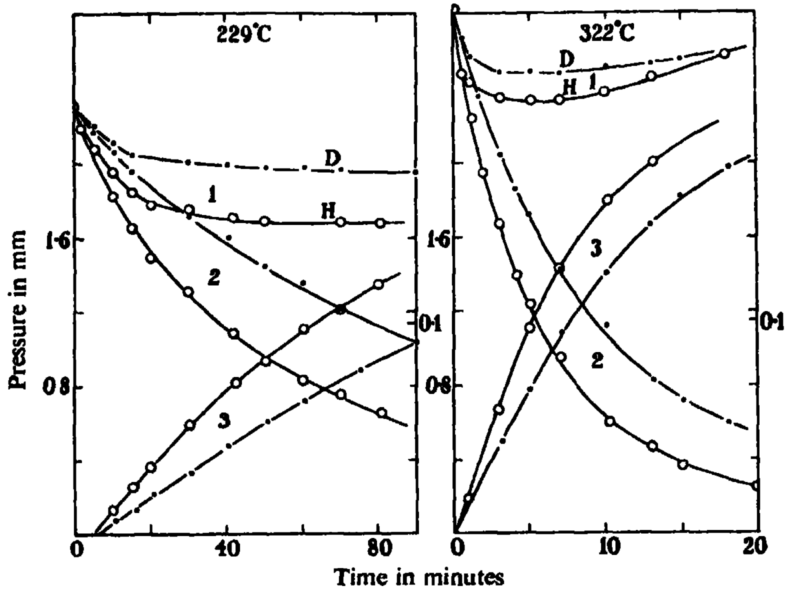

FIG. 2—Diffusion through palladium—gas measured on both sides. Curve 2 shows the pressure on the high pressure side. Curve 3 shows the pressure on the low pressure side, calculated for a volume equal to that on the high pressure side. The actual low pressures are indicated on the left side of the diagrams. ● deuterium; ○ hydrogen.

Except for the last run at high temperatures where the short period of measurement precluded accurate evaluation we obtain as energy of activation for diffusion a value of $E = 17\cdot8$ kg cal/mol and $E_{D_2} - E_{H_2} = 0\cdot75$ kg cal/mol.*

---

* *Cf.* A. and L. Farkas, 'Proc. Roy. Soc.,' A, vol. 144, p. 477 (1934), when $E = 16\cdot5$ kg cal and $E_{D_2} - E_{H_2} = 0\cdot83$ kg cal/mol.

The energy of activation for diffusion is unexpectedly high for the tube, the disc proved to be much more porous than the tube, although on standing, even when sealed up *in vacuo* and maintained at room temperature, it steadily became less porous. The decrease in porosity was not due to poisoning of the surface, for great care was taken to keep the liquid air trap at −183° C throughout the experiments; the activity could in part be restored by long heating in air or oxygen and then passing hydrogen through it. Similar diffusion experiments were carried out on the disc at low temperatures, the results of which are given in Table V.

TABLE IV

Area of palladium tube 1·51 cm^2, thickness 0·1 mm volume of system 41 cc.

Temperature °C	Gas	Initial pressure mm	$t_{0\cdot25}$ min	$t_{0\cdot5}$ min	$t_{0\cdot75}$ min	Ratio H/D	$E_{D_2} - E_{H_2}$ kg cal
228	H	2·30	16·7	42·2	—	1·80	0·76
228	D	2·31	30·0	79·0	—		
281	H	2·85	2·55	8·0	18·4	1·58	0·68
281	D	2·87	4·40	12·7	29·0		
322	H	2·81	1·40	4·0	8·95	1·73	0·86
322	D	2·85	2·52	6·6	15·1		
363	H	2·87	0·65	1·76	3·95	1·26	0·4
362	D	2·92	0·80	2·30	4·95		

TABLE V

Area of Pd disc 0·78 cm^2, thickness 0·075 mm. Volume of system 44·1 cc.

Temperature °C	Initial pressure mm	$t_{0\cdot5}H$	$t_{0\cdot5}D$	$\frac{t_{0\cdot5}D}{t_{0\cdot5}H}$	$E_{D_2} - E_{H_2}$
106	3·03	6·2	—	—	—
154	3·03	3·30	8·0	2·42	1·04
167	3·03	2·31	4·41	1·90	0·90
189	3·05	2·15	3·75	1·75	0·83

The energy of activation for the palladium disc is found to be 5·0 kg cal/mol.* It seems clear that the energy of activation for diffusion through the palladium varies with the crystalline state of the palladium.

---

* *Cf.* Smithells and Ransley, 'Proc. Roy. Soc.,' A, vol. 150, p. 182 (1935), compared with a value of about 4·14 kg cal from the data of Lombart and Eichner, 'Bull. Soc. Chim.,' vol. 53, p. 1176 (1933).

In a general way the rate of diffusion through metals may be represented by

$$R = k\sqrt{T}\,e^{-\frac{E}{RT}}$$

that is a non-temperature dependent factor k which may include a function of the available area and other characteristics of the metal and an exponential involving an energy of activation. It will be shown that k is actually a composite quantity. It is of interest to compare the value of k for the tube and disc in order to see whether the exponential factor alone is responsible for the difference in the rates.

For the tube we find with E = 17·8 kg cals and hydrogen at 2·30 mm in a volume of 41 cc at 229° C a half life of 44·2 minutes. With a disc at an initial pressure of 3·03 mm and a volume of 44·1 cc the calculated half life at 229° C is 1·26 minutes. Since the geometrical areas and thicknesses of the tube and disc are approximately equal we obtain

$$\frac{k\text{ tube}}{k\text{ disc}} = \frac{1}{10^4}.$$

Thus the value of E does not wholly control the facility of passage of hydrogen through the metal and some intrinsic difference in the apparent porosity of the metal is indicated.

The measurement of the initial relative rates of solution was found impracticable on account of the great rapidity of the reaction, but a series of desorption runs were made, the original pressures of the two gases being adjusted so that equal amounts of the two gases were dissolved.

For this purpose the palladium tube was coated on the outside with a thick layer of copper to prevent diffusion right through. Hydrogen was admitted and the solution followed until the pressure remained stationary. The system was then connected to a large evacuated bulb so that the pressure fell instantly to 1/20 of its equilibrium value (the time allowed was 5 seconds), the bulb was then shut off and the rise in pressure followed until equilibrium was once more reached. The results for a temperature of 275° are shown in fig. 3.

It is evident that hydrogen and deuterium at this temperature initially desorb at the same speed, although at equilibrium the pressure of the deuterium is rather larger owing to the greater solubility of the hydrogen.

DIFFUSION THROUGH COPPER AND NICKEL ON PALLADIUM SUPPORTS

In adopting the procedure of employing thin films of copper or nickel on palladium several possible complications arose which had to be examined. The possibility of there being holes in the electro-deposited copper or nickel was checked by comparing the energy of activation for palladium and for copper. To show that during the experimental runs copper did not diffuse into the palladium, the copper was afterwards stripped off electrolytically and the porosity of the palladium redetermined. The fact that palladium is in contact with the copper and that hydrogen in the form of atoms in the palladium is migrating into the copper instead of molecular hydrogen from the gas may alter the facility with which hydrogen enters the copper. To eliminate this factor the palladium tube was first coated with copper, then palladium was deposited on the copper so that the copper film was surrounded on both sides with palladium. Conversely using the disc, first one side was plated and the rate of diffusion measured and then the other side was covered with the same thickness of copper, the measurements being repeated. Anticipating the results it may be said that the experiments revealed the important fact that the palladium functioned as an inert support. In fig. 4 is shown the effect of depositing a layer of copper 3·4 × 10^{-3} cm thick (*ca.* 3 × 10^{4} atoms) with a current density of 1 × 1·10 ^{2} amps/cm^{2}.

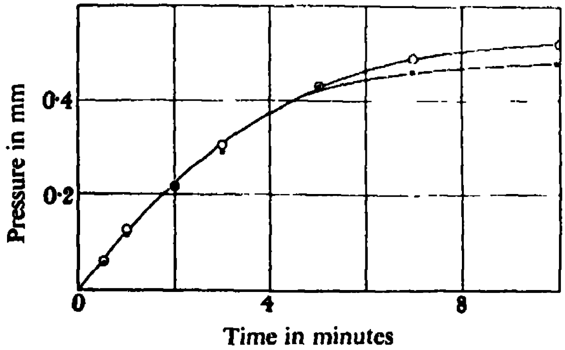

FIG. 3—Rate of desorption of hydrogen and deuterium from palladium at 275°. ○ 63% D; ● H_2.

Curve A represents the diffusion of hydrogen through uncovered palladium at 362° C, whilst B is that with copper deposited. The half life of the hydrogen has increased about 40 times. The other runs were done in the mentioned order at different temperatures to estimate the energy of activation which was found to be E = 13·7 kg cal/mol compared with 17·8 kg cal/mol for palladium. The diffusion took place from the copper to the palladium. To check these results the volume of gas emerging from the palladium was measured by a McLeod gauge, and the same value for the energy of activation obtained.

In Table VI are summarized a number of runs with hydrogen and a 70% deuterium mixture.

On removal of the copper the diffusion rate returned to its original value for the palladium; traces of water vapour were found to be without effect.

With thick films of copper about 10^{-1} mm the diffusion rate decreased with the time, at 360° C the rate falling to a constant value in 20 hours, probably due to sintering of the films. Similar observations were made with the disc and are shown in fig. 5.

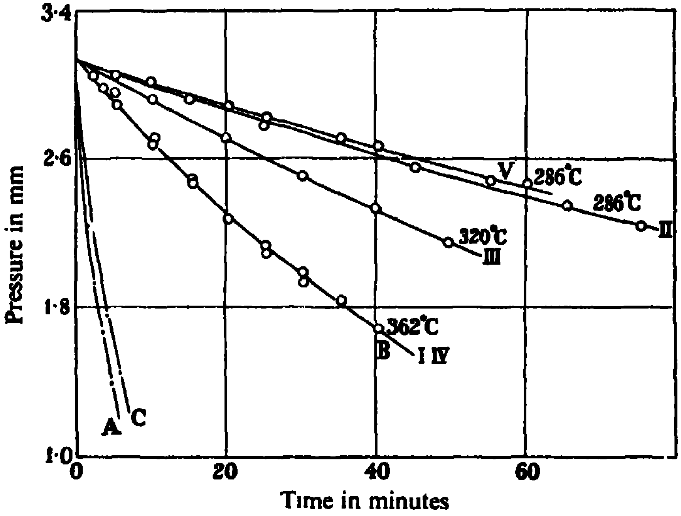

Fig. 4—Diffusion of hydrogen through copper film $3\cdot4 \times 10^{-3}$ cm thick plated on one side of the palladium tube. I and IV at 362° C; III, 320° C; II and V, 286° C.

A layer of copper $8\cdot4 \times 10^{-5}$ cm thick was deposited on one side and the diffusion rate measured, next a layer of the same thickness was placed on the other side, the rate being halved. Building up progressively thicker films reduced the rate in proportion to the thickness.

These experiments indicated that palladium does not in any way modify the characteristics of a copper film so far as diffusion is concerned. The energy of activation for diffusion of hydrogen through copper on the disc was found to be 11·4 kg cal, a little lower than 13·7 obtained for the tube. The variation of the rate of diffusion with pressure was measured for copper on palladium and on plotting log (rate) against log (pressure) a straight line having a slope of 0·7 was obtained.

TABLE VI

Temperature °C	Gas	Initial pressure mm	High pressure time for ΔP − − 1·0 mm	Low pressure time for ΔP − + 0·1 mm	Average ratio H/D	$E_{D_2} - E_{H_2}$
310	H	3·18	18·5	16·0	1·78	0·9
310	D	3·19	33	28·2		
320	H	3·14	29·7	25·7	1·53	0·69
320	D	3·13	44·8	39·5		
				(t for ΔP = 0·03 m)		
356*	H	3·35	—	60·7	1·52	0·71
	D	3·36	—	91·5		
362†	H	3·55	--	44·8	1·63	0·78
	D	3·55	—	73·0		
						(Av. 0·77)

* Thick film $17 \cdot 10^{-5}$ cm. † Composite film Pd–Cu–Pd.

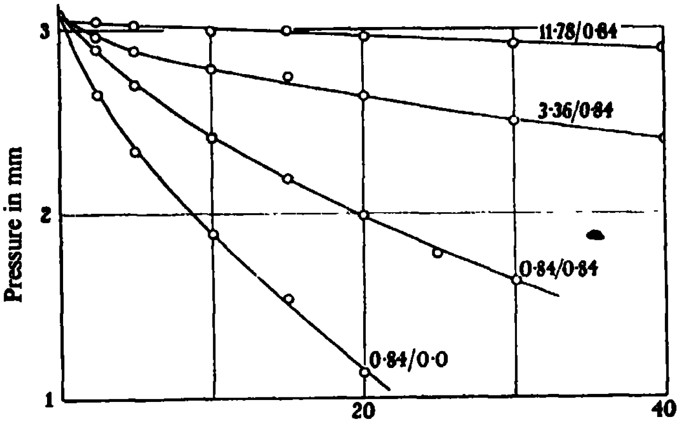

FIG. 5—Diffusion of hydrogen through palladium disc coated on one and also on both sides with copper. Thicknesses in units of 10^{-4} cm shown on the curves.

DIFFUSION THROUGH NICKEL

Analogous experiments were made with nickel films plated on the palladium tube. A typical set of data is given in Table VIII to show the temperature coefficient and the ratio of the velocities of diffusion of hydrogen and deuterium. The pressure on both sides of the tube was measured to act as a double check on the results, the direction of flow being nickel → palladium. The nickel films proved to be more stable than copper in that the diffusion rate did not decrease on prolonged baking at 360°. It will be seen that the degree of separation is similar to that obtained with copper and palladium, and what is of greater significance, equal, within the experimental error, to the difference in the energy of activation for hydrogen and deuterium in the catalytic hydrogenation of oxygen and of nitrous oxide on a nickel surface.

TABLE VII

External pressure	Rate (mm/min) into a volume of 327 cc
3·2	0·00042
12·0	0·00112
110·0	0·00423
183·0	0·00601

TABLE VIII

Thickness of Ni film $3·8 \times 10^{-4}$ cm. Area $1·5$ cm^2. Initial pressure 3·50 mm

Gas	H	D	H	H	H	H	H	D	H
t for Δp −0·8, volume 38·5 cc	16·5	23·7	17·0	9·0	40·5	33·3	56	93·5	60
t for Δp | 0·09, volume 327 cc	13·0	21·0	14·2	7·0	32·0	27·5	---	79	52
Temperature ° C	323	320	323	363	279	293	228	228	228

	kg cal
Energy of activation for H_2	14·3
Energy of activation for D_2	14·9
Difference	0·6

DISCUSSION OF THE DATA

From the foregoing experiments an attempt may be made to picture the two essential processes which govern the diffusion of hydrogen through metals. The first process involves the penetration of hydrogen just inside the metal. This reaction certainly requires activation, and, as will be shown later, this energy required is less than that for diffusion in the metal. It does not appear to involve molecular hydrogen because the rate is unaffected if the gas phase be replaced by a metal like palladium (*cf.* Table VI), *i.e.*, if atoms instead of molecules are presented to the metal. Two observations must also be borne in mind, namely, that the rate of diffusion is inversely proportional to the thickness (*cf.* fig. 5) and nearly directly proportional to the square root of the external pressure. The former implies that there is a concentration gradient set up in the body of the metal, the latter probably means that atoms are concerned in the diffusion through the metal. From the experiments of Roberts,* we may now regard a copper surface (for example) exposed to hydrogen gas as consisting of an almost but not quite complete monolayer of CuH chemi-adsorbed on the surface (A), fig. 6; above this layer there exists a molecular layer (B), held on to the surface especially strongly over these portions of the hydride surface where the gaps occur. The formation of the primary chemi-adsorbed monolayer (B) proceeds with an undetectable energy of activation and the same holds good for the formation of the molecular layer above (A).

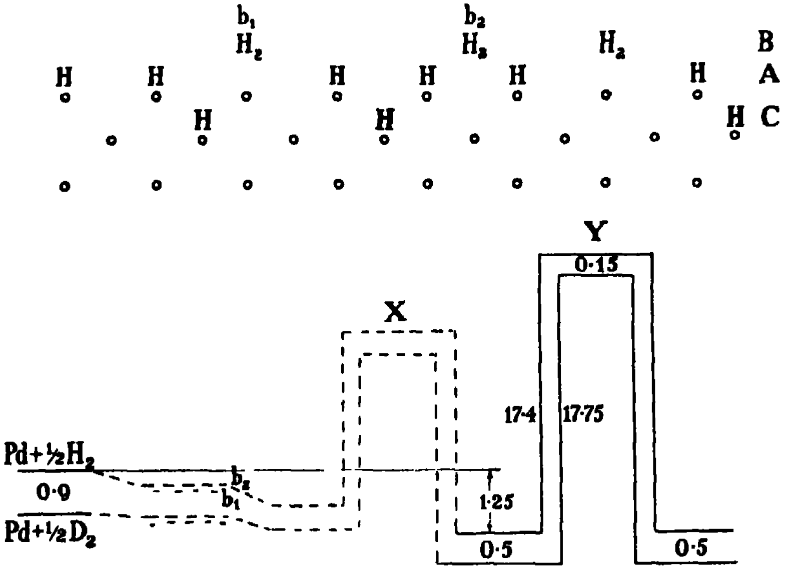

FIG. 6.

If we imagine one of the surface copper hydride molecules at the edge of a gap to undergo an exchange or " platzwechsel " with an atom in the second layer, or to undergo a rotation so that the hydrogen atom is now underneath, forming a second layer (C) this is equivalent to penetration. The probability of this process occurring is dependent directly on the concentration of H_2 molecules in layer B; moreover, the experiments on activated sorption would appear to indicate that the rate of the primary penetration is the same for hydrogen and deuterium, if we identify activated adsorption with this transition. When two gaps are formed in juxtaposition in the top layer A they are filled by the dissociation of a molecule from layer B. Diffusion into the interior now takes place from layer C. Atoms from layer C must also revert to layer A, ultimately forming molecules in layer B. In order to obtain the square root relationship between rate of diffusion and pressure the rate of transition $C \rightarrow A \rightarrow B$ must be proportional to the square root of the concentration of atoms in C. The extent of the surface layer A may also control the concentration of atoms in C, and consequently the rate of diffusion will be affected by heat treatment in so far as A is altered. For example, sintering by heating copper films to high temperatures decreases the rate (*cf.* p. 96). Palladium, however, appears to be exceptional in this respect, the disc and tube differing in porosity to an extent greater than that reasonably expected from this factor alone, and suggest that grain boundaries or intercrystalline cracks play an important part in the diffusion process.

---

* 'Nature,' vol. 135, p. 1037 (1935).

We can develop a formal equation for the rate of diffusion as follows. If [H] be the concentration in the layer C and the concentration of atoms at the low pressure side be considered negligibly small, then in the steady state the rate of diffusion is given by

$$k_3\,[\mathrm{H}]\,e^{-\frac{E_3}{RT}}.$$

In the steady state [H] is maintained by dissociation of H_2 molecules adsorbed on the top of the chemi-adsorbed CuH layer at a rate given by

$$k_1\,[\mathrm{H}_2]\,e^{-\frac{E_1}{RT}},$$

where $[H_2]$ is the surface concentration of molecular hydrogen in the layer B; a fraction of the atoms in the second layer must return to the top layer in pairs and can there recombine and re-evaporate at a rate:

$$k_2\,[\mathrm{H}]^2\,e^{-\frac{E_2}{RT}}.$$

The equilibrium concentration of [H] just inside the metal, *i.e.*, in this second layer is defined by

$$k_1\,[\mathrm{H}_2]\,e^{-\frac{E_1}{RT}} - k_2\,[\mathrm{H}]^2\,e^{-\frac{E_2}{RT}} - k_3\,[\mathrm{H}]\,e^{-\frac{E_3}{RT}} = 0.$$

If the rate of diffusion be slow compared with the rate of penetration this reduces to

$$[\mathrm{H}] = [\mathrm{H}_2]^{\frac{1}{2}}\, e^{-\left(\frac{E_1-E_2}{2RT}\right)} \left(\frac{k_1}{k_2}\right)^{\frac{1}{2}}, \tag{2}$$

and the rate of diffusion reduces to

$$-\frac{d\,[\mathrm{H}]}{dt} = k_3 \left(\frac{k_1}{k_2}\right)^{\frac{1}{2}} e^{-\left(\frac{E_1-E_2}{2RT}\right)} \cdot e^{-\frac{E_3}{RT}}\, [\mathrm{H}_2]^{\frac{1}{2}}, \tag{3}$$

i.e., the rate is proportional to the square root of the amount of gas adsorbed.

On the other hand, if we are measuring the rate under conditions when the layer penetrated is relatively bare, *i.e.*, at low pressures or high rates of diffusion, we obtain

$$[\mathrm{H}] = [\mathrm{H}_2]\, e^{-\left(\frac{E_1-E_3}{RT}\right)} \frac{k_1}{k_3},$$

and the rate of diffusion reduces to

$$-\frac{d\,[\mathrm{H}]}{dt} = k_1\, e^{-\frac{E_1}{RT}}\, [\mathrm{H}_2],$$

i.e., the rate is proportional to the amount of gas adsorbed. We may note that if P is the partial pressure of the gas then in general

$$[\mathrm{H}_2] = \frac{a\mathrm{P}}{1 + b\mathrm{P}}.$$

In equation (2) $E_1 - E_2$ is the heat evolved when one mole of H_2 dissolves in the metal, for palladium this was found to be $E_{1H_2} - E_{2H_2} = 2{\cdot}50$ kg cal, and for D_2 1·72 kg cal, the difference being 0·78 kg cal.

The true energy of activation for migration is therefore $E_{\mathrm{Diff}} - \frac{E_1 - E_2}{2}$ or $17{\cdot}8 - 0{\cdot}4 = 17{\cdot}4$ kg cal, where E_{Diff} is that measured for the total diffusion process. The difference in E_{Diff} for H_2 and D_2 is 0·75 kg cal. Of this 0·40 kg cal is due to the difference in solubilities and therefore $E_3(\mathrm{D}) - E_3(\mathrm{H})$ is only 0·35 kg cal.

The difference in the zero point energies of metal hydride and deuteride in the activated state during the migration is 0·15 kg cal compared with 0·5 in the initial and final states. This is what might be expected, for the difference in the activated state could only be zero if the atoms were removed from the metal and re-deposited. On p. 91 it was estimated that about 50 kg cal are required to remove a hydrogen atom from the metal. Since the energy required for migration is 17·4 kg cal the atom is comparatively tightly bound even in the activated state.

No direct information can be obtained as to the height of the barrier CX and AX, fig. 6, *i.e.*, the barrier controlling activated penetration of the metal, except it would appear that the inner surface equilibrium for copper, nickel, and palladium sets in more rapidly than the diffusion process and thus the height AX must be less than CY, *i.e.*, less than 17·4 kg cals for palladium.

Similar potential energy diagrams could be constructed for nickel and copper, but the solubility data at low temperatures employed for these experiments are uncertain. The observed difference in the energy of activation for H and D are thus composite. Estimates have been made of the difference in zero point energy of Ni–H and Ni–D of 0·7 kg cal and CuH and CuD 0·8 kg cal. If these are identical with the values when the hydrogen atoms are attached to a metal lattice the difference in E for migrating in Ni is 0·6 kg cal, and 0·7 kg cal in copper, the respective differences in the activated states being about 0·1. In hydrogenation reactions these two facts no doubt contribute to the determined difference in energy of activation, both favouring the reactivity of the hydrogen.

We have to thank the Commissioners for the Exhibition of 1851 for a grant to one of us (H. W M.).

SUMMARY

The diffusion of hydrogen and of deuterium through palladium, copper, and nickel has been investigated at temperatures from 150 to 350° C and at pressures from 1 to 200 mm. For each metal hydrogen diffuses more quickly, the difference in energy of activation for diffusion being 0·8 for palladium, 0·6 for nickel, and 0·8 kg cal for copper respectively. The copper and nickel were supported on palladium.

In copper, it has been shown by employing composite films Cu–Pd–Cu and Pd–Cu–Pd that the rate determining step, and therefore the step responsible for the difference in the velocity of diffusion, is not due to any process connected with the gas metal interface.

With palladium measurements of the solubility of the two isotopes were also made, hydrogen being the most soluble. Combining these results with the diffusion measurements it is shown that the difference in velocities

of diffusion is due partly to the greater solubility as well as to the greater mobility of hydrogen in palladium.

Potential barriers have been constructed from diffusion and solubility data, and it is shown that there exists a definite barrier for the penetration of hydrogen from the surface to the interior. The barrier has the same height for both hydrogen and deuterium and a mechanism for the transfer of gas is suggested.

Pro-knocks and Hydrocarbon Combustion

By A. R. UBBELOHDE, J. W. DRINKWATER, and A. EGERTON, F.R.S.

(*Received August* 6, 1935)

1—INTRODUCTION

Evidence has been collected* which shows that knock in an internal combustion engine cylinder is intimately connected with the presence of peroxidic substances of characteristic structure formed in the last part of the charge to burn. Such peroxides might be formed either in the primary oxidation of the hydrocarbon, or from aldehydes which are known to be an intermediate product. The experiments described, in the paper cited, left somewhat undecided the question whether or not peroxides arising from aldehydes formed during combustion are responsible for engine knock, although there was evidence against such a conclusion. It was also left uncertain to what extent aldehydes other than formaldehyde were present in the gases sampled from the engine cylinder. The purpose of this note is to describe some further experiments on these questions, which make it very unlikely that aldehyde peroxides are those that are mainly responsible for knock; this conclusion strengthens the evidence for the primary formation of peroxides in the oxidation of the higher hydrocarbons.

First, experiments on various fuels show that aldehydes other than formaldehyde are formed in amounts inadequate to account for the knock observed; and formaldehyde is shown not to cause knock even when its concentration is much greater than ever arises from the combustion of fuels which knock. Furthermore, there is no correlation between the amount of higher aldehydes formed by any fuel and its tendency to knock. Secondly, experiments were made to test whether fuels which do not readily knock fail to do so on account of their not forming sufficient primary peroxide of suitable structure, or because of a radically different mechanism of combustion. The results suggest that the former is the reason; for instance, amylene containing appreciable amounts of olefine peroxide (p. 112) did not knock, whereas an addition to it of small quantities of amyl nitrite had a pro-knock effect even more pronounced than its effect on a fuel such as petrol.

---

* Egerton, Smith, and Ubbelohde, 'Phil. Trans.,' A, vol. 234, p. 433 (1935)

Another matter which was left undecided as the result of the previous work (*op. cit.*) is the source of the nitrogen peroxide which is found in the gases sampled from the engine cylinder. Some of the experiments indicated that the NO_2 was formed at the surface of the hot exhaust valve; but it was also possible, and *prima facie* seemed more likely, that the NO_2 was formed in the flame. There were, in fact, three possibilities:

(*a*) That the NO_2 was formed in the flame or in the small flamelets projected from the flame, and, if so, there was the further possibility that some of the NO in the residual gas could form NO_2 during the latter part of the compression stroke;

(*b*) That the NO_2 was formed by chemical reaction associated with the chain reactions occurring in the hydrocarbon combustion; or

(*c*) That the NO_2 was formed by catalysis at the active surface of the hot exhaust valve.

The experiments here described rule out the possibility (*a*), but process (*c*), catalysis at the exhaust valve, apparently plays a prominent role. It is uncertain yet to what extent process (*b*) is important.

2—EXPERIMENTAL PROCEDURE

The single cylinder Delco engine used in these experiments has already been described, together with the valve for sampling the products of combustion at different parts of the cycle (*op. cit.*). In order to compare the products when the mixture was spark ignited with those when it was merely compressed by the piston travel, an alternative sparking mechanism was built on to the engine. This was actuated by a magneto driven at one quarter of the engine speed, so that firing only occurred after every second suction stroke. Cams on a shaft rotating at one quarter the speed of the engine alternately interposed or removed a steel block between the hammer and the tappet of the sampling valve, so that samples were recovered either exclusively from the sparked or the non-sparked mixture, according to which cam was used, fig. 1. By increasing the

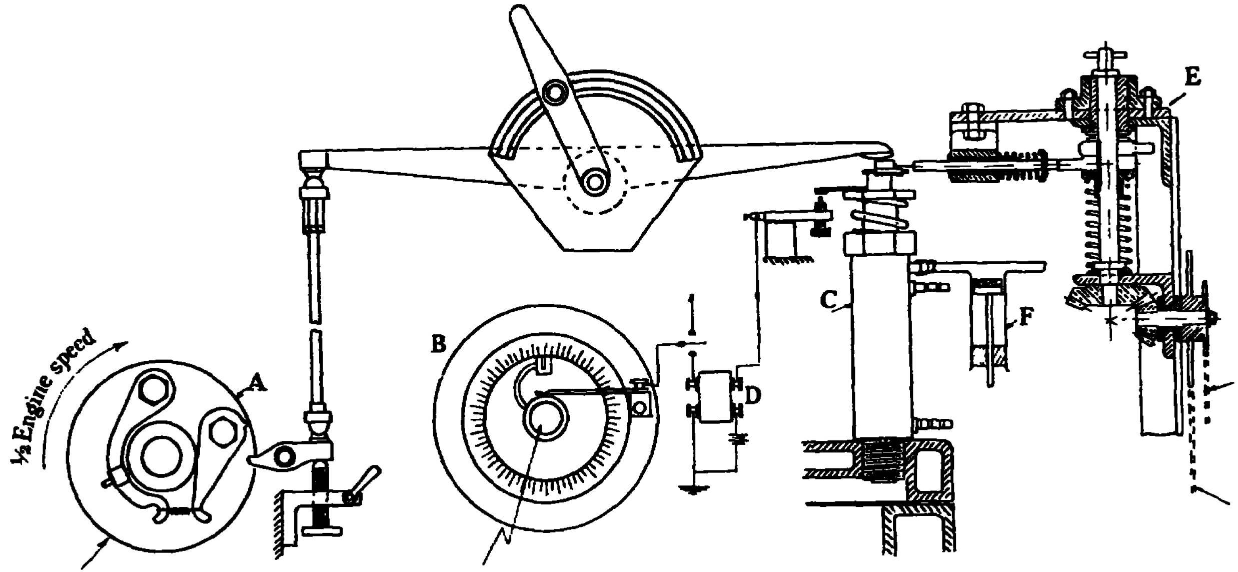

FIG. 1—General arrangement of sampling apparatus. A, trigger plate and phasing gear; B, electrical indicator; C, sampling valve; D, induction coil; E, alternate cycle mechanism; F, droplet disc and holder.

mass of the fly wheel the engine could be run at the same spark advance (−22½°) and the same speed 600 revs/min on the alternatively sparked cycle as on the normal cycle; but the power was, of course, very much less. The temperature and other conditions in the engine must obviously also be rather different.

The aldehydes in the combustion products were analysed by the "droplet" method previously described (*op. cit.*). In order to obtain definite information as to the proportion of formaldehyde and of higher aldehydes, the Schiff's reagent was modified as follows:

Reagent B—25 cc 0·04% rosaniline hydrochloride, 10 cc N/10 potassium metabisulphite, 1·75 cc 20% $KHSO_4$ 36·75 cc distilled water.

This reagent reacted with both formaldehyde and the higher aldehydes.

Reagent A—The proportions were the same as for B, except that 36·75 cc of 10% H_2SO_4 by volume were used in the place of distilled water. The time of coloration of the "droplet" to standard tint (0·002% rosaniline in 0·05% $KHSO_4$) was established for each of these reagents. Both formaldehyde and acetaldehyde vapour were used in establishing the calibration curve for the B reagent; the time of coloration was practically the same for both aldehydes. Acetaldehyde vapour has no effect on the A reagent in concentrations which arise in these experiments, and the time of coloration of the A reagent using formaldehyde was greater than for the B reagent at the same concentration. If t is the time of coloration of the A reagent, the concentration of formaldehyde would be that read from the calibration curve for the B reagent at a time $t' = 0{\cdot}52t$. Using each of these reagents in turn at the various settings, estimates of the relative amounts of formaldehyde and higher aldehydes are recorded graphically. (At concentrations between 20 and 2×10^{-4}, the results are probably within $0{\cdot}5 \times 10^{-4}$ mol fraction.)

EXPERIMENTAL RESULTS

(*a*) *Aldehydes*—Graph 1, fig. 2, records the results at various settings of the sample valve when running the engine on Shell petrol at 600 revs/min, throttle 9°. The residual gas present in the cylinder contains about 1½ parts in 10,000 of formaldehyde; this increases along with higher aldehydes up to T.D.C., after which the higher aldehydes increase very little, but the formaldehyde concentration (over 20×10^{-4}) increases rapidly till the flame reaches the valve when the concentration of aldehydes decrease. The higher aldehydes disappear altogether, but even at the end of the working stroke some formaldehyde is detectable. (The thick curve refers to total aldehydes, the thin to formaldehyde, and the dash and dot to higher aldehydes.)

Graph 2, fig. 2, gives the " total " aldehydes formed when using the alternate spark device at the same speed and spark advance. The upper curve (*a*) refers to sampling in the firing stroke, and curve (*b*) to the non-fired compression and expansion strokes. Aldehydes are formed during the non-firing strokes, but not nearly to the same extent as when the flame is present; this shows that the flame enhances precombustion of the charge. Owing to the small concentration, the percentage of formaldehyde in the aldehydes formed in the non-firing stroke was not ascer-

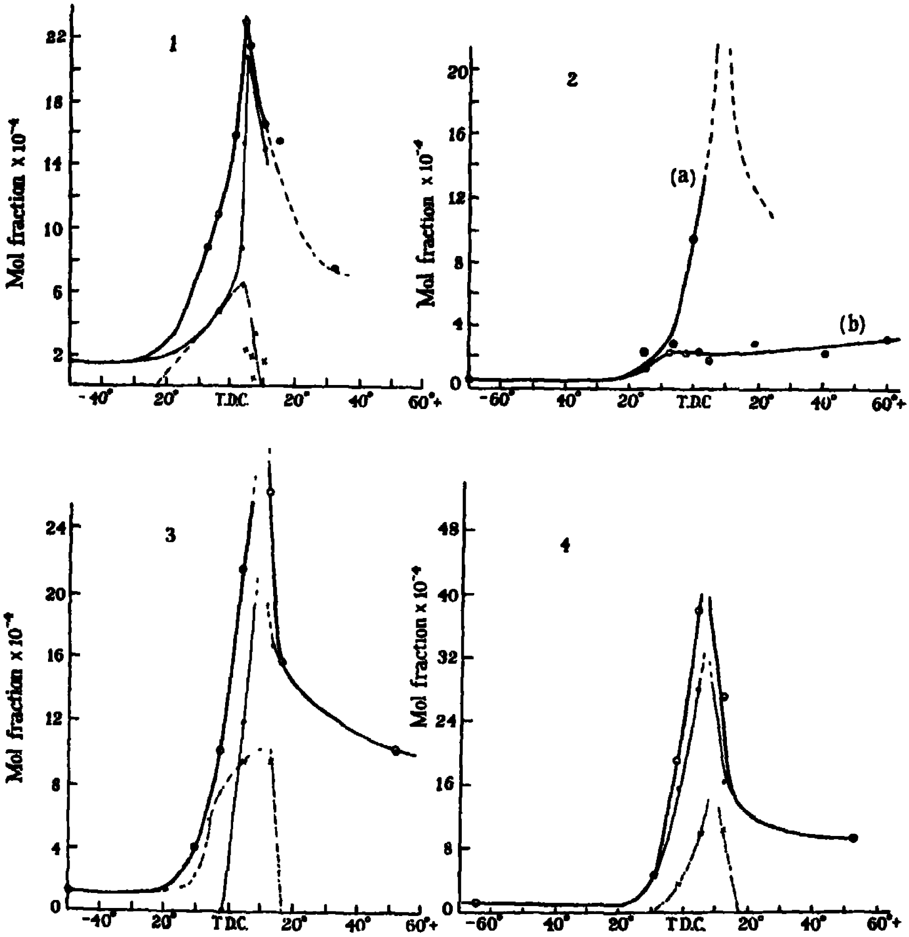

FIG. 2—1 and 2, petrol; 3, cyclohexane; and 4, hexane.

tained; but it is probable from the other results that higher aldehydes were also present. The pressures against which the valve had to operate after T.D.C. in the firing stroke were too high for satisfactory sampling, but the curve would be similar to that shown in graph 1.

Graphs 3 and 4, fig. 2, give the results obtained when the engine is using cyclohexane and hexane respectively. The largest part of the increase in aldehyde content of the gases before the flame reaches the valve is due to the production of formaldehyde. The higher aldehydes decrease very rapidly as the flame approaches the valve.

Graph 5, fig. 3, refers to an experiment under similar engine conditions when 6% freshly distilled acetaldehyde was added to petrol and used as a fuel. The mixture knocked to about the same extent as when petrol was used alone at the same load. The arrow indicates the estimated concentration of acetaldehyde obtained from the known percentage in the liquid fuel. The total higher aldehydes (inclusive of the acetaldehyde added) at first increase (from −20° to −3° before T.D.C.) and then they rapidly disappear; formaldehyde, however, increases from −20° to the moment when flame reaches the valve (about 10°), after which the quantity decreases. Similar results were obtained with 7% *iso*-valeric aldehyde petrol mixture, only the valeraldehyde disappeared even more rapidly after −20°.

Graphs 6 and 9, fig. 3, show somewhat similar results to those obtained with hexane using the non-knocking fuels, amylene and acetone respectively. (This amylene contained approximately 10^{-3} mols of amylene peroxide per litre.)

Graphs 7 and 8, fig. 3, show results obtained with butyl and ethyl alcohols. Probably owing to the slower flame travel and cooler flame, the higher aldehydes do not decrease till later in the stroke and no formaldehyde is formed till after T.D.C.; in fact, a minimum appears in the formaldehyde curve in the neighbourhood of T.D.C. Another feature of these experiments with alcohols was that no peak appeared in the formaldehyde curve, the concentration increasing to a value a little greater than that obtained after passage of the flame in the experiments when hexane was used.

Graph 10, fig. 3, benzene (pure A.R.) gave only a small quantity of total aldehydes (maximum 7×10^{-4} at +10°); owing to the small concentration, the higher aldehyde content was not measured.

Iso-octane gives rise to very little formaldehyde, mainly higher aldehydes are formed, the maximum concentration observed was about 17×10^{-4} at +10°; apparently very little formaldehyde is formed in this case even in the expansion stroke.

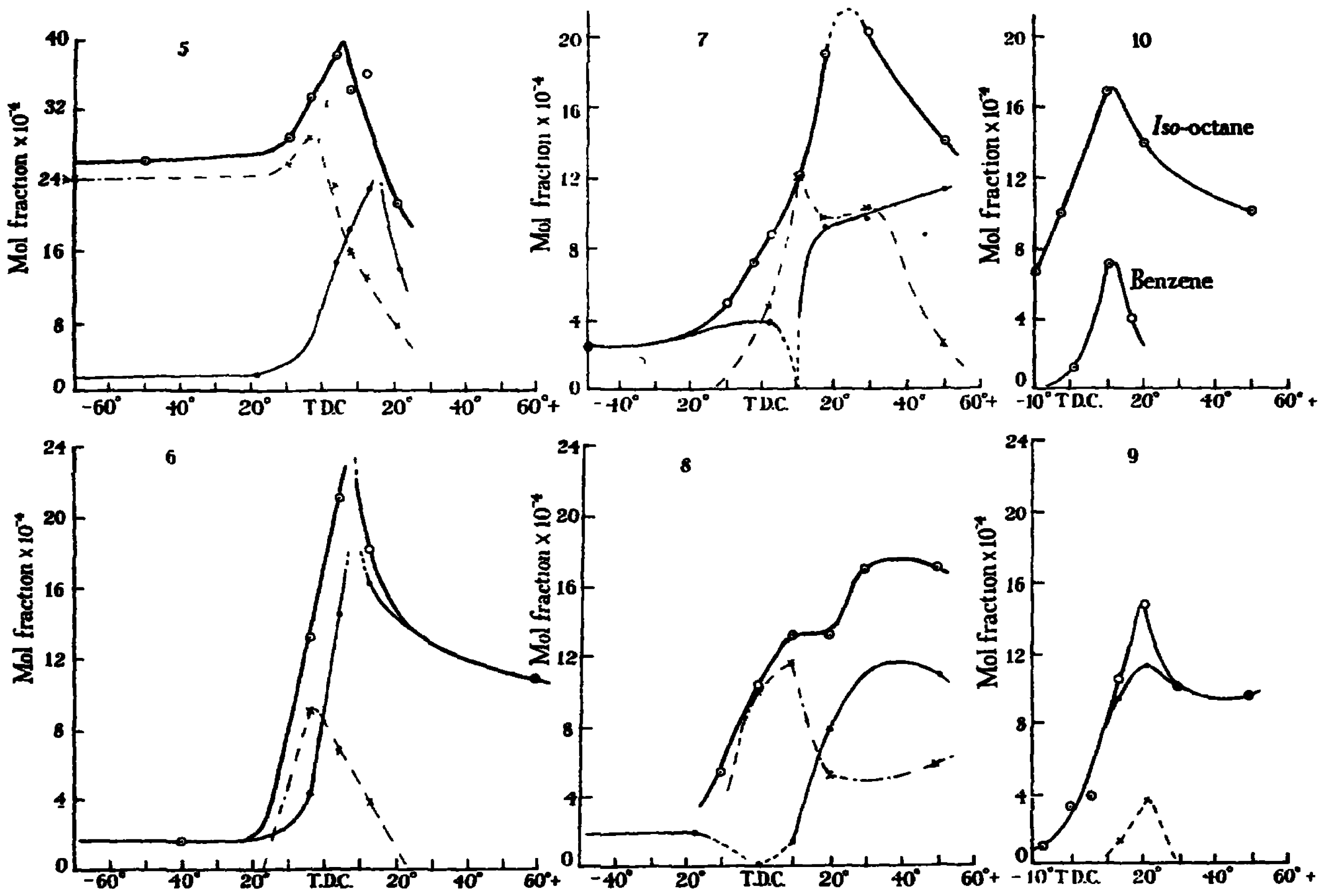

FIG. 3—5, acetaldehyde and petrol; 6, amylene; 7, butyl alcohol; 8, ethyl alcohol; 9, acetone.

The engine conditions in these experiments: spark —22½, speed 600 revs are given in Table I.

TABLE I

Fuel	Throttle opening °	Power in watts	Fuel consumption cc/min	Notes
Petrol	9	368	10·7	C.M.D.
Petrol	9	—	—	V.D.
Cyclohexane (b.p. 79–80·5°)	9	415	7·07	Just not knocking
Hexane (b.p. 66·5–68·5°)	8	478	7·95	C.M.D.
Petrol + 6% acetaldehyde (b.p. 121°)	9	368	—	„
Amylene (b.p. 34·5–36·5°)	10	427	10·45	No knock
Acetone* (b.p. 56°)	9	414	10·48	„
n Butyl alcohol* (b.p. 116·5–117·5°)	10	480	9·03	„
Ethyl alcohol* (97·6°)	10	460	10·5	„
Benzene (A.R.)	10	430	7·4	„
Iso-octane	9	400	7·7	„

* Smaller throat for carburettor choke tube.

The mixture strengths for all the fuels, except petrol, were weak.

Before discussing the above results, another experiment must be mentioned. When attempts are made to run the engine using pure acetaldehyde vapour as fuel, knock is too violent for stable running; however, no appreciable increase of knock is observed until the concentration of acetaldehyde exceeds 10% of the total fuel. But an increase of knock is observable with only 0·05% acetyl peroxide added to the fuel, so that clearly less than 0·05% of acetyl peroxide is formed in the time available in any one stroke, unless the acetaldehyde concentration exceeds at least 10%, or the mol fraction of acetaldehyde in the cylinder is greater than about 40×10^{-4}. (With higher aldehydes still greater concentrations would be necessary.)

Formaldehyde peroxidizes even less readily than acetaldehyde, and it should therefore be possible to run the engine on still higher concentrations of formaldehyde vapour. Liquid formaldehyde was prepared by the method of Spence and Wild.* The vapour was gradually introduced into a mixing chamber attached to the induction pipe with the engine running on a butane-air mixture. As the flow of formaldehyde increased, the butane supply was cut off, till finally the engine was running on pure formaldehyde vapour at about 300 revs/minute. Under these conditions, even increasing the load produced no knock, either when running on pure formaldehyde or on mixtures with butane. (A single loud knock was once heard when some of the liquid formaldehyde was allowed to splash into the cylinder.) These amounts of formaldehyde exceed those isolated from the various fuels, during their combustion in the engine cylinder, by some 400 times, while the amounts of "higher aldehydes," which can be added without causing a perceptible increase of knock, exceed the maximum amounts isolated (10×10^{-4}) some four times. It can be concluded, therefore, that any aldehydes which are formed in the engine cylinder do not form sufficient aldehyde peroxides during the short time available before the flame arrives for the knock to be due to their influence. Graph 5, fig. 3, shows that added aldehydes are undergoing combustion before the flame reaches the sampling valve, so that it cannot be held that these aldehydes are not undergoing the combustion that would occur if they were formed from the hydrocarbon in the course of its combustion. Furthermore, the experiments on cyclohexane, amylene, *iso*-octane, and even alcohols show that amounts of higher aldehydes are formed in the precombustion of fuels which are much the same whether or not the fuel gives rise to knock; in fact, for different fuels there is no correlation between the amount of higher aldehydes and the tendency to knock. It follows that if knock is connected with the formation of peroxides (Egerton and others, *op. cit.*) some source other than the aldehydes must be responsible, and it has been held that they result from the earliest stages of oxidation of the hydrocarbon. In this connexion some further experiments may be mentioned.

---

* ‘J. Chem. Soc.,’ p. 335 (1935).

It has been suggested that the pro-knock hydroperoxides, etc., can disrupt in such a manner that the reaction which gives rise to them may develop a branching character.* There is evidence† that an activated molecule of H_2O_2 breaks down into two OH radicals, while alkyl peroxides almost certainly disrupt to give OR groups (or OR and OH groups) and alkyl nitrites have been shown by Steacie‡ to provide OR radicals. Each radical so formed could operate a reaction chain, branching would thus be facilitated. A simple nitrocompound, like nitrobenzene, does not dissociate into such radicals, and it is also unlikely that the molecule of an olefine peroxide should split in such a way as to give rise to them, and these substances do not act as potent pro-knocks.

---

* Ubbelohde and Egerton, ' Nature,' vol. 135, p. 67 (1935).

† Hinshelwood, Williamson, and Wolfenden, ' Proc. Roy. Soc.,' A, vol. 147, p. 48 (1934).

‡ ' Proc. Roy. Soc.,' A, vol. 146, p. 388 (1934).

Even though the normal combustion of different fuels may involve the same chain carriers (alkyl peroxide, and acyl radicals), the phenomena of knock depend on the temporary production of *sufficient* of the peroxides for establishment of this characteristic mode of chain branching. Although certain fuels such as amylene or benzene may give rise to practically no such peroxide, yet added pro-knocks which disrupt on the approach of flame will lead to greatly enhanced combustion if the same free radicals which they produce can initiate sufficiently long chains. The effect of added pro-knocks therefore indicates whether or not similar combustion chains can be initiated in various hydrocarbons and substitution products such as alcohols, aldehydes, and ketones.

Owing to the small amount of the pure fuels available, the experiments were carried out by spraying into the induction pipe the fuels containing the pro-knock; the effect on knock is shown in Table II.

TABLE II

Fuel	Throttle °	Spray % in fuel	Approximate mol fraction	Result
Petrol	6	14% amyl nitrite	2×10^{-4}	Loud knock.
Hexane	6	,,	2×10^{-4}	,,
Amylene	6	,,	2×10^{-4}	Louder knock.
Cyclohexane	9	,,	2×10^{-4}	Sharp knock.
Benzene	10	,,	2×10^{-4}	Definite but not so loud.
Ethyl alcohol	10	,,	2×10^{-4}	Practically nil.
Butyl alcohol	10	,,	2×10^{-4}	Loud knock.
Acetone	11	,,	2×10^{-4}	No knock, speed drops.

The only fuels in Table II which knock under normal circumstances are petrol and hexane (though cyclohexane would knock in this engine at throttle 12°). On the other hand, the only fuels not susceptible to the added pro-knock are ethyl alcohol and acetone. Even ethyl alcohol with throttle open 24° and 40% amyl nitrite spray (6×10^{-4}) gives a heavy knock. With such substances containing only a few C atoms, even when a chain is initiated, the length before stabilized products are formed is likely to be short, so that larger amounts of pro-knock substances are needed. The inference from the experiments is that similar chains can be initiated in a wide variety of fuels by similar means.

It has already been pointed out* that although the phenomena of knock and of ignition have many characteristics in common, that the time-factor is very different in the two cases. Aldehydes, alcohols, and even water lower the ignition temperature of hydrocarbons, but their effect may take a number of seconds to develop, whereas the time available in the engine cylinder to occasion knock is only of the order of about a thousandth of a second. Aldehydes are able to initiate combustion chains in pure hydrocarbons probably through the intervention of radicals RCO and $RCOO_2$ formed during their own oxidation; the phenomena of knock, on the other hand, seems more closely associated with chain branching owing to the disruption of peroxides RO—OH, etc., which are only formed as a by-product during the combustion of aldehydes under suitable conditions; high concentration of the aldehyde favours their production. A scheme according to which these peroxides may be formed has been presented by one of the authors.*

---

* Egerton and others, 'Phil. Trans.,' A, vol. 234, p. 433 (1935).

(*b*) *Nitrogen Peroxide*—Some further experiments have been made on the other question left undecided by the previous work, viz., the source of the nitrogen peroxide found in the gases sampled from the cylinder.

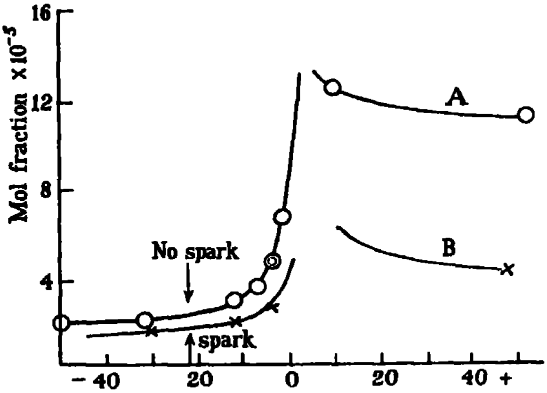

Fig. 4.

(1) Hexane (b.p. 67–69°) was used as a fuel (throttle open 8°, continuous and fairly heavy knock), and the NO_2 in the gases sampled from the cylinder was determined by the Greiss reagent in a "droplet." The engine was fired every alternate cycle and the valve was operated first in the non-firing stroke with the results shown in curve A, fig. 4, and then in the firing stroke, curve B. (The second point at −4° was a check in the non-firing stroke done after the measurements in the firing stroke.) From these results, it is quite definite that NO_2 is formed in the non-sparked stroke and even more is produced in this stroke than in the normal stroke. Clearly, then, the NO_2 is not a product of the flame.

---

* Ubbelohde, 'Proc. Roy. Soc.,' A, vol. 152, p. 372 (1935).

(2) *Iso*-octane was next used (throttle 9°, no knock) and very little NO_2 was detected in either the non-firing or the firing strokes ($< 2 \times 10^{-5}$ at $-1°$). A small quantity of an acetaldehyde/acetylperoxide mixture was added to the *iso*-octane; the iodine titration showing that about 3×10^{-4} mol fraction of acetylperoxide was present in the " doped " *iso*-octane. When the engine was run on this fuel, appreciable amounts of NO_2 ($4 \cdot 5 \times 10^{-5}$) were formed even at $-30°$ before T.D.C. When sprayed in along with the fuel, acetyl peroxide causes *iso*-octane to knock, but the quantity (5×10^{-6} mol fraction acetyl peroxide in cylinder gases) in the above experiment was quite insufficient to cause any detectable difference in the running of the engine, and yet the presence of the peroxide is able to induce production of NO_2 in the non-firing stroke. This experiment confirms the first one, and also the observation quoted in p. 482 *of the former paper,** in which acyl peroxides were shown to assist the production of NO_2 quite early in the stroke, in this case with a fuel which otherwise gives very little nitrogen peroxide.

(3) The suggestion that NO in the residual gas is present in sufficient amount to form gradually the NO_2 found towards the end of the compression stroke is disproved by the following experiment.† The gases from the sample valve were led through a glass tube 24 cm long before passing over the droplet. Oxygen, or nitrogen, could be passed into the gas stream with which it mixed in the long tube. No appreciable difference was made to the time of coloration of the droplet whether oxygen or nitrogen was added, provided that the dilution was the same; this was controlled by the flow meter measuring the rate of flow of the oxygen or the nitrogen, while the flow from the sampling valve was maintained as constant as possible. The valve setting was chosen at $-10°$ before T.D.C., it having been shown beforehand that the concentration of NO_2 at this point in the stroke was commencing to increase. (The time of coloration for the mixture with oxygen was 10 min 36 secs, and with nitrogen 10 min 20 secs.)

(4) Finally an attempt has been made to settle whether the surface of the hot exhaust valve is active in catalysing the formation of NO_2. A spare exhaust valve was electro-plated with gold. The engine was operated under precisely similar conditions, (*a*) with the silchrome valve in its usual state, then (*b*) with the gold-plated valve in position, then (*c*) again with the silchrome valve. The load was the same in each case, the gilding survived but was covered with a thin deposit of carbon. The following were the times of coloration of the droplets: (*a*) 1 min 35 secs,

---

* Egerton and others, ' Phil. Trans.,' A, vol. 234, p. 482 (1935).

† *Ibid.*, p. 484.

(*b*) 3 min 3 secs, (*c*) 1 min 38 secs. The corresponding NO_2 concentrations were 13×10^{-5} and 5×10^{-5}. If the temperature of the valve controls the process and thermal equilibrium were established, the valve surface temperature would have to differ by 100° to account for such a difference in concentration, and there seems no reason for the two valves to differ in temperature so much. It is therefore probable that the main reason for the reduction in concentration of NO_2 is that the catalytic activity of the surface is lessened by the coating of gold.

The above experiments indicate that the source of the NO_2 in the gases sampled from the engine is not the flame, but that the surface of the hot exhaust valve appears to play a prominent part in its production. Whether the peroxides which give rise to larger concentrations of NO_2, when added to the fuel, do so by activating the surface of the valve or by facilitating reaction in the gas as well as at the surface will require further experiments to settle definitely; the experiments described in the former paper,* in which diminishing quantities of amyl nitrite were added without much affecting the maximum concentration of NO_2 formed, indicates that the main effect is a surface one.

SUMMARY

The experiments were designed to clear up certain points left unsettled by the earlier investigation.

The former arrangement for sampling the gases from the engine cylinder has been so modified that the samples can be taken when ignition is made to occur every alternate cycle either in the firing or non-firing strokes.

Aldehydes are formed at the end of the compression stroke in the non-fired cycle, but the concentration is much smaller than in the firing stroke.

The quantities of formaldehyde and of total aldehydes have been measured when running on petrol, hexane, cyclohexane, amylene, acetone, butyl and ethyl alcohols, benzene, *iso*-octane, and also mixtures of aldehydes and petrol.

It is shown that the amounts of aldehydes produced are insufficient to account for " knock," and for this another source of peroxides is therefore needed.

Experiments are described which suggest that most hydrocarbon fuels can be made to " knock " provided molecules which can disrupt and give rise to a branched chain reaction are produced or made available.

The main source of the nitrogen peroxide found in the previous experiments is probably the hot active surface of the exhaust valve, and the experiments indicate that it is not the flame.

---

* ' Phil. Trans.,' A, vol. 234, p. 481 (1935).

Reactions in Monolayers of Drying Oils

I— The Oxidation of the Maleic Anhydride Compound of β-Elaeostearin

By G. Gee and Eric K. Rideal, F.R.S., Laboratory of Colloid Science, Cambridge

(*Received August* 6, 1935)

Introduction

The mechanism by which a film of a drying oil becomes converted in the course of drying to a hard solid, and in particular the role played by oxygen, is still a matter requiring elucidation. The original hypothesis of a direct oxidation has been replaced by a process involving a primary oxidation followed by a polymerization of the oxidized body. Fahrion[*] and Ellis[†] regarded the primary oxidation as the formation of hydroxy ketones which condense with the elimination of water. The work of Elm,[‡] and especially of Morrell,[§] suggests that the oxidation product which polymerizes is a peroxide, although the lability of this peroxide seems well established by the identification of dihydroxy and ketol bodies.

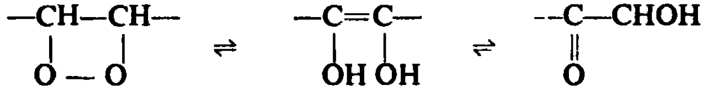

$$\begin{array}{c}-\text{CH}-\text{CH}-\\ \mid\qquad\mid\\ \text{O}-\text{O}\end{array} \rightleftharpoons \begin{array}{c}-\text{C}=\text{C}-\\ \mid\quad\;\mid\\ \text{OH}\;\text{OH}\end{array} \rightleftharpoons \begin{array}{c}-\text{C}-\text{CHOH}\\ \|\\ \text{O}\end{array}$$

Staudinger[||] further considers the peroxide to be preceded by a less stable moloxide —CH—CH—, and evidence for the existence of some such unstable body has been presented by Hilditch and Lea[¶] in the oxidation of methyl oleate.

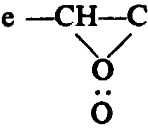

$$\begin{array}{c}-\text{CH}-\text{CH}-\\ \diagdown\;\diagup\\ \text{O}\\ \cdot\cdot\\ \text{O}\end{array}$$

---

[*] 'Z. angew, Chem.,' vol. 23, p. 722 (1910).

[†] 'J. Soc. Chem. Ind.,' vol. 44, pp. 401T, 463, 409, 486 (1925); vol. 45, p. 193T (1926).

[‡] 'Ind. Eng. Chem.,' vol. 23, p. 881 (1931).

[§] Morrell, 'Ind. Chem.,' vol. 1, p. 68 (1925); 'J. Oil. Col. Chem. Ass.,' vol. 12, p. 183 (1929); vol. 13, p. 84 (1930); 'J. Soc. Chem. Ind.,' vol. 50, p. 27T (1931); vol. 52, p. 130T (1933); "Chemistry of Drying Oils."

[||] 'Ber. deuts. chem. Ges.,' vol. 58B, p. 1075 (1925).

[¶] 'J. Chem. Soc.,' p. 1576 (1928).

Opinions differ as to the nature of the polymer. This is regarded by Elm as an associated compound, whereas Morrell and Staudinger regard it as a true polymeride or macromolecule. The further possibility of polymerization of the more stable oxidized forms of the glyceride is not to be overlooked, however, for Petrov and Kasterina* have shown that linseed oil oxidized with potassium chromate dries at substantially the same rate as a "blown" oil, although in the former case the product is mainly the dihydroxide. These reviews do not take into account the possibilities of the polymerization of the unoxidized glyceride, although it is clear that this is the main reaction in the process of " heat bodying " of an oil. Some workers, notably Scheifele† and Scheiber,‡ consider that in low-temperature drying the role of oxygen is limited to the formation of a polymerization catalyst, while Stephens§ and others|| regard both oxidation and polymerization as chain reactions, both taking a place in the finished product. The various studies of the reaction kinetics of the oxidation process for the oil in bulk or when spread as a thin layer on various surfaces have led to somewhat conflicting results; the total quantity of oxygen absorbed appears to vary considerably, probably on account of the variation in the magnitude of the disruptive oxidation which accompanies such bulk oxidation. The observation of a period of induction at the commencement of the reaction has led most workers to regard the reaction as auto-catalytic (*see e.g.*, Morrell), but the curves given by Long¶ represent a pseudo-unimolecular reaction after a short period of induction, and Coffey** obtained a similar result for linoleic acid. The cause of the induction period has been ascribed by Hilditch†† to the presence of natural anti-oxidants, for freshly distilled simple esters do not exhibit this phenomenon.

It appeared possible that some further insight into the mechanism of what is evidently a series of complex reactions might be gained by carrying

---

* 'Masloboino Zhirovoe Delo,' vol. 10, p. 30 (1931).

† 'Farben. Z.,' vol 33, p. 739 (1927); 'Z. angew. Chem.,' vol. 42, p 787 (1929).

‡ 'Z. angew. Chem.,' vol. 40, p. 1279 (1927); 'Farbe u. Lack,' vol. 33, p. 518 (1928); vol. 34, p. 284 (1929); vol. 34, p. 477 (1929); vol. 36, p. 511 (1931).

§ 'Ind. Eng. Chem.,' vol. 24, p. 918 (1932).

|| Eibner, 'Z. angew. Chem.,' vol. 39, p. 38 (1926); 'Chem. Umsch. Fette,' vol. 33, pp. 188, 201, 213 (1926); vol. 34, pp. 89, 101 (1927); vol. 35, p. 241 (1928); Miller and Claxton, 'Ind. Eng. Chem.,' vol. 20, p. 43 (1928).

¶ 'Ind. Eng. Chem.,' vol. 21, p. 950 (1929); vol. 23, p. 786 (1931); vol. 25, p. 1086 (1933).

** 'J. Chem. Soc.,' pp. 1152, 1408 (1921); p. 18 (1922); 'J. Oil. Col. Chem. Ass.,' vol. 6, p. 2 (1923).

†† 'J. Soc. Chem. Ind.,' vol. 51, pp. 39T. 411T (1932).

out the reaction in monolayers on the surface of water by the methods outlined in previous communications, especially as Long has shown that such monolayers can readily be formed with linseed oil.

EXPERIMENTAL

The apparatus designed to permit of simultaneous measurements of the surface pressure and phase boundary potential followed closely that described in previous communications, but was improved by substitution for the polonium source of a thin glass tube containing 1·0 mg mesothorium (attached to the air electrode) and a valve potentiometer based upon a circuit described by Compton and Haring* in place of the Lindemann electrometer. Such a system was found to possess several advantages in speed and flexibility of action over the previous design. The trough was enclosed in a metal-covered wooden thermostat, and the electrode for exploring the phase boundary potential, the glass slide for compressing the film, and the torsion head of the Langmuir trough could all be operated from outside.

The torsion wire employed gave a sensitivity of about 10° per dyne per cm, and film pressures could be measured with an accuracy of about 0·2 dyne per cm. The material investigated was the maleic anhydride compound of β-elaeostearin described by Morrell. We are indebted both to Dr. Morrell and to the British Dyestuffs Corporation for preparations which gave similar results. The β-elaeostearin preparation in the latter case was obtained from tung oil, and recrystallized from dry acetone as far as possible in an atmosphere of carbon dioxide (m.p. 60–60·5° C). The maleic anhydride was prepared by Mason's method, the product being fractionated under reduced pressure and recrystallized from chloroform (m.p. 53–53·5° C). The condensation was carried out as described by Morrell.

It was discovered at once that a monolayer spread from petrol ether on dilute acid (N/100 HCl or H_2SO_4) was unstable, and underwent expansion when maintained at constant pressure, but fairly consistent force-area and phase boundary potential curves could be obtained by rapid examination. On 0·1% hydroquinone the films were found to be perfectly stable and the values obtained agreed with those obtained without the inhibitor.

The force-area and potential curves are shown in fig. 1 together with

---

[*] 'Trans. Electrochem. Soc.,' vol. 62, p. 345 (1932).

the mean value of the vertical component of the effective molecular dipole moment derived with the aid of the equation

$$\Delta V = 4\pi n \mu.$$

The information provided by these curves serves to interpret the effect of compression of the film on the molecular orientation. Several structures have been proposed for the maleic anhydride compound of β-elaeostearin. Our results are most readily interpreted on the structure given by Morrell, which can be represented as a cis-glyceride, fig. 2.

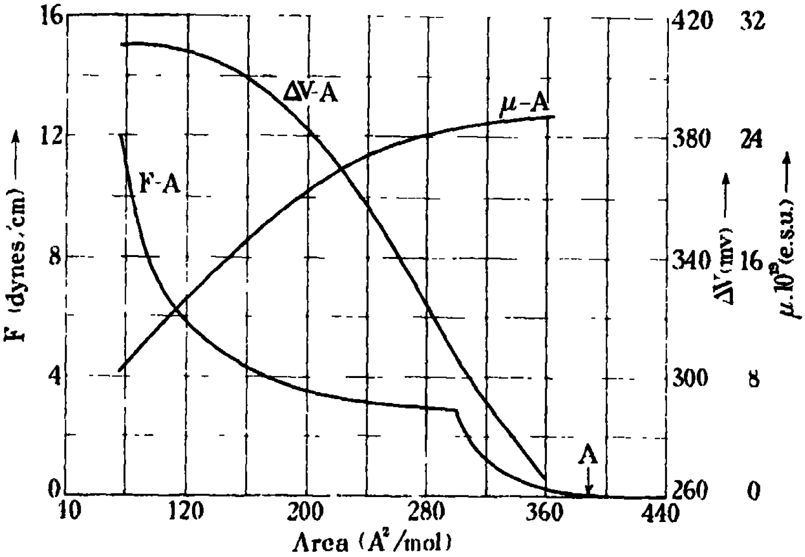

FIG. 1—F — ΔV — μ - A curves of maleic anhydride β-elaeostearin on N/100 H_2SO_4.

The effective width of the tilted double ring system is found to be about 6·5 A. Hence if these are just in close contact at A, the point on the compression curve where the pressure becomes sensible is:

For the area as far as the double bonds	$19{\cdot}5 \times \frac{1}{2}(10 + 3 \times 6{\cdot}5)$	$= 287{\cdot}5$ A²
For the terminal C_4H_9 chains..	$5 \times 19{\cdot}5$	$= 97{\cdot}5$ A²
Total		385 A²

which is very close to the limiting area observed experimentally, viz., 380 A².

On compression of the chains the molecule may be regarded as passing through the following stages:

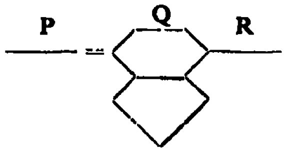

I

Area calc. = 385 A^2
Area obs. ~ 380 A^2
F obs. = 0·2 dynes/cm
μ obs. = $25 \cdot 4 \times 10^{-19}$ e.s.u.

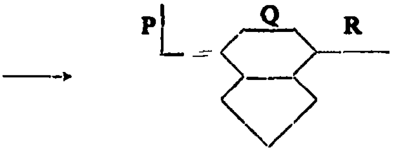

II

Area calc. = 290 A
Area obs. = 300 A
F obs. = 2·9 dynes/cm
μ obs. = $24 \cdot 6 \times 10^{-19}$ e.s.u.

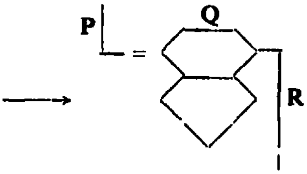

III

This position does not correspond with a sharply defined point on the curve.

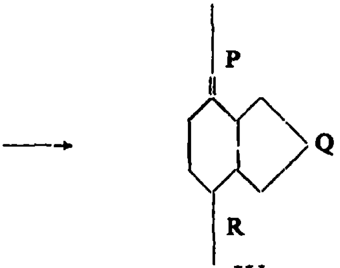

IV

Area at final collapse
Area calc. = 110 A^2 (ring system)
Area at F = 12 is 80 A^2
Area extrapolated to F = 0 is 120 A^2
μ obs. = $8 \cdot 2 \times 10^{-19}$ e.s.u.

During the final stage the double bond leaves the surface and a marked fall in the reaction velocity occurs.

The polar portions of the molecule consist of the glyceride molecule in R, the anhydride ring system Q, and the double bonds in Q and P. The value of μ obtained for a typical glyceride such as tripalmitin is $\mu = 10 \cdot 0 \times 10^{-19}$ e.s.u., while that for the ring system can be evaluated from the known value for an etheric oxygen of $\mu = 2 \cdot 5 \times 10^{-19}$ e.s.u., and of a ketonic oxygen $\mu = 3 \cdot 0 \times 10^{-19}$ e.s.u. In the anhydride ring the ketonic oxygen atoms form an angle of approximately

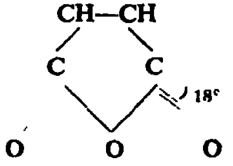

18° with the horizontal. Hence the contribution to the total vertical component of the dipole system due to the three rings in the glyceride molecule is

$$\mu = 3 \times \{2{\cdot}5 + 2 \times 3 \sin 18°\}\, 10^{-19} \cong 13 \times 10^{-19} \text{ e.s.u.}$$

Each double bond in the system contributes some $0{\cdot}3 \times 10^{-19}$ e.s.u. (*e.g.*, μ of myristic acid $1{\cdot}8 \times 10^{-19}$, oleic acid $2{\cdot}1 \times 10^{-19}$ e.s.u.). Hence the six double bonds in the molecule contribute $1{\cdot}8 \times 10^{-19}$ e.s.u.

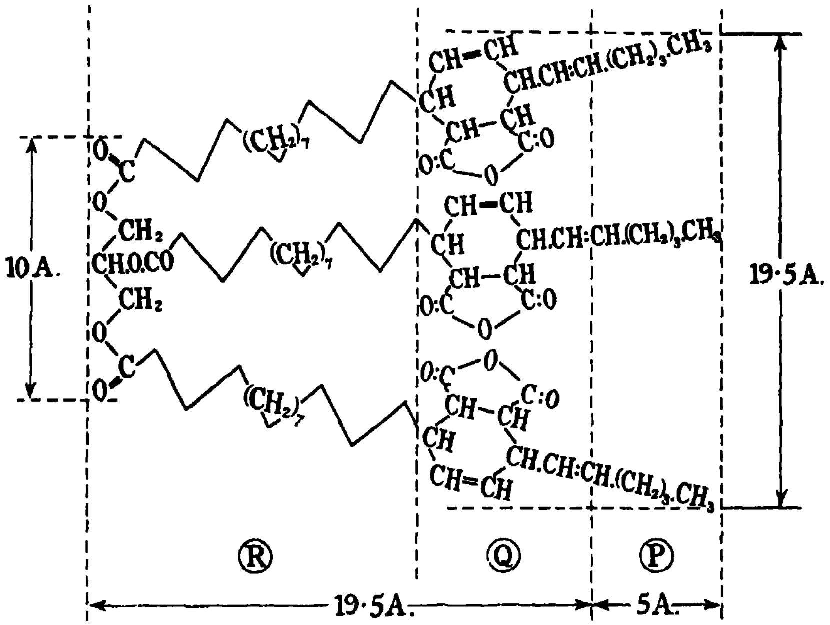

FIG. 2.

We thus obtain for the total value of the vertical components of the effective electric moments per molecule of the trigylceride the following values:

	$\mu \times 10^{-19}$ e.s.u.
The glyceride group	10·0
Ring system	13·0
Double bonds	1·8

Total, $\mu = 24{\cdot}8 \times 10^{-19}$ e.s.u.

a value to be compared with that experimentally determined of $25{\cdot}4 \times 10^{-19}$ e.s.u.

On submergence of the glyceride (position III) the value of the moment falls to about 15 × 10^{-19} e.s.u. and finally, on compression to the erect state the moment might be expected to fall still further, a limiting value of $\mu = 8\cdot2 \times 10^{-19}$ being actually obtained.

It may be concluded that both the limiting areas and phase boundary potentials support the structural formula proposed by Morrell for this compound, and further support is obtained from the changes in these molecular properties on compression of the film.

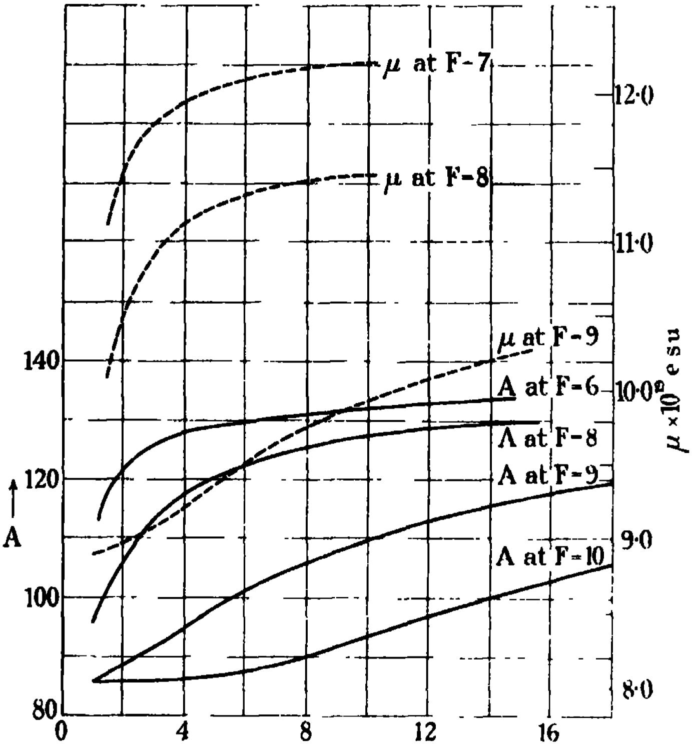

Fig. 3—Rate of oxidation on N/100 H_2SO_4.

In fig. 3 are presented a series of curves showing the increase of area at several surface pressures on N/100 H_2SO_4 solution at 287° K. It is evident that the reaction velocity begins to fall off markedly at high pressures. The reactive groups in the molecule are the double bonds in each chain remote from the glyceride group, and the interpretation already given of the force area curve is consistent with the view that this bond is being removed from the surface at high pressures, the reaction velocity thus falling as in the compression of films of oleic acid examined by

Hughes and Rideal.* The reaction thus apparently involves the double bond, and that the oxidation of this glyceride is indeed accompanied by expansion of the film was shown by spreading the film on 0·001% solution of $KMnO_4$. On this substrate the areas measured initially were somewhat higher than those of the unoxidized material, but fell rapidly and continuously practically to zero. It is clear that the primary oxidation is almost instantaneous but is followed by a disruptive oxidation leading to soluble products.

Further evidence that the reaction on dilute acids is an oxidation process is provided by the fact that like films of α- and β-elaeostearic acids the reaction is completely stopped by the presence of 0·1% hydroquinone in the substrate; whilst the reaction can be accelerated by the salts of the heavy metals such as cobalt sulphate which are used as oxidation catalysts.

The reaction at constant pressure is accompanied not only by an increase in area but also by a rise in the vertical component of the effective dipole moment. This quantity is calculated from the measured values of the phase boundary potential, and the compression by the Helmholtz equation $\Delta V = 4\pi n\mu$. The variation of μ with time is also given in fig. 3.

Owing to the fact that the variation in the area as oxidation proceeds is greater than the change in the phase boundary potential, the former has generally been used to calculate the velocity and order of the reaction, although experimentally it was found that both methods of computation gave the same values. The reactions have been followed at constant pressure to preserve identical molecular configuration during the run.

Some typical results of plotting $\partial A/\partial t$ against the area are shown in fig. 4.

It is clear that the reaction velocity is extremely sensitive to variations in pressure. At high pressures, we note that the curves are unimolecular over the greater part of their course with deviations both at the commencement and end of the reaction, the causes of which will be discussed later.

The temperature coefficient of the reaction was determined by carrying out runs at 275·5° K and 287° K. Some of the data obtained are given in Table I, yielding a value for the energy of activation of the reaction of $E = 6500$ cals.

With another sample of material the values obtained at $F = 8$ were: at 275° K, $k = 0·49$ min^{-1}, at 303° K, $k = 1·5$ min^{-1}, giving a value again of $E = 6500$ cals. In fig. 5 are plotted the mean values of the velocity constant in reciprocal minutes reduced in all cases to that at 275° K as a function of the two-dimensional pressure F.

---

* 'Proc. Roy. Soc.,' A, vol. 140, p. 253 (1933).

TABLE I

F dynes/cm	k in min^{-1}		k 287/k 275·5
	At 275·5° K	At 287° K	
8	0·34	0·53	1·6
7	0·67	1·04	1·6
6	0·87	1·5	1·7

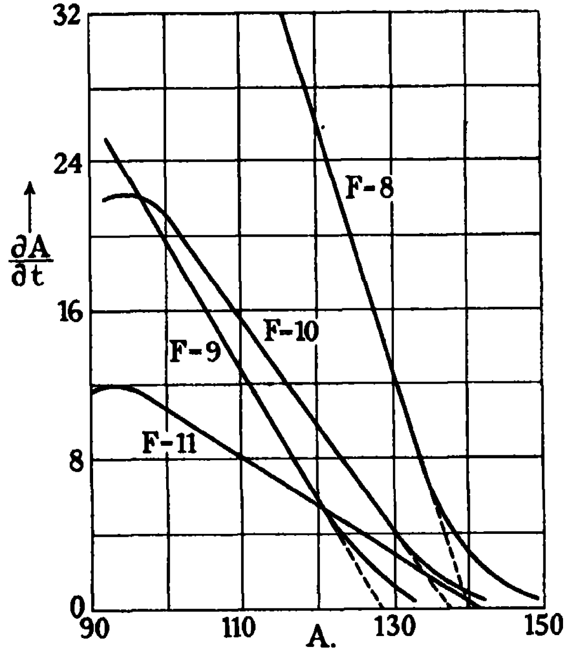

FIG. 4—Velocity constants for oxidation stage, N/100 H_2SO_4, 290·5° K.

In addition to this change in the velocity constant as a function of F another effect of pressure is evident; the total increase in area at high pressures is greater than at low, and similar differences are found in the values of the dipole moment. Typical values are shown in Tables II and III.

It should be noted that the areas and moments given in Table II refer to the pressure of the experiment: an area of 130 A^2 at F = 10 is approximately equivalent to 160 A^2 at F = 6.

It must be concluded that the reaction product varies with the reaction pressure, a high pressure giving a product of high area and low moment.

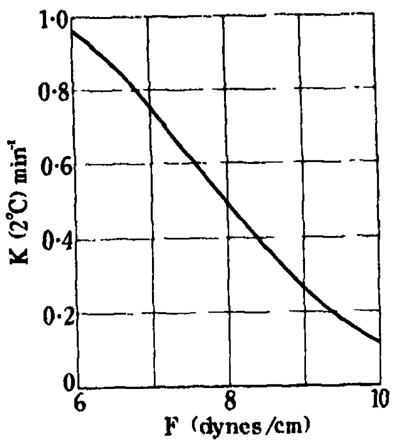

FIG. 5—Effect of pressure on oxidation velocity constant, N/100 H_2SO_4, 275° K.

TABLE II—FINAL AREAS (A_∞) AND MOMENTS (μ_∞) OBTAINED BY EXTRAPOLATION OF THE LINEAR PORTION OF ($\partial A/\partial t$—A) AND ($\partial\mu/\partial t$—μ) CURVES

Oxidation pressure F in dynes/cm	A_∞ in $Å^2$ at 275·5° K	A_∞ in $Å^2$ at 287° K	$\mu_\infty \times 10^{19}$ at 275·5° K	$\mu_\infty \times 10^{19}$ at 287° K
10	119	130	10·5	
9	119·5	128	10·55	10·5
8	122	124·5		11·4
7	119·5	124·5		12·0
6	127·5	124·5		12·6

TABLE III—FILM CHARACTERISTICS AFTER OXIDATION AT DIFFERENT PRESSURES

F in dynes/cm	A in $Å^2$ after oxidation at F = 5	A in $Å^2$ after oxidation at F = 10	$\mu \times 10^{19}$ after oxidation at F = 5	$\mu \times 10^{19}$ after oxidation at F = 10
5	157	173	14·15	12·8
6	142	157	13·25	11·8
7	132	146	12·5	11·2
8	129	140	11·8	10·85
9	110	133·5	10·55	10·45
10	106	128·5	10·15	10·15

This variability clearly suggests that the primary oxidation product is not stable but can undergo a subsequent reaction or reactions, the extent of which depends on the pressure. Provided such reaction is rapid compared with the primary oxidation, the reaction would remain pseudo-unimolecular except that the initial velocity would be lower than that required by the unimolecular law. Inspection of the curves indicates that this behaviour is actually observed.

From the bulk properties of drying oils it seems likely that the primary peroxide is capable of undergoing at least two types of reaction, isomerization and polymerization, so that we may represent the total reaction schematically as follows:

$$\begin{tikzcd} & & \text{Polymer} \\ X \arrow[r] & XO'_2 \arrow[ur] \arrow[dr] & \\ & & XO_2 \end{tikzcd}$$

where X is the initial unoxidized material, XO'_2 the unstable primary peroxide, and XO_2 the isomer.*

We might anticipate that the rate of polymerization should be pressure sensitive but that the rate of isomerization might be independent of the pressure. The observed variation of the oxidation product with the conditions of reaction is thus understandable. Further, at low pressures the rate of polymerization may fall to values commensurate with the rate of oxidation and the reaction will no longer be pseudo-unimolecular; this behaviour is already evident at pressures as low as $F = 6$ dynes/cm. Finally, if we carry out the oxidation at low enough pressures, the polymerization should become negligible and it will be possible to produce only the isomer. The film, however, is no longer homogeneous when expanded to such a high degree and the pressure is too small to measure; but the reaction can be studied by compression of the film at intervals to measure either the area or the potential under a standard pressure ($F = 8$ dynes/cm was actually employed). As soon as the film, consisting of a mixture of XO'_2 and XO_2, is compressed the XO'_2 commences to polymerize, necessitating rapid measurement and forming a fresh film for each determination. At these large areas the oxidation proceeds extremely rapidly so it is possible to construct a curve giving the rate of conversion of the unstable peroxide XO'_2 into the stable isomer XO_2. The results are shown in fig. 6.

[*Note added in proof, October* 15, 1935—An alternative possibility is that the peroxide may loose oxygen with the formation of a monoxide XO. This reaction has been shown to occur in bulk (Morrell, private communication); the present experiments do not permit of a decision between the two possibilities.]

Two series of measurements are given for readings at 295° K and 303° K. The experimental points at 295° K obey a unimolecular law accurately; the results at the higher temperature, while not so reproducible, are well

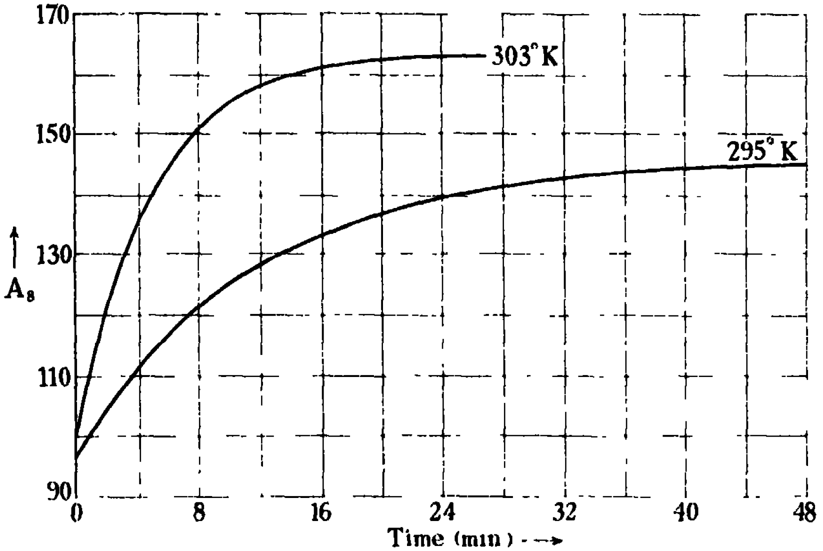

FIG. 6—Rate of isomerization ($XO_2' \rightarrow XO_2$) N/100 H_2SO_4.

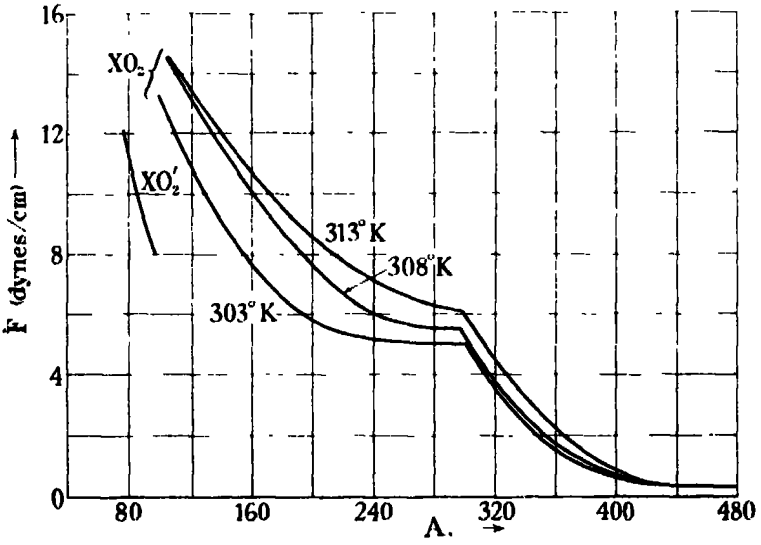

FIG. 7—F-A curves of XO_2 and XO_2' on N/100 H_2SO_4.

represented by the curve drawn. The velocity constants are $k_{295} = 0{\cdot}089$ min^{-1}, $k_{303} = 0{\cdot}21$ min^{-1}, and the calculated energy of activation is $E = 19{,}000$ cal/mol. In fig. 7 are shown the force area curves for the stable isomer of the unstable peroxide. The force area curves for the latter, on account of its reactivity, are extremely difficult to determine, but a few points which appear to be reliable are plotted in the same figure. Comparison of this curve with the one for the unoxidized material shows that there is no appreciable change in area involved in the primary oxidation. Further examination of the properties of the stable isomer of the peroxide revealed the fact that it could slowly undergo a reaction like the unstable peroxide to form apparently a similar polymer, the kinetics of which will be discussed in the next section.

We may conclude that the mechanism of "drying" of the maleic anhydride compound of β-elaeostearin in the form of a monolayer on dilute acid may be represented by the following series of changes,

$$\begin{tikzcd}
 & & \text{Polymer} \\
X \arrow[r, dashed, "k_1"] & XO'_2 \arrow[ur, "k_2"] \arrow[dr, "k_3"'] & \\
 & & XO_2 \arrow[uu, "k_4"']
\end{tikzcd}$$

and we have already established the fact that the reactions denoted by k_1 and k_3 are unimolecular with energies of activation of 6500 cal/mol and 19,000 cal/mol respectively.

Reactions in Monolayers of Drying Oils
II—Polymerization of the Oxidized Forms of the Maleic Anhydride Compound of β-Elaeostearin

By G. GEE, Laboratory of Colloid Science, Cambridge

(*Communicated by E. K. Rideal, F.R.S.—Received August* 6, 1935)

In Part I it was shown that the preliminary stages in the " drying " of a monolayer of the maleic anhydride compound of β-elaeostearin extended on dilute acid substrates consisted in the formation of an unstable peroxide, which in turn could form either a stable isomer or be converted into a polymer. The stable isomer in turn was likewise found capable of undergoing polymerization. The evidence that the reaction subsequent to the formation of the peroxide is a species of polymerization is based upon the following observations. Films of β-elaeostearin when the reaction is completed are continuous and gel-like in nature; those of the maleic anhydride compound are highly viscous and cannot be extended without becoming inhomogeneous. It is clear that cross-linkage in the formation of the polymer is readily possible in β-elaeostearin; but this tendency is much reduced in the maleic anhydride compound, especially when the most probable molecular configuration is considered (Part I).

[*Note added in proof, October* 15, 1935.—The position of the reaction double bonds immediately above the double ring system must introduce difficulties in the formation of oxygen bridges during polymerization. As successive molecules are added, the bulky rings must be forced progressively outwards, causing both a progressive expansion of the film as the molecular complexity increases and a diminution in the case of addition of further molecules.]

We have seen that at low temperatures and high pressures the polymerization of XO_2' occurs so rapidly that the whole reaction is pseudo-unimolecular. At higher temperatures and at pressures of the order of $5 \sim 6$ dynes per cm this is no longer true, and the two processes can be observed to proceed successively; the separation is particularly well marked if the substrate contains a little cobalt sulphate. Some typical curves are given in fig. 1 where $\partial A/\partial t$ is plotted as a function of A. It will be noted that the curve for $F = 7$ dynes/cm gives the best illustration of this separation into two portions and that the second section is roughly parabolic in shape.

The effect of inhibitors is also worthy of note; the presence of a little hydroquinone in the substrate causes the reaction to come to an end at a much smaller area than usual, but in addition dilution of the film by mixing the glyceride with small amounts of a stable body such as ethyl myristate also exerts a profound effect on the shape of the curve. In fig. 1 is included a curve for a mixture containing 10% ethyl myristate allowed to react at F = 9 dynes/cm. It is evident that this addition has greatly decreased the velocity of reaction. These observations are readily interpreted on the view that the subsequent reaction is one of polymerization; that this polymerization is a chain reaction in the film, and that the chains are capable of being broken either by chain-breaking materials in the substrate such as hydroquinone or incorporated like ethyl myristate in the actual film itself. A few observations on the photo-sensitivity of the oxidation process occurring in these films likewise support the view that two distinct stages in the process can be identified: the primary oxidation sensitive to short wave ultra-violet light and the polymerization process sensitive to long wave ultra-violet light.

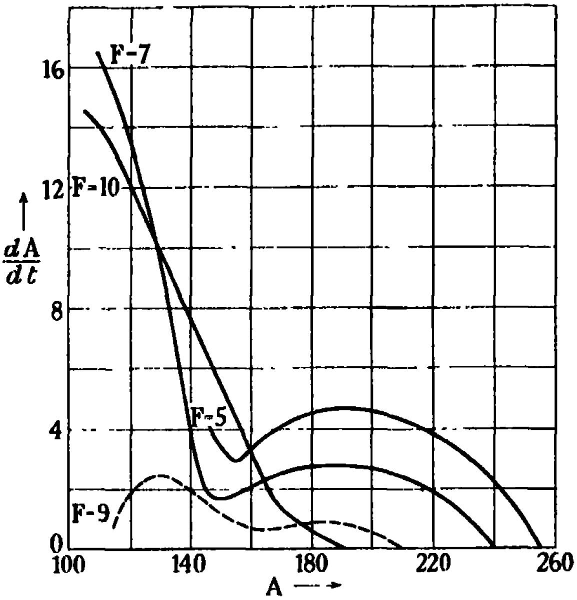

FIG. 1—Velocity of reaction on N/100 H_2SO_4 + 5 × 10^{-4} M. $CoSO_4$ at 299° K.

An analysis of the kinetics of polymerization has been published elsewhere,* in which the mechanism of these processes is discussed. It is concluded that the reaction proceeds by the primary activation of monomer (a slow process), followed by the rapid reaction of the active material with successive molecules of inactive monomer, so that the reaction is terminated by the disappearance of monomer. Evidence is presented to show that the decreasing activity of the growing polymer may be adaquately accounted for on the basis of an increasing steric factor.

---

* Gee and Rideal, 'Trans. Faraday Soc.,' vol. 31, p. 969 (1935). [*Note added in proof, October* 15, 1935. The analysis given there derives the velocities in terms of the number of molecules n_r of the polymer M_r reckoned in terms of monomer. To transform to the usual convention involves the insertion of a factor $1/r$; all results quoted here have been altered in this way.]

$$\begin{array}{ll} M \rightarrow M^1 & (k_1) \\ M + M^1 \rightarrow M_2 & (k_2) \\ M + M_2 \rightarrow M_3 & (k_3) \\ \dots\dots\dots\dots\dots\dots & \\ M + M_r \rightarrow M_{r+1} & (k_{r+1}) \\ \dots\dots\dots\dots\dots\dots & \end{array}$$

If the reaction system be represented by a set of equations as above, k_{r+1} may thus be written as a function of r and a parameter K. Two possibilities are considered:

$$\left\{ \begin{array}{ll} k_{r+1} = K & \quad (1\text{A}) \\ k_{r+1} = K/r. & \quad (1\text{B}) \end{array} \right.$$

Writing $k_1 = \alpha n_0 K$, where n_0 is the original number of molecules present and α a numerical constant, the reaction velocity is derived in terms of the total number of molecules N, and the mean chain-length ν of the fraction which has polymerized. It is shown that for the two steric factors given above:

$$\left\{ \begin{array}{ll} -\dfrac{\partial N}{\partial t} = \dfrac{K}{(\nu - 1)^2}(n_0 - N)(N\nu - n_0) & \quad (2\text{A}) \\ -\dfrac{\partial N}{\partial t} = \dfrac{K}{\nu(\nu - 1)^2}(n_0 - N)(N\nu - n_0). & \quad (2\text{B}) \end{array} \right.$$

It is further demonstrated that there are two limiting cases to be considered:

(1) when $\alpha \rightarrow 0$ (long chains) the reaction degenerates to a pseudo-unimolecular form,

(2) where the chain length remains constant during the reaction, the equation becomes identical with one proposed by Semenoff* for

---

* 'Z. phys. Chem.,' B, vol. 11, p. 464 (1933); 'Phys. Z. Sowjet,' vol. 4, p. 906 (1933).

thermal gaseous chain reactions and gives a parabolic curve for $\partial N/\partial t$ against N. In practice, it is pointed out that this condition will be approached for large values of α and/or a large steric factor.

Intermediate cases give an asymmetrical $\partial N/\partial t - N$ curve, the maximum being increasingly displaced towards the start of the reaction as the chain length of the product becomes greater.

Before this analysis can be applied to the present experiments, it is necessary to know how the molecular area A changes as the polymer grows.

The simplest assumption to make is that the area of the polymer molecule changes by a constant amount δA for each unit added, so that if A is the area per monomer molecule of the polymer M, we have

$$A_r = A_0 + \frac{r-1}{r} . \delta A. \tag{3A}$$

This assumption is, however, in the present case inadequate, as the variation in area during reaction $(A_\infty - A_0)$ could only lie in the range $\frac{1}{2}\delta A$ to δA, *i.e.*, 1 : 2, whereas experimentally values covering a range of 1 : 7 have been found. If the growth is irregular and not linear then for *short* chains there will be a progressive increase in area which may be expressed in the form:

$$A_r = A_0 + r\delta A. \tag{3B}$$

Two other possible relations between the extension of the film and the chain length may be noted. It is possible that the formation of the dimer takes place with only a small expansion δA, but that in each subsequent addition an area increment of $(1 + p)\,\delta A$ is involved, whence

$$A_r = A_0 + \left\{1 + \frac{r-2}{r} p\right\} \delta A. \tag{3C}$$

Finally we may imagine that the expansion increases progressively for the first few units, but ultimately reaches a finite limit, the complete variation being expressed by a symmetrical curve of the form

$$A_r = A_0 + \lambda\,(1 - e^{-qr}), \tag{3D}$$

whence $(A_r)_{r\to\infty} = A_0 + \lambda$, λ and q being constants. The last three possibilities have been examined in some detail, and all are consistent with the present experimental data. It will, however, be pointed out later how a separate determination of the mean chain-lengths of the polymers formed under different conditions would enable a decision to be made between them.

Taking the three alternatives for A_r we can find the relationship between the mean molecular area A at time t and N. Let the numbers of molecules of M, M^1, M_2, .., M_r at time t be n_1, n^1, n_2, .., n_3, reckoned in terms of the monomer, so that we have

$$n_0 = n_1 + n^1 + n_2 + n_3 + \, .. + n_r + \, .. \tag{4}$$

$$N = n_1 + n^1 + \tfrac{1}{2}n_2 + \tfrac{1}{3}\, n_3 + \, .. + \frac{1}{r}\, n_r + \, .. \tag{5}$$

If ν is the mean chain-length of the fraction $\frac{(n_0 - n_1)}{n_0}$ polymerized then also $N = n_1 + n^1 + \frac{n_0 - n_1 - n^1}{\nu}$ and approximately

$$n_1 = \frac{N\nu - n_0}{\nu - 1}. \tag{6}$$

If the areas of the various molecular species are A_0, A_2, A_3, .., A_r *per monomer*, then

$$n_0A = n_1A_0 + n^1A_0 + n_2A_2 + n_3A_3 + \, .. + n_rA_r + \, .. \tag{7}$$

The equations relating A to N are now easily derived and are found to be:

$$n_0 (A - A_0) = \frac{\nu^2 \, . \, \delta A}{\nu - 1} (n_0 - N), \tag{8B}$$

$$n_0 (A - A_0) = \delta A \, . \frac{\nu}{\nu - 1}\left[1 + p \, . \frac{\nu - 2}{\nu}\right](n_0 - N), \tag{8C}$$

$$n_0 (A - A_0) = \lambda q \, . \frac{\nu^2}{\nu - 1} (1 - \tfrac{1}{2}q) (n_0 - N). \tag{8D}$$

(8D) is based on the approximate expansion $1 - e^{-qr} \cong qr - \frac{1}{2}q^2r^2$.

We are now in a position to derive a series of equations relating the reaction velocity as measured by dA/dt with the observed area. For this purpose we may combine any of the expansion laws with any steric factor, but no useful purpose would be served by giving details as the procedure does not differ fundamentally from that outlined in the paper already referred to.* The results are illustrated by equations obtained by combining the law $A_r = A_0 + r \,.\, \delta A$ with a zero steric factor ($k_{r+1} = K$). We find:

---

* Gee and Rideal, 'Trans. Faraday Soc.,' vol. 31, p. 969 (1935).

$$n_0 \frac{dA}{dt} = (2\nu + 1)\, \delta A \,.\, K n_1 (n_0 - n_1) \tag{9}$$

and by definition of ν,

$$A - A_0 = \left(1 - \frac{n_1}{n_0}\right) \nu \,.\, \delta A, \tag{10}$$

whence

$$\frac{dA}{dt} = \frac{(2\nu + 1) K n_0}{\nu^2 \,.\, \delta A} (A_0 + \nu \,.\, \delta A - A)(A - A_0). \tag{11}$$

This reduces to the " Semenoff " parabolic form if ν is equated to ν_∞, its value at the end of the reaction, and the same property is found whatever expansion and steric laws are considered. The general properties of the curves are also similar and are strictly analogous to those of the dN/dt, N curves, as given above.

It is easily shown that the initial slope of the dA/dt A curve is proportional to Kn_0, but the constant of proportionality obtained depends on which of the possible expansion laws is employed. Having obtained Kn_0, α is then derivable from the initial value of d^2A/dt^2,* but the experiments described here scarcely permit of the determination of these quantities with sufficient accuracy to justify the use of such methods.

In practice it has been found most convenient to interpret the results in terms of the equation to the parabolic " Semenoff "† curve, a form which is closely approached by many of the experiments. The equation was originally given in the form:

$$\xi = \frac{1}{1 + e^{-\phi\tau}}, \tag{12}$$

where ξ is the fraction of the original material which has undergone reaction at the time τ, reckoned from the time of half-reaction, and ϕ is a function of temperature and pressure of the form

$$\phi = Bp^n e^{-E/RT}. \tag{13}$$

On the assumption that the change in area is proportional to the fraction which has reacted, we may write:

$$\xi = \frac{A - A_0}{A_\infty - A_0}. \tag{14}$$

---

* *See* Gee and Rideal, *loc. cit.*

† 'Z. phys. Chem.,' B, vol. 11, p. 464 (1933).

Combining equations (12) and (14) it is easily shown that

$$\frac{dA}{dt} = \frac{k_2}{A_\infty - A_0}(A_\infty - A)(A - A_0), \tag{15}$$

where k_2 is written instead of ϕ.

A form of equation more suitable for the purposes of computation is obtained by inserting in (15) the condition for dA/dt to be a maximum, which is clearly $A = \frac{1}{2}(A_0 + A_\infty)$, when we find:

$$\left(\frac{dA}{dt}\right)_{max} = \frac{k_2(A_\infty - A_0)}{4}. \tag{16}$$

This equation has been used to compute velocity constants from the data of the experiments described below.

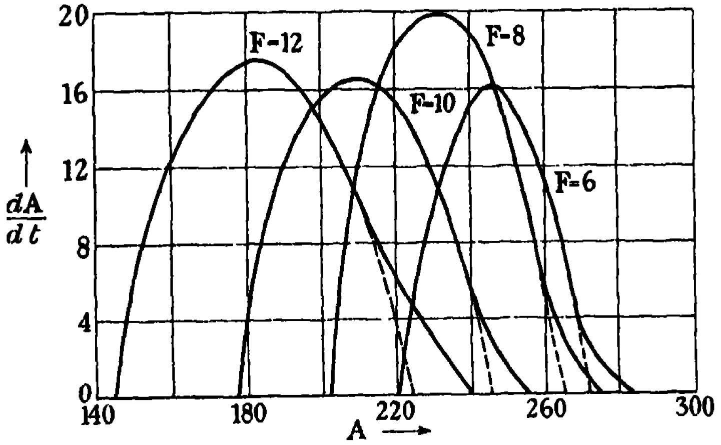

FIG. 2—Kinetics of polymerization of stable isomer on N/100 H_2SO_4 at 40° C.

POLYMERIZATION OF THE STABLE ISOMER XO_2 OF THE PEROXIDE XO_2'

A film of nearly pure isomer of the active peroxide is produced by permitting the glyceride to oxidize at a large area and allowing it to stand thus extended for the length of time required to complete the isomerization. The film can then be compressed and its polymerization studied at any convenient pressure. Some typical results are given in fig. 2.

The curves plotting dA/dt against A are seen to be nearly parabolic, from which form they only deviate at large areas. From the curves the values of A_0 and $\left(\frac{dA}{dt}\right)_{max}$ are readily obtained, and combining with these the values of A_∞ given by the smooth curve the velocity constants are calculated with the aid of equation (16). The effect of varying the surface pressure F and the temperature are represented in fig. 3 where k_s is plotted against F for three different temperatures.

The increase in velocity constant at the highest temperature 313° K and low pressures is most probably due to a phase change, condensed to expanded, occurring at a pressure which lies within the range 8–12 dynes/cm at 313° K but below it at 303° and 308° K. In fig. 7, Part I, it will be noted that for the stable isomer the transition at 313° K from expanded to condensed is so gradual that it is difficult to say when the film is completely condensed. If we accept this interpretation the energy of activation of the process in the condensed film at 12 dynes/cm is found to be of the order E = 20,000 cals/gm mol.

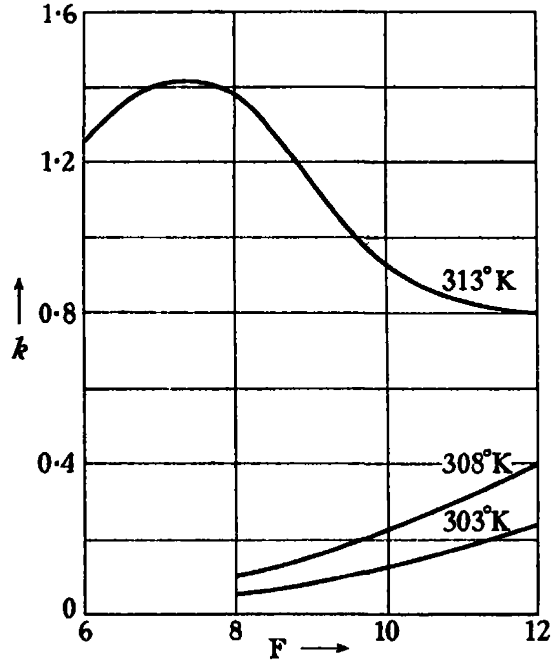

FIG. 3—Velocity constants for polymerization of stable isomer.

The effect of pressure on the velocity constant has been obtained from a series of measurements at 303° K on substrates containing 2 × 10^{-3} M cobalt sulphate. A plot of log k_s, log F gives a straight line for F = 8, 10, 12, showing that $k_s \propto F^3$. At F = 6 a higher value is obtained, again suggesting that the film is partly expanded.

This law of pressure variation also holds for the experiments on N/100

TABLE I—VELOCITY CONSTANTS FOR POLYMERIZATION OF ISOMER ON N/100 $H_2SO_4 + 2 \times 10^{-3}$ M $CoSO_4$ AT 303° K

F (dynes/cm)	k_s (min^{-1})	$10^4 k_s/F^3$
6	0·195	9·0
8	0·312	6·1
10	0·595	6·0
12	1·07	6·2

H_2SO_4 at 303° K and 308° K recorded in fig. 3, for taking the observed values at F = 12 we can calculate the constants at F = 8, with the results obtained in Table II.

TABLE II

Temp. (° K)	k_{12} (min^{-1})	k_8 (min^{-1})	
		Calculated	Observed
303	0·24	0·07	0·05
308	0·40	0·12	0·10

The agreement is within the experimental error. The complete variation of the velocity constant with temperature and pressure may thus be written:

$$k = k_0 \, F^3 \, e^{-20{,}000/RT}.$$

It may be noted that this is of the same form as the equation (13) given by Semenoff (*loc. cit.*).

POLYMERIZATION OF THE UNSTABLE PEROXIDE XO_2'

If a film of glyceride be spread at high expansions (> 400 A^2/mol) and allowed to stand long enough for oxidation to be complete we obtain a mixture of the peroxide and its more stable isomer in proportions depending on the time for which the film was expanded and which can be calculated from the known velocity of isomerization. On compression such a film will commence to polymerize while the process of isomerization will also continue. It is possible to choose a temperature range over which the process of isomerization and the polymerization of the isomer proceed at rates negligible in comparison with the velocity of polymerization of the unstable peroxide. The velocity curves obtained in this way are similar to those obtained for the polymerization of the stable isomer, and velocity constants can be calculated in a similar manner.

On decreasing the ratio of the unstable peroxide to stable isomer by increasing the time of expansion, we note a diminution in total expansion and a simultaneous decrease of velocity constant. The simplest explanation of this is that the stable isomer, being unable to form chains under the experimental conditions, is acting like ethyl myristate, fig. 1, as a chain-breaking inhibitor. Now the variation of the velocity constant k with the concentration C of an inhibitor should for a chain process be given by an equation of the form

$$k = \frac{k_0}{1 + \alpha C}$$

or

$$\frac{1}{k} = \frac{1}{k_0} + \frac{\alpha C}{k_0},$$

where α is a specific constant depending on the efficiency of the inhibitor.

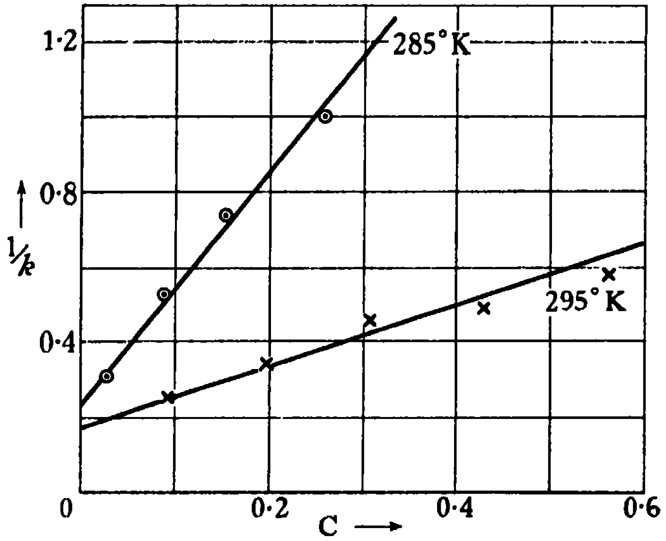

FIG. 4—Velocity constants, k, for the polymerization of XO_2' on N/100 H_2SO_4 at F = 8. C = concentration of XO_2 (moles per 1 mole of XO_2').

In fig. 4 are given the mean results of a series of experiments at two temperatures. It is clear from the linearity of the curves that the formation of the active peroxide at high expansions must be an extremely rapid process.

By extrapolation to $c = 0$ we obtain the energy of activation:

$$\text{F} = 8 \text{ dynes/cm} \quad \left.\begin{array}{l} k_0 \text{ at } 285^\circ \text{ K} = 4{\cdot}3 \text{ min}^{-1} \\ k_0 \text{ at } 295^\circ \text{ K} = 5{\cdot}9_5 \text{ min}^{-1} \end{array}\right\} \text{E} = 5000 \text{ cal}$$

and

$$\alpha \text{ at } 285^\circ \text{ K} = 0{\cdot}71,$$

$$\alpha \text{ at } 295^\circ \text{ K} = 0{\cdot}14.$$

The marked decrease in efficiency of the inhibitor with rise in temperature is to be anticipated, as we know in fact that the polymerization velocity of the stable isomer becomes appreciable at temperatures higher than 303° K. The effect of varying the pressure is rather complex, as will be seen from fig. 5.

It will be seen that the maximum value of dA/dt falls and that the total expansion increases with increase of pressure and at the highest pressures there is a complete change in the type of curve.

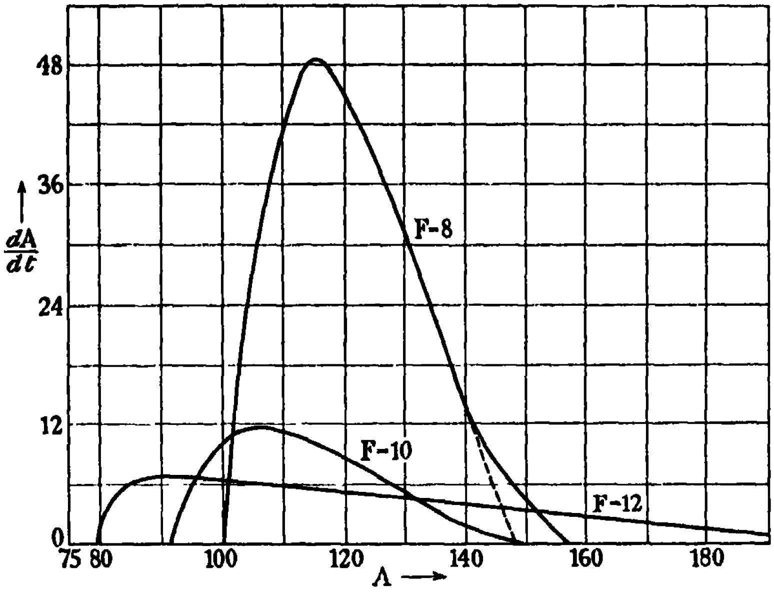

FIG. 5—Effect of pressure on polymerization of XO_2' on N/100 H_2SO_4 at 295° K (1 minute allowed for oxidation at high expansion).

From the analysis given on pp. 131–133 this change in form of curve is to be attributed to an increase in the length of the chain as the pressure is increased. Taking any law relating the expansion to the chain-length (*see* above) the total expansion accompanying the reaction can be interpreted in terms of the mean chain-length of the product, but the results obtained naturally depend on which law is chosen. Hence a separate determination of the chain-length would enable the law governing the expansion to be deduced. Tables III and IV give the observed expansions for a series of polymerizations under varying conditions of temperature and pressure.

The effect of pressure and temperature on the chain-length of the unstable peroxide polymer is very marked, the total variation being about 6 to 1, so that the largest polymer produced would appear on this basis to contain approximately 12 units (assuming a linear law of expansion). As a contrast, the chain-length of the polymer from the stable isomer is scarcely affected by the temperature but increases with the pressure.

We wish to thank Dr. R. S. Morrell for his kindness in providing us with specimens of the anhydride and the British Dyestuffs Corporation for financial and material assistance to one of us (G. G.) which rendered this work possible.

TABLE III—POLYMER FROM UNSTABLE PEROXIDE

Temperature °K	F (dynes/cm)	Expansion (A^2/mol) corrected to pressure of F = 8
285	8	33
290	8	47
290	10	49
295	8	66
295	10	66
295	12	175

TABLE IV—POLYMER FROM STABLE ISOMER

Temperature °K	F (dynes/cm)	Expansion (A^2/mol) corrected to pressure of F = 8
313	12	134
	10	89
	8	74
	6	59
308	12	130
	10	100
	8	80
303	12	124
($CoSO_4$ sustrate)	10	106
	8	77
	6	64

SUMMARY

The mechanism of the " drying " of the maleic anhydride compound of β-elaeostearin in the form of monolayers on aqueous substrates has been examined by means of determination of the surface pressure and phase boundary potentials. These data support the structure proposed by Morrell. Evidence is brought forward to support the view that in

"drying" a primary unstable peroxide is formed, and this can undergo conversion to a more stable isomer or undergo direct polymerization. The energies of activation for oxidation and isomerization are 6500 and 19,000 cal per gm molecule respectively. The kinetics of polymerization are discussed and evidence is presented for the view that a steric factor alone is sufficient to account for the form of the curves obtained; Semenoff's equation for gaseous chain reactions is shown to be one of a number applicable to these condensed chains. Chain-breaking materials may be of two kinds; those inserted in the substrate like hydroquinone and those inserted in the film itself like ethyl myristate. The polymerization of the unstable peroxide, as well as its more stable isomer, has been examined and found to possess energies of activation of the order of 5000 cal/gm mol and 20,000 cal/gm mol respectively.

Quantitative Spectrographic Analysis of Biological Material.

I—A Method for the Determination of Lead in Cerebrospinal Fluid

By J. S. FOSTER, D.Sc., F.R.S., Professor of Physics, G. O. LANGSTROTH, Ph.D., and D. R. MCRAE, Ph.D., Research Associates, McGill University

(*Received August* 14, 1935)

[PLATE 1]

INTRODUCTION

This is the first of a series of papers which deal with the development of quantitative methods of spectrographic analysis as applied to biological problems. In addition to the importance attached to the development of suitable physical methods, some emphasis is placed upon the solution of specific biological or medical problems, and the investigations are carried out with the full co-operation of colleagues whose main interests lie in the associated science. The procedure described in this article has been developed and applied to the determination of lead concen-

trations in the cerebrospinal fluid of humans and animals.[*] We have already learned, however, that it can be adapted as well to problems involving other body fluids and other metallic elements.

It is essentially a method of analysis for "trace" elements, since it is applicable for concentrations between 1×10^{-8} and 2×10^{-6} gm/cc. The precision of a determination is better than 15%. The procedure is microanalytic in that a sample of 1 cc is sufficient for several determinations, and a semi-quantitative measurement can be made with 0·08 cc. This is of considerable importance in certain investigations, since it makes possible the analysis of substances which can be obtained only in small quantities.

The method is based on the fact that when the atoms of a sample are excited by a direct current spark under suitable conditions, the intensity of a lead line is proportional to the lead concentration, if it is small. The spectrum of the fluid to be analysed is photographed before and after the addition of a known amount of lead, and the intensity of a lead line with reference to an "internal standard" line is measured in each exposure. From these data it is possible to calculate the lead concentration of the untreated fluid. The determination is unique for each sample, and consequently the difficulties which may be associated with the use of a predetermined standard intensity-concentration curve do not arise. Two samples can be analysed semi-quantitatively in half an hour and quantitatively in about 3 hours.

It is well known that contamination and loss are usually exceedingly troublesome in analysing for small quantities of an element. One of the chief advantages of the present method lies in the ease with which these troubles are avoided. This is due to the simplicity of the procedure, which requires no ashing or previous treatment for fluids similar to the spinal fluid. Moreover, the small quantity required for a determination makes repeated checks possible even for substances obtainable in limited quantities.

The spectrographic method appears to possess several advantages over the most refined chemical method available for this problem.[†] The latter is qualitative only and requires relatively large samples. It is neither so sensitive nor so fast. Moreover, it is susceptible to contamination owing to the involved procedure and the number of reagents used.

---

[*] An investigation of lead as a possible cause of multiple sclerosis was initiated by Dr. W. Cone and Dr. C. K. Russel of the Neurological Institute, Montreal. The results of medical interest will be published separately.

[†] Harwood and Brophy, 'J. Ind. Hyg.,' vol. 16, p. 25 (1934).

§ 1 of this paper is concerned with a discussion of the general principles underlying this type of spectrographic analysis. § 2 describes the procedure used for the spinal fluid analyses, and § 3 contains the data which justify it.

1—GENERAL CONSIDERATIONS

The procedure for the spinal fluid analyses consists essentially of three operations; the preparation of the sample for excitation, the excitation, and the photographic measurement of the intensities of lead and internal standard lines. A small quantity of the sample to be analysed is placed on the movable plane electrode of a point-plane pair, dried at low pressure, and sparked with a D.C. spark. Intensity measurements are made by the methods developed by Professor Ornstein and his colleagues at Utrecht.*

We have chosen this method of preparing the sample for excitation because accurate results of high sensitivity may be obtained with only a small sample. This makes it possible to analyse substances obtainable in limited quantities, a problem which arises, for example, in work with small animals. Moreover, the importance of using the untreated sample cannot be overestimated in view of the dangers of contamination or loss.

The D.C. spark has been chosen for the excitation because of its high sensitivity, concentration of radiation energy in the arc spectrum, low intensity of background and air lines, and other advantages peculiar to the method of loading the electrodes. In these respects we have found it to be superior to either the arc or the A.C. spark.

Other methods which are sometimes used depend upon the sparking of *solutions* with an A.C. spark, or the introduction of the ashed material into an arc. Both require relatively large samples, and the former is relatively insensitive. The latter is susceptible to contamination and loss in ashing, and is, quantitatively at least, not very reliable even if a rotating arc is used. The justification for the use of any procedure, of course, depends on the accuracy required in the results.

It is important to recognize the fact that a spectroscopic method which is suitable for the analysis of one biological substance may not be equally successful when employed for the analysis of another substance of characteristically different composition. Indeed, marked variations in technique are sometimes necessary. This is so because the results obtained are strongly influenced by the mechanical nature of the material placed on the electrode. For moderately accurate work it appears to be essential that the material adhere strongly to the electrode surface. If ashed or dried material is placed loosely on an arc or spark electrode the results are almost certain to be erratic owing to the scattering action of the discharge. Even when the condition of adherence is fulfilled; the mechanical nature of the load strongly influences the intensities. This is also true of the incidental chemical composition of the material to be tested. For example, the intensity of a lead line obtained by sparking a dried biological sample differs considerably from that obtained by sparking a dried aqueous solution of a lead compound containing the same concentration of lead. This is certainly true of D.C. and A.C. spark excitation, and probably also of arc excitation. Any subsidiary experiments should therefore be carried out with material similar in composition to the material to be tested. For these reasons a thorough investigation into the characteristics of a spectroscopic method should be made for each new type of material examined.

---

* Ornstein, Moll, and Burger, " Objektive Spektralphotometrie " (Vieweg, 1932).

Apart from the speed of the optical apparatus which gives the required dispersion, the sensitivity of a spectroscopic method is limited by the background intensity. It is therefore important for high sensitivity to choose a source which radiates the line spectrum of a sample strongly relative to the background. The accuracy of a quantitative method is principally limited by the degree of reproducibility of the radiation from the source, and the error in the measurement of line intensity. If the errors due to the former can be reduced to a point where those due to the latter predominate (as in the present method), the accuracy is limited by the precision of the intensity measurements. These can be made by the usual photographic methods with an accuracy of 7 or 8%, and under certain conditions with an accuracy of 5%.

One other point should be mentioned. The relative intensity of two lines from different elements, as well as the absolute intensities, depends upon the region of the arc or spark from which the light incident on the plate is radiated. If, in two exposures with the same material, different regions of the source are focussed on the spectrograph slit, the results obtained will not agree. The present method depends upon the statistical distribution on the slit of the light from a large number of sparks. This results in a statistical constancy of the light incident on the plate. If only a few sparks are used the results are worthless for any moderately accurate determination.

2—PROCEDURE

The method of handling the sample before testing is important in view of the danger of contamination. It is stored in Pyrex tubes with

FIG. 1—The point-plane sparking electrodes.

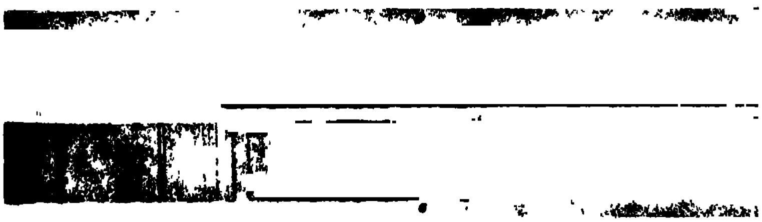

FIG. 4—Typical spectra of spinal fluid in the wave-length region about λ 2833, photographed with the most sensitive optical conditions used in this work. The upper spectrum is that for a fluid containing less than 1×10^{-8} gm/cc of lead, and the lower that for one containing 25×10^{-8} gm/cc. The lead line λ 2833 is marked by a dot.

Pyrex caps. All pipettes and containers, and the apparatus for distilling cleaning acid and water are of Pyrex. All glassware is cleaned before use with boiling concentrated HNO_3 and distilled water. Soft glass apparatus is to be avoided, since lead dissolves from it into the solution. For example, 5 cc of spinal fluid which contained no detectable lead was found to contain 5×10^{-8} gm/cc after a 4-day storage in a carefully cleaned soft glass tube.

The electrodes consist of a point-plane pair as illustrated in fig. 1, Plate 1. The plane electrode on which the load is placed is easily detached from its support for purposes of cleaning and loading. It is about 9 mm long and 6 mm wide. When the crank is rotated the plane electrode moves steadily in a direction parallel to the crank axis, and also backward and forward with an eccentric motion in a direction perpendicular to the crank axis. In several turns of the crank the spark from the fixed point electrode passes over practically the entire surface of the plane. A convenient electrode separation is 3·2 mm, and the point electrode is lined up with the spectrograph slit. Lead-free copper, silver, and aluminium have been used as electrode material. It has been found sufficient to clean the electrodes in concentrated HNO_3 at an appropriate temperature, and in distilled water.

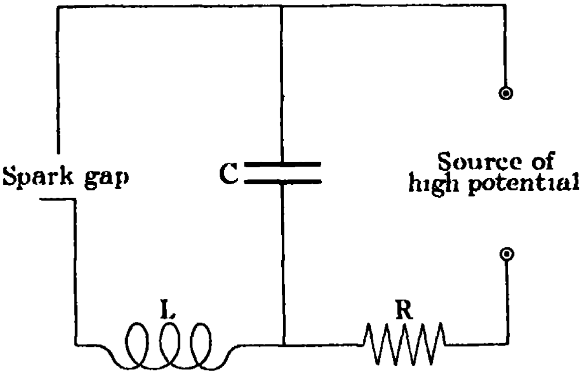

FIG. 2—Sparking circuit.

The sparking circuit is shown in fig. 2. The condenser C has a capacity of about 0·1 mfd, R is a high water resistance, and L an inductance sufficient to eliminate air lines. The circuit is connected to a D.C. source capable of supplying 0·1 ampere at 10 kV. This arrangement produces intermittent sparks at the rate of two or three per second.

A Hilger E2 spectrograph and a spherical condensing lens are used. All optical parts are of quartz.

In testing, a sample of definite quantity (0·08 cc) is placed on the plane electrode with a special capillary loading pipette, and dried at low pressure. This results in a layer of dried organic material which sticks fast to the electrode surface. An exposure of 1·5 minutes is made, in which the spark passes twice over the electrode surface. A second exposure is taken with a sample of the same fluid to which a definite quantity of a known lead solution has been added. The quantity added should be as small as possible compared with the quantity of the fluid in order to make the dilution factor as small as possible. Intensity-blackening calibration marks are then put on the plate with the aid of a step-slit and quartz standard lamp.

It is necessary in accurate work to compare the lead line intensities with those of a line due to some other element which serves as an internal standard. We have found it advantageous to use one of the elements occurring naturally in the sample for this purpose. In the present application intensity measurements were made in all cases on the persistent lead line* $(6p^2)\,^3P_0$—$[6p\,(^2P_{\frac{1}{2}})\,7s]\,2_1^{\circ}$, ($\lambda$ 2833·1). The internal standard line chosen was one of the magnesium lines† $(3s3p)\,^3P_1$—$(3p^2)\,^3P_2$, (λ 2776·8); $(3s3p)\,^3P_0$—$(3p^2)\,^3P_1$, (λ 2778·4), or $(3s3p)\,^3P_{2,1}$—$(3p^2)\,^3P_{2,1}$, (λ 2779·9). The intensities of the lead and the magnesium lines and of the background are determined with the aid of a Moll microphotometer, using the standard methods which have been described elsewhere.‡ A considerable saving of time and labour in making the intensity analyses of the microphotometer records is achieved by use of a ratiometer.§ The intensity measurements are not "heterochromatic," even if the measured lines have a considerable wave-length difference, since essentially the intensities of corresponding lines in different exposures are compared. The intermittency effect introduces no troubles, since reproducibility of results is sought for and, as shown in § 3, may be obtained.

Having determined the relative intensity of the lead to the magnesium line for each exposure in arbitrary but constant units, the concentration of lead in the sample tested is given by

$$R_1/R_2 = C/(C + C_1\Delta v/v), \qquad (1)$$

where R_1 and R_2 are the measured Pb/Mg intensity ratios for the untreated and treated samples, C is the unknown Pb concentration of the untreated sample, and C_1 is the known Pb concentration of the standard solution added. Δv represents the known volume of standard solution added to a volume v of the sample. If the concentration of the internal standard element is high, as it is in the present application, equation (1) is valid only when the dilution factor $\Delta v/v$ is small. In practice the addition of 0·1 cc of the standard solution to 1·0 cc of the sample can easily be made to within 2%.

---

* Geiseler and Grotian, 'Z. Physik,' vol. 34, p. 374 (1925); vol. 39, p. 377 (1926); Bacher and Goudsmit, "Atomic Energy States" (McGraw-Hill, 1932).

† Kayser, "Handbuch der Spectroscopie," vol. 7 (Hirzel, 1934).

‡ Ornstein, Moll, and Burger, *op. cit.*

§ Langstroth, 'Rev. Sci. Instr.,' vol. 5, p. 255 (1934).

3—JUSTIFICATION OF THE PROCEDURE

The following data were obtained either with spinal fluid or with a synthetic imitation containing glucose, urea, sodium chloride, and magnesium sulphate. Magnesium concentrations were of the order of 1×10^{-5} gm/cc, and lead concentrations varied from 6×10^{-8} to 2500×10^{-8} gm/cc.

The examples of Table I show that the Pb/Mg intensity ratio can be repeated with an error which is not more than that introduced in making the intensity measurements. This is the first requisite in developing accurate quantitative methods.

TABLE I—REPRODUCIBILITY OF Pb/Mg INTENSITY RATIOS FOR VARIOUS SOLUTIONS

Observed intensity ratio	0·058 0·051	0·298	0·149	0·575	0·830	1·36	1·25	1·47	2·56
Repeat	0·056	0·325	0·149	0·561	0·750	1·21	1·30	1·43	2·44
Average	0·055	0·312	0·149	0·568	0·790	1·29	1·28	1·45	2·50
Deviation from the mean (%) ..	7	4	0	1	5	6	2	1	2

The relation between the Pb/Mg intensity ratio and the lead concentration is shown in fig. 3. The results for several solutions have been plotted. Since the magnesium content was not identical in each, a number of straight lines which pass through the origin is obtained. It is evident that for any one sample the ratio is proportional to the amount of lead present. This characteristic is the basic foundation for equation (1), § 2. Its application leads to a unique determination for each sample, *i.e.*, there is no necessity for determining initially a standard intensity-concentration curve and using it in the analysis of all subsequent samples. Such a procedure may give rise to difficulties, since it is necessary to keep conditions strictly standard over long periods of time.

As a practical test of the ability of the method to give correct results, samples of spinal fluid and of synthetic solutions containing known concentrations of lead were analysed, and the known and determined values compared. The examples of Table II show the degree of consistency found. The largest discrepancy is 11%, which is satisfactory, in view of the fact that the errors in measurement may be as high as 15%.

A semi-quantitative analysis may be made from a single exposure of the unknown material, by visual comparison of the lead line blackening with those of a standard plate representing various lead concentrations *in a similar solution*. This is possible since under the most favourable conditions the absolute intensity is reproducible to 20%, as shown by the photometrically determined values in Table III. Lead concentrations may be determined with an accuracy depending upon this factor, and upon the degree to which the blackenings may be visually matched or interpolated. An experienced operator can get rather good results when the blackenings are not too great, *e.g.*, for concentrations up to 30 or 40×10^{-8} gm/cc with the most sensitive experimental conditions. The

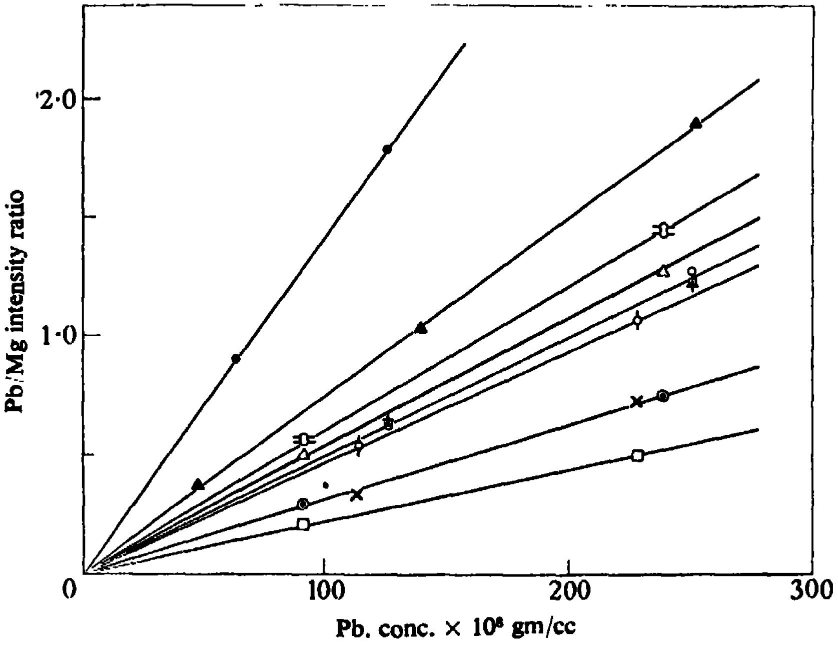

Fig. 3—Relation between the Pb/Mg intensity ratio and the Pb concentration for various solutions. The abscissae and ordinates for the points represented by ⊙ and + should be multiplied by 2, those for the points represented by Δ by 4, and those for the points represented by ▲, ● by 20 and 1·5 respectively.

method is useful for investigations in which the concentrations do not vary over a wide range, since only one-tenth of a cubic centimetre of the unknown is required and the results may be obtained in half an hour.

TABLE II—COMPARISON OF KNOWN AND DETERMINED LEAD CONCENTRATIONS FOR VARIOUS SOLUTIONS

Solution	Pb concentration, gm/cc ($\times 10^{-8}$)			
	$C_1 . \Delta v/v$	Determined	Known	% difference
Synthetic	147	0·00	0	—
		94	91	3
Spinal fluid	138	99	91	10
Synthetic	147	0·00	0	—
		94	91	3
Spinal fluid	147	0·00	0	—
		93	91	2
Synthetic	147	0·00	0	—
		96	91	6
Spinal fluid	113	102	114	11
Spinal fluid	113	117	114	3
Synthetic	250	272	250	8
Synthetic	250	244	250	2
	250	265	250	6
Synthetic	819	189	191	1
	455	542	555	2
Synthetic	1250	1270	1250	2

The degree to which the " absolute " intensity can be reproduced is illustrated by the examples given in Table III. We define "absolute" intensity in this instance as the intensity of a line determined in terms of the radiation at the same wave-length of a band lamp operated under standard conditions. The optical conditions for the exposure, and the excitation conditions are, of course, standard also. The results of Table III were obtained with various synthetic and spinal fluids, and each set of figures refers to a particular sample.

The remainder of this section is devoted to an account of the effect of altering the experimental conditions or the nature of the solution on he line intensities.

TABLE III—PHOTOMETRICALLY DETERMINED REPRODUCIBILITY OF ABSOLUTE INTENSITY FOR VARIOUS SOLUTIONS

Element	Intensities								
				Average			% deviation from mean		
	T	B	L	T	B	L	T	B	L
Mg	71·0	9·6	61·4	70·5	10·1	60·4	1	5	2
	70·0	10·5	59·5						
	55·0	3·6	51·4	53·7	3·7	50·0	7	16	7
	50·0	3·7	46·3						
	55·0	4·3	50·7						
	55·0	3·4	51·6						
	45·0	7·4	37·6	43·8	7·3	36·5	3	1	4
	42·5	7·2	35·3						
	58·0	3·5	54·5	71·8	4·2	67·6	18	20	19
	69·0	4·3	64·7						
	85·0	4·5	80·5						
	75·0	4·5	70·5						
	39·0	6·0	33·0	44·2	7·0	37·1	11	13	11
	49·3	7·9	41·4						
	20·5	2·8	17·7	20·8	2·9	18·0	1	3	2
	21·1	2·9	18·2						
Pb	52·3	7·9	44·0	50·7	8·0	42·7	3	1	4
	49·0	8·0	41·0						
	16·7	12·0	4·7	15·9	11·5	4·4	6	5	7
	15 0	10·9	4·1						
	12·1	4·1	8·0	12·0	4·4	7·7	1	6	5
	11·9	4·6	7·3						
	65·0	5·8	59·2	64·0	6·0	58·0	2	4	2
	63·0	6·2	56·8						
	24·0	9·2	14·8	21·5	8·0	13·5	10	15	10
	19·0	6·8	12·2						
	36·0	6·8	29·2	35·5	6·8	28·6	2	2	2
	35·0	7·0	28·0						
	45·0	4·5	40·5	54·5	4·7	49·8	17	4	19
	64·0	4·9	59·1						
	24·5	4·2	20·3	36·5	4·4	22·2	8	4	8
	28·5	4·5	24·0						

T, B, and L denote respectively the total intensity of line plus background, background, and net line intensity.

Three exposures in which the electrode separations were 3·2, 2·6, and 1·8 mm gave absolute intensities which deviated from the mean by less than 7%, and Pb/Mg intensity ratios which deviated from the mean by less than 10%. Four exposures, in which the point electrode was varied from " very sharp " in the first to " very dull " in the last, gave intensities which varied by less than 8% from the mean.

Naturally the absolute intensities vary with the quantity of the sample placed on the electrode. It is perhaps surprising that the Pb/Mg intensity ratio depends to some extent on this factor. It is therefore necessary to keep the load as accurately constant as possible. The maximum deviation from the mean in a series of weighed loads was 1·6%. Since a 10% variation in the load changes the ratio by only 2 or 3% for the quantity used in these experiments, there can be no question of the entrance of spurious effects due to this cause.

Within certain limits changes in the incidental chemical composition of the sample have no detectable effect on the Pb/Mg intensity ratios.* For example, solutions which were identical except in their sodium content (which varied in the ratio 1 : 4 : 12), gave ratios which varied from the mean by less than 6%. The absolute intensities, however, may vary considerably, depending on the nature of the original substance and the extent of the changes in incidental composition.

The molecular form in which the lead is present in the sample has no detectable effect upon the intensities. This conclusion was reached after the examination of similar samples containing the lead as the acetate, chloride, or sulphate. These three lead compounds were chosen because of their difference in boiling-point. The melting- and boiling-points are respectively acetate 75° C and 280° C, chloride 501° C and 950° C, and sulphate 1170° C (b.p. unknown).

In view of the results of these subsidiary experiments, we believe that the small differences in conditions which may occur from time to time do not seriously affect the reliability of the method. This conclusion is upheld by the consistency of the results obtained with known solutions.

We are indebted to the other members of the group concerned with the study of lead pathology, namely Dr. W. Cone, Dr. C. K. Russel, Dr. R. U. Harwood, and Miss D. Brophy, for their helpful cooperation. We are also indebted to the Rockefeller Foundation for financial assistance.

---

* This refers only to solutions, such as the spinal fluid, which contain appreciable quantities of other compounds to aid in carrying the spark current. It must be kept in mind that the results obtained also depend upon the mechanical nature of the dried material on the electrode, and that the method as presented here is not suitable for the examination of every biological fluid, *e.g.*, whole blood.

SUMMARY

A quantitative spectroscopic method for the determination of small concentrations of lead in certain biological material is described. It is valid for concentrations between 1×10^{-8} and 2×10^{-5} gm/cc, and the precision of a determination is better than 15%.

The ability to make determinations with very small samples, and to use the material without previous treatment, are important features of the method.

The general considerations on which this type of analysis is based are discussed.

The Oxygen Afterglow

By ERIC M. STODDART

(*Communicated by F. G. Donnan, F.R.S.—Received June* 28, 1935)

Lord Rayleigh[*] has drawn attention to an early paper of his[†] which deals with the problem of whether or not, at low pressures, pure oxygen possesses an afterglow. The present author made no reference to this early paper, in an investigation on this same problem,[‡] owing, as Lord Rayleigh conjectures, to the inexplicit title of the early paper. Incidentally, this early paper of his seems to have been completely ignored by other workers in this field, Herzberg[§] and Lewis.[||]

Lord Rayleigh believes that if I had made certain slightly different experiments, I would have been led to conclusions identical with his own. He points out that the electrodeless ring discharge and the high frequency electrodeless discharge differ from each other in nature, and he considers that I did not appreciate their difference. He was led to this erroneous conclusion by the inexplicitness of my paper.

A short time previously, I[¶] had made an investigation on the hydroxyl radicle particularly with reference to its formation in the presence of

[*] 'Proc. Roy. Soc.,' A, vol. 150, p. 34 (1935).

[†] 'Proc. Phys. Soc.,' vol. 24, p. 4 (1911).

[‡] 'Proc. Roy. Soc.,' A, vol. 147, p. 454 (1934).

[§] 'Z. Physik,' vol. 46, p. 878 (1928).

[||] 'J. Amer. Chem. Soc.,' vol. 51, p. 654 (1929).

[¶] 'Phil. Mag.,' vol. 18, p. 409 (1934).

oxygen atoms. During this work, I had constantly observed the oxygen afterglow, and at that time believed that oxygen free from nitrogen could possess this afterglow, provided the apparatus had poisoned surfaces. That this was so seemed to be shown by the experiments of Lewis,[||] and I attempted to repeat Lewis's work.

Reference to Lewis's paper (p. 656) will show that he employed a powerful ring discharge in his experiments, and a repetition of them, using very similar apparatus, seemed to show that (i) pure oxygen in de-gassed vessels did not possess an afterglow, (ii) contrary to the observations of Lewis, pure oxygen in vessels with surfaces poisoned by water vapour was also glowless, (iii) oxygen containing up to 5% nitrogen was glowless in vessels with unpoisoned walls, (iv) oxygen containing 5% nitrogen possessed a weak afterglow in vessels with walls poisoned by water vapour. In all my experiments, both forms of electrodeless discharge were employed and the results were identical. Details of the discharges appear in my paper.[*]

Consideration of these experiments after their completion seemed to show that the glass apparatus was capable of considerable improvement. The chief objections were that (*a*) the metal filament used for synthesis of the water vapour[†] was very close to the observation bulb (capacity of 4 litres), and it was possible for stray discharge currents to be set up, (*b*) although the gases were prepared by the thermal decomposition of potassium permanganate and sodium azide, there was no means of decomposing these bodies without passing all of the evolved gases through the main apparatus.

Experimental result (iv) using a ring discharge was first verified under these original conditions, and then the apparatus was redesigned to overcome these objections. The redesigned apparatus was used for a repetition of the whole work, and the convenient high frequency discharge was used in place of the ring discharge since the results of the two discharges had been found to be identical. In the repeated work, findings (i), (ii), and (iii) were unaffected, but the gases in (iv) were found to be glowless. Little mention of the early work using ring discharges was made in my paper, thus Lord Rayleigh was led to believe that I would have obtained different results with their aid.

In his communication[‡] he writes that his work was in " substantial agreement " with my experiments using the high frequency discharge. I would like to point out the observations of other investigators, all using

[*] ' Proc. Roy. Soc.,' A, vol. 147, p. 455 (1934).

[†] ' Proc. Roy. Soc.,' A, vol. 147, p. 457 (1934).

[‡] ' Proc. Roy. Soc.,' A, vol. 150, p. 35 (1935).

electrodeless ring discharges: (i) Thomson* observed the yellow afterglow in pure oxygen; (ii) Herzberg (*loc. cit.*) observed the glow in oxygen only when it contained at least 1–2% nitrogen, using poisoned vessels; (iii) Lewis (*loc. cit.*) observed the glow in oxygen free from nitrogen, in poisoned vessels; (iv) whilst the present writer, using high frequency discharges, never observed the glow with oxygen containing up to 40% nitrogen, in poisoned vessels; and other observations made with ordinary vacuum tubes are: (v) Strutt† found that when " oxygen perfectly free from nitrogen " was used, " the afterglow is very faint compared with that observed when nitrogen is present "; and (vi) the present author found that pure oxygen in an electrode tube with poisoned walls possessed no glow until it contained a trace of nitrogen. Taking these conclusions together, it is seen that little agreement exists. I previously pointed out (*loc. cit.*) that in the experiments of Lewis it was possible that traces of nitrogen were present in his oxygen. Assuming this to be true for the experiments of Thomson (i) and to a minor degree in the case of Strutt (v), then my conclusion--viz., that an afterglow is only obtained in oxygen which contains a trace of nitrogen provided (*a*) that the walls of the system are poisoned, and (*b*) that the discharge is of a form which can synthesize nitric oxide and ozone during the time of its duration—allows these facts to be understood. Whereas my electrodeless high frequency discharges were quite incapable of synthesizing nitric oxide, the ring discharges of Herzberg were able to do so provided the oxygen contained over 1–2% nitrogen, and those of the other workers were very efficient in this process. That the electrodeless discharge can vary in its proficiency in this respect is indicated by my experiments (*loc. cit.*, p. 464).

Strutt† found that when oxygen perfectly free from nitrogen was run through a vacuum tube, the afterglow was very faint compared with that observed when nitrogen was present. Use of a condensed discharge or an electrodeless ring discharge under these conditions produced a white afterglow. Since the white afterglow was destroyed when the gas was dried over phosphoric anhydride, whereas the yellow oxygen-nitrogen glow was unaffected by this process, Strutt concluded that the white afterglow depended upon the presence of moisture in the gas phase. Certain spectroscopical observations also lead to this view. The following experiments show the relationship between the yellow glow and water vapour, and are of interest regarding these observations by Strutt.

The apparatus, fig. 1, consisted of a simple discharge-tube A fitted with aluminium electrodes, the exit gases leaving by the spectroscopic observation tube B, fitted with a quartz window. The system was protected from vapours arising from the oil pumps, by a liquid air trap inserted into the pumping line C. Electrolytic oxygen, supplied by the British Oxygen Company in cylinders, could be passed through the bubbler D, containing vacuum distilled water, or alternatively, through the tube E containing phosphoric anhydride. When the oxygen was passed through D, the trap F and the coil G were immersed in refrigerants, thereby controlling the amount of water vapour carried into the apparatus by the gas stream. Manipulation of the gas regulator H enabled the oxygen to stream through the apparatus, the equilibrium pressure being maintained at about 0·2 mm. The amount of water vapour carried by the oxygen was varied, whilst an uncondensed or a condensed discharge was maintained in the discharge-tube. It was found that the oxygen contained sufficient nitrogen to enable a powerful afterglow to be obtained. The glowing exit gases travelled a considerable distance towards the pumps before extinction, and this distance varied with the amount of water vapour present in the gas. In an uncondensed discharge, the approximate measurements given in Table I were obtained.

---

* 'Phil. Mag.,' vol. 32, p. 321 (1891).

† 'Proc. Phys. Soc.,' vol. 24, p. 4 (1911).

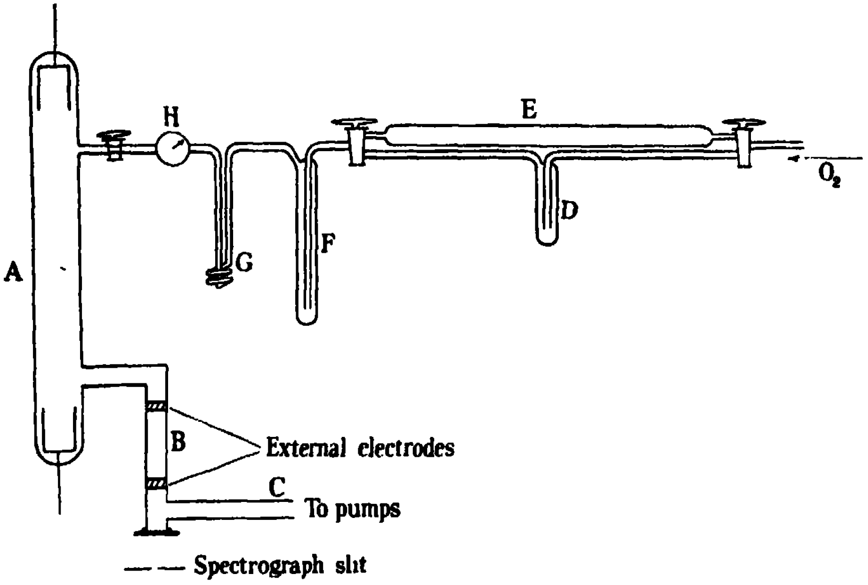

FIG. 1.

TABLE I

Temp. of refrigerant, ° C	−180	−80	−60	−40	−22	0
Distance from tube, cm........	80	80	80	75	38	20

It must be noted that a very powerful " cleaning-up " by the discharge occurred, thereby making it difficult to obtain identical surface conditions for each experiment. Usually, the entire apparatus was filled with damp oxygen and allowed to stand overnight. When the measurements were required, low temperatures were used to start with and the amount of water vapour carried by the oxygen gradually increased. The discharge current was passed for a few seconds only, for each measurement, the cleaning-up action of the discharge thus being minimized. Although such measurements can only be approximate, the quenching effect of water vapour in the gas phase on the afterglow is well marked.

The oxygen was now dried by being passed through the tube E, the vessels G and F being cooled in liquid air. At first, the afterglow was intense, but it quickly diminished in intensity, as the discharge current was continually passed, Table II.

TABLE II

Time, min	0	5	10	15	20	25	30
Distance glow travelled from tube, cm	75	34	18	8	2	1	1

This effect is clearly due to the cleaning-up action of the discharge. Water vapour adsorbed by the glass surfaces is slowly removed; consequently the surfaces are soon in a clean condition, thereby enabling wall reactions to take place in preference to gas phase reactions, the latter being made manifest by the presence of an afterglow.

During this cleaning-up process, the gases travelling through the observation tube B were excited by a subsidiary discharge, supplied from a small valve oscillator (using a Marconi L.S.5 valve), and spectrally examined with a small quartz spectrograph. It was found that while an afterglow was existent, the principal Balmer lines of hydrogen, the principal hydroxyl bands, and bands due to nitric oxide, were all observable. Once the afterglow had disappeared, due to the cleaning action of the main discharge, the hydrogen lines and the hydroxyl bands almost vanished, but the nitric oxide bands remained. Thus it is clear that the yellow oxygen afterglow is best obtained with (*a*) a minimum of water vapour in the gas phase and (*b*) a maximum amount of water vapour adsorbed on the glass surfaces, a conclusion which is in agreement with my previous experiments, as well as the observations of Copeland,* Crewe and Hulbert,† and Lewis (*loc. cit.*).

When gases are dried by standing over phosphoric anhydride, it is usually believed that the water vapour adsorbed on the surface of the glass is removed. Strutt found, however, that the yellow glow was unaffected by this drying process; an observation which is in direct contradiction to the above experiments.

---

* 'Phys. Rev.,' vol. 36, p. 1221 (1930).

† 'Phys. Rev.,' vol. 30, p. 124 (1927).

Again, it is seen that although Strutt found the white afterglow to be destroyed by drying over phosphoric anhydride, this is not conclusive proof that it owes its origin to water vapour in the gas phase, since the drying will undoubtedly clean the poisoned surfaces of the apparatus by removal of the adsorbed water vapour, thus leading to the non-existence of the glow.

In my previous paper (p. 462), it was shown that pure oxygen in electrode tubes with poisoned walls was perfectly glowless. Addition of a trace of nitrogen, by the heating of a platinum filament, the surface of which contained adsorbed nitrogen, restored the glow. The glow thus obtained was very pale—almost white, and in general my observations on the yellow afterglow indicate that as the nitrogen content decreases the glow becomes paler, particularly at pressures below 0·16 mm. This seems to indicate that Strutt's white afterglow may be a very weak yellow glow which has been enhanced by a condensed discharge.

In conclusion, the author wishes to thank Professor F. G. Donnan, C.B.E., F.R.S., for the interest with which he followed this work.

SUMMARY

It is shown that many of Lord Rayleigh's criticisms of my earlier paper are untenable. A survey of observations concerning the oxygen afterglow is given, and my earlier conclusions are justified. Experiments are described showing the effect on the oxygen afterglow of water vapour in the gas phase and adsorbed on the surfaces of the vessels. These observations are in agreement with the results of other workers.

The Dielectric Loss Characteristics of a Chlorinated Diphenyl

By WILLIS JACKSON, D.Sc., A.M.I.E.E., Magdalen College, Oxford

(*Communicated by E. V. Appleton, F.R.S.—Received June* 28, 1935)

INTRODUCTION

Considerable attention has been devoted of recent years to the development of synthetic insulating materials devoid of the uncertainties and limitations of naturally occurring dielectrics and their modifications (such as cellulose, rubber, oil, and wax compounds). Into this category falls a range of non-inflammable chlorinated diphenyl compounds known in this country as Permitol. The members of this range consist of a double benzene ring as basis with which chlorine atoms have been combined. By controlling the degree of chlorination, it is possible to produce compounds ranging at room temperatures from crystalline solids to liquids of relatively low viscosity. The present paper deals with a study of the dielectric behaviour over the frequency range 50 to 10^7 cycles per second and at temperatures extending from − 20 to + 80° C of a sample of chlorinated diphenyl classed as suitable for condenser impregnation. Its viscosity at 60° C is that of a light transformer oil, but with temperature decrease the viscosity increases very rapidly until the material becomes a glassy solid about − 10° C.

One of the most desirable characteristics of a material to be used for this purpose is a high dielectric constant (permittivity) allied to freedom from dielectric loss. A high permittivity is usually associated, however, with the presence of polar molecules in the material, and these, according to the Debye theory of dielectric absorption, must be responsible for dielectric loss in alternating electric fields under suitable conditions of temperature and frequency. For a dilute solution of polar molecules in a non-polar solvent, the power factor passes through a maximum at a frequency given by

$$f = kT/8\pi^2 a^3 \eta, \qquad (1)$$

where k is Boltzmann's constant, T is the absolute temperature, a is the radius of an equivalent sphere representing the dipole molecule or group, and η is the viscosity opposing molecular orientation. The power factor becomes zero at both zero and infinite frequency. At sufficiently low frequency the polar molecules orient freely in sympathy with the electric field variations ; the power factor is therefore low and the dielectric constant high ; but at high frequencies the sympathetic orientation of the polar molecules is prevented by their viscous environment, their contribution to the total dielectric polarization becomes negligible, and the power factor and dielectric constant are together low. Similar power factor and permittivity changes result on variation of the temperature, and with it the viscosity at constant frequency. It is evident that maximum dielectric constant and low dielectric loss for a given polar material can exist simultaneously by a suitable choice of the operating conditions of temperature and frequency.

The partially chlorinated diphenyl molecule is a permanent electric dipole, and while it is not to be expected that the Debye theory of dilute solutions can be accurately applied to its behaviour in bulk, the above type of loss characteristic is to be expected, and is, in fact, demonstrated very emphatically by the experimental work recorded in the paper. It is found that the power factor-temperature curve for the material is extremely sensitive to temperature variation, so much so that a 20° C change is sufficient to convert it from a good to a quite useless dielectric medium.

It has frequently been doubted whether the necessary physical conditions for the appearance of a Debye power factor maximum at frequencies as low as 50 cycles per second can arise at normal temperatures. Since it has been possible in the present work to follow this maximum throughout the frequency range from 10^7 to 50 cycles per second within the temperature span from $+ 40$ to $- 5°$ C, this doubt can no longer be maintained.

THE METHODS ADOPTED FOR POWER FACTOR MEASUREMENT

The frequency range mentioned was covered in steps and a power factor-temperature curve for the dielectric obtained at each of the chosen frequency values. Over the range $10^6 - 10^7$ cycles per second, the method employed was a resonance substitution one, the circuit diagram of which is shown diagrammatically in fig. 1. In order to avoid any assumptions regarding zero loss in the comparison air condenser, and at the same time to allow for any residual loss in the test condenser not arising from the inserted dielectric, use was made of two condensers C and C_x identical in construction. A description of these condensers and of the arrangements for their temperature variation has been given elsewhere.* The dielectric to be investigated was poured into C_x and the capacitance of C, having air dielectric, was then adjusted until it equalled that of C_x. When this adjustment had been made the circuit remained in tune to the chosen frequency when the condenser was changed from C_x to C at the switch S. The power factor of the dielectric of C_x was derived from the difference between the total circuit power factor when the capacitance was formed by C_x and by C. In the higher part of this frequency range the power factor was deduced from the width of the resonance curve delineated on the thermionic voltmeter V by suitable incremental changes in the oscillator frequency, but in the lower part it was more convenient to employ resistance insertion at the resonant adjustment.

---

* Jackson, ' Proc. Roy. Soc.,' A, vol. 150, p. 197 (1935).

In the audio frequency range the dielectric power factor was determined by arranging the test and air condensers to form in turn one arm of a low-voltage Schering bridge. The 50-cycle measurements included in the paper are due to the British Thomson Houston Company and were also obtained on a Schering bridge, but at much higher voltage gradients.

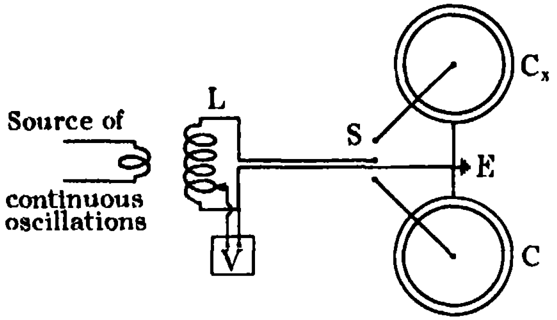

FIG. 1—C_x, test condenser; C, identical air condenser; S, change-over switch; V, thermionic voltmeter; E, earthpoint.

STATEMENT AND DISCUSSION OF THE RESULTS

The combined results of the power factor measurements are shown in fig. 2. It is seen somewhat surprisingly that in a frequency change from 50 to 10^7 cycles per second the position of the power factor maximum is shifted upwards in the temperature range by only about 45° C, and also, but quite analogously, that the power factor-temperature curves are exceedingly sharp. With the exception of the 50-cycle curve A, the curves at the several frequencies are of closely the same height. The maximum power factor, 21·5%, is so large as to render the material valueless for dielectric purposes in the immediate vicinity. Only a 20° C temperature displacement from this point is necessary, however, to improve the power factor to a desirable value of less than 1%. The discrepancy in the height of the 50-cycle curve can probably be accounted for in the fact that this curve relates to a different sample of the same material, and the author is informed that such differences are to be expected from sample to sample. This observed independence of the power factor maximum of frequency and temperature is in agreement with the existing Debye theory. The theory would lead to the expectancy of an increase in height of the curve with decrease in temperature; but for the 10% change in absolute temperature from the peak of curve H to that of B this effect would not be very important.

The expression (1) giving the condition for the appearance of the power factor maximum as a function of the frequency, the temperature and the physical constants of the dielectric medium, and also the corresponding expressions for the variation of the power factor with frequency and temperature separately have been derived by Debye for the case of dilute solutions of polar molecules in non-polar solvents. The treatment for a polar material in bulk has not yet been developed, and this fact should be borne in mind during the subsequent discussion of the results.

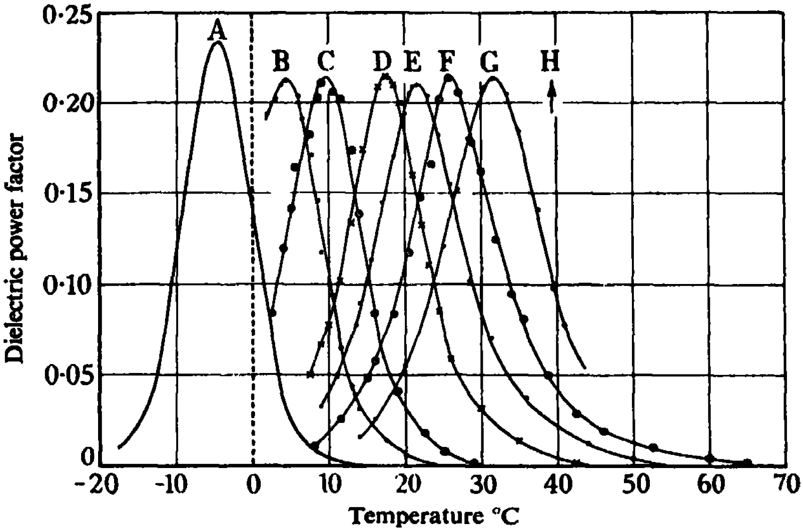

FIG. 2—Frequency values in cycles per second—A, 50; B, 10^3; C, 6×10^3; D, 10^5; E, $2 \cdot 95 \times 10^5$; F, $9 \cdot 5 \times 10^5$; G, $2 \cdot 75 \times 10^6$; H, $1 \cdot 09 \times 10^7$.

The Debye theory gives the power factor as a function of frequency in the form

$$\tan \delta = \frac{\varepsilon_0 - \varepsilon_\infty}{\sqrt{\varepsilon_0 \varepsilon_\infty}} \cdot \frac{A\omega\tau}{A^2 + \omega^2\tau^2}, \tag{2}$$

where $\tau = \frac{4\pi a^3 \eta}{kT}$ is the relaxation time of the polar molecules in the viscous environment concerned; A = $\sqrt{\frac{\varepsilon_0}{\varepsilon_\infty}}\cdot\left(\frac{\varepsilon_\infty+2}{\varepsilon_0+2}\right)$ and ε_0, ε_∞ are the dielectric constant values at zero and infinite frequency ($\omega/2\pi$) respectively. The power factor has its maximum value

$$\tan\delta_m = \frac{\varepsilon_0-\varepsilon_\infty}{2\sqrt{\varepsilon_0\varepsilon_\infty}}, \tag{3}$$

at the frequency for which

$$\omega = 2\pi f = \frac{A}{\tau} = \frac{kT}{4\pi a^3\eta}\cdot\sqrt{\frac{\varepsilon_0}{\varepsilon_\infty}}\left(\frac{\varepsilon_\infty+2}{\varepsilon_0+2}\right). \tag{4}$$

The important criterion governing the magnitude of the power factor maximum is the factor ($\varepsilon_0-\varepsilon_\infty$), and this may be estimated from a curve such as that of fig. 3, in which the dielectric constant is plotted as a function of the temperature at a constant frequency of 0·95 × 10^6 cycles per second. This curve corresponds to the power factor-temperature curve F of fig. 2 and demonstrates that the region of dielectric constant change coincides with that of appreciable power factor. As previously implied, ε_∞ corresponds to a state where, at a given frequency, the temperature is so low that the movement of the dipole molecules is completely restricted and they are unable to make any resultant contribution to the total polarization; this may be said to occur in the portion AB of the curve of fig. 3, so that ε_∞ may be taken as 2·80. Similarly, it may be inferred that the polar molecules are able to orient in perfect sympathy with the alternating electric field in the portion CD of the curve. The maximum value of the dielectric constant may be taken, therefore, as a measure of ε_0, although this is likely to be an underestimate. If these values for ε_0 and ε_∞ are substituted in equation (3), the maximum power factor tan δ_m is given as 0·233, which is in fair agreement with the experimental value 0·216.

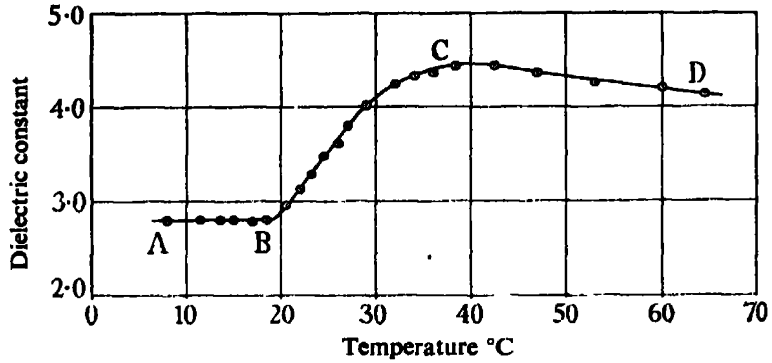

FIG. 3—Frequency of measurement, 9·50 × 10^5 cycles per second.

Consideration of equation (4) permits an examination of the physical factors controlling the position of the power factor maximum in the spectrum of frequency and temperature. As mentioned previously, the equation as it stands cannot be expected to apply rigorously to a perfectly concentrated polar material, but in general form it should be correct. Thus the frequency of maximum power factor can reasonably be written as a function of the absolute temperature T, the viscosity opposing dipole orientation η and the volume of the orienting dipole V, in the form

$$f = K \cdot \frac{T}{V\eta} \cdot \qquad (5)$$

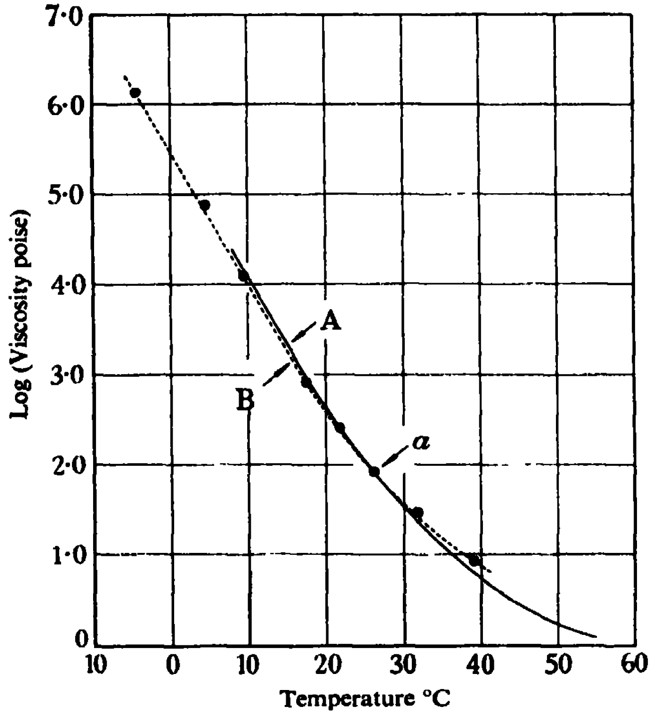

FIG. 4—A —— measured viscosity-temperature curve; B - - ⊙ - - calculated curve as determined from the position of the peaks of the curves in fig. 2. For the purpose of comparison the curves have been made to coincide at the point *a*.

The volume V being a characteristic of the material may be expected to be a constant, and since several corresponding values of f and T are given by the power factor-temperature curves of fig. 2, a quantity proportional to η can be calculated and its variation with temperature studied. This quantity has been calculated from the position of each of the peaks of the curves, and its logarithm plotted against the temperature in curve B, fig. 4.

Each of the points on this curve corresponds to a different frequency, and a certain amount of evidence is available to suggest that the viscosity decreases with rise in frequency. The possibility of a frequency dependence may be investigated by comparing the viscosity-temperature variation derived as above with an independent determination of this variation by viscometric measurements. These latter measurements were carried out over the temperature range 13–55° C in an equipment, of which a description will be published later, developed by Professor R. V. Southwell and Dr. A. Gemant. The logarithm of the measured viscosity values is plotted as a function of the temperature in curve A, fig. 4. The derivations from equation (5) give only a quantity proportional to the viscosity, but for the purpose of comparing the temperature variation, curve B has been made coincident with curve A at the point *a*. It is seen that the two curves are very similar in shape, with the calculated curve of somewhat smaller slope. If the viscosity were dependent on frequency in the manner suggested, the calculated curve B would be expected to have a greater slope than that of curve A, and it seems, therefore, that there is no such frequency dependence for this material.

TABLE I

Frequency c.p.s.	Temperature of power factor maximum		Viscosity poise	Apparent volume V in cu A	Apparent equivalent radius "*a*" A
	°C	°abs			
6×10^3	9·5	282·5	$1{\cdot}45 \times 10^4$	22·0	1·77
10^5	17·5	290·5	$9{\cdot}10 \times 10^3$	22·0	1·77
$2{\cdot}95 \times 10^5$	21·8	294·5	$2{\cdot}55 \times 10^2$	26·5	1·85
$9{\cdot}5 \times 10^5$	26·0	299·0	83·2	26·0	1·84
$2{\cdot}75 \times 10^6$	31·7	304·7	24·5	30·5	1·94
$1{\cdot}09 \times 10^7$	39·0	312·0	6·20	31·5	1·96

If the experimentally determined viscosity value at the position of the peak of a power factor-temperature curve be substituted in equation 4, along with other known data, an apparent value can be obtained for the dimension "*a*," or the volume $V = 4/3 \, . \, \pi a^3$, of the orienting portion of the chlorinated diphenyl molecule. This process has been carried out for each of the curves of fig. 2, and the results of the calculations are given in Table I.

The variation observed in the computed value of V is consistent with the disagreement between the two curves of fig. 4. The mean value of V is about 26·5 cu A, and the corresponding apparent value of the equivalent radius for the orienting portion of the molecule is $1{\cdot}85 \times 10^{-8}$ cm.

The apparent molecular volume found here is of the right order of magnitude, but somewhat too small. The volume of the molecule may be estimated by use of Sugden's parachor values; thus taking $V = 2 \cdot 0 \times 10^{-25}$ P cc, the volume of a monochlorodiphenyl molecule $C_{12}H_9Cl$ is 83·4 cu A. This is to be increased by 7·4 cu A for each extra chlorine atom substituted in the molecule. An analysis of the permitol by sodium peroxide fusion in a Parr bomb gave the chlorine content of the material as 56·3% by weight. This suggests an average of about 4 chlorine atoms per molecule. (The Carius method of determining the chlorine content gave a very low figure—36%.)

The smallest possible polar group in the molecule capable of independent orientation is monochlorphenyl with a volume of 45·4 cu A. The substitution would have to be ortho- or meta- for this independent rotation, and even then the independence would only apply for rotation of the group about one axis, and still but partially. The actual mixture presumably contains substituents mainly in ortho- and para-positions. The latter require the full volume, or something even larger, since the dipole is parallel to the long axis of the molecule. It follows that the mean value to be taken for the volume of the molecule cannot be much less than 80 cu A, as compared with the mean value of 26·5 cu A derived from the experimental results.

It is observed from the preceding table that the apparent volume rises somewhat with increasing temperature (and frequency) from 23 cu A at 10° C (10^4 cycles) to about 33 cu A at 40° C (10^7 cycles). This sort of behaviour is fairly characteristic. The outstanding example is, of course, glycerol with an apparent molecular volume of 0·18 cu A. Debye is now studying the possibility of attributing such results to the "quasi-crystalline" structure of liquids. It is in agreement with this theory that the apparent molecular volume approaches the true value as the temperature is raised, since rise of temperature tends to destroy any quasi-crystalline structure present.

The experimental work recorded was carried out in the Engineering Laboratory, Oxford. The author is indebted to the British Thomson Houston Company for supplying the chlorinated diphenyl sample, to Mr. F. C. Frank for undertaking the chemical analysis, and to the Department of Scientific and Industrial Research for a grant which enabled the research to be performed under the direction of Mr. E. B. Moullin.

SUMMARY

The paper describes a series of power factor measurements on a chlorinated diphenyl over the frequency range 50 to 10^7 cycles per second and at temperatures from − 15 to + 80° C. The results are discussed in terms of the Debye theory and related to the chemical constitution of the material. It has frequently been doubted whether the necessary physical conditions for the appearance of a Debye power factor maximum at frequencies as low as 50 cycles can arise at normal temperatures. Since it has been possible with this material to follow the maximum through the above frequency range within the temperature span − 5 to + 40° C, and relate this behaviour to the variation of the measured viscosity coefficient, this doubt can no longer be maintained.

The Crystal Structure of Ice at Low Temperatures

By E. F. BURTON, F.R.S.C., and W. F. OLIVER, M.A., The McLennan Laboratory, Department of Physics, University of Toronto

(*Communicated by Sir John McLennan, F.R.S.—Received July* 8, 1935)

[PLATE 2]

1—INTRODUCTION

The use of X-rays in the study of the mechanism of crystal growth showed that if the vapour of a substance came in contact with a cold surface, it condensed to form a solid, the structure of which depended on the temperature of the condensing surface.[*][†] The authors announced recently[‡] that ice formed by condensation at low temperatures and pressures also changed form with temperature. Details of the apparatus and the results follow in this paper.

2—METHOD AND PRELIMINARY WORK

Analysis was carried out by the Hull-Debye-Scherrer method, using the K_α doublet of copper. With a camera of 5 cm radius, photographs were obtained in 4 to 6 hours, using a Shearer tube operated at 30 kV (R.M.S.) and 10 mA. The K_β line was removed from the radiation by a filter of nickel foil.

---

[*] Ingersoll and De Vinney, ' Phys. Rev.,' vol. 26, p. 86 (1925).

[†] *See* reference in Clarke's paper, " Symposia on Quantitative Biology," vol. 11, p. 6 (1934).

[‡] Burton and Oliver, ' Nature,' vol. 135, p. 505 (1935).

The method of forming the ice was essentially that described in § 3. In the preliminary work, the ice was formed by condensation of water molecules at low pressure on a small copper tube, through which liquid air, or methyl alcohol cooled by solid carbon dioxide, had been circulated.

A marked change was observed in the form of the ice, the structure depending on the temperature of the condensing surface. At the higher temperature, the X-ray pattern consisted of sharp diffraction maxima characteristic of the close-packed hexagonal structure, while at the lower temperature there were two very diffuse lines indicating the amorphous character of the condensate.

Considerable difficulty was encountered in determining the temperature at which the change in structure occurred. Attempts to maintain some intermediate temperature at a constant value for 4 hours, by the circulation of dry air which had been cooled previously by a liquid air bath, were unsuccessful. It was therefore necessary to devise some other means of maintaining the condensing surface at intermediate temperatures. The method described in the second paragraph of § 3 proved satisfactory.

3—APPARATUS

The apparatus is shown diagrammatically in fig. 1. The camera (right in plan and elevation) consisted of a brass cylinder, about 10 cm in diameter, closed at the bottom and fitted with a ground lip LL at the top. A German silver flask (left) of special design was constructed; it had a ground lip L′L′ arranged to fit the lip of the camera. With a liberal application of vacuum grease this made an air-tight joint.

The vapour was condensed on a small copper rod v, soldered into the Dewar flask at x and y. Heater coils h_1, h_2, constructed of constantan wire, which had been oxidized for insulation purposes, were wound on the rod in the position shown on the diagram. A coating of shellac between the rod and the coils increased the insulation. The current through each coil was adjusted so that the temperature at both ends of the sample was the same, as measured by the thermo-couples t_1 and t_2. All leads were brought out through bakelite stoppers waxed into cup-shaped tubes inserted in the outer wall of the Dewar flask. A thin film of wax was allowed to flow round each wire. With this arrangement, a constant temperature of any value could be maintained almost indefinitely.

With a rod 0·2 cm in diameter, and a metal of high thermal conductivity such as copper, the temperature gradient over the sample was small.

The vapour entered the camera from a glass tube B, which was sealed into the bottom of the camera. Water placed in the tube B was frozen by means of liquid air, during evacuation of the camera. When evacuation was complete the liquid air was replaced by a bath of ice and water. The temperature of the ice in B did not rise above −25° C, as indicated by the thermo-couple t_3. The ice which was formed by the condensation of the vapour on the rod between the thermo-couples t_1 and t_2 was used as the specimen. When a layer of the order of 10^{-3} cm was formed, the tube B was surrounded again by liquid air, to prevent further sublimation.

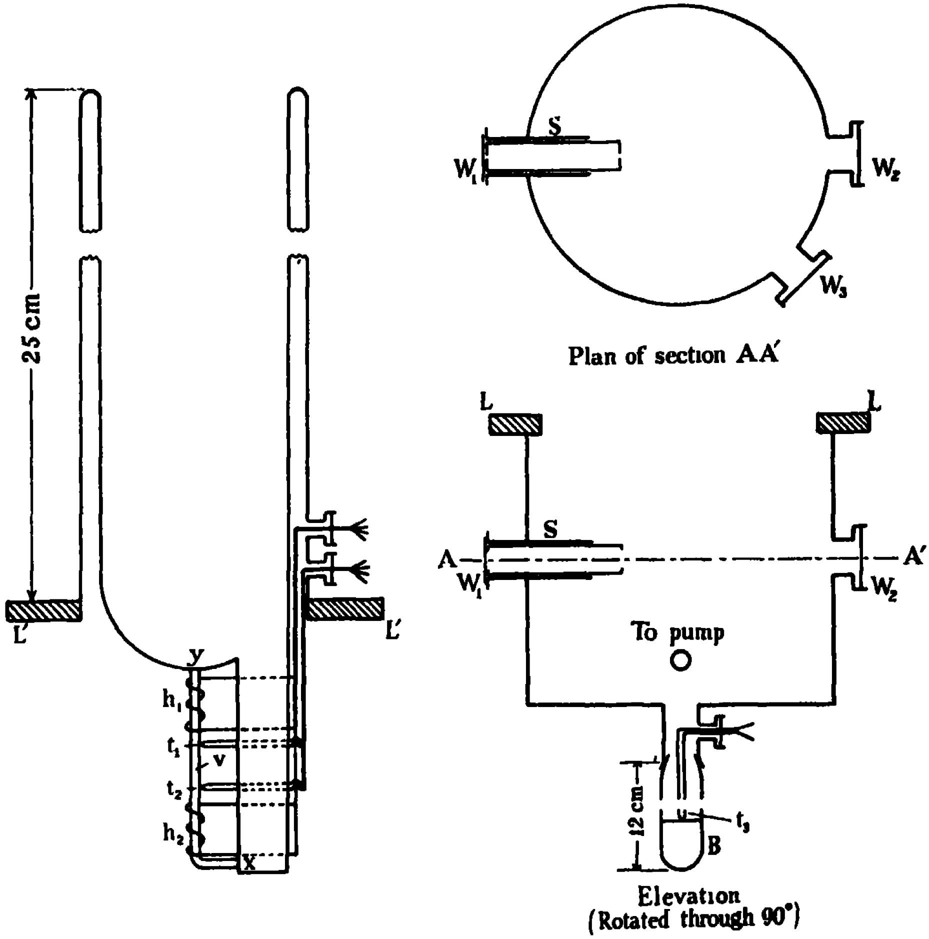

Plan of section AA′

Elevation (Rotated through 90°)

FIG. 1—Apparatus used in the study of the structure of ice formed from the vapour.

When the ice was allowed to form slowly, it was assumed that the temperature of the condensing surface was that indicated by the thermo-couples. The camera was connected to the pumps continuously. The air pressure in the camera was of the order of 10^{-5} cm mercury.

The X-ray beam passed through an aluminium window W_1, was defined by the slit system, S, and was allowed to fall on one edge of the specimen. A thin glass window, W_2, diametrically opposite, was used for aligning the camera. A glass window, W_3, extending the full height of the camera, provided for observation of the specimen.

The film holder (not shown in the diagram) was a brass cylinder which fitted into a groove in the camera, the film itself being held in position by spring clips.

4—RESULTS

A series of representative photographs is given in fig. 2, Plate 2. The lines due to diffraction by copper are indicated in the photographs, the other lines being those due to ice. In Table I are listed the interplanar spacings, together with the observed intensities of the corresponding lines.

It was noted that if the condensing surface was maintained above −80° C, the ice crystallized in a close-packed hexagonal structure, with the dimensions of the unit cell as follows:

$$c = 7 \cdot 32 \text{ A}, \quad a = 4 \cdot 46 \text{ A}, \quad \text{whence } c/a = 1 \cdot 62.$$

Within experimental error, these values are in good agreement with the lattice constants of ice formed by the freezing of water. Furthermore, the relative intensities of the lines are of the same order of magnitude as those observed by Dennison.*

If the temperature of the condensing surface was lower than −80° C there was apparently a marked change in the regularity of the arrangement of the molecules. The interference became less perfect in some cases, and at −90° C there remained only four sharp lines corresponding to the planes, (10·0), (00·1), (11·0), and (11·2). If the temperature of formation was −105° C, the interference again became less perfect, as indicated by a broadening of the lines. At −115° C there were only two very diffuse diffraction lines corresponding to a spacing of 3·7 A and 2·1 A respectively. The line at 2·1 A was very faint, and appeared as a slight darkening about the diffraction line arising from the (111) plane of copper ($d/n = 2 \cdot 08$ A). To obtain more definite proof of the existence of this line, the copper rod was replaced by one of lead which gave no diffraction at 2·1 A. Because of the relatively high temperature gradient along a lead rod, this was the only case in which lead was used.

---

* 'Phys. Rev.,' vol. 17, p. 20 (1921).

The results indicated that there was a temperature about −110° C, below which the condensate was vitreous, and above which a semi-crystalline or a crystalline solid was formed.

TABLE I—OBSERVED VALUES OF THE INTERPLANAR SPACINGS OF ICE FORMED FROM THE VAPOUR AT VARIOUS TEMPERATURES

Miller indices	−50° to −80° C		−85° C		−90° to −105° C		−115° to −175° C	
h k l	Intensity*	*d*/*n* in A	Intensity*	*d*/*n* in A	Intensity*	*d*/*n* in A	Intensity*	*d*/*n* in A
10·0	w	3·90	w	3·87	w	3·90	m	3·7
00·1	vvs	3·63	vvs	3·69	vs	3·66		
10·1	m	3·40	m	3·42				
10·2	m	2·64	m	2·66				
11·0	w	2·26	vw	2·28	s	2·25	w	2·1
10·3	vs	2·05	vs	2·05				
11·2	w	1·90	w	1·92	m	1·91		
10·1 (2)	w	1·71						
20·3	w	1·51	w	1·52				
12·0	m	1·45						
10·5 12·2	m	1·35	m	1·37				
12·3	vw	1·26						
30·2 00·1 (3)	vw	1·21						
20·5	vw	1·17	vw	1·17				

* vvs, very, very strong; vs, very strong; s, strong; m, medium; w, weak; vw, very weak.

Some photographs were taken of ice which, after being formed at a temperature T_1 (about −160° C), had its temperature increased to a value T_2 (*e.g.*, −95° C or −50° C), at which temperature it was maintained during the exposure. The structure was the same as if the ice had been formed at T_2. A few photographs were also taken, when the ice had been maintained at the temperature T_2 (−95° C, or −105° C) for

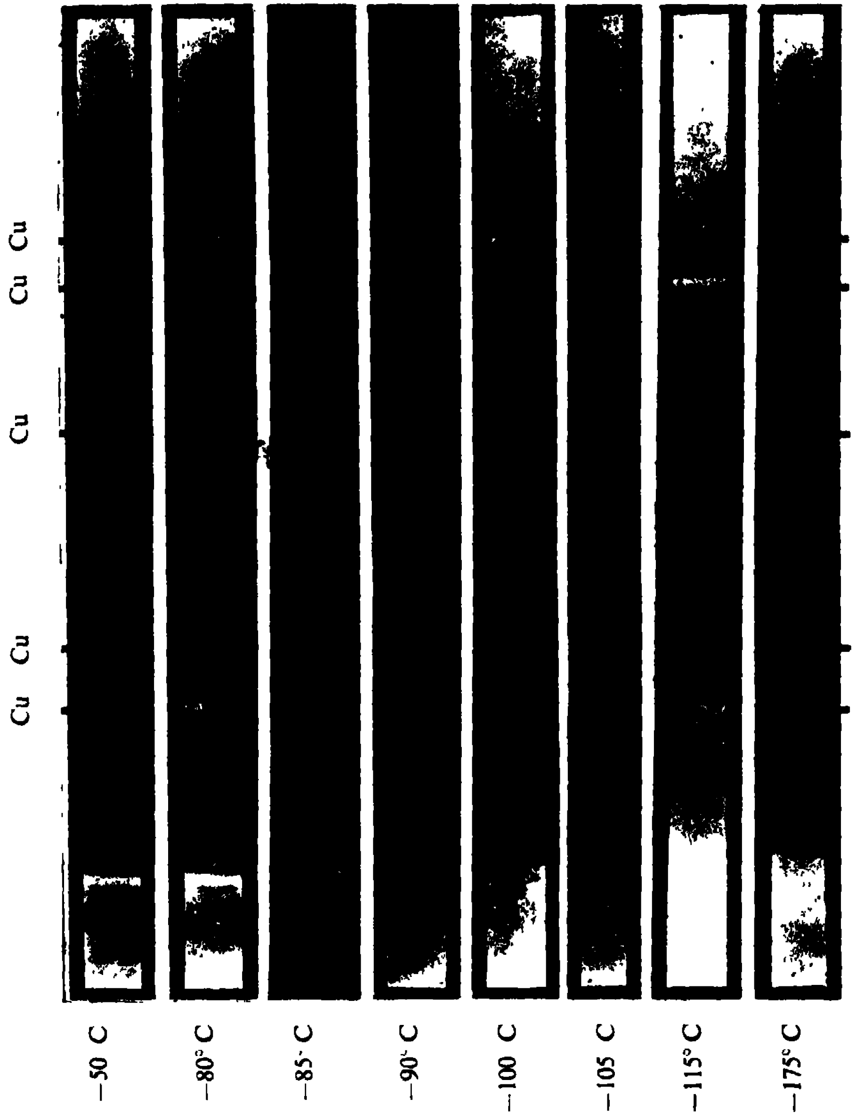

Fig. 2—Typical Hull-Debye-Scherrer diffraction patterns of ice formed from the vapour.

only a short time, and then the temperature was lowered to T_1, at which temperature the photograph was taken. There were indications that there was a slight time lag in the forming of crystalline ice. The spectrogram exhibited a structure similar to that of ice formed at a temperature a few degrees below T_2.

If ice was formed at some temperature T' (above −110° C) and the temperature allowed to fall to a value T'' (below −110° C), the structure was that corresponding to the temperature T'.

5—DISCUSSION

These facts may be explained by assuming that if the temperature of the condensing surface is sufficiently low, the molecules stick when they strike the surface. If the temperature is high enough the condensed molecules migrate on the surface to positions of minimum potential energy which are those positions favourable for crystal formation.

It was found that at temperatures above −80° C, the molecules had sufficient energy to arrange themselves into the highly organized state of a crystalline solid. If the ice was formed at −90° C the energy of the molecules in the condensate was just enough to build up crystals along certain planes. At temperatures immediately below the critical temperature −110° C there were just sufficient molecules arranged in parallel planes to give rise to two very diffuse diffraction maxima, the size of the particles probably being of the order of 10^{7} cm. In this last case, if the temperature of the ice was raised above −110° C the molecules would migrate to positions on a crystal lattice, the time required for such migration being less than 2 minutes.

From the results obtained, it was thought that if some of the kinetic energy of the molecules of a gas was transferred to the molecules of ice at temperatures below −110° C a crystal lattice would be built up. A few experiments were carried out, in which ice was formed on a surface maintained at approximately −140° C, in the presence of air. These experiments indicated that within certain limits increasing the pressure of air in the camera caused the critical temperature to drop below −110° C. The study of this feature is being continued.

The authors wish to thank Professor H. J. C. Ireton and Mr. J. O. Wilhelm for assistance in the carrying out of this work.

6—SUMMARY

An investigation is reported of the structure of ice formed from the vapour at low temperatures and pressures, using the method of X-ray diffraction. When the vapour was condensed on a surface maintained at a temperature below $-110°$ C, the condensate was vitreous, and above this temperature a semi-crystalline or crystalline solid was formed.

Iron of High Purity

By FRANK ADCOCK, M.B.E., D.Sc., and CHARLES A. BRISTOW, A.R.S.M., B.Sc., A.Inst.M.M., of the Metallurgy Department, National Physical Laboratory

(*Communicated by C. H. Desch, F.R.S.—Received July* 11, 1935)

[PLATE 3]

INTRODUCTION

During the past eleven years (1925–35) several equilibrium diagrams involving iron as one of the components have been investigated at the National Physical Laboratory. The provision of the numerous alloys required for these researches has necessitated the production of quantities of high purity iron. Tritton and Hanson,* when they began work on the iron-oxygen system at the National Physical Laboratory, considered that the best commercial iron then obtainable was unsuitable for their work, and in the period 1922–24 prepared iron electrolytically according to the method of Cain, Schram, and Cleaves.† At first the present authors produced iron in a somewhat similar manner, but when improvements in analytical methods revealed impurities in samples originally considered satisfactory, alterations were made in the method of preparation. Comprehensive analyses indicate that the latest batch of iron prepared by the authors is very low in impurities, yet the physical properties of this material suggest that some disturbing factor may still be present. The problem is apparently complex and a rapid solution appears unlikely.

---

* 'J. Iron and Steel Inst.,' vol. 110, p. 90 (1924).

† 'Bull. Bur. Stands.,' vol. 13, p. 1 (1916–17).

In these circumstances it was thought that the present publication of data concerning several batches of iron prepared at the National Physical Laboratory would serve a useful purpose. In addition to information obtained by the authors, particulars of a batch of iron prepared by Mr. W. E. Prytherch, M.Sc., also of the Metallurgy Department, N.P.L., are included, together with occasional results obtained by other members of tde staff. The results of Tritton and Hanson (*loc. cit.*) are omitted, however, as these have already been published.

PREPARATION

The mode of preparation of five batches is briefly described below and the analyses are given in Table I.

Batches 1 *to* 3 (1926–29)—These batches were prepared electrolytically according to the method adopted by Hanson and Tritton (*loc. cit.*), anodes of " Armco " iron and an electrolyte containing ferrous chloride and sodium chloride being used. The crude electro-deposited metal was then melted in a high-frequency furnace and a stream of hydrogen passed over the surface of the liquid metal to remove oxide. As experience was gained refinements and modifications were introduced. Prytherch, in his preparation of batch 2 iron, endeavoured to lessen the impurities in the electrolytic iron by wrapping the anodes in linen, thus retaining sludge. Vacuum melts, when allowed to solidify in the crucible, were low in oxygen content but were not always suitable for subsequent mechanical treatment, owing to the lack of control of the position of the shrinkage cavity. Sounder ingots of batch 2 metal were obtained by a system of bottom pouring *in vacuo.* In batch 3 iron the removal of oxide from the liquid metal was effected by the continuous circulation of hydrogen instead of passing a stream of fresh gas over the melt.

One melt of batch 3 iron, weighing 3 kilogrammes, was found to be quite brittle in the cold, although ductile when hot. Fig. 1, Plate 3, is a photomicrograph of the brittle iron, and it will be noted that elongated cavities exist (after etching) at the crystal boundaries.

Batch 4 (1930–31)—A further quantity of iron was prepared electrolytically and given a short preliminary hydrogen treatment at 600–700° C in a high-frequency furnace to remove chlorine and some of the oxides. Fig. 2 shows the arrangement inside the furnace chamber. The iron, which had now become soft, was briquetted and vacuum-melted in china-clay crucibles yielding slag-covered ingots each weighing nearly a kilogramme. After the careful removal of all slag the ingots were subjected to a rigorous hydrogen treatment which was later adopted for batch 5 iron and is described in detail under that heading. Much of this material was reduced to 6 mm diameter rod suitable for spectroscopic electrodes, great care being taken to avoid contamination in the rolling and swaging operations.

Batch 5 (1932-33)—The analyses of three batches of commercially pure iron available as anode material in the electrolytic bath disclosed the presence of appreciable quantities of nickel (0·014–0·087%). A sample of purchased ferrous chloride, on the other hand, contained only 0·002% of this impurity. As the electrolytic preparation of the iron did not remove all the nickel the method was abandoned, the metal being prepared directly from ferrous chloride in the following manner. An alumina

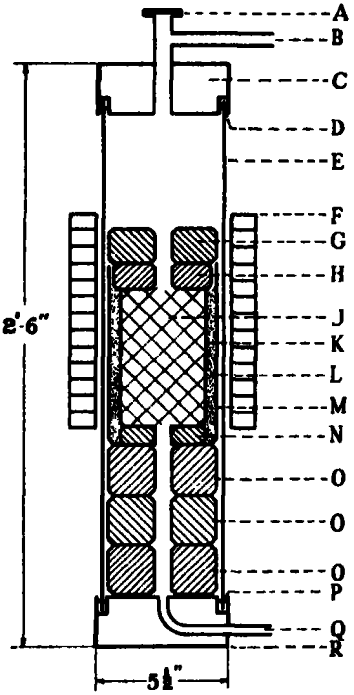

FIG. 2—Preliminary hydrogen treatment of electrolytic iron.

Arrangement inside high-frequency furnace. A, glass window; B, gas inlet tube; C, gas-tight head (water-cooled); D, upper wax seal; E, silica tube forming melting chamber; F, high-frequency furnace coil (diagrammatic); G, refractory cylinder (perforated); H, alumina cylinder (perforated); J, charge of solid iron undergoing treatment; K, crucible of china-clay alumina (perforated); L, powdered alumina lagging; M, outer sleeve of carborundum refractory; N, block of alumina (perforated); O, refractory cylinders; P, lower wax seal; Q, gas outlet tube; R, gas-tight base (water-cooled).

crucible 6 cm diameter and 15 cm high (approximate) was filled with ferrous chloride and heated to 300° C in a vertical furnace. The mass darkened and a considerable contraction in volume took place. Further additions of ferrous chloride were then made and steam injected into the crucible by means of a vertical silica tube. After several hours of this treatment hydrochloric acid fumes ceased to be evolved and the contents of the crucible became reddish-black. After cooling, the residue was washed with distilled water and dried at 110° C. The dark iron oxide* was then packed into a shallow alumina boat which was heated to 400° C in a horizontal tube furnace. Hydrogen was then passed through the furnace and the temperature gradually raised to 800° C. At this stage reduction of the iron oxide was practically complete, but the spongy iron so formed was too fragile for convenient handling. The apparatus was accordingly washed out with nitrogen and the temperature raised to 1050° C for a short time in order to sinter the metal. At high temperatures hydrogen attacks silica in contact with iron, hence the presence of hydrogen was avoided in the final sintering treatment. In order to extract from the hydrogen impurities which otherwise might accumulate in the charge undergoing reduction, the gas was first passed over hot turnings of high purity iron. The reduced iron was briquetted and vacuum melted in alumina crucibles in a high-frequency induction furnace.

Final Hydrogen Treatment—After removal of adhering slag, etc., the ingots, each weighing nearly a kilogramme, were subjected to the final hydrogen treatment, which is described at some length, as it was only after much attention to detail that a high purity product was obtained. It is well known that the exposure of a substance to a large quantity of gas may result in some hardly perceptible impurity in the gas being extracted and concentrated in the substance. Chiefly on this account a method of continuously purifying and circulating a relatively small volume of hydrogen was adopted. The apparatus shown in fig. 3 was similar to that used in the treatment of electro-deposited chromium,† and consisted essentially of a closed circuit through which the hydrogen was propelled by means of a magnetically-operated piston pump.‡ On emerging from the pump the gas first passed over asbestos impregnated with palladium and heated to 165° C, in order to ensure the combination of any free oxygen present in the hydrogen. A gas-flow indicator was next included in the circuit. Sulphur which had been removed from the iron by the hydrogen was extracted from the gas by exposing silver turnings, the surfaces of which had been amalgamated. Calcium chloride was used to absorb the bulk of the water vapour, and the final traces were removed from the gas by freezing. The hydrogen was passed successively through

---

* Roscoe and Schorlemmer, "Treatise on Chemistry," vol. 2, 'Metals,' 5th Ed., p. 1228, state that magnetic oxide is formed according to equation $3\ FeCl_2 + 4\ H_2O = Fe_3O_4 + 6\ HCL + H_2$. The black oxide obtained by the authors was not attracted by a magnet.

† Adcock, 'J. Iron and Steel Inst.,' vol. 115, p. 389 (1927).

‡ Adcock, 'J. Sci. Instr.,' vol. 5, p. 290 (1928).

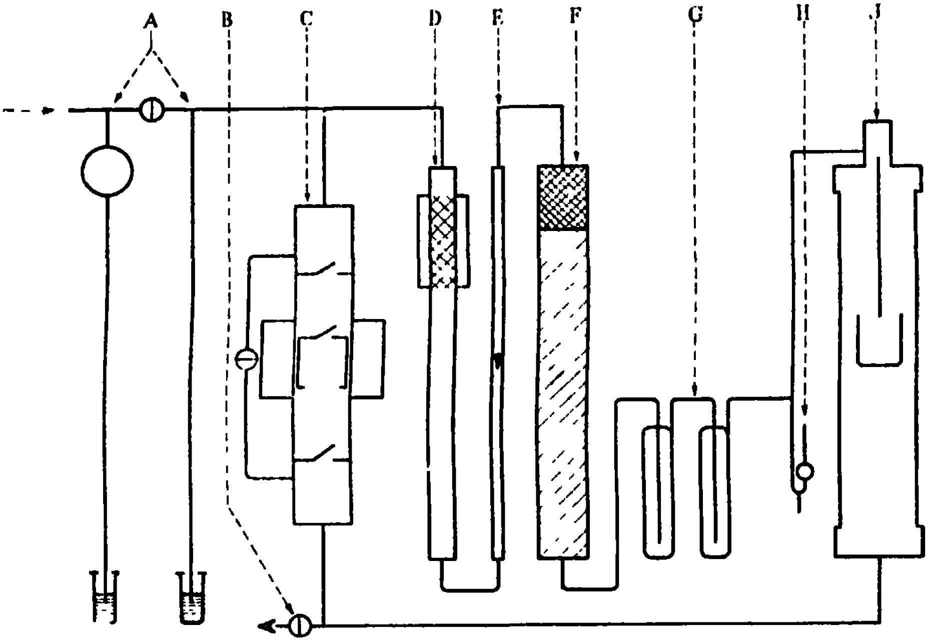

Fig. 3—Arrangement of apparatus for circulating hydrogen (diagrammatic). A, apparatus for admitting hydrogen to closed circulatory system. Comprises : excess pressure reliefs, reservoir, needle valve, and barometer column; B, branch to vacuum pump, normally closed by stopcock; C, magnetically operated gas circulation pump; D, small furnace containing heated asbestos impregnated with palladium; E, gas flow indicator (float in tapered tube); F, metal vessel containing amalgamated silver to remove sulphur and calcium chloride for rough drying; G, traps for removing traces of moisture from gas by freezing; H, vacuum gauge; J, furnace chamber, shown in detail in fig. 4.

two freezing traps, the first cooled with a mixture of ice and brine, the second by means of acetone to which carbon dioxide snow had been added. Bircumshaw* has shown that the formation of aerosols is avoided and that the removal of water vapour is very effective when the gas is cooled in stages. Next the gas passed downwards through the furnace and then returned to the circulating pump, thus completing the circuit. A vacuum connexion, a gas inlet, and subsidiary apparatus were also provided. The hydrogen was supplied from a high-pressure cylinder, and experience had shown that the gas storage bulb, needle valve, and excess pressure relief tubes of more than barometric height, see fig. 3, were all essential if gas was to be admitted safely to the circulatory system.

---

* 'J. Chem. Soc.,' p. 2213 (1930).

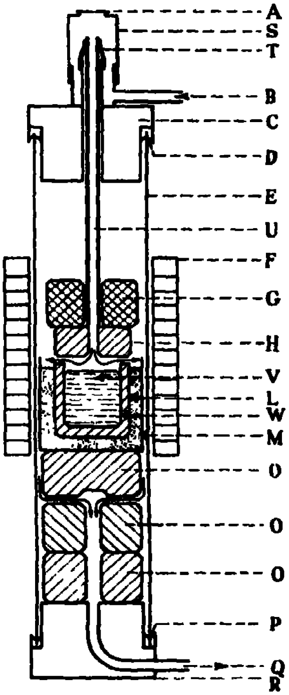

FIG. 4—Hydrogen treatment of liquid iron. Arrangement inside high-frequency furnace. S, removable brass cap; T, rubber joint between silica tube and metal head; U, silica tube down which hydrogen passes; V, molten iron under treatment; W, alumina crucible. Other lettering as in fig. 2.

The arrangement inside the actual furnace is shown in fig. 4. Each ingot, which had been previously vacuum-melted and cleaned, was placed inside a soft alumina crucible* of such dimensions that only a small space would exist over the metal when molten. Owing to the fragility of the crucible it was necessary to leave ample room around the solid ingot to avoid risk of cracking of the crucible as a result of the expansion of the metal on heating.

---

* Two varieties of alumina crucibles were available—" soft " crucibles made from raw alumina as received, and " hard " crucibles prepared from alumina which had been subjected to a crushing process. Some iron was introduced into the alumina during crushing, but was mostly removed by treatment in a magnetic separator. " Soft " alumina crucibles contained less than 0·006% carbon, while the " hard " crucibles gave figures of 0·03–0·06% carbon. For this reason in all melting operations " soft " alumina crucibles, although friable, were employed in preference to the more robust " hard " crucibles.

The hydrogen passed down the central vertical silica tube, the lower end of which was snugly seated in a perforated block of pure alumina which acted as a crucible cover. Silica at high temperatures is reduced by hydrogen, and it was necessary to shield in this manner the lower end of the silica tube from the full heat radiation of the hot metal charge. Outlets were provided for the hydrogen by slotting the lip of the crucible.

The procedure in the case of a charge weighing one kilogramme approximately was as follows : the system was evacuated and then filled with hydrogen. After standing overnight to allow the hydrogen to diffuse throughout the refractories the system was again evacuated and filled once more with hydrogen. Finally, the system was evacuated for the third time and hydrogen admitted until an absolute pressure of approximately 200 mm was attained. This pressure was indicated by the barometer column which was incorporated in that part of the apparatus used for admitting gas to the system (*see* letter A, fig. 3). The hydrogen circulation pump was then started, and the charge of iron gradually heated by means of the high-frequency induction furnace.

During the hydrogen treatment the gas pressure in the system was noted at five-minute intervals. As will be seen from fig. 5, which shows the changes in gas pressure for a typical " run," the pressure first increased and then fell rapidly. When the pressure had fallen to 140 mm a fresh quantity of gas was admitted to the system to restore the original pressure of 200 mm, and the circulation continued until the fall in pressure became extremely slow (less than $\frac{1}{2}$ mm Hg in five minutes). The surface of the liquid iron was visible down the central silica tube, and in the early stages of the treatment was almost covered with an immiscible liquid. This layer gradually disappeared and was presumed to be mainly iron oxide.

Undercooling, as shown by " flashing " of the surface when the melt was allowed to freeze, became pronounced towards the end of the hydrogen treatment. The thin frozen layer quickly vanished on restarting the furnace current, which was regulated so as to avoid risk of overheating and consequent contamination of the charge. The top surface of the ingot after cooling and removal from the furnace was bright and revealed the presence of three distinct systems of crystal grain boundaries. A slight degree of slag formation had occurred where the melt had been in contact with the crucible. The sides and bottom of the ingot, although bright, were covered with a loosely adhering layer of slightly altered alumina. Silicon appears to be removed from the iron as a result of reaction with the alumina of the crucible. Thus the silicon content of one iron ingot dropped during the hydrogen treatment from 0·009% to 0·002%. The removal of silicon by this means also takes place in the absence of hydrogen, since an experimental iron ingot containing 0·003% silicon gave only 0·0002% on analysis after vacuum melting in an alumina crucible.

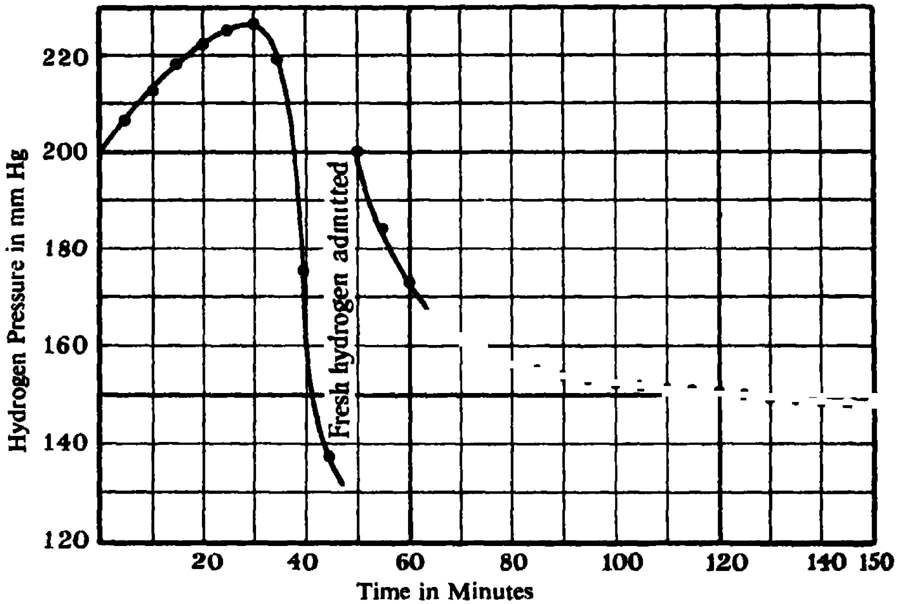

Fig. 5—Variations of pressure inside apparatus during hydrogen treatment of molten iron.

Final Vacuum Melting—Several ingots of 1100 gm average weight from this batch of iron were hydrogen-treated. The pure metal was ultimately required in bars up to 3 cm diameter, and for this reason it was necessary to prepare ingots weighing from 3–4 kilogrammes. Several of the hydrogen-treated ingots were machined so as to remove a thin outer skin of metal and then vacuum-melted together in a large alumina crucible. The temperature of the iron charge was very slowly raised in stages while a high-speed vacuum pump, connected to the furnace chamber by a wide bore tube, rapidly removed liberated gases. Rapid heating of the charge or the slow removal of gas might result in contamination of the iron due to gases evolved from the hot refractories being absorbed by the melt. Ultimately the iron melted with a slight effervescence, and was maintained in the liquid state for 15 minutes. A special procedure was adopted during solidification in order to limit the shrinkage cavity to the top of the ingot. The furnace tube and contents were first lowered until the top of the liquid charge was level with the bottom of the furnace inductor coil and the furnace current gradually reduced until signs of solidification appeared. The upper part of the charge was then alternately melted and frozen several times by periodically increasing and decreasing the furnace current, and in this way an ingot containing over 80% of sound metal was obtained.

During the whole process of vacuum melting and solidification, which lasted over six hours, the gas pressure in the furnace chamber was noted. In the cold a reading as low as 0·0003 mm Hg was obtained, and although at one stage of melting the pressure rose to 0·063 mm the final reading of the gauge when the melt solidified was 0·006 mm. Fig. 6, Plate 3, shows a typical ingot, the top of which was characterized by a matt surface and large crystal grain structures. The microstructure of the metal prepared in this manner, fig. 7, Plate 3, shows the crystal boundaries to be practically free from either cavities or inclusions.

It was found that iron containing appreciable quantities of both carbon and oxygen (0·01–0·03%) lost a proportion of both these impurities when held liquid for a time under vacuum conditions. In the later stages of the investigation this method of carbon and oxygen removal was not employed.

CHEMICAL ANALYSES

In the accompanying analyses, Table I, it will be noted that very few impurities were determined in the earlier batches, chiefly on account of the small quantity of iron available. It was only in batches 4 and 5 that the analysis could be carried out in a comprehensive manner. The chemical estimation of such small traces of impurities in these irons has in most cases involved the use of large samples, and in addition its success has been dependent on a definite technique developed as the result of experience and experiment.

Rods of batch 4 iron, 6 mm in diameter, were submitted to Dr. S. Judd Lewis* for spectroscopic analysis. The results for nickel, copper, chromium, cobalt, and tin were obtained by comparison with previously known standards. For vanadium, titanium, aluminium, and boron there were no suitable standards for comparison. A special search was made for arsenic, barium, calcium, gallium, magnesium, manganese, molybdenum, sodium, lead, strontium, tungsten, and zinc, but met with negative results. The foreign lines of the spectra were generally of feeble intensity owing to the small proportions of impurities present in the metal. For nickel, however, the spectrum lines were stronger. Figures were also obtained by purely chemical methods for silicon, aluminium, copper, nickel, manganese, and molybdenum, and were in close agreement with the spectrographic results. Carbon, sulphur, and phosphorus were determined by chemical methods only. In all cases the analyses were made on the actual 6 mm diameter rods as prepared for spectrographic standards. Both spectrographic and chemical analyses of batch 5 iron were carried out at the N.P.L. on samples taken from 13 mm diameter rods as prepared for the investigation of sundry physical properties, and the results of check chemical analyses made on different samples were found to be in good agreement.

---

* Report on the spectrographic analysis of a supply of exceptionally pure iron rods prepared at the National Physical Laboratory, Teddington, London, on behalf of Messrs. Adam Hilger, Ltd., to whom thanks are due for permission to make use of this analysis.

In both batch 4 and batch 5 the figures for oxygen, and hydrogen plus nitrogen, were obtained by the vacuum fusion* of massive samples in a high-frequency furnace. Graphite crucibles were used and the evolved gases were pumped off and analysed. The results obtained with duplicate samples agreed within close limits. Some oxygen determinations were also made by passing hydrogen over the hot finely divided samples. The surface occlusion of gases on the sample at room temperature was believed to be a serious disturbing factor in this method, and for this reason the values obtained have not been given in Table I.

X-RAY ANALYSIS

In an early determination (at room temperature) of the lattice parameter of batch 2 iron, Preston (Metallurgy Department, N.P.L.) arrived at a figure of $2 \cdot 860_8$ A for the length of the side of the body-centred cube. Later he obtained a corresponding figure of $2 \cdot 8600 \pm 0 \cdot 0005$ at 17° C† for a sample of batch 3 iron. The values of λ used in calculating this result were Cr.Kα_1 $2285 \cdot 033 \times 10^{-11}$ cm, and Cr.Kα_2 $2288 \cdot 907 \times 10^{-11}$ cm, as given in 'I. C. T.,' vol. VI, p. 36. Mr. C. Wainwright (Metallurgy Department, N.P.L.) also examined samples of iron from batches 4 and 5, and a comparison of his values with those of Mr. Preston for batch 3 iron failed to show any differences in the lattice parameter.

---

* Analyses conducted and apparatus arranged by H. A. Sloman, of the Metallurgy Department, N.P.L.

† Preston, 'Phil. Mag.,' vol. 13, p. 419 (1932).

TABLE I—ANALYSIS OF IRONS

Figures indicate weight percentages of impurities

Element	Batch 1 1926	Batch 2 1927	Batch 3 1929	Batch 4 1930–31		Batch 5 1932–33	
				Spectroscopic (Judd Lewis)	Chemical aided by spectroscopic	Spectroscopic N.P.L.	Chemical
				*		*	
C	n.d.	0·006	0·01	—	0·006	xx	0·0045
Si	trace	0·0004	0·003	0·0005	trace	x	0·0002
S	n.d.	0·0006	0·0015	—	nil	n.d.	0·0015
P	0·015	0·003	0·003	—	under 0·001	n.d.	0·001
Ni	n.d.	n.d.	n.d.	0·022	0·022	xx	0·0006
Cu	n.d.	trace	n.d.	0·0008	trace	x	nil
Cr	n.d.	n.d.	n.d.	0·003	trace	x	nil
Co	n.d.	n.d.	n.d.	0·004	trace	o	n.d.
Sn	n.d.	n.d.	n.d.	0·0001	n.d.	o	n.d.
V	n.d.	n.d.	n.d.	x	faint trace	o	n.d.
Ti	n.d.	n.d.	n.d.	x	v. faint trace	o	n.d.
Al	n.d.	n.d.	n.d.	x	v. faint trace	xx	trace
B	n.d.	n.d.	n.d.	x	n.d.	x	n.d.
Ca	n.d.	n.d.	n.d.	x	faint trace	xx	nil
As	n.d.	n.d.	n.d.	o	trace	o	n.d.
Ba	n.d.	n.d.	n.d.	o	trace	o	n.d.
Ga	n.d.	n.d.	n.d.	o	n.d.	o	n.d.
Mg	n.d.	n.d.	n.d.	o	n.d.	n.d.	trace
Mn	n.d.	trace	n.d.	o	nil	xx	0·002
Mo	n.d.	n.d.	n.d.	o	nil	o	nil
Na	n.d.	n.d.	n.d.	o	v. v. faint trace	o	n.d.

Pb	n.d.	n.d.	n.d.	o	? v. faint trace	o	n.d
Sr	n.d.	n.d.	n.d.	o	n.d.	o	n.d.
W	n.d.	n.d.	n.d.	o	n.d.	o	n.d.
Zn	n.d.	n.d.	n.d.	o	n.d.	o	n.d.
Au	n.d.	n.d.	n.d.	n.d.	n.d.	n.d.	Absent in parent ferrous chloride
Ag	n.d.	n.d.	n.d.	n.d.	n.d.	n.d.	
Ge	n.d.	n.d.	n.d.	n.d.	n.d.	n.d.	
H	n.d.	n.d.	n.d.	—	under 0·001	—	under 0·001
N	n.d.	n.d.	0·002	—			
O	n.d.	n.d.	n.d.	—	0·0003	—	0·0005
Total impurities					0·0387 ÷ traces (28 elements)		0·0113 + traces (31 elements)

* xx, Trace of element present; x, slight trace of element present; o, element sought for with negative results; ?, presence doubtful; n.d., not determined.

It is of interest to compare the observations made at the National Physical Laboratory with those made elsewhere. Using a camera of 16·65 cm radius, Blake[*] determined the lattice parameter of iron as 2·8603 ± 0·0002 A, while Neuberger[†] gives it as 2·8610 ± 0·0004 A.

Table II gives the density of iron calculated from the above figures, making use of the following data :

Atomic weight of iron	55·84.
Atomic weight of hydrogen	1·0077.
Mass of hydrogen atom	$1\cdot663 \times 10^{-24}$ grammes.

The lattice parameter of the body-centred cube has also been calculated as 2·860 A by Wever[‡] from Gumlich's figure of 7·876 gm/cc for the density of iron.

TABLE II

Lattice parameter A	Temperature °C	Calculated density gm/cc
2·8600 ± 0·0005	17	7·878 ± 0·004[§]
2·8603 ± 0·0002	—	7·876 ± 0·002[‖]
2·8610 ± 0·0004	22	7·870 ± 0·003[¶]

[§] Preston, 'Phil. Mag.,' vol. 13, p. 419 (1932).

[‖] 'Phys. Rev.,' vol. 26, p. 60 (1925).

[¶] 'Z. Kristallog., vol. 86, p. 405 (1933).

As shown in Table III, the density of iron as obtained in the more recent direct determinations is 7·871.

DENSITY

No appreciable difference could be found between the density of specimens cut from the ingot as cooled and that of specimens from the same ingot which had been cold-worked and subsequently annealed at 950° C. A severely cold-worked rod from batch 5 (cold-rolled from 3 cm diameter down to 1 cm diameter), however, had a density of 7·867 gm/cc. After annealing, its density was found to be 7·871 gm/cc. The density figures given in Table III were determined in the Metrology Department of the National Physical Laboratory, and the value for the purest iron was 7·871 ± 0·002 gm/cc at 19° C.

COEFFICIENT OF EXPANSION

The coefficient of expansion of batch 5 iron was determined in the Physics Department, N.P.L., on a rod 1·2 cm in diameter and 30 cm in length. For this purpose the previously annealed specimen was placed in a vertical silica tube of slightly larger diameter and rested on the bottom, or closed end of the tube. The latter was considerably longer than the specimen, and permitted the insertion of a silica distance piece which transmitted the movement of the upper end of the rod to the plunger of a dial indicator rigidly attached to the top of the tube. Table IV shows the results obtained over a temperature range of 0–250° C.

---

[*] 'Phys. Rev.,' vol. 26, p. 60 (1925).

[†] 'Z. Kristallog.,' vol. 86, p. 405 (1933).

[‡] 'Mitt. K.-Wilh. Inst. Eisenforsch.,' vol. 3, p. 51 (1921).

TABLE III

Batch number	Temperature °C	Density gm/cc (± 0·002)	Remarks
1	11	7·874	
2	18	7·868	Probably contained traces of oxide.
3	17	7·866	
4	19	7·871	Ingot as cooled in furnace.
5	19	7·871	Ingot as cooled in furnace.
		7·871	Rod cold-rolled 3 cm to 1 cm diameter, then annealed 2 hours at 950° C.

TABLE IV—COEFFICIENT OF EXPANSION FOR BATCH 5 IRON

Temperature range °C	Coefficient of expansion per °C
0–100	0·0000112 ± 0·0000005
0–150	0·0000118 ± 0·0000005
0–200	0·0000120 ± 0·0000002
0–250	0·0000124 ± 0·0000002

APPROXIMATE SMOOTHED VALUES DERIVED FROM ABOVE RESULTS

Mean temperature °C	Coefficient of expansion per °C × 10^6
0	(10·4)
25	(10·8)
50	11·2
75	11·6
100	12·0
125	12·4
150	12·8
175	(13·2)

Somewhat lower values for the coefficient of expansion were obtained at an earlier date for iron of batch 1, which was less pure than batch 5 material. These results suggest that the increased purity of batch 5 iron may be responsible for the slightly higher coefficient of expansion.

ELECTRICAL RESISTIVITY

The specific electrical resistivities of four batches of iron were measured at room temperature by the Electricity Department, N.P.L., and the results are indicated in Table V. A known current was passed through a rod sample of constant cross-section, and the resistivity deduced from the resulting potential gradient in the specimen.

TABLE V

Batch	*Temperature* °C	Resistivity ohm–cm × 10^{-6}	Remarks
1	20	$9{\cdot}9_0$	Annealed.
2	20	$9{\cdot}7_5$	Annealed.
3	20	$9{\cdot}4_0$	Annealed.
5	20	$9{\cdot}9_0$	Cold-rolled, unannealed.
		$9{\cdot}8_8$	Cold-rolled and annealed.
		$9{\cdot}8_4$	Cold-rolled and annealed. Taken from curve plotted from Table VI.

Determinations of the specific electrical resistivity of batch 5 iron at elevated temperatures were also made in the Physics Department, N.P.L. In these experiments a bar specimen was heated as uniformly as possible in a suitable enclosure, temperatures being measured by means of thermocouples pegged into holes in the bar. The figures obtained for the resistivity as measured at room temperature, both before and after the tests at elevated temperatures, agreed within the limits of experimental error. Table VI gives the smoothed values at 50° C intervals over the temperature range 0–200° C. The specific resistivity and temperature coefficient of resistance at any definite temperature within this range can be estimated by using the following equation:

$$R_t = (8{\cdot}8 + 0{\cdot}051\, t + 0{\cdot}00006\, t^2) \times 10^{-6},$$

where t is the temperature in degrees centigrade and R_t the specific resistivity.

THERMAL CONDUCTIVITY

The thermal conductivity of batch 5 iron was measured in the Physics Department, N.P.L., by Mr. R. W. Powell,* and some details of the method have already been published. For this purpose the sample, in the form of a rod (1 cm diameter × 15 cm long), was heated electrically at one end and water-cooled at the other, suitable arrangements being made to minimize lateral dissipation of heat. Once steady conditions were achieved, the flow of heat along the rod was readily ascertained and the temperature gradient measured by means of thermo-couples pegged into holes in the rod. The energy supplied to the heating element and the heat energy removed by the cooling water at the other end of the rod were found to agree to within 2%. It may therefore be presumed that the results obtained have this degree of accuracy. Table VII gives the smoothed values of thermal conductivity for 25° C intervals, and it will be observed that figures are higher than those usually atrributed to iron.

---

* 'Engineer,' vol. 159, p. 68 (1935).

TABLE VI—ELECTRICAL RESISTIVITY OF BATCH 5 IRON AT VARIOUS TEMPERATURES

Temperature °C	Electrical resistivity ohm-cm × 10^{-6}
0	(8·8)*
50	11·5
100	14·5
150	17·8
200	(21·5)

* Values in brackets have been obtained by slight extrapolation.

TABLE VII

Mean Temperature °C	Thermal conductivity in c.g.s. units Batch 5
0	$(0{\cdot}19_4)$*
25	$0{\cdot}18_9$
50	$0{\cdot}18_5$
75	$0{\cdot}18_0$
100	$0{\cdot}17_6$
125	$0{\cdot}17_2$
150	$0{\cdot}16_7$
175	$(0{\cdot}16_2)$
200	$(0{\cdot}15_8)$

* The values in brackets have been obtained by extrapolation.

TRANSFORMATIONS IN IRON AT HIGH TEMPERATURES

The melting-point of iron has been determined optically by Dr. C. H. M. Jenkins and Dr. Marie L. V. Gayler,† of the Metallurgy Department, N.P.L. Values have also been given for the melting-point and other transformations (including the " gamma-delta ") for iron of moderate purity by one of the authors* in a study of the chromium-iron constitutional diagram. The thermal arrests and the dilatometric changes associated with the lower transformations in five batches of iron are shown in Table VIII. Thermal analysis was conducted *in vacuo*, but an atmosphere of purified argon was maintained in the furnace used for dilatometric observations.† The thermal and dilatometric results were not strictly comparable, since the former indicated the maximum rate of heat evolution or absorption, while the latter clearly showed transformations extending over definite temperature ranges. As will be seen from fig. 8, which is reproduced from an autographic record of the Ac3 transformation, in batch 4 the upper and lower limits are sharply defined. At first it was thought that this temperature range was only apparent and due to some defect in the method employed. Consequently, care was taken to avoid appreciable temperature gradients in the specimen and to maintain intimate contact between the specimen and the junction of the thermocouple used for temperature measurements. In one experiment the temperature of a sample of iron undergoing dilatometric test was raised at about one-third the usual rate (2–2½° C instead of 7° C per minute), but this procedure had no marked influence on the position or extent of the

---

† 'Proc. Roy. Soc.,' A, vol. 129, p. 91 (1930).

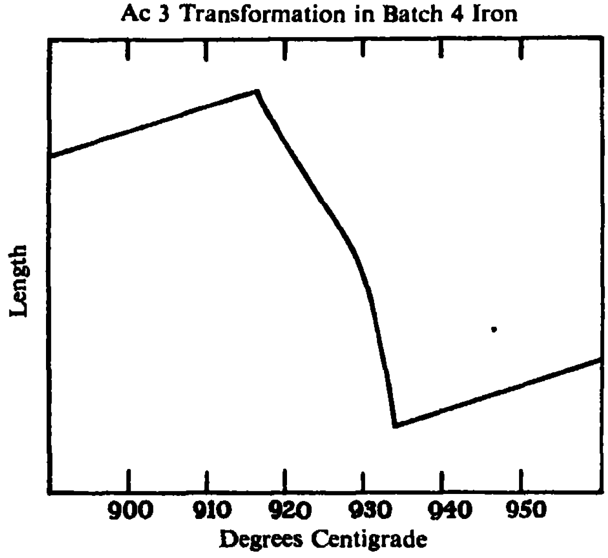

FIG. 8.

---

* Adcock, 'J. Iron and Steel Inst.,' vol. 124, p. 110 (1931).

† Haughton and Adcock, 'J. Sci. Instr.,' vol. 10, p. 178 (1933).

transformation range. The average values for the $\alpha-\gamma$ transformation was decidedly higher for batch 5 than for the previous batches. This is of interest, as Yensen* has suggested that no transformations below the melting-point exist in really pure iron. On the other hand, another sample of iron (not prepared by the authors) possessed a relatively high transformation range—mean value Ac3 and Ar3 = 924° C—in spite of the fact that this material contained the following impurities :

Carbon	0·008%
Nickel	0·035%
Silicon	0·035%

It is difficult to account for this high figure for the A3 transformation, unless the lowering action of the carbon is more than balanced by the effect of the silicon present. It will also be noticed that although batch 4 iron only differed from batch 5 in containing slightly more carbon (0·006 instead of 0·0045%) and 0·022% nickel, the transformation in batch 4 was on an average 9° C lower than that in the latter material. Esser and Cornelius† have reported the presence of double A3 thermal arrests in electro-deposited iron treated with hydrogen. Batches 4 and 5 used by the authors contained very little hydrogen, however, and the spreading of the dimensional changes associated with the A3 transformations over definite temperature ranges could not be attributed to the presence of this gas. Hansel and Larsen,‡ who conducted a dilatometric investigation on iron, found that a previous high-temperature treatment of the metal with hydrogen raised the A3 transformation from 10° C–30° C.

The variations found in the thermal determinations of the " Curie " or A2 point for the different batches of iron hardly exceeded the limits of experimental error. Further, the values obtained for the A2 thermal arrests were almost identical, whether the determinations were made with rising or falling temperatures. In this respect the A2 and A3 transformations in iron were markedly different, as will be seen from Table VIII. The sensitivity of the dilatometer was normally adjusted for the convenient delineation of the A3 range, and under such conditions no dimensional changes were detected in connexion with the " Curie " or A2 transformation in iron.

MAGNETIC PROPERTIES

Magnetic tests on several samples of high purity iron were undertaken by Mr. C. E. Webb, assisted by Mr. L. H. Ford, of the Electricity Depart-

---

* ' J. Amer. Inst. Min. and Met. Engineers,' Iron and Steel Division, p. 320 (1929).

† ' Amer. Soc. Steel Treat.,' vol. 21, p. 733 (1933).

‡ ' Metals and Alloys,' vol. 4, p. 37 (1933).

TABLE VIII

			Batch		
	1	2	3	4	5
			Thermal Arrests		
Ac3	916	915	919	—	—
Ar3	902·5	902	907	—	—
Mean $\frac{Ac3 + Ar3}{2}$	909	908·5	913	—	—
Ac2	766·5	769	769	—	—
Ar2	765	769	767	—	—
			Dilatometric Critical Ranges		
Ac3 range	—	—	917–938	917–934	924–950
Ac3 mean	—	—	927·5	925·5	937
Ar3 range	—	—	914–900	911–899	917–905
Ar3 mean	—	—	907	905	911
Mean $\frac{Ac3 + Ar3}{2}$	—	—	917	915	924

All temperatures in °C.

ment, N.P.L. Rings were used in all tests, and preliminary heat-treatments were conducted under vacuum conditions (usually 0·001–0·0003 mm Hg pressure). Table IX shows the magnetic properties of the five batches of iron as measured on rings which had been held at a temperature of approximately 1000° C for 15 minutes and furnace-cooled. It will be seen that the maximum permeability obtained with batch 5 iron was relatively low in spite of the high purity of this sample. The influence of impurities on the maximum permeability of iron has already received the attention of investigators,[*] and with a view to obtaining further evidence on this subject the maximum permeability figures of a number of high purity irons and of irons containing known impurities have been determined, Table X. The highest value (31,400 at $H = 0{\cdot}3$ Oersted) was derived from batch 3 iron, which contained appreciable amounts of carbon, oxygen, and probably nickel. Batch 4 possessed a maximum permeability of 28,600, but this relatively high figure was not due to the presence of 0·022% nickel in the material, as was shown when nickel was deliberately added to some high purity iron of batch 5. The final melt contained 0·057% nickel, and gave only a maximum permeability of 16,800. The value of 26,500 was obtained for batch 1, in spite of the presence of 0·015% phosphorus, *see* Table X. On the other hand, sample " D," which con-

---

[*] Yensen, 'Phys. Rev.,' vol. 39, p. 358 (1932); Cioffi, *Ibid.*, vol. 45, p. 742 (1934); Cioffi, *Ibid.*, vol. 39, p. 363 (1932); McKeehan, *Ibid.*, vol. 39, p. 376 (discussion) (1932).

TABLE IX—MAGNETIC PROPERTIES OF FIVE BATCHES OF HIGH PURITY IRON

(Extracted from results obtained by Mr. C. E. Webb, assisted by Mr. L. H. Ford.)

Values of Flux Density (B) and Permeability (μ) for different values of Magnetic Force (H)

Batch / Magnetic force H Oersted	1		2		3		4		5	
	B gauss	μ	B gauss	μ	B gauss	μ	B gauss	μ	B gauss	μ
0·05	140	2800	120	2400	240	4800	300	6000	—	—
0·1	500	5000	620	6200	770	7700	1500	15000	300	3000
0·2	4200	21000	4790	24000	4970	24900	5480	27400	1500	7500
0·3	7950	26500	8680	28900	9420	31400	8580	28600	3390	11300
0·4	9950	24880	10720	26800	—	—	10320	25800	5380	13450
0·5	—	—	—	—	12330	24700	—	—	7180	14360
0·6	11790	19650	12400	20700	—	—	12090	20150	—	—
1	13200	13200	13440	13440	14100	14100	13180	13180	12000	12000
10	15380	1538	15030	1503	15610	1561	14710	1471	15500	1550
100	17830	178	—	—	—	—	17370	174	17820	178

	1	2	3	4	5
Maximum permeability ..	26500 at H = 0·3 Oe.	28900 at H = 0·3 Oe.	31400 at H = 0·3 Oe.	28600 at H = 0·3 Oe.	14360 at H = 0·5 Oe.
Hysteresis loss (ergs/cc/cycle)	$0{\cdot}00022\ B^{1{\cdot}6}$	$0{\cdot}000183\ B^{1{\cdot}6}$	$0{\cdot}000191\ B^{1{\cdot}6}$	—	—
Remanence (gauss)	8500	8580	8440	8800	8700
Coercivity (Oersted)	0·183	0·147	0·162	0·115	0·271

tained 0·02% carbon, possessed the relatively low maximum permeability of 8500. Under the microscope most of the crystal grains in this material were found to be separated by thin strips of cementite—a fact which perhaps explains the low permeability value. One difficulty of making comparisons between the various samples of iron was due to changes which occurred at room temperature in the magnetic properties during the time which elapsed between the heat-treatment and the magnetic test.

TABLE X—EFFECT OF IMPURITIES ON MAXIMUM MAGNETIC PERMEABILITY

	Maximum permeability		Outstanding impurities
		at H =	
Batch 3	31400	0·3 Oe.	C = 0·01%, visible oxide under microscope, probably Ni = 0·02%.
„ 4 ..	28600	0·3 „	Ni = 0·022%.
„ 1 ..	26500	0·3 „	P – 0·015%
Sample A ..	18600	0·5 „	Si = 0·016%, probably Ni – 0·02%.
„ B ..	16800	0·4 „	Ni – 0·057%.
„ C ..	14460	0·7 „	C = 0·015, Ni = 0·011. Iron made by carbonyl process, not melted.
Batch 5 ..	14360	0·5 „	No outstanding impurity.
Sample D ..	8500	1·0 „	C = 0·02. Visible cementite under microscope.

Curve 1, fig. 9, shows the B–H curve for a specimen of iron, containing as chief impurities 0·011% carbon and 0·022% nickel, several months after heating to 1000° C and furnace-cooling. Curve 2, fig. 9, demonstrates the effect on the magnetic properties after two and one-third years' ageing at room temperature, and it will be noticed that a considerable fall in flux-density has occurred for values of H ranging from 0·2–3·0. The specimen was then heated to 1000° C, cooled to room temperature in three hours, then tested magnetically within a further two hours. Curve 3, fig. 9, indicates the result of this test. For values of H within the limits 0·2–1·0 Oersted, the flux-density is greater than that obtained in the original test, but for high values of H the flux-density is somewhat diminished. Further magnetic tests were then made on the sample over a period of a month, during which the flux-density fell slightly at low values of H and increased somewhat for high values of H. This slow magnetic change was not appreciably accelerated by holding the sample at 100° C for one week. Further, a short treatment at a temperature of minus 70° C had no effect on the magnetic properties as measured at room temperature.

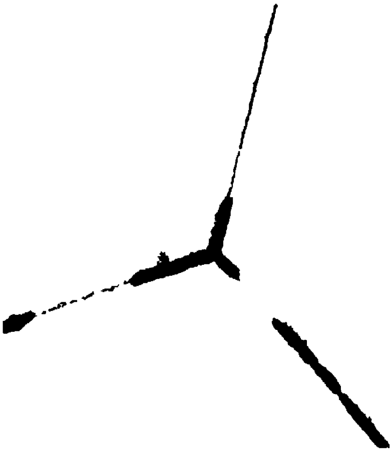

Fig. 1—Microstructure of brittle iron. 1500.

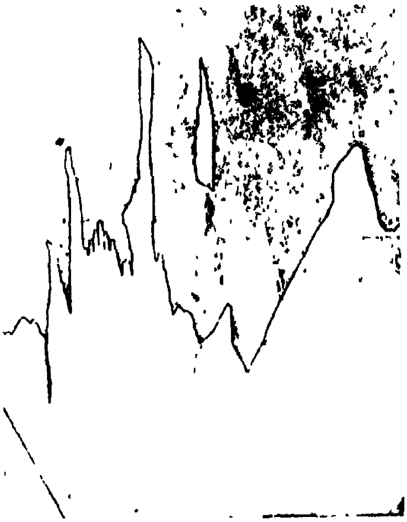

Fig. 7—Microstructure of batch 5 iron. × 112.

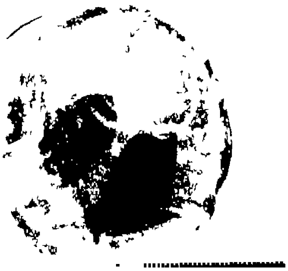

Fig. 6 -Top surface of vacuum melted ingot (batch 5) as removed from furnace. ¾.

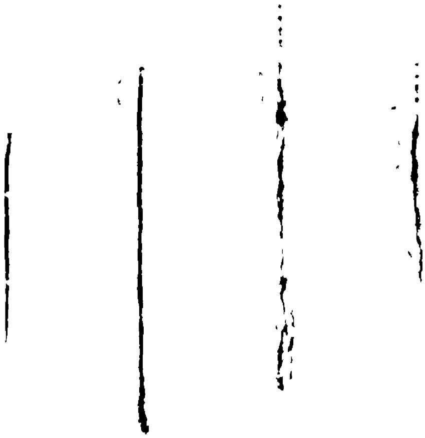

Fig. 11- -Two tensile test-pieces of batch 5 iron, after test. Natural size.

Similar changes in magnetic properties occurred under the same conditions with another sample of high purity iron and also an iron containing 0·16% silicon. This behaviour is not, however, characteristic of all solid solution iron alloys. Three alloys containing respectively 14·8, 16·7, and 25·0 atomic % chromium were re-tested after ageing at room temperature for approximately two years, but no important change in the magnetic properties was observed. The 25·0 atomic % chromium alloy possessed at low values of H a permeability comparable with that of iron.

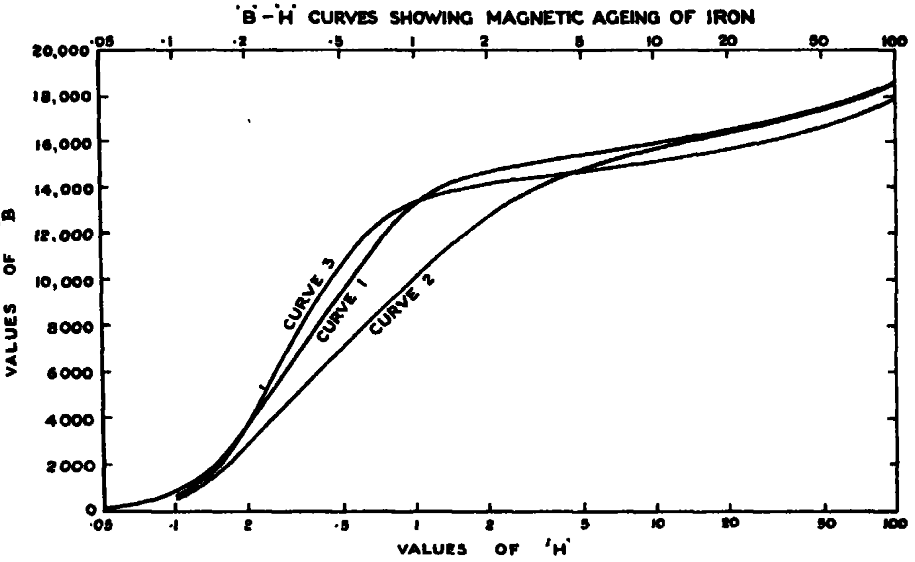

Fig. 9—" B "—" H " Curves.

Unfortunately the irons used for the ageing tests did not possess the purity subsequently attained in batches 4 and 5. It is therefore possible that the falling off in magnetic permeability for low and moderate values of H may be due to the slow separation of fine particles of a second phase. Magnetic ageing cannot be due simply to the gradual escape of hydrogen from the iron sample, otherwise the permeability would not be raised again on vacuum annealing. Cioffi* has obtained a maximum permeability of 280,000 for a sample of iron subjected to a treatment with pure hydrogen at high temperatures. This remarkable figure may be due either to the removal of certain impurities by the action of the hydrogen or to the actual absorption of hydrogen by the metal. The latter possibility is supported by the moderate values of maximum permeability obtained by the authors for batches 4 and 5, both of which were known to be low in hydrogen.

---

* 'Phys. Rev.,' vol. 45, p. 742 (1934).

Investigators in America* have shown that the slow cooling in a magnetic field of a 65% nickel-iron alloy greatly increases the magnetic permeability of the material at room temperature. It was considered desirable to ascertain if the magnetic properties of iron are modified by a similar treatment. Accordingly a ring made from batch 5 iron was heated to 800° C under vacuum conditions, slowly cooled and tested magnetically. The ring was then heated again to 800° C and slowly cooled, while a direct current of 160 amperes was maintained in a copper rod which passed axially through the ring. The magnetic results obtained for this ring after this and further treatments are shown in Table XI. It will be seen that cooling in a magnetic field increased the permeability for low and moderate values of H. A further increase in permeability occurred when the cooling in a magnetic field was repeated. Finally the specimen was slowly cooled in the absence of the magnetic field, and was found still to possess a permeability greater than that of the specimen when slowly cooled in the absence of the magnetic field on the first occasion. The effect of slow cooling in a magnetic field on the magnetic properties at room temperature was much less for iron than that claimed for the nickel-iron alloy. Nevertheless, in these experiments which were of an exploratory nature, the permeability value was in one instance raised by more than 50%.

TABLE XI—MAGNETIC PERMEABILITY OF RING OF BATCH 5 IRON AFTER SUCCESSIVE TREATMENTS

All cooled from 800° C to 550° C at 100° C per hour

H in Oersteds	Current in axial conductor: Nil	160 amperes	160 amperes	Nil
	Permeability			
0·25	10160	14080	15600	12320
0·5	16000	19800	20800	19000
1·0	12700	13450	13500	13250
2·0	7190	7265	7265	7240
10	1555	1557	1557	1555

The observations so far made relate in most cases to single specimens, and the results are not necessarily representative. In general, however, it is evident that the magnetic properties of high purity iron are strongly influenced by factors other than chemical composition. Further, the results do not support the view that a high magnetic permeability for low values of H are necessarily associated with iron of great purity. It is hoped that circumstances will permit of a fuller investigation of the magnetic properties of high purity iron at an early date.

---

* Bozorth, Dillinger, and Kelsall, 'Phys. Rev.,' vol. 45, p. 742 (1934).

MECHANICAL PROPERTIES

Hardness—A difficulty was encountered in the exact determination of the hardness of iron samples owing to the irregular impressions produced by both the diamond pyramid and the Brinell ball. Specimens of iron cut from ingots as solidified in the crucible were coarse grained and presented the greatest obstacle in this respect. Attempts made to obtain a fine-grained material by heavily cold-working and subsequently annealing the ingot metal met with only partial success with the high purity batch 5 iron, owing to the excessive growth of the crystal grains. In arriving at the hardness values the average of four measurements of diameters inclined to one another at 45° was accepted for the Brinell impressions, while the mean of the two diagonals was taken in the case of the impressions of the diamond pyramid.

The results for the various batches of iron are shown in Tables XII and XIII. Many factors were found to influence the hardness figures which, in spite of the precautions adopted in making the measurements, could only be regarded as approximate. For example, elongated crystal grains were usually found in ingots as solidified in the crucible, and the hardness figure deduced from impressions made on a surface cut at right angles to the long axes of the crystals was invariably 5 to 10 points lower than the corresponding values derived from surfaces cut parallel to the length of the crystals. With small impressions the effect of work on the surface was very marked. Thus, a Brinell hardness figure of 96 and a diamond pyramid hardness of 115 were obtained from batch 4 iron when the surface was prepared in the usual way by sawing, grinding, and polishing. After a vacuum annealing at 950° C for 30 minutes the hardness figure, as determined on the same surface by both methods, had fallen to 55. The hardness values were also dependent on the grain size of the material, since crystal-grain boundaries appeared to exert a definite stiffening action.

TABLE XII—BRINELL HARDNESS

Batch	Description of specimen	Load time 30 seconds		Number of impressions	Average Brinell hardness number	Maximum divergence from average
		Diameter of ball mm	Load kg			
1	Slightly worked and annealed	10	1000	2	60	±1
		5	250	2	64·5	±0·5
2	Worked. Annealed 2 hours *in vacuo*	5	250	2	64·7	±0·5
3	Annealed *in vacuo* for 24 hours at 1300–1350° C	2	40	2	47·0	±1·5
4	Unworked. Cut from ingot. Annealed after preparation ½ hour at 950° C	2	40	2	50·3	±0·1
		2	20	8	54·7	+1·3 −2·7
4	Severely cold-worked and annealed 1 hour at 950° C	2	20	3	61	+0·5
5	Unworked. Cut from ingot. Unannealed..............	5	250	2	56·5	±1·7
		2	40	7	54·5	+1·4 −1·6
		2	20	3	54·0	+1·0 −3·0
5	Severely cold-worked and annealed 2 hours at 950° C. Large crystal grain size	2	20	2	49	±1·0
5	Reduced 75% in thickness by cold-rolling. Tested in hardened condition	2	40	—	169 approx.	

N.B.—Hardness numbers obtained from Tables of Brinell Hardness Numbers given in British Standard Specification No. 240 (1926).

TABLE XIII—DIAMOND PYRAMID HARDNESS

(Angle of diamond pyramid, 136°; load, 10 kg; time of loading, 30 secs)

Batch	Description of Specimen	Number of impressions	Average diamond pyramid hardness number	Maximum divergence from average
4	Unworked. Cut from ingot. Annealed after preparation ½ hour at 950° C	8	54·1	+ 1·9 − 3·1
4	Severely cold-worked and annealed 1 hour at 950° C	4	62	+ 3 − 4
5	Severely cold-worked and annealed 2 hours at 950° C. Large crystal grain size	2	48	± 3

N.B.—Hardness numbers obtained from Tables of Diamond Pyramid Hardness Numbers given in British Standard Specification No. 427 (1931).

MALLEABILITY

Samples of iron containing oxide visible under the microscope (portions of batch 3) were often cold short. On the other hand, high purity specimens containing no visible oxide proved to be very malleable at room temperatures. A reduction in thickness approaching 99% was attained by cold-rolling both batch 4 and 5 material which had already been subjected to a moderate degree of hot-working. The specimens were not annealed at any stage in the cold-rolling, and there was no indication that the limit in reduction had been reached.

TENSILE PROPERTIES

Tensile tests were conducted on small cylindrical specimens of batch 2 and 5 materials by the Engineering Department, N.P.L., and the results are given in Table XIV and fig. 10. Owing to the low loads involved, it was not possible to determine the modulus of elasticity with an accuracy greater than ± 2%. It was observed that test-piece " B," batch 5, was drawn down to a single chisel edge at the fracture, a fact which suggests that a large crystal grain had existed in this region of the test-piece. Fig. 11, Plate 3, shows both test-pieces of batch 5 after test. Neither test-piece of batch 5 iron showed a well-defined yield point. The significance of this unusual feature is doubtful, however, since the test-pieces

TABLE XIV—TENSILE PROPERTIES

	Batch 2, iron		Batch 5, iron	
	A	B	A	B
Diameter of test piece, in.....	0·280	0·281	0·250	0·251
Area of cross-section, sq in ..	0·0616	0·0619	0·0491	0·0495
Gauge length, in, $4 \times \sqrt{\text{area of section}}$	1	1	0·88	0·89
Approximate limit of proportionality, stress in tons/sq in	8·44	9·85	2·04	2·42
kg/mm^2	13·25	15·5	3·2	3·8
Ultimate stress, tons/sq in ..	15·6	16·0	11·9	9·1
kg/mm^2	24·5	25·2	18·7	14·3
Reduction in area at fracture %	92	90·5	100	100
Elongation on gauge length %	66	72	49	36
Modulus of elasticity, lb/sq in	27·8 × 10^6	27·1 × 10^6	29·7 × 10^6	28·0 × 10^6
kg/mm^2	19·5 × 10^3	19·0 × 10^3	20·8 × 10^3	19·7 × 10^3

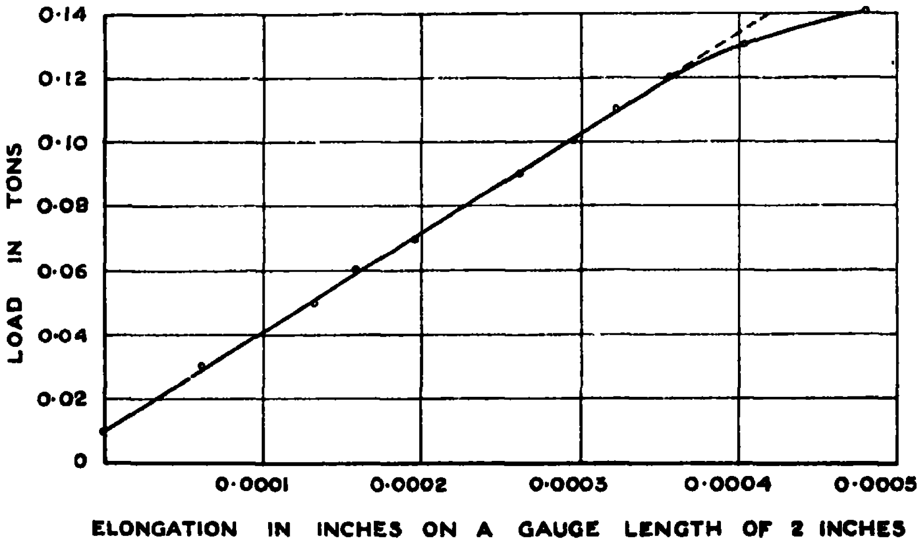

FIG. 10.—Load-elongation curve, batch 5 iron, test-piece B.

possessed extremely coarse crystal grain structures, and it is probable that a well-defined yield point is essentially an attribute of polycrystalline material.

CONCLUSIONS

The authors have deliberately refrained from speculative explanations in connexion with their observations. A comparison of the results for different batches of iron shows that measurable differences existed in some of the physical properties. Thus the higher purity batch 5 iron possessed a slightly higher electrical resistivity than two of the earlier batches. This does not confirm the usually accepted view that the lowest electrical resistance is associated with an element in the purest form. Again, the observations of the magnetic permeability for low and moderate values of magnetizing force do not indicate that the purest iron possesses the highest magnetic permeability. Jones,* in commenting on Yensen's hypothesis,† suggested that de-oxidation of iron would suppress " gamma " iron. The present work does not support this view, however, since it was found that the alpha-gamma transformation was neither suppressed nor raised to any great extent in batch 5 iron, which contains very little oxygen or other impurities.

It is significant that the " alpha-gamma " transformation in the later batches of iron, as indicated by the dilatometric observations, does not take place at a constant temperature, but occupies a definite temperature range. If this temperature interval is attributed to the action of known foreign elements, then the minute traces of impurities found in batch 5 iron must be credited with an extraordinarily powerful influence ; an assumption which should only be admitted when other explanations have failed. Comprehensive analyses have been conducted on this material, and the effect can hardly be attributed to some unidentified impurity. It would appear that the " alpha-gamma " transformation in high purity iron is not a simple phase change occurring at a constant temperature but is a more complex transformation. Further work is desirable, since a full understanding of this change is probably of great importance in connexion with commercial iron alloys.

The high purity iron samples mentioned in this paper have been prepared and investigated at intervals over a period of about eleven years. The late Dr. W. Rosenhain, F.R.S., was responsible for the general

---

* ' J. Iron and Steel Inst.,' vol. 2, p. 429 (1934).

† ' J. Amer. Inst. Min. and Met. Engineers,' Iron and Steel Div., p. 320 (1929).

supervision of the work in the earlier stages, while Dr. C. H. Desch, F.R.S., who succeeded Dr. Rosenhain as Superintendent of the Metallurgical Department, N.P.L., more recently undertook the general supervision of the research. Thanks are also due to Dr. J. L. Haughton, D.Sc., in this connexion. Most of the chemical analyses were carried out by Mr. T. E. Rooney, A.M.S.T., F.I.C., and Mr. P. G. Ward, B.Sc., A.R.C.S., assisted by Mr. A. G. Stapleton and other members of the staff of the Chemical Division of the Metallurgy Department. Dr. G. Barr, B.A., D.Sc., assisted by Mr. H. R. Sullivan and Mr. A. L. Thorogood, B.Sc., undertook those spectroscopic analyses which were conducted at the National Physical Laboratory. The provision of suitable refractories, without which progress would have been impossible, was taken in hand by Mr. D. Turner, B.Sc., assisted by Mr. A. Hatcher and Mr. W. Crowhurst. Acknowledgment is given as far as possible in the text of the paper where important sections of the work have not been undertaken by the authors, but it has not been possible to refer separately to members of the staff who have rendered occasional assistance. The authors are indebted to the staff of the Metallurgy Department workshop for the construction of apparatus, and wish to record their appreciation of the general assistance of Mr. C. Harvey and Mr. A. J. Cook.

Isotherms of CO_2 Between 0° and 150° and Pressures from 16 to 250 Atm (Amagat Densities 18-206)

By A. Michels and Mrs. C. Michels

42nd Publication of the van der Waals Fund

(*Communicated by F. A. Freeth, F.R.S.—Received July* 16, 1935)

In a previous publication* results of measurements were given of the dielectric constant of CO_2 under pressure. In the calculation of the Clausius-Mosotti function, $\frac{\varepsilon - 1}{\varepsilon + 2} \cdot \frac{1}{d}$, from these results and the isotherm data as published by Amagat† doubt arose as to the reliability of the latter, and isotherm measurements have therefore been carried out up to 3000 atm at the same temperatures at which the dielectric constant was measured. The results will be given in a series of papers, of which the present one describes the measurements up to 250 atm. In this range the method published in previous papers‡ could be used.

The apparatus is shown diagrammatically in fig. 1. A is the glass piezometer containing the gas under investigation. It is enclosed in the steel vessel C, which contains some mercury, the remainder being filled with oil. The piezometer consists of a large reservoir B and several small reservoirs connected by narrow capillaries. Through each of these capillaries is sealed a platinum wire, and these all make contact with another platinum wire wound round the outside of the capillary and connected to an insulated lead E through the top of the steel vessel. The volumes from each of the contacts to the top of the tube are calibrated by weighing with mercury, using the method described by Michels and Gibson.§ The volume of gas with which the piezometer is filled is determined separately at 25° and a pressure of about 1 atm, as described by Michels, Wouters, and de Boer.‡ The steel vessel is placed in a thermostat, the temperature of which is electrically regulated in the way previously described by the authors.* The temperature is read with thermometers divided in hundredths of a degree and compared with thermometers calibrated at the P.T.R. (Berlin). They were totally immersed in the thermostat and read with the help of a periscope.* For the isotherm measurements, pressure is applied to the oil through D, forcing the mercury up inside the piezometer and compressing the gas till the mercury surface makes contact with the platinum wires. This contact is indicated by a drop in the electrical resistance of the platinum wire wound round the capillary. The equilibrium pressure, at which contact is made, is measured with a pressure balance. Corrections must be applied for the height of the mercury column inside the glass piezometer and the hydrostatic head of the oil. From the data thus obtained for p, v, and T, the isotherms can be calculated if the total amount of gas contained in the piezometer is known in standard units.

---

* Michels and Michels, ' Phil. Trans.,' A, vol. 231, p. 409 (1933).

† *See* " Critical Tables," vol. 3, p. 11.

‡ Michels, Wouters, and de Boer, ' Physica,' vol. 1, p. 587 (1934); Otto, Michels, and Wouters, ' Phys. Z.,' vol. 35, p. 97 (1934).

§ ' Ann. Physik,' vol. 87, p. 850 (1928).

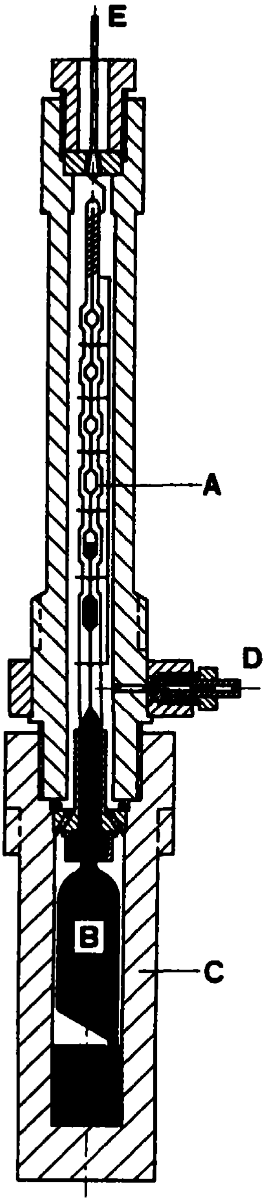

Fig. 1.

The Normal Volume

Isotherm data are in general expressed in Amagat units. In this system the unit of volume is the volume of gas used at 1 atm at 0° C (the so-called normal volume). The quantity of gas is, however, to be determined from the volume measurements at 25° and about 1 atm, and the normal volume must therefore be calculated from those data. For most gases the value of pv is a linear function of p with sufficient accuracy in the pressure range from 0 to 1 atm, so that

$$pv = (pv)_{p=0} + \beta p.$$

If the slope of the isotherms, β, can be obtained from the literature for 0° and 25°, the calculation can be carried out in the following way:

$$(pv)_{p=0,\,t=25} = (pv)_{p,\,t=25} - \beta_{25}p$$

$$(pv)_{p=0,\,t=0} = (pv)_{p=0,\,t}\,\frac{273\cdot15}{273\cdot15 + t}$$

$$(pv)_{p=1,\,t=0} = (pv)_{p=0,\,t=0} + \beta_0.$$

For CO_2 a sufficiently accurate value of β is not available nor can pv *a priori* be assumed to be a linear function of p within the limits wanted.

---

* Michels and Michels, 'Phil. Trans.,' A, vol. 231, p. 419 (1933).

If, however, compressibility data are measured at 0° and 25° and at pressures not too far above 1 atm, the difficulty can be overcome by combining these data with the data obtained at 25° and about 1 atm.

As this procedure can be applied for other gases where the same difficulty holds, a description of the method will be given.

Preliminary figures are taken for β_0 and β_{25}, either from the results published by other experimenters or using the law of corresponding states, and with these a preliminary value is calculated for the volume of the gas at 0° and 1 atm. This volume expressed in cm³ will be called v_N. If the volumes of the piezometer above the different contacts, expressed in *cm*³, are v_1, v_2, v_3, . ., v_x, the Amagat volumes are by definition:

$$v_{1_A} = \frac{v_1}{v_N} \qquad v_{x_A} = \frac{v_x}{v_N}$$

and the Amagat densities:

$$d_{1_A} = \frac{v_N}{v_1} \qquad d_{x_A} = \frac{v_N}{v_x}.$$

The data obtained in the isotherm measurements at 25° together with the data found at 1 atm are evaluated as a series of the type:

$$pv_A = A_{25} + B_{25}d_A + C_{25}d_A^2 + D_{25}d_A^4,$$

using the method of mean squares.

The value of A_{25} is identical with $(pv)_{25}$ for infinite volume, hence the Gay-Lussac law can be applied to give:

$$A_0 = A_{25}\frac{273{\cdot}15}{273{\cdot}15 + 25}$$

where A_0 is the value of pv_A at 0° for zero density and is the first term of the corresponding series for 0° C.

$$pv_A = A_0 + B_0d_A + C_0d_A^2 + D_0d_A^4,$$

A_0 now being known B_0, C_0, and D_0 can again be calculated from the data of the isotherm measurements at 0° with mean squares. If the right value for β_0 and β_{25}, and thus also for the normal volume, has been taken, substitution of $d_A = 1$ must lead by definition to:

$$pv_{A_0} = 1 = A_0 + B_0 + C_0 + D_0.$$

If the equation, however, gives another value, *e.g.*, Y, this means that the volume taken as unit was 1/Y times too large. Hence all the previous values must be multiplied by 1/Y to obtain the volumes expressed in Amagat units. The procedure can then be repeated to make sure that the equation

$$pv_{A_0} = A_0 + B_0 + C_0 + D_0 = 1$$

holds. For CO_2 A_0 was found to be 1·006824.

THE MEASUREMENTS

The CO_2 used was prepared from commercial gas by a three-stage distillation.* The measurements were carried out in two different piezometers, one with a total volume of about 1·500 cm^3 for 8 densities between 18 and 51 Amagat and one with a total volume of 100 cm^3 for 9 densities between 45 and 206 Amagat. The isotherms were measured at 0°, 25°, 30°, 31°, 32°, 40°, 50°, 75°, 100°, 125°, 140°, 145°, and 150° except for the points in the coexistence region or close to the critical point where the method used will not give accurate results. The densities and volumes at the same contact at different temperatures are not exactly the same owing to the compression and thermal expansion of the glass. To facilitate the interpolation for other densities and temperatures, the values have therefore been reduced to standard densities, viz., those at 75°. The correction to be applied is

$$\int_{d_t}^{d_{75}} \left(\frac{\partial pv}{\partial d}\right)_T . \delta d.$$

This term is never greater than 1/600 of the value of *pv* and could therefore be determined graphically.

RESULTS

Pressures between 16 and 66 atm (Amagat densities 18–51).

The results as obtained after being corrected to equal densities are given in Table I.

The values obtained for the seven lowest densities at each temperature have been evaluated in series equations of the type

$$pv = A + Bd + Cd^2 + Dd^4$$

using the method of mean squares. A has been calculated for each temperature from $A_0 = 1·006824$ using the Gay-Lussac relation

$$A_t = A_0 \frac{t + 273·15}{273·15} .$$

---

* Michels and Michels, 'Phil. Trans.,' A, vol. 231, p. 409 (1933).

TABLE I

	d in Amagat units	p in int. atm	pv	$(pv_{\text{calc.}} - pv_{\text{exp.}}) \cdot 10^5$
		T = 0°		
1	18·7500	16·5488	0·88260	−1
2	23·4609	20·0042	0·85266	1
3	28·1756	23·1918	0·82312	−2
4	32·7823	26·0553	0·79480	4
5	37·6251	28·7979	0·76539	−1
6	42·4239	31·2562	0·73676	−2
7	47·1236	33·4202	0·70920	1
		T = 25·053°		
1	18·7500	18·5374	0·98866	2
2	23·4609	22·5716	0·96209	1
3	28·1756	26·3707	0·93594	−6
4	32·7823	29·8654	0·91102	2
5	37·6251	33·3074	0·88524	1
6	42·4239	36·4942	0·86023	0
7	47·1236	39·4066	0·83624	−1
8	51·9162	42·1695	0·81226	
		T = 29·900°		
1	18·7500	18·9142	1·00876	3
2	23·4609	23·0572	0·98279	0
3	28·1756	26·9725	0·95730	−4
4	32·7823	30·5845	0·93296	1
5	37·6251	34·1582	0·90786	2
6	42·4239	37·4781	0·88342	−1
7	47·1236	40·5267	0·86001	0
8	51·9162	43·4302	0·83655	
		T = 31·037°		
1	18·7500	19·0023	1·01346	−4
2	23·4609	23·1728	0·98772	2
3	28·1756	27·1155	0·96238	1
4	32·7823	30·7548	0·93815	6
5	37·6251	34·3530	0·91304	−4
6	42·4239	37·7033	0·88873	−4
7	47·1236	40·7834	0·86546	3
8	51·9162	43·7249	0·84222	
		T = 32·075°		
1	18·7500	19·0843	1·01783	0
2	23·4609	23·2753	0·99209	−2
3	28·1756	27·2422	0·96687	0

TABLE I—(continued)

	d in Amagat units	p in int. atm	pv	$(pv_{\text{calc.}} - pv_{\text{exp.}}) \cdot 10^5$
		T = 32·075°—(continued)		
4	32·7823	30·9057	0·94276	6
5	37·6251	34·5310	0·91777	−2
6	42·4239	37·9095	0·89359	−3
7	47·1236	41·0194	0·87046	2
8	51·9162	43·9873	0·84728	
		T = 40·105°		
1	18·7500	19·7049	1·05093	−2
2	23·4609	24·0750	1·02618	2
3	28·1756	28·2269	1·00182	−3
4	32·7823	32·0819	0·97864	5
5	37·6251	35·9179	0·95463	1
6	42·4239	39·5101	0·93132	−6
7	47·1236	42·8401	0·90910	3
8	51·9162	46·0366	0·88675	
		T = 49·712°		
1	18·7500	20·4459	1·09045	0
2	23·4609	25·0260	1·06671	2
3	28·1756	29·3972	1·04336	−6
4	32·7823	33·4756	1·02115	2
5	37·6251	37·5594	0·99826	6
6	42·4239	41·4000	0·97586	−6
7	47·1236	44·9823	0·95456	2
8	51·9162	48·4512	0·93326	
		T = 75·260°		
1	18·7500	22·3956	1·19443	−5
2	23·4609	27·5246	1·17321	5
3	28·1756	32·4664	1·15229	−1
4	32·7823	37·1221	1·13238	3
5	37·6251	41·8318	1·11181	−3
6	42·4239	46·3237	1·09192	−1
7	47·1236	50·5569	1·07286	1
8	51·9162	54·7133	1·05388	
		T = 99·767°		
1	18·7500	24·2483	1·29325	−3
2	23·4609	29·8914	1·27409	2
3	28·1756	35·3693	1·25532	0
4	32·7823	40·5672	1·23747	6

Table I—(continued)

	d in Amagat units	p in int. atm	pv	$(pv_{calc} - pv_{exp}) . 10^5$
T = 99·767°—(continued)				
5	37·6251	45·8633	1·21896	−6
6	42·4239	50·9585	1·20117	−1
7	47·1236	55·7976	1·18407	1
8	51·9162	50·5903	1·16708	
T = 125·007°				
1	18·7500	26·1449	1·39439	−7
2	23·4609	32·3124	1·37729	5
3	28·1756	38·3316	1·36046	1
4	32·7823	44·0758	1·34450	5
5	37·6251	49·9670	1·32802	−4
6	42·4239	55·6672	1·31217	−5
7	47·1236	61·1248	1·29712	3
T = 139·832°				
1	18·7500	27·2629	1·45402	−1
2	23·4609	33·7360	1·43797	4
3	28·1756	40·0701	1·42216	−5
4	32·7823	46·1341	1·40729	4
5	37·6251	52·3711	1·39192	−2
6	42·4239	58·4258	1·37719	1
7	47·1236	64·2354	1·36313	0
T = 145·049°				
1	18·7500	27·6502	1·47468	−2
2	23·4609	34·2283	1·45895	−2
3	28·1756	40·6771	1·44370	7
4	32·7823	46·8464	1·42902	−3
5	37·6251	53·2068	1·41413	2
6	42·4239	59·3798	1·39968	−4
7	47·1236	65·3144	1·38602	2
T = 150·140°				
1	18·7500	28·0309	1·49498	2
2	23·4609	34·7130	1·47961	1
3	28·1756	41·2661	1·46461	−4
4	32·7823	47·5473	1·45040	−1
5	37·6251	54·0256	1·43589	5
6	42·4239	60·3181	1·42179	−2
7	47·1236	66·3704	1·40843	0

The values of *d* for the different points measured have been substituted in the equation, and the last column of Table I gives the difference between the values so obtained for *pv* and the experimental ones, showing that the series evaluation fits the experiments within $\pm \frac{1}{20,000}$. The values obtained at the highest density were not used in the series evaluation as they were not measured for some of the temperatures. Table II gives the values of the coefficients A, B, C, and D. When plotted as a function of temperature B gives a smooth curve, fig. 2, in contrast with C and D. The reason for this will be discussed in a later paper.

TABLE II

Temp.	A	$B\,.\,10^{3}$	$C\,.\,10^{-6}$	$D\,.\,10^{12}$
0°	1·006824	−6·8370459	11·392053	151·42345
25·053	1·099169	−6·1003636	10·935636	53·63504
29·900	1·117035	−5·9935436	11·629296	83·19171
31·037	1·121226	−5·9614836	11·565534	−112·15987
32·075	1·125052	−5·9274260	11·126705	1·73649
40·105	1·154650	−5·7480687	11·618127	−102·41663
49·712	1·190062	−5·5334588	11·831728	−210·17999
75·260	1·284231	−5·0003078	11·476013	−251·45923
99·767	1·374563	−4·5490179	11·520446	−349·45185
125·007	1·467597	−4·1002219	10·727025	−227·08611
139·832	1·522241	−3·8127583	9·349572	− 41·49212
145·049	1·541471	−3·7403400	9·593405	−103·98110
150·140	1·560237	−3·6601313	9·587843	−125·14100

Pressures between 38 and 242 atm (Amagat densities 45–206).

The results obtained after being corrected to equal densities are given in Table III.

The series evaluation of the results is discussed in a separate paper.

For the interpolation of intermediate temperatures use can be made of the value of $\Delta pv/\Delta T$. This function was therefore calculated for each density measured, 75·26° taken as reference temperature.

Substitution of the values of *pv* at $d = 18{\cdot}75$ and $t = 0°$ and 75·26° in $\frac{pv_t - pv_{75\cdot26}}{t - 75\cdot26}$ gives f.i.:

$$\frac{\Delta pv}{\Delta T} = \frac{0{\cdot}882601 - 1{\cdot}194433}{0 - 75{\cdot}260} = \frac{0{\cdot}311832}{75{\cdot}26} = 414{\cdot}34 \times 10^{-5}.$$

The results obtained are plotted in figs. 3 and 4 as a function of temperature. From the slope of the lines conclusions can be drawn as to the

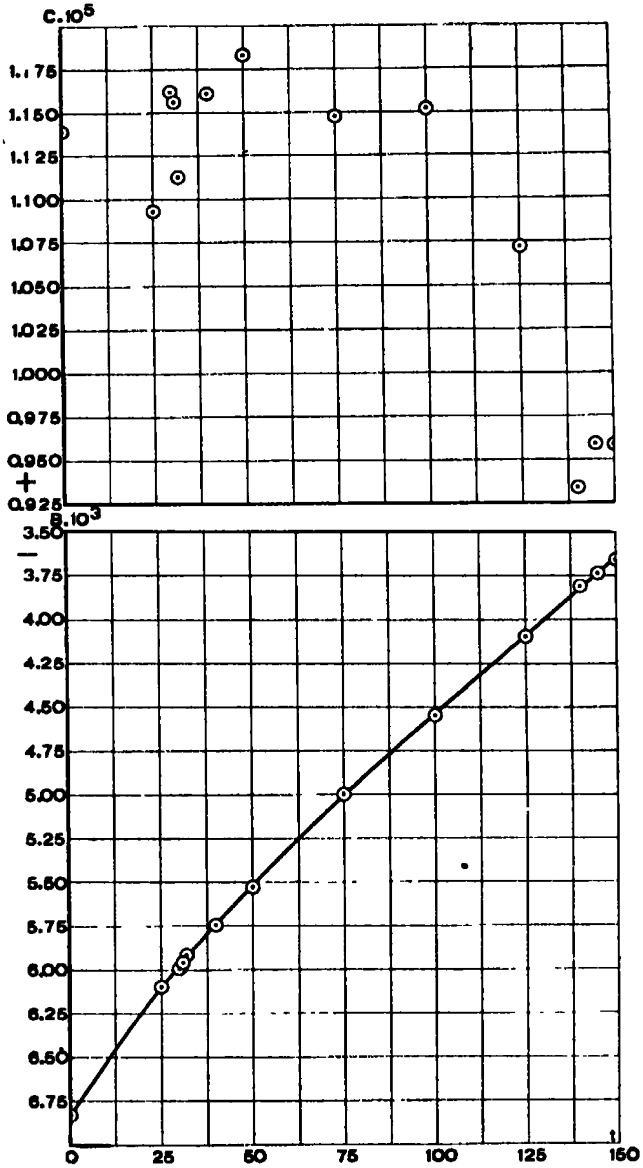
C.10⁵
1.175
1.150
1.125
1.100
1.075
1.050
1.025
1.000
0.975
0.950
+
0.925
B.10³
3.50
—
3.75
4.00
4.25
4.50
4.75
5.00
5.25
5.50
5.75
6.00
6.25
6.50
6.75
t
0
25
50
75
100
125
150

FIG. 2.

TABLE III

	d in Amagat units	*p* in int. atm	*pv*
		T = 0°	
9	45·7631	32·8104	0·71696
		T = 25·053°	
9	45·7631	38·5848	0·84314
10	69·1536	50·4894	0·73011
11	91·1131	57·8714	0·63516
12	112·181	62·1547	0·55406
		T = 29·900°	
10	69·1536	52·3024	0·75632
11	91·1131	60·4925	0·66393
12	112·181	65·6621	0·58532
		T = 31·037°	
9	45·7631	39·9116	0·87214
10	69·1536	52·7335	0·76256
11	91·1131	61·1005	0·67060
12	112·181	66·4466	0·59232
13	133·474	69·7944	0·52291
14	153·793	71·5656	0·46534
15	170·439	72·3269	0·42436
		T = 32·075°	
9	45·7631	40·1351	0·87702
10	69·1536	53·1108	0·76801
11	91·1131	61·6445	0·67657
12	112·181	67·1831	0·59888
13	133·474	70·7150	0·52981
14	153·793	72·6751	0·47255
		T = 40·105°	
9	45·7631	41·8949	0·91547
10	69·1536	56·0660	0·81075
11	91·1131	65·8679	0·72292
12	112·181	72·7142	0·64819
13	133·474	77·6808	0·58199
14	153·793	81·0225	0·52683
15	170·439	83·0491	0·48727

TABLE III—(continued)

	d in Amagat units	*p* in int. atm	*pv*
	T = 49·712°		
9	45·7631	43·9632	0·96067
10	69·1536	59·5247	0·86076
11	91·1131	70·7822	0·77686
12	112·181	79·1582	0·70563
13	133·474	85·7385	0·64236
14	153·793	90·6827	0·58964
15	170·439	94·0488	0·55180
16	88·541	97·2327	0·51571
17	206·448	100·111	0·48492
	T = 75·260°		
9	45·7631	49·3542	1·07847
10	69·1536	68·4200	0·98939
11	91·1131	83·3944	0·91528
12	112·181	95·6316	0·85248
13	133·474	106·367	0·79692
14	153·793	115·505	0·75104
15	170·439	122·438	0·71837
16	188·541	129·654	0·68767
17	206·448	136·724	0·66227
	T = 99·767°		
9	45·7631	54·4127	1·18901
10	69·1536	76·7447	1·10977
11	91·1131	95·1297	1·04408
12	112·181	110·947	0·98900
13	133·474	125·564	0·94074
14	153·793	138·669	0·90166
15	170·439	149·054	0·87453
16	188·541	160·256	0·84998
17	206·448	171·567	0·83105
	T = 125·007°		
9	45·7631	59·5642	1·30158
10	69·1536	85·1721	1·23164
11	91·1131	106·991	1·17426
12	112·181	126·402	1·12677
13	133·474	144·979	1·08620
14	153·793	162·163	1·05442
15	170·439	176·137	1·03343
16	188·541	191·499	1·01569
17	206·448	207·249	1·00388

TABLE III—(continued)

	d in Amagat units	p in int. atm	pv
	T = 139·832°		
9	45·7631	62·5508	1·36684
10	69·1536	90·0439	1·30209
11	91·1131	113·845	1·24949
12	112·181	135·354	1·20657
13	133·474	156·231	1·17050
14	153·793	175·791	1·14304
15	170·439	191·864	1·12571
16	188·541	209·677	1·11210
17	206·448	228·042	1·10460
	T = 145·049°		
9	45·7631	63·6203	1·39021
10	69·1536	91·7867	1·32729
11	91·1131	116·284	1·27627
12	112·181	138·536	1·23493
13	133·474	160·226	1·20043
14	153·793	180·635	1·17453
15	170·439	197·461	1·15854
16	188·541	216·150	1·14644
17	206·448	235·454	1·14050
	T = 150·140°		
9	45·7631	64·6284	1·41224
10	69·1536	93·4256	1·35099
11	91·1131	118·587	1·30154
12	112·181	141·534	1·26166
13	133·474	164·001	1·22872
14	153·793	185·206	1·20425
15	170·439	202·746	1·18955
16	188·541	222·250	1·17879
17	206·448	242·450	1·17439

behaviour of the specific heat at constant volume (c_v) at the higher densities.

$$dS = \frac{c_v}{T}\,dT + \left(\frac{\partial p}{\partial T}\right)_v dv,$$

$$\frac{1}{T}\frac{\partial c_v}{\partial v} = \frac{\partial^2 p}{\partial T^2} = \frac{1}{v}\left(\frac{\partial^2 pv}{\partial T^2}\right)_v,$$

where S is the entropy.

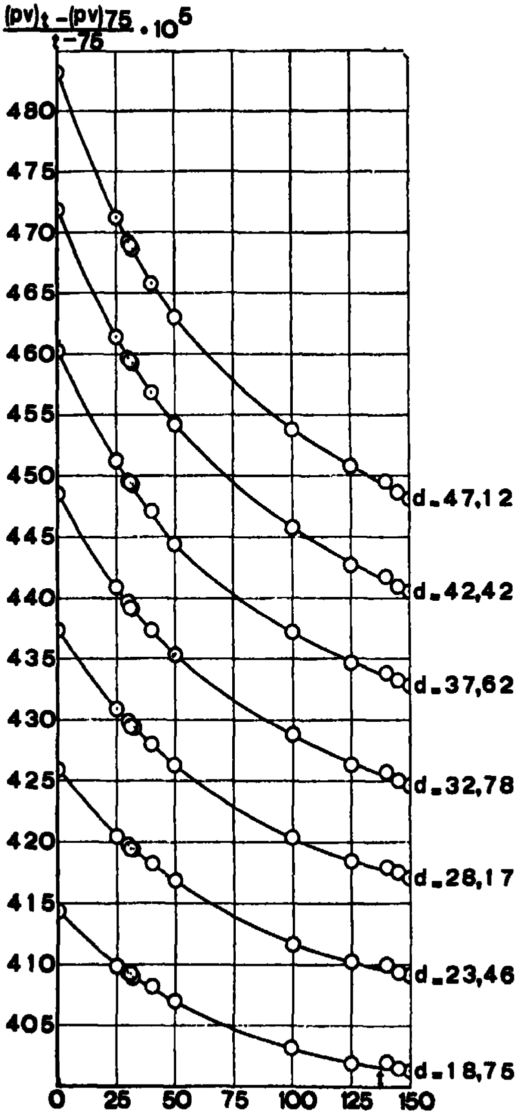
$\frac{(pv)_t - (pv)_{75}}{t-75} \cdot 10^5$
480
475
470
465
460
455
450
445
440
435
430
425
420
415
410
405
0
25
50
75
100
125
150
t
d = 47,12
d = 42,42
d = 37,62
d = 32,78
d = 28,17
d = 23,46
d = 18,75

FIG. 3.

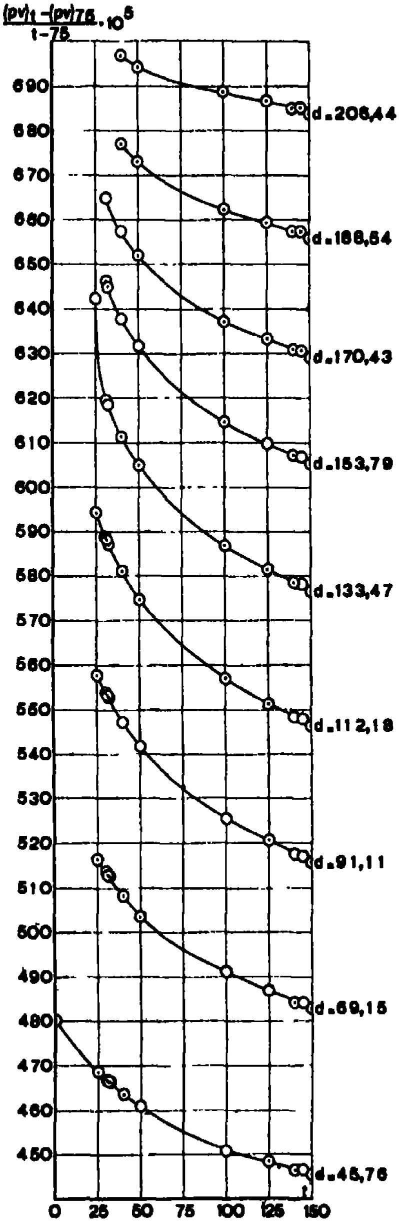
$\frac{(pv)_t - (pv)_{75}}{t-75} \cdot 10^5$
690
680
670
660
650
640
630
620
610
600
590
580
570
560
550
540
530
520
510
500
490
480
470
460
450
0
25
50
75
100
125
150
t
d = 206,44
d = 188,54
d = 170,43
d = 153,79
d = 133,47
d = 112,18
d = 91,11
d = 69,15
d = 45,76

FIG. 4.

The slope of the lines drawn is given by

$$\frac{\partial \frac{\Delta pv}{\Delta T}}{\partial T}$$

which is negative in the whole range measured, hence $(\partial^2 pv/\partial T^2)_v$ can be expected to be negative and

$$\frac{\partial c_v}{\partial d} = -\frac{1}{d^2}\frac{\partial c_v}{\partial v} = -\frac{T}{d}\left(\frac{\partial^2 pv}{\partial T^2}\right)_v$$

will be positive.

The specific heat will therefore increase with increasing density. Thermodynamical conclusions which can be derived from the figures given will be discussed in a separate paper.

Isotherms of CO_2 Between 70 and 3000 Atmospheres (Amagat Densities between 200 and 600)

By A. Michels, Mrs. C. Michels, and H. Wouters

43rd Publication of the van der Waals Fund

(*Communicated by F. A. Freeth, F.R.S.—Received July* 16, 1935)

In the previous paper the technique and results of isotherm measurements up to densities of 200 Amagat units were described. For higher densities, however, the method used has the disadvantage that either the final volumes of the gas will be very small or the initial volume must be very large. The first would lead to inaccurate density-measurements, the second to an enlargement of the steel container, which must stand 3000 atmospheres pressure so that the apparatus would be rather bulky.

The apparatus was therefore altered so that the piezometer could be filled and the normal volume determined under pressure, but, by taking this pressure between 20 to 50 atmospheres, use could be made of the isotherm measurements described in the previous paper.

The Apparatus

The apparatus as assembled and filled, is shown in fig. 1. The top half of the glass piezometer, B to C, containing the contacts for the isotherm measurements is of the same shape as in the previous design. The bottom half is changed to allow the piezometer to be filled under pressure through the capillary D, while a contact at A is sealed in for the determination of the normal volume. The volume above A was 75 cc, the volume above B, the first measuring contact, was 7·5 cc, and the top volume above the highest contact about 4·5 cc. If, therefore, the amount of gas with which the piezometer is filled is chosen so that when the mercury reaches contact A the density $d = 20$, measurements can be carried out between density $d = 200$ and $d = 340$. With a second filling giving a density $d = 34$ at A, the range can be extended up to a density of 580. The piezometer is filled with gas at I through the valve E. The spindle of this valve is controlled with the rod F, which fits tightly in the tube G. The packing is fitted at the top H of this tube projecting out of the thermostat so that it is not attacked by the hot oil.

Special precautions had to be taken to avoid mercury entering the capillary D when pressure, applied to the oil at K, forces the mercury level inside the piezometer above the top of this capillary. A steel hood, L, is therefore placed over the top of the capillary. As the ratio of the density of the gas when the mercury surface is at the bottom of the hood to the density when it is at the top contact is about 1/20, the volume of the hood must be at least 20 times the total volume of the capillary and the passages to the point of the valve spindle. It is thus essential to keep these volumes as small as possible, and steel rods, along which a groove was cut for letting the gas pass, were therefore placed in the capillary and passages. The dimensions of

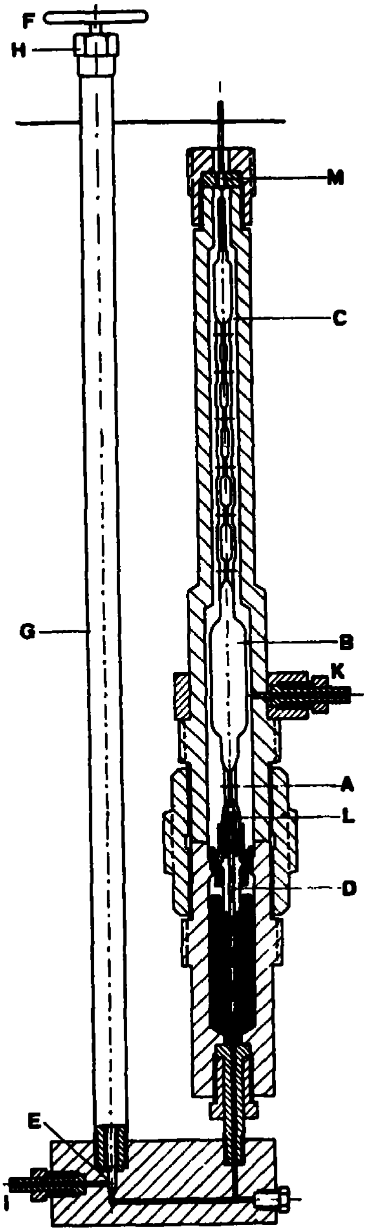

FIG. 1.

the apparatus and the amount of mercury are so chosen that the mercury is about 5 cm below the bottom edge of the hood when it has the same level inside and outside the glass piezometer.

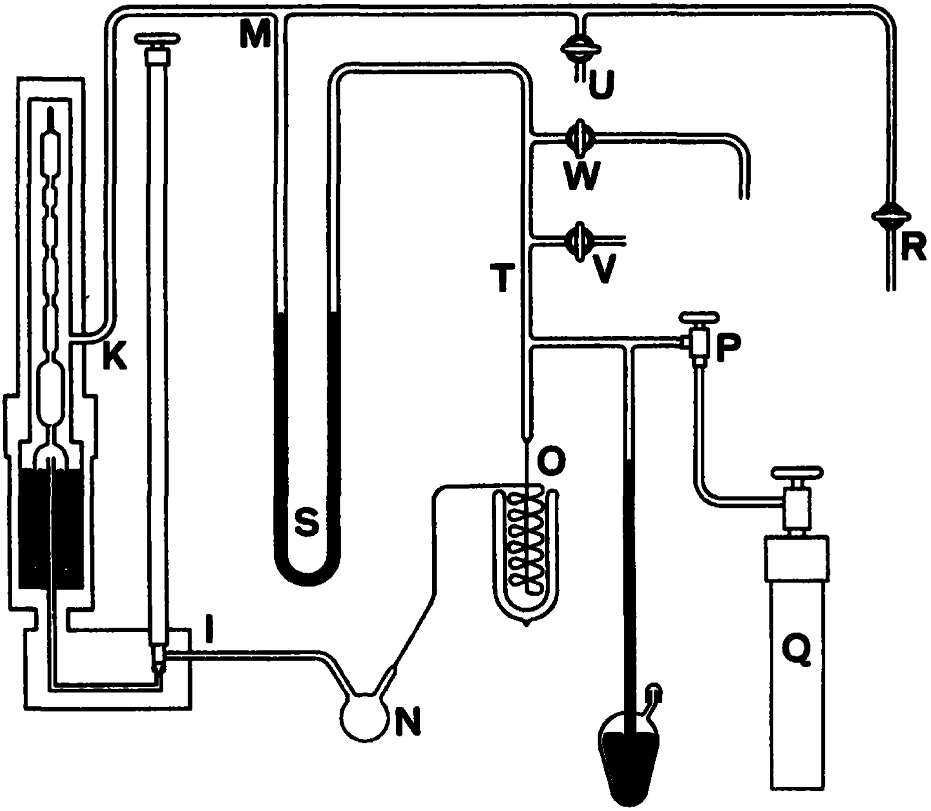

Fig. 2.

The Filling of the Piezometer with Gas

The filling is carried out in two stages: first to a gas pressure of a little over 1 atmosphere, and in the second stage the filling is completed to the required density.

During the first stage, there is no oil above the mercury in the steel container, which is not placed in the thermostat but is coupled to a filling apparatus shown in fig. 2. A copper capillary is connected at K, the other end of which is soldered to the glass T-piece M leading to the glass tap R and the differential mercury manometer S. The filling tube I is connected through the mercury trap N, the cooling coil O and the throttling valve P to the storage cylinder Q. A side tube T leads to the other end of the differential manometer S. V is connected to a mercury diffusion pump, W and R to a rotary oil pump, U opens to the atmosphere. The apparatus is first pumped inside and outside the glass piezometer with the oil pump. To avoid getting mercury in the steel hood, the pumping speed on either side is regulated with the taps R and W, so that the pressure outside the piezometer is always slightly less than the pressure inside. The pressure difference is controlled by the differential manometer S. When the pressure is less than a few millimetres, R and W are shut and the inside is pumped for a day or two with the diffusion pump; during this pumping O is cooled with liquid air to prevent mercury vapour from reaching the soldered joint near N. Then V is shut, gas is slowly let in to the inside of the piezometer, and air to the outside while again the pressure outside is kept rather less than inside. This procedure is repeated several times to wash out the piezometer. It is then finally filled to a pressure a few centimetres above atmospheric.

The first stage of the filling being finished, the steel vessel is filled with oil, placed in the thermostat, and the apparatus assembled as shown in fig. 3 for the second stage. Here Q is the storage cylinder, P and V are metal throttling valves. M is a high pressure steel tube, L is a hydraulic press, R a pressure balance, U and W are spring manometers reading up to 50 atmospheres, S is a glass differential manometer which can stand 10 atmospheres. All the other tubes are steel capillaries. The tube M is filled with oil. With the valves I and T shut, the tube system between I, T, and S is pumped through V with a diffusion pump. Gas is let in from the storage cylinder to atmospheric pressure and the procedure repeated till all residual gas is sufficiently washed out. The system is then filled slightly above atmospheric pressure and the valve I opened. More gas is supplied very slowly through the throttling valve T. The oil pressure on the outside of the piezometer is simultaneously increased with the oil press L, but is always kept slightly less than the gas pressure to prevent mercury entering the steel hood. The pressure difference is controlled with the mercury differential manometer. When a pressure of about 10 atmospheres is reached, valves P and N are shut and the differential manometer dismantled. Gas can now be let in without danger, as the displacement of the mercury level inside the piezometer is negligible owing to the small compression of the oil outside the piezometer and in the press. When about the right amount of gas is let in, I is shut, the thermostat regulated at 25°, the oil pressure is increased with the press L till the mercury reaches the normal volume contact A, and the pressure measured with the pressure balance. From this pressure, the temperature, the calibrated volume above the contact A, and the isotherm data available, the amount of gas in the piezometer is calculated. The quantity of the gas can be altered at will after lowering the mercury below the steel hood.

THE MEASUREMENTS

The temperature control and measurement is carried out in the same way as described in the previous paper.

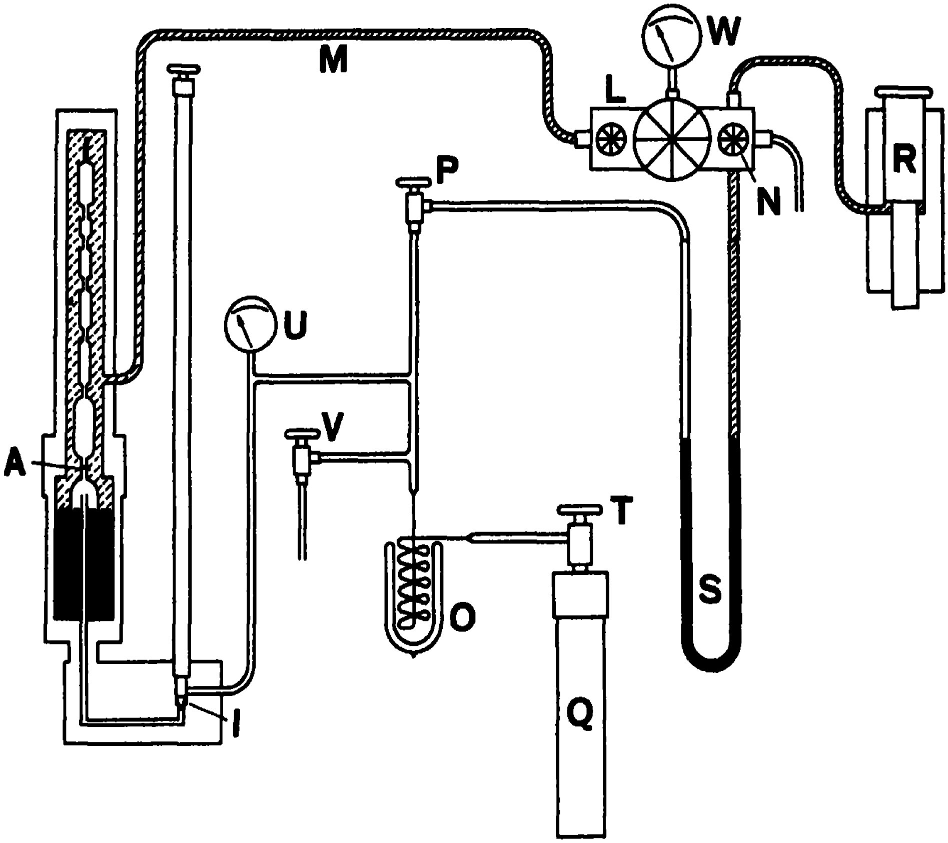

FIG. 3.

Above 2000 atmospheres the accuracy in the results decreases gradually owing to the increase in the viscosity of the oil. At the highest pressure it is not above 1 : 2000. After the second filling, contact 6 disappeared, for temperatures above 75°, while the first contact at 100°, 125°, and 150° showed signs of deterioration, the reproducibility for this point at those temperatures being not better than 1 : 2000. At the highest densities no measurements were made at 140° and 145°, as the results at lower densities showed sufficiently clearly that nothing peculiar happened at those temperatures, so that the values could as well be calculated from the results at 125° and 150°.[*] In the immediate neighbourhood of the critical point, no measurements were made as the method used is not suitable in this region.

The results reduced to equal densities and temperatures are given in Table I. A possible change in the effective area of the piston of the pressure balance is not taken into account as this has not yet been determined.

TABLE I

	d[†] in Amagat units	p in int. atm.	pv
		T = 0°	
32	563·322	537·348	0·95389
		T = 25·053°	
27	386·741	74·739	0·19325
28	422·259	109·870	0·26020
29	457·002	180·783	0·39558
30	491·852	308·620	0·62747
31	527·299	523·452	0·99270
32	563·322	864·844	1·53526
33	596·455	1325·17	2·22175
		T = 29·900°	
26	352·168	77·500	0·22006
27	386·741	95·133	0·24599
28	422·259	136·228	0·32262
29	457·002	214·196	0·46870
30	491·852	350·240	0·71208
31	527·299	575·031	1·09052
32	563·322	927·543	1·64656
33	596·455	1399·97	2·34715
		T = 31·037°	
26	352·168	81·261	0·23075
27	386·741	99·928	0·25838
28	422·259	142·458	0·33737
29	457·002	221·968	0·48570
30..	491·852	359·953	0·73183
31	527·299	586·799	1·11284
32	563·322	942·145	1·67248
33	596·455	1417·40	2·37637

[†] The numbering of the densities measured starts at 18 as a continuation of the one published in the previous paper.

[*] *See* Ibbs and Wakeman, 'Proc. Roy. Soc.,' A, vol. 134, p. 613 (1932).

TABLE I—(continued)

	d in Amagat units	*p* in int. atm.	*pv*
		T = 32·075°	
26	352·168	84·715	0·24055
27	386·741	104·352	0·26983
28	422·259	148·113	0·35076
29	457·002	228·958	0·50100
30	491·852	368·433	0·74907
31	527·299	597·131	1·13243
32	563·322	954·615	1·69462
33	596·455	1431·91	2·40069
		T = 40·105°	
18	206·465	86·197	0·41749
19	226·708	87·587	0·38634
20	247·482	89·060	0·35986
21	267·766	90·768	0·33898
22	288·060	93·074	0·32311
23	308·608	96·583	0·31296
24	329·365	102·084	0·30994
25	348·296	109·778	0·31519
26	352·168	111·891	0·31772
27	386·741	138·903	0·35916
28	422·259	192·012	0·45473
29	457·002	284·037	0·62152
30	491·852	436·706	0·88788
31	527·299	681·094	1·29167
32	563·322	1056·92	1·87623
33	596·455	1553·06	2·60381
		T = 49·712°	
18	206·465	100·118	0·48492
19	226·708	103·257	0·45546
20	247·482	106·665	0·43100
21	267·766	110·491	0·41264
22	288·060	115·297	0·40026
23	308·608	121·776	0·39460
24	329·365	130·848	0·39727
25	348·296	142·376	0·40878
26	352·168	145·229	0·41239
27	386·741	180·898	0·46775
28	422·259	245·038	0·58030
29	457·002	350·279	0·76647
30	491·852	518·686	1·05456
31	527·299	781·537	1·48215
32	563·322	1178·98	2·09291
33	596·455	1697·79	2·84647

TABLE I—(continued)

	d in Amagat units	*p* in int. atm.	*pv*
	T = 75·260°		
18	206·465	136·755	0·66236
19	226·708	144·999	0·63958
20	247·482	154·134	0·62281
21	267·766	164·233	0·61332
22	288·060	176·119	0·61140
23	308·608	190·823	0·61834
24	329·365	209·486	0·63603
25	348·296	231·033	0·66332
26	352·168	236·152	0·67057
27	386·741	294·160	0·76061
28	422·259	386·643	0·91565
29	457·002	525·234	1·14930
30			
31	527·299	1043·50	1·97896
32	563·322	1495·84	2·65539
33	596·455	2071·69	3·47334
	T = 99·767°		
18	206·465	171·567	0·83097
19	226·708	184·991	0·81599
20	247·482	199·951	0·80794
21	267·766	216·386	0·80812
22	288·060	235·395	0·81717
23	308·608	258·216	0·83671
24	329·365	286·180	0·86888
25	348·296	317·264	0·91090
26	352·168	324·641	0·92184
27	386·741	403·553	1·04347
28	422·259	522·315	1·23695
29	457·002	691·824	1·51383
30			
31	527·299	1289·39	2·44528
32	563·322	1792·29	3·18164
33	596·455	2419·97	4·05726
	T = 125·007°		
18	206·465	207·180	1·00346
19	226·708	226·052	0·99710
20	247·482	247·204	0·99887
21	267·766	270·324	1·00955
22	288·060	296·782	1·03028
23	308·608	328·050	1·06300
24	329·365	365·592	1·10999

TABLE I—(continued)

	d in Amagat units	*p* in int. atm.	*pv*
	T = 125·007°—(continued)		
25	348·296	406·517	1·16716
26	352·168	416·089	1·18151
27	386·741	516·195	1·33473
28	422·259	661·080	1·56558
29	457·002	861·320	1·88472
30			
31	527·299	1537·59	2·91597
32	563·322	2090·21	3·71051
33	596·455	2772·13	4·64768
	T = 139·832°		
18	206·465	227·971	1·10416
19	226·708	250·070	1·10305
20	247·482	274·861	1·11063
21	267·766	301·942	1·12763
22	288·060	332·811	1·15536
23	308·608	369·052	1·19586
24	329·365	412·253	1·25166
25	348·296	458·836	1·31738
	T = 145·049°		
18	206·465	235·402	1·14015
19	226·708	258·675	1·14100
20	247·482	284·778	1·15070
21	267·766	313·261	1·16991
22	288·060	345·718	1·20016
23	308·608	383·741	1·24346
24	329·365	428·928	1·30229
25	348·296	477·593	1·37123
	T = 150·140°		
18	206·465	242·478	1·17443
19	226·708	266·859	1·17710
20	247·482	294·204	1·18879
21	267·766	324·034	1·21014
22	288·060	357·992	1·24277
23	308·608	397·723	1·28876
24	329·365	444·846	1·35062
25	348·296	495·431	1·42244
26	352·168	507·212	1·44026
27	386·741	628·422	1·62492
28	422·259	799·215	1·89271
29	457·002	1030·05	2·25393
30			
31	527·299	1782·41	3·38027
32	563·322	2384·27	4·23251
33	596·455	3117·01	5·22590

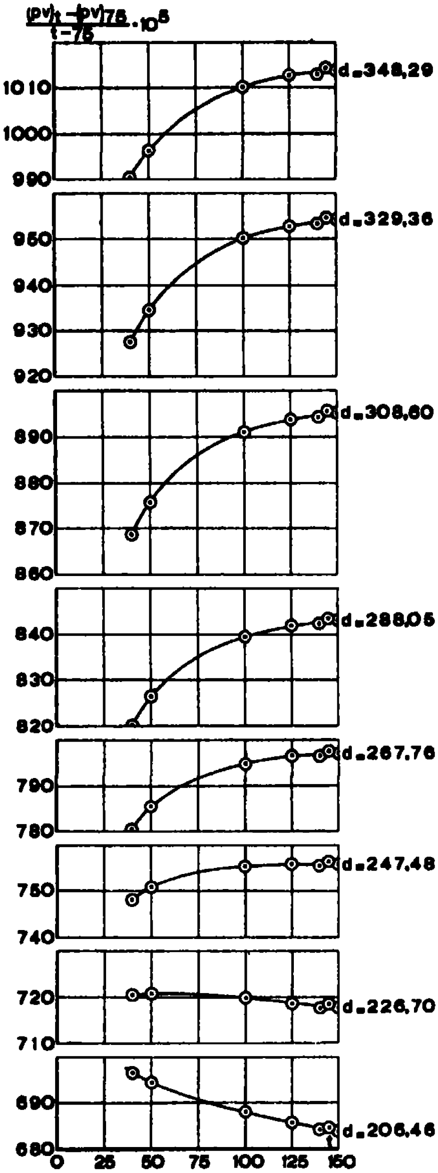

FIG. 4.

The series evaluation will be discussed in a separate paper. As in the previous paper, the values of $\frac{pv_{75} - pv_t}{75 - t}$ were calculated and are plotted against t.

From the slope of the curves it can be seen, as explained in the previous paper, that at a density of 206 A the specific heat c_v still increases with increasing density to a maximum for $d = 226 \cdot 7$ A, then decreases and passes through a minimum at a density between 390 A and 460 A. It may be noted that the position of the maximum at the density of 226 coincides with the density of the critical point. The existence of a maximum of c_v in the direct neighbourhood of the critical point was already found by W. H. Keesom.* Numerical data will be given in a separate paper.

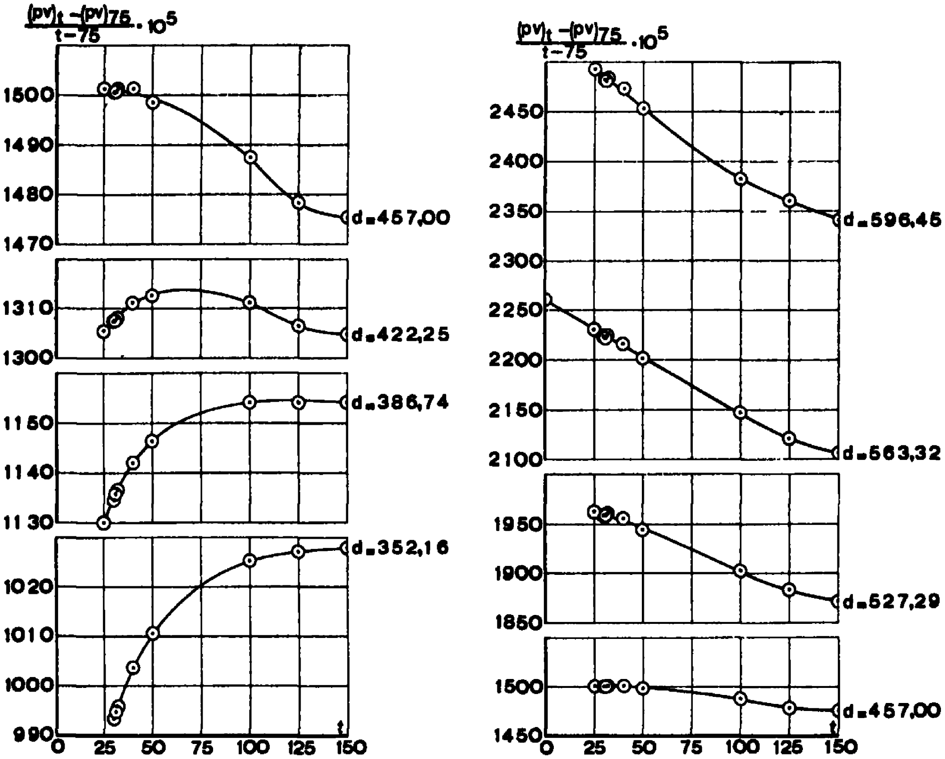

FIG. 5.

---

* ‘Comm. Phys. Lab. Leiden,’ No. 88.

The Crystal Structure of Para-Dinitrobenzene

By R. W. James, G. King, and H. Horrocks, Manchester University

(*Communicated by W. L. Bragg, F.R.S.—Received July* 20, 1935)

The crystallography and optical properties of para-dinitrobenzene were first studied by Bodewig* in 1876. Investigations by means of X-rays have recently been made by Hertel,† who determined the unit cell and the space group and tentatively proposed a structure, and by Banerjee,‡ who applied the method of Fourier synthesis and gave a set of atomic parameters. A brief examination of the intensities of a few X-ray spectra shows that the structure proposed by Hertel cannot be correct, and it was therefore decided to attempt a full analysis, with a view to determining the size and shape of the nitro group in aromatic compounds. During the course of the work Banerjee's paper was published. We are, however, unable to agree with his conclusions, and the structure proposed as a result of the work to be described here differs radically from his.

CRYSTALLOGRAPHY AND OPTICAL PROPERTIES

Very beautiful crystals of para-dinitrobenzene may be obtained by the slow evaporation of a solution in acetone. They are pale lemon-yellow in colour, and the smaller ones are very clear and free from flaws, and have brilliantly reflecting faces. Crystals several millimetres across may easily be grown, but these are usually less perfect than the smaller ones. The crystals belong to the monoclinic holohedral class, and Bodewig gives for the monoclinic angle and the axial ratios

$$\beta = 90^\circ\ 18', \quad a : b : c = 2\cdot038 : 1 : 1\cdot043,$$

values which are closely confirmed by goniometer measurements made during the course of this work.

The crystals grown from solution in acetone usually show the prism faces $\{110\}$, and the faces (100) and $(\bar{1}00)$ in the zone $[001]$. In the zone $[010]$, the faces (101) and $(\bar{1}01)$ are usually well developed. Plates with surfaces parallel to $(\bar{1}01)$, having (101) relatively small, frequently form; but there is considerable variation in habit, and crystals longer in the

---

* 'Ann. Physik,' vol. 158, p. 239 (1876).

† 'Z. phys. Chem.,' B, vol. 7, p. 188 (1930).

‡ 'Phil. Mag.,' vol. 18, p. 1004 (1934).

c direction than in the *a* and *b* directions are not uncommon. The faces (001) and (010) are rarely, if ever, formed, and it would be more correct structurally to regard ($\bar{1}01$) as the *c* face, corresponding to a monoclinic angle $\beta = 115° \, 7'$; for the crystal is truly monoclinic, and not pseudo-rhombic, as the value $\beta = 92° \, 18'$ might suggest. We have, however, retained the standard indexing of the faces.

As an aid in guessing a provisional structure, the three principal refractive indices of the crystal were determined. Small crystals, immersed in solutions of potassium mercuric iodide of different concentrations, were examined under the polarizing microscope, the concentration of the solution being altered until the crystal became nearly invisible.

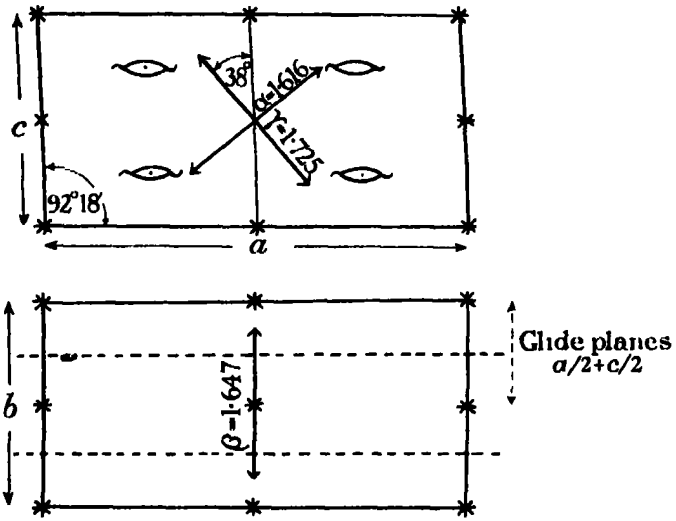

Fig. 1—Symmetry elements, and refractive indices.

The Becke line phenomenon was used as an indication of the direction in which the concentration had to be altered in any given case. By suitable manipulation of the crystals all three refractive indices were measured in this way, and the values

$$\alpha = 1 \cdot 61_6, \quad \beta = 1 \cdot 64_7, \quad \gamma = 1 \cdot 72_5$$

were obtained with sodium light. The crystal is thus positively birefringent. The optic-axial plane is the symmetry plane (010) ; and the intermediate axis of the optical ellipsoid, corresponding to β, lies along the *b* axis of the crystal. The longest axis of the ellipsoid, corresponding to γ, lies in the plane (010), and is inclined at an angle of about 38° to the *c* axis, as shown in fig. 1.

THE UNIT CELL AND THE SPACE-GROUP

A series of oscillation photographs was made with CuKα radiation. The dimensions of the unit cell determined from these are

$$a = 11 \cdot 05 \text{ A}, \quad b = 5 \cdot 42 \text{ A}, \quad c = 6 \cdot 56 \text{ A}.$$

According to Barker,* the density of the crystal is 1·546 ; v. Groth† quotes values of 1·625 obtained by Lobry de Bruyn,‡ and 1·623 obtained by Brandl. From these values, it follows that the unit cell must contain two molecules of $C_6H_4(NO_2)_2$, and, assuming this, we find the true density to be 1·64.

General reflexions *hkl* of all types occur, showing that the unit cell having the above dimensions is primitive. Reflexions 0*k*0 are absent if *k* is odd, and reflexions *h*0*l* are absent if $h + l$ is odd. There are no other systematic absences. If we assume the crystal to be holohedral, an assumption confirmed by the crystallographic evidence, and by the absence of any pyro-electric effect when it is cooled in liquid aid, this fixes the space-group as C_{2h}^5, or P $2_1/n$ in the Hermann-Maugin notation. This group possesses, in addition to centres of symmetry, screw axes parallel to [010], and glide planes, with glide components $a/2 + c/2$, parallel to (010). The unit cell and the symmetry elements are shown in fig. 1.

A general position in the group P $2_1/n$ has a multiplicity of four, and the four equivalent points have fractional co-ordinates, referred to a symmetry centre as origin,

$$\pm (u, v, w) \; ; \; \pm (u + \tfrac{1}{2}, \tfrac{1}{2} - v, w + \tfrac{1}{2}).$$

Since the unit cell contains only two molecules, we must conclude that the molecules themselves have centres of symmetry, evidently the centres of the benzene rings, which lie at centres of symmetry of the structure as a whole. Suppose now each corner of the unit cell to be occupied by a symmetry centre, which is also the centre of a molecule. This accounts for one of the molecules of the unit cell. The screw axes give rise to another set of symmetry centres, lying at the mid-points of the unit cells formed by the first set. At each of these is the centre of a molecule which may be derived from a molecule of the first set by the action of a screw axis. This is as far as one can go in the determination of the structure, using purely geometrical reasoning.

---

* 'Z. Kristallog.,' vol. 44, p. 154 (1908).

† 'Chem. Kristallog.,' vol. 4, p. 14.

‡ 'Rec. trav. chim. Pays-bas,' vol. 13, p. 111 (1894).

THE PRELIMINARY ESTIMATE OF THE STRUCTURE

In deciding what is the probable structure of the crystal, we may use first our knowledge of the optical properties, and secondly the information as to the size and shape of the benzene ring that has been provided by the work of Mrs. Lonsdale,* Robertson,† and others. The crystal has one large refractive index and two smaller ones, which are nearly equal. We should infer from this that the direction of vibration for the largest refractive index, which lies in the *ac* plane in the direction indicated by γ in fig. 1, is nearly parallel to the plane of the benzene ring ; while the directions of vibration corresponding to the two smaller indices, which lie along the directions marked α and β in fig. 1, are roughly equally inclined to the plane of the ring.

The benzene ring is known to approximate very closely to a regular hexagon of edge 1·4 A, and the closest approach of neighbouring rings in such compounds as have been investigated is 3·6 to 3·8 A. We had, to begin with, no definite knowledge of the size and shape of the nitro group, but assumed that it would be similar to the NO_2 group in $NaNO_2$, as determined by Ziegler,‡ with an O — O distance of 2·09 A, and N — O distances of 1·13 A. The distance C — N was unknown, but 1·35 A, the value in urea, was assumed as likely. With these dimensions, scale models of the molecules were constructed of cardboard. It was found possible to pack these models into the unit cell in such a way as to fulfil the symmetry conditions, and to satisfy the demands of the refractive indices, only if the planes of the rings were inclined at about 50° to the *ac* plane, and if the lines joining the pairs of oxygen atoms in the nitro groups were parallel, or nearly parallel to the *ac* plane. The type of arrangement to which this reasoning leads may be seen from fig. 3, which represents the projection of the final structure on the *ac* plane ; for more detailed work based on intensity measurements shows these preliminary ideas to be very near the truth.

THE FOURIER SYNTHESIS OF THE STRUCTURE

For the accurate determination of the structure we have used the method of the double Fourier series, developed by W. L. Bragg,§ which has already been applied to a number of aromatic compounds by Mrs. Lonsdale,* Robertson, *loc. cit.*, and others.

---

* ' Proc. Roy. Soc.,' A, vol. 123, p. 494 (1929).

† ' Proc. Roy. Soc.,' A, vol. 140, p. 79 (1933); vol. 142, p. 674 (1933).

‡ ' Phys. Rev.,' vol. 38, p. 1040 (1931).

§ ' Proc. Roy. Soc.,' A, vol. 123, p. 537 (1929).

If the whole electron density of the crystal be supposed projected on the face *ab*, the direction of projection being parallel to *c*, then $\rho\ (xy)$, the density of this projection at the point (x, y) in the *ab* plane, is given by

$$\rho\ (x, y) = 1/\mathrm{A}\ (ab) \sum^{h} \sum^{k} \mathrm{F}\ (hk0) \cos 2\pi \{(hx/a + ky/b)\}, \qquad (1)$$

where A (*ab*) is the area of the side *ab* of the unit cell, and F (*hk*0) is the structure factor of the spectrum *hk*0. The sums are to be taken over all values of *h* and *k*, positive and negative. The series can be written in the form (1) only if the projection on the *ab* plane has a centre of symmetry, which is also the origin of the co-ordinates *x* and *y*. Corresponding series give the projections on the other axial planes. The areas of the faces *ab* and *ac* of the unit cell are approximately double that of the face *bc*. There is thus much less chance of interference between the maxima corresponding to the different atoms in the projections for $\rho\ (x, y)$ and $\rho\ (x, z)$ than for $\rho\ (y, z)$. The projection $\rho\ (x, z)$ was determined first of all, since the provisional structure promised clear resolution of the atoms in the *ac* plane.

ABSOLUTE INTENSITY MEASUREMENTS

In order to evaluate the series for $\rho\ (x, z)$, it was necessary to determine in absolute measure the structure factors F (*h*0*l*) for all spectra of appreciable strength having indices of the type *h*0*l*, and arising from crystal planes belonging to the zone [010]. For this a crystal with opposite (110) faces strongly developed, which formed a parallel-sided plate about 1·8 mm in thickness, was used. The plate was mounted at the centre of the vertical circle of the crystal holder of the ionization spectrometer, the *b* axis of the crystal being parallel to the axis of the circle, and so horizontal. By rotating the vertical circle in its own plane, all planes of type (*h*0*l*) could be brought in turn parallel to the axis of the spectrometer. An X-ray beam narrow enough to be received completely by the face of the crystal plate was used, and the integrated intensity of each spectrum was measured by finding the area beneath the curve giving the relation between crystal setting and reflected intensity. The intensities were standardized in terms of the reflexion from a rock salt crystal giving a known integrated reflexion. Molybdenum Kα radiation was used. The observations were controlled by oscillation photographs, to ensure that no spectra not belonging to the zone were measured in the ionization chamber. This is a desirable precaution when one of the crystal axes is long.

---

* 'Proc. Roy. Soc.,' A, vol. 133, p. 536 (1931).

For spectra of type (*h*0*l*) the zone axis is [010], and this is not perpendicular to the planes (110) that formed the faces of the crystal plate. The usual formula for the integrated reflexion ρ through a crystal plate, which assumes the reflecting planes to be perpendicular to the surface of the plate, cannot be used without modification. We find the general formula for a crystal plate of thickness t to be

$$\rho = \frac{Qq}{\mu} \cdot \frac{e^{-pt} - e^{\ qt}}{q - p}, \tag{2}$$

where $p = \mu \sec \chi \,.\, \sec (\theta - \eta)$, $q = \mu \sec \chi \,.\, \text{sec.}\ (\theta + \eta)$. Here μ is the linear absorption coefficient of the crystal, χ is the angle between the normal to the plate and the plane of reflexion, which always contains the zone axis, and η is the angle between the projection of the normal on the plane of reflexion and the zone axis. The angles actually measured are α, the angle between the normal and the zone axis, which is constant, and ϕ, the setting of the vertical circle. If ϕ is taken as zero when the normal to the slip lies in the plane of reflexion, we have

$$\sin \chi = \sin \phi \,.\, \sin \alpha \ ; \ \cos \eta = \cos \alpha \,.\, \sec \chi \,. \tag{3}$$

The formula (2) is not very convenient for computation, but if pt and qt are small, which is usual with organic crystals, we may write with sufficient accuracy

$$\rho = \frac{Qqt}{\mu} \left\{ 1 - \frac{p+q}{2} \,.\, t \right\}, \tag{4}$$

which we have found quite accurate enough for the present work. Although formula (2) becomes indeterminate when $\alpha = 0$, it may easily be shown to have as a limit the usual value $Qt \sec \theta \,.\, e^{-\mu t \sec \theta}$.

The absorption coefficient occurs in equation (4) only in the product μt, which was determined experimentally for the actual crystal plates used in the experiments. The equations given above apply to a crystal showing no primary or secondary extinction. The agreement between the observed and finally calculated structure factors seems to show that extinction plays no important part in the crystals used in our experiments, except for two or three of the stronger spectra. The formulae have accordingly been used without correction. Q has the usual value

$$N^2\lambda^3 \,.\, |F|^2 \,.\, (e^2/mc^2)^2 \,.\, (1 + \cos^2 2\theta)/2 \sin 2\theta \,.$$

For the *hk*0 spectra a crystal plate with surfaces parallel to ($\bar{1}01$) was used. Again the zone axis is not perpendicular to the surface of the plate, and formula (4) must be used in calculating Q. The agreement between the corresponding value of |F (*h*00)| and |F (0*k*0)| obtained from the two sets of spectra *h*0*l* and *hk*0, which was of the order of 5%, is evidence that the methods used in reducing the observations to absolute measure were sound.

No suitable crystal plate could be found for measuring the spectra 0*kl*. A small crystal was bathed in the radiation, and the assumption was made that the integrated reflexion was proportional to the volume of the crystal. The spectra 0*k*0 and 00*l*, which had been measured in the other zones, were taken as known, and the other integrated reflexions were calculated from these. The measurements in this zone are probably less accurate than those in the others. The measured values of |F| for all the spectra used in the calculation of the Fourier series are shown in column 4 of Table I.

TABLE I—OBSERVED AND CALCULATED STRUCTURE FACTORS

	λ = 0·71 A			
hkl	θ		F (calc.)	F (obs.)
	°	'		
200	3	42	10·4	10·0
400	7	17	− 20·0	18·5
600	11	6	− 14·0	10·3
800	14	48	11·2	6·0
10,00	18	42	1·6	1·9
12,00	22	36	− 7·2	3·0
020	7	30	36·4	26·4
040	15	12	− 3·2	6·0
060	23	0	− 2·4	—
002	7	12	1·2	2·8
004	14	36	− 14·0	12·4
006	22	5	− 3·2	2·4
011	5	12	6·0	8·4
012	8	12	12·0	9·6
013	11	30	− 13·6	12·8
014	15	6	1·2	3·2
015	18	42	6·4	3·6
016	22	30	4·0	2·4
021	8	18	− 13·2	8·8
022	10	30	5·2	2·8
023	13	18	− 10·0	6·8
024	16	30	− 5·6	4·4
025	19	54	3·6	3·2
026	23	36	0·4	—
031	11	54	− 6·8	7·6
032	13	30	− 2·8	3·2
033	15	48	− 4·8	4·8
034	18	36	− 4·4	6·0
035	21	48	—	—
036	25	12	7·2	2·8
041	15	36	− 14·0	8·8
042	16	54	8·4	5·6
043	18	48	11·6	10·0
044	21	18	1·6	—
045	24	12	0·4	—
051	19	30	1·6	—
052	20	30	− 4·0	5·6
053	22	13	− 0·8	—
054	24	24	2·4	—
061	23	24	2·4	—
062	24	18	2·0	—
063	25	48	− 1·2	—
101	4	6	− 4·0	1·6
$10\bar{1}$	4	0	44·4	22·2
103	11	6	− 25·6	18·4
$10\bar{3}$	11	0	8·8	3·6
105	18	30	0·4	—
$10\bar{5}$	18	24	4·8	2·8

TABLE I—(continued)

λ = 0·71 A					λ = 0·71A				
hkl	θ		F (calc.)	F (obs.)	*hkl*	θ		F (calc.)	F (obs.)
	°	′				°	′		
107	26	18	− 4·4	2·8	$80\bar{4}$	20	36	− 4·4	2·8
$10\bar{7}$	26	12	− 1·6	1·6	806	27	42	7·2	2·8
202	8	12	− 9·2	8·0	$80\bar{6}$	26	42	− 2·4	2·0
$20\bar{2}$	8	0	− 24·8	16·4	901	17	24	− 0·8	4·0
204	15	12	− 1·6	3·6	$90\bar{1}$	16	54	4·0	5·6
$20\bar{4}$	14	54	− 3·2	—	903	20	36	− 1·6	2·8
206	22	42	− 6·0	3·6	$90\bar{3}$	19	42	4·0	3·6
$20\bar{6}$	22	18	5·2	2·0	905	25	48	4·0	2·0
301	6	42	− 7·2	6·4	$90\bar{5}$	24	42	− 1·6	3·2
301	6	24	3·2	4·8	10,02	20	30	3·2	7·2
303	12	24	− 3·6	2·0	$10,0\bar{2}$	19	48	0·0	1·2
303	12	0	− 3·6	2·4	10,04	24	30	− 2·0	—
305	19	24	4·4	—	10,04	23	30	− 1·2	1·2
$30\bar{5}$	19	0	− 6·4	1·6	11,01	21	12	− 2·4	6·0
402	10	36	17·2	13·4	$11,0\bar{1}$	20	42	− 3·6	4·0
$40\bar{2}$	10	6	− 1·2	3·2	11,03	24	10	− 1·2	1·6
404	16	42	10·8	4·8	$11,0\bar{3}$	23	12	1·2	—
$40\bar{4}$	16	6	14·8	12·4	11,05	28	48	− 1·6	2·0
406	23	48	− 0·4	—	11,05	27	30	− 3·6	2·4
$40\bar{6}$	23	12	− 4·0	2·8	12,02	24	12	7·6	7·6
$50\bar{1}$	10	6	− 3·6	9·6	12,02	23	30	− 5·6	4·4
501	9	42	24·0	21·6	13,01	25	12	8·0	6·0
503	14	42	− 6·0	7·6	$13,0\bar{1}$	24	42	− 4·0	1·6
$50\bar{3}$	14	0	14·4	10·4					
505	21	0	4·4	2·5	110	4	12	− 2·4	1·0
$50\bar{5}$	20	18	3·2	6·8	120	7	42	20·0	19·6
507	28	18	− 0·4	—	130	11	30	− 16·4	14·8
507	27	26	− 2·8	2·4	140	15	24	12·4	8·4
602	13	36	− 22·4	21·6	150	19	12	− 0·8	2·4
$60\bar{2}$	13	0	6·0	2·0	210	5	12	− 29·6	26·0
604	18	48	− 8·4	5·6	220	8	24	− 19·2	16·8
$60\bar{4}$	18	6	19·2	14·8	230	11	54	− 22·0	16·4
606	25	30	7·2	5·6	240	15	36	− 7·6	8·8
$60\bar{6}$	24	36	− 2·0	—	250	19	30	− 6·8	1·2
701	13	42	− 4·4	6·4	310	6	42	43·2	28·0
$70\bar{1}$	13	18	− 25·6	20·0	320	9	18	− 4·0	6·8
703	17	24	− 6·8	4·8	330	12	36	2·4	—
$70\bar{3}$	16	42	0·4	—	340	16	12	0·8	2·4
705	23	12	6·0	6·8	350	19	54	− 1·2	2·4
$70\bar{5}$	22	18	6·4	3·6	360	23	48	− 3·6	4·0
802	16	54	− 4·4	4·4	410	8	12	− 0·8	—
802	16	18	− 4·0	1·6	420	10	30	− 10·0	7·2
804	21	30	− 1·6	—	430	13	30	9·6	8·0

TABLE I—(continued)

	λ – 0·71A					λ = 0·71A			
hkl	θ		F (calc.)	F (obs.)	*hkl*	0		F (calc.)	F (obs.)
	°	′				°	′		
440	16	54	1·2	2·4	850	24	30	1·6	4·8
460	24	18	2·8	1·6	860	27	54	2·8	2·4
510	9	54	– 5·6	6·4	910	17	6	– 6·8	5·2
520	11	54	– 8·4	7·2	920	18	24	10·4	10·8
530	14	36	– 1·2	3·6	940	22	54	4·0	2·0
540	17	48	0·0	3·2	950	25	48	– 3·6	2·8
550	21	18	– 1·2	3·6	10,10	19	0	0·8	1·6
610	11	42	6·4	9·6	10,20	20	12	2·4	3·2
620	13	24	– 0·4	2·8	10,30	22	0	– 4·4	2·4
630	15	54	11·6	9·6	10,40	24	18	0·8	3·2
640	18	54	– 2·4	4·0	10,50	27	12	4·8	2·4
670	29	42	– 4·4	2·4	11,10	20	54	8·4	1·6
710	13	30	– 7·2	6·4	11,20	22	0	2·8	2·0
720	15	0	3·6	6·0	11,30	23	42	4·0	2·0
730	17	18	4·4	7·6	11,40	25	54	– 1·2	2·0
740	20	6	1·2	1·6	12,10	22	52	4·0	2·8
750	23	18	0·4	2·0	12,20	23	54	– 3·2	2·8
810	15	18	4·0	5·6	13,10	24	54	– 1·6	1 6
820	16	42	10·0	10·0	13,40	29	18	– 0·8	1·2
830	16	42	7·2	2·4	13,50	31	54	2·4	1·6
840	21	24	– 0·8	2·0	15,30	31	12	0·8	1·6

THE EVALUATION OF THE FOURIER SERIES

The coefficients F in the Fourier series, when the origin of co-ordinates is a symmetry centre, may be either positive or negative, and the observations, since they give only $|F|^2$, cannot determine which. For the first evaluation of the series for $\rho\,(x, z)$, approximate values of the parameters u and w were taken from the provisional structure described above, and the structure factors for the spectra ($h0l$) were calculated, using the expression

$$F\,(hkl) = 4 \sum_{s} f_s \cos 2\pi \left\{hu + lw + \frac{h+k+l}{4}\right\} . \cos 2\pi \left\{kv - \frac{h+k+l}{4}\right\}, \qquad (5)$$

the sum being over all the atoms in the unit cell.

For the atomic scattering factors f, values for N and O were taken from the tables of James and Brindley,* a slight estimated allowance for the temperature factor being made. For the carbon atoms of the benzene ring a set of values recently published by Robertson* was used, and we are much indebted to him for allowing us to have these values before their publication. It was found that the assumed parameters gave a general agreement between observed and calculated structure factors for the stronger spectra, and that the signs of the larger structure factors were not altered by small changes in the values of the parameters. The series was therefore evaluated with only the stronger half of the measured coefficients, whose signs were those determined from the assumed structure. The projection so obtained, although not very clean, gave definite maxima and minima from which improved values of the parameters u and w could be estimated. With these, the structure factors were recalculated, and a few of the coefficients changed sign. The series was again evaluated with the corrected signs, the weaker coefficients being now also included. The maxima in the projection were now very clear, but a further calculation was made with the slightly changed para-

---

* 'Phil. Mag.,' vol. 12, p. 81 (1931).

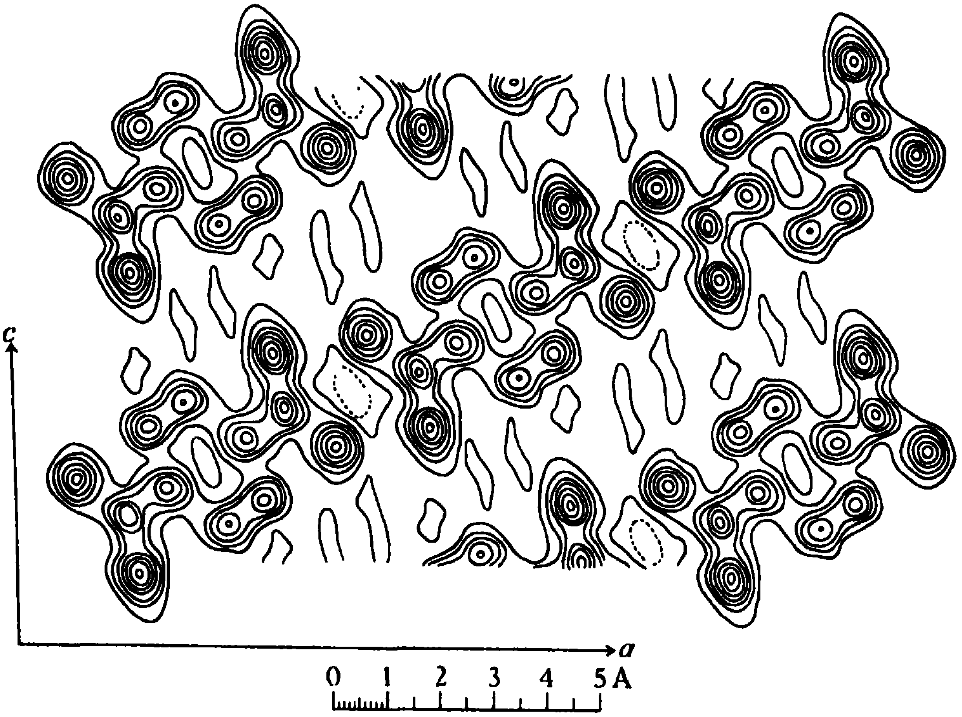

FIG. 2—Fourier projection of the structure in direction of b axis on to the ac plane. Contours at intervals of one electron per A^3. The dotted line is the three-electron contour.

---

* 'Proc. Roy. Soc.,' A, vol. 150, p. 106 (1935).

meters deduced from the second projection. This led to minor adjustments of sign, and the calculation of the projection was emended accordingly. The contour diagram drawn from the final values of ρ (x, z) for the projection on the *ac* face, viewed parallel to *b*, is shown in fig. 2. This contour diagram may be interpreted with the help of the key diagram, fig. 3, which shows the structure projected on the *ac* plane.

The $(h0l)$ projection shows clearly the benzene ring and the nitro groups, and is evidently consistent with the view that the former is a regular hexagon. Assuming this, we may calculate the size and orientation of the ring, and so determine the v parameters of the carbon atoms. It is also plain that the line joining C to N is nearly parallel to a diameter of the ring, and that the lines joining O to O in a nitro group are nearly parallel to the *ac* plane. These considerations enabled us to make an estimate of the v parameters of O and N. The u parameters were already known from the *ac* projection. It was therefore possible to calculate the signs of the coefficients F $(hk0)$ for the projection parallel to c on to the

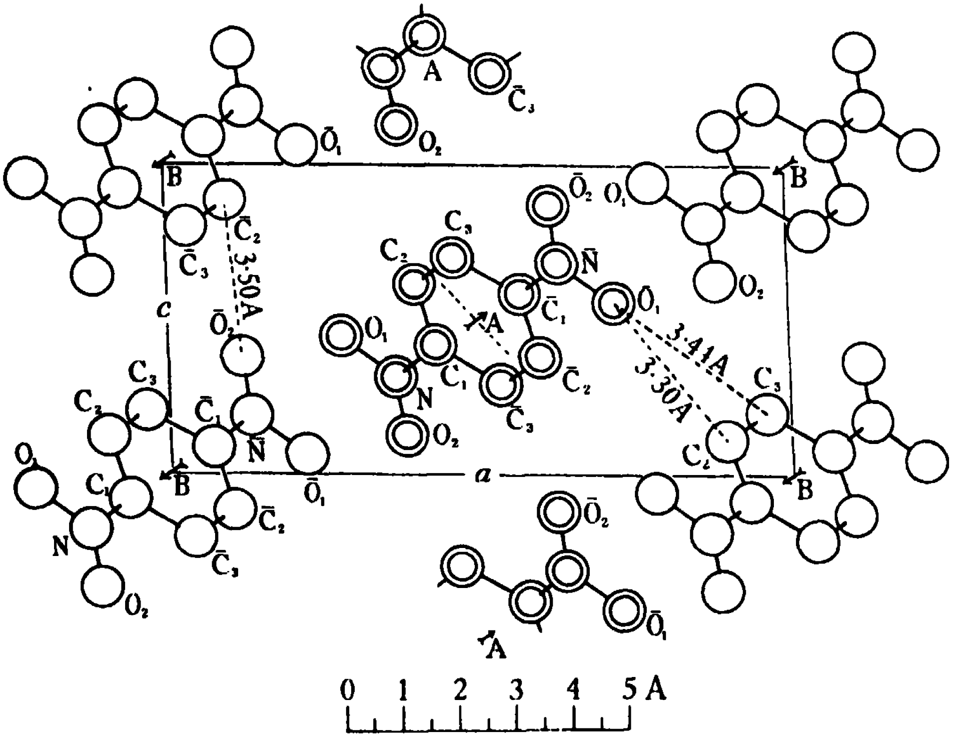

FIG. 3—Projection of the structure in direction *b* axis on to the *ac* plane. The planes containing the centres of the A molecules (double circles) lie *b*/2 above or below those containing the centres of the B molecules.

ab face, and then to proceed exactly as before. The contour diagram and key diagram corresponding to the values of ρ (*x*, *y*) are given in figs. 4 and 5.

Finally, the series for ρ (*y*, *z*) was evaluated from the 0*kl* spectra. The results are illustrated by the contour diagram, fig. 6, and the key diagram, fig. 7.

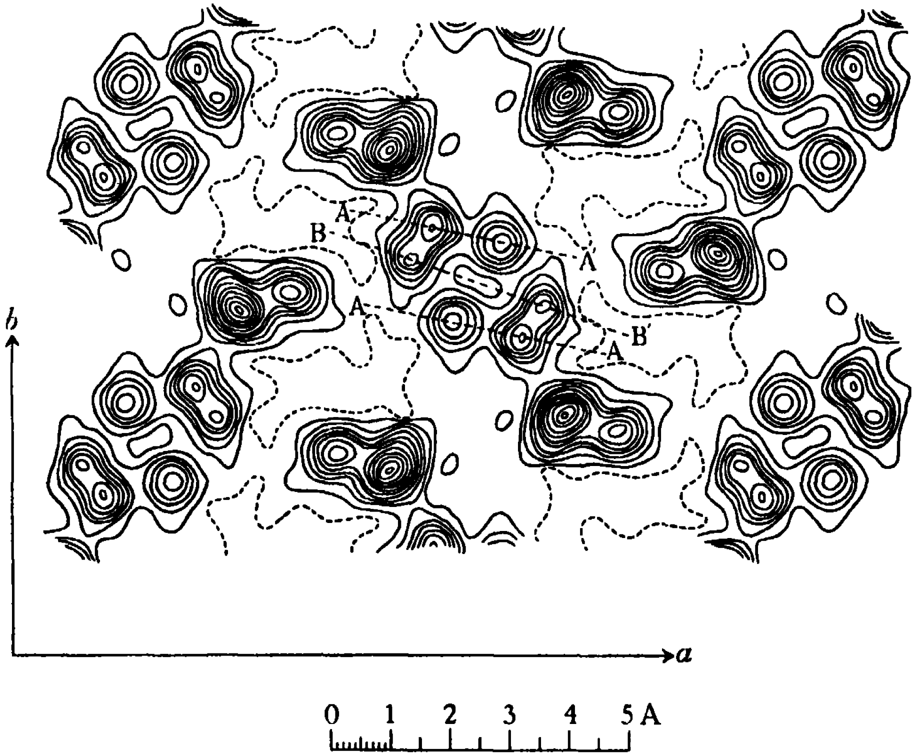

FIG. 4—Fourier projection of the structure in *c* direction on to face *ab*. Contours at intervals of one electron per A^2. The four-electron contour is dotted.

ESTIMATION OF THE PARAMETERS FROM THE CONTOUR DIAGRAMS

In the projection on the *ac* face, figs. 2 and 3, the peaks representing the different atoms are well resolved and are fairly circular in outline. The parameters *u* and *w* estimated from this projection should therefore be fairly reliable. In the projection on *ab*, figs. 4 and 5, the atoms of the benzene ring still show clearly-separated maxima, although those marked C_1 and C_2 are not quite clearly resolved. The N atom, and the atom O_2 are, however, so nearly in line as to form one large maximum of slightly elliptical outline. If we assume the separation of the atoms to be along the axis of this ellipse, and take the *u* parameters as known from the *ac* projection, we can make fairly good estimates of the *v* parameters for these two atoms. The *v* parameters of the other atoms in the structure are clearly defined. A list of the parameters as finally deduced from the projections *ac* and *ab* is given in Table II.

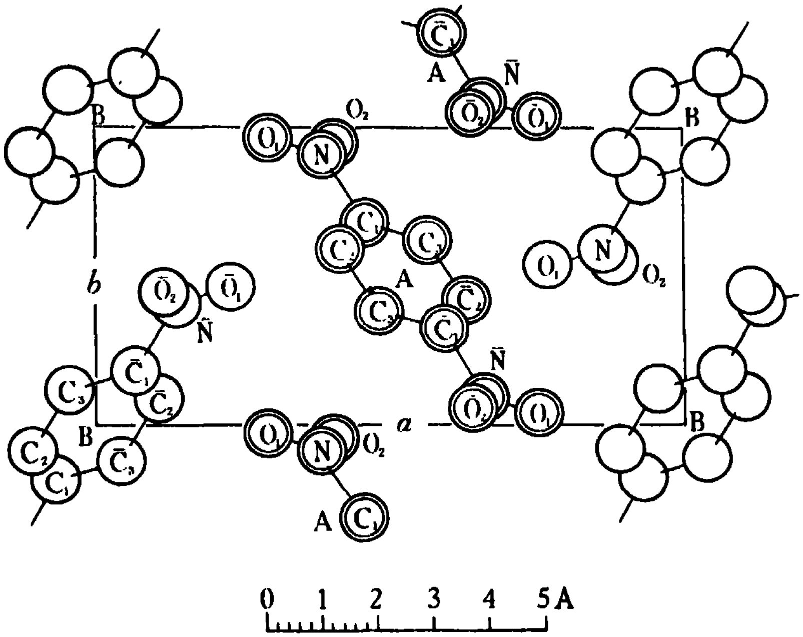

FIG. 5—Projection of the structure on the *ab* plane. Molecules of type A lie in planes *c*/2 above and below those of type B.

TABLE II—PARAMETERS OF ATOMS AS FRACTIONS OF THE CORRESPONDING LATTICE TRANSLATIONS

	u	*v*	*w*
C_1	− 0·069	0·180	− 0·084
C_2	− 0·100	0·085	0·120
C_3	− 0·036	− 0·120	0·206
N	− 0·134	0·41 ± 0·01	− 0·185
O_1	− 0·220	0·464	− 0·056
O_2	− 0·120	0·45 ± 0·01	− 0·372

The fractional co-ordinates of the 4 equivalent atoms in the unit cell are

$$\pm (u, v, w);\ \pm (u + \tfrac{1}{2}, \tfrac{1}{2} - v, w + \tfrac{1}{2}).$$

The projection on the *ac* plane is consistent, within the limits of experimental error, with a plane regular benzene ring. The same is, however, not true of the projection on *ab*. Lines that in the projection of a regular hexagon should be parallel, such as AA′ and BB′ in fig. 4, are definitely not parallel. Now a careful investigation shows that it is the v parameter of the atom C_1, which is joined to the nitro group, that causes the departure from regularity. An increase in the value of v for C_1 from 0·18 to 0·20 would give a ring consistent in both projections with a regular hexagon of side 1·40 A, within the limits of error. The question now arises as to whether we are to consider this departure from regularity as real. We may first note that the differences between the values of the u parameter of the same atom, determined independently from the two projections *ac* and *ab*, are always much smaller than the change in the

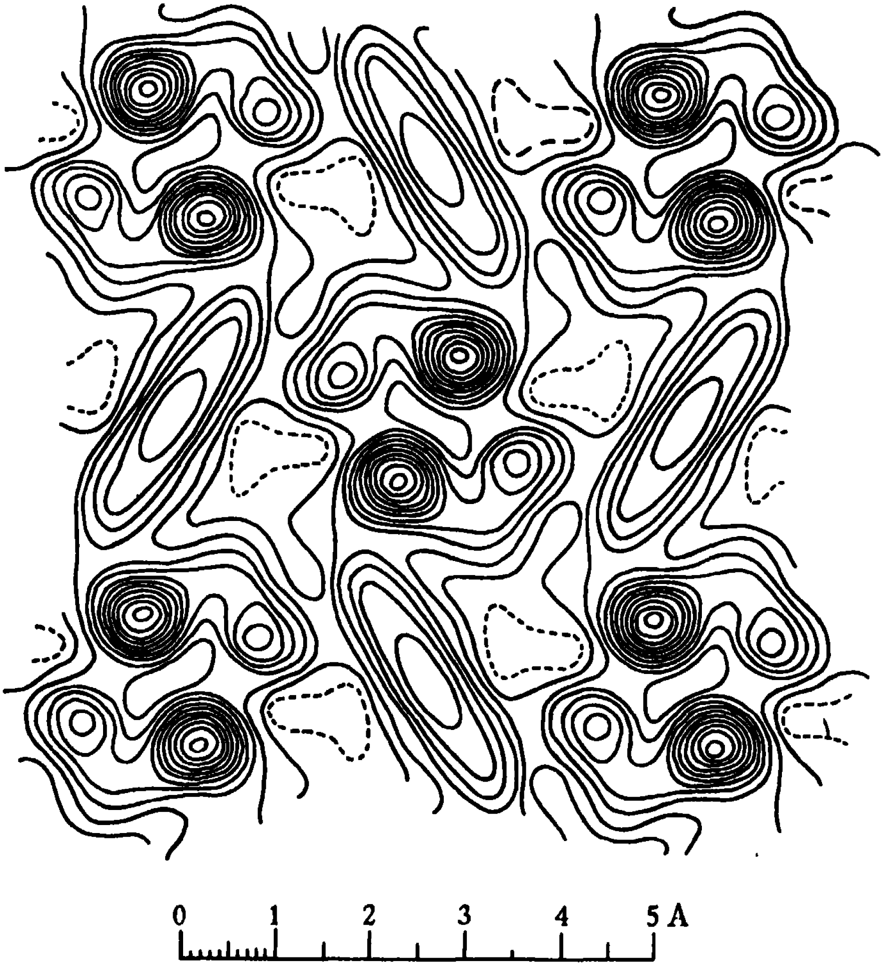

FIG. 6—Fourier projection along *a* axis on to plane *bc*.

v parameter of C_1 necessary to give a regular ring. The peaks C_1 and C_2 in fig. 4 are not entirely resolved. Nevertheless, the two maxima are quite distinct, and trial shows that the drawing together of two maxima in a combined peak owing to the overlapping of two peaks is quite small so long as the combined peak shows two distinct maxima. Moreover, any displacement due to lack of resolution should affect C_1 and C_2 equally; but to make the ring regular we must displace C_1 alone.

To obtain, if possible, a check on the v parameters the third projection on the plane *bc* was made. This is a much less favourable projection than the other two. It is based on a smaller number of spectra, owing to the smaller spacing, and its area being only about half those of the other projections, the atoms are not well resolved. The atom C_2 is almost coincident with the atom O_2 of the nitro group of a neighbouring molecule; the atom C_3 shows no definite maximum, and may be disturbed by the presence of the large C_2 — O_2 peak in its neighbourhood; the atoms N and O_1, and their inversions across the symmetry centres of the projection, appear as long ridges without separate maxima. The C_1 atoms do, however, show clear maxima, and these entirely confirm the parameter $v = 0{\cdot}18$ obtained from the *ab* projection, and make it very hard to

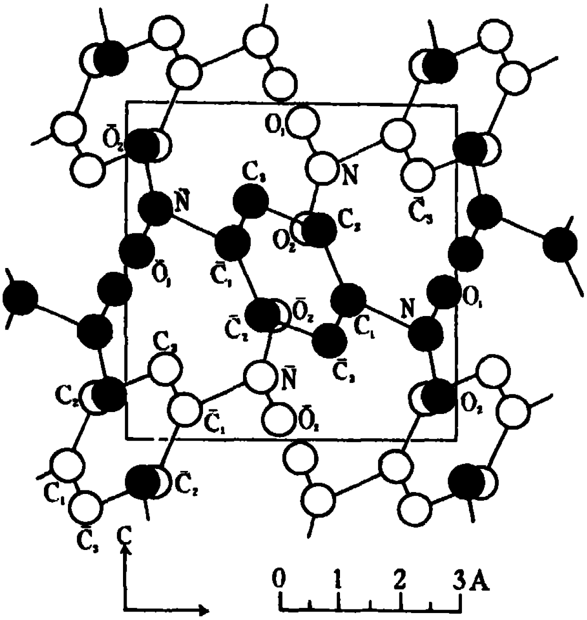

FIG. 7—Projection of the structure in *a* direction on to the plane *bc*. The molecules with black atoms have their centres in planes *a*/2 above and below those of the molecules with white atoms.

allow a value as high as 0·20. The evidence for the parameters as given in Table II is thus strong, and we shall employ them in our discussion of the structure. At the same time it must be emphasized that we are working very near the limit of optical resolution. The spectra fall off rapidly with increasing glancing angle θ, and little advantage is gained by using molybdenum radiation, particularly as the crystals used were, owing to their small absorption coefficient for the radiation, much below the optimum size for intensity measurement. The rapid decrease of intensity with θ probably corresponds to a large thermal motion of the molecules, which causes lack of definition in the projection, an idea which is confirmed by the fairly uniform, but very high, background in the projections. There is, however, always the danger that a number of spectra, each of which is in itself too weak to measure, may conspire in certain parts of the projection to produce measurable distortion and false detail. The general roundness of the peaks in the projections indicates that such effects are probably small in the present case; but the possibility of their occurrence cannot be entirely excluded, and must be borne in mind in any discussion of the fine details of a structure.

THE DESCRIPTION OF THE STRUCTURE

(*a*) *The Molecule*—Corresponding atoms in the unit cell are marked in the same way in all the key diagrams. The carbon atoms linked to the nitro groups are denoted by C_1 and $\bar{C}_1$, and the CH units by C_2, $\bar{C}_2$ and C_3, $\bar{C}_3$, the bar denoting inversion across the symmetry centre of the molecule. The dimensions of the molecule, as calculated from the parameters in Table I, are as follows :

$$C_2 - C_3 = \bar{C}_2 - \bar{C}_3 = 1{\cdot}39 \text{ A}$$

$$C_1 - \bar{C}_3 = \bar{C}_1 - C_3 = 1{\cdot}41 \text{ A}$$

$$C_1 - C_2 = \bar{C}_1 - \bar{C}_2 = 1{\cdot}32 \text{ A}$$

$$C_1 - N = \bar{C}_1 - \bar{N} = 1{\cdot}53 \text{ A}$$

$$N - O_1 = \bar{N} - \bar{O}_1 = 1{\cdot}25 \text{ A}$$

$$N - O_2 = \bar{N} - \bar{O}_2 = 1{\cdot}10 \text{ A}$$

$$O_1 - O_2 = \bar{O}_1 - \bar{O}_2 = 2{\cdot}14 \text{ A}$$

The interatomic distances and the angles between the interatomic links are shown in fig. 8*a*.

Symmetry requires that the four CH units C_2, C_3, $\bar{C}_2$, $\bar{C}_3$ should all lie in one plane. They are found to form a rectangle and to occupy, within the errors of measurement, the positions proper to a regular hexagon of side 1·39 to 1·40 A. It will be convenient in what follows to refer briefly to the plane of this hexagon as the " plane of the ring."

The atoms C_1 and $\bar{C}_1$ are displaced from their positions in the regular hexagon. The displacement is such as to shorten one of each pair of sides adjacent to a C — N link. These sides $C_1\ C_2$ and $\bar{C}_1\ \bar{C}_2$, become 1·32 A, and the corresponding radii to the two carbon atoms from the centre of the ring are reduced to 1·32 A also. The shortened distances are shown by dotted lines in fig. 8*a*. If the plane of the paper in fig. 8*a* is the plane of the ring, C_1 lies slightly above it, and $\bar{C}_1$ slightly below it, the actual distances being about 0·10 A. The radii to C_1 and $\bar{C}_1$ are inclined at about 5° to the plane of the ring.

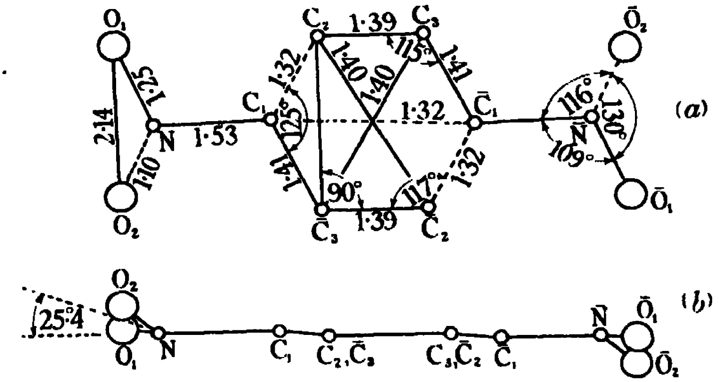

FIG. 8—The molecule of *p*-dinitrobenzene.

The radius from the centre of the molecule to N makes an angle of about 2° with the plane of the ring. In fig. 8*a*, N lies about 0·10 A above the plane of the paper, and $\bar{N}$ the same distance below. The link C_1 — N is thus nearly parallel to the plane of the ring, and slightly above it. The bonds $C_1 — C_2$, $C_1 — \bar{C}_3$, and C_1 — N accordingly lie very nearly, but not quite, in one plane ; but the departure from a plane is almost within the errors of measurement. The length of the link C_1 — N is 1·53 A, considerably longer than that assumed in the provisional structure.

The direction of the radius to N from the centre of the ring is perpendicular to the breadth $C_2\ \bar{C}_3$ of the ring, while the direction C_1 — N makes an angle of 93° with it. All these departures from regularity are small, and all depend on the displacement of the atoms C_1 and $\bar{C}_1$.

The distances of the two oxygen atoms of the nitro group from the nitrogen are not equal. N — O_2 is 1·10 A and N — O_1, 1·25 A. These distances should be fairly accurately determined, since they depend almost entirely on the *ac* projection, in which the atoms are clearly resolved. The distance $O_1 - O_2$ is 2·14 A, and the angle between $N - O$ and $N - O_2$ is 130°, while that between NC_1 and NO_1 is 109°, and between $N - C_1$ and $N - O_2$, 116°.

The plane of the nitro group NO_1O_2 is not parallel to the plane of the ring, but is inclined to it at a large angle. The angle between the direction C_1N, and the line joining N to the point midway between O_1 and O_2 is 25·4°, and the mid point lies above the plane of the ring in fig. 8*a* for N, and below it for $\overline{N}$. The projection of $O_1 - O_2$ on the plane of the ring is parallel to the breadth $C_2\overline{C}_3$ of the ring within the errors of determination, but $O_1 - O_2$ is inclined to the plane of the ring at an angle of about 11°, O_1 being lower than O_2 and $\overline{O}_1$ higher than $\overline{O}_2$ in fig. 8*a*. In fig. 8*b* a projection of the molecule on a plane normal to the plane of the ring, and parallel to C_2C_3, is shown, which should help to make clear the geometry of the molecule.

It is to be understood that this description refers to the molecule as a unit of the crystal structure; it must not be assumed that a free molecule will necessarily have the same configuration.

(*b*) *The Packing of the Molecules in the Crystal*—We must now consider how a number of molecules such as the one we have described pack together to form the crystal structure. This is most easily understood by considering first the projection on the *ac* plane, fig. 3. Suppose that we are looking at the *ac* projection in the direction of the *b* axis, and that *y* increases positively below the plane of the paper in figs. 2 and 3. Let the centre of the unit cell be chosen as origin, and let such a molecule as we have discussed have its centre at this origin. We shall refer to this molecule, and to others derived from it simply by the translations of the lattice, as A molecules. The other molecules, derived from the A molecules by the action of the glide planes or screw axes, we shall call B molecules. These have their centres, in projections on all three axial planes, in planes half a lattice spacing above and below those containing the centres of the A molecules. The diagrams are labelled so that all atoms derived from one another by a lattice translation, or by a single operation of a glide plane, are denoted by the same letter, while atoms differing in their marking merely by a bar are derived from one another by the action of a screw axis, or by inversion across a centre of symmetry.

The plane of the ring of any molecule is inclined to the *ac* plane at an angle of 53·7°. The line of intersection of the plane of the ring with the *ac* plane passing through its centre is inclined at 46·1° to the *a* axis, and at 41·7° to the *c* axis. The direction of vibration corresponding to the largest refractive index of the crystal is inclined at 38° to the *c* axis, fig. 1, and is thus in fact nearly parallel to the plane of the ring, as we inferred at the outset. The projection of the breadth $C_2\,\bar{C}_3$ of the ring makes angles of 48·2° and 39·7° with the *a* and *c* axes respectively, and is thus nearly parallel to the intersection of the plane of the ring with the *ac* plane. The direction of this intersection is shown by the dotted line for the A molecule in the middle of fig. 3.

The projections of molecules of types A and B on the *ac* plane are identical. In fig. 3 molecules of type A must, however, be thought of as sloping upwards to the right, and those of type B as sloping downwards to the right. These slopes are indicated by an arrow in fig. 3. It must be remembered, too, that the centres of the A molecules lie in planes half the *c*-spacing above and below those containing the centres of the B molecules.

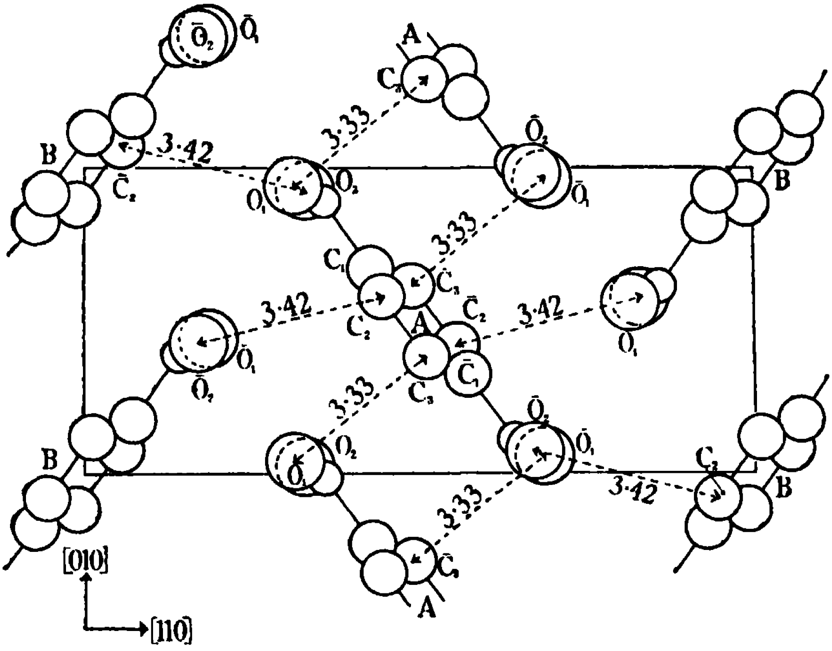

FIG. 9—Projection of the structure on the plane $(\bar{1}01)$.

A characteristic feature of the *ac* projection is the arrangement of the A and B molecules in diagonal rows, or really sheets, parallel to the plane $(\bar{1}01)$. It is perhaps significant that the face $(\bar{1}01)$ is always the most prominent one in the actual crystal of para-dinitrobenzene. In fig. 9 is shown a projection of the molecules constituting *one* such sheet on to the $(\bar{1}01)$ plane, to illustrate the linkages in the sheet itself. The centres of all molecules, whether of type A or B, now lie in the plane of the diagram;

the rings appear nearly but not quite edge-on, and the two oxygen atoms in each nitro group nearly end-on. The bending of the planes of the nitro groups out of the plane of the ring is clearly shown.

It will be seen that the oxygen atoms form zig-zag chains whose links pass between the $\dot{\bar{O}}_2$ atoms of the B molecules lying in one vertical column parallel to the *b* axis, and the O_1 atoms of the A molecules in an adjacent column ; and also between the $\bar{O}_1$ atoms of the B molecules and the O_2 atoms of the A molecules. The links of these chains are the distances of closest approach of oxygen atoms in different molecules in the structure. Each chain has links which are alternately 3·19 A and 3·32 A. These distances are greater than the distances of closest approach of oxygen atoms in inorganic structures, which are of the order of 2·7 A, and this indicates that the linkage between the molecules which holds the structure together is not mainly oxygen to oxygen.

There are, however, a number of close links between oxygen and CH, whose lengths are of the order of 3·3 to 3·4 A, and these probably represent the main binding of the structure. Let us consider the A molecule in the middle of fig. 9. Each CH unit of this molecule approaches within less than 3·5 A of an oxygen atom in a neighbouring molecule. C_3 and $\dot{\bar{C}}_3$ approach to within 3·33 A of O_1 and $\bar{O}_2$ respectively of the A molecules above and below in the same column; and C_2 and $\bar{C}_2$ to within 3·42 A of $\dot{O}_2$ and O_1 respectively of B molecules in adjacent columns. In addition, the oxygen atoms of the molecule considered approach the CH units of adjacent molecules to within the same two distances, 3·33 and 3·42 A, the links being O_1C_3 and $\bar{O}_1\bar{C}_3$ to A molecules in the same column, and $O_2\bar{C}_2$ and $\bar{O}_2C_2$ to B molecules in adjacent columns. This set of linkages is indicated by the dotted lines in fig. 9. Each molecule has thus eight links of the type O — CH of approximately equal length, distributed among six neighbouring molecules lying in the same $(\bar{1}01)$ plane.

We have next to consider the linkages between the molecules lying in adjacent $(\bar{1}01)$ planes. For this purpose we return to the consideration of fig. 3. We find again fairly close approaches of O atoms to CH. Atoms O_1 in A molecules approach $\dot{\bar{C}}_2$ and $\dot{\bar{C}}_3$ in B molecules (or $\bar{O}_1$ in A, C_2 and C_3 in B) within 3·30 A and 3·44 A respectively. For example, $\bar{O}_1$ in A in the middle of fig. 3 approaches C_2 and C_3 in the molecule B at the lower right-hand corner of the figure whose centre lies at half the *b* spacing above the centre of A.

The approach of the atoms O_2 and $\bar{O}_2$ to CH units in adjacent $(\bar{1}01)$ planes is not quite so close as that of O_1 and $\bar{O}_1$. The atom O_2 in the B molecule at the top right-hand corner of fig. 3 approaches C_2 in molecule B at the lower corner whose centre is at the same level, and C_3

of the B molecule whose centre is *b* above, each within 3·5 A; and each atom of type O_2 or $\bar{O}_2$ in every molecule makes corresponding approaches.

To sum up, every oxygen atom approaches to within 3·5 A or less of three CH units, one such close approach is between molecules in the same $(\bar{1}01)$ plane, and two are between molecules in adjacent planes. Each NO_2 group, considered as a unit, thus makes six such contacts.

The closest approach of CH units in adjacent molecules is 3·63 A, between C_3 and $\bar{C}_3$ of pairs of adjacent molecules of type A or type B. This may be compared with the value 3·60 to 3·72 for naphthalene, and 3·77 to 3·80 A for anthracene, obtained by Robertson;* and 3·42 A obtained by Iball† for chrysene.

We have used the term link between O and CH in a purely geometrical sense, as denoting a close approach of the atoms. It seems, however, likely that such links are responsible for a considerable part of the forces binding the crystal together. The whole structure is a very compact one, the crystal has a high density, 1·64, and is, for a crystal of an organic substance, hard and well defined, and it is tempting to relate these properties with this type of linkage. It is, of course, possible that there are forces between the adjacent nitro groups which, as we have seen, approach to within about 3·2 A of one another.

In conclusion, we wish to thank Professor W. L. Bragg, F.R.S., for his constant interest and encouragement. We should also like to express our indebtedness to Mr. C. W. Bunn, of Imperial Chemical Industries, Northwich, for advice and help in connexion with the measurement of refractive indices, and to Mr. W. J. Whitehouse, who helped with some of the observations in the earlier stages of the work. One of us (G. K.) is in receipt of a grant from the Department of Scientific and Industrial Research.

SUMMARY

The method of double Fourier series has been applied to determine the crystal structure of para-dinitrobenzene. Projections of the electron density on the three axial planes have been made, and the 18 independent parameters of the structure have been measured. The space-group is P $2_1/n$, and the unit cell contains two molecules. The molecule must therefore have a centre of symmetry.

The benzene ring, although nearly a regular hexagon of side 1·40 A, appears slightly distorted to an extent which should rather be greater than

---

* 'Proc. Roy. Soc.,' A, vol. 140, p. 79 (1933).

† 'Proc. Roy. Soc.,' A, vol. 146, p. 140 (1934).

the experimental error. The length of one of each of the pairs of sides adjacent to the C — N link is shortened to 1·32 A. The distortion appears to be due to the displacement of the carbon atoms which are linked to the nitro groups.

The C — N link lies nearly in the plane of the ring, but is inclined at about 25° to the plane of the NO_2 group. The N — O distances are not quite equal, being 1·10 A and 1·25 A. The O — O distance is 2·14 A. The closest approach of O to CH in adjacent molecules is 3·30 A. A discussion of the packing of the molecules in the structure is given.

Address of the President,
Sir Frederick Gowland Hopkins, O.M.,
at the Anniversary Meeting, November 30, 1935

It is my traditional duty to remind you of the losses the Society has suffered in the death of eighteen members. Four of these, Theobald Smith, Hugo de Vries, Friedrich Went, and H. F. Osborn, were distinguished Foreign Members. Among the fourteen Fellows are two who were active members of the Council, Dr. H. H. Thomas and Sir John McLennan.

By the death of Sir **Horace Lamb**, the Society has lost a Fellow who for more than forty years was one of the most prominent and successful among the many workers in applied mathematics in this country. He was fortunate in his generation; Maxwell had shown the importance of the wave equation in electromagnetic theory; the work of Stokes, Rayleigh, and Thomson had aroused fresh interest in problems in heat and hydrodynamics, in all of which it was of importance. Lamb realized this and utilized his mathematical ability in the development of some of its many consequences. His papers on hydrodynamics and elasticity added to our knowledge in a marked degree. And in addition he was a great teacher. His text-book on "*Hydrodynamics*," the outcome of a course of lectures to undergraduates at Cambridge in 1875, is a model of what such a book should be, and the distinction of many of his pupils is clear evidence of the value of his work as a Professor at Manchester. To quote from a resolution of the Council and Senate, " He inspired all who knew him in the University with respect and esteem, and his many friends with warm affection."

Theobald Smith was born at Albany, New York, on July 31, 1859. In 1884, he went to the Bureau of Animal Industry, U.S. Department of Agriculture as Assistant, and was made Director of the Pathological Laboratory in 1885. In 1895, at the age of 35, he went to Harvard as Professor of Applied Zoology, his chair being changed to one of Comparative Pathology in 1896. He also became Director of the Antitoxin and Vaccine Laboratory and Pathologist to the State Board of Health of Massachusetts. In 1915, at the age of 55, he became Director of the Department of Animal Pathology of the Rockefeller Institute for Medica Research at Princeton, New Jersey, where he stayed 20 years, retiring in 1929 at the age of 70. In each of the three foregoing environments (Washington, Boston, and Princeton) he built up great institutions and carried out investigations of great scientific importance. He died in New York on December 10, 1934, in his 75th year.

A list of his scientific publications, covering a period of 51 years, contains 255 titles. He did fundamental work on pathogenic organisms, their variability, adaptibility, mutations, differentiation, biochemical reactions, and advanced our knowledge of culture media and technique. He discovered that fluid cultures of the hog cholera bacillus, when injected into pigeons after being killed by heat (58–60° C), rendered them immune to inoculation with living cultures which killed control birds; this proved of much importance, for killed cultures have since been used on a vast scale for immunizing man against plague, cholera, typhoid, and paratyphoid fevers. He was the first clearly to differentiate tubercle bacilli of human and bovine origin. The results of his work on the toxin of the diphtheria bacillus and on antitoxin production, on accurately balanced toxin-antitoxin mixtures producing immunity for years without immediate or remote ill-effects, the finding that an excess of toxin in a mixture induced a much higher degree of immunity, etc., proved of great value when applied to man. He was the first to observe serum anaphylaxis (referred to by Otto as the " Theobald Smith phenomenon ").

His work on Redwater (" Texas fever ") of cattle, in which he discovered the causative protozoal parasite (*Babesia*) and its mode of transmission by ticks (*Boophilus*), followed by the successful application of preventive measures, has been of incalculable economic importance in many parts of the world. His discovery of the protozoal parasite (*Histoplasma*), causing " Black-head ", a deadly disease of turkeys in the United States, also of economic importance, was, like Redwater, of great scientific interest.

Finally, he was the first to demonstrate the significance of colostrum (first milk) to the new-born calf and why calves deprived of first milk are prone to die. He found that the blood plasma of the calf is devoid at birth of antibodies against common organisms like the colon bacillus. The colostrum contains such protective substances in high concentration, and, when ingested by the new-born animal, they are absorbed very readily into its blood which is thus armed against bacterial invasion. He was elected Foreign Member of the Society in 1932 and received the Copley Medal in 1933.

By the death of Sir ALFRED EWING on January 17, we have lost a colleague of rare distinction in many walks of life. He was in turn Professor in three Universities, Director of Naval Education, Principal and Vice-Chancellor of the University of Edinburgh, and in each position did educational work of the highest value. An Engineering laboratory he claimed, endeavours, as all University Laboratories, to contribute to the common stock of knowledge by furnishing opportunities and appliances for original research. Magnetic hysteresis, re-discovered and so named by him when in Japan—he had been forestalled, though he did not know it, by Warburg, and some other German writers—will ever be linked with his name, while the discovery of slip bands made in conjunction with Rosenhain has been of great importance to metallurgists. His own view was that these results were due to good fortune rather than to any special merit. If he had any particular faculty it was that, he said, of grasping at the skirts of happy chance when they presented themselves; "They seemed to present themselves oftener when I was a young man than they do to young men now, but I dare say happy chance, like other women, wears her skirts shorter now."

In addition to his eminence as an investigator and teacher, he was a great administrator. To our own council, to the councils of other societies, and of the Department of Scientific and Industrial Research, he gave valued help; the National Physical Laboratory owes much to his continued interest in its progress. As a chairman he was most efficient. One who knew him well has written that "to work under Ewing was no sinecure; under a genial manner he had an infinity of driving power." Nor must a reference be omitted to his work for the nation in Room 40 during the war, when he deciphered, with the aid at first of ladies, "personal and family friends whose intelligence I knew and whose discretion I could trust," wireless messages picked up from enemy sources, an achievement characterized by Lord Fisher as one of the crowning glories of the Admiralty work during the war. The Society and the nation owe much to Sir Alfred Ewing.

Dr. FREDERICK AUGUSTUS DIXEY died in his eightieth year on January 16, as the result of injuries inflicted by a motor car in Park Lane. His earliest researches, on anatomical and medical subjects, were conducted at University College, London, where he collaborated with his brother-in-law, Sir Edward Sharpey-Schafer. Returning to Oxford in 1883, a chief interest of his youth was revived and he began, in the Hope Department of the Oxford University Museum, the long series of important researches on Lepidoptera, especially the Pierines (or "White Butterflies") of the world, on which he became the leading authority. His investigations, first published in 1890 and continuing with unabated energy until his death, were devoted to the evolution of wing-markings; the differences between wet- and dry-season forms; mimicry; the epigamic aroma of male butterflies; and to the structure and development of the scent-producing scales and of the wings which bear them. He will be long remembered as one who gave constant and efficient help to diverse causes, and whose presence promoted the pleasure and success of social activities in the scientific community.

By the death, in March this year, of Professor JOHN JAMES RICKARD MACLEOD medical science lost a man who, by his work, had contributed to the prolongation of the lives, in comfort and happiness, of hundreds of thousands of sufferers, otherwise doomed to an early death, from *Diabetes mellitus*. In 1921 the isolation of insulin, the active principle of the pancreas which, in some way, controls the utilization of sugar in the body, by a team of workers in the Toronto laboratory of which Macleod was head, added to the medical armamentarium a unique and potent product. Macleod's main research interest throughout his academic life was the metabolism of carbohydrate in the animal organism. No one more fitted both by experience and temperament could have been found to interest himself in the project of Banting when he suggested a fresh attack on the age-long problem of the relation of the pancreas to diabetes. The whole story of the discovery, isolation, and purification of insulin in the relatively short period it took is an outstanding example of what may be attained by the activities of a research team ably directed and concentrated on a single end.

By the death of Sir EDWARD SHARPEY-SCHAFER the Society loses its second oldest member. Elected in 1878, he twice served on the Council, and received the Copley and Royal Medals. Inspired by the teaching of Sharpey, he made his name first as a histologist, and became assistant Professor, and then Jodrell Professor of Physiology, at University College, London, and there became famous for his researches and in particular for those on endocrinology. Discovering the remarkable action of an extract of supra-renal gland on the blood pressure, he and George Oliver opened up a new field of physiological research which had important clinical applications. He became widely known to the general public as the initiator of the Schafer system of artificial respiration, which has been almost universally adopted for purposes of resuscitation. Transferred to the Chair at Edinburgh, Schafer gave his best in furthering both the interests of that University and the science of Physiology, and inspired his assistants with enthusiasm and affection. These are now scattered over the world and fill chairs in American, Dominion, and even Chinese Universities. On his retirement at the age of 83, twenty-nine of these contributed researches to an honour volume of the '*Quarterly Journal of Experimental Physiology*' which Schafer himself had founded and edited for many years. In the preface to this volume it is well stated that " there is no need to speak of what he has done; his contributions to physiological science are stored in the libraries and utilized daily by research workers in furthering the boundaries of knowledge which he has himself done so much to advance." A man of the highest integrity of mind, Schafer showed great power of lucid exposition, both in his text-books and as an oral teacher. Few men lived so long a life of usefulness to their fellows.

Sir JOHN ROSE BRADFORD was a great teacher of clinical medicine and he attained the highest office among clinicians, that of the President of the Royal College of Physicians. To University College and its Hospital he gave life-long service and was justly beloved by all who had been his pupils or patients. But at the beginning Bradford had been a physiologist and, to the great advantage of medicine, he never lost that outlook. His own research work dealt chiefly with the nature and distribution of what are now known as the autonomic nerves and it had no direct reference to problems of disease; its scientific merit was recognized by his election to our Fellowship at the age of 31. Later he passed over to clinical medicine and then, except for some thoughtful studies of the effects on metabolism of removing portions of the kidney, his experimental work ceased. But he kept in the closest touch with the biological sciences and deliberately gave himself to every administrative plan by which their advances could be used to help the progress of medicine in its own clinical science.

As a Secretary of our Society from 1907 to 1915, he was keenly interested in the work of the committees on Tropical Medicine and especially on sleeping sickness. His unique position of authority alike in science and in practical medicine made it natural that his advice and guidance should be sought for in all the movements that from 1900 onwards so greatly transformed the opportunities for medical research in London. His fairness in judgment, his straightforwardness and sense of honour, and finally his resolution gave him great power in persuading others to the changes that he desired. Had it not been for Bradford's influence, medicine in our islands would have moved all too slowly in the rear of physiology and the other sciences that were opening fresh roads for her advance, and the Medical Research Council at its creation would have found fewer men in the country to do its work.

CHARLES FREDERICK CROSS, who passed away at the age of 80, was one of those gifted individuals who combined the scientific spirit with technical ability and withal possessed an artistic temperament. His contributions to the subject of cellulose were many and important and for many years he was the leading scientific investigator into its nature and properties. At the same time his technical work led to continuous progress in the cellulose-using industries, particularly the paper industry. Outstanding for all time is his discovery of viscose and the development from it of artificial silk, which in its effect on the world at large is probably the most fruitful scientific discovery in its practical application since those of Faraday. Cross lived to see the people around him largely clothed in rayon, though the structure of cellulose is still only partly elucidated. He was a pioneer also in the field of cellulose acetate. The many scientific writings of Cross, particularly his original and now classical book on cellulose, showed an unusual gift of imagination, his technical work was of the highest precision and his consulting practice enjoyed a world-wide renown.

HERBERT BRERETON BAKER was born at Livesey near Blackburn in 1862 and during a long and active life carried out research work which materially advanced our knowledge of inorganic chemistry, especially in connexion with the inhibition of reactions in the absence of moisture. He was one of the few schoolmasters who, like Sir William Tilden, was able to reach high distinction both in Scholastic and Academic life, for he was elected a Fellow in 1902 while still a science master at Dulwich College. He was very fortunate in his teachers, because in early life he came under the influence of Francis Jones of the Manchester Grammar School, and later, when he was appointed Lee's Reader at Christ Church, Oxford, he became associated with H. B. Dixon who imparted to him some of the enthusiasm for research with which he was so amply endowed. After the German gas attack in 1915 Baker was sent with Dr. J. S. Haldane to carry out an investigation on the spot. He devised temporary measures of protection both against chlorine and phosgene, and although his methods have long been replaced by more perfect protective agents they were undoubtedly instrumental in giving adequate protection at a time when it was most needed. He was created C.B.E. for his war services in 1917.

JAMES WALKER was the first British student to be attracted to the new school of physical chemistry under Wilhelm Ostwald at Leipzig in 1887, and for nearly half a century thereafter sustained, through his research work and text-books, the role of the leading advocate of the subject in this country. Several of the more significant chapters of the van 't Hoff-Arrhenius theory of solutions—for example, those on hydrolysis and amphoteric electrolytes—were largely based on Walker's original work. He was also a skilled organic chemist, and rendered valuable service in the manufacture of T.N.T. during the Great War. The new department of chemistry at King's Buildings, completed in 1924, constitutes a fitting memorial to his twenty years' occupancy of the Edinburgh Chair. He was elected a Fellow in 1900, and served as Vice-President of the Society in 1930–31. In 1926 he received the Davy Medal.

HERBERT HENRY THOMAS belonged to that class of geologist which, through the inevitable expansion of the science, is becoming rare; for he combined a wide and expert knowledge of field stratigraphy with specialization in more than one branch of his subject.

After leaving Cambridge in 1898, with high honours, he acted for a time as Assistant to Professor Sollas at Oxford. In 1901 he joined the Geological Survey and was assigned to the South Wales district where Strahan was in charge. There his work lay amongst the igneous and sedimentary rocks of Lower Palaeozoic age. In country that had known De la Beche, Murchison, Logan, Phillips, Ramsay, and others, he was able with his colleagues to adopt Lapworth's threefold classification of the rocks and apply intensive zonal methods to their subdivision. On completion of the survey in South Wales in 1909, Thomas was transferred to the Flintshire Coalfield until 1911, when he was appointed Petrographer to the Survey and Museum. During the War his specialist knowledge was invaluable in the solution of various urgent problems for Government Departments, and in furthering the preparation of memoirs on the Mineral Resources of Great Britain. Thereafter he took an important share in the work of the Scottish branch of the Survey on the Tertiary igneous rocks of the Mainland and the Western Isles, the results of which have brought about one of the most impressive advances in British Geology made in recent years. Besides being the author of many important papers on stratigraphy, petrology, and mineralogy, his interest in pre-History was intense, as evidenced by his determination of the source of the "bluestones" of Stonehenge. Through his knowledge of mineralogy he became a pioneer in the study of the heavy minerals of sediments, his first thesis on this subject being the essay that won him the Sedgwick Prize in 1904. He was ever ready with advice, help, and encouragement; and his lovable personality secured him a host of friends. He became a Fellow in 1927, and at the date of his untimely death was a member of Council.

HECTOR MUNRO MACDONALD, who died on May 16 last at the age of 70, was a Royal Medallist of the Society in 1916, President of the London Mathematical Society in 1916–18, an Honorary Fellow of Clare College, Cambridge, and an Honorary LL.D. of Glasgow. He occupied the Chair of Mathematics in Aberdeen University for thirty years, and was an influential member of the University Court and of the governing bodies of many scientific and educational institutions in the North of Scotland. To pure mathematicians he was known as an investigator in the Theory of Functions, particularly the Theory of Bessel Functions; but most of his work was in Mathematical Physics. His rigorous solution of the difficult problem of diffraction by a prism was one of the most fruitful achievements in Optics in this century; and his determination of the effect, at a distant point of the earth's surface, due to a Hertzian oscillator emitting waves of a definite frequency, was the first important step towards an understanding of the propagation of wireless waves round the earth. He was elected a Fellow in 1901 and served on the Council in 1908–10.

HUGO DE VRIES died on May 21 at the age of 87. His early work on vegetable physiology culminated in a series of investigations on the causes of turgor in plant cells, by which he showed that it is due to osmotic pressure determined by the numbers of molecules and not by the weight of the solute. He thus provided independent demonstrations of the kinetic theories of solution associated with van 't Hoff and Arrhenius. Later he turned his attention to the experimental study of inheritance in plants and became one of the founders of the then infant science of genetics. He perceived that the material basis of heredity lay in the nucleus of the cell and as a consequence of his study of a chance population of *Oenothera* naturalized among the sand dunes near Hilversum he introduced the conception of ' Mutations '—large heritable variations in the organism by which varieties and presumably species originated, instead of the smooth flow of change by the accumulation of insensible steps which Darwin had postulated. This conception has become a permanent part of genetic theory. To de Vries as to few men was given the distinction of laying two foundation-stones in different branches of science.

JULIUS BEREND COHEN was one of the pioneers of this country in the teaching of organic chemistry. In his earliest days as a teacher he introduced practical courses in the subject and subsequently through the medium of his books was able to direct the steps of many students in their training as organic chemists. In addition to his great work as a teacher he was an enthusiastic research worker and was happiest when working himself or instructing others in his laboratory. His chief investigations were in the field of substitution in aromatic compounds, in problems concerning optical activity, and in the relation of chemical structure to antiseptic and trypanocidal action. He was one of those who as early as the beginning of the present century realized the contribution that chemistry could make in the study of biological problems, and many of his research students were directed into the field of biochemistry at a time when there were few workers in the subject. In some of his leisure time he sought by direct investigations on atmospheric pollution to convince his fellows of the ravages wrought by smoke in our industrial areas, and his work on this subject has been of great value. He was elected a Fellow in 1911.

Professor FRIEDRICH AUGUST FERDINAND CHRISTIAN WENT (1863–1935) began his career as a pupil of Hugo de Vries; after graduation he worked under Strasburger at Bonn and van Tieghem in Paris. After spending five years in Java he was elected Professor of Botany at Utrecht, a post which he held until 1934. In 1930, when the International Botanical Congress met at Cambridge, Professor Went received an Honorary Doctorate; shortly afterwards he was chosen by his Dutch colleagues to be President of the next International Congress, which was held in Amsterdam this year (1935). He looked forward with the keenest pleasure to the presidential duties and, despite failing health, he continued to exercise a controlling influence until a few days before his death, which occurred about a month before the date of the Congress. He was in an exceptional degree internationally minded and took advantage of every opportunity of promoting friendly co-operation and good feeling among biologists throughout the world.

The earliest important work undertaken by Went was a study of the distribution of sugars throughout the life history of crops of sugar cane in Java (1898), made on behalf of the growers in the Dutch East Indies. Went collected an imposing mass of analytical data for all parts of the cane, and for all ages and stages of growth. These data demonstrated the striking specific differences of behaviour between cane-sugar and the hexose sugars as the tissues of the plant develop. Thus was provided the first picture of the developmental drift of the carbohydrate metabolism of the plant. From this work in Java Went returned to Holland to take up the professorship of Botany and to direct the physiological research work of the Botanical Institute at Utrecht. On retiring from his professorship in 1934 he wrote an account in English (‘*Biological Reviews*,’ 1935) of the scores of investigations carried through in his Institute on the influence of the so-called “growth-substances” upon growth-rates and growth-curvatures. It is in connexion with this fine organization of continuous work on the first discovered hormone in plants that Went's name will be most widely known. This scheme of work progressively took up the measurement of the production of this hormone, the path and conditions of its transport, and the determination of its precise effect upon the complex phenomenon of cell-growth. Thereby it was made clear how the plant by its slower grade of transport and reactivity lends itself to the elucidation of certain fundamental problems of general physiology.

HAROLD WARD DUDLEY, who died before he had completed his 48th year, had acquired a wide influence in scientific circles concerned with biochemistry by his already fine record of investigation in that field, and by the unselfish devotion of his time and his work to the interests of his colleagues. He was one of a series of pupils of the late J. B. Cohen, who have won distinction in British biochemistry. He became early associated with H. D. Dakin at the Herter laboratory in New York, where from 1912 to 1914 they were jointly responsible for a series of brilliant investigations, particularly on the enzyme glyoxalase, which they discovered, and on the racemization of proteins. Dudley served with distinction during the war in the special organization dealing with protection against chemical warfare. After the war, he joined the staff of the National Institute for Medical Research as chief biochemist in the Department directed by Sir Henry Dale. He was there responsible for an important series of investigations on pituitary hormones, insulin, spermine, histamine, acetylcholine, and ergometrine, a new and important alkaloid from ergot which he isolated early in the present year, and of which his complete description was published in our '*Proceedings*' on the day of his death. Dudley did great service to biochemistry as Secretary of the Biochemical Society, and as Co-Editor of the '*Biochemical Journal*' at different periods. His early death removes a man whose personal qualities and unselfish devotion to the interests of all concerned with his subject had endeared him to a wide circle of workers in biochemistry and physiology.

In Sir JOHN CUNNINGHAM MCLENNAN we lose one who in a special degree linked the rapidly growing scientific activities of Canada with those of the Mother Country. He began at Toronto University, with which he remained associated until the end. In his youth he came to Cambridge and gained a training in original research under Sir J. J. Thomson. Returning to Toronto, he took a prominent part in the development of physical teaching and research there, displaying an activity which can only be described as prodigious. After his appointment as director of the laboratory (1904) and professor (1907), nearly all that was done was under his inspiration and in many cases his personal direction as well. During the war his glowing patriotism showed itself. He developed processes for separation of helium from natural gas, and surveyed the available sources in Canada with a view to its use in airships and pilot balloons. Later, coming to England he developed methods of great practical value in the anti-submarine campaign. After the war he returned to Toronto, and did what was perhaps his best work. A cryogenic laboratory was set up, with arrangements for the liquefaction of hydrogen and helium, and he added notably to our knowledge of supraconductivity, showing that it is not in evidence when the current alternates rapidly. Further, he solved the long-standing mystery of the green line of the auroral spectrum, showing that it is due to oxygen and establishing the nature of the spectroscopic energy levels concerned. For this work he was awarded a Royal Medal in 1927. He received the K.B.E. in the present year (1935). His university recognized his services by appointing him Emeritus Professor and by giving the physical laboratory his name. His last years were spent in this country.

HENRY FAIRFIELD OSBORN will be widely regretted in this country, where he was well known, as well as in America. He has a special tie with London in that he attended a course on comparative anatomy given by Huxley fifty-six years ago. The American Museum of Natural History early recognized Osborn's value and under his curatorship the department of vertebrate paleontology became what it is to-day. His enthusiasm, professional skill, and adroit use of opportunity enabled him both in expeditionary work and in research to perform an almost incredible amount of successful work, well exemplified in his beautiful memoirs on Equidae and Titanotheres, while his numerous published papers deal with almost every branch of zoology and paleontology. He received the Darwin Medal in 1918 and was elected a Foreign Member in 1926.

This year's Report of Council reproduces the loyal Address of the Society to its Patron the King on the occasion of His Majesty's Jubilee, and also the gracious acknowledgment it received.

The Report as a whole makes it clear that the normal activities of the Society have proceeded during the year on satisfactory lines.

The Society remains fortunate in being entrusted with successive benefactions for the furtherance of research. A gift of £10,000 has been recently received at the instance of Professor P. E. Newberry and Mrs. Newberry from the trustees of the late William Johnston, shipowner of Liverpool, for the foundation of a fellowship or studentship devoted to research on the problems of Health, and, as its Report states, Council have been informed that the Society appears in the will of Mr. J. J. Jaffe as a possible beneficiary. The executors are at present seeking the authorization of the Courts before dealing with the estate. It is a striking fact that the Society's present expenditure in support of research is nearly tenfold that of twenty-five years ago.

Noteworthy also is the circumstance that in the last ten years the Society's publications have more than doubled in bulk; this is true of the '*Philosophical Transactions*' as well as of the '*Proceedings*.'

Under the wise guidance of the Treasurer, the system of accounting as applied to our funds as a whole has been reorganized and simplified. The change of method has already proved satisfactory and it will add to the convenience of all who wish to appraise the position of the Society's finances.

The problems associated with Dr. Kapitza's position, which has aroused interest and provoked comments in many countries besides our own, have now been solved on lines which the Royal Society, from its own standpoint, should, I think, regard as satisfactory. All Fellows of the Society will take pleasure in learning of the complete success which has attended the efforts of those responsible for the establishment of the memorial to Sir Charles Parsons.

The last few years have brought forth much discussion concerning the social responsibilities of science. One aspect of that theme has indeed become so familiar of late that I should hesitate to refer to it on such an occasion as this but for a particular circumstance. As most here will remember, the British Association recently listened to successive presidential addresses containing references to the misuse of the gifts of science. To discuss such matters is certainly proper to the defined functions of the Association, and, influenced chiefly by the circumstance just mentioned, and perhaps to some degree also by pressure from the lay press, which traditionally concerns itself in its own particular way with the business of the Association, its Council thought it well two years ago to invite various sections to devote part of their time to such discussion. At Aberdeen last year the problems involved certainly received some attention. Unfavourable comments have been made, however, because this year at Norwich it seems to have been already forgotten or neglected.

'*The Times*' itself in an article dealing with the Norwich meeting expressed regret for the neglect in question, and the writer ventured to say, apropos, that the Association revealed "a real hiatus" in its activities "in not studying science itself by scientific methods." This remark when first read seems to be an impressive one, at once an accusation and a suggestion for a line of action; but an endeavour to understand precisely what it means reveals, I think, considerable difficulties. Many, and not journalists alone, have called upon devotees of science to play some special part in helping to correct the social dislocations which their work is held to have caused, but I know of no concrete suggestions as to how, if as specialists, and not merely as good citizens, they are to set about it.

I will venture to quote very briefly from the presidential addresses which helped to bring this question so much to the front.

There came first certain striking remarks in the brilliant oration delivered by General Smuts at the centenary meeting of the Association in London. You will doubtless remember that he was dealing on broadest lines with the scientific world picture of to-day, but at one point he was led to remind his audience that " a serious lag has already developed between our rapid scientific advance and our stationary ethical development," a lag, he said, " which has already found expression in the greatest tragedy of history." In these words he provided the text for much subsequent discussion. He then went on to urge that Science itself must help to close this dangerous gap in our advance which threatens the disruption of our civilization and the decay of our species. "Its final and perhaps most difficult task," he concluded, "may be found just here." General Smuts, however, though in these words he emphasized the social responsibilities of science, spoke, as I shall immediately remind you, in a spirit of complete optimism concerning its ability to bear them. His immediate successor, Sir Alfred Ewing, perhaps because he was feeling the burden of the years, for his life of fine service was unhappily nearing its end when he delivered his address at York, spoke in a spirit less hopeful. He again emphasized the view that man is unprepared for the great bounty which science had provided for him, and expressed, you will remember, his own consequent disillusion when watching to-day the sweeping pageant of discovery and invention, in which as a young man he had taken unbounded delight. He expressed no hope that science itself could provide the remedy, but rather a failure to see from whence it was to come. We cannot fail to feel the pathos of such disillusionment in one whose death after a life of great accomplishment we mourn this year. We may believe that it was but a mood which, could he have lived to see the future growing brighter, might well have changed.

It was my privilege to follow these two distinguished men in the Chair of the Association, and I could not wholly forgo reference to the problems they had raised. I found, however, that from a humbler standpoint I could do little more than suggest that the inadvertent sins of science should be viewed in correct perspective, and to claim that biological science at any rate had done little to aid man's destructive impulsives but provided teaching that, were he willing to learn, might do much to correct these as well as other faults in his complex nature. This faith certainly remains with me.

Owing to what would seem to be a confusion in thought, the supposed social harms created by science have been vaguely attributed in some not unprejudiced quarters to its own unethical character. The conclusion reached by General Smuts, as we learnt from his address, is greatly different from this. He holds that among the values gradually recognized by the developing human mind, science ranks with religion and art, and that while to-day religion, art, and science are separate values, they may not always remain so. Indeed he thinks—so he told us—that one of the greatest tasks before the human race will be to link up science with ethical values. He admitted, it is true, that in speaking thus he was going beyond the scope of science as at present understood, but he expressed the belief that the conception of science itself is bound to be affected by its eventual integration with the other great values. I make no apology for recalling his words, for I think they should remain in our minds.

It is perhaps not quite easy to follow closely his thought concerning the future extension of the scope of science, but his own assurance that its teaching can be linked up with ethical values is a corrective for some of the accusations from which science is apt to suffer.

Indeed, possible future developments apart, the gap between what science provides for humanity and what are usually spoken of as values in religion, literature, and art, has been and is less wide than some assume. History itself shows that it is wrong to deny ethical influence, even if it be indirect, to the scientific spirit. While, for instance, the earlier stages of the Renaissance enriched men's minds by restoring to them the literary and philosophical heritage of antiquity, we all know that not until later, when the awakening scientific spirit demanded a courageous inquiry into the actual facts of Nature did human thought begin its release from the shackles of Authority and traditional dogma. This release was surely ethical in its effects. In later times throughout the years of the Royal Society's existence the growth of intelligent interest in the material universe was slowly preparing the ground for that last great step in the progress of intellectual freedom which came in the middle years of the last century. The influence of Darwin and Lyell did more, of course, than establish a new outlook for science itself. It re-orientated all thought. It caused heart-searchings where there had been mere complacency in the acceptance of tradition, and its impacts subtly encouraged the growth of that intellectual honesty for which Huxley and others then so nobly fought. The history of those days is familiar enough, but we sometimes forget the debt we owe to them.

It was the influence of science which, more than any other influence, established the idea of Progress, replacing as it did a static by an evolving universe, and incidentally a faith that man himself has an inherent capacity for advance. There are not a few to-day, including one very able and very articulate theologian, who profess to disbelieve in progress; but for the majority it is now a faith ingrained if sometimes only subconsciously held. Evolution we know may not at each step tend upwards, but we have reason to believe that in the long run it does, and that in spite of occasional disillusions we may believe in the upward tendencies of mankind. By this faith hope is fed, human efforts towards betterment are encouraged, and ethical values emerge. The depressing belief that Man and the social fabric he has contrived for himself, while so imperfect, are yet incapable of ultimate betterment, was the one excuse for that particular form of professed otherworldliness which from time to time has been an essential part of narrow religious ideals, but which was surely evil in its almost contemptuous indifference to social wrongs and to the urgent problems of this world.

With regard to values of the kind claimed in particular by art and literature, it is a prejudiced assumption that science must remain incapable of contributing to these. It is indeed right to insist, as Sir William Bragg has recently insisted in the course of a public lecture, that our perception of beauty need not be limited to that which appeals to our ordinary senses. The extension of the senses which science provides adds new beauties to the old without in the least degree supplanting them. There can be very few among true devotees of science who fail to feel this intensely. Sir Richard Gregory, indeed, in an eloquent Address on the " Interpretation of Science," urged the poets themselves to qualify for the emotional interpretation of these new beauties. He reminded his audience that at the beginning of the last century Wordsworth expressed his own assurance that when the right moment should come, the poet would find in the revelations of science a proper object for his Art, and went on to show by quotations that since Wordsworth's day many of our greater poets have had moments at least when the emotional value of those revelations has inspired them. General Smuts's faith that if to-day religion, art, and science are still separate values they may not always remain so, has a basis which is surely not unreal.

I will return for a moment to the circumstance from which I started and the criticisms it has called forth. You will have realized that the tendency of late has been not so much to reiterate the theme of science's gifts to the powers of destruction, but rather, with the supposed default of the British Association in illustration, to urge in a more general sense that scientific workers have not shown sufficient interest in the social implications of their work, or in the public responsibilities of their calling. We have only to look closely into this view as usually expressed to realize that, after all, its basis is vague, and, did it involve any charge against the individual worker, unreal.

It is after all not surprising, though the attempt was fully justified, that in the final issue members of the Association failed to find grounds for any very serious discussion of the subject. The individual investigator must realize that, *quà* scientist at least, he has little opportunity for effective action. Commonly he concludes that he will be most useful, even to society, by continuing his chosen work in its proper environment.

It is, I think, impossible not to sympathize with this view. The special endowments acquired by the scientific investigator are not those of a politician or of a missionary. Needless to say, it remains his duty to give his skilled services to the public whenever they are legitimately required and invited, and in so giving them he may do much to promote the interests of Science itself.

Although one may well believe that the recent extensive public discussion of the less happy social repercussions of science has had its uses, it has now fulfilled any purpose it may have had, and one may hope that on present lines at least it will now cease.

What seems to be really desirable is some method of closing the gap between the mind and outlook of the publicist and those of the trained scientist. It is a just claim that in a civilization so largely based on science as that of to-day, the scientist should have more influence on policy than he has hitherto been allowed. Not long ago the gap in question was wide; it is now, I think, lessening. Occasionally at least, modern statesmen do seek scientific guidance, and, I think, know better than they did how rightly to obtain it. But it is time, perhaps, that the building of a bridge should begin on the scientific side of the gap. This is a task for organized scientific effort and the pooling of knowledge. As John Stuart Mill urged, knowledge before it can assist public action must somewhere be concentrated.

Thirty years ago Sir William Huggins devoted the whole of a presidential address to a discussion of the advisory relations of the Royal Society to the State, pointing out how important these relations had been throughout the history of the Society. It must be recognized that during quite recent years its advice and assistance have been less sought by Government departments, or sought upon matters of relatively small importance. It is perhaps not difficult to understand why this should be the case. Other bodies, State-supported and qualified for advisory functions, have arisen; notably the three Research Councils under the Privy Council. The main business of these is to control nationally endowed research, but together they are highly qualified to give advice over a wide ground of technical problems, and they or their officials are in close touch with Government Departments. Moreover, the appointment of *ad hoc* Government Committees to deal with problems essentially scientific has lately become a very common policy.

It must be admitted that in these connexions the status of the Royal Society has been so far recognized that under the original Charters of the three Research Councils each election to their personnel must have the approval of your President *ex officio*; doubtless on the understanding that in any position of difficulty he would consult the Society through its Council. It is again because he represents the Society that the President sits on some of the Government Committees that I have mentioned. Naturally, many others among its Fellows are found on such committees. I do not indeed think that the Society should resent, or even regret that, as a body, it is less consulted than formerly on merely technical and highly specialized questions; but on broad general questions which bring science into contact with the State its constitution and prestige give it the right to be so consulted. I personally believe that such questions exist to-day, and with the growing influence of science on social developments they may well arise with greater urgency in the future. Should not the Society, with its unique authority, while always prepared to advise, be also perpared on appropriate occasions to approach the Government on its own initiative, and even at times make its own appeal to the public conscience?

There is a branch of scientific inquiry which can claim to yield knowledge of unqualified benefit to humanity, and one in which investigators, though inspired by the extreme scientific interest of the problems involved, have, I feel, always had the public importance of their solution in view, and have themselves done their best to encourage the practical applications of the knowledge they have won. I refer to the study of the nutritional needs of the body.

It must be confessed that up to the end of the last century this country had contributed too little to this side of knowledge, but British workers have since fully made up for that neglect.

The last two decades have seen a quite remarkable activity in research upon nutritional problems, and it is now even increasing. Publications describing original work upon various aspects of these come from almost every country where science is pursued, and have amounted to many hundreds during the course of each single year. A valuable journal, '*Nutrition Abstracts and Reviews*,' devoted, it is true, to animal as well as human nutrition, published in its first volume, issued in 1932, summaries of over 3000 papers and in its last completed volume over 4000.

In this country much research on nutrition has been generously endowed, organized, and encouraged by our Medical Research Council, and it has received financial support from various other sources. We have begun to follow the example of the United States in founding Chairs in Dietetics, and emphasis is being placed upon the subject in physiological and biochemical teaching at the Universities, while at centres where domestic science is taught, such as that at King's College, London, adequate knowledge is being supplied to students who afterwards in various capacities are imparting its essentials to the public. The excellent work of scores of infant welfare centres has educational value for mothers of the poorer classes. The British Medical Association has made it clear that the importance of nutrition is recognized by the profession, and clinical literature displays an increasing consciousness of the influence of malnutrition in the causation of ill-health. The Ministry of Health has now constituted a fully representative Committee on Nutrition, with advisory functions, and we may believe from many indications that the Government has awakened to the importance of the problems it involves.

Behind all these and other practical activities has been a somewhat sudden realization of the importance of right nutrition on the part of the educated community at large, and a consequent awakening of the public conscience and public concern with regard to it. There are but few to-day who doubt that it is the duty of the State to see that in this country no man or woman and, especially for the sake of the future, no child shall suffer inadequate nourishment unless for reasons beyond public control. It is much to be hoped that national interests of such importance will not be further exploited in party politics.

A desirable happening at the present moment is the international approach at Geneva for full discussion of the nutritional problems of the world; for, viewed broadly, the problems are undoubtedly international. As you doubtless know, on a demand from the representatives of twelve nations including Great Britain and Australia (which has played a leading part in the movement), the Health Organizations of the League have set machinery in motion for securing full and intimate discussion. Policies concerned respectively with the production, transport, distribution, and consumption of foods will all, we may hope, be discussed. They seem to be the very proper business of the League, and if discussion goes deep enough and is frank enough, it may well do no small service to the interests of peace itself.

Many are concerned just now to know the truth concerning the degree and extent of malnutrition as it exists among the less fortunate sections of the community at the present time. They have seen certain desirable steps taken to mitigate whatever may exist, as, for instance, the diversion of surplus milk to the schools; but they yet ask how far is an extension of such measures an urgent need of the moment. That underfeeding and ill-feeding exist is sure, but to measure their extent is, for reasons to which I will allude, a task of some difficulty.

We have only to read the successive annual reports from numerous Medical Officers of Health to believe that, in the case of children at least, nutrition, inadequate for one reason or another, exists in various districts to an extent which is far indeed from being negligible. Nevertheless, we have to realize that the numerical data supplied from different centres are based upon varying standards, and the opinions expressed depend to no small degree on the temperament and perhaps on the acuity of individual officers. The difficulty before all concerned is that there is no clear definition of the term "malnutrition," and no satisfactory objective methods for measuring its degrees. Sir George Newman, the late Chief Medical Officer to the Ministry of Health, always felt justified in taking an optimistic view concerning the available food supply of children in this country, and he was wont to insist upon the circumstance that though under-nourishment may be due in part to an insufficient quantity of food, it depends also on other factors. "The principal cause," he once wrote, "is a body unable to assimilate the food supplied to it." In certain cases this must, of course, be true, but we are entitled to ask whether in many of such cases the disability of the body when observed has not followed upon malnutrition at an earlier period. What we know to-day justifies this view. In any case the essential question is whether food adequate in quantity and quality is within the reach of all. In the Annual Report for 1934 issued by the present Chief Medical Officer of the Ministry, it is made clear in a section devoted to the effect of unemployment on national health and dealing with evidence based upon a conjoint investigation by officers of the Ministry and the Board of Education into conditions in certain depressed areas in Durham, that the statistics of actual diseases there do not indicate unfavourable effects of present economic conditions. We may conclude from this, and take comfort from the fact, that malnutrition even in such areas has not been at its severest, but it may be highly deleterious in its ultimate effects when not such as to affect the current statistics of disease. Moreover, full normal nutrition was only claimed for some 70 to 80 per cent. of the children, varying between these figures in different areas, and though, as I have said, criteria for establishing the existence of subnormal nutrition are not satisfactory, it is difficult to be content with such figures. The Ministry's investigators admit further that in the areas studied the condition of adolescent youths, especially those aged 14 and 15 years, was found unsatisfactory. These are years when good nutrition is quite specially desirable. As a measure of the state of health of younger adults at the present time, the results of medical examinations for recruiting are not without importance. The War Office Report on the Health of the Army for 1933 shows that in that year nearly 38 per cent. of the prospective recruits were rejected as unfit. Although, as the Report points out, many of these rejections were on account of disabilities which unfitted them for military service in particular, and therefore did not reflect on their general health, yet a glance at the stated reasons for rejection shows that a large proportion of the men suffered from defects which might well be due to faulty nutrition in childhood or adolescence, and a considerable proportion in which it almost certainly contributed to their unfitness.

I have read most of the available literature bearing on this important matter, and have tried to appraise the value of the evidence it offers. I am left with a strong impression that the situation calls for further and immediate action.

The current interest in the subject of the national food supply and in right feeding is doubtless largely due to the awakening of the public conscience to this and other kindred social responsibilities; but it has also been stimulated, I think, by the nature of the results which scientific studies during the last twenty years have revealed. They have shown, as you know, that our nutritional needs are so much more numerous, subtle, and specific than was earlier thought, and they have shown how extraordinarily potent and how entirely indispensable material may be, even though consumed in infinitesimal amounts. We know now that a fault in quality may be as deleterious as a failure in quantity. This fact the general public is now rapidly assimilating though not always to its profit. Indeed, a certain vocal section of the public is (as it has always been) so perverse in its views concerning food that it is almost necessary to remind it that after all quantity still counts. We cannot live on vitamins alone! A more intelligent section of the public seems, I notice, to assume with impatience that so much scientific talk about food may lead to individuals being dragooned with respect to what they shall or shall not eat. A self-constituted Committee whose propaganda against malnutrition I respect for its wisdom and fairness has appreciated this attitude, and in a recent memorandum made the following wise statement: " certain diet habits, must be classed as cultural, and of personal and psychological necessity, and to upset these in the service of protein or vitamin content is to provoke a natural reaction against " the advice that science can legitimately give. It is, of course, unthinkable that there should be any such dragooning. The intelligent public will learn to apply the newer knowledge of nutrition without discomfort to itself.

The same memorandum says—again wisely—" to a working class housewife with restricted purchasing power, education in food values alone can only add one further problem to an already insoluble series of anxieties and worries." This of course is true, and so long as we see that foods of the right variety are all within her purchasing power, elementary instruction in terms of the foods themselves and not in technical food values will set the housewife on the right path. I am tempted to add that what the English housewife in the poorer classes needs most to be taught is the art of simple but good cooking ! It is not beneath the dignity of nutritional science or of administrative policy to take note of the circumstance that in this country more than in perhaps any other is good food ruined, and its nutritional value impaired, by unintelligent treatment in the home.

One last consideration before I release you. Is the time yet ripe for the initiation of a comprehensive National Food Policy; one that will endeavour to adjust production, in a qualitative as well as a quantitative sense, to right consumption, and at the same time organize all the details of distribution on national lines ?

I note that those responsible for the contents of that very impressive book entitled " *The Next Five Years*," which has appeared under the aegis of many influential names, hold that no administrative action less comprehensive than a national policy of the kind in question could deal adequately with existing problems. They suggest that it should now be taken in hand. Others have urged that, apart from the almost prohibitive magnitude of effort the policy would require, it is one which should await the arrival of more knowledge. The latter suggestion has, I think, but little point. There is doubtless much more scientific knowledge to be gained about nutrition and food production, but we know enough to guide administration on to the right lines.

More to be thought of perhaps is the fact that if we take a long range view any policy concerned with food production must ultimately, if it is to be ideal, become part of a world policy. You may have noticed that at Geneva Mr. Bruce, speaking of such a world policy, said that its aim would be to " marry agriculture to health." Such a marriage, if ever properly consummated, would greatly profit the world. The interests of both partners must be equally guarded, however, in the marriage contract. In this country one may venture to say the first mentioned is at present receiving preferential treatment.

My last official duty as your President will be the pleasant one of distributing the medals of the year. Before proceeding to this, however, I would like to express my deep gratitude to the Society for having entrusted me with an office so highly privileged and so much to be coveted. If I have fulfilled its duties with any success it has been due to the continuous support and help I have received from my fellow officers to whose unremitting care for the interests of the Society I wish to testify. To all members of Council who during my term of office have shared in the heavy responsibilities which ultimately fall to that body my gratitude is also due. Finally, I wish to thank the Assistant Secretary, Mr. Winckworth, and all the members of the office staff for their loyal and efficient services.

My retirement is associated with that of Sir Henry Dale, whose ten years of fine service as Secretary will remain outstanding in the records of the Society. I am sure he joins with me in wishing success to those whom for the moment I must call our probable successors.

Awards of Medals, 1935

Professor CHARLES THOMSON REES WILSON is awarded the COPLEY MEDAL. He has contributed fundamentally to the progress of modern physics by his work on the use of clouds in advancing our knowledge of atoms and their properties. How wide the field of his work has been can be seen from the following summary of his researches. He studied the phenomena of condensation of vapour to form drops by the use of expansion apparatus—which he designed. He discovered the existence of " rainlike " and " cloudlike " condensation of water vapour and measured the corresponding supersaturations and the corresponding critical expansions. He also measured the supersaturations requisite to produce condensation of water vapour in ions of both signs produced in various ways. He devised and constructed various types of electrometers and with them and with his cloud apparatus demonstrated the so-called natural ionization of air and other gases. Later he made valuable contributions to our knowledge of atmospheric electricity. With a new form of expansion apparatus, he photographed the tracks of ionizing particles and radiations traversing gases. He next developed methods of measurements which he applied to the study of thunderstorm electricity. In this work the main phenomena relating to the electric field changes produced by lightning discharges were observed for the first time, studied quantitatively, and the principles of their interpretation outlined. He further extended the use of the cloud-chamber method. Stereoscopic methods of photographing ionization tracks were applied successfully to the investigation of the properties of photo-electrons and Compton recoil electrons including their ranges. In recent years he has continued to make numerous and important contributions to the study of atmospheric electricity and, by introducing important improvements and modifications into his cloud-chambers, he has greatly extended their use.

A ROYAL MEDAL is awarded to Professor CHARLES GALTON DARWIN, F.R.S., for his researches in mathematical physics, especially in quantum-mechanics, optics, and statistical mechanics.

His papers on the reflexion of X-rays are now regarded as the fundamental researches on the subject. In his first paper he obtained the formula which is now accepted as generally applicable. There emerged, however, a contradiction: the theory predicted an intensity far less than the experimental. This caused him to discuss the subject more deeply; he traced the discrepancy to its source, and was thus led to investigate the imperfection of crystals, a subject which he was the first to treat effectively.

In a series of papers on statistical mechanics, written in collaboration with R. H. Fowler, he published a new mathematical technique by which the relation of thermodynamics to statistics was placed on a satisfactory basis, and the way was opened for extensive subsequent developments.

Perhaps the most original and influential of Darwin's papers have been those concerned with quantum-mechanics. The quantum theory of the motion of an electron in an electromagnetic field, as it had been developed before 1925, gave results not in accordance with experiment. To obviate this, in 1925 the assumption was introduced that the electron has a mechanical angular momentum and a magnetic moment; but this conception did not admit of the application of wave-theory, since the waves corresponding directly to such an electron would be in space of six dimensions. It was Darwin who in February, 1927, put forward the idea which led ultimately to the solution of these difficulties; he assumed that, just as there are two independent polarized components in a wave of light so there are two independent components in the wave of an electron. He then constructed a pair of equations to represent the fine structure of the hydrogen spectrum, obtaining all the levels correctly except the *s*-levels, and showed how the equations could be expressed in vectorial form, so that, as he expressed it, the electron was a vector wave. This paper was the first important contribution to the modern wave-mechanics of the electron.

Among the quantum papers is also numbered the celebrated memoir on *Free motion in wave mechanics*, in which he took up the general question of aperiodic phenomena and dealt with it in masterly fashion, the principles of description and interpretation which are now universally accepted being formulated and applied to the free motion of electrons and atoms in various types of field. Coming as it did at a critical time, this paper had a great influence.

The reader of Darwin's papers is impressed by his original and powerful mind, his immediate penetration to the heart of a problem, and his combination of deep intuition in physics with mastery of analytical methods.

A ROYAL MEDAL is awarded to Dr. ALFRED HARKER as the greatest British petrologist since that subject became a science; his original contributions have had a profound influence throughout the world. In 1886 he published a paper on Slaty Cleavage, which added considerably to the better understanding of the nature and laws of cleavage phenomena. His next important contribution was the Sedgwick Prize Essay of 1889 on the Bala Volcanic Series of Carnarvonshire. In collaboration with his colleague, J. E. Marr, he published a notable work on the Shap Granite and associated rocks. It is probably true to say that Harker's greatest achievement is the geological mapping of the island of Skye from 1895 to 1901, the results of which were published as a Memoir of the Geological Survey in 1904. This monumental work has had a very wide influence upon the science of petrology: in this Memoir and in the subsequent Memoir on the Smaller Islands of the Inner Hebrides, Harker set a high standard of work both in the field and in the laboratory; he settled the long-standing controversy between Geikie and Judd, and his results have been confirmed by subsequent workers. His book on the "*Natural History of Igneous Rocks*," published in 1909, has been described as "a work which has had a greater effect than any geological publication in the last fifty years." He has also made contributions of great value to the subject of differentiation of rock magmas, etc. His latest book on "*Metamorphism*," published in 1932, is the best contribution to the subject written in any language.

Professor ARTHUR HARDEN is awarded the DAVY MEDAL in recognition of his distinguished work in biochemistry and especially of his fundamental discoveries in the chemistry of alcoholic fermentation.

His researches form a landmark in the history of the organic chemistry of biological processes.

In 1904, in collaboration with his colleague W. J. Young, he showed that the alcoholic ferment of active cell-free yeast juice, the preparation of which had been achieved a few years earlier by E. and H. Buchner, could be separated into two components, a thermolabile non-dialysable enzyme complex and a thermostable dialysable co-enzyme, both of these being essential for the fermentation of sugar. They observed that the fermentation of sugars by this yeast juice was profoundly affected by an addition of inorganic phosphate and followed up this discovery by a detailed and systematic investigation of the carbon balance, from which they showed that for each hexose molecule broken down to carbon dioxide and alcohol another molecule became esterified with phosphoric acid. From the fermentation products, hexosediphosphoric and hexosemonophosphoric esters were subsequently isolated by Harden and his colleagues. These discoveries have been the foundation upon which much of our present knowledge of the intermediate changes in the enzymic breakdown of carbohydrate has been established. In muscle and other glycolytic systems, utilization of carbohydrate is effected by processes closely similar to those occurring in yeast and involving the intervention of phosphate and formation of phosphoric esters. Harden's monograph on alcoholic fermentation is a masterly discussion of this problem of yeast metabolism.

Harden has made important contributions to our knowledge of chemical reactions effected by bacterial enzymes, especially those concerned in carbohydrate metabolism. He has also taken an active part in the development of vitamin research in this country, while as editor of the '*Biochemical Journal*' since 1911 he has influenced deeply the development of this branch of chemistry.

A HUGHES MEDAL is awarded to Dr. CLINTON JOSEPH DAVISSON for his discovery that electrons are diffracted like waves of light. Like many other discoveries, that one disclosed itself gradually; but its origin can certainly be traced to some experiments on the scattering of electrons by nickel made by Davisson and Kunsmann in 1921. Davisson recognized at the time that the observed effects did not harmonize with the existing theories of matter and electrons. Owing to the polycrystalline nature of the metals investigated, the correct interpretation to be put upon the results was not at all clear. Davisson fully recognized the importance of this discrepancy, and this he and his assistants proceeded to investigate with great pertinacity and skill.

Towards the end of 1926 Davisson and Germer succeeded in making similar experiments with a single metallic crystal surface so that the results were simple enough to be interpreted easily. It was then at once seen that the electrons were diffracted like waves of light of the wave-length required by the theory which had in the meanwhile been put forward by M. de Broglie towards the end of 1924. The first announcement of Davisson and Germer's results was published in '*Nature*,' April 16, 1927. This publication was the first clear experimental proof of the wave character of the electron.

Davisson and his associates, principally Germer, have confirmed, amplified, and extended these results in numerous later publications. Davisson has also made important contributions to thermionics.

The Distortion of β-Brass and Iron Crystals

By C. F. ELAM (Mrs. G. H. Tipper)

(*Communicated by G. I. Taylor, F.R.S.—Received June* 5, 1935)

[PLATES 4–7]

Experiments on the distortion of metal crystals having cubic face-centred or hexagonal lattices have given very consistent results, and in every experiment the slip-plane has proved to be the crystal plane of greatest atomic density, which is subjected to the maximum shear stress. The direction of shear on this plane is represented by the line of atoms in closest formation nearest to the line of maximum slope. There is still considerable diversity of opinion concerning the actual mechanism of distortion in crystals having a body-centred cubic lattice. Goucher,[*] using tungsten crystals in the form of a fine wire (maximum diameter 0·195 mm), concluded that planes of type {112} were the most probable slip-planes, the direction of slip being [111].

Distortion combined with X-ray measurements on iron[†] indicated that the pole of the slip-plane was usually nearest to a {112} plane, but tended to lie on the great circle perpendicular to the direction of slip, which was a [111] direction, between a {110} and {112} plane. The slip plane was determined by stress considerations. This work was confirmed by Taylor's[‡] similar investigation of the distortion of β-brass crystals; but with this material the slip-plane tended to be closer to a {110} plane.

Gough's[§] alternating torsion tests on iron seemed to show that the direction of slip was close to a [111] direction but the slip-bands might be resolved into pairs of planes of the type {110} and {123} or {112} and {123}.

Fahrenhorst and Schmid[||] consider {123} planes to be the most probable slip-planes in iron. Their work was confined to the measurement of the movement of the test-piece axis relative to the crystal axes during a tensile test, which they compared with the calculated movement, assuming that the slip-plane was {110}, {112}, {123}, or a random plane, all in a

---

[*] 'Phil. Mag.,' vol. 48, pp. 229, 800 (1924).

[†] Taylor and Elam, 'Proc. Roy. Soc.,' A, vol. 112, p. 337 (1926).

[‡] 'Proc. Roy. Soc.,' A, vol. 118, p. 1 (1928).

[§] 'Proc. Roy. Soc.,' A, vol. 118, p. 498 (1928).

[||] 'Z. Physik,' vol. 78 p. 383 (1932).

[111] direction. These figures are reproduced in fig. 1 as they have a definite bearing on the present investigation. They also compared the observed with the calculated shear stress at the yield point and again thought that a {123} plane most nearly agreed with experiment. They found no slip bands and no broadening of the bar, which would be expected unless the slip-plane had a random orientation.

v. Göler and Sachs* record one instance of slip-bands on a round β-brass crystal, made by Bridgman's method, agreeing with a {110} plane and the change in dimensions was consistent with a [111] slip direction.

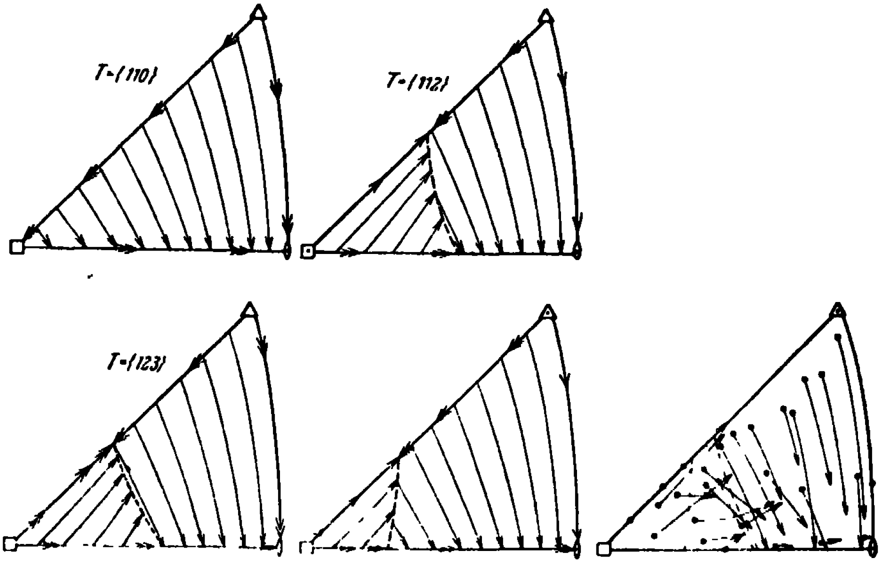

Fig. 1—From Fahrenhorst and Schmid. Movement of crystal axes in extension of cubic face-centred crystals, direction of slip — [111], for possible slip-planes. 1, {110}; 2, {112}; 3, {123}; 4, random; 5, experimental, iron crystals.

The cleavage of both iron and tungsten is known to be along {100} planes. Further, both iron† and β-brass‡ appear to form twin lamellae when subjected to shock. In iron, the twin plane is {112} and the direction of shear [111]. The form of twinning in β-brass has not been determined.

In order to attempt to clear up some of these obscurities, further experiments were carried out with β-brass, and the results were again compared with tests on iron crystals. Crystals of β-brass were prepared by the method of straining and heat treatment, and by Bridgman's method, *i.e.*, from the melt. The brass was very kindly supplied by Thomas Bolton & Sons, Ltd., and prepared under the supervision of Dr. W. E. Alkins, to whom I wish to convey my thanks. I am also indebted to this firm for undertaking the analysis of the crystals. I was fortunate in having a strip of the brass used by Professor Taylor, who also gave me one of his original compression specimens for a further X-ray examination. The iron crystals were remains of the original pieces given by Professor Edwards and Dr. Pfeil.

---

* 'Naturwiss.,' vol. 22, p. 412 (1928).

† Mügge, 'Neu. Jahrb. Min.,' vol. 2, p. 55 (1899); Pfeil, 'J. Iron and Steel Inst. Carnegie Schol. Mem.,' vol. 25, Nos. 1–26, p. 319.

‡ Johnson, 'J. Inst. Met.,' vol. 24, p. 301 (1920); Clarke, 'Amer. Inst. Min. Met. Eng. Inst. Met. Div.,' p. 253 (1927).

Tests on β-brass will be described first.

TABLE I—β-BRASS CRYSTALS*

No.	Copper %	Remarks
1	53·82	All cut from same strip.
2	53·82	
3	53·82	
5	53·38	
6	49·92	Over 1% Pb. Quenched from 800° C.
7	50·12	
8	54·02	Piece of original strip used by Professor Taylor.
9	54·02	
10	55·20	Prepared from melt. Brass melted in nitrogen. Low percentage of zinc due to loss by volatilization.
11	55·39	
12	54·48	
13	Not analysed	

* The analyses were made on the crystals after extension. Where more than one was cut from the same strip only one was analysed.

With the exception of Nos. 6 and 7, all the crystals were cooled in the furnace; those made by the melting method from the highest temperatures reached, *i.e.*, 1000–1050° C and those annealed after straining from 800° C. It has long been known that some change takes place in β-brass over a range of temperature reaching a climax about 450–470° C, which causes a slight change in volume, electrical conductivity, etc.* X-ray investigation† has shown that there is no allotropic change involving a change in space lattice, but recent information obtained from other similar alloys points to a re-orientation of atoms in the lattice.‡ No information is available of the effect of such a change on the distortion of a crystal. which seems to be chiefly dependent on the structure of the lattice. As the quenched crystals did not deform uniformly—due probably to stresses set up during quenching—it was not possible to obtain any evidence on this point. The slow cooling of the other crystals was intended to allow them to reach a condition of stability, and to ensure that they were, as far as possible, similarly treated.

---

* Carpenter and Edwards, 'J. Inst. Met.,' vol. 5, p. 127 (1911); Matsuda, 'Sci. Rep. Tohoku Imp. Univ.,' p. 223 (1922).

† Westgren and Phragmen, 'Phil. Mag.,' vol. 50, p. 311 (1925); Phillips and Thelin, 'J. Franklin Inst.,' vol. 204, p. 359 (1927); v. Göler and Sachs, 'Naturwiss.,' vol. 22, p. 412 (1928).

‡ Straumanis and Weerts, 'Z. Physik,' vol. 78, p. 1 (1932) ; 'Metallwirt.,' vol. 10, p. 1929 (1931); Bragg and Williams, 'Proc. Roy. Soc.,' A, vol. 145, p. 699 (1934).

The crystals were filed into the form of small strips or square bars and very carefully polished. Tensile specimens were chosen in preference to compression in order to make the fullest possible use of any surface markings, such as slip-bands, that might appear. It is admitted that the distortion is probably more uniform in compression specimens. On the other hand, some of the measurements are more accurate in tensile specimens, notably the change in length. The crystal axes were determined by means of X-rays and the marking and measuring carried out as in previous investigations. The crystals were then extended and a complete series of measurements made at each stage. Three entirely separate sets of measurements can be obtained: (1) traces of surface markings, such as slip-bands on two adjacent faces; (2) movements of test-piece axis relative to crystal axes (determined by means of X-rays); (3) calculation of the position of lines of particles in the strained and unstrained state which are unchanged in length by the deformation.

1—A well-marked yield point coincided with the first appearance of broad bands on the surface. In most cases they were confined to one pair of faces only, no marks of any kind being visible on the other pair. Typical examples are shown in figs. 13, 14, and 15, Plate 4. The inclination of such bands to the vertical axis may vary considerably on the same face, but it is possible to obtain a rough average figure representative of the majority. As the extension proceeds, a large number of very fine lines appears, usually making a small angle with the wider bands, and the fine bands are also to be found on the pair of faces previously free from markings, fig. 16, Plate 4.

In the early stages it was rare to find more than one set of slip-bands. Occasionally two sets were visible on first straining but only one persisted subsequently.

After an extension varying from 20–40% a new series of bands appeared. As in the first instance, they were wide and visible to the naked eye while the specimen was under test. They generally started from one end and rapidly spread along the specimen, closely resembling the behaviour of α-brass crystals* when slip suddenly changed from one plane to another.

* Elam, 'Proc. Roy. Soc.,' A, vol. 115, p. 148 (1927).

Sometimes three stages were observed before fracture. Some typical examples of these slip-bands are shown in figs. 17, 18, and 19, Plate 5. It is probable that the broad bands represent alternate regions of slip and non-slip when they first become visible. Later the " gaps " close up and the whole surface becomes covered with extremely fine, regular bands. There was a marked yield point coinciding with the onset of the formation of each new set of bands, presumably caused by the sudden reduction of cross-sectional area of the test-piece.

The position of the principal crystal planes was determined before extension and at different stages during test. The traces of the slip-bands on the faces were also measured and the two compared. The first broad bands did not always agree with any likely crystal plane, but the first fine bands agreed very closely with a possible {110} plane, with one or two exceptions, the most important being No. 10, in which the slip-bands appeared to be on a {112} plane. The slip-bands tended to deviate from the position of traces of possible crystal planes as the distortion proceeded, but when a new set appeared they again agreed with another possible {110} plane. Intermediate polishing removed all traces of the bands, but they appeared again in approximately the same position on re-straining. Data from both sets of measurements are included in Table II, and the positions of slip-bands are marked in the stereographic diagrams where they may be compared with the distortion figures. Allowing for errors in measurement, the deviation of the actual slip-bands from traces of crystal planes is still often large. This can only mean that they do not represent true crystal planes, and since the crystal does not remain constant in relation to them, their exact significance is somewhat obscure. One can only say that in the first instance they are caused by some kind of movement on planes of type {110}. It was characteristic of iron crystals that the slip-bands varied in appearance according to the position of the specimen surface relative to the direction of slip. The same effect is found here. The slip-bands were always difficult to see and were straighter on faces parallel with the direction of slip.

2—*Movement of Test-piece Axis During Extension*—This information is derived entirely from X-ray measurements and is thus independent of calculations of the distortion. It is known that with shear on one plane only, the test-piece axis moves relative to the crystal axes towards the direction of shear.* The distance moved along the great circle joining

---

* Mark, Polanyi, and Schmid, ' Z. Physik,' vol. 12, p. 58 (1927); Taylor and Elam, ' Proc. Roy. Soc.,' A, vol. 102, p. 643 (1923).

the direction of shear and the original position of the axis is also related to the extension. The results are shown in stereographic projection in fig. 2. To avoid confusion, the crystals are not all put into one triangle, but each triangle is crystallographically similar. According to Taylor,† the points representing the axis at each stage of the deformation should

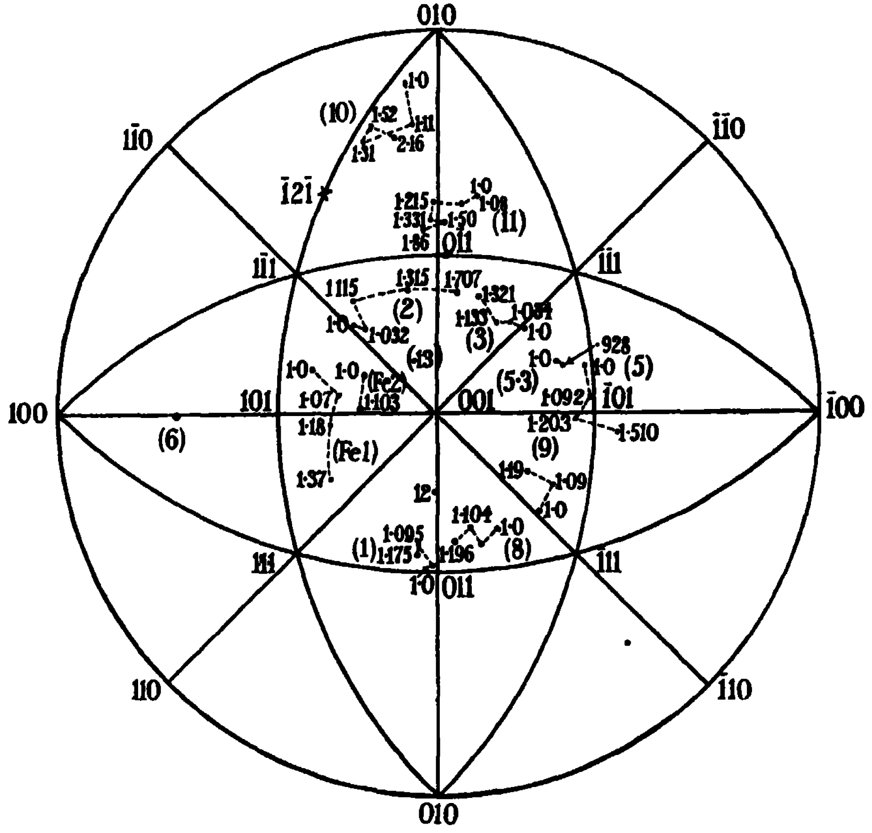

Fig. 2.*

---

* The direction of slip depends on the orientation of the slip-plane and is generally the crystallographic direction nearest to the line of maximum slope in the plane. In fig. 2, according to Taylor's theory, if the axis of the specimen is in the triangle [001], [011], $[\bar{1}11]$, the direction of slip is [111] and the axis should move towards this direction if the direction of slip on the slip-plane is towards [111]. Similarly in the triangle [001], [111], [011] the direction of slip is towards $[\bar{1}\bar{1}1]$, and so on for every triangle. As it was found necessary, to avoid confusion, to make use of several triangles in the diagram, corresponding indices have been assigned to the figures representing X-ray and distortion measurements in later diagrams. If the axis moves out of its first triangle the indices are not altered.

† 'Proc. Roy. Soc.,' A, vol. 118, p. 1 (1928).

lie on a great circle through the original point and the [111] direction which is the direction of slip, *see* footnote to fig. 2. This conclusion is arrived at from distortion measurements to be described later. Owing to the fact that he worked with small amounts of deformation and did not always determine the positions before and after straining, his results are not suitable for comparison with the above. One may, however, compare them with Fahrenhorst's and Schmid's for iron, remembering that the tests were carried out all in one stage in their experiments. There is very considerable variation in direction, although in a number of the crystals the average movement is towards a [111] direction. Only one crystal was obtained in which the test-piece axis was near the [100] axis (No. 10), and this crystal proved an exception in other respects (*see* also p. 285); but it agreed with certain of Fahrenhorst's and Schmid's and also with the predicted behaviour of crystals in that position for certain planes of slip, *i.e.*, {112}, {123}, or random.

Allowing for errors of measurement, the points lie far off the predicted line, sometimes taking on a zig-zag motion on either side of it. The full significance of these results will be referred to again.

It is also clear that at certain stages the movement is less than would be expected for slip on one plane. During the later stages, we know that other planes participate, but this certainly does not apply to the first 20% extension.

3—*Distortion Measurements and Calculations*—Previous calculations of the distortion of β-brass and iron crystals have shown that the lines of particles unchanged in length during the deformation lie in two planes. This type of distortion in the face-centred cubic metals has a simple interpretation, *i.e.*, one plane is the slip-plane and is related to the crystal structure and consists of the same particles throughout the distortion. In the body-centred cubic metals it is the exception rather than the rule to find that either plane coincides with a crystal plane. This is confirmed by the present investigation. In order to obtain the fullest possible information from these measurements, calculations were made of the directions in both strained and unstrained positions at each stage, not only in reference to the original unstrained state but also between intermediate stages up to the appearance of a second set of slip-lines. Calculations beyond this point generally gave a figure indicating that slip was definitely not confined to one plane. In the majority of cases, the calculations gave two planes with differing degrees of accuracy. There seemed to be a tendency for the crystals that were made from the melt to give better results than those grown in the solid. With few exceptions there

TABLES II AND III—TABLES GIVING SPHERICAL CO-ORDINATES OF DISTORTION PLANES, DIRECTION OF SLIP, ETC., AND NEAREST CRYSTAL PLANES AND DIRECTIONS FOR REPRESENTATIVE β-BRASS CRYSTALS AND IRON CRYSTALS

ε = ratio of extended to initial lengths. In column 2, the stages in the extension are referred to in values of ε.
θ = angle between test-piece axis and pole of plane.
ψ = angle between reference plane (Face I of specimen) and plane containing θ. ψ is measured anti-clockwise.
η = angle between direction of slip and line of greatest slope on slip plane.

Except in special cases, unless a crystal plane or direction is within 10° radius of the corresponding points determined from distortion measurements or slip-bands, they are not given in the table.

Where figures are given for slip-bands in "unstrained" material, they refer to their position when they first appeared at an extension of 1–2%.

Both strained and unstrained positions were not calculated for every stage.

TABLE II

No.	ε	Distortion planes		Direction of slip		η	Slip-bands		Crystal plane		Crystal direction	
		θ	ψ	θ	ψ		θ	ψ	θ	ψ	θ	ψ
	Strained											
3	1·0 to	32	286	62	75	26						
	1·034	60	76	34	288	17	33	83	{110} 33	75		
	1·034 to	52	286	39	94	7·5						
	1·072	44	95	46	286	8	42	85	{110} 41	90·5	[111] 50	286·5
	1·072 to	51·5	276	40·5	73	14						
	1·133	32·5	68	60	273·5	21	42	85	{110} 36·5	82	[111] 56	284
	Unstrained											
	1·034 to	51·5	278	39	85	8						
	1·133	38	91	53	279	6·5	33	83	{110} 33	75	[111] 60	283

	Strained											
	1·034 to	58	270	33	81	10						
	1·133	40·5	84	51	283	14	42	85	{110} 37	82	[111] 56	284
	Unstrained											
	1·133 to	45·5	293	48	88	18						
	1·321	37	82	57	291	24			{110} 37	82	[111] 56	284
	Strained											
	1·133 to	58	292	37	78	19						
	1·321	42	84	52	294	24	55	80	{110} 45	80	[111] 48	284
							12	254	{110} 15	248		
5	**Unstrained**											
	1·0 to	36·5	281	57·5	81	16	48	290	{110} 48	298	[111] 48	81
	1·035	24	67	68	272	22	—	—	—	—	—	—
	1·035 to	52	280·5	45	62	26	48	288	No X-ray analysis done corresponding to $\varepsilon = 1{\cdot}035$.			
	1·092	41·5	60	55	279	31						
	Strained											
	1·035 to	54	280	40	67	20	51	288	{110} 54	278	[111] 38	65
	1·092	42	69	52	281	24						
	Re-polished and Re-marked											
	Unstrained											
	1·092 to	49	268	50	109	16	51	288	{110} 54	276	[111] 38	65
	1·203	44	111	48	269	16						
	Strained											
	1·092 to	48	290	45	85	16·5	54	283	{110} 58	288	36	79
	1·203	38	88	41	293	16						

TABLE II—(continued)

No.	ε	Distortion planes		Direction of slip		η	Slip-bands		Crystal plane		Crystal direction	
		θ	ψ	θ	ψ		θ	ψ	θ	ψ	θ	ψ
	Re-polished and Re-marked—(continued)											
5	Strained											
	1·203 to	67·5	275·5	25	70	11	58	278·5	{110} 67	288	[111] 30	60
	1·320	33	76·5	59	278	18						
	1·320 to	Not two planes					58	279	{110} 66	277 (old)		
	1·510						52	41	{110} 60	30·5 (new)		
10	Unstrained											
	1·0 to	42·5	321	48	139	2	39·5	319·5	{112} 44·5	317	[111] 49·5	135
	1·11	42	139	46	322	2						
	Strained											
	1·0 to	50	316·5	40·5	139·5	2	47	318	{112} 49	325	[111] 42	136
	1·11	42	138·5	42	317·5	2						
	Unstrained											
	1·11 to	50	316·5	39·5	138	1	47	318	{112} 49	325	[111] 42	136
	1·525	20	139	70	316·5	2·5						
	Strained											
	1·11 to	68	308·5	22	124	2	63	313	{112} 55	311·5	[111] 39	128·5
	1·525	44	126	46	309	2						
	1·525 to	Nearly circular cone					51	313·5	{112} 55	317		
	2·16					Fracture	45	61	{110} 39·5	63		

11	Unstrained												
	1·0 to	44·5	266·5	50	58	21		46	262	{110} 44	260	[111] 45	66
	1·081	46	56	48	266	21							
	1·0 to	38	266	52	68·5	14							
	1·331	36	63·5	55	271	14							
	Strained												
	1·0 to	50	269·5	45	58	21		51	269·5	{110} 50	261	[111] 41	64
	1·081	49	60	45	273	22							
	Unstrained												
	1·081 to	48	269	43·5	72·5	12·5		51	269·5	{110} 50	261	[111] 41	64
	1·215	36	68	56	267	16							
	Strained												
	1·215							54	268	{110} 54	263		
	1·331						Old S_1	59·5	269	{110} 58	263		
							New S_2	46·5	19	{110} 54	23		
	1·50						S_2	56	20	{110} 57	21		
	1·86						S_2	57·5	33	{110} 53	32		
							S_2	59	274	{110} 59	273	Same as S_1 ?	
							Fracture	45	31			Same as S_2 ?	

were generally some outward signs of non-uniformity or more than one set of slip-bands in those crystals which gave a distortion figure not consisting of two planes. The two possible directions of slip were found as usual, by marking off on the stereographic diagram points on each plane 90° to their line of intersection. Consequently, if the calculated directions did not lie accurately on two planes, the directions of slip could not be determined with certainty. Which of the two directions is the true direction of slip can only be determined by other measurements. In Table I the results are given for a number of typical crystals and a note is made if the " cone " did not consist of two planes.

Thirteen crystals were tested and 43 calculations made. In the majority, one of the planes is near a {110} plane, which is also the nearest crystal plane to that formed by the slip-bands. No. 10 is an exception, the nearest crystal plane being {112}, and one other instance of a {112} plane functioning as a possible slip-plane is recorded, *i.e.*, the first stage of crystal 2.

Turning now to the direction of slip in that plane which, on general grounds, appears to be most closely related to the crystal structure. Only 14 slip directions were coincident with or near, *i.e.*, within 5° of, a [111] direction. In a few cases, the direction of slip could not be obtained accurately. Of the remainder the deviation from a [111] direction varied considerably and was greater than could be attributed to error in measurement. Stereographic projections were made of all stages, but it is impossible to give more than a few representative examples. Reference may also be made to the previous papers on iron and β-brass where typical diagrams are shown of the figure obtained when the direction of slip coincides with a [111] direction. In such cases the pole of the plane of distortion lies on an arc of the great circle at 90° to this direction and coincides with a {112} or {110} plane or lies between them. There is no such simple relationship if the direction of slip is also variable, and it will be seen in some of the following diagrams that both slip-plane and direction of slip vary within wide limits. The strained position of one extension and the unstrained of the following extension refer to the same position of the crystal axes and it is possible to put the results of these two calculations into one figure. This has been done for crystal No. 3 in fig. 3. The strained position of the first stage, $\epsilon = 1 \cdot 0$ to $\epsilon = 1 \cdot 034$, shows that more than one plane had contributed to the distortion, *i.e.*, the figure does not consist of two planes. Traces of several sets of slip-bands appeared on first straining, but they were not all visible on two faces, only one set agreeing with a {110} plane persisted, so that probably movement on the others was only small, but sufficient to affect the distortion figure. On the same diagram is the result of the unstrained position for $\epsilon = 1\cdot034$ to $\epsilon = 1\cdot133$. Here, the figure clearly consists of two planes, but the agreement with a crystal plane and direction are only approximate. On the other hand, the slip-bands agree fairly well with a {110} plane. Similarly in fig. 4 one can compare the strained position of $\epsilon = 1\cdot034$ to $\epsilon = 1\cdot133$ with the unstrained of $\epsilon = 1\cdot133$ to $\epsilon = 1\cdot321$. If one of the planes represents a plane of shear which has continued to function throughout both stages of the deformation it should occupy the same position relative to the reference plane, *i.e.*, face I, in both stages. In no stages of crystal 3 were these conditions fulfilled. On the other hand, crystal 10 provides an example of this type of deformation. This crystal differed from most of the others in that the slip-bands and distortion measurements indicated slip on a {112} plane. Fig. 5 shows that throughout the whole extension up to $\epsilon = 1\cdot525$ one plane remained undistorted. In this case also, the direction of slip,

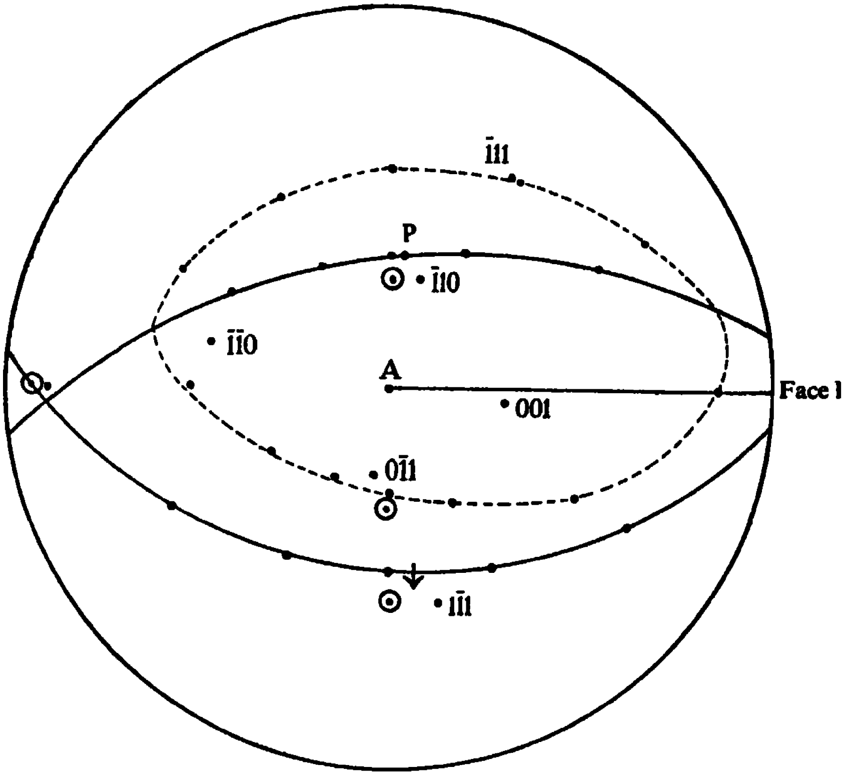

FIG. 3—β-brass-3. $\epsilon = 1\cdot0$ to $\epsilon = 1\cdot034$ strained— — · — —; $\epsilon = 1\cdot034$ to $\epsilon = 1\cdot133$ unstrained— · —; traces of slip-bands marked thus ⊙ ; direction of slip →.

which was a [111] direction, also remained constant. Quite another result is obtained if the strained position of the cone is calculated for the extension $\epsilon = 1\cdot11$ to $\epsilon = 1\cdot525$, fig. 6. Here are still two planes, but they have deserted the crystal planes and directions and no longer agree with slip-band measurements. Crystal 11 illustrates a similar phenomenon, but in this one the slip-plane is nearest to {110}, fig. 7.

One other example may be given. At one stage of the extension of crystal 2 from $\epsilon = 1\cdot115$ to $\epsilon = 1\cdot32$, in the strained position one plane and slip-direction agreed very closely with a {110} plane and [111] direction and slip-bands supported the normal conclusion that this crystal was deforming by slip in the ordinary way. In the next stage, $\epsilon = 1\cdot32$ to $\epsilon = 1\cdot632$ however, there appeared to be no relationship. Fig. 8. When the specimen was carefully examined, traces of a new set of slip-bands were just visible and these agreed with another {110} plane. The appearance of a new set of slip-bands agreeing with a possible crystal plane was invariably met with and served to check the X-ray measure-

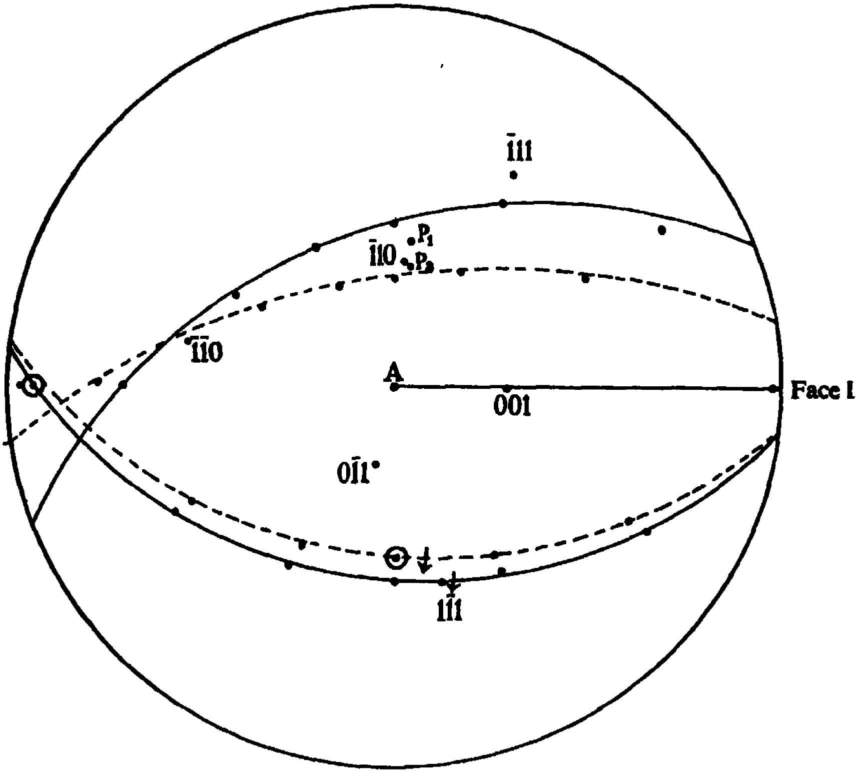

FIG. 4—β-brass 3. $\epsilon = 1\cdot034$ to $\epsilon = 1\cdot133$ strained — — · — — P_1; $\epsilon = 1\cdot133$ to $\epsilon = 1\cdot321$ unstrained — · — P_2.

ments. The discrepancy between the plane calculated from distortion measurements and the crystal planes cannot be explained by attributing it to slip on the new plane. This would result in an entirely different type of figure, *i.e.*, it would not consist of two planes.

If the deformation is due to shear on a plane there is a relationship between the amount of extension and the final and initial positions of the slip-plane, $\cos \theta_1 = \varepsilon \cos \theta_0$.

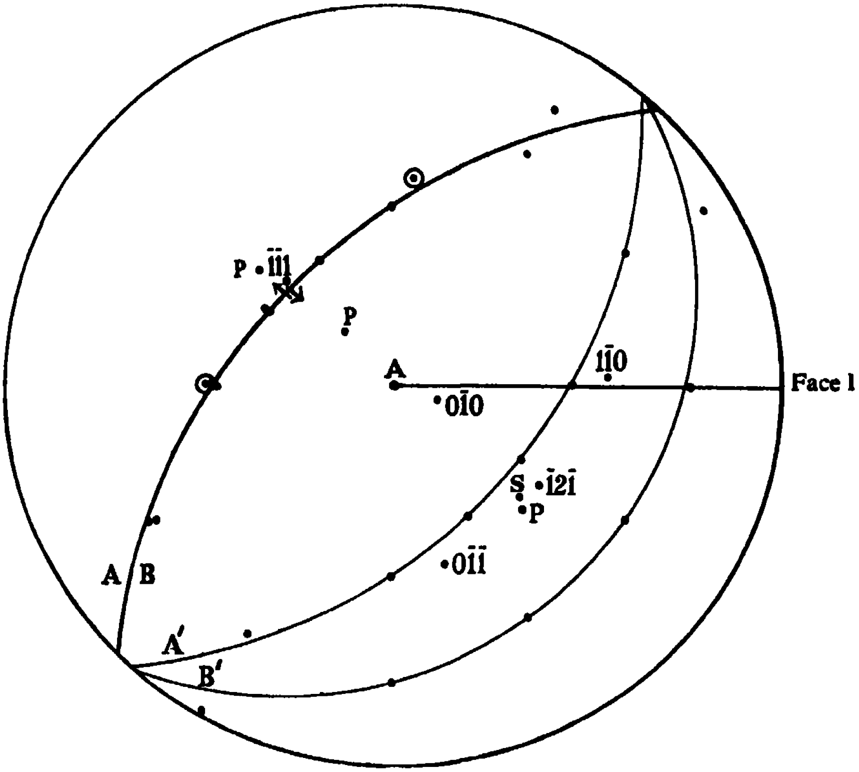

FIG. 5—β-brass 10. $\varepsilon = 1{\cdot}0$ to $\varepsilon = 1{\cdot}11$ strained (A) A′; $\varepsilon = 1{\cdot}11$ to $\varepsilon = 1{\cdot}525$ unstrained (B) B′.

Table II gives the particulars required for making this calculation and it is clear that this relationship does not hold whether the distortion plane, slip-band plane, or the most likely crystal plane, *e.g.*, {110} or {112}, are considered.

There are certain other interesting features about some crystals. One, No. 6, became divided into two parts immediately straining began, giving the appearance of a twin, fig. 20, Plate 5. The axis of this specimen lay in a {100} plane (*see* fig. 2) and the " twin " plane was parallel to this plane. Examination of the surface showed two sets of slip-bands divided by the "twin" plane, the bands agreeing closely with two {110} planes, which were equally inclined to the axis. Evidently the "twin" was caused by deformation related to both these planes. Although the plane of union is a {100} plane at the beginning of the test it will cease to be so as soon as extension has taken place.* Other examples of this occurrence were not infrequently met with, particularly near a crystal boundary, where the distortion was not uniform. In some crystals there were alternate bands, resembling lamellar twinning. These bands persisted when a crystal section was polished and etched, unlike slip-bands which are usually purely surface markings (*see* p. 277). In all the tensile specimens examined the plane of union was near a possible {100} plane and three sets, belonging to all three possible {100} planes, have been found in the same crystal.

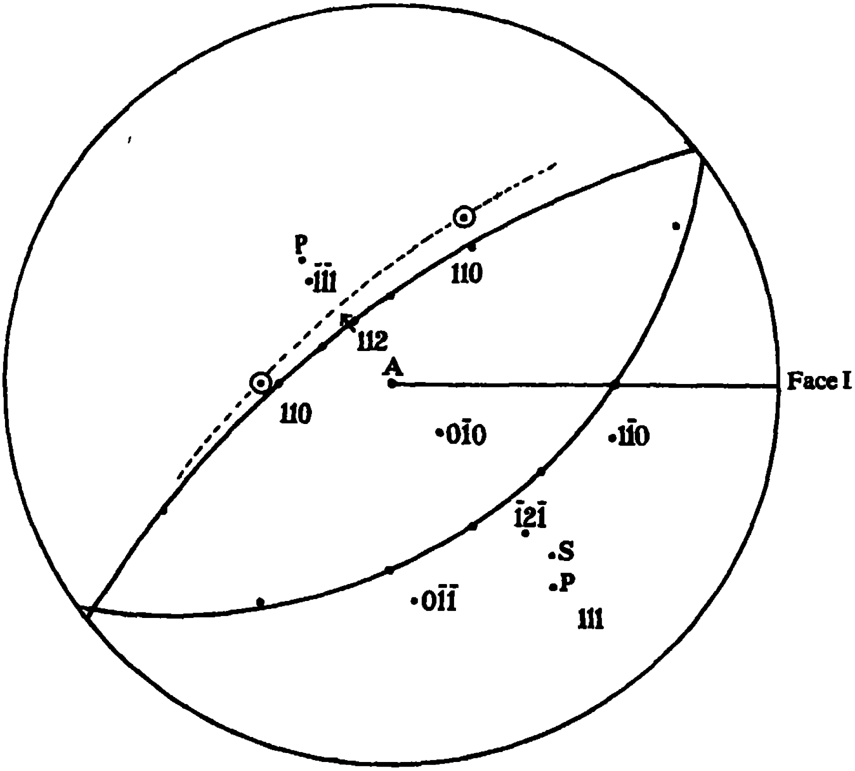

FIG. 6—β-brass 10. ϵ — 1·11 to ϵ = 1·525 strained.

---

* A similar structure is described for an aluminium crystal. Elam, 'Proc. Roy. Soc.,' A, vol. 121, p. 237 (1928).

Iron Crystals—In view of the results obtained with β-brass crystals, it was decided to repeat some tests with iron and to carry on the investigation until fracture occurred. Calculation of the distortion had previously been confined to comparatively small extensions or compressions. The same procedure was adopted as for the brass crystals and the results are given in Table III and in figs. 9 and 10. The first slip-bands were hardly visible on one pair of faces. Their appearance on two faces at right angles after an extension corresponding to $\varepsilon = 1{\cdot}077$ is illustrated in figs. 21 and 22, Plate 6. The nearest crystal plane was {110}. No other slip bands appeared before the crystal broke at about 63% extension. The movement of the test-piece axis was definitely not towards a [111] direction at the beginning of extension but later tended to approach this direction. Calculations of the distortion showed a slight variation in

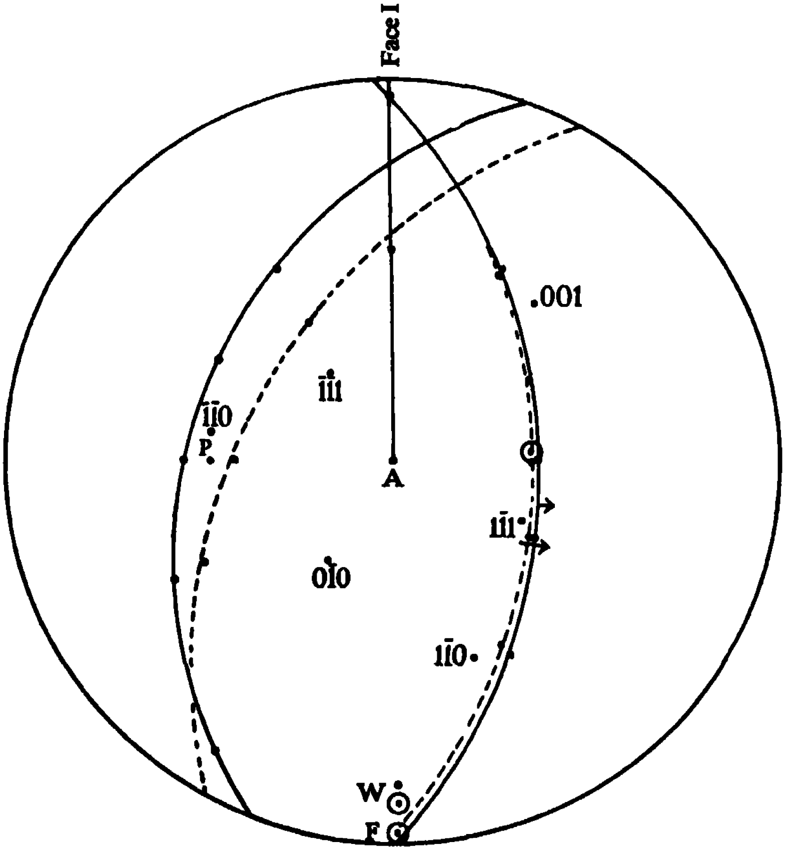

FIG. 7—β-brass 11. $\varepsilon = 1{\cdot}081$ strained - - · - -; $\varepsilon - 1{\cdot}081$ to $\varepsilon = 1{\cdot}215$ unstrained —·—.

position of the planes in the unstrained material according to the extension, fig. 9. This is contrary to what would be expected if the whole of the distortion is due to slip on one of these planes. At the beginning of the test, one of the planes agreed fairly closely with a {110} plane and with the plane obtained from the slip-bands. After straining, the slip-bands agreed with the distortion plane, but neither agreed with the {110} plane, nor with any other simple crystal plane, fig. 10. Neither was the direction of slip obtained from these measurements near a [111] direction, but seemed to be along the line of greatest slope in the plane. Very similar results were obtained with another crystal, which, however, did not show such a uniform distortion from the start. In this case, slip-bands agreed very closely with a {110} plane. One of the distortion planes, which were not perfect planes, was only approximately near the

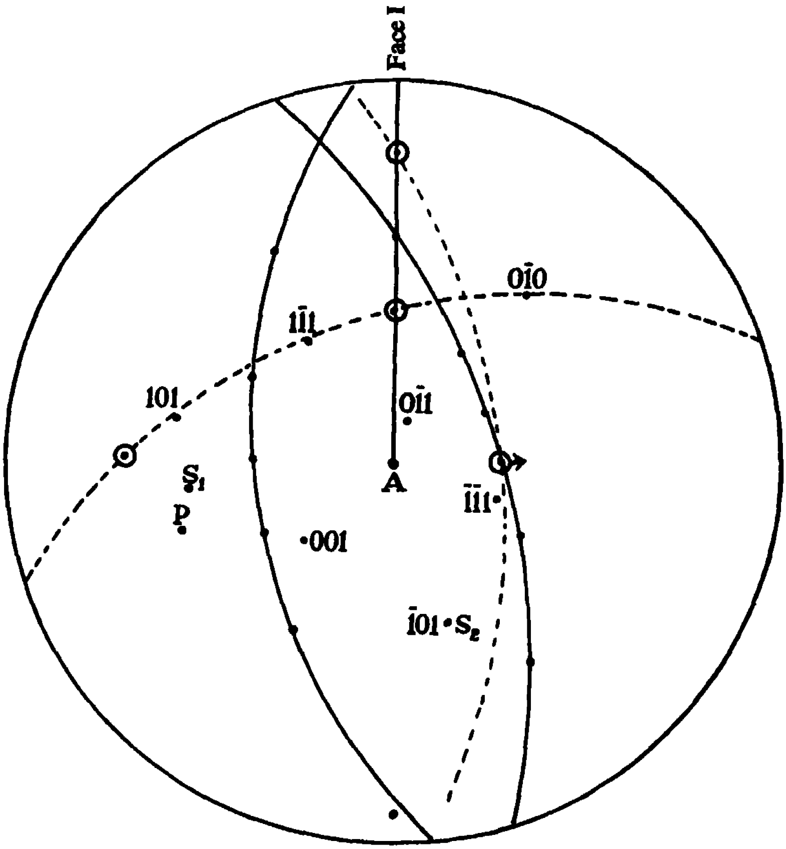

FIG. 8—β-brass 2. $\epsilon = 1\cdot205$ to $\epsilon = 1\cdot517$ strained. S_1 = original slip-bands; S_2 = new slip-bands, appearing just at $\epsilon = 1\cdot517$.

TABLE III—Iron

No.	ε	Distortion planes		Direction of slip		η	Slip-bands		Crystal plane		Crystal direction	
		θ	ψ	θ	ψ		θ	ψ	θ	ψ	θ	ψ
1	Unstrained											
	1·0 to	44	183	46	355	5·5	46	179	{110} 47	176	[111] 46	16
	1·077	42	355	48	175	5						
	1·0 to	42	179	48	359	0	Same					
	1·181	39	0	51	181	0						
	1·0 to	39	181·5	50·5	0	0	Same					
	1·367	33	1	55	179							
	Strained											
	1·0 to	48	183	48	357	4	50	179	{110} 48	186·5	[111] 42	10
	1·077	45	357	45	182	3						
	1·0 to	57	178	33	1·5	2	57	179	{110} 70	188	[111] 22	4
	1·367	40	0	40	0	1						
	1·181						52	175	{110} 56	179	[111] 34	2·5
2	Unstrained											
	1·0 to	34·5	69·5	56	250	0	41·5	63·5	{110} 40	66·5	[111] 50	246
	1·103	40	248	45	67	3·5						
	1·0 to	38·5	68	50·5	248	0	Same					
	1·23	51	250	50	65	3·5						

{110} plane, but the direction of slip was close to a [111] direction. This direction happened to be also the direction of greatest slope.

FRACTURE OF β-BRASS CRYSTALS

Most of the crystals that were broken in tension did not show well-defined cleavage planes, but Nos. 10 and 11 both gave regular cleavage fractures at 45° to the axis, Table II. Allowing for considerable local distortion at the point of fracture, these planes were fairly close to {110} planes. For No. 10 the type of plane was confirmed by obtaining direct X-ray reflexions from it corresponding to a {110} plane. Further information on the cleavage plane of β-brass crystals was obtained by rolling strips consisting of large crystals occupying the whole cross-

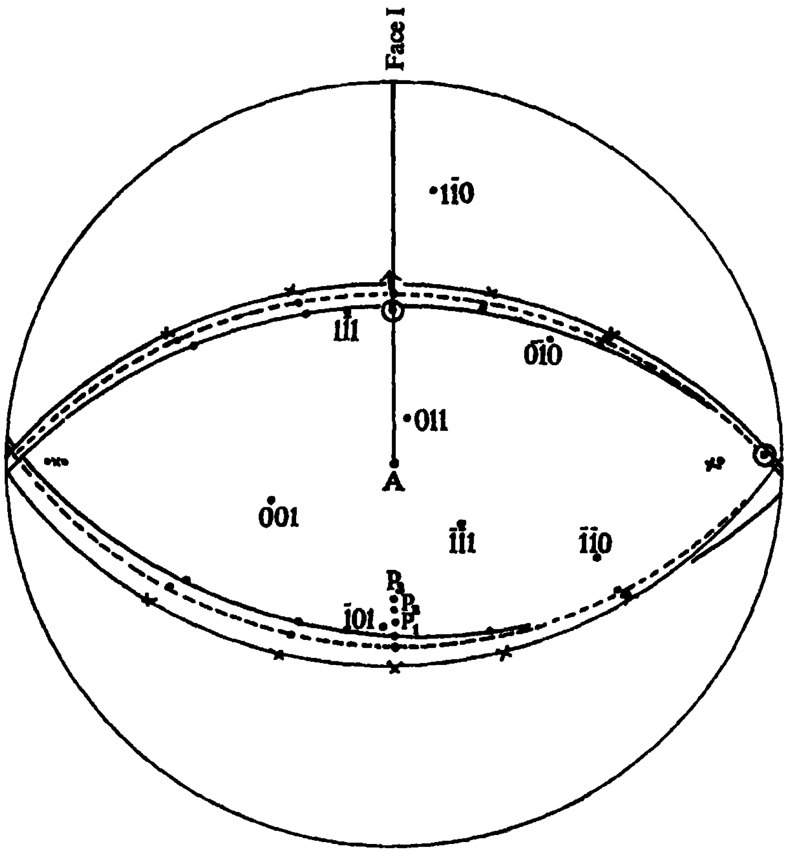

FIG. 9—Fe 1. $\varepsilon = 1 \cdot 077$ P_1 ——•; $\varepsilon = 1 \cdot 181$ P_2 – – • – –; $\varepsilon = 1 \cdot 367$ P_3 ——× unstrained.

section. The metal is extremely tough when cold and was rolled in a small hand roll with very small reductions between each pass. There was very little lateral spread in the strip. At about 20% reduction in thickness some crystals began to crack. The cracking was quite audible and sometimes took place after the strip was removed from the rolls, the warmth of the hand appearing to increase the liability to crack. In extreme cases, the metal disintegrated into small pieces having almost perfect plane faces. A general appearance of the cracks on the rolled surface after polishing is illustrated in fig. 23, Plate 7. Where two cleavage planes intersected, the edge was very clear-cut and straight. Fig. 24, Plate 7, shows such a cleavage face and edge and also shows striations on the face which were often met with. Unlike slip-bands, these striations were not removed by polishing. Fig. 23, Plate 7, shows some of them in the neighbourhood of a crack, the section having been polished and

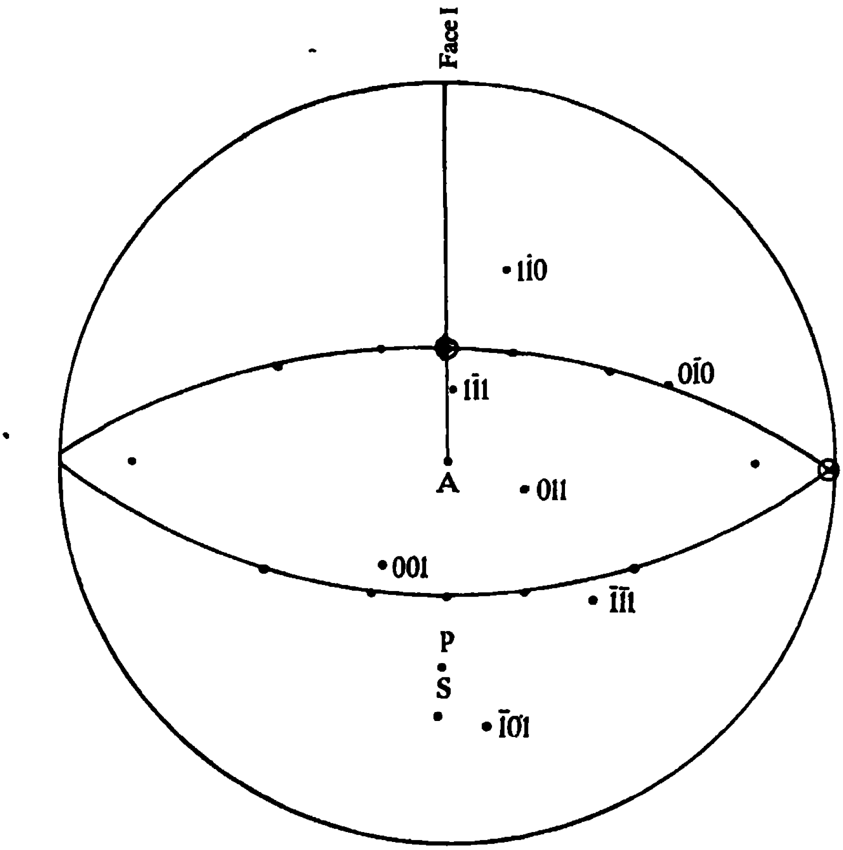

Fig. 10—Fe 1. ε — 1·367 strained.

lightly etched with ammonia. Measurements of the angles between cleavage planes were carried out in a goniometer. The angles were usually 60° or 120° and the two planes were most frequently arranged so that they were equally inclined to the rolling plane.

The angle 60° suggested that the planes were crystal planes of type $\{110\}$, planes of this form making angles of 60° with each other or 90°. X-ray photographs were accordingly made and confirmed the fact that the cleavage planes were always of this type.

The striations on the cleavage planes and on polished faces of rolled specimens proved to be sections of planes which at first sight seemed to be twin lamellae. They were approximately parallel to $\{100\}$ planes or $\{111\}$ planes in the crystal. Structures such as these are very common in rolled metal. It has already been explained how such structures may arise in tension on planes parallel to $\{100\}$ planes, *see* p. 288. Striations parallel to $\{111\}$ planes were never found in tensile specimens and only in one compression specimen. X-ray photographs did not show a duplex orientation. Therefore, one may conclude that any differences of orientation which may exist between neighbouring lamellae are small. After annealing at 200° C, fig. 25, Plate 7, however, one rolled specimen now gave two sets of spots, one set clear and undistorted, indicating that they were obtained from recrystallized metal, the other being unaltered. The new series suggested a rotation of 10° in relation to the old, about an axis representing approximately a direction at right angles to the direction of rolling in the plane of the strip. The striations seem to be layers of material more strained than intermediate layers, but not layers of different orientation. They are not in this respect like the structures described above which are parallel to $\{100\}$ planes.

Fig. 11 is a stereographic diagram illustrating these points. The cleavage planes were $(1\bar{1}0)$ and (101) respectively. Striations on their faces and on the plane of rolling agreed approximately with the $(1\bar{1}1)$ and $(\bar{1}11)$ planes. The normals of these planes are the probable slip-directions of the respective $\{110\}$ planes and the planes themselves are perpendicular to them. If, for example, the deformation takes place by slip along the plane of maximum shear stress $(\bar{1}01)$ and in a direction $[\bar{1}11]$, there will be a complementary shear stress at 90° to this plane, *i.e.*, along the plane $(1\bar{1}1)$. This is not one of the usual slip-planes and in a tensile test the need for any adjustment on this plane probably does not arise. But in rolling, the metal is compressed in one direction while being extended in the other, therefore faulting along planes perpendicular to the plane of shear becomes necessary. Clearly the deformation is not simple slip, otherwise there would be no sign of it after polishing. The

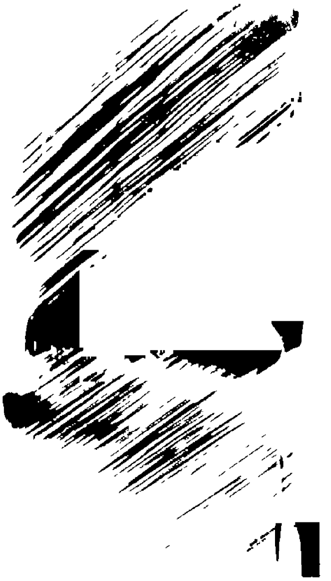

Fig. 13—Strip consisting of 2 crystals, extended 5 %.

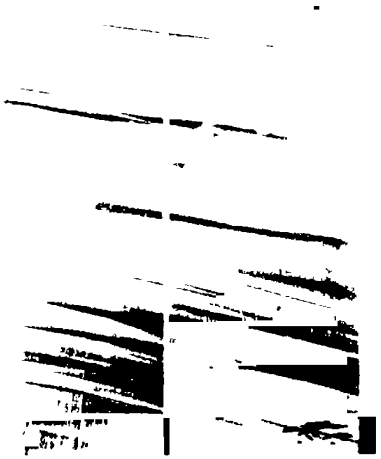

Fig. 14—β-brass 8, ε = 1·06.

Figs. 13 and 14, illumination slightly oblique.

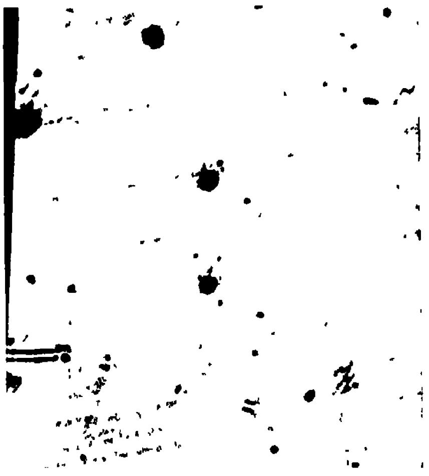

Fig. 15—No. 13, extension 2%.

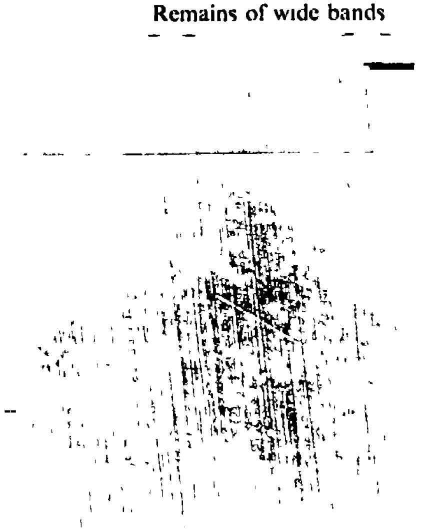

Fig. 16 No. 3, ε = 1·034

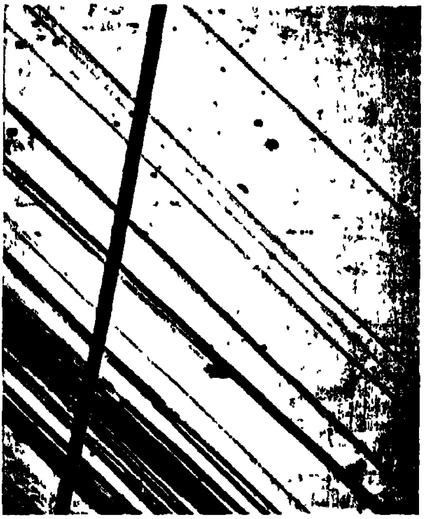

× 90

Fig. 17—No. 11, ε = 1·4 – 1·50

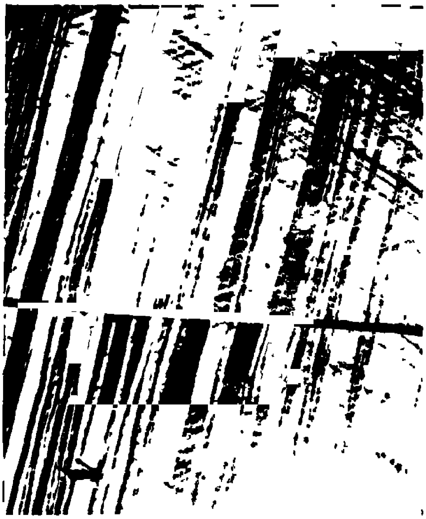

× 90

Fig. 18—No. 11, ε = 1·50.

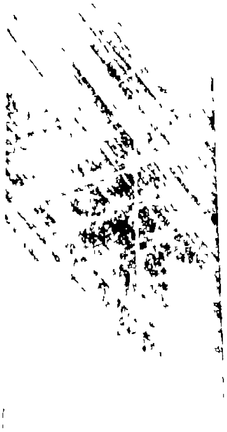

× 2·7

Fig. 19—No. 3 broken.
Last set of slip bands formed just before fracture.

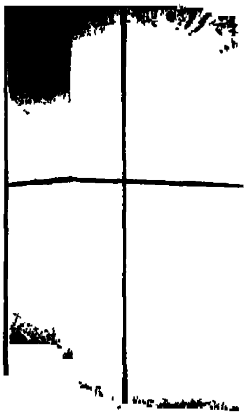

× 2·7

Fig. 20—No. 6, formation of twin.

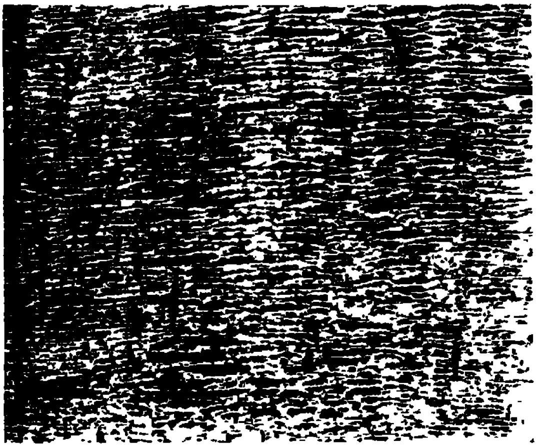

× 90

FIG. 21—Fe 1, $\varepsilon = 1\cdot077$, face II.

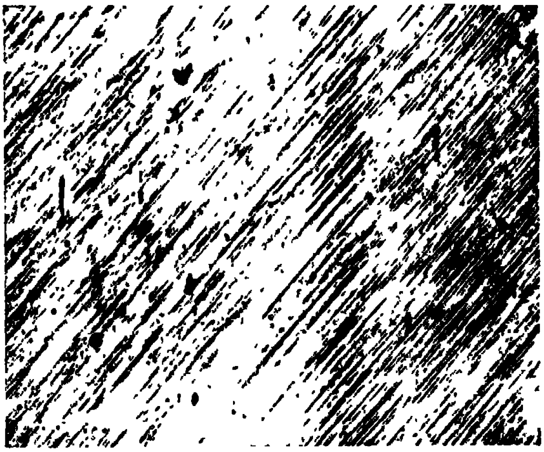

× 90

FIG. 22—Fe 1, $\varepsilon = 1\cdot077$, face III.

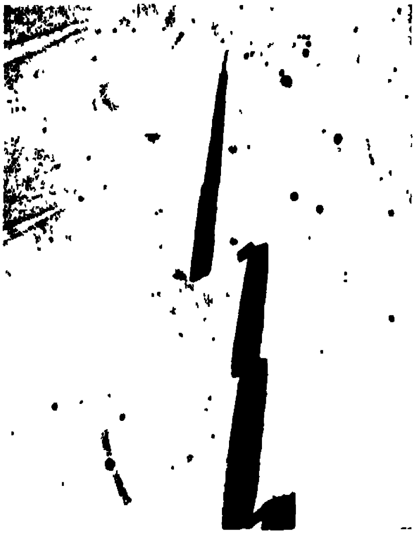

× 135

FIG. 23—Crack in rolled β-brass crystal.

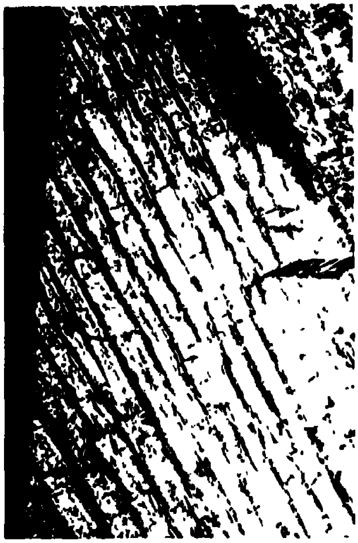

× 135

FIG. 24—Cleavage face of rolled β-brass crystal.

× 135

FIG. 25—Striations in rolled crystals after annealing at 200° C.

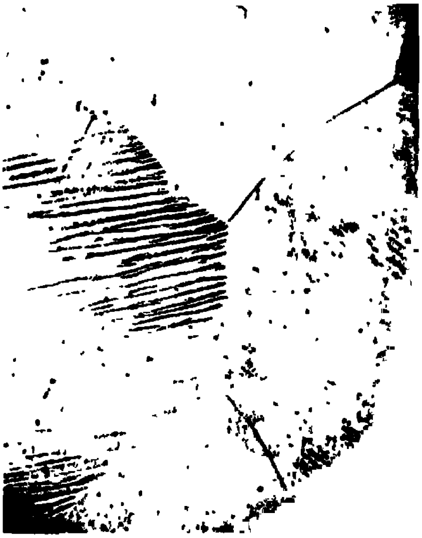

× 135

FIG. 26—Striations in rolled polycrystalline β-brass.

metal must be somewhat seriously broken up along these planes and it was not uncommon to find the striations coinciding with interruptions in the cracks such as are shown in fig. 23, Plate 7. In the crystal of fig. 11, two cleavage planes were formed and both had corresponding markings on the {111} planes at 90° to them.

Most of the crystals examined were of the orientation shown in fig. 11. Some crystals did not crack until a later stage in the rolling. It is possible that their orientation was such that the plane at 90° to the shear plane was also a {110} plane, which took part in the distortion without serious disintegration of the crystal. In this connexion one may refer to the structure of rolled polycrystalline metals of body-centred cubic structure. The most usual form* is for a [110] direction to lie in the direction of rolling and a {100} plane or {112} plane in the plane of rolling. The second of these arrangements agrees with most of the crystals investigated

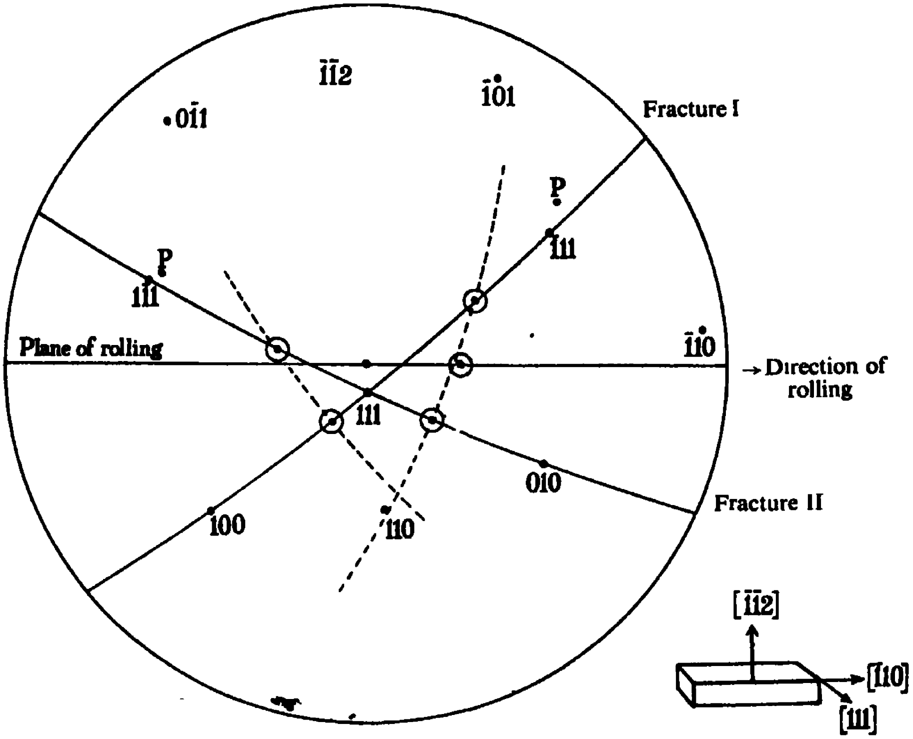

FIG. 11—β-brass, crystal I rolled.

---

* v. Göler and Sachs, 'Z. Physik,' vol. 56, p. 477 (1929).

in the present work. An alternative* is for a [112] direction to be in the direction of rolling and a {111} plane in the plane of rolling.

STRESS MEASUREMENTS

The load required to give each extension was measured. Both brass and iron crystals had a definite yield point coincident with the first appearance of slip-bands and, for brass, with any subsequent formation for a new set of slip-bands. These points would have been marked on a continuous record of load and extension, but there is no indication of them in the stress-strain curves, nor is there any change of direction to coincide with the appearance of new planes. This is in agreement with previous results. Particulars for all the crystals are plotted in fig. 12.

The composition of the brass crystals was different, but reference to Table III shows that the variation in yield point, for example, does not agree with variations in composition. One must conclude, therefore, that it is connected with structural differences and the inclination of slip-planes, etc., to the axis of loading. As we do not know the slip-plane with certainty, and as the evidence indicates that there is no constant slip-plane throughout the extension, it is not possible to calculate the shear stress on it and in the direction of slip, and to compare it with the amount of shear. If correct assumptions are made, the figures for different crystals should be close, due allowance being made for differences in composition. Calculations of the shear stress at the yield point on the most likely {110} plane, Table IV, and the plane derived from distortion measurements were made and did not show the usual agreement. With the exception of No. 10, the stress-strain curves are very similar. This agrees with the hypothesis that there is no marked difference between the crystals made by recrystallization and those grown from the melt. Dehlinger† has found a difference for aluminium in the early stages of test, but the present tests were not sufficiently accurate to show the small differences that he found in the character of the yield point.

CONCLUSION

It is quite clear that no simple kind of distortion can explain the facts described above. One can, however, now say that there is no material difference between iron and β-brass. None of the present results is inconsistent with those of previous workers except that the direction of

---

* Kurdjumow and Sachs, 'Z. Physik,' vol. 62, p. 592 (1930).

† 'Phys. Z.,' vol. 34, p. 836 (1933).

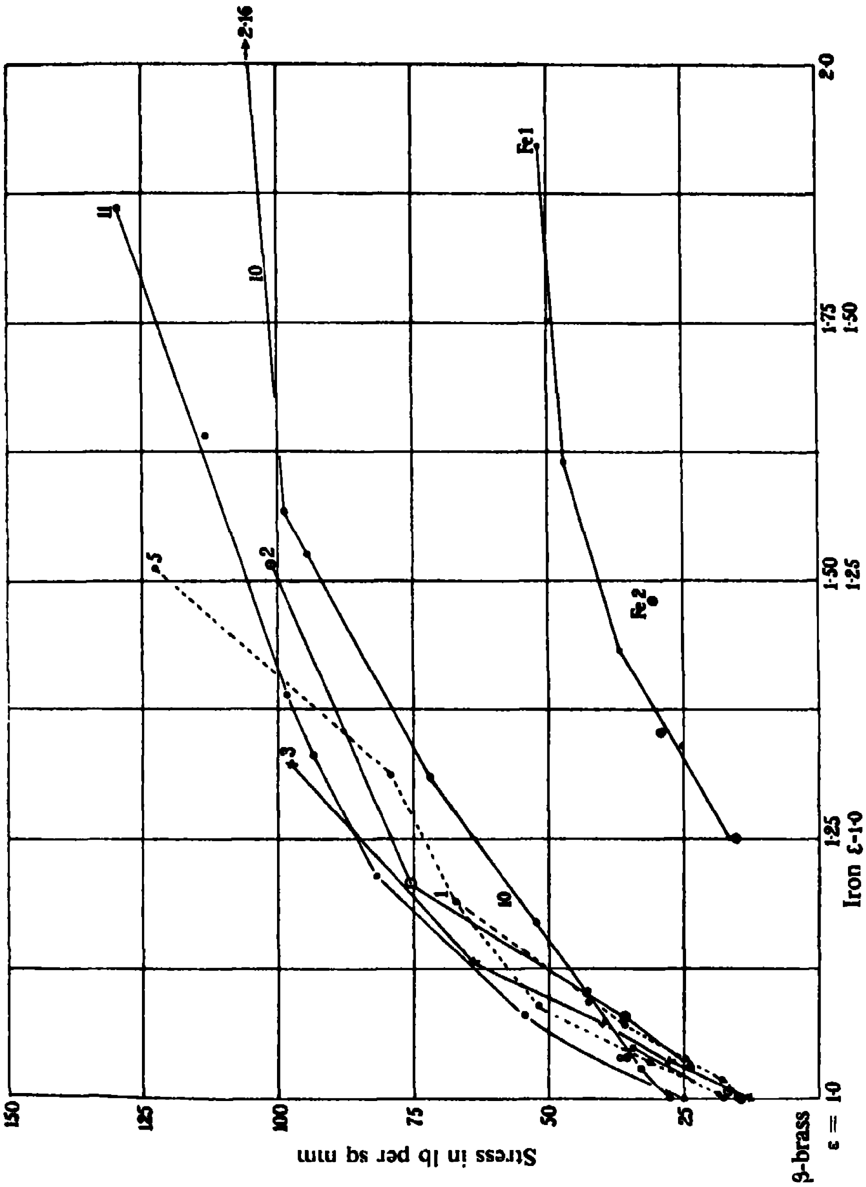
150
125
100
75
50
25
Stress in lb per sq mm
β-brass ε = 1·0
1·25
1·50
1·75
2·0
Iron ε-1·0
1·25
1·50
→2·16
11
10
Fe1
Fe2
5
2
3
1
10

FIG. 12.

slip is not always a [111] direction. Fig. 1, however, which gives the results of Fahrenhorst and Schmid, shows that several of their crystals did not slip in this direction, and it is doubtful if Gough's methods were sufficiently accurate to decide this question if the deviation were not great. Taylor's measurements, on the other hand, were accurate and one can only suppose that distortion is slightly different for small amounts of compression or it may be by chance that all his crystals deformed similarly. This is not so improbable, as reference to Tables II and III shows that a [111] direction was the *nearest* crystal direction even if it did not actually coincide with the direction of slip. But there is some evidence that if he had carried his investigations further different results would have been obtained, because in the present case the distortion planes became farther and farther away from a crystal plane as the crystal elongated. Moreover, his curves* showing relationship between shear stress and amount of shear, all of which were calculated on the assumption that the distortion proceeded on the same plane and in the same direction, gave such different results that one can only conclude that the distortion did not take this simple form. If all the results, including those just described and previous investigations, are considered together one fact stands out, viz., that the *whole* of the deformation of these body-centred cubic latticed crystals cannot be explained by slip on a single crystal

TABLE IV

No.	Composition Cu %	Stress at yield point lbs per mm^2	Shear stress on {110} plane and in [111] direction in closest agreement with slip-bands	
1	53·82	15·0	—	(Slip-bands not agreeing with any plane.)
2	53·82	14·6	5·93	{112} plane ?
3	53·82	12·9	5·42	
5	53·38	18·6	8·39	
6	49·92	17·2	—	(" Twin," uneven).
7	50·12	22·4	7·96	(Uneven).
8	54·02	18·0	8·40	
9	54·02	18·0	6·48	
10	55·20	25·4	12·75	{112} plane.
11	55·39	17·6	8·75	
12	54·48	14·9	7·44	
13	—	15·1	7·15	
	Iron			
1	—	17·1	8·30	
2	—	15·6	7·69	

---

* Taylor, 'Proc. Roy. Soc.,' A, vol. 118, p. 17 (1928), fig. 9.

plane or any other plane subjected to the maximum shear stress and along a direction in that plane related to the structure. On the other hand, the deformation is definitely related to both crystal structure and stress. It was noticeable in all these crystals that the X-ray reflexions did not become seriously distorted,* and a Laue photograph through a fracture still showed well-defined spots and approximately correct angle between the planes. Attention has already been drawn to the regularity of later formed slip-bands and their close agreement with possible crystal planes. Therefore, the distortion must have been uniform and plates or rods must have moved parallel with each other so as not to break up the crystal. In most of the crystals a {110} plane is the nearest plane to the distortion plane, while a {112} plane is less frequently met with. These are the two planes in the lattice of highest atomic density. There are eight {110} planes to choose from and twelve {112} planes, but in actual fact most of them are ruled out by the maximum shear stress law. The tendency seems to be to slip first of all on the plane of maximum shear stress coincident with or near to a {112} or {110} plane, but it also seems probable that the crystal can and does slip on planes which are not necessarily crystal planes but are planes of maximum shear stress. This is not so improbable if it is remembered that the direction of slip may not be a crystal direction. It is tentatively suggested that the broad bands and possibly the distortion planes, which are not crystal planes, correspond to what are known as Lüder's Lines in the aggregate. Many of the photographs of deformed crystals, notably figs. 13, 14, and 15, Plate 4, show broad bands which resemble Lüder's Lines in iron and mild steel very much more than they do slip-bands. The fact that both kinds are visible together and make small angles with each other tends to support the view that they are different. If it is admitted that the body-centred cubic crystals can deform on planes other than crystal planes the formation of Lüder's Lines in the aggregate may be more easily explained. Even if the lines are in some way related to the crystal planes of type {110} and {112}, there are so many possibilities for slip, whatever the orientations of the crystals in the aggregate, that the plane of maximum shear stress will find its way across the specimen without any great deviation of angle between crystal and crystal. If this idea is correct, it would be expected that β-brass in the aggregate would show Lüder's Lines equally well as iron. So far, attempts to produce them have been unsuccessful, but it is well known that a fine grained structure is necessary to show them in iron, and no such fineness in structure has yet been obtained in β-brass to make comparable tests. Further investigations are in progress.

---

* Burger ('Metallwirtschaft,' vol. 11, p. 251 (1932)) maintains that there is less distortion when slip takes place on a number of planes than if it is confined to one.

The change of orientation of the crystal and the relationship of the crystal planes to the distortion planes are difficult to explain. The figures show that they do not remain fixed relative to one another nor to the slip-bands. The movement on crystal planes which will give the distortion figures found are: (1) the whole of the distortion takes place by means of shear on one crystal plane in a fixed direction; (2) two or more planes may take part provided they have the same direction of slip; (3) if two planes slip in different directions, they must be so related that their poles and the directions of slip are perpendicular to one another and all lie in one plane. It is probable that all these types of deformation occur at different times and in different crystals. If we assume that the most favourable direction of slip is [111], the possibilities of No. 3 are limited to certain pairs of {112} planes. For example, $(1\bar{1}2)$ slipping in the direction $[\bar{1}11]$ and $(\bar{1}12)$ in the direction $[1\bar{1}1]$. This condition is fulfilled in crystal No. 10, but not in the others. On the other hand, there is no such possibility if slip is on {110} planes. But if we admit that the direction of slip is not always a crystal direction, a similar type of distortion could occur, and if, as seems probable, there is no rigid adherence to any particular crystal planes with this type of lattice, a still wider range of possibilities is opened up.

In connexion with a possible explanation of variation in slip-direction reference may be made to the work of Yamaguchi.* He counted the number of slip-bands formed during the extension of aluminium crystals and concluded that although new planes appeared with each extension some additional slip must have occurred on planes already formed. If the structure is destroyed by slip on a plane, any subsequent slip on that plane may not follow the original arrangement of atoms, but rather the direction of stress. Another error may be introduced by the fact that slip-bands tend to break off and start again, causing a series of small discontinuities as they pass across a section of a crystal; an extreme example is iron, fig. 21, Plate 6. In these circumstances the planes of slip cannot possibly coincide with layers parallel with a perfect crystal plane.

The data available in the present work are not sufficient to distinguish between the dfferent types of deformation referred to above, and the problem of the distortion of the body-centred cubic lattice is still unsolved. As Taylor† has pointed out, this lattice does not readily divide into planes, but into hexagonal rods, so that it is not altogether surprising that the distortion follows a complicated pattern.

---

* 'Sci. Pap. Inst. Phys. Chem. Res.,' Tokyo, vol. 8, p. 289 (1928).

† 'Proc. Roy. Soc.,' A, vol. 118, p. 1 (1928).

I wish to thank the Leverhulme Research Committee for a grant in aid of this investigation. Professor C. E. Inglis, F.R.S., has very kindly given me facilities for research in the Cambridge University Engineering Department, and I am indebted to Professor R. S. Hutton for allowing me to take the microphotographs in the Goldsmith's Laboratory. Professor G. I. Taylor, F.R.S., has helped me in various ways and particularly in allowing me to discuss my results with him.

SUMMARY

Some further experiments on the distortion in tension of the body-centred cubic metals, iron and β-brass, are described and the conclusion arrived at that there is no essential difference between them. Although slip-bands agreeing with possible crystal planes—chiefly {110} planes, less frequently {112} planes—are usual, calculations of the distortion do not agree with slip on these planes throughout the extension. Moreover, the direction of slip is not always a [111] direction, although this is the most common direction found. It is suggested that the deformation does not take place by slip on any definite crystal plane but that the distortion is brought about by movements of a complicated nature originally related to the structure, but finally having no obvious connexion with it. The fact that the distortion cone usually consists of two planes limits the possibilities, but no definite conclusion has been arrived at as to the details of the distortion. Stress-strain curves of the crystals are given and the fracture of β-brass crystals in tension and in rolling are described.

Breaking up of a Drop of Viscous Liquid Immersed in Another Viscous Fluid which is Extending at a Uniform Rate

By S. TOMOTIKA, D.Sc.

(*Communicated by G. I. Taylor, F.R.S.—Received July* 13, 1935)

INTRODUCTION

1—In a previous paper[†] the present writer has discussed the instability of a long cylindrical column of an incompressible viscous liquid surrounded by another viscous fluid under the action of both surface tension and viscous forces. In this work the fluids were at rest except for the small disturbances which were assumed to develop slowly. It was shown that if the ratio of viscosities of the two fluids is neither zero nor infinity the maximum instability always occurs at a certain definite value of the wave-length of the assumed initial varicosity so that the formation of drops of definite size would be expected. A comparison of the theory with observation has also been made and satisfactorily good agreement between them was found.

Now, in his experimental studies[‡] on the mode of formation of a cylindrical thread from a drop of a viscous liquid by the disruptive effect of the viscous drags of a surrounding liquid, Professor G. I. Taylor observed that when a drop of black lubricating oil was surrounded by syrup, the thread formed by pulling out the drop did not at once break up into small drops but remained cylindrical for some time and finally broke up into small drops, the diameters of which were about 1/10th of the diameter of the original drop. On the other hand, if as soon as the cylindrical thread was formed the apparatus was stopped the thread immediately began to break up in the manner described above. Thus, if the apparatus were kept going very much smaller drops were formed than if it were stopped as soon as the initial drop had been pulled out into a cylindrical thread.

These observations seem to show that the flow in the surrounding fluid may have some stabilizing effect which inhibits the formation of drops until the thread has been considerably reduced. The drops which are ultimately formed correspond in the newly formed cylindrical thread to varicosity of very short wave-length, which is initially stable, but as the oil thread is drawn out by the motion of the surrounding syrup its wave-length increases till it becomes equal to the circumference of the thread when it becomes unstable.

[†] 'Proc. Roy, Soc.,' A, vol. 150, p. 322 (1935).

[‡] 'Proc. Roy. Soc.,' A, vol. 146, p. 501 (1934).

As in the previous paper, the writer now considers a long, straight cylindrical column with uniform small circular cross-section of a viscous liquid of viscosity μ', in an infinite mass of another viscous fluid of viscosity μ, and assumes that the thread and surrounding fluid are being stretched at a uniform rate as they were in Professor Taylor's apparatus when it was kept in motion after the drop had begun to burst. Further assumption is made that the effects of inertia of the fluids are insensible and negligible in comparison with those of viscosity. Symmetry about the axis of the thread is assumed and only disturbances which are simple harmonic with respect to z, the co-ordinate parallel to the axis, are considered. By performing various calculations the writer investigates the effect of the flow of the surrounding fluid on the stability of small motions of the thread caused by the small disturbances.

The writer shows that the effect of the flow of the surrounding fluid is to limit the increase in any initial disturbance to a finite value. Thus, true instability does not occur when the drop is surrounded by the field of flow which causes a drop to pull out into a cylindrical thread. On the other hand, disturbances formed at various stages in the process of drawing out can increase in very different proportions. Thus, varicosity which begins as soon as the cylindrical thread is just formed from the initial drop can only increase in relative amplitude in the ratio 1 : 20·89, but varicosity which forms when the cylindrical thread has been drawn out to 1/8th of its initial diameter can increase in relative amplitude in the ratio $1 : 2{\cdot}26 \times 10^{10}$. This seems to explain why the thread does not immediately break up into drops but remains cylindrical till it has extended sufficiently to form drops which are about 1/1000th of the volume of the initial drop.

The writer wishes to express his cordial thanks to Professor G. I. Taylor, who suggested the present problem, for his continued valuable suggestions and criticisms during the course of this investigation.

A FIELD OF UNIFORM RATE OF STRAIN

2—Taking the axis of the cylindrical column as the z-axis and the r-axis perpendicular to it, we consider in the fluids a field of uniform rate of strain represented by equations:

$$\mathrm{U} = -\tfrac{1}{2}\mathrm{C}r, \qquad \mathrm{W} = \mathrm{C}z, \tag{1}$$

where U and W are respectively the r- and z-components of velocity and C is a constant. U and W obviously satisfy the equation of continuity of an incompressible fluid, *i.e.*, $\frac{\partial \mathrm{U}}{\partial r} + \frac{\mathrm{U}}{r} + \frac{\partial \mathrm{W}}{\partial z} = 0$.

Let (r, z) be the co-ordinates of a particle in either of the fluids. Then,

$$\frac{dr}{dt} = \mathrm{U} = -\tfrac{1}{2}\mathrm{C}r, \qquad \frac{dz}{dt} = \mathrm{W} = \mathrm{C}z.$$

Integrating these equations and denoting the initial co-ordinates of the particle under consideration by (r_0, z_0), we get

$$r = r_0 e^{-\frac{1}{2}\mathrm{C}t}, \qquad z = z_0 e^{\mathrm{C}t}. \tag{2}$$

It is easily seen from these results that if the column has initially a uniform circular cross-section it remains always in the form of a cylinder with uniform circular section and that the radius a of the column at any time is connected with its initial value a_0 by

$$a = a_0 e^{-\frac{1}{2}\mathrm{C}t}. \tag{3}$$

Also, we easily see that if varicosity of uniform wave-length λ_0 is supposed to be formed initially on the column, then the column has always the varicosity of uniform wave-length, the magnitude of which varies with time according to the law:

$$\lambda = \lambda_0 e^{\mathrm{C}t}. \tag{4}$$

Thus, if we introduce, as in the previous paper, a variable x defined by $x = 2\pi a/\lambda = ka$ which will be used in order to specify varicosity throughout this paper, and denote its initial value by x_0, we get

$$x = x_0 e^{-\frac{3}{2}\mathrm{C}t}. \tag{5}$$

SOLUTIONS OF EQUATIONS OF SUPERPOSED SMALL MOTIONS AND BOUNDARY CONDITIONS

3—Now consider that we superpose on the flow (1) small motions by giving small disturbances and suppose that they are symmetrical about the axis of the column, *i.e.*, the z-axis and also simple harmonic with respect to z. Let u and w be the r- and z-components of velocity and ψ the Stokes current function for the small motions. Then,

$$u = \frac{1}{r}\frac{\partial \psi}{\partial z}, \qquad w = -\frac{1}{r}\frac{\partial \psi}{\partial r}, \tag{6}$$

and when the effects of inertia of the fluids are insensible and negligible compared with those of viscosity, the function ψ satisfies the partial differential equation†:

$$\left(\frac{\partial^2}{\partial r^2} - \frac{1}{r}\frac{\partial}{\partial r} + \frac{\partial^2}{\partial z^2}\right)\left(\frac{\partial^2}{\partial r^2} - \frac{1}{r}\frac{\partial}{\partial r} + \frac{\partial^2}{\partial z^2}\right)\psi = 0. \tag{7}$$

In the present case, r and z are both functions of time and vary according to the laws given in (2).

To solve the above equation (7), we put

$$\frac{\partial^2\psi}{\partial r^2} - \frac{1}{r}\frac{\partial\psi}{\partial r} + \frac{\partial^2\psi}{\partial z^2} = \psi_*, \tag{8A}$$

then

$$\frac{\partial^2\psi_*}{\partial r^2} - \frac{1}{r}\frac{\partial\psi_*}{\partial r} + \frac{\partial^2\psi_*}{\partial z^2} = 0. \tag{8B}$$

In accordance with the assumptions made at the beginning of this paragraph, we put

$$\psi = \phi \sin kz, \qquad \psi_* = \phi_* \sin kz, \tag{9}$$

where ϕ and ϕ_* are functions of r and t, and $k = 2\pi/\lambda$, λ being the wavelength of varicosity, and we have

$$\frac{d^2\phi}{dr^2} - \frac{1}{r}\frac{d\phi}{dr} - k^2\phi = \phi_*, \tag{10A}$$

and

$$\frac{d^2\phi_*}{dr^2} - \frac{1}{r}\frac{d\phi_*}{dr} - k^2\phi_* = 0. \tag{10B}$$

The general solution of (10B) is easily found to be

$$\phi_* = A_* r I_1(kr) + B_* r K_1(kr), \tag{11}$$

in which A_*, B_* are arbitrary functions of time t.

Putting (11) in the right-hand side of (10A), we get

$$\frac{d^2\phi}{dr^2} - \frac{1}{r}\frac{d\phi}{dr} - k^2\phi = A_* r I_1(kr) + B_* r K_1(kr), \tag{12}$$

the general solution of which is obtained in the form:

$$\phi = \{A_1 r I_1(kr) + A_2 r^2 I_1'(kr)\} + \{B_1 r K_1(kr) + B_2 r^2 K_1'(kr)\}, \tag{13}$$

where A_1, A_2, B_1, B_2 are all arbitrary functions of time t. A_2, B_2 are connected with A_*, B_* as $A_2 = A_*/2k$, $B_2 = B_*/2k$ respectively. Thus we get finally the general solution of equation (7), namely:

$$\psi = [\{A_1 r I_1(kr) + A_2 r^2 I_1'(kr)\} \\ + \{B_1 r K_1(kr) + B_2 r^2 K_1'(kr)\}] \sin kz. \tag{14}$$

---

† This equation can easily be obtained from equation (6) of the previous paper (*loc. cit.*) by putting $\rho = 0$.

The appropriate form of the current function ψ' for the motion inside the column is therefore

$$\psi' = \{A_1 r I_1(kr) + A_2 r^2 I_1'(kr)\} \sin kz, \tag{15}$$

and the corresponding function for the surrounding fluid, which is simply denoted by ψ, is given by

$$\psi = \{B_1 r K_1(kr) + B_2 r^2 K_1'(kr)\} \sin kz. \tag{16}$$

The velocity components, the tangential stress (p_{zr}), and the normal stress (p_{rr}) in the fluids can easily be calculated by using the well-known formulae as in the previous paper, and the results are as follows.

(i) For the fluid inside the column:

$$\left.\begin{aligned} u' &= [A_1 I_1(kr) + A_2 r I'_1(kr)]\, k \cos kz, \\ w' &= -[A_1 k I_0(kr) + A_2\{kr I_1(kr) + I_0(kr)\}] \sin kz, \\ p'_{zr} &= -2k^2\mu' [A_1 I_1(kr) + A_2 r I_0(kr)] \sin kz, \\ p'_{rr} &= 2k\mu' [A_1 k I_1'(kr) \\ &\qquad + A_2\{I_1'(kr) + kr I_1''(kr) - I_0(kr)\}] \cos kz; \end{aligned}\right\} \tag{17}$$

(ii) For the surrounding fluid:

$$\left.\begin{aligned} u &= [B_1 K_1(kr) + B_2 r K_1'(kr)]\, k \cos kz, \\ w &= -[-B_1 k K_0(kr) + B_2\{kr K_1(kr) - K_0(kr)\}] \sin kz, \\ p_{zr} &= -2k^2\mu [B_1 K_1(kr) - B_2 r K_0(kr)] \sin kz, \\ p_{rr} &= 2k\mu [B_1 k K_1'(kr) \\ &\qquad + B_2\{K_1'(kr) + kr K_1''(kr) + K_0(kr)\}] \cos kz. \end{aligned}\right\} \tag{18}$$

These quantities must satisfy at any time certain boundary conditions at the interface of the two fluids, *i.e.*, at the surface of the cylindrical column, the radius of which is generally denoted by a. The conditions are, as mentioned in the previous paper, as follows:

(1) the velocity components are continuous at the surface of the column;

(2) the tangential stress is continuous at the surface; and finally

(3) the difference in the normal stress between the inside and outside of the column is due to the interfacial surface tension.

Remembering that if the displacement in the r-direction of a particle at the surface of the column be denoted by ξ, the variable part in the pressure due to the surface tension T, assumed to be constant, is given by

$$\frac{T\xi(k^2a^2-1)}{a^2}, \tag{19}$$

and that if we further denote by ε the amplitude of varicosity, the displacement ξ can be written as:

$$\xi = \varepsilon \cos kz, \tag{20}$$

because u is proportional to $\cos kz$, we can write, by (17) and (18), these boundary conditions in the following forms:

$$\left.\begin{aligned}
&A_1 k I_1(ka) + A_2 ka I_1'(ka) - B_1 k K_1(ka) - B_2 ka K_1'(ka) = 0,\\
&A_1 k I_0(ka) + A_2\{ka I_1(ka) + I_0(ka)\} + B_1 k K_0(ka)\\
&\qquad\qquad\qquad - B_2\{ka K_1(ka) - K_0(ka)\} = 0,\\
&A_1(\mu'/\mu) k I_1(ka) + A_2(\mu'/\mu) ka I_0(ka) - B_1 k K_1(ka)\\
&\qquad\qquad\qquad + B_2 ka K_0(ka) = 0,\\
&A_1(\mu'/\mu) k I_1'(ka) + A_2(\mu'/\mu)\{I_1'(ka) + ka I_1''(ka) - I_0(ka)\}\\
&\quad - B_1 k K_1'(ka) - B_2\{K_1'(ka) + ka K_1''(ka) + K_0(ka)\}\\
&\qquad\qquad\qquad = T\varepsilon(1 - k^2a^2)/(2k\mu a^2).
\end{aligned}\right\} \tag{21}$$

Rate of Change of Relative Amplitude

4—Next, we shall calculate the rate of change of the amplitude ε of varicosity with time, or more appropriately, the rate of change with time of the relative amplitude ε/a, *i.e.*, the ratio of the amplitude ε to the radius a. Suppose that at any time t the mean radius of the column and the amplitude of varicosity are respectively given by a and ε, and denote by u'_m the r-component of velocity at that time of a particle on the crest of the varicosity where $\cos kz = 1$. Then, if we suppose that during the subsequent very short interval of time δt the amplitude is increased by $\delta\varepsilon$, the amplitude at time $t + \delta t$ is $\varepsilon + \delta\varepsilon$ and it is given by

$$\begin{aligned}
\varepsilon + \delta\varepsilon &= \{(a+\varepsilon)e^{-\frac{1}{2}C\delta t} + u'_m\,\delta t\} - ae^{-\frac{1}{2}C\delta t}\\
&= \varepsilon e^{-\frac{1}{2}C\delta t} + u'_m\,\delta t.
\end{aligned}$$

Thus,

$$\delta\varepsilon = \varepsilon(e^{-\frac{1}{2}C\delta t} - 1) + u'_m\,\delta t,$$

or, since δt is very small, we have

$$\frac{\delta\varepsilon}{\delta t} = (-\tfrac{1}{2}C\varepsilon + u'_m) + O(\delta t).$$

Hence, we get the rate of change of the amplitude with time in the form:

$$\frac{d\varepsilon}{dt} = \left(\frac{\delta\varepsilon}{\delta t}\right)_{\delta t \to 0} = -\tfrac{1}{2}\mathrm{C}\varepsilon + u'_m, \tag{22}$$

which, however, can be put into a more convenient form, as follows:

By the first equation in (17) we have

$$u'_m = \mathrm{A}_1 k \mathrm{I}_1(ka) + \mathrm{A}_2 ka \mathrm{I}_1'(ka),$$

or, using the variable $x = ka$,

$$u'_m = \mathrm{A}_1 k \mathrm{I}_1(x) + \mathrm{A}_2 x \mathrm{I}_1'(x). \tag{23}$$

Solving next the equations (21), which are now regarded as simultaneous linear equations with four variables A_1, A_2, B_1, B_2, we easily obtain A_1, A_2 in the forms:

$$\left.\begin{aligned} \mathrm{A}_1 &= \frac{\mathrm{T}\varepsilon(1-x^2)}{2\mu x}\,\frac{\Delta_1}{\mathrm{D}(x)}, \\ \mathrm{A}_2 &= -\frac{\mathrm{T}\varepsilon(1-x^2)}{2\mu a}\,\frac{\Delta_2}{\mathrm{D}(x)}, \end{aligned}\right\} \tag{24}$$

where $x = ka$ as usual, and

$$\begin{aligned} \mathrm{D}(x) = {} & (\mu'/\mu)\{x\mathrm{I}_0(x) - \mathrm{I}_1(x)\}\,\Delta_1 - (\mu'/\mu)\{(1+x^2)\,\mathrm{I}_1(x) - x\mathrm{I}_0(x)\}\,\Delta_2 \\ & - \{x\mathrm{K}_0(x) + \mathrm{K}_1(x)\}\,\Delta_3 - \{(1+x^2)\,\mathrm{K}_1(x) + x\mathrm{K}_0(x)\}\,\Delta_4, \end{aligned}$$

which was used in the previous paper. Δ_1, Δ_2, Δ_3, and Δ_4 are all functions of x containing μ'/μ as a parameter, expressed conveniently in the determinantal forms, the expressions of which were given in the previous paper (pp. 332–333).

Substituting (24) in (23) we get

$$\begin{aligned} u'_m &= \frac{\mathrm{T}(1-x^2)}{2\mu a}\,\frac{\varepsilon}{\mathrm{D}(x)}\left[\mathrm{I}_1(x)\,\Delta_1 - \{x\mathrm{I}_0(x) - \mathrm{I}_1(x)\}\,\Delta_2\right] \\ &= \frac{\mathrm{T}(1-x^2)}{2\mu a}\,\frac{\mathrm{N}(x)}{\mathrm{D}(x)}\,\varepsilon, \end{aligned}$$

where we put

$$\mathrm{N}(x) = \mathrm{I}_1(x)\,\Delta_1 - \{x\mathrm{I}_0(x) - \mathrm{I}_1(x)\}\,\Delta_2.$$

This function $\mathrm{N}(x)$ was also used in the previous paper.

Thus, writing, as in the previous paper,

$$\Phi(x) = \left(\frac{\mathrm{N}(x)}{\mathrm{D}(x)}\right),$$

we have

$$u'_m = \frac{T}{2\mu a}(1 - x^2)\,\Phi(x)\,\epsilon, \tag{25}$$ †

and the substitution of this in (22) gives

$$\frac{1}{\epsilon}\frac{d\epsilon}{dt} = -\tfrac{1}{2}C + \frac{T}{2\mu a}(1 - x^2)\,\Phi(x),$$

or

$$\frac{d}{dt}(\log \epsilon) = -\tfrac{1}{2}C + \frac{T}{2\mu a}(1 - x^2)\,\Phi(x). \tag{26}$$

We have, however, by (3),

$$\frac{d}{dt}(\log a) = -\tfrac{1}{2}C.$$

Thus, taking this into account, we get

$$\frac{d}{dt}\left[\log\left(\frac{\epsilon}{a}\right)\right] = \frac{T}{2\mu a}(1 - x^2)\,\Phi(x). \tag{27}$$

Since x and a are both functions of time, this equation gives the rate of change with time of the logarithm of the relative amplitude as a function of time.

It may not be useless to indicate here that in a special case when there is no stretching field in the fluids so that C is equal to zero, equation (27) yields immediately the result obtained in the previous paper. In effect, in such a special case a and x are both independent of time and therefore the direct integration of (27) with respect to t is possible and we get

$$\frac{\epsilon}{a} = \frac{\epsilon_0}{a}\,e^{qt}, \qquad q = \frac{T}{2\mu a}(1 - x^2)\,\Phi(x), \tag{28}$$

agreeing with the result in the previous paper.

5—Now the quantity $x = ka$ varies with time according to the law (5) and in every case it varies from a certain initial value x_0 to the ultimate value $x = 0$. Thus, it seems to be more appropriate to use x as the variable instead of t. Then remembering (3) and (5), we can put equation (27) in the form:

$$\frac{d}{dx}\left[\log\left(\frac{\epsilon}{a}\right)\right] = -\frac{Tx_0^{1/3}}{3\mu a_0 C}\Psi(x), \tag{29}$$

---

† The value of the function $(1 - x^2)\,\Phi(x)$ for $\mu'/\mu = 0{\cdot}91$ and for the range $0 \leqq x \leqq 1{\cdot}0$ is tabulated in Table III of the previous paper (*loc. cit.*) and the corresponding graph is shown in fig. 1 there. In the present investigation, further calculations of the value of this function have been carried out for the range $1{\cdot}0 \leqq x \leqq 2{\cdot}0$, taking $\mu'/\mu = 0{\cdot}91$ as before.

where we put for simplicity

$$\Psi(x) = x^{-4/3}(1 - x^2)\,\Phi(x), \tag{30}$$

and $T/3\mu a_0 C$ is a non-dimensional quantity. The graph of the function $\Psi(x)$ for $\mu'/\mu = 0{\cdot}91$ and for the range $0 \leq x \leq 2{\cdot}0$ is shown in fig. 1 by a dotted-line curve.

The radius a of the column is connected with x by the relation:

$$a/a_0 = (x/x_0)^{1/3}, \tag{31}$$

which is easily obtained from (3) and (5).

Denoting by ε_0, a_0 the initial values of ε, a respectively and integrating (29) with respect to x from x_0 to x, we have

$$\log\left[\left(\frac{\varepsilon}{a}\right)\Big/\left(\frac{\varepsilon_0}{a_0}\right)\right] = \frac{Tx_0^{1/3}}{3\mu a_0 C}\int_x^{x_0}\Psi(x)\,dx, \tag{32}$$

which may also be written as:

$$\log\left[\left(\frac{\varepsilon}{a}\right)\Big/\left(\frac{\varepsilon_0}{a_0}\right)\right] = \frac{Tx_0^{1/3}}{3\mu a_0 C}\left\{\int_x^1\Psi(x)\,dx - \int_{x_0}^1\Psi(x)\,dx\right\}. \tag{33}$$

This gives the logarithm of the magnification of relative amplitude at any moment.

The graph of the integral

$$\int_x^1\Psi(x)\,dx \quad \text{for} \quad \mu'/\mu = 0{\cdot}91$$

is given in fig. 1 by a full-line curve, which has been constructed from the graph of $\Psi(x)$ by graphical integration. It will be noticed that the integral in question has the finite value of $1{\cdot}52$ at $x = 0$, as shown in fig. 1.

In effect, the function $\Psi(x)$ is everywhere continuous and vanishes at $x = 1$ irrespective of the value of the ratio μ'/μ, and, on the other hand, it behaves as the function $-x^{2/3}\log x$ when x is very small,† so that

$$\lim_{x\to 0}\,[\Psi(x)] = \lim_{x\to 0}\,[-x^{2/3}\log x] = 0,$$

as shown in fig. 1, provided that the ratio μ'/μ is neither zero nor infinity.‡

---

† It is easily seen that $\Phi(x) = O(-x^2\log x)$ when x is very small, and therefore we have for the function $\Psi(x)$, which is equal to $x^{-4/3}(1 - x^2)\,\Phi(x)$,

$$\Psi(x) = O[-x^{2/3}(1 - x^2)\log x] = O[-x^{2/3}\log x],$$

when x is very small.

‡ We leave these limiting cases out of consideration because they are not interesting and also not important from either experimental or theoretical points of view (*see* the previous paper, *loc. cit.*).

Thus, when μ'/μ takes a definite value, the integral $\int_0^1 \Psi(x)\,dx$ has a certain definite value, A say, namely:

$$\int_0^1 \Psi(x)\,dx = \mathrm{A}, \tag{34}$$

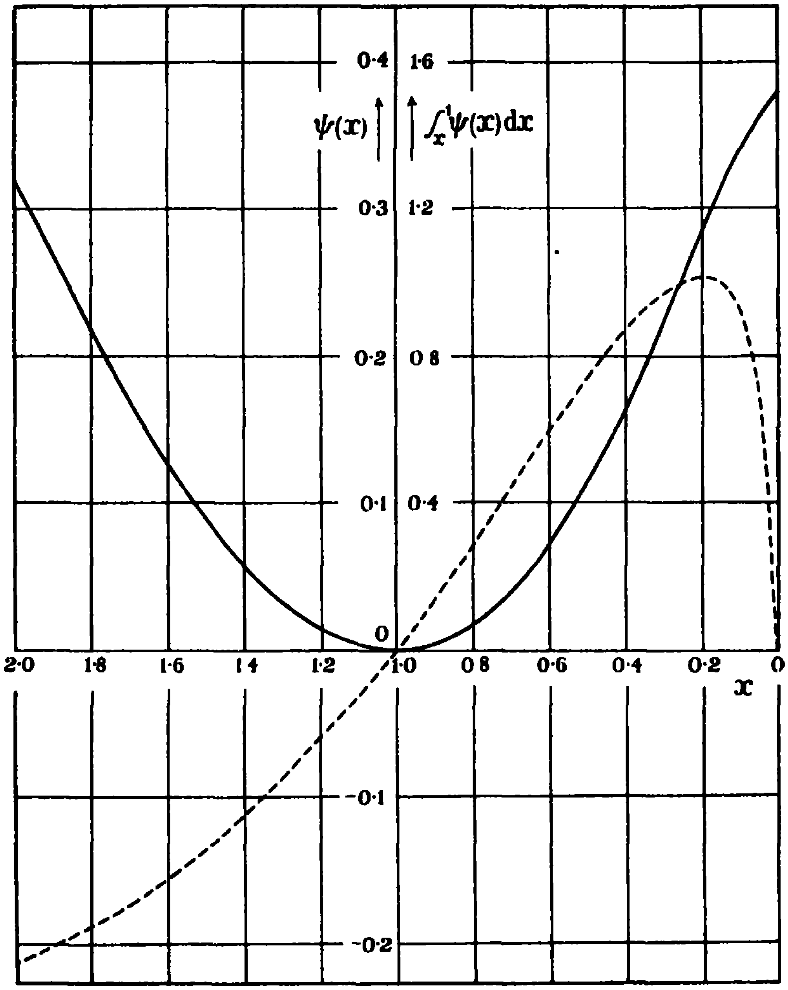

FIG. 1 – – –, curve of $\Psi(x) = x^{-4/3}(1 - x^2)\,\Phi(x)$; —— curve of $\int_x^1 \Psi(x)\,dx$.

and for the particular case when $\mu'/\mu = 0\cdot91$ we have already seen that $\mathrm{A} = 1\cdot52$.

6—We are now in a position to consider the physical property of the non-dimensional quantity $T/3\mu a_0 C$. In his experimental studies on the bursting of a drop (radius $= R_0$) of a viscous liquid of viscosity μ in a uniformly stretching field of flow of another viscous liquid of viscosity μ, Taylor[†] observed that when the speed of distortion of the surrounding fluid increased till a non-dimensional quantity $F = 2\mu R_0 C_*/T$[‡] attained a certain critical value, the drop began to burst into a cylindrical form and that such a critical value depends very much on the ratio μ'/μ. For a drop of black lubricating oil in the field of syrup for which $\mu'/\mu = 0{\cdot}91$, the said critical value of $2\mu R_0 C_*/T$ was found experimentally to be $0{\cdot}39$.

Now, in visualizing the breaking extension of a drop of radius R_0 we may as an approximation imagine arbitrarily that when the rate of strain in the surrounding fluid is such that

$$\frac{2\mu R_0 C_*}{T} = 0{\cdot}39, \tag{35}$$

the drop becomes a portion of a cylinder of radius a_0 and length $2a_0$. Then, we have

$$2\pi a_0^3 = \frac{4}{3}\pi R_0^3,$$

which gives

$$\frac{R_0}{a_0} = \left(\frac{3}{2}\right)^{1/3} = 1{\cdot}145. \tag{36}$$

Combining this with (35) we get

$$\frac{2\mu a_0 C_*}{T} = 0{\cdot}34. \tag{37}$$

As mentioned already, we may put $C = C_*$ approximately, and therefore we get

$$\frac{3\mu a_0 C}{T} = 0{\cdot}51. \tag{38}$$

Thus we see that if we make the above-mentioned assumption about an oil drop in the field of syrup, the drop begins to extend when the non-dimensional quantity $3\mu a_0 C/T$ attains the constant value 0·51.

[†] 'Proc. Roy. Soc.,' A, vol. 146, p. 501 (1934).

[‡] To avoid confusion, some of Taylor's notations are replaced here by other notations. C_* is a constant specifying the speed of distortion in the field of flow produced by Taylor's apparatus, which was approximately represented by equations $u = C_* x$, $v = -C_* y$, and T is the interfacial surface tension. The constant C_* in Taylor's case is not exactly equal to the constant C used in the present paper, since our constant C specifies the speed of distortion of the three-dimensional flow represented by equations (1) which, though very similar, is not exactly equal to the flow produced by Taylor's apparatus. However, we may roughly take $C = C_*$ in our numerical computations which follow.

Similar conclusions can be drawn in any case, irrespective of the value of the ratio μ'/μ, and it will be seen generally that the non-dimensional quantity $3\mu a_0 C/T$ is a definite constant specifying the beginning of extension of a drop, the value of which depends on the ratio μ'/μ, as can be seen from Taylor's experiments.

7—Considering, as in Taylor's experiment, black lubricating oil in syrup for which $\mu'/\mu = 0{\cdot}91$ we may now enquire how the maximum possible magnification of an initial disturbance varies with its wavelength.

Denoting the ultimate relative amplitude at $x = 0$, *i.e.*, at $t \to \infty$ by $(\varepsilon/a)_\infty$ and remembering (34) and (38), we get from (33)

$$\log\left|\left(\frac{\varepsilon}{a}\right)_\infty\Big/\left(\frac{\varepsilon_0}{a_0}\right)\right| = \frac{x_0^{1/3}}{0{\cdot}51}\left\{1{\cdot}52 - \int_{x_0}^{1}\Psi(x)\,dx\right\}. \qquad (39)$$

Taking x_0 as 0·8, 1·0, 1·2, 1·4, the corresponding values of $0{\cdot}51\log\left|\left(\frac{\varepsilon}{a}\right)_\infty\Big/\left(\frac{\varepsilon_0}{a_0}\right)\right|$ are 1·35, 1·52, 1·55, 1·43 respectively. All other values of x_0 give smaller magnification, so that there is a maximum approximately at $x_0 = 1{\cdot}2$. The magnification then is

$$\left(\frac{\varepsilon}{a}\right)_\infty\Big/\left(\frac{\varepsilon_0}{a_0}\right) = e^{1{\cdot}55/0{\cdot}51} = 20{\cdot}89.$$

In order to show clearly the way in which the magnification of initial disturbance varies with x_0, the graphs of

$$\frac{3\mu a_0 C}{T}\log\left|\left(\frac{\varepsilon}{a}\right)\Big/\left(\frac{\varepsilon_0}{a_0}\right)\right| = 0{\cdot}51\log\left|\left(\frac{\varepsilon}{a}\right)\Big/\left(\frac{\varepsilon_0}{a_0}\right)\right|$$

are plotted, by using (33), against x as shown in fig. 2 for various values of x_0. It will be seen that the highest point of this series of curves occurs at $x = 0$ for $x_0 = 1{\cdot}2$.

EFFECT OF THE FLOW IN THE SURROUNDING FLUID ON THE STABILITY OF SMALL MOTIONS OF THE THREAD

8—We have seen for a thread of black lubricating oil in syrup that the relative amplitude of any initial varicosity cannot increase to more than 20·89 times as great as the initial value. These results therefore do not afford any indication that there is any type of initial varicosity which will become magnified to such an extent that the thread may be expected to break up into small drops. In other words, the stretching flow of the surrounding fluid inhibits the formation of small drops by great increase of initial disturbances.

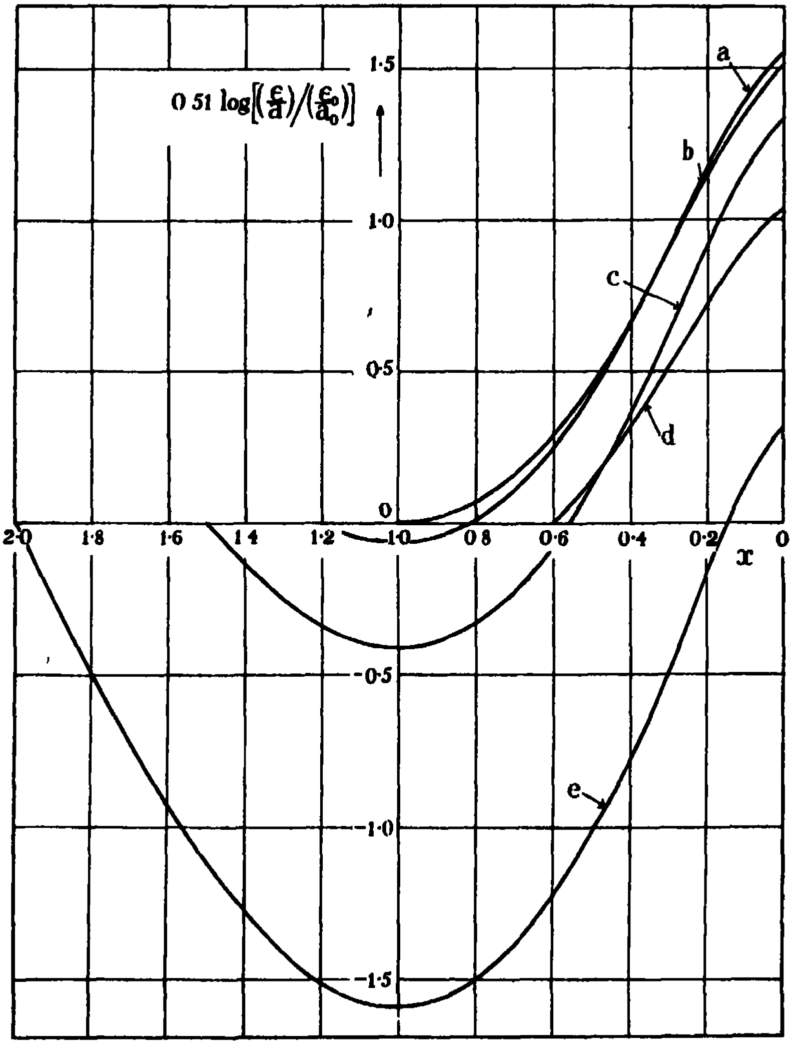

FIG. 2—*a*, $x_0 = 1{\cdot}2$; *b*, $x_0 = 1{\cdot}0$; *c*, $x_0 = 1{\cdot}5$; *d*, $x_0 = 0{\cdot}6$; *e*, $x_0 = 2{\cdot}0$.

On the other hand, observations show that a drop which has been stretched into a thread by Taylor's apparatus does, in fact, break up into small drops after the thread has been reduced to a small fraction of its initial diameter.

Although the maximum magnification of initial disturbance is very small, yet it will be seen from fig. 2 that when x_0 is greater than 1·0 the disturbance initially decreases, only beginning to increase again when $x = 1\cdot0$. Thus the final disturbance when $x \to 0$ may be much greater than 20·89 times as great as the disturbance when it is at its minimum value at $x = 1\cdot0$. For instance, when $x_0 = 2\cdot0$ we have

$$\left(\frac{\varepsilon}{a}\right)_x \Big/ \left(\frac{\varepsilon_0}{a_0}\right) = e^{0\cdot31/0\cdot51} = 1\cdot84,$$

but if ε_* / a_* represents the disturbance when $x = 1\cdot0$,

$$\left(\frac{\varepsilon}{a}\right)_x \Big/ \left(\frac{\varepsilon_*}{a_*}\right) = e^{1\cdot01/0\cdot51} = 42\cdot31.$$

Thus, if disturbances were initiated not when the drop begins to burst but at a later stage in the process of drawing out, the magnification might be much greater than 20·89.

9—We shall now investigate the maximum magnification of varicosity which is supposed to be initiated at various stages in the process of pulling out the thread with wave-length equal to the circumference of the thread ($x = 1$). We denote by a_* and ε_* respectively the radius of the thread and the amplitude when $x = 1$, so that the initial relative amplitude when the varicosity is first formed is ε_* / a_*.

It is desired to express the magnification in terms of the time which has elapsed since the initial drop burst before the varicosity ($x = 1$) with relative amplitude ε_* / a_* was initiated. This time is proportional to $\log (a_0 / a_*)$. It is desirable, therefore, to express the maximum magnification $\left(\frac{\varepsilon}{a}\right)_\infty \Big/ \left(\frac{\varepsilon_*}{a_*}\right)$ in terms of a_0 / a_*, and for this purpose we may use the equations already given which contain x_0. x_0 is now a virtual value of x when $a = a_0$ corresponding with $x = 1$ when $a = a_*$. Thus

$$x_0^{1/3} = \frac{a_0}{a_*}, \quad \text{or} \quad x_0 = \left(\frac{a_0}{a_*}\right)^3. \tag{40}$$

Remembering this and (38), the integration of (29) with respect to x from 1 to x gives

$$\log \left| \left(\frac{\varepsilon}{a}\right) \Big/ \left(\frac{\varepsilon_*}{a_*}\right) \right| = \frac{1}{0\cdot51} \left(\frac{a_0}{a_*}\right) \int_x^1 \Psi(x)\, dx, \tag{41}$$

and therefore the maximum magnification is given by

$$\log \left[\left(\frac{\varepsilon}{a}\right)_x \Big/ \left(\frac{\varepsilon_*}{a_*}\right) \right] = \frac{1\cdot52}{0\cdot51} \left(\frac{a_0}{a_*}\right). \tag{42}$$

The maximum magnification of disturbances initiated when $x = 1$ has been calculated by this formula for various values of a_0/a_* and is shown in Table I.

TABLE I

x_0	$\dfrac{a_0}{a_*}$	$\left(\dfrac{\varepsilon}{a}\right)_\infty \Big/ \left(\dfrac{\varepsilon_*}{a_*}\right)$
8	2	$3 \cdot 88 \times 10^{2}$
27	3	$7 \cdot 64 \times 10^{3}$
64	4	$1 \cdot 50 \times 10^{5}$
125	5	$2 \cdot 96 \times 10^{6}$
216	6	$5 \cdot 83 \times 10^{7}$
343	7	$1 \cdot 15 \times 10^{9}$
512	8	$2 \cdot 26 \times 10^{10}$
729	9	$4 \cdot 46 \times 10^{11}$
1000	10	$8 \cdot 78 \times 10^{12}$

We see from this table that the magnification of disturbance $x = 1$ initiated when the diameter of the thread has been considerably reduced is very great. For instance, varicosity $x = 1$ which is formed when the thread has been pulled out to 1/8th of its initial diameter can increase in relative amplitude in the ratio $1 : 2 \cdot 26 \times 10^{10}$.

The results of supposing that small disturbances represented by $x = 1$ are liable to be introduced at any stage in the process of drawing out the thread are illustrated in fig. 3, where the abscissae are proportional to the time which has elapsed since the moment of bursting of the drop and the ordinates represent, on a logarithmic scale, the magnification. The full-line curves represent the magnification of disturbances which were initiated when $Ct/(2 \log 2) = 0,\ 1 \cdot 0,\ 1 \cdot 58,\ 2 \cdot 0,\ 2 \cdot 58,\ 3 \cdot 0,\ 3 \cdot 58,\ 4 \cdot 0$, *i.e.*, when $a_0/a_* = 1, 2, 3, 4, 6, 8, 12, 16$ respectively. The envelope of this series of curves, shown by a dotted-line curve in fig. 3, represents the maximum possible magnification at various times after the bursting of the drop.

SUMMARY AND CONCLUSIONS

10—In the present paper the writer discusses the mode of breaking up of a drop of one viscous liquid immersed in another viscous fluid which is extending at a uniform rate in one direction and contracting symmetrically in all directions at right angles to this.

Taylor observed that when the rate of distortion in the outer fluid reaches a certain value the drop becomes unstable and stretches out into a thin thread. The present writer has shown in a previous paper that a thread of one viscous liquid at rest in another breaks up into drops of a more or less definite size and in a thread of black lubricating oil surrounded by syrup the diameters of the drops produced are about $\{3\pi/(2 \times 0\cdot568)\}^{1/3} = 2\cdot02$ times the diameter of the thread. In Taylor's experiment on the bursting of a big drop to form little ones he found that

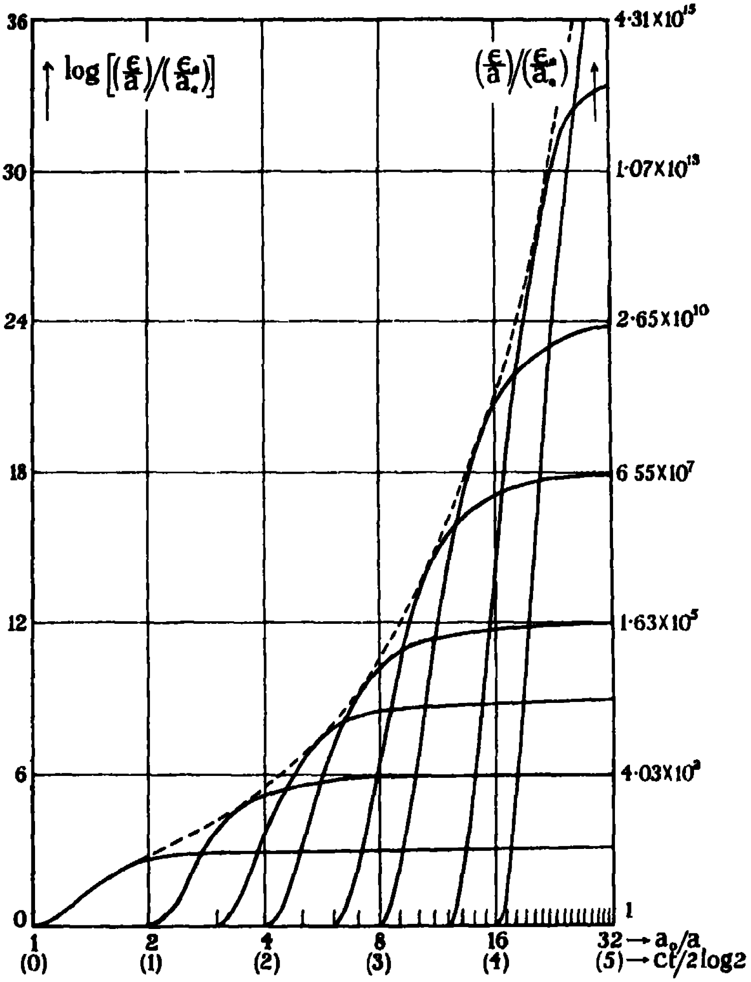

Fig. 3.

for an oil-drop in syrup the diameters of the final small drops were only about 1/10th of the diameter of the initial drop. It seems, therefore, that the action of the field of flow is to inhibit the instability mentioned above.

In the present paper it is shown for a drop of black lubricating oil in syrup that any initial disturbance which is initiated as soon as the thread is just formed from the original drop cannot increase to more than 20·89 times as great as the initial disturbance. True instability therefore does not occur when the drop is surrounded by the field of flow which causes the drop to burst into a thread-like form. It is further shown that although the maximum possible magnification of initial disturbances is very small, yet disturbances formed at a later stage in the process of drawing out, when the diameter of the thread has been considerably reduced, can increase in a very great ratio. For instance, a disturbance first formed when the thread has been reduced in the ratio 10 : 1 can increase in relative amplitude in the ratio $1 : 8\cdot78 \times 10^{12}$.

These theoretical results seem to explain satisfactorily the observed fact that in the stretching field of flow the thread does not immediately break up into drops but remains cylindrical till it has extended sufficiently to form small drops, the volumes of which are about 1/1000th of the volume of the initial drop.

The Infra-Red Absorption Spectra of Quartz and Fused Silica from 1 to 7·5 μ. I—Experimental Method

By D. G. Drummond, Ph.D., Armstrong College, Newcastle-on-Tyne

(*Communicated by W. E. Curtis, F.R.S.—Received July* 22, 1935)

INTRODUCTION

A critical examination of the published data on the near infra-red spectra of silica shows that these are much less complete than appears commonly to be supposed. The absorption spectra of fused silica and of the ordinary ray in quartz have certainly been roughly examined over the whole region from 1 to $7\cdot5$ μ, but these results have been so frequently quoted that an impression may be formed that many more independent measurements are on record than is actually the case.

McGinnety* has collected the more important original figures and reduced them to common terms (*i.e.*, absorption coefficients—wave numbers), from which it is clear that there are serious discrepancies between the results of different investigators—no one of whom has covered the whole region—not only with regard to the values of the absorption coefficients and wave numbers but also with regard to the shapes of the curves and the existence or non-existence of certain bands. There is therefore room for a new and comprehensive experimental survey of the region.

---

* 'Proc. Univ. Durham Phil. Soc.,' vol. 8, p. 337 (1931).

It is a survey of this nature which is the subject of the present papers, and the absorption spectrum of the extraordinary ray in quartz has been added to those of the ordinary ray and of fused silica. The resolution attained in the measurement of these spectra is a marked improvement on that of previous work, although the spectrometer was only a rather small prism instrument. The bands found have, where possible, been examined in at least two thicknesses of material, so that there is reasonably convincing confirmation of their existence.

The number and the range of thicknesses of the specimens used in the investigation far exceeds that of any previous work on solid materials, and it is hoped that the results will form a sound basis for theories of the spectra of silica in particular and of solid bodies in general.

The wave-length measurements are based on the dispersion data of Paschen* and others for the various prism materials and are correct to within about 0·005 μ when checked against well-known bands of CO_2 and water vapour. The percentage transmissions are correct to at least 1%, and in much of the work the probable error is appreciably less than this.

Absorption coefficients derived from these observed transmissions are probably correct to about 3%.

BRIEF DESCRIPTION OF APPARATUS

The apparatus consisted essentially of four parts: (*a*) the source of radiation; (*b*) an optical system into which the specimen to be examined could be introduced; (*c*) the spectrometer; (*d*) instruments for the detection and measurement of radiation.

Several sources were tried, of which a small electric furnace or "hohlraum" and a Nernst filament proved the most useful.

The optical system consisted of two concave mirrors focusing the source on the slit, the specimen being introduced by means of a solidly constructed rocker into the parallel beam between the mirrors. This beam was limited in aperture by a stop placed immediately after the specimen.

---

* Fluorite: Paschen, 'Ann. Physik,' vol. 53, p. 325 (1894); vol. 4, p. 299 (1901); vol. 41, p. 670 (1913); Liebreich, 'Verh. deuts. phys. Ges.,' vol. 13, pp. 1, 700 (1911). Quartz: Paschen, 'Ann. Physik,' vol. 35, p. 1005 (1911); Rubens, *ibid.*, vol. 53, p. 273 (1894); Carvallo, 'C.R. Acad. Sci.,' Paris, vol. 126, p. 728 (1898).

The spectrometer was a small Hilger infra-red instrument (D33) used with either a quartz or a fluorite prism.

The thermopile was connected to a Moll thermal relay, in connexion with which Moll galvanometers were used in both the primary and secondary circuits.

The source, optical system, and spectrometer were all set up on a large slate slab laid over the ordinary bench and were either rigidly fixed to the slate or mounted on massive bases to avoid accidental relative movements.

The whole apparatus was operated by a single observer, and it was necessary, therefore, that all controls and all scales to be read should be grouped together at a suitable point, in the interests of accuracy no less than of convenience. In this respect it is worth particular mention that the scale of the Nernst current control galvanometer was placed where it could be watched practically simultaneously with the scale of the main galvanometer, the rheostats being also conveniently placed to hand so that the Nernst current could be adjusted up to the moment of reading a deflexion.

SOURCES OF RADIATION

The furnace mentioned above was made with Nonpareil fire bricks and alundum cement, with silit rod heating elements.

Its disadvantages were:

(i) A long time was required to attain a steady temperature.
(ii) The intrinsic brightness was comparatively low.

These disadvantages were not shared by the Nernst filament which was, accordingly, used for much of the work. To keep off the draughts, to which a Nernst filament is peculiarly susceptible, a housing was constructed of celotex and provision made, as recommended by Robertson, Fox, and Hiscocks,* for a continuous flow of air through the housing from inlets at the bottom to a chimney on the top. This was, however, found to be unsatisfactory, and considerably greater steadiness of emission was obtained when the air flow was cut off. The housing was made on a wedge plan with a shutter at the apex. It could be pushed in among the other apparatus with the shutter well clear of the filament, so that its operation did not disturb the air about the filament.

An accumulator battery of 160 volts and 60 ampere hours' capacity was used to run the filament at 95 volts and 1 ampere through a control circuit on the lines of that described by Robertson, Fox, and Hiscocks. The current was controlled to 3 milliamp, *i.e.*, to 0·3%.

---

* 'Proc. Roy. Soc.,' A, vol. 120, p. 128 (1928).

OPTICAL SYSTEM EXTERNAL TO SPECTROMETER

The optical system between the source and the spectrometer required more careful consideration than was at first realized, and errors occurred which were due in part to bad design of this section of the apparatus. A discussion of these errors has appeared in another place* and will not be repeated in full. It may be stated, however, that they occurred in regions of the spectrum where the dispersing prism itself absorbed radiation, and were due to differential absorption of the two beams to be compared. This arose from a change produced in the direction of the beam entering the spectrometer by the introduction of the specimen. Such an effect could not occur if the aperture of the spectrometer was in each case filled by a beam of uniform intensity over its cross-section, but in the present work this condition was not readily fulfilled as many of the specimens were of rather small area. It was necessary to place a sufficiently small, rigidly fixed stop between the specimen and collimator slit and to make sure that this was filled with a uniform beam both with and without the specimen in position.

Setting up the Specimen—In setting up a specimen on the " rocker " it was the normal practice to adjust the surfaces to be perpendicular to the mean axis of the beam. This was ensured by receiving on a screen the inverted image formed by back-reflexion from the specimen surfaces and first mirror and adjusting to make the image of the upper half cover the position of the lower half of the source.

One or twice a double image was observed, indicating that the specimen surfaces were not parallel and that in consequence the transmitted beam must be deviated. When the lack of parallelism was excessive the specimen was re-ground, but in milder cases it was merely rotated until the back-reflected images overlapped on a vertical line. The deviation of the beam was then confined to a vertical direction and the transmitted image only moved slightly up or down the slit and not across it. If the image were allowed to move sideways, serious error might occur because the two beams to be compared would have come from quite different parts of the source—in effect from different sources.

Care was taken to keep the specimens clean, as it was found that after standing for three days in the atmosphere of the laboratory (with surfaces vertical) a specimen transmitted about 1% less than when freshly cleaned. All specimens up to the 63·1 mm thickness of crystalline quartz were mounted on the rocker and adjusted as above described. The bigger specimens, however, could not be so treated and special experimental arrangements were made for each case; these will be described later.

---

* Drummond, ' Proc. Univ. Durham Phil. Soc.,' vol. 9, p. 55 (1933).

Standard Wave-length for Setting Prisms—For setting the prism on the spectrometer most previous workers have used as a standard the mercury emission line at 1·014 μ. This has been abandoned in the present work for several reasons.

(i) It involves the use of an extra source of radiation, *i.e.*, a mercury arc.

(ii) Difficulty was experienced in running a mercury arc sufficiently steadily for infra-red work.

(iii) The line 1·014 μ is not very far out of the visible region and its use in setting the prism when work is to be done at long wave-lengths implies a long extrapolation.

It was found more convenient to set the prisms to the CO_2 absorption bands in the neighbourhood of 2·7 μ. Moderate resolution shows two bands in this region, but higher resolution splits each of these into a doublet. With the quartz prism used under optimum conditions it was just possible to show this doubling.

The wave-lengths of these bands are known with sufficient accuracy for the purpose and are given by Barker* as:

$$\left.\begin{array}{l}2\cdot677\ \mu\\ 2\cdot698\ \mu\end{array}\right\}\ 2\cdot688\ \mu$$

$$\left.\begin{array}{l}2\cdot753\ \mu\\ 2\cdot776\ \mu\end{array}\right\}\ 2\cdot765\ \mu$$

To make this setting the ratios of the deflexions through a CO_2 tube about 5 cm long and a corresponding dummy tube were observed.

THE SPECTROMETER AND PRISMS

The D33 Hilger spectrometer was enclosed in an approximately cubical housing, through the sides of which projected a low power microscope, for reading the drum, and a handle by means of which the drum could be set. A thermometer was fixed through the lid for reading the prism temperature.

To facilitate adjustment of the instrument and ensure permanency of the setting it was found necessary to replace the setting screw for the Wadsworth mirror by one with a much finer thread and to fit this with a lock nut.

---

* 'Astrophys. J.,' vol. 55, p. 391 (1922); Schaefer and Philips, 'Z. Phys.,' vol. 36, p. 641 (1926); *cf.* Schaefer and Matossi, "Das Ultrarote Spektrum," p. 226 (1930).

Mirror Surfaces—The original mirror surfaces were silvered on glass and were replaced, when tarnishing had become excessive, as follows:

Telescope and collimator—platinized on glass.
Wadsworth—stainless steel.

Unfortunately, the reflexion coefficients of these metals are relatively low* and at 2·7 μ, for example, the loss of efficiency relative to the three silvered mirrors amounted to over 33%. Silvered surfaces were quickly reverted to.

Calibration—As both quartz and fluorite prisms were to be used the reading drum was engraved with uniformly spaced graduations instead of wave-lengths.

The relation between drum reading and prism table rotation was obtained by measurement using a telescope and a carefully calibrated scale set up at 5 metres distance as described by Robertson and Fox. The telescope magnification was increased to a suitable value by replacing the eyepiece with a low power microscope and substituting glue thread crosswires† for the original crosswires.

The accuracy attained in this measurement was about ± 3 seconds of arc being limited by the insufficient rigidity of the wooden floor between the spectrometer and the measuring scale.

Wave-length calibration of the prisms was then based on the standard dispersion data‡ and carried out on the lines suggested by Rawlins and Taylor.§

Probable Errors—The estimated probable error of wave-length reading arising out of inaccuracy of the drum calibration depends on the dispersion of the prism material and is given by:

$$\delta\lambda = \frac{d\lambda}{dn} \cdot \delta n, \tag{1}$$

where $d\lambda/dn$ is the reciprocal of the slope of the n, λ curve at the wave-length in question, and δn is the uncertainty in the refractive index corresponding to an uncertainty of about ± 3 seconds of arc in the angular setting of the prism table.

---

* Lecomte, " Le Spectre Infra rouge," p. 424 (1928).

† Drummond, 'J. Sci. Instrum.,' vol. 10, p. 258 (1933).

‡ Fluorite: Paschen, 'Ann. Physik,' vol. 53, p. 325 (1894); vol. 4, p. 299 (1901); vol. 41, p. 670 (1913); Liebreich, 'Verh. deuts. phys. Ges.,' vol. 13, pp. 1, 700 (1911). Quartz: Paschen, 'Ann. Physik,' vol. 35, p. 1005 (1911); Rubens, *ibid.*, vol. 53, p. 273 (1894); Carvallo, 'C.R. Acad. Sci.,' Paris, vol. 126, p. 728 (1898).

§ " Infra-red Analysis of Molecular Structure," p. 117 (1929).

For quartz and fluorite the values of $\delta\lambda$ are given in Table I.

TABLE I

Quartz		Fluorite	
λ	$\delta\lambda$	λ	$\delta\lambda$
μ	μ	μ	μ
4·0	±0·0005	8·0	±0·0009
3·5	±0·0006	7·0	±0·0011
3·0	±0·0007	6·0	±0·0013
2·5	±0·0009	5·0	±0·0016
2·0	±0·0012	4·0	±0·0021
1·5	±0·0015	3·0	±0·0029
1·0	±0·0014	2·0	±0·0039
		1·5	±0·0044
		1·0	±0·0031

This is not, of course, the only source of wave-length error, and uncertainties in the refractive index data themselves will account for errors of the same, or even much greater order. In quartz at 3·5 μ, in particular, there appears to be uncertainty amounting to 0·025 μ due to inaccurate refractive index data.*

Other sources of wave-length error have been discussed before.†‡

Prisms—The quartz prism used was not of the Cornu type; but this is of less importance in the infra-red than it would be in the visible because the rotatory power of quartz decreases as the wave-length increases. At 1·0 μ the separation of the right- and left-handed circularly polarized beams is 3 or 4 seconds; at 2 μ it is less than 1 second of arc and is growing rapidly smaller. Even through the dichroic region at 2·9 μ the rotatory power continues to fall uniformly.§

The fluorite prism was rather cloudy by comparison with the quartz and there were several flaws in it which tended to obscure the beam. Probably in consequence of this the resolution in the 3 μ region was much less good than elementary calculation would have led one to expect, but at longer wave-lengths, where its dispersion is higher, this prism gave very satisfactory results.

THE MEASURING INSTRUMENTS

The Thermopile—The thermopile was a standard Hilger instrument of receiving area 10 × 0·5 mm and was placed in an airtight holder with rocksalt window as designed by Robertson, Fox, and Hiscocks.* The window supplied was covered with protecting films of pyroxylin, a substance which is rich in intense absorption bands in the infra-red, and it was necessary to dissolve this off in amyl acetate before use.

---

* Drummond, 'Nature,' vol. 134, p. 937 (1934).

† Bailey, Cassie, and Angus, 'Proc. Roy. Soc.,' A, vol. 130, p. 133 (1930).

‡ A. Hilger, Ltd., "Notes on the Use of the Infra-red Spectrometer."

§ Lowry and Snow, 'Proc. Roy. Soc.,' A, vol. 127, p. 271 (1930); *see* Sosman, "Properties of Silica," p. 660 (1927).

Thermal Relay—The thermopile was connected to a Moll thermal relay and so to a Moll secondary galvanometer. The thermal relay and its connexions were a source of much unsteadiness of the galvanometer spot. The effects may be divided into two classes, mechanical and electrical.

MECHANICAL DISTURBANCES OF THE RELAY

It was found that the relay was sensitive, not so much to vibration as to tilting of its support, and since it originally stood on a shelf on a partition wall at the top of a three-story building the zero was never steady. Serious disturbances were produced by people moving about the building or by wind exerting pressure on the external walls. The trouble was largely overcome by suspending the relay in an independent framework from a wall bracket and enclosing the whole system with a draught-proof housing.

With this arrangement it was possible, during the night, to take readings of an accuracy of about ½ mm at a sensitivity of about 3×10^{11} amp per millimetre at 1 metre; as the scale distance from the secondary galvanometer was almost 2 metres, the effective sensitivity was roughly twice the above.

The adjustment of the relay on the swinging cage was a matter of some little difficulty on account of the oscillations set up by touching it. The final adjustment of the galvanometer spot to a convenient zero point on the scale was effected by dropping small weights on to the edge of the slate base of the suspension, thus turning to good account the effect of tilts of the relay on the zero of the system. The method was simple and entirely reliable, the zero shift being quantitatively proportional to the added weight. The angular tilt produced by 1 gm placed on the edge of the base was about 0·75 seconds and the zero shift so caused was 4 cm—figures which give some idea of the extraordinary sensitiveness of the relay to this form of disturbance.

To avoid the transmission of tilts to the suspension through the connecting wires it was necessary to take off all leads from as close as possible to the point of suspension.

---

* 'Proc. Roy. Soc.,' A, vol. 120, p. 128 (1928).

ELECTRICAL AND MAGNETIC DISTURBANCES OF THE RELAY

Electro-magnetic Effects—Electro-magnetic effects fortunately had an almost negligible effect on the relay itself but were troublesome in the connecting circuits. The effects could be very greatly reduced by eliminating magnetic loops as far as possible, and in particular by connecting direct from thermopile to primary galvanometer with twisted twin flex.

Electro-magnetic Radiation—High-frequency oscillators, used for the excitation of gas spectra in the same laboratory as the infra-red apparatus, produced large deflexions of the galvanometer. The direction of deflexion was always that corresponding to heating of the thermopile junctions, and the mechanism of the effect appeared to be that electro-magnetic radiation was picked up by the leads, the small currents so produced resulting in a differential heating of the junctions. The " hot " junctions were of much lower heat capacity than the " cold " junctions and the result was a pseudo-rectification of the high-frequency currents.

The thermal relay element includes two junctions, but no direct effect of the H.F. oscillators on this was detected. Presumably, this was because the junctions in this case were of equal heat capacity and no differential effect was possible.

It is likely that a thermopile with equal hot and cold junctions would be free from this defect in an electro-magnetic radiational field and possibly also from susceptibility to adiabatic fluctuations of air pressure when not in an airtight holder. With the Hilger thermopile readings have only been taken when no oscillators were working.

Disturbances of Uncertain Origin—When the source was glowing, deflexions were occasionally produced by touching any metal part of the spectrometer, rocker, or mirror stands. The effect could be eliminated by earthing all metal parts of the system. It occurred both with the furnace and the Nernst, though it was more consistently present with the latter.

Disturbances Due to the Relay Lamp—The relay lamp was run from high-capacity accumulators which were kept well charged, and no further precautions were taken to ensure steadiness except that the connecting wires and knife switch were kept in good condition.

The lamps used on the relay were rated at 4 volts, 25 watts, though the true consumption at 4 volts was only 14·4 watts. At the maximum lamp current zero fluctuations were excessive and for all accurate work it was necessary to insert a resistance of about 1/3rd ohm in the circuit, thereby increasing stability though halving the sensitivity.

Thermo-electric and Leakage Current Disturbances—Thermo-electric and leakage current effects also gave some trouble but were dealt with in the usual ways.

Zero Drifts—Zero drifts were almost invariably present and under normally favourable conditions a drift of 3 to 4 cm per hour could be expected. Since about 90 deflexions per hour were read this drift was not a serious drawback.

Acknowledgments and thanks are due to the Government Grant Committee of the Royal Society for a grant made to Professor W. E. Curtis, F.R.S., for the purchase of the spectrometer used in this work.

SUMMARY

A description is given of apparatus for the measurement of the near infra-red absorption spectra of solid sections. Indications are given of the accuracy attainable and of some of the precautions necessary to ensure this accuracy.

The Infra-Red Absorption Spectra of Quartz and Fused Silica from 1 to 7·5 μ

II—Experimental Results

By D. G. Drummond, Ph.D.

(*Communicated by W. E. Curtis, F.R.S.—Received July* 22, 1935)

The accuracy of calibration, as already mentioned, was checked against CO_2 and water vapour bands. With the quartz prism the instrument could be set to show the 2·7 μ CO_2 bands resolved and within about 0·003 μ of their known wave-lengths*; *i.e.*, within 4 cm^{-1}. With the fluorite prism, resolution at 2·7 μ was inferior, but the structure of the water vapour band centred at 6·3 μ provided about 20 points for the checking of wave-lengths.† Here the maximum discrepancy was 5 cm^{-1}, and the mean discrepancy about 1·5 cm^{-1}. The wave-number error, therefore, is not likely to exceed 5 cm^{-1} in any part of the range investigated.

The fraction of radiation transmitted by a specimen was measured to three figures and a mean of two or three observations at least taken for each wave-length setting. The accuracy varies from specimen to specimen and from point to point throughout the spectrum, depending on the magnitude of the galvanometer deflexions obtainable. The error is, however, nowhere likely to be greater than 0·01 and for much of the work is of the order of 0·002.

The curves in graphs I, II, and III are all adequately populated with experimental points, the standard interval adopted being 0·02 μ. This, for the most part, was sufficient to give at least two points per slit width, the latter being defined as the wave-length range which would be embraced by the thermopile slit if the collimator slit were infinitely narrow. In practice the collimator slit width was, in all cases, equal to that of the thermopile slit. In the region 2·8 μ to 3·1 μ the curves for the crystalline specimens were obtained with reduced slit widths, and to bring out the improved resolution so rendered possible the readings were taken at intervals of only 0·005 μ. In several other cases bands suspected of structure were examined at reading intervals of 0·01 μ and with slits of suitably reduced width, but it was only in the region just mentioned that any finer structure than that shown with the standard reading interval was revealed.

---

* Barker, ' Astrophys. J.,' vol. 55, p. 391 (1922).

† Sleator and Phelps, *ibid.*, vol. 62, p. 28 (1925).

It is believed that every inflexion shown on the curves is significant and that finer structure than this is either absent or will require a very considerable increase in resolving power for its detection.

THE SPECIMENS EXAMINED

The specimens examined are listed and briefly described in Table I.

Grateful acknowledgments and thanks are due to The Thermal Syndicate, of Wallsend-on-Tyne, for all the fused silica specimens, which were

TABLE I—FUSED SILICA SPECIMENS

Specimen	Thickness mm	Description	Remarks
A	3060	In the form of a drawn rod 9 mm diam. Full of striae and imperfections so that no image could be transmitted.	Impracticable to mount this on the rocker. The specimen and comparison beam were accommodated simultaneously within the aperture of the mirrors and obscured alternately by a rocking shutter. The axes of the two beams were arranged to lie in one vertical plane so that both passed through equal thicknesses of prism material. The ordinates of the curve are plotted to an arbitrary scale.
B	458	Drawn rod, 20 mm diam. Full of striae as above and no image could be transmitted.	Mounted on rocker and swung into beam alternately with small stop chosen to give deflexions of similar order of magnitude. Ordinates of curve plotted to an arbitrary scale.
C	29·85	Cylinder cut from melt *a* (April, 1931). Contained many striae and transmitted a blurred though recognizable image.	Had had additional heat treatment to that of the other specimens cut from melt *a*, to try to improve homogeneity. Standard optical system used for measurements.

TABLE I—continued

Specimen	Thickness mm	Description	Remarks
D_1 E_1 F G	6·01 1·60 0·605 0·28	Discs cut from melt *a*. Optical quality not specially good, but fair visible images transmitted.	Sections E_1, F, and G were used for relatively long wave-length work where scattering was small so that the effective optical quality was reasonably good.
D_2 E_2	5·970 1·484	Squares cut from melt *b* (March, 1932). Optical quality good and striae imperceptible.	—
H	0·109	Section cut from melt *c* (June, 1933). Too thin to show striae if present.	Thickness measured by observing fringes crossing the spectrum of white light which had passed through the section. (Edser-Butler fringes.)
J	0·005?	Portion of blown bubble of fused silica. Had considerable curvature and was non-uniform in thickness.	Results qualitative only.
CRYSTALLINE QUARTZ SPECIMENS CUT PERPENDICULAR TO AXIS			
K	690	Train of five large, rough blocks of quartz. Assorted as regards sign of optical rotation and ends only approximately perpendicular to the axis and roughly polished. Ends not in all cases parallel.	Train set up on special sliding carriage and moved as one unit in and out of beam. The blocks were set up in turn working back from slit to source and making the faces of each as nearly as possible perpendicular to the beam, the wedge angles being vertical and opposed to minimize the resultant deviation and confine it to the vertical plane.
L	63·1	Single piece of crystal optically worked. In polarized (transmitted) light it appeared somewhat mottled.	—

TABLE I—(continued)

Specimen	Thickness mm	Description	Remarks
M	12·09	Single piece of crystal optically worked. In monochromatic (not white) polarized light a thin vein of twinned material was detectable.	Readings taken with a stop covering the perfect portion only or overlapping the twinning vein were indistinguishable, the area of twinned material being only a minute fraction of the area of the stop.
N	3·20	Single piece of crystal optically worked. Showed several parallel twinning veins in polarized light.	Absorption coefficients obtained from this specimen in the strongly dichroic region were definitely lower than those for specimen M and were therefore rejected.
P	0·582	Single piece of crystal optically worked. Untwinned.	—
Q	0·0845	Single piece of crystal, polished. 25 mm square.	An unusually large area for so thin an unmounted specimen so that reliable readings were readily obtainable. Thickness measured by Edser-Butler fringes.
CRYSTALLINE QUARTZ SPECIMENS CUT PARALLEL TO AXIS			
R	34·6	Single piece of crystal optically worked. Actually the same piece as section M above, but viewed through the edge instead of the main faces.	To cut off light reflected back internally into the beam from the main faces, a long narrow aperture was used as stop. This reduced the deflexions and therefore the accuracy of individual readings. A large number of readings was taken to ensure a good mean value.
S	6·053	Single piece of crystal. Optically perfect.	—
T	1·129	Single piece of crystal. Optically perfect.	—

TABLE I—(continued)

Specimen	Thickness mm	Description	Remarks
U	0·104	Polished plate, 25 mm square. Parallel sided but very slightly warped. Unfortunately it was cracked right across. The pieces were mounted in a wooden frame with their edges in contact.	As the reflexion coefficient is much less at 5–7·5 μ than in the visible, the loss of light due to the crack was negligible. Thickness measured by Edser-Butler fringes (*see* below).

supplied by them free of charge, and for the loan of a Moll galvanometer; also to Messrs. A. Hilger, Ltd., for the loan of the large quartz blocks used for specimen K.

The experimental transmission curves for the specimens are shown in graphs I, II, and III, the lettering there corresponding to the lettering in Table I.

The curve for specimen K, graph II, has been corrected for the incomplete filling of the stop by the extreme component pencils of the beam, caused by the unusually great length of path between the first mirror and the stop of the optical system. The extent of this deficiency was altered by the introduction of the quartz train and a correction of 10·2% on all the observed deflexion ratios was necessary.

None of the curves is corrected for reflexion losses. For specimen K, again, 10 surfaces are involved and the loss is considerable.

In the measurement of crystalline specimens cut parallel to the axis an additional precaution was taken to ensure accuracy. Readings were taken both with the optic axis horizontal and with it vertical and the mean of the two sets of results found. The ordinary and extraordinary rays were thus given equal treatment and the effect of instrumental polarization eliminated. This technique precluded the use of any section whose faces were not very nearly parallel, as the consequent deviation of the beam could not be confined to the vertical direction in both positions of the specimen. One minute of arc departure from parallelism was the limit of tolerance allowed in these specimens. In practice the effect of instrumental polarization proved negligible except in a region of strong dichroism of the specimen.

With regard to results previously published,* on absorption in a thickness of 83·1 mm of quartz cut parallel to the axis, it must be mentioned that some of the precautions now described were omitted in making the measurements and that the curve must be discarded in favour of that for specimen R of the present series.

---

* Drummond, 'Nature,' vol. 130, p. 928 (1932).

The measurement of the thickness of specimen U by means of Edser-Butler fringes presented a point of interest. In unpolarized light, sets of fringes due to the ordinary and extraordinary rays were superposed, giving the effect of a single set of fringes of fluctuating visibility. By making measurements in polarized light and assuming a knowledge of the two refractive indices, two independent values for the thickness were obtained and also, incidentally, the direction of the optic axis in the crystal slice was revealed.

CALCULATION OF ABSORPTION COEFFICIENTS

Absorption coefficients have been calculated from the fundamental equation:

$$\frac{\mathrm{I}}{\mathrm{I}_0} = e^{\kappa d} . \rho = \mathrm{m}, \tag{1}$$

where

I_0 = incident intensity of radiation.
I = transmitted intensity of radiation.
d = thickness of specimen in millimetres.
κ = absorption coefficient.
ρ = correction for losses by reflexion at the surfaces.
m = measured deflexion ratio.

The value of ρ depends on the nature of the specimen.

(*a*) For a simple section with two parallel surfaces ρ is given approximately by the expression:

$$\rho = (1 - r)^2, \tag{2}$$

where r = reflexion coefficient.

When successive internal reflexions are taken into account the more accurate expression obtained is:

$$\rho = \frac{(1 - r)^2}{1 - \dfrac{m^2r^2}{(1 - r)^4} + \text{. . smaller terms}} . \tag{3}$$

Equation (1) is then most simply manipulated in the following form:

$$\kappa = \frac{1}{d \log_{10} e} . \log_{10} \frac{(1 - r)^2}{m} + \frac{m^2r^2}{(1 - r)^4 d} . \tag{4}$$

It will be noticed that $\frac{(1 - r)^2}{m}$ is always greater than unity and the logarithm remains positive, and further that $(1 - r)^2$ remains sensibly constant over an appreciable wave-length range. This is a great convenience when long columns of figures are to be calculated as, by using a slide rule which embodies a reciprocal scale on the slide and a logarithm scale below the fixed scale on the face of the rule, a whole series of values of $\log \frac{(1-r)^2}{m}$ can be obtained, at a single setting of the slide to $(1-r)^2$, by merely running the cursor to the values of m on the reciprocal scale and reading straight across to the logarithm scale.

The term $\frac{m^2 r^2}{(1-r)^4}\, d$ constitutes the small correction for successive internal reflections and may usually be neglected. It becomes of importance only when κ itself is very small.

(*b*) Where the specimen consists of a number of pieces of the material in a train the complete expression for ρ is very complicated. An approximation to it may, however, be obtained by neglecting:

(i) Absorption in the specimen.

(ii) Terms in r^4 and higher powers of r.

Then

$$\rho = p^{2n}\left\{1 + \frac{(1-p)^2}{1-p^2}\left[2n - 1 - \frac{p^2\,(1-p^{4n-2})}{1-p^2}\right]\right\}, \tag{5}$$

where

$$p = 1 - r,$$

and

n = number of pieces of material in train.

This expression can be applied only when the reflexion losses are much greater than the absorption losses. For the long train of crystalline quartz blocks (specimen II K) approximate absorption coefficients may be calculated using this value of ρ, but there is not sufficient agreement between the values so obtained and those from specimen II L to justify reproducing the results.

(*c*) With optically imperfect specimens such as the long rods of fused silica there were losses due to scattering and to diffusion of the image as well as to reflexion at the surfaces. All these can be included in the factor ρ which becomes an unknown. Assuming, however, that it is constant in the spectral range involved, its value may be determined by inserting in the equation a particular value of κ obtained independently by measurements on a more optically perfect specimen. Rough values of κ may then be calculated throughout the range of the curve in question.

THE ABSORPTION COEFFICIENTS FOR THE EXTRAORDINARY RAY

In extracting values for κ_ϵ from the transmission figures for sections cut parallel to the axis it has been assumed that the absorption coefficient for the ordinary ray (κ_ω) is constant for all directions in quartz. This is certainly not far from the truth, although, as is shown by the results obtained for Iceland spar by Le Roux,* such an assumption is not justified in general. Time and circumstances have not permitted of a more rigorous examination of the point, but no serious discrepancies have appeared in the results for κ_ϵ. These results are presented with the reservation implied in the above remarks.

It has already been mentioned that the sections cut parallel to the axis were measured both with the axis placed horizontally and vertically to eliminate effects of instrumental polarization. If m' and m'' are the deflexion ratios for the two positions it is not difficult to show that

$$m' + m'' - m_\omega = m_\epsilon, \tag{6}$$

where m_ω and m_ϵ are the fractions transmitted of the ordinary and extraordinary rays respectively.

r_ω being known, and κ_ω having been determined from the results for sections cut perpendicular to the axis, m_ω could be calculated and thence m_ϵ found. κ_ϵ was then derived from the formula:

$$m_\epsilon = e^{\kappa_\epsilon d} . (1 - r_\epsilon)^2.$$

REFLEXION DATA

The principal source of the reflexion data required in order to calculate absorption coefficients was Reinkober's paper of 1911.† The results are given there in the form of small scale graphs which were measured up as accurately as possible and redrawn on a larger scale so that values of r could easily be read off. The limits of error in the values of ρ so derived were less than the error of measurement of m.

For crystalline quartz r was also calculated from the refractive indices

$$r = \left(\frac{n-1}{n+1}\right)^2, \tag{7}$$

and for the ordinary ray excellent agreement with Reinkober's values was found in the region 1 to 4 μ. The results for the extraordinary ray were not in such close agreement, but even here the discrepancy only amounted to 1/5th of 1% in the value of $(1 - r)^2$.

---

* 'Ann. Physique,' vol. 20, p. 518 (1933).

† 'Ann. Physik,' vol. 34, p. 343 (1911).

Nichols* has also given values of r for the ordinary ray in the region 4 to 8 μ and these were taken into account.

For fused silica there are no checks on Reinkober's results, as neither confirmatory direct measurements nor refractive index data are available.

PROBABLE ACCURACY OF κ

It was found that concordant values of κ were obtained from results for specimens of different thicknesses only when the fraction transmitted, at the wave-length in question, lay somewhere towards the middle of the possible range in each case. (Reflexion losses prevent the range of possible values extending right up to 1·0.)

For fractional transmissions lying nearer to the limits of this range the calculated values of κ tended to be erratic and were invariably low, a fact which finds its explanation in the following discussion of the curve of probable error.

From equation (1) we have

$$\frac{m}{\rho} = e^{\kappa d}.$$

Assuming now that m/ρ can be measured to within a given standard range, $\delta\left(\frac{m}{\rho}\right)$, of error, then the percentage probable error in κd is given by:

$$100\frac{\delta(\kappa d)}{\kappa d} = -\frac{100}{\kappa d}\cdot\frac{\delta\left(\frac{m}{\rho}\right)}{e^{\kappa d}},$$

$$= \frac{100\delta\left(\frac{m}{\rho}\right)}{\frac{m}{\rho}\log_e\left(\frac{m}{\rho}\right)}. \tag{8}$$

In fig. 1 the expression $\dfrac{1}{\frac{m}{\rho}\log_e\left(\frac{m}{\rho}\right)}$ is plotted against m/ρ and shows the form of the curve of percentage error in κd if a constant error in m/ρ is assumed. In the present work the accuracy of ρ and d is to about four figures, which is much higher than that for m and κ, and the curve may be taken as relating the errors of m and κ directly. It has already been stated that the values of m are correct to at least 1%. We may therefore write $\delta\left(\frac{m}{\rho}\right) = 0{\cdot}01$ and the ordinates in fig. 1 become actual percentage probable errors in κ.

---

* 'Ann. Physik,' vol. 60, p. 401 (1897); 'Phys. Rev.,' vol. 4, p. 297 (1897).

It is immediately obvious that when m lies between 0·10 and 0·65 the probable error in κ does not exceed 4% but that it increases very rapidly outside these limits.

Calculation from suitably overlapping experimental curves gives values of κ agreeing to within 3%, but where there are additional overlapping curves in which the values of the transmission, m, do not lie within the " safe " range, the additional values of κ are invariably erratic and low. This suggests that m tends to be too high, a tendency which will probably persist through the " safe " range making even the values of κ obtained here slightly low.

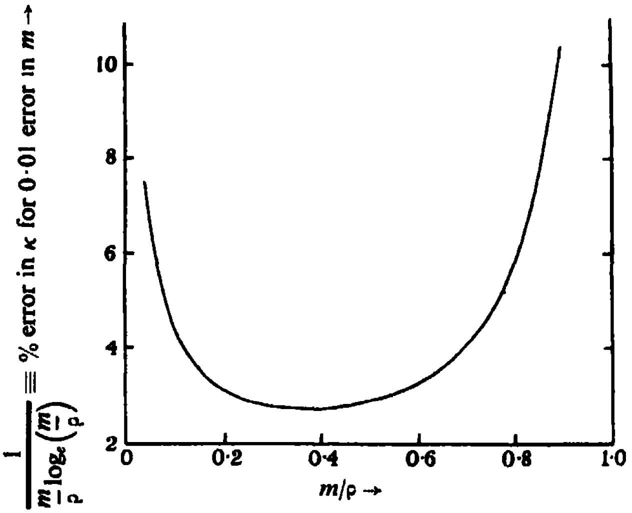

FIG. 1—" Error curve for equation $\frac{m}{\rho} = e^{-\kappa d}$."

The reason for the high values of m is, almost certainly, the presence of residual scattered light in the spectrometer. This is a not uncommon fault and is only successfully eliminated by the use of a double spectrometer. The scattering in the instrument used for the present results was small, however, and has only been detected by examination of the results on the lines indicated above. This appears to form a sensitive test of the performance of an instrument in this respect.

The optimum value of m/ρ for the purpose of calculating κ is $1/e$, that is 0·37, and not 0·50 as is commonly assumed.

NUMERICAL VALUES OF ABSORPTION COEFFICIENTS

The results for the absorption coefficients in the three substances (*i.e.*, fused silica, and the ordinary and extraordinary rays in quartz) are given in graph IV where, for convenience of representation, a logarithmic scale has been used for κ, which is plotted against frequencies instead of wave-lengths. The curves are continued as far down towards the visible as they may be regarded as reliable. In the region 1 to 2 μ it is to be noticed that there is evidence in both curves IA and IIK of a maximum of transmission at about 2 μ and an increase of absorption towards the visible as well as towards longer wave-lengths. From 2 to 1 μ the increase in the absorption coefficient appears to amount to 0·0002 in fused silica and 0·0006 in quartz (ω), though the former figure is the better substantiated of the two.

As to the absolute absorption coefficients at 2 μ it appears unlikely that these are greater than 0·001 for fused silica or 0·0002 for quartz (ω).

Heymans and Allis,* using a Lummer Brodhun photometer, found κ for fused silica in the visible to be 0·00696. If this were correct the fraction transmitted through the 10-foot (3060-mm) rod would be about 10^{-9}, but since, in fact, the emergent visible light was quite bright the coefficient quoted must be much too high. Even the value of 0·001 suggested above for fused silica at 2 μ only allows of 5% transmission through such a thickness, but it must not be forgotten that in curve IA the scale of ordinates is arbitrary and that the maximum may not represent more than 5%.

I wish to express my grateful thanks to Professor W. E. Curtis, F.R.S., for his continued interest and advice over a period of five years, and for the laboratory facilities placed at my disposal; also to Dr. J. J. Fox, of the Government Laboratory, for advice and discussion of the experimental details, especially in the early part of the work. My thanks are also due to the Armstrong College Post Graduate Research Committee for a Studentship and a grant awarded during the course of the research, which made possible its completion.

* 'J. Math. Phys. Mass. Inst. Techn.,' vol. 2, p. 216 (1923); *see also* Sosman, "Properties of Silica," p. 733 (1927).

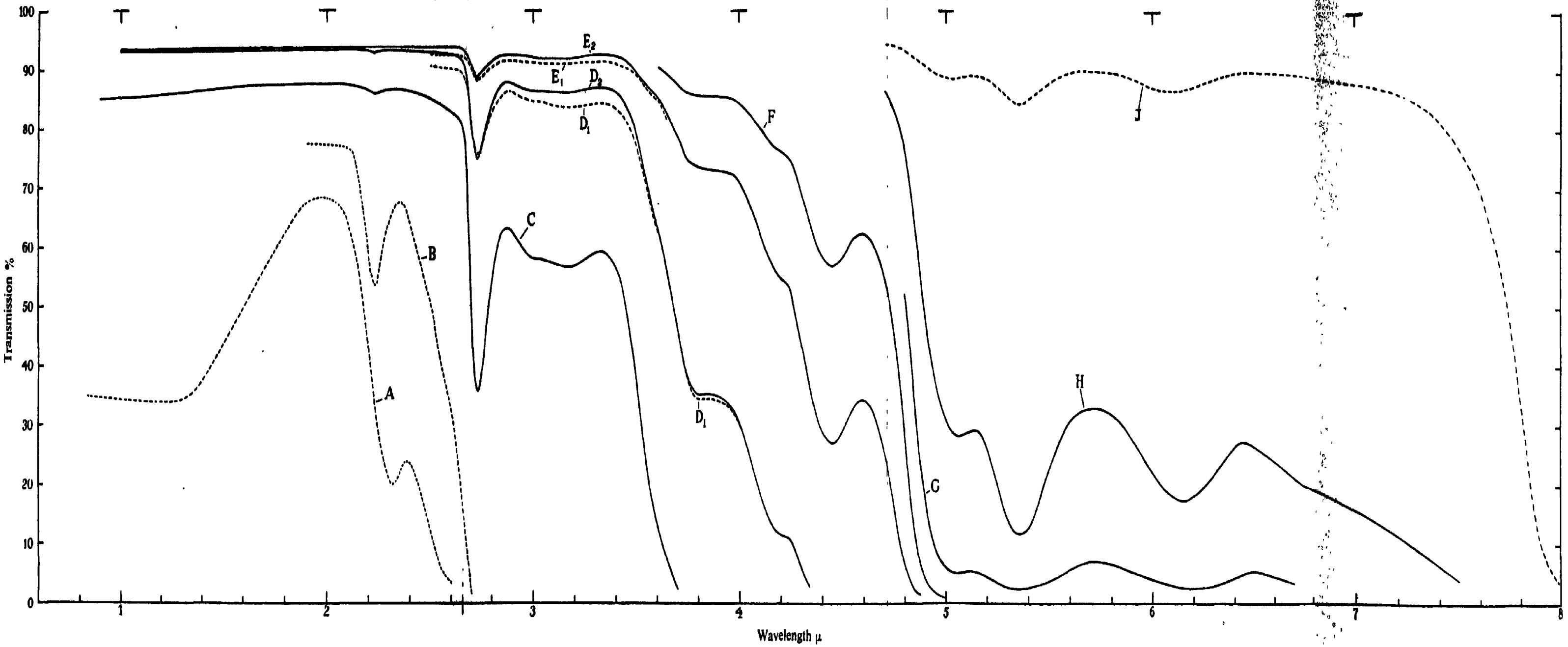

GRAPH I—Results for fused silica specimens.

	mm		mm
A	3060	E_2	1·484
B	458	F	0·605
C	29·85	G	0·28
D_1	6·01	H	0·109
D_2	5·970	J	0·005 ?
E_1	1·60		

(Facing p. 338)

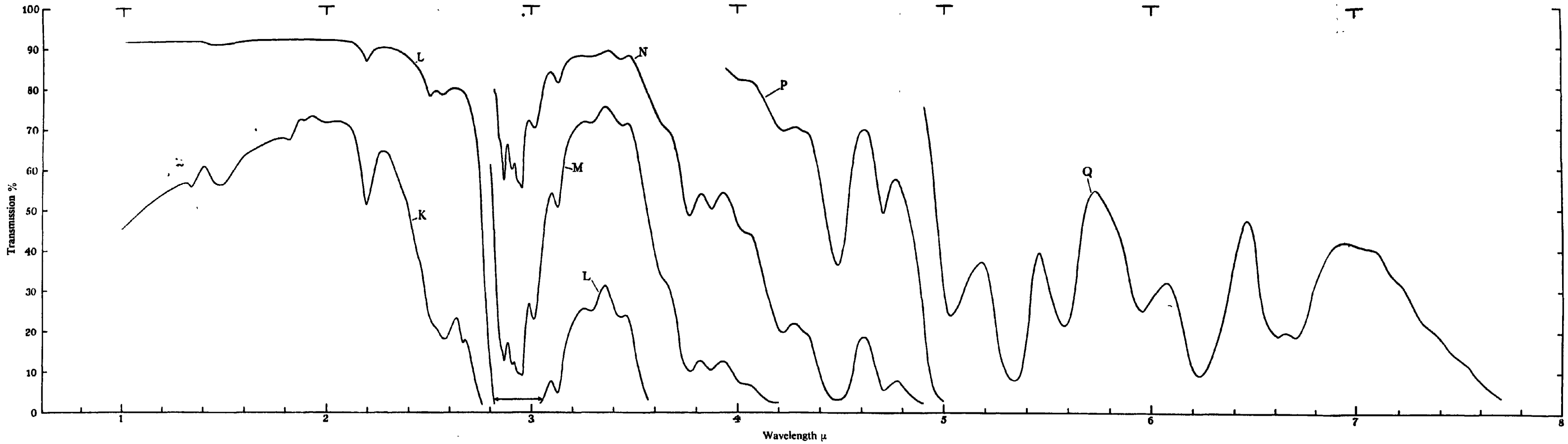

Graph II—Results for quartz specimens cut perpendicular to the axis. K, 690 mm; L, 63·1 mm; M, 12·09 mm; N, 3·20 mm; P, 0·582 mm; Q, 0·0845 mm.

Drummond Proc. Roy. Soc., A, vol. 153

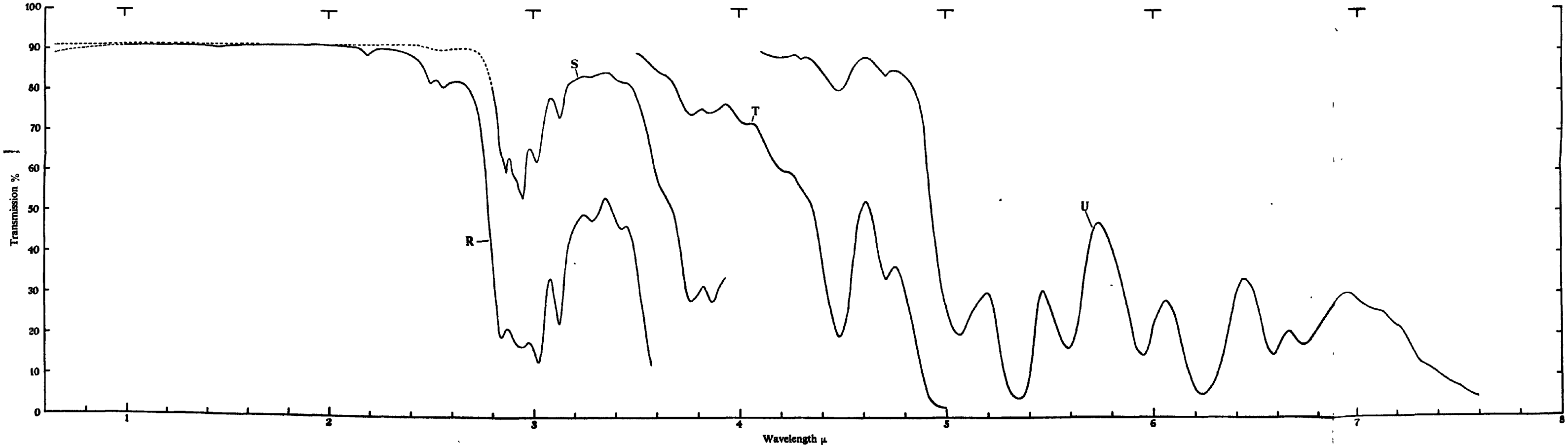

Graph III—Results for quartz specimens cut parallel to the axis. R, 34·6 mm; S, 6·053 mm; T, 1·129 mm; U, 0·104 mm.

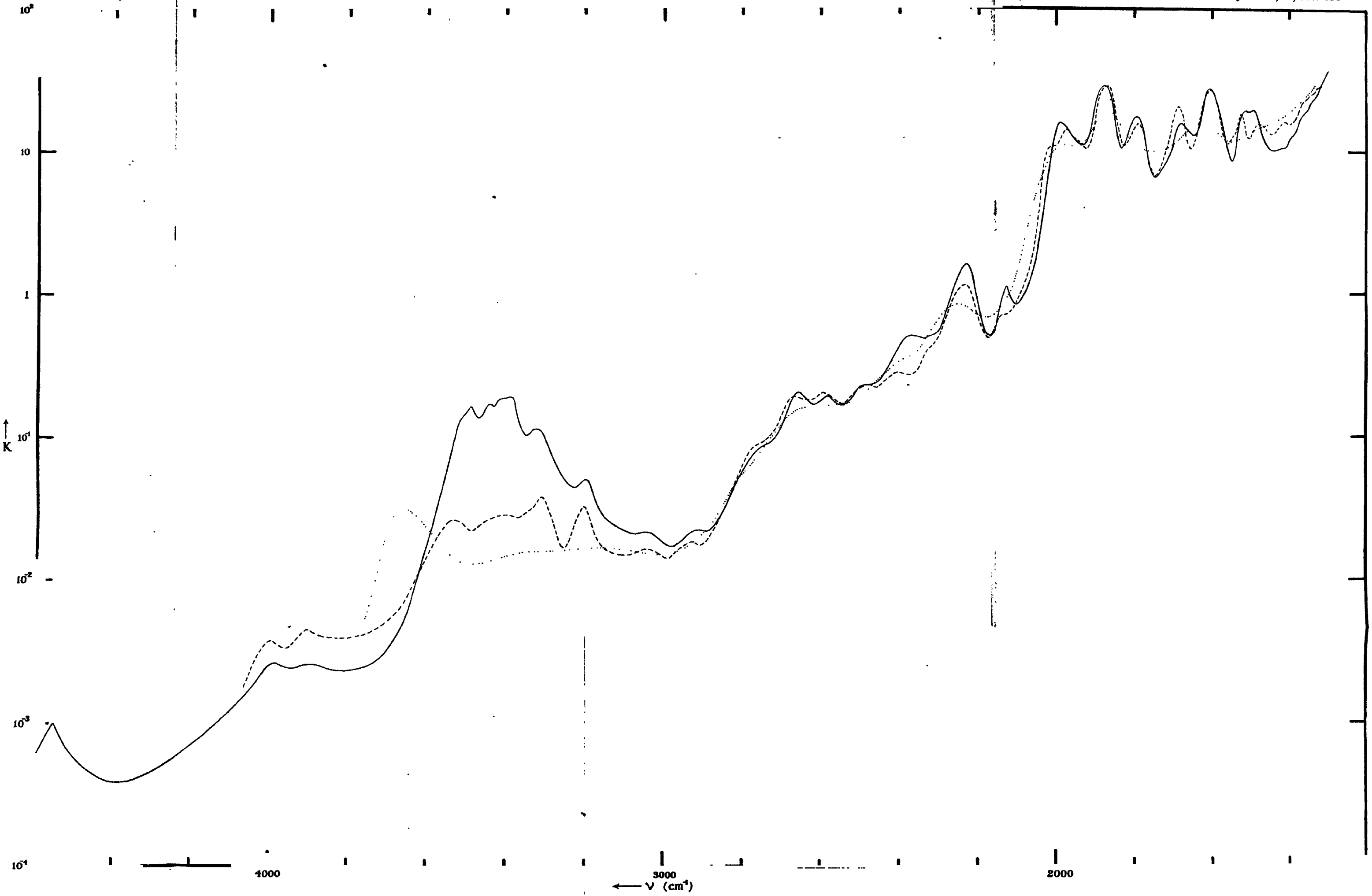

GRAPH IV—Absorption coefficients for fused silica, the ordinary ray in quartz and the extraordinary ray in quartz. —— quartz (ω); - - - quartz (ε); · · · · fused silica.

SUMMARY

Results are given, in graphical form, of absorption measurements on a wide range of thicknesses of fused silica and quartz (ordinary and extraordinary rays) between 1 and 7·5 μ in the near infra-red.

The methods of calculating absorption coefficients, κ, taking account of reflexion corrections, are indicated and a section on the probable accuracy of κ included. The absorption coefficients also are given in graphical form.

On the Theory of Optical Activity

III—A Regular Tetrahedron Twisted through a Small Angle about a Binary Axis

By B. Y. OKE, St. John's College, Cambridge

(*Communicated by T. M. Lowry, F.R.S. -Received July* 22, 1935)

INTRODUCTION

The problem of optical activity of a molecule, which is built up of several groups to each of which is attributed an isotropic resonator, has been treated by Born* in a paper with the same title (Part I and II). The method of approximation used there depends on the assumption of small coupling forces, *i.e.*, large distances between the resonators. It seems of some interest to investigate whether active models can be found which may be treated without this assumption of large distances.

A regular tetrahedron, the corners of which carry identical isotropic resonators, is not optically active. If, however, changes of shape and therefore of mechanical properties are introduced which exclude a plane of symmetry, the system can be optically active. In this paper we consider a change brought about by a small twist of the regular shape of the tetrahedron. Two of the corners of the regular tetrahedron are kept fixed and the other two are rotated through a small angle, along a binary

* Born, ' Proc. Roy. Soc.,' A, vol. 150, p. 84 (1935).

axis connecting the centres of the two edges. Such a system has evidently no plane of symmetry and it can be optically active.* The rotatory power can be calculated by a method of approximation. In this the regular tetrahedron is taken as the zero order approximation. We shall show that the optical activity is proportional to the third power of the small angle of twist.

Such considerations may be of some value for estimating the influence of deviations of a system from a regular shape, on the optical activity of the system.

1—POSITIONS OF THE RESONATORS AND THEIR INTERACTION FORCES

We consider a set of four mass points, having masses, m_1, m_2, m_3, m_4, situated at the corners of a regular tetrahedron. The co-ordinate axes are so chosen that the resonators have the following co-ordinates:

$$\left.\begin{array}{ll} (1) & \frac{l}{2\sqrt{2}}\ (\ \ 1,\ \ \ 1,\ \ \ 1) \\ (2) & \frac{l}{2\sqrt{2}}\ (\ \ 1, -1, -1) \\ (3) & \frac{l}{2\sqrt{2}}\ (-1,\ \ \ 1, -1) \\ (4) & \frac{l}{2\sqrt{2}}\ (-1, -1,\ \ \ 1) \end{array}\right\} \qquad (1.1)$$

where l is the length of an edge of the tetrahedron.

We assume that each resonator performs small vibrations about its position of equilibrium given in (1.1).

As shown by Born in the paper cited above [refer equation (1.11) therein], the hamiltonian of the system is

$$\mathbf{H} = \frac{1}{2}\sum_{k}\left\{\sum_{x} m_k (\dot{u}_x^k)^2 + \sum_{x,y}(\mathrm{P}_{xy}^k - \mathrm{Q}_{xy}^{kk})\, u_x^k u_y^k\right\} - \frac{1}{2}\sum_{xy}\sum_{k,l}{}' \mathrm{Q}_{xy}^{k,l}\, u_x^l u_y^l. \qquad (1.2)$$

---

* A rhombic bisphenoid with similar elements of symmetry has been suggested by F. M. Faeger ("Optical Activity and High Temperature Measurements," Cornell Lectures, 1930, p. 51) as a configuration for the atoms of the sulphur family in dis-

symmetric deviations of the type $\frac{R_1}{R_2}\Big\rangle L = 0$, etc.

Making the following substitutions

$$\left.\begin{aligned} \sqrt{m_k}\,\{u_x^k, u_y^k, u_z^k\} &= u_k, v_k, w_k \\ \frac{1}{m_k}(P_{xy}^k - Q_{xy}^{kk}) &= S_{xy}^k \\ \frac{1}{\sqrt{m_k m_l}} Q_{xy}^{kl} &= S_{xy}^{kl} \end{aligned}\right\}, \tag{1.3}$$

the hamiltonian can be expressed as:

$$\mathbf{H} = \tfrac{1}{2} \sum_{k=1}^{4} \left\{ \sum_{x} (\dot{u}_k)^2 + \sum_{x,y} S_{xy}^k u_k v_k \right\} - \tfrac{1}{2} \sum_{k,l}' \sum_{xy} S_{xy}^{k,l} u_k v_l. \tag{1.4}$$

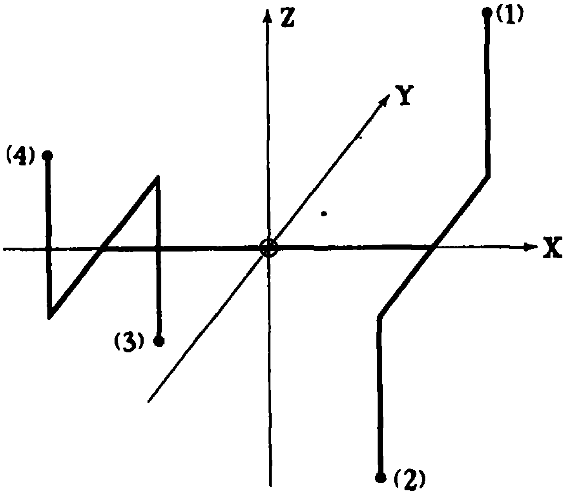

FIG. 1.

The coefficients $S_{xy}^{k,l}$ for $(k \neq l)$ can be expressed by the geometrical configuration of the system. These are given by

$$S_{xy}^{kl} = \frac{e_k e_l}{\sqrt{m_k m_l}} \frac{1}{r_{k,l}^3} \left(\frac{3 x_{kl} y_{kl}}{r_{k,l}^2} - \delta_{x,y} \right). \tag{1.5}$$

We consider the harmonic vibrations of an uncoupled single resonator with the frequency ω (per 2π seconds); putting

$$\mu = \omega^2 \tag{1.6}$$

the equations of motion are:

$$\mu_k u_k = \sum_{y} S_{xy}^k v_k, \tag{1.7}$$

giving three equations for each resonator k.

We assume that none of the vibrators has an intrinsic anisotropy, so that the tensor S^k_{xy} is isotropic. All the three roots of the characteristic equations are equal. If the roots be denoted by $\mu_{0\,k}$ we have

$$\mathbf{H} = \tfrac{1}{2} \sum_{k=1}^{4} \left\{ \sum_x (\dot{u}_k)^2 + \mu_{0k} \sum_x (u_k)^2 \right\} - \tfrac{1}{2} \sum_{k,l}' \sum_{xy} S^{kl}_{xy} u_k v_l. \tag{1.8}$$

2—Normal Vibrations of the Coupled System

If all the four vibrators are identical, they have the same masses and carry equal charges, and the roots of the characteristic equations are the same in each case. We put:

$$e_k = e; \quad m_k = m; \quad \mu_{0k} = \mu \quad \text{for } k = 1, 2, 3, 4. \tag{2.1}$$

Let

$$\left.\begin{aligned} \frac{\mu_0 - \mu}{\frac{1}{2}\frac{e^2}{m}\frac{1}{l^3}} &= \lambda, \\ a^{kl}_{xy} &= \frac{1}{(\frac{1}{2})\frac{e^2}{m}\frac{1}{l^3}} S^{k,l}_{xy} \end{aligned}\right\}. \tag{2.2}$$

From (1.5) the values of $a^{k,l}_{xy}$ are obtained as follows:

$$\left.\begin{aligned} a^{1,2}_{yy} = a^{1,2}_{zz} = a^{1,3}_{zz} = a^{1,3}_{xx} &= a^{1,4}_{xx} = a^{1,4}_{yy} = 1, \\ a^{3,4}_{yy} = a^{3,4}_{zz} = a^{2,4}_{zz} = a^{2,4}_{xx} &= a^{2,3}_{xx} = a^{2,3}_{yy} = 1, \\ a^{1,2}_{xx} = a^{3,4}_{xx} = a^{1,3}_{yy} = a^{2,4}_{yy} &= a^{1,4}_{zz} = a^{2,3}_{zz} = -2, \\ a^{1,2}_{yz} = a^{1,3}_{zx} = a^{1,4}_{xy} = -a^{3,4}_{yz} &= -a^{2,4}_{zx} = -a^{2,3}_{xy} = 3; \end{aligned}\right\} \tag{2.3}$$

all coefficients not given here vanish.

The equations of motion of the coupled system are:

$$\left.\begin{aligned} \lambda u_k &= \sum_l{}' \sum_y a^{kl}_{xy} v_l, \\ \lambda v_k &= \sum_l{}' \sum_z a^{kl}_{yz} w_l, \\ \lambda w_k &= \sum_l{}' \sum_x a^{kl}_{zx} u_k, \end{aligned}\right\} \tag{2.4}$$

for $k = 1, 2, 3, 4$; their number is 12.

We make the following substitutions:

$$\left.\begin{aligned}
&X_1 = \tfrac{1}{2}(u_1 + u_2 + u_3 + u_4), \quad Y_1 = \tfrac{1}{2}(v_1 - v_2 - v_3 + v_4),\\
&\qquad Z_1 = \tfrac{1}{2}(w_1 + w_2 - w_3 - w_4);\\
&X_2 = \tfrac{1}{2}(u_1 - u_2 + u_3 - u_4), \quad Y_2 = \tfrac{1}{2}(v_1 + v_2 - v_3 - v_4),\\
&\qquad Z_2 = \tfrac{1}{2}(w_1 + w_2 + w_3 + w_4);\\
&X_3 = \tfrac{1}{2}(u_1 - u_2 - u_3 + u_4), \quad Y_3 = \tfrac{1}{2}(v_1 + v_2 + v_3 + v_4),\\
&\qquad Z_3 = \tfrac{1}{2}(w_1 - w_2 + w_3 - w_4);\\
&X_4 = \tfrac{1}{2}(u_1 + u_2 - u_3 - u_4), \quad Y_4 = \tfrac{1}{2}(v_1 - v_2 + v_3 - v_4),\\
&\qquad Z_4 = \tfrac{1}{2}(w_1 - w_2 - w_3 + w_4).
\end{aligned}\right\} \qquad (2.5)$$

Combining together the four equations given by each of the equations in (2.4) we obtain the following simplified system of equations:

$$\left.\begin{aligned}
&\lambda A_i - 3B_i - 3C_i = 0\\
&-3A_i + (\lambda - 2)B_i + 3C_i = 0\\
&-3A_i + 3B_i + (\lambda - 2)C_i = 0\\
\text{for}\quad & i = 1;\ A_1 = X_1;\ B_1 = Y_1;\ C_1 = Z_1,\\
& i = 2;\ A_2 = Z_2;\ B_2 = X_2;\ C_2 = Y_2,\\
& i = 3;\ A_3 = Y_3;\ B_3 = Z_3;\ C_3 = X_3,\\
\text{and}\quad &(\lambda + 4)X_4 + 3Y_4 + 3Z_4 = 0\\
&3X_4 + (\lambda + 4)Y_4 + 3Z_4 = 0\\
&3X_4 + 3Y_4 + (\lambda + 4)Z_4 = 0
\end{aligned}\right\} \qquad (2.6)$$

The original secular equation of the 12th degree in λ is thus resolved into four cubic equations. The roots are:

$$\left.\begin{aligned}
&\lambda_1 = \lambda_2 = \lambda_3 = \lambda_{\mathrm{I}} = 5\\
&\lambda_4 = \lambda_5 = \lambda_6 = \lambda_{\mathrm{II}} = -\frac{\alpha + 1}{2}\\
&\lambda_7 = \lambda_8 = \lambda_9 = \lambda_{\mathrm{III}} = \frac{\alpha - 1}{2}\\
&\lambda_{10} = \lambda_{\mathrm{IV}} = -10 \quad \text{and} \quad \lambda_{11} = \lambda_{12} = \lambda_{\mathrm{V}} = -1;
\end{aligned}\right\} \qquad (2.7)$$

where

$$\alpha = \sqrt{73}. \qquad (2.8)$$

The equations of motion (2.4) can be written in a normal form. The normal co-ordinates, which will be functions of X, Y, Z, can be expressed in terms of u_k, v_k, w_k ($k = 1, 2, 3, 4$) by means of the equations (2.5).

To each λ_j (for $j = 1, 2, \ldots 12$) corresponds an eigenvector $e_j^{(0)\,k}$ satisfying the identity

$$\lambda_j\, e_{j,x}^{(0)\,k} = \sum_l{}' \sum_y a_{xy}^{k,\,l}\, e_{j,y}^{(0)\,l}. \tag{2.9}$$

The normalized eigenvectors satisfy the orthogonality conditions:

$$\left.\begin{aligned} \sum_{k=1}^{4} e_j^{(0)\,k} \,.\, e_h^{(0)\,k} &= \delta_{jh} \\ \sum_{j=1}^{12} e_{jx}^{(0)\,k}\, e_{jy}^{(0)\,l} &= \delta_{k,\,l}\, \delta_{xy} \end{aligned}\right\} . \tag{2.10}$$

Now we have only one eigenvector in a 12-dimensional configuration space instead of four eigenvectors $e_j^{(0)\,k}$ ($k = 1, 2, 3, 4$) in the usual space. One such eigenvector belongs to each eigen-value λ_j and we obtain an orthogonal co-ordinate system in a 12-dimensional configuration space.

We introduce 12 variables ξ_j with the help of the orthogonal transformation:

$$\left.\begin{aligned} u_k &= \sum_{j=1}^{12} e_{jx}^{(0)\,k}\, \xi_j \\ \text{whence} \qquad & \\ \xi_j &= \sum_{k=1}^{4} \Big(\sum_x e_{jx}^{(0)\,k}\, u_k \Big) \end{aligned}\right\} . \tag{2.11}$$

The equations of motion are

$$(\lambda - \lambda_j)\, \xi_j = 0, \quad \text{for } j = 1, 2, \ldots 12. \tag{2.12}$$

The values of the components of the eigenvectors are given in Table I. We put, for brevity:

$$\left.\begin{aligned} \beta = \frac{6\sqrt{2}}{\alpha - 1}, \quad \beta_1 = \frac{1}{2\sqrt{1+\beta^2}}, \quad \beta_2 = \frac{\beta}{2\sqrt{2}\sqrt{1+\beta^2}}, \\ \beta_3 = \frac{\beta}{2\sqrt{1+\beta^2}}, \quad \beta_4 = \frac{1}{2\sqrt{2}\sqrt{1+\beta^2}}. \end{aligned}\right\} \tag{2.13}$$

3—THE MOTION OF INDIVIDUAL VIBRATORS

We shall discuss the geometrical properties of the different types of vibrations.

TABLE I

λ	ξ	u_1	v_1	w_1	u_2	v_2	w_2	u_3	v_3	w_3	u_4	v_4	w_4
5	ξ_1	0	$\frac{1}{2\sqrt{2}}$	$-\frac{1}{2\sqrt{2}}$	0	$-\frac{1}{2\sqrt{2}}$	$\frac{1}{2\sqrt{2}}$	0	$-\frac{1}{2\sqrt{2}}$	$-\frac{1}{2\sqrt{2}}$	0	$\frac{1}{2\sqrt{2}}$	$\frac{1}{2\sqrt{2}}$
5	ξ_2	$-\frac{1}{2\sqrt{2}}$	0	$\frac{1}{2\sqrt{2}}$	$\frac{1}{2\sqrt{2}}$	0	$\frac{1}{2\sqrt{2}}$	$\frac{1}{2\sqrt{2}}$	0	$-\frac{1}{2\sqrt{2}}$	$-\frac{1}{2\sqrt{2}}$	0	$-\frac{1}{2\sqrt{2}}$
5	ξ_3	$\frac{1}{2\sqrt{2}}$	$-\frac{1}{2\sqrt{2}}$	0	$-\frac{1}{2\sqrt{2}}$	$-\frac{1}{2\sqrt{2}}$	0	$\frac{1}{2\sqrt{2}}$	$\frac{1}{2\sqrt{2}}$	0	$-\frac{1}{2\sqrt{2}}$	$\frac{1}{2\sqrt{2}}$	0
$-\frac{1+\alpha}{2}$	ξ_4	β_1	$-\beta_2$	$-\beta_2$	β_1	β_2	β_2	β_1	β_2	$-\beta_2$	β_1	$-\beta_2$	β_2
$-\frac{1+\alpha}{2}$	ξ_5	$-\beta_2$	β_1	$-\beta_2$	β_2	β_1	$-\beta_2$	β_2	β_1	β_2	$-\beta_2$	β_1	β_2
$-\frac{1+\alpha}{2}$	ξ_6	$-\beta_2$	$-\beta_2$	β_1	β_2	$-\beta_2$	β_1	$-\beta_2$	β_2	β_1	β_2	β_2	β_1
$\frac{\alpha-1}{2}$	ξ_7	β_3	β_4	β_4	β_3	$-\beta_4$	$-\beta_4$	β_3	$-\beta_4$	β_4	β_3	β_4	$-\beta_4$
$\frac{\alpha-1}{2}$	ξ_8	β_4	β_3	β_4	$-\beta_4$	β_3	β_4	$-\beta_4$	β_3	$-\beta_4$	$+\beta_4$	β_3	$-\beta_4$
$\frac{\alpha-1}{2}$	ξ_9	β_4	β_4	β_3	$-\beta_4$	β_4	β_3	β_4	$-\beta_4$	β_3	$-\beta_4$	$-\beta_4$	β_3
-10	ξ_{10}	$\frac{1}{2\sqrt{3}}$	$\frac{1}{2\sqrt{3}}$	$\frac{1}{2\sqrt{3}}$	$\frac{1}{2\sqrt{3}}$	$-\frac{1}{2\sqrt{3}}$	$-\frac{1}{2\sqrt{3}}$	$-\frac{1}{2\sqrt{3}}$	$\frac{1}{2\sqrt{3}}$	$-\frac{1}{2\sqrt{3}}$	$-\frac{1}{2\sqrt{3}}$	$-\frac{1}{2\sqrt{3}}$	$\frac{1}{2\sqrt{3}}$
-1	ξ_{11}	0	$\frac{1}{2\sqrt{2}}$	$-\frac{1}{2\sqrt{2}}$	0	$-\frac{1}{2\sqrt{2}}$	$\frac{1}{2\sqrt{2}}$	0	$\frac{1}{2\sqrt{2}}$	$\frac{1}{2\sqrt{2}}$	0	$-\frac{1}{2\sqrt{2}}$	$-\frac{1}{2\sqrt{2}}$
-1	ξ_{12}	$\frac{1}{\sqrt{6}}$	$-\frac{1}{2\sqrt{6}}$	$-\frac{1}{2\sqrt{6}}$	$1\ \sqrt{6}$	$\frac{1}{2\sqrt{6}}$	$\frac{1}{2\sqrt{6}}$	$-\frac{1}{1/\sqrt{6}}$	$-\frac{1}{2\sqrt{6}}$	$\frac{1}{2\sqrt{6}}$	$-1/\sqrt{6}$	$\frac{1}{2/\sqrt{6}}$	$-\frac{1}{2\sqrt{6}}$

From (1.6) and (2.2) we have

$$\omega_j^2 = \omega_0^2 - \frac{1}{2}\frac{e^2}{m}\frac{1}{l^3}\lambda_j. \tag{3.1}$$

or, introducing the frequency per second, ν:

$$\nu_j^2 = \nu_0^2 - \frac{e^2}{8\pi^2 m}\frac{1}{l^3}\lambda_j. \tag{3.2}$$

Instead of l, we introduce a frequency of coupling given by

$$\nu_c = \sqrt{\frac{e^2}{8\pi^2 m l^3}}\,\sec^{-1}, \tag{3.3}$$

so that

$$\nu_j^2 = \nu_0^2 - \lambda_j\,\nu_c^2. \tag{3.4}$$

While the system possesses 12 degrees of freedom, it is degenerate in that we get only five distinct frequencies corresponding to the five distinct roots of the secular equation.

(1) λ_{I}—Comparison of the first three lines in the scheme of the components of the eigenvectors with the equilibrium co-ordinates given in (1.1) shows that these vibrations represent rotations around the co-ordinate axes.

(2) λ_{II}—This frequency corresponds to a triple root of the secular equation. We consider, for instance, the motion denoted by ξ_4. This motion consists of a displacement of each particle parallel to the x-axis, and a simultaneous displacement of particles 1 and 2 and 3 and 4, respectively along the lines joining them, the first pair moving towards each other while the second moves away from each other and *vice versa.*

The motions denoted by ξ_5 and ξ_6 will be similar with respect to the y and z axes instead of the x axis.

(3) λ_{III}—This also corresponds to a triple root of the secular equation, the motion will be identical in character to that corresponding to λ_{II} except for the differences in the amplitude and phase.

(4) λ_{IV}—This corresponds to a single root of the secular equation. The motion is always such that the four vibrators lie at the corners of a regular tetrahedron. The vibration is completely symmetrical.

(5) λ_{V}—This corresponds to a double root of the secular equation. The distance of each vibrator k from the origin is always r_k, the equilibrium distance, provided we neglect the squares of the

amplitude. The motion of the vibrators is confined to the surface of a sphere.

4—TWISTING OF THE REGULAR TETRAHEDRON

The x-axis is the line of centres of the pairs 1 and 2 and 3 and 4; about this line of centres the pair 3 and 4 is twisted through a small angle ϕ. The changed co-ordinates of the points 3 and 4 will be

$$\left.\begin{array}{ll} (3) & \frac{l}{2\sqrt{2}}(-1, (1+\phi);\ -(1-\phi)) \\ (4) & \frac{l}{2\sqrt{2}}(-1;\ -(1+\phi);\ (1-\phi)) \end{array}\right\} \tag{4.1}$$

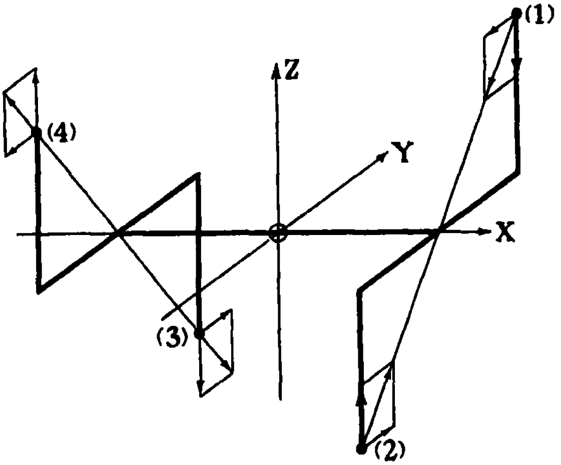

FIG. 2.

This twist introduces a small change in the potential energy of the original system. Denoting the new values of the coupling forces by S'^{kl}_{xy}, we shall obtain an expansion of the type

$$S'^{kl}_{xy} = S^{kl}_{xy} + \phi\,\Delta_1(S^{k,l}_{xy}) + \dots \tag{4.2}$$

We have, for example:

$$\begin{aligned} S'^{1,3}_{xx} &= \frac{e^2}{m}\frac{1}{r'^5_{kl}}(3x'_{1,3}x'_{1,3} - r'^2_{1,3}) \\ &= \frac{e^2}{m}\frac{l^2}{l^5\left(1-\frac{\phi}{2}\right)^{5/2}}\left\{\tfrac{3}{2} - \left(1-\frac{\phi}{2}\right)\right\} \\ &= S^{1,3}_{xx} + \frac{e^2}{ml^3}\tfrac{9}{8}\,\phi, \end{aligned}$$

therefore

$$\Delta_1 (S^{1,3}_{xx}) = \frac{e^2}{ml^3}\tfrac{9}{8}. \tag{4.3}$$

Putting

$$a'^{kl}_{xy} = \frac{1}{\tfrac{1}{2}\dfrac{e^2}{m}\dfrac{1}{l^3}} S'^{kl}_{xy}, \tag{4.4}$$

we have

$$\Delta_1 (a'^{1,3}_{xx}) = \tfrac{9}{4}. \tag{4.5}$$

The perturbation function will be given by

$$\tfrac{1}{2}\phi \sum_{k,l}{}' \sum_{x,y} \Delta_1 (a'^{kl}_{xy})\, u_k v_l. \tag{4.6}$$

Substituting the values of $\Delta_1 (a'^{kl}_{xy})$ the perturbation function is

$$\begin{aligned}\phi\, [&\tfrac{9}{4}(u_1u_3 - u_1u_4 - u_2u_3 + u_2u_4) + \tfrac{3}{2}(-v_1v_3 + w_1w_4 + w_2w_3 - v_2v_4)\\ &+ \tfrac{3}{4}(-w_1w_3 + v_1v_4 + v_2v_3 - w_2w_4) + 6\,(v_3v_4 - w_3w_4)\\ &+ \tfrac{3}{2}\{(u_1 + u_2 + w_1 - w_2)(v_4 - v_3) + (u_1 + u_2 + v_1 - v_2)(w_4 - w_3)\\ &+ (v_1 + v_2 + w_1 + w_2)(u_4 - u_3)\}].\end{aligned} \tag{4.7}$$

The (u_k, v_k, w_k) are expressed in terms of the ξ's with the help of (2.11), and the perturbation function will be obtained in the form

$$\phi \sum_{j,h=1}^{12} \alpha_{jh}\xi_j\xi_h. \tag{4.8}$$

The values of the α's are found to be as follows:

$$\alpha_{ii} = 0,$$

$$\alpha_{ij} = 0 \quad \text{for} \quad i = 1, 4, 7, 10, 11 \text{ or } 12$$
$$\text{and} \quad j = 2, 3, 5, 6, 8 \text{ or } 9.$$

$$\alpha_{1,4} = \left\{\frac{3\beta}{4\sqrt{1+\beta^2}} + \frac{3}{\sqrt{2}\sqrt{1+\beta^2}}\right\}; \quad \alpha_{1,7} = \left\{-\frac{3}{4\sqrt{1+\beta^2}} + \frac{3\beta}{\sqrt{2}\sqrt{1+\beta^2}}\right\};$$

$$\alpha_{1,10} = \frac{5\sqrt{3}}{\sqrt{2}}; \quad \alpha_{1,12} = -\sqrt{3};$$

$$\alpha_{4,11} = -\frac{3}{\sqrt{2}\sqrt{1+\beta^2}}; \quad \alpha_{7,11} = -\frac{3\beta}{\sqrt{2}\sqrt{1+\beta^2}};$$

$$\alpha_{10,11} = -\frac{9\sqrt{3}}{2\sqrt{2}}; \quad \alpha_{11,12} = \frac{9}{4\sqrt{3}};$$

$$\alpha_{2,2} = -\alpha_{3,3} = -\tfrac{45}{16}; \quad \alpha_{5,5} = -\alpha_{6,6} = \frac{-21\beta^2 + 18}{16(1+\beta^2)} - \frac{3\beta}{2\sqrt{2}(1+\beta^2)};$$

$$\alpha_{8,8} = -\alpha_{9,9} = \frac{18\beta^2 - 21}{16(1+\beta^2)} + \frac{3\beta}{2\sqrt{2}(1+\beta^2)};$$

$$\alpha_{2,5} = \alpha_{3,6} = -\left\{\frac{3\beta}{8\sqrt{1+\beta^2}} + \frac{3}{2\sqrt{2}\sqrt{1+\beta^2}}\right\};$$

$$\alpha_{2,6} = \alpha_{3,5} = \frac{3\beta}{2\sqrt{1+\beta^2}} + \frac{3}{2\sqrt{2}\sqrt{1+\beta^2}};$$

$$\alpha_{2,8} = \alpha_{3,9} = \frac{3}{8\sqrt{1+\beta^2}} - \frac{3\beta}{2\sqrt{2}\sqrt{1+\beta^2}};$$

$$\alpha_{2,9} = \alpha_{3,8} = \frac{3\beta}{2\sqrt{2}\sqrt{1+\beta^2}} - \frac{3}{2\sqrt{1+\beta^2}};$$

$$\alpha_{5,8} = -\alpha_{6,9} = \frac{3(1-\beta^2)}{2\sqrt{2}(1+\beta^2)} + \frac{39\beta}{8(1+\beta^2)};$$

$$\alpha_{5,9} = -\alpha_{6,8} = -\frac{9}{2\sqrt{2}}.$$

From these values we have the following relations:

$$\begin{aligned} \alpha_{1,4} + \alpha_{2,5} + \alpha_{3,6} &= 0, \\ \alpha_{1,7} + \alpha_{2,8} + \alpha_{3,9} &= 0. \end{aligned} \tag{4.9}$$

Instead of ξ_{11} and ξ_{12} we introduce ξ'_{11} and ξ'_{12} given by

$$\xi'_{11} = \frac{\xi_{11} + \xi_{12}}{\sqrt{2}}; \qquad \xi'_{12} = \frac{\xi_{11} - \xi_{12}}{\sqrt{2}}. \tag{4.10}$$

The new corresponding coefficients will be given by

$$\alpha'_{h,11} = \frac{1}{\sqrt{2}}(\alpha_{h,11} + \alpha_{h,12}); \qquad \alpha'_{h,12} = \frac{1}{\sqrt{2}}(\alpha_{h,11} - \alpha_{h,12})$$

for $h = 1, 2, 3, \ldots 10$.

$$\alpha'_{11,11} = -\alpha'_{12,12} = \frac{\alpha_{11,12}}{2} \qquad \text{and} \qquad \alpha'_{11,12} = 0.$$

We shall now denote these new ξ's and the new α's without the dashes. Making the following substitutions:

$$\left.\begin{aligned} &\left\{\begin{aligned} \lambda_1^0 &= \lambda_{\mathrm{I}}, & \lambda_7^0 &= \lambda_{\mathrm{III}}. \\ \lambda_2^0 &= \lambda_{\mathrm{I}} + 2\alpha_{2,2}\phi, & \lambda_8^0 &= \lambda_{\mathrm{III}} + 2\alpha_{8,8}\phi, \\ \lambda_3^0 &= \lambda_{\mathrm{I}} - 2\alpha_{2,2}\phi, & \lambda_9^0 &= \lambda_{\mathrm{III}} - 2\alpha_{9,9}\phi, \end{aligned}\right. \\ &\left\{\begin{aligned} \lambda_4^0 &= \lambda_{\mathrm{II}}, & \lambda_{10}^0 &= \lambda_{\mathrm{IV}}, \\ \lambda_5^0 &= \lambda_{\mathrm{II}} + 2\alpha_{5,5}\phi, & \lambda_{11}^0 &= \lambda_{\mathrm{V}} + 2\alpha_{11,11}\phi, \\ \lambda_6^0 &= \lambda_{\mathrm{II}} - 2\alpha_{5,5}\phi, & \lambda_{12}^0 &= \lambda_{\mathrm{V}} - 2\alpha_{11,11}\phi. \end{aligned}\right. \end{aligned}\right\} \tag{4.11}$$

The equations of motion of the perturbed system will be given by

$$(\lambda - \lambda_j^0)\,\xi_j = \phi \sum_h{}' \alpha_{jh}\xi_h, \tag{4.12}$$

where the dash over the summation sign denotes that the term $j = h$ does not occur.

ϕ is a small angle; treating the right-hand sides of (4.12) as small perturbation terms, the equations can be solved by a method of approximation.

The zero order approximation is given by

$$\lambda = \lambda_i^0; \quad \xi_{ij}^{(0)} = \delta_{ij}. \tag{4.13}$$

The first order approximation is determined by the equation

$$(\lambda_i^0 - \lambda_j^0)\,\xi_j^{(1)} = -\lambda_j^{(1)}\,\xi_i^{(0)} + \phi\alpha_{ji}. \tag{4.14}$$

The solutions are

$$\lambda_i^{(1)} = \phi\alpha_{ii} = 0, \qquad \text{if } i = j, \tag{4.15}$$

$$\xi_i^{(1)} = \phi\,\frac{\alpha_{ji}}{\lambda_i^0 - \lambda_j^0}, \qquad \text{if } i \neq j. \tag{4.16}$$

The normalizing condition

$$\sum_j (\xi_{ij})^2 = \sum_j \{(\xi_{ij}^{(0)})^2 + 2\,\xi_{ij}^{(0)}\,\xi_{ij}^{(1)} + \dots\} = 1 \tag{4.17}$$

gives

$$\xi_{ii}^{(1)} = 0. \tag{4.18}$$

$\xi_{ji}^{(1)}$ denotes the amplitude of ξ_j for the vibration having the frequency ν_i.

We define eigenvectors e_i^k given by

$$e_i^k = \Sigma\,(e_{ij}^{(0)k} + e_{ij}^{(1)k}), \tag{4.19}$$

where

$$e_{ij}^{(0)k} = e_i^{(0)k}\,\delta_{ij}, \tag{4.20}$$

and

$$e_{ij}^{(1)k} = \phi\,\frac{\alpha_{ij}}{\lambda_i^0 - \lambda_j^0}\,e_j^{(0)k}. \tag{4.21}$$

The values of the components of $e_j^{(0)k}$ are given in Table I.

5—The Rotation Parameter and Optical Activity

Defining the vectors $\mathbf{L}_i$ and $\mathbf{R}_i$ as follows:

$$\mathbf{L}_i = \frac{e}{\sqrt{m}} \sum_{k=1}^{4} e_i^k, \tag{5.1}$$

$$\mathbf{R}_i = \frac{e}{\sqrt{m}} \sum_{k=1}^{4} [e_i^k \times r_k]. \tag{5.2}$$

The rotation parameter is given by*

$$g = \frac{2\pi}{\lambda} \frac{1}{3} \sum_{i=1}^{12} \frac{L_i R_i}{\omega_i^2 - \omega^2}. \tag{5.3}$$

Substituting from (4.19) we have

$$L_i R_i = \frac{e^2}{m} \sum_k \sum_j \left(e_i^{(0)k} \delta_{ij} + \phi \frac{\alpha_{ij} e_j^{(0)k}}{\lambda_i^0 - \lambda_j^0} \right) \sum_k \sum_j \left[\left(e_i^{(0)k} \delta_{ij} + \phi \frac{\alpha_{ij} e_j^{(0)k}}{\lambda_i^0 - \lambda_j^0} \right) \times r_k \right].$$

Since

$$e_i^{(0)k} [e_i^{(0)k} \times r_k] = 0,$$

we get

$$L_i R_i = \frac{e^2}{m} \phi \left\{ \left(\sum_k e_i^{(0)k}\right) . \sum_k \sum_j{}' \frac{\alpha_{ij}}{\lambda_i^0 - \lambda_j^0} [e_j^{(0)k} \times r_k] \right.$$

$$\left. + \sum_k \sum_j{}' \frac{\alpha_{ij}}{\lambda_i^0 - \lambda_j^0} e_j^{(0)k} \sum_k [e_i^{(0)k} \times r_k] \right\}.$$

The 12 terms in g ($i = 1, 2, .., 12$) can be divided into five different groups corresponding to five distinct frequencies of the untwisted tetrahedron model. We expand the difference terms in the denominator, binomially in power series of ϕ, so that only the differences of the five frequencies given in (3.4) and of the five roots given in (2.7) occur. On account of the equal values of some of the α's and the relations (4.9), the terms in ϕ and ϕ^2 are found to be zero. Thus retaining only the first non-vanishing term we obtain

$$g = \frac{2\pi}{3\lambda} \times \frac{1}{4\pi^2} \frac{e^2}{m} l \phi^3 \sum_{i \; \mathrm{I}}^{\mathrm{V}} \frac{F_i}{\nu_i^2 - \nu^2}. \tag{5.4}$$

The values of F_i for $i = \mathrm{I}, \mathrm{II}, \mathrm{III}, \mathrm{IV}$, and V are

$$\left.\begin{aligned}
F_{\mathrm{I}} &= \left\{ -40{\cdot}3 - 41{\cdot}44 \frac{\nu_c^2}{\nu_{\mathrm{I}}^2 - \nu^2} - 50{\cdot}5 \left(\frac{\nu_c^2}{\nu_{\mathrm{I}}^2 - \nu^2} \right)^2 \right\}, \\
F_{\mathrm{II}} &= \left\{ 0{\cdot}1 + 0{\cdot}37 \frac{\nu_c^2}{\nu_{\mathrm{II}}^2 - \nu^2} + 0{\cdot}63 \left(\frac{\nu_c^2}{\nu_{\mathrm{II}}^2 - \nu^2} \right)^2 \right\}, \\
F_{\mathrm{III}} &= \left\{ 41{\cdot}8 - 9{\cdot}0 \frac{\nu_c^2}{\nu_{\mathrm{III}}^2 - \nu^2} + 1{\cdot}89 \left(\frac{\nu_c^2}{\nu_{\mathrm{III}}^2 - \nu^2} \right)^2 \right\}, \\
F_{\mathrm{IV}} &= 0, \\
F_{\mathrm{V}} &= \left\{ -0{\cdot}01 - 0{\cdot}43 \frac{\nu_c^2}{\nu_{\mathrm{V}}^2 - \nu^2} \right\}.
\end{aligned}\right\} \tag{5.5}$$

The factor F_{IV} is zero, so that the contribution to the rotation parameter by the frequency ν_{IV} is nil. This is to be expected from the symmetrical nature of the vibrations corresponding to this frequency.

---

* Born, "Optik," § 99 (7).

The angle of rotation of the plane of polarization per unit length is given by

$$\chi = \frac{8\pi^2}{3} \mathbf{N} \frac{n^2+2}{n\lambda_0} g, \tag{5.6}$$

where $\mathbf{N}$ is the number of active molecules per unit volume, λ_0 the wavelength in vacuum, and n the index of refraction.

The molar rotation per unit length is defined as

$$\chi_M = \frac{\mu}{\rho} \frac{3}{n^2+2} \chi, \tag{5.7}$$

where μ and ρ are the molecular weight and the density. From (5.6) we get

$$\chi_M = \frac{8\pi^2}{n\lambda_0} \mathrm{N} g, \tag{5.8}$$

where the Avogadro's number

$$\mathrm{N} = \frac{\mu \mathbf{N}}{\rho}. \tag{5.9}$$

Defining an absolute frequency, the molar frequency, which occurs in all dispersion problems, by

$$\nu_M = \sqrt{\frac{\mathrm{N}e^2}{\pi m}} \tag{5.10}$$

and substituting the value of g from (5.4), we get

$$\lambda_0 \chi_M = \frac{4\pi^2}{3} \frac{d}{\lambda_0} \phi^3 \nu_M^2 \sum_{i=1}^{5} \frac{F_i}{\nu_i^2 - \nu^2}, \tag{5.12}$$

both sides of which are dimensionless.

Since the angle of rotation depends on the cube of ϕ, its sign will depend on the cense of this angle of twist.

I wish to thank Professor M. Born for his very great help and guidance in writing this paper.

SUMMARY

A system of four identical vibrators at the corners of a tetrahedron, mutually interacting, gives five different characteristic frequencies. If one pair of vibrators is twisted round the line of centres, the distorted system becomes optically active. The angle of optical rotation is calculated in terms of the five characteristic frequencies, the edge of the tetrahedron, and the angle of twist.

The Scattering of Fast β-Particles by Nitrogen Nuclei

By F. C. CHAMPION, M.A., Ph.D., Lecturer in Physics, King's College, London

(*Communicated by E. V. Appleton, F.R.S.—Received July* 23, 1935)

INTRODUCTION

Of the many conflicting experiments* which have been performed on the single scattering of fast β-particles by atomic nuclei, it is generally accepted that the most reliable are those of Chadwick and Mercier,† and of Neher.‡ The former experimenters used the annular ring method and an ionization chamber to examine the scattering of the non-homogeneous β-rays from RaE by an aluminium foil, between angles of 20° and 40°. The results were in fair agreement with Darwin's classical relativistic formula§:

$$q = \pi n t \left(\frac{Ze^2}{m_0 c^2}\right)^2 . \frac{(1-\beta^2)}{\beta^4} . \beta^2 \operatorname{cosec}^2 \psi, \qquad (1)$$

where

q = fraction scattered through an angle greater than θ,

Z, t and n = atomic number, number of atoms per cc, and thickness of scatterer respectively,

e and m_0 = charge and rest mass of electron,

$\beta = v/c$ = ratio of velocity of β-particle to that of light, and

ψ is defined by the relation

$$\beta \cot \psi = \tan \left[\pi - \tfrac{1}{2}(\pi + \theta) \cos \psi\right]. \qquad (2)$$

The experiments of Neher, however, using cathode rays with energies up to 145 kV, corresponding to $\beta = 0 \cdot 63$, showed that the number of β-particles scattered by aluminium nuclei between angles $\theta_1 = 95°$ and $\theta_2 = 172°$ was only about one-third that predicted by Darwin's formula. That the classical theory would fail under these conditions was to be expected since the de Broglie wave-length associated with the cathode rays was much longer than the closest distance of approach as calculated on classical mechanics. The results were in much better agreement with the following formula deduced on the basis of wave mechanics by Mott*

---

* Rutherford, Chadwick, and Ellis, "Radiations from Radioactive Substances," p. 215 *et seq*. (1930).

† 'Phil. Mag.,' vol. 50, p. 208 (1925).

‡ 'Phys. Rev.,' vol. 38, p. 1321 (1931).

§ 'Phil. Mag.,' vol. 25, p. 201 (1913).

$$q = \pi nt \left(\frac{Ze^2}{m_0c^2}\right)^2 . \frac{(1-\beta^2)}{\beta^4}\left[\cot^2 \tfrac{1}{2}\theta_1 - \cot^2 \tfrac{1}{2}\theta_2 - 2\beta^2 \log \frac{\sin \frac{1}{2}\theta_2}{\sin \frac{1}{2}\theta_1}\right]. \qquad (3)$$

In the investigation described below, a study has been made of the scattering of fast β-particles by nitrogen nuclei over the whole range of angles between 20° and 180° for known velocities lying between $\beta = 0\cdot828$ and $\beta = 0\cdot950$.

EXPERIMENTAL

The present work completes the analysis of the 20,000 tracks of fast β-particles in nitrogen, photographed with an automatic expansion chamber.† The experimental work has already been described; it should be mentioned, however, that the analysis of the nuclear scattering of fast β-particles is infinitely more lengthy and tedious than that of electron scattering. With the latter, the heavily ionized recoil track greatly facilitates the process of searching for collisions, but with the former the eye must be cast along each track individually. As a further precaution against missing collisions, it was found necessary to count only those collisions in which the β-particle was deflected in a direction opposite to the original direction of curvature of the β-particle in the applied magnetic field. The collision is then indicated by a cusp in an otherwise smooth curve. With this criterion the number of collisions to be expected is one-half that given by equations (1) or (3).

RESULTS

In 875 metres of track, 201 collisions of fast β-particles with nitrogen nuclei have been observed in which the β-particle is scattered through more than 20°. Values of θ below 20° were not considered, partly owing to the greatly increased number of measurements which would be involved and partly owing to the increased difficulty in fixing a definite value of the lower limit.

A general survey of the results is afforded by the statistical diagram in fig. 1 in which each dot corresponds to an observed value of θ and β.

---

* 'Proc. Roy. Soc.,' A, vol. 124, p. 426 (1929).

† Champion, 'Proc. Roy. Soc.,' A, vol. 134, p. 672 (1932); *ibid.*, vol. 136, p. 630 (1932); *ibid.*, vol. 137, p. 688 (1932).

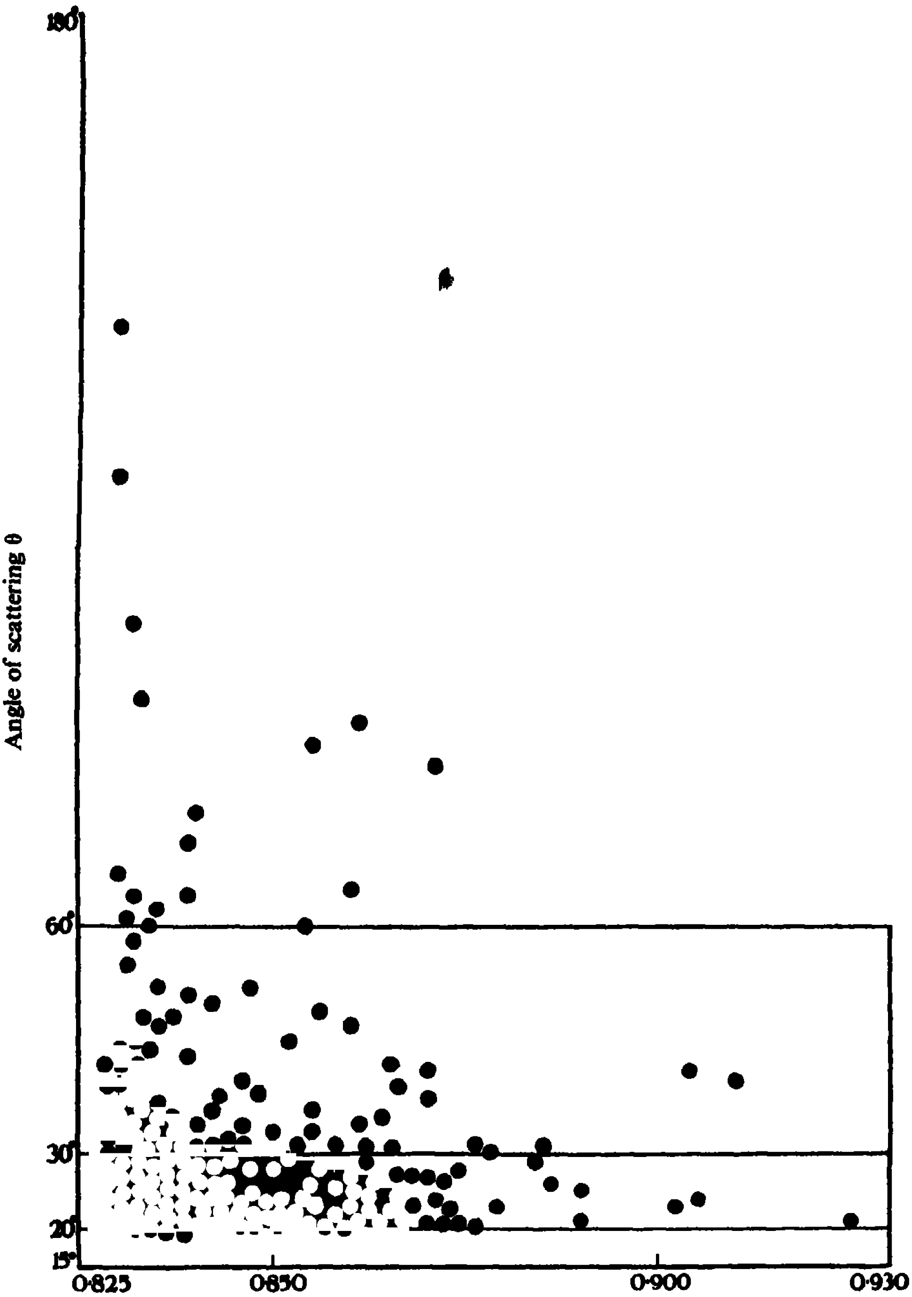
180°
60°
30°
20°
15°
Angle of scattering θ
0·825
0·850
0·900
0·930
Velocity β = v/c

FIG. 1.

The density of the dots then represents the intensity of the scattering. The number of collisions is observed to fall off rapidly with increasing value of θ, but it should be noted that the chief factor influencing the decrease in the number of dots in passing from left to right across the scattering diagram is the distribution of velocity in the β-ray spectrum of RaE and not simply the smaller chance of scattering for a higher velocity.

For comparison between theory and experiment the statistical diagram has been divided into three cells with angular limits 20° to 30°, 30° to 60°, and 60° to 180° respectively. The scattering formulae of equations (1) and (3) have then been integrated between the limits of $\beta = 0\cdot828$ to the end of the β-ray spectrum of RaE at about $\beta = 0\cdot95$ (Champion, *loc. cit.*). The final results are collected in Table I, column 1 giving the angular limits of θ and column 2 the observed number of dots in each cell. The numbers predicted on Mott's theory and Darwin's formula are given in columns 3 and 4 respectively. Column 5 gives the numbers predicted on non-relativistic classical theory, while column 6 gives the values obtained by substituting $m_0/(1 - \beta^2)^{\frac{1}{2}}$ for m_0 in the non-relativistic classical formula.

TABLE I

1 θ	2 Obs.	3 Mott	4 Darwin	5 Classical	6 $C(1 - \beta^2)$
20°–30°	111	142	146	579	145
30°–60°	73	80	108	347	86
60°–180°	17	16	50	95	26
20°–180°	201	238	304	1021	257

DISCUSSION

It will at once be seen that over the entire range the most satisfactory agreement is with Mott's formula, Darwin's formula predicting a scattering 50% larger than that observed between angles of 30° and 60° and nearly 300% greater than that occurring between 60° and 180°. For the large angle scattering, therefore, the results are in substantial agreement with those of Neher. For smaller angles of scattering, however, the results support those of Chadwick and Mercier; but this is to be expected since the values predicted by the two theoretical formulae converge in this region. The ordinary classical non-relativistic formula gives results many times too large; but it is interesting to note that even at large angles, the classical formula, multiplied by a factor $(1 - \beta^2)$, gives results in fair agreement with experiment. The same empirical adjustment of the classical formula has been shown previously to be of use in giving a quick approximation when the scattering of fast β-particles by electrons is under consideration.* Between the angles of 20° and 30° the results are considerably less than those predicted by any of the formulae. Too much stress must not be laid on this disagreement as it is possible that it is due to the difficulty of determining which collisions shall be rejected at the lower limit.†

Owing to statistical fluctuations, it is not possible to say whether the present results support Neher in finding that to within 5% the number of β-particles scattered between 95° and 172° was 1·32 times that predicted by Mott's theory. On the other hand, the advantages of the expansion method are that it may be stated with certainty that none of the scattered β-particles was a secondary electron and that no plural scattering occurred. Further, if energy is lost during the nuclear encounter, it has the possibility of being registered in three ways. First, if the loss in energy were greater than 15% of that of the incident β-particle, the difference in the curvature of the track in the magnetic field before and after collision would be easily detectable. Measurements on 100 suitable collisions failed to detect any energy loss. Second, if the loss were greater than 20%, the increase in specific ionization after collision would be observable: none was found. Finally, it is possible that the radiation might be absorbed in the extra-nuclear structure of the same atom and give rise, by the Auger effect, to a photo-electron. One such case has been observed, the β-particle suffering a deflexion of about 120° and giving rise simultaneously to a short branch track. Owing to scattering and to the presence of the magnetic field, the branch track is very irregular; but from range considerations its energy may be approximately estimated as 40,000 volts, that is about 5% of that of the incident β-particle. Kramer's‡ classical radiation theory is not applicable when fast β-particles are deflected through even moderately large angles; but a treatment by Mott§ on the quantum theory has been applied to deduce the probability of a loss of energy greater than 15% for β-particles with $\beta = 0 \cdot 85$ incident upon nitrogen nuclei and scattered through angles greater than 20°. For all angles the probability is much less than 1%. The present results therefore support Mott in regarding radiation as a factor unlikely to influence the scattering formula.

It may be remarked that there is no evidence for the creation of positive electrons such as have been observed by Skobeltzyn and Stepanowa* when fast β-particles make nuclear encounters. It is very unlikely that the one short branch track observed is due to the creation of a positive electron since the original β-particle would then have lost over 50% of its energy, whereas no marked increase in specific ionization or curvature was observed after the collision. It is possible that the probability of the creation of positive electrons increases rapidly as the energy of the incident β-particles is increased above one million volts.

---

* Champion (*loc. cit.*).

† *Cf.* Blackett and Champion, 'Proc. Roy. Soc.,' A, vol. 130, p. 380 (1931).

‡ 'Phil. Mag.,' vol. 46, p. 826 (1923).

§ 'Proc. Camb. Phil. Soc.,' vol. 27, p. 255 (1931).

The writer wishes to express his thanks for a Government Grant from the Royal Society which enabled him to purchase a microscope for the analysis of the photographs.

SUMMARY

Using an automatic expansion chamber, the scattering of fast β-particles by nitrogen nuclei is examined between 20° and 180°. The results were in good agreement with the formula deduced by Mott on the basis of wave mechanics and justify the neglect of radiation losses in deducing the scattering law.

---

* 'J. Phys. Rad.,' vol. 6, p. 1 (1935).

The Formation of Mercury Molecules

By F. L. ARNOT, Ph.D., Lecturer in Natural Philosophy, and J. C. MILLIGAN, M.A., B.Sc., The University, St. Andrews

(*Communicated by H. S. Allen, F.R.S.—Received July* 25, 1935)

INTRODUCTION

Mercury molecules in the vapour state have never been directly detected. The ratio of the specific heats and vapour density determinations all show that mercury vapour is strictly monatomic, so that so far as chemical evidence is concerned mercury vapour molecules do not exist. However, the occurrence of quite strong bands in the absorption and emission spectra of mercury vapour at high pressure demand the presence of molecules in considerable number.

We have obtained definite evidence that diatomic molecules are formed in mercury vapour by the attachment of excited atoms to normal atoms. The formation of the molecules in this way clearly reconciles the chemical evidence of their non-existence with the band spectra evidence of their presence; for, unless the atoms are excited by light or electron impact, the vapour may remain practically monatomic.

APPARATUS

Fig. 1 is a scale drawing of the apparatus which consists essentially of an ionization chamber and a magnetic analyser. The analyser was constructed of brass sheet with the exception of the soft ion tube T. This tube was fitted with a water cooler C, on top of which was a trough containing Lilliendahl's white vacuum wax No. 849A, into which the end of the ionization chamber was set. The wax could be melted by passing steam through the water cooler. After construction the entire analyser, including the ion tube T and the Faraday cylinder A, was electroplated, first with copper and then with a coat of nickel, which adheres well to a copper surface. In order to make the copper adhere to the soldered joints of the analyser, it was found necessary to use an electrolyte of cuprocyanide of sodium.* The nickel coating prevents amalgamation of mercury with the solder and brass of the analyser, besides ensuring that the latter is vacuum tight.

---

* *See* Richard Threlfall's "Laboratory Arts," p. 313.

The Faraday cylinder A was supported on a quartz tube passing through an ebonite cap containing a ring of sulphur. The right-hand outlet tube of the analyser was connected through a liquid air trap of large diameter to a mercury diffusion pump backed by a Hyvac pump. The left-hand outlet tube was connected through another liquid air trap to a McLeod gauge. The connexions to both liquid air traps were as short as possible (10 cm), so as to reduce the pressure of mercury vapour in the analyser to a minimum.

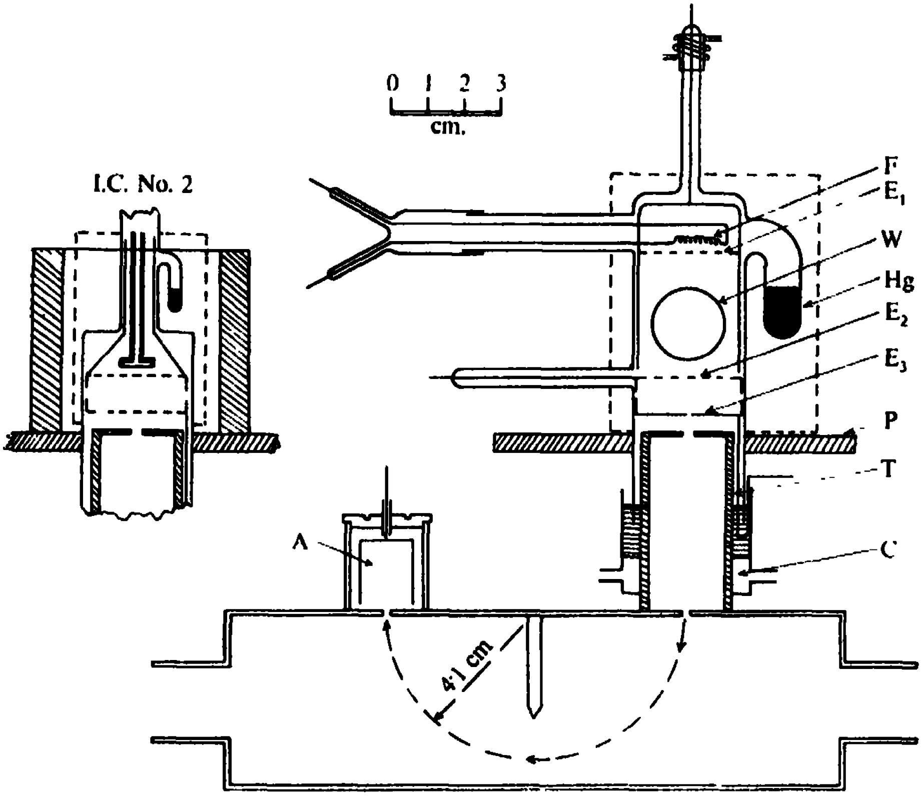

Fig. 1.

The analyser was set in a gap of 1 cm between the poles of a large electromagnet. When accelerated into the analyser by a potential drop of 100 volts the mercury molecular ion required a field of 7020 gauss for it to be brought into the Faraday cylinder. This required a current of 2·27 amps in the magnet coils. Since the battery supplying this current was not otherwise used during any of the runs recorded here, the magnet current remained absolutely steady.

The analysis of the ions was made by varying the magnet current, and not by varying the accelerating potential, as is the usual practice. The reason for this procedure was to keep the thickness of the positive ion sheath on E_3 constant; and more especially since scattering of the ions, including loss by neutralization, in the analyser would vary considerably with the accelerating potential.

Calibration of the magnet was made with a search coil and Grassot fluxmeter. The field was found to be accurately proportional to the current in the coils up to a value of 10,000 gauss, and the field produced by any given current was always the same provided the current was first taken to a higher value and then reduced to the required value.

The ionization chamber was made of clear fused quartz with an optically plane window W, 2 cm in diameter, in one side and a conical light trap on the opposite side. These adjuncts, which were not used in the present work, were added to the chamber to enable a study of photoionization of the vapour by the resonance line 2537 A to be carried out.

The electrodes E_1 and E_2 are nickel cylinders open at the lower end and covered with nickel gauze at the other end. E_3 is a short nickel cylinder having its lower end closed by a nickel plate with a slit 1 mm × 8 mm in the centre. This electrode was pressed out of a single piece of nickel, and was made to fit very tightly into the quartz tube, thus effectively dividing the ionization chamber into two parts, the narrow slit being the only opening between them. The object of this was to decrease to a minimum the diffusion of mercury vapour from the upper or high-pressure side of the slit to the low-pressure side. A high-pressure of mercury vapour was maintained on the upper side of this slit by an electric furnace, outlined in fig. 1 by the broken line. The vapour which diffused through the slit was condensed on the top and sides of the tube T which was kept cold by the water cooler C. Very little condensation of mercury occurred on the electrode E_3, for this was practically at the temperature of the furnace, since it was thermally insulated from the cold tube T by the whole length of quartz down to the wax joint.

The slit in the top of the tube T was 3 mm × 10 mm, and the two other slits in the analyser were 2 mm × 8 mm. The magnetic field in the ionization chamber due to the stray field of the magnet was considerably reduced by the soft ion plate P. The electric furnace was non-inductively wound, and no alteration in the ion currents could be detected when it was switched off and on. The leads to the electrodes entered through hard wax seals, the seal on top of the chamber being water-cooled.

The tungsten filament F was 0·15 mm in diameter, and had various lengths on different occasions. The results shown in figs. 2, 3, 4, 5 were obtained with a close-coiled filament having a potential drop across it of 14 volts. The results shown in figs. 6, 7, 8 were obtained with a short straight filament having a potential drop across it of less than 2 volts.

The potential used to accelerate the electrons to E_1 will be denoted throughout this paper by V_0. This potential drop will all occur across a very thin positive ion sheath formed over the surface of the filament, except when V_0 is below the ionization potential. In general, a small potential of 10 volts was put between E_1 and E_2. This potential drop, denoted by V_1, will also all be concentrated in a very thin positive ion sheath on the surface of E_2, so that nearly all the space between F and E_2 will be field-free. The potential drop V_2 between E_2 and E_3 was in nearly all cases about 90 volts. E_3 was connected to the ion tube T and earthed. Certain results given in fig. 2 show that for high values of V_0 the whole of the potential drop V_2 occurs across a very thin positive ion sheath formed on the surface of E_3. The positive ion sheaths will, of course, be absent when V_0 is below the ionization potential, and will not be so thin when V_0 is just above the ionization potential as they are when V_0 is large (30 to 200 volts), for the ionization produced will then be much less. The actual values of these potentials will be given when discussing the results.

In order to obtain the appearance potential for the Hg_2^+ ion the intensity of the ion currents were considerably increased by using a smaller ionization chamber, shown as an inset in fig. 1. The essential differences between this and the original ionization chamber are (1) the distance between filament and first slit cf analyser is reduced from 5 cm to 2 cm; (2) the narrow slit in the electrode E_3 was replaced by nickel gauze; and (3) improved magnetic shielding of the ionization chamber was obtained by addition of a soft ion cylinder 8 mm thick resting on the plate P. The potential V_2 was placed between the iron tube T and the electrode immediately above it. The results shown in figs. 7 and 8 were obtained with this ionization chamber No. 2.

The electrometer was worked at a voltage sensitivity of 800 mm per volt, the capacity of the insulated system being 86 cm. For all runs the pressure of residual gas shown on the McLeod gauge was below 5×10^{-6} mm of Hg.

RESULTS

1—*Analysis of the Ions*

In fig. 2 is shown a set of eight ion-analysis curves for various values of V_0, the electron accelerating potential. These curves were all taken with

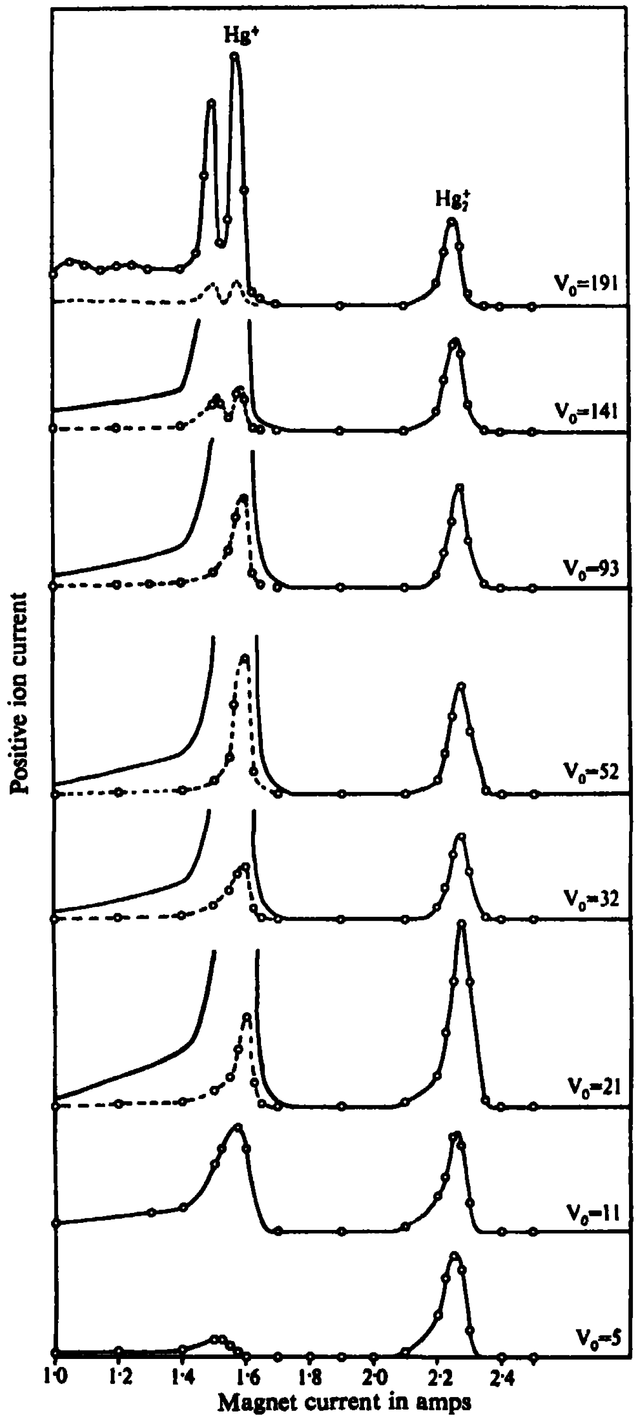

FIG. 2—Ion-analysis curves showing presence of Hg_2^+ for various electron energies.

the same filament, having a potential drop across it of 14 volts. The value of V_0 is the mean energy of the electrons, so that in the curve for $V_0 = 11$ volts the electrons had initial energies between 4 and 18 volts.* The curves for 5 and 11 volts were taken at a temperature of 82° C. The 21-volt curve is for 77° C. The temperature for the other curves was 72° C. The filament emission for the three lower curves was about 1 milliamp. That for the other curves was 0·4 milliamp.

The peak on the right shows the presence of the diatomic molecular ion Hg_2^+; that on the left is for the atomic ion Hg^+. The broken line under the atomic peak represents the ordinates reduced by a factor of 10.

It will be noticed that in the curves for $V_0 = 141$ volts and $V_0 = 191$ volts the atomic peak consists of two sharp peaks occurring at values of the magnet current equal to 1·50 amp and 1·58 amp. The peak at 1·58 amp is due to ionization in the field-free space between the positive ion sheath on F and the positive ion sheath on E_2. The ions produced here are accelerated by $V_1 + V_2 = 100$ volts. The peak at 1·50 amp is due to ionization between E_2 and E_3. These ions are accelerated by $V_2 = 90$ volts. The value of the magnetic field H required to bend the ions into the Faraday cylinder is given by

$$H^2\rho^2 = \frac{2Vmc^2}{300e}, \tag{1}$$

where V is the accelerating potential in volts, ρ the radius of the path, e the charge in e.s.u., and m the mass of the ion. We have from (1)

$$\frac{H_1}{H_2} = \left(\frac{V_1}{V_2}\right)^{\frac{1}{2}} = \left(\frac{90}{100}\right)^{\frac{1}{2}} = \frac{1\cdot50}{1\cdot58}.$$

The fact that the peak at 1·50 amp is as sharp as that at 1·58 amp shows that there is a very thin positive ion sheath over the surface of E_3 in which the whole 90 volts potential drop is concentrated. This positive ion sheath over E_3 will occur only when $V_0 > V_1 + V_2 > 100$ volts, for when $V_0 < 100$ volts the electrons will be brought to rest in the 90-volt potential drop between E_2 and E_3; and since they are more numerous than the positive ions their negative space charge would destroy any positive ion sheath on E_3. When $V_0 > 100$ volts the electrons are not brought to rest, and their negative space charge is then negligible compared with that of the positive ions, even though the latter are less numerous.*

---

* In a preliminary report of this work in 'Nature,' vol. 135, p. 999 (1935), the values given for V_0 were the *maximum* energies of the electrons. The energy spread for these curves was also 14 volts.

Since the peak at 1·50 amp is almost the same size as that at 1·58 amp, we conclude that of the atomic ions entering the analyser nearly as many are produced in the 1-cm space between E_2 and E_3 as are formed in the 4-cm space between F and E_2 for high values of V_0.

We see that when the mean energy is 5 volts, the electrons having a range of energy from 0 to 12 volts, the molecular peak is considerably larger than the atomic peak, which suggests that the appearance potential for the molecular ion is below that for the atomic ion. The reason for the molecular peak being so much larger than the atomic peak will be evident when we come to consider the variation in the ratio of Hg_2^+ to Hg^+ with electron energy shown in figs. 6 and 7. This point will also be referred to in discussing fig. 8 (*see* p. 372).

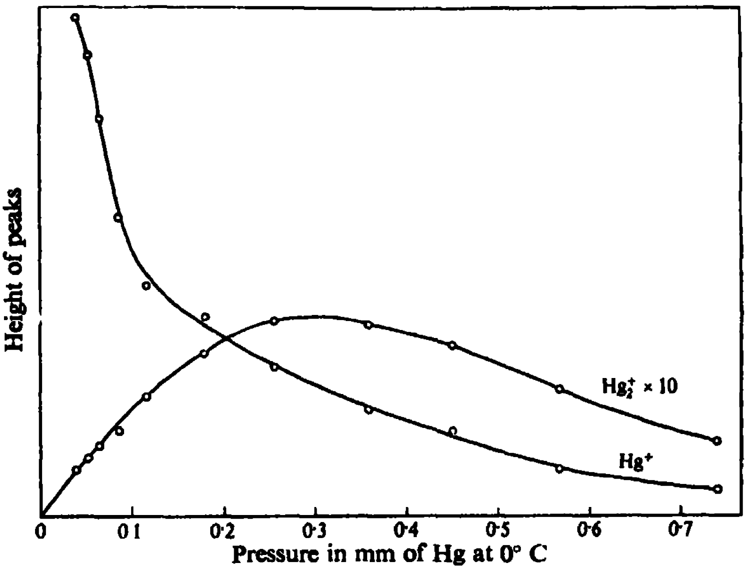

FIG. 3—Showing the number of atomic and molecular ions recorded as a function of the pressure of mercury vapour.

2—*Variation of Peaks with Pressure*

Fig. 3 shows the variation in the heights of the atomic and molecular peaks with pressure. The saturation vapour pressures corresponding to the temperature of the furnace were taken from the International Critical

---

* For a treatment of space charge sheaths in positive ray analysis *see* Gurney and Morse, 'Phys. Rev.,' vol. 33, p. 789 (1929).

Tables and reduced to 0° C. In order to allow for any possible movement of the peaks during the run the heights were determined by taking several readings over the top of the peaks at slightly different magnet currents. The mean energy of the electron stream was 91 volts with an energy spread of 14 volts. V_1 was 10 volts and V_2 was 90 volts. The filament emission was kept constant at 0·4 milliamp.

We see that over the whole pressure range measured the atomic peak decreases as the pressure is increased. This decrease is caused by multiple scattering and absorption of the ions and ionizing electrons. On decreasing the pressure to zero, the atomic peak would rise to a maximum and then decrease to zero at the origin. At very low pressures the atomic curve is a straight line. The fact that the molecular peak is increasing at pressures such that the atomic peak is decreasing means that the number of molecular ions formed is proportional to a higher power of the pressure than that which governs the formation of the atomic ions.

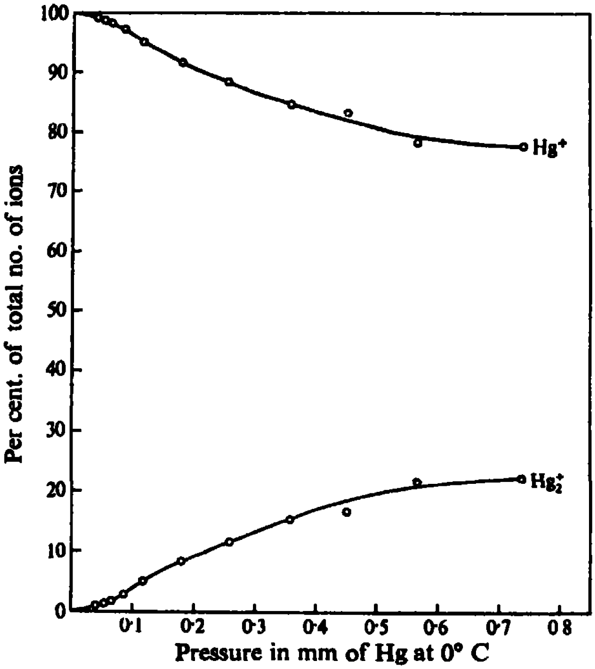

FIG. 4—Percentage of atomic and molecular ions recorded as a function of the pressure of mercury vapour.

These curves are similar to those found in hydrogen* and other molecular gases, but with the important difference that the Hg^+ curve corresponds to the H_2^+ curve, while the Hg_2^+ curve corresponds to the H^+ curve.

---

* Smyth, 'Phys. Rev.,' vol. 25, p. 452 (1925).

The usual method of showing pressure variation curves is to plot for any one ion ordinates representing its percentage of the total number of ions formed. These results, which are obtained from fig. 3, are shown in fig. 4. These curves are of the same type as those found for hydrogen and nitrogen,* with again the important difference that the Hg^+ curve corresponds to the N_2^+ curve, while the curve for Hg_2^+ corresponds to that for N^+.

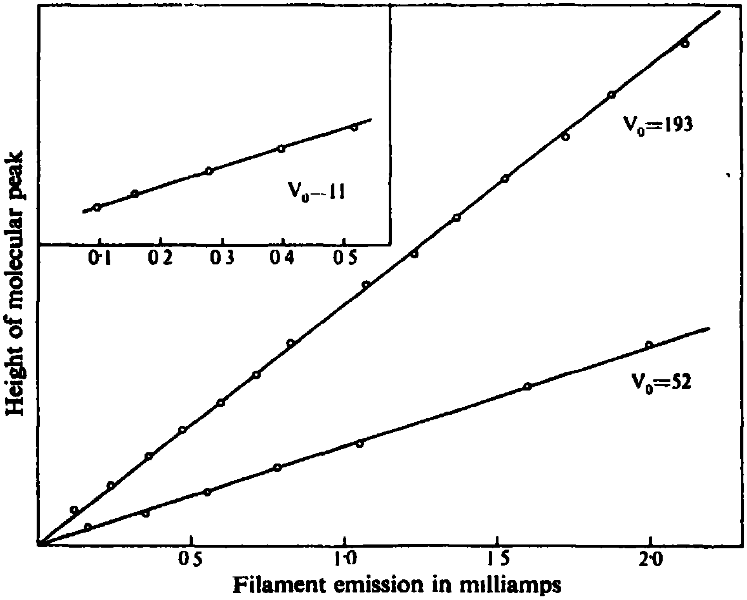

FIG. 5—Variation of molecular peak with filament emission.

Interpreting these curves in the usual way, we have here definite evidence that the molecular ion Hg_2^+ is formed by a secondary process, since the molecular curve extrapolates to the origin, while the atomic ion is the primary process. This shows that the molecular ion is not due to direct ionization of mercury molecules but is formed in the vapour by an attachment process which will be discussed later.

3—*Variation of Peaks with Filament Emission*

The variation in the height of the molecular ion peak with filament emission is shown in fig. 5 for three different energies of the ionizing electrons, 11, 52, and 193 volts. The above values for V_0 represent the mean energy of the electrons, the energy spread being 14 volts for the two higher-energy curves, and 1 volt for the 11-volt curve. The temperature for all three curves was 75° C. The 11-volt curve was taken, using ionization chamber No. 2, with $V_1 = 100$ volts and $V_2 = 0$. The other two curves were taken, using chamber No. 1, with $V_1 = 10$ volts and $V_2 = 90$ volts.

---

* Smyth, 'Rev. Mod. Phys.,' vol. 3, p. 347 (1931).

We see that the number of molecular ions formed is strictly proportional to the first power of the filament emission for all three values of V_0. This shows that in the attachment process leading to the formation of the molecular ion only one of the atoms is excited or ionized, the other atom being in the normal state. As would be expected, a strictly linear variation in height with filament emission was also obtained for the atomic peak.

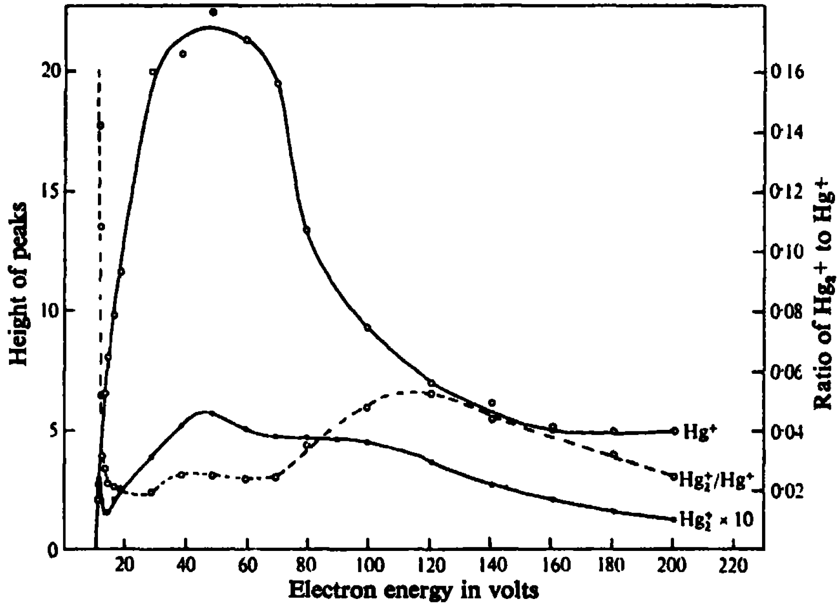

FIG. 6—Variation in atomic and molecular peaks with electron energy obtained with ionization chamber No. 1.

4—*Variation of Peaks with Electron Energy*

Fig. 6 shows the variation with electron energy V_0 in the heights of the atomic and molecular peaks. The broken curve represents the ratio of the molecular peak to the atomic peak. In order to allow for any possible movement of the peaks during the run, the heights were determined by taking several readings over the top of the peaks at slightly different magnet currents. No appreciable movement of the peaks was observed.

A short filament 1 cm in length having a potential drop of 1·6 volts across it was used, the emission being kept constant at 1 milliamp throughout the run. Owing to the cooling of the ends of the filament by the heavy leads the potential drop across the effective part of the filament was probably not much more than 1 volt. As in all results recorded here, V_0 represents the mean energy of the electrons. The temperature during the run was 84° C. V_1 was 10 volts and V_2 was 90 volts. Ionization chamber No. 1 was used.

We see that the curve for the atomic ion rises rapidly from the ionization potential, 10·4 volts, to a maximum at about 50 volts, after which it falls off rather rapidly. The curve is very similar to Bleakney's curve* for ionization by single electron impact, the maxima occurring at 50 volts in both curves. However, our curve falls off more steeply on the high-energy side of the maximum. We should not expect the curves to be identical since Bleakney's curve is for single electron impact, whereas in our apparatus the electrons make several collisions. At $V_0 = 50$ volts the experimental mean free path† is 2·3 mm, so that the electrons make at least 17 collisions before reaching E_2, assuming they are scattered forward at each collision. They will, in fact, make more than this number, for as they lose energy their mean free path decreases. At $V_0 = 200$ volts the mean free path is 3·9 mm, so that at least 10 collisions will be made.

The most interesting feature of these results is the way the molecular curve reaches a minimum at about 14 volts, after which it increases as V_0 is decreased, so causing the ratio curve (broken curve) to rise steeply. The molecular curve reaches a maximum at 11·4 volts, two identical readings being obtained at 11·2 and 11·6 volts. This feature has been carefully checked and occurs in all curves. The fact that it does not appear in any atomic curve definitely shows that it is not a spurious effect due to some peculiarity in the apparatus, such as reflexion of the ions.

It was not found possible to obtain readings below 11 volts with this ionization chamber owing to the fact that below the ionization potential the emission from the filament was so limited by space charge that sufficient intensity could not be obtained. To overcome this difficulty, an extra grid was inserted between the filament and E_1. The electrons were then accelerated up to the grid by a potential well above the ionization potential and retarded to the required velocity between the grid and E_1. It was found, however, that owing to a thin positive ion sheath forming over E_1 many of the electrons could pass through the centre of the holes in the gauze on E_1 without passing through the sheath, and so without suffering retardation. The ineffectiveness of the electrode E_1 in retarding the electrons was due to the same cause as that which makes the grid in a thyratron ineffective once the arc has struck.

---

* 'Phys. Rev.,' vol. 35, p. 139 (1930).

† Brode, 'Proc. Roy. Soc.,' A, vol. 125, p. 134 (1929).

In order to increase the intensity of the ion currents to a value which would enable readings to be obtained below the ionization potential, even when the filament emission was limited by space charge to a low value, the ionization chamber No. 2, shown as an inset in fig. 1, was constructed.

Using this ionization chamber at a temperature of 76° C and with a filament 8 mm in length, the results shown in figs. 7 and 8 were obtained. The potential drop across the filament was 1·2 volts. V_1 was zero and V_2 was 100 volts. The left-hand ordinate scales in figs. 6 and 7 are both marked in the same arbitrary units.

Comparing figs. 6 and 7, we see that both the atomic and the molecular curve is of the same form in each figure, but in fig. 7 the curves are extended in the direction of the V_0 axis. This extension is the same for the atomic as for the molecular curve, so that the ratio curve for Hg_2^+/Hg^+ remains of the same shape except for a similar extension. These curves in figs. 6 and 7 were checked several times and found to be reproducible, so that the extension of the curves produced by ionization chamber No. 2 is quite genuine.

The conditions in an ionization chamber at high pressure are so complicated that possibly several factors contribute to this extension of the curves. The essential point, however, is that the curves are of the same relative shape, and that the curve showing the ratio of Hg_2^+ to Hg^+ is of about the same magnitude and of the same form relative to the atomic curve at all values of V_0 in both figures.

The rise in the molecular curve at low energies is not so pronounced relative to the rest of the curve in the results obtained with ionization chamber No. 2. It is, however, quite definite, as is shown by fig. 8, and the maximum occurs at 11·5 volts in excellent agreement with the value 11·4 volts obtained with ionization chamber No. 1, and shown in fig. 6. As the absolute intensity of the ion currents was much greater with chamber No. 2, the molecular curve could be traced down to the appearance potential.

In fig. 8 the voltage scale has been adjusted by 1·4 volts so as to make the atomic ion curve extrapolate to 10·4 volts. Most of this correction

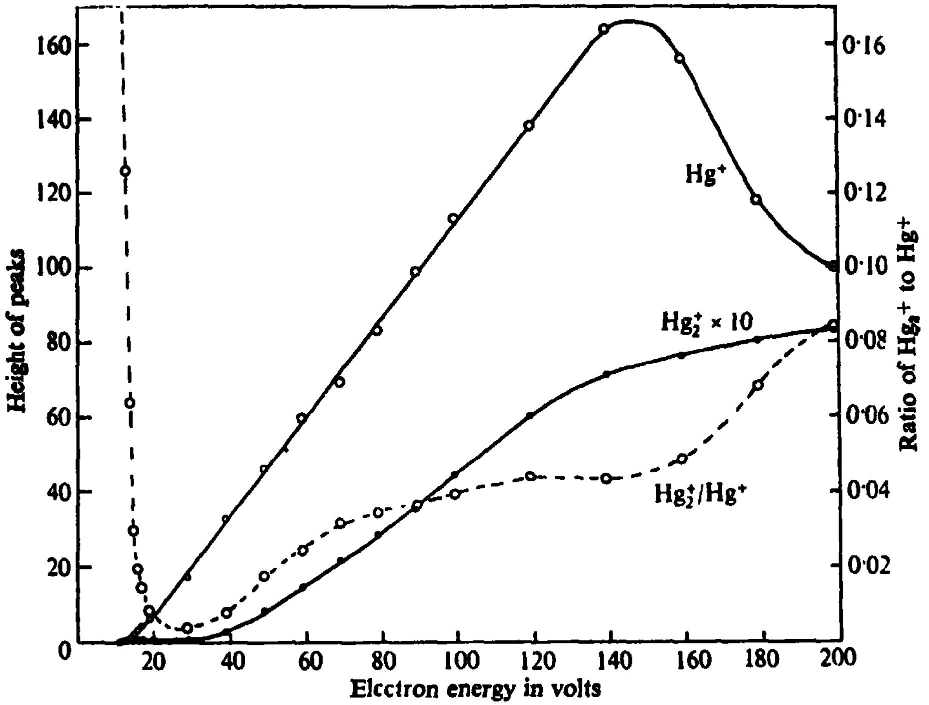

FIG 7—Variation in atomic and molecular peaks with electron energy obtained with ionization chamber No. 2.

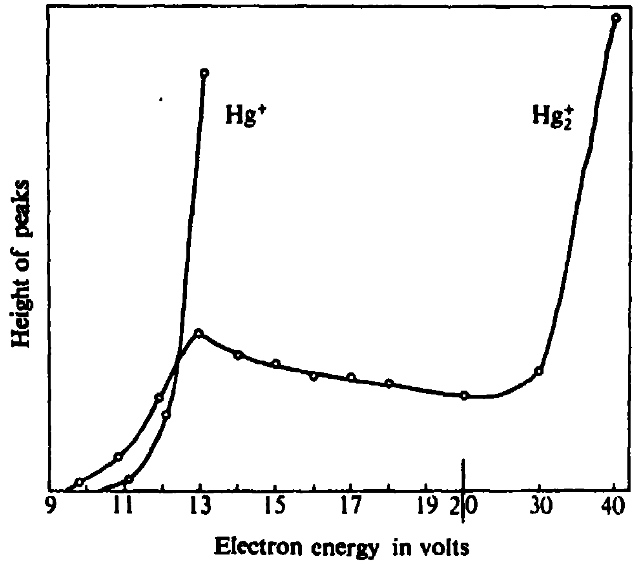

FIG. 8—Appearance potentials for the atomic and molecular ions.

is due to the energy spread of the electron stream, as is shown by the curvature of the graphs where they meet the voltage axis, and the correction has consequently not been applied to the curves in figs. 6 and 7.

The appearance potential for the molecular ion is seen to be 9·5 volts, which is in excellent agreement with the limits 9·32 to 9·52 which can be deduced from the results of Houtermans, on the assumption that the ionization observed in mercury vapour when irradiated by its resonance radiation 2537 A is due to the formation of molecular ions (*see* p. 375).

We also see from fig. 8 that, over the range of energy from 0 to 12 volts, the molecular ionization is everywhere greater than the atomic ionization. This fact is confirmed by the results shown in fig. 2 for $V_0 = 5$ volts, which corresponds to an energy range of 0 to 12 volts, for the molecular peak in this curve is considerably greater than the atomic peak.

THE PROCESS OF FORMATION OF THE MOLECULE

As stated above, the results shown in fig. 4 provide definite evidence that the molecular ionization is a secondary effect, and therefore that the molecular ion is formed by an attachment process. The fact that the molecular ionization varies with the first power of the filament emission, as shown in fig. 5, proves definitely that in the attachment process only one of the atoms is excited or ionized, the other atom being in the normal state. We have therefore the two following possible processes, depending upon whether the atom is excited or ionized.

$$\mathrm{Hg}' + \mathrm{Hg} \rightarrow \mathrm{Hg}_2^+ + \varepsilon, \tag{1}$$

$$\mathrm{Hg}^+ + \mathrm{Hg} \rightarrow \mathrm{Hg}_2^+. \tag{2}$$

The fact that the appearance potential of the molecular ion is definitely below the ionization potential of the atom, as shown in fig. 8, proves that process (1) at least occurs, but does not exclude the possibility of process (2) also occurring at higher electron energies. However, an examination of the optical excitation functions for lines of the mercury spectrum, measured by Crozier* and by Schaffernicht,† indicates that process (1) can account for the formation of the molecules over the entire range of electron energies used.

The optical excitation functions are determined by measuring the intensity of certain spectral lines as a function of the energy of the exciting electrons. The number of atoms in a certain excited state is then proportional to the intensity of the lines that originate in transitions from that state. The optical excitation function of a certain state does not in general represent the probability of excitation from the ground state, for the higher state may be excited by indirect means, such as collisions of the second kind or by recombination. However, for our purpose we require to know the number of atoms in the excited state, irrespective of how they got there, and therefore it is the optical excitation functions that we require.

---

* 'Phys. Rev.,' vol. 31, p. 800 (1928).

† 'Z. Physik,' vol. 62, p. 106 (1930).

Since the appearance potential of the molecular ion is 9·5 volts, we conclude that the excited atom must possess 9·5 volts energy before it can combine by process (1) to form an ionized molecule. Now the lowest state of the mercury atom which has more than this amount of energy is the $6s7d\,^1D_2$ state which has 9·506 volts energy. Just above this singlet state there is the triplet state $6s7d\,^3D_{1,2,3}$, of which the energies are 9·508, 9·515, 9·517 volts.*

Schaffernicht gives optical excitation functions for these four states. Those for the $4\,^3D_1$ and $4\,^3D_3$ states, obtained from the transitions $2\,^3P_0$—$4\,^3D_1$ and $2\,^3P_2$—$4\,^3D_3$, both rise steeply from the excitation potential to a sharp maximum at 12 volts and 11·2 volts respectively, after which they fall off sharply. These would account for the sharp maximum in our molecular curve at 11·5 volts. The excitation functions for the $4\,^1D_2$ and $4\,^3D_2$ states, obtained from the transitions $2\,^3P_2$—$4\,^1D_2$ and $2\,^1P_1$—$4\,^3D_2$, both rise to a broad maximum at about 30 volts. These could account for the broad maximum in our molecular curve at higher energies.

To illustrate this we can combine these four excitation functions into a single curve to represent the probability of formation of molecules by process (1) as a function of the electron energy. Now to do this accurately we require to know in what proportion we are to combine the excitation functions. This requires a knowledge of the relative probability of attachment of the atom in the four given states as well as the absolute magnitude of the excitation functions. The former we do not know. The latter can only be found by adding together the excitation functions for all possible transitions from the given state. Since the excitation functions for all possible transitions from the given states have not been measured we do not know in what proportion the four excitation functions should be combined to give the correct curve.

It is, however, of definite value to see if the experimental curve can be reproduced approximately in shape by any reasonable combination of the excitation functions given above. This has been done as follows. The two excitation functions having maxima at 12 volts and 11·2 volts, which are almost identical in shape, were added together in a 1 to 1 ratio and then reduced to fit the maximum at 11·5 volts in the molecular curve shown in fig. 6. The excitation function for the $^1D_2$ state was then reduced so that its maximum at 30 volts was of the same height as the maximum in the molecular curve at 47 volts. This function was then added to the sum of the other two, and the resultant plotted as a broken curve in fig. 9, together with the molecular curve of fig. 6. The excitation function for the $^3D_2$ state has not been used. If it is included in any but a small proportion the agreement is not so good, although the curve is still of the correct form. It has the effect of raising the maximum at 11·5 volts relative to that at 30 volts.

---

* Bacher and Goudsmit, " Atomic Energy States," p. 228 (1932).

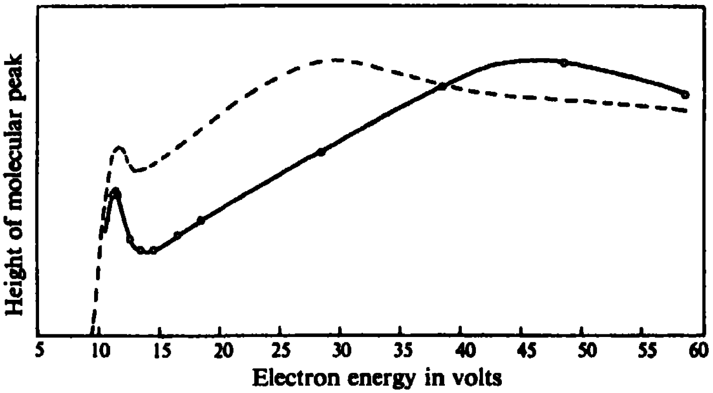

FIG. 9—Broken curve represents an approximate theoretical curve for the probability of formation of molecular ions as a function of the electron energy. Continuous curve is the experimental curve of fig. 6.

The agreement in shape is sufficiently good to suggest that the attachment process (1) can account for the formation of the molecules over the entire energy range. The two curves should not be identical, for the true theoretical curve, to which the curve in fig. 9 is an approximation, would represent the probability of formation of a molecule, whereas the experimental curve represents the probability of formation of only those molecules which pass through the apparatus and reach the Faraday cylinder, and the proportion of these to the total number of molecules formed is probably dependent to a certain extent upon the electron energy, this dependence itself being also affected by the dimensions of the apparatus, as is shown by the extension of the curves in fig. 7 relative to those in fig. 6 in the direction of the electron energy axis.

Further evidence against process (2) occurring is given by figs. 6 and 7, for if the molecule is formed by attachment of atomic ions to normal atoms we should expect the ratio of Hg_2^+ to Hg^+, shown by the broken curves in figs. 6 and 7, to be independent of the energy of the electrons, which is clearly not so.

It was found by Rouse and Giddings,* whose results were checked and developed by Houtermans† and Foote,‡ that mercury vapour is ionized by its resonance radiation 2537 A, of which the photons have only 4·86 volts energy. The ionization was found to be proportional to the *square* of the intensity of the light. To explain these results Houtermans suggested that an excited atom in the $2\,^3P_1$ state of 4·86 volts energy may combine with a metastable atom in the $2\,^3P_0$ state of 4·66 volts energy to form an ionized molecule and a free electron. The energy available for ionization of this molecule is (4·86 + 4·66) volts plus the energy of dissociation of the normal molecule, which Winans§ gives from band spectra data as 0·15 volt, making a total energy of 9·67 volts.

Houtermans also obtained evidence to show that a collision between two atoms, both of which are in the metastable state $2\,^3P_0$, does *not* lead to ionization. We may therefore conclude that the ionization potential of the molecule is greater than 9·32 + D and less than 9·52 + D, where D is the energy of dissociation of the normal molecule. These limits are in excellent agreement with our value of 9·5 volts for the appearance potential. We therefore conclude that the ionization potential of the molecule is 9·50 + 0·15 = 9·65 volts. The energy of dissociation of the ionized molecule is then

$$\begin{aligned} D_i &= I_a - I_m + D \\ &= 10{\cdot}4 - 9{\cdot}65 + 0{\cdot}15 \\ &= 0{\cdot}9 \text{ volt,} \end{aligned}$$

where I_a is the ionization potential of the atom, and I_m that of the molecule.

We infer from the very low energy of dissociation of the normal molecule that the binding in the fundamental state is due simply to the polarization or van der Waals forces of attraction, whereas the value for the energy of dissociation of the ionized molecule indicates that in the molecular ion ordinary rigid binding occurs.

* 'Proc. Nat. Acad. Sci. Wash.,' vol. 11, p. 514 (1925); vol. 12, p. 447 (1926).

† 'Z. Physik,' vol. 41, p. 619 (1927).

‡ 'Phys. Rev.,' vol. 29, p. 609 (1927).

§ 'Phys. Rev.,' vol. 37, p. 897 (1931).

A very low value for the energy of dissociation of the molecule in the fundamental state is also to be inferred from the fact that the absorption bands which occur in the spectrum of mercury vapour at high pressure appear in association with the atomic lines. The shading off of these bands on the short wave-length side shows that the internuclear distance in the fundamental state is greater than in the excited state.

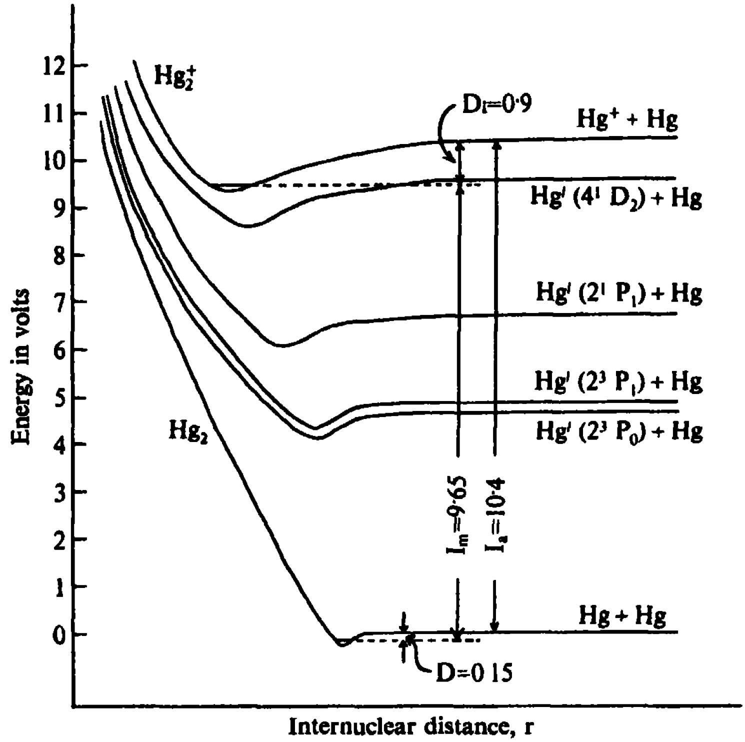

FIG. 10—Approximate Frank-Condon diagrams for various states of the diatomic mercury molecule.

With the above data we can now draw approximate Frank-Condon diagrams for various states of the molecule. These are shown in fig. 10. The products into which the molecule dissociates are given on the right of each curve. When no specific excited state is given the ground state $1\,^1S_0$ is to be understood.

We can now picture the formation of an ionized molecule by considering the curve for the collision of an excited atom in the $4\,^1D_2$ state with a normal atom. When the atoms are far apart their energy is represented by a point on the flat portion of the curve; or, to be precise, just above the flat portion of the curve by an amount equal to their combined thermal energy.* The total energy of the atoms is then slightly greater than the energy of the lowest vibrational state of the ionized molecule represented by the broken line. The collision process is represented by a horizontal movement to the left. Association of the atoms into the lowest vibrational state of the ionized molecule can then occur with the loss of the excess energy of the atoms above that of the quantized state of the molecular ion.

There are two ways in which this excess energy can be carried away, (1) by infra-red radiation, and (2) in the form of kinetic energy of the ejected electron. The latter seems to be far the more likely mechanism, since no spectrum due to association of atoms has ever been observed.

The formation of ionized molecules by collision of atoms in higher vibrational states than the $4\,^1D_2$ state with normal atoms can then occur in a similar way to that described above, the molecular ion formed in these cases being possibly in a higher vibrational state.

If the excited atom is in a lower state than the $4\,^1D_2$ state then attachment to a normal atom will lead to an excited molecule. In this way many molecules in various states of excitation may be formed when mercury vapour is irradiated by ultra-violet light or subjected to electron impact, thus accounting for the quite strong bands that have been observed in the absorption and emission spectra of the vapour.

The formation of an ionized molecule by the attachment of an excited atom in the $2\,^3P_1$ state to a metastable atom in the $2\,^3P_0$ state is also seen to be possible, for the combined energy of the two excited atoms is then 9·52 volts. Since the probability of collision between an excited atom and a metastable atom is very much less than the probability of collision between an excited atom and a normal atom, the number of molecules formed in this way will be very much smaller than the number formed by process (1), which would account for their not having been observed in this work, *see* fig. 8.

Now let us consider the possibility of the formation of an ionized molecule by the attachment of an atomic ion to a normal atom, as in process (2), p. 372. There is now no electron set free to carry away the energy of the colliding particles in excess of that of a quantized state of the molecular ion. Since we do not consider radiation of the excess energy to be at all likely attachment becomes impossible. Consequently, on the basis of the experimental evidence as well as on the above theoretical discussion, we conclude that the molecular ions of mercury observed by us are formed over the entire range of electron energy by the attachment of excited atoms to normal atoms.

---

* The combined mean thermal kinetic energy of the two atoms at a temperature of 76° C is 0·1 volt.

It should be mentioned that in all other association processes involving ions that have been observed, such as the formation of H_3^+ and I_3^+, the balance of evidence shows that the triatomic molecular ion is formed by a collision between a diatomic molecular ion and a normal diatomic molecule, in which the latter is dissociated by the process, so that in this case an atom is set free to carry away the excess energy.

One of us (J. C. M.) wishes to thank the Carnegie Trust for the Universities of Scotland for a Research Scholarship.

SUMMARY

Diatomic molecular ions of mercury have been observed for the first time by magnetic analysis of the ions produced in mercury vapour by electron impact. Pressure variation curves show that the molecular ions are formed by a secondary process. The number of molecular ions produced is directly proportional to the first power of the filament emission. The appearance potential of the molecular ion is 9·5 volts. Since this is less than the atomic ionization potential the molecular ion must be formed by the attachment of an excited atom to a normal atom by the process

$$Hg' + Hg \rightarrow Hg_2^+ + \epsilon.$$

As the energy of the electrons is increased the molecular ionization rises from zero at 9·5 volts to a maximum at 11·5 volts, falls to a minimum at about 14 volts, then rises to a second maximum at about 40 volts, after which it decreases up to 200 volts energy. Optical excitation functions for states above 9·5 volts energy indicate that the maximum at 11·5 volts is due to triplet excitation, while that at about 40 volts is due mainly to singlet excitation of the atom which goes to form the molecular ion. The ionization potential of the molecule is 9·65 volts, using Winans's value of 0·15 volt for the energy of dissociation of the normal molecule.

The formation of molecules by attachment of excited atoms to normal atoms, which has been shown definitely to occur in this work, clearly reconciles the chemical evidence of their non-existence with the band spectra evidence of their presence; for, unless the atoms are excited by light or by electron impact, the vapour may remain practically monatomic.

Refractive Dispersion of Organic Compounds

VII—The Refractive Indices of Hexane and the Refractivities of Hydrogen and Carbon. Significance of the Dispersion Constants

By C. B. ALLSOPP, M.A., Ph.D., and H. F. WILLIS, M.Sc., Laboratory of Physical Chemistry, Cambridge University

(*Communicated by Professor T. M. Lowry, F.R.S.—Received July* 25, 1935)

INTRODUCTION

The law of additivity as applied to molecular refractions is based on two empirical observations, both of which were first established quantitatively by Landolt,* namely, (i) the constancy of the increment of molecular refraction corresponding to each addition of CH_2 in a homologous series, and (ii) the identity of the molecular refractions of isomeric compounds. With the help of this law the refractivity of a molecule may be resolved into the sum of a series of atomic refractivities. Thus Eisenlohr in 1910 calculated the refractivities of carbon and hydrogen, for the D-line of sodium and for the three visible lines of hydrogen, from measurements of the refractive indices at these wave-lengths of 145 open-chain hydrocarbons, aldehydes, ketones, acids, alcohols, and esters, as follows:

(i) The refractivity of the *methylene radical* $R[CH_2]$ was deduced from the mean increment between consecutive members of various homologous series.

(ii) The refractivity of *hydrogen* was deduced by extrapolation from the refractivities of the series of paraffins by means of the relation

$$R[H_2] = R[C_nH_{2n+2}] - nR[CH_2].$$

(iii) The refractivity of *carbon* was deduced from the difference

$$R[C] = R[CH_2] - 2R[H].$$

As is well known, the additive relationship can only be maintained by taking different values for oxygen and nitrogen in different states of combination, whilst the influence of double and triple bonds is allowed for by assigning a definite increment to each type of multiple bond; but, even when this has been done, the additive relationship is still only approximately valid. Thus, in the homologous series studied by Eisenlohr, the increment for CH_2 varied from $M_D = 4 \cdot 606$ in the esters to 4·634 in the alcohols; and the measurements of Voellmy* show that, when the refractivities of two homologous ketones are compared in the neighbourhood of an absorption band, this increment undergoes grotesque variations, since the displacement of the wave-length of maximum absorption throws the two dispersion curves completely out of alignment, and the differences between them reproduce all the anomalies which are characteristic of refractive dispersion in a region of absorption. An additive law is therefore only plausible in regions remote from an absorption band.

---

* 'Pogg. Ann.,' vol. 117, p. 353 (1862); vol. 122, p. 545 (1864); vol. 123, p. 595 (1864); vol. 213, p. 75 (1882). Similar, but only semi-quantitative, observations had been made by earlier workers.

In its present form, however, the additive relationship has no logical physical basis, since there is no justification for expecting that the contribution of a given atom to the refractivity of a molecule will be independent of the way in which it is bound to other atoms. On the contrary, if the refractivity cf the atom could be dissected out, we should expect it to be made up of a series of partial refractivities, the characteristic frequencies of which would be determined by the various energies of excitation of the atom, as represented by a series of absorption bands in different regions of the spectrum. Thus the refractivity of the carbonyl radical (*see* Part VI)† includes (i) a small anomalous refractivity with a characteristic frequency in the middle ultra-violet, corresponding with the familiar ketonic absorption band, and (ii) a much larger refractivity (about 100 times greater) with a characteristic frequency in the Schumann region. Since the frequency of the ultra-violet absorption band is known to be influenced by the radicals to which the carbonyl group is linked, we cannot expect that the sum of these partial refractivities will be constant.

Since all atomic refractivities are obviously complex aggregates of partial refractivities with diverse frequencies, a much more promising method of analysis is provided by resolving the refractivity of the molecule into a series of partial refractivities corresponding to the different absorption bands which it exhibits. Thus, the refractivity of the molecule will include partial refractions due to—

(i) the electrons of the outer shells of valency electrons,

(ii) the electrons of the inner shells.

---

* 'Z. phys. Chem.,' vol. 127, p. 305 (1927).

† 'Proc. Roy. Soc.,' A, vol. 146, p. 313 (1934).

Each set of similar electrons will have its own characteristic absorption frequencies, and the total refractivity of the molecule will be the sum of the partial refractivities which these contribute.

The absorption bands of the latter class of electrons fall without exception in the distant Schumann region of the spectrum. Some of them will be excited only by radiation of X-ray frequencies, and will therefore contribute little or nothing to the refractivity in the visible and near ultra-violet regions. Those which do contribute, however, may be expected to be influenced but little by the mode of coupling of the outer valency electrons; and the contributions of these electrons of the kernel may be expected to be independent of the state of combination of the atoms. On the other hand, the outer valency electrons will obviously be influenced by the way in which they are coupled together to form either "lone-pairs" of electrons or single, double, or triple bonds. It is therefore more logical to assign partial refractivities to (i) the kernel of each atom, (ii) its lone pairs of electrons, and (iii) the shared electrons of the single, double, and triple bonds between atoms of given types than to assign fixed values to the atoms themselves.

On this basis, the resolution of the molecular refractivities of organic compounds into atomic refractions is seen to be a merely formal process. Thus, the method of deriving the refractivity of hydrogen, as half the difference between the refractivities of hexane and *cyclo*-hexane, which is described below, is really equivalent to measuring the difference between the refractivities of the electrons forming two C—H bonds and those of one C—C bond:

$$2R[H] = 2R[C\text{—}H] - R[C\text{—}C];$$

whereas the value derived from the refractive index of gaseous hydrogen is

$$2R[H] = R[H\text{—}H].$$

The dispersion of the refractivity will not therefore be represented by a simple curve corresponding to a single characteristic frequency but by the *difference* of two such curves; and it may therefore contain anomalies analogous to those in the curves of rotatory dispersion of substances such as ethyl tartrate, whose rotatory powers are given by the difference of two terms of the Drude type.* On the other hand, the dispersion of the refractivity of the hydrogen molecule may be expected to be made up of contributions from electronic frequencies which are characteristic of that molecule alone, and will thus be represented in general by the *sum* rather than the *difference* of a series of terms. In these circumstances, it is not surprising that the value deduced for the refractivity of atomic hydrogen in organic compounds is quite different from the value deduced by halving the observed refractivity of molecular hydrogen, and that neither of these values agrees with that which has been predicted for the free hydrogen atom.* An attempt by Samuel† to reconcile the first two of these values involves the assumption that the two atoms composing a molecule of hydrogen are not equivalent to one another, and reduces in practice to transferring to hydrogen the constitutional variations in the refractivities of other atoms, *e.g.*, oxygen and nitrogen.

---

* Lowry and Dickson, 'Trans. Faraday Soc.,' vol. 10, p. 99 (1914).

Since additive relationships appear to be rendered impossible by the near neighbourhood of an absorption band, and are only probable when all the characteristic frequencies are in the same region of the spectrum, we have adopted a working rule that only those molecular refractivities are suitable for mathematical analysis which can be expressed by dispersion formulae of the simplest possible type, *i.e.*, by a Ketteler-Helmholtz or Lorentz-Lorenz formula containing only a single characteristic frequency and two other arbitrary constants. Since this characteristic frequency always lies in the Schumann region of the spectrum, the additive law may be restated on this basis as follows: " The molecular refraction of a molecule may be expected to be equal to the sum of the refractivities of its constituent atoms (or electrons) only when its refractive dispersion can be represented by an equation containing only one variable term, this being the partial refraction contributed by a characteristic frequency lying in the Schumann region of the spectrum."

In the present paper, this principle has been used in order to determine the refractivities of carbon and hydrogen over a wide range of wavelengths, as a sequel to the determination in Part VI of values for the oxygen, carbonyl, and carboxyl radicals. The refractive indices used for this purpose were those of two saturated hydrocarbons, whose refractive dispersions fulfil the condition set out above, namely (i) *hexane*, C_6H_{14}, for which data are given in the present paper, and (ii) *cyclo*-hexane, C_6H_{12}, for which data were given in Part II.‡ The atomic refractivity of *hydrogen* is derived as half the difference between the molecular refractions of these two compounds:

$$2R[H] = R[C_6H_{14}] - R[C_6H_{12}].$$

---

* Podolsky, ' Proc. Nat. Acad. Sci. Wash.,' vol. 14, p. 253 (1928).

† ' Z. Physik,' vol. 49, p. 95 (1928); vol. 53, p. 380 (1929).

‡ ' Proc. Roy. Soc.,' A, vol. 133, p. 36 (1931).

As in Part VI, the refractivity of the methylene radical is taken to be one-sixth of that of the *cyclo*hexane molecule:

$$R[CH_2] = \tfrac{1}{6}R[C_6H_{12}].$$

The atomic refractivity of *carbon* is then obtained as the simple difference

$$R[C] = R[CH_2] - R[H_2].$$

The method is at once justified by the results, since the value now deduced for the refractivity of the methylene radical, $M_D = 4{\cdot}618$, is identical with the *mean* value deduced by Eisenlohr from his measurements of many series of open-chain compounds. The use of the cyclic compound, therefore, does not lead to any abnormality, an observation which is confirmed by the work of Eisenlohr himself,* and also by the measurements of Willstätter and Bruce.† Whereas, however, Eisenlohr only deduced values for three other wave-lengths, in addition to the D-line, the values now recorded include 57 wave-lengths extending over the whole range from 6708 to 2451 A.

EXPERIMENTAL

(*a*) *Materials*—The hexane used for the present measurements was supplied by Professor Timmermanns, from the *Bureau d'Etalons Physico-chimiques* in Brussels. Its density was $d_4^{20} = 0{\cdot}6595$.

(*b*) *Method*—The methods of measurement were those previously described.‡

(*c*) *Refractive Indices of Hexane*—The refractive indices at 20° are set out, for 19 visual wave-lengths in Table I, and for 38 photographic readings in Table II. The dispersion curve is drawn in fig. 1, A.

(*d*) *Comparison with Previous Observations*—The refractive indices of hexane at wave-lengths in the visible spectrum have been measured by Brühl§ and by Landolt and Jahn.|| Our molecular refractivities are uniformly 0·02 units higher than those of Brühl, but are identical, at wave-lengths in the green and blue, with those recorded by Landolt. Values at visible and ultra-violet wave-lengths are also tabulated by

---

* "Spektrochemie Organischer Verbindungen," 1912, p. 86.

† 'Ber. deuts. chem. Ges.,' vol. 40, p. 3979 (1907).

‡ Lowry and Allsopp, 'Proc. Roy. Soc.,' A, vol. 126, p. 165 (1929); vol. 133, p. 26 (1931).

§ 'Liebig's Ann.,' vol. 200, p. 183 (1880).

|| 'Z. phys. Chem.,' vol. 10, p. 302 (1892).

Voellmy.* At the D-lines, Voellmy's value, $M_D = 29 \cdot 88$, is almost identical with the present value, $M = 29 \cdot 89$, but his values increase rather more rapidly at shorter wave-lengths, reaching $M_{2500} = 33 \cdot 53$ as compared with 33·41 at $\lambda = 2500$ A. The direction of this divergence is the same as in the other similar cases previously recorded.†

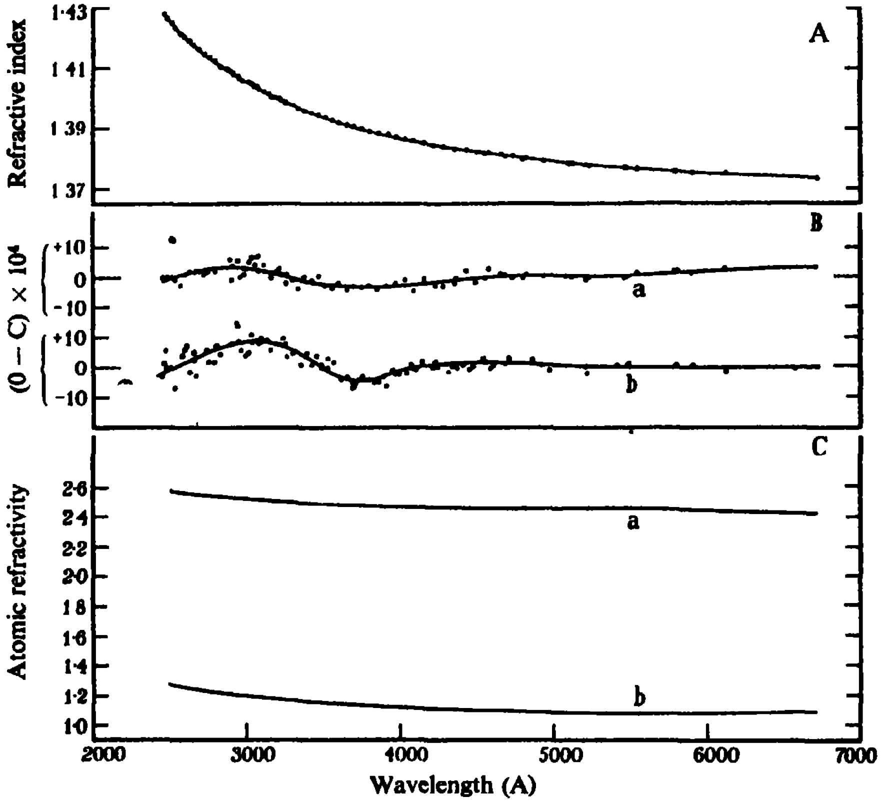

FIG. 1—A, Refractive indices of hexane; B, difference curves, *a*, hexane, *b*, *cyclo*-hexane; C, atomic refractivities, *a*, carbon, *b*, hydrogen.

REFRACTIVITIES OF HYDROGEN AND CARBON

The molecular refractions of hexane and of *cyclo*-hexane, and the refractivities of the methylene radical and of the hydrogen and carbon atoms deduced from them, are set out in Table III. In the visual region, where the same wave-lengths were used for all the different series of

* 'Z. phys. Chem.,' vol. 127, p. 305 (1927).

† *E.g.*, *cyclo*hexane and benzene, Parts II and III.

TABLE I—REFRACTIVE INDICES OF HEXANE AT 20° C VISUAL READINGS

λ*	Refractive index			Molecular refraction
	n observed	*n* calculated	Difference $(O - C) \times 10^4$	$R[C_6H_{14}]$
Li 6707·86	1·37297	1·37260	+3·7	29·745
Li 6103·6	1·37447	1·37417	+3·0	29·853
Na 5895·93	1·37498	1·37482	+1·6	29·888
Hg 5790·66	1·37540	1·37518	+2·2	29·919
Cu 5782·15	1·37543	1·37521	+2·2	29·921
Ba 5535·5	1·37626	1·37615	+1·1	29·979
Ag 5471·51	1·37641	1·37641	±	29·990
Hg 5460·73	1·37645	1·37646	−0·1	29·993
Cu 5220·06	1·37753	1·37755	−0·2	30·070
Ag 5209·04	1·37755	1·37761	−0·6	30·071
Cu 5105·55	1·37813	1·37813	±	30·112
Cd 5085·82	1·37826	1·37823	+0·3	30·121
Ba 4934·10	1·37909	1·37908	+0·1	30·180
Zn 4810·53	1·37987	1·37982	+0·5	30·236
Cd 4799·91	1·37986	1·37989	−0·3	30·235
Zn 4722·16	1·38036	1·38040	−0·4	30·271
Cd 4678·15	1·38075	1·38070	+0·5	30·298
Ba 4554·04	1·38156	1·38159	−0·3	30·356
Hg 4358·34	1·38322	1·38316	+0·6	30·473

* Wave-lengths for the visual readings in Table I are taken from the 'International Critical Tables,' vol. 5 (1929).

TABLE II—REFRACTIVE INDICES OF HEXANE AT 20° C PHOTOGRAPHIC READINGS

λ*	Refractive index			Molecular refraction
	n observed	*n* calculated	Difference $(O - C) \times 10^4$	$R[C_6H_{14}]$
4349·5	1·3830	1·3832	−2	30·458
4279·8	1·3835	1·3838	−3	30·494
4213·1	1·3842	1·3845	−3	30·542
4148·4	1·3850	1·3851	−1	30·599
4084·5 Fe	1·3853	1·3858	−5	30·622

* The wave-lengths of the photographic readings in Table II are coincidence wave-lengths which have been interpolated, correct to the first decimal place, from those of neighbouring iron or tungsten lines, except where the coincidence falls on a line marked Fe or W respectively. The wave-lengths of the iron lines are taken from Burns ('Z. wiss. Photogr.,' vol. 12, p. 207 (1913)) and of the tungsten lines from Belke ('Z. wiss. Photogr.,' vol. 17, p. 132 (1917), and vol. 17, p. 144 (1918)).

TABLE II—(continued)

λ*	Refractive index			Molecular refraction $R[C_6H_{14}]$
	n observed	*n* calculated	Difference $(O - C) \times 10^4$	
4024·7 Fe	1·3863	1·3864	−1	30·690
3965·4	1·3869	1·3871	−2	30·734
3907·9	1·3875	1·3878	−3	30·777
3851·9	1·3881	1·3885	−4	30·817
3798·5 Fe	1·3889	1·3892	−3	30·873
3745·9 Fe	1·3896	1·3899	−3	30·924
3695·1 Fe	1·3903	1·3906	3	30·972
3645·8 Fe	1·3910	1·3914	−4	31·023
3598·0	1·3919	1·3921	−2	31·086
3550·8	1·3925	1·3929	−4	31·129
3505·9	1·3934	1·3937	−3	31·192
3462·3	1·3944	1·3944	±	31·263
3419·1	1·3951	1·3952	−1	31·311
3377·2	1·3960	1·3960	±	31·374
3335·8 Fe	1·3965	1·3969	−4	31·408
3296·7	1·3976	1·3977	−1	31·486
3258·2	1·3986	1·3985	+1	31·556
3204·2	1·4000	1·3997	+3	31·654
3156·3 Fe	1·4009	1·4009	±	31·716
3111·1 W	1·4024	1·4020	+4	31·821
3045·8	1·4042	1·4038	+4	31·948
2981·2	1·4060	1·4057	+3	32·072
2949·3	1·4066	1·4066	±	32·114
2900·5 W	1·4081	1·4082	−1	32·218
2864·6	1·4098	1·4095	+3	32·336
2789·6	1·4123	1·4121	+2	32·511
2754·5 W	1·4136	1·4134	+2	32·601
2687·4	1·4164	1·4162	+2	32·795
2623·5 Fe	1·4192	1·4190	+2	32·987
2562·5 Fe	1·4217	1·4220	−3	33·159
2533·8 Fe	1·4234	1·4235	−1	33·278
2505·8 W	1·4250	1·4250	±	33·386
2451·5 W	1·4281	1·4281	±	33·601

TABLE III—ATOMIC REFRACTIVITIES OF HYDROGEN AND CARBON

λ*	Molecular refractions		Atomic refractions				
	$R[C_6H_{14}]$	$R[C_6H_{12}]$	R[H] Obs.	R[H] Calc.	(O − C) × 10^2	$R[CH_2]$	R[C]
Li 6708	29·745	27·574	1·086	1·075	+1·1	4·596	2·425
Li 6104	29·853	27·658	1·098	1·083	+1·5	4·610	2·415
Na 5896	29·888	27·710	1·089	1·087	+0·2	4·618	2·440
Hg 5791	29·919	27·732	1·094	1·089	+0·5	4·622	2·435
Hg 5461	29·993	27·819	1·087	1·096	−0·9	4·637	2·463
Cu 5220	30·070	27·889	1·091	1·102	−1·1	4·648	2·467
Cd 5086	30·121	27·933	1·094	1·105	−1·1	4·656	2·468
Zn 4811	30·236	28·018	1·109	1·114	−0·5	4·670	2·452
Zn 4722	30·271	28·067	1·102	1·117	−1·5	4·678	2·474
Cd 4678	30·298	28·079	1·110	1·119	−0·9	4·680	2·461
Ba 4554	30·356	28·128	1·114	1·124	−1·0	4·686	2·460
Hg 4358	30·473	28·223	1·125	1·133	−0·8	4·704	2·454
……							
4300	30·50	28·25	1·13	1·14	−1	4·71	2·46
4200	30·56	28·31	1·13	1·14	−1	4·72	2·47
4100	30·63	28·37	1·13	1·15	−2	4·73	2·47
4000	30·70	28·43	1·14	1·15	−1	4·74	2·47
3900	30·79	28·50	1·15	1·16	−1	4·75	2·46
3800	30·87	28·57	1·15	1·16	−1	4·76	2·46
3700	30·97	28·66	1·16	1·17	−1	4·78	2·46
3600	31·09	28·77	1·16	1·18	−2	4·795	2·47
3500	31·21	28·88	1·17	1·19	−2	4·81	2·48
3400	31·34	29·01	1·17	1·20	−3	4·83	2·50
3300	31·48	29·14	1·17	1·21	4	4·86	2·52
3200	31·65	29·29	1·18	1·22	−4	4·88	2·52
3100	31·84	29·46	1·19	1·24	−5	4·91	2·53
3000	32·04	29·62	1·21	1·25	−4	4·94	2·52
2900	32·25	29·81	1·22	1·27	−5	4·97	2·53
2800	32·49	30·01	1·24	1·28	−4	5·00	2·52
2700	32·75	30·24	1·26	1·31	−5	5·04	2·53
2600	33·06	30·52	1·27	1·33	−6	5·09	2·55
2500	33·41	30·85	1·28	1·36	−8	5·13	2·58

* The ultra-violet values in this table are interpolated from neighbouring photographic readings for purposes of comparison.

readings, the molecular refractivities were deduced directly from the observed refractive indices; the ultra-violet refractivities are interpolated at regular intervals of wave-length from closely-spaced photographic readings of refraction.

Table III also contains values of the refractivity of the hydrogen atom calculated as half the difference of the two equations of molecular refraction, namely

$$\mathrm{R[Hexane]} = 29\cdot1900 + \frac{0\cdot218079}{\lambda^2 - 0\cdot00710}$$

$$\mathrm{R}[\mathit{cyclo}\mathrm{Hexane}] = 27\cdot0927 + \frac{0\cdot197918}{\lambda^2 - 0\cdot009475}.$$

These two equations both exhibit small systematic deviations from the observed values, as shown by shallow loops in the difference curves for the two hydrocarbons (fig. 1 of Part II, and fig. 1, B, of the present paper), but these cancel out when the refractivities of C_6H_{14} and C_6H_{12} are subtracted from one another in order to deduce a value for the refractivity of H_2, with the result that there is no loop to be seen in the curve for R[H], fig. 1, C. No explanation can be given, however, either of the origin of these loops, or of the identity of form which results in their cancellation.

SIGNIFICANCE OF DISPERSION CONSTANTS

Born has pointed out an important contrast between the significance of the dispersion constants of the two equations:

$$n^2 = a + \sum_{r=1}^{m} \frac{b_r}{\lambda^2 - c_r} \qquad \text{(i)}$$

(Ketteler-Helmholtz)

$$\frac{n^2 - 1}{n^2 + 2} = \alpha + \sum_{r=1}^{m} \frac{\beta_r}{\lambda^2 - \gamma_r} \qquad \text{(ii)}$$

(Lorentz-Lorenz)

by which refractive indices are commonly expressed, arising from the fact that the former equation is strictly valid only for gases, whilst the latter is equally applicable to liquids, since the function $\frac{n^2 - 1}{n^2 + 2} \cdot \frac{1}{d}$ (where d is the density) is almost independent of the state of aggregation. Thus in equation (i) the dispersion-constants c_r are identical with the squares of the wave-lengths of the true characteristic frequencies of the medium only in *gases*, and have no intrinsic physical significance for the molecule when applied to *liquids*, the true characteristic frequencies of which can only be deduced from the constants γ_r of equation (ii).

The errors thus introduced are surprisingly large. Thus the refractive indices of hexane (Tables I and II) can be represented equally well over the range from 6708 to 2451 A by the equations

$$n^2 = 1\cdot86380 + \frac{0\cdot008906}{\lambda^2 - 0\cdot00940} \tag{iii}$$

and

$$\frac{n^2-1}{n^2+2} = 0\cdot223563 + \frac{0\cdot0017897}{\lambda^2 - 0\cdot00710}. \tag{iv}$$

The dispersion constants of the two equations, however, correspond with characteristic frequencies at 970 and 843 A respectively, so that the former is in error by as much as 127 A. In the same way the refractive indices of *cyclo*-hexane can be represented equally well by the equations:

$$n^2 = 2\cdot00519 + \frac{0\cdot0098035}{\lambda^2 - 0\cdot011923} \tag{v}$$

and

$$\frac{n^2-1}{n^2+2} = 0\cdot250972 + \frac{0\cdot0018334}{\lambda^2 - 0\cdot009475}. \tag{vi}$$

The characteristic frequencies are 1092 and 973 A with an error in the former of 119 A. Corresponding errors of 115 A, 130 A, and 133 A are obtained for *cyclo*-hexanone, *cyclo*-hexanol, and ethyl hexahydrobenzoate respectively. It is therefore clear that frequencies deduced by means of the simple Ketteler-Helmholtz equation are subject to errors of the order of 100 A, and that trustworthy values can only be derived from the more complex equation of Lorentz and Lorenz.

Since the labour of calculation is enormously increased by using the latter equation, and the values of the constants are subject to greater errors, it is of value to notice that the three-constant equations

$$n^2 = a + \frac{b}{\lambda^2 - c} \quad \text{and} \quad \frac{n^2-1}{n^2+2} = \alpha + \frac{\beta}{\lambda^2 - \gamma}$$

are interconvertible by means of the relations

$$a = \frac{1+2\alpha}{1-\alpha} \qquad b = \frac{3\beta}{(1-\alpha)^2} \qquad c = \gamma + \frac{\beta}{1-\alpha} \tag{vii}$$

and

$$\alpha = \frac{a-1}{a+2} \qquad \beta = \frac{3b}{(a+2)^2} \qquad \gamma = c - \frac{b}{a+2}. \tag{viii}$$

All the preliminary work can therefore be carried out with the simpler and more precise equation, and the constants of the more complex correct equation can then be deduced by an easy transformation.

When there is more than one characteristic frequency, the calculations are more complicated, but may be simplified by postulating that one of the terms is much smaller than the other, as is nearly always true, since the refractivities associated with the weak ultra-violet bands are always small compared with those of the very strong bands in the Schumann region.* In the equations

$$n^2 = a + \frac{b_1}{\lambda^2 - c_1} + \frac{b_2}{\lambda^2 - c_2} \tag{ix}$$

and

$$\frac{n^2 - 1}{n^2 + 2} = \alpha + \frac{\beta_1}{\lambda^2 - \gamma_1} + \frac{\beta_2}{\lambda^2 - \gamma_2}, \tag{x}$$

we can then postulate that

$$b_2 \ll b_1 \qquad \beta_2 \ll \beta_1.$$

It is then found that

$$c_1 - \gamma_1 = \frac{b_1}{a+2} + \frac{b_1 b_2/(a+2)^2}{\left(c_2 - \frac{b_2}{a+2}\right) - \left(c_1 - \frac{b_1}{a+2}\right)} \tag{xi}$$

and

$$c_2 - \gamma_2 = \frac{b_2}{a+2} - \frac{b_1 b_2/(a+2)^2}{\left(c_2 - \frac{b_2}{a+2}\right) - \left(c_1 - \frac{b_1}{a+2}\right)}. \tag{xii}$$

The second term in each of these expressions is negligible, so that the differences are given with reasonable accuracy by $b_1/(a+2)$ and $b_2/(a+2)$ respectively. In practice, b_2 is so small that the error in the calculated characteristic wave-length of the ultra-violet absorption band is only of the order of a few A, whilst for the Schumann band it is again of the order of 100 A, the value for *cyclo*-hexene being 158 A and for 1 : 3-*cyclo*-hexadiene, 140 A.

It remains to compare this error with that which may occur in deducing the constants, a, b, and c, or α, β, or γ from experimental data which are subject to a known probable error. For this purpose, we have assumed that the average error in the value of n^2 is not likely to exceed $1\cdot5 \times 10^{-4}$ in the visible and 7×10^{-4} in the ultra-violet. It is then found that such errors would introduce variations in *a*, *b*, *c*, of the following order of magnitude:

---

* Lowry and Allsopp, 'Proc. Roy. Soc.,' A, vol. 133, p. 48 (1931), benzene; vol. 143, p. 618 (1934), *cyclo*hexene and *cyclo*hexadiene; 'J. Chem. Soc.,' p. 1613 (1932), nicotine.

$$\delta a = 3 \times 10^{-5}, \quad \delta b = 4 \times 10^{-5}, \quad \text{and} \quad \delta c = 2 \times 10^{-4}.$$

The dispersion constant *c* can thus be determined correctly to 1 part in 50, *i.e.*, with a possible error in the calculated characteristic frequency of about 10 A as contrasted with an error of 100 A which arises from the use of the wrong dispersion-equation.

SUMMARY

The physical basis of the law of additivity as applied to molecular refractions is examined. The refractivity of a molecule may be expected to be the sum of the refractivities of its component atoms only when its refractive indices can be represented by a dispersion equation containing a single variable term with a characteristic frequency in the Schumann region of the spectrum.

Refractive indices of hexane are recorded at 57 visual and ultra-violet wave-lengths between 6708 and 2450 A, and the atomic refractivities of hydrogen and carbon over the same spectral range are deduced with the help of data previously recorded for *cyclo*-hexane.

The use of the Ketteler-Helmholtz equation instead of the Lorentz-Lorenz equation for determining the characteristic frequencies of the molecules of a liquid from its refractive dispersion involves an error of the order of 100 A in frequencies in the Schumann region. The error arising from experimental inaccuracy in the refractive indices is not greater than 10 A.

Refractive Dispersion of Organic Compounds

VIII—Isomers of the Formula $C_4H_8O_2$: Dioxan, Ethyl Acetate, *iso*-Butyric Acid, and Acetoin

By C. B. Allsopp, M.A., Ph.D., and H. F. Willis, M.Sc., Laboratory of Physical Chemistry, Cambridge

(*Communicated by Professor T. M. Lowry, F.R.S.—Received July* 25, 1935)

Introduction

In the preceding paper, Part VII, the law of additivity of atomic refractivities was discussed in the light of the *first* of the two fundamental observations on which it was based, namely, the constancy of the increment of molecular refraction in homologous series. The present Part VIII contains an account of an examination of the *second* of these observations, namely, the identity of the molecular refractivities of isomeric compounds. Whilst the conclusions drawn by Landolt* in this connexion were largely confirmed by later workers, notably by Brühl and by Eisenlohr,† they were lacking in one essential feature, since they were based on measurements which were confined to a few wave-lengths in the visible spectrum only. In the present paper this limitation has been overcome by using the interference method, by means of which measurements of the refractivities of a series of isomers have been extended from the visible into the ultra-violet spectrum up to the limits of transparency of thin films of the materials.

Absorption Spectra

The compounds selected were four isomers of the formula $C_4H_8O_2$, namely:

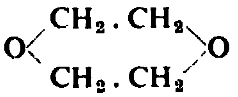

I. Dioxan

$CH_3 . CO . O . C_2H_5$

II. Ethyl acetate.

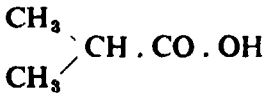

III. *iso*-Butyric acid.

$CH_3 . CO . CHOH . CH_3$

IV. Acetoin

---

* 'Pogg. Ann.,' vol. 117, p. 353 (1862); vol. 122, p. 545 (1864); vol. 123, p. 595 (1864); vol. 213, p. 75 (1882).

† *Cf.* "Spektrochemie Organischer Verbindungen," Stuttgart, 1912, pp. 32, *et seq.*

The absorption spectrum of the acid III has already been recorded*; that of acetoin was examined by Lowry and Baldwin†; those of the other isomers were determined as a part of the present research. The molecular extinction coefficients are plotted in fig. 1, together with comparable values for *cyclo*-hexanone. In the middle ultra-violet, acetoin shows the usual weak ketonic absorption band at 2800 A; but this is absent in the

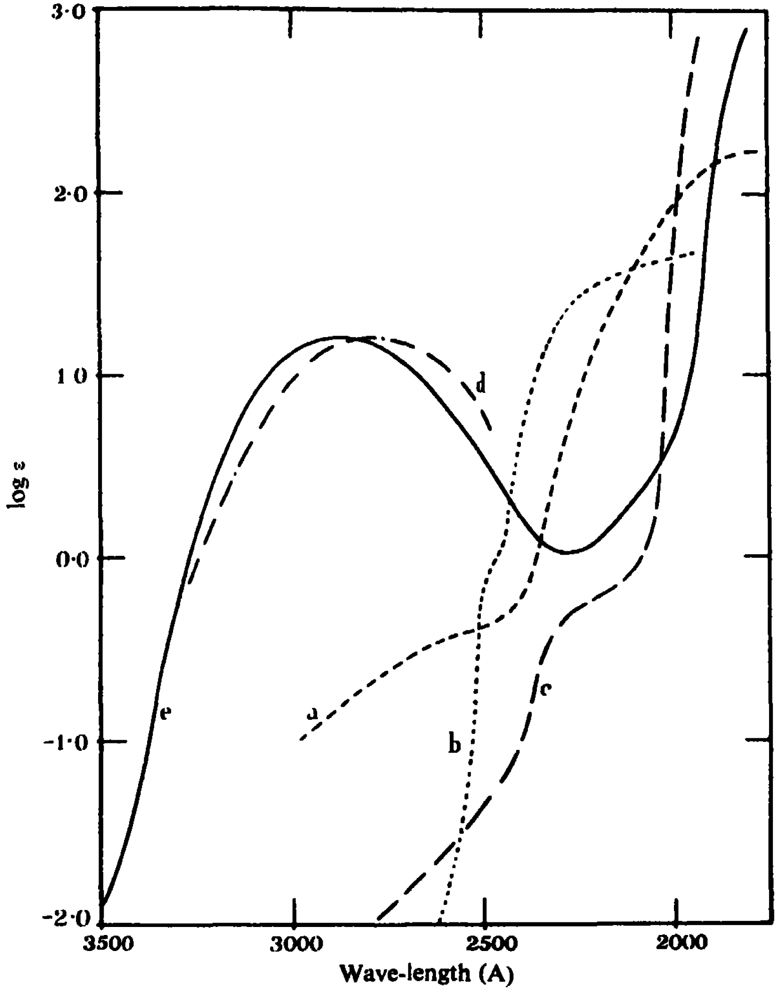

Fig. 1—Molecular extinction coefficients of *a*, *iso*-butyric acid, *b*, ethyl acetate; *c*, dioxan; *d*, acetoin; *e*, *cyclo*-hexanone.

---

* Part V, 'Proc. Roy. Soc.,' A, vol. 146, p. 300 (1934).

† 'J. Chem. Soc.' (1935), p. 704.

two carboxyl-compounds and in dioxan. Down to 2500 A ethyl acetate and dioxan are almost completely transparent, whilst *iso*-butyric acid shows only weak general absorption at wave-lengths less than 3000 A. All four compounds, however, have an absorption band of moderate strength near the limit of the accessible ultra-violet spectrum at 1850 A. This band is a well-known property of the carboxyl group,* and a similar absorption is not unexpected in acetoin; but it is more surprising to find an even stronger absorption in dioxan (*e.g.*, $\log \varepsilon = 2\cdot76$ at 1930 A), in view of the fact that alcohols and ethers have so often been used as transparent solvents for measurements of absorption up to the limit of strong emission by the iron arc at 2327 A. It is, however, now well-established that alcohols and ethers exhibit a strong general absorption as the Schumann region is approached, although the maximum is not accessible by the methods which are now most commonly used for measurements of absorption in the ultra-violet region.

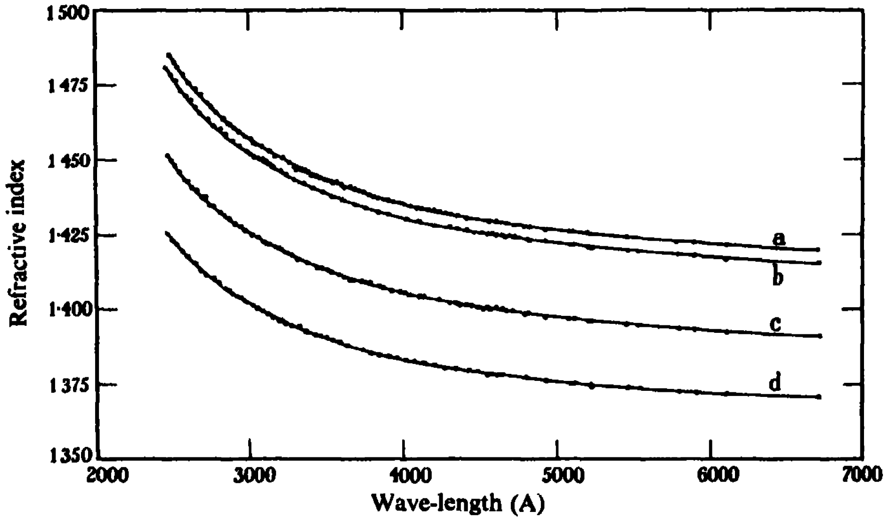

FIG. 2—Refractive indices of *a*, dioxan; *b*, acetoin; *c*, *iso*-butyric acid; *d*, ethyl acetate.

REFRACTIVE DISPERSION

The curves of refractive dispersion are drawn in fig. 2. They all follow a similar course, and tend asymptotically towards an absorption frequency at wave-lengths in the Schumann region. By using a very thin film, the refractive dispersion of acetoin was followed right through the ketonic absorption band, just as in the case of *cyclo*-hexanone.† The measurements, however, reveal no trace of a " ripple " of anomalous dispersion inside the absorption band. This band has therefore little or no influence on the refractive dispersion, although it dominates the rotatory dispersion exhibited by the same substance.*

---

* Bielecki and Henri, 'Phys. Z.,' vol. 14, p. 516 (1913).

† Part V.

Dispersion Equations

The refractive indices of the four compounds can be represented accurately over the whole range of the measurements by equations containing only one variable term, as follows:

Dioxan : $$\frac{n^2-1}{n^2+2}\cdot\frac{M}{d} = 21\cdot2161 + \frac{0\cdot148862}{\lambda^2 - 0\cdot014843}$$

Ethyl acetate: $$\frac{n^2-1}{n^2+2}\cdot\frac{M}{d} = 21\cdot772 + \frac{0\cdot158451}{\lambda^2 - 0\cdot012466}$$

iso-Butyric acid : $$\frac{n^2-1}{n^2+2}\cdot\frac{M}{d} = 21\cdot7067 + \frac{0\cdot15937}{\lambda^2 - 0\cdot012789}$$

Acetoin: $$\frac{n^2-1}{n^2+2}\cdot\frac{M}{d} = 21\cdot6941 + \frac{0\cdot164736}{\lambda^2 - 0\cdot01106}.$$

The characteristic frequencies of these equations lie in the Schumann region of the spectrum at wave-lengths of the order of 1100 A. The ultraviolet absorption bands associated with the —O—, $—CO.OC_2H_5$, —CO . OH, and —CO . CHOH— radicals therefore make no essential contribution to the refractive indices of the molecules, in striking contrast with the effect of the absorption bands in *cyclo*-hexanol, ethyl hexahydrobenzoate, and *cyclo*-hexanone,† which were quite appreciable at short wave-lengths, although their contributions were negligible in the visible spectrum.

Refractivities

Curves of molecular refractivity are of little value for the purpose of comparing the four isomers, since the differences cannot be shown on a sufficiently large scale. In fig. 3, therefore, the differences themselves are plotted against wave-lengths, with dioxan as an arbitrary standard, since it is the least refractive of the four compounds. Its refractivity is thus represented by the zero axis, whilst the other curves represent the increments of refractivity on passing from dioxan to ethyl acetate, acetoin, and *iso*-butyric acid. If the additivity law were valid at all wave-lengths, the four curves would coincide along the zero axis throughout their whole length. In reality the curves for ethyl acetate, acetoin, and *iso*-butyric acid are all displaced by about 0·5 units from the zero axis. Such a displacement might be expected in view of the fact that each of the two oxygen atoms of dioxan is linked by single bonds to two carbon atoms, whereas in the other compounds one of the oxygens is linked to carbon by a double bond. The molecular refraction of dioxan therefore includes contributions from *two* electronic systems of the type [C—O—C], as compared with [C—O—H] + [C=O] in *iso*-butyric acid and in acetoin, and [C—O—C] + [C=O] in ethyl acetate.

---

* Lowry and Baldwin, *loc. cit.*

† Part VI, ' Proc. Roy. Soc.,' A, vol. 146, p. 313 (1934).

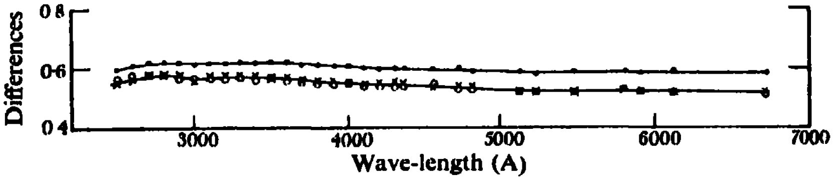

Fig. 3—Comparison of molecular refractivities. ● ethyl acetate; > acetoin; ○ *iso*-butyric acid; zero axis represents dioxan.

Influence of Conjugation and Coordination

It was shown in Part VI* that the refractivity of the carboxyl group in the visible spectrum is less than that of the constituent carbonyl and oxygen radicals $R[CO\,.\,O] < R[CO] + R[O]$. As the carboxylic band is approached, however, this effect is reversed, and the carboxyl-group exhibits a positive optical exaltation. Similar deviations from the additive law have also been observed in the parachors of the esters, which are 3 units less than the calculated values.† These anomalies are generally attributed to the close association of the >C=O and —OR groups, which Robinson (by an extension of Thiele's theory) regards as a modified form of *conjugation*,‡ so that a positive optical exaltation would usually be expected. On the other hand, in the carboxylic acids, the *coordination* of the acidic hydrogen atoms with two atoms of oxygen is widely admitted as an explanation both of their abnormal physical properties and of their readiness to form into polymeric molecules.§

The data recorded in fig. 3 are remarkable in that *the curves for* iso-*butyric acid and for acetoin are almost coincident throughout the whole*

---

* Part VI, 'Proc. Roy. Soc.,' A, vol. 146, p. 313 (1934).

† Sugden, 'J. Chem. Soc.,' vol. 125, p. 1179 (1924).

‡ 'J. Chem. Soc.,' vol. 109, p. 1038 (1916).

§ Pfeiffer, 'Liebig's Ann.,' vol. 398, p. 137 (1913); Lowry and Burgess, 'J. Chem. Soc.,' vol. 123, p. 2111 (1923).

range of the spectrum, whilst the curve for ethyl acetate is uniformly higher. The refractivity of this pair of compounds is therefore not affected when the two oxygens are attached to contiguous carbon atoms instead of to the same atom. This remarkable observation suggests that, whilst the peculiarities of the carboxyl group in the esters may perhaps be associated with a modified form of conjugation, those of the carboxylic acids cannot be interpreted in this way. On the other hand, they may be associated with a coordination of hydrogen, which would be even easier in acetoin than in a monocarboxylic acid, since it would lead to the formation of an unstrained ring of 5 atoms.

The curve for ethyl acetate lies uniformly 0·06 units above those for *iso*-butyric acid and for acetoin. This result is compatible with an additive law, if we assign a higher value to ethereal than to alcoholic oxygen. On this basis the conversion of ethereal into carboxylic oxygen would be accompanied by an increment of 0·58 units, whilst its conversion into hydroxylic oxygen would produce a decrement of 0·06 units, thus:

ethyl acetate – dioxan, R[C=O] – R[C—O—C] = 0·58 units.
ethyl acetate – *iso*-butyric acid, R[C—O—C] – R[C—O—H] = 0·06 units.

In addition to differences of refractivity, fig. 3 also discloses a difference between the *dispersive powers* of dioxan and of the other three isomers, the curves for which are slightly inclined to the zero axis. This difference may perhaps be attributed to an increased dispersion under the influence of the absorption band of dioxan, which lies at the limit of the accessible ultra-violet spectrum. This deduction is supported by the fact that the dispersion constant in the equation for dioxan is rather larger than those for the other isomers, and may thus represent a mean frequency of two bands, as in the cases of *cyclo*-hexanol and ethyl hexahydrobenzoate, where the influence of a second band has been detected in a region of incipient absorption but is too small to require an additional term in the dispersion equations for longer wave-lengths, Part V.

The results of the present investigation of the molecular refractions of isomeric compounds indicate that if allowance is made for the variations in the refractivity of oxygen, according to the manner in which it is linked in the molecule, *the law for additivity of atomic refractions is valid at all wave-lengths* for those compounds whose refractive dispersions can be represented by equations containing only one variable term, with a characteristic frequency in the Schumann region of the spectrum. They thus support the point of view which was set out in the preceding paper.

THE RELATIONSHIP BETWEEN ABSORPTION AND REFRACTIVE DISPERSION

A point of considerable theoretical importance is raised by the observation that the ultra-violet " ketonic " absorption band of acetoin makes no measurable contribution to the refractive indices, even in the spectral region covered by the band, although the corresponding band in *cyclo*-hexanone gives rise to a ripple of " anomalous " dispersion. The refractive dispersion of free molecules is represented, both on electromagnetic and on quantum theories, by an expression of the form:

$$n^2-1 = \frac{Le^2}{\pi m} \Sigma \frac{f_k}{\nu_k^2 - \nu^2},$$

in which

$$f_k = \frac{mc}{\pi e^2} \frac{1}{L} \int \mu_r d\nu$$

is a constant measuring the " strength " of the absorption due to the characteristic frequency ν_k. The partial refraction due to the frequency ν_k is therefore directly proportional to $\int \mu_r \, d\nu$, *i.e.*, to the area under the absorption curve. In fig. 1, the absorption curve for *cyclo*-hexanone is reproduced for comparison with that of acetoin, to which it shows a very close resemblance. The *f*-values deduced from these curves are almost identical at 0·00038 for $C_6H_{10}O$ and 0·00037 for $C_4H_8O_2$, but the partial refractions in the absorption band, which are easily detected in one case, were not observed in the other. This result indicates clearly that the theory of refractive dispersion, which has been repeatedly confirmed for the *line* absorption of metallic vapours, may not be valid when applied to the absorption *bands* of organic molecules.*

THE REFRACTIVITY OF OXYGEN

In accordance with the experimental observations of Gladstone,† Brühl,‡ and Conrady,§ Eisenlohr's tables contain refractivities for oxygen in three states of combination, as follows:

carbonyl oxygen, R[O''], from aldehydes and ketones,

$$R[O''] = R[C_nH_{2n}O''] - nR[CH_2];$$

---

* For literature, *see* Born, " Optik," pp. 495, 498; Lowry, " Optical Rotatory Power " (1935), p. 462.

† ' Proc. Roy. Soc.,' vol. 18, p. 49 (1870).

‡ ' Liebig's Ann.,' vol. 203, p. 1 (1880).

§ ' Z. phys. Chem.,' vol. 3, p. 210 (1889).

hydroxyl oxygen, R[O′], from acids,

$$R[O'] = R[C_nH_{2n}O''O'] - nR[CH_2] - R[O''];$$

ethereal oxygen, R[O<], from ethers or esters,

$$R[O<] = R[C_nH_{2n}O<] - nR[CH_2]$$

or

$$R[O<] = R[C_nH_{2n}O<O'] - nR[CH_2] - R[O'].$$

Eisenlohr's value for hydroxyl oxygen therefore depends on the assumption that the refractivity of the carboxyl radical is the sum of those of carbonyl and hydroxyl. This assumption is justified by the equality of the molecular refractions of *iso*-butyric acid and acetoin, although it is contradicted by the results described in Part VI. A determination of the *dispersion* of the refractivities of oxygen in its three types of linkage can therefore be based on the present measurements of refractive indices, as follows:

$$2R[O<] = R[\text{dioxan}] - \tfrac{2}{3}R[\textit{cyclo}\text{-hexane}].$$
$$R[O''] + R[O<] = R[\text{ethyl acetate}] - \tfrac{2}{3}R[\textit{cyclo}\text{-hexane}].$$
$$R[O'] + R[O''] = R[\textit{iso}\text{-butyric acid}] - \tfrac{2}{3}R[\textit{cyclo}\text{-hexane}].$$

The results are set out in Table I, and the dispersion curves are drawn in fig. 4. These have an almost constant separation throughout the whole range of wave-lengths, and appear to approach asymptotically to frequencies in the extreme ultra-violet spectrum, which, however, are at much longer wave-lengths than in the case of carbon or of hydrogen.

For comparison with the values which would be obtained, *on the same basis of calculation*, from the data recorded in Parts VI and VII, the refractivities now obtained at the D-lines are set out in Table II, which also contains Eisenlohr's values.

There is a striking contrast between the data now recorded for open-chain compounds, where the additive law seems to be true to a very close approximation, and those given by Lowry and Allsopp for ring compounds, where the additive law was shown to be invalid. This suggests that, although the optical behaviour of a saturated hydrocarbon ring is of the same simple type as that of an open-chain hydrocarbon, the introduction of a chromophoric group into the system gives rise to more complex relationships. This view is supported by the fact that the refractive dispersions of the substituted ring compounds cannot be represented, like those of open-chain compounds containing the same chromophoric groups, by dispersion equations containing only a single partial refraction. Some of the " anomalies " in the molecular refractions of cyclic compounds which are recorded in the literature may perhaps

TABLE I—REFRACTIVITIES OF THE OXYGEN ATOM

	Molecular refractions					Atomic refractions		
λ	Dioxan	Ethyl acetate	*iso*-Butyric acid	Acetoin	$\frac{2}{3}$R[C_6H_{12}]	Ethereal R[O<]	Carbonyl R[O″]	Hydroxyl R[O′]
6708	21·552	22·128	22·069	22·068	18·382	1·585	2·160	1·526
6104	21·633	22·217	22·153	22·151	18·438	1·597	2·181	1·533
5896	21·663	22·241	22·183	22·180	18·474	1·595	2·173	1·537
5791	21·680	22·273	22·203	22·205	18·488	1·596	2·189	1·526
5461	21·746	22·331	22·262	22·271	18·546	1·600	2·185	1·531
5220	21·800	22·382	22·320	22·323	18·592	1·604	2·185	1·542
5086	21·831	22·418	22·355	22·362	18·622	1·605	2·191	1·542
4800	21·907	22·501	22·434	22·446	18·686	1·611	2·204	1·544
4722	21·931	22·527	22·463	22·473	18·712	1·610	2·206	1·546
4678	21·944	22·542	22·485	22·485	18·720	1·613	2·210	1·556
4554	21·989	22·594	22·535	22·532	18·752	1·619	2·223	1·560
4358	22·063	22·675	22·608	22·614	18·816	1·624	2·236	1·557
4300	22·09	22·69	22·63	22·65	18·84	1·63	2·23	1·57
4200	22·14	22·74	22·68	22·69	18·87	1·635	2·235	1·575
4100	22·19	22·79	22·73	22·74	18·91	1·64	2·24	1·58
4000	22·24	22·85	22·79	22·79	18·95	1·645	2·255	1·585
3900	22·30	22·91	22·85	22·86	19·00	1·65	2·26	1·59
3800	22·37	22·98	22·92	22·93	19·05	1·66	2·27	1·60
3700	22·44	23·05	22·99	23·00	19·11	1·665	2·275	1·605
3600	22·51	23·13	23·07	23·08	19·18	1·665	2·285	1·605
3500	22·60	23·22	23·16	23·17	19·25	1·675	2·295	1·615
3400	22·69	23·31	23·26	23·27	19·34	1·675	2·295	1·625
3300	22·80	23·42	23·37	23·38	19·43	1·685	2·305	1·635
3200	22·92	23·54	23·49	23·50	19·53	1·695	2·315	1·645
3100	23·05	23·67	23 62	23·63	19·64	1·705	2 325	1·655
3000	23·20	23·82	23·77	23·76	19·79	1·725	2·345	1·655
2900	23·37	23·99	23·94	23·95	19·87	1·75	2·37	1·70
2800	23·56	24·18	24·14	24·14	20·06	1·775	2·395	1·735
2700	23·78	24·40	24·36	24·36	20·16	1·81	3·43	1·77
2600	24·04	24·65	24·62	24·61	20·34	1·85	2·46	1·82
2500	24·34	24·94	24·91	24·90	20·57	1·885	2·52	1·82

TABLE II—REFRACTIVITIES OF OXYGEN

	R[O″]	R[O<]	[RO′]
Open-chain compounds (Eisenlohr) ……	2·211	1·643	1·525
Open-chain compounds (Allsopp and Willis, Part VIII) ……………………	2·173	1·595	1·537
Ring compounds (Lowry and Allsopp, Part VI) …………………………	2·401	1·551	1·625

also be attributed to the same disturbing influence of a chromophoric group on their optical properties.

EXPERIMENTAL

Materials—Dioxan and *ethyl acetate* were supplied by Professor Timmermanns from the *Bureau D'Etalons Physico-chimiques* in Brussels. Their densities were $d_4^{20} = 1{\cdot}03361$ and $0{\cdot}90055$ respectively. *iso*-Butyric acid was the sample used previously for measurements of absorption spectra, Part V. It boiled at 154° and had $d_4^{20} = 0{\cdot}9486$. Acetoin was the specimen described elsewhere by Lowry and Baldwin (*loc. cit.*). After each redistillation, crystals of a polymer invariably formed, and it was therefore necessary to make all the measurements rapidly with small quantities of freshly distilled material. Accurate determination of the density at 20° proved to be difficult, since polymerization occurred during the short time necessary for the exact temperature to be attained. It was found possible, however, to measure the coefficient of expansion at neighbouring temperatures with sufficient accuracy for the density at 20° to be interpolated, and a mean value $d_4^{20} = 1{\cdot}000$ was finally adopted, agreeing closely with the *mean* of the widely differing

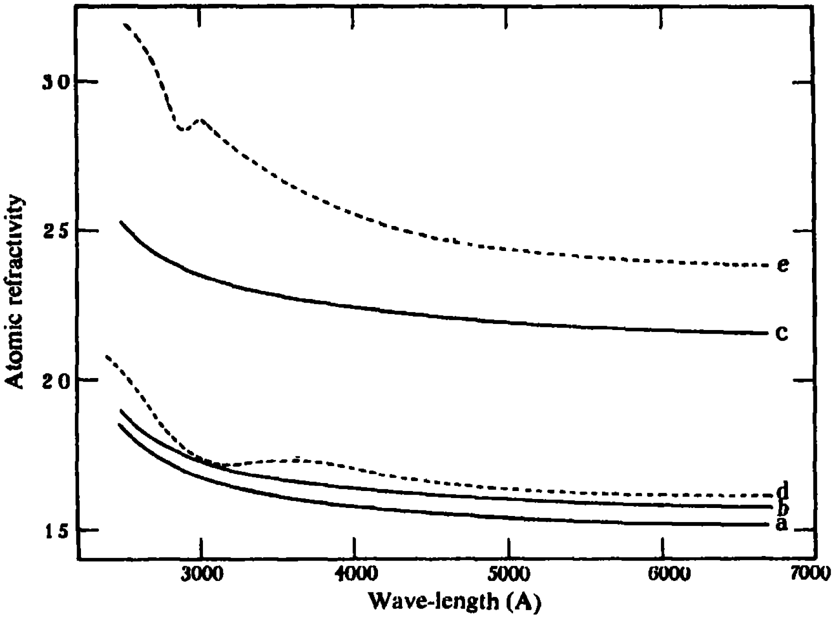

FIG. 4—Atomic refractivity of oxygen: *a*, hydroxyl; *b*, ethereal; *c*, carbonyl; *d*, hydroxyl; *e*, carbonyl (*d* and *e*, Lowry and Allsopp, Part VI).

TABLE III—REFRACTIVE INDICES, AT 20° C, AND MOLECULAR REFRACTIONS OF DIOXAN, ACETOIN, *iso*-BUTYRIC ACID, AND ETHYL ACETATE. VISUAL READINGS

	Refractive indices								Molecular refractions			
	Dioxan		Acetoin		*iso*-Butyric acid		Ethyl acetate		Dioxan	Acetoin	*iso*-Butyric acid	Ethyl acetate
λ*	*n* observed	(O − C) × 10⁴	*n* observed	(O − C) × 10⁴	*n* observed	(O − C) × 10⁴	*n* observed	(O − C) 10⁴				
Li 6707·86	1·41979	−1·5	1·41532	−0·4	1·39124	−0·5	1·37018	−1·6	21·552	22·068	22·069	22·128
Li 6103·6	1·42159	+0·1	1·41710	+0 2	1·39294	+0·8	1·37185	+0·6	21·633	22·151	22·153	22·217
Na 5895·93	1·42227	−0·1	1·41774	−0·8	1·39352	±	1·37229	−1·1	21 663	22·180	22·183	22·241
Hg 5790·66	1·42265	−0·1	1·41826	+0·5	1·39393	+0·5	1·37289	+1·5	21·680	22·205	22·203	22·273
Cu 5782·15	1·42269	±	1·41831	+0·7	1·39390	−0·2	1·37283	+0·6	21 682	22·207	22·201	22·270
Ba 5535·5			1·41930	+0·3	1·39475	−1·0	1·37367	+0·3		22·253	22·243	22·315
Ag 5471·51	1·42405	+0·8	1·41960	+0·3	1·39509	−0·3	1·37388	−0·1	21·743	22·267	22·261	22·325
Hg 5460·73	1·42413	−1·1	1·41969	+0·7	1·39513	−0·4	1·37399	+0·5	21·746	22·271	22·262	22·331
Cu 5220·06	1·42532	+1·4	1·42081	−0·3	1·39628	±	1·37494	−0·3	21·800	22·323	22·320	22·382
Ag 5209·04	1·42526	+0·2	1·42088	−0·1	1·39624	−0·9	1·37499	−0·3	21·797	22·327	22·318	22·385
Cu 5105·55	1·42581	±	1·42144	−0·3	1·39684	−0·2	1·37543	−0·8	21·822	22·353	22·348	22·408
Cd 5085·82	1·42602	+1 0	1·42164	+0 5	1·39698	+0·1	1·37561	+0·1	21·831	22·362	22·355	22·418
Ba 4934·10	1·42684	+0·2	1·42248	−0·4	1·39788	+0·5	1·37633	−0·7	21·868	22·401	22·400	22·456
Zn 4810·53	1·42761	−0·2	1·42330	−0 6	1·39867	+0·8	1·37708	−0·3	21·903	22·439	22·439	22·496
Cd 4799·91	1·42771	+0·1	1·42344	+0·1	1·39857	−0·9	1·37717	±	21·907	22·446	22·434	22·501
Zn 4722·16	1·42824	−0·1	1·42404	+0·4	1·39915	−0·3			21·931	22·473	22·463	
Cd 4678·15	1·42854	−0·4	1·42429	−0·4	1·39959	+1·0			21·944	22·485	22·485	
Li 4603·0	1·42912	−0·3	1·42496	+0·3	1·40017	+1·4	1·37865	+2·1	21·970	22·516	22·514	22·580
Ba 4554·04	1·42955	±	1·42530	−0·3	1·40059	+1·9	1·37891	+1·2	21·989	22·532	22·535	22·594
Hg 4358·34	1·43120	−0·7	1·42707	−0·3	1·40207	+0·5	1·38044	+1·5	22·063	22·614	22·608	22·675

* Wave-lengths from 'International Critical Tables,' vol. 5 (1929).

values which have been recorded for this substance. The sample had a specific rotatory power $[\alpha]^{20}_{5461} = 8{\cdot}04°$.

REFRACTIVE INDICES

The refractive indices of all four isomers at 20 wave-lengths in the visible spectrum are recorded in Table III, and Tables IV to VII contain the ultra-violet values obtained photographically for dioxan, ethyl acetate, *iso*-butyric acid, and acetoin. Table I contains the molecular refractions, the values at ultra-violet wave-lengths being interpolated from neighbouring photographic readings together with the refractivities of the oxygen atom derived from them.

TABLE IV—REFRACTIVE INDICES OF DIOXAN AT 20° C—PHOTOGRAPHIC READINGS

λ	Refractive index		Molecular refraction	λ	Refractive index		Molecular refraction
	n observed	(O − C) × 10^4			*n* observed	(O − C) × 10^4	
4683·6 W	1·4284	1	21·937	3493·2	1·4434	±	22·605
4636·4	1·4292	+3	21·973	3441·0 Fe	1·4444	−1	22·650
4587·7	1·4293	+	21·978	3391·1 W	1·4457	+1	22·706
4540·5 W	1·4294	−3	21·983	3342·2 Fe	1·4467	−1	22·750
4495·6	1·4300	±	22·009	3295·0	1·4479	±	22·804
4450·3	1·4302	−2	22·019	3260·7	1·4489	+1	22·848
4364·8 W	1·4314	+2	22·072	3199·5 Fe	1·4501	−3	22·901
4281·4	1·4321	+1	22·103	3130·3 W	1·4526	+1	23·010
4202·0 Fe	1·4331	+2	22·148	3085·7	1·4539	±	23·068
4124·1	1·4336	−1	22·170	3031·2 Fe	1·4554	−3	23·134
4049·5	1·4342	−4	22·196	2979·9 W	1·4576	±	23·230
3980·0	1·4357	+2	22·263	2930·0	1·4595	±	23·313
3910·8 Fe	1·4364	±	22·294	2866·6 Fe	1·4618	−3	23·415
3844·5	1·4372	−1	22·330	2790·9	1·4653	−2	23·567
3780·8 W	1·4382	−1	22·374	2727·2	1·4686	−1	23·711
3719·9 Fe	1·4395	+3	22·433	2647·1 W	1·4730	−2	23·901
3660·4	1·4405	+3	22·476	2573·1	1·4780	+1	24·118
3602·5 Fe	1·4413	±	22·512	2503·0	1·4826	−3	24·315
3547·6	1·4426	+3	22·570	2487·1 Fe	1·4844	+3	24·392

The authors desire to place on record their indebtedness to Professor T. M. Lowry, F.R.S., for his continued advice and encouragement, and to the Council of the University of Wales for a Fellowship held by one of them (H. F. W.) during the period in which the investigations described in the present papers (Parts VII and VIII) were carried out.

SUMMARY

Molecular extinction coefficients, refractive indices, and molecular refractivities at a large number of visible and ultra-violet wave-lengths are recorded for the following isomers of the formula $C_4H_8O_2$: dioxan, ethyl acetate, *iso*-butyric acid, and acetoin. Atomic refractivities for ethereal, carbonyl, and hydroxyl oxygen are deduced.

TABLE V—REFRACTIVE INDICES OF ACETOIN AT 20° C—PHOTOGRAPHIC READINGS

λ	Refractive index *n* observed	Refractive index (O − C) × 10^4	Molecular refraction	λ	Refractive index *n* observed	Refractive index (O − C) × 10^4	Molecular refraction
4709·2	1·4246	+5	22·500	3421·5	1·4407	2	23·241
4647·4 Fe	1·4249	+3	22·513	3359·9	1·4422	±	23·310
4587·0 W	1·4251	±	22·522	3299·4	1·4432	−5	23·356
4528·6 Fe	1·4255	−1	22·542	3243·0	1·4451	±	23·443
4471·1	1·4256	−4	22·545	3188·2	1·4467	+1	23·515
4417·6	1·4267	+2	22·597	3136·1	1·4487	+6	23·607
4363·4	1·4270	−1	22·610	3082·0 W	1·4502	+4	23·676
4310·9	1·4275	−1	22·634	3034·3 W	1·4513	±	23·726
4208·2	1·4279	−7	22·652	2987·3 Fe	1·4532	+2	23·812
4113·4	1·4293	−5	22·717	2938·3	1·4548	+1	23·884
4021·9 Fe	1·4304	−4	22·767	2894·3	1·4566	+1	23·966
3934·8	1·4316	−4	22·823	2810·4	1·4604	+4	24·138
3850·8 Fe	1·4325	−6	22·865	2730·7 Fe	1·4637	±	24·287
3771·7	1·4339	−5	22·930	2656·8 Fe	1·4675	−1	24·459
3695·1 Fe	1·4350	−6	22·979	2586·8	1·4712	−4	24·623
3623·2 Fe	1·4367	−1	23·058	2523·2	1·4764	+7	24·854
3552·6	1·4378	−4	23·109	2491·5	1·4782	+3	24·937
3486·1	1·4394	−1	23·182	2445·3	1·4808	−5	25·053

The refractive indices of each compound can be represented by a dispersion equation containing a single variable term, contributed by a frequency in the Schumann region of the spectrum; and the molecular refractivities are in accordance with a law of additivity of atomic refractivities which is valid throughout the whole range of spectrum.

The *f*-value of the ketonic absorption band of acetoin is almost identical with that of the corresponding band of *cyclo*-hexanone, but the partial refraction in the absorption band, which was easily detected for the latter compound, is not now observed. The partial refractions of the absorption bands of organic molecules are therefore not necessarily proportional to the *f*-values.

TABLE VI—REFRACTIVE INDICES OF *iso*-BUTYRIC ACID AT 20° C—PHOTOGRAPHIC READINGS

λ	Refractive index		Molecular refraction	λ	Refractive index		Molecular refraction
	n observed	(O − C) × 10^4			*n* observed	(O − C) × 10^4	
4693·0	1·3994	±	22·475	3382·4 Fe	1·4157	+1	23·282
4610·1	1·3998	−2	22·495	3320·4 W	1·4170	+1	23·346
4531·2 Fe	1·4007	+1	22·541	3281·1	1·4182	+4	23·405
4455·0 Fe	1·4015	+3	22·580	3232·7 W	1·4194	+4	23·464
4378·5 W	1·4014	−5	22·575	3174·3	1·4208	+3	23·533
4307·9 Fe	1·4024	−1	22·624	3117·6 W	1·4219	−2	23·586
4238·8 Fe	1·4031	±	22·660	3064·7	1·4238	+2	23·679
4139·8	1·4043	+2	22·720	3029·8	1·4247	±	23·724
4043·9 Fe	1·4049	−3	22·748	2979·9 W	1·4266	+3	23·816
3984·0 Fe	1·4059	±	22·799	2915·1 W	1·4286	±	23·914
3924·4	1·4063	−3	22·819	2869·3 Fe	1·4305	+2	24·006
3868·0 W	1·4073	−1	22·868	2809·6 W	1·4326	−2	24·108
3786·7 Fe	1·4088	+3	22·942	2753·3 Fe	1·4351	−1	24·229
3733·3 Fe	1·4094	+1	22·971	2699·6 W	1·4377	−1	24·356
3680·8 Fe	1·4097	−4	22·987	2661·0	1·4398	+1	24·440
3632·0 Fe	1·4109	±	23·045	2611·1 Fe	1·4423	−1	24·578
3583·3 Fe	1·4115	−2	23·075	2552·1 W	1·4459	±	24·751
3536·6 Fe	1·4125	±	23·125	2496·0 W	1·4495	±	24·925
3468·8 Fe	1·4139	+1	23·193	2474·8 Fe	1·4512	+2	25·006

TABLE VII—REFRACTIVE INDICES OF ETHYL ACETATE AT 20° C—PHOTOGRAPHIC READINGS

λ	Refractive index		Molecular refraction	λ	Refractive index		Molecular refraction
	n observed	(O − C) × 10⁴			*n* observed	(O − C) × 10⁴	
4650·0	1·3782	+1	22·555	3415·1	1·3917	−5	23·270
4570·7 W	1·3789	+2	22·594	3373·8 W	1·3928	−2	23·329
4493·4	1·3794	+2	22·619	3314·1	1·3945	+3	23·417
4418·8	1·3798	±	22·640	3272·9	1·3947	−4	23·429
4347·1	1·3804	±	22·673	3214·0 Fe	1·3964	±	23·517
4277·2	1·3809	−1	22·700	3156·3 Fe	1·3977	−1	23·587
4210·4 Fe	1·3816	±	22·736	3101·5	1·3994	+2	23·675
4145·8	1·3824	+2	22·778	3047·6 Fe	1·4005	−2	23·733
4083·0 W	1·3830	+2	22·811	2996·1	1·4019	−3	23·805
4020·5	1·3831	−4	22·817	2947·9	1·4039	+2	23·910
3962·4	1·3841	±	22·868	2899·9	1·4053	±	23·984
3905·1	1·3847	−1	22·901	2854·7	1·4073	+4	24·088
3850·0 Fe	1·3856	+1	22·949	2810·0	1·4087	+1	24·160
3794·3 Fe	1·3856	−6	22·949	2767·5 Fe	1·4106	+3	24·260
3743·3 Fe	1·3868	−1	23·012	2724·9 Fe	1·4116	−5	24·311
3642·8	1·3882	−1	23·092	2684·8 Fe	1·4133	−6	24·400
3595·3	1·3891	±	23·133	2647·1 W	1·4155	2	24·513
3548·6	1·3898	±	23·169	2574·4 Fe	1·4197*	+2	24·730
3503·3	1·3906	±	23·213	2504·7 W	1·4231	−4	24·906
3459·1	1·3914	1	23·255	2473·2 Fe	1·4259	+5	25·051

The Band Spectra of the Lead Halides, PbF and PbCl

By G. D. ROCHESTER, M.Sc., Earl Grey Fellow of Armstrong College,
Newcastle-upon-Tyne

(*Communicated by W. E. Curtis, F.R.S.—Received July* 27, 1935)

[PLATE 8]

INTRODUCTION

In the course of a series of investigations on the halides of Groups IV and V of the Periodic Table, Howell and Rochester* reported that high-frequency discharges through the vapours of lead and bismuth halides excited in each case large systems of bands degraded to the red and noted the striking similarity in general appearance of the spectra of corresponding lead and bismuth compounds. Such similarity was seen, especially when spectrograms of the fluorides or the chlorides were compared. Two of the lead halide spectra, namely, those ascribed to the diatomic molecules PbF and PbCl, have been analysed and are described in the present paper. It is shown that their similarity to the corresponding spectra of the bismuth halides is a consequence of the identity of the vibrational constants. No previous observations on the band spectrum of PbF appear to have been made. The fluorescent spectrum of PbCl has been photographed and partly analysed by Popov and Neujmin,† using spectrographs of low dispersion (20 — 80 A per mm).

EXPERIMENTAL

Lead Fluoride (PbF)

The most satisfactory source of the spectrum of PbF was a high-frequency discharge through the vapour of the lead salt (PbF_2) in a quartz tube of the form shown in fig. 1.

The middle portion of the tube was of clear quartz 5 cm long × 0·5 cm internal diameter and was joined to wider pieces of quartz vitreosil tubing. One end of the discharge tube was covered with a plane quartz window. A small well had been blown in the clear quartz tube B and into this were melted about three grams of pure anhydrous lead fluoride. The discharge, readily started by exhausting and heating the tube strongly with a bunsen-burner, was of a deep blue colour. By continuous pumping and appropriate heating of different parts of the tube, no difficulty was experienced in maintaining a fairly constant vapour pressure for a considerable time. Exposures longer than two hours were, however, impossible because of the destructive action of the molten salt on the walls of the tube.

---

* 'Proc. Univ. Durham Phil. Soc.,' vol. 9, p. 126 (1934).

† 'Phys. Z. Sowjet.,' vol. 2, p. 394 (1932).

Preliminary photographs taken on a Hilger small quartz spectrograph in the region 2000 to 6800 A revealed a spectrum extending from 4200 to 5400 A. Photographs on larger dispersion were taken on a Hilger E52 spectrograph, having a dispersion varying from 5·5 A per mm to 12 A per mm in the region covered by the spectrum, using Ilford Monarch and Hypersensitive Panchromatic plates. Exposure times ranged from ¼ to 2 hours.

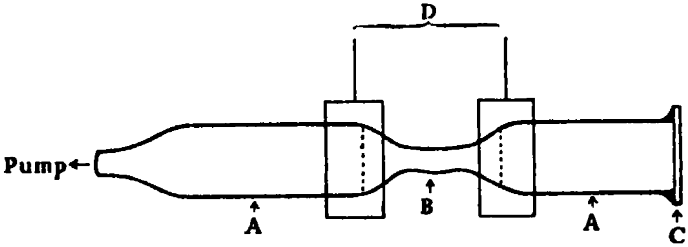

FIG. 1—A, vitreosil quartz; B, clear quartz; C, quartz window; D, high-frequency oscillator. 2 kW λ — 180 m.

Lead Chloride (PbCl)

(*a*) *Emission*—Whereas hot lead fluoride was extremely destructive of quartz, no such action of lead chloride was observed; a much more energetic discharge could therefore be used to excite its spectrum. The most satisfactory was found to be an uncondensed transformer discharge through lead chloride vapour, using an H-shaped tube with side-limbs in which were long water-cooled tungsten electrodes. The tube carrying the discharge was 15 cm long × 0·3 cm internal diameter, and it had a deep well at one end containing 20 grams of pure anhydrous lead chloride, so that when in operation a current of vapour could be drawn into the discharge. It was always necessary to keep the lead chloride gently boiling and to heat the discharge tube. With a voltage of 5000 and a current of approximately 0·2 amperes the discharge was of a bluish-white colour, and when photographed on a Hilger small quartz spectrograph showed a spectrum confined to the region 4200 to 5700 A. Photographs were also taken in the second order of a small plane grating having a dispersion of 5 A per mm. Ilford Monarch and Special Rapid

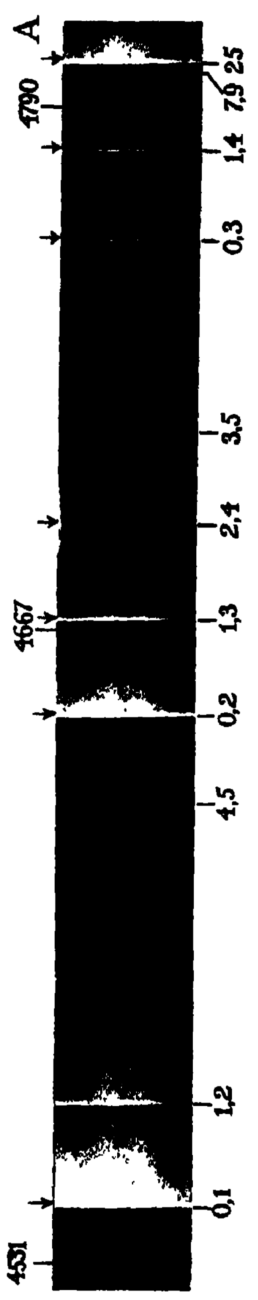

Fig. 2—Lead fluoride emission bands. × 8. Band origins are indicated by an arrow head.

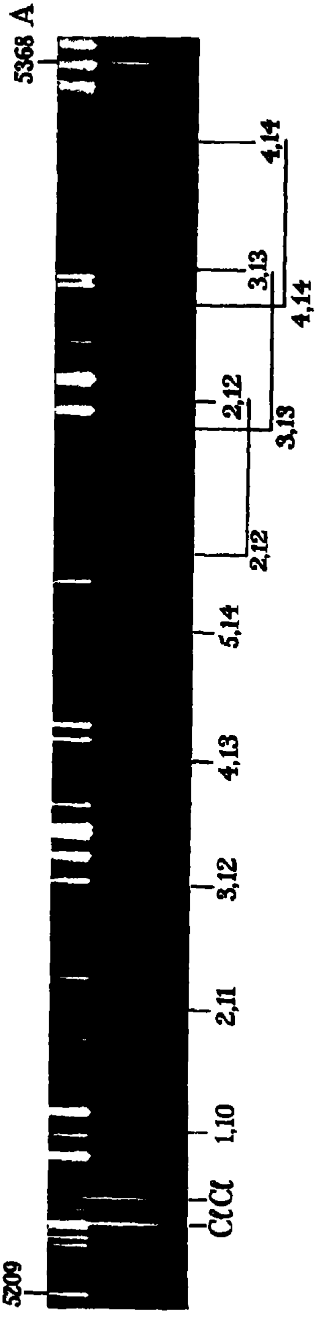

Fig 3—Lead chloride emission bands. × 8.

Panchromatic plates were used throughout with exposure times varying from one to two hours.

(*b*) *Absorption*—Many PbCl bands were obtained in absorption with fairly good contrast even with low vapour pressures of lead chloride by using a long column of absorbing vapour. The absorption tube, an iron tube 3·5 feet long × 1 inch internal diameter, had a length of 2·5 feet heated by a gas furnace capable of giving a maximum temperature of approximately 750° C (v.p. of PbCl at 750° C is 40 mm). No windows covered the ends of the tube, as these were found by experiment to be unnecessary.

With a Philips tungsten band lamp (taking 15 amperes at 12 volts) as the source of continuum exposure times ranged from one to two hours.

Three plates covered the whole of the PbF spectrum and four the PbCl (emission) spectrum with such large regions of overlap that almost all bands were photographed twice. Measurements of the band-heads were made on a Zeiss comparator and were reduced to wave-lengths, using iron arc wave-length standards and methods of reduction appropriate to the type of spectrograph. The PbF band-heads were very sharp, and results from different plates for strong bands seldom differed by more than 0·5 cm^{-1}. On the other hand, PbCl band-heads were not so sharp and well defined; for these bands measurements from different plates seldom differed by more than 1 cm^{-1}.

Intensities were assigned visually on the usual 0–10 scale, no attempt being made to correlate the scales for the two spectra.

DESCRIPTION OF THE SPECTRA

Representative photographs exhibiting the main features of both spectra are reproduced in Plate 8.

Lead Fluoride (PbF)

Fig. 2, Plate 8, shows clearly that these bands are grouped in well-marked sequences and have intense, line-like heads, wide gaps at the origin, and fairly strong and in some cases well-resolved branches on the low-frequency sides of the band-origins. It is possible that these well-resolved branches may be P branches, since they do not form sharp heads. Since the bands degrade to the red the line-like heads must be R heads.

Lead Chloride (PbCl)

Fig. 3, Plate 8, shows part of the emission spectrum of PbCl. The line-like heads and prominent sequences of PbF are absent, and, especially at the violet end of the spectrum, much overlapping of one band by another occurs. The principal bands in the spectrum are due to the molecule $PbCl^{35}$. When these are intense and remote from the system-origin, they are accompanied by weaker bands due to the molecule $PbCl^{37}$.

The absorption spectrum consists of a set of narrow discrete bands, lying in the region 4300 – 4800 A, identical with emission bands of small v'' number, and a broad region of strong continuous absorption beginning at 4300 A and extending into the ultra-violet. Since free chlorine, resulting from the dissociation of the lead chloride ($PbCl_2$), must have been present in the absorption tube, it is probable that the observed continuum is the well-known chlorine absorption band lying in that region.

VIBRATIONAL ANALYSES AND INTENSITY DISTRIBUTIONS

The Deslandres schemes for both molecules have been constructed, the presence of long "bounding" progressions of strong bands indicating unambiguously how the quantum allocations were to be made. In PbCl the chlorine isotope effect confirms the v enumeration. For both spectra and all electronic states graphs of $G(v):v$ are sensibly straight; the vibrational constants have been derived from these in the usual way. Mean ΔG values are shown in the square arrays of Tables I and II. The formulae for the R band-heads are:

$$\text{PbF} \quad \nu = 22{,}566\cdot6 + 397\cdot75\,(v' + \tfrac{1}{2}) - 1\cdot77\,(v' + \tfrac{1}{2})^2 - 507\cdot5\,(v'' + \tfrac{1}{2}) + 2\cdot32\,(v'' + \tfrac{1}{2})^2 \,.. \qquad (1)$$

$$\text{PbCl} \quad \nu = 21{,}863\cdot1 + 228\cdot8\,(v' + \tfrac{1}{2}) - 0\cdot795\,(v' + \tfrac{1}{2})^2 - 303\cdot6\,(v'' + \tfrac{1}{2}) + 0\cdot875\,(v'' + \tfrac{1}{2})^2 + \ldots. \qquad (2)$$

The O – C (observed – calculated) values given in Tables V and VI show that these formulae represent the wave numbers of the observed bands with an accuracy of the same order as that of measurement. The residuals for PbCl seem to show a small continuous change with v'', probably indicating that a small term in $(v'' + \tfrac{1}{2})^3$ should be added to (2). Both systems have similar intensity distributions (*see* Tables I and II), consisting of the usual Condon curve with one long and one short limb as commonly found for transitions involving relative ω values such as occur in this case.

Popov and Neujmin* have observed numerous PbCl bands in fluorescence and have proposed an analysis differing appreciably from the one

---

* 'Phys. Z. Sowjet.,' vol. 2, p. 394 (1932).

TABLE I—INTENSITIES AND VIBRATIONAL ANALYSIS OF PbF BANDS

v' \ v''	0	1	2	3	4	5	6	7	8	9	10	11	12	13	ΔG′
0	(8)	(10)	(9)	(7)	(4)										394·3
1	(10)		(4)	(9)	(7)	(6)									390·3
2	(5)		(3)		(8)	(7)	(6)	(2)							386·6
3	(2)	(3)		(2)		(2)	(5)	(4)	(2)	(0)					384·1
4		(3)	(1)		(1)	(2)		(4)	(3)	(2)	(1)				380·1
5			(2)						(0)	(1)	(2)	(1)			376·4
6			(1)						(2)		(2)	(2)	(1)		372·5
7										(1)		(1)	(1)	(1)	369·1
8											(0)			(1)	
9												(0)			
ΔG″	501·4	498·1	493·3	488·7	484·6	479·1	474·8	471·0	465·6	461·5	456·3	453·1	448·8		
v''	0	1	2	3	4	5	6	7	8	9	10	11	12	13	

TABLE II—INTENSITIES AND VIBRATIONAL ANALYSIS OF PbCl^{35} BANDS

v' \ v''	0	1	2	3	4	5	6	7	8	9	10	11	12	13	14	15	16	17	18	ΔG′
0		(2)	(7)	(8)	(9)	(10)	(10)	(10)	(1)	(2)										
1	(2)	(10)	(10)	(8)					(9)	(10)	(5)									226·9
2	(4)	(10)	(7)		(5)	(6)	(0)			(5)	(10)	(8)	(4)							225·7
3	(8)	(6)		(0)								(6)	(8)	(8)						224·3
4	(10)	(1)		(3)										(6)	(8)	(8)	(6)			221·7
5	(10)		(3)												(1)	(8)	(8)	(6)		221·0
6	(8)		(2)														(2)	(8)	(3)	219·6
7	(5)																			216·8
8	(1)	(2)																		215·0
9																				
10																				
ΔG″	302·4	300·0	298·2	296·0	296·0	292·8	292·1	290·6	286·3	285·8	285·4	282·1	280·9	278·9	277·2	276·7	273·8	271·6		
v''	0	1	2	3	4	5	6	7	8	9	10	11	12	13	14	15	16	17	18	

given here. Two main differences appear; in the first place a difference of 4 units in the v' numeration leading to a value of ω_e' of 250 cm^{-1} as against 229 cm^{-1}, and in the second an entirely different value of ω_e'', namely, 540 cm^{-1} as against 304 cm^{-1} (from present observations). In order that reliance can be placed on any vibrational analysis, it is in general essential that the first differences in the Deslandres scheme should agree to within a few wave numbers. First differences in the work under consideration often vary by as much as 15 cm^{-1}, and in consequence a difference approximately equal to $\omega_e' + \omega_e''$ has been mistaken for a first difference. The analysis presented here fulfils the requirement just outlined and in addition receives support from the chlorine isotope effect and the intensity distribution.

THE ISOTOPE EFFECTS

Since lead and chlorine are known to have several isotopes (*vide* Table III), one might expect to be able to observe lead isoptic band-heads in the spectrum of PbF and lead and chlorine isotopic heads in PbCl.

TABLE III—ABUNDANCES AND MASSES OF THE PRINCIPAL ISOTOPES OF LEAD AND CHLORINE*

Lead	Masses	206	207	208
	Abundances	4	3	7
Chlorine	Masses	35	37	
	Abundances	3	1	

* Aston, "Isotopes," pp. 134, 151. Arnold (1933).

The Lead Isotope Effect

In only one previous observation, namely, that of Bloomenthal* on the spectrum of PbO, has definite evidence of lead isotope effects been found. Bloomenthal was able to identify rotational lines due to the three most abundant isotopic molecules and to show that the separations of these lines were as predicted by Mulliken's theory. The dispersion used in the present work is much less than Bloomenthal's; thus the most one can hope to observe is a vibrational isotope effect at the band-heads. The conditions favouring the detection of the effect are that the heads must be intense and must lie on the short-wave side of the system-origin to ensure that the heads due to the less abundant isotopic molecules are not hidden by those due to the more abundant.

Very few bands in the spectrum of PbF fulfil these requirements; in the most suitable case, 2,0, the calculated separation of the heads due to the molecules $Pb^{206}F$ and $Pb^{208}F$ is $0 \cdot 3$ cm^{-1}, a separation which is much too small to observe; in fact, an examination of enlargements of the bands reveals no sign of diffuseness in any band-head.

---

* 'Phys. Rev.,' vol. 35, p. 34 (1930).

The spectrum of PbCl is much more suitable for the observation of the lead isotope effect because of the occurrence of a long progression of strong bands on the short-wave side of the system-origin. For the most favourable band, 6,0, the calculated separation, $Pb^{206}Cl^{35} - Pb^{208}Cl^{35}$ is $0 \cdot 9$ cm^{-1}, the $Pb^{207}Cl^{35}$ head being approximately midway between these heads. No sign of structure has been observed, but there is a slight diffuseness which might be an isotope effect.

The Chlorine Isotope Effect

Numerous observations concerning the chlorine isotope effect in band spectra have been made. Jevons* cites twelve different molecules for which the effect has been observed, and to this list at least another six recent observations can be added, *i.e.*, in the spectra of AlCl,† BeCl,‡ BiCl,§, GaCl§, InCl§ and SiCl.‖ Since the theory of isotopy has been amply verified for the chlorine isotopes, new observations are of use only in bringing out new points in the theory or of using the isotope effect to confirm the v numerations, as in the present case. The observed vibrational isotope separations, together with the theoretical separations, are collected in Table IV, the theoretical separations being calculated from the formula¶:

$$\nu^{i}_{v} - \nu_{v} = -0 \cdot 02339\,[228 \cdot 8\,(v' + \tfrac{1}{2}) - 303 \cdot 6\,(v'' + \tfrac{1}{2})] + 0 \cdot 04620\,[0 \cdot 795\,(v' + \tfrac{1}{2})^2 - 0 \cdot 875\,(v'' + \tfrac{1}{2})^2].$$

The symbol " i " refers, as usual, to the less abundant molecule. It is seen that the agreement between the observed and calculated values is fairly good when account is taken of the difficulty of measuring weak PbCl band-heads. Such agreement is not obtained if the v numerations are altered in any way. So far as could be ascertained, when there was little overlapping the intensities of the isotopic bands were of the order of one-third of the main heads. Bands, other than those in the Table, in which it was not possible to detect isotopic heads because of an intense fortuitous line structure, included the following

---

* Jevons, " Report on Band Spectra of Diatomic Molecules," p. 226 (1932).

† Bhaduri and Fowler, ' Proc. Roy. Soc.,' A, vol. 145, p. 321 (1934).

‡ Fredrickson and Hogan, ' Phys. Rev.,' vol. 46, p. 455 (1934).

§ Table VIII.

‖ Datta, ' Z. Physik,' vol. 78, p. 486 (1933).

¶ Jevons, " Report," p. 213.

4,0: 3,1 : 2,1 : 1,3 and 0,3.

Classified Bands

Classified bands are arranged in order of wave-lengths in Tables V and VI. A few faint unclassified PbCl bands are to be found in Table VII.

THE VIBRATIONAL CONSTANTS OF HEAVY MOLECULES

In this section it is proposed to outline in some detail the relations of the vibrational constants of the lead halides to those of other heavy molecules. The ω_e's of the lowest electronic states of all the heavy molecules so far investigated are tabulated in Table VIII, according to the Periodic Classification. Where doubt exists about the lowest state observed being the ground state an asterisk is placed near the number.

Several interesting features regarding the relations between ω_e, the number of electrons in the molecule, and the type of molecule, *i.e.*, whether MO, MS, MCl, or M_2 are illustrated by the Table. The first is the almost invariable rule that in any group of related elements, *e.g.*, Ge, Sn, and Pb, the ω_e's for a given type of molecule decrease as the molecular weight increases. Thus (GeS): (SnS): (PbS): 576: 488: 428. This relation between ω_e and the size of the molecule is expressed in several empirical rules of which Morse's $\omega_e r^3_e$ = constant is the best known. r_e must increase with the size of the molecule and therefore ω_e must decrease. The compounds of Group I metals, *i.e.*, Cu, Ag, and Au, form an exception to this rule so far as ω_e (AgCl) $<$ ω_e (AuCl). A similar exception occurs in the ω_e's of the ground states of the hydrides and is no doubt associated, as Knave* has pointed out, with the greater stability of the d^{10} electron shell in silver than in copper and gold.

Further, the spectra of groups of related molecules such as the one just instanced move towards longer wave-lengths as the size of the molecule increases, *e.g.*, the spectra of GeS, SnS, and PbS occur in the regions 2500 – 3400 A, 2600 – 5000 A, and 3200 – 7700 A. On the assumption that the spectra are due to similar electronic transitions, this means that the larger the molecule becomes the less is the energy difference between the energy levels corresponding to similar electronic states.

Secondly, starting at Group I and moving along any row of the Table, the ω_e's of the halides appear firstly to decrease to Group II or III and

---

* 'Diss. Stockholm,' p. 45, 1932.

TABLE IV—PbCl

(Theoretical sep

v′ \ v″	0	1	2	3	4	5	6	7	8
0			14·7 (14·9)	—	28·2 (28·5)	34·1 (35·2)	42·4 (41·8)	47·5 (48·3)	
1		3·2 (2·6)	10·5 (9·5)	—					51·4 (49·5)
2			5·0 (4·3)						
3	−14·0 (−14·8)								
4	—								
5	−23·6 (−24·8)								
6	−28·0 (−29·7)								

* Covered by

TABLE V—PbF BANDS. R HEADS AND ORIGINS

ν (cm⁻¹)	I	O − C	Classification	ν (cm⁻¹)	I	O − C	Classification
23,822·9	1	0·0	R 6, 2	21,599·8	2	0·3	R 4, 5
23,681·1	2	−2·7	R 3, 0	21,510·2	9	−0·6	R 0, 2
23,676·4			3, 0	21,500·8			0, 2
23,565·2	3	0·6	R 4, 1	21,411·3	9	−0·1	R 1, 3
23,447·2	2	0·8	R 5, 2	21,402·0			1, 3
23,294·6	5	−2·1	R 2, 0	21,313·3	8	0·2	R 2, 4
23,287·0			2, 0	21,305·5			2, 4
23,180·6	3	−0·4	R 3, 1	21,215·6	2	−0·3	R 3, 5
23,172·7			3, 1	21,017·3	7	0·1	R 0, 3
23,066·8	1	0·4	R 4, 2	21,007·6			0, 3
22,904·3	10	−1·7	R 1, 0	20,932·2	2	1·1	R 6, 8
22,895·6			1, 0	20,922·8	7	0·4	R 1, 4
22,510·3	8	−1·5	R 0, 0	20,913·5			1, 4
22,502·1			0, 0	20,838·3	1	−0·1	R 7, 9
22,294·7	3	−1·0	R 2, 2	20,829·2	7	0·4	R 2, 5
22,189·3	2	0·1	R 3, 3	20,820·1			2, 5
22,085·4	1	1·6	R 4, 4	20,746·4	0	−0·3	R 8, 10
22,008·0	10	−1·0	R 0, 1	20,736·8	5	0·4	R 3, 6
21,999·2			0, 1	20,728·3			3, 6
21,905·0	4	0·0	R 1, 2	20,655·8	0	−0·3	R 9, 11

ISOTOPE SEPARATIONS

arations in brackets)

9	10	11	12	13	14	15	16	17	18
—* (55·8)	—* (62·1)								
	—* (57·0)	—* (63·2)							
			66·0 (64·1)	68·8 (70·2)					
					71·3 (71·1)	75·2 (76·0)			
						73·3 (72·0)			

intense bands.

TABLE V—(continued)

ν (cm⁻¹)	I	O − C	Classification	ν (cm⁻¹)	I	O − C	Classification
20,645·5	4	0·6	R 4, 7	19,875·4	2	1·2	R 2, 7
20,555·6	0	1·0	R 5, 8	19,790·6	2	−0·3	R 3, 8
20,528·5	4	0·3	R 0, 4	19,709·7	2	0·9	R 4, 9
20,438·7	6	0·6	R 1, 5	19,627·8	2	0·0	R 5, 10
20,428·9			1, 5	19,548·2	2	0·4	R 6, 11
20,349·9	6	0·6	R 2, 6	19,467·6	1	−1·4	R 7, 12
20,339·8			2, 6	19,387·9	1	−3·3	R 8, 13
20,261·8	4	0·5	R 3, 7	19,325·7	0	0·5	R 3, 9
20,174·8	3	0·3	R 4, 8	19,247·8	1	0·1	R 4, 10
20,088·9	1	0·0	R 5, 9	19,171·0	1	−0·3	R 5, 11
20,004·0	2	−0·3	R 6, 10	19,094·9	1	−1·1	R 6, 12
19,920·4	1	−0·4	R 7, 11	19,018·8	1	−3·0	R 7, 13

then gradually to increase. Thus, to take a typical row ω_e(AgCl): ω_e(InCl): ω_e(SnCl): ω_e(ICl):: 344: 316: 350: 385. The validity of this conclusion depends very largely upon the reliability of the determinations of the ω_e's of GaCl, InCl, and TlCl; the first two determinations by Miescher and his co-workers appear to be quite reliable, but the last by Butkow must be taken with some reservations, as an examination of the

TABLE VI—PbCl CLASSIFIED BANDS

ν (cm^{-1})	I	O − C	Classification	ν (cm^{-1})	I	O − C	Classification
23,598·8	1	0·0	R 8, 0	20,334·2	10	0·2	R 0, 5
23,382·0	5	−0·7	R 7, 0	20,084·1	2		R^i 0, 6
23,297·0	2	0·0	R 8, 1	20,041·7	10	0·8	R 0, 6
*23,167·0	8	2·0	R 6, 0	19,797·1	4		R^i 0, 7
23,139·0	3		R^i 6, 0	19,749·6	10	0·1	R 0, 7
*22,947·9	10	2·1	R 5, 0	19,736·3	2		R^i 1, 8
22,924·3	3		R^i 5, 0	19,684·9	9	−1·2	R 1, 8
*22,726·2	10	1·3	R 4, 0	19,623·9	5	−1·0	R 2, 9
*22,563·7	2	0·6	R 6, 2	19,459·0	1	−0·9	R 0, 8
*22,504·4	8	1·9	R 3, 0	19,399·1	10	−0·2	R 1, 9
22,490·4	2		R^i 3, 0	19,338·8	10	0·0	R 2, 10
*22,423·4	1	0·3	R 4, 1	19,277·6	6	−0·8	R 3, 11
*22,343·7	3	−0·2	R 5, 2	19,172·3	2	0·2	R 0, 9
*22,279·5	4	0·8	R 2, 0	19,112·7	5	−0·5	R 1, 10
*22,201·1	6	0·4	R 3, 1	19,061·0	3		R^i 3, 12
*22,054·0	2	1·1	R 1, 0	19,053·4	8	−1·0	R 2, 11
*21,977·1	10	0·4	R 2, 1	18,995·0	8	−0·9	R 3, 12
*21,824·3	3	−0·3	R 4, 3	18,936·3	6	−1·1	R 4, 13
21,755·3	3		R^i 1, 1	18,878·2	1	−1·1	R 5, 14
*21,752·1	10	1·0	R 1, 1	18,782·9	2		R^i 3, 13
21,683·9	2		R^i 2, 2	18,771·9	4	0·0	R 2, 12
*21,678·9	7	2·3	R 2, 2	18,728·7	3		R^i 4, 14
*21,603·7	0	1·5	R 3, 3	18,714·1	8	−0·9	R 3, 13
21,462·4	4		R^i 1, 2	18,674·5	2		R^i 5, 15
*21,451·9	10	0·9	R 1, 2	18,657·4	8	−1·0	R 4, 14
21,239·2	2		R^i 0, 2	18,601·2	8	−0·7	R 5, 15
*21,224·5	7	0·7	R 0, 2	18,544·6	2	−0·9	R 6, 16
*21,154·2	8	1·6	R 1, 3	18,455·3	2		R^i 4, 15
21,082·7	5	1·1	R 2, 4	18,380·1	8	−0·9	R 4, 15
*20,925·8	8	0·2	R 0, 3	18,324·2	8	−2·1	R 5, 16
20,786·4	6	−0·4	R 2, 5	18,270·0	8	−1·7	R 6, 17
20,658·0	4		R^i 0, 4	18,103·8	6	−1·6	R 4, 16
*20,629·8	9	1·0	R 0, 4	18,051·2	6	−1·3	R 5, 17
20,493·4	0	−0·3	R 2, 6	17,998·4	3	−1·2	R 6, 18
20,368·3	3		R^i 0, 5				

* Obtained in absorption only.

TABLE VII—PbCl UNCLASSIFIED BANDS

ν (cm^{-1})	I	ν (cm^{-1})	I
20,424·6	1	18,976·1	0
20,090·1	1	18,583·4	1
19,168·2	1		

TABLE VIII—VIBRATIONAL CONSTANTS OF THE LOWEST STATES OF MOLECULES OF THE TYPES M_2, MF, MCL, MO, AND MS

I	II	III	IV	V	VI	VII
29 Cu 64	Zn	31 Ga 70	32 Ge 73	33 As 75	34 Se 79	35 Br 80
		(39) GaO 768*	(40) GeO 984	(41) AsO 968		
			(48) GeS 576			
(46) CuCl 417		(48) GaCl 365	(49) GeCl —	(50) AsCl —		
				(66) As_2 432	(68) Se_2 388	(70) Br_2 324
47 Ag 108	Cd	49 In 115	50 Sn 119	51 Sb 122	52 Te 127	53 I 127
			(58) SnO 822	(59) SbO 810*		
			(66) SnS 488			
			(67) SnCl 353*	(68) SbCl —		
		(66) InCl 316				(70) ICl 385
(64) AgCl 344						
				(102) Sb_2 268	(104) Te_2 251	(106) I_2 214
79 Au 197	Hg	81 Tl 204	82 Pb 207	83 Bi 209		
			(90) PbO 722	(91) BiO 493*		
			(91) PbF 507	(92) BiF 512		
			(98) PbS 428			
(96) AuCl 383		(98) TlCl 285	(99) PbCl 304	(100) BiCl 309		
				(166) Bi_2 173		

NOTES

1—* Indicates that the ground state is not known.

2—Numbers in brackets placed before the chemical symbol indicate the number of electrons in the molecule.

3—References. For all except the following, *see* Jevons, "Report," p. 276, *et seq.*—GaO: Guernsey, 'Phys. Rev.,' vol. 46, p. 114 (1934). GaCl, InCl: Wehrli, 'Helv. Phys. Act.,' vol. 7, p. 298 (1934). GeO: Shaw, 'Phys. Rev.,' vol. 43, p. 1043 (1933). SnO: Connelly, 'Proc. Phys. Soc.,' vol. 45, p. 780 (1933). SnS: Rochester, 'Proc. Roy. Soc.,' A, vol. 150, p. 668 (1935). PbF, PbCl: Rochester (present paper). PbS: Rochester and Howell, 'Proc. Roy. Soc.,' A, vol. 148, p. 157 (1935). AsO: Connelly, 'Proc. Phys. Soc.,' vol. 46, p. 790 (1934). As_2: Gibson, etc., 'Phys. Rev.,' vol. 46, p. 1059 (1394). Sb_2: Naudé, 'Phys. Rev.,' vol. 45, p. 280 (1934). BiF: Howell (unpublished work). Bi_2: Almy and Sparks, 'Phys. Rev.,' vol. 44, p. 365 (1933).

Deslandres scheme, from which ω_e'' is derived, reveals that $\omega_e' \gg \omega_e''$ and yet all the bands degrade to the red. Further, $x_e'\omega_e'$ is of the order of 290 cm^{-1}, an impossibly large value for a molecule like TlCl.*

The last feature to which attention may be drawn is the remarkable similarity of the ω's of the spectra of similar compounds of metals of Groups IV and V. Thus the following pairs of molecules (one from each Group) have ω's as under:

TABLE IX—VIBRATIONAL CONSTANTS OF CORRESPONDING COMPOUNDS

Molecule	GeO	AsO *	SnO	SbO	PbF	BiF†	PbCl	BiCl
No. of electrons	40	41	58	59	91	92	99	100
ω_e'	648	685	579	586	398	382	229	221
ω_e''	984	966	822	824	507	512	304	309
ν_e	37,760	31,200	29,630	29,630	22,570	22,960	21,860	21,800

All degrade to Red.

* Doublet spectrum: ν_e is a " mean " value.

† Data relating to this molecule have been kindly supplied by H. G. Howell, of Armstrong College, Newcastle-upon-Tyne.

Also included in the Table are the wave numbers of the system origins to help in forming some idea of the regions in which the spectra lie. It will be noted that the ν_e's of corresponding pairs of molecules are often extremely close.

The pair of molecules PbO, BiO form an apparent exception to this relationship, the ω's of BiO being much below those of PbO.

Both these relationships lead to the conclusion that although the difference in electronic structure of adjacent metals of Groups III to VII is the same, *i.e.*, one "*p*" electron, these "*p*" electrons cause different changes in ω_e, and therefore must have different functions in the molecules. Evidently the first produces a relatively large change and the second very little. It is not possible to say what the effect of other "*p*" electrons will be because of insufficient data. A further fact which may be pointed out (*vide* Table IX) is that the constants of corresponding pairs of molecules become more nearly equal as the number of electrons in the molecules increase, *e.g.*, Cf. PbF, BiF and PbCl, BiCl; GeO, AsO and SnO, SbO. This is to be expected, for if it be assumed that the addition of an electron to the electronic configuration of, say PbF, to form the electronic configuration of BiF produces a certain change in ω_e, the addition of the same electron to the electronic configuration of PbCl to form BiCl must produce a smaller change. PbCl being a larger molecule than PbF, the electron will move in a larger orbit, and in consequence will usually be at greater distances from the nuclei and therefore have a smaller effect on the nuclear field and hence on ω_e.

---

* An unpublished analysis of TlCl by Howell and Coulson, of Armstrong College, Newcastle-upon-Tyne, indicates that $\omega_e'' = 283$ cm^{-1} and $\omega_e' = 203$ cm^{-1}.

This work was begun at Armstrong College, Newcastle-upon-Tyne, and completed at the Stockholm Högskola. It is again a great pleasure to acknowledge my indebtedness to the directors of the departments of physics of both of these institutes, Professors W. E. Curtis, D.Sc., F.R.S., and Erik Hulthén, fil. dr., for their interest and generous assistance at all times.

SUMMARY

An account is given of the emission band spectra of PbF and PbCl. Each spectrum is found to consist of one large system which includes all the observed bands except a few in the case of PbCl.

The vibrational constants are as follows in cm^{-1} :

	State	ν_e	ω_e	$x_e\omega_e$
PbF	A	22,566·6	397·75	1·77
	X	0	507·5	2·32
PbCl^{35}	A	21,863·3	228·8	0·795
	X	0	303·6	0·875

Popov and Neujmin's analysis of PbCl is shown to be incorrect.

Many PbCl bands of small v'' value are observed in absorption also. No definite evidence of lead isotope effects is obtained, presumably because of insufficient resolving power; but large chlorine isotope effects are observed. Some discussion of the relation between the vibrational constants of certain heavy molecules is given.

The Emission of Positive Ions by Platinum when Heated in Oxygen

By T. B. RYMER, Ph.D., King's College, London

(*Communicated by O. W. Richardson, F.R.S.—Received July 29, 1935*)

1—INTRODUCTION

It has long been known that platinum when heated in a gas emits positive ions derived from the gas molecules. The principal investigation of this subject is that of Richardson,* who examined the emission in a number of gases and studied with particular care oxygen, which, by reason of the large emission it produces, is well suited for observation. In the paper referred to, Richardson derived an expression for the positive ion current emitted by the platinum as a function of the gas pressure. This expression was obtained on the assumption that the ions were derived from atoms of oxygen which were adsorbed on to the platinum and subsequently emitted as positive ions. It was further supposed that molecular oxygen was incapable of being adsorbed. The following is the quantitative formulation of this theory.

Let A be the area of the platinum surface and p the partial pressure of the atomic oxygen. Then if θ be the fraction of the surface covered with adsorbed oxygen the rate of adsorption of oxygen will be proportional to $A(1-\theta)p$, provided we assume that oxygen can be adsorbed only on the free platinum. The rate of liberation of oxygen from the platinum will be proportional to the quantity adsorbed, *i.e.*, to $A\theta$. Hence, in equilibrium

$$aA(1-\theta)p = bA\theta.$$

Whence

$$\begin{aligned} bA\theta &= \frac{Abp}{b/a+p} \\ &= \frac{Abf(P)}{b/a+f(P)}, \end{aligned} \tag{1}$$

where P is the total oxygen pressure. The quantity on the left of equation (1) is the rate of liberation of oxygen from the platinum. A certain fraction of the liberated oxygen will be in the form of ions. It is reasonable to suppose that the magnitude of this fraction will depend on the temperature of the platinum through a factor of the form $T^{\lambda}e^{-B/T}$, where λ and B are constants. The positive ion current will therefore be given by

---

* 'Phil. Trans.,' A, vol. 207, p. 1 (1906).

$$i \propto \frac{Abf(P)}{b/a + f(P)} T^{\lambda}e^{-B/T}. \tag{2}$$

At low temperatures the degree of dissociation of the oxygen will be small and we may write $f(P) \propto P^{\frac{1}{2}}$. At high temperatures, on the other hand, the degree of dissociation is large and $f(P) \propto P$. Richardson found that the variation of emission with pressure was satisfactorily represented by equation (2) when $f(P)$ had the above form.

We have now to consider how the quantities a and b in equation (2) depend on the temperature of the platinum and the other conditions. The quantity a, which measures the rate of adsorption, will depend on the temperature of the gas and possibly to a slight extent on the temperature of the platinum. To a first approximation, however, we may take it as independent of the temperature of the platinum. The quantity b, on the other hand, which measures the rate of liberation of oxygen, may be expected to increase rapidly with the temperature through a factor of the form $e^{-W/kT}$, where W is the heat of adsorption of an oxygen atom. We may therefore write equation (2) in the form

$$i \propto \frac{e^{-W/kT} f(P)}{\alpha e^{\;W/kT} + f(P)} T^{\lambda}e^{-B/T},$$

where α is a constant. At high temperatures ($\alpha e^{\;W/kT} \gg f(P)$) this reduces to

$$i \propto f(P)\, T^{\lambda}e^{-B/T}, \tag{3A}$$

while at low temperatures it becomes

$$i \propto T^{\lambda}e^{-(W/k+B)/T}. \tag{3B}$$

It is to be expected, therefore, that if the logarithm of the emission be plotted against the reciprocal of the absolute temperature in the usual way a curve will be obtained consisting of two straight line portions (since over the range of temperatures examined T^{λ} will vary but little compared with the exponential factor) united by an intermediate curved portion corresponding to the range $\alpha e^{-W/kT} \sim f(P)$.

In view of the fact that concepts very similar to the above have frequently been used in discussing the adsorption of gases by solids, it appeared to be of interest to see whether the variation of emission with temperature was, in fact, in accord with equations (3A) and (3B), and the present work was initially undertaken to this end. This attempt to verify the equation experimentally, however, revealed unexpected difficulties. In the first place it appears that the range of temperature that can usefully be employed is rather limited. For oxygen pressures of the order of 3 mm it appears that at temperatures much above 1050° C the platinum undergoes disintegration, making observations at such temperatures unreliable. On the other hand, if the temperature be much below 700° C, it is almost impossible to obtain reproducible results owing to the extreme slowness with which the metal reaches equilibrium. Another fact that makes the study of the effect of the gas pressure on the temperature variation of the emission difficult is that over the range of pressures and temperatures examined (1–10 mm; 400°–1100° C) no evidence could be found of a dependence of the emission on the pressure. This is rather remarkable in view of the fact that a great part of Richardson's original paper is taken up with an investigation of the effect of the prèssure on the emission. The difference between these two results may be tentatively ascribed to a difference in the heat treatment of the platinum. These facts have prevented the verification of equations (3A) and (3B).

The ionization produced by hot metals in gases has been most studied for tungsten in caesium vapour, the pioneer experiments being those of Langmuir and Kingdon,* who have given an elegant treatment of the subject based on the Saha equation for the reaction isochore. In the present paper it is shown that a similar treatment can be applied to platinum in oxygen, although there are certain complications.

The most important fact which emerges from such a treatment is that in using the method of the Saha equation to link together the electron and ion emissions from a metal, it is not in general permissible to make use of the experimentally determined electron emission, even though this may have been determined under conditions identical with those of the ion emission. Thus in the present work the Saha equation does not link the emission of positive ions with the electron emission as measured under the same condition of oxygen pressure, but with the emission of those electrons which leave the surface in the immediate neighbourhood of an adsorbed oxygen atom—and these form but a minute fraction of the total emission. The reason for this is that the measurements of electron emission are not made under the equilibrium conditions contemplated by the Saha theory.

A consideration of the results of the present work, together with the earlier results of Richardson, in the light of the theory to be given, shows that a consistent interpretation can be given to both if it be assumed that the platinum used in the present work adsorbed oxygen as molecules, while that used by Richardson was able to adsorb only oxygen atoms. It is known that platinum ordinarily adsorbs oxygen but sparingly, but that by suitable treatment it becomes "activated" and is then able to take up much more oxygen. It therefore seems probable that the platinum used in the present work was activated, while that used by Richardson was not, and that the process of activation consists in causing the platinum to adsorb molecular oxygen, the unactivated form of platinum being capable of adsorbing only atomic oxygen.

---

* 'Proc. Roy. Soc.,' A, vol. 107, p. 61 (1925).

2—GENERAL THEORY

The treatment to be given is based on that of Langmuir and Kingdon,* with the modifications that appear to be necessary to account for the peculiar features of ionization in oxygen. The discussion to be given is applicable in its present form to the ionization produced by a wire heated in a monatomic gas. With oxygen there is some evidence that in certain circumstances the emitted ions are charged oxygen atoms. We have seen that Richardson obtained a satisfactory explanation of the experimental results by considering the equilibrium of a platinum wire heated in a gas of oxygen atoms, the pressure of the gas being taken equal to the partial pressure of the dissociated oxygen near the filament. Such a procedure is equivalent to assuming that oxygen *molecules* are not adsorbed. Whether such an assumption is strictly justified is perhaps doubtful. However, to modify the theory to take account of the simultaneous adsorption of oxygen atoms and molecules would add considerably to its complexity and is hardly worth attempting in the present state of our experimental knowledge of the subject. In this case, therefore, the theory is to be applied by writing for the gas pressure the partial pressure of the dissociated oxygen.

In the present experiments, on the other hand, conditions are rather different from those prevailing in Richardson's experiments, and we shall see that there are indications that the oxygen is adsorbed and re-emitted in the form of molecules, while the ions are molecular ions. In this case the oxygen molecule is effectively acting as an elementary particle, and the theory may be applied directly, the gas pressure to be used in the equations being the actual measured gas pressure.

---

* 'Proc. Roy. Soc.,' A, vol. 107, p. 61 (1925).

Consider an enclosure having walls of platinum at temperature T and containing a gas. When equilibrium is attained, let ν_-, ν_+, and ν_0 be the number of electrons, ionized gas atoms, and neutral gas atoms respectively per unit volume of the enclosure. Then the law of mass action states that

$$\frac{\nu_-\nu_+}{\nu_0} = \mathrm{K}, \tag{4}$$

where K is a constant at constant temperature. K has been calculated as a function of the temperature by Saha. According to a slightly modified form of Saha's equation due to Fowler,* K is given by

$$\mathrm{K} = \frac{(2\pi mk\mathrm{T})^{\frac{3}{2}}}{h^3}\, e^{-\chi\varepsilon/k\mathrm{T}}, \tag{5}$$

where m is the mass of an electron, ε its charge, χ the ionization potential of the gas, and k and h are the Boltzmann and Planck constants.

Now ν_- is determined from the electronic emission of the platinum. We have†

$$\nu_- = \frac{2\,(2\pi mk\mathrm{T})^{\frac{3}{2}}}{h^3}\, e^{-\phi\varepsilon/k\mathrm{T}}, \tag{6}$$

where ϕ is the thermionic work function in electron volts. The precise interpretation of ϕ will be considered in the next section in the discussion of the experimental results, but for the present we may note that ϕ obviously refers not to pure platinum but to platinum contaminated by the gas in question.

ν_+ is determined from the positive ionization current I. When there is equilibrium, the number of ions which strike unit area of the platinum in unit time is

$$\frac{(2k\mathrm{T})^{\frac{1}{2}}}{2\,(\pi\mathrm{M})^{\frac{1}{2}}}\,\nu_+,$$

where M is the mass of the gas atom. Of these, a fraction r_+ will be reflected and a fraction $1 - r_+$ adsorbed. If we assume that the observed positive ion current I is equal to the number of positive ions adsorbed in unit time under the equilibrium conditions contemplated in the above discussion (this is justifiable provided recombination of ions and electrons in the gaseous space is negligible), we have

$$\mathrm{I} = \frac{(2k\mathrm{T})^{\frac{1}{2}}}{2\,(\pi\mathrm{M})^{\frac{1}{2}}}\,\nu_+\,\varepsilon\,(1 - r_+)$$

* "Statistical Mechanics," p. 281, Cambridge (1929).

† "Statistical Mechanics," p. 266.

or

$$\nu_+ = \frac{2(\pi M)^{\frac{1}{2}} I}{(2kT)^{\frac{1}{2}} \varepsilon (1 - r_+)}. \tag{7}$$

We have now to consider the value of ν_0. Up to the present we have considered the whole mass of gas to be at temperature T. Actually, however, we measure the emission from a filament immersed in a gas at temperature T′ and pressure p'. The number of gas atoms per unit volume is therefore

$$\frac{Np' T_0}{p_0 T'},$$

where N is the Loschmidt number and p_0, T_0 are standard pressure and temperature. The number of atoms which strike unit area of the wire in unit time is therefore

$$\frac{Np'T_0}{p_0T'} \frac{(2kT')^{\frac{1}{2}}}{2(\pi M)^{\frac{1}{2}}}. \tag{8}$$

Conditions at the surface of a wire are practically the same as if the whole mass of gas were at temperature T and the concentration of gas atoms were such that the number striking unit area of the surface were given by (8). If ν_0' be this effective concentration we have

$$\nu_0' \frac{(2kT)^{\frac{1}{2}}}{2(\pi M)^{\frac{1}{2}}} = \frac{Np'T_0}{p_0T'} \frac{(2kT')^{\frac{1}{2}}}{2(\pi M)^{\frac{1}{2}}},$$

therefore

$$\nu_0' = \frac{Np'T_0}{p_0\sqrt{TT'}}. \tag{9}$$

ν_0' is not the value of the effective concentration of the gas atoms which appears in equation (4), for of the atoms striking the wire a fraction r_0 is reflected and plays no part in the reaction at the platinum surface. The effective concentration ν_0 of the gas molecules is therefore not ν'_0 but

$$\begin{aligned} \nu_0 &= (1 - r_0)\, \nu'_0 \\ &= \frac{Np'T_0}{p_0 \sqrt{TT'}} (1 - r_0). \end{aligned} \tag{10}$$

From equations (4), (5), (6), (7) , and (10) we obtain

$$I = \frac{1}{2} \left(\frac{k}{2\pi M}\right)^{\frac{1}{2}} \frac{Np'T_0}{p_0T'^{\frac{1}{2}}} \varepsilon (1 - r_+)(1 - r_0)\, e^{-(\chi - \phi)\varepsilon/kT}. \tag{11}$$

In this equation we may provisionally write $r_+ = 0$ in the absence of any evidence as to the reflexion of positive ions.

We now have to consider the term $(1 - r_0)$ in equation (11). Consider a gas atom approaching the wire. Then we make the fundamental assumption that the probability of the atom being reflected is directly proportional to the amount of adsorbed gas, so if μ be the number of adsorbed atoms per unit area of surface the probability of reflexion will be $\xi\mu$. If μ_∞ be the limit to which μ tends as the gas pressure is increased, we can show that $\xi = 1/\mu_\infty$. For the number of gas molecules striking unit area of the wire in unit time is proportional to the pressure p'. Since the probability of reflexion is $\xi\mu$, the rate of adsorption is proportional to

$$p'(1 - \xi\mu).$$

Since $\mu \rightarrow \mu_\infty$ as $p' \rightarrow \infty$ the above expression tends to a limit as $p' \rightarrow \infty$. This will occur only if $1 - \xi\mu \rightarrow 0$ as $p' \rightarrow \infty$. We conclude that $\xi = 1/\mu_\infty$, at any rate for large values of μ. Assuming, therefore, that ξ does not vary perceptibly with μ we may write

$$1 - r_0 = 1 - \mu/\mu_\infty. \tag{12}$$

The determination of the form of $1 - r_0$ is therefore equivalent to the determination of the amount of adsorbed gas as a function of the filament temperature and of the gas pressure. This question was first attacked by Richardson, as described in § 1, and his treatment was later amplified by Langmuir. The problem may also be attacked by postulating a certain equation of state for the adsorbed film and considering the equilibrium between the adsorbed film and the surrounding gas. A useful discussion of the subject from this point of view has been given by Frumkin.* The following results are taken from his paper:

Let

Π = spreading force or negative surface tension of the adsorbed film,

μ = number of adsorbed molecules per unit area of the wire.

$\mu_\infty = \underset{p' \rightarrow \infty}{\mathrm{Lt}}\ \mu$,

δ = thickness of adsorbed film,

W = heat of adsorption per molecule in electron volts,

ν'_0 = effective number of molecules per unit volume of the gas as given by equation (9).

Π is the two-dimensional analogue of a gas pressure. If we take for the relation between Π and ν'_0 an equation of the form

$$\Pi = b \log(\nu'_0/c + 1),$$

---

* 'Z. phys. Chem.,' vol. 116, p. 466 (1925).

(*b*, *c* constants) which was discovered empirically by Szyszkowski from experiments on the surface tension of solutions, we obtain for the relation between the amount of gas adsorbed and the concentration of the external gas

$$\mu = \frac{\beta\mu_\infty \nu'_0}{\beta\nu_0' + \mu_\infty}, \tag{13}$$

where

$$\beta/\delta = e^{W\epsilon/kT}.$$

This is of the same form as that obtained by Richardson from very different considerations.

We are now in a position to consider the way in which the gas pressure and temperature influence the emission. An examination of equation (11) shows that the gas pressure and temperature are involved through the factor

$$P = \frac{p'}{T'^{\frac{1}{2}}}(1 - r_0). \tag{14}$$

Now from equation (12)

$$1 - r_0 = 1 - \mu/\mu_\infty.$$

Hence from (13)

$$P = \frac{p'}{T'^{\frac{1}{2}}}\left(1 - \frac{\beta\nu'_0}{\beta\nu'_0 + \mu_\infty}\right).$$

The quantity to be used for the concentration of the gas is the quantity ν_0' of equation (9).

Hence

$$P = \frac{\mu_\infty p' T'^{-}}{\dfrac{\beta N p' T_0}{p_0\sqrt{TT'}} + \mu_\infty}. \tag{15}$$

The quantity P may be calculated in a variety of ways depending on the precise assumptions that are made as to the mechanism of the adsorption of the gas on to the platinum, but it will be found that almost all methods lead to an expression that is practically identical with (15).

When T is small β is large and (15) reduces to

$$P = \frac{\mu_\infty p_0}{NT_0}\frac{T^{\frac{1}{2}}}{\beta}$$

$$= \frac{\mu_\infty p_0}{NT_0\delta}T^{\frac{1}{2}}e^{-W\epsilon/kT}.$$

Hence

$$I \propto T^{\frac{1}{2}}e^{-(\chi-\phi+W)\epsilon/kT}. \tag{16}$$

At high temperatures, on the other hand, β is small and (15) reduces to

$$P = p' T'^{-\frac{1}{2}}.$$

Hence

$$\mathrm{I} \propto \mathrm{T}'^{-\frac{1}{2}} p' e^{-(\chi-\phi)\epsilon/k\mathrm{T}}. \tag{17}$$

A comparison of (16) with (17) shows that it is to be expected that a curve connecting log I with 1/T will consist of two straight lines connected by an intermediate curved portion. As has been mentioned, no evidence of this transition region has been found over the range of temperatures and pressures examined.

3—EXPERIMENTAL

The design of the apparatus employed followed closely that of Richardson. The hot platinum was in the form of a wire 0·1 mm diameter and was heated electrically, the leads being platinum wires 0·165 cm in diameter. The collecting electrode, in the form of a cylinder surrounding the looped filament, was also of platinum, and before use the whole electrode system was treated with boiling nitric acid and distilled water. The tube itself was of quartz and was rinsed with boiling nitric acid and distilled water before use.

The temperature of the filament was determined from its resistance in the usual manner. No correction was made for lead loss, and the results are therefore of a rather rough nature. The emission was measured by a quadrant electrometer shunted with a suitable capacity. For the measurement of the ion current the collecting electrode was made 60 volts negative with respect to the filament.

The results obtained for the variation of the ion emission with temperature at various pressures are given in figs. 1 and 2 for two different filaments. In these figures the common logarithm of the ion current in amperes divided by the square root of the absolute temperature is plotted against the reciprocal of the absolute temperature. If the ion emission obeys equation (16), the curves will be straight lines. The first thing to be noticed is that at temperatures above about 700° C the curves corresponding to pressures of 3 mm and 10 mm coincide in fig. 1. As mentioned in § 1, this result is contrary to that of Richardson. The magnitude of this discrepancy may readily be calculated. At 820° C ($1/\mathrm{T} = 9{\cdot}16$) Richardson's results give for the emission at 3 mm and 10 mm pressure the values $1{\cdot}7 \times 10^{-11}$ and $2{\cdot}5 \times 10^{-11}$ amperes respectively. At $1/\mathrm{T} = 9{\cdot}16$, therefore, according to Richardson's results, the 10 mm curve should lie above the 3 mm one by an amount $\log_{10} \frac{2{\cdot}5}{1{\cdot}7} = 0{\cdot}17$. A glance at fig. 1 shows that a separation of the 3 and 10 mm curves by this amount is quite unjustified by the present results.

It might at first be supposed that the coincidence of the 3 and 10 mm curves in the present experiments is due to the surface of the platinum having undergone a change between the taking of the 3 and 10 mm curves, and that this caused a decrease in the emission which happened just to compensate the increase to be expected on account of the higher pressure. An examination of fig. 3 shows that this explanation is untenable. In this figure the points marked with crosses are those of the 3 mm curve of fig. 1, while those marked with circles represent readings taken at the same pressure about two months later. During this time the wire had been heated in oxygen at 10 mm pressure at temperatures up to 1500° C; in the course of this heating sufficient of the wire had disintegrated to increase its resistance by 14%. It is evident that the two sets

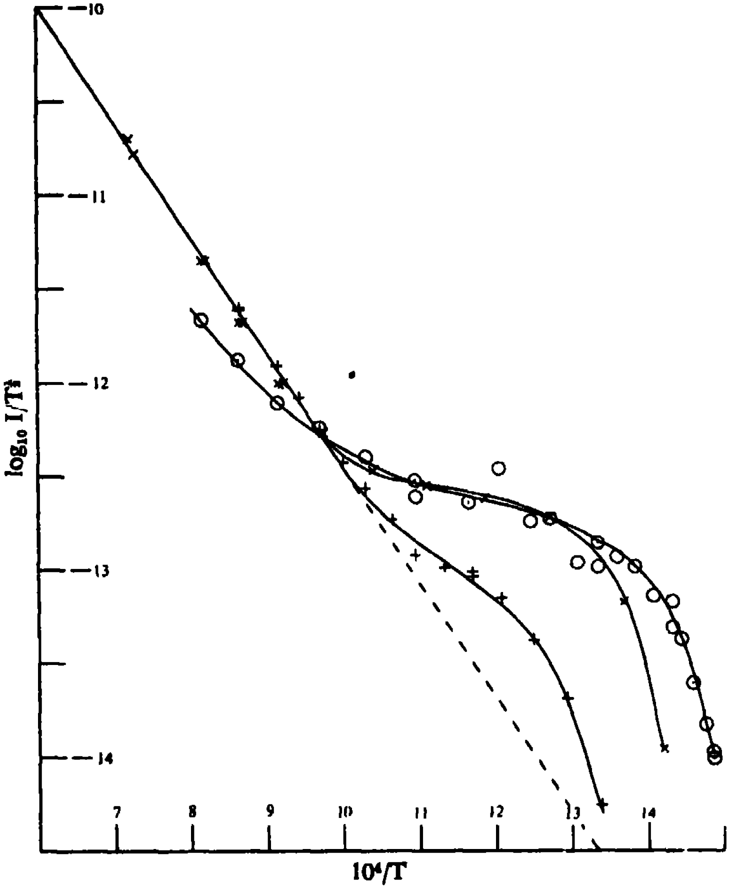

Fig. 1—Filament No. 1, 7·4 cm long. × pressure, 3 mm; ⊦ pressure, 10 mm; ⊙ pressure, 1 mm.

of points fall on the same curve, showing that they correspond to a property inherent in the platinum and do not represent a casual condition of the surface.

In this connexion the results obtained with the second filament are inconclusive. Here, readings were taken at 1·47 mm and afterwards at 3·00 mm. The 3 mm curve is found to lie nearly parallel to and 0·32 above the 1·47 mm curve corresponding to a ratio of 2·1 : 1 in the emissions at the two pressures. Richardson's results would require a ratio of 1·3 : 1 at 820° C, and, moreover, they also require the separation of the two curves, instead of remaining constant at all temperatures, to increase with the temperature. It is probable, therefore, that the difference between the two curves is due not to the effect of pressure but to a change in the surface of the platinum. This is rendered the more plausible since the last reading to be taken at 1·47 mm before the readings at 3 mm commenced (the point A in fig. 2) lies considerably above the 1·47 mm curve and close to the 3·00 mm one. It was intended to repeat these observations after running the filament for some hours at a very high temperature —a process which it will be seen may be expected to stabilize the wire—but, unfortunately, the filament burnt out before this could be done.

The experiments therefore show that there is no reason to suppose that the ion emission in oxygen is affected by the external pressure, at any rate over the range of pressures examined. Since the emission is determined by the amount of oxygen adsorbed, it follows that this also is independent of the pressure. This conclusion has also recently been reached by Reischaur* from direct measurement of the amount of oxygen adsorbed on to platinum foil.

According to the discussion in § 2, the fact that the emission is independent of the pressure in the present experiments indicates that the platinum must have been saturated with oxygen ($\mu \simeq \mu_\infty$). The platinum used by Richardson, on the other hand, must have contained a relatively small amount of adsorbed oxygen, since the emission was markedly influenced by the pressure. This view is confirmed by measurements of the electron emission. In the present series of experiments, extensive measurements of the electronic emission were not made. The electron emission was tested from time to time, but at most of the temperatures employed it was found to be too small to measure. The few measurements that were made, however, showed that it was from 0·01 to 0·001 of the value found by Richardson. The positive ion emission, however, was not very different in the two cases. It follows, therefore, from equations (4), (7), (10), and (12) of the previous section that μ, the number of adsorbed atoms per square centimetre of surface, is much greater in the present experiments in agreement with the conclusions we have reached from a consideration of the effect of pressure on the emission.*

---

* 'Z. phys. Chem.,' B, vol. 26, p. 399 (1934).

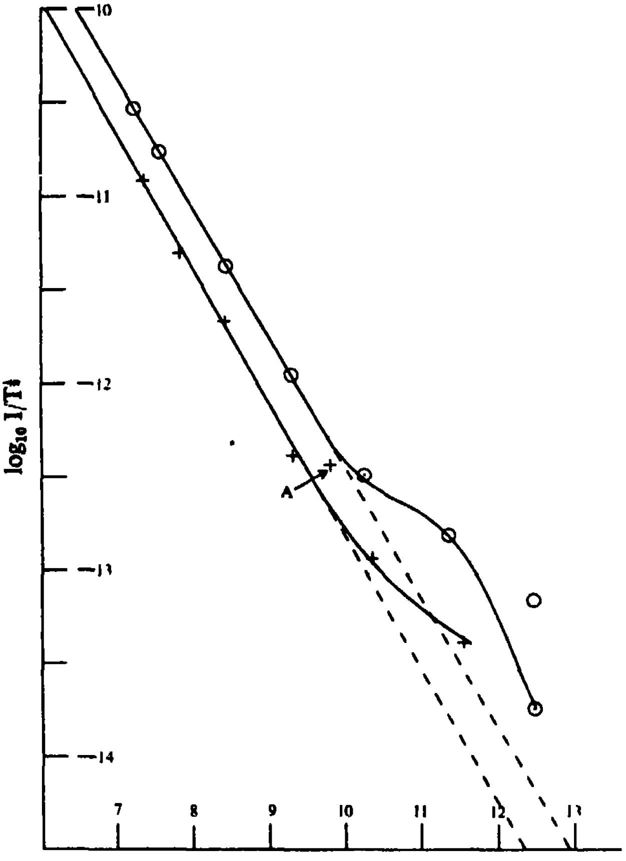

FIG. 2—Filament No. 2, 14·1 cm long; + pressure, 1·47 mm; ⊙ pressure, 3·00 mm.

It seems highly probable that the difference between the two sets of results is due to a different heat treatment of the wire, for it seems fairly certain that the wire used in the present work was heated in oxygen to a considerably higher temperature than any used by Richardson. This is particularly the case of the filament used for the results of fig. 1, which affords the most convincing evidence of the saturation of the platinum in the present experiments. The filament used for the results of fig. 2 had undergone a less extensive preliminary heating and does not appear to have become completely saturated—the emission having increased on raising the pressure from 1·47 mm to 3·00 mm. This result is in conformity with the conclusions of a number of observers* that the quantity of oxygen adsorbed by platinum increases with the temperature.

---

* An alternative, and possibly more acceptable, explanation of the low value of the electron emission found in the present experiments is that the value of the electronic work function for the platinum, as determined from measurements of the electron emission, is nearer to the value of the work function for platinum completely covered with adsorbed oxygen than was the case in Richardson's experiments. This point will become clearer in the subsequent discussion. However, it may readily be seen that this explanation also requires that more oxygen should be adsorbed in the present experiments than was the case in Richardson's.

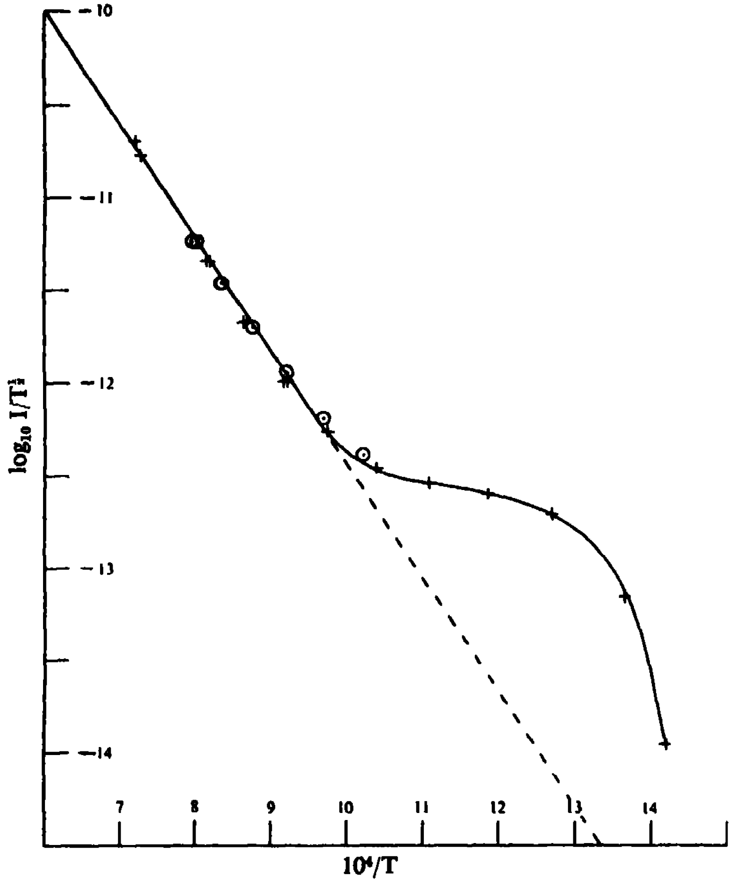

Fig. 3—Filament No. 1. 7·4 cm long; pressure, 3 mm.

---

* Langmuir, 'J. Amer. Chem. Soc.,' vol. 40, p. 1393 (1918); Reischaur, 'Z. phys. Chem.,' B, vol. 26, p. 399 (1934); Neumann and Goebel, 'Z. Elektrochem.,' vol. 40, p. 754 (1934).

The very consistent nature of Richardson's results shows that the wire he used was in a stable, or at any rate a metastable, condition, and it therefore appears to be necessary to postulate separate adsorption processes to account for Richardson's and the present results. This is in agreement with the adsorption measurements of a number of workers.* The general result of such measurements is to show that platinum at ordinary temperatures sorbs only imperceptible quantities of oxygen. By suitable processes, however, it may be " activated " and is then able to sorb far more oxygen. The process of activation usually consists in heating the platinum in electrolytic gas. It appears from the above results that heating in oxygen alone to a sufficiently high temperature suffices to activate the platinum. On this view, Richardson's platinum is to be regarded as unactivated or partially activated, and the platinum used in the present experiments as activated.

The deviations from straight lines observed in the results given in figs. 1 and 2 at low temperatures are to be ascribed to the slowness with which the wire attains equilibrium. This is shown by the fact that it is found that the longer a wire is kept at any particular temperature the less is the deviation from the normal. Thus the deviations are less in fig. 2 than in fig. 1. In the latter case the wire was seldom kept for more than an hour at any particular temperature, while in the former the majority of the observations were made after at least 10 hours heating at each temperature. The fact that the 10 mm curve in fig. 1 deviates less from the normal than the others is just what we should expect, for the attainment of equilibrium would be expected to be the more rapid the higher the pressure. It may be that the difficulty of attaining equilibrium at low temperatures is due to a partial transition to unactivated adsorption. Such a supposition affords a satisfactory explanation of several facts. In the first place, a transition from one type of adsorption to another will certainly give rise to an anomaly in the variation of the current with the temperature since it corresponds to a variation of the quantity W of equation (16). Again, we have said that the platinum used in the present experiments showed activated adsorption, at any rate at the higher temperatures. It is therefore to be expected that any transition to unactivated adsorption will be of a transitory character and will not correspond to any equilibrium condition of the platinum. As we have seen, the deviations from straight lines of figs. 1 and 2 do not represent an equilibrium condition.

The difference between activated and unactivated adsorption is that, for a given external gas pressure, more gas is adsorbed in the former case than in the latter. Now the rate at which gas molecules are adsorbed on to a platinum surface is equal to the rate at which gas molecules strike the surface multiplied by the probability that a molecule striking the surface is adsorbed. This probability is $1 - r_0$, which from equation (12) is equal to $1 - \mu/\mu_\infty$. Thus, for a platinum surface at a given temperature in equilibrium with a gas at a given pressure, the rate of adsorption of molecules (and therefore the rate of evaporation also) must be less if the platinum is activated than if it is unactivated. Activated platinum is therefore distinguished by the fact that it has more molecules adsorbed on it and at the same time the rate of evaporation is less than for unactivated platinum. This requires that the average life of an adsorbed molecule be greater for activated adsorption than for unactivated. If, therefore, we have a given amount of gas adsorbed on a platinum surface and the adsorption forces suddenly change from those characteristic of activated adsorption to those characteristic of unactivated adsorption, there will be an increase in the rate of evaporation of the adsorbed gas. A partial temporary transition from activated to unactivated adsorption is therefore characterized by an increased positive ion current. This conclusion is in agreement with the fact that, as may be seen from figs. 1 and 2, the deviation of the current from the normal at low temperatures is always in the direction of larger currents.

---

* Langmuir, *loc. cit.*; Schaaff, ' Z. phys. Chem.,' B, vol. 26, p. 413 (1934).

We come now to a consideration of the slopes of the two curves. According to equation (16) of the previous section, the constant V in the equation

$$i \propto T^{\frac{1}{2}} e^{-V_e/kT} \tag{18}$$

for the positive ion emission should satisfy the equation

$$V = \chi - \phi + W. \tag{19}$$

In deriving equation (16) we assumed that we were dealing with a monatomic gas. Two possibilities therefore present themselves. Either we deal with oxygen molecules which are adsorbed and re-emitted as molecules and molecular ions (in which case the oxygen is acting effectively as a monatomic gas) or we deal with dissociated oxygen atoms which are adsorbed and re-emitted as such, the oxygen molecules playing no part in the process. It appears that the hypothesis that best fits the facts is that in the present experiments the oxygen is adsorbed mainly in the molecular form, while in Richardson's experiments it was the atomic form that was effective. It will be remembered that Richardson found that the variation of the emission with pressure was best explained on the view that atomic oxygen alone was capable of being adsorbed. The fact that a different type of adsorption is postulated for the present experiments is in agreement with our previous conclusion that Richardson's platinum was unactivated and ours activated. It seems likely, therefore, that activation consists in the transition from adsorption of oxygen atoms to oxygen molecules.

In applying equation (19) then, we must write for χ the ionization potential for molecular oxygen. This has recently been given by Mulliken and Stevens* as 12·2 volts. ϕ, the work function for platinum saturated with adsorbed oxygen, is given by Cassel and Glückauf† as 8·46 volts, while W, the heat of adsorption of oxygen, has been determined calorimetrically by Maxted and Hassid‡ as 2·6 volts. Substituting these values in equation (19) gives $V = 6 \cdot 34$ volts. The value determined from fig. 1 is 1·21 volts and that from fig. 2 is 1·37 volts. The latter is probably the more accurate, since it will be less disturbed by lead loss. There is evidently a discrepancy that can hardly be accounted for by experimental errors but must be due to an erroneous application of the theory.

The error lies in the fact that our observations are not made under the equilibrium conditions contemplated by the preceding theory.

Consider an enclosure having walls of platinum and containing oxygen. Some of the oxygen will be adsorbed on to the platinum, and those parts of the platinum where oxygen is adsorbed will have a higher work function than the clean parts. The parts of the platinum where oxygen is adsorbed are represented schematically by black patches in fig. 4. Now the work that must be done to remove an electron from a point A inside the metal to a point B within the enclosure is the same whether the electron be taken along the path ACB, ACDB, or ADB. On the other hand, the work that must be done to remove the electron from A to a point D just outside a part of the platinum that is covered with adsorbed oxygen is greater than the work that must be done to remove the electron to a point C just outside a clean part of the platinum. It follows that D will be at a negative potential to C, the potential difference being equal to the difference of the work functions at C and D. There will therefore be electric fields directed from the clean parts of the platinum to the parts covered with a film of adsorbed oxygen, and these will prevent all but a small portion of the electrons ejected from the clean platinum from reaching the centre of the enclosure. The electron density at the centre of the enclosure will therefore be determined almost entirely by the electron emission from the parts of the platinum that are covered with adsorbed oxygen. It is this electron concentration that appears in the theory given in the previous section.

---

* 'Phys. Rev.,' vol. 44, p. 720 (1933).

† 'Z. phys. Chem.,' B, vol. 18, p. 347 (1932).

‡ 'Trans. Faraday Soc.,' vol. 29, p. 698 (1933).

When we measure the electron emission, however, we apply a strong electric field to draw the electrons to the collecting plate. Under these conditions electrons are drawn from the whole of the surface. The de Broglie wave-length of the emitted electrons is always large compared with the distance between neighbouring adsorbed atoms, and therefore the local inequalities of work function are smoothed out. If ϕ_1, ϕ_2 are the work functions of clean platinum and of platinum coated with oxygen respectively, then ϕ, the average work function for the surface, is given by

$$\phi = (1 - \theta)\,\phi_1 + \theta\phi_2, \tag{20}$$

where θ is the fraction of the surface covered by oxygen. This equation, which was first given by Langmuir, is true provided the forces between the adsorbed atoms are small compared with the forces between an adsorbed atom and the metallic surface. This is probably true for

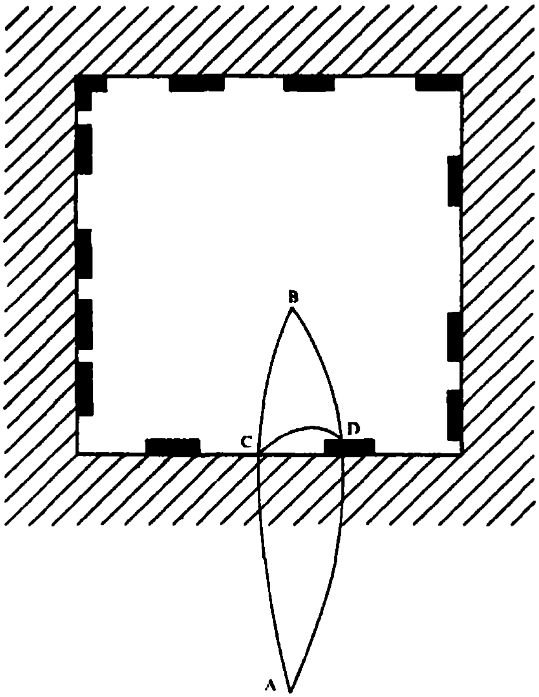

FIG. 4.

oxygen even when the surface is saturated, since the great difficulty experienced in freeing a platinum surface from adsorbed oxygen shows that the adsorption forces must be more than usually powerful. Additional confirmation of this view is provided by the observation of Maxted and Hassid (*loc. cit.*) that the heat of adsorption of oxygen on platinum black is independent of the amount adsorbed.

The electronic work function determined experimentally is the quantity ϕ of equation (20), while the work function that appears in equation (19) is the quantity ϕ_2, since we have seen that it is this that determines the equilibrium concentration of electrons in the enclosure of fig. 4.

The same result may be derived from another point of view. The behaviour of an adsorbed atom at D in fig. 4 is determined by the forces holding it to the platinum and therefore by the nature of the part of the platinum surface to which it is bound. The constants of the remainder of the surface, *i.e.*, the part that is free from adsorbed atoms, play no part in determining the behaviour of the adsorbed atom. It follows that a theory of positive ion emission relates the ion emission to the electronic work function of the part of the surface that is covered with oxygen, *i.e.*, to the quantity ϕ_2 of equation (20).

Let us now consider this question from another angle. Consider a beam of electrons falling on a platinum surface coated with oxygen. We have seen that the oxygen-coated portions of the surface are at a negative potential with respect to the remainder of the surface. It follows that electrons will be unable to reach them if their energy be less than that corresponding to the potential difference between the oxygen-coated and clean portions of the surface. If every electron reaching the oxygen-coated portion of the surface causes the desorption of an oxygen atom, the efficiency of the electrons in causing desorption will be small if their energy be less than this critical value. The efficiency of electrons of this critical energy in causing desorption will be equal to the fraction of the surface that is covered with oxygen.

Let us now apply these ideas to our experimental results. Substituting in equation (19) the values $V = 1 \cdot 37$, $\chi = 12 \cdot 2$, $W = 2 \cdot 6$ (*see* p. 437), we obtain $\phi = 13 \cdot 43$ volts. This, the work function of the oxygen-coated portions of the platinum surface, is $7 \cdot 16$ volts greater than the value $6 \cdot 27$ volts obtained by Du Bridge* for pure platinum. There is, therefore, a potential difference of $7 \cdot 16$ volts between the oxygen-coated portions of a platinum surface and the remainder. Now Kobosew and Anochin* have measured the efficiency of electrons in causing desorption of oxygen from a platinum surface saturated by anodic polarization. They find that the efficiency has a sharp maximum for electrons of energy $7\cdot0 \pm 0\cdot3$ volts. This is the same as the value $7\cdot16$ volts determined from the present experiments for the potential difference between oxygen-coated and clean platinum.

---

* 'Phys. Rev.,' vol. 32, p. 961 (1928). We use the value found by Du Bridge instead of the later value 5·29 volts proposed by Van Velzer ('Phys. Rev.,' vol. 44, p. 831 (1933)), because the heat treatment of the platinum used in the present work resembled that used by Du Bridge rather than that used by Van Velzer.

We see that the electronic work function of the part of the platinum surface that is covered with adsorbed oxygen (the quantity ϕ_2 of equation (20)) is $13\cdot43$ volts, while that of pure platinum (ϕ_1) is $6\cdot27$ volts, and that of platinum saturated with oxygen (ϕ) is $8\cdot46$ volts.† Substituting these values in equation (20), we find that platinum saturated with oxygen has a fraction $\theta = 30\cdot6\%$ of its surface covered. The greatest value recorded by Kobosew and Anochin for the efficiency of 7-volt electrons in causing desorption is $29\cdot5\%$, which is in good agreement with the result just obtained.

It may perhaps be mentioned that in addition to the maximum in the efficiency of desorption for electrons of 7 volts energy, Kobosew and Anochin also found maxima at $10\cdot0$ and $12\cdot4$ volts. The greatest efficiencies of desorption recorded at these two voltages were $8\cdot8\%$ and $10\cdot8\%$ respectively. It may be that these voltages correspond to critical voltages for the emission of secondary electrons from the oxygen-coated portions of the platinum. This might account for the efficiency of desorption at these voltages being less than at 7 volts, for although there are no data available for oxygen-coated platinum, it has been found in a number of instances that the probability of reflexion of an electron from a metallic surface increases as the velocity of the electron is increased from zero.

The experiments of Richardson may be interpreted in a similar manner. In these experiments the emission varies with the pressure, and therefore, according to equation (17) of the previous section, the constant V of the equation $i \propto e^{-\mathrm{V}e/k\mathrm{T}}$ is given by

$$\mathrm{V} = \chi - \phi. \tag{21}$$

Richardson found $\mathrm{V} = 1\cdot37$ volts and therefore, writing $\chi = 13\cdot56$ volts as the ionization potential of atomic oxygen—we saw in § 1 that Richardson found it necessary to assume that oxygen is adsorbed in the atomic form—we obtain $\phi = 12\cdot19$ volts. If we assume, as before, that the difference in the electronic work function of oxygen-coated and clean platinum is 7·16 volts, whether the platinum is activated or not, we obtain 5·03 volts as the electronic work function of the pure metal. This differs from Du Bridge's determination (6·27 volts) of this quantity. This, however, is not surprising. for not only was the platinum available in 1906 of a different degree of purity to the modern product but also the heat treatment of Richardson's platinum was probably different from both that used by Du Bridge and that used in the present work.

---

* 'Z. phys. Chem.,' B, vol. 13, p. 18 (1931).

† Cassel and Glückauf, *loc. cit.*

The measurements of Richardson of the variation of the emission with pressure enable us to calculate the ratio of the amount of oxygen adsorbed at any pressure to that adsorbed at saturation. We find that at a pressure of 1·47 mm (the pressure at which Richardson measured the variation of the positive emission with temperature) this ratio has the values 0·238, 0·233, 0·234 at temperatures 730°, 820°, and 1170° C respectively. Combining this value with the results either of Kobosew and Anochin, or of the present work for the fraction of the surface that is covered at saturation, we obtain by a method similar to that used above the value

$$5{\cdot}03 + 0{\cdot}234\,(7{\cdot}16 \times 0{\cdot}30) = 5{\cdot}54$$

volts as the electronic work function of the platinum under the conditions of the experiment. This agrees, within the limits of experimental error, with the value 5·72 volts found by Richardson.

The fact that Langmuir and Kingdon were able to use the experimentally determined electronic work function in their discussion, by means of the Saha equation, of the positive ion emission from tungsten heated in caesium vapour suggests that the sharp delimitation of the areas of the metallic surface covered with adsorbed atoms which is visualized in fig. 4 does not obtain for caesium adsorbed on tungsten. This is what we should expect, since the forces of adsorption in the case of alkali atoms appear to be of the long-range type (image forces, van der Waals forces), while for oxygen they are probably short-range valence forces. The fact that the influence of adsorbed caesium atoms is less localized than that of adsorbed oxygen atoms might have been foreseen from more general considerations. For suppose that the influence of a caesium atom adsorbed on tungsten is localized, as are oxygen atoms adsorbed on platinum, then the state of affairs is as represented in fig. 4, where the black patches now represent regions of lower electronic work function. The argument given on p. 437 leads to the conclusion that the electron density in the centre of the enclosure (which is what appears in the Saha equation for the positive ion emission) depends on the work function of the clean portions of the metal surface. This is contrary to the conclusion reached by a different method on p. 439 that the electron density that appears in the Saha equation is determined by the work function of the part of the surface that is covered by adsorbed atoms. This contradiction can be resolved only by supposing that the influence of adsorbed electropositive atoms extends over a considerable range and that there are therefore no local inequalities of work function such as are visualized in fig. 4. The electron density that appears in the Saha equation is then determined by a work function for the whole surface which is given approximately by equation (20).

In conclusion, I wish to thank Professor O. W. Richardson for suggesting this investigation and for his helpful advice during the progress of the work.

SUMMARY

The variation with temperature of the positive ion emission from platinum heated in oxygen has been examined. The results are compared with the earlier work of Richardson and are discussed in the light of the Saha equation. Satisfactory agreement with the theory is obtained, but, owing to the discontinuous nature of the emitting surface, it is necessary to assume a different value for the electronic work function from that determined experimentally. The difference is quantitatively accounted for.

On the Production of Electron Pairs

By J. C. JAEGER, Trinity College, Cambridge, and H. R. HULME, Gonville and Caius College, Cambridge

(*Communicated by R. H. Fowler, F.R.S.—Received July* 30, 1935)

1—INTRODUCTION AND METHOD

The production of positive-negative electron pairs by a beam of γ-rays traversing matter has been examined by various authors,* the most comprehensive treatment being that of Bethe and Heitler.† These authors employ the usual " Born Approximation " method, and justify its use for such elements as lead by pointing out that for γ-rays in the region $h\nu/mc^2 - 3$ to 11, the results obtained are in fairly good agreement with experiments. We reproduce some of their results below, namely, the ratio of the absorption due to combined Compton and photo-electric effects to that due to production of electron pairs.

	Lead			Aluminium
Energy in units of mc^2	2–4·4	5·2	10–12	10–12
Experimental ratio	(0·03)	0·22	(0·67)	(0·06)
Theoretical ratio	0·03	0·20	0·95	0·17

The theoretical ratios are calculated for energies $h\nu/mc^2 = 3, 5\cdot2$, and 11. The values in brackets refer to measurements made in rather thick plates of lead, whereas the value for the $5\cdot2\, mc^2$ γ-radiation is reduced to infinitely thin plates. Even so, the calculation of the absorption in a thin plate from experiments in thick plates involves a good deal of uncertainty. The agreement in the first column is not of any great significance, owing to the further uncertainty of the distribution of the energy in the γ-rays used. The results for aluminium are somewhat disturbing, as one would expect the Born Approximation to be more accurate here.

It therefore seems desirable to treat the problem rigorously, using spherical wave functions and not employing any approximation except those occurring in the numerical work, in which one can estimate the error involved.

---

* Plesset and Oppenheimer, ' Phys. Rev.,' vol. 44, p. 53 (1933); Heitler and Sauter, ' Nature,' vol. 132, p. 892 (1933); Nishina, Tomonaga, and Sakata, ' Sci. Pap. Inst. Phys. Chem. Res., Tokyo,' vol. 24, p. 1 (1934).

† Bethe and Heitler, ' Proc. Roy. Soc.,' A, vol. 146, p. 83 (1934).

The method employed here is an extension of that used by the authors to calculate the internal conversion of γ-rays with the production of electron pairs.* The γ-ray is treated as a perturbation acting on an electron in a state of negative energy, in the presence of a nucleus, represented by a wave function $\psi\,(E', k', u')$, where E' ($< -mc^2$) is the energy, k' and u' the azimuthal and magnetic quantum numbers respectively. It can then be shown† that the rate of absorption of energy, due to creation of electron pairs, from a beam of unity intensity travelling along the z-axis is given by

$$\frac{2\pi ce^2}{h\nu}\sum_{k,u}|\,(E, k, u\,|\,-\,\rho_2\sigma_y\,e^{2\pi i\nu z/c}\,|\,E', k', u')\,|^2 \tag{1}$$

per unit energy range, where ν is the frequency of the γ-ray. The above expression is a sum of squares of matrix elements representing transitions from the state $\psi\,(E', k', u')$ to states $\psi\,(E, k, u)$, and it is assumed that there is one electron per unit energy range in the state $\psi\,(E', k', u')$ entering a large sphere about the nucleus per second. $\rho_1\sigma_y$ is one of Dirac's matrices, and the wave functions have four components. Actually there are $1/h$ electrons per unit energy range for each value of k', u', so that the total absorption is

$$\frac{2\pi ce^2}{h^2\nu}\int_{E_1'}^{-mc^2} dE'\sum_{\substack{k,\,u\\ k',\,u'}}|\,(E, k, u\,|\,-\,\rho_1\sigma_y\,e^{2\pi i\nu z/c}\,|\,E', k', u')\,|^2 \tag{2}$$

where $E'_1 = -h\nu + mc^2$. Electrons with energies less than E'_1 cannot be excited by a γ-ray of energy $h\nu$.

The calculation of the matrix elements in (2) is difficult, and can only be done numerically. As stated, the method used is an extension of that given by the authors (*loc. cit.*) for internal conversion. We expand the perturbation term $\exp\,(2\pi i\nu z/c)$ as

$$e^{2\pi i r\cos\theta/\lambda} = \sum_{n=0}^{\infty}(2n+1)\frac{i^n}{n!}\left(\frac{\pi}{2\,.\,2\pi r/\lambda}\right)^{\frac{1}{2}} J_{n+\frac{1}{2}}\,(2\pi r/\lambda)\,P_n{}^0\,(\cos 0), \tag{3}$$

putting $z = r\cos\theta$. Here $P_n{}^0$ is the Legendre function as defined by Darwin and is $n\,!$ times the ordinary one. The matrix elements (2) are of the form

$$\iiint \psi^*\,(E, k, u)\,e^{2\pi i r\cos\theta/\lambda}\,\rho_1\sigma_y\,\psi\,(E', k', u')\,r^2\sin\theta\,d\theta\,d\phi\,dr,$$

---

* Jaeger and Hulme, 'Proc. Roy. Soc.,' A, vol. 148, p. 708 (1935), referred to as J. and H.

† *See*, for example, Hulme, 'Proc. Roy. Soc.,' A, vol. 133, p. 390 (1931), expression (33).

and an integration over ϕ yields immediately $u = u' \pm 1$. There is no selection rule for k' and for any given transition $k' \rightarrow k$ we have, using (3), an infinite sum of integrals involving the product of three Legendre functions, one from the perturbation term and one from each of the wave functions. On integrating over θ these vanish except for a finite number, and we are left with an integration over r, involving the radial parts of the wave functions and a number of Bessel functions. It is difficult to give general formulae, and we shall be content with giving as an example the matrix elements for transitions from $k' = 0$, $u' = 0$, the simplest case. These are

$$m^a{}_{-1,k} = i^k (k+1)^{\frac{1}{2}} \int_0^\infty \Big\{ \mathrm{F}_k \mathrm{G}_{0'} \mathrm{J}_{k+1+\frac{1}{2}}(qr) + \mathrm{F}_{0'}\mathrm{G}_k \Big| \frac{(k+1)\,\mathrm{J}_{k+1+\frac{1}{2}}(qr) - k\mathrm{J}_{k-1+\frac{1}{2}}(qr)}{2k+1} \Big| \Big\} \times \mathrm{L}_k(r)\,dr,$$

$$m^a{}_{1,k} = -\,i^k \int_0^\infty \Big\{ \mathrm{F}_{0'}\, G_k \,[\mathrm{J}_{k+1+\frac{1}{2}}(qr) + \mathrm{J}_{k\;1+\frac{1}{2}}(qr)] \frac{\{(k)(k+1)(k+2)\}^{\frac{1}{2}}}{2k+1} \Big\} \mathrm{L}_k(r)\,dr,$$

$$m^b{}_{-1,k} = i_k\, k^{\frac{1}{2}} \int_0^\infty \Big\{ \mathrm{F}_{-k-1}\, \mathrm{G}_{0'}\, \mathrm{J}_{k-1+\frac{1}{2}}(qr) - \mathrm{G}_{-k-1}\, \mathrm{F}_{0'} \Big| \frac{(k+1)\,\mathrm{J}_{k+1+\frac{1}{2}}(qr) - k\,\mathrm{J}_{k-1+\frac{1}{2}}(qr)}{2k+1} \Big| \Big\} \times \mathrm{L}_{-k-1}(r)\,dr,$$

$$m^b{}_{1,k} = -\,i^k \int_0^\infty \Big\{ \mathrm{G}_{-k-1}\, \mathrm{F}_{0'}\, [\mathrm{J}_{k+1+\frac{1}{2}}(qr) + \mathrm{J}_{k-1+\frac{1}{2}}(qr)] \frac{\{(k-1)\,k\,(k+1)\}^{\frac{1}{2}}}{2k+1} \Big\} \mathrm{L}_{-k-1}(r)\,dr,$$

where

$$q = 2\pi\nu/c,$$

and

$$\mathrm{L}_k(r) = (\pi/2qr)^{\frac{1}{2}}\, \xi(\mathrm{E}', 0')\, \xi(\mathrm{E}, k)\, r^2.$$

$m^a{}_{-1,k}$ is the matrix element when the final state is of type A (*see* J. and H.) with $u = -1$ and azimuthal quantum number k. The quantities F_k, G_{-k-1}, etc., are the radial parts of the Dirac wave functions as given by Darwin.* Convenient forms for these and for the normalizing factors $\xi(\mathrm{E}', 0')$ and $\xi(\mathrm{E}, k)$ are given in J. and H. To evaluate the integrals in (4) we express the Bessel functions as follows:

$$\mathrm{J}_{k+\frac{1}{2}}(qr) = \frac{1}{(2\pi qr)^{\frac{1}{2}}} \left[e^{iqr} \sum_{l=0}^{k} \frac{i^{l-k-1}(k+l)\,!}{l\,!\,(k-l)\,!\,(2qr)^l} + \begin{matrix}\text{conjugate}\\ \text{complex}\end{matrix} \right].$$

---

* 'Proc. Roy. Soc.,' A, vol. 118, p. 654 (1928).

The problem is now reduced to the evaluation of a number of convergent integrals of the form

$$\int_0^\infty r^\lambda e^{\mp iqr} G_{k'} G_k \, dr$$

(or with F_k instead), and a full account of the evaluation of integrals of this type is given in J. and H. The numerical work involved is great, but for fairly low energies of the γ-ray only small values of k and k' are required. For high energies the method is quite impracticable.

2—RESULTS

We have calculated the cross-section per atom (σ) for absorption by electron pair production in lead, for γ-rays of energies 3 mc^2 and 5·2 mc^2, and also the quantity $\bar{E}_+ - \bar{E}_-$ where $\bar{E}_+$ and $\bar{E}_-$ are the mean energies of the positron and electron respectively. This gives some idea of the asymmetry of the energy distribution. It will be seen that the positrons always have a higher mean energy than the electrons, owing to the fact that they are repelled from the nucleus, whereas the electrons are attracted. In Table I we give Bethe and Heitler's results for comparison.

TABLE I

$h\nu/mc^2$	$\sigma \times 10^{24}$	$\sigma \times 10^{24}$ (B. and H.)	$\bar{E}_+ - \bar{E}_-$
3	0·67	0·34	0·33
5·2	3·1	2·5	0·55

The values for 5 mc^2 are not so accurate as could be desired, as about 25% of the absorption comes from transitions involving high k-values, and these have been calculated by extrapolation. The error in σ, however, should not be more than about 10%.

It will be seen that the present method yields results somewhat higher than those of Bethe and Heitler. It shows, however, that *even for heavy elements we may expect the Born Approximation to give good results for γ-rays of high energy.* The same is presumably true for the radiative energy losses suffered by fast particles traversing matter, though not for the photo-electric effect, where the Born Approximation gives far too large a result even for high energies. As regards the absolute magnitude of the absorption coefficient, the agreement with experiment is not improved, but as yet no reliable results are available for absorption in thin sheets of lead.

The energy distribution of positrons created in thin sheets of lead (25 μ thick) has been examined by Alichanow, Alichanian, and Kosodaew,* using ThC″ γ-rays ($h\nu = 5 \cdot 2\,mc^2$). We reproduce their experimental points and curve below (I), together with the theoretical curve obtained by us (II). The latter stops abruptly at the end point shown, 1600 kV, corresponding to point where the positron takes up all the energy liberated by the γ-ray.

---

* 'Nature,' vol. 136, p. 475 (1935). We are greatly indebted to these authors for the opportunity of seeing their results before publication.

The agreement between the two curves is not very close, but they do show the same characteristics, a maximum in the region of 1000 kV, and a very sudden drop at the end of the range. The scale of the ordinate is arbitrary, and the curves have been adjusted to give the same value for the maximum number of positrons.

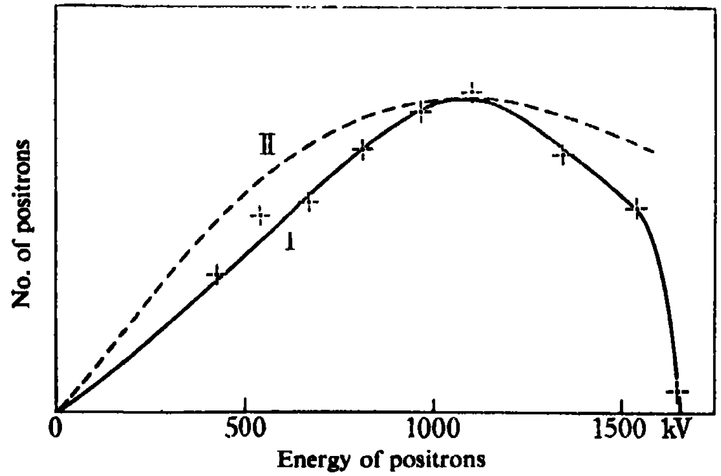

FIG. 1.

In conclusion, we should like to thank Professor R. H. Fowler for his interest in the work, and the Council of Trinity College, Cambridge, for a grant from the Rouse Ball Fund.

SUMMARY

A method is given for finding the number of pairs created by a γ-ray traversing matter. The use of the Born Approximation is avoided by using the exact wave functions for an electron in the presence of a heavy nucleus, but it is not possible to obtain closed formulae for the absorption. The results obtained for γ-rays of energies 3 mc^2 and 5·2 mc^2 give an absorption coefficient greater than that found by the Born Approximation method. The present method also gives the energy distribution of the positrons, which shows the same characteristics as the experimental distribution found for the positrons created by Th C″ γ-rays in thin plates of lead.

The Oxidation of Aromatic Hydrocarbons at High Pressures

I—Benzene. II—Toluene. III—Ethyl Benzene

By D. M. NEWITT, D.Sc., and J. H. BURGOYNE, B.Sc.

(*Communicated by W. A. Bone, F.R.S.—Received July* 30, 1935)

It has been shown in previous papers of this series* that during the slow combustion of the aliphatic hydrocarbons at high pressure conditions are particularly favourable to the isolation of the intermediate compounds involved, and that such oxidations take place by successive stages of hydroxylation. The work has now been extended to include the aromatic hydrocarbons, and the present paper embodies the results for benzene, toluene, and ethyl benzene.

The homogeneous slow oxidation of benzene in the vapour phase has been studied by Fort and Hinshelwood,† who concluded that at atmospheric pressure it proceeds by a chain mechanism somewhat analogous to that which they postulated for ethylene. Although a complete analysis of the products of combustion was not made, other circumstances suggested that during an " apparent period of induction " the first products were formed without pressure increase, and that, to quote their words, " hydroxylation of the double bonds may be assumed to occur, followed by rapid further oxidation of the open chain unsaturated compound so produced to a substance like glyoxal. The remaining stages would then be analagous to the oxidation of acetylene—

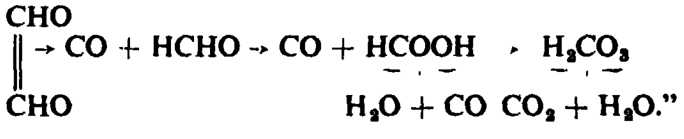

$$\begin{matrix}\text{CHO}\\ \|\\ \text{CHO}\end{matrix} \rightarrow \text{CO} + \text{HCHO} \rightarrow \text{CO} + \underbrace{\text{HCOOH}}_{\text{H}_2\text{O} + \text{CO}} \rightarrow \underbrace{\text{H}_2\text{CO}_3}_{\text{CO}_2 + \text{H}_2\text{O}."}$$

No similar data are available for toluene or ethyl benzene, although there is evidence that the side chains undergo oxidation by successive stages in a manner resembling that of the paraffin hydrocarbons. Thus, for example, at atmospheric pressure toluene yields on oxidation benzaldehyde and benzoic acid, whilst at high pressures the presence of benzyl alcohol has also been reported.

---

* 'Proc. Roy. Soc.,' A, vol. 134, p. 591 (1932); A, vol. 140, p. 427 (1932).

† 'Proc. Roy. Soc.,' A, vol. 127, p. 218 (1930).

Our experiments at high pressures have shown a marked difference in behaviour between benzene and its alkyl derivatives; for whilst at suitable temperatures and pressures the oxidation of the former proceeds smoothly without any induction period or sudden change in reaction velocity, both toluene and ethyl benzene exhibit well-defined induction periods, and in each case oxidation of the nucleus and side chains occurs simultaneously. Indeed, both alkyl derivatives exhibit many of the characteristic features of paraffin hydrocarbon combustion. Chemical analyses of the products also show that combustion takes place by hydroxylation either of the ring or the side chain, giving as primary products phenol in the one case and alcohols in the other.

The course of combustion up to the point at which rupture of the ring occurs may be represented as follows:

Benzene

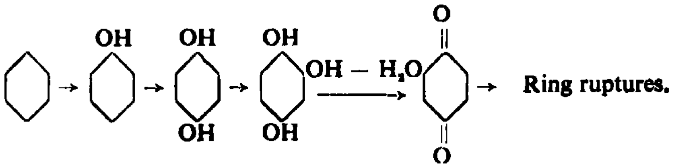

Toluene

Side chain oxidation

$C_6H_5\cdot CH_3 \rightarrow C_6H_5\cdot CH_2OH \rightarrow C_6H_5CH(OH)_2 \rightarrow H_2O + C_6H_5CHO$

Oxidation of the nucleus gives mainly

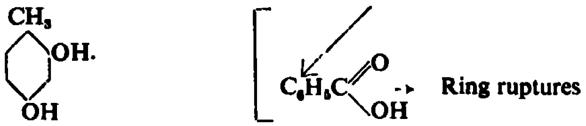

Ethyl Benzene

Side chain oxidation

Oxidation of the nucleus gives mainly

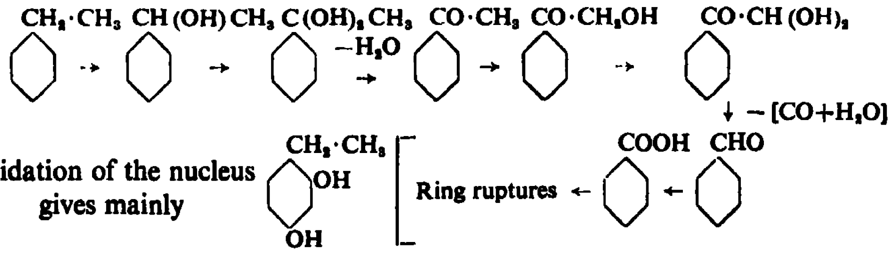

EXPERIMENTAL

Procedure—A description of the apparatus employed and the experimental method have been given in previous papers. Briefly, the procedure was to introduce successively into a cylindrical steel reaction vessel, of 500 cc capacity, maintained at a suitable temperature, the components of the reacting medium in the requisite proportions. The progress of oxidation could then be followed by the changes in temperature as indicated by a thermocouple situated axially in the reaction chamber, and by means of analyses of samples taken at periodic intervals. At the conclusion of the reaction or at some predetermined time, the contents of the vessel were passed through a train of cooling and scrubbing coils to remove condensable and soluble products, and the gaseous residue was collected, measured, and analysed.

When the products contained substances of high boiling-point it was sometimes necessary to cool the reaction vessel and extract any residual condensable material with a suitable solvent.

From the ascertained composition of the initial mixture and the products a balance could be drawn up showing how the carbon in the hydrocarbon oxidized was distributed in the products.

Slow Oxidation of Benzene

(1) At pressures of about 50 atm benzene reacted readily with oxygen at temperatures of 280° C and upwards, the principal products for mixtures containing an excess of the hydrocarbon being phenol, the two oxides of carbon and steam. Hydroquinone, quinone, maleic acid, and formaldehyde were also found in small quantities. At high temperatures when combustion proceeded rapidly with liberation of heat, some tarry matter and free carbon were deposited in the reaction vessel and the gaseous products included hydrogen, methane, and occasionally higher hydrocarbons. Diphenyl formed by the pyrolysis of benzene was also found in small quantities.

Unlike the aliphatic hydrocarbons, reaction was not preceded by any marked induction period, but began almost immediately the mixture was admitted to the heated vessel. With comparatively rich mixtures it passed rapidly beyond the stage at which the ring structure breaks down, and only small quantities of aromatic derivatives survived. When, however, a large excess of the hydrocarbon was present in the reacting medium oxidation was partially arrested during its earlier stages, and considerable quantities of phenol were found in the products.

(2) Thus, in a series of experiments at 312° with mixtures in which the benzene-oxygen ratio was varied between 20: 1 and 1·9: 1, the partial pressure of hydrocarbon being kept constant at 20 atm, the percentages of the benzene burnt appearing as phenol are given in Table I:

TABLE I

Ratio C_6H_6/O_2	% of the C_6H_6 burnt appearing as phenol
1·9	12·8
3·7	37·7
9·9	24·9
20·0	38·3

Only inconsiderable amounts of diphenyl, hydroquinone, and quinone could be detected in the remaining products which consisted principally of the oxides of carbon and steam.

(3) Further experiments with benzene-air mixtures containing a large excess of the hydrocarbon were carried out over a temperature range including both slow and rapid rates of reaction, and comparisons made between the amounts of phenol surviving, Table II.

TABLE II—THE AMOUNTS OF PHENOL SURVIVING IN THE PRODUCTS FROM VARIOUS BENZENE-AIR MIXTURES

Reaction temperature °C	% of the benzene burnt appearing as phenol from		
	$20C_6H_6 + 2O_2 + 7{\cdot}5N_2$ Pressure = 30 atm	$40C_6H_6 + 2O_2 + 7{\cdot}5N_2$ Pressure = 50 atm	$60C_6H_6 + 3O_2 + 11{\cdot}3N_2$ Pressure = 75 atm
291	34·2	29·8	—
309	24·9	—	—
312	39·2	—	39·9
332	—	36·3	40·4
362	—	53·5	—
513	—	26·7*	—

* Some inflammation occurred during this experiment.

It will be seen that the most favourable conditions in respect of phenol formation occurred with the $40\,C_6H_6/9{\cdot}5$ air mixture at temperatures sufficiently high to give rapid reaction without inflammation. Thus, at 362° it accounted for upwards of 50% of the benzene burnt, and even at higher temperatures, where reaction was very vigorous and accompanied by flame formation, considerable quantities still survived.

The percentage distribution of oxygen in the products from this experiment was:

Phenol	10·6
Hydroquinone and quinone	trace
Maleic acid	2·8
Formaldehyde	3·0
Carbon monoxide	26·2
Carbon dioxide	29·8
Water	27·6
	100·0

It is noteworthy that in no instance have aromatic oxidation products other than phenol been found in anything but traces, a circumstance suggesting that the introduction of the first hydroxyl group into the nucleus undermines its resistance to oxidation. The presence of hydroquinone and quinone, however, have some significance in that they point to further oxidation occurring by successive stages of hydroxylation as follows :

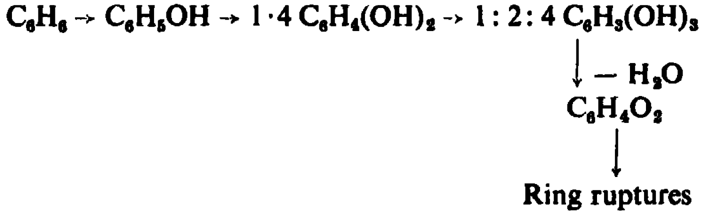

$$\begin{array}{l} C_6H_6 \rightarrow C_6H_5OH \rightarrow 1\cdot4\ C_6H_4(OH)_2 \rightarrow 1:2:4\ C_6H_3(OH)_3 \\ \qquad\qquad\qquad\qquad\qquad\qquad\qquad\qquad \downarrow -H_2O \\ \qquad\qquad\qquad\qquad\qquad\qquad\qquad\qquad C_6H_4O_2 \\ \qquad\qquad\qquad\qquad\qquad\qquad\qquad\qquad \downarrow \\ \qquad\qquad\qquad\qquad\qquad\qquad\qquad \text{Ring ruptures} \end{array}$$

It will be noticed that in passing from hydroquinone to quinone the intervention of a trihydroxy derivative is postulated. This compound was not isolated in the products, but it could be detected by qualitative tests, and its presence constitutes a logical step in the transition from hydroquinone to quinone.

(4) When the concentration of oxygen in the reacting medium was increased, the earlier stages of combustion were rapidly passed and there was a considerable diminution in the amount of phenol surviving. Thus, with a 2: 1 benzene-oxygen mixture undergoing reaction at 30 atm and temperatures between 274° and 333°, upwards of 97% of the oxygen used appeared in the products as oxides of carbon and steam (*see* Table III).

TABLE III—DISTRIBUTION OF OXYGEN IN THE PRODUCTS FROM THE REACTION OF A 2: 1 BENZENE-OXYGEN MEDIUM AT 30 ATM AND VARIOUS TEMPERATURES

Temp. °C	% oxygen used appearing in products as Phenol	Maleic acid	Form-aldehyde	CO_2	CO	H_2O*
274	0·9	3·2	0·2	59·3	8·2	28·2
296	1·5	2·1	0·2	35·6	22·8	37·8
313	1·8	0·3	0·2	22·2	55·5	20·0
333	2·5	0·7	—	18·7	60·1	18·0

* This figure includes, in addition to steam, aromatic oxidation products present in traces only.

The temperature range covered by these experiments was sufficiently wide to include both very slow rates of reaction and almost instantaneous inflammation. At 274°, for example, only 64% of the oxygen contained in the initial mixture was used up in 2¾ hours, whilst at 333° reaction took place during the filling operation. The phenol surviving represented between 7·9 and 12·8% of the benzene burnt, the amount increasing with the reaction temperature.

Slow Combustion of Toluene

The products of the slow combustion of toluene at high pressures may be divided into three groups, according as they result from oxidation of the side chain, oxidation of the nucleus, or rupture of the ring structure with subsequent oxidation of the resultant " fragments." The relative proportions in which each group survives depends *inter alia* upon temperature, pressure, and mixture composition. The principal products are (1) from side chain oxidations—benzyl alcohol, benzaldehyde, and benzoic acid; (2) from nucleus oxidation—*p*-cresol, 2:4 dihydroxy-toluene; and (3) from rupture of the ring—aliphatic acids, formaldehyde, the two oxides of carbon and steam.

In addition dibenzyl is formed by pyrolysis of toluene, and small quantities of benzene arise probably from thermal decomposition of benzoic acid.

These substances have been isolated or identified by means of their derivatives, but owing to their number and complexity it was not possible to make a quantitative estimate of those occurring in small quantities only. In all cases, however, the greater part (upwards of 75%) of the carbon of the toluene burnt has been accounted for in the analyses.

At pressures of 20 atm and upwards toluene-oxygen mixtures containing excess of the hydrocarbon reacted slowly at 210° and at a measurable and increasing rate up to temperatures of about 275°. Beyond this point, inflammation was liable to occur with some tar formation and liberation of carbon. Between these temperature limits the products consisted largely of aromatic derivatives containing oxygen in the nucleus or side chain, although some oxide of carbon, steam, and traces of aliphatic acids and aldehydes were always present. As an example, the data for a toluene/oxygen = 1·5/1 mixture reacting at a pressure of 18·3 atm and various temperatures between 216°–276° C is summarized in Table IV.

It will be seen from an inspection of the table that at all temperatures up to 268° benzoic acid was the principal product of the oxidation; the amount surviving increased from 34·4% at 216°, at which temperature the rate of reaction was very slow, to a maximum of 55·4% at 260° and thereafter diminished. The amount of benzaldehyde surviving showed a rapid decrease from 18·8% at 216° to 4·9% at 276°, whilst benzyl alcohol, although present in much smaller quantities, behaved in a similar manner.

TABLE IV—PRODUCTS FROM THE REACTION OF A $1\cdot5\,\mathrm{C_6H_5\cdot CH_3} + \mathrm{O_2}$ MIXTURE AT 18·8 ATM AND VARIOUS TEMPERATURES

Temp. °C	Products as % of the carbon of the toluene burnt					
	Benzyl Alcohol	Benzaldehyde	Benzoic acid	2·4 hydroxy-toluene	$\mathrm{CO_2}$	CO
216	2·6	18·8	34·4	5·8	9·3	2·6
222	1·8	17·6	28·2	4·2	7·5	2·2
240	1·1	10·2	45·0	1·2	15·1	2·9
249	1·2	8·6	47·1	5·1	19·6	3·3
260	1·2	5·9	55·4	6·7	26·0	5·8
268	1·5	6·2	49·5	6·7	21·2	6·2
276	1·7	4·9	1·7	5·4	3·0	9·7*

* Inflammation occurred with liberation of carbon. The gaseous products contained, in addition to oxides of carbon, 11·1% of methane and a small quantity of a higher hydrocarbon, probably ethane.

The only product present in any quantity resulting from the direct oxidation of the nucleus was 2·4 dihydroxy-toluene, but traces (less than 1%) of salicylic acid and *p*-cresol could be detected at the lower temperatures. Even under the most favourable conditions, however, the greater part of the oxygen was used in forming side chain derivatives; thus, on calculating its percentage distribution between the nucleus and side chain at the various temperatures the figures given in Table V were obtained:

TABLE V

Temperature °C	% distribution of oxygen	
	Side chain	Nucleus
215	72·0	28·0
249	91·5	8·5
260	89·5	10·5
268	88·5	11·5

If, as we suppose, oxidation of the side chain proceeds by successive hydroxylations through benzyl alcohol and benzaldehyde to benzoic acid

$$-\mathrm{CH_3} \rightarrow \overset{(1)}{-\mathrm{CH_2OH}} \rightarrow \overset{(2)}{\underbrace{-\mathrm{CH(OH)_2}}_{\mathrm{H_2O} + -\mathrm{CHO}}} \rightarrow \overset{(3)}{-\mathrm{COOH}}$$

it is evident from the above results that combustion had proceeded to a large extent beyond the first two stages. In the next series of experiments, therefore, the toluene-oxygen ratio of the reacting medium was varied over a wide range, keeping always an excess of the hydrocarbon, in order to ascertain whether more favourable conditions could be found for the isolation of the initially formed products in greater quantity. In all the experiments the total pressure of the system was kept constant at 20 atm, and the reaction temperatures were varied so as to give approximately equal rates of reaction for all the mixtures.

The results are summarized in Table VI and are shown by means of curves in fig. 1.

It is evident that mixture composition had a marked effect upon the combustion, particularly as regards the side-chain derivatives. Thus, for example, whilst the comparatively rich 1 : 1 toluene-oxygen mixture gave 59·3% of benzoic acid in the products and only in considerable amounts of benzyl alcohol and benzaldehyde, the 30 : 1 mixture yielded 50·6% of benzaldehyde, 6·2% of benzyl alcohol, and only 16·3% of benzoic acid. The curves in fig. 1, indeed, show clearly that with increasing hydrocarbon concentration there was a tendency for a partial " hold-up " to occur at the benzaldehyde stage.

Oxidation of the nucleus was also favourably effected by increasing toluene concentration, and the percentage distribution of oxygen between the nucleus and side chain indicated that a more equitable division took place with the weaker mixtures. Attention may also be drawn to the fact that with a 30: 1 mixture, not less than 83% of the carbon of the toluene burnt appeared in the form of aromatic compounds in the products.

A further series of experiments was carried out to determine the influence of reaction temperature upon the products. 20: 5 and 30: 5 toluene-air mixtures were used, the partial pressure of oxygen being maintained constant at 1 atm and temperatures being varied so as to include both slow and rapid rates of reaction. The results for the two mixtures are recorded in Table VII.

The most noticeable feature of the results is the progressive increase in the amount of benzyl alcohol surviving with rising reaction temperature. With the 20: 5 mixture at 400°, for example, it constituted one of the most important products of the combustion and was present in larger amounts than either benzaldehyde or benzoic acid. Both the aldehyde and acid appeared in diminishing quantities as the temperature was increased, the effect being particularly marked with the acid.

It can thus be seen that by suitable variations of temperature and mixture composition any one of the three side chain derivatives may be obtained

TABLE VI—PRODUCTS OF COMBUSTION OF VARIOUS TOLUENE-OXYGEN MIXTURES

		Products as % of the carbon of the toluene burnt						% distribution of oxygen in	
Ratio $C_6H_5CH_3/O_2$	Temp. °C	Benzyl alcohol	Benzaldehyde	Benzoic acid	2:4 hydroxy toluene	CO_2	CO	Side chain	Nucleus
30*	337	6·2	50·6	16·3	9·9	5·2	5·4	81·5	18·5
20*	276	5·9	36·1	12·1	14·7	3·0	1·4	71·0	29·0
3·7	250	2·8	21·9	26·2	6·1	17·9	6·0	86·5	13·5
3·2	250	1·6	18·1	53·0	6·3	18·3	4·7	91·0	9·0
1·5	250	1·2	8·6	47·1	5·1	19·6	3·3	91·0	9·0
1	250	0·7	3·0	59·3	7·1	25·8	3·8	89·5	10·5

* These mixtures contained, in addition to toluene and oxygen, 3·76 atm of nitrogen.

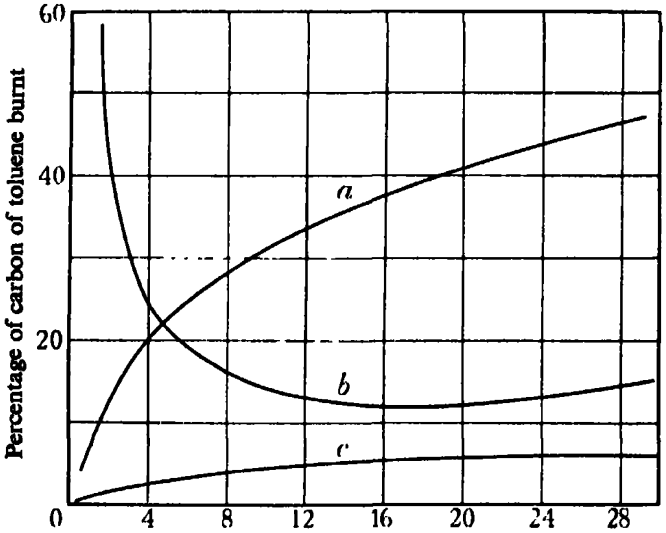

FIG. 1—*a*, benzaldehyde; *b*, benzoic acid; *c*, benzylalcohol.

in optimum quantities. Moreover, the conditions for bringing about this selective action are such as can best be explained on the assumption that benzyl alcohol is the primary product and that its further oxidation yields in turn the aldehyde and acid.

SLOW OXIDATION OF ETHYL BENZENE

The oxidation of ethyl benzene has hitherto not been studied in the vapour phase. In the liquid phase, however, Stephens* has found that it

* 'J. Amer. Chem. Soc.,' vol. 18, p. 2920 (1926).

combines readily with oxygen at temperatures of 100°–120° C, yielding acetophenone and the oxides of carbon but no alcohol or aldehyde. Under similar circumstances, but in the presence of a manganese oxide catalyst, Senseman and Stubbs* reported that the products contain, in addition to the above, phenyl methyl carbinol, benzoic acid, and formaldehyde.

In discussing the mechanism of the reaction, Stephens concludes that the hydrogen attached to the carbon atom in the *alpha* position to the ring is first removed and that oxygen tends to substitute in the same position as do the halogens, giving acetophenone. The alcohol is regarded not as an intermediate product of the combustion but as arising from some independent secondary reaction.

TABLE VII—PRODUCTS FROM THE COMBUSTION OF 20:5 AND 30:5 TOLUENE-AIR MIXTURES AT VARIOUS TEMPERATURES. PARTIAL PRESSURE OF OXYGEN = 1 ATM.

Temperature °C	Products as percentages of the carbon of the toluene burnt					
	Benzyl alcohol	Benz-aldehyde	Benzoic acid	2:4 hydroxy-toluene	CO_2	CO
			$20\ C_6H_5CH_3 + 5$ Air			
276	5·9	36·1	12·1	14·7	3·0	1·4
304	5·6	38·6	17·7	15·0	3·5	3·0
331	6·0	40·4	19·4	17·9	4·5	3·8
375	15·8	30·0	10·2	—	14·4	5·3
400	31·1	30·1	8·1	10·2	14·7	4·2
			$30\ C_6H_5CH_3 + 5$ Air			
337	6·2	50·6	16·3	9·9	5·2	5·4
358	8·3	45·4	10·6	10·7	4·0	5·5
391	16·6	31·0	9·7	9·3	4·2	3·9
503*	6·6	3·2	3·6	3·9	3·5	9·8

* Inflammation occurred with carbon deposition, and the gaseous products were found to contain about 14% of methane and a lesser quantity of some higher hydrocarbon.

Our results do not support this view, but show that the homogeneous vapour phase oxidation takes place by successive hydroxylations of the hydrogen attached to the carbon atom in the *alpha* position, yielding as a primary product phenyl methyl carbinol which in turn gives acetophenone. The further oxidation of acetophenone then occurs by hydroxylation of the hydrogen attached to the carbon in the *beta* position, giving benzaldehyde and benzoic acid. The intermediate stages resulting in the formation of the acid are therefore as follows:

---

* 'J. Ind. Eng. Chem.,' vol. 25, p. 1287 (1933).

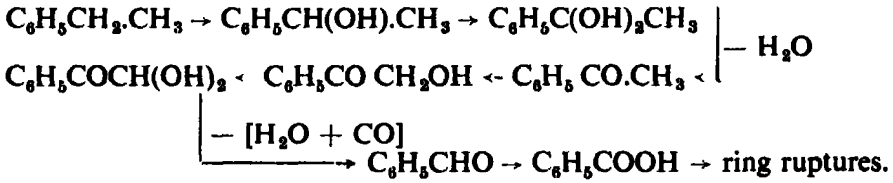

$$
\begin{array}{l}
C_6H_5CH_2.CH_3 \rightarrow C_6H_5CH(OH).CH_3 \rightarrow C_6H_5C(OH)_2CH_3 \\
\qquad\qquad\qquad\qquad\qquad\qquad\qquad\qquad\qquad\quad \big| - H_2O \\
C_6H_5COCH(OH)_2 \leftarrow C_6H_5CO\,CH_2OH \leftarrow C_6H_5\,CO.CH_3 \leftarrow \\
\quad \big| - [H_2O + CO] \\
\quad \longrightarrow C_6H_5CHO \rightarrow C_6H_5COOH \rightarrow \text{ring ruptures.}
\end{array}
$$

In the vapour phase ethyl benzene was found to oxidize readily at temperatures in the neighbourhood of its boiling point (136·15° C). It was therefore not feasible to study its slow combustion at very high pressures; the maximum partial pressure that could be obtained at any temperature below the critical temperature being limited by the saturated vapour pressure. As no determination of the vapour pressure above the boiling-point nor of the critical constants have hitherto been published, it was necessary at the outset of the investigation to obtain the required data by direct measurements. The results are given in Table VIII.

TABLE VIII—VAPOUR PRESSURE OF ETHYL BENZENE ABOVE 136·5° C

Temp. °C	Pressure atms	Temp. °C	Pressure atms
136·15	1	250·0	10·05
190·0	3·77	270·0	12·80
200·0	4·50	280·0	14·70
210·0	5·36	290·0	17·00
220·0	6·39	300·0	19·50
230·0	7·45	310·0	22·10
240·0	8·65	320·0	24·90
		330·0	28·30

Critical temperature 335·0 ± 0·2 °C
Critical pressure 30·2 ± 0·2 atm

Preliminary experiments showed that the principal products of the vapour phase oxidation were: (*a*) aromatic—phenyl methyl carbinol, acetophenone, benzaldehyde, benzoic acid, and 2:4 dihydroxy ethyl benzene, and (*b*) resulting from ring rupture—oxalic acid, formaldehyde, the two oxides of carbon and steam. In addition, small quantities of *p*-hydroxy ethyl benzene, benzene, and toluene were detected.

All the above products were identified but, owing to the complexity of the mixture, it was not found practicable to estimate quantitatively those present in small quantities only. In all cases, however, upwards of 75%

of the carbon of the ethyl benzene burnt has been accounted for in the analyses.

As previous work on the oxidation of benzene and toluene had shown that the conditions most favourable to the survival of the initially formed products of combustion were (1) a reacting mixture containing a large excess of the hydrocarbon and (2) a rapid rate of reaction, the first series of experiments was made with a 20: 7·5 ethyl benzene-air mixture at various temperatures between 322° and 437° C, the total pressure of the reacting medium being 27·5 atm.

It will be seen from the results, Table IX, that of the aromatic products only phenyl methyl carbinol increased to any marked extent with increasing reaction temperature, a circumstance which points to its being the initial product of the combustion.

TABLE IX—PRODUCTS FROM THE COMBUSTION OF A 20: 7·5 ETHYL BENZENE-AIR MIXTURE AT 27·5 ATM AND VARIOUS TEMPERATURES

Reaction temp. °C	322°	385°	437°
	Products as % of the carbon of the ethyl benzene burnt:		
Phenyl methyl carbinol	8·9	11·5	27·7
Acetophenone	13·4	trace	trace
Benzaldehyde	54·0	52·3	23·6
Benzoic acid	6·4	8·9	8·7
2: 4 dihydroxy ethyl benzene	10·3	9·2	6·8

Acetophenone diminished from 13·4% at 322° to a trace at the higher temperatures, whilst benzaldehyde and 2: 4 dihydroxy ethyl benzene behaved in a similar manner. Benzoic acid increased from 6·4 to 8·9% when the temperature was raised from 322° to 385°, but thereafter remained constant. The distribution of oxygen between the side chain and the nucleus at the three temperatures is shown in Table X.

TABLE X

	% distribution of oxygen in—	
Temp. °C	Side chain	Nucleus
322	77·0	23·0
385	75·0	25·0
437	69·0	31·0

On employing mixtures containing a much larger proportion of oxygen and temperatures at which reaction proceeded at a comparatively slow rate the amounts of ketone and acid surviving were considerably increased whilst the alcohol and aldehyde showed a corresponding diminution.

At 222°, for example, the products from 1·05: 1, 1·4: 1, and 2·2: 1, ethyl benzene-oxygen mixtures are shown in Table XI.

TABLE XI—RATIO OF ETHYL BENZENE/OXYGEN IN INITIAL MIXTURE (PARTIAL PRESSURE OF ETHYL BENZENE = 6·6 ATM)

	1·05	1·4	2·2
	Products as % of the carbon of the ethyl benzene burnt—		
Phenyl methyl carbinol	1·9	1·2	0·8
Acetophenone	26·8	38·1	20·6
Benzaldehyde	4·9	4·4	5·7
Benzoic acid	28·3	28·7	29·0
2·4 dihydroxy ethyl benzene	4·6	6·0	6·3

These results, in conjunction with those of the previous series, afford evidence that the initial course of the side chain oxidation is through phenyl methyl carbinol to acetophenone, as already stated. The remaining products—benzaldehyde and benzoic acid—might arise from further oxidation of the ketone and/or directly from ethyl benzene by successive hydroxylations of the hydrogen attached to the carbon in the *beta* position; in the former case the first step would be the formation of oxyacetophenone and in the latter of phenyl ethyl alcohol. Neither of these substances has been identified, although traces of some primary alcohol could always be detected in the products.

When, however, acetophenone was oxidized under suitable conditions, it gave large yields of both benzaldehyde and benzoic acid. Thus the products from a acetophenone, 15·1%, oxygen, 7·0%, nitrogen, 77·9% mixture at 8·6 atm, reacting at 290° C, are given in Table XII.

TABLE XII

Product	% of the carbon of the acetophenone burnt
Benzoic acid	64·5
Benzaldehyde	26·0
Carbon dioxide	7·1
Carbon monoxide	2·4
	100·0

It therefore seems most probable that the greater part of the aldehyde and acid resulted from further oxidation of acetophenone rather than from an independent reaction based upon the initial oxidation of the hydrogen attached to the end methyl group.

A COMPARISON OF SOME CHARACTERISTIC FEATURES OF THE SLOW COMBUSTION OF BENZENE, TOLUENE, AND ETHYL BENZENE AT HIGH PRESSURE

Whilst the main purpose of the present investigation was to trace the course of the slow combustion of some typical aromatic hydrocarbons, certain observations having a bearing upon the mechanism of their oxidation may be mentioned briefly.

One of the characteristic differences noted between benzene and its alkyl derivative was that whereas benzene-oxygen mixtures at high pressures, when admitted to a container maintained at a suitably high temperature, began to react immediately, neither toluene nor ethyl benzene in like circumstances reacted appreciably until after the lapse of a definite "induction" period which in some cases extended to five or more minutes. Once reaction had started, however, it proceeded with relative rapidity until the greater part of the free oxygen had been consumed.

It was also found that for comparable rates of reaction, benzene-oxygen mixtures required a higher temperature than either toluene or ethyl benzene-oxygen mixtures of similar composition. Thus in the 1·5:1 hydrocarbon-oxygen mixtures the comparative figures, given in Table XIII, were obtained:

TABLE XIII

	Reaction temp. °C	Duration of induction mins	Duration of reaction mins
Benzene	293	nil	3
Toluene	251	6	2
Ethyl benzene	239	6	2

This accords with the observation that during the combustion of toluene and ethyl benzene by far the greater part of the oxygen consumed was found in the side chain derivatives.

On increasing the surface exposed to the reacting medium by packing the vessel with metal shavings, it was found that whilst in the benzene-oxygen mixtures there was a noticeable retardation in the rate of reaction, with toluene and ethyl benzene no appreciable alteration took place. The effect of additions of nitrogen to the reacting media was always to slow down the rate of reaction.

These observations suggest that a "chain" mechanism is involved in the combustion of all three compounds but that a difference exists in the chain propagating reactions according to whether oxidation of the nucleus or the side chain is taking place; further experiments are being undertaken with a view to obtaining more information upon this aspect of the subject.

SUMMARY AND CONCLUSIONS

It has been shown that during the slow combustion at high pressures of benzene-oxygen or air mixtures containing an excess of the hydrocarbon, the primary product is phenol and that in suitable circumstances as much as 53·5% of the carbon of the benzene burnt appears as phenol in the products. The progressive oxidation of the nucleus is by hydroxylation giving phenol, hydroquinone, and quinone, after which the ring ruptures.

With alkyl derivatives oxidations of the side chain and nucleus occurs simultaneously. Thus toluene gives benzyl alcohol, benzaldehyde, and benzoic acid from side chain oxidation and 2·4 dihydroxy toluene from the nucleus. By suitably varying the concentration of oxygen in the reacting medium, and the pressure and temperature of the reaction either one of the side chain derivatives may be obtained in optimum amounts.

The oxidation of the side chain in ethyl benzene occurs by hydroxylation of the hydrogen attached to the carbon in the *alpha* position, giving phenyl methyl carbinol, acetophenone, benzaldehyde, and benzoic acid. Oxidation of the nucleus occurs simultaneously, giving principally 2·4 dihydroxy ethyl benzene.

Usually upwards of three-quarters of the oxygen found in the aromatic products of combustion of toluene and ethyl benzene are accounted for by side chain derivatives.

Whereas the slow combustion of benzene at high pressures is not characterized by an induction period, both its alkyl derivatives show well-defined induction periods.

Increased surface retards the rate of oxidation of benzene but has no appreciable effect upon toluene or ethyl benzene, whilst the addition of a diluent gas (nitrogen) retards all three reactions equally. These observations suggest that chain mechanisms are concerned in the oxidation but that the chain propagating reaction for benzene is different from that of the two alkyl derivatives.

The Electrical Resistance of Aluminium at Low Temperatures

By H. A. Boorse,* Ph.D., and H. Niewodniczański,† Ph.D., The Royal Society Mond Laboratory, Cambridge

(Communicated by Lord Rutherford, O.M., F.R.S.—Received August 2, 1935)

1—INTRODUCTION

The electrical resistance of aluminium at low temperatures has been the subject of numerous investigations. The general results of the studies made previous to 1926 have been summarized by Tuyn and Kamerlingh Onnes.‡ Subsequent researches have been mainly concerned with measurements at liquid helium temperatures. These have been made by Tuyn and Kamerlingh Onnes,§ by Meissner and Voigt,|| and by Keesom,¶ who discovered that aluminium becomes superconducting at about 1·14° K.

The data given by Meissner and Voigt for Al, as well as for several other metals (*e.g.*, Mo, Co, and Mg), appear to show that the resistance in the range 4·2° K to 1·3° K is not constant, but increases slightly with decreasing temperature. The measurements of Tuyn and Kamerlingh Onnes and of Keesom show no such phenomenon, the resistance of their aluminium specimens remaining constant, within the experimental error, between these temperatures. However, the resistance ratio $R_{4\cdot2^\circ \mathrm{K}}/R_{0^\circ \mathrm{C}}$ for the specimen used by Tuyn and Kamerlingh Onnes was 0·067 and for the specimens of Keesom 0·073 and 0·039, while the four specimens used by Meissner and Voigt show considerably smaller values, viz., 0·0197, 0·0148, 0·0079, and 0·0065, suggesting that their aluminium was of higher purity than that used by Tuyn and Kamerlingh Onnes and by Keesom.

---

* Lydig Fellow of Columbia University.

† Docent of Experimental Physics, Stefan Batory University, Wilno, Poland; Fellow of the Rockefeller Foundation.

‡ 'Comm. Phys. Lab., Leiden,' Suppl., No. 58 (1926).

§ 'Comm. Phys. Lab., Leiden,' No. 181 (1926).

|| 'Ann. Physik,' vol. 7, p. 761 (1930).

¶ 'Comm. Phys. Lab., Leiden,' No. 224c (1933).

Recently de Haas, de Boer, and van den Berg* have carefully examined the resistance of two specimens of gold at liquid helium temperatures and have found that the resistance of both passes through a minimum value at about 3·7° K and thereafter increases with decreasing temperature.

Such a behaviour of the electrical resistance of metals is of considerable interest since it is not to be expected on the basis of the recent theories of metallic conduction. Since we had at our disposal samples of aluminium of exceptional chemical purity, we decided to reinvestigate the electrical resistance of this metal at low temperatures, with special reference to the liquid helium region.

2—EXPERIMENTAL

The specimens used in our experiments consisted of polycrystalline aluminium wires of 0·15 mm diameter, ranging in length from 68 to 86 cm. The specimens hereafter referred to as Nos. 1 and 2 were prepared from wires supplied by Hartmann and Braun, no analysis of the metal being given. Those hereafter designated by Nos. 3, 4, 5, and 6 were prepared from a sample of aluminium generously given to this laboratory by the British Aluminium Company who specified the material to be at least 99·995% pure. In order to ascertain whether or not impurities were introduced by drawing the metal into wires, condensed spark discharge spectrograms were taken before and after drawing. No difference was observable in the plates which showed, besides the fully developed aluminium spectrum, only the *raies ultimes* of Mg, Ca, and Cu, the two Cu lines, 3274·0 and 3247·5 A, being extremely weak.

The drawing was carried out by pressing the metal through steel dies until a short wire of 2·2 mm diameter was formed. This wire was then boiled in a 20% solution of HCl, after which it was drawn down to a diameter of 1·0 mm. After again boiling in HCl solution, it was drawn through acid-cleaned agate dies to 0·15 mm diameter. No lubricant was applied to the dies or the wire until the latter reached a diameter of 0·5 mm. As further drawing almost always resulted in breakage, the final diameter was reached by the application of a small amount of paraffin to the dies.

Extended preliminary experiments were carried out in order to find the most suitable method of mounting the specimens. A convenient arrangement consistent with the use of a relatively small quantity of liquefied gas and absence of mechanical strain in the wires was effected by coiling them in loose spirals of about 8 mm diameter. The coils were then placed in thin-walled Pyrex glass tubes of about 1 cm internal diameter and about 5 cm long and supported by passing the ends of the coils through small holes made in the glass near the ends of the tubes. This method of mounting, fig. 1, not only allows the wires to expand and contract freely but also protects them from external mechanical damage.

---

* 'Physica,' vol. 1, p. 1115 (1934).

Since we wished to prepare specimens of the smallest possible resistance at low temperatures and to compare their resistance with that of the untreated pure metal, several of the specimens were annealed. For this purpose the Pyrex tube, containing the specimen to be heated, was placed in a fused silica tube surrounded by an electric furnace. The open end of the silica tube was connected by a vacuum-tight joint to a Holweck molecular pump backed by a Hyvac pump. By using a molecular pump instead of an oil or mercury diffusion pump it was possible to secure a very high vacuum without any traces of oil or mercury being deposited on the specimens. We were guided in choosing the annealing time and temperature by data previously published.* Specimens Nos. 2 and 4 were annealed for 3 hours in high vacuum at 275° C, and Nos. 5 and 6 at 250° C; Nos. 1 and 3 were not annealed. The cooling from the annealing temperature to room temperature was made by reducing the current in the furnace to zero over a period of not less than 3 hours, the specimens remaining in high vacuum.

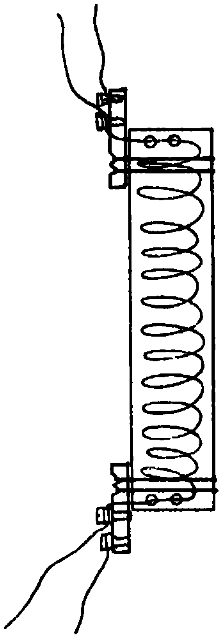

FIG. 1—The specimen mounting.

After annealing, two short pieces of aluminium rod, about 4 mm square in section, were tied by thread to each Pyrex tube. Each of the ends of a specimen wire was clamped to a rod by means of an aluminium screw and washer and the necessary electrical connexions made as shown in fig. 1. The resistance of four specimens was investigated in one experiment, the method of mounting them in the Dewar flask being shown in fig. 2. For the sake of clarity, only one specimen is shown in position in the figure.

The temperature of the specimens was regulated by immersing them directly in a liquefied gas, the temperature of the latter being determined from measurements of the vapour pressure of the gas in equilibrium with the liquid. Vapour pressures in the flask (varied by means of a vacuum pump) were calculated from the readings of a mercury manometer connected to the flask and a barometer. The corresponding temperatures were read from vapour pressure-temperature curves plotted for nitrogen from the data given by Cath,* for hydrogen from the data of Keesom, Bijl, and Miss van den Horst,† and for helium from the data given by Keesom.‡ In all cases where these data are given in degrees Centigrade we have calculated the corresponding absolute temperatures by assuming 0° C = 273·16° K.

---

* Tuyn and Kamerlingh Onnes, 'Comm. Phys. Lab., Leiden,' Suppl., No. 58 (1926); Meissner and Voigt, 'Ann. Physik,' vol. 7, p. 761 (1930).

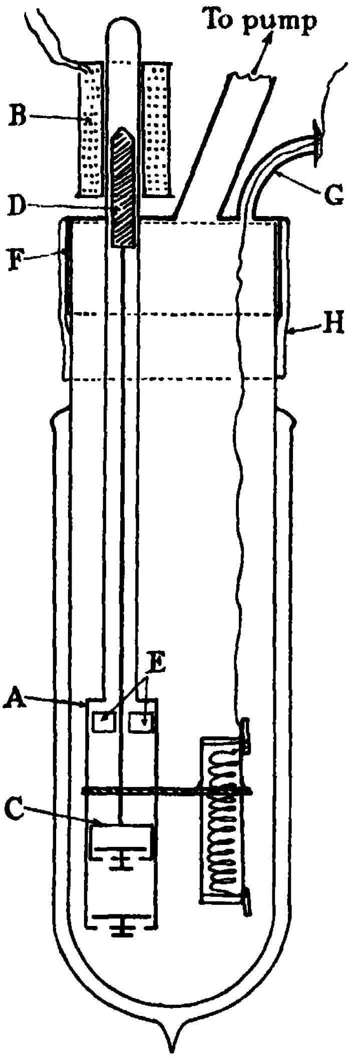

Fig. 2—Cross-section of the apparatus.

To determine the temperature of a bath of liquid nitrogen, liquid hydrogen, or liquid helium in this way, it is necessary to stir the bath very thoroughly. The natural boiling of the liquid in our Dewar flasks was found quite insufficient for this purpose, especially when the vapour pressure over the liquid was allowed to increase after previous experiments at more reduced pressures. Liquid helium is especially troublesome in this respect as had also been observed by Meissner and Voigt (*loc. cit.*). By circulating the liquid with the small lift pump temperature gradients in the bath were prevented. The pump A is shown in fig. 2. The piston C of the pump is drawn up by the attraction of the solenoid on the iron piece D of the piston rod, a periodic motion being produced by the use of an adjustable automatic interruptor to make and break the current in the solenoid. Circulation of the liquid is brought about by the arrangement of the valves in the pump; on the up-stroke liquid enters at the bottom, the succeeding up-stroke causes it to be discharged at the top, through the holes E. The pump casing was made of thin "Staybrite" steel tubing. The heat conductivity of this material is so small that no marked increase of the rate of evaporation of the liquefied gas was observed due to the immersion of the pump.

---

* 'Comm. Phys. Lab., Leiden,' No. 152d (1918).

† *Ibid.*, No. 217a (1931).

‡ *Ibid.*, Suppl., No. 71d (1932).

By soldering the pump casing to the brass cap F, the pump, specimens, and connecting wires could be removed from the flask as a unit. This arrangement proved to be very advantageous, since in changing Dewar flasks the specimen wires were not bent or disturbed in any way likely to change their resistance. By leading the connecting wires through the tube G, sealed with black wax, and by using tap grease under the rubber sleeve H, squeezed against the brass cap and the glass by wire bands, it was possible to make the flask vacuum tight.

The efficiency of the pump was tested at various pressures over the liquid by immersing a resistance thermometer, wound on a flat ring, at various depths in the liquid; with the pump in operation the temperature was found to be quite constant at all depths.

In making the resistance measurements at 0 °C, the specimen unit was removed from the Dewar flask, as described above, and immersed in a bath of CCl_4 contained in a glass tube. The CCl_4 was circulated by the pump just as with the liquefied gases, the bath in this case being cooled externally by surrounding the glass tube with a Dewar flask containing ice and water. The temperature of the bath was determined by a calibrated mercury thermometer, and by taking several sets of measurements close to 0° C the resistance at this temperature could be accurately computed.

The measurements of the electrical resistance of the specimens were made by the usual potentiometric method. The specimens were connected in series to an external series circuit composed of a variable resistance of the plug type, a fixed "standard" resistance, and an accumulator battery of large capacity. From a practical standpoint, it is convenient to have the measured resistance and the fixed "standard" resistance approximately equal, this arrangement being also favourable to greater accuracy in the measurements. Three different "standard" resistances were therefore used, a Tinsley standard ohm for measurements at 0° C, a specially prepared fixed resistance made of short length of manganin wire soldered to heavy copper terminals, for measurements at liquid nitrogen temperatures, and another of this description for the resistance determinations at both liquid hydrogen and liquid helium temperatures. The resistance of these three "standards" was very carefully measured in terms of the standards of the Cavendish Laboratory by Dr. C. D. Ellis, to whom we extend our thanks for this kind assistance. The values found were respectively: $0\cdot9998_2$ ohms, $0\cdot10684_4$ ohms, and $0\cdot01572_6$ ohms at 20° C.

The potential drops across the resistances were determined by a Tinsley ionization potentiometer used in connexion with a galvanometer of the moving-coil type designed by Kapitza. The sensitivity of the galvanometre was such as to give about 1 mm deflexion at a distance of 1 meter for a potential difference of 10^{-7} volts. Experiments carried out to determine the linearity of the potentiometer scale showed that there were no deviations larger than 0·1% over the range used in the measurements. Since other errors occurring in the measurements were estimated to be of this magnitude, the potentiometer readings were not corrected and the final results are not considered to be more precise than 1 part in 1000.

The presence of thermal E.M.F's. in the circuits was investigated with the specimens at various temperatures by (1) reversing the current through the specimens, (2) reversing the current in the fixed comparison resistance, and (3) reversing the current in the potentiometer. By eliminating soldered electrical connexions as far as possible and by suitable thermal shielding it was found possible to eliminate this source of error. The measuring currents used to determine the resistance of the specimens varied between 10 and 40 milliamp.

The experiments made at liquid helium temperatures were carried out with the Dewar flask connected to the helium liquefier developed by Kapitza.*

3—RESULTS AND DISCUSSIONS

The results of the measurements on specimens Nos. 1 and 2 are shown in Table I, r denoting the resistance ratio $R_T/R_{0^\circ C}$. The values of r at liquid nitrogen temperatures are plotted in fig. 3 and those for liquid hydrogen temperatures in fig. 4. Both these specimens when compared with Nos. 3, 4, 5, and 6 show relatively large values of r in the liquid hydrogen region, indicating a large residual resistance. Therefore no measurements were carried out on these wires at liquid helium temperatures.

According to Matthiessen's rule, the specific resistance ρ of a metal is given by the equation:

$$\rho = \rho_{\text{ideal}} + \rho_{\text{residual}},$$

the ideal resistivity being the same for all samples of the same metal at any given temperature and the residual resistivity being a constant which depends on the chemical purity and physical structure of the metal. If we neglect the change with temperature of the ratio l/a, where l is the length and a the area of cross-section of the wire, it follows from the above for any two specimens of the same metal at the same temperature that $r_1 - r_2 = z_1 - z_2$, where z denotes the ratio $R_{\text{residual}}/R_{0^\circ C}$.

---

* 'Proc. Roy. Soc.,' A, vol. 147, p. 189 (1934).

The annealed specimen, No. 2, shows, as might be expected, smaller values of r. From figs. 3 and 4 it may be seen that r, T curves are parallel within the limits of error of the measurements, and from Table I that the differences $r_1 - r_2 = z_1 - z_2$ below 77·8° K are very nearly constant. The results therefore indicate that in the given temperature range Matthiessen's rule is valid for these two specimens.

TABLE I—AL FROM HARTMANN AND BRAUN

Specimen	No. 1	No. 2	
Length	68 cm	68 cm	
Heat treatment	Not annealed	Annealed 3 hours at 275° C	
Resistance in Ω at 0° C	1·0317	1·0252	
Temperature ° K	r_1	r_2	$r_1 - r_2$
273·16	1	1	
77·2	0·1859	0·1649	0·0210
74·9	0·1790	0·1577	0·0213
73·5	0·1747	0·1534	0·0213
72·3	0·1711	0·1499	0·0212
70·6	0·1659	0·1448	0·0211
65·6	0·1509	0·1294	0·0215
20·32	$0{\cdot}0930_0$	$0{\cdot}0720_9$	$0{\cdot}0209_1$
19·37	$0{\cdot}0928_1$	$0{\cdot}0719_0$	$0{\cdot}0209_1$
19·12	$0{\cdot}0927_8$	$0{\cdot}0718_5$	$0{\cdot}0209_3$
18·63	$0{\cdot}0927_0$	$0{\cdot}0718_0$	$0{\cdot}0209_0$
17·65	$0{\cdot}0925_5$	$0{\cdot}0716_3$	$0{\cdot}0209_2$
17·22	$0{\cdot}0924_6$	$0{\cdot}0715_4$	$0{\cdot}0209_2$
16·93	—	$0{\cdot}0715_2$	—
16·90	$0{\cdot}0924_4$	—	—
16·12	—	$0{\cdot}0714_2$	—
15·98	$0{\cdot}0923_3$	—	—
15·95	$0{\cdot}0923_2$	$0{\cdot}0713_9$	$0{\cdot}0209_3$
14·25	$0{\cdot}0921_6$	$0{\cdot}0712_1$	$0{\cdot}0209_5$

The results obtained from measurements on specimens Nos. 3, 4, 5, and 6 are shown in Table II. The numbers denoted $[r]$ refer to the "reduced" resistance of the specimens and were calculated by means of the Matthiessen-Nernst formula

$$[r] = \frac{r_{\text{obs}} - z}{1 - z},$$

the residual resistance ratio z being computed as $R_{1.\,\text{Helium}}/R_{0^\circ\text{C}}$. The values given in the last column of Table II, denoted by $[r]_{\text{calc}}$ represent the values of the ideal resistance ratio for aluminium calculated from the expression:

$$[r]_{\text{calc}} = \frac{\rho_{\text{T}}}{\rho_{0^{\circ}\text{C}}} = \frac{\text{T}\,\sigma_{\text{T}}/\sigma_{\infty}\,[1 + \alpha_1\text{T} + \alpha_2\text{T}^2]}{273\cdot16\,\sigma_0/\sigma_{\infty}\,[1 + 273\cdot16\alpha + (273\cdot16)^2\,\alpha_2]},$$

which follows from the formula:

$$\rho_{\text{T}} = \text{T}\sigma_{\text{T}}\,(1 + \alpha_1\text{T} + \alpha_2\text{T}^2),$$

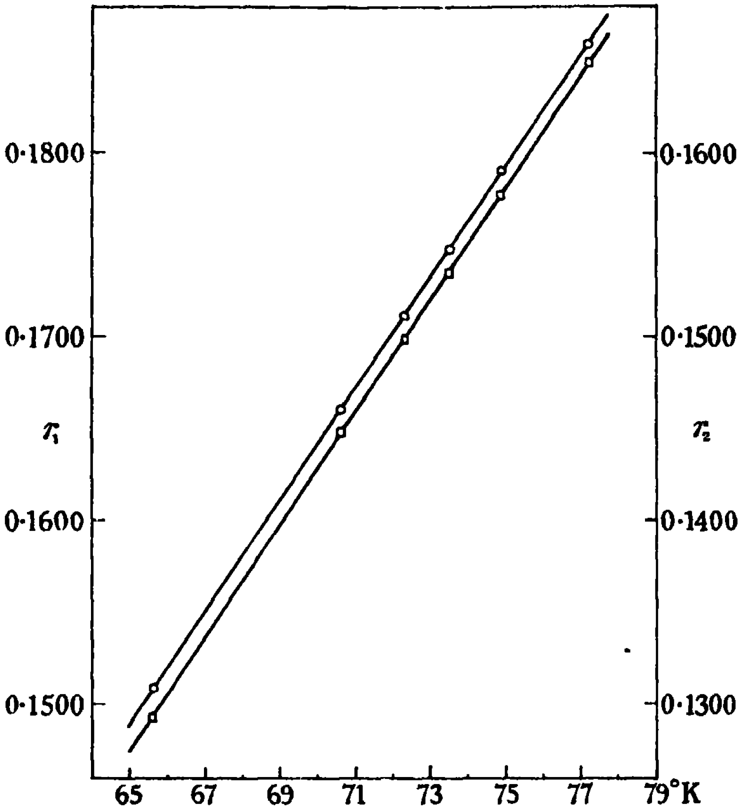

FIG. 3—*r*, T curves for specimens Nos 1 and 2 in liquid nitrogen temperatures; ○ specimen 1; □ specimen 2.

proposed by Grüneisen.* The coefficients α_1 and α_2 for aluminium were given by the latter as $\alpha_1 = +\,2\cdot95 \times 10^{-4}$ and $\alpha_2 = -\,1\cdot38 \times 10^{-7}$ and represent empirical constants used for bringing the resistivities calculated from the formula of Bloch into better agreement with experimental data. The values of the integrals represented by $\sigma_{\text{T}}/\sigma_{\infty}$ were obtained from the table given by Grüneisen, assuming for the characteristic temperature of aluminium $\theta = 395°$ K.

---

* ' Ann. Physik,' vol. 16, p. 530 (1933).

The values of r for specimens Nos. 3, 4, 5, and 6 at liquid nitrogen temperatures are plotted in fig. 5 and for liquid hydrogen temperatures in fig. 6. The curves show clearly that the values r are very sensitive to a relatively small change in the annealing temperature.

The curves for r in liquid helium region are shown in fig. 7. The curves which best fit the values of r are straight lines parallel to the temperature axis. The absolute experimental error in the ratios we estimate to be not greater than 0·00002. According to the data of Meissner and Voigt (*loc. cit.*), we could expect an increase in r of between 0·00007 and 0·00014 in the temperature interval from 4·2° to 2·2° K. Since two of our specimens, Nos. 5 and 6, show smaller values of r in this temperature region than any previously reported for Al, we conclude that within the accuracy of our measurements there is no increase in the resistance of very pure aluminium down to 2·2° K.

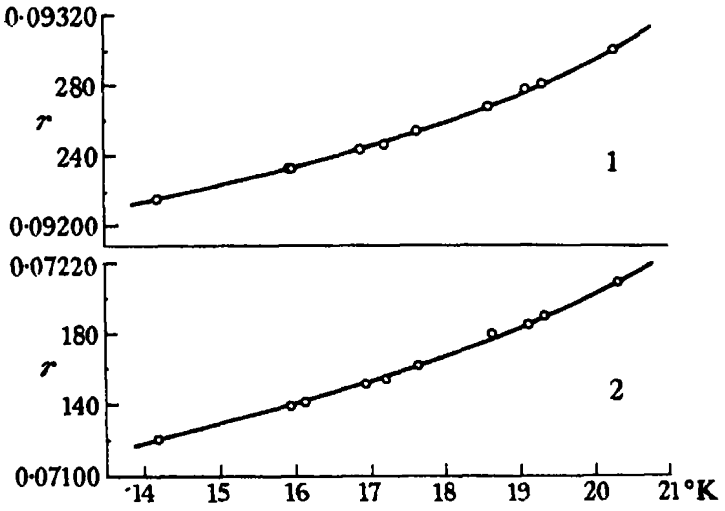

FIG. 4—r, T curves for specimens Nos. 1 and 2 in liquid hydrogen temperatures.

The Matthiessen-Nernst formula, given above, implies that $[r]$ should, at any given temperature, be the same for all specimens of any particular metal. From Table II it may be seen that at liquid nitrogen temperatures the values of $[r]$ for all four specimens are almost equal and are also in reasonably good agreement with the values of $[r]_{\text{calc}}$ obtained from the Grüneisen formula. At liquid hydrogen temperatures, however, the values of $[r]$ show very large differences for any value of T given in the

TABLE II—AL FROM BRITISH ALUMINIUM COMPANY; PURITY AT LEAST 99·995%

Specimen Length Heat treatment		No. 3 ~ 75 cm Not annealed		No. 4 ~ 75 cm Annealed 3 hours at 275° C		No. 5 ~ 86 cm Annealed 3 hours at 250° C		No. 6 ~ 80 cm Annealed 3 hours at 250° C		
Resistance in Ω at 0° C		0·9856		0·9015		1·0825		1·0280		
Vapour pressure of He mm Hg	Temperature °K	r_3	$[r_3]$	r_4	$[r_4]$	r_5	$[r_5]$	r_6	$[r_6]$	$[r]_{calc}$
—	273·16	1	1	1	1	1	1	1	1	—
—	77·3	0·1036$_1$	0·0937$_0$	0·0990$_5$	0·0924$_0$	0·0981$_7$	0·0925$_2$	0·0968$_0$	0·0924$_0$	0·0931
—	75·5	0·0974$_5$	0·0873$_7$	0·0927$_7$	0·0860$_7$	0·0921$_0$	0·0864$_1$	0·0906$_2$	0·0861$_9$	0·0869
—	73·4$_5$	0·0909$_6$	0·0808$_7$	0·0862$_3$	0·0794$_8$	0·0854$_2$	0·0796$_9$	0·0840$_1$	0·0795$_5$	0·0801
—	69·6	0·0782$_6$	0·0680$_6$	0·0738$_6$	0·0670$_0$	0·0726$_3$	0·0668$_2$	0·0712$_3$	0·0665$_5$	0·0676
—	66·8	0·0688$_7$	0·0585$_7$	0·0640$_2$	0·0571$_1$	0·0632$_5$	0·0573$_8$	0·0616$_4$	0·0570$_6$	0·0589
—	20·49	0·01158	0·00065	0·00799	0·00066	0·00709	0·00087	0·00561	0·00074	0·00029
—	19·54	0·01150	0·00057	0·00794	0·00061	—	—	—	—	0·00023
—	19·51	—	—	—	—	0·00700	0·00078	0·00552	0·00065	0·00023
—	18·40	0·01139	0·00046	0·00782	0·00049	0·00691	0·00068	0·00542	0·00055	0·00017
—	17·47	0·01133	0·00039	0·00774	0·00041	—	—	0·00535	0·00048	0·00013
—	17·41	—	—	—	—	0·00681	0·00058	—	—	0·00013
—	16·16	—	—	0·00768	0·00035	—	—	—	—	0·00009
—	16·07	0·01124	0·00030	—	—	0·00672	0·00049	0·00526	0·00039	0·00009
—	14·45	0·01111	0·00017	0·00755	0·00022	0·00661	0·00038	0·00516	0·00029	0·00005
793	4·27	0·01093	—	0·00734	—	0·00623	—	0·00487	—	—
793	4·27	—	—	0·00734	—	—	—	—	—	—
778	4·25	—	—	—	—	0·00624	—	0·00487	—	—
412	3·62	0·01095	—	0·00732	—	0·00621	—	0·00488	—	—
266	3·27	—	—	—	—	—	—	0·00487	—	—
263	3·26	—	—	0·00733	—	—	—	—	—	—
260	3·25	0·01093	—	—	—	0·00623	—	—	—	—
46	2·26	0·01094	—	0·00735	—	—	—	0·00487	—	—
41	2·21	—	—	—	—	0·00624	—	—	—	—

table. It seems, therefore, necessary to conclude that for very pure aluminium the supposition of an ideal specific resistance, common for all specimens at a given temperature, obtainable by subtracting from the measured resistivity the residual resistivity (constant specific resistance at liquid helium temperatures), is not valid at temperatures of about 20° K and below. It is also evident from Table II that there is a wide discrepancy between the values $[r]_{\text{calc.}}$ predicted by the Bloch-Grüneisen formula and $[r]$ obtained from experimental data, the former being much too small.

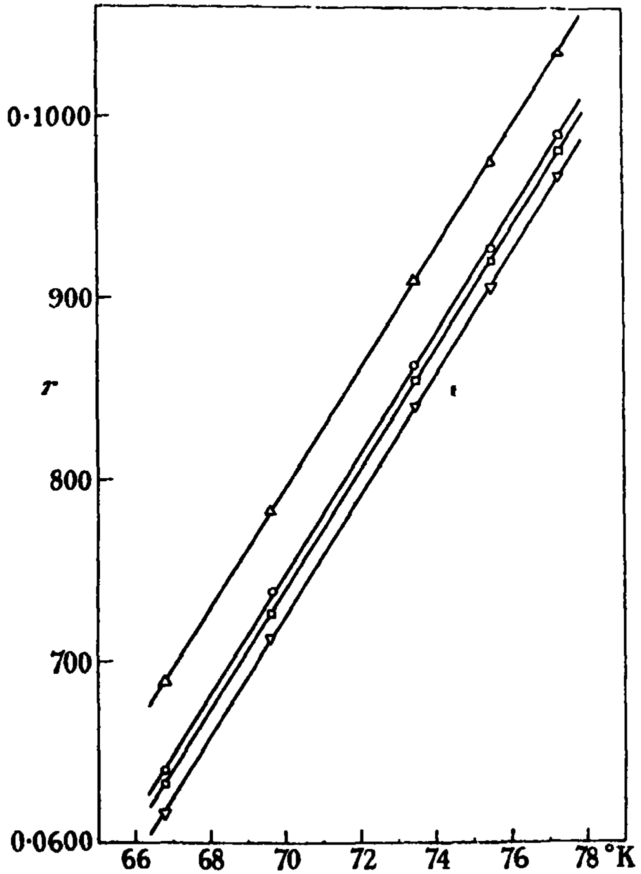

FIG. 5—r, T curves for specimens Nos. 3 = △, 4 = ○, 5 = □, and 6 = ▽, in liquid nitrogen temperatures.

We are much indebted to Lord Rutherford for placing the facilities of the Royal Society Mond Laboratory at our disposal and for his interest in the work.

It is a pleasure to extend our thanks to Professor P. Kapitza for the privilege of using the hydrogen and helium liquefiers designed by him, and also to Dr. J. D. Cockcroft for helpful suggestions and continuous interest.

Our thanks are also due to Mr. H. Pearson and Mr. E. Laurman for their technical assistance, the former for aid in constructing the apparatus and the latter for drawing the aluminium wires and making spectral analysis of them.

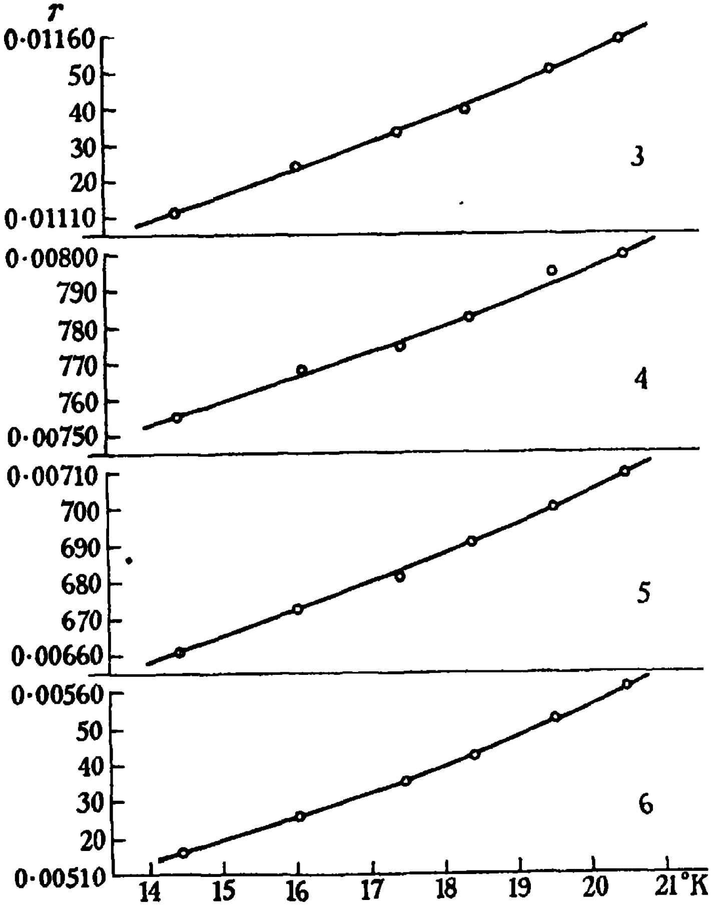

FIG. 6—r, T curves for specimens Nos. 3, 4, 5, and 6 in liquid hydrogen temperatures.

One of us (H. A. B.) wishes further to acknowledge his indebtedness to Columbia University, and the other (H. N.) to The Rockefeller Foundation for the award of fellowships which have enabled us to carry out this work.

4—SUMMARY

The electrical resistance of six polycrystalline aluminium wires was measured at 0° C and at liquid nitrogen and liquid hydrogen temperatures. Measurements at liquid helium temperatures were also made on four of the wires which were drawn from very pure aluminium. The resistances of these four specimens were found to be constant, within the experimental errors, between 4·2° and 2·2° K. Reduced resistivities of these wires were computed by means of the Matthiessen-Nernst formula and then compared with those calculated from an expression proposed by Grüneisen. Satisfactory agreement was found for liquid nitrogen temperatures but not for liquid hydrogen temperatures.

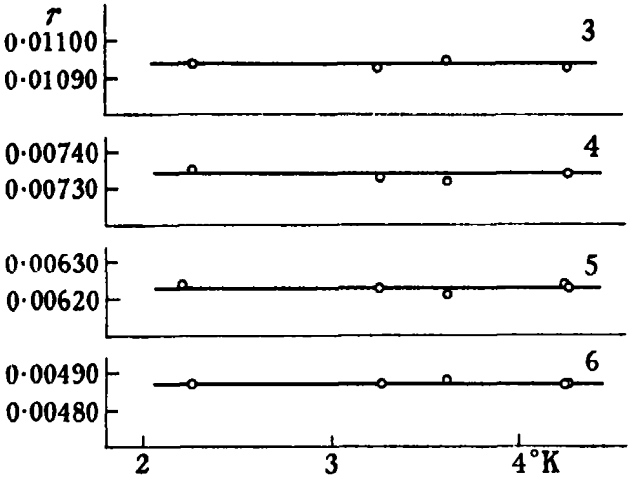

FIG. 7—*r*, T curves for specimens Nos. 3, 4, 5, and 6 in liquid helium temperatares.

Neutrons of Thermal Energies

By P. B. Moon and J. R. Tillman, Beit Scientific Research Scholar,
Imperial College of Science and Technology

(*Communicated by G. P. Thomson, F.R.S.—Received November* 4, 1935)

If fast neutrons, such as those emitted by beryllium under alpha-particle bombardment, are allowed to pass through a considerable bulk of material rich in hydrogen, they rapidly lose energy by collisions with protons, so that the neutrons present in the medium have energies which are, on the average, very much less than those with which they left the source. Fermi and his collaborators* have shown that these slow neutrons are strongly absorbed by the nuclei of a large number of elements; frequently this absorption results in the formation of a radioactive nucleus. They suggested that when the hydrogen-containing medium through which the neutrons pass is free from such strongly absorbing elements, the elastic scattering of the neutrons may preponderate so much over absorption that a considerable fraction of the original neutrons may become reduced to thermal velocities before becoming absorbed.

In the hope of verifying this suggestion, they irradiated specimens of rhodium and of silver within a large volume of a mixture of liquid hydrocarbons at room temperature, and again at 200° C in order to find whether the intensity of artificial radioactivity showed any dependence upon the " temperature " of the neutrons. Possible effects of thermal expansion were eliminated by the use of different mixtures at the two temperatures, the density and atomic composition being kept constant. Although the measurements had an accuracy of $\pm 2\%$, no such temperature-dependence was found. We, too, had made similar experiments, also with negative results. Our measurements were inferior in accuracy, mainly because we attempted to correct rather than to eliminate the effects of expansion; but our conditions of irradiation were perhaps more favourable than those employed in Rome: the distance of the specimen from the source was greater (5 cm instead of 2 cm), and we worked up to 250° C.

Now there are three obvious explanations of the apparent absence of such a temperature effect. We may suppose (i) that there are, in fact, no " thermal " neutrons present; (ii) that the cross-section for capture of a neutron by a silver or a rhodium nucleus, though so large for neutrons slower than those emitted by the original source, becomes negligible again at thermal velocities; or (iii) that the capture cross-section, though still large, is independent of velocity in the thermal region of about 3×10^6 cm/sec.

---

* 'Proc. Roy. Soc.,' A, vol. 149, p. 522 (1935).

Thinking that *(iii)* might well prove to be the true explanation, we proceeded with some experiments in which the presence of thermal neutrons could nevertheless be detected. A radon-beryllium source of neutrons was maintained at a distance of about 10 cm from a specimen of silver and the two were moved at a speed of 3×10^3 cm/sec in the gap between two large tanks of water, the specimen preceding the source. The β-ray activity of the silver was compared with that obtained in the same time at low speeds. The number of neutrons reaching the silver should be lessened by the continual recession of the specimen from the diffusing neutrons. The condition that the activity should be appreciably less than if source and specimen were at rest can be seen to be that the specimen should have moved appreciably in the " time of relaxation " of the non-uniform distribution of neutrons which surrounds the source. This time of relaxation, as calculated from the known free paths of slow neutrons and the assumption that the disappearance of the neutron cloud is due to diffusion with thermal velocities, comes out to be of the order of 10^{-3} sec, during which time the specimen would move through 3 cm; we were thus hoping for a quite noticeable effect of motion. We found none, to within limits of error of ± 4%, and were therefore more inclined to the belief that the neutrons which are so readily absorbed by silver have velocities greater than those of thermal agitation.

We were, however, at that time engaged in some measurements of the transmission of slow neutrons through various materials, measuring the fraction of neutrons transmitted by way of the radioactivity induced in different detectors. We found the absorption coefficient of a block of iodine to be two or three times greater when an iodine detector was used than when the detector was either silver or rhodium. Now this means that the relation between absorption cross-section and velocity for collisions of neutrons with iodine nuclei is different from that which holds for collisions of neutrons with silver or rhodium nuclei. The absorption cross-section therefore cannot be independent of velocity for all three nuclei, so that if no temperature effect indeed exists with any of the three elements as detector it is to be presumed that in at least one of the three cases the neutrons responsible for the radioactivity are not of thermal velocity.

It seemed, then, worth while to reinvestigate the effect of temperature upon the activity produced by slow neutrons, using various elements as detectors. We were, moreover, encouraged to do this by the kindness of Messrs. Bjerge and Westcott in telling us that their then unpublished experiments* showed the absorption of slow neutrons by water, though not enough to prevent a large number of neutrons from reaching thermal velocities, to be so large that the mean life of a neutron in water cannot very much exceed 10^{-4} second. This at once renders inconclusive our experiment with the moving source and detector.

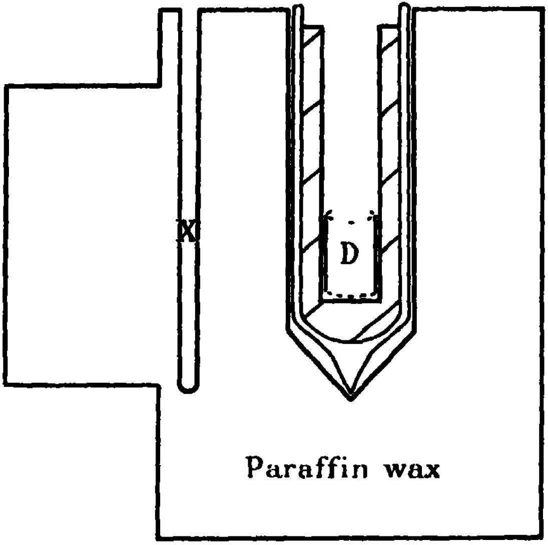

FIG. 1.

EXPERIMENTS AT LOW TEMPERATURES

For the new attempt we decided to use paraffin wax as the medium through which the neutrons were to pass, and to carry out the experiment by cooling that portion of the wax which immediately surrounds the detector from room temperature 290° K to the temperature of liquid oxygen, 90° K. The ratio of these two temperatures (3·2: 1) is greater than can be obtained by heating any substance equally rich in hydrogen from room temperature to its boiling point.

The experimental arrangement was as follows. A long cylinder of paraffin wax, of external radius 3·7 cm and wall thickness 1·6 cm fitted closely within a cylindrical glass Dewar vessel, which was in turn surrounded by wax to an average thickness of 7 cm, fig. 1. The source of fast neutrons, a glass bulb packed with powdered beryllium and containing about 60 millicuries of radon, was placed at X in a cavity in the outer wax. A thin cylinder of silver, rhodium, or iodine was placed at D, within the inner wax cylinder, and exposed for a suitable time to the neutrons. The β-ray activity of the specimen was then measured by placing it around a Geiger-Müller counter. The design of the counter will be sufficiently clear from fig. 2; the aluminium foil was of thickness equivalent to about 10 cm of air. The counter was connected to a valve amplifier, thyratron relay, and mechanical recorder. The sensitivity of the counter was regularly and frequently checked with the aid of a constant source of γ-rays placed in a standard position, and the necessary corrections for "naturals" and for finite resolution were determined by separate experiments. When several sets of readings had been obtained under the conditions described above, the inner wax cylinder was cooled by pouring liquid oxygen into the vessel. When temperature equilibrium had been attained, any remaining liquid was removed, the specimen (which had been previously cooled) was replaced at D, and the irradiation and β-particle count repeated. The specimen was allowed to regain room temperature before being presented to the counter. A thermocouple junction imbedded in the wax served to verify that no appreciable rise of temperature occurred during the irradiation. Separate experiments were made to make certain that the glass of the Dewar vessel was practically non-absorbent to slow neutrons.

---

* 'Proc. Roy. Soc.,' A, vol. 150, p. 709 (1935).

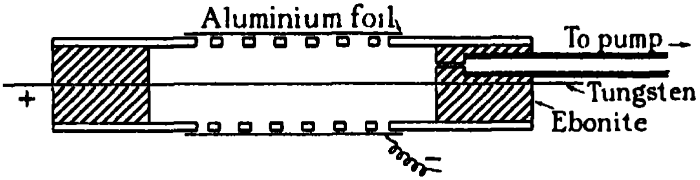

FIG. 2.

The results of the first sets of measurements, made with silver (25-second half-period), were as follows. Thirteen measurements were made at room temperature, during which 3700 particles were counted, and ten, involving the counting of 3600 particles, at the temperature of liquid oxygen. The final value for the ratio of the activity obtained at 90° K to that obtained at 290° K (which ratio we shall for brevity denote by the symbol J^{90}) was, after correction for the decay of the source, 1·31. The statistical standard deviation of this result, calculated from the numbers of particles counted during the measurements and during the calibration of the counter, was ± 0·05. The agreement between the separate runs was as good as could be expected on statistical grounds and showed the absence of any other important random error. We may safely adopt ± 0·05 as the probable error of this set of experiments, so it seems that under these conditions there exists a very definite effect of temperature on the absorption of neutrons into silver nuclei. Another set of experiments made during the following week gave $J^{90} = 1 \cdot 21 \pm 0 \cdot 06$, the final mean ratio thus being $J^{90} = 1 \cdot 26 \pm 0 \cdot 04$.

We concluded,* therefore, that a considerable proportion of the neutrons traversing the wax and effective in producing radioactivity in silver had velocities at least comparable with those of thermal agitation; for otherwise it would be impossible that their properties should be so markedly influenced by the temperature of the medium. Effects of temperature observed by Dunning and others,† though very much smaller than those which we have found, have inclined these authors to the same conclusion: this conclusion has since been confirmed by Fermi ‡ and his collaborators who, quite without knowledge of our unsuccessful experiment with the moving source, carried out an experiment almost identical but of greater refinement and at much higher speed, and were able to establish a small but definite effect of motion.

THE INFLUENCE OF GEOMETRICAL CONDITIONS

Now the value $J^{90} = 1 \cdot 26$ can refer only to the particular arrangement of source, wax, and specimen which were used in the experiments in question, and it soon became evident that J^{90} does, in fact, vary very greatly with the geometrical conditions of the experiment.§ It will be well to discuss this matter at once, so that we may see what conditions may most appropriately be taken as standard for the comparison of temperature effects obtained with different elements.

We approached the problem first from the experimental side. To begin with, we replaced the thin silver specimen hitherto used by a thick-walled (1·0 gm/cm²), hollow silver cylinder. The irradiation was carried out under conditions not quite identical with those described above, the principal difference being that the inner wax cylinder, whose temperature was altered as before from 290° K to 90° K, had walls 2·2 cm in thickness. Under these conditions J^{90} for a very thin specimen was 1·17, while the *inner* surface of the thick specimen gave $J^{90} = 1 \cdot 02$. The explanation is clear; the increased absorption coefficient of the colder neutrons in silver, to which is due the increased activity of a thin specimen, has involved a decrease in the number which penetrate to the inner surface—a decrease which in this particular case is just about enough to offset their increased chance of being captured there. In order to avoid complications of this sort, it is necessary to use specimens which are so thin as to absorb only a small fraction of the incident neutrons; the activity observed after exposure to any set of neutrons will then be proportional to $\int N(v)\,\sigma(v)\,dv$, where $N(v)$ is the number of neutrons which strike the specimen with velocity v and $\sigma(v)$ the absorption cross-section for this velocity. An alternative procedure would be to use a specimen so thick that practically all neutrons striking it are absorbed; the *average* activity of the specimen, which could be measured by powdering or dissolving it and presenting a thoroughly mixed sample to the counter, would then be a measure of the total number of neutrons incident upon it; that is, $\int N(v)\,dv$. It is here assumed that the material does not scatter neutrons appreciably, and that the absorption is due entirely to the production of the radioactive body whose β-radiation is measured.

---

* 'Nature,' vol. 135, p. 904 (1935).

† 'Phys. Rev.,' vol. 48, p. 265 (1935).

‡ 'Ric. Sci.,' June (1935).

§ 'Nature,' vol. 136, p. 66 (1935).

It may be mentioned that the temperature of the specimen, as distinct from that of the neutrons striking it, may usually be disregarded, for the velocities of agitation of heavy atoms in a crystal lattice are small in comparison with those of neutrons at a comparable temperature, and substantial changes of velocity of a neutron through elastic collisions with heavy atoms will be rare even if the specimen is thick.

In order to study the effect of varying the wall-thickness of the wax cylinder whose temperature is altered, we cast a large block of wax, 20 cm × 20 cm × 33 cm with a central cylindrical hole 6·5 cm in diameter and 20 cm in length. Several hollow wax cylinders were also cast, 20 cm long and of external diameter 6 cm so that they fitted easily into the large block; their walls were of different thicknesses, ranging from 0·2 cm to 2·0 cm. Each cylinder was bound with a thin tape to prevent its crumbling in liquid oxygen. The source of neutrons was placed as before in the large block, about 8 cm from the centre. One of the hollow cylinders was cooled by immersion in a flask of liquid oxygen and then rapidly transferred to the hole in the main block. A thin silver specimen was quickly inserted into the cylinder and left there for 30 seconds, during which time no serious change of temperature took place. The β-ray activity of the silver was compared with that obtained with the whole apparatus at room temperature, and the process repeated with the remaining hollow cylinders.

Fig. 3 shows the relation between J^{90} and the wall thickness of the cylinder. The point indicated by the dotted circle is not strictly comparable with the others, as in order to accommodate so thick a cylinder we had to enlarge the cavity. There seems little doubt how the explanation of this curve must be sought. If the layer of wax whose temperature is altered be thin in relation to the mean free path for *scattering* of the thermal neutrons, they will pass through the cold layer without acquiring a new temperature; if, on the other hand, the layer be so thick that there is a large chance that a thermal neutron will be absorbed in passing through it, the observed change in the induced activity will be a differential effect of the changes in the absorption coefficients of the wax and of the material of the specimen. Now the mean free path for scattering of slow neutrons in paraffin is known to be a few millimetres, so it is reasonable that the effect of temperature should increase very little after a thickness of a centimetre has been reached. The fall in J^{90} at greater thicknesses requires rather more detailed consideration, and here it is useful to introduce some theoretical predictions as a basis for discussion. On certain simple assumptions regarding the interactions of neutrons with nuclei, it may be shown[*][†] that, for collisions of neutrons with any given nucleus at energies less than about 1000 electron-volts, the cross-section

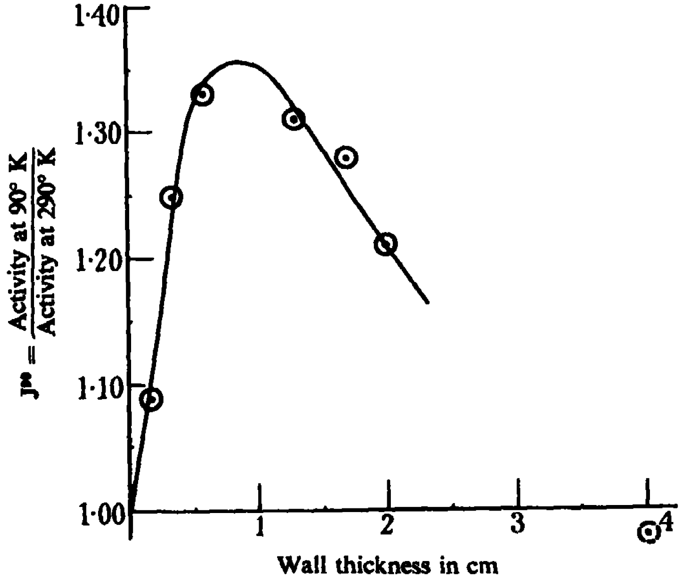

FIG. 3.

---

[*] Amaldi and others, 'Proc. Roy. Soc.,' A, vol. 149, p. 535 (1935).

[†] Bethe, 'Phys. Rev.,' vol. 47, p. 747 (1935).

for *elastic scattering* is independent of the velocity of collision, while the cross-section for *capture* is inversely proportional to the velocity. Put into other words, this means that in a given substance all slow neutrons will have a constant mean free path and a constant mean life. The chance that a given atom shall absorb a neutron in a given interval of time depends upon the nature of the atom, but is simply proportional to the number of neutrons present in unit volume and is independent of the velocities of the neutrons and of the nucleus.

What is important for our immediate purpose is not so much the precise form of these laws as the suggestion that the ratio of the probabilities that a neutron shall be captured by each of two different nuclei should be independent of velocity. If this be true, it means that a neutron introduced anywhere into an infinite uniform mixture of two or more kinds of atoms (for example, an aqueous solution of a silver salt) has a probability of ending its life by capture by any one kind of nucleus (say, silver). This depends only upon the nature and relative number of each kind of atom present, but is at every instant independent of the velocities of the neutron and of the nuclei and is therefore independent of the temperature of the mixture. The average intensity of activation of the silver in such a solution should therefore be independent of temperature. It does not quite follow, however, that the amount of radioactive silver formed in any given small region of the solution will be independent of temperature, for at low temperatures the total length of path traversed by a neutron before its capture will be less than at high temperatures, so that the activity will be slightly more concentrated in the neighbourhood of the source. A fall in temperature of the whole medium should thus result in a slight increase in the amount of radioactive silver at places near the source and a corresponding slight decrease at distant places. Fortunately, it is not difficult to calculate an upper limit to these changes from a knowledge of the free path for scattering of fast neutrons and the average thickness of wax through which a thermal neutron diffuses before its capture. If we take for these two quantities 5 cm and 2 cm respectively, we find that at distances from the source greater than about 10 cm the fractional decrease becomes independent of distance and cannot exceed about 3%. Clearly it cannot matter whether the silver is in solution or in the solid form, provided that its distribution is such as not to interfere perceptibly with the spatial distribution of neutrons; we thus conclude that if, for neutrons of thermal energies, the variation of absorption cross-section with velocity follows the same law for silver as for wax, a thin silver specimen placed in a large block of wax at a considerable distance from the source of neutrons (say, 10 cm) should acquire an activity which is very nearly independent of the temperature of the block. We have so far ignored the question of thermal expansion. The effect of this will differ according to whether the distance between source and specimen is supposed to remain fixed (as, for instance, if they are held at fixed places in an expanding liquid) or whether they are supposed to move apart as the medium expands, as would occur if each were placed in a separate cavity in an expanding solid. If the linear expansion of the medium is in the ratio $1 + \alpha$, where α is small, then the expansion may be shown to multiply the activity induced at a distance R from the source by the factor $\left(1 - 6\alpha - \frac{3\alpha \mathrm{R}}{\mathrm{C}} \frac{d\mathrm{C}}{d\mathrm{R}}\right)$ in the former case, and $\left(1 - 6\alpha - \frac{2\alpha \mathrm{R}}{\mathrm{C}} \frac{d\mathrm{C}}{d\mathrm{R}}\right)$ in the latter, C being the concentration of neutrons at distance R from the source. Thus at small distances from the source, where the diminution of intensity with distance is slow, the effect of expansion will in either case be to decrease the activity. At very large distances, where the variation of intensity with distance must necessarily be greater than inverse square (owing to the absorption of the fast neutrons) the last term in the bracket will become numerically greater than the second, and will increase without limit as the distance increases, so that at large distances an expansion of the medium will entail an increase in the observed activity. There must be in either case an intermediate region in which the effect of expansion is small. If we estimate values of $\frac{\mathrm{R}}{\mathrm{C}} \frac{d\mathrm{C}}{d\mathrm{R}}$ from Bjerge and Westcott's* paper, we find that this will occur at about 10 cm from the source if the specimen is supposed to move with expanding material, and at about 15 cm if the specimen is held at a fixed distance from the source.

We may therefore say that at moderate distances, of the order of 10 cm, the effect of expansion is of the order of magnitude of the *linear* expansion α; even very close to the source it cannot exceed 6α. In the experiments which we have described and those which we shall mention later, the medium was not infinite nor was the whole of it cooled, but the distances involved were of the order of 10 cm, and we shall make no large error in neglecting the effect of expansion and contraction, since the linear contraction of wax over the range 290° K–90° K is only 1%.

It seems, therefore, that if the absorption cross-section does, in fact, vary in the same way for all elements, the observed temperature effects must, apart from the small secondary effects which we have just been considering, be regarded as transition effects occurring in the neighbourhood of a temperature gradient. This would help to explain the failure to find any large effect of temperature when a large bulk of material is heated or cooled.

---

* 'Proc. Camb. Phil. Soc.,' vol. 31, fig. 6 (p. 150) (1935).

Since the measurement of temperature effects within a large bulk of wax provides a possibility of testing the ubiquity of the law connecting absorption with velocity, we proceeded to fill a large copper Dewar vessel, of internal diameter about 8 cm, with small pieces of paraffin wax, leaving a narrow cylindrical opening which extended from the neck to just below the centre. This opening was kept free from wax by a thin-walled brass tube. The mass of wax was such as to be equivalent to a solid sphere of 7 cm radius. The apparatus and the source were immersed in a large tank of water, the distance of the source from the centre of the wax being 24 cm. The activity induced in a thin specimen of silver (25-second period) at the centre of the wax was measured, with the wax firstly at room temperature and secondly at the temperature of liquid oxygen. Care was taken that the whole of the wax should be thoroughly cooled, but that only a trace of liquid oxygen should remain at the bottom of the flask. The activity obtained at the lower temperature was found to be less in the ratio of 0·80 ± 0·04. It seems, therefore, that the absorption of neutrons by wax increases more rapidly with decreasing temperature than does the absorption of neutrons by silver.

TEMPERATURE EFFECTS WITH VARIOUS ELEMENTS

It appears to us that the values of J^{90} which may most advantageously be quoted at the present stage of our knowledge would be those for which the thickness of the cooled layer is (*a*) about 0·8 cm, which corresponds to the maximum of fig. 3, and (*b*) as large as possible. One would naturally desire to extrapolate the descending limb of the curve of fig. 3 back to zero thickness so as to obtain the effect of a change in the temperature of the neutrons free from the change in their number which arises from absorption. Since, at thicknesses of the order of a few free paths, the average number of collisions made by a neutron in diffusing through the cold layer varies approximately as the square of the thickness of the layer, it would probably be fairer to plot J^{90} against the square of the thickness of the cylinder wall. When this is done, the curve descends much less rapidly, and a reasonable extrapolation shows that the intercept is not very much in excess of the maximum of the curve, being about 1·42 for silver. For comparative purposes it seems best to take the maximum ordinate, which is much more certain. In either case the amount of surrounding wax and the distance of the source ought to be specified, and it would seem best that both should be very large. As regards (*b*), the only careful measurement which we have so far made is that which we have just described, but we have investigated (*a*) much more fully. We have made experiments with surrounding layers of wax (or water) of thicknesses from 7 cm to 12 cm, and with distances between silver specimen and source ranging from 8 cm to 20 cm. In none of these experiments has J^{90} been found to differ appreciably from the value of 1·34 shown in fig. 3, so we have some confidence in adopting this figure as reasonably independent of surrounding bulk of wax and of the distance of the source, provided that both are tolerably large; this ratio, then, represents the effect of altering the temperature of the neutrons from 290° K to 90° K without seriously altering their number. Table I shows comparable values for several elements, and makes it very clear that J^{90} varies from one element to another. A specimen of dysprosia was kindly lent to us by Professor S. Sugden.

TABLE I

Element	J^{90}	Element	J^{90}
Silver (25 sec) ……	$1{\cdot}34 \pm 0{\cdot}03$	Iodine (25 min) ….	$1{\cdot}19 \pm 0{\cdot}03$
Silver (2·5 min) ….	$1{\cdot}35 \pm 0{\cdot}05$	Dysprosium (2·5 hr)	$1{\cdot}32 \pm 0{\cdot}04$
Copper (5 min) ….	$1{\cdot}47 \pm 0{\cdot}05$	Rhodium (44 sec) ..	$1{\cdot}25 \pm 0{\cdot}04$
Vanadium (225 sec) ..	$1{\cdot}47 \pm 0{\cdot}05$		

This means that the law of dependence of absorption cross-section upon velocity varies from one element to another; it does not tell us, however, whether these differences lie within the thermal region. For example, the relatively high value for copper might mean that the absorption of *thermal* neutrons varies more rapidly with their velocity than with, say, iodine. But it could be explained equally well by supposing that iodine absorbs a greater proportion of neutrons whose velocities are well above the thermal range, so that the effect of changing the temperature of the thermal neutrons though identical with the corresponding effect in copper, is more " diluted " by the larger constant effect of the faster neutrons. The latter explanation is the one which is required by the suggested theory. On this basis, if we take the values of J^{90} for a simple change of temperature without any change in the number of neutrons incident to be as given in Table I,* we may easily calculate what fraction of the activity induced at room temperature must be attributed to thermal neutrons; for if all the neutrons absorbed were in thermal equilibrium the value of J^{90} should (on the $1/v$ law) be $\sqrt{290/90}$

---

* This value is a little too low, but not enough to cause an error of more than about 5% in the percentage to be attributed to thermal neutrons.

or very nearly 1·80. The amount of dilution by non-thermal neutrons must be chosen to fit the observed values which are all smaller than this. Calculation shows that with copper most of the activity (about 60%) must be ascribed to thermal neutrons, while with iodine they contribute only about 25%.

It would be possible to decide between the two possible explanations (or at least to test the suggestion that the absorption law is the same for all elements in the thermal range of velocities) by making measurements at room temperature and at *two* other temperatures. It is easy to show that $(J^{T_1} - 1)/(J^{T_2} - 1)$ should be the same for all elements, provided only that the same law of absorption holds for all elements *in the thermal region*, and no matter what differences may be present at higher velocities. Unfortunately, an adequate test of this point requires very accurate measurements of activities unless the range of temperature, and hence the variation of activity, can be considerably extended. In view of the apparent difference between the behaviour of silver and that of wax, the matter seems to deserve attention, and it is much to be hoped that accurate measurements at temperatures below 90° K will not long be lacking.

SELECTIVE ABSORPTION OF SLOW NEUTRONS

We shall now describe in more detail some experiments, already very briefly mentioned on p. 477, on the absorption of slow neutrons. Our first measurements were made with the neutrons emerging from one face of a roughly cubical block of wax of 12 cm side, at the centre of which was placed the source. The face in question was covered with a block of iodine (2·8 gm/cm^2) and measurements made of the activity produced in detectors of silver and of iodine placed just outside this absorbent layer; the activity was in each case expressed as a fraction of that obtained at the same place and for the same time of irradiation when the iodine block was absent. For the iodine detector the fraction was found to be 0·56 ± 0·05, while for the silver detector it had the definitely larger value of 0·83 ± 0·07. Similar experiments with an absorber of silver (2·0 gm/cm^2) gave transmission factors of 0·37 ± 0·03 (silver detector) and 0·55 ± 0·05 (iodine detector). The difference here is less marked but still quite definite, and it seemed worth while to pursue the matter further. We then decided to use absorbers and detectors in the form of hollow cylinders, and to carry out the irradiation within a cavity in a block of wax; this arrangement has practical advantages, since a cylindrical specimen is the most convenient for presenting to the counter. The geometrical conditions were now very similar to those shown in fig. 1

under which the temperature experiments were made, though there was one important difference: in order to reduce the effect of neutrons entering through the open ends of the absorbing cylinder, the specimen was always lined with a layer of cadmium sufficiently thick to absorb practically all slow neutrons incident upon it. Table II shows the results obtained; at the head of each column of figures is given the nature and mass of the absorber, while the detectors are specified in the first column. The figure of 0·41 given in the bottom row of the table shows the result of measurements made at 90° K with the silver absorber, the thickness of wax cooled being 1·5 cm. The increase of the absorption with respect to its value at room temperature is just about what might be expected from the value of J^{90} for silver. We have also found the absorption by boron (as measured by detectors of silver and of iodine) to be greater for "cold" than for "warm" neutrons.

TABLE II

Absorber / Detector	Iodine 2·0 gm/cm^2	Silver 1·0 gm/cm^2	Copper 4·5 gm/cm^2
Silver—25 sec	0·85 ± 0·05	0·50 ± 0·03	0·71 ± 0·04
Silver—150 sec	0·95 ± 0·06	0·51 ± 0·03	0·70 ± 0·04
Copper—5 min	0·89 ± 0·06	0·62 ± 0·05	0·72 ± 0·045
Copper—10 hr	0·90 ± 0·07		0·62 ± 0·05
Iodine—25 min	0·68 ± 0·03	0·72 + 0·025	0·76 ± 0·025
Rhodium—44 sec	0·90 ± 0·04	0·63 ± 0·025	0·75 ± 0·04
Silver—25 sec. "cold" neutrons		0·41 ± 0·03	

Selective absorption appears most pronounced with the iodine absorber; the activity of the iodine detector is reduced by 32%, while the other detectors show decreases of the order of 10% only. With the silver absorber the differences are somewhat less striking though still very well marked, and here again the apparent absorption is greatest when the detector is identical with the absorber. The copper absorber, on the other hand, shows differences which are very small; the experiments were, however, rather unsatisfactory in view of the relatively small absorption. In order to obtain larger absorption we reverted to the use of plane absorbers, which could be more conveniently obtained in the rather large thicknesses required. The source was placed at the centre of a block of wax, 20 cm × 20 cm × 33 cm. Two layers of copper, each of 8·2 gm/cm^2, were placed on top of one of the rectangular faces of the block, the detector being placed in a small gap between them; the gap was so small that it was possible to ignore the chance of neutrons reaching the detector without going through the copper, and there was no need to introduce the complication of cadmium screens. The whole arrangement was backed by a further 5 cm of wax, fig. 4. When the activity of the specimen had been measured under these conditions, the copper absorbers were removed and the detector irradiated again in its original position; the ratio of the activity in the presence of the copper absorber to that with no absorber is given below for several detectors:

Cu (10 hr), 0·37 ± 0·03; Cu (5 min), 0·33 ± $0{\cdot}02_5$; Ag (25 sec), 0·36 ± 0·02; Rh (44 sec), 0·36 ± 0·02; I (25 min), 0·43 ± $0{\cdot}02_5$; Dy (2·5 hr), 0·26 ± 0·02.

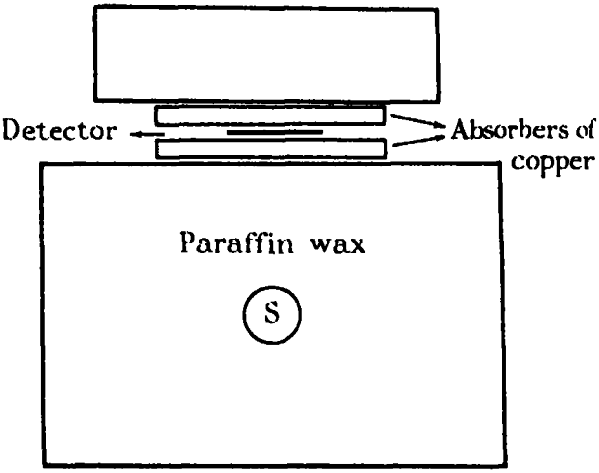

Fig. 4.

It will be seen that the differences are once again so small as to be not entirely beyond the range of experimental error, though we feel that with the iodine detector the figures quoted above, together with those previously given in Table II, make it very probable that the absorption is genuinely less than that measured with a copper detector.

Discussion

We can say, therefore, that as a general rule the absorption is apparently greatest when measured with the same element as detector; this is what one would naturally expect if the absorption cross-section depends upon the velocity of the neutron in a manner which varies from one element to another. After passing through the absorber, the neutrons will be deficient in just those velocities which are the most readily absorbed into the nuclei of the same element. It is fundamentally impossible to deduce from experiments of this nature anything about the velocities in question; we cannot even decide which element prefers, on the whole, the faster neutrons and which the slower. All that can be done is to use these measurements as a check upon any suggested laws of variation of absorption cross-section with velocity. Now, as we have already mentioned, the suggestion of the simple theory is that any differences between one element and another must be confined to velocities immensely greater than those of thermal agitation. Let us, with this in mind, consider the experiments with copper and iodine. We have to explain the following observations: (i) copper is at least twice as sensitive to changes of temperature as is iodine, the respective values of J^{90} being 1·47 and 1·19; (ii) iodine appears to absorb neutrons two or three times as strongly when an iodine detector is used as when the detector is of copper; (iii) the absorption of copper appears only very slightly greater when measured with a copper detector than with an iodine detector. (ii) and (iii) refer to room temperature.

To interpret (i) in accordance with the theoretical predictions we must, as has already been seen, assume that the greater part of the activity of copper is due to neutrons of thermal velocities, but that with iodine the activity is mainly due to neutrons whose energies are greater than those of thermal agitation. We must postulate that these faster neutrons which affect iodine must, in fact, be very fast, for the theory forbids any difference between the absorption laws of different elements (and therefore any selective absorption) until energies of some thousands of electron-volts are reached. This is compatible with (ii). Now (iii) tells us that the average absorption coefficient of copper for the fast neutrons which affect iodine is not very different from its absorption coefficient for the average of the thermal neutrons which are the main source of the activity of copper. Since this is the *average* and not the *greatest* value of the absorption, it is probable that for some of the fast neutrons which affect iodine the absorption cross-section of the copper nucleus is actually greater than for the average of the thermal neutrons. Now this is certainly not true for the very fastest neutrons which have been studied—that is to say, for neutrons whose energies are of the order of a million electron-volts or more, so it seems that in order to explain the absorption and temperature experiments on the basis of the proposed theory we require that the absorption cross-section of copper shall show a maximum value (probably greater than that for thermal velocities) at velocities corresponding to energies somewhere between, say, a thousand and a million volts. Such a complicated law of absorption as a function of velocity may actually hold, but so far we have no evidence that the increase of absorption cross-section with decreasing velocity is other than monotonic. Until such evidence appears, the necessity for postulating a rather unexpected behaviour in a region of velocity which has not yet been investigated either experimentally or theoretically must be counted somewhat inauspicious for the ultimate success of the simple theory which has formed the basis of the present discussion. We ought, moreover, to add that, even if we free ourselves from the restriction that the absorption shall vary inversely with velocity for all nuclei at low velocities, we have so far failed to devise a pair of *monotonic* laws of absorption which explain the observations summarized in (i), (ii), and (iii). If we abandon the restriction that the laws shall be monotonic with velocity, the problem presents no special difficulty and may be solved in a variety of ways.

Professor G. P. Thomson, who took an active part in some of the earlier experiments, has throughout this work given us very great help in the planning of experiments and in the discussion of their results, and we are glad to take this opportunity of expressing our thanks to him. The radon was given to us by the Radium Committee of the Medical Research Council through Professor S. Russ of the Middlesex Hospital. We are very grateful to Professor Russ for arranging the supplies and to his technical assistants, Messrs. B. A. and G. W. Spicer, for their skilful preparation of the sources.

SUMMARY

The conclusions drawn from the experiments which we have described above may be summarized as follows:

A considerable proportion of the "slow" neutrons produced when fast neutrons pass through water or paraffin have thermal velocities.

The cross-sections for the absorption of thermal neutrons by all the nuclei which we have so far investigated (Cu, V, Dy, Ag, Rh, I, B) increase when the temperature of the neutrons is reduced to 90° K. The increases depend very much upon the particular geometry of that portion of the hydrogen-containing medium whose temperature is altered, being greatest when it is a layer surrounding the detector, and having a thickness of about two free paths (about 8 mm of paraffin wax). Under these conditions the increases range from about 50% for copper to about 20% for iodine. It has not yet been possible to determine whether these differences are to be ascribed to variations in the proportion of the activity which, in the several cases, is due to fast neutrons or to differences between the laws connecting cross-section and velocity for *thermal* neutrons.

The apparent absorption of neutrons by iodine and by silver depends greatly upon the nature of the detector used to measure the intensity of the transmitted beam, being greatest when the detector is the same element as the absorber. An absorber of copper, on the other hand, shows only very slight selectivity. It seems difficult, though not necessarily impossible, to reconcile these results and those of the temperature experiments with the suggestion that the absorption cross-section at low velocities should for all elements vary inversely as the velocity, or, indeed, with any monotonic relation between cross-section and velocity.

Intended Substitution of the Practical Absolute System of Electrical Units for the Existing International System

Following a revision in 1921 of the International Treaty known as the Convention du Mêtre, under which at present 32 nations co-operate in the maintenance of the international prototype standards of the metre and kilogramme, the Conférence Générale des Poids et Mesures in 1927 gave authority to the Comité International des Poids et Mesures to take up also the question of electrical units. An advisory electrical Committee, including representatives of the principal National Laboratories, was appointed, and acting on the advice of this Committee, the International Committee in 1933 recommended, and the Conférence Générale of that year approved in principle, the eventual substitution of the Practical Absolute System of electrical units for the present "International" system. The Conférence further instructed the Comité International to take the necessary steps to give effect to this decision.

At its meeting in October, 1935, the Committee decided that the work on the subject which has been in progress for so many years in the various National Laboratories had reached a stage at which it was possible to fix a date for the change, and authorized the publication of the following statement (translated from the original French text):

1. In accordance with the authority and responsibility placed upon it by the General Conference of Weights and Measures in 1933, the International Committee of Weights and Measures has decided that the actual substitution of the absolute system of electrical units for the internatonal system shall take place on the 1st January 1940.

2. In collaboration with the national physical laboratories, the Committee is actively engaged in establishing the ratios between the international units and the corresponding practical absolute units.

3. The Committee directs attention to the fact that it is not at all necessary for any existing electrical standard to be altered or modified with a view to making its actual value conform with the new units. For the majority of engineering applications the old values of the international standards will be sufficiently close to the new for no change, even of a numerical nature, to be required. If for any special reason a higher precision is necessary numerical corrections can always be applied.

4. The following table gives a provisional list of the ratios of the international units to the corresponding practical absolute units, taken

to the fourth decimal place. Since differences affecting the fifth decimal place exist between the standards of the international units held by the various national laboratories and also because all the laboratories which have undertaken determinations of the values of their standards in absolute measure have not yet obtained final results, the Committee does not consider it desirable for the present to seek a higher precision. At the same time it hopes that it will be possible to extend the table of these ratios with a close approximation to the fifth decimal place well before the date fixed for the actual substitution of the practical absolute system for the international system.

TABLE

1 Ampere international = 0·999 9 Ampere Absolute
1 Coulomb ,, = 0·999 9 Coulomb ,,
1 Ohm ,, = 1·000 5 Ohm ,,
1 Volt ,, = 1·000 4 Volt ,,
1 Henry ,, = 1·000 5 Henry ,,
1 Farad ,, = 0·999 5 Farad ,,
1 Weber ,, = 1·000 4 Weber ,,
1 Watt ,, = 1·000 3 Watt ,,

The Structure of Atomic Nuclei

By H. A. Wilson, F.R.S., Rice Institute, Houston, Texas

(*Received September* 17, 1935)

In a previous paper* it was shown that the energies of nuclear reactions are multiples of $q = 0{\cdot}000415$ in atomic weight units and that the atomic weights of the light elements may be supposed equal to $N(1 + b) + sq$, where N and s are integers and b is a small quantity the same for all elements. In the reaction equations the terms $N(1 + b)$ cancel out so that the reaction energies are given by $nq = \Sigma sq$. Thus the equation ${}_4Be^9 + {}_1H^1 = {}_4Be^8 + {}_1H^2 + nq$ gives

$$9(1 + b) + 33q + 1 + b + 19q = 8(1 + b) + 17q + 2(1 + b) + 34q + nq,$$

so that $33q + 19q = 17q + 34q + nq$ which gives $52 = 51 + n$, or $n = 1$. The number of independent reaction equations is two less than the number of elements involved so that two of the values of the energy integer s can be selected. In the previous paper the values of s for ${}_2He^4$ and ${}_1H^1$ were taken to be 8 and 19 respectively and the values of s for the other elements were calculated by means of the reaction equations.

Any atom, of atomic number z and atomic weight integer w, may be supposed formed by the combination of z protons and $w - z$ neutrons according to the reaction equation

$$z\,{}_1H^1 + (w - z)\,{}_0n^1 = {}_zA^w + E, \tag{1}$$

where E denotes the energy of formation of the atom ${}_zA^w$ in atomic weight units. If ${}_zs^w$ denotes the energy integer for ${}_zA^w$ then equation (1) gives

$$z\,{}_1s^1 + (w - z)\,{}_0s^1 = {}_zs^w + E/q. \tag{2}$$

By means of this equation the energies of formation† may be calculated using the values of ${}_zs^w$ given in the previous paper. Table I gives the values of E/q obtained in this way.

---

* 'Proc. Roy. Soc.,' A, vol. 152, p. 497 (1935).

† The energies of formation obtained in this way are uniquely determined by the reaction energies and are independent of the values chosen for the energy integers of ${}_2He^4$ and ${}_1H^1$.

TABLE I—ENERGIES OF FORMATION IN TERMS OF q AS UNIT

$_1H^2$	5	$_3Li^6$	78	$_4Be^{10}$	160	$_8O^{16}$	312
$_1H^3$	20	$_3Li^7$	96	$_5B^{10}$	161		
$_2He^3$	17	$_4Be^8$	139	$_5B^{11}$	188		
$_2He^4$	70	$_4Be^9$	143	$_7N^{14}$	255		

The energy integers of N^{14} and O^{16} were taken equal to 18 and 0 respectively.

The energies of formation, of course, can also be calculated directly from the atomic weights but the values so obtained are probably not as reliable as those got from the reaction energies. The atomic weights calculated from the reaction energies give the same energies of formation as the reaction energies.

The energies of formation and reaction energies are expressed in terms of q as unit in this paper.

The equation (1) gives the atomic weights in terms of the atomic weights of $_0n^1$ and $_1H^1$. If we take $_0n^1 = 1{\cdot}00830$ and $_1H^1 = 1{\cdot}007885$, this equation gives the same atomic weights as were obtained in the previous paper with $_2He^4 = 4{\cdot}00332$.

Atoms regarded as combinations of neutrons and hydrogen atoms are somewhat analogous to ordinary chemical compounds of, for example, carbon and hydrogen. The difference is mainly that the energy of formation of an atom is much greater than the energy of formation of a chemical compound. The energy of formation of hydrocarbons can be calculated very approximately by supposing that the formation of each chemical bond between two atoms represents a definite amount of energy so it seems natural to try to explain the energies of formation of atoms out of neutrons and hydrogen atoms in a similar way.

The neutrons and protons may be supposed to attract each other when very near together so that the energy of formation should depend simply on the numbers of pairs of particles connected. Since the energies of formation are multiples of q the energies of formation of such pairs should also be multiples of q.

Such a theory, if valid, should enable the energies of formation of atoms to be calculated by assuming a suitable structure or arrangement and suitable energy values for the three sorts of pairs. Also the structures adopted should be such as to allow the observed reactions to occur with as little rearrangement of the neutrons and protons as possible. The energies of formation should also be as large as possible because an atom in which the particles could be rearranged so as to increase the energy of formation would be expected to change with emission of energy.

The energy of formation of $_1H^2$ is 5 which suggests that the energy of a bond or connexion between a neutron and a proton should be 5. However, in the other atoms, with the exception of $_2He^3$, a proton never appears to be connected to only one neutron but always to two or more neutrons or to another proton, and when a proton is connected to two or more neutrons the energy appears to be 10 for each connexion.

The energy of formation of $_2He^3$ is 17. We may suppose that in $_2He^3$ there are three bonds two between a neutron and a proton each with energy 5 as in $_1H^2$ and one between the two protons with energy 7. In the other atoms the energy of a bond between two protons appears to be 21 or three times that in $_2He^3$. The energy of formation of $_1H^3$ is 20 and may be supposed to be that of two bonds between a proton and a neutron.

The energy of formation of $_2He^4$ is 70 and we may suppose the four particles at the corners of a tetrahedron so that there are four proton-neutron bonds, one proton-proton bond, and one neutron-neutron bond. The proton-neutron bonds give 40 so if we take the energy of the proton-proton bond equal to 21 and that of the neutron-neutron bond equal to 9 we get the required total of 70.

The energy of formation of $_3Li^6$ is 78. We may suppose each proton connected to two neutrons giving energy 60 so that there should be two neutron-neutron bonds each with energy 9.

The energy of formation of $_3Li^7$ is 96 or 18 more than for $_3Li^6$. We therefore suppose $_3Li^7$ to have four neutron-neutron bonds and six proton-neutron bonds giving $6 \times 10 + 4 \times 9 = 96$.

The energy of formation of $_4Be^8$ is 139 which is equal to $21 + 2 \times 9 + 10 \times 10$ and that of $_4Be^9$ is 143 which is $7 \times 9 + 8 \times 10$. The energy of formation of $_4Be^{10}$ is 160 which is 16×10, or $2 \times 21 + 2 \times 9 + 10 \times 10$.

Fig. 1 shows possible arrangements of the neutrons and protons in these atoms. A neutron is indicated by a small circle and a proton by a black disc.

It is possible that the energy of formation of $_4Be^8$ is 140 instead of 139 and the value 140 is supported by the simple cubical arrangement in fig. 1 which gives 140 and may be regarded as two $_2He^4$ atoms connected together.

The energy of formation of $_4Be^9$ is smaller than might have been expected, and there is no very obvious reason why a neutron should not be connected to two of the neutrons in the cubical $_4Be^8$ atom which would give a $_4Be^9$ atom with energy of formation 158 and so atomic weight 9·00747 which is much smaller than the accepted value 9·0137. To explain why a $_4Be^9$ atom with energy of formation 158 cannot be formed it is necessary to assume something analogous to valency. We may suppose, for example, that a neutron which is attached to two connected protons, as in a helium atom, cannot be attached to more than one other neutron. This would make the $_4Be^9$ atom with energy of formation 158 impossible.

The energy of formation of $_5B^{10}$ is 161 which is equal to $21 + 14 \times 10$, and that of $_5B^{11}$ is 188 which is $2 \times 21 + 4 \times 9 + 11 \times 10$. The energy of formation of oxygen $_8O^{16}$ is 312 which is equal to $8 \times 9 + 24 \times 10$.

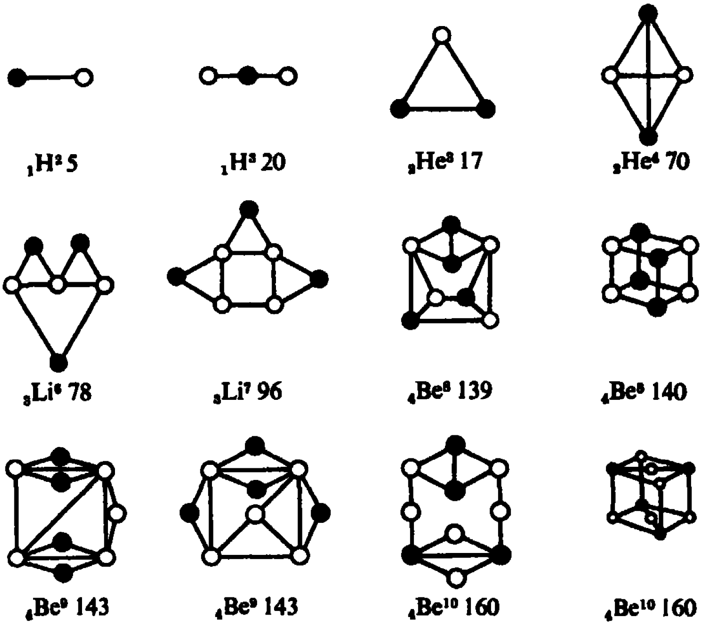

$_1H^2$ 5 $_1H^3$ 20 $_2He^3$ 17 $_2He^4$ 70

$_3Li^6$ 78 $_3Li^7$ 96 $_4Be^8$ 139 $_4Be^8$ 140

$_4Be^9$ 143 $_4Be^9$ 143 $_4Be^{10}$ 160 $_4Be^{10}$ 160

FIG. 1.

Fig. 2 shows possible arrangements of the neutrons and protons in $_5B^{10}$, $_5B^{11}$, and $_8O^{16}$.

Figs. 3, 4, 5, 6 show how the neutrons and protons may be supposed to be rearranged in a number of nuclear reactions. The reactions are numbered as in the list of 17 reactions given in the previous paper. In the initial state, the bonds which remain unchanged are represented by thick lines and those which disappear by thin lines. The new bonds to be formed are indicated by dotted lines.

It appears that the observed reactions can be explained by the assumed nuclear constitutions. Since the atoms have the correct energies the reaction energies must be correct also. The reactions (5), (8), (9), (16), and (17) not shown in figs. 3, 4, 5, 6 may be represented in the same way.

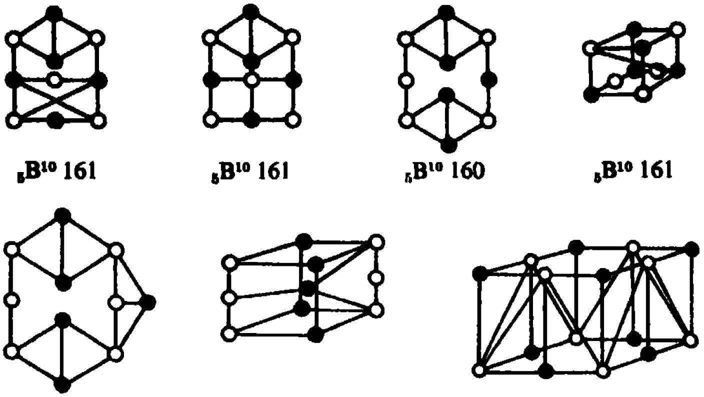
$_5B^{10}$ 161 $_5B^{10}$ 161 $_5B^{10}$ 160 $_5B^{10}$ 161

$_5B^{11}$ 188 $_5B^{11}$ 188 $_8O^{16}$ 312

FIG. 2.

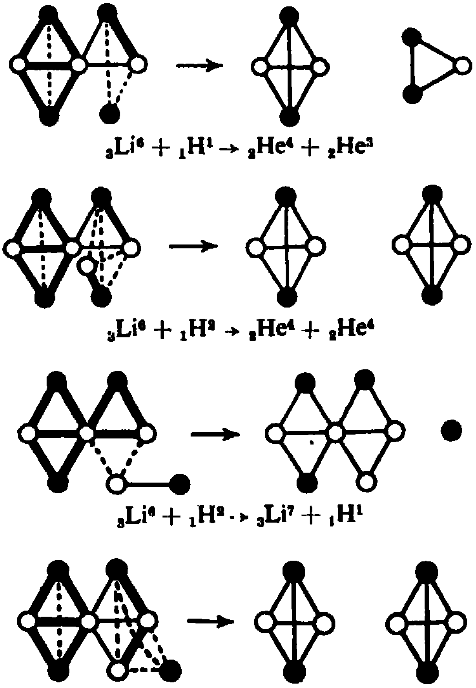
$${}_3Li^6 + {}_1H^1 \rightarrow {}_2He^4 + {}_2He^3 \quad (1)$$

$${}_3Li^6 + {}_1H^2 \rightarrow {}_2He^4 + {}_2He^4 \quad (2)$$

$${}_3Li^6 + {}_1H^2 \dashrightarrow {}_3Li^7 + {}_1H^1 \quad (3)$$

$${}_3Li^7 + {}_1H^1 \rightarrow {}_2He^4 + {}_2He^4 \quad (4)$$

FIG. 3.

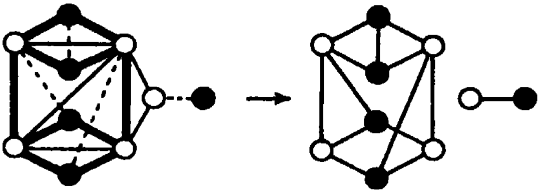

$${}_4\mathrm{Be}^9 + {}_1\mathrm{H}^1 \rightarrow {}_4\mathrm{Be}^8 + {}_1\mathrm{H}^2 \qquad (6)$$

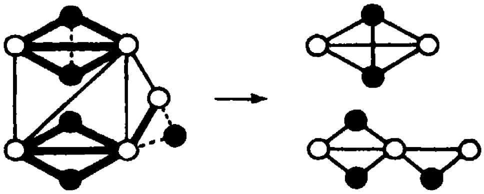

$${}_4\mathrm{Be}^9 + {}_1\mathrm{H}^1 \rightarrow {}_2\mathrm{He}^4 + {}_3\mathrm{Li}^6 \qquad (7)$$

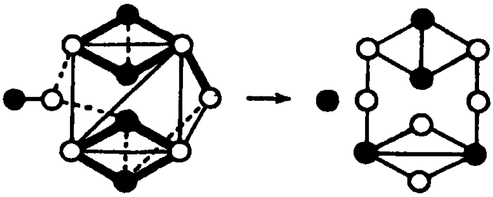

$${}_1\mathrm{H}^2 + {}_4\mathrm{Be}^9 \rightarrow {}_1\mathrm{H}^1 + {}_4\mathrm{Be}^{10} \qquad (10)$$

FIG. 4.

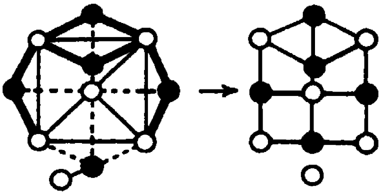

$${}_4\mathrm{Be}^9 + {}_1\mathrm{H}^2 \rightarrow {}_5\mathrm{B}^{10} + {}_0n^1 \qquad (11)$$

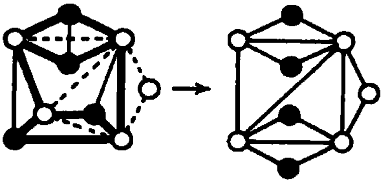

$${}_4\mathrm{Be}^8 + {}_0n^1 \rightarrow {}_4\mathrm{Be}^9 \qquad (12)$$

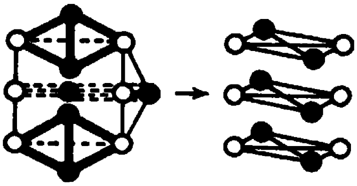

$${}_5\mathrm{B}^{11} + {}_1\mathrm{H}^1 \rightarrow 3\,{}_2\mathrm{He}^4 \qquad (13)$$

FIG. 5.

They are either so similar to those shown or so simple as not to be worth showing.

The reaction $_8O^{16} + {}_1H^2 \rightarrow {}_7N^{14} + {}_2He^4$ is shown in fig. 7. The two neutrons on the right-hand side of the N^{14} atom are assumed to be separated from the adjacent neutrons since otherwise the atomic weight of the N^{14} atom would be exactly 14. This makes the energy of formation of $_7N^{14}$ equal to 255 and so $_7s^{14} = 18$ which gives $_7N^{14} = 14{\cdot}00747$. This agrees nearly with Bethe's* value which is 14·0076. The energy of the reaction is given by $0 + 34 = 18 + 8 + E$, which gives $E = 8$.

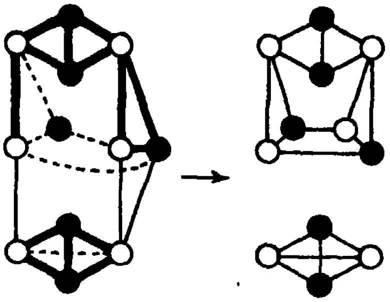

$_5B^{11} + {}_1H^1 \rightarrow {}_4Be^8 + {}_2He^4$ (14)

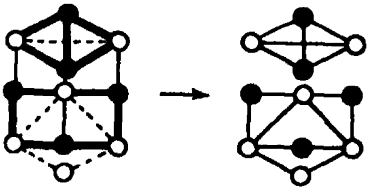

$_5B^{10} + {}_0n^1 \rightarrow {}_2He^4 + {}_3Li^7$ (15)

FIG. 6.

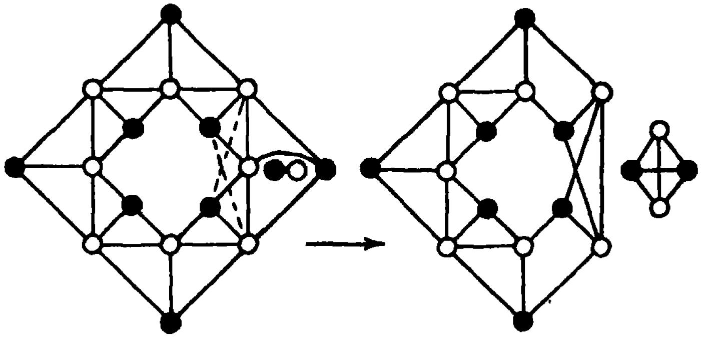

$_8O^{16} + {}_1H^2 \rightarrow {}_7N^{14} + {}_2He^4$

FIG. 7.

---

[*] Bethe, 'Phys. Rev.,' vol. 47, p. 634 (1935).

If we suppose a helium atom $_2He^4$ split off from an oxygen atom as in fig. 8 we get a carbon atom $_6C^{12}$. If the bond shown dotted is present the $_6C^{12}$ atom has energy of formation 234 and so atomic weight exactly 12. If the dotted bond is not present then the atom has energy of formation 225 and atomic weight 12·003735 which agrees well with Bethe's value 12·0037. The energy of the reaction $_6C^{12} + {}_2He^4 \rightarrow {}_8O^{16}$ is given by $9 + 8 = 0 + E$ which gives $E = 17$.

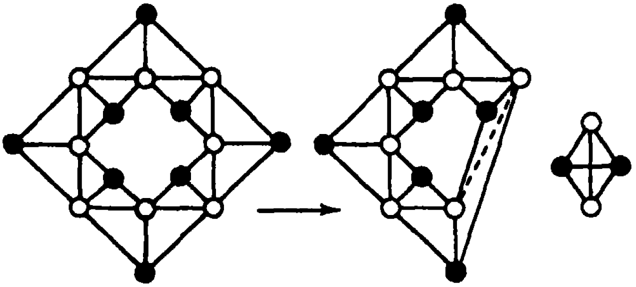

$_8O^{16} \rightarrow {}_6C^{12} + {}_2He^4$

Fig. 8.

The atom $_8O^{17}$ may be supposed to have the constitution shown in fig. 9. This gives $_8O^{17} = 17 + 10q = 17·00415$ which is slightly less than Bethe's value 17·0040.

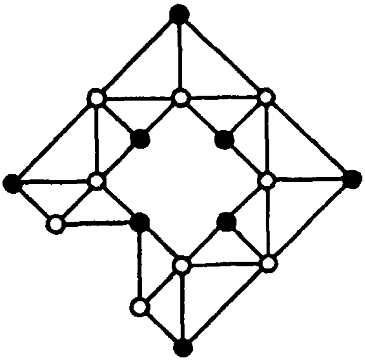

$_8O^{17}$ 322

Fig. 9.

The reaction $_0n^1 + {}_7N^{14} \rightarrow {}_2He^4 + {}_5B^{11}$ is shown in fig. 10. The energy of the reaction is given by $18 + 20 = 8 + 27 + E$, which gives $E = 3$.

Fluorine $_9F^{19}$ may be supposed formed by adding one proton and two neutrons to $_8O^{16}$ as shown in fig. 11. This makes the energy of formation of $_9F^{19}$ equal to 371 which gives $_9s^{19} = 0$ and $_9F^{19} = 19$ exactly.

If the helium atom on the right of the $_9F^{19}$ atom is removed we get $_7N^{15}$. This atom may be supposed to have the constitution shown in fig. 12, which makes its energy of formation 280 and its atomic weight 15·005395, which agrees well with Bethe's value 15·0053.

The reaction $_5B^{11} + {}_1H^2 \rightarrow {}_6C^{12} + {}_0n^1$ is shown in fig. 13. This makes the energy of formation of $_6C^{12}$ equal to 224 so that $_6s^{12} = 10$ and the energy of the reaction is given by $34 + 27 = 20 + 10 + E$ which gives

E = 31. According to Lauritsen and Crane,* the energy of this reaction is 12·1 mV or 31·27.

The energy of formation 224 for ${}_6C^{12}$ gives ${}_6C^{12}$ = 12·00415 which is

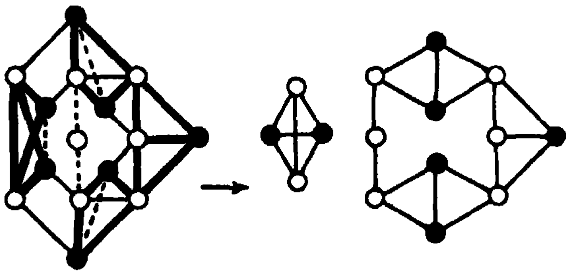

${}_7N^{14} + {}_0n^1 \rightarrow {}_2He^4 + {}_5B^{11}$

FIG. 10.

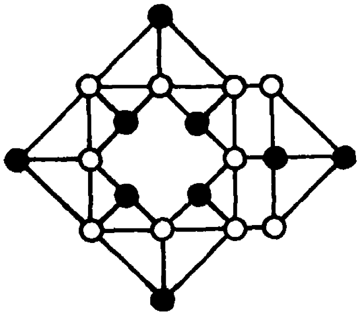

${}_9F^{19}$ 371

FIG. 11.

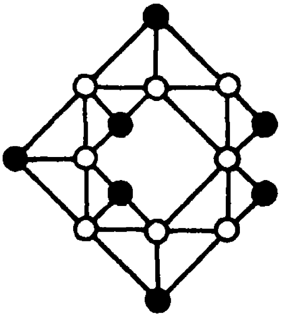

${}_7N^{15}$ 280

FIG. 12.

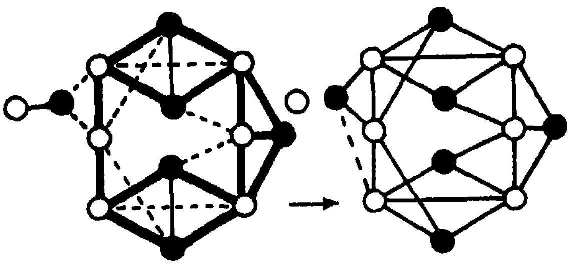

${}_1H^2 + {}_5B^{11} \rightarrow {}_0n^1 + {}_6C^{12}$

FIG. 13.

higher than Bethe's 12·0037. If we suppose one of the neutron-neutron bonds removed and the proton-neutron bond, shown dotted in ${}_6C^{12}$ added the energy of formation becomes 225 and the atomic weight 12·003735;

---

* 'Rep. Int. Conf. Nuclear Phys. London,' p. 141 (1935).

but this makes the energy of the reaction 32. We might have expected to have both the dotted bond and all six neutron-neutron bonds making the atomic weight exactly 12 but this makes the reaction energy much too large.

The reaction ${}_9F^{19} + {}_1H^1 \to {}_8O^{16} + {}_2He^4$ is shown in fig. 14. The energy of the reaction is given by $0 + 19 = 0 + 8 + E$, which gives $E = 11$. This is less than the energy found by Henderson, Livingstone, and Lawrence,* which was about 17.

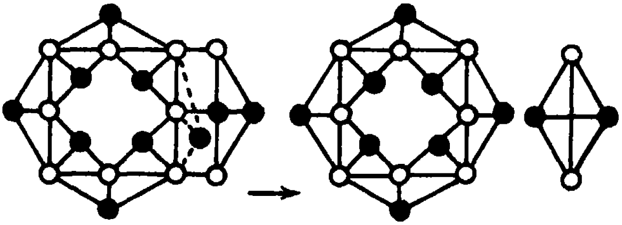

${}_9F^{19} + {}_1H^1 \to {}_8O^{16} + {}_2He^4$

Fig. 14.

Another possible constitution of ${}_9F^{19}$ is shown in fig. 15. This makes the energy of formation 367 so that ${}_9s^{19} = 371 - 367 = 4$, and ${}_9F^{19} = 19{\cdot}00166$. The energy of the reaction ${}_9F^{19} + {}_1H^1 \to {}_8O^{16} + {}_2He^4$ is then given by $4 + 19 = 0 + 8 + E$ which gives $E = 15$.

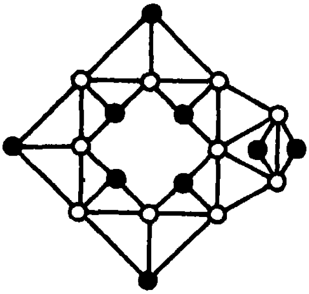

${}_9F^{19}$ 367

Fig. 15.

It does not seem to be possible to make the reaction energy equal to 17 without giving up the simple relation between the ${}_8O^{16}$ and ${}_9F^{19}$ atoms. The reaction ${}_6C^{13} + {}_1H^1 \to {}_5B^{10} + {}_2He^4$ is shown in fig. 16. We suppose that the neutron at A is displaced by the proton and that it then combines with the two protons B and C and the neutron D. The energy of formation of the ${}_6C^{13}$ atom is 237, so that ${}_6s^{13} = 254 - 237 = 17$, and ${}_6C^{13} = 13{\cdot}007055$, which is slightly greater than Bethe's value $13{\cdot}0069$. The energy of the reaction is given by $17 + 19 = 34 + 8 + E$, so that $E = -6$.

The neutrons and protons in many of the atoms considered may be arranged in many ways with energies of formation less than that of the normal atoms. Atoms with such lower energies of formation are excited atoms and should change to normal atoms with the emission of gamma rays. When the energy levels of the atoms are known it may be possible to deduce the arrangements for such excited atoms. Fig. 17 shows several excited $_4Be^9$ atoms.

---

* 'Rep. Int. Conf. Nuclear Phys. London,' p. 125 (1935).

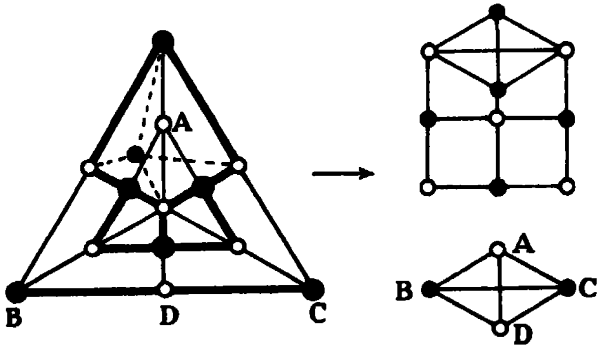

$_6C^{13} + {}_1H^1 \rightarrow {}_5B^{10} + {}_2He^4$
FIG. 16.

It appears that series of excited states with energies of formation differing by q may be possible. Series of energy levels with energy differences roughly equal to q have been observed with several light elements.

Since almost any energy of formation, within certain limits, can be obtained with some of the atoms it is clear that the fact that arrangements can be found having the correct energies of formation, for such atoms, should not be regarded as providing much support for the present theory. The way in which the assumed arrangements offer simple explanations of the observed reactions is of much greater weight.

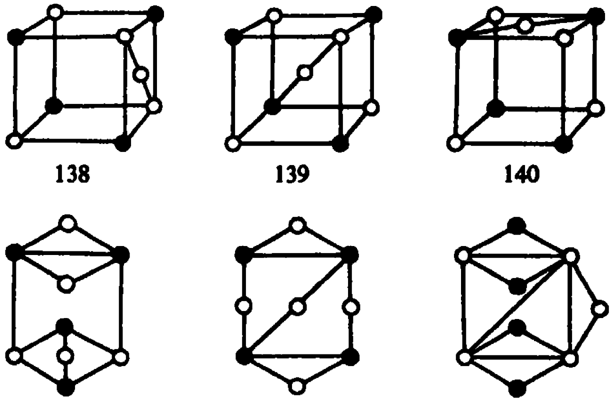
138 139 140
141 142 143

$_4Be^9$
FIG. 17.

It is possible that other values of the bond energies with different arrangements could be found which would equally well explain the observed energies and reactions. The writer has tried several other sets of bond energies but was not able to find arrangements giving the correct energies of formation, of all the atoms considered, with them.

SUMMARY

The energies of formation of several atoms, from neutrons and protons, are calculated from nuclear reaction energies. It is suggested that the energies of formation may be supposed due to the formation of bonds or connexions between the neutrons and protons. Arrangements of the neutrons and protons and bond energies are found which give the correct energies of formation. The observed reactions may be explained by means of the assumed nuclear arrangements or constitutions and the bond energies.

The Diffusion of Hydrogen through Copper

By E. O. BRAATEN and G. F. CLARK*

(*Communicated by Sir John McLennan, F.R.S.—Received July* 18, 1935)

INTRODUCTION

At temperatures higher than about 400° C, several observers have determined the rates of *diffusion* of hydrogen through copper, and only recently has a paper by Smithells and Ransley appeared,† giving measurements on *diffusion* as low as 225° C. Sieverts,‡ Deming and Hendricks,‡ and Lombard‡ have shown that the copper tubes and plates used in the experiments at high temperatures tend to crystallize and become fissured, so that the measurements are of little value.

The *adsorption* of hydrogen by copper has been thoroughly studied over a large temperature range. Ward§ has shown that, at low temperatures, the immediate initial *adsorption* is followed by a slow solution of the hydrogen in the copper. Solution increases very rapidly with temperature, and above 160° C is so large and so rapid that the initial *adsorption* cannot be accurately determined.

---

* Holder of Fellowship, Graduate School, University of Toronto, 1934–35.

† ' Proc. Roy. Soc.,' A, vol. 150, p. 172 (1935).

‡ *See* McBain, J. W., " The Sorption of Gases by Solids," p. 263.

§ ' Proc. Roy. Soc.,' A, vol. 133, p. 506 (1931).

Lennard-Jones* has treated the problem of *diffusion* and solution theoretically, and the theory developed for solution gives a satisfactory explanation of Ward's investigations.

THEORY

It has been found for most cases of the *diffusion* of a gas through a metal that the rate of *diffusion* can be expressed as a function of the temperature and pressure by means of the empirical relation

$$\mathrm{M} = \mathrm{K}p^{\frac{1}{2}}e^{-b/\mathrm{T}}, \tag{1}$$

where M is the mass of gas diffusing per second, K and b are constants, p is the pressure, and T is the absolute temperature.

From consideration of the kinetic theory of diffusion of an adsorbed atom moving over the surface of a crystalline solid and eventually diffusing into the interior of the solid through narrow surface cracks, Lennard-Jones has shown that the diffusion of a gas into a solid is described by the equation

$$\mathrm{M} = \mathrm{K}n_0e^{-\mathrm{E}_0/k\mathrm{T}} \quad \text{if} \quad \mathrm{E}_0 \gg k\mathrm{T} \tag{2}$$

$$\mathrm{M} = \mathrm{KT}n_0e^{-\mathrm{E}_0/k\mathrm{T}} \quad \text{if} \quad \mathrm{E}_0 \ll k\mathrm{T}, \tag{3}$$

where M is the mass of gas *diffusing* per second, K is a constant, T is the absolute temperature, k is Boltzmann's constant, n_0 is the amount of gas *adsorbed* per unit surface area, and E_0 is the " energy of activation," *i.e.*, the minimum energy required by an atom for it to move freely over the surface. Since *diffusion* occurs, *e.g.*, at 300° C, equation (2) would apply where E_0 is of the order of 5000 cals per gram atom or more and equation (3) would apply where E_0 is about 100 cals per gram atom.

Ward has determined the energy of activation of hydrogen *adsorbed* on copper and has found it to be 14,100 cal/gram atom. Thus, the first of the two equations should apply to the *diffusion* of hydrogen through copper. The difficulty of applying the equation is due to our inability to make an exact determination of n_0 the amount of gas *adsorbed* on the surface. Where the rate of *diffusion* is appreciable, the *adsorption* cannot be measured experimentally. If, however, we assume that the connexion between *adsorption* and gas pressure is given by Langmuir's " Isotherm," then n_0 is given by the equation

$$n_0 = \frac{c_1c_2p}{1 + c_2p} \tag{4}$$

---

* 'Trans. Faraday Soc.,' vol. 28, p. 333 (1932).

where c_1 and c_2 are functions of the temperature only. Substituting for n_0 the *diffusion* equation will become

$$M = K \frac{c_1 c_2 p}{1 + c_2 p} e^{-E_0/kT}. \tag{5}$$

It is found by Ward that (1) and (5) represent the experimental results, equally well wherever the values of c_1 and c_2 are known.

In the recent paper by Smithells and Ransley* a modified type of expression has been proposed

$$M = C p^{\frac{1}{2}} \frac{c_2 p}{1 + c_2 p} e^{-E_0/kT}, \tag{6}$$

where E_0 and k have values† as described previously. They point out that the rate of *diffusion* is not exactly proportional to $p^{\frac{1}{2}}$ and that by introducing Langmuir's isotherm into equation (1), one can account for the rapid increase in *diffusion* over the low-pressure range. As p increases, the factor $c_2p/1 + c_2p$ approaches unity so the variation of *diffusion* should proceed according to the $p^{\frac{1}{2}}$ law.

EXPERIMENTAL

The arrangement of the apparatus is shown in fig. 1. A thin, cold-drawn copper tube,‡ 0·14 mm wall thickness, 0·79 cm in diameter, and of surface area 31·42 sq cm was sealed to a pyrex tube and mounted in the glass system shown. Hydrogen 99·9% pure was admitted to the tube through A, the pressure being measured with a manometer. The gas diffusing through the copper tube C was collected in B and the pressure measured with a sensitive McLeod gauge. The system was placed in an electric furnace and the temperature, measured by a calibrated mercury thermometer, was kept constant to 1° C by means of a brass-invar thermostat.

To reduce any copper oxide formed in constructing the apparatus, the tube was maintained for 100 hours at 200° C in an atmosphere of hydrogen. It was later found that the tube could be heated to 350° C without altering the reproducibility of the measurements at lower temperatures. The system was tested for leaks at 250° C by using nitrogen and helium. With nitrogen the rate of increase on the low-pressure side was of the same order as the rate of desorption from the glass, or about 1/50 of the smallest rate of diffusion measured in the experiment. For helium the rate was that of diffusion through the short pyrex tube forming the seal to the copper.

---

* 'Proc. Roy. Soc.,' A, vol. 150, p. 152 (1935).

† Smithells and Ransley preferred to use b instead of E_0/k, where b is the temperature coefficient of diffusion.

‡ Supplied by the French Manufacturing Co., Waterbury, Conn., U.S.A.

The mass of gas diffusing per hour was calculated from the volumes of the different parts of the system and the densities of the gas in the parts. Calculations show that no corrections were necessary for thermo-molecular flow.

RESULTS

Table I gives the values of the mass of gas in grams diffusing per hour through 1 sq cm of surface at different pressures. Measurements were made for pressures from 5 to 76 cm at a constant temperature of 254° C. When the temperature is constant, Smithells and Ransley's equation may be written

$$1 + c_2 p = c' p^{3/2}/\mathrm{M}, \qquad (7)$$

and if p is plotted against $p^{3/2}/\mathrm{M}$ a straight line should be obtained, fig. 2.

The variation of the rate of diffusion with temperature was determined at two pressures. Table II gives the values obtained at a pressure of 76·0 cm, Table III the values at a pressure of 17·3 cm.

When the pressure is constant and the variation of *adsorption* with temperature is so small that the *adsorption* factor $(c_2 p/1 + c_2 p)$ may be treated as a constant, we may write equation (6) in the form

$$\log \mathrm{M} = \mathrm{C} - \mathrm{E}_0/k\mathrm{T}. \qquad (8)$$

Log M is plotted against 1/T in fig. 3. From the graph the value of the energy of activation, E_0, is calculated to be 19,700 cal/gm atom.

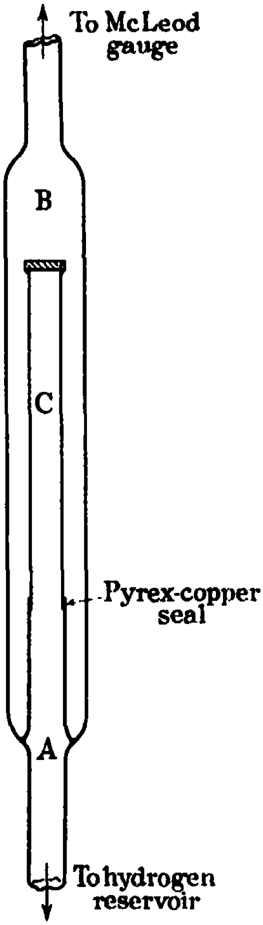

FIG. 1 — Apparatus used for measuring the diffusion of hydrogen through copper.

DISCUSSION

It has been shown that the rate of diffusion varies with the pressure in a manner consistent with the equation of Smithells and Ransley. Quite as good agreement would be obtained using equation (5), with T constant,

TABLE 1

Pressure in cm of Hg	Mass in gm × 10^{10}
77·4	87·4
60·1	79·0
43·2	66·5
25·9	50·5
12·1	29·0
5·0	14·0

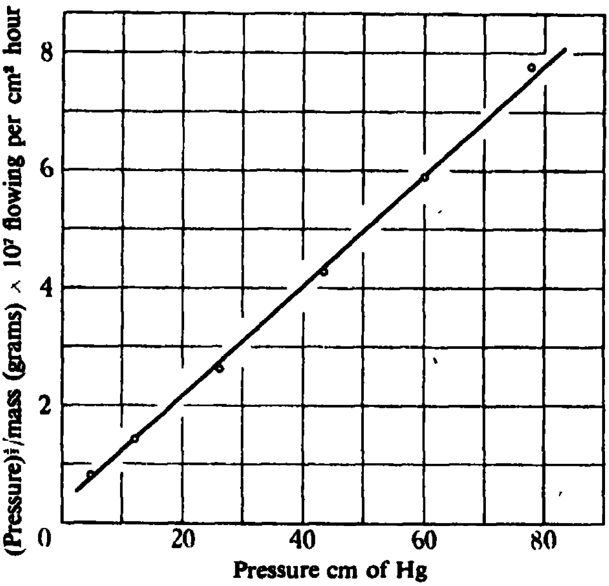

FIG. 2—The relation between the rate of diffusion and pressure at a fixed temperature ($p^{3/2}$/M plotted against p). H_2 — Cu 528° K.

TABLE II—PRESSURE CONSTANT AT 76 CM

Temperature °C	Mass in gm × 10^{10}
166	1·7
177	3·3
198	9·0
227	32·0
254	86·6
285	246·8
321	622·6

TABLE III—PRESSURE CONSTANT AT 17·3 CM

Temperature °C	Mass in gm × 10^{10}
195	3·3
220	8·8
254	38·5
289	105·4
319	259·4

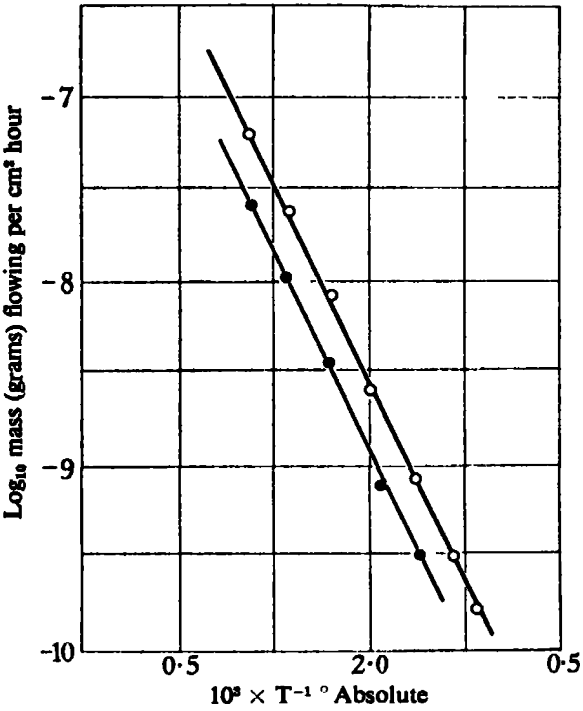

FIG. 3—The relation between log (diffusion) and the reciprocal of the absolute temperature at constant pressures. ● 17·3 cm; ○ 76·0 cm; E_0— 19,700 cal/gm atom.

as is illustrated if one plots P/M against *p*. However, equation (6), which agrees better with most experimental results and which appears to have a somewhat better theoretical significance, has been adopted.

The method used in fig. 2 to plot the results has an advantage over that of Smithells and Ransley; since the resulting expression as an equation between p and $p^{3/2}/M$ is linear, one may readily detect any deviation from the straight line. The results obtained by Smithells and Ransley for the *diffusion* of H_2 through copper and iron (for which a greater accuracy was assured) have been plotted in fig. 4 in the method similar to fig. 2. A departure from the straight line occurs at about 2 mm pressure, the amount of gas diffusing being in both cases larger than required by the equation.

The validity of Langmuir's expression for *adsorption* as applied to the data obtained by Ward* on the *adsorption* of H_2 on copper has been tested by plotting p/n_0 against p, where n_0 is the amount of gas *adsorbed*, fig. 5.

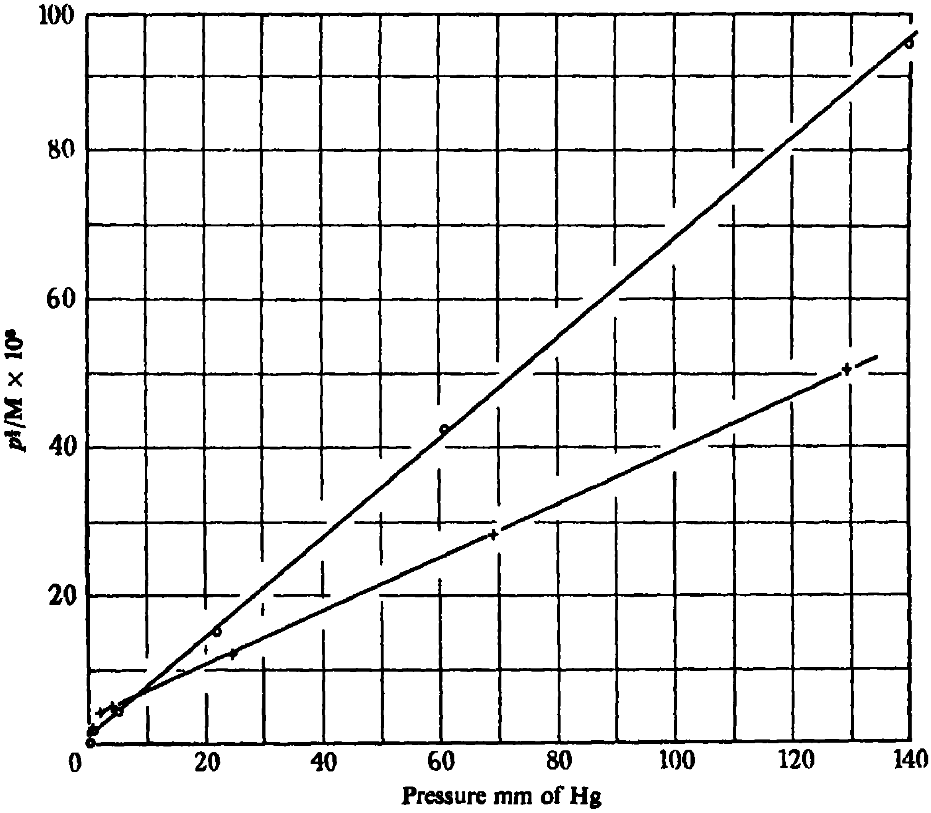

Fig. 4—The variation with pressure of the rates of diffusion of hydrogen through iron and copper for fixed temperatures. O H_2 – Fe 686°K, Smithells and Ransley; + H_2 – Cu 723°K, Smithells and Ransley.

There is a departure from a straight line at about 2 mm pressure,† below which the amount of gas *adsorbed* is greater than required by the adsorption isotherm.

---

* Fig. 4, 'Proc. Roy. Soc.,' A, vol. 133, p. 515 (1931).

† If the method of treating Langmuir's equation, as proposed by Cunningham ('J. Phys. Chem.,' vol. 39, p. 69 (1935)), is applied to Ward's data, a similar conclusion would be reached.

It would thus appear that the inadequacy of equation (6) to give the rate of *diffusion* when p is small may be partly attributed to the failure of Langmuir's isotherm to express accurately the amount of gas *adsorbed* per unit area at low pressures. These considerations lend added support to the idea that *diffusion* through most metals begins from an *adsorbed* layer.

Smithells and Ransley obtained a value of $b = 8300$ for the diffusion coefficient of H_2 through copper which had been previously oxidized and reduced at 600° C. According to the notation used above, this corresponds to an activation energy of 16,200 cal/gram atom and compares favourably with the authors' results on copper whose highest temperature did not exceed 350° C.

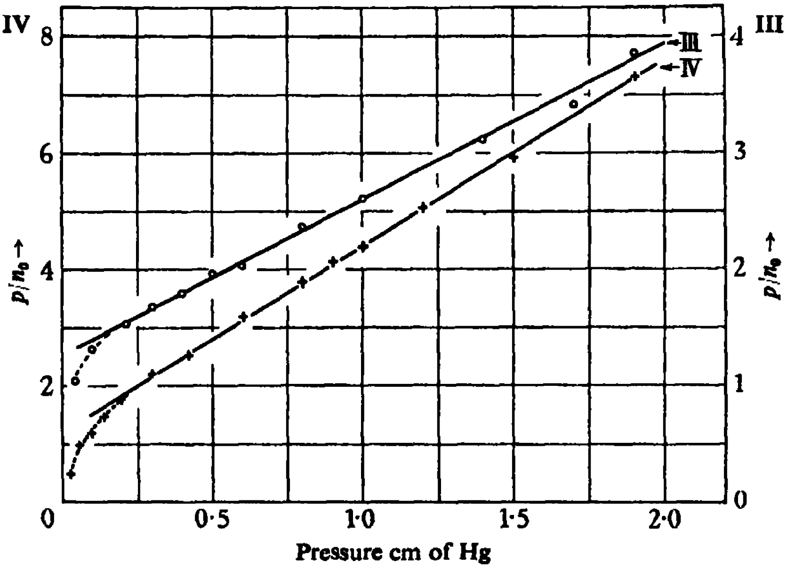

FIG. 5—Curves showing the variation with pressure for the amount, n_0, of hydrogen adsorbed on copper (using Ward's data), where p/n_0 is plotted against p. Ward gives four sets of results, of which III and IV are chosen here. Ordinates on the right for III and on the left for IV.

In (8) the *adsorption* is assumed to be independent of temperature. If it be supposed (6) that the *adsorption* varies as, say $1/T^n$, then at constant pressure (6) becomes

$$\log M = C + n \log \frac{1}{T} - E_0/kT. \qquad (9)$$

Within the limits of experimental error the graph between log M and 1/T will still be linear, but will lead to a somewhat larger value of E_0, depending on the (small) positive value of n chosen. If it should be found necessary to assume an *adsorption* depending on T, the consequent change in E_0 is easily computed.

An attempt was made to extend the experiment to higher temperatures by using a metal apparatus, but no accurate measurements could be made because of the large adsorption on the metal surfaces.

It is a pleasure to thank Professor E. F. Burton for his valuable advice and encouragement throughout this work, and Mr. Chappell for his assistance in constructing the apparatus.

SUMMARY

The rate of diffusion of H_2 through copper has been determined for several temperatures and pressures.

The effect of temperature is represented by the usual exponential relation, and an activation energy of 19,700 cal/gram atom was obtained.

The effect of pressure can be nearly represented by the equation

$$M \propto p^{\frac{1}{2}} \frac{c_2 p}{1 + c_2 p}.$$

The small departure from the above equation which occurs at about 2 mm pressure is thought to be partly due to the adsorption factor.

The Theory of the Surface Photoelectric Effect in Metals—II

By K. MITCHELL, Department of Mathematics, The University, Leeds

(*Communicated by R. H. Fowler, F.R.S.—Received August* 7, 1935)

INTRODUCTION

1—It is usual to divide observed photoelectric effects into two general categories, known as the selective and normal effects. The former, of the occurrence of which there can be no doubt, is so named from the form of the spectral distribution curve, the photoelectric emission passing through a well-defined maximum for a frequency usually at about one and a half times the threshold frequency. The normal effect, on the other hand, shows no such maximum, and was given its rather unhappy name by the early experimenters who observed it when using light polarized with its electric vector perpendicular to the plane of incidence.

The use of the term normal for this effect is unfortunate for two reasons. In the first place, the effect is of very rare occurrence, and is not clearly shown by pure metals in a solid state. Secondly, the term is really needed to describe the " usual " photoelectric effect, which is theoretically predicted,[*] and which is actually found to occur with metals in a very pure or nearly pure state. This effect has a maximum in the spectral distribution curve, the emission at the maximum being of the order of $1\text{-}5 \times 10^{-4}$ Coulombs per calorie.[†] Now there would be no harm in calling this effect the selective effect without further qualification, were it not that it needs to be distinguished from a more violent type of selective effect, which is observed only when the surface of the metal is specially sensitized. The maximum is then much sharper, and the order of magnitude as much as 100 times greater.

Now the essential difference between these effects must be realized, and ideally they should be called the normal and selective effects, the present " normal " effect being a rather different problem. Since, however, the term normal is already in use, the best course seems to be to distinguish the two selective effects as the high order and low order spectral selective effects.*

---

[*] Mitchell, 'Proc. Roy. Soc.,' A, vol. 146, p. 442 (1934), and references there given. This will be referred to as I in the present paper.

[†] With the very pure metals other than the alkalis the observed curves show no such maxima. The frequency ranges covered do not, however, extend as far as the predicted maximum, so that there is no justification for calling these normal curves, in the accepted sense of the term.

The present paper is concerned mainly with the low order selective effect, partly too with the normal effect. The theory of the surface photoelectric effect in metals presented in I is further discussed, and some refinements are introduced which enable us to forecast the results which would be obtained with a less idealized model. The discussion of the results, which in I only touched on the spectral distribution curve for unpolarized light, is extended here to cover polarization phenomena, and the normal and total energy distribution curves. The temperature dependence has in the meantime been discussed by the author in a separate paper.†

REFINEMENTS OF THE THEORY

2.1—In I the photoelectric current liberated from Sommerfeld's ideal model metal with a simple discontinuity of potential at its surface, by a light wave with scalar and vector potentials

$$\left.\begin{aligned}\phi &= 0\\ \mathbf{A} &= 2\mathbf{a}\cos 2\pi\nu\left\{t + (x\cos\theta + y\sin\theta)/c\right\}\end{aligned}\right\}, \tag{1}$$

was calculated, and it was shown that the current normal to the surface is of amount

$$\mathrm{J}_x = \frac{e^3\mathbf{a}_x^{\,2}\nu_a}{2\pi^3 m^2 c^2 \nu^3}\int_{0,\,[\mu(\nu_a-\nu)]^{\frac{1}{2}}}^{(\mu\bar{\nu})^{\frac{1}{2}}} dk\,.\,\frac{k^2(\mu\bar{\nu}-k^2)\{k^2+\mu(\nu-\nu_a)\}^{\frac{1}{2}}}{[(k^2+\mu\nu)^{\frac{1}{2}}+\{k^2+\mu(\nu-\nu_a)\}^{\frac{1}{2}}]^2}, \tag{2}$$

the components of current tangential to the surface vanishing.

Here *e*, *m* denote the charge and mass of an electron, *c* the velocity of light, ν the frequency of the light wave and $\mathbf{a}_x$ the *x*-component of $\mathbf{a}$, while $\mu = 8\pi^2 m/h$, where *h* is Planck's constant. The height of the potential jump at the surface of the metal is $h\nu_a$, and $h\bar{\nu}$ is the Fermi critical energy, given by

$$\mu\bar{\nu} = (3\pi^2 n)^{\frac{2}{3}}, \tag{3}$$

n being the number of conducting electrons in unit volume of the metal.

---

* Suhrmann ('Ergebn. exakt. Naturwiss.,' vol. 13, p. 148 (1934)) distinguishes between "*Der lichtelektrische Effekt an einfach adsorbierten Schichten*" and "*an zusammengesetzten Schichten.*" These terms, however, define the metal surface rather than its photoelectric properties.

† 'Proc. Camb. Phil. Soc.,' vol. 31, p. 416 (1935).

Further, k denotes the wave number of an electron in the x-direction, connected with the corresponding part of the total energy by the relation

$$k^2 = 8\pi^2 m\mathrm{E}/h^2. \tag{4}$$

The lower limit of integration in (2) is 0, if $\nu > \nu_a$, and $[\mu(\nu_a - \nu)]^{\frac{1}{2}}$, if $\nu < \nu_a$.

Now the idealizations made in deriving (2) are two in number, and concern the treatment of the metal, and of the light wave. Taking the metal first, let us consider what alterations there would be if we replaced Sommerfeld's model metal by the more accurate quantum mechanical model, taking into account the lattice structure. The electrons inside the metal are now no longer free, and a volume effect can occur: Tamm and Schubin* have shown, however, that the threshold for this effect is higher than that for the surface effect, since the possible transitions are restricted by a selection rule. Near the threshold, the volume effect may then be neglected, and we need only consider the modifications produced directly by band structure, and by the fact that the "surface" of the metal is no longer plane.

Taking into account band structure, it is evident that the transition probabilities between given states will be given effectively, for the surface effect, by the ordinary Sommerfeld wave functions, which approximate to the more accurate wave functions for a periodic lattice: the only modification due to the band structure will then be that due to the change in width of the band of energies occupied by the conducting electrons at the absolute zero. On the strict Sommerfeld theory, the band is of width $h\bar{\nu}$, where $\bar{\nu}$ is given by (3). If we assume, however, that on account of lattice structure the band width becomes $h\nu_0$, then, since this band must contain still the same total number of electrons, we must suppose the average electron density in any state† to be multiplied by a factor $(\bar{\nu}/\nu_0)^{\frac{3}{2}}$. Thus to get the modified result we must replace $\bar{\nu}$ in (2) by ν_0, and multiply through by the factor $(\bar{\nu}/\nu_0)^{\frac{3}{2}}$. We thus have

$$\mathrm{J}_x = \frac{e^3 \mathrm{a}_x{}^2 \nu_a}{2\pi^3 m^2 c^2 \nu^2}\left(\frac{\bar{\nu}}{\nu_0}\right)^{\frac{3}{2}} \int_{0,\,[\mu(\nu_a-\nu)]^{\frac{1}{2}}}^{(\mu\nu_0)^{\frac{1}{2}}} dk\, \frac{k^2(\mu\nu_0 - k^2)\{k^2 + \mu(\nu - \nu_a)\}^{\frac{1}{2}}}{[(k^2 + \mu\nu)^{\frac{1}{2}} + \{k^2 + \mu(\nu - \nu_a)\}^{\frac{1}{2}}]^2}. \tag{5}$$

The ν_a occurring here must also be altered, so as to keep the threshold frequency $\nu_g = \nu_a - \nu_0$ unaltered.

---

* 'Z. Physik,' vol. 68, p. 97 (1931).

† In the Kronig-Penney model ('Proc. Roy. Soc.,' A, vol. 130, p. 499 (1931)) the electron states are no longer uniformly distributed in k-space. We cannot take this into account without a more thorough investigation.

The fact that in a three-dimensional model taking into account internal potential variations the surface cannot be plane is of greater importance, as it is evident that this opens up the possibility of contributions to the photo-current from the components of vector potential absent from (2) and (5), which are tangential to the macroscopic surface. The same possibility arises also from the fact that the surface of the metal will show small roughnesses, as a result of which the direction of the microscopic normal at any point will not in general be that of the general normal to the surface. Now although no simple method of attacking the first point presents itself, the second can be discussed by an averaging process, and we may adopt the modifications reached on this basis as taking into account both of these effects.

Let us assume that the microscopic normal at any point is inclined to the mean position of the normal, and that its direction cosines are l, m, n relative to axes Ox along the mean normal, and Oy and Oz tangential to the surface, the plane Oxy being the plane of incidence. If $\mathbf{A}_x$, $\mathbf{A}_y$, $\mathbf{A}_z$ denote the components of vector potential of the light wave relative to these axes, the component along the microscopic normal will be

$$l\mathbf{A}_x + m\mathbf{A}_y + n\mathbf{A}_z, \tag{6}$$

and it is this quantity which is effective in producing the photoelectric emission from a small element of surface about the point considered. The current from an element of area dS will then be

$$\mathbf{J}_0 = \frac{e^3\,|l\mathbf{A}_x + m\mathbf{A}_y + n\mathbf{A}_z|^2\,\nu_a\,dS}{2\pi^3 m^2 c^2 \nu^2}\left(\frac{\nu}{\nu_0}\right)^{\frac{1}{2}} \times \int_{0,\,\{\mu(\nu_a-\nu)\}^{\frac{1}{2}}}^{(\mu\nu_0)^{\frac{1}{2}}} dk\,\frac{k^2(\mu\nu_0 - k^2)\{k^2 + \mu(\nu - \nu_a)\}^{\frac{1}{2}}}{[(k^2+\mu\nu)^{\frac{1}{2}} + \{k^2 + \mu(\nu-\nu_a)\}^{\frac{1}{2}}]^2}, \tag{7}$$

and this is in the direction of the microscopic normal, and hence has a component $l\mathbf{J}_0$ along the average normal. Since $l d\text{S} = dydz$, we see that the total emission per unit area will be given by replacing $|\mathbf{a}_x|^2$ in (5) by the average value of the square of the modulus of expression (6). The tangential components of $\mathbf{J}_0$ will obviously vanish on summing over the whole surface.

Now we cannot obtain an exact value for the average required, and we must content ourselves by remarking that it will be of the form

$$\mathbf{a}_x^2 \cos^2 \varpi + \tfrac{1}{2}(\mathbf{a}_y^2 + \mathbf{a}_z^2)\sin^2 \varpi, \tag{8}$$

where ϖ is a parameter defining the roughness of the surface. Increasing ϖ corresponds to increasing roughness.

2.2—The other respect in which the simple theory must be modified is its treatment of the light wave. In deriving (2) the effect of refraction and reflexion of the light at the metal surface was neglected altogether. Now it was shown in I that this neglect was not justifiable, and a further formula,

$$\mathrm{J}_x = \frac{e^3\nu_a}{2\pi^3 m^2 c^2 \nu^2}\int_{0,\,[\mu(\nu_a-\nu)]^{\frac{1}{2}}}^{(\mu\bar{\nu})^{\frac{1}{2}}} dk\,\frac{k^2(\mu\bar{\nu}-k^2)\{k^2+\mu(\nu-\nu_a)\}^{\frac{1}{2}}}{[(k^2+\mu\nu)^{\frac{1}{2}}+\{k^2+\mu(\nu-\nu_a)\}^{\frac{1}{2}}]^2} \times \frac{|(k^2-ipq)\,\mathbf{a}_{tx}+p\,(p+iq)\,(\mathbf{a}_{ix}+\mathbf{a}_{rx})|^2}{\mu^2{\nu_a}^2}, \quad (9)$$

was derived. Here

$$\left.\begin{aligned} p^2 &= \mu\nu_a - k^2 \\ q^2 &= k^2 + \mu(\nu-\nu_a) \end{aligned}\right\}, \quad (10)$$

and $\mathbf{a}_{ix}$, $\mathbf{a}_{rx}$, $\mathbf{a}_{tx}$ refer to the incident, reflected, and transmitted beams respectively. It was assumed in deriving (9) that the light wave could be represented by three beams of type (1), the vectors $\mathbf{a}_i$, $\mathbf{a}_r$, $\mathbf{a}_t$, being constant, and the change from $\mathbf{a}_i + \mathbf{a}_r$ outside the metal to $\mathbf{a}_t$ inside taking place abruptly at the surface. It was further assumed that the values of $\mathbf{a}_r$ and $\mathbf{a}_t$ could be calculated in terms of $\mathbf{a}_i$ and the optical constants of the metal by using the classical electromagnetic theory.

Now this is by no means the only course that could be followed at this point. It is evident that in reality the change from $\mathbf{a}_i + \mathbf{a}_r$ outside the metal to $\mathbf{a}_t$ inside will be gradual, and because of this the author suggested in I that a better result might be obtained by assuming the sudden change to take place at a point not at the actual surface, and averaging for different positions of the point. An alternative suggestion is as follows. From the calculation by the method of variation of constants in I it is seen that the major portions of the matrix elements all come from a region within a few electron wave-lengths of the surface. At such a short distance within the metal, it can be argued, the gradual change from $\mathbf{a}_i + \mathbf{a}_r$ to $\mathbf{a}_t$ will not have proceeded far, and it may give better results to use $\mathbf{a}_i + \mathbf{a}_r$ inside and outside the metal, in calculating the emission. This suggestion has the further advantage of simplifying the final results considerably, and was made the basis of further calculations by the author. It appeared, however, to affect the agreement with experiment rather deleteriously than otherwise.*

The three suggestions so far make use of the classical electromagnetic theory to calculate $\mathbf{a}_r$ and $\mathbf{a}_t$; better results would, however, be expected if we could use a quantum theory of metallic reflexion. Such a theory has now been published by Schiff and Thomas,* who apply it to the photoelectric effect. They find that the classical electromagnetic theory gives approximately correct results for the components of vector potential parallel to the surface, as well as for the perpendicular component beyond an immediate neighbourhood extending some electron wave-lengths into the surface. Within this region the perpendicular component fluctuates widely, and it is just from this region that the greater parts of the matrix elements come. This theory then argues against the acceptance of any of the three above proposals; unfortunately, however, its application demands very troublesome calculations, and hence the course adopted in I has been followed again here. The detailed calculations necessary may be worth making when there is a better body of experimental fact with which to compare the results, but in the present position we may content ourselves with quoting the above authors' conclusion that for the case of potassium, discussed in I, the agreement with experiment would be improved by replacing the classical theory by the quantum theory of metallic reflexion.

---

* A calculation for potassium, with the same values of n, κ, ν_g, etc., as in I, gives a curve only about one-half the height of the curve there given, I, fig. 2.

SPECTRAL DISTRIBUTION CURVES AND POLARIZATION PHENOMENA

3.1—Combining the various modifications discussed above, it is evident that we must replace $\bar{\nu}$ in (9) by ν_0, and multiply through by $\bar{\nu}/\nu_0)^{\frac{1}{2}}$, as well as replace the quantity

$$\mathbf{a}_{tx}(k^2 - ipq) + (\mathbf{a}_{ix} + \mathbf{a}_{rx})\,p\,(p + iq),$$

by

$$(l\mathbf{a}_{tx} + m\mathbf{a}_{ty} + n\mathbf{a}_{tz})(k^2 - ipq) + p\,(p + iq)\,\{l\,(\mathbf{a}_{ix} + \mathbf{a}_{rx}) + m\,(\mathbf{a}_{iy} + \mathbf{a}_{ry}) + n\,(\mathbf{a}_{iz} + \mathbf{a}_{rz})\}, \qquad (11)$$

in the contribution to (9) from a small surface element, as in (7). Taking the square of the modulus of (11), we shall get a homogeneous quadratic expression in l, m, n, and upon averaging over differently directed surface elements, the product terms lm, mn, nl, will go out. Using also the fact that the tangential components of vector potential are continuous, we obtain the final result in the form

$$\mathrm{J}_x = \frac{e^3\nu_a}{2\pi^3 m^2 c^2 \nu^2}\left(\frac{\bar{\nu}}{\nu_0}\right)^{\frac{1}{2}} \int_{0,\,[\mu(\nu_a-\nu)]^{\frac{1}{2}}}^{(\mu\nu_0)^{\frac{1}{2}}} dk\, \frac{k^2(\mu\nu_0 - k^2)\{k^2 + \mu(\nu - \nu_a)\}^{\frac{1}{2}}}{[(k^2 + \mu\nu)^{\frac{1}{2}} + \{k^2 + \mu(\nu - \nu_a)\}^{\frac{1}{2}}]^2} \times \left[\frac{\cos^2\varpi\,|(k^2 - ipq)\,\mathbf{a}_{tx} + p\,(p + iq)(\mathbf{a}_{ix} + \mathbf{a}_{rx})|^2}{\mu^2\nu_a^2} + \tfrac{1}{2}\sin^2\varpi\,\{|\mathbf{a}_{ty}|^2 + |\mathbf{a}_{tz}|^2\}\right]. \qquad (12)$$

---

* 'Phys. Rev.,' vol. 47, p. 860 (1935).

We can now proceed to derive expressions for the current per unit incident energy, for light polarized with the electric vector parallel or perpendicular to the plane of incidence. We shall use the symbols $E_{\parallel}$ and $E_{\perp}$ for these cases, and write $P_{\parallel}$, $P_{\perp}$, for the currents per unit incident energy. We may note first that the rate at which energy is incident upon unit area of the surface, when the light vector is given by (1), is

$$\frac{2\pi\nu^2 \cos\theta}{c} |\mathbf{a}|^2. \tag{13}$$

3.2. $E_{\parallel}$ *case*—Taking for the vector potentials of the incident, reflected and transmitted beams the expressions given in I, equation (77), the emission per unit incident energy is found to be

$$\begin{aligned} P_{\parallel} = \frac{e^3 \nu_a \sin^2\theta}{4\pi^4 m^2 c \nu^4 \cos\theta} \left(\frac{\bar{\nu}}{\nu_0}\right)^{\frac{1}{2}} \int_{0,\,[\mu(\nu_a-\nu)]^{\frac{1}{2}}}^{(\mu\nu_0)^{\frac{1}{2}}} dk\, \frac{k^2(\mu\nu_0 - k^2)\{k^2 + \mu(\nu - \nu_a)\}^{\frac{1}{2}}}{[(k^2 + \mu\nu)^{\frac{1}{2}} + \{k^2 + \mu(\nu - \nu_a)\}^{\frac{1}{2}}]^2} \\ \times \left[\frac{\cos^2\varpi}{\mu^2\nu_a^2} \left| (k^2 - ipq)\frac{\mathbf{a}_{tx}}{\mathbf{a}_{ix}} + p(p + iq)\frac{\mathbf{a}_{ix} + \mathbf{a}_{rx}}{\mathbf{a}_{ix}} \right|^2 \right. \\ \left. + \tfrac{1}{2}\sin^2\varpi \frac{n^2 + \kappa^2}{\sin^2\theta} \left|\frac{\mathbf{a}_{tx}}{\mathbf{a}_{ix}}\right|^2 \right], \end{aligned} \tag{14}$$

θ being the angle of incidence. The values of $\mathbf{a}_{rx}$ and $\mathbf{a}_{tx}$ are obtained in I in terms of the optical constants by making the tangential components of electric and magnetic intensity continuous at the surface. Using the results of I, equation (78), introducing the notation

$$\left.\begin{aligned} \nu_g &= \nu_a - \nu_0 \\ k^2 &= \mu\nu_g X^2 \\ \nu_0 &= \varepsilon\nu_g \\ \nu &= \eta\nu_g \end{aligned}\right\}, \tag{15}$$

and converting the emission into Coulombs per calorie by multiplying by $1{\cdot}395 \times 10^{-2}$, we find

$$\begin{aligned} P_{\parallel} = C \frac{\varepsilon^{-\frac{1}{2}}\nu_g^{-1}(\bar{\nu}/\nu_g)^{\frac{1}{2}}}{(n^2+\kappa^2+\sin^2\theta)^2\cos^2\theta + 2n(n^2+\kappa^2+\sin^2\theta)\cos\theta + n^2 + \kappa^2\cos^2 2\theta} \\ \times \{\cos^2\varpi \sin^2\theta\cos\theta\,[\{(n^2+\kappa^2)^2 - 2(n^2-\kappa^2)\cos^2\theta + \cos^4\theta\}\,\zeta_1(\eta,\varepsilon) \\ + \{2(n^2 - \kappa^2 - \cos^2\theta) + 1\}\,\zeta_2(\eta,\varepsilon) + n\kappa\zeta_3(\eta,\varepsilon) + \zeta_4(\eta,\varepsilon)] \\ + \tfrac{1}{2}\sin^2\varpi\cos\theta\,(n^2 + \kappa^2)\,[\zeta_2(\eta,\varepsilon) + \zeta_4(\eta,\varepsilon)]\}. \end{aligned} \tag{16}$$

Here

$$C = \frac{64e^3}{h^2c} \,.\, 1{\cdot}395 \,.\, 10^{-2} = 7{\cdot}537 \times 10^{18}, \tag{17}$$

and the $\zeta_i(\eta, \epsilon)$ are certain integrals involving η and ϵ, defined in I, equations (84) to (87).

3.3. $E_\perp$ *case*—In the $E_\perp$ case, the only component of vector potential occurring is the *z*-component. Taking for the vector potentials of the incident, reflected, and transmitted beams the real parts of the products of $2\mathbf{a}_{iz}$, $2\mathbf{a}_{rz}$, $2\mathbf{a}_{tz}$, with the same exponential factors as in the $E_\parallel$ case, we find with the same boundary conditions

$$\left.\begin{aligned} \frac{\mathbf{a}_{rz}}{\mathbf{a}_{iz}} &= -\frac{(n - i\kappa) - \cos\theta}{(n - i\kappa) + \cos\theta} \\ \frac{\mathbf{a}_{tz}}{\mathbf{a}_{iz}} &= \frac{2\cos\theta}{(n - i\kappa) + \cos\theta} \end{aligned}\right\}, \tag{18}$$

and the emission per unit incident energy is found to be

$$P_\perp = C\frac{1}{\nu_g}\left(\frac{\bar{\nu}}{\nu_g}\right)\epsilon^{-\frac{1}{2}}\{\zeta_2(\eta, \epsilon) + \zeta_4(\eta, \epsilon)\}\frac{\frac{1}{2}\sin^2\varpi\cos\theta}{n^2 + \kappa^2 + 2n\cos\theta + \cos^2\theta}, \tag{19}$$

with the same notation as before.

Dependence upon Angle of Incidence

3.4—With these results we pass on to consider the dependence of $P_\parallel$ and $P_\perp$ upon the angle of incidence θ, the frequency being fixed. The experimental results on this point are all very similar in general trend. For perpendicular incidence the emissions are the same, the distinction between the two cases vanishing, and as the angle of incidence increases $P_\perp$ decreases steadily to zero. The emission $P_\parallel$ on the other hand increases at first slowly, then more rapidly, passes through a maximum for an angle of incidence in the neighbourhood of 60° to 80°, and then falls rapidly to zero at glancing incidence. These general results are always obtained, but there are very large variations in the values of the ratio of the greatest emission for $E_\parallel$ to that at normal incidence. This ratio, which we can take as measuring the polarization selectivity, can be as great as 200, or it may be as small as 2 or 3. Further, for the same specimen, it may show quite large variations with frequency, in many cases increasing rapidly with increasing frequency near the threshold, and subsequently decreasing. This is, however, connected with the phenomenon of spectral selectivity, and we shall not consider it further at the moment.

The theoretical results, given by (16) and (19), agree very well with the experimental results in general form, and the variation in the magnitude of the polarization ratio can be reproduced by allowing ϖ to vary suitably.

A further indication that the theory is on the right track is the fact that the higher observed values of the polarization ratio occur for highly reflecting surfaces, when a small value of ϖ would be expected. However, it must be admitted that to explain the smaller values of the polarization ratio we must postulate values of ϖ in the neighbourhood of 45°, and such values are not very plausible.

We must content ourselves with the above general remarks. A detailed comparison with experimental results would be of interest, but is not worth making until careful experiments have been made with properly outgassed metals.

SPECTRAL DISTRIBUTION CURVES WITH POLARIZED LIGHT

3.5—In the introduction we have mentioned briefly the experimental results obtained. In general, for the $E_{\parallel}$ case, the emission shows low order selectivity, while the normal effect is usually (though not invariably) observed in the $E_{\perp}$ case. It is unfortunate that no results have been obtained with thoroughly clean metals, but in the present section we accept the observed differences between the spectral distribution curves for $P_{\parallel}$ and $P_{\perp}$, and try to explain them in terms of the theory.*

We cannot proceed so rapidly as in the previous section on account of the necessity of knowing the values of the optical constants n and κ over a fairly wide range of frequencies. Unfortunately, this demands a much wider knowledge than experiment provides:† there are few metals whose optical constants are known with any precision for more than three frequencies above their photoelectric thresholds, and with such meagre results it is a hazardous matter to attempt to connect the points by a smooth curve, even without attempting extrapolation into the ultraviolet. Some such process must, however, be attempted if we are to explain the observed differences between the forms of the spectral distribution curves for the $E_{\parallel}$ and $E_{\perp}$ cases, which constitute one of the most puzzling aspects of photoelectricity. The only factors which can give rise to these differences are the optical constants n and κ, unless the roughness parameter ϖ is supposed to vary. Now there is a certain amount of justification for assuming ϖ to increase with frequency, when of course $J_{\perp}$ would increase more rapidly than $J_{\parallel}$. As the frequency increases, so the wave-length of the most energetic electron decreases, and the surface roughness then becomes greater compared with the mean wave-length of the emitted electrons, corresponding to an increase of ϖ. It is evident, however, that this increase of ϖ would hardly be sufficient to mask the theoretical maximum, for the $E_\perp$ case.

---

* It must be mentioned, however, that these differences are most pronounced for thin layers of metals only some molecules thick. Their occurrence for pure metals in bulk is doubtful, as it seems to be a general result that large values for the polarization ratio are not observed for bulk metals.

† Silver, of course, is exceptional, but its photoelectric properties have been studied only over a very small frequency range.

Now although experimental values of the optical constants are very scanty, there is no lack of theoretical values for these quantities: accordingly the possibility presents itself, of using theoretical values in place of the experimental values. Upon closer investigation, however, we find that this course does not lead us to any useful conclusions. We consider only the alkali metals, these being at the same time the most interesting, and the most thoroughly investigated.

Wood* has described the experimental optical properties of alkali metals, showing that beyond a certain threshold in the ultra-violet (3000 A for K, 4300 A for Cs) each metal becomes almost completely transparent, having a fairly high reflectivity at first, which falls off fairly rapidly. Unfortunately, he gives no measurements of n and κ, and we must call upon theory to fill in the gap. Without taking actual theoretical values, which are not in any good agreement with the experimental results, where such exist, we can say that theory† indicates that in the region of frequencies less than the critical frequency in the ultra-violet n is small, and κ in the neighbourhood of 1 to 3, while beyond this critical frequency, the position is reversed. Now had this frequency been close to the frequency of the observed spectral maximum for the particular metal considered, we might have expected the variation of the optical constants to produce the differences between the spectral distribution curves for the two planes of polarization: as it is the critical frequency lies too far in the ultra-violet, and the changes in the optical constants near the spectral maximum are not rapid enough to introduce a factor sufficient to cut out the maximum for the $E_\perp$ case.

Even if suitable variations of the optical constants were to occur, we should not necessarily expect to obtain agreement between theory and experiment along these lines, for rapidly varying optical constants would give evidence of the occurrence of a photoelectric volume effect, comparable with the surface effect. Conversely, the absence of such rapid changes in the optical constants indicates that the volume effect is inappreciable, and we cannot ascribe to its influence the observed behaviour of the metal towards polarized light.

---

* 'Nature,' vol. 131, p. 582 (1933); 'Phys. Rev.,' vol. 44, p. 353 (1933).

† *See*, for example, Wilson, 'Proc. Roy. Soc.,' A, vol. 151. p. 274 (1935), where a full discussion will be found.

It thus appears that the theory presented here can give no explanation of observed differences between the $E_{\parallel}$ and $E_{\perp}$ spectral distribution curves. It is, of course, possible that a rigid quantum mechanical treatment of the light wave, following Schiff and Thomas (*loc. cit.*), might yield the explanation desired,* but the complicated calculations required are not worth making until the experimental results are more definite. A prime necessity before any finality can be reached is a detailed study of the photoelectric properties and the optical constants of some thoroughly outgassed metal in bulk, over an adequate frequency range. When that is to hand, we can see just what features really do need explanation.

SPECTRAL DISTRIBUTION CURVES WITH UNRESOLVED LIGHT

3.6—We will conclude this section with a consideration of the spectral distribution curves for unresolved light. Here the experimental results must be compared with the mean of our expressions (16) and (19) for $P_{\parallel}$ and $P_{\perp}$, and hence the undetermined quantity ϖ occurs in the final result. We cannot then give one definite theoretical curve for a given metal, but must compare the experimental results with a set of curves obtained by varying the quantities ν_0 and ϖ. We shall show that in spite of the variability of these quantities, the order of magnitude of the emission (for angles of incidence *circa* 60°), and the general form of the spectral distribution curves, do not vary much, and that both features are in excellent agreement with such experimental results as are available.

We gave in fig. 1 of Paper I a series of curves showing the variation with frequency of the quantities $\zeta_i(\eta, \varepsilon)$, for the case $\bar{\nu} = \nu_g$. The same curves apply here for $\nu_0 = \nu_g$, and the general sense of the variation with ν_0 can be seen from fig. 1*a* here, which gives $\varepsilon^{\frac{1}{2}}\{\zeta_2(\eta, \varepsilon) + \zeta_4(\eta, \varepsilon)\}$ as a function of η $(= \nu/\nu_g)$, for a series of values of ν_0/ν_g, from 0·4 to 2·0. It will be seen that the effect of reducing ν_0 is to make the maximum sharper, and to shift it towards the threshold, while at the same time very slightly increasing the order of magnitude.

Now it is evident that this decrease of ν_0, taken by itself, could markedly improve the agreement between the theory and the experimental results of Suhrmann and Theissing† for potassium, already discussed in I. Unfortunately, however, it appears from more recent work that Suhrmann and Theissing's results cannot be taken as characteristic of pure potassium.

---

* This course may lead to an explanation of the peculiar photoelectric properties of thin films.

† 'Z. Physik,' vol. 52, p. 453 (1928–29).

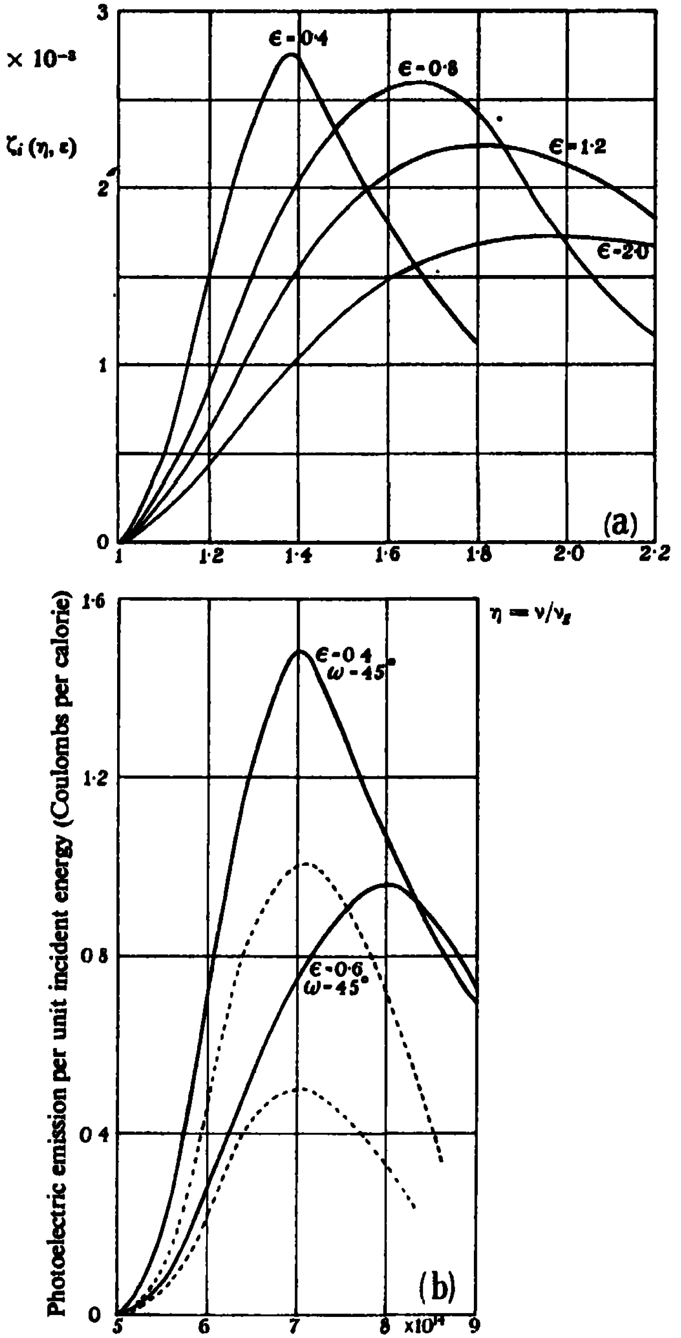

FIG. 1—(*a*) The function $\epsilon^{-\frac{1}{2}}\{\zeta_2(\eta, \epsilon) + \zeta_1(\eta, \epsilon)\}$ for various values of ε. (*b*) Theoretical and experimental spectral distribution curves for potassium, with unpolarized light. —— theoretical; - - - experimental.

Klauer† prepared clean surfaces of potassium by repeated distillations *in vacuo*, and obtained results with freshly distilled surfaces, shown dotted in fig. 1, *b*. These are of a lower order of magnitude than the results obtained by Suhrmann and Theissing, and Klauer observed further that the emission increased up to about the same values as these authors report, when his surfaces had stood for some hours. It seems likely, then, that the very low order of magnitude is characteristic of the pure metal, and we shall make Klauer's curves the basis for further comparison.

The experimental results, shown dotted in fig. 1, *b*, are given in two positions, corresponding to Klauer's estimate of the maximum order of magnitude as lying about 5–10 × 10^{-5} Coul/cal. The theoretical curve, calculated with the values $\theta = 60°$ (assumed), $\nu_u = \nu = 5 \times 10^{14}$, $n = 0{\cdot}068$,‡ $\kappa = 1{\cdot}5$,‡ $\varepsilon = 0{\cdot}4$, $\varpi = 45°$, shows good agreement in general form with the experimental results, but the order of magnitude is slightly too great, and the maximum perhaps not steep enough. The second theoretical curve, for $\varepsilon = 0{\cdot}6$, and the same values of the other quantities, shows the right order of magnitude, but a maximum too far from the threshold. If the Schiff and Thomas correction§ brings this maximum towards the threshold without altering the order of magnitude, this will evidently give very good agreement. The dubious point here is the value of ϖ. Taking $\varpi = 0$ gives a curve of approximately double the height of the curve shown, which spoils the agreement, and a value of ϖ as great as 45° seems to have very little meaning, though it is perhaps significant that a value of ϖ of this order is required to give results showing no polarization selectivity (*i.e.*, a polarization ratio of about 2 or 3).

3.61—We may ask ourselves now what interpretation is to be put upon the quantity ν_0 which is determined by getting the best possible fit with experimental results. Were our theory less idealized, we could expect to determine the " effective mass " m^* of the electrons in the metal, defined by the equation analogous to (3),

$$(8\pi^2 m^*/h)\,\nu_0 = (3\pi^2 n)^{\frac{1}{3}}, \tag{20}$$

so that

$$m^*/m = \nu/\nu_0. \tag{21}$$

Regarded in this way, the effective mass for potassium is seen to be about $2{\cdot}5m$.

Now there are three factors here which can affect the value of ν_0/ν_u. In the first place, the optical constants have been assumed independent of frequency in calculating the theoretical curves. Their variation over the range considered is slow, and would hardly affect the results appreciably. Secondly, it is doubtful to what extent the use of more accurate wave functions inside the metal, and of a less idealized potential barrier, would affect the results. With an effective mass of $2 \cdot 5m$ some difference would certainly be expected, but with smaller values it should not be very great. Thirdly, Schiff and Thomas (*loc. cit.*) have shown that the quantum mechanical treatment of the light wave introduces a correcting factor, which tends to bring about the same changes as does lessening ν_0. This fact must be considered, and in view of it it is evident that we must regard the value of m^*, obtained above, as an upper limit to the effective mass of a conducting electron in potassium. The true effective mass is probably much nearer m, and the corrections above, other than the Schiff and Thomas correction, inappreciable.

---

† 'Ann. Physik,' vol. 20, p. 909 (1934).

‡ 'Int. Critical Tables,' vol. 5, p. 249.

§ *See* § 3.61.

3.62—Further comparison with experiment would be interesting, but is hardly worth making without more information as to the absolute order of magnitude of the photo-current. Kluge† gives suitable results for carefully outgassed caesium, finding a threshold near 6000 A, a weak spectral maximum at 4400 A, and an order of magnitude only 3×10^{-5} at maximum. It is evident without going into greater detail that these results are in reasonably good agreement with our theory.

Suhrmann‡ also gives results for platinum, gold, and silver; but these, unfortunately, cannot be used, in the case of the first two because of lack of knowledge of the optical constants, and in the case of silver because Suhrmann's results are certainly not characteristic of the pure metal. His threshold value is 2970 A, whereas the accepted value for the pure metal§ is 2610–2700 A. It is unfortunate that the absolute order of magnitude has not been given for the heavy metals in a very pure state, as this is the only point with which the theory may be compared, the range of frequencies over which experiments can be made being very small.

ENERGY AND VELOCITY DISTRIBUTION FUNCTIONS

4.1—The usual experimental methods enable us to obtain three distinct velocity or energy distribution functions. Using the method of retarding potentials with concentric spheres or parallel plates we obtain voltage current curves, from which by differentiation the total and normal energy distribution functions can be obtained. These functions give the numbers of electrons emitted with given total energy, or with a given normal energy, understanding by the latter term the kinetic energy of the normal component of velocity. The third distribution function, obtained by magnetic deflexion of the emitted electrons, gives the total velocity distribution for electrons emitted in a certain direction from the (plane) cathode.

---

† 'Z. Physik,' vol. 93, p. 636 (1934–35).

‡ *See* the curves given in Hughes and Du Bridge, "Photoelectric Phenomena," fig. 3.3 (McGraw Hill, 1932).

§ Winch, 'Phys. Rev.,' vol. 37, p. 1269 (1931).

None of these distribution functions has been discussed fully from the theoretical side, if we except Fröhlich's† discussion of the total energy distribution for thin films, and Du Bridge's‡ discussions of the temperature-dependent high energy tails of the curves, for the normal and total energies. To the latter we have nothing to add, since the assumptions made by Du Bridge in deriving his results are seen to be valid in terms of the exact theory.

TOTAL ENERGY DISTRIBUTION§

4.2—Let $g(\mathrm{E})\,d\mathrm{E}$ denote the number of emitted electrons with total energy between the limits E, E + dE. Modifying I, equation (33), by removing the signs of integration, we find the number of electrons emitted from bound states with wave numbers in the ranges k to $k + dk$, etc., will be proportional to

$$\frac{k^2\{k^2+\mu(\nu-\nu_a)\}^{\frac{1}{2}}}{[(k^2+\mu\nu)^{\frac{1}{2}}+\{k^2+\mu(\nu-\nu_a)\}^{\frac{1}{2}}]^2} \times \frac{dk\,dk_y\,dk_z}{1+\exp h^2(k^2+k_y^2+k_z^2-\mu\bar{\nu})/8\pi^2mk\mathrm{T}}. \tag{22}$$

The corresponding total energy is

$$\mathrm{E} = h^2(k^2+k_y^2+k_z^2)/8\pi^2m + h(\nu-\nu_a). \tag{23}$$

Introducing spherical polar coordinates $\mathrm{E}^{\frac{1}{2}}$, ϑ, ϕ, such that

$$\left.\begin{aligned} &\left(\frac{8\pi^2m}{h^2}\mathrm{E}\right)^{\frac{1}{2}}\cos\vartheta = \{k^2+\mu(\nu-\nu_a)\}^{\frac{1}{2}} \\ &\left(\frac{8\pi^2m}{h^2}\mathrm{E}\right)^{\frac{1}{2}}\sin\vartheta\cos\phi = k_y, \qquad \left(\frac{8\pi^2m}{h^2}\mathrm{E}\right)^{\frac{1}{2}}\sin\vartheta\sin\phi = k_z \end{aligned}\right\}, \tag{24}$$

---

† 'Ann. Physik,' vol. 7, p. 103 (1930).

‡ 'Phys, Rev.,' vol. 43, p. 727 (1933).

§ To obtain a simple result it is essential to neglect the effect of refraction and reflexion of the light wave. The various expressions occurring in the integrands of $\zeta_l(\eta, \epsilon)$ do not differ sufficiently for this course to introduce any serious errors. This remark applies equally to all three distribution functions. For the total energy only, surface roughness has no effect.

we have

$$\{k^2 + \mu(\nu - \nu_a)\}^{-\frac{1}{2}}\, k\, dk\, dk_y\, dk_z = \tfrac{1}{2}\mathrm{E}^{\frac{1}{2}}\, d\mathrm{E} \sin\vartheta\, d\vartheta\, d\phi \left(\frac{8\pi^2 m}{h^2}\right)^{\frac{3}{2}}, \quad (25)$$

and making this substitution above and integrating with respect to ϑ and ϕ, we shall have

$$g(\mathrm{E})\, d\mathrm{E} \propto \int_0^{\pi/2} d\vartheta \int_0^{2\pi} d\phi \frac{\{\mathrm{E}\cos^2\vartheta + h(\nu_a - \nu)\}^{\frac{1}{2}}\, \mathrm{E}^{\frac{1}{2}} \cos^2\vartheta \sin\vartheta\, d\mathrm{E}}{\{\mathrm{E}^{\frac{1}{2}}\cos\vartheta + (\mathrm{E}\cos^2\vartheta + h\nu_a)^{\frac{1}{2}}\}^2 \left\{1 + \exp\dfrac{\mathrm{E} - h(\nu - \nu_a)}{k\mathrm{T}}\right\}},$$

i.e.,

$$g(\mathrm{E})\, d\mathrm{E} \propto \frac{\mathrm{E}^{\frac{1}{2}}\, d\mathrm{E}}{1 + \exp\{\mathrm{E} - h(\nu - \nu_a)\}/k\mathrm{T}}$$

$$\times \int_0^{\pi/2,\ \cos^{-1}\left\{\frac{h(\nu - \nu_a)}{\mathrm{E}}\right\}^{\frac{1}{2}}} \frac{\{\mathrm{E}\cos^2\vartheta + h(\nu_a - \nu)\}^{\frac{1}{2}} \cos^2\vartheta \sin\vartheta\, d\vartheta}{\{\mathrm{E}^{\frac{1}{2}}\cos\vartheta + (\mathrm{E}\cos^2\vartheta + h\nu_a)^{\frac{1}{2}}\}^2}, \quad (26)$$

where the upper limit of integration is $\pi/2$, if $\nu < \nu_a$, and

$$\cos^{-1}\{h(\nu - \nu_a)/\mathrm{E}\}^{\frac{1}{2}},$$

if $\nu > \nu_a$. Introducing a new variable y in place of $\cos\vartheta$, we have

$$g(\mathrm{E})\, d\mathrm{E} \propto \frac{\mathrm{E}^{\frac{1}{2}} d\mathrm{E}}{1 + \exp\{\mathrm{E} - h(\nu - \nu_a)\}/k\mathrm{T}} \int_{0,\ \left\{\frac{h(\nu - \nu_a)}{\mathrm{E}}\right\}^{\frac{1}{2}}}^{1} \frac{y^2\{\mathrm{E}y^2 + h(\nu_a - \nu)\}^{\frac{1}{2}}\, dy}{\{\mathrm{E}^{\frac{1}{2}}y + (\mathrm{E}y^2 + h\nu_a)^{\frac{1}{2}}\}^2}. \quad (27)$$

The function g (E) is shown in fig. 2, *a*, for the case of potassium, ($\nu_0 = 5 \,.\, 10^{14}$, $\nu_a = 10^{15}$, T = 300° K), and may be compared with recent results of Brady† for this metal in a very highly outgassed state, shown in fig. 2, *b*, for two wave-lengths of the incident light. The abscissae in fig. 2, *b*, represent electron-volts, and the curves have not been reduced to relative energy values, as the threshold of Brady's specimen was not known. The comparison thus is somewhat indefinite, but the agreement in general form is seen to be excellent. Earlier curves, however, obtained with less well outgassed metals,‡ were of rather a different form, having a maximum at an energy in the neighbourhood of one-half or less of the greatest energy. Lukirsky and Prilazaev,§ in fact, found this form to be characteristic of a metal in bulk, while a thin layer gave a curve more like the theoretical curve. These results are, however, in

---

† 'Phys. Rev.,' vol. 46, p. 768 (1934).

‡ *See* the general discussion in Hughes and Du Bridge, "Photoelectric Phenomena," chap. IV (McGraw Hill, 1932).

§ 'Z. Physik,' vol. 49, p. 236 (1928).

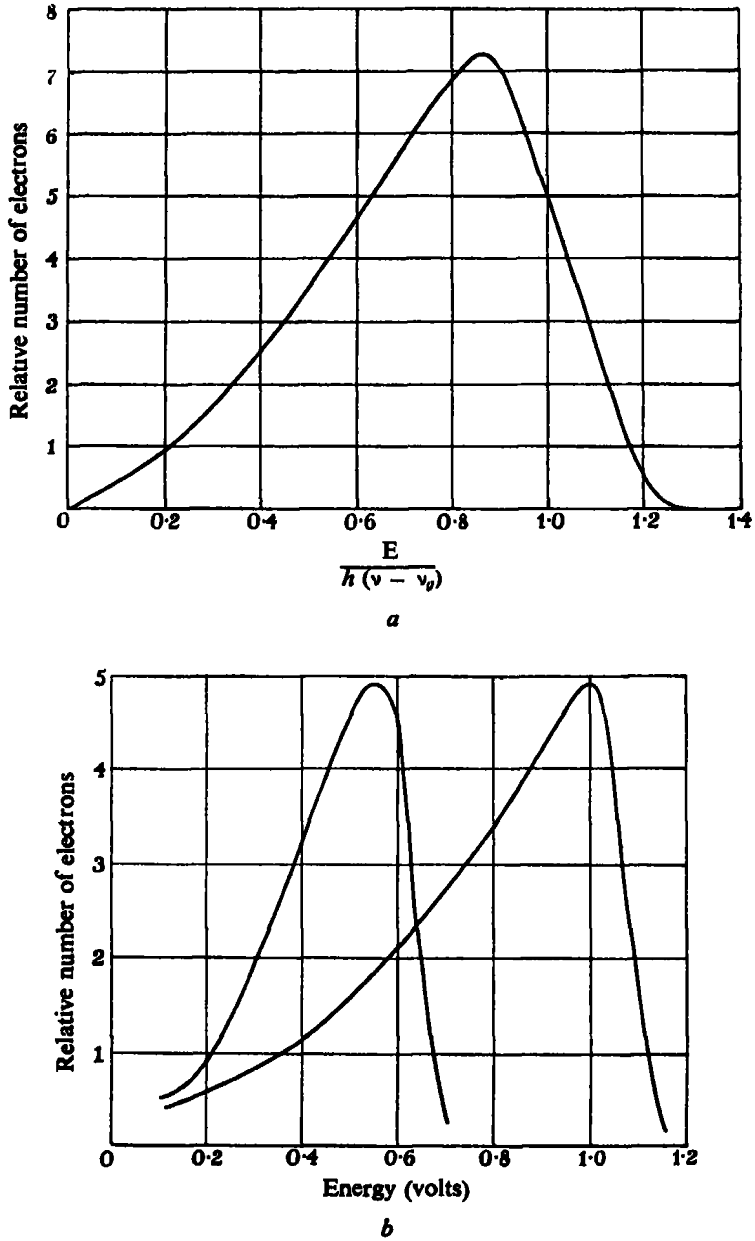

FIG. 2—(*a*) Total energy distribution curve for potassium. Theoretical. (*b*) Experimental total energy distribution curves for potassium (Brady).

direct contradiction to those of Brady, who found the energy distribution curves to be almost independent of film thickness up to about 30 molecular layers, at which thickness he had found earlier† that the thin film possessed the photoelectric characteristics of the metal in bulk.

ENERGY DISTRIBUTION BY MAGNETIC DEFLEXION‡

4.3—When the energy distribution is observed by magnetic deflexion experiments, only those electrons are observed which leave the metal surface in a definite direction, depending upon the experimental arrangement, inclined at an angle ϑ, say, with the normal. If we take this direction as lying in the *xy*-plane, and consider an electron escaping with velocity v, its component wave numbers inside the metal will be

$$\left.\begin{array}{l} k = \{(2\pi m v \cos\vartheta/h)^2 + \mu\nu_a - \mu\nu\}^{\frac{1}{2}} \\ k_y = 2\pi m v \sin\vartheta/h, \qquad k_z = 0 \end{array}\right\} . \tag{28}$$

The number of electrons with k, k_y, k_z, inside ranges dk, dk_y, dk_z, being given by (22), we replace $k\,dk$ by $r\,dr$, where $r^2 = k^2 + \mu\nu - \mu\nu_a$, and $dr\,dk_y$ by $v\,dv\,d\vartheta$, omitting numerical factors. The elements $d\vartheta$ and dk_z are then numerical constants, which may be omitted, and we shall have for the number of electrons emitted in the given direction with total velocity between v and $v + dv$

$$\mathrm{F}(v)\,dv \propto \frac{k\,(k^2 + \mu\nu - \mu\nu_a)\,v\,dv}{(q+r)^2\{1 + \exp h^2(k^2 + k_y^2 + k_z^2 - \mu\nu)/8\pi^2 mk\mathrm{T}\}}, \tag{29}$$

which gives, expressed in terms of v,

$$\mathrm{F}(v)\,dv \propto \frac{v^3\{v^2 + 2h(\nu_a - \nu)/m\cos^2\vartheta\}^{\frac{1}{2}}\,dv}{\{v + (v^2 + 2h\nu_a/m\cos^2\vartheta)^{\frac{1}{2}}\}^2\{1 + \exp[\frac{1}{2}mv^2 - h(\nu - \nu_g)]/k\mathrm{T}\}}. \tag{30}$$

The function $\mathrm{F}(v)$ is plotted as a function of v for a typical case (potassium, $\nu_g = 5 \times 10^{14}$, $\nu_a = 10^{15}$, $\mathrm{T} = 300°$ K) in fig. 3, *a*. The curve there given is for $\nu = 6 \times 10^{14}$, and $\vartheta = 0$, but curves for other values of ϑ, and for $\nu = 8\text{–}10 \times 10^{14}$, lie so close to the curve given as to be indistinguishable from it, except in the fact that the drop on the high velocity side becomes steeper the greater the frequency.

---

† 'Phys. Rev.,' vol. 41, p. 613 (1932).

‡ Here, and in the next section, we should take into account the effect of surface roughness, but the calculations, unfortunately, are rather complicated.

These results are in qualitatively good agreement with experiment[†] both as regards the form of the curves and the approximate independence

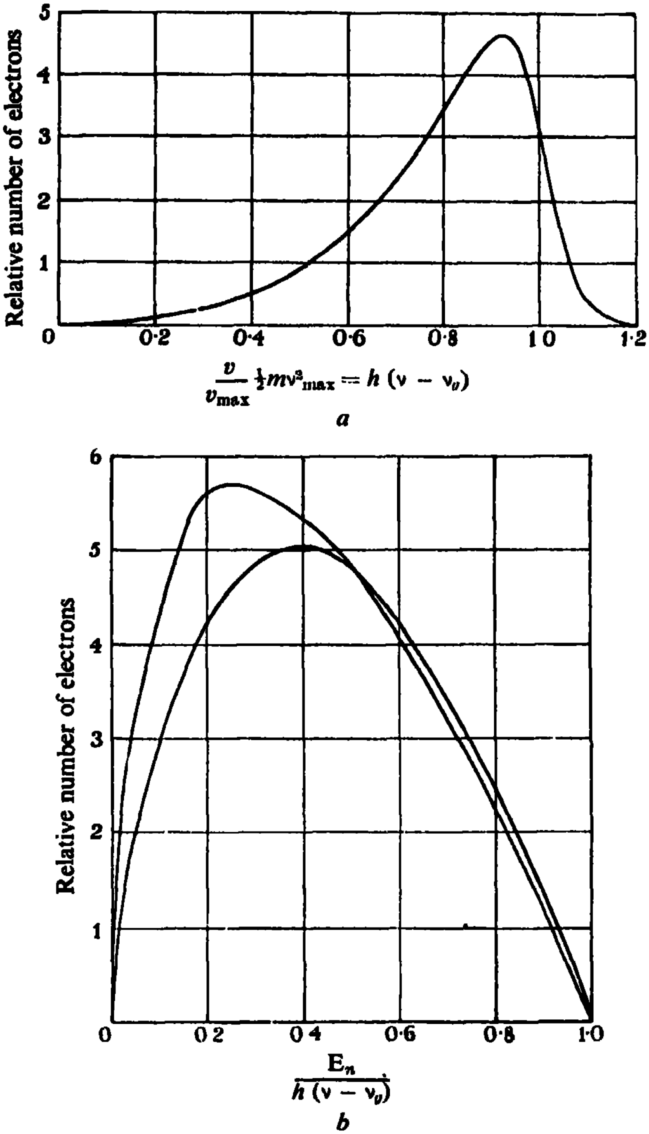

FIG. 3—(*a*) Theoretical velocity distribution curves for magnetic deflexion experiments. (*b*) Theoretical normal energy distribution.

of form and frequency. It is a further experimental result that curves for different metals can be brought into approximate coincidence by plotting $v/v_{\max}$ and adjusting the scale suitably: this, too, appears from our results, as it is evident that (30) is given effectively by

---

[†] *See* Hughes and Du Bridge, § 4.2, figs. 4.4, 4.5, 4.6.

$$\mathrm{F}(v) \propto \frac{v^3 \text{ or } v^4}{1 + \exp\{\frac{1}{2}mv^2 - h(\nu - \nu_a)\}/k\mathrm{T}}. \tag{31}$$

It must be remarked that the theoretical ratio of the most probable to the highest velocity is rather too high, but against this we must balance the fact that the experimental results have been obtained with imperfectly outgassed metals.

NORMAL ENERGY DISTRIBUTION

4.4—Defining normal energy to mean the kinetic energy

$$h^2(k^2 + \mu\nu - \mu\nu_a)/8\pi^2m,$$

associated with the velocity component normal to the surface, of the escaping electron, let $f(\mathrm{E}_n)\,d\mathrm{E}_n$ denote the number of electrons emitted with normal energy between the limits E_n to $\mathrm{E}_n + d\mathrm{E}_n$. Then from (2) the number of escaping electrons for which k lies in the range k to $k + dk$ is proportional to

$$\frac{k^2(\mu\bar{\nu} - k^2)\{k^2 + \mu(\nu - \nu_a)\}^{\frac{1}{2}}\,dk}{[(k^2 + \mu\nu)^{\frac{1}{2}} + \{k^2 + \mu(\nu - \nu_a)\}^{\frac{1}{2}}]^2}, \tag{32}$$

neglecting temperature dependence.

Now

$$\mathrm{E}_n = h^2(k^2 + \mu\nu - \mu\nu_a)/8\pi^2m, \tag{33}$$

$$d\mathrm{E}_n = h^2k\,dk/4\pi^2m, \tag{34}$$

hence

$$f(\mathrm{E}_n)\,d\mathrm{E}_n \propto \frac{\mathrm{E}_n^{\frac{1}{2}}\{\mathrm{E}_n + h(\nu_a - \nu)\}^{\frac{1}{2}}\{h(\nu - \nu_a) - \mathrm{E}_n\}\,d\mathrm{E}_n}{[\mathrm{E}_n^{\frac{1}{2}} + (\mathrm{E}_n + h\nu_a)^{\frac{1}{2}}]^2}. \tag{35}$$

Typical curves are shown in fig. 3, *b*, again for the case of potassium, and can be seen to differ considerably from the two energy distribution curves previously given. The two curves shown, calculated for widely different values of the frequency, lie close together, showing that this distribution curve, like the others, is almost independent of frequency.

The author wishes to take this opportunity of repeating his thanks to Professor R. H. Fowler and Mr. A. H. Wilson for their constant interest in and encouragement with the work.

SUMMARY

5—The theory of the surface photoelectric effect in metals, due to the author, is applied to calculate spectral distribution curves for polarized and unpolarized light, and energy distribution curves. It is shown that a selective maximum, and a high degree of polarization selectivity, are immediate consequences of the theory, as originally proposed; further, by taking into account surface roughness, a possible explanation of the absence of polarization selectivity is given. This modification, however, can throw no light on the difference between the spectral distribution curves obtained for light polarized parallel and perpendicular to the plane of incidence, nor indeed on the so-called " normal " spectral distribution curves, which show no maxima.

Excellent agreement with experimental results on alkali metals is found for the spectral distribution curves with unpolarized light, both as regards order of magnitude and the general form of the curve. For other metals comparison cannot be made, as the appropriate experimental results are lacking.

The total energy distribution curves are given, and are in excellent agreement with the recent work of Brady, though not with some earlier results. They show a most probable energy quite close to the maximum energy of emission, agreeing with Fröhlich's results for thin films. The magnetic deflexion velocity distribution curves are also in satisfactory agreement with experiment, and the normal velocity distribution curves are also given.

Ultra-Violet Absorption of Ice

By E. J. CASSEL

(*Communicated by F. A. Lindemann, F.R.S.—Received August* 7, 1935)

[PLATE 9]

INTRODUCTION

It was proposed to compare the absorption spectra of condensed substances with their absorption in the gaseous state, as little is known of the nature of the light absorption process in solids, and it was hoped to discover the effect upon the molecular terms of embedding the molecules in a crystal lattice.* A vacuum spectrograph was used with fluorite prisms and lenses transparent down to a wave-length of 1400 A.

Water was first employed as a test substance because the technique is simple. As a gas it has no discrete bands in this region—or to be more accurate, only very weak and diffuse ones, superimposed on a broad absorption continuum.† However, the results proved of some interest—especially as the spectra of light and heavy ice could be compared in the same way as has been done by Franck and Wood‡ for water vapour.

EXPERIMENTAL PROCEDURE

Water vapour was condensed on a fluorite window cooled in the following way. The inner member of the Dewar vessel D, fig. 1, containing liquid air, has a chrome-steel bottom C sealed to the glass in the way developed by Philips of Eindhoven. It was found that liquid air could be safely poured onto the joint. Screwed to the chrome steel is a copper block B, surrounding the fluorite window W—15 mm in diameter—on which the vapour is condensed. B is cut away on one side, so that the window may be observed. The whole inner part of the Dewar vessel is inserted into the outer part by means of a ground joint G, and can be removed to clean and inspect the window. For the experiments with water vapour the vessel was silvered.

---

* Vegard ('Z. Physik,' vol. 75, p. 30 (1932)) has investigated the emission spectrum of solid N_2 down to the temperature of liquid helium, and P. Pringsheim and Kronenberger ('Z. Physik,' vol. 40, p. 75 (1927)) the absorption of solid benzene at liquid air temperatures. The light absorption of solid oxygen was investigated by McLennan, Smith, and Wilhelm, 'Trans. Roy. Soc. Canada,' vol. 24, III, p. 65 (1930), and Prikhotko, Ruhemann, and Frederitenko, 'Phys. Z. Sowjet,' vol. 7, p. 410 (1935).

† S. W. Leifson, 'Astrophys. J.,' vol. 63, p. 73 (1926); G. W. Rathenau, 'Z. Physik,' vol. 87, p. 32 (1933).

‡ J. Franck and Wood, 'Phys. Rev.,' vol 45, p. 667 (1934).

The window was illuminated by the hydrogen discharge tube H, the continuous spectrum of hydrogen being used as a background. The light then passed into the spectrograph *s*. This was a fluorite prism spectrograph of the type described by Cario and Schmidt-Ott.* The dispersion at 1600 A is about 15 A/mm, and the spectrum is of fairly high intensity. The lines of the molecular hydrogen spectrum and the mercury line 2537 were used as standards. The photographs were taken on Schumann plates from Hilger. In an experiment liquid air was put in the vessel and the window allowed to cool for about 4 hours. Water vapour was then admitted through the glass jet J and condensed on the fluorite.

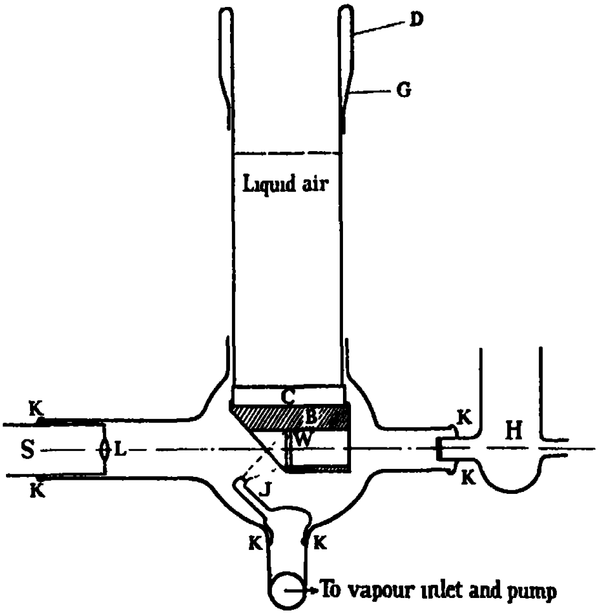

FIG. 1. — · — Light path; KKK wax seals.

The chief difficulty was to make an estimate of the thickness of the film. This was done finally in the following way. Water in the vessel A, fig. 2, was distilled *in vacuo* into B. The bottle C, of known volume, was then evacuated and the tap between B and C opened. The temperature in B was kept constant (by a jacket of melting ice), and 1 hour was allowed for the vapour to attain equilibrium. Then the tap between B and C was shut and the known mass of vapour in C admitted through the glass jet J to the Dewar vessel. In order to arrive at the lowest possible limit for the thickness of the film it was assumed that if ω be the solid angle subtended by the window W at J, the fraction of the vapour coming from C condensed on the window is $\omega/2\pi$. The justification for this is discussed later.

---

* 'Z. Physik,' vol. 69, p. 719 (1931).

The estimated thickness of the film made in this way was 3–4 μ. It was invisible on the window. However, a film about five times as thick showed many cracks, and one could not be certain that the observed weakening of the light was not due to irregularity of the film.

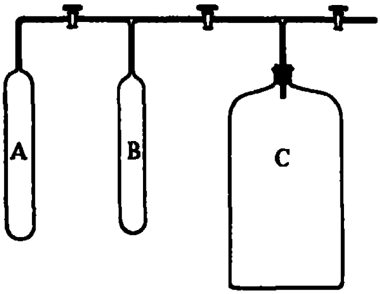

Fig. 2.

Results

The thin films of ice used showed a continuous absorption with a long wave-length limit at about 1670 A, which varied only slowly with the thickness of the film, indicating an abrupt rise in the coefficient of absorption. The limit for heavy ice was slightly displaced towards short waves, as may be seen from fig. 5, Plate 9.

That there is a shift is very clear, but it is not easy to measure owing to the number of hydrogen lines in this part of the spectrum. The value obtained was

$$\Delta\nu = 1300 \pm 250 \text{ cm}^{-1}.$$

This is definitely of the same order as that found by Franck and Wood for water vapour (about 1100 cm^{-1}).

The films of heavy and light ice were distilled in the way described under identical conditions, so that uncertainty in the estimated thickness makes no difference here—the two films must have been equally thick. The spectra were recorded on the same plate with the same exposure and discharge current in the hydrogen tube.

The absorption spectra of ordinary water vapour and ordinary ice were also recorded on the same plate with the same exposure, fig. 6, Plate 9. The long wave limit of the vapour absorption lay between 1780–1790 A, as was found by Leifson and Rathenau (*loc. cit.*). The limit of the ice absorption was displaced towards short waves by an amount

$$\Delta\lambda > 120 \text{ A}$$

or

$$\Delta\nu > 4700 \text{ cm}^{-1}$$

or

$$\Delta w > 0{\cdot}58 \text{ volt.}$$

The error in the measurement of the plate may be expected to amount to about 10%. The figures given must be regarded as a lower limit, owing to the uncertainty about the thickness of the film, but this would lead if anything to a rather higher value.

For instance, the volume of vapour, at 0° C, admitted through the jet J was 2·7 litres. The fraction condensing on the window, according to the estimate given above, was 1/30. Since the area of the window was about 1·5 cm^2, the equivalent length of the column of vapour (at 5 mm pressure) condensed on the window was $l = 60$ cm. The length of the absorption path in the vapour photograph (also taken at 5 mm pressure) was $l' = 16$ cm.

Thus the absorbing mass of ice in fig. 6, *d*, Plate 9, is at least four times more than that of vapour in *b*, apart from the uncertainty in the estimate of the fraction condensed on the window. To get a rough idea of the effect of different film thicknesses on the absorption limit, experiments were made which showed that the edge moved about 500 cm^{-1} for a factor of 3 to 4 in the thickness. One has to consider the factor 4 mentioned above and a further factor k, due to the assumption about the jet, which may well be of the same order. For the jet was directed at the middle of the window, and one would expect that, if anything, a greater proportion of the vapour would condense on this than is given by the solid angle. For both these reasons the value of 0·6 volts for the displacement must be regarded as a lower limit—the true value is, however, unlikely to exceed 0·7 volts.

While investigating different film thicknesses some very thin films were photographed in the hope of finding discrete bands corresponding to those reported by Leifson and Rathenau for vapour, but without success. However, these discrete bands are stated to be extremely weak and diffuse.

So far the displacement has been considered from the point of view of the long wave limit, and it must be pointed out that the possibility of measuring it depends on the steepness of the absorption curve.

Of course, to make a true comparison of the two bands would involve photometric measurements, which cannot be made with Schumann plates.

But one may get further purely qualitative evidence of the reality of the shift by considering the absorption maximum. In photographs of vapour at low pressures, fig. 6, *c*, Plate 9, the centre of the band is seen to be somewhere about 1650–1700 A, while the strong hydrogen lines in the neighbourhood of 1600 A come through somewhat weakened. *See* rough diagram fig. 3 of absorption curve, which is only intended to be qualitative. In a corresponding photograph of a thin ice film in which the lines at 1600 A are transmitted at about the same strength as in the vapour experiment, there is no absorption in the region 1700 A. Fig. 6, *e* and *f*, Plate 9, of thin films of ice show very markedly the stronger absorption near 1600 A, compared with vapour absorption *c*, and the weaker absorption near 1700 A. Now, unless in ice the maximum of the absorption band is shifted considerably towards short waves, a film which partly absorbs the lines at 1600 A should certainly completely absorb the continuum at 1700 A, for the lines are much stronger than the continuum.

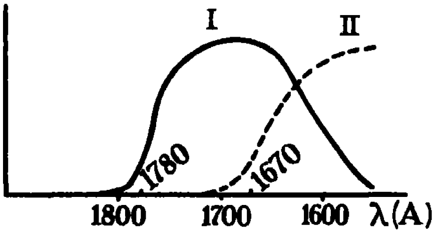

FIG. 3. —— vapour; - - - ice.

The dotted curve in fig. 3 is meant to give a qualitative idea of the ice absorption curve.

DISCUSSION

Since very little is known of the structure of solids and of the nature of the light absorption process in them, it is impossible to give an exact explanation of the phenomena. Nevertheless, one may attempt to account for them in the following qualitative way.

The observation that the absorption of heavy ice begins at a shorter wave-length than that of light ice, and that the amount of the displacement is of the same order as that found by Franck and Wood for water vapour, make it reasonable to seek to explain the mechanism of absorption in a similar way. Franck and Wood regard the absorption as taking place from a lower stable state, the ground state of the molecule, to an upper unstable state, characterized by a repulsion curve, and leading to dissociation into neutral H and OH. They account for the different absorption of heavy water vapour by the different zero point energies present in the two isotopes in the ground state.

The assumption that the molecules in ice still have, to some extent, a separate existence would be in agreement with the theory of ice postulated by Fowler and Bernal,* while the work of Plyler† also shows that the infra-red frequencies of ice do not differ greatly from those of vapour water.

Fig. 4, used by Franck and Wood to explain the absorption of vapour, has only a very limited validity in our case, but probably sufficient for the following rough deductions.

The curves of fig. 4, *a*, represent the potential energies V of the ground state and of an excited state (repulsion curve) in ice as a function of the distance *r* between the H and OH. The right-hand part of the curve is dotted to indicate the increasing uncertainty at large distances. The line AB represents the energy $h\nu$ corresponding to the long wave limit. In fig. 4, *b*, the transition for vapour is shown. Here CD represents the energy absorbed at the long wave limit. For simplicity only the levels are given. To provide an explanation of the facts we try the following assumptions.

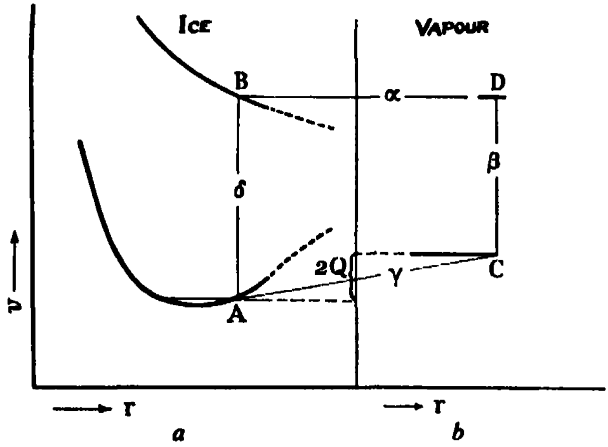

FIG. 4.

1—The equilibrium distances *r* are roughly the same both in ice and vapour.

2—The final state, which exists only in the moment of the electron transition, has a negligible dipole moment compared with the ground state. This is the hypothesis we wish to test by comparison with the observations.

---

* Fowler and Bernal, 'J. Chem. Phys.,' vol. 1, p. 515 (1933).

† Plyler, 'J. Amer. Opt. Soc.,' vol. 9, p. 545 (1924).

3—The part of the lattice energy of a molecule due to forces other than electrostatic ones (van der Waals's forces—forces of repulsion, etc.) is small compared with the binding energy due to the electric moment, and does not change greatly in the transition to the excited state.

To quote Fowler and Bernal, by far the greater part of the cohesion of ice is due to the electrostatic interaction of the molecules.

The energy states in ice can be compared with those in water vapour by means of a cyclic process ($\alpha\beta\gamma\ \delta$) in fig. 4.

The step AB—as before mentioned—represents excitation of a molecule in the lattice. In the moment of the transition the molecules in the neighbourhood will not have time to change their positions much, so that the energy of orientation of the surrounding lattice may be regarded as constant. This is an assumption of the same kind as that made in deriving the Franck-Condon principle for transitions between molecular terms.

The step AC represents the removal of a normal lattice molecule from the interior of the crystal to infinity. As the surroundings are supposed to be left unchanged, this is twice the heat of sublimation Q, where $Q = 0 \cdot 5$ volts. (The factor 2 is due to the fact that in finding the lattice energy per molecule, or heat of sublimation, the mutual energy of each molecule pair is counted twice.) CD represents the energy of excitation of a free gas molecule, the lattice still remaining unchanged, while DB represents the replacing of an excited molecule in the hole in the lattice which is waiting to receive it. According to assumptions 2 and 3, this requires only a negligible amount of work.

Thus the process would give a shift of the ice absorption limit towards higher frequencies by 2Q or 1 volt. The experiment gives a probable value between $0 \cdot 6$ and $0 \cdot 7$ volt.

If the inaccuracy of assumption 1 is allowed for, the calculated value would probably be rather lower. This would introduce into the cycle a step of expanding the H and OH in the excited state before putting it back in the lattice—since the molecules in ice are probably larger than those in vapour. A change of size in the ground state would not involve an appreciable energy change.

Therefore, provided that the whole method of argument is justifiable, we conclude that assumption 2 is not far from the truth, *i.e.*, the electronic excitation produces a marked decrease in the dipole moment. Although this was originally only postulated *ad hoc* to explain the facts it can now be regarded, to some extent, as a conclusion from experiment.

However, there is an analogy to it in the absorption of the alkali halides.* In that case the ground state is an ionic one, with certainly a

---

* Franck, Kuhn, and Rollefson, 'Z. Physik,' vol. 43, p. 155 (1927).

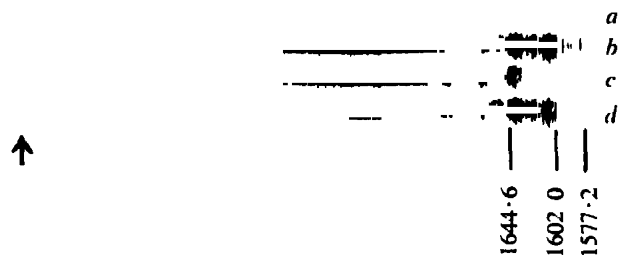

Fig. 5—*a*, light ice; *b*, comparison spectrum; *c*, heavy ice; *d*, comparison spectrum. The arrow marks the position of the line 2537 A, which is not visible here.

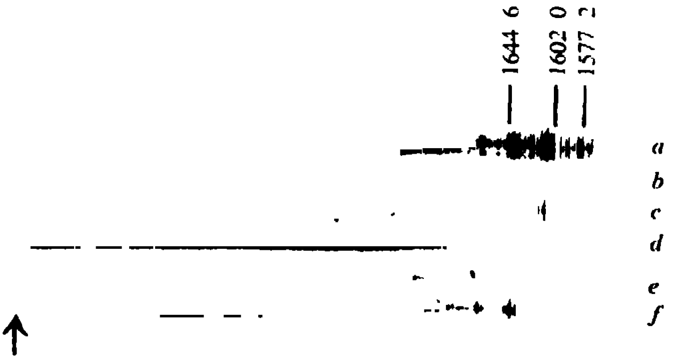

Fig. 6—*a*, comparison spectrum; *b*, vapour absorption, to be compared with *d*; *c*, vapour absorption, low pressure; *d*, ice absorption; *e* and *f*, thin films of ice. The arrow marks the position of the line 2537 A, which is not visible here.

strong dipole moment, and the final state of the absorption is an unstable state leading to dissociation into neutral atoms. It is quite safe to assume that this upper state has a very small dipole moment. Although in water the bond is certainly not a purely ionic one, a strong decrease of the polarity during the electron jump is by no means improbable.

Finally, since the absorption of heavy ice lies further in the ultra-violet than that of plain ice the dispersion of heavy ice in the visible might be expected to be less than of plain ice. The same should apply to water because the arrangement of the molecules in water is known to be very like that in ice. This has actually been found by Luten* and others who have compared the dispersion of light and heavy water.

In conclusion, my thanks are due to Professor J. Franck (late of Gottingen University) for proposing the problem, to Professor F. A. Lindemann, F.R.S., of Oxford, for assistance in the discussion of the results, and to Dr. H. Kuhn for continued advice and encouragement.

SUMMARY

The absorption of thin films of ice has been measured in the extreme ultra-violet. The absorption band of ice is found to be shifted towards short waves, relatively to that of vapour by 0·6 to 0·7 electron volts.

Further, the absorption of heavy and light ice has been compared and a shift of the heavy ice absorption towards short waves found, amounting to about 1300 cm^{-1} (= 0·16 electron volts)—*i.e.*, of the same order as was observed by Franck and Wood for water vapour.

These results are discussed in the light of existing theories of the structure of ice and a tentative explanation is put forward. It is then shown that these results were compatible with measurements on the dispersion of light and heavy ice made elsewhere.

---

* Luten, 'Phys. Rev.,' vol. 45, p. 167 (1934); Tilton and Taylor, 'Bur. Stand. J. Res.,' vol. 13, p. 207 (1934).

Investigations on the Preliminary Stages of Spark Formation in various Gases by the use of the Wilson Chamber

By U. Nakaya, D.Sc., Professor of Experimental Physics, and F. Yamasaki, Lecturer in Physics, Faculty of Science, Hokkaido Imperial University, Sapporo, Japan

(*Communicated by C. T. R. Wilson, F.R.S.—Received August* 12, 1935)

[Plates 10–17]

1—Introduction

Since the appearance of Rogowski's investigation of the spark discharge by a cathode ray oscillograph as well as those of Dunnington and others using a Kerr cell, the physical investigations on the spark formation have undergone almost a complete transformation. The previous theory of the ionization by collision of positive ions was modified to the theory of the electron avalanche proposed by Frank, v. Hippel, and others. In this stage of the investigation it is most important to get thorough knowledge on the preliminary stages of spark formation immediately preceding the main spark. For this purpose the authors* have tried to study the production and distribution of ions associated with the initial stages of spark formation by using the Wilson chamber, and have confirmed the possibility of its application. Almost simultaneously Snoddy and Bradley,† and Kroemer‡ published the results of their experiments which were quite similar to those in our investigation.

In our previous experiments an influence machine was used as the high voltage source and a pendulum for the synchronization of the expansion of the chamber and the application of the voltage impulse. It was difficult, however, by these methods to keep the voltage constant and to avoid undesirable distributed inductance of the circuit. In the new series of experiments the influence machine was replaced by a system of transformer, kenotron, and condenser, and an apparatus of special design was used for the purpose of the synchronization in place of the pendulum. With this apparatus thus developed cloud photographs were taken of sparks in various gases and air mixed with small quantities of some organic vapours, the results of which will be described in this paper. Raether's recent paper* deals with similar experiments in nitrogen, carbonic oxide, and hydrogen. Some of his photographs are similar to ours, but most of them are quite different, as will be described below.

---

* ' Nature,' vol. 134, p. 496 (1934); ' Proc. Roy. Soc.,' A, vol. 148, p. 446 (1935).

† ' Phys. Rev.,' vol. 45, p. 432 (1934); vol. 47, p. 541 (1935).

‡ ' Arch. Elektrotech.,' vol. 28, p. 403 (1934).

2—EXPERIMENTAL APPARATUS

This series of experiments was carried out with a larger cloud chamber than that used in the previous study. The chamber was 17 cm in diameter and 7·5 cm in depth, and into it point and plate electrodes of the same dimension as the previous ones were introduced through two quartz tubes. The distance between the electrodes was kept at 25 mm throughout the experiment, and the electrode surface was polished with the finest emery paper and cleaned carefully almost every time before the beginning of a series of experiments.

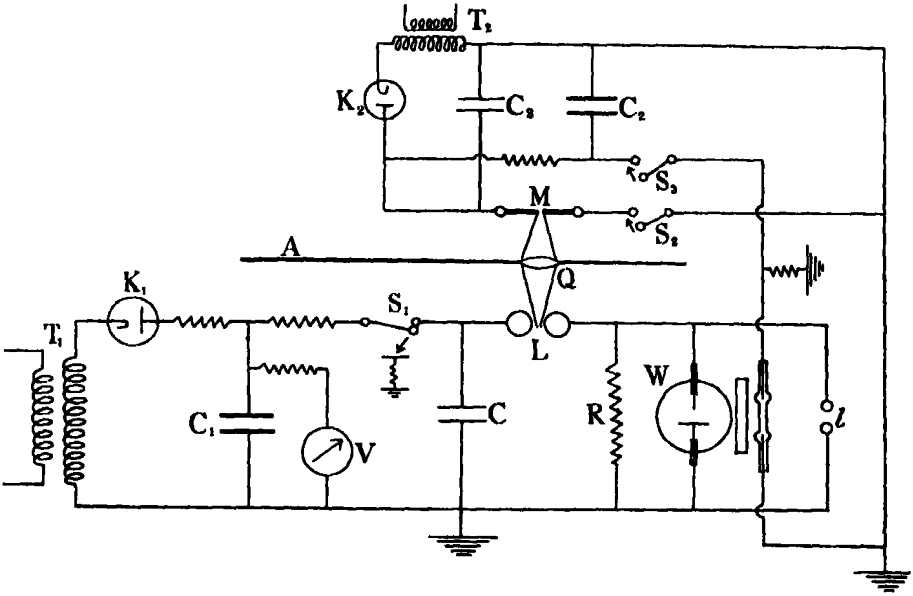

FIG. 1.

The electrical circuit is shown in fig. 1. The principle is the same as in the previous experiment, that is, the successive stages of the suppressed spark are examined by varying the distance of the secondary gap *l*. The system consisting of transformer T_1, kenotron K_1, and the condenser C_1

---

* ' Z. Physik,' vol. 94, p. 567 (1935).

of the capacity 0·25 mF is the source of the required high voltage, which is measured by an electrostatic voltmeter V. C is a Leiden jar of 30 m capacity and this is the source of the electricity whose discharge is to be examined. S_1 is a switch with a spring operated by an electromagnet: it serves to cut off the system of the high voltage source just before the Leiden jar is discharged. The electrodes of gap L consist of two brass spheres each 6 cm in diameter, and this gap is used as a gap switch to send the voltage impulse. In this series of experiments L is usually kept at 10 mm and the potential is gradually raised to the corresponding sparking potential 30 kV. At that point the voltage is still maintained for a short duration owing to the time lag of the spark. When a strong beam of ultra-violet light from the magnesium gap M is focussed onto the electrode L through a quartz lens Q at a moment within this time duration, a spark passes at L and the impulse is sent to the chamber, this being synchronized with the expansion of the chamber. This method was also used independently by Snoddy and Bradley (*loc. cit.*) in their experiment on the same problem. For the nice operation of this mechanism it is necessary to raise the voltage applied to L very slowly and the surface of the cathode of L is left in an uncleansed condition. The method of illumination is by a heavy discharge of a condenser through mercury vapour using a source of 0·25 mF and 20 kV. C_3 is a Leiden jar of 60 m capacity and serves as the source of the ultra-violet light. S_2 and S_3 are the switches operated with electromagnets and springs and are constructed to lessen the time lag of operation to as short a time as possible, S_2 being used for sending ultra-violet light and S_3 for illumination. A metal screen A is set between the main circuit and that for illumination in order to prevent a mutual induction of the circuits. For the expansion of the chamber a vacuum method was used, and the gum bung connexion to the vacuum was suddenly pulled apart by a mechanism using strong springs. A metal rod was projected from the side of the piston of the chamber so that by its motion the circuit of the electromagnet S_2 was first closed, and then that of S_3. The time interval between the closures of these two circuits was adjusted by trial to give the best result. The voltage applied to the ceiling of the chamber was cut off just before the expansion by the motion of the rod that pulls apart the gum bung.

When taking the photographs, it is only necessary to watch the gradual rise of the needle of the voltmeter V, and when it reaches 30 kV to throw in a switch. Then switch S_1 is operated to cut off the circuit of the high voltage source and after a suitable time interval the chamber is expanded automatically, and as a result of the motion of the piston first the ultra-violet light is sent to the gap to send the impulse to the chamber and then the illuminating discharge takes place. The mechanism of operating the switches was so adjusted that the impulse was sent to the chamber immediately after the expansion was completed.

For the nice operation of the mechanism above described it is important that the switches be constructed to work with definite and shortest time lag. Special precautions, were taken in their construction, two of them are shown in figs. 2 and 3. Fig. 2 shows the design of the trigger for the expansion of the chamber. The mode of operation will be understood by the arrows shown in the diagram. The piece A is made of tempered steel, the sharp edge of which acts as a trigger. The arm B serves to cut off the voltage applied to the ceiling of the chamber. This mechanism is almost similar to that used by Professor Nishina, by whose kind advice

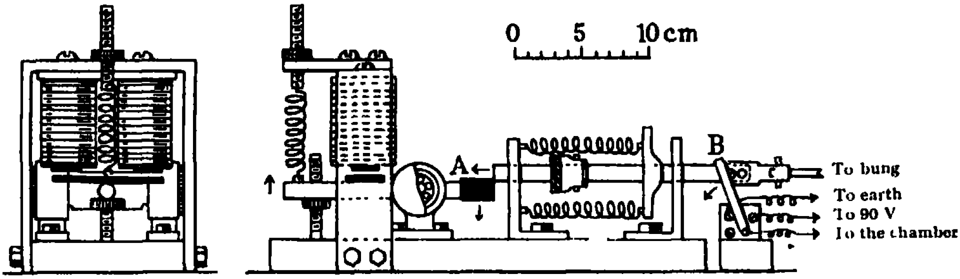

FIG. 2.

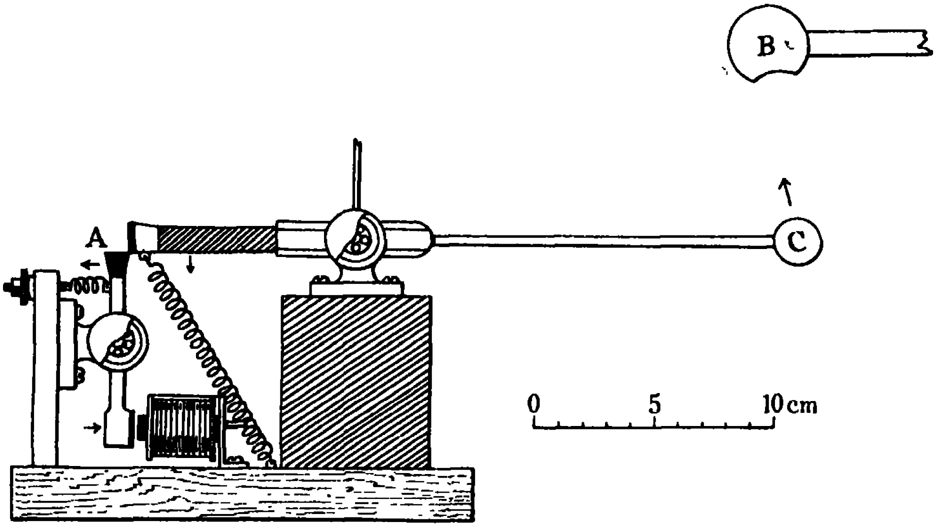

FIG. 3.

it has been constructed. As the synchronization of sending the ultra-violet light and the expansion of chamber is most important, the switch S_2 must be constructed with care. A diagram of it is shown in fig. 3. The principle is similar to that shown in fig. 2. A is a piece of tempered steel and the shaded parts are made of bakelite. The ball B is made of lead in order to lessen the mechanical shock when it receives the brass ball C.

3—PRELIMINARY EXPERIMENTS IN AIR

Preliminary experiments in air were carried out with the gap distances 15 mm and 25 mm and many photographs of positive and negative discharges were taken for various distances of l, increasing from $l = 1$ mm up to 10 mm at every 1 mm step.

In order to study the effect of changing the expansion ratio, photographs were taken for positive discharges with the ratio $s = 1\cdot33$ and then the ratio was decreased step by step to 1·07, keeping the other conditions as constant as possible. An unexpected result was obtained, viz., the ion cloud was observed with a value as small as $s = 1\cdot07$ and its form remained qualitatively almost the same. Between $s = 1\cdot33$ and $s = 1\cdot20$ no difference was observed at all, and below 1·18 it was noticed that the ion cloud was less dense and the streamers became shorter in length. It is well known that the expansion ratio below 1·25 is too small for the condensation of water vapour on ordinary ions. Most of the nuclei, therefore, produced by the preliminary discharge of spark are to be considered as different from ordinary ions, being probably larger. C. T. R. Wilson* observed similar nuclei in point discharge or when the air was illuminated by strong ultra-violet light. He suggested that these nuclei may be due to some chemical compounds as nitric acid in the former case and hydrogen peroxide in the latter. It is quite natural to consider that those chemical compounds are produced by the discharge in our case, and act as the condensation nuclei with smaller expansion ratio. Most of the photographs were taken with $s = 1\cdot22$ except those for hydrogen and carbon dioxide, for which the ratio 1·31 was chosen.

Photographs of the positive and negative clouds in air without inserting any special resistance or inductance in the circuit are shown in fig. 4*a*, *b*, and fig. 5*a*–*c*, Plate 10. The distance between the needle and plate electrodes was always kept at 25 mm in these and also in the following experiments, the potential applied to L being 30 kV throughout. With the present apparatus the reproducibility and the fineness of the form and structure of the cloud were much improved over those reported in the previous paper. When the needle is positive and l is shorter, the cloud takes the form of a small spindle or a bundle of spindles with a few branched streamers of well-defined form, one example for $l = 4$ mm being shown in fig. 4*a*. Increasing the value of l the spindle is extended and tends to be divided into a bundle of thin spindles or bands. The streamers increase in number and grow in length, many branchings occurring along the paths. The case when $l = 8$ mm is reproduced in fig. 4*b*. The characteristics of the branched streamers are similar to those of the gliding brush discharge on a photographic plate. When the discharge develops to this state, faint luminous brushes of bluish violet tint are observed in darkness between the electrodes. When l is increased to 9 mm, the form of the ion cloud is not much altered, the photograph of this stage is reproduced in fig. 15*a*, Plate 16. The comparison of these two pictures will show the order of the reproducibility of the form of ion cloud with the present apparatus. The condition when $l = 9$ mm shows the state of the distribution of ionized canals just before the main spark occurs. With $l = 10$ mm a brilliant spark passes the gap in the chamber instead of l, when a dense fog appears in the chamber and the streamers are blown away by an electric wind. This state will be described later when describing the conditions for nitrogen.

---

* 'Phil. Trans.,' A, vol. 192, p. 410 (1899).

When the needle is negative, the form of the cloud is quite different. The photographs for $l = 3$, 6, 8, and 9 mm are shown in fig. 5*a*–*c*, Plate 10, and fig. 15*d*, Plate 16. A few small spindles grow from the point of the electrode when l is shorter and they develop into a bundle of ribbons for larger values of l, all being diffuse in character without sharp boundaries. Some short streamers with branchings, seen in the photographs, we consider at present are due to an electrical oscillation of the circuit.

4—PRELIMINARY DISCHARGES IN VARIOUS GASES

The mode of the preliminary discharges in various gases was studied under the same conditions as in air, which were kept as constant as possible throughout the experiments both in electrical and mechanical senses. The gases examined were nitrogen, oxygen, hydrogen, carbon dioxide, and nitrogen oxide, each of which was purified by washing with suitable reagents.

1. *Nitrogen*—A cylinder of commercial nitrogen was used as the source. The oxygen admixed was removed by washing with a solution of ammonia containing pieces of metallic copper and then by passing it over heated

copper. The residual oxygen was again removed by bubbling the gas through an alkaline solution of pyrogallol. The gas was finally washed with a dilute solution of sulphuric acid and passed into the previously evacuated chamber.

The form of the preliminary discharge in nitrogen is very beautiful with a delicate and complicated structure. The positive clouds for various l are shown in fig. 6*a–d*, Plate 11, and the negative clouds in fig. 8*a–c*, Plate 12. When the needle is positive, a small and diffuse cloud of brush form appears on the tip of the needle for $l = 1$ or 2 mm. The picture of this state is not reproduced in the Plate, but the appearance is quite similar to the negative cloud of oxygen for $l = 3$ mm, fig. 10*a*, Plate 13. Increasing l to 3 mm, thin and sharply defined streamers with distinct branchings develop from the electrode, as shown in fig. 6*a*, Plate 11. These streamers appear also for $l = 2 \cdot 5$ mm but not for $l = 2$ mm, and it seems that the limit of the voltage for producing these streamers is rather sharply defined. When l is increased further, these streamers develop in length and branchings and at the same time some ribbons of fair width but distinct boundaries begin to appear. These ribbons also show some branchings, and it appears that the stem part of the streamers of tree-like branchings grow wider and form the ribbons. This state of things is clearly shown in the photographs of clouds for $l = 5$ mm and 7 mm, fig. 6*b*, *c*, Plate 11. The branched streamers develop into their extremely complicated forms at $l = 10$ mm, as is shown in fig. 6*d*. They are 20–30% greater in length than those in air and the branching is remarkable. This picture shows the state of things immediately preceding the occurrence of the main spark discharge. Sometimes by chance the main spark passes this gap with the same l, when a dense fog is formed along the track of the spark and it is blown aside in an explosive manner by the strong electric wind. The mode of propagation of the wind is clearly shown in fig. 7, Plate 12. It is of interest to see that ions formed by the spark are scattered over such a wide range, although only the bright line of the spark track can be observed by the naked eye or by taking a photograph. When once a spark passes in the chamber, the nuclei persist for a long time, say 1 hour, giving a dense background for the succeeding photographs. At least some of these persisting nuclei may be the aerosol of metals detached from the electrode. It is well known that the occurrence of spark is much facilitated after the first spark has passed the gap, especially in a closed chamber. Our photograph suggests that the abundant nuclei produced by the preceding spark may play some important role in addition to the known fact that the electrode surface is modified by the spark.

In the negative discharge, the branched streamers characteristic of the positive cloud do not show themselves at all. The photographs for $l = 3$, 7, and 9 mm are shown in fig. 8*a*–*c*, Plate 12. These negative clouds in nitrogen appear quite different from those in air in that no spindle is observed in this case and the discharge takes a short branched form, showing a plume-like appearance. The plumes are extended in length for increasing l. The state just before sparking over is shown in fig. 8*c*.

2. *Oxygen*—The gas from a cylinder of commercial oxygen was washed with a solution of potassium hydroxide and sent into the chamber. The appearance of the clouds in oxygen is quite different from those in air or nitrogen both in positive and negative cases. The positive discharge takes the form of branched streamers with minute zigzag structures, and it is decidedly shorter than that in nitrogen, being less than one-half in length. No ribbon-like streamer is observed. Three photographs of positive clouds are reproduced in fig. 9*a*–*c*, Plate 13. More marked difference is observed with a negative cloud; in all cases for $l = 2$–9 mm they are very short in point of length and consist of needle-like lines radiating out from the surface of the electrode. Even for $l = 9$ mm the longest track extends only 8 mm from the point of the electrode. The features of the clouds are well shown in fig. 10*a*–*c*, Plate 13. Comparing the clouds in air, nitrogen, and oxygen, it may be seen that those in air and nitrogen are to some extent similar to each other but that in oxygen the cloud is far different from any in either air or nitrogen both in magnitude and in character.

3. *Carbon Dioxide*—Carbon dioxide was manufactured from pieces of marble and hydrochloric acid in the usual way. It was more difficult to cause the cloud to appear in this gas than in the other gases examined, and the expansion ratio that gave the best result was 1·31. Three photographs of positive clouds and the corresponding negative ones taken with this ratio are reproduced in figs. 11*a*–*c*, and 12*a*–*c*, Plate 14. The mode of the discharge in this gas was characterized by the facts that the positive and negative clouds bear resemblance with each other in their forms and the negative cloud is always larger in size than the corresponding positive one. In both cases of the positive and negative discharges, the clouds consist of branched streamers, which have complicated structure, but the shape is not distinctly defined. The ramifications are more intricate in the negative discharge, which appears exceptional to the apparent rule that the branchings occur with the positive discharge.

4. *Hydrogen*—Hydrogen was made by a Kipp's apparatus from zinc and sulphuric acid in the usual manner and sent into the chamber after bubbling through solutions of silver nitrate, potassium permanganate, and pyrogallol. It was also difficult to cause the cloud to appear in this gas, and the expansion ratio was chosen as 1·31. The positive cloud takes the form of a bundle of thick, smooth bands with diffuse boundaries, as shown in fig. 13*a–c*, Plate 15. The band appears to keep itself constant in length and the bands increase in number for increasing l; for example, one band is seen for $l = 5$ mm, four for 7 mm, and seven for 9 mm. It is well known that a long spark in hydrogen takes the form of a smooth line while the corresponding one in air takes a zigzag form like a lightning path. The form of the preliminary discharge in hydrogen indicates the smoothness of the spark track. It must be remarked that very often a small dot of cloud appears at the tip of the electrode as shown in fig. 13, *a* and *b*, being a feature peculiar to hydrogen. Increasing l further, a bright spark passes in the chamber at $l = 10$ mm, as shown in fig. 14*a*, Plate 15. In this case the fog is, as with nitrogen, blown away by an electric wind, but it is much lighter in density and no trace of streamer is observed. The negative cloud in hydrogen is more difficult to obtain than the positive, and usually no cloud is observed, or light cloud appears all over the space in the chamber, especially when l is shorter. For larger l a diffuse broad band appears in the gap. One example for l - 10 mm is shown in fig. 14*b*, Plate 15.

5. *Nitrogen Oxide*—Nitrogen oxide was manufactured from metallic copper and nitric acid. This gas was chosen for discovering the effect, if any, of nitrogen combined with other elements. Clouds with any definite form were very difficult to obtain in this gas both for positive and negative discharges. Usually a dense fog appeared in a wide range surrounding the needle electrode, and it was sometimes observed that a small cloud of a brush form, say 5 mm in length, appeared on the tip of the needle. Many photographs were taken, but without success, by varying the expansion ratio between 1·25 and 1·31.

5—THE EFFECT OF ADMIXTURE OF ORGANIC VAPOUR TO AIR

It is well known that a long spark in air takes the form of a zigzag or lightning path when the electric field is sufficiently non-homogeneous. In previous experiments it was found that this form can be turned into a smooth curved line by admixing a small quantity of some organic vapour

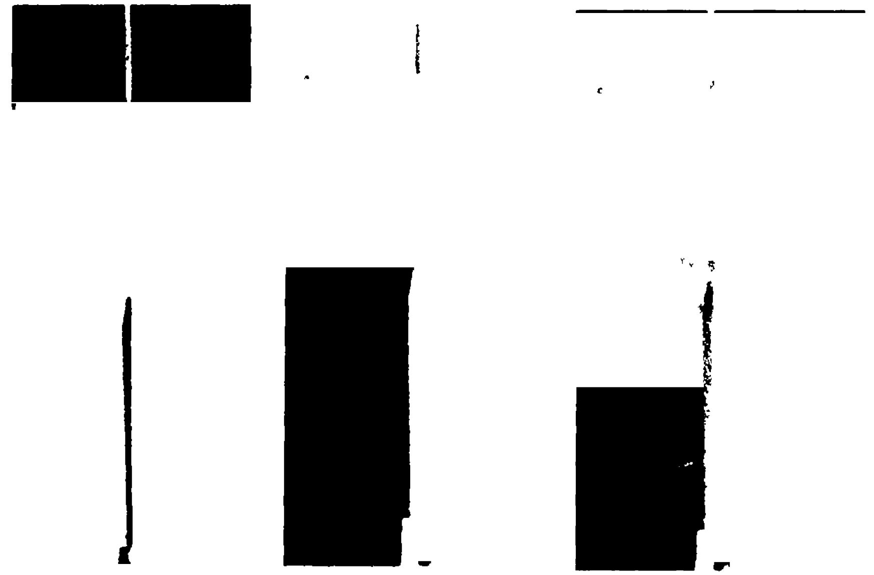

a $l = 3$ mm

b $l = 6$ mm

c $l = 8$ mm

Fig. 5—*a–c*, air negative.

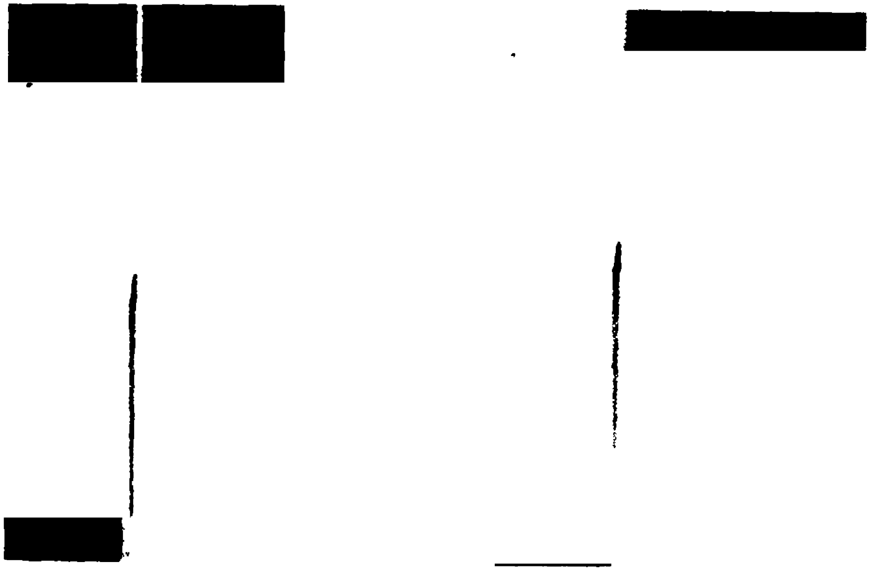

a $l = 4$ mm

b $l = 8$ mm

Fig. 4—*a*, *b*, air positive.

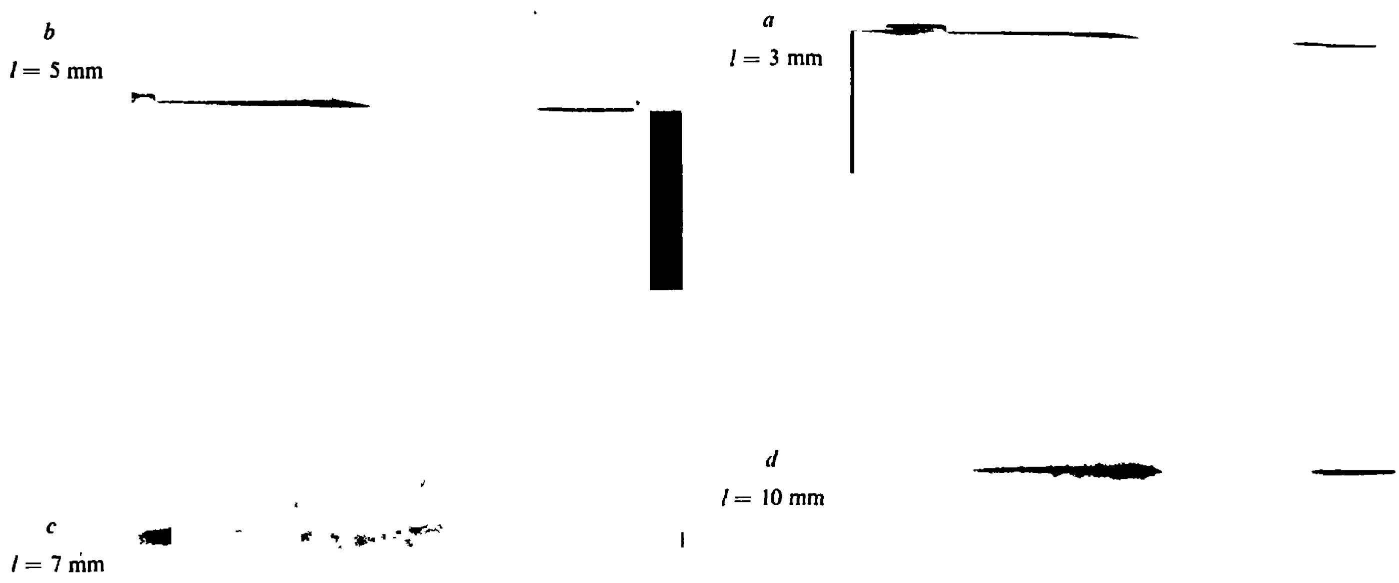

FIG. 6—*a–d*, nitrogen positive.

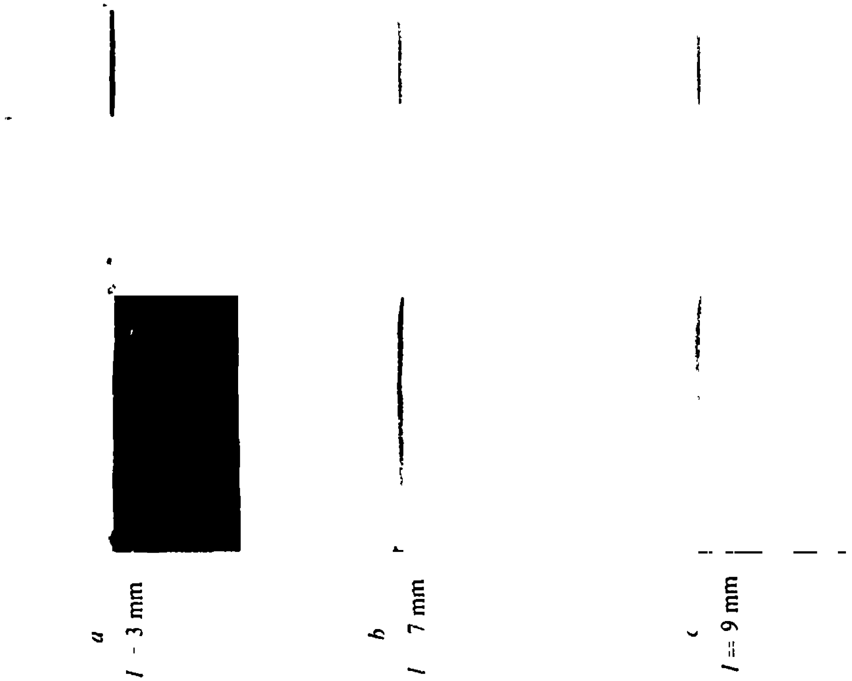

FIG. 8—*a–c*, nitrogen negative.

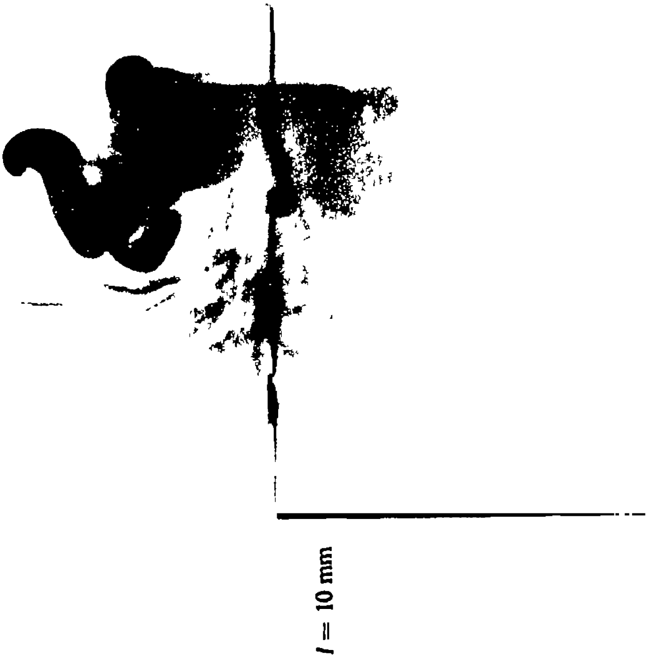

FIG. 7—Nitrogen positive.

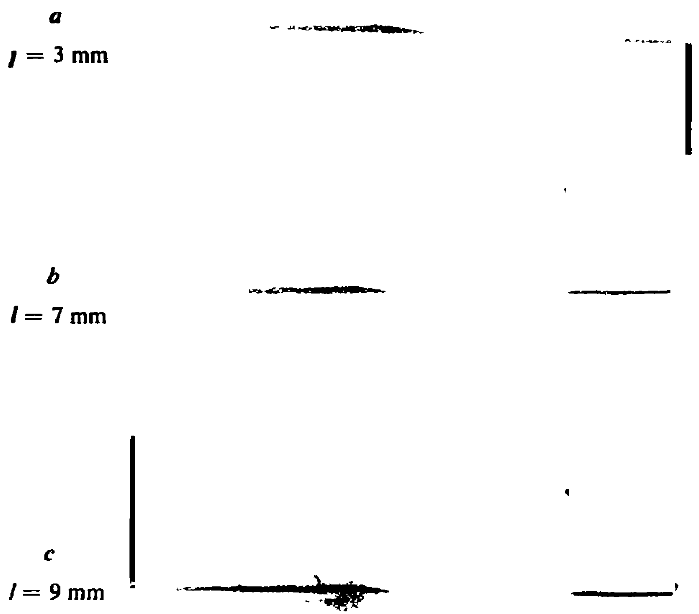

FIG. 9—*a–c*, oxygen positive.

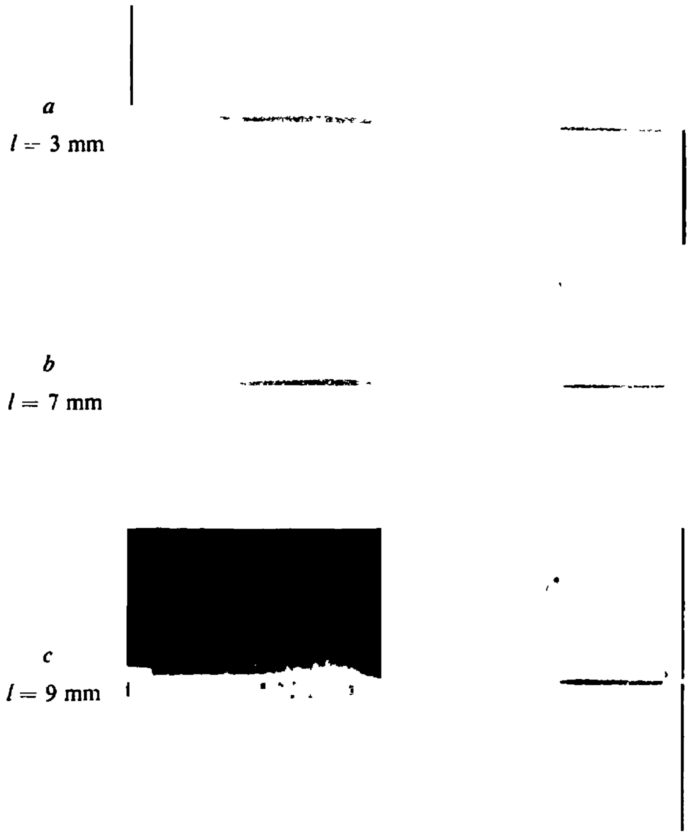

FIG. 10—*a–c*, oxygen negative.

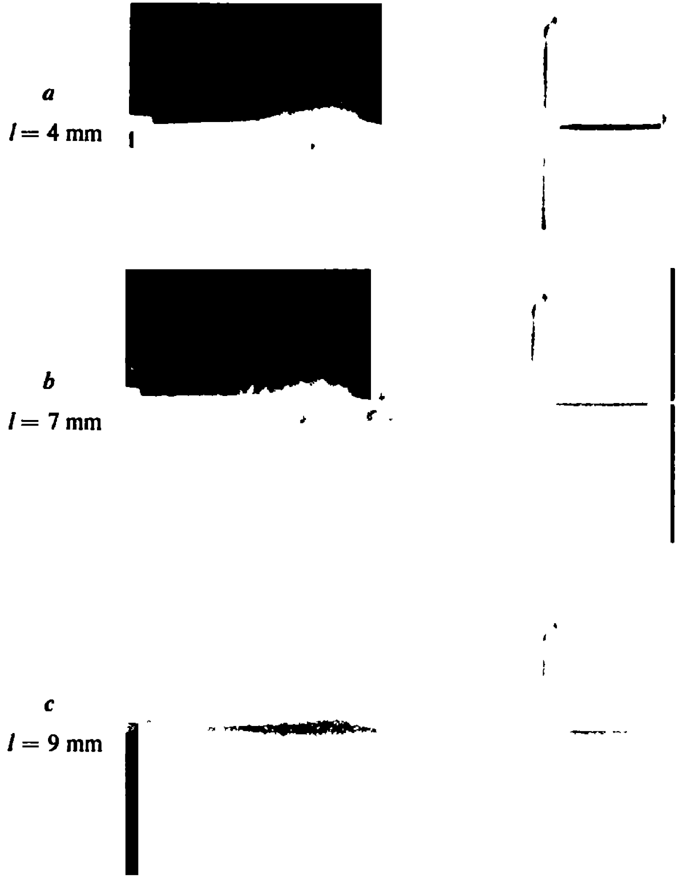

a $l = 4$ mm

b $l = 7$ mm

c $l = 9$ mm

FIG. 11—*a–c*, CO_2 positive.

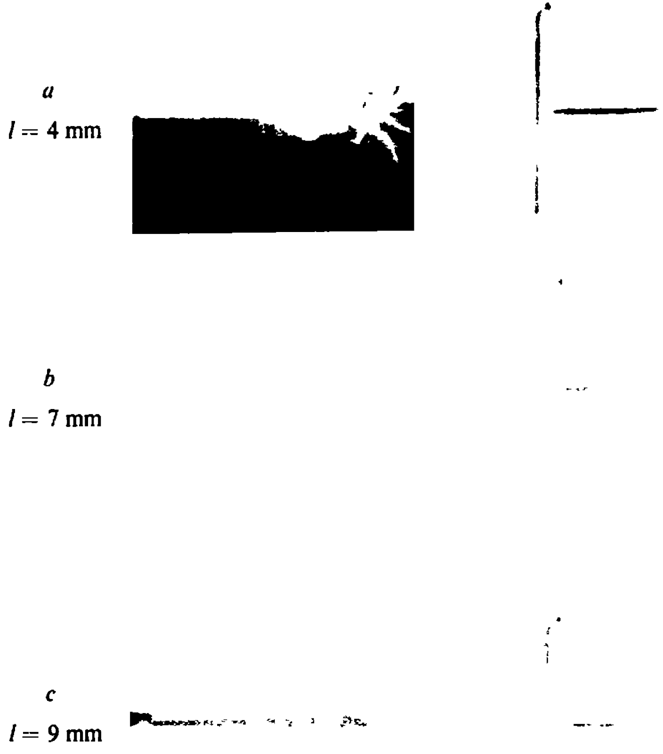

a $l = 4$ mm

b $l = 7$ mm

c $l = 9$ mm

FIG. 12—*a–c*, CO_2 negative.

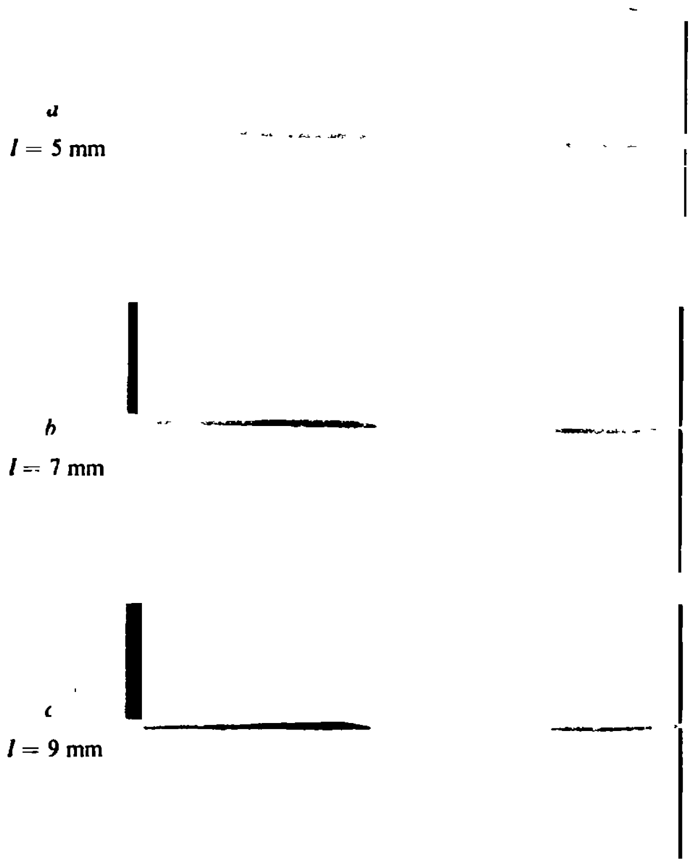

FIG. 13—*a–c*, hydrogen positive.

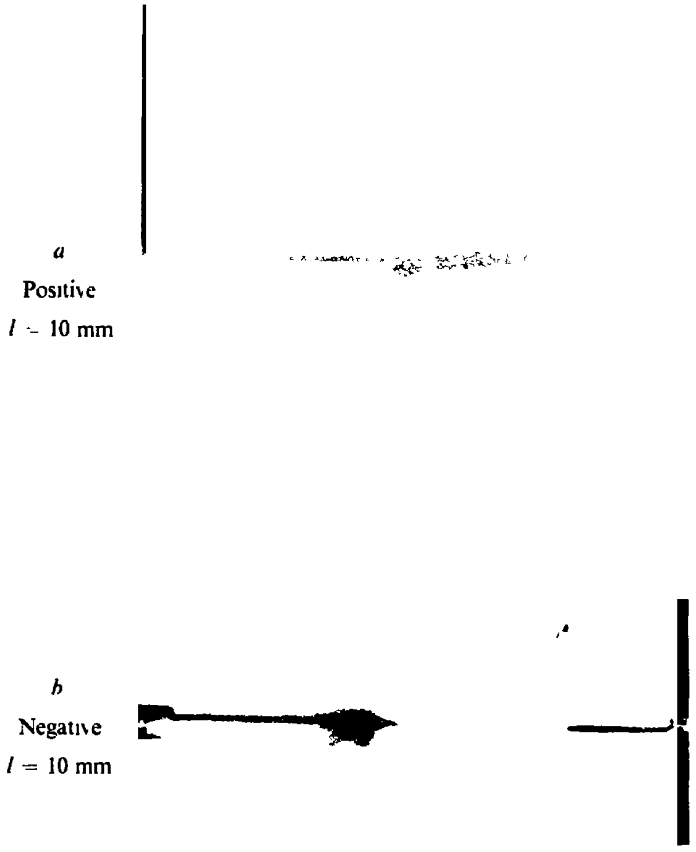

FIG. 14—*a*, *b*, hydrogen.

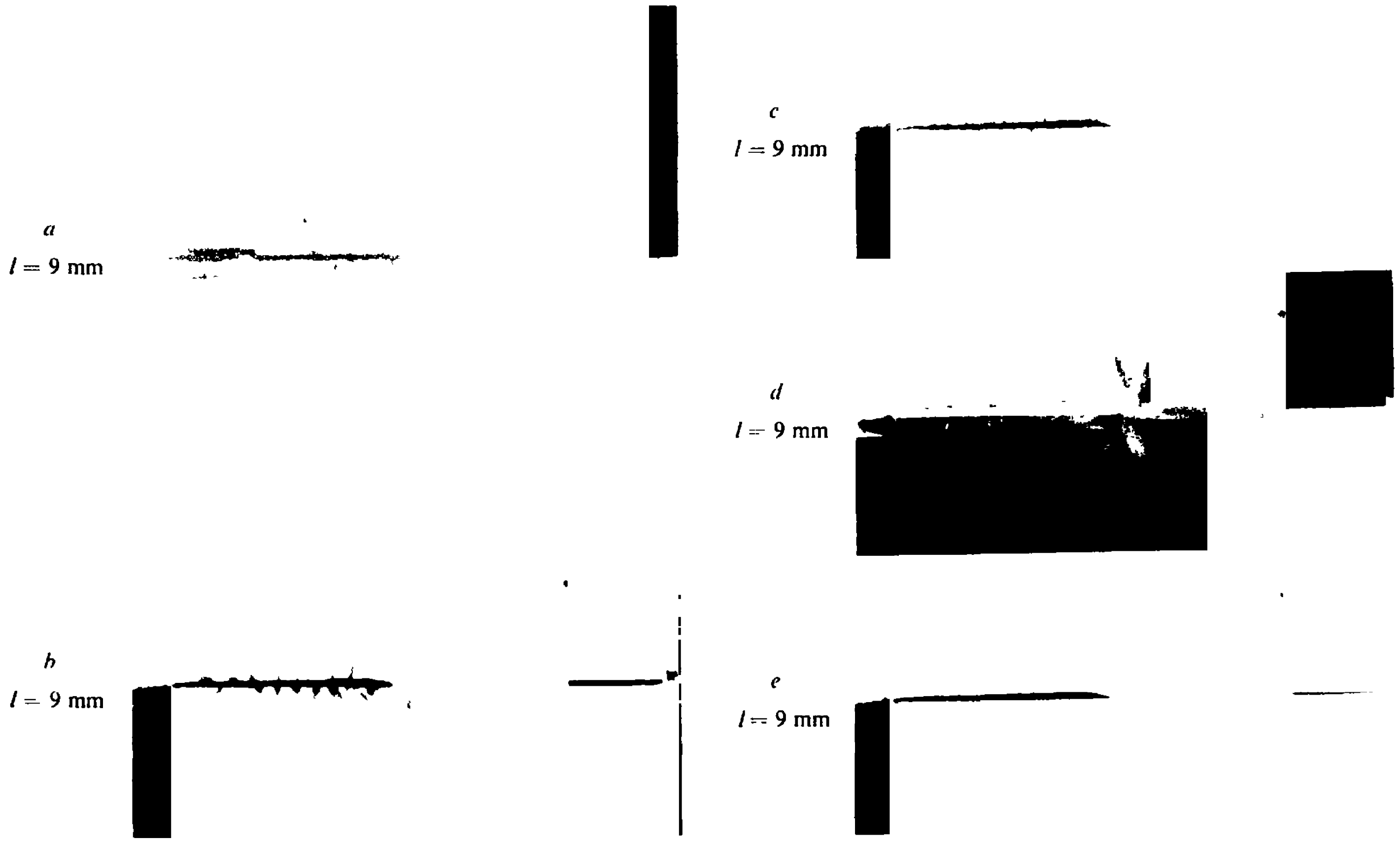

FIG. 15—Air mixed with chloroform vapour. *a*, air without chloroform, positive; *b*, chloroform 0·2% positive; *c*, chloroform 1% positive; *d*. air without chloroform, negative; *e*, chloroform 1% negative.

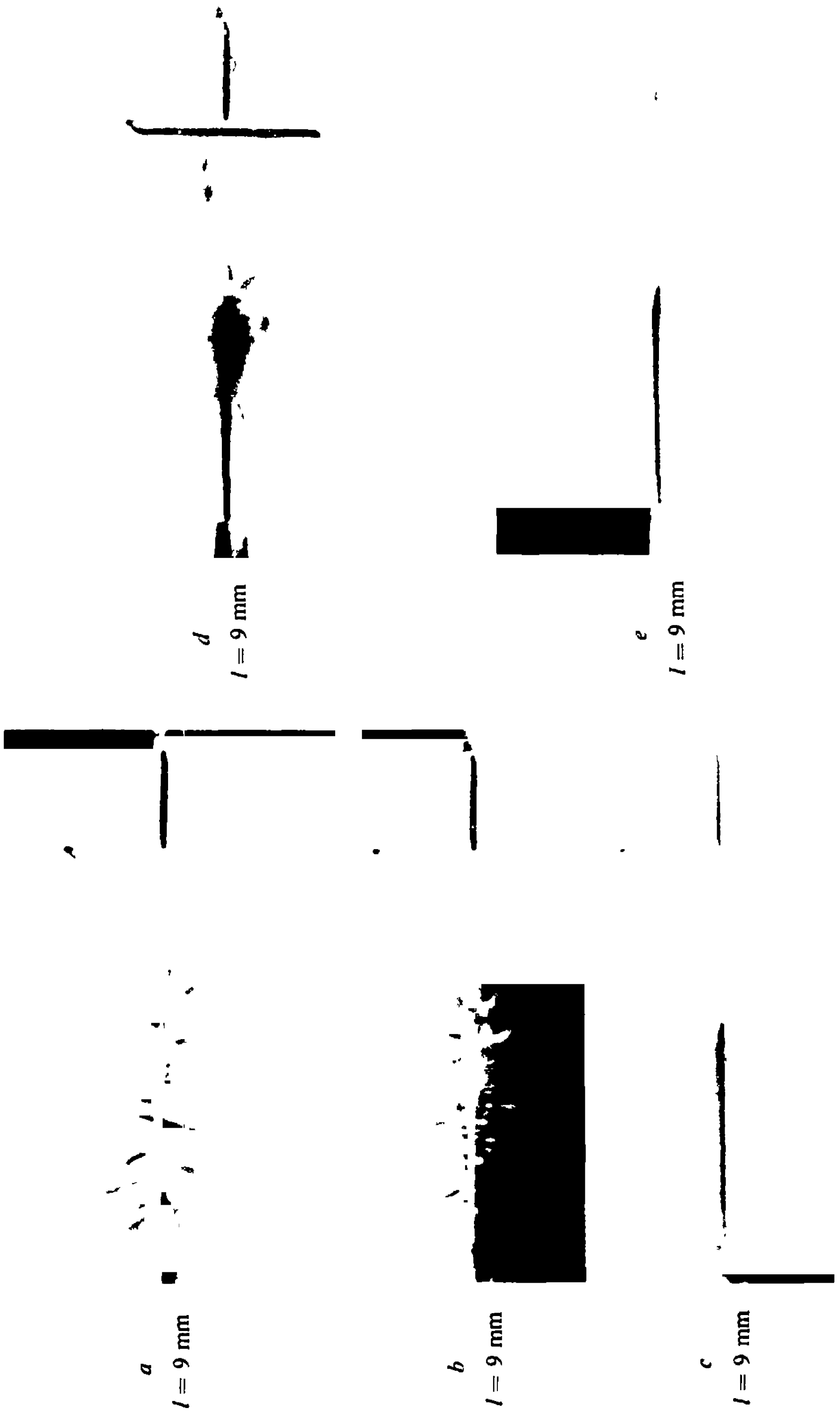

FIG. 16—Air mixed with other organic vapours. *a*, CH_3I 1% positive; *b*, CH_3I 1% negative; *c*, CCl_4 0·2% positive; *d*, C_2H_5Cl 2% positive; *e*, C_2H_5Cl 2% negative.

to air.[*] The vapours which facilitate this action were those of chain compounds containing iodine or chlorine. This action was at that time attributed to the change in form of preliminary discharge, and that point was confirmed by this cloud method.

The substances chosen are obtained all in the liquid state at the ordinary temperature except CH_2Cl_2 and may be volatilized completely after introduction into the chamber. A small quantity of the substance is placed by means of a pipette in a U-tube, and its volume is calculated from the length of the capillary tube occupied by the liquid. This U-tube is then connected to the chamber previously evacuated. After the liquid is completely dried up, the dry filtered air is introduced into the chamber up to the atmospheric pressure. The molecular percentage of mixture is then calculated from the density, molecular weight of the liquid, and volume of the chamber. The substances examined are tabulated in Table I, where the numbers are molecular percentages, and parentheses indicate the presence of the smoothing effect on the form of the preliminary discharge. It may be seen that $CHCl_3$, CCl_4, CH_3I, and C_2H_5I are effective, and this result agrees well with that obtained in the study of the spark form.

TABLE I

Cl-compound	CH_2Cl_2	0·2	1	2
	$CHCl_3$	(0·2)	(1)	
	CCl_4	(0·2)	(0·5)	
	C_2H_5Cl		1	2
	$CHCl_2CHCl_2$		0·5	
	$N_2 + CCl_4$		(0·5)	
I-compound	CH_3I		(1)	
	C_2H_5I		(1)	(2)
Br-compound	C_2H_5Br		0·5	2
No halogen	C_2H_5OH		1	
	$C_2H_5OC_2H_5$		1	

The change in form of the preliminary discharge with the admixture of chloroform $CHCl_3$ is illustrated in fig. 15*a–e*, Plate 16. Fig. 15*a* shows the cloud in air for comparison and *b* the effect of admixture of only 0·2% of chloroform, other conditions being kept constant. A remarkable change is observed in the appearance of the streamers; they become reduced in length, smooth in form, and branching becomes very simple. When the vapour content is increased to 1%, the characteristics above mentioned are emphasized and no more branching is observed, fig. 15*c*. For smaller *l*, a similar cloud of shorter extension is observed and its length increases with increasing *l*. This type of positive discharge is peculiar to the organic vapour, and no resemblance is seen with any of the simple gases studied before. With a negative discharge the cloud become still shorter and a simple brush extends out about 5 mm from the surface of the needle electrode. The negative cloud for $l = 9$ mm in air with 1% of chloroform is shown in fig. 15*e*. The cloud in air under the same conditions is represented in fig. 15*d* for comparison.

---

[*] Terada, Nakaya, and Yamamoto, 'Sci. Pap. Inst. Phys. Chem. Res., Tokyo,' vol. 10, p. 271 (1929).

Fig. 16*a*, *b*, Plate 17, show the positive and negative clouds in air with 1% of methyl iodide, CH_3I. It is seen that the effect of this vapour is quite similar to that of chloroform. A difference may exist in the effectiveness of the vapour; that is, 0·2% of chloroform gives the same order of effect as 1% of methyl iodide, compare fig. 15*b* and fig. 16*a*. Carbon tetrachloride, CCl_4, is more effective than chloroform, 0·2% of the former giving a similar effect to 1% of the latter as shown in fig. 16*c*. A similar result was also obtained when carbon tetrachloride was mixed with nitrogen gas, when the intricate structure of the positive streamers in nitrogen, as shown in fig. 6*d*, was suddenly transformed into a group of short straight lines.

CH_2Cl_2 or C_2H_5Cl was examined with care, increasing the percentage up to 2%, but no smoothing effect was observed, although CH_3I and C_2H_5I have marked smoothing effects. The strange fact that bromine compounds are not effective was observed in the previous studies on spark form, and this point was again confirmed by the present experiments. Accordingly, this smoothing action cannot be explained in a simple manner by something like the relative volume ionizations of the vapours measured for α-, β-, or X-rays.

When a small quantity of the " ineffective " vapour is mixed, the positive streamer remains almost constant in length and the branching is still observed, the mode of ramification being a little simplified. If the amount of vapour is increased further, say, up to 2%, the positive cloud usually becomes diffuse in character, having a constitution of branched streamers inside the diffuse cloud. As an example, the case for 2% of C_2H_5Cl is shown in fig. 16*d*, Plate 17. The corresponding negative cloud is represented in fig. 16*e*, in which one sees that the cloud becomes decidedly lighter along the tracks of the preliminary discharge, but its length is not much affected. The form of cloud in other " ineffective " vapours such as C_2H_5Br, C_2H_5OH, etc., is qualitatively the same as the case represented above.

So far as our present data are concerned, the organic vapours are in the main classified into two kinds, the effective and the ineffective. No essential difference in the form of the cloud is observed among the vapours belonging to one kind.

6—CONCLUDING REMARKS

The most remarkable effect observed in the present series of experiments is that many long streamers with complicated branchings are extended in the positive discharge in air or nitrogen. This type of streamer is seen only in air and nitrogen, and at present it will be natural to consider this streamer as a special characteristic of nitrogen. According to v. Hippel,* the tree-like branching of the positive brush discharge in air is explained as being produced by the flowing of free electrons in the gap into the positive electrode. This theory is convenient for explaining the reason why the streamers are long and fully developed in nitrogen which is an electro-positive gas, and why they are shortened by the admixture of a small quantity of an electro-negative vapour such as chloroform. The positive preliminary discharge in hydrogen, however, shows no long branched streamer in spite of the electro-positive nature of the gas, and in carbon dioxide the negative discharge is more elongated and ramified than the positive. These phenomena may be very difficult to explain in a simple manner by a theory that attributes the preliminary discharge of a spark to a stream of electrons only.

The effect of an abundant existence of free electrons in the gap was studied by applying γ-rays of a radium preparation to the chamber and taking cloud photographs. No further complication of the form of the positive streamers, which might be expected from the existence of abundant free electrons, was observed. The positive streamers of ordinary form were photographed overlapped with an almost continuous background of cloud due to Compton electrons of γ-rays.

One important point omitted in the present investigation is the problem of the form of surge front and oscillation of the circuit. In order to get a rough estimation of this effect, small inductance or non-inductive resistance was introduced in the various places of the circuit. The influence of the inductance was most remarkable and a coil of only two turns was enough to produce a sensible change in the form of the cloud. The systematic study was hindered by the lack of space, as the room was not suitable for setting long transmission lines. Experiments on this problem are now in progress, but the result will be postponed for a later communication.

---

* ' Z. Physik,' vol. 80, p. 19 (1933).

In conclusion, the authors express their best thanks to Hattori Hôkôkai, by whose aid a considerable part of the apparatus used in this experiment was obtained. Their thanks are also due to Professor Terada for his kind assistance in obtaining the gift. They are indebted to Mr. Takano for his kind help during the course of the experiments.

SUMMARY

The previous experiments on the application of the Wilson chamber to the study of spark discharge were developed with improved equipment both in electrical and mechanical designs. With the present apparatus the authors succeeded in taking reproducible photographs of the cloud tracks of preliminary discharge of spark in non-homogeneous fields. Discharge clouds were obtained in air, nitrogen, oxygen, carbon dioxide, hydrogen, and nitrogen oxide, and it was found that the form and structure of the preliminary discharge were quite different for different gases, each gas showing a characteristic feature peculiar to itself. The effect of admixture of a small quantity of some organic vapour was studied. Some chain compounds containing chlorine or iodine, such as chloroform, methyl iodide, etc., were very effective in transforming the positive branched streamers in air into a smooth track.

The Structure of the near Infra-Red Bands of Methane
I—General Survey, and a New Band at 11,050 A

By W. H. J. CHILDS, B.Sc., Ph.D.

(*Communicated by Sir William Bragg, O.M., F.R.S.—Received August* 15 —*Revised October* 18, 1935)

INTRODUCTION

Methane is the most important of the relatively few polyatomic molecules which may be expected to give rise to spectra suitable for investigation in that portion of the near infra-red which is as yet available to photography. To the chemist it is the simplest organic molecule, whilst to the theoretical physicist the four directed valencies and their symmetry properties are its most interesting features. From a technical point of view its importance lies in the fact that its low moment of inertia gives to the band structure a coarseness which brings it within reach of the diffraction grating. The amount of information which we possess of the spectrum is already fairly considerable. The first to make a resolution of the fine structure was Cooley,[*] who investigated the bands at 7·7 μ and 3·3 μ and the measurements have since been extended, with the usual type of thermojunction infra-red spectrometer, by Ellis,[†] Moorhead,[‡] and Norris and Unger.[§] In the photographic infra-red, measurements at wave-lengths shorter than 1 μ have been made by Dennison and Ingram,[||] and Vedder and Mecke.[¶] The present series of papers presents measurements made by the writer in the region λ10,000–12,000 A. They thus overlap into part of the region covered by Norris and Unger and include the bands found by them at λ 11,350, λ 11,620, and λ 11,870. The resolving power of the grating is of course far higher than that employed by them, and much new detail not shown in their curves is now revealed for the first time. The regularities which they abstract from their measurements prove to be spurious, the result merely of the smoothing out of a many-lined spectrum by the use of too low a resolving power.

[*] 'Astrophys. J.,' vol. 62, p. 73 (1925).

[†] 'Proc. Nat. Acad. Sci. Wash.,' vol. 13, p. 202 (1927).

[‡] 'Phys. Rev.,' vol. 39, p. 83 (1932).

[§] 'Phys. Rev.,' vol. 43, p. 467 (1933).

[||] 'Phys. Rev.,' vol. 36, p. 1451 (1930).

[¶] 'Z. Physik,' vol. 86, p. 137 (1933).

Two new bands have also been discovered at λ 11,050 and λ 11,230. The first has the simplest structure of any of the overtones, or indeed of any band except that at 3·3 μ, and it is with it that the present paper is concerned. The measurements of the other bands will be presented in a subsequent paper.

GENERAL SURVEY

Vibration Structure

Before dealing with the relation of this band with the rest of the methane spectrum it is necessary briefly to review the present position of our knowledge, and to point out some peculiarities which so far seem to have escaped notice. The evidence of stereo-chemistry all points to the regular tetrahedron as the appropriate model for the methane molecule. As further evidence the absence of a dipole moment is often quoted, although it must be admitted that in view of the extremely small inherent moment of the C—H bond this is not a very sensitive criterion of symmetry. With the assumption of regular tetrahedral structure it is easy to predict what the spectrum should be. Because of the symmetry the nine fundamental frequencies of a five-atom molecule are reduced to four, one single (ν_s), one double (δ_s), and two triply degenerate (δ_a), (ν_a).* For ν_s the carbon atom remains at rest and the four hydrogen nuclei move in phase along the lines joining them to the carbon atom, for δ_s the carbon atom is again at rest, but now the four hydrogens move in circles on the surface of a sphere. For δ_a and ν_a the carbon atom also takes part in the motion, but here the corresponding Planck oscillator is three dimensional and not, as for δ_s, two dimensional. The general motion cannot easily be described, but special cases may be derived from a consideration of molecules with axial symmetry. Only δ_a and ν_a are active. Overtones of δ_a and ν_a are active, overtones of δ_s and ν_s inactive. Any combination tone including an active fundamental will also be active or, rather, will have at least one active sub-band. Similar predictions may be made for the Raman effect; in particular all four frequencies are Raman active, ν_s probably most strongly. With these four frequencies, and bearing in mind the predicted activities, it should be possible to explain the whole of the observed spectrum. The agreement between observation and prediction is shown in Table I which includes all measurements below $\nu = 10{,}000$ cm^{-1} and all the expected bands for transitions up to three quantum numbers. It will be noticed that only three of the frequencies appear in the Raman spectrum, and one of these only as the first overtone, which is strengthened by its proximity to ν_s. It is clear from Table I that the band now under discussion is the second overtone of ν_a. The fact that it does not fit into a smooth series with $\nu_a = 3020$ and $2\nu_a = 6009$ is a consequence of the fact that ν_a consists of three sub-bands of which only one is active, whilst $2\nu_a$ consists of four sub-bands of which two are active (one only has been found). When the vibrations are harmonic the sub-bands coincide, but on the introduction of anharmonicity not only is the whole group shifted (by an amount $\propto n^2$) but a splitting up of the group occurs of the same order of magnitude as the shift. As it is only the active members of the group which are observed in the infra-red, smooth series do not necessarily occur. For this reason and until more is known of the interaction constants of the sub-bands, the assignations given in Table I must remain to a certain extent ambiguous.

---

* The notation is that of Mecke ('Z. phys. Chem.,' B, vol. 16, p. 409 (1932)). ν, δ refer respectively to valency and deformation vibrations; the former involve predominantly displacements of the nuclei in the direction of the valency bonds, the latter displacements at right angles to the valency bonds. Strictly speaking, such a notation is permissible only for the linear type of molecule and has little point when applied to the tetrahedron, but it is retained for the sake of uniformity.

*Rotation Structure**

The interpretation of the detailed structure of the bands presents considerable difficulties. The rotational energy levels of a regular tetrahedron are given by $B'' J(J+1)$ in the ground state and $B' J(J+1)$ in any higher state, so that each band should consist of P, Q, and R branches of very simple structure; the P, R, lines in the neighbourhood of the origin being spaced by an amount $B' + B'' \hat{=} 2B''$. In the Raman spectrum several branches are expected, but the strongest lines should be spaced $B' + 3B'' \hat{=} B'' + 3B' \hat{=} 4B''$. As is well known, the structures actually observed differ considerably from these simple patterns. The spacing of the band at $\nu = 1306$ is approximately half that of the band at 3020, whilst the spacing of the latter in the Raman spectrum is not the same as it is in the infra-red. An explanation of these discrepancies has recently been advanced by Teller,† who has investigated the consequences of the interaction of an internal moment of momentum ζ arising from a degenerate vibration, with the rotational moment of momentum. The introduction of the vibrational moment of momentum removes the triple degeneracy and the rotational levels split into three,

---

* The notation throughout this section of the paper, where the discussion is concerned with rotation structure, is that of Jevons's "Report on Band Spectra."

† 'Hand. und Jahrbuch der Chemischen Physik,' vol. 9

TABLE I

Type and predicted activity		(Calc.)	(Obs.)
δ_a	Active	(1306)	1306*
δ_s	Ra-active	(1536)	?
ν_s	Ra-active	(2915)	2915
ν_a	Active Ra-active	(3020)	3020
$\nu_a - \delta_a$	Active	1714	1720†
$2\delta_a$	,,	2612	2600
$\delta_a + \delta_s$	,,	2842	2825
$2\delta_s$	Ra-active	(3072)	3072
$\delta_a + \nu_s$	Active	4221	4217
$\delta_a + \nu_a$	,,	4326	4315
$\delta_s + \nu_a$	,,	4556	4543
$\nu_s + \nu_a$	,,	5935	5865
$2\nu_a$	,,	6040	6009
$3\delta_a$	Active	3918	—
$2\delta_a + \delta_s$	,,	4148	4122
$\delta_a + 2\delta_s$	,,	4378	—
$2\delta_a + \nu_s$	,,	5527	—
$2\delta_a + \nu_a$	,,	5632	5589
$\delta_a + \delta_s + \nu_s$	,,	5757	—
$\delta_a + \delta_s + \nu_a$	,,	5862	5768
$\nu_a + 2\delta_s$	,,	6092	—
$\delta_a + 2\nu_s$	,,	7136	—
$\delta_a + \nu_a + \nu_s$	,,	7241	—
$\delta_a + 2\nu_a$	,,	7346	—
$\nu_a + \nu_s + \delta_s$	,,	7471	—
$2\nu_a + \delta_s$	,,	7576	7516
$\nu_a + 2\nu_s$	,,	8850	8800
$2\nu_a + \nu$	,,	8955	8900‡
$3\nu_a$	,,	9060	9047‡
$2\delta_a + 2\nu_s$	,,	8442	8423
$2\delta_a + 2\nu_a$	,,	8652	8606

* This is frequently given incorrectly as 1320, from a misprint in Cooley's paper.

† Measurements of Coblentz, " Investigation of Infra-red Spectra—I," p. 43 (1906).

‡ New bands of this paper.

The observations, except where otherwise stated, are from the sources given in the introduction. The Raman observations are by Dickinson, Dillon, and Rasetti, 'Phys. Rev.,' vol. 34, p. 582 (1929)

( ) indicate the assumed values for the four fundamentals. δ_s is not directly observed, but obtained from $2\delta_s$. The second column is calculated with these four values, but no attempt has been made to include anharmonicity factors. The assignments of the observations differ somewhat from those of Vedder and Mecke (*loc. cit.*).

having energies respectively of $B'(J+\zeta)(J+\zeta+1)$, $B'J(J+1)$, $B'(J-\zeta)(J-\zeta+1)$. For transitions from the ground state the election rules are:—

R branch (positive branch) $J \rightarrow J - \zeta + 1$
Q branch (zero branch) $J \rightarrow J$
P branch (negative branch) $J \rightarrow J + \zeta - 1$,

whilst for the Raman spectrum the strongest lines are given by

positive branch $J \rightarrow J + \zeta + 2$,
negative branch $J \rightarrow J - \zeta - 2$.

This "crossing over" in the infra-red band explains at once the differences in the infra-red and Raman structure of the band at 3020, whilst the two different spacings of the bands at 1306 and 3020 correspond to two different values of the vibrational moment of momentum ζ. By an extension of the theory, it is found that the sum of the ζ values for the two bands is 1/2 (in units of $h/2\pi$). If ζ is small for the band at 3020 (and thus approximately equal 1/2 for the band at 1306) we have an interpretation of the fact that the spacings in the two bands are approximately as 2 to 1. In testing this theory use is frequently made of the measurements of Cooley, or rather, of the formulae which Cooley gives as a derivation from his measurements.

The writer has found that an expression of the type

$$\nu = \nu_0 \pm (B' + B'')J + (B' - B'')J^2$$

does not best fit these measurements, and that there is a considerable systematic deviation from the expressions given by Cooley. This may be shown most clearly by plotting the quantities (*a*) $(R_J + P_J)/2$, and (*b*) $(R_J - P_J)/_{2J}$ as a function of J. The first extrapolates to ν_0 and gives the magnitude of $(B' - B'')$ whilst the second is constant and equal to $(B' + B'')$. The deviation is particularly apparent for (*b*) (*see* figs. 1 and 2) and is, moreover, not included in the first-order effect of the interaction of vibration and rotation. The important point, however, is that this method of treating Cooley's measurements is much more suitable for deriving the value of $(B' + B'')$ (apparent) at the centre of the band, and thus for applying to the test of the theory, than any root-mean-square fit to a quadratic formula. The values derived in this way for the quantity $B' + B'' - 2\zeta B'$ are 5·74 for 1306 and 9·93 for 3020 (*cf.* 5·41 and 9·77 Cooley) with corresponding values for ζ of 0·4497 and 0·0503. The value of ζ computed from 3020 Raman and 3020 infra-red is 0·0476, so that the agreement may be considered satisfactory. The value of

B″ derived in this way is 5·252 with a corresponding moment of inertia of $5{\cdot}267 \times 10^{-4}$ gm cm^2.* It must be emphasized, however, that the second-order effect shown in Cooley's measurements remains unexplained; extra terms in J^3 are necessary in the rotational energy expression. The empirically determined terms then become:—

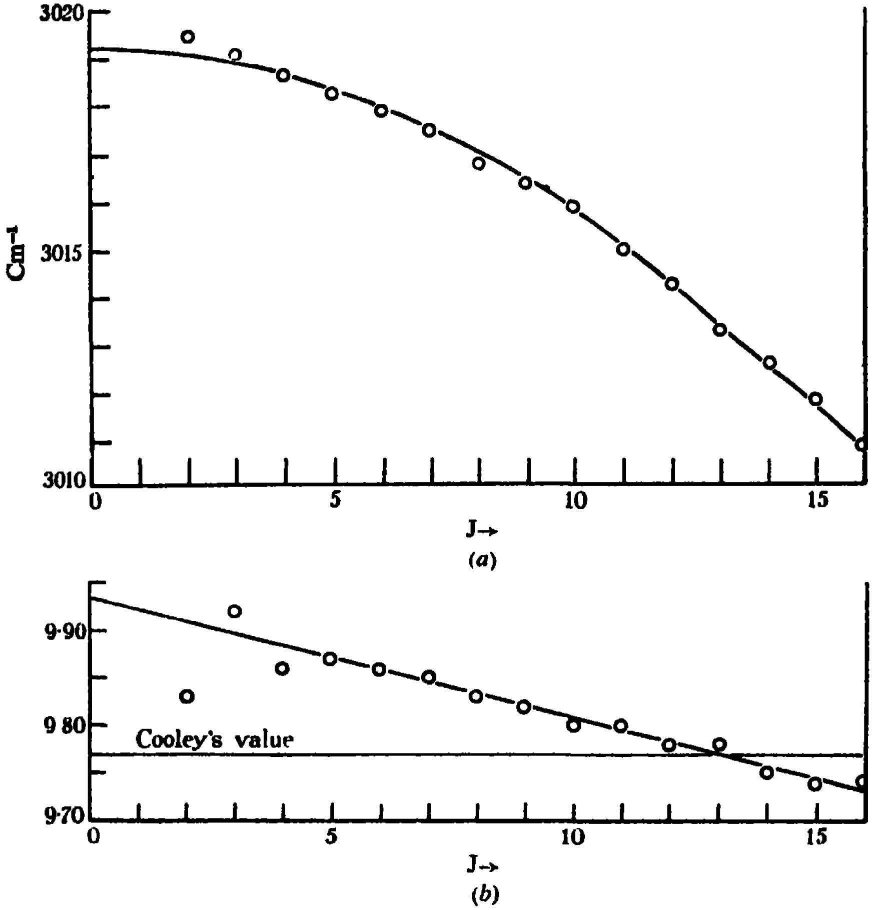

Fig. 1—The band at 3020 (*a*) the quantity $\dfrac{R(J) + P(J)}{2}$ plotted as a function of J. The small deviations J = 2, 3 are probably experimental errors due to proximity of the Q branch; (*b*) the quantity $\dfrac{R(J) - P(J)}{2J}$ plotted as a function of J.

$$1306 \quad \nu = 1306{\cdot}6 \pm (5{\cdot}74)\,J \mp (0{\cdot}033)\,J^2 - (0{\cdot}038)\,J^3$$
$$3020 \quad \nu = 3019{\cdot}3 \pm (9{\cdot}93)\,J \mp (0{\cdot}012)\,J^2 - (0{\cdot}035)\,J^3$$

---

* This differs from the value given by Dennison, 'Phys. Rev.,' vol. 47, p. 93 (1935), who apparently has also used Cooley's formulae.

but more refined measurements on these bands must be awaited before any definite conclusions on this point may be reached.

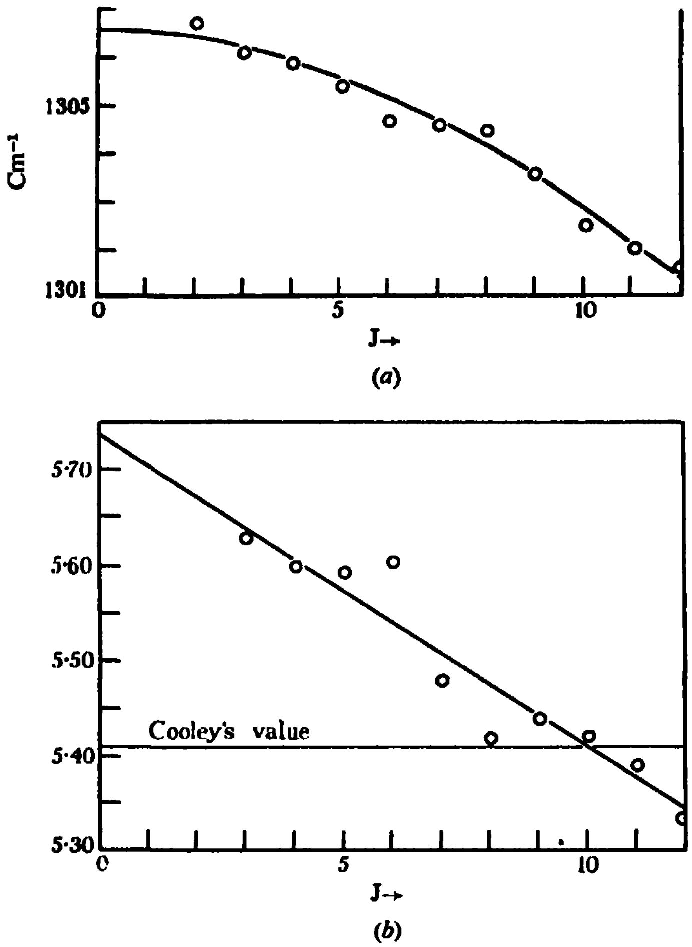

FIG. 2—The band at 1306. (*a*) The quantity $\frac{R(J) + P(J)}{2}$ plotted as a function of J; (*b*) the quantity $\frac{R(J) - P(J)}{2J}$ plotted as a function of J.

THE BAND AT λ 11,050 A

Experimental

The plates have been obtained with the Rowland grating which has recently been mounted at the Royal Institution.* It has proved to be

---

* 'J. Sci. Instr.,' vol. 10, p. 272 (1933).

excellent, giving a very strong first order at 1 to 1·5 μ with very good definition, and eminently suited to work of this nature. The mounting has behaved satisfactorily in every way, and even with the longest exposures of 8 hours there has been no evidence of shifts or lack of resolution due to temperature changes. The absorption tube was 6·1 metres long and 10 cm diameter with a collimator lens and red filter (to suppress higher order spectra than the first) acting as windows at the source and grating end of the tube respectively. The methane was approximately 90% pure, with only traces of foreign gases (an analysis, for which I am indebted to Sir Robert Robertson, showed some 2% of CO_2, 1% of O_2, and 3% of N_2). A fractional distillation performed with liquid nitrogen showed a negligible ethane or other hydrocarbon content (less than 5%). No pressure higher than atmospheric was used, as with the path length employed the absorption was amply strong and an increase would have succeeded only in blurring the details. Agfa Rapid 1060 plates were used, hypersensitized in the usual way with ammonia. With a slit width of 0·08 mm, which is the optimum value for the mounting at this wave-length, the exposure times ranged from 2 to 9 hours. The longest wave-length to which lines can be measured is λ 12,100 A; the mean dispersion is 5·46 A, or approximately 4·5 cm^{-1}, per mm.

The Measurements

The plates were measured with a Hilger comparator, against third order iron arc lines. An intercomparison of the results shows that the stronger lines should be accurate to 0·05 cm^{-1}; the error for the lines marked with intensity 0 (Table II), and especially for those marked 00, may be as much as 0·10 cm^{-1}. The lines are all sharp and well defined and none shows any evidence of pressure broadening. On the long wave-length side there is some overlapping with lines which appear to belong to the band at 11,230 A and many of the lines with frequencies smaller than 9020, included in Table II for the sake of completeness, undoubtedly belong to that band. The intensities are merely eye estimations, and the scale has been so chosen that an intensity of 1 or greater indicates lines which are plainly visible; 0 indicates lines which present some difficulty of measurement and 00 are doubtful lines. The general appearance of the band may be gathered from fig. 3.

The rotation structure of the 9047 band is by far the simplest of any of the methane bands as yet photographed, and is obviously closely connected with that of its fundamental. The band is peculiar in several respects. First of all, the P branch is very much weaker than the R

TABLE II

Intensity	ν Vac.		Intensity	ν Vac.	
00	9168·40		3	9100·45 br.	R(4)
00	66·61		1	9099·91	
0	63·54		0	94·84	
0	56·17		2	93·53	
0	54·93	R(9)	1	92·40	
0	54·06		3	89·64 br.	R(3)
1	52·70		0	88·10	
1	51·87		0	86·83	
1	50·81		0	85·38	
0	49·68		0	84·48	
0	48·62		0	82·54	
1	47·12		0	81·01	
1	45·51		0	80·12	
2	43·82	R(8)	2	79·17	R(2)
1	41·90		0	77·91	
2	41·14		0	77·01	
0	39·84		0	75·84	
0	38·65		0	73·91	
0	37·19		1	72·92	
0	36·23		2	71·43 br.	
0	34·53		1	69·95 br.	
1	32·29	R(7)	2	68·65 br.	R(1)
1	31·06		0	66·91	
1	30·65		0	66·36	
0	29·51		0	65·75	
0	28·27		0	65·35	
0	27·13		0	63·48	
0	23·48		0	60·77	
0	22·57		0	60·21	
3	21·52	R(6)	0	59·39	
3	20·37		0	58·70	
0	19·19		1	57·79	R(0)
0	18·05		0	56·81	
0	16·73		0	55·87	
0	15·55		0	54·91	
0	14·13		0	53·88	
0	13·45		0	52·71	
2	10·91	R(5)	0	51·59	
1	10·08		0	50·81	
0	06·91		0	49·85	
0	05·22		0	49·23	
0	04·59		1	9045·47 br.	Q
00	02·50		1	44·67 br.	
00	01·68		2	43·48	

TABLE II—(continued)

Intensity	ν Vac.	Intensity	ν Vac.
1	9042·63 } Q	1	8995·76
2	41·64	1	94·57
00	40·41	1	93·33
00	39·77	3	92·44
00	38·36	5	91·02 br. P(6) ?
00	37·24 P(1) ?	1	90·53
0	36·30	2	89·59
0	35·36	1	88·75
00	33·99	2	87·74
0	33·05	1	86·96
00	31·85	3	86·24
00	27·82 P(2) ?	1	85·26
00	27·20	0	84·78
00	26·30	0	83·88
00	25·77	0	83·14
00	24·84	2	82·25
00	23·94	6	81·77 P(7) ?
00	22·79	1	80·70
0	19·89	1	80·00
0	18·78 P(3) ?	1	78·94
0	17·84	1	77·92
0	16·42	3	77·12
1	15·66	3	76·16
2	14·74	1	75·59
1	14·06	1	75·14
2	13·27	2	74·39
0	12·46	1	73·42
0	11·61	2	72·76 P(8) ?
1	10·73	7	71·57
2	09·57 P(4) ?	1	70·15
1	08·87	1	69·71
1	07·44	0	68·87
1	06·60	0	67·99
1	06·09	2	67·06
1	05·19	1	65·79
2	04·32 + w.v.	1	65·25
1	03·53	0	64·51 w.v.
1	02·77	5	63·84 P(9) ?
2	01·67 + w.v.	5	63·18
2	01·00	1	61·60
2	00·28 P(5) ?	1	60·72
1	8999·54	2	59·80
1	98·59	1	58·83 w.v.
1	97·67	0	58·04 w.v.
1	96·78 w.v.	4	57·38

TABLE II—(continued)

Intensity	ν Vac.	Intensity	ν Vac.
1	8956·28 w.v.	2	8952·71
0	55·74	2	52·01
0	55·00 w.v.	1	51·48
0	54·25	3	50·25 + w.v.
3	53·46 + w.v.		

br. = broad.
w.v. = water vapour.
+ w.v. = blend with water vapour line.

branch; there are no lines which stand out as obviously belonging to the P branch. Secondly, the lines of the R branch show a splitting which increases in magnitude and complexity with the rotational quantum number. Lastly, the spacing in the R branch is not regular, but after an initial decrease begins to increase again (*see* fig. 4). The Q branch is also comparatively weak. The first step in the interpretation of the measurements must be the determination, by an application of the appropriate combination relationships, of the energy of the levels concerned in the transitions. It will be clear that since the selection rules are J to $J - \zeta + 1$ for the positive branch, and J to $J + \zeta - 1$ for the negative branch, no exact combination will hold. For example, the combination $R(J-1) - P(J+1)$ which normally gives the initial term differences $F''(J+1) - F''(J-1)$ is now defective by an amount $2B'\zeta(2J+1)$, so that we have

$$R(J-1) - P(J+1) + 2B'\zeta(2J+1) = F''(J+1) - F''(J-1)$$
$$= 2B''(2J+1).$$

By making use of this relationship, and assuming that ζ is not very much different from 0·05, it is possible to find seven or eight lines which may belong to the negative branch. The process is straightforward enough for the first few lines of the positive branch, which are single, but when the splitting becomes appreciable it is the low frequency component of each line which has to be used. The negative branch lines found in this way have been indicated in Table I. The agreement between the combination differences for fundamental and overtone is quite good, Table III.

If this agreement is real and not fortuitous it indicates that ζ has closely the same value in the overtones as it has in the fundamental. As one would expect from the anomalous spacings in the R branch the

F′ terms are quite irregular, but their trend indicates that the reason must lie in an unexpectedly large vibration-rotation interaction. For this reason there can be no point, when dealing with the complicated structure of these overtone and combination bands, of looking for the regular line spacings of the fundamentals. The line splitting increases with the rotational quantum number and is clearly due to the removal of degeneracy by the rotation (each rotational level is $(2J + 1)$ fold degenerate *in the molecule*), but the weakness of the P branch, and the breakdown of the combination relationships, together make it impossible for the present to trace the phenomenon back to the levels concerned. It should perhaps be emphasized that we are here only at the beginning of the detailed analysis of a spectrum showing pronounced interaction effects and much remains to be done on the theoretical as well as on the experimental side before we can be in a position to explain them.

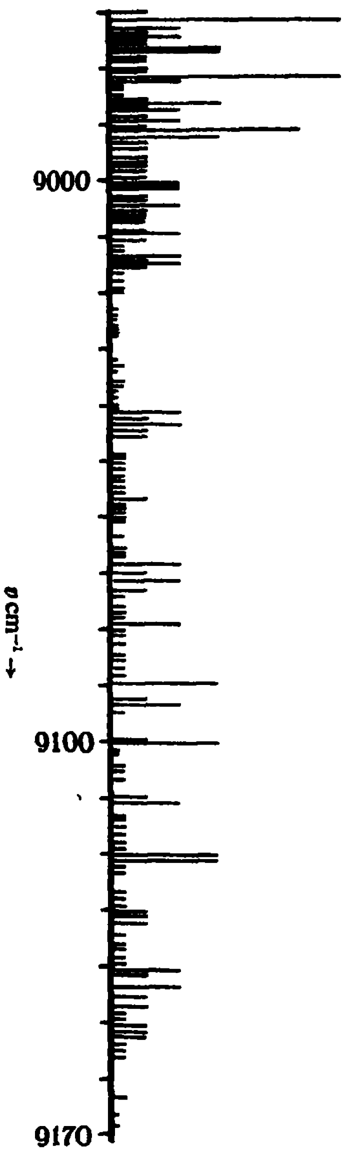

Fig. 3—The general appearance of the band at λ 11,050.

In conclusion, I wish to thank Sir William Bragg, O.M., F.R.S., and the Managers of the Royal Institution for the facilities afforded at the Davy Faraday Laboratory where this work was carried out.

SUMMARY

The near infra-red bands of methane, in the region 10,000 to 12,000 A, have been investigated photographically under high dispersion (4·5 cm^{-1} per mm). Two new bands have been discovered, at λ 10,050 A and λ 11,230 A, and much new detail obtained in the bands at λ 11,350, λ 11,620, and λ 11,870 A. The new band at λ 10,050 is investigated in detail and interpreted as the second harmonic of the fundamental at 3·3 μ. From a critical discussion of the spacings

in the bands measured by Cooley it has been possible to point out several inaccuracies in the constants of the methane molecule hitherto derived from them. The moment of inertia in the ground state is found to be $5{\cdot}267 \times 10^{-40}$ gm cm^2, whilst the vibration moment of momentum in

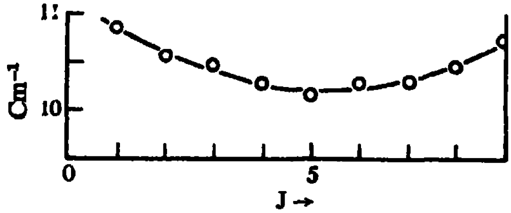

FIG. 4—First-order differences, R (J) − R (J − 1), in the 9047 band. The low frequency component only of each line has been used.

TABLE III

R (J − 1) − P (J + 1)

J	3020	9047
1	29·4	29·97
2	49·8	49·87
3	69·6	69·60
4	89·2	89·36
5	109·0	108·89
6	128·5	128·31
7	148·2	147·61
8	167·4	166·81

the 7·7 μ and 3·3 μ bands is respectively 0·45 and 0·050 (0·048 from Raman spectrum). All the bands, however, show a second-order effect involving terms in Jl which is not included in the theory. The value of ζ is the same in the overtone as in the fundamental.

The Disintegration of Boron

By D. Roaf

(*Communicated by F. A. Lindemann, F.R.S.—Received August* 16, 1935)

[Plate 18]

Introduction

The nuclei of the lighter elements, owing to their relatively large masses and low potential barriers, can be penetrated by charged particles of low energy. The probability of a disintegration taking place in such circumstances is comparatively great.

Since beryllium and boron emit neutrons when bombarded with α-particles it appeared to be particularly interesting to endeavour to follow the process of disintegration of one of these substances. As borontrifluoride is a comparatively stable gas it appeared possible to use it in a Wilson chamber and to record the reaction.

By the time the apparatus was ready for use Fermi's work on artificial radioactivity had been published and it was decided in the first place to attempt to record the reaction between boron and neutrons, as the yield of disintegrations with neutrons was much greater than with α-particles.

Clearly, owing to their rapid reactions with BF_3, neither water nor alcohol could be used to form the cloud in the chamber. In order to test the various liquids a preliminary expansion chamber was therefore constructed similar to that described by Blackett,* using flexible metal bellows instead of a diaphragm. Various specimens of the lighter paraffins were tried but the tracks obtained in their vapours were never sharp, possibly owing to the difficulty in obtaining really pure specimens. Carbondisulphide was unsuitable since no cement or washers could be found capable of withstanding its solvent action. Chloroform and carbon tetrachloride proved satisfactory, the latter being chosen as it is more stable and contains no hydrogen, collisions with which, though rare, might cause difficulties in interpreting the results. The considerable drop in temperature required to form tracks with CCl_4 combined with the small ratio of the specific heats of BF_3 (1 : 2) made a comparatively large expansion ratio necessary. This caused considerable technical difficulties.

It was not possible to obtain a large expansion ratio with the preliminary chamber because (*a*) the metal bellows could not be stretched to the necessary degree, and (*b*) the tracks ceased after a few hundred expansions. This was ultimately traced to the solution of the gas in the liquid and its boiling out after each expansion.

---

* 'J. Sci. Instr.,' vol. 4, p. 433 (1927).

In order to reduce the stopping power of the gas and thus obtain longer tracks, which could be more accurately measured, and also in order to reduce the expansion ratio to a more convenient value, the borontrifluoride was mixed with about three times its volume of helium, which was kindly supplied clean and dried from Dr. Kürti's liquefier.

In the meantime a synthetic rubber-like substance, ethylene polysulphide, insoluble in CCl_4, which could be obtained thin enough to be used as an elastic diaphragm, was developed by the Dunlop Rubber Company. Using this a simple diaphragm type of Wilson chamber was designed permitting an expansion ratio of at least 2: 1 and constructed of materials which were neither attacked by CCl_4 nor BF_3 and which did not absorb slow neutrons. The chamber was built of brass and its piston made gas-tight by the ethylene polysulphide diaphragm. It was made shallow so that a Be-Rn source could be put immediately below the gas. Thus, when it was desired to bombard the BF_3 with neutrons, these would only have to penetrate 3 mm of brass and not the glass of the chamber which might contain boron and absorb them.

An expansion ratio of 2: 1 entailed such large forces that a chamber of only 5 cm diameter was built. To achieve such a large expansion ratio with a manageable movement of the piston the initial volume of the chamber had to be small. The final design is shown in fig. 1. The chamber consists of a glass ring 5 mm deep and 5 cm in diameter, which is clamped on to the main block by four bolts.

The piston P, constructed of a thin brass disc, is sealed at the edges by an elastic diaphragm made of ethylene polysulphide which, as mentioned above, is insoluble in carbontetrachloride. The piston rises as far as the gauze G so that, before expansion, the diaphragm fitted tightly to the upper walls of the lower part of the chamber leaving for the initial volume only the space above the gauze. After expansion the diaphragm fitted tightly to the lower walls of the chamber so that a large increase in the volume was obtained without undue movement of the piston.

Of course, an expansion ratio as large as this makes it very difficult to avoid distortion of the tracks, and great care has to be taken to see that the piston moves symmetrically. In order to prevent eddies the gauze G has to be very fine and the inside of the chamber has to be smooth.

To produce the expansion a valve in the two pipes B connecting the space below the diaphragm with an evacuated chamber is opened automatically by the timing mechanism which actuates the cameras, the field for clearing ions, and the spark to illuminate the chamber.

The tracks were recorded by two 35-mm cinema cameras with the films at right angles as described by Blackett.*

PRODUCTION OF BF_3 AND FILLING OF CHAMBER

The method is that described by German and Booth.†

Boric oxide was heated in a Fletcher furnace until it melted and all the water was driven off. The glass-like boric oxide was ground into a fine powder and dissolved in sulphuric acid in the proportions 75 gm boric oxide to 400 cc H_2SO_4. 200 gm CaF_2 were added to this and the hydrogen fluoride allowed to escape into a flue.

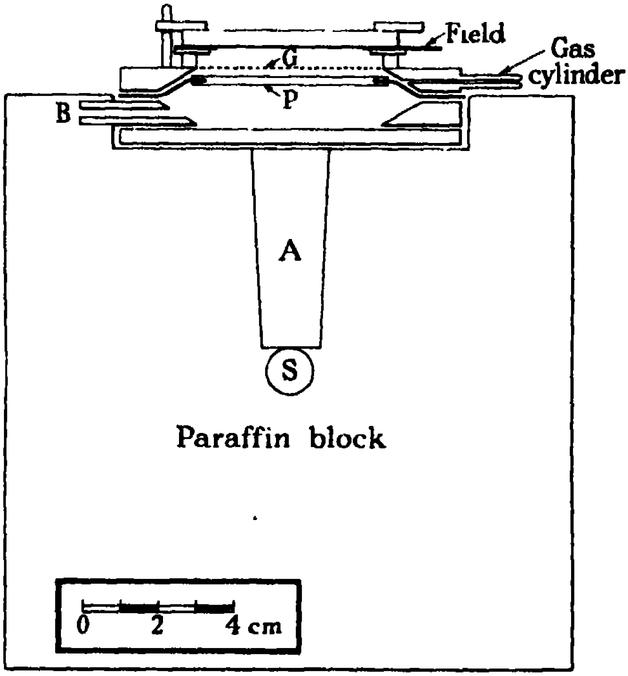

FIG. 1—Experimental arrangement.

The mixture was then put into a flask and the reaction started by heating.

The BF_3 was purified by fractionation in liquid air, and collected at a pressure of 4 atmospheres in a cast steel cylinder.

---

* 'Proc. Roy. Soc.,' A, vol. 123, p. 613 (1929).

† 'J. phys. Chem.,' p. 369 (1926).

The chamber was tested for leaks and evacuated to 1/100 mm for 6 hours; vapour from CCl_4 dried by P_2O_5 was then admitted from a side tube and the apparatus left evacuated over night.

The chamber was filled with a mixture of equal volumes of BF_3 and He and the apparatus set in motion. Successive quantities of helium were added until sharp tracks were formed.

It was found that a clearing field of 1000 volts/cm across the chamber was necessary if good tracks were to be obtained.

EXPERIMENTAL

Whilst the preliminary part of this work was in progress the tracks produced by the disintegration of the heavier elements carbon, oxygen, and nitrogen when bombarded with neutrons had been photographed by Feather.*

As these neutron disintegrations proved to be of considerable interest, it was decided in the first place to examine the disintegration of boron by neutrons.

The source of neutrons, S, was a glass bulb filled with powdered beryllium and radon. This was surrounded by 8 cm of paraffin wax in order to obtain neutrons slowed up by collisions with the hydrogen nuclei. A wedge of lead, A, 8 cm thick was used to screen the chamber from γ-rays.

About 400 pairs of photographs were taken; upon examination a number of single tracks similar to those of α-particles were found in the gas. The lengths of these were calculated from measurements on the negatives and in three cases checked by reprojecting the films through the cameras.

CALCULATION OF ENERGY

Of the possible disintegrations discussed by Chadwick the only reaction which fits the observations is

$$B_5^{10} + n_0^1 = Li_3^7 + He_2^4.$$

This is confirmed by the work of Taylor and Goldhaber.†

It is important to convert the range of the recoils into energy as then a correction to the atomic mass of the B_5^{10} nucleus can be made.

To do this it is necessary to know: (*a*) the stopping power of the BF_3-He

* 'Proc. Roy. Soc.,' A, vol. 136, p. 709 (1932); vol. 142, p. 689 (1933).

† 'Nature,' vol. 135, p. 341 (1935).

mixture; (*b*) the energy range relation in air for one of the recoiling atoms; and (*c*) the proportion of the observed track due to each recoil.

These points are now considered.

(*a*) As an accurate calculation of the stopping power of the He-BF_3 mixture was difficult it was measured directly.

To do this α-rays from a polonium source were allowed to enter the chamber through a thin mica window and the reduction in the length of the tracks in the He-BF_3 mixture was measured when the polonium source was moved away so that the α-particles had to pass through a greater length of air of known stopping power.

(*b*) We have accurate experimental data for the energy range relation of a He recoil in air.*

(*c*) It is impossible by a visual examination to decide which part of a track is due to the He nucleus and which part to the Li nucleus because (1) it is not possible to distinguish between a He and a Li recoil by their difference in density of ionization, and (2) as the disintegration is in general due to a slow neutron of negligible momentum the He and Li recoils lie in a straight line and there is no geometrical starting point for their tracks. From the one bent track observed it was impossible to get an accurate measurement, but it was estimated that the ratio of the lengths of the recoils was about 1 : 1.

If we knew the range of the recoil of the He atom we could, even without knowing the range velocity relation for Li, calculate accurately the energy involved in the reaction.

For the tracks observed this was not possible, but on certain assumptions we can make an estimate of the range of a lithium recoil. As far as is known the ionization due to a heavy particle depends only on its charge and velocity. The charge, of course, is frequently changing, but an estimate of the mean charge on the recoil atom at any velocity may be made from Fowler's† calculation on the capture and loss of electrons by swift nuclei.

In this paper the thermal equilibrium of an atom with a stream of electrons is considered and the ratio of the length of path in an ionized state to the path in a neutral state is calculated. The excellent agreement of this theory with experiment for helium justifies its application to lithium.

A rough calculation of the greatest possible velocity of the helium recoil gives a value about 8×10^8 cm/sec. Therefore the velocity of

---

* Blackett and Lees, 'Proc. Roy. Soc.,' A, vol. 134, p. 658 (1931).

† 'Phil. Mag.,' vol. 47, p. 416 (1924).

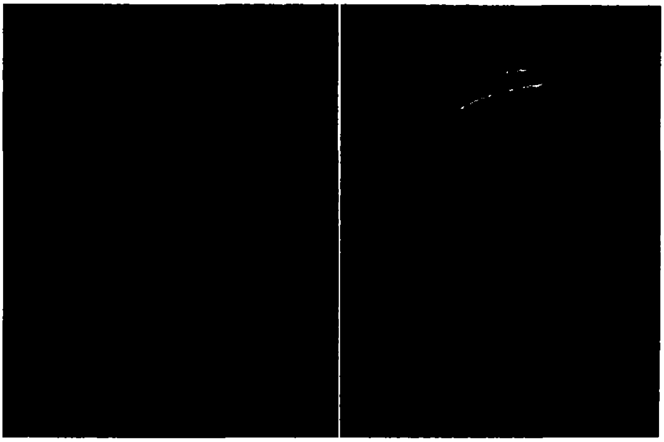

Stereoscopic pair of photographs of the He–Li recoil.

He–Li recoil due to fast neutron showing angle between tracks.

the lithium nucleus relative to the electrons is 5 × 10^8 cm/sec, or about 75 volts.

Since the ionization potential for doubly ionized lithium is 75·2 volts, it is apparent that the Li atom is not more than singly charged.

Fowler's formula applied to Li^+ and Li^0 gives:

$$\frac{[Li^+]}{[Li^0]} Ve = 3 \cdot 87 \times 10^{21} \frac{W - E_0}{WE_0} . W^{\frac{1}{2}} . (W + E)^2$$

where

Ve = density of electrons, taken as 4 × 10^{24}

W = relative velocity of electrons, in volts.

E_0 = ionization potential of the atom.

It is obvious from the high ionization potential of helium that this formula breaks down for the last few millimetres of its range. In this region, however, a calculation of the mean charge on a helium recoil can be made from the experiments of Kapitza* on the curvature of α-particles in a strong magnetic field. For Li^+, $E_0 = 4 \cdot 5$ volts. This corresponds to a recoil velocity of 10^8 cm/sec, so that the formula can probably be relied upon within 0·5 mm of the end of the range of the lithium recoil. Table I shows values of W against the mean charge on a lithium recoil for velocities 4·5 × 10^8 to 2 × 10^8 cm/sec, and also the mean charge on a He recoil calculated from the experimental results of Kapitza.

TABLE I

W	$\frac{[Li^+]}{[Li^0]}$	Mean charge Li Z_{Li}	Mean charge He Z_{He}
5	—	—	—
10	0·07	0·065	0·1
15	0·21	0·17	0·59
20	0·31	0·23	0·65
40	2·1	0·68	1·02
50	4·0	0·80	1·05
60	5·8	0·87	—

From Blackett's empirical relationship for recoiling nuclei ($R \alpha MZ^{-\frac{1}{2}} f(v)$) we have over a small equal range of velocity

$$\frac{\Delta R_{He}}{\Delta R_{Li}} = \frac{M_{He}}{M_{Li}} \left(\frac{Z_{He}}{Z_{Li}}\right)^{-\frac{1}{2}}, \qquad (1)$$

thus eliminating the velocity function.

---

* 'Proc. Roy. Soc.,' A, vol. 106, p. 602 (1924).

The variation of Z_{He}/Z_{Li} with velocity can be obtained from Table I. Using equation (1) and Blackett and Lees's* curves for the range velocity relation of a helium recoil, a range velocity graph for a Li recoil can be constructed, fig. 2.

For this disintegration according to the law of the conservation of momentum the initial velocities of the helium and lithium atoms are in the ratio 7 : 4. Since the combined length of the recoils is known we can therefore derive the range of either nucleus from the graph.

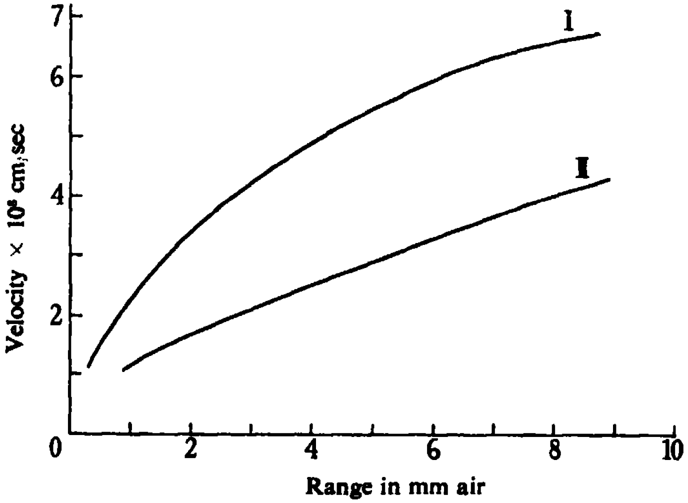

FIG. 2—Range-velocity curves for He and Li. I, helium from Blackett; II, lithium calculated on Fowler's theory from data of Kapitza and Blackett.

DISCUSSION OF RESULTS

Out of the 32 tracks recorded, 8 of the clearest were measured; the mean of their lengths on the negative was 3·91 ± 0·03 mm.

Six separate measurements of the stopping power of the gas were made, and it was found that a range of 1 cm in air corresponded to a track of the length 0·34 ± 0·01 cm on the negative.

Hence the length of the helium-lithium recoil reduced to air is 1·15 ± 0·04 cm. According to our graphs 0·55 ± 0·02 cm of the combined recoil track must be attributed to the helium recoil. Using Blackett's (*loc. cit.*) energy range data, therefore, the disintegration must be accompanied by an energy release of $1 \cdot 50 \pm 0 \cdot 05 \times 10^{-3}$ units of atomic mass. Using Rutherford's* latest values of the atomic masses in question, one finds for the mass of B_5^{10} $7 \cdot 0170 \pm 0 \cdot 0007$, $+ 4 \cdot 0034 \pm 0 \cdot 0004$, $+ 0 \cdot 00150$, $- 1 \cdot 0083 \pm 0 \cdot 0003$, $= 10 \cdot 0136 \pm 0 \cdot 0014$.

---

* 'Proc. Roy. Soc.,' A, vol. 134, p. 658 (1931).

The total length of the track agrees with that obtained in photographic emulsion by Taylor and Goldhaber† and the range of each recoil calculated on the above assumptions is consistent with the range of 5 mm found in an ionization chamber by Chadwick and Goldhaber.‡

It is not in agreement, however, with the recoil ranges for this reaction measured by B. and J. Kurtchatov and Latychev.§

Only a rough estimate of the cross-section of the boron atom for slow neutrons can be made as the time of track formation and the percentage of slow neutrons were uncertain. It was estimated that in each cm^3 of the gas there were 10^{18} atoms of B_5^{10}.

Allowing 1/100 sec for the time during which tracks could be formed and using Fermi's estimate that 1000 neutrons/sec come from 1 mC source, of which 20% are slow, the effective cross-section of the B_5^{10} nucleus is $1 \cdot 6 \times 10^{-21}$ sq cm.

One track was recorded with an angle of about 18° between the two recoils. If this angle is due to the momentum of the neutron the disintegration must have been caused by a neutron of energy greater than 10^5 e.v.

Of the remainder, those tracks which were sharp enough for accurate measurement, were straight within an angle of 5°. The maximum energy of the neutrons causing these reactions is therefore 2×10^4 e.v.

Two obvious proton tracks were observed in the chamber which may have been due to a disintegration of zinc in the walls.

In conclusion, I wish to thank Professor Lindemann and Mr. C. H. Collie for their constant interest and help, and also the Czechoslovak Government for the loan of the 1½ gm of radium from which the sources were prepared.

SUMMARY

A Wilson expansion chamber has been built for use with borontrifluoride and with it the recoils from the disintegration of B_5^{10} by neutrons have been photographed and their energy measured.

The energy released in the reaction $B_5^{10} + n_0^1 = Li_3^7 + He_2^4$ is found to

---

* 'Proc. Roy. Soc.,' A, vol. 150, p. 253 (1935).

† 'Nature,' vol. 135, p. 341 (1935).

‡ 'Nature,' vol. 135, p. 65 (1935).

§ *See* 'C.R. Acad. Sci., Paris,' vol. 200, p. 1199 (April 1, 1935).

be $1\cdot50 \pm 0\cdot05 \times 10^{-3}$ units of atomic mass and a correction to the B_5^{10} mass has been made ($B^{10} = 10\cdot0136 \pm 0\cdot0014$). The effective B_5^{10}-neutron cross-section is estimated at $1\cdot6 \times 10^{-21}$ sq cm.

Most of the disintegrations were caused by neutrons of energy less than 2×10^4 e.v., but one was observed due to a neutron of energy greater than 1×10^6 e.v.

On Condensed Helium at Absolute Zero

By F. LONDON, Clarendon Laboratory, Oxford

(*Communicated by F. A. Lindemann, F.R.S.—Received August* 16, 1935)

The properties of helium at very low temperatures have recently been the subject of many investigations.*† Helium is the only substance which cannot be transformed into the solid state merely by cooling. It has, it is true, at 2·19° abs a thermal anomaly, the so-called λ-point. At this temperature the specific heat has a discontinuity, indicating that liquid helium undergoes at this point that characteristic type of phase transition which, in Ehrenfest's well-known classification, corresponds to a phase equilibrium of the "second kind." But even below this temperature helium remains liquid; moreover, it has been found‡ that its viscosity decreases suddenly to about a tenth when passing through the λ-point. It is only under pressure that the solid state can exist. Extrapolated to the absolute zero, this pressure amounts to about 25 atmospheres. The entropy difference between the liquid and the solid phase tends towards zero with falling temperature,§ which means that the liquid phase goes into a peculiar ordered state.|| This change towards an ordered state begins immediately below the λ-point and is associated with a large loss of energy which occurs continuously in a relatively small temperature range.

---

* Keesom and co-workers, 'Comm. Phys. Lab. Leiden,' Nos. 184*b*, 190*b*, 216*b*, 219*e*, 221*e*, Suppl. Nos. 67*b*, 71*e*, 76*b*; 'Physica,' vol. 1, pp. 128, 161 (1934).

† Simon, 'Nature,' vol. 133, pp. 460, 529 (1934); *see also* Bennewitz and Simon, 'Z. Physik,' vol. 16, p. 197 (1923).

‡ Burton, 'Nature,' vol. 135, p. 265 (1935).

§ Keesom, 'Comm. Phys. Lab. Leiden,' Suppl. No. 61*b*.

|| Simon, 'Z. Physik,' vol. 41, p. 808 (1927); 'Ergebn. exact. Naturwiss.,' vol. 9, pp. 235, 247 *ff.* (1930); 'Z. anorg. Chem.,' vol. 203, p. 222 (1931).

Simon[*] has shown that near 0° abs the liquid state has less energy than the solid state. Using the Θ_{Debye} of the specific heat he presumed that this peculiarity may be interpreted as due to an unusually large zero point energy (in comparison with the " Van der Waals energy ") and to its rapid variation with the molecular volume, and he has proposed that this presumption should be examined in greater detail. It would be interesting to know what kind of order the liquid state may have, and in what respect it is different from the solid state. In this note we shall only deal with helium at the absolute zero; thermal properties will not be considered.

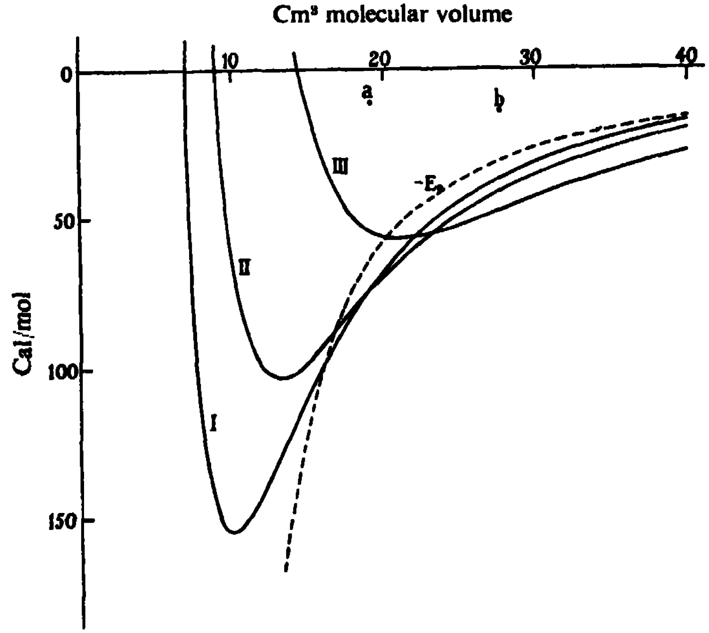

Fig. 1—Potential energy of various helium lattices and zero point energy. I, cubic face-centred; II, simple cubic; III, diamond; *a*, solid 25 atm (exp.); *b*, liquid (exp.).

The particular difficulty which stands in the way of treating the He lattice by the usual methods of lattice theory is the fact that its zero point energy is of the same order of magnitude as the interaction energy and has an effect of decisive importance for the constitution of the lattice.

How unusual the situation with helium is, can be seen from fig. 1. There, for different types of regular lattices, the energy has been plotted as a function of the molar volume. (The body-centred cubic structure, which always gives a slightly higher energy than at least one of the others, has been omitted.) The forces between two isolated He-atoms have been calculated on a quantum-mechanical basis by various authors.* We have used the expression given by Slater and Kirkwood* for the energy of two helium atoms at a fixed distance r:

---

[*] *See* † footnote, p. 576.

$$\phi = \left(77 \,.\, e^{-4,6r} - \frac{0\cdot 149}{r^6}\right) 10^{-11}\,\mathrm{erg} \qquad (r \text{ in A})$$

which is found to give good agreement when used to calculate the second virial coefficient of the gas equation.† Nevertheless, the neglect of the attractive terms proportional to R^{-8} and to higher powers of $1/R$ ‡ implies an uncertainty of about 20–50% which may be partly compensated by the simplified form of the repulsive term; in any case, we must be content with a rough qualitative discussion, and cannot aim at any great numerical exactitude.

The curves in fig. 1 are calculated by summing ϕ over all atoms of the different lattices. Here one relies on the additivity which is characteristic of the molecular forces and which follows from quantum mechanics in the same degree of approximation as the forces are defined themselves. One obtains the following expressions for the lattice energy per mol (the repulsion term is only summed over the nearest and the second nearest neighbours):

For the face-centred cubic lattice:

$$\left[669\cdot 6\, e^{-5\cdot 16R}\left(1 + \tfrac{1}{2} \,.\, e^{-2\cdot 13R}\right) - \frac{0\cdot 780}{R^6}\right] 10^5\,\frac{\mathrm{cal}}{\mathrm{mol}}$$

For the body-centred cubic lattice:

$$\left[446\cdot 4\, e^{-5\cdot 02R}\left(1 + \tfrac{3}{4} \,.\, e^{-0\cdot 784R}\right) - \frac{0\cdot 784}{R^6}\right] 10^5\,\frac{\mathrm{cal}}{\mathrm{mol}}$$

For the simple cubic lattice:

$$\left[334\cdot 8\, e^{\;4\cdot 6R}\left(1 + 2 \,.\, e^{-1\cdot 905R}\right) - \frac{0\cdot 907}{R^6}\right] 10^5\,\frac{\mathrm{cal}}{\mathrm{mol}}$$

For the diamond lattice:

$$\left[223\cdot 2\, e^{-3\cdot 98R}\left(1 + 3 \,.\, e^{-2\cdot 52R}\right) - \frac{1\cdot 31}{R^6}\right] 10^5\,\frac{\mathrm{cal}}{\mathrm{mol}}.$$

---

* London, 'Z. Physik,' vol. 63, p. 245 (1930); 'Z. phys. Chem.,' B, vol. 11, p 222 (1930); Slater and Kirkwood, 'Phys. Rev.,' vol. 37, p. 682 (1931).

† Kirkwood and Keyes, 'Phys. Rev.,' vol. 37, p. 832 (1931).

‡ Margenau, 'Phys. Rev.,' vol. 38, p. 897 (1931).

Here R^3 is the volume per atom, R is measured in A.

In fig. 1 are also shown the experimental values of the density and of the energy content of the liquid state, *b*, and of the solid state (under pressure), *a*. One sees that a volume expansion up to almost three times the "classical" volume and a compensation of about 90% of the "potential" energy content are to be attributed to the zero point energy, and it is evident that an attempt to calculate the lattice in the usual way by adding $9/8\, h\nu_{\text{Debye}}$ for the zero point energy could not succeed.*

Nor does the Einstein model, which considers every individual atom as oscillating in its potential hollow formed by the forces of its neighbours, apply because with such great interatomic distances it leads to a potential hump half-way, *i.e.*, just where there should be minimum at the "equilibrium" position. The atom would prefer to stick to the wall of its hollow unless it were permanently removed by its zero point motion. The energy of the latter therefore cannot be calculated even approximately from the classical proper frequency at the equilibrium position.

As an exact treatment of the simultaneous interaction of many helium atoms taking into account their wave nature is scarcely possible, one might try to start from the opposite limiting case and consider first the zero point energy of rigid spheres of finite diameter, and then superimpose the interaction energy. The quantization of the translatory motion of rigid spheres (or of their mean free path) was a famous problem never definitely solved in the older Quantum Theory. Its lowest eigenvalue has been estimated by Heitler† and afterwards by Lenz‡ on a quantum-mechanical basis to be

$$E_0 = \frac{h^2 d}{2\pi m R^3} \qquad (R \gg d), \tag{1}$$

d being the diameter of the spheres, R the mean distance between the atoms ($N_L R^3$ = mol volume). But this estimate only applies for $R \gg d$. For the limiting case of very high density we estimate roughly

$$E_0 = \frac{h^2}{8m\,(r-d)^2} \qquad r \approx d, \tag{2}$$

where r is the shortest interatomic distance in closest packing ($r = 2^{1/6}R$). Equation (2) gives the lowest eigenvalue of a mass m which is confined to the interior of a sphere of a radius $r - d$. The intermediate case can scarcely be treated rigorously. We have used the formula

---

* Herzfeld and Göppert-Meyer, 'Phys. Rev.,' vol. 46, p. 996 (1934).

† 'Z. Physik,' vol. 44, p. 161 (1927).

‡ 'Z. Physik,' vol. 56, p. 778 (1929).

$$E_0 = \frac{h^2 d}{2\pi m (R - 2^{-1/6} d)^2 (R + kd)} \qquad k = \frac{2^{7/3}}{\pi} - 2^{-1/3} = 0{\cdot}713, \quad (3)$$

which merges into the formulae (1) and (2) in the two limits of large and small values of R. The negative value of the zero point energy, $-E_0$, calculated by formula (3) has been plotted in fig. 1, dotted curve. The quantity d in (3), the diameter of the helium atoms, cannot of course be sharply defined. We have used the value $d = 2{\cdot}35$ A, which was found most suitable and is near the value where ϕ vanishes (2·6 A). (In gas theory one uses $d = 1{\cdot}95$ A; there $\phi = 6{\cdot}79 \times 10^{-14}$ erg $= 3/2\, k \,.\, 335°$ abs.)

One sees that this amount of zero point energy can account for the expansion of the volume to three times its original value and the reduction of the energy content to one-tenth of the energy of the "classical" equilibrium position. It is doubtful how far one is entitled to deduce anything further from these curves. One is tempted simply to superimpose this zero point energy on the different potential curves in order to estimate the total energy.* This is shown in fig. 2. Accordingly not the closest packed structure but the diamond structure would have the lowest energy.† The molecular volume (28 cm^3) and energy (17 cal/mol) of the equilibrium position A correspond fairly well with the experimental values for the liquid state (27·6 cm^3) and about 14 cal/mol respectively. Compression down to 24·9 cm^3 (experimental value 23·2 cm^3) leads to a state B which has the energy of 16 cal/mol (experimentally about 13 cal/mol), which is in equilibrium with the state C (possibly the solid state), connected with B by the common tangent BC. The slope BC gives the equilibrium pressure of about 42 atmospheres (experimental value 25 atmospheres). C has the volume 20·6 cm^3 (19·2 cm^3 by experiment) and the energy 12·4 cal (about 11 cal by experiment).

One should not, however, over-estimate the exactitude which can properly be expected. The curves, fig. 2, are the result of subtracting two quantities of the same order of magnitude; an inexactitude of only

---

* In this approximation there is no particular influence of the Bose Statistics of the He-atoms to be considered.

† *Note added in proof, November* 18, 1935—This result depends entirely upon the fact that the zero point energy has been considered to be a function of the molecular volume only, independent of the configuration, an assumption which seems roughly justified since the zero point energy is not based upon a simple interaction between pairs of atoms like, for example, the Van der Waals forces.

20% in the zero point energy or in the potential ϕ would give rise to deviations of about 50% in the total energy. Furthermore, we have chosen the best fitting value of d.

According to fig. 2, one would expect further compression to change the simple cubic structure into a closest packed modification. But it is quite possible that in reality curve II, belonging to the simple cubic structure, does not project enough to cut the tangent joining the two other curves. Then the diamond configuration would change under sufficient pressure immediately into the closest packed configuration which in any case is stable for high pressures. The existence of a simple cubic modification—it would be the first example of an atom lattice of this type—cannot therefore be predicted with certainty. In Table I the figures in brackets show the values which would result from assuming a direct transition from the diamond to the closest packed structure if for these two structures one uses the same energy curves as plotted in fig. 2 and for the cubic structure one only slightly higher.

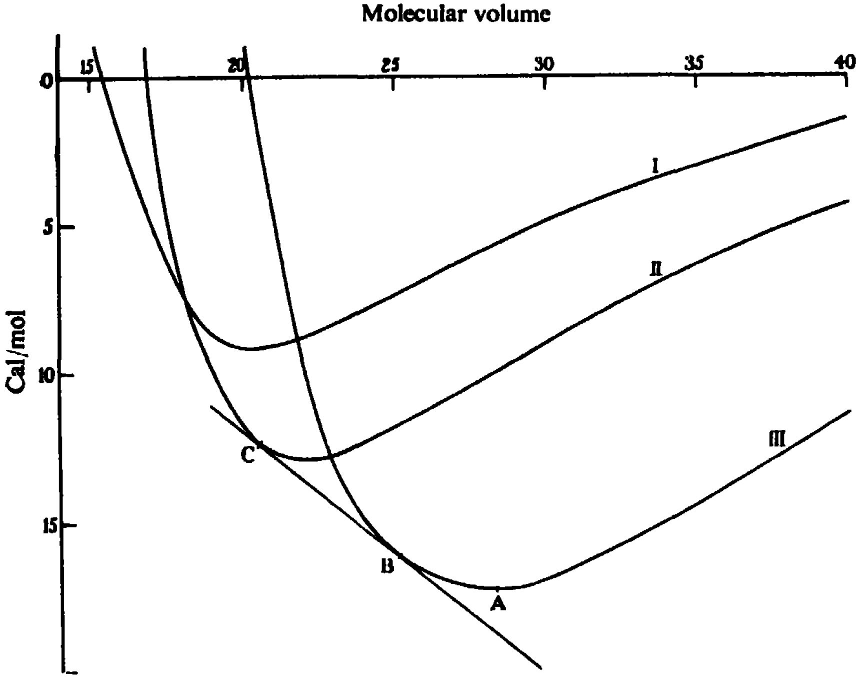

FIG. 2—Estimate of the total energy of various helium lattices. I, face-centred cubic; II, simple cubic; III, diamond.

Is liquid helium below the λ-point to be simply interpreted as going into the ordered state of a diamond lattice? From the zero point energy of

Table I—Observed and Calculated Dates of He at 0° Abs

	Theoretical	Experimental
Pressure 0 -		
Liquid—		
Molecular volume	28 cm^3	27·6 cm^3
Energy	17 cal/mol	14 cal/mol
Equilibrium pressure—		
Liquid—		
Molecular volume	24·9 (24·2) cm^3	23·2 cm^3
Energy	16 (15·2) cal/mol	13 cal/mol
Solid—		
Molecular volume	20·6 (18·7) cm^3	19·2 cm^3
Energy	12·4 (8·3) cal/mol	11 cal/mol
Equilibrium pressure	42 (62) atm	25 atm

this state we may estimate the range ρ which according to the uncertainty principle is required for the zero point motion. If the zero point energy were merely kinetic energy, we should obtain (*cf.* equation (2)):

$$E_0 = \frac{h^2}{8m\rho^2}.$$

Assuming the zero point energy in the liquid state to be about 34 cal/mol we obtain:

$$\rho = 1\cdot85 \text{ A}.$$

That means that each He-atom, here imagined as a ball of 2·35 A diameter, is spread over a region of at least $2\cdot35 + 2 \times 1\cdot85 = 6$ A diameter. That is considerably more than is left in the tetrahedron with edges 5 A in length formed by the four nearest neighbours in the diamond configuration. But possibly this estimate is too pessimistic. The 6 A would mean the minimum diameter of a *closed* sphere which in its interior contains a He-atom of not more than 34 cal/mol. If we ask only for the mean uncertainty Δx of the position of an helium atom with momentum

$$p_x \approx \sqrt{\frac{2mE_0}{3}},$$

we get

$$\Delta x \approx \frac{h}{4\pi}\sqrt{\frac{3}{2mE_0}} = 0\cdot53 \text{ A}.$$

This gives a "mean" diameter of $0\cdot53 + 2\cdot35 = 2\cdot9$ A which has plenty of room in the tetrahedron. Nevertheless, one sees that at the best one can speak of a statistical preference for the equilibrium position.

There will be a considerable probability of finding every atom outside its tetrahedron, and this signifies that one cannot definitely localize the helium atoms in a spatial lattice.

One may of course speak of the *probability function of the atomic distances*, and one will gather from our calculations of the energy that this statistical distribution of the atomic distances cannot differ very much from that of a diamond lattice, which of course is very characteristically different from the distribution function of the closest packed structure. This conception, which could be tested by an X-ray analysis, seems not to be so unsatisfactory in view of the very small viscosity of this phase, which is hardly to be understood by assuming that it is simplya common crystallized state.

For the closest packed state the zero point energy of about 60 cal/mol implies a range of only $\rho \simeq 1 \cdot 4$ A. The shortest distance is comparatively large in the closest packed structure, namely $3 \cdot 55$ A for a molecular volume of $19 \cdot 2$ cm^3,* so that there is no difficulty in localizing a helium atom between its 12 neighbours in the solid state.

In conclusion, I wish to express my thanks to Professor F. A. Lindemann, F.R.S., for his kind interest in this work and to Imperial Chemical Industries, Limited, whose generosity made it possible for me to continue my researches in Oxford.

SUMMARY

It is shown why the application of the customary methods of lattice theory to condensed helium could not succeed and how one can roughly take account of the decisive contribution of the zero point energy which is due to the quantization of the mean free path. Closest packed structure has been found to be stable only under pressure and this seems to explain why solid helium can only exist, even at the absolute zero, under pressure.

If no external pressure is applied a configuration with the coordination number four has proved to have considerably lower energy. In seems that this configuration gives a rough model of the liquid modification of helium which is stable at the absolute zero.

---

* With the diamond structure, and a molecular volume of the liquid state of 28 cm^3, the shortest distance is only $3 \cdot 09$ A.

Studies on Gas-Solid Equilibria
VI—Adsorption from Binary Gas Mixtures by Silica Gel

By Bertram Lambert and Herbert Stone Heaven

(*Communicated by F. Soddy, F.R.S.—Received August* 19, 1935)

In Part V* of this work, an experimental method was described for the study of pressure-concentration equilibria between adsorbent solids and binary gas mixtures. This technique has made it possible to obtain experimental values of high accuracy and reliability for (*a*) gas volumes admitted to an adsorption system (which is maintained at a constant temperature); (*b*) the total volume and the total pressure of the gaseous phase within the system at equilibrium; (*c*) the total volume of gas adsorbed by the solid adsorbent; (*d*) the exact composition of the gaseous phase at equilibrium.

The amount of *each* gas in the adsorbed phase and the partial pressure of *each* gas in the gaseous phase can therefore be determined with certainty; and reliable data can consequently be obtained for the examination of the problem of adsorption from binary gas mixtures by adsorbent solids.

The results already published (Part V) on the adsorption from oxygen-nitrogen mixtures by silica gel are notable in that they could not have been predicted from considerations of current hypotheses on adsorption. The procedure followed in those experiments was selected with a view to obtaining " ascending " and " descending " points on pressure (partial)-concentration isothermals; it was too complicated to allow simple theoretical deductions to be drawn from the results, although it clearly showed the reality and essential stability of the remarkable equilibrium conditions found to exist in the system.

In this part of the work the following simplified procedure has been adopted for the study of the pressure-concentration equilibria between silica gel and binary mixtures of two gases X and Y :

(i) The pressure-concentration equilibria for the *separate* pure gases are determined, at 0° C, and at pressures up to one atmosphere; isothermals are plotted.

(ii) A known volume of gas X is introduced into the evacuated adsorption system, maintained at 0° C, and left for 12 hours. A pressure reading having shown that true equilibrium has been reached (the equilibrium point falling exactly on its own isothermal), a known and approximately equal volume of gas Y is introduced. After a further 12 hours the equilibrium gas (total) pressure is read and a sample of the true equilibrium gaseous phase withdrawn and analysed.

---

* 'Proc. Roy. Soc.,' A, vol. 144, p. 205 (1934).

(iii) A separate, independent experiment is then carried out exactly as in (ii), except that larger volumes of the gases are added and, consequently, larger equilibrium pressures obtained.

(iv) Separate, independent experiments are now carried out exactly as in (ii) and (iii), except that gas Y is introduced prior to gas X.

(v) Separate, independent experiments are finally carried out exactly as in (ii) and (iii), except that measured volumes of *a mixture containing known and approximately equal volumes of X and Y* are used throughout.

The results so obtained make it possible to determine, with certainty, the volumes of X and Y adsorbed and the partial pressures of X and Y in the equilibrium gaseous phase: (*a*) when X is given priority of contact with the solid adsorbent; (*b*) when Y is given priority of contact with the solid adsorbent; (*c*) when X and Y, in approximately equal concentrations, reach the solid adsorbent simultaneously.

Comparison of these values with those obtained from experiments with the separate, pure gases shows how the adsorption of *each* of the constituents of a binary gas mixture is affected by the presence of the other under the above simple conditions, when the two gases are present in the adsorption system in approximately equal amounts.

Using this procedure, the pressure-concentration equilibria between silica gel and the following binary gas mixtures have been investigated—(1) oxygen-argon; (2) oxygen-nitrogen; (3) oxygen-helium.

The silica gel was the same as that used in the earlier experiments, and the pressure-concentration isothermals for the separate pure gases oxygen and nitrogen are given in Part V. The gel shows no measureable adsorptive power for helium at 0° C.

The pressure-concentration equilibria between the gel and pure argon at 0° C and at pressures up to one atmosphere have been determined, and the values are given in the Table I.

These results are plotted in fig. 1 and the isothermals for pure nitrogen and for pure oxygen are given alongside for comparison.

The adsorption isothermals for all these three gases are nearly linear, and the ratio *volume of gas adsorbed/pressure of gas*, shows a high degree of constancy; it may therefore be taken that each of these gases is adsorbed by silica gel at 0° C in amounts directly proportional to the pressure. The equilibria in all three gases are isothermally reversible down to quite low pressures, and the gel shows no sign of having reached saturation even at the higher pressures.

Since it was essential to know whether the intrinsic adsorptive power of the silica gel for the separate, pure gases remained constant during the whole course of these experiments, independent check determinations of its adsorptive power for each gas were carried out at intervals spread over the three years occupied by the work; these determinations have shown that the adsorptive power of the gel has undergone no change whatever during the whole period.

TABLE I—SILICA GEL-ARGON EQUILIBRIA AT 0° C

No.	Volumes of argon adsorbed in cc at S.T.P.	Equilibrium pressures in mm of Hg at 0° C	$\frac{\text{Volume adsorbed}}{\text{Pressure}}$
1	1·50	67·86	0·022
2	3·14	143·62	0·022
3	4·83	221·11	0·022
4	6·49	296·73	0·022
5	8·13	373·05	0·022
6	9·74	448·84	0·022
7	11·36	525·58	0·022
8	12·74	590·51	0·022
9	13·86	643·78	0·022
10	15·12	704·94	0·021
11	16·34	764·26	0·021
12	14·85	689·70	0·022
13	13·33	617·52	0·022
14	11·93	550·67	0·022
15	10·30	472·69	0·022
16	8·91	408·06	0·022
17	7·23	329·76	0·022
18	5·86	265·86	0·022
19	4·30	194·09	0·022
20	2·91	131·11	0·022
21	1·77	78·95	0·022
22	0·84	37·35	0·022
23	0·52	22·37	0·023

The equilibrium points are numbered in the order in which they were obtained. " Ascending " points—Nos. 1 to 11; " Descending points "—Nos. 12 to 23.

If a measured volume of any one of these pure gases is introduced into the evacuated adsorption system, maintained at 0° C, the equilibrium point invariably falls exactly on the originally determined isothermal for that gas *provided that the gel has first been adequately* " *washed out* " *with* *the same pure gas.* In experiments on the adsorption of gases by solids the importance of the proper pre-treatment of the solid adsorbent—adequate evacuation, heating and "washing out" with the gas to be studied—cannot be exaggerated; very large errors may arise from neglect in any detail of this operation. It has been found that the only safe criterion of the reliability of measurements of gas-solid equilibria is that they can be repeated (and fresh equilibrium points found to fall exactly on the same isothermal) in independent experiments.

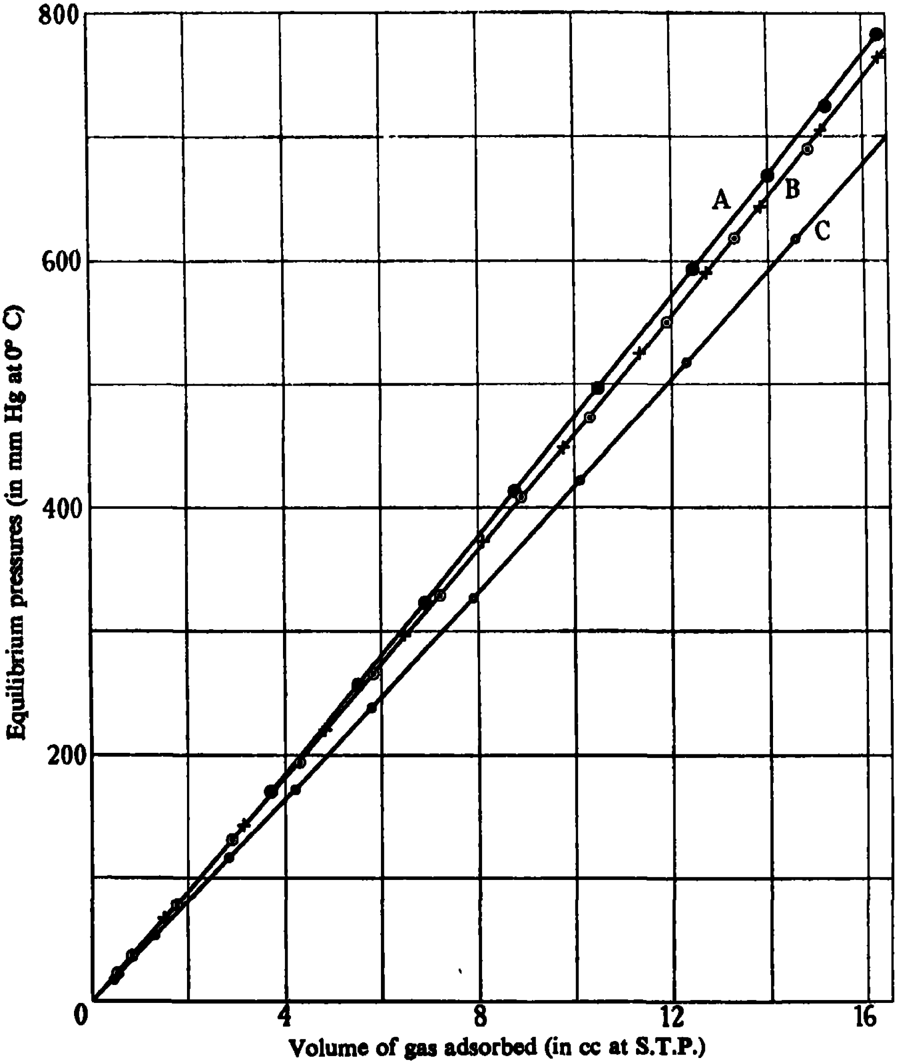

FIG. 1—A, oxygen; B, argon; C, nitrogen.

The proper pre-treatment for any particular adsorbent solid—so that repeatability of results is obtained without altering the intrinsic adsorptive power of the solid—can only be found by careful experiment. The proper pre-treatment of the silica gel used in this work is as follows:

(*a*) The adsorption system is thoroughly evacuated (to a steady, maintained pressure of less than 10^{-4} mm mercury) by means of a Gaede two-stage mercury vapour pump backed by a Gaede rotary oil pump.

(*b*) The silica gel is then heated to 150° C by means of a small electric resistance furnace made to fit closely round the vessel containing it; the temperature of the gel is maintained at 150° C for 1½ hours and then allowed to fall slowly, the pumps running all the time.

(*c*) The adsorption system is next cooled to 0° C and about 10 cc of the gas to be studied is introduced; the gas is left in contact with the gel for at least half an hour. The system is again thoroughly evacuated and heated exactly as in (*a*) and (*b*).

(*d*) The whole detailed process of " washing out " with the gas to be studied, followed by evacuation and heating is then repeated.*

Careful experiments have shown that the silica gel, at 0° C, has a negligible adsorptive power for pure helium and this gas has been used to measure the volume, free gas space, of the adsorption system (*vide* Part V). It might have been expected, therefore, that, after the gel had been in contact with pure helium, a thorough evacuation and heating would be a sufficient pre-treatment before the subsequent study of the adsorption of oxygen; but it has been found that most fictitious values are obtained if this is done; an oxygen equilibrium point can only be made to fall on its own isothermal if the proper *full* pre-treatment of the gel is carried out. This matter is dealt with later.

ADSORPTION BY THE SILICA GEL FROM OXYGEN-ARGON MIXTURES AT 0° C

1*st Series*—The gel was " washed out " with *argon* as described above; a measured volume of argon was then added and the system left overnight to come to equilibrium, the equilibrium being checked by the point falling exactly on the pure argon isothermal; a measured, approximately equal, volume of *oxygen* was then added and the system again left overnight to come to equilibrium.

The total pressure having been read and checked some hours later, a sample of the equilibrium gaseous phase was then withdrawn and analysed;

---

* In those experiments involving the introduction of *mixed* gases, containing approximately equal volumes of the two constituents, into the adsorption system, this mixture is used in the " washing out " process.

the volume of each gas taken into the adsorbed phase and the partial pressure of each gas in the equilibrium gaseous phase could then be calculated.

Two separate, independent experiments, A and B, were carried out in this series at different total pressures; the results obtained are given in Table II.

TABLE II

Experiment	Volume of oxygen adsorbed*	Partial pressure of oxygen	Volume of argon adsorbed*	Partial pressure of argon
		1st Series		
A	2·1 (−1·0)	141·3	4·0 (+1· 1)	132·2
B	3·2 (−1·8)	231·8	7·0 (+2·15)	218·9
		2nd Series		
C	4·6 (+1·75)	129·0	1·5 (−1·65)	143·5
D	7·9 (+3·05)	224·3	2·5 (−2·9)	245·9
		3rd Series		
E	3·3 (+0·25)	137·5	3·1 (+0·1)	134·7
F	5·1 (+0·4)	215·3	5·0 (+0·05)	224·2

* Volumes of gas are given in cc at S.T.P. Pressures (partial) are given in mm of mercury at 0° C. After each value given for the amount of gas adsorbed from the *mixture*, there is stated (in brackets with a + or − sign) the *difference* between this amount and the amount which would be adsorbed from *the pure gas alone at the same pressure*. The + sign indicates that more (and the − sign less) of the gas is adsorbed from the mixture than from the single pure gas.

2nd Series—The gel was " washed out " with *oxygen* and *oxygen added first*; otherwise the procedure was the same as in the 1st Series.

Two separate independent experiments, C and D, were carried out; the results are given in Table II.

3rd Series—The gel was " washed out " with a *mixture* (containing about equal proportions of oxygen and argon) and measured volumes of *a mixture of oxygen and argon* (in known and approximately equal proportions) added to the system throughout; otherwise the procedure was the same as in the 1st and 2nd Series. Two separate, independent experiments, E and F, were carried out; the results are given in Table II.

The results of these experiments are plotted in fig. 2 and fig. 3 to show how the adsorption of each gas is affected by the presence of the other: (*a*) when argon is given priority of contact with the gel; (*b*) when oxygen is given priority of contact with the gel; (*c*) when both gases reach the gel simultaneously.

In all the experiments the two constituent gases of the mixture are present in approximately equal proportions at the equilibrium points.

It will be seen that the two independent experiments carried out in each series, at different pressures, afford a good confirmation of one another.

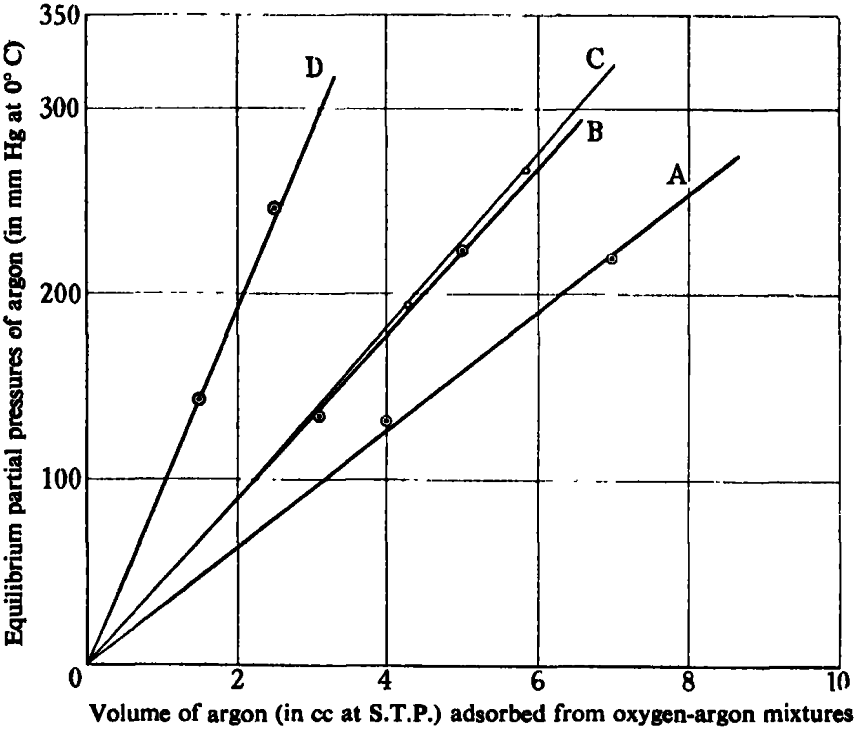

FIG. 2—Argon isothermals, at 0° C, in the presence of oxygen. A, gel "washed out" with argon; argon added first. B, gel "washed out" with oxygen-argon mixture; mixture added throughout. C, Pure argon isothermal. D, gel "washed out" with oxygen; oxygen added first. In A, B, and D approximately equal volumes of oxygen and argon are present at all equilibrium points.

The results show that when silica gel comes into contact with mixtures of oxygen and argon in approximately equal concentrations, the amount of each gas adsorbed depends to a very marked degree on which of the two gases has been given priority of contact with the gel.

(*a*) When argon is given priority of contact, the addition of oxygen causes an increase of about 40% in the amount of argon adsorbed, while the oxygen is adsorbed about 35% less than it would be in the absence of the argon. *The actual amount of argon in the adsorbed phase is double the amount of oxygen.*

(*b*) When oxygen is given priority of contact, the situation is reversed and the effect is even more marked; the addition of argon causes an increase of over 60% in the amount of oxygen adsorbed, while the argon is adsorbed about 50% less than it would be in the absence of the oxygen.

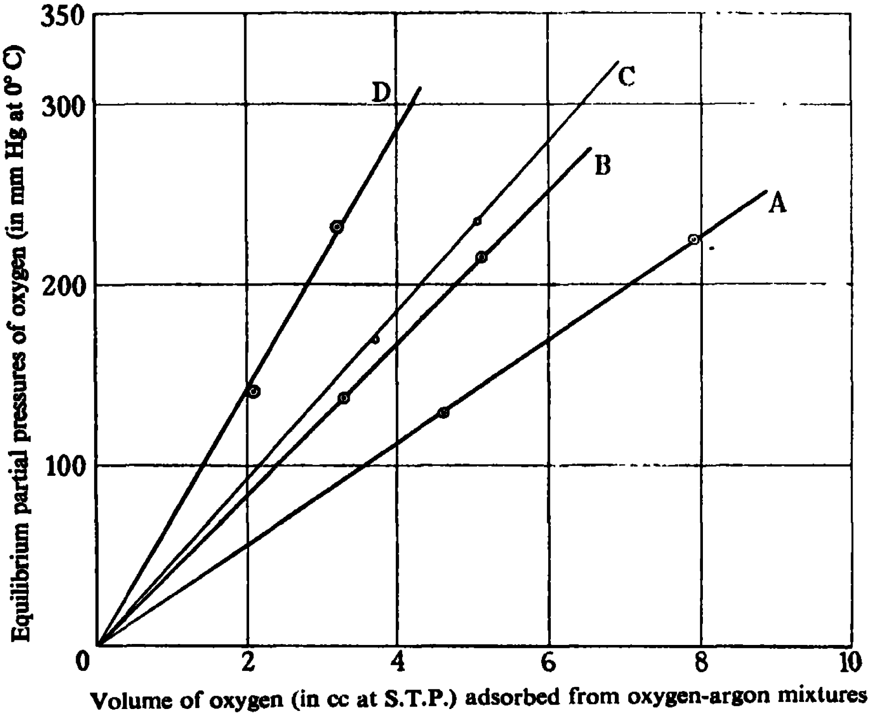

FIG. 3—Oxygen isothermals, at 0° C, in the presence of argon. A, gel " washed out " with oxygen; oxygen added first. B, gel " washed out " with oxygen-argon mixture; mixture added throughout. C, Pure oxygen isothermal. D, gel " washed out " with argon; argon added first. In A, B, and D approximately equal volumes of oxygen and argon are present at all equilibrium points.

The actual amount of oxygen in the adsorbed phase is three times the amount of argon.

(*c*) When, however, the two gases in equal concentration reach the gel simultaneously, each of them is adsorbed in an amount nearly the same as if it alone were present, *i.e.*, the gases are adsorbed in amounts nearly in direct proportion to the partial pressures. *There are actually equal amounts of the two gases in the adsorbed phase.*

In all experiments the *added amounts* of argon and oxygen adsorbed from the mixtures are greater than the *sum of the separate amounts* of the pure gases adsorbed singly at the same pressures; in some experiments this increase in the total amount of gas adsorbed is nearly 10%.

ADSORPTION BY THE SILICA GEL FROM OXYGEN-NITROGEN MIXTURES AT 0° C

The procedure was the same as in the investigation of the oxygen-argon mixtures.

1st Series—The gel was "washed out" with *nitrogen* and *nitrogen was added first*. Two separate, independent experiments, G and H, were carried out; the results are given in Table III.

TABLE III

Experiment	Volume of oxygen adsorbed	Partial pressure of oxygen	Volume of nitrogen adsorbed	Partial pressure of nitrogen
		1st Series		
G	5·8 (+0·2)	259·4	6·2 (−0·3)	268·3
H	4·25 (+0·1)	188·2	4·5 (−0·2)	193·2
		2nd Series		
I	2·8 (+0·4)	107·5	2·3 (−0·45)	112·4
J	5·6 (+0·9)	213·9	4·6 (−0·9)	224·8
		3rd Series		
K	2·6 (+0·05)	116·2	2·5 (−0·25)	112·5
L	5·0 (+0·2)	220·4	5·2 (−0·4)	230·3

2nd Series—The gel was "washed out" with *oxygen* and *oxygen was added first*. Two separate, independent experiments, I and J, were carried out; the results are given in Table III.

3rd Series—The gel was "washed out" with a *mixture* (containing about equal proportions of oxygen and nitrogen), and measured volumes of *a mixture of oxygen and nitrogen*, in known and approximately equal proportions, added throughout. Two separate, independent experiments, K and L, were carried out; the results are given in Table III.

The results of these experiments on the adsorption from oxygen-nitrogen mixtures are plotted in fig. 4 and fig. 5 to show how the adsorption of each gas is affected by the presence of the other: (*a*) when nitrogen is given priority of contact with the gel; (*b*) when oxygen is given priority of contact with the gel; (*c*) when both gases reach the gel simultaneously.

In all experiments the two constituents of the mixture are present in approximately equal proportions at the equilibrium points.

The results show that when silica comes into contact with mixtures of oxygen and nitrogen in approximately equal concentrations (i) the amount of *oxygen* adsorbed is always *greater* than it would be in the absence of the nitrogen; (ii) the amount of *nitrogen* adsorbed is always smaller than it would be in the absence of the oxygen; (iii) the *added amounts* of oxygen and nitrogen adsorbed from the mixtures is slightly *smaller* than the *sum of the separate amounts* of the pure gases adsorbed singly at the same pressures.

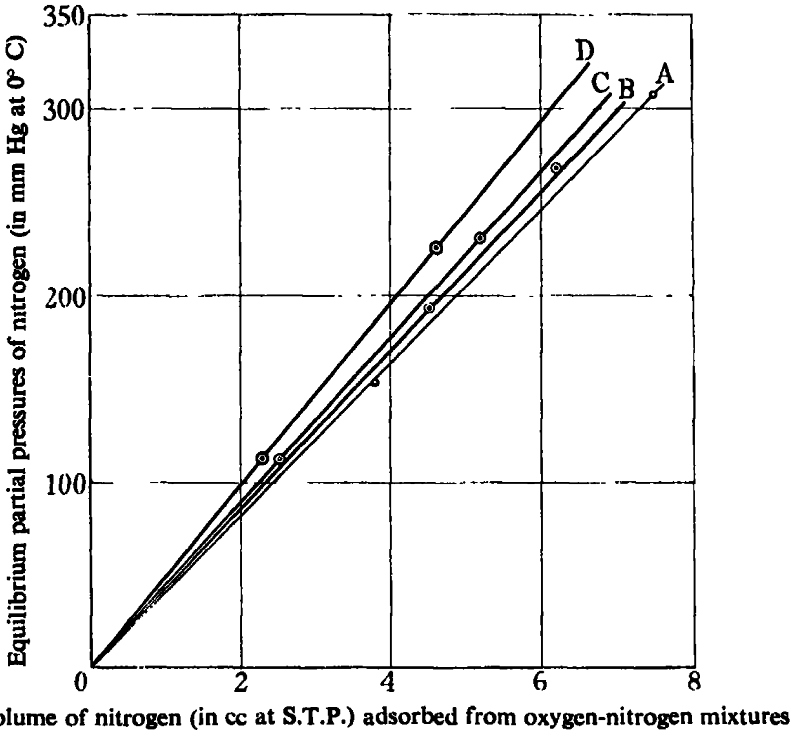

FIG. 4—Nitrogen isothermals, at 0° C, in the presence of oxygen. A, Pure nitrogen isothermal. B, gel " washed out " with nitrogen; nitrogen added first. C, gel " washed out " with oxygen-nitrogen mixture; mixture added throughout. D, gel " washed out " with oxygen; oxygen added first. Approximately equal volumes of oxygen and nitrogen are present at all equilibrium points.

Under the above conditions of experiment, the adsorption of *oxygen* by silica gel is, then, *always increased by the presence of nitrogen*, and the adsorption of *nitrogen is always decreased by the presence of oxygen.*

It is only the *degree* of increase (or decrease) which is affected by the order in which the gases come into contact with the gel. When oxygen is given priority of contact, the amount adsorbed shows the greatest increase; and this increase is least when nitrogen is given priority of contact; while the increase has an intermediate value when the two gases reach the gel simultaneously.

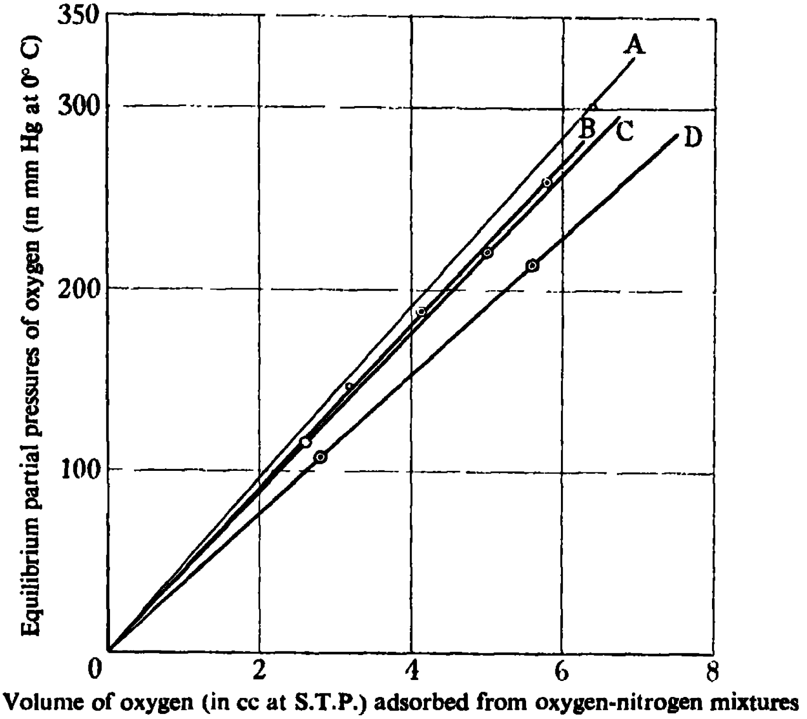

FIG. 5—Oxygen isothermals, at 0° C, in the presence of nitrogen. A, Pure oxygen isothermal. B, gel " washed out " with nitrogen; nitrogen added first. C, gel " washed out " with oxygen-nitrogen mixture; mixture added throughout. D, gel " washed out " with oxygen; oxygen added first. Approximately equal volumes of oxygen and nitrogen are present at all equilibrium points.

When nitrogen is given priority of contact, the amount adsorbed shows the smallest decrease; and this decrease is greatest when oxygen is given priority of contact; while the decrease has an intermediate value when the two gases reach the gel simultaneously.

The results of the earlier experiments on this same equilibrium (Part V) are thus amply confirmed, although the experiments were carried out under quite different conditions. The earlier experiments do, however, afford valuable evidence of the reality and essential stability of the equilibrium. The measurements were spread over many weeks. During this period, the equilibrium was temporarily disturbed by occasional additions of gas and by the occasional withdrawal of gas samples for analysis; after each such disturbance, the system was allowed to stand for 12 hours before the next point was taken. The fact that, in these circumstances, the relative amounts of oxygen and nitrogen in the adsorbed phase remained the same throughout, and that twelve equilibrium points (from two separate, independent experiments) fell on almost linear partial pressure-concentration isothermals, affords very convincing evidence of the accuracy of the experimental technique and the stability of the equilibrium reached in 12 hours.

It is important to note that the *total pressure* in all these systems becomes steady within a short space of time after the addition of gas mixtures. Total pressures read immediately after the addition of any of the above gases (or mixtures) show no measurable alteration the next day or even, as careful experiments have shown, after several weeks. While this must mean that the process of adsorption is very rapid for binary mixtures, as it is well known to be for single pure gases, it does not, of course, imply that real equilibrium is equally rapidly attained in the adsorption layer. This point is dealt with in the discussion.

ADSORPTION BY THE SILICA GEL FROM OXYGEN-HELIUM MIXTURES AT 0° C

Many experiments have been carried out on the adsorption by the silica gel from mixtures of oxygen and helium, and it has been proved that the amount of oxygen adsorbed is not affected by the presence of helium *provided that the gel has previously been given the full " washing out " treatment with oxygen.*

If this has been done, it does not matter whether the oxygen or the helium is added first; when mixtures of the two gases are left overnight in contact with the gel, it is found that the amount of oxygen adsorbed is directly proportional to its partial pressure and that the oxygen equilibrium point falls exactly on its own isothermal; this has been shown in five separate, independent experiments.

If, however, the gel has first been given the full " washing out " pretreatment with helium before being put into contact with oxygen-helium mixtures, the results show that the amount of oxygen adsorbed is *not* directly proportional to its partial pressure; most variable results have been obtained for the amounts of oxygen adsorbed after the system has been left to stand overnight at 0° C.

This matter may have a most important significance and requires further investigation before any opinion can be expressed upon it. It is to be remembered that the silica gel has a negligible adsorptive power for pure helium at 0° C.

In all these experiments the partial pressures of the two gases in the equilibrium gas phase have been calculated from determinations of the composition of that phase; this involves the assumption that Dalton's Law of Partial Pressures is rigidly true for the binary mixtures studied—oxygen-argon, oxygen-nitrogen, and oxygen-helium—at pressures up to one atmosphere.

Masson and Dolley* point out that " The rigid statement of the law of partial pressures, namely, that the pressure of a gaseous mixture is the sum of the contributions made by the several varieties of molecule actually present in it, does not lend itself to direct experimental proof. For practical purposes, Dalton's law is usually taken to imply that the total pressure is the sum of those which can be experimentally measured by enclosing each constituent in turn by itself in the volume of the mixture ": they call this modified form the Law of Additive Pressures. The law in either form covers the cases of gases which deviate from Boyle's Law, but it involves the assumption, as Dalton himself stated, that each constituent of the mixture retains its individual character and does not, by its presence, affect the pressure of the others.

The validity of the law of additive pressures has been very carefully investigated for the gas mixtures used in this work, and it has been proved that the law is rigidly obeyed by all these mixtures at pressures up to one atmosphere.

The method of calculating the partial pressures of the constituent gases in the equilibrium gas phase is therefore justified, and it becomes clear that the remarkable equilibrium conditions found to exist in these gas-solid systems cannot be caused by abnormalities in the gaseous phase; the cause must therefore be sought in the nature of the adsorbed phase.

Theoretical considerations of the problem of adsorption of gases by solids have hitherto been founded on experimental work dealing with the adsorption of single gases and, usually, the underlying basis of these considerations has been the conception, due to Langmuir, that the adsorbed phase consists of a monomolecular gas layer. The remarkable equilibrium conditions found to exist between silica gel and oxygen-argon mixtures are quite incompatible with the existence of an adsorbed gas layer only one molecule thick.

---

* 'Proc. Roy. Soc.,' A, vol. 103, p. 524 (1923).

The physical properties of oxygen and argon are very similar; their critical temperatures and pressures are almost identical, and there are only small differences between their van der Waals constants. The pure gases are adsorbed singly to very nearly the same extent by silica gel, and the amounts adsorbed, at 0° C, and at all pressures up to one atmosphere, are directly proportional to their pressures. Although their chemical properties are very different, it is difficult to conceive of chemical interaction between oxygen and argon or between argon and silica gel. It would thus appear that the system silica gel—oxygen-argon (studied at 0° C at pressures below one atmosphere, and using equal proportions of the two gases) afforded an almost ideally simple case for the study of adsorption from binary gas mixtures. Further, the amounts of gas adsorbed at 0° C are sufficiently large to permit of accurate measurements being made.

If, when silica gel is put in contact with a mixture containing equal volumes of oxygen and argon, the adsorbed phase consists of a gas layer only one molecule thick, then *all* the adsorbed molecules must be in direct and uninterrupted contact with the gaseous phase. In these circumstances, with a system of such simplicity, it would be expected that neither gas would have any marked effect on the adsorption of the other. *Since the adsorptive power of the gel is the same for each gas and the gases are present in equal concentration, both adsorbed phase and gaseous phase should always contain equal amounts of oxygen and argon, at equilibrium*; the order in which the two gases are brought into contact with the gel should have no influence on the final state of equilibrium and the total added amounts of the two gases adsorbed from the mixture should be the same as the sum of the separate amounts adsorbed singly from the pure gases at the same pressures. But the experimental results show, quite definitely, that *the composition of the adsorbed phase is very markedly influenced by the order in which the two gases are brought into contact with the silica gel*:

(*a*) When oxygen is given priority of contact with the gel, the composition of the adsorbed phase is given by the ratio:

$$\frac{\text{Number of oxygen molecules adsorbed}}{\text{Number of argon molecules adsorbed}} = \frac{3}{1}$$

(*b*) When argon is given priority of contact with the gel, the composition of the adsorbed phase is given by the ratio:

$$\frac{\text{Number of oxygen molecules adsorbed}}{\text{Number of argon molecules adsorbed}} = \frac{1}{2}$$

(*c*) When the two gases (in admixture) reach the gel simultaneously, the composition of the adsorbed phase is actually identical with that of the gaseous phase and

$$\frac{\text{Number of oxygen molecules adsorbed}}{\text{Number of argon molecules adsorbed}} = 1$$

There is no doubt about the reality and essential stability of the equilibrium conditions in the different systems, and they are obviously incompatible with an adsorbed phase consisting only of a monomolecular gas layer in which all the adsorbed molecules are in uninterrupted contact with the gaseous phase.

A possible explanation of these experimental facts may be founded on the assumption that the adsorbed phase consists of a *double* layer of gas molecules—a first, fundamental layer of strongly adsorbed gas molecules which is effectively shielded from contact with the free gaseous phase by a second layer of much less strongly adsorbed gas molecules.

If such a state of things were possible, the introduction of a measured volume of oxygen into the adsorption system would result in the formation, at the gas-solid interface, of a double layer of adsorbed oxygen molecules directly proportional in amount to the pressure of the oxygen. The subsequent addition of an equal volume of argon would double the gas pressure and, *temporarily*, until the argon had diffused to the gas-solid interface, *the concentration of the oxygen molecules in the immediate neighbourhood of this interface would also be doubled.* Since the process of adsorption (at any rate for single gases) is instantaneous, the result would be that the adsorbed phase—now increased in amount to correspond with the doubled pressure—would be made up entirely of oxygen molecules. This state of affairs would persist until the argon had diffused to the gas-solid interface. Oxygen would then desorb from the second layer and be replaced by argon until a state of equilibrium had been reached between the free gas phase and the second layer of adsorbed molecules; the first, strongly adsorbed and effectively shielded, layer of adsorbed oxygen molecules would, however, not be affected, and the final equilibrium would be one set up between the free gas phase and the second layer of adsorbed molecules in uninterrupted contact with it.

Since the adsorptive power of silica gel is the same for oxygen as it is for argon, and the two gases are present in equal proportions, it follows from the theory—assuming equal numbers of molecules in the two adsorbed layers—that the composition of the adsorbed phase should be given by the ratio:

$$\frac{\text{Number of oxygen molecules adsorbed}}{\text{Number of argon molecules adsorbed}} = \frac{3}{1}$$

This is exactly what is shown by experiment.

This ratio should be exactly reversed when argon is given priority of contact with the silica gel; but the experimental results show that the *two* molecules of argon are adsorbed for each molecule of oxygen.

When the two gases, in admixture in equal proportions, reach the gel simultaneously, the amounts of oxygen and argon adsorbed should be equal; the experimental results show that this is actually what happens. It would be expected from the theory that the total added amounts of the two gases adsorbed from the mixture would be the same as the sum of the separate amounts adsorbed singly from the pure gases at the same pressures; the experimental results show, however, that this total is always greater (up to 10% more) than would be expected.

The theory of adsorption outlined above takes no account of any interaction between the molecules in the adsorbed phase except such as would contribute towards the effective shielding of the first layer of adsorbed molecules from the free gas phase. One conceives this shielding effect as being caused by heteropolar forces, and, on the evidence at present available, it would seem that the forces involved in the adsorption of gases by solids are *chiefly* van der Waals forces and heteropolar forces. Homopolar forces cannot, however, be entirely excluded from consideration. Our experiments on the adsorption by silica gel of the single pure gases oxygen, argon, and nitrogen, have shown that the equilibria are isothermally reversible down to pressures of 20 to 30 mm. But the necessity for the drastic pre-treatment of the adsorbent (in order to ensure repeatability of results) in all adsorption experiments, even when the solid has been in contact only with a negligibly adsorbed gas like helium, points to the conclusion that adsorption at very low pressures is not an easily reversible process. Other workers on the subject have drawn attention to the abnormal character of adsorption processes at low pressures, and it seems probable that adsorption under these conditions is associated with very much higher heats of adsorption than those found experimentally for the *whole* adsorption process. Such values are undoubtedly the *mean* of the heats of adsorption associated with the different forces involved.

The close concordance between the experimental results and those predicted from the above theory seem to indicate that the silica gel-oxygen-argon system is very simple in character, as would be expected from the close similarity between the physical properties of the two gases. The marked difference shown to exist between the silica gel-oxygen-argon system and the silica gel-oxygen-nitrogen system is quite unexpected in the absence of any very large differences between the physical properties of the three gases involved. The priority of contact factor, so definite in the former case, is overshadowed in the latter case by what, for the present, must be vaguely termed a mutual interaction factor. Further accurate work—using different gas mixtures and different adsorbent solids—is required before a clearer light can be thrown on the parts played by the factors involved in what seems to be a very complex process.

Thanks are tendered to Messrs. The Imperial Chemical Industries for a grant which helped to defray the cost of apparatus used in this work.

SUMMARY

The adsorption by silica gel at 0° C from the following binary gas mixtures has been studied: oxygen-argon, oxygen-nitrogen, and oxygen-helium. The binary gas mixtures contained equal proportions of the two gases in all cases.

It has been shown that with oxygen-argon mixtures the composition of the adsorbed phase is greatly affected by the order in which the two gases reach the gel surface. When the oxygen is given priority of contact with the gel, the adsorbed phase at equilibrium contains three times as much oxygen as argon; when argon is given priority of contact the adsorbed phase at equilibrium contains only half as much oxygen as argon; and when the two gases (previously mixed) reach the gel simultaneously, the adsorbed phase contains equal amounts of oxygen and argon. These results are shown to be incompatible with a monomolecular adsorbed phase; a theory of adsorption is outlined, involving the assumption of an adsorbed phase consisting of two layers of gas molecules.

With oxygen-nitrogen mixtures, oxygen is always adsorbed more, and nitrogen less, than each of them would be in the absence of the other; the order of priority of contact with the gel only affects the degree of these differences.

With oxygen-helium mixtures, oxygen is adsorbed in the same amount as it would be in the absence of the helium, provided that the gel has previously been adequately " washed out " with oxygen. The adsorptive power of silica gel for helium at 0° C is negligible.

The Rotation of Molecules in Fields of Octahedral Symmetry

By A. F. DEVONSHIRE, University Chemical Laboratory and Trinity Hall, Cambridge

(*Communicated by J. E. Lennard-Jones, F.R.S.—Received August* 19, 1935)

1—INTRODUCTION

A problem in quantum mechanics which has important applications in the theory of specific heats and dielectric constants of solids, is that of determining the rotational energy states of a molecule in a potential field, such as occurs in a crystal.

A mathematical treatment of the rotation of molecules in crystals was first given by Pauling,[*] and the theory has since been extended by several other authors.[†] In these discussions, however, either the potential energy has been assumed to depend only on one angular coordinate or the term involving the second angular coordinate has been supposed to be sufficiently small to be treated as a perturbation.

In this paper we shall discuss the rotation of molecules in a field of octahedral symmetry, as this is a more accurate representation of the field in which molecules move in solids, particularly in crystals of cubical symmetry. The problem is first discussed generally for any field of octahedral symmetry and then more specifically for a special field of this type.

A similar mathematical problem occurs in the theory of electronic orbitals in molecules of the type XY_6, of which SF_6 may be quoted as an example. The calculation of the excited levels of such molecules cannot yet be carried out by the methods which have proved useful for the ground states,[‡] and it is likely that in such cases the method of molecular orbitals, as developed by Lennard-Jones[§] and Mulliken,[||] will prove of increasing value. The analysis of this paper provides an essential step in this development.

---

[*] 'Phys. Rev.,' vol. 36, p. 430 (1930).

[†] For example, by Stern, 'Proc. Roy. Soc.,' A, vol. 130, p. 551 (1930); Fowler, 'Proc. Roy. Soc.,' A, vol. 149, p. 1 (1935); Nielsen, 'J. Chem. Phys.,' vol. 3, p. 189 (1935).

[‡] Slater, 'Phys. Rev.,' vol. 37, p. 481 (1931); vol. 38, p. 1109 (1931).

[§] 'Trans. Faraday Soc.,' vol. 25, p. 668 (1929); vol. 30, p. 70 (1934).

[||] 'Phys. Rev.,' vol. 40, p. 55 (1932); vol. 41, pp. 49, 751 (1932); vol. 43, p. 279 (1933); 'J. Chem. Phys.,' vol. 1, p. 492 (1933); vol. 3, p. 375 (1935).

The problem is also of mathematical interest for it deals with a differential equation which is, in a sense, the analogue in two angular coordinates of Mathieu's equation, which has received so much attention from mathematicians.

2—Formulation of the Problem

Schrödinger's equation for a diatomic molecule is

$$\frac{1}{\sin\theta}\frac{\partial}{\partial\theta}\left(\sin\theta\frac{\partial\psi}{\partial\theta}\right)+\left(\frac{1}{\sin\theta}\right)^2\frac{\partial^2\psi}{\partial\phi^2}+\frac{8\pi^2 I}{h^2}\{E-V(\theta,\phi)\}\psi=0, \qquad (1)$$

where θ and ϕ are the usual Eulerian coordinates, I the moment of inertia of the molecule, and V is the potential energy in which it moves; in the case we are considering, it is a function of octahedral symmetry.

Being a single-valued function of θ and ϕ, V can always be expanded in a series of surface harmonics. If, therefore, we wish to assume an explicit form for V, the simplest and most natural one is the first non-constant term in the general expansion, in surface harmonics, of any function of θ and ϕ having octahedral symmetry.

Now it is shown in a paper by Bethe* that there are no surface harmonics of degree less than four which have octahedral symmetry (except the trivial case of a constant), and that the only surface harmonic of degree four having octahedral symmetry is

$$P_4^0(\cos\theta)+(1/168)\,P_4^4(\cos\theta)\cos 4\phi,$$

where

$$P_l^m(\mu)=\frac{1}{l!\,2^l}(1-\mu^2)^{m/2}\frac{\partial^{l+m}}{\partial\mu^{l+m}}(\mu^2-1)^l, \qquad (2)$$

and the axes of symmetry are the lines

$$\theta=0 \text{ or } \pi; \quad \theta=\tfrac{1}{2}\pi, \quad \phi=0, \pm\tfrac{1}{2}\pi \text{ or } \pi.$$

We shall therefore use as an explicit expression for V:

$$-K\{P_4^0(\cos\theta)+(1/168)\,P_4^4(\cos\theta)\cos 4\phi\}, \qquad (3)$$

where K is a constant.

No generality is gained by adding a constant term, as this only increases the energy by a constant amount without otherwise altering the problem.

The expression for V can also be written in the forms:

$$-K\{\tfrac{1}{8}(3-30\cos^2\theta+35\cos^4\theta+5\sin^4\theta\cos 4\phi)\}$$

---

* 'Ann. Physik,' vol. 3, p. 133 (1929).

or

$$-K\left\{-\tfrac{3}{2}+\tfrac{5}{2}\,\frac{x^4+y^4+z^4}{r^4}\right\}.$$

In fig. 1 we show the orthogonal projection of the equipotential lines on the plane $\theta = \frac{1}{2}\pi$, and in fig. 2 we show the conical projection of the equipotential lines on the plane $x + y + z = \text{const.}$, the vertex of projection being the centre of the sphere.

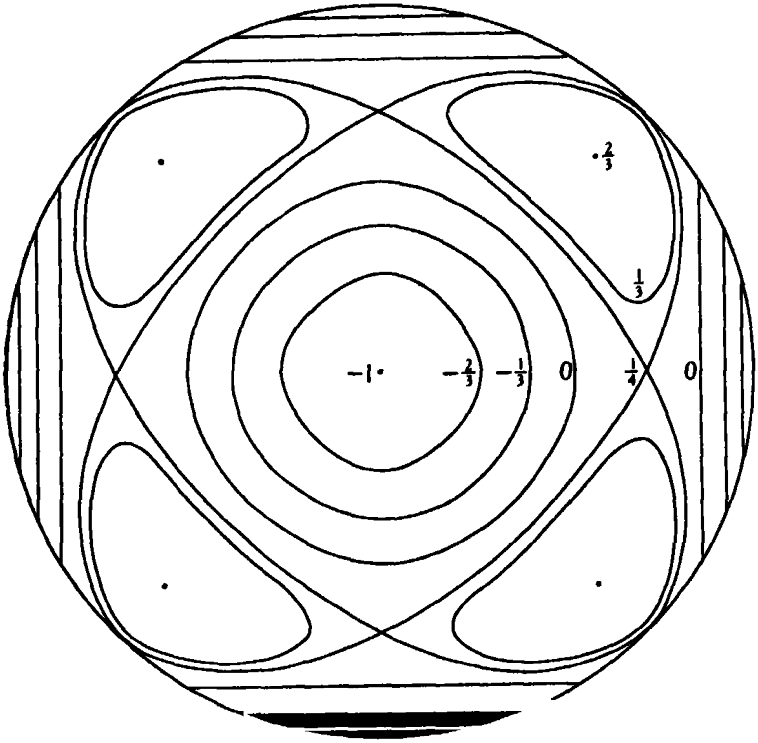

FIG. 1—Equipotential lines for K - 1.

For K positive V has six minima, equal to $-K$, at the points:

$$\theta = 0 \text{ or } \pi;$$

$$\theta = \tfrac{1}{2}\pi, \quad \phi = 0, \pm \tfrac{1}{2}\pi \text{ or } \pi;$$

and eight maxima, equal to $\frac{2}{3}K$, at the points:

$$\theta = \cos^{-1} \pm 1/\sqrt{3}, \quad \phi = \pm \tfrac{1}{4}\pi \text{ or } \pm \tfrac{3}{4}\pi.$$

The equipotential curve having double points is $V = \frac{1}{4}K$. This curve is the dividing line between the potential maxima and minima, so that there are six potential hollows of depth $1\frac{1}{4}$K and eight potential hills of depth (5/12)K, the positions of the hills and hollows being, of course, interchanged if K is negative.

3—DISCUSSION OF THE GENERAL EQUATION

In this section we shall discuss the equation (1), where V is any function having octahedral symmetry, without assuming an explicit expression for V.

As the equation is invariant under the operations of the octahedral group, the solutions must belong to representations of this group. These representations, with their group characteristics, are given in Table I, in the notation used by Mulliken.*

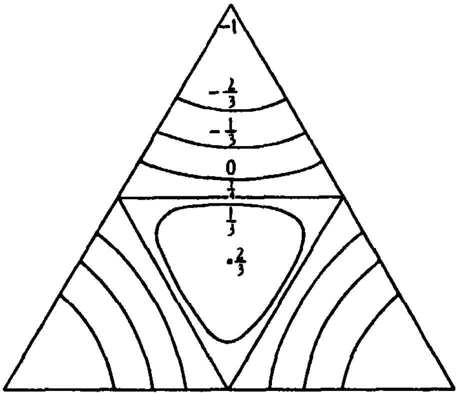

FIG. 2—Equipotential lines for K = 1.

TABLE I—THE REPRESENTATIONS OF THE O_h GROUP

O_h	E	$3C_2$	$6C_4$	$6C_2$	$8C_3$	iE	$3iC_2$	$6iC_4$	$6iC_2$	$8iC_3$
A_{1g}	1	1	1	1	1	1	1	1	1	1
A_{1u}	1	1	1	1	1	−1	−1	−1	−1	−1
A_{2g}	1	1	−1	−1	1	1	1	−1	−1	1
A_{2u}	1	1	−1	−1	1	−1	−1	1	1	−1
E_g	2	2	0	0	−1	2	2	0	0	−1
E_u	2	2	0	0	−1	−2	−2	0	0	1
T_{1g}	3	−1	1	−1	0	3	−1	1	1	0
T_{1u}	3	−1	1	−1	0	−3	1	−1	1	0
T_{2g}	3	−1	−1	1	0	3	−1	−1	1	0
T_{2u}	3	−1	−1	1	0	−3	1	1	−1	0

If V = 0, which corresponds to the case of free rotation, the solutions are the surface harmonics and are degenerate, all the surface harmonics of degree l corresponding to the same value of E, namely $l(l+1)$; but, under the influence of a field of octahedral symmetry, the degeneracy is partly removed, and they split up as shown in Table II.*

---

* 'Phys. Rev.,' vol. 43, p. 278 (1933).

TABLE II—SPLITTING OF ROTATIONAL ENERGY LEVELS IN A FIELD OF OCTAHEDRAL SYMMETRY

l		l	
0	A_{1g}	1	T_{1u}
2	$E_g + T_{2g}$	3	$A_{2u} + T_{1u} + T_{2u}$
4	$A_{1g} + E_g + T_{1g} + T_{2g}$	5	$E_u + 2T_{1u} + T_{2u}$
6	$A_{1g} + A_{2g} + E_g + T_{1g} + 2T_{2g}$	7	$A_{2u} + E_u + 2T_{1u} + 2T_{2u}$
8	$A_{1g} + 2E_g + 2T_{1g} + 2T_{2g}$	9	$A_{1u} + A_{2u} + E_u + 3T_{1u} + 2T_{2u}$
10	$A_{1g} + A_{2g} + 2E_g + 2T_{1g} + 3T_{2g}$	11	$A_{2u} + 2E_u + 3T_{1u} + 3T_{2u}$
12	$2A_{1g} + A_{2g} + 2E_g + 3T_{1g} + 3T_{2g}$	13	$A_{1u} + A_{2u} + 2E_u + 4T_{1u} + 3T_{2u}$

Since any solution ψ has to be unique it must be possible to express it in a series of surface harmonics, so that one method of solution is to assume that ψ is equal to such a series, with coefficients to be determined. Just as there are four types of solution of Mathieu's equation, so there are twenty types of solution of this equation, corresponding to the group representations in Table I, though there are only ten sets of energy values, as some of the solutions are degenerate.

It is, however, inconvenient to divide the solutions into these twenty types, if we are using expansions in surface harmonics, as the simple surface harmonics $P_l^m(\cos\theta)\cos m\phi$ cannot, in general, be assigned to any particular representation of the O_h group, and we should have to use the correct linear combinations of them. Instead, we divide the solutions into the twelve types shown in Table IV. These types correspond to the representations of the tetragonal group D_{4h}†; as the equation has the complete symmetry of this group, it follows that the solutions can be divided up in this manner.

Since the O_h group has the complete symmetry of the D_{4h} group, any representation of the first must correspond to one or more representations of the second, the nature of the correspondence being shown in Table III.‡

Now the series in Table IV must belong to representations of the O_h group when the coefficients are chosen so that they are solutions of equation (1), and from Table III we can deduce to which representation a particular solution will belong, though not always unambiguously. For instance, a solution which belongs to the representation A_{1g} of the D_{4h} group will belong either to the representation A_{1g} of the O_h group, or be one of a pair of solutions, with the same energy values, which belong to the representation E_g of that group. Hence in Table IV we show opposite each series the representation of the D_{4h} group to which it belongs, and also the representation or representations of the O_h group, to one of which it will belong when the coefficients are chosen so that it is a solution of equation (1).

---

* *Cf.* Bethe, *loc. cit.*, Table II, and Mulliken, *loc. cit.*

† For the notation, *see* Mulliken's paper, and for the method of finding the representation to which a given surface harmonic belongs *see* Bethe, *loc. cit.*, p. 143.

‡ Mulliken, *loc. cit.*, Table IV.

TABLE III—CORRESPONDENCE BETWEEN REPRESENTATIONS OF O_h AND D_{4h} GROUPS

O_h	D_{4h}	O_h	D_{4h}
$A_{1g} \longrightarrow$	A_{1g}	$A_{1u} \longrightarrow$	A_{1u}
$A_{2g} \longrightarrow$	B_{1g}	$A_{2u} \longrightarrow$	B_{1u}
$E_g \longrightarrow$	$A_{1g} + B_{1g}$	$E_u \longrightarrow$	$A_{1u} + B_{1u}$
$T_{1g} \longrightarrow$	$A_{2g} + E_g$	$T_{1u} \longrightarrow$	$A_{2u} + E_u$
$T_{2g} \longrightarrow$	$B_{2g} + E_g$	$T_{2u} \longrightarrow$	$B_{2u} + E_u$

TABLE IV—REPRESENTATIONS OF THE O_h AND D_{4h} GROUPS TO WHICH THE DIFFERENT TYPES OF SOLUTION OF EQUATION (1) BELONG

O_h	D_{4h}	Series
A_{1g} or E_g	A_{1g}	$a_0^0 + a_2^0 P_2^0 + a_4^0 P_4^0 + a_4^4 P_4^4 \cos 4\phi + \ldots$
A_{2g} or E_g	B_{1g}	$a_2^2 P_2^2 \cos 2\phi + a_4^2 P_4^2 \cos 2\phi + \ldots + a_6^6 P_6^6 \cos 6\phi +$
T_{1g}	A_{2g}	$b_4^4 P_4^4 \sin 4\phi + b_6^4 P_6^4 \sin 4\phi + \ldots$
T_{1g} or T_{2g}	E_g	$a_2^1 P_2^1 \cos \phi + a_4^1 P_4^1 \cos \phi + a_4^3 P_4^3 \cos 3\phi + \ldots$ $b_2^1 P_2^1 \sin \phi + b_4^1 P_4^1 \sin \phi + b_4^3 P_4^3 \sin 3\phi + \ldots$
T_{2g}	B_{2g}	$b_2^2 P_2^2 \sin 2\phi + b_4^2 P_4^2 \sin 2\phi + \ldots$
A_{1u} or E_u	A_{1u}	$b_5^4 P_5^4 \sin 4\phi + b_7^4 P_7^4 \sin 4\phi + \ldots$
A_{2u} or E_u	B_{1u}	$b_3^2 P_3^2 \sin 2\phi + b_5^2 P_5^2 \sin 2\phi + \ldots$
T_{1u}	A_{2u}	$a_1^0 P_1^0 + a_3^0 P_3^0 + a_5^0 P_5^0 + a_5^4 P_5^4 \cos 4\phi + \ldots$
T_{1u} or T_{2u}	E_u	$a_1^1 P_1^1 \cos \phi + a_3^1 P_3^1 \cos 3\phi + \ldots$ $b_1^1 P_1^1 \sin \phi + b_3^1 P_3^1 \sin 3\phi + \ldots$
T_{2u}	B_{2u}	$a_3^2 P_3^2 \cos 2\phi + a_5^2 P_5^2 \cos 2\phi + \ldots$

4—SOLUTION OF PARTICULAR EQUATION: GENERAL METHOD

We shall now apply the method of the previous section to the solution of equation (1), when V has the value given by equation (3). In subsequent sections we shall use two other methods of solving the equation, the first being applicable when K is large, and the second being suitable for finding the higher energy levels when K is not too large.

In order to use the method of § 3 it is necessary to be able to express $\{P_4^0 + (1/168)\,P_4^4 \cos 4\phi\}\,P_l^m \cos m\phi$ as a sum of surface harmonics, P_l^m being defined by equation (2). From the well-known recurrence relation

$$\mu P_l^m = \{1/(2l+1)\}\,\{(l+m)\,P_{l-1}^m + (l+1-m)\,P_{l+1}^m\}, \tag{4}$$

we infer that

$$\left.\begin{aligned}\mu^2 P_l^m = {} & \{1/(2l+1)\}\,[\{(l+m)/(2l-1)\}\{(l+m-1)\,P_{l-2}^m \\ & + (l-m)\,P_l^m\} + \{(l+1-m)/(2l+3)\}\{(l+m+1)\,P_l^m \\ & + (l+2-m)\,P_{l+2}^m\}] = \frac{(l+m)(l+m-1)}{(2l+1)(2l-1)}\,P_{l-2}^m \\ & + \frac{2l^2+2l-1-2m^2}{(2l-1)(2l+3)}\,P_l^m + \frac{(l+1-m)(l+2-m)}{(2l+1)(2l+3)}\,P_{l+2}^m\end{aligned}\right\}, \tag{5}$$

and similarly

$$\left.\begin{aligned}\mu^4 P_l^m = {} & \frac{(l+m)(l+m-1)(l+m-2)(l+m-3)}{(2l-5)(2l-3)(2l-1)(2l+1)}\,P_{l-4}^m \\ & + \frac{2(l+m)(l+m-1)(2l^2-2l-7-2m^2)}{(2l-5)(2l-1)(2l+1)(2l+3)}\,P_{l-2}^m \\ & + \frac{3\{2l^4+4l^3-6l^2-8l+3-2m^2(2l^2+2l-5)+2m^4\}}{(2l-3)(2l-1)(2l+3)(2l+5)}\,P_l^m \\ & + \frac{2(l+2-m)(l+1-m)(2l^2+6l-3-2m^2)}{(2l-1)(2l+1)(2l+3)(2l+7)}\,P_{l+2}^m \\ & + \frac{(l+1-m)(l+2-m)(l+3-m)(l+4-m)}{(2l+1)(2l+3)(2l+5)(2l+7)}\,P_{l+4}^m\end{aligned}\right\}. \tag{6}$$

Since $$P_4^0 = \tfrac{1}{8}(35\mu^4 - 30\mu^2 + 3),$$

we have

$$\left.\begin{aligned}P_4^0 P_l^m = {} & \frac{(l+m)(l+m-1)(l+m-2)(l+m-3)}{(2l-5)(2l-3)(2l-1)(2l+1)}\cdot\frac{35}{8}\,P_{l-4}^m \\ & + \frac{(l+m)(l+m-1)(l^2-l-2-7m^2)}{(2l-5)(2l-1)(2l+1)(2l+3)}\cdot\frac{5}{2}\,P_{l-2}^m \\ & + \frac{3l^4+6l^3-3l^2-6l-5m^2(6l^2+6l-5)+35m^4}{(2l-3)(2l-1)(2l+3)(2l+5)}\cdot\frac{3}{4}\,P_l^m \\ & + \frac{(l+1-m)(l+2-m)(l^2+3l-7m^2)}{(2l-1)(2l+1)(2l+3)(2l+7)}\cdot\frac{5}{2}\,P_{l+2}^m \\ & + \frac{(l+1-m)(l+2-m)(l+3-m)(l+4-m)}{(2l+1)(2l+3)(2l+5)(2l+7)}\cdot\frac{35}{8}\,P_{l+4}^m\end{aligned}\right\}. \tag{7}$$

Since

$$\cos 4\phi \cos m\phi = \tfrac{1}{2}\{\cos(m-4)\,\phi + \cos(m+4)\,\phi\},$$

$P_4^4\, P_l^m$ has to be expressed in two different forms, namely $\Sigma a_s P_s^{m+4}$ and $\Sigma b_s P_s^{m-4}$.

From the well-known recurrence relation

$$P_l = \frac{1}{2l+1}\left\{\frac{\partial P_{l+1}}{\partial\mu} - \frac{\partial P_{l-1}}{\partial\mu}\right\}, \qquad (8)$$

we infer

$$\left.\begin{aligned} P_l = {} & \frac{1}{(2l+1)(2l+3)}\left\{\frac{\partial^2 P_{l+2}}{\partial\mu^2} - \frac{\partial^2 P_l}{\partial\mu^2}\right\} \\ & - \frac{1}{(2l+1)(2l-1)}\left\{\frac{\partial^2 P_l}{\partial\mu^2} - \frac{\partial^2 P_{l-2}}{\partial\mu^2}\right\} \\ = {} & \frac{1}{(2l+1)(2l+3)}\frac{\partial^2 P_{l+2}}{\partial\mu^2} - \frac{2}{(2l-1)(2l+3)}\frac{\partial^2 P_l}{\partial\mu^2} \\ & + \frac{1}{(2l-1)(2l+1)}\frac{\partial^2 P_{l-2}}{\partial\mu^2} \end{aligned}\right\}, \qquad (9)$$

and similarly

$$\left.\begin{aligned} P_l = {} & \frac{1}{(2l+1)(2l+3)(2l+5)(2l+7)}\frac{\partial^4 P_{l+4}}{\partial\mu^4} \\ & - \frac{4}{(2l-1)(2l+1)(2l+3)(2l+7)}\frac{\partial^4 P_{l+2}}{\partial\mu^4} \\ & + \frac{6}{(2l-3)(2l-1)(2l+3)(2l+5)}\frac{\partial^4 P_l}{\partial\mu^4} \\ & - \frac{4}{(2l-5)(2l-1)(2l+1)(2l+3)}\frac{\partial^4 P_{l-2}}{\partial\mu^4} \\ & + \frac{1}{(2l-5)(2l-3)(2l-1)(2l+1)}\frac{\partial^4 P_{l-4}}{\partial\mu^4} \end{aligned}\right\}. \qquad (10)$$

Now we have

$$P_4^4 = 105\,(1-\mu^2)^2,$$

and

$$P_l^m = (1-\mu^2)^{m/2}\,(\partial^m/\partial\mu^m)\,P_l.$$

Hence if we differentiate both sides of equation (10) m times, and then multiply by $105\,(1-\mu^2)^{(m+4)/2}$, we obtain

$$\left.\begin{aligned} P_4^4\, P_l^m = {} & 105\,(1-\mu^2)^2\, P_l^m \\ = {} & \frac{105}{(2l-5)(2l-3)(2l-1)(2l+1)}\, P_{l-4}^{m+4} \\ & - \frac{4\times 105}{(2l-5)(2l-1)(2l+1)(2l+3)}\, P_{l-2}^{m+4} \end{aligned}\right\}. \qquad (11)$$

$$\left.\begin{aligned}
&+\frac{6\times 105}{(2l-3)(2l-1)(2l+3)(2l+5)}\,P_l^{m+4}\\
&-\frac{4\times 105}{(2l-1)(2l+1)(2l+3)(2l+7)}\,P_{l+2}^{m+4}\\
&+\frac{105}{(2l+1)(2l+3)(2l+5)(2l+7)}\,P_{l+4}^{m+4}
\end{aligned}\right\}\begin{array}{c}(11)\\ \text{(cont.)}\end{array}$$

Now if we write $P_4^4\,P_l^m = \Sigma a_l^s\,P_s^{m-4}$, multiply both sides of the equation by P_s^{m-4}, and integrate from $\mu = -1$ to $\mu = +1$, we find that

$$\int_{-1}^{1} P_s^{m-4}\,P_4^4\,P_l^m\,d\mu = a_l^s\cdot\frac{2}{2s+1}\,\frac{(s+m-4)\,!}{(s-m+4)\,!}. \qquad (12)$$

We also have $P_4^4\,P_s^{m-4} = \Sigma b_s^l\,P_l^m$, where b_s^l is known from equation (11). If we multiply both sides of the equation by P_l^m, and integrate from $\mu = -1$ to $\mu = +1$, we have

$$\int_{-1}^{1} P_s^{m-4}P_4^4\,P_l^m\,d\mu = b_s^l\cdot\frac{2}{2l+1}\,\frac{(l+m)\,!}{(l-m)\,!},$$

and hence, using equation (12), we obtain

$$a_l^s = \frac{2s+1}{2l+1}\,\frac{(s-m+4)\,!\;(l+m)\,!}{(s+m-4)\,!\;(l-m)\,!}\,b_s^l. \qquad (13)$$

Since b_l^s is known a_l^s can be calculated, and therefore we can deduce the equation,

$$\left.\begin{aligned}
P_4^4\,P_l^m = {}&\frac{(l+m)\,!}{(l+m-8)\,!}\,\frac{105}{(2l-5)(2l-3)(2l-1)(2l+1)}\,P_{l-4}^{m-4}\\
&-\frac{(l+m)!\,(l-m+2)!}{(l+m-6)!\,(l-m)!}\,\frac{4\times 105}{(2l-5)(2l-1)(2l+1)(2l+3)}\,P_{l-2}^{m-4}\\
&+\frac{(l+m)!\,(l-m+4)!}{(l+m-4)!\,(l-m)!}\,\frac{6\times 105}{(2l-3)(2l-1)(2l+3)(2l+5)}\,P_l^{m-4}\\
&-\frac{(l+m)!\,(l-m+6)!}{(l+m-2)!\,(l-m)!}\,\frac{4\times 105}{(2l-1)(2l+1)(2l+3)(2l+7)}\,P_{l+2}^{m-4}\\
&+\frac{(l-m+8)\,!}{(l-m)}\,\frac{105}{(2l+1)(2l+3)(2l+5)(2l+7)}\,P_{l+4}^{m-4}
\end{aligned}\right\}.(14)$$

Since

$$\cos 4\phi\,\cos 2\phi = \tfrac{1}{2}\,(\cos 2\phi + \cos 6\phi),$$

it is also necessary to know the expansion of $P_4^4\,P_l^2$ in the form $\Sigma a_s P_s^2$.

Since

$$P_4^4 = 105\,(1-\mu^2)^2,$$

we can deduce the required result from equations (5) and (6), and we thus get

$$\left.\begin{aligned}P_4^4 P_l^2 = 105(l-1)l(l+1)(l+2)\Big[&\frac{1}{(2l-5)(2l-3)(2l-1)(2l+1)}P_{l-4}^2\\ &-\frac{4}{(2l-5)(2l-1)(2l+1)(2l+3)}P_{l-2}^2\\ &+\frac{6}{(2l-3)(2l-1)(2l+3)(2l+5)}P_l^2\\ &-\frac{4}{(2l-1)(2l+1)(2l+3)(2l+7)}P_{l+2}^2\\ &+\frac{1}{(2l+1)(2l+3)(2l+5)(2l+7)}P_{l+4}^2\Big]\end{aligned}\right\}. \quad (15)$$

Now the equation we wish to solve is

$$\frac{1}{\sin\theta}\frac{\partial}{\partial\theta}\left(\sin\theta\frac{\partial\psi}{\partial\theta}\right)+\left(\frac{1}{\sin\theta}\right)^2\frac{\partial^2\psi}{\partial\phi^2}$$
$$+\left[W+k\left\{P_4^0(\cos\theta)+(1/168)P_4^4(\cos\theta)\cos 4\phi\right\}\right]\psi=0, \quad (16)$$

where

$$W = 8\pi^2 IE/h^2,$$

and

$$k = 8\pi^2 IK/h^2.$$

If, in this equation, we substitute for ψ one of the series given in Table IV, use formulae (7)–(15) to express all the terms in the equation as sums of surface harmonics, and then equate the coefficient of each surface harmonic to zero, we obtain a set of equations between the coefficients, a typical set being

$$a_0^0 W + \qquad a_4^0 k(1/9) + a_4^4 k(40/3) = 0,$$

$$a_2^0\{W - 6 + k(2/7)\} + a_4^0 k(100/693) - a_4^4 k(800/33)$$
$$+ a_6^0 k(25/143) + a_6^4 k(9000/143) = 0,$$

. . . .

The condition that these equations shall be consistent determines W in the form of a determinantal equation. It is possible to obtain approximately a few of the lowest roots of W, for not too large values of k, by taking only the first few rows and columns of the infinite determinant. Even then the calculations would be very laborious if carried out directly. They can be done, however, with the aid of an electrical calculating

$$\left.\begin{array}{ccccccccc}
\theta & 0 & 0\cdot0111 & 0\cdot0079 & 0 & 0 & 0 & 0 & 0 \\
0 & \begin{pmatrix}\theta-0\cdot6\alpha\\+0\cdot0286\end{pmatrix} & 0\cdot0144 & -0\cdot0144 & 0\cdot0175 & 0\cdot0113 & 0 & 0 & 0 \\
0\cdot1000 & 0\cdot0260 & \begin{pmatrix}\theta-2\alpha\\+0\cdot0162\end{pmatrix} & 0\cdot0090 & 0\cdot0140 & -0\cdot0272 & 0\cdot0202 & 0\cdot0056 & 0 \\
0\cdot1000 & -0\cdot0364 & 0\cdot0126 & \begin{pmatrix}\theta-2\alpha\\-0\cdot0126\end{pmatrix} & -0\cdot0028 & -0\cdot0381 & 0\cdot0003 & 0\cdot0079 & 0\cdot0144 \\
0 & 0\cdot0455 & 0\cdot0202 & -0\cdot0029 & \begin{pmatrix}\theta-4\cdot2\alpha\\+0\cdot0150\end{pmatrix} & 0\cdot0243 & 0\cdot0142 & -0\cdot0153 & 0 \\
0 & 0\cdot0100 & -0\cdot0133 & -0\cdot0133 & 0\cdot0082 & \begin{pmatrix}\theta-4\cdot2\alpha\\-0\cdot0171\end{pmatrix} & -0\cdot0026 & -0\cdot0064 & -0\cdot0290 \\
0 & 0 & 0\cdot0381 & 0\cdot0004 & 0\cdot0186 & -0\cdot0100 & \begin{pmatrix}\theta-7\cdot2\alpha\\+0\cdot0146\end{pmatrix} & 0\cdot0156 & 0 \\
0 & 0 & 0\cdot0100 & 0\cdot0100 & -0\cdot0189 & -0\cdot0239 & 0\cdot0099 & \begin{pmatrix}\theta-7\cdot2\alpha\\-0\cdot0097\end{pmatrix} & 0\cdot0147 \\
0 & 0 & 0 & 0\cdot0500 & 0 & -0\cdot0028 & 0 & 0\cdot0003 & \begin{pmatrix}\theta-7\cdot2\alpha\\+0\cdot0211\end{pmatrix}
\end{array}\right\} = 0. \qquad (17)$$

machine,* which is capable of solving numerically a determinantal equation in which the determinant has up to nine rows and columns, and the unknown appears only on the diagonal.

In equation (17) we give a typical example of a determinantal equation which had to be solved, arranged in the most convenient form for solution by means of the machine. In it we have written $\theta = E/(10k)$, $k = 1/\alpha$, and arranged the coefficients so that they all lie between -1 and $+1$. They can then be set to three places of decimals, and the equation for determining the lowest roots of W corresponding to the representations A_{1g} and E_g becomes equation (17), p. 611.

5—Solution of Particular Equation: Method for k Large

We now proceed to consider asymptotic expansions of W and ψ in descending powers of $k^{\frac{1}{2}}$, by a method similar to that used for asymptotic solutions of the Mathieu equation.†

In this method we assume that ψ is small except near a position of potential minimum, and it corresponds to the case when the molecule is oscillating about a position of equilibrium. It may be expected to give fairly good results provided the energy values obtained, reckoned from the position of potential minimum, are less than the depth of the potential hollow.

We shall first consider the case when k is positive, and find the solution for which ψ is small except near $\theta = 0$. In equation (16) write $W' = W + k$, and $y = \sin^2 \theta$, then the equation becomes

$$\left\{4y(1-y)\frac{\partial^2}{\partial y^2} + 2(2-3y)\frac{\partial}{\partial y} + \frac{1}{y}\frac{\partial^2}{\partial \phi^2} + W' + k\left(-5y + 4\tfrac{3}{8}y^2 + \tfrac{5}{8}y^2\cos 4\phi\right)\right\}\psi = 0. \qquad (18)$$

Putting $z = y\sqrt{(5k)}$, we have

$$\left\{\sqrt{(5k)}\left(4z\frac{\partial^2}{\partial z^2} + 4\frac{\partial}{\partial z} + \frac{1}{z}\frac{\partial^2}{\partial \phi^2} - z\right) - \left(4z^2\frac{\partial^2}{\partial z^2} + 6z\frac{\partial}{\partial z} - \tfrac{7}{8}z^2 - \tfrac{1}{8}z^2\cos 4\phi\right) + W'\right\}\psi = 0. \qquad (19)$$

---

* For a full description of this machine, *see* Mallock, 'Proc. Roy. Soc.,' A, vol. 140, p. 457 (1932). I am indebted to Professor Lennard-Jones for suggesting and arranging for the use of this machine, and should like to express my thanks to Mr. Mallock and the Cambridge Scientific Instrument Company for allowing me to use it, and for instruction in the method of doing so.

† Goldstein, 'Trans, Camb. Phil. Soc.,' vol. 23, p. 303 (1927).

Write $\psi = e^{-z/2}\, v$, and we get,

$$\Big[\sqrt{(5k)}\left\{4z\frac{\partial^2}{\partial z^2}+4(1-z)\frac{\partial}{\partial z}+\frac{1}{z}\frac{\partial^2}{\partial \phi^2}-2\right\}$$
$$-\left\{4z^2\frac{\partial^2}{\partial z^2}+2z(3-2z)\frac{\partial}{\partial z}+\tfrac{1}{8}z^2(1-\cos 4\phi)-3z\right\}$$
$$+\,W'\Big]v=0. \qquad (20)$$

If we now write

$$\left.\begin{aligned} v &= f_0+(5k)^{-\frac{1}{2}}f_1+(5k)^{-1}f_2+\,.. \\ W' &= (5k)^{\frac{1}{2}}a+a_0+(5k)^{-\frac{1}{2}}a_1+\,.. \end{aligned}\right\}, \qquad (21)$$

substitute in equation (20), and equate the coefficients of powers of $(5k)^{\frac{1}{2}}$ to zero, we obtain the following set of equations:

$$\left\{4z\frac{\partial^2}{\partial z^2}+4(1-z)\frac{\partial}{\partial z}+\frac{1}{z}\frac{\partial^2}{\partial \phi^2}+(a-2)\right\}f_0=0, \qquad (22\text{A})$$

$$\left\{4z\frac{\partial^2}{\partial z^2}+4(1-z)\frac{\partial}{\partial z}+\frac{1}{z}\frac{\partial^2}{\partial \phi^2}+(a-2)\right\}f_1$$
$$+\left\{-4z^2\frac{\partial^2}{\partial z^2}-2z(3-2z)\frac{\partial}{\partial z}-\tfrac{1}{8}z^2(1-\cos 4\phi)\right.$$
$$\left.+\,3z+a_0\right\}f_0=0, \qquad (22\text{B})$$

etc.

In equation (22A) put

$$f_0=\left.\begin{matrix}\cos m\phi\\ \sin m\phi\end{matrix}\right\}z^{m/2}\,u(z),$$

where m must be an integer (which we may assume to be positive or zero), since otherwise f_0 would not be single-valued on the surface of a sphere, and we get

$$4z\frac{d^2u}{dz^2}+4(m+1-z)\frac{du}{dz}+(a-2-2m)\,u=0. \qquad (23)$$

If we attempt to solve this equation by assuming a solution in series, we find that the solution is of the order e^z for large z, unless $a=4r-2m+2$, where r is a positive integer greater than or equal to m. Since ψ, and therefore f_0, has been assumed to be small for large z, a must have this value, and then the equation becomes

$$z\frac{d^2u}{dz^2}+(m+1-z)\frac{du}{dz}+(r-m)\,u=0, \qquad (24)$$

which is known to have the solution

$$u = \frac{d^m}{dz^m} \mathrm{L}_r(z),$$

where $\mathrm{L}_r(z)$ is the Laguerre polynomial defined by the equation

$$\mathrm{L}_r(z) = e^z \frac{d^r}{dz^r}(z^r e^{-z}). \tag{25}$$

If we now write

$$\mathrm{L}_r^m(z) = z^{m/2} \frac{d}{dz}(\mathrm{L}_r(z)), \tag{26}$$

then

$$f_0 = \sin m\phi \, \mathrm{L}_r^m(z),$$

or

$$f_0 = \cos m\phi \, \mathrm{L}_r^m(z).$$

Hence the required solution of equation (22A) is given by

$$a = 2n + 2,$$

$$f_0 = \sum_{r,m} \mathrm{L}_r^m(z) \{b_r^m \cos m\phi + c_r^m \sin m\phi\}, \tag{27}$$

where r, n, and m are positive integers,

$$r \geqslant m, \quad \text{and} \quad 2r - m = n.$$

If we substitute these values in equation (22B), and express the second line as a sum of terms of the form $\mathrm{L}_s^p \cos p\phi$ by means of recurrence relations, it becomes

$$4z \frac{\partial^2 f_1}{\partial z^2} + 4(1 - z)\frac{\partial f_1}{\partial z} + \frac{1}{z}\frac{\partial^2 f_1}{\partial \phi^2} + 2nf_1 - \Sigma \, \mathrm{L}_s^p \{b_s^p \cos p\phi + c_s^p \sin p\phi\} = 0, \tag{28}$$

where b_s^p, c_s^p are linear functions of the b_r^m, c_r^m of equation (27).

We can immediately obtain a particular integral of this equation, namely

$$f_1 = \Sigma \{1/(2n - 4s + 2p)\} \mathrm{L}_s^p \{b_s^p \cos p\phi + c_s^p \sin p\phi\},$$

provided none of the s's and p's are connected by the relation $n = 2s - p$. If, however, some of the s's and p's are connected by this relation, the particular integral will have logarithmic terms, involving a singularity at the origin. Hence we equate the coefficients of these terms to zero, and this will give us $2n + 1$ linear homogeneous equations connecting the $2n + 1$ coefficients b_r^m and c_r^m. The condition that these equations are consistent gives us a determinantal equation, having $2n + 1$ roots, to determine a_0. By a similar process we could determine a_1, a_2, etc., but in practice the calculation is too laborious.

From the nature of equation (22B) we can see that it is not necessary to assume a completely general form for f_1, but that we can divide the solutions up into four types if n is even (in which case all the m's are even), and into two types if n is odd (in which case all the m's are odd). These types are given in Table V. We notice that types (e) and (f) are degenerate, giving the same set of values of W, as a solution of one type can be transformed into a solution of the other by the operation of increasing or decreasing ϕ by $\frac{1}{2}\pi$, which does not alter the original equation.

TABLE V—TYPES OF ASYMPTOTIC SOLUTIONS OF EQUATION (16)

Solution		Group representation
n even		
$\Sigma\, b_r^{4m} \cos 4m\phi$	(a)	$A_{1g} + E_g + T_{1u}$
$\Sigma\, c_r^{4m} \sin 4m\phi$	(b)	$A_{1u} + E_u + T_{1g}$
$\Sigma\, b_r^{4m+2} \cos (4m + 2)\, \phi$	(c)	$A_{2g} + E_g + T_{2u}$
$\Sigma\, c_r^{4m+2} \sin (4m + 2)\, \phi$	(d)	$A_{2u} + E_u + T_{2g}$
n odd		
$\Sigma\, b_r^{2m+1} \cos (2m + 1)\, \phi$	(e)	$T_{1g} + T_{1u} + T_{2g} + T_{2u}$
$\Sigma\, c_r^{2m+1} \sin (2m + 1)\, \phi$	(f)	

All the solutions are degenerate, however; for to each solution in which ψ is small except near $\theta = 0$ correspond five equivalent solutions, in which ψ is small except near one of the other potential minima. If we take these six (or in the case of types (e) and (f) twelve) solutions together we can determine their characteristic system under the operations of the O_h group, and hence from Table I the representations of that group to which they belong. These are the same for the solutions of any particular type, and are shown in Table V.

In order to evaluate a_0 and the coefficients b_r^m, we must determine the recurrence relations connecting the polynomials $L_r^m(z)$.

Now

$$\begin{aligned} L_{r+1} &= e^z \{d^{r+1}/dz^{r+1}\,(z^{r+1}\,e^{-z})\} \\ &= ze^z \{d^{r+1}/dz^{r+1}\,(z^r e^{-z})\} + (r + 1)\, L_r \\ &= z dL_r/dz - zL_r + (r + 1)\, L_r. \end{aligned} \tag{29}$$

Differentiating this and using equation (24) we get

$$\begin{aligned} dL_{r+1}/dz &= -L_r + (r+2)\,dL_r/dz - z\,dL_r/dz + z\,d^2L_r/dz^2 \\ &= (r+1)\,(dL_r/dz - L_r). \end{aligned} \tag{30}$$

From equations (29) and (30) we infer

$$z\,dL_r/dz = rL_r - r^2L_{r-1}, \tag{31}$$

and

$$zL_r = -L_{r+1} + (2r+1)\,L_r - r^2L_{r-1}. \tag{32}$$

Differentiating equations (31) and (32) m times and multiplying by $z^{m/2}$, we get

$$z\,dL_r^m/dz = (r - m/2)\,L_r^m - r^2L_{r-1}^m, \tag{33}$$

and

$$zL_r^m = \{1 - m/(r+1)\}\,L_{r+1}^m + (2r+1-m)\,L_r^m - r^2L_{r-1}^m, \tag{34}$$

from which follows

$$\begin{aligned} z^2L_r^m = {} & \{1 - m/(r+1)\}\{1 - m/(r+2)\}\,L_{r+2}^m \\ & - 2\{1 - m/(r+1)\}(2r+2-m)\,L_{r+1}^m \\ & + \{2(3r^2+3r+1) - 3(2r+1)\,m + m^2\}\,L_r^m \\ & - 2r^2(2r-m)\,L_{r-1}^m + r^2(r-1)^2\,L_{r-2}^m. \end{aligned} \tag{35}$$

Equation (33) is equivalent to

$$z^{\frac{1}{2}}L_r^{m+1} = (r-m)\,L_r^m - r^2L_{r-1}^m, \tag{36}$$

from which follows

$$zL_r^{m+2} = (r-m-1)(r-m)\,L_r^m - 2r^2(r-m-1)\,L_{r-1}^m + r^2(r-1)^2L_{r-2}^m. \tag{37}$$

Similarly from equation (30) we infer

$$z^{\frac{1}{2}}L_r^{m-1} = L_r^m - \{1/(r+1)\}\,L_{r+1}^m, \tag{38}$$

and hence

$$zL_r^{m-2} = L_r^m - \frac{2}{r+1}\,L_{r+1}^m + \frac{1}{(r+1)(r+2)}\,L_{r+2}^m. \tag{39}$$

With the aid of these recurrence relations we can evaluate a_0 and hence determine the first three terms in the asymptotic expansion of W, the results being given in Table VI.

Although the formulae are too complicated to permit a general expression for a_0 to be obtained, we can obtain the average value of a_0 corresponding

TABLE VI—ASYMPTOTIC EXPANSION OF W FOR k LARGE

W	Group representation
$-k + 2\sqrt{(5k)} - 2\frac{3}{4}$	$A_{1g} + E_g + T_{1u}$
$-k + 4\sqrt{(5k)} - 7\frac{1}{4}$	$T_{1g} + T_{2g} + T_{1u} + T_{2u}$
$-k + 6\sqrt{(5k)} - 17\frac{1}{4}$	$A_{1g} + E_g + T_{1u}$
$-k + 6\sqrt{(5k)} - 14\frac{1}{4}$	$A_{2g} + E_g + T_{2u}$
$-k + 6\sqrt{(5k)} - 12\frac{3}{4}$	$A_{2u} + E_u + T_{2g}$
$-k + 8\sqrt{(5k)} - 29$	$T_{1g} + T_{2g} + T_{1u} + T_{2u}$
$-k + 8\sqrt{(5k)} - 21\frac{1}{2}$	$T_{1g} + T_{2g} + T_{1u} + T_{2u}$

to a given value of n, and hence the average value of W as far as the first three terms. It is

$$-k + 2(n + 1)\sqrt{(5k)} - (1\tfrac{1}{2}n^2 + 3n + 2\tfrac{3}{4}).$$

If k is large and negative we can solve the equation in a similar manner. In this case, since there are eight potential minima, the solutions are eight- or sixteen-fold degenerate, and are of three types, with the group representations:

$$A_{1g} + A_{2u} + T_{2g} + T_{1u},$$
$$A_{2g} + A_{1u} + T_{1g} + T_{2u},$$
$$E_g + E_u + T_{1g} + T_{2g} + T_{1u} + T_{2u}.$$

Values of W as far as the first three terms are given in Table VII, the average value for given n in this case being

$$\tfrac{2}{3}k + 2(n + 1)\sqrt{(-3\tfrac{1}{3}k)} - (n^2 + 2n + 2\tfrac{1}{2}).$$

TABLE VII—ASYMPTOTIC EXPANSION OF W FOR k LARGE AND NEGATIVE

W	Group representation
$\frac{2}{3}k + 2\sqrt{(-3\frac{1}{3}k)} - 2\frac{1}{2}$	$A_{1g} + A_{2u} + T_{2g} + T_{1u}$
$\frac{2}{3}k + 4\sqrt{(-3\frac{1}{3}k)} - 5\frac{1}{2}$	$E_g + E_u + T_{1g} + T_{2g} + T_{1u} + T_{2u}$
$\frac{2}{3}k + 6\sqrt{(-3\frac{1}{3}k)} - 11$	$E_g + E_u + T_{1g} + T_{2g} + T_{1u} + T_{2u}$
$\frac{2}{3}k + 6\sqrt{(-3\frac{1}{3}k)} - 9\frac{1}{2}$	$A_{1g} + A_{2u} + T_{2g} + T_{1u}$

6—METHOD OF SOLUTION FOR HIGH ENERGY VALUES

In this section we determine W as an ascending series in powers of k by an adaptation of a method used for solving the Mathieu equation.*

---

* Whittaker and Watson, "Modern Analysis," p. 421 (1920); *cf.* Lennard-Jones and Pike, 'Trans. Faraday Soc.,' vol. 30, p. 837 (1934).

For a given value of k the terms in the series converge more rapidly for the higher values of W.

In equation (16), which for brevity we shall write

$$\Delta\psi + (\mathrm{W} - \mathrm{U})\,\psi = 0,$$

put

$$\mathrm{W} = l(l+1) + \mathrm{R}.$$

It then becomes

$$\Delta\psi + l(l+1)\,\psi = (-\,\mathrm{R} + \mathrm{U})\,\psi. \tag{40}$$

As a first approximation we neglect the right-hand side of equation (40), and then the solution is

$$\psi_1 = \sum_m a_m \mathrm{P}_l^m \cos m\phi + \sum_m b_m \mathrm{P}_l^m \sin m\phi,$$

where the a's and b's are arbitrary coefficients. The second approximation is obtained by substituting ψ_1 for ψ in the right-hand side of equation (40), expressing $(-\,\mathrm{R} + \mathrm{U})\,\psi_1$ as a sum of surface harmonics by means of formulae (7)–(15), and then adding an expression of the form

$$\Sigma\, \alpha_1^m \mathrm{P}_l^m \cos m\phi + \Sigma\, \beta_1^m \mathrm{P}_l^m \sin m\phi,$$

where the α's and β's are so chosen that all the surface harmonics of degree l are cancelled. This ensures that the second approximation, which we write ψ_2, is single-valued. It can immediately be written down as a sum of surface harmonics.

If we continue to derive successive approximations in this manner, and then add together the equations from which they were derived we get

$$\begin{aligned} &\{\Delta + l(l+1) + \mathrm{R} - \mathrm{U}\} \sum_{s=1}^{r+1} \psi_s \\ &= (-\,\mathrm{R} + \mathrm{U})\,\psi_{r+1} + \sum_m \mathrm{P}_l^m \{\cos m\phi \sum_s \alpha_s^m + \sin m\phi \sum_s \beta_s^m\}. \end{aligned} \tag{41}$$

If $\Sigma\,\psi_s$ is convergent it will, therefore, satisfy equation (40) provided the right-hand side of equation (41) vanishes. Now if $\Sigma\,\psi_s$ is convergent, $(-\,\mathrm{R} + \mathrm{U})\,\psi_{r+1}$ is negligible for r large. Hence the right-hand side will vanish if

$$\sum_s \alpha_s^m = 0, \qquad \sum_s \beta_s^m = 0, \qquad \text{for all } m. \tag{42}$$

The α's and β's are linear homogeneous functions of the a's and b's, and also depend on R. Hence the a's and b's can be determined from equations (42), and the condition that the equations are consistent determines R in the form of a determinantal equation.

The calculations may be simplified by noting that it is not necessary to assume the most general expression for ψ_1, but that the possible expressions can be classified into the types shown in Table IV. The solutions will then also be of these types.

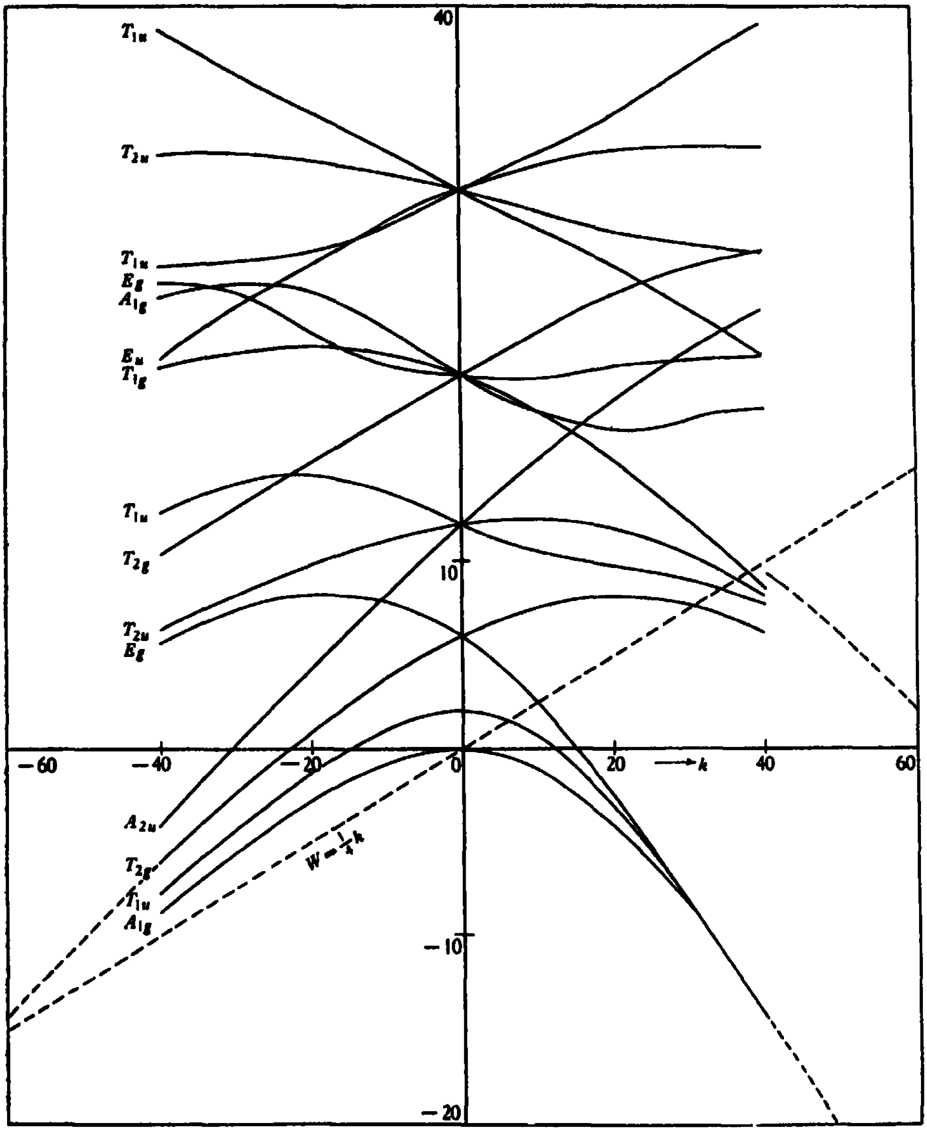

FIG. 3—Energy levels as a function of *k*.

7—DISCUSSION OF RESULTS

In fig. 3 are drawn curves showing the variations of the values of W as *k* changes over the range $k = -60$ to $+60$. The points on the full curves were obtained by the method of § 4, in most cases with the aid of the calculating machine, while the points on the dotted curves are asymptotic values calculated from Tables VI and VII.

For the lowest roots of W the asymptotic values fit on to the values obtained by other methods, so that W is determined for all values of k, but the agreement is much better for positive values of k than for negative values. The reason for this is clear if we remember* that the depth of the potential hollows is $(5/4)k$ for k positive and $-(5/12)k$ for k negative. The dividing line between the potential maxima and minima in each case corresponds to a potential energy $-\frac{1}{4}k$. In fig. 3 we have plotted the line $W = \frac{1}{4}k$. Roughly speaking, for values of W to the left of this line the molecule is rotating, and for values of W to the right it is oscillating. It is only in this latter region that we should expect the asymptotic values to be even approximately correct.

In Tables VIIIA and VIIIB are given the energy levels of the equation

$$\frac{1}{\sin\theta}\frac{\partial}{\partial\theta}\left(\sin\theta\,\frac{\partial\psi}{\partial\theta}\right)+\left(\frac{1}{\sin\theta}\right)^2\frac{\partial^2\psi}{\partial\phi^2}$$
$$+\left[W+k\left(1-5\sin^2\theta+4\tfrac{3}{8}\sin^4\theta+\tfrac{5}{8}\sin^4\theta\cos 4\phi\right)\right]\psi=0, \quad (43)$$

from which the curves in fig. 3 have been calculated.

TABLE VIIIA—ENERGY VALUES FOR POSITIVE VALUES OF k

	k = 0	10	15	20	25	33⅓	40	50
A_{1g}	0	−1·05	−2·40	−4·25	−6·34	−10·9	−14·8	−21·0
T_{1u}	2	0·63	−1·18	−3·25	−5·80	−10·6	−14·7	−21·2
E_g	6	2·33	−0·02	−2·74	−5·57	−10·7	−15·0	−21·8
T_{2g}	6	7·50	7·88	8·05	7·95	7·2	6·0	3·4
A_{2u}	12	15·48	17·09	18·59	20·01	22·0	23·3	24·7
T_{1u}	12	10·60	10·22	9·90	9·45	8·7	7·6	5·3
T_{2u}	12	12·28	12·14	11·76	11·17	9·7	8·1	5·4
A_{1g}	20	17·99	17·47	17·27	17·4	17·8	18·1	
E_g	20	18·04	20·24	20·48	20·7	21·0		
T_{1g}	20	18·36	17·27	16·02	14·6	11·9	9·6	
T_{2g}	20	22·29	23·40	24·45	25·1	26·2	26·6	
E_u	30	31·30	31·77	32·12	32·3	32·4	30·7	
T_{1u}	30	32·03	33·04	33·94	35·6	37·6	39·1	
T_{1u}	30	28·07	27·18	26·35	25·9	25·1	24·6	
T_{2u}	30	28·93	28·41	27·91	27·5	27·2	26·4	

---

* *See* figs. 1 and 2.

TABLE VIIIB—ENERGY VALUES FOR NEGATIVE VALUES OF k

	$k = 0$	-10	-15	-20	-25	$-33\frac{1}{3}$	-40	-50
A_{1g}	0	−0·83	−1·74	−2·85	−4·13	−6·7	−8·8	−12·3
T_{1u}	2	1·00	−0·03	−1·30	−2·75	−5·4	−7·7	−11·5
E_g	6	7·93	8·22	8·19	7·87	7·1	5·6	3·7
T_{2g}	6	3·73	2·44	0·86	−1·24	−3·6	−6·2	−10·1
A_{2u}	12	8·23	6·26	4·24	2·17	−1·4	−4·3	− 8·7
T_{1u}	12	13·72	14·40	14·62	14·5	13·9	12·7	10·5
T_{2u}	12	11·12	10·50	9·79	9·0	7·5	6·3	4·2
A_{1g}	20	22·64	23·79	24·56	25·0	24·7	24·2	
E_g	20	21·07	21·52	21·94	22·3	22·8	23·1	
T_{1g}	20	20·87	20·99	20·95	20·8	20·2	19·3	
T_{2g}	20	17·62	16·39	15·22	14·0	12·1	8·6	
E_u	30	28·25	27·23	26·13	24·9	22·8	20·7	
T_{1u}	30	28·08	27·25	26·56	26·6	26·2	25·9	
T_{1u}	30	32·09	30·17	34·26	35·5	37·3	38·6	
T_{2u}	30	30·94	31·43	31·60	31·8	32·2	31·9	

In conclusion, I should like to express my thanks to Professor Lennard-Jones for suggesting this problem, and for his help in developing the methods used in its solution.

SUMMARY

The solution of Schrödinger's equation for a diatomic molecule rotating in a potential field having octahedral symmetry is discussed, firstly in the general case, and then when the field has a particular form. In the latter case the energy values are plotted against a parameter determining the strength of the field.

A Quantum Mechanical Calculation of the Elastic Constants of Monovalent Metals

By K. Fuchs, H. H. Wills Physical Laboratory, University of Bristol

(*Communicated by A. M. Tyndall, F.R.S.—Received August* 22, 1935)

1—Introduction

The present paper is based on the results of the investigations of Wigner and Seitz* and Seitz† on the cohesive forces in metallic sodium and lithium and the extension of their work to copper by the present author.‡ These calculations have shown that quantum mechanics is capable of accounting in a satisfactory way for the lattice energy and compressibility of these metals. It is the object of the present paper to give an extension of the theory from which their elastic constants can be calculated.

Following Wigner and Seitz, we divide the lattice into polyhedra, one polyhedron surrounding each atom. We shall call each polyhedron a "unit polyhedron." The wave functions of the valence electrons extend throughout the whole lattice and have certain periodicity properties, which lead to boundary conditions for the wave function at the surface of each unit polyhedron. For the state of lowest energy, the wave function is obtained, in each unit polyhedron, by solving the Schrödinger equation

$$\nabla^2 \phi_0 + \frac{8\pi^2 m}{h^2} (W - V) \phi_0 = 0 \tag{1}$$

with the boundary condition

$$\partial \phi_0 / \partial n = 0, \tag{1A}$$

where $\partial/\partial n$ denotes the normal derivative at the boundary of the unit polyhedron. $V(r)$ is here the potential of the ion.

The calculations quoted have shown that ϕ_0 is nearly independent of position in the neighbourhood of the boundaries of the polyhedron ($\partial \phi_0/\partial n = 0$, $\partial^2 \phi_0/\partial n^2$ small). Therefore if the shape of the polyhedron is altered by elastic distortion, the same wave function ϕ_0 will nearly satisfy the new boundary conditions.

---

* 'Phys, Rev.,' vol. 43, p. 804 (1933); vol. 46, p. 509 (1934). Cited as I and II.

† 'Phys. Rev.,' vol. 47, p. 400 (1935).

‡ 'Proc. Roy. Soc.,' A, vol. 151, p. 585 (1935). Cited as III.

Now the energy of the crystal is the sum of the kinetic energy

$$-\frac{h^2}{8\pi^2 m}\int \Psi^*(x_1, x_2, \ldots) \sum_i \nabla_i^2 \Psi(x_1, x_2, \ldots)\, d\tau_1\, d\tau_2 \ldots$$

and the potential energy

$$\tfrac{1}{2}\sum_s \sum_t \int \Psi^*(x_1, x_2, \ldots)\left[\frac{e^2}{|\mathbf{R}_s - \mathbf{R}_t|} + \frac{e^2}{|\mathbf{r}_s - \mathbf{r}_t|} - \frac{2e^2}{|\mathbf{R}_s - \mathbf{r}_t|}\right] \times \Psi(x_1, x_2, \ldots)\, d\tau_1\, d\tau_2 \ldots$$

where $\mathbf{R}_s$ is the position of an ion, $\mathbf{r}_s$ that of an electron, and the term $\mathbf{R}_s = \mathbf{R}_t$ is excluded. Ψ is the wave function of the whole system of electrons in the crystal. The kinetic energy per electron is conveniently divided into

(1) The kinetic energy of the lowest electronic state

$$-\frac{h^2}{8\pi^2 m}\int \phi_0^*\, \nabla^2\, \phi_0\, d\tau. \tag{2}$$

(2) The "Fermi energy," $W,^{(F)}$ *i.e.*, the extra energy which arises because the electrons obey the Pauli principle and hence are not all in the lowest state.

Now as regards the former term, the integrand is large only towards the centre of the unit polyhedron; therefore, by what has been said above, *in any distortion of the lattice in which the volume is unchanged,* (2) is unaltered. (If the volume is changed the normalization factor of ϕ_0 alters, and this is no longer true.)

As regards the second term, the calculations quoted show that it is given by the Sommerfeld formula, multiplied by a factor f,

$$W^{(F)} = \frac{3}{5}\,\frac{h^2}{8\pi^2 m}\left(\frac{3\pi^2}{\Omega}\right)^{2/3} \qquad \Omega = \text{atomic volume.} \tag{3}$$

The factor f is nearly independent of the atomic volume, and it is of the order of magnitude 1.

It is probably safe to assume that, even if formula (3) is not satisfied, $W^{(F)}$ depends only on the atomic volume for monovalent metals, though for metals with more than one valence electron per atom this is probably not true, the shape of the "Brillouin zones" becoming important.†

Such metals will not be considered here.

To obtain the change in the energy in any elastic distortion in which the volume is unchanged, therefore, we have only to calculate the change in the potential energy, and since the wave functions are unchanged and constant near the boundaries of the unit cell, this can be done by a purely classical electrostatic method (§ 3).

---

† *Cf.* Jones, 'Proc. Roy. Soc.,' A, vol. 147, p. 396 (1934).

For copper, furthermore, the " exchange " interaction between the closed shells of the ions is considerable (*cf.* III), and the present calculation shows that for the alkalis, too, it is not entirely negligible (§ 4).

It will be convenient to divide up the total energy W of the lattice in the following way.

We denote by $W^{(0)}$ the energy of the lowest electronic state in the field of the ion in each unit polyhedron, calculated by solving the Schrödinger equation (1) and satisfying the boundary condition (1A) on the boundaries of a sphere of radius r_0 ($4\pi r_0^3/3 = \Omega =$ atomic volume); $W^{(0)}$ depends on Ω only; it includes the kinetic energy and part of the potential energy, namely, that part due to the interaction of an ion with "its own" electron. By " its own " electron we understand here the negative charge inside the sphere of radius r_0. (Since the wave function is practically constant in that part of the sphere which does not belong to the unit polyhedron and vice versa, the sphere contains the same amount of charge as the unit polyhedron, *i.e.*, one electron.)

By $W^{(L)}$ we denote the rest of the potential energy; this has been calculated for an undistorted lattice (*cf.* II and III) and found to be small, but its change on distortion is shown in this paper to be large.

By $W^{(F)}$ we denote the Fermi energy of the valence electrons; it is given by equation (3) and it depends on the atomic volume only.

By $W^{(I)}$ we denote the " exchange " energy between the closed shells of the ions.

If we now consider those elastic distortions which change the shape of the unit cell, but leave the atomic volume unaltered, the energies $W^{(0)}$ and $W^{(F)}$ remain the same. The change in $W^{(L)}$ will be dealt with in § 3. The change in $W^{(I)}$ can easily be calculated, if the energy between two ions as a function of their distance is known, § 4.

As we shall see in § 2, there are two distortions of this type which together with the uniform compression constitute a complete set of independent distortions; by considering these three distortions, the elastic constants can be calculated. It will be seen that for copper the calculation gives satisfactory agreement with the observed values of the elastic constants. For lithium, sodium, and potassium the elastic constants have not been measured. We therefore used the theoretical values to calculate the characteristic temperature, the results being in satisfactory agreement with the values observed at low temperatures (§ 5).

We included potassium into our calculation, although no calculations such as those mentioned for the other metals have yet been done. Gombas[*] has made calculations using a statistical method, supposing the electron distribution to be entirely uniform, and has obtained good agreement with experiment at least for the lattice constant and lattice energy. We may therefore expect that for potassium, too, the wave functions are practically plane waves.

2—THE ELASTIC POTENTIAL ENERGY

We shall now consider the relation between the elastic constants and the change in the energy of the lattice by distortion. We take Cartesian axes parallel to the cube edges of the lattice. Let ε_x, ε_y, ε_z be the relative displacements of the lattice points in the x, y, z directions and γ_{xy}, γ_{yz}, γ_{zx} the angles of distortion in the xy, yz, zx planes. The elastic potential energy per atom for a regular crystal can then be written in the form

$$\mathrm{W} = \mathrm{W}_0 + \tfrac{1}{2}c_{11}(\varepsilon_x^2 + \varepsilon_y^2 + \varepsilon_z^2) + c_{12}(\varepsilon_x\varepsilon_y + \varepsilon_y\varepsilon_z + \varepsilon_z\varepsilon_x) \\ + \tfrac{1}{2}c_{44}(\gamma_{xy}^2 + \gamma_{yz}^2 + \gamma_{zx}^2), \quad (4)$$

where c_{11}, c_{12}, c_{44} are the three independent elastic constants. We shall consider two types of distortion, which we choose as follows:

A—Compression and expansion in two directions parallel to two of the cube edges, keeping the volume unchanged. There is one independent variable, say ε_x, the second, say ε_y, being determined by

$$1 + \varepsilon_y = 1/(1 + \varepsilon_x) \quad (5)$$

and ε_z remaining unchanged.

We shall denote by 2A the second total differential coefficient of W with respect to ε_x at the equilibrium position

$$\mathrm{A} = \tfrac{1}{2}\frac{d^2\mathrm{W}}{d\varepsilon_x^2}. \quad (5\text{A})$$

B—Shear in one plane parallel to one surface of the cube. We define

$$\mathrm{B} = \tfrac{1}{2}\frac{d^2\mathrm{W}}{d\gamma_{xy}^2}. \quad (6)$$

Finally we define for uniform compression, which has been dealt with in the papers quoted in the introduction,

$$\mathrm{C} = \tfrac{1}{2}\frac{d^2\mathrm{W}}{d\varepsilon_v^2} \qquad 1 + \varepsilon_v = (1 + \varepsilon_x)(1 + \varepsilon_y)(1 + \varepsilon_z). \quad (7)$$

---

[*] 'Z. Physik,' vol. 94, p. 473 (1935).

The equations connecting A, B, and C with the elastic constants are, as may easily be verified from equation (4),

$$A = c_{11} - c_{12} \qquad 2B = c_{44} \qquad 2C = \tfrac{1}{3}(c_{11} + 2c_{12}). \tag{8}$$

For an isotropic substance, $A = 4B$.

The last of these equations gives the well-known relation between the compressibility $\kappa = 1/2C$ and the elastic constants for a regular lattice.

As explained in § 1, the total energy is the sum of a number of terms $W^{(1)}$, $W^{(2)}$, etc., $W = \sum_i W^{(i)}$. We shall deal with these terms separately, and therefore we define correspondingly to (5A) and (6)

$$\left.\begin{aligned} A &= \sum_i A^{(i)} \quad A^{(i)} = \tfrac{1}{2}\frac{d^2W^{(i)}}{d\varepsilon_x^2} \\ &= \tfrac{1}{2}\left[\frac{\partial^2}{\partial\varepsilon_x^2} + 2\frac{d\varepsilon_y}{d\varepsilon_x}\frac{\partial^2}{\partial\varepsilon_x\partial\varepsilon_y} + \left(\frac{d\varepsilon_y}{d\varepsilon_x}\right)^2\frac{\partial^2}{\partial\varepsilon_y^2} + \frac{d^2\varepsilon_y}{d\varepsilon_x^2}\frac{\partial}{\partial\varepsilon_y}\right]W^{(i)} \\ B &= \sum_i B^{(i)} \quad B^{(i)} = \tfrac{1}{2}\frac{d^2W^{(i)}}{d\gamma_{xy}^2} \end{aligned}\right\}. \tag{9}$$

In the next section we shall consider the differential quotients (9) resulting from the electrostatic energy of the lattice (the ions being considered as point charges), in § 4 those resulting from the exchange energy between the closed shells of the ions.

3—THE ELECTROSTATIC ENERGY OF THE LATTICE (THE IONS CONSIDERED AS POINT CHARGES)

As already explained, only the energy $W^{(L)}$ will give non-vanishing differential quotients A and B. This term is the potential energy of the lattice, excluding that of the electrons in the field of their own ions. Wigner and Seitz (*cf.* II) have shown that $W^{(L)}$ is equal to the difference between the energy $W^{(1)}$ of a lattice with positive point charges $+e$ embedded in a uniform negative charge distribution (one electron per unit polyhedron), and the energy $W^{(s)}$ of a spherical uniform negative charge distribution of radius r_0 with a positive point charge $+e$ at the centre ($4\pi r_0^3/3$ = atomic volume). $W^{(s)}$ depends on r_0 only and therefore changes with the atomic volume only; $A^{(s)}$ and $B^{(s)}$ vanish. By an extension of Ewald's method of calculating the electrostatic energy of a lattice, $W^{(1)}$ can be expressed in the form (*cf.* III)

$$W^{(1)} = \frac{e^2}{2}\left\{\frac{1}{\pi\Omega}\sum_l{}' \frac{\exp\left(-\frac{\pi^2}{E^2}h_l^2\right)}{h_l^2} + \sum_l{}' \frac{1-\phi(ER_l)}{R_l} - \frac{\pi}{E^2\Omega} - \frac{2E}{\sqrt{\pi}}\right\}, \tag{10}$$

where

$$\phi(x) = \frac{2}{\sqrt{\pi}}\int_0^x \exp(-t^2)\,dt.$$

$\mathbf{R}_l$ = lattice vector joining any two points of the lattice.

$\mathbf{h}_l$ = vector of the reciprocal lattice.

Ω = atomic volume.

E = arbitrary parameter of the dimensions of a reciprocal length.

The dash on the summation signs indicates that the terms where $h_l = 0$, $R_l = 0$ respectively are to be excluded.

Writing $X^{(l)}$ for $A^{(l)}$ or $B^{(l)}$ in definition (9) and ϵ for the independent variable defining the distortion (*i.e.*, ϵ_x for distortion A, γ_{xy} for distortion B), we obtain from equation (10)

$$\left.\begin{aligned} X^{(l)} &= \tfrac{1}{2}\frac{d^2W^{(l)}}{d\epsilon^2} \\ &= \left\{\begin{aligned} &\frac{e^2}{4\pi\Omega}\sum_l{}' \exp\left(-\frac{\pi^2}{E^2}h_l^2\right)\left[\left(\frac{\pi^4}{E^4}\frac{1}{h_l^2} + 2\frac{\pi^2}{E^2}\frac{1}{h_l^4} + \frac{2}{h_l^6}\right)\left(\frac{dh_l^2}{d\epsilon}\right)^2\right. \\ &\qquad\qquad\qquad\left. - \left(\frac{\pi^2}{E^2}\frac{1}{h_l^2} + \frac{1}{h_l^4}\right)\frac{d^2h_l^2}{d\epsilon^2}\right] \\ &+ \frac{e^2}{4}\sum_l{}'\left[\frac{2\exp(-E^2R_l^2)}{\sqrt{\pi}}\left\{\left(2E^3 + \frac{2E}{R_l^2}\right)\left(\frac{dR_l}{d\epsilon}\right)^2 - \frac{E}{R_l}\frac{d^2R_l}{d\epsilon^2}\right\}\right. \\ &\qquad\qquad\left. + \frac{1-\phi(ER_l)}{R_l^2}\left\{\frac{2}{R_l}\left(\frac{dR_l}{d\epsilon}\right)^2 - \frac{d^2R_l}{d\epsilon^2}\right\}\right] \end{aligned}\right. \end{aligned}\right\} \quad (10\text{A})$$

In a lattice which has undergone distortion A, the lattice vectors R_l and the vectors of the reciprocal lattice h_l have the form

$$\left.\begin{aligned} R_l &= \frac{\delta}{2}\sqrt{\left[n_1^2(1+\epsilon_x)^2 + \frac{n_2^2}{(1+\epsilon_x)^2} + n_3^2\right]} \\ h_l^2 &= \frac{1}{\delta^2}\left[\frac{m_1^2}{(1+\epsilon_x)^2} + m_2^2(1+\epsilon_x)^2 + m_3^2\right] \\ n &= \sqrt{(n_1^2 + n_2^2 + n_3^2)} \\ m &= \sqrt{(m_1^2 + m_2^2 + m_3^2)} \end{aligned}\right\} \quad (11)$$

where δ is the lattice constant; $\mathbf{n} = (n_1, n_2, n_3)$, $\mathbf{m} = (m_1, m_2, m_3)$ are sets of integers such that $\frac{1}{2}\mathbf{n}\delta$, $\mathbf{m}/\delta$ are points of the lattice and the reciprocal lattice respectively. We obtain from equation (11)

$$\left.\begin{aligned}
\left(\frac{d\mathrm{R}_l}{d\epsilon_x}\right)_{\epsilon_x=0} &= \frac{\delta}{2}\frac{n_1^2-n_2^2}{n}\\
\left(\frac{dh_l^2}{d\epsilon_x}\right)_{\epsilon_x=0} &= \frac{2}{\delta^2}(m_2^2-m_1^2)\\
\left(\frac{d^2\mathrm{R}_l}{d\epsilon_x^2}\right)_{\epsilon_x=0} &= \frac{\delta}{2}\left[\frac{n_1^2+3n_2^2}{n}-\frac{(n_1^2-n_2^2)^2}{n^3}\right]\\
\left(\frac{d^2h_l^2}{d\epsilon_x^2}\right)_{\epsilon_x=0} &= \frac{2}{\delta^2}(3m_1^2+m_2^2)
\end{aligned}\right\}. \quad (12)$$

For distortions of the type B we obtain correspondingly

$$\left.\begin{aligned}
\left(\frac{d\mathrm{R}_l}{d\gamma_{xy}}\right)_{\gamma_{xy}=0} &= \frac{\delta}{2}\frac{n_1n_2}{n} & \left(\frac{dh_l^2}{d\gamma_{xy}}\right)_{\gamma_{xy}=0} &= -\frac{2}{\delta^2}m_1m_2\\
\left(\frac{d^2\mathrm{R}_l}{d\gamma_{xy}^2}\right)_{\gamma_{xy}=0} &= \frac{\delta}{2}\left(\frac{n_2^2}{n}-\frac{n_1^2n_2^2}{n^3}\right) & \left(\frac{d^2h_l^2}{d\gamma_{xy}^2}\right)_{\gamma_{yz}=0} &= \frac{2}{\delta^2}m_1^2
\end{aligned}\right\}. \quad (13)$$

Inserting (12) and (13) into equation (10A), we obtain

$$\left.\begin{aligned}
\mathrm{X}^{(l)} = &\left\{\begin{aligned}
&\frac{e^2\delta^2}{2\pi\Omega}\sum_{\mathbf{m}}{}'\exp(-m^2\xi^2)\Big[2\xi^4\alpha(\mathbf{m})\\
&\qquad\qquad+\left(\frac{\xi^2}{m^2}+\frac{1}{m^4}\right)(4\alpha(\mathbf{m})-\beta(\mathbf{m}))\Big]\\
&+\frac{e^2}{2\delta}\sum_{\mathbf{n}}{}'\Big[\frac{2\exp(-n^2\eta^2)}{\sqrt{\pi}}\left\{2\eta^3\alpha(\mathbf{n})+\frac{\eta}{n^2}(3\alpha(\mathbf{n})-\beta(\mathbf{n}))\right\}\\
&\qquad\qquad+\frac{1-\phi(\eta n)}{n^3}\{3\alpha(\mathbf{n})-\beta(\mathbf{n})\}\Big]
\end{aligned}\right.\\
&\begin{aligned}
\eta &= \mathrm{E}\frac{\delta}{2} \\
\xi &= \frac{\pi}{\mathrm{E}\delta}
\end{aligned}
\qquad \alpha(\mathbf{n}) = \begin{cases}\dfrac{(n_1^2-n_2^2)^2}{n^2}\\[2ex] \dfrac{n_1^2n_2^2}{n^2}\end{cases}
\qquad \beta(\mathbf{n}) = \begin{cases} n_1^2+3n_2^2 & \text{for } \mathrm{X}^{(l)}=\mathrm{A}^{(l)}\\[2ex] n_2^2 & \text{for } \mathrm{X}^{(l)}=\mathrm{B}^{(l)}\end{cases}
\end{aligned}\right\}. \quad (14)$$

The numerical values obtained for face-centred (F.C.) and body-centred (B.C.) cubic structure are given in Table I in units of $e^2/2\delta$, δ being the lattice constant.

TABLE I

	Face centred	Body centred
$\mathrm{A}^{(l)}$	0·2115	0·1994
$2\mathrm{B}^{(l)}$	0·9479	0·7423

The formulae of Table I hold only if the electron density at the boundary of the unit polyhedra in the metal is equal to that in the lattice with a uniform electron distribution, *i.e.*, if

$$|\phi_0(r_0)|^2\Omega \tag{14A}$$

is equal to unity. A simple consideration shows that, if this is not true, the values of Table I have to be multiplied with the factor (14A). For sodium and copper this factor has been found to be equal to unity (*cf.* II and III). We shall assume this to be true for all the metals which we are considering here.

4—THE EXCHANGE ENERGY BETWEEN THE CLOSED SHELLS OF THE IONS

In (*cf.*) III we found that the force between the closed shells of the copper ions has a very important effect on the compressibility. We expressed there the opinion that this effect would probably be negligible for the alkali metals. In the course of the present investigation, however, we found on this assumption certain discrepancies between the theoretical and experimental results (*see* § 6). We shall therefore consider the exchange interaction between the closed shells of the alkali ions too. It will be seen that, although this effect is smaller than for copper, it is not negligible.

The forces between the closed shells of the ions are the sum of an attractive force, the van der Waals force, and a repulsive force which is due to the overlapping of the closed shells; since the overlapping is small, the overlapping of more than two shells in the same space element will be negligible and the repulsive forces can be treated as additive central forces. We may therefore denote by $w(r)$ the energy per ion (so that $2w(r)$ is the whole interaction energy for two ions) between the closed shells of two ions at a distance r apart (excluding the electrostatic energy between the ions considered as point charges). $w(r)$ decreases so rapidly with r that it is sufficient to consider nearest and next nearest neighbours only. For the lattice the energy $W^{(I)}$ per atom is thus

$$W^{(I)} = \sum_r w(r) \tag{15}$$

where the summation is over all distances r between nearest and next nearest neighbours.

Writing again $X^{(I)}$ for the elastic constants $A^{(I)}$ and $B^{(I)}$ in definition

(9) and ε for the independent variable defining the distortion, we obtain from equation (15)

$$X^{(1)} = \frac{1}{2} \sum_{r} \frac{d^2w}{dr^2}\left(\frac{dr}{d\varepsilon}\right)^2 + \frac{dw}{dr}\frac{d^2r}{d\varepsilon^2}. \tag{16}$$

The values of $dr/d\varepsilon$ and $d^2r/d\varepsilon^2$ are contained in the equations (12), (13). The summation yields for face-centred and body-centred structures respectively the values given in Table II.

TABLE II

	Nearest neighbours		Next nearest neighbour's (face and body centred)
	Face centred	Body centred	
$A^{(1)}$	$\rho^2 \frac{d^2w}{d\rho^2} + 7\rho \frac{dw}{d\rho}$	$8\rho \frac{dw}{d\rho}$	$2\delta^2 \frac{d^2w}{d\delta^2} + 2\delta \frac{dw}{d\delta}$
$2B^{(1)}$	$\rho^2 \frac{d^2w}{d\rho^2} + 3\rho \frac{dw}{d\rho}$	$2\rho^2 \frac{d^2w}{d\rho^2} + \frac{8}{3}\rho \frac{dw}{d\rho}$	$2\delta \frac{dw}{d\delta}$

Here ρ is the interatomic distance and δ the lattice constant.

The numerical values of $dw/d\rho$ and $d^2w/d\rho^2$ for the repulsive force between the copper ions are (*cf.* III)

$$\frac{dw}{d\rho} = -\,0{\cdot}0051\ \mathrm{R}\, a_0^{-1} \quad \frac{d^2w}{d\rho^2} = 0{\cdot}018\ \mathrm{R}\, a_0^{-2} \tag{17}$$

where a_0 is the atomic unit of length (0·528 A) and R the Rydberg unit of energy. The repulsion between the next nearest copper ions is negligible. The values (17) were calculated in III by a statistical method. Although this method could not be expected to give very reliable results, the values (17) gave rather close agreement with the observed value of the compressibility. These values should therefore be a good estimate and they should give a fair test of the present theory.

The repulsive energy between the alkali ions was taken from the calculations of Born and Mayer,* Mayer and Helmholz,† and Huggins and Mayer‡ on the cohesion in the alkali-halides. Born and Mayer assume a repulsive potential between two ions of the type

$$w^{(\mathrm{R})} = C_{12}\, b\, e^{(r_1+r_2-r)/\rho}. \tag{17A}$$

C_{12} represents, according to Pauling,§ the dependence of the repulsive potential on the charge of the ions. For two alkali ions it has the value 1·25, except for lithium, where it is 2·00. r is the distance between the ions. r_1 and r_2 are the two ionic radii, b and ρ are two constants, which Born and Mayer calculate from the volume and the compressibility, assuming that they are the same for the interaction of two positive, two negative or a positive and a negative ion, and that they do not change with the distance. These two assumptions seem to be justified by the results of the calculation: Born and Mayer found that ρ is the same for all alkali halides; Huggins and Mayer (*loc. cit.*) succeeded in deriving a consistent set of ionic radii with one constant b for the interaction between all the ions in question. We therefore feel justified in using these repulsive potentials in our calculations. The corresponding calculations of Mayer and Levy* for the cuprous halides cannot, however, be used in the same way, for there the value of ρ changes with the type of ion. They therefore give no indication of the interaction between two copper ions.

---

* 'Z. Physik,' vol. 75, p. 1 (1932).

† 'Z. Physik,' vol. 75, p. 19 (1932).

‡ 'J. Chem. Phys.,' vol. 1, p. 643 (1933).

§ 'Z. Kristallog.,' vol. 67, p. 377 (1928).

The van der Waals potential between two ions

$$w^{(a)} = -\frac{c}{r^6} \tag{18}$$

has been computed by Mayer and Helmholz (*loc. cit.*) for the alkalis and by Mayer and Levy* for the copper ions from the formulae of London.† The van der Waals force for the copper ions is in our case negligible compared with the repulsive force, and therefore the results of (*cf.*) III are not affected.

The values of the repulsive potential and the van der Waals potential taken from the papers mentioned are given in Table III.

TABLE III

	Li	Na	K
$c \times 10^{60}$ erg cm^6	0·55	2·5	30
Ionic radius $\times 10^8$ cm	0·475	0·875	1·185

$b = 10^{-12}$ erg $\rho = 0{\cdot}345 \times 10^{-8}$ cm

The elastic constants $A^{(I)}$ and $2B^{(I)}$ obtained from the formulae of this paragraph will be given later, § 6, Table V.

5—THE CHARACTERISTIC TEMPERATURE OF THE ALKALIS

From the results of the preceding paragraphs, the elastic constants of copper and the alkalis can be calculated. For copper we may make a comparison with the observed values. For the alkalis no experimental data exist, except for the compressibility; but from the Debye characteristic temperature Θ as found from the measured specific heat at sufficiently low temperatures, a relation between the elastic constants can be deduced. We shall therefore use our data to calculate Θ.

---

* 'J. Chem. Phys.,' vol. 1, p. 647 (1933).

† 'Z. phys. Chem.,' B, vol. 11, p. 222 (1930).

According to the theory of Born and Karman* for non-isotropic crystals, the value of Θ at low temperatures may be obtained as follows: Let p, q, r be the direction cosines; to each direction correspond three velocities $v_i\,(p, q, r)$ $(i = 1, 2, 3)$, one for longitudinal, two for transverse waves. Then Θ is given by

$$\left.\begin{aligned}\Theta &= \frac{h}{k}\left(\frac{3}{4\pi\Omega}\right)^{1/3}\bar{v}\\ \frac{1}{\bar{v}^3} &= \tfrac{1}{3}\sum_{i=1}^{3}\frac{1}{4\pi}\iint\frac{1}{v_i^3}\,dw\end{aligned}\right\} \tag{19}$$

where the integration is over all directions in the crystal. At low temperatures we require only the values of the velocities for long wave-lengths; these can be calculated from the elastic constants. If we substitute

$$\left.\begin{aligned}z_i &= \frac{\rho v_i^2 - c_{44}}{c_{11} - c_{44}} & \mathrm{D} &= \frac{c_{44}}{c_{11} - c_{44}}\\ \mathrm{D}' &= \frac{c_{12} + c_{44}}{c_{11} - c_{44}} & \mathrm{D}'' &= c_{11} - c_{44}\end{aligned}\right\} \tag{20}$$

where ρ is the density, then the z_i as functions of p, q, r are the three roots of the equation†

$$\left.\begin{aligned}z^3 - z^2 + (1 - \mathrm{D}'^2)\,z\alpha - (1 - 3\mathrm{D}'^2 + 2\mathrm{D}'^3)\,\beta = 0\\ \alpha = p^2q^2 + q^2r^2 + r^2p^2 \qquad \beta = p^2q^2r^2.\end{aligned}\right\} \tag{21}$$

Substituting (20) into equation (19), we obtain

$$\frac{1}{\bar{v}^3} = \tfrac{1}{3}\sum_{i=1}^{3}\frac{1}{4\pi}\left(\frac{\rho}{\mathrm{D}''}\right)^{3/2}\iint\frac{1}{(z_i + \mathrm{D})^{3/2}}\,dw. \tag{22}$$

This integral was evaluated by a method due to Hopf and Lechner‡: if we approximate to the integrand by a power series of z and sum over all i, we obtain a series of expressions of the form $z_1^\nu + z_2^\nu + z_3^\nu$; these functions can be expressed in terms of the coefficients of equation

---

* 'Phys. Z.,' vol. 14, p. 15 (1913).

† *Cf.* Born and Karman, *loc. cit.*

‡ 'Ber. deuts. phys. Ges.,' vol. 15, p. 643 (1914).

(21). The integrands occurring are then simply products of powers of α and β, which can easily be calculated.

The final result obtained is (the first six terms are those calculated by Hopf and Lechner, but the accuracy thus obtained was not sufficient in our case):

$$\frac{1}{\bar{v}^3} \cong \frac{1}{3}\left(\frac{\rho}{D''}\right)^{3/2} \left\{ \begin{aligned} & 3a_0 + a_1 + \frac{a_2}{5}[3 + 2D'^2] \\ & + \frac{a_3}{35}[15 + 18D'^2 + 2D'^3] \\ & + \frac{a_4}{105}[35 + 52D'^2 + 8D'^3 + 10D'^4] \\ & + \frac{a_5}{231}[63 + 100D'^2 + 16D'^3 + 46D'^4 + 6D'^5] \\ & + \frac{a_6}{5005}[1155 + 1830D'^2 + 272D'^3 + 1338D'^4 \\ & \qquad + 276\,D'^5 + 134D'^6] \\ & + \frac{a_7}{2145}[429 + 658D'^2 + 86D'^3 + 634D'^4 \\ & \qquad + 154D'^5 + 162D'^6 + 22D'^7] \\ & + \frac{a_8}{255255}[45045 + 66136D'^2 + 7408D'^3 \\ & \qquad + 75220D'^4 + 37008D'^5 + 32712D'^6 \\ & \qquad + 7536D'^7 + 2142D'^8] \end{aligned} \right\} \tag{23}$$

where the a_ν are the coefficients of the approximating power series

$$\frac{1}{(z + D)^{3/2}} \cong \sum_{\nu=0}^{8} a_\nu z^\nu. \tag{23A}$$

6—DISCUSSION OF THE RESULTS

In Table IV the resulting elastic constants are given in Voigt's notation. They are obtained from those defined by equation (4) for the elastic potential energy per atom and calculated from Tables I and II, by dividing by the atomic volume Ω.

The quantities 2C, A, and 2B given in the first three columns represent an independent set of elastic constants, from which c_{11}, c_{12}, and c_{44} may be deduced.

The values of A and 2B shown in bold faced type, represent the new results of this paper, being obtained directly from Tables I and II. They

TABLE IV—THE ELASTIC CONSTANTS (C.G.S.-UNITS × 10^{11})

		2C $=1/\kappa$	A $=c_{11}-c_{12}$	2B $=c_{44}$	c_{11}	c_{12}	$\delta \times 10^8$ cm (experimental)
Li		1·30*	0·279	1·605	1·49	1·21	3·40
Na		0·85*	0·106	0·770	0·92	0·81	4·22
K		0·40*	0·0541	0·882	0·44	0·38	5·15
Cu	theoretical	14·1	5·1	8·9	17·5	12·4	—
	experimental: room temperature	12·7	4·7	7·5	17·0	12·3	—
	experimental: absolute zero	13·9	5·1†	8·2†	18·6	13·5	3·60

* Experimental values.

† These extrapolated values are in good agreement with certain preliminary observations made by Dr. Goens at low temperatures. I wish to thank Professor N. F. Mott, and hence Dr. Goens, for allowing me to see these values.

both represent distortions in which the volume is unchanged, and therefore, for the reasons discussed in § 1, should be more accurate than the calculated compressibility, at least for the alkali metals (the compressibility depends, for instance, on the field of the ion which, especially for heavier atoms, has not been obtained accurately). In the calculation of A and 2B the experimental values of the lattice constants (column 6) at the absolute zero of temperature were used. They were extrapolated from the values observed at room temperatures, using the observed expansion coefficients,* which for Cu is known to fairly low temperatures. For the alkalis the expansion coefficients at room temperatures only are known, but since the amount of the extrapolation is less than 2%, this is not serious.

The elastic constants c_{11}, c_{12}, and c_{44} can only be calculated from A and 2B if the compressibility $\kappa = 1/2\text{C}$ is known. The theoretical values for the alkalis, obtained from the calculations mentioned in § 1, are mostly not very accurate. We therefore extrapolated for this purpose the observed values† to the absolute zero of temperature (column 1); this extrapolation is rather uncertain, since no observations of the temperature dependence of the compressibility at low temperatures exist for the alkalis.

The experimental values of the elastic constants at room temperature are obtained from the coefficients of elasticity observed by Goens and Weerts.‡ In order to obtain an idea of the order of magnitude of the extrapolation to the absolute zero of temperature an extrapolation proportional to that of 2C, observed by Grüneisen, was made (last line).

---

* 'Landolt-Börnstein Tables,' 5 ed., vol. 2 and 2*b*.

† *Ibid*, vol. 1*a*.

‡ 'Z. InstrumKde.,' vol. 52, p. 167 (1932).

The Cauchy Relations—If the lattice is considered as a system of point centres of force, certain relations between the elastic constants, the "Cauchy relations," can be derived. For a regular lattice the only Cauchy relation is $c_{12} = c_{44}$. It is known that for many monatomic metals, including copper, the Cauchy relations do not hold. The explanation, suggested by various workers, that the crystal structure consists of various simple lattices, which are displaced against each other as a whole by the distortion, cannot apply to monatomic metals,* since here every lattice point is a centre of symmetry. It has therefore been suggested by Geckeler* that the structure of these monatomic metals is not that of a simple lattice. As a result of the present calculation, it follows that this hypothesis is unnecessary, but that the model of point-like centres of force must be abandoned in order to account for the elastic behaviour of these metals. According to our calculation, in the displacements of the type A and B, central forces only are called into play, *e.g.*, the electrostatic and exchange energy between the ions; but for the compressibility forces are important which depend on the atomic volume only: the kinetic and part of the potential energy of the electrons. This accounts for the fact that the Cauchy relations are not satisfied.

In Table V we give separately the various contributions to the elastic constants A and 2B. In (*cf.*) III we concluded that the repulsion between the ions is much more important in determining the compressibility for copper than for the alkalis. This is the case for the other elastic constants, as is apparent from Table V.

The characteristic temperatures of the alkalis calculated from equations (19), (22) are given in Table VI, together with the experimental values at the lowest temperatures at which they have been measured. The value for lithium is that given by Simon and Swain† at 15° K; the values for sodium and potassium were calculated from the specific heat observed by Simon and Seidler‡ at 17° K and 14·7° K respectively.

The comparison with the Θ-values obtained from measurements of the specific heat is somewhat uncertain, since these values for Li and Na change considerably even at these low temperatures. Simon§ attributed this change to the excitation of higher energy levels, and by subtracting a

---

* *Cf.* 'Handb. d. Physik,' vol. 6, p. 414 (1928).

† 'Z. phys. Chem.,' B, vol. 28, p. 189 (1935).

‡ 'Z. phys. Chem.,' A, vol. 123, p. 383 (1926).

§ *Loc. cit.* and 'S.B. preuss. Akad. Wiss.,' p. 477 (1926).

TABLE V—COMPOSITION OF THE ELASTIC CONSTANTS (C.G.S.-UNITS × 10^{11})

Terms contributing	Li		Na		K		Cu	
	A	2B	A	2B	A	2B	A	2B
Electrostatic lattice energy of ions and valence electrons	0·339	1·263	0·143	0·532	0·0644	0·240	0·573	2·57
Repulsive energy of ions	−0·068	0·369	−0·042	0·255	−0·0202	0·127	$4{\cdot}5_4$	$6{\cdot}3_8$
The van der Waals energy of ions	0·008	−0·027	0·005	−0·017	0·0099	−0·035	−0·012	−0·034
Total	0·279	1·605	0·106	0·770	0·0541	0·332	5·1	8·9

suitable amount for the specific heat of this effect, he obtained constant Θ-values which are considerably higher. The recent work of Blackman,* however, has shown that such variations can be accounted for by a theory of the specific heat which takes into account the atomic structure. The variations of Θ are shown in fig. 1. Curve I indicates the observed values taken from the papers mentioned above. Curve II indicates a tentative extrapolation such as might be expected from Blackman's theory and has been found for other substances. This extrapolation seems to be qualitatively safe for sodium and lithium, where the further decrease of the Θ-value is indicated by the observed values. In order to see that this decrease is not due to the specific heat of the electrons, a correction was made according to Sommerfeld's† formula

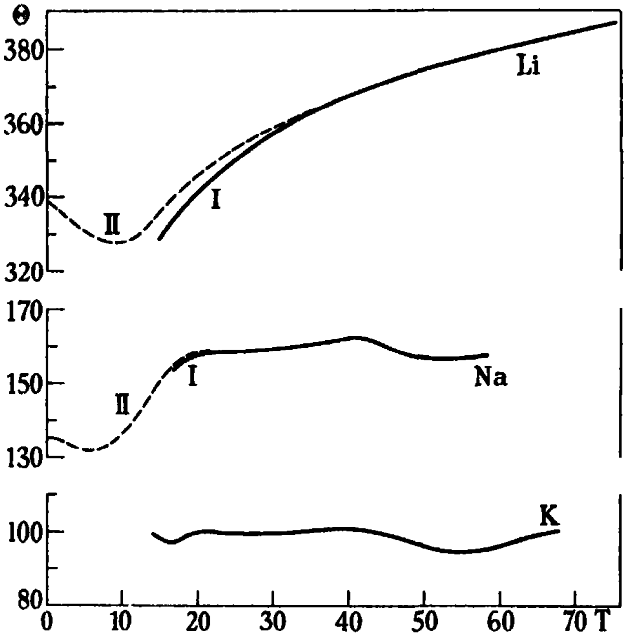

FIG. 1—The characteristic temperatures of Li, Na, and K. Curve I shows the observed values, and curve II the effect of the specific heat of the electrons, and also a possible extrapolation to the zero of temperature.

$$C_{\text{electr}} = \frac{\pi^2 mk}{h^2} n \left(\frac{8\pi}{3N}\right)^{2/3} RT,$$

where n is the number of electrons per atom (for the alkalis $n = 1$), N the number of electrons per unit volume; this correction is the difference between curve II and I at the temperatures at which experiments have been made. It seems possible, therefore, that the agreement between the theoretical and experimental Θ-values is even better than that expressed by the figures given in Table VI.

---

* 'Proc. Roy. Soc.,' A, vol. 148, p. 365; vol. 149, p. 117 (1935).

† 'Z. Physik,' vol. 47, p. 1 (1928).

TABLE VI—THE CHARACTERISTIC TEMPERATURES OF THE ALKALIS

Calculated from	Li	Na	K
Theoretical elastic constants without interaction of the ions	354	131	76
Theoretical elastic constants with interaction of the ions	339	135	90
Observed specific heat	328	154	99·5
Compressibility by Einstein's formula	274	137	79

On the other hand, not too much reliance can be laid on the theoretical values. There are two uncertain factors: firstly, the extrapolation of the compressibility; we tested this effect for sodium, where the error introduced will not be more than 5°. Secondly, in the calculation of the repulsion between the ions we neglected entirely the fact that the size of the ions is bigger in the metal than in the ionic lattice, since in the metal the valence electrons penetrate the alkali ions. Our estimate of the repulsion is therefore probably an under-estimate.

It seemed desirable to see how far the agreement in the Θ-values is simply due to the various experimental values (lattice constant, compressibility) entering the formulae (19) and (22) and how far to the anisotropy expressed by the elastic constants. This can be seen from the values given in the last row of Table VI and calculated from Einstein's formula

$$\Theta = \frac{13 \cdot 25 \times 10^{-4}}{A^{1/3}\,\rho^{1/6}\,\kappa^{1/2}}, \tag{25}$$

where A is the atomic weight, ρ the density, and κ the compressibility. The ratio of the Θ-values calculated from this formula and from the elastic constants is a function of the ratios of the three elastic constants only. It can be seen that this ratio is important for the agreement.

In the first row of Table VI we give the Θ-values obtained by neglecting the interaction between the ions. The disagreement with the observed values is much greater and, almost certainly for potassium, probably for lithium, too, greater than the change of Θ which may be expected at lower temperatures from Blackman's theory.

I have great pleasure in acknowledging my indebtedness to Professor N. F. Mott, who suggested the present problem to me, for his kind advice on many occasions. My thanks are also due to Professor A. M. Tyndall for granting me facilities to work in this laboratory and to Dr. H. Jones for the interest he has taken in the present work.

SUMMARY

The method developed by Wigner and Seitz for calculating the lattice energy and compressibility of monovalent metals is extended to account for their other elastic properties. The elastic constants of Li, Na, K, and Cu are calculated. For Cu satisfactory agreement with the observed values is obtained. As the elastic constants of the alkalis have not been measured, the Debye characteristic temperatures of Li, Na, and K are calculated from the theoretical elastic constants and compared with the values observed at low temperatures. It is shown further that the elastic constants of metals do not obey the Cauchy relations.

Some Measurements of the Reflexion Coefficient of the Ionosphere for Wireless Waves

By F. W. G. WHITE, M.Sc., Ph.D., and L. W. BROWN, B.Sc., Halley Stewart Laboratory, King's College, London

(*Communicated by E. V. Appleton, F.R.S.—Received August* 27, 1935)

1—INTRODUCTION

The first measurements of the attenuation of wireless waves in the ionized regions of the upper atmosphere were made by Appleton and Ratcliffe* in 1930. The results of their measurements were expressed in terms of the "reflexion coefficient" of the reflecting region, this coefficient being so defined as to be a measure of the total absorption suffered by the atmospheric wave in its passage from the sender to the receiver. It was pointed out that in order to estimate the reflexion coefficient it is necessary to know (1) the intensity of the waves starting out in an upward direction from the transmitting station towards the ionized regions, and (2) the intensity of the waves coming down to the ground after deviation by the region. The intensity of the waves at the

* 'Proc. Roy, Soc.,' A, vol. 128, p. 133 (1930).

receiver may readily be found, but it is much more difficult to measure the intensity of the waves leaving the sender. In the experiments of Appleton and Ratcliffe, the calculated value of the latter factor was used.

In recent papers by one of us[*] an account has been given of measurements of the amplitude of wireless waves refracted by the ionized regions of the earth's atmosphere. In these papers the development of the Breit and Tuve method for this purpose has been described and its advantages emphasized. The chief advantage of the method is that the waves which have been once reflected by the ionized regions may be received separated from those which have been more than once reflected between the ionized regions and the surface of the earth, thus permitting the reflexion coefficient to be directly calculated from the relative amplitude of these waves.[†] Since, however, it is not always possible to observe double reflexions it is desirable to calibrate the apparatus so that the reflexion coefficient may be calculated from the amplitude of the first reflexion. A method of doing this is described in this paper.

In all investigations of the electrical structure of the ionized regions it is of advantage to ensure that the experiments yield data relating to one particular set of conditions in the upper atmosphere. An outstanding example of this is Appleton's method of investigating the equivalent height-frequency relationship.[‡] In this paper an account is given of experiments in which the variation of the reflexion coefficient with the frequency of the waves is investigated. The total absorption suffered by the waves is plotted against the frequency, such curves being referred to as absorption-frequency curves. This type of measurement is analogous to the equivalent height-frequency investigations, and the interpretation of the results is very much assisted by a knowledge of the latter relationship which, in our experiments, is simultaneously determined. From these measurements it is possible to estimate the factors which influence the absorption and to make measurements of the collisional frequency of the electrons with gas molecules in the upper atmosphere.

While the present investigations were in progress, the results of experiments, carried out by Eckersley[§] and by Farmer and Ratcliffe,[||] dealing with the variation of the reflexion coefficient with time (as distinct from the multi-frequency method used here) have been published. These authors have estimated from their results a value for the collisional frequency of the electrons with gas molecules, which is not very different from the measurements given below.

---

[*] White, 'Proc. Phys. Soc. Lond.,' vol. 46, pp. 91, 805 (1934).

[†] Appleton, 'J. Inst. Elect. Engr.,' vol. 71, p. 645 (1932).

[‡] Appleton, 'Proc. Phys. Soc., Lond.,' vol. 45, p. 673 (1933).

[§] 'Nature,' vol. 135, p. 435 (1935).

[||] 'Proc. Roy. Soc.,' A, vol. 151, p. 370 (1935).

2—THE TRANSMISSION COEFFICIENT

In measurements of the type described in this paper, advantage is taken of the fact that energy, radiated in the form of an electromagnetic wave from the transmitting station (T) may reach the receiving station (R) by two or more paths. These are respectively the direct or ground path, and the atmospheric paths of single or multiple reflected waves. The relative amplitudes of the direct wave and the atmospheric waves will depend upon:

(1) The attenuation of the direct wave travelling over the earth's surface.
(2) The attenuation of the atmospheric waves in the ionized regions.
(3) The relative distances travelled by each of the waves (the amplitude decreasing inversely as the distance).
(4) The relative amplitudes of the waves radiated by the transmitting aerial at different angles to the vertical.

It has been previously shown* that these factors may be related to the amplitudes of the direct wave G and the reflected wave F'† by

$$\frac{F'}{G} = \frac{\beta d_0 \rho}{\alpha d_1}, \tag{1}$$

where $F' = \frac{\beta}{d_1}\rho$, β being the constant involving the amplitude of the wave sent upwards from the aerial, d_1 the actual distance travelled by the atmospheric wave, and ρ the reflexion coefficient of the ionized regions; while $G = \frac{\alpha}{d_0}$, where α describes the amplitude of the direct wave and its attenuation by the ground, and d_0 the actual distance between the sender and the receiver over the direct path.

If the path between T and R is one involving double reflexions between the ionized regions and the earth's surface, then $F'' = \frac{\beta\rho^2\rho_g}{2d_1}$ and therefore $\frac{F''}{F'}\frac{\rho\rho_g}{2}$, where ρ_g is the reflexion coefficient of the earth's surface. If it is assumed that, to a first approximation, ρ_g is equal to unity, then

$$\rho = \frac{2F''}{F'} = Kd_1\frac{F'}{G} \tag{2}$$

---

* White, 'Proc. Phys. Soc. Lond.,' vol. 46, pp. 91, 805 (1934).

† The nomenclature F', F'' has been used in this paper to denote first and second orders of reflexion.

where K is a quantity, called the "transmission coefficient" defined by

$$K = \frac{\alpha}{\beta d_0} = \frac{2\,F''G}{(F')^2\,d_1}. \tag{3}$$

Under suitable conditions, when double reflexions are observed, the Breit and Tuve method permits F′ and F″ to be measured. If at the same time the amplitude of the ground wave (G) is found then the transmission coefficient K may be calculated.

For the conditions under which the present experiments were carried out, it is known that when the atmospheric wave enters the ionized regions it is resolved into two component waves which return to the receiver circularly polarized with right- and left-handed senses of rotation. Also for certain ionospheric conditions these components return to the receiver with different delay times and can be separately examined by the Breit and Tuve method. It is assumed in the present measurements that the upgoing wave, on entering the ionosphere, is plane polarized, so that the two circularly polarized components have equal amplitudes, namely, half that of the incident wave. For the component waves the reflexion coefficients are therefore given by

$$\rho_0 = \frac{2F''_0}{F'_0} = K\,d_{10}\,\frac{F'_0}{G} \qquad \text{(ordinary wave)}$$

$$\rho_x = \frac{2F''_x}{F'_x} = K\,d_{1x}\,\frac{F'_x}{G}, \qquad \text{(extraordinary wave).}$$

According to this definition, a reflexion coefficient of unity clearly is measured for either component if it suffers no absorption.

Experimental Determination of the Transmission Coefficient.—The measurements to be described were made with wireless signals emitted from King's College, London, and received at the Halley Stewart Laboratory, Hampstead, a distance of 6 kilometres away. The sending system employed was that described by Pulley,* the aerial being a horizontal dipole of length 16 metres. With this arrangement the sender was used over the frequency range from 2·8 to 6·5 Mc/s. At the receiving station the aerial consisted of a single length of wire coupled to a superheterodyne receiver, the output of which was recorded on a cathode ray oscillograph. Since the voltage output of the receiver was linearly related to the amplitude of the signal received, the deflexion of the oscillograph measured in arbitrary units could be taken as a measure of the signal amplitude.

---

* 'Proc. Phys. Soc. Lond.,' vol. 46, p. 853 (1934).

The method by which the transmission coefficient K was measured is as follows. At suitable times when double reflexions were obtained the ratios F′/G and F″/F′ were measured for either or both components and from these ratios the transmission coefficient was calculated as explained above. There were several difficulties which had to be overcome before the final value of the coefficient could be obtained. The criticism which follows applies not only to the determination of K but also to the measurements of the reflexion coefficient, ρ, which are discussed below.

First it is important to allow for the random fading of the signal at the receiver. This phenomenon is well known and its effect on the measurements has to be eliminated by averaging the fluctuations. Two conflicting considerations influence the choice of the method of averaging. It is desirable that observations over the whole range of frequency should be made as quickly as possible in order that the results may be assumed to relate to a particular set of ionospheric conditions. However, in order to be certain that a correct average value is obtained, many observations on each frequency should be taken. A compromise had thus necessarily to be adopted.

The whole frequency range was divided into 85 steps, each frequency on which observations were made being separated from the next by about 0·05 Mc/s. In making the observations, one half-minute was spent on each frequency, and during that period two snapshot pictures were taken at random times. From measurements of these pictures the average value of K for each frequency was calculated. Such observations were repeated as often as possible. When all the available readings were plotted on squared paper, it was obvious that although some readings were considerably in error, due principally to fading, on the average a mean curve could satisfactorily be drawn.

A further uncertainty arises from the fact that, for the lower part of the frequency range, the two magneto-ionic components were not separated or only partially separated in our method of echo-delineation. Since in the second order the separation is always twice that in the first order, the variations in amplitude of the second order reflexion, due to mutual interference of the component waves, is liable to be quite different from that of the first order. These irregularities were eliminated by the method of averaging described above.

A difficulty also presents itself in the determination of the distance d_1, since only the equivalent path P′ could be measured. It was considered sufficiently accurate, in these measurements to assume that, for the flat portion of the P′-f curve, the actual length of the trajectory was equal to the equivalent distance. Where the P′-f curve departs from the flat portion, the value of d_1 corresponding to the flat portion was taken, since it is known that a large change in P′ is accompanied by a much smaller change in the actual path. It is considered that the error involved in this estimate is of the same order of magnitude as that in obtaining the average amplitude.

The results of the measurements are shown in fig. 1. This curve shows the variation of $K = \alpha/\beta d_0$ with frequency. This result has an added interest for the following reason. Expressed more fully, the coefficient K is equal to the relative amplitude of the radiation from the aerial in a vertical and a horizontal direction (this being implied in α/β), multiplied by the ground attenuation factor (included in α), and divided by the distance d_0. If the two latter factors were measured, the frequency variation of the ratio of the vertical to horizontal radiation of the aerial could be calculated. Moreover, by using a transportable receiver so that the distance d_0 may be varied, and working with one frequency only, a similar set of measurements would give the vertical polar diagram of the sending aerial for spatial radiation.

3—ABSORPTION-FREQUENCY MEASUREMENTS

It is shown above that, with the aid of the transmission coefficient K, the reflexion coefficient ρ may be obtained from measurements of the ratio F′/G and of d_1. In the measurements described below, the coefficient ρ, together with the equivalent height of reflexion, was found, at noon, during the months November 1934 to May 1935, over the frequency range from 2·8 to 6·5 Mc/s. Since results of this nature have not previously been described, the experimental results are first presented, the discussion following in a later section of the paper. The results are given in the form of curves showing both the equivalent path P′ and the reflexion coefficient as a function of frequency. Since the reflexion coefficient is generally a measure of the absorption suffered by the wave, it may be conveniently expressed in terms of the absorption coefficient k by the statement that

$$\rho = e^{-\int k\, ds} \tag{4}$$

or that

$$\log \rho = -\int k \,.\, ds. \tag{5}$$

the integral referring to the whole trajectory of the wave. It is thought advisable in these curves to plot log ρ in preference to ρ, since the former quantity is more directly involved in the calculations and discussion.

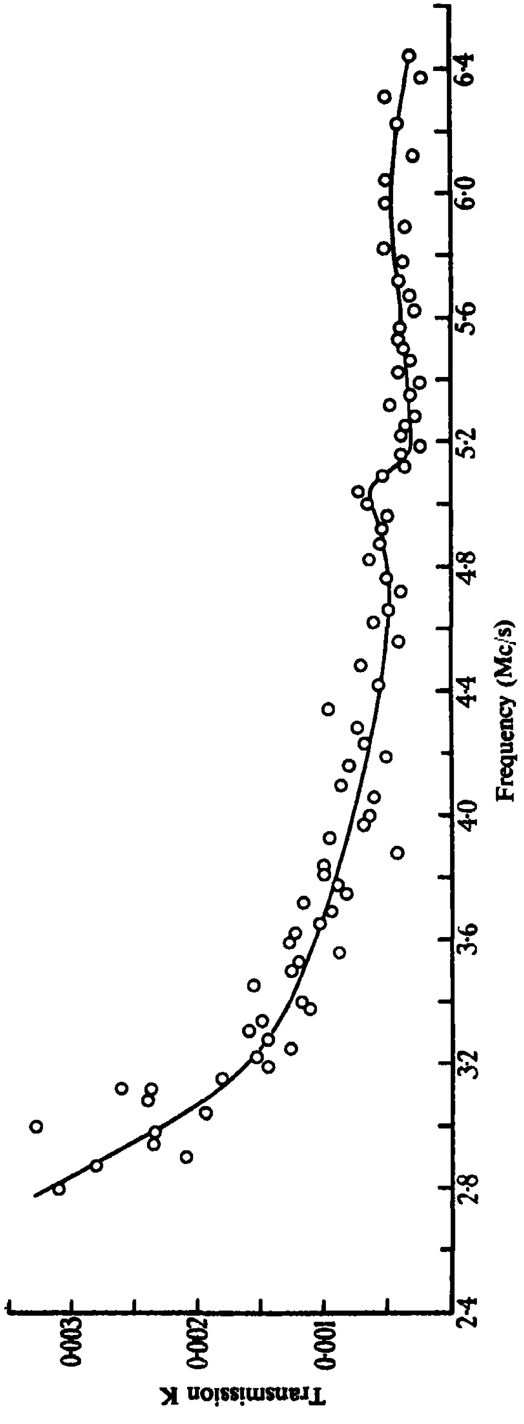
Transmission K
0·003
0·002
0·001
2·4
2·8
3·2
3·6
4·0
4·4
4·8
5·2
5·6
6·0
6·4
Frequency (Mc/s)

FIG. 1.

One or two general remarks about these curves may be made here. No attempt has been made to draw a smooth curve through the values of log ρ, but in endeavouring to elucidate the absorption phenomena the general trend of the values of log ρ has been studied, for in this manner the mean value of a number of consecutive readings may be estimated.

No means of observing separately the two magneto-ionic components, when the equivalent height for each is the same has been adopted. Thus some of the readings are to be interpreted as the average value of log ρ for both components taken together. These values are plotted as though they are for the ordinary ray, but it is quite obvious that an inspection of the P′-*f* curve will show when the components are overlapping. The only part of the curve for which this is not so is that part, at the low frequency end, before the extraordinary ray is first observed reflected from the F region. It is well known that the extraordinary ray should appear at about 0·70 Mc/s after the ordinary ray, but in most cases this frequency separation cannot be observed on account of the marked absorption suffered by the former component. These facts eliminate to some extent any doubt as to the identity of the components. Although no measurements of polarization have been made in order to distinguish the components it is felt that the observed general trend of the P′-*f* curve is sufficient for this purpose, in view of the very close study of such curves that has been made by Appleton and others.

4—EXPERIMENTAL RESULTS

There are presented below a number of curves which have been selected as representative of the results obtained at mid-day during the months November 1934 to May 1935.

Example No. 1, *January* 29, 1935—The results obtained on this occasion are shown in fig. 2, the upper part of which shows the values of P′ and the lower those of log ρ. On the first five frequencies a small echo of equivalent height 150 km is recorded, evidently the intermediate region E_2. At 2·70 Mc/s there is an abrupt increase in P'_0 of magnitude 50 km at the transition from E_2 to F region. The equivalent height then shows two small minima at about 2·85 and 3·20 Mc/s but remains very constant over the range 3·40 to 4·80 Mc/s, just before it finally rises on penetrating F region.

The pronounced minimum in the values of log ρ_0 is coincident with a small maximum in equivalent height, but at the higher frequency, about 3·30 Mc/s, a similar change in height is not accompanied by such a

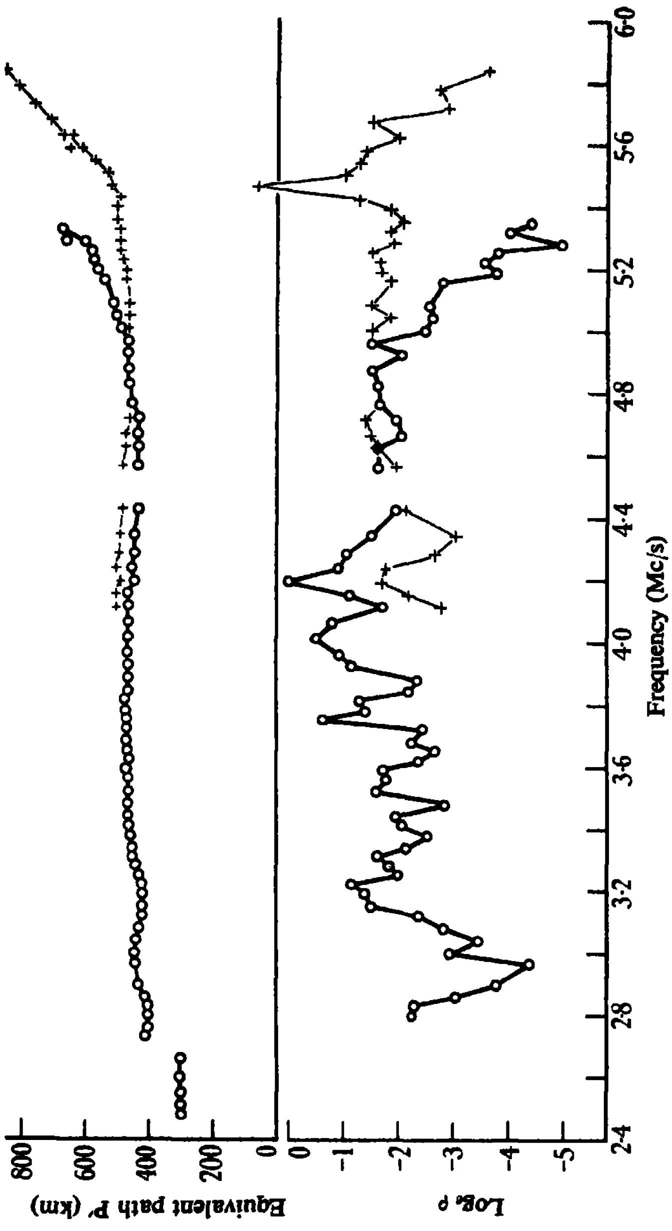

FIG. 2—January 29, 1935, 13.00 G.M.T.

marked change in log ρ_0. This change in log ρ_0 just after transition from E to F regions is further discussed below.

The extraordinary ray does not appear separated from the ordinary ray until the frequency 4·10 Mc/s is reached, and although the amplitude of this component increases the change is not so marked as for the ordinary ray. It is probable that the values of log ρ_0 just before this, from 3·7 to 4·1 Mc/s, are to some extent affected by the extraordinary ray, although only the ordinary component is shown.

At the high frequency end of the curve the decrease in amplitude associated with the penetration of the F region is clearly shown. The sharp maximum at 5·46 Mc/s is, no doubt, due to random fading.

Example No. 2, *March* 7, 1935—This run, fig. 3, begins at 3·2 Mc/s with an appreciable decrease in height for the F region. This is accompanied by a very rapid decrease in absorption. The extraordinary ray appears at 4·06 Mc/s and, from the nature of the curves, it may be assumed that the readings for the lower frequencies are for the ordinary ray only. Log ρ_x, between 4·06 and 4·23 Mc/s, decreases and it is unfortunate that this component cannot be separately distinguished in the next few readings for this decrease may be similar to that usually found in the case of log ρ_0 just after the transition from E to F region. The pronounced increase in log ρ_0 at 4·56 Mc/s may be due to the interference of the two components.

In this example the change in P′ at about 5·1 Mc/s is associated with the transition from F_1 to F_2 region described by Appleton. As is to be expected, the transition is accompanied by a decrease in log ρ. This transition is more obvious for the extraordinary ray than for the ordinary.

As the critical frequency for F_2 region is approached the equivalent height increases much more slowly with frequency than is usual.

Example No. 3, *March* 12, 1935—At the low frequency end of this curve, fig. 4, the transition from E_1 region to the intermediate region, E_2, and then to the F_1 region is shown. From 3·00 to 3·40 Mc/s the decrease in P′ due to decreasing group retardation in the lower regions occurs, and is accompanied by an increase in the reflexion coefficient.

Although the extraordinary ray reflected from the lower regions is not observed, it is of sufficient intensity at 3·65 Mc/s to be recorded. The curve shows a gradual increase in the intensity of this component between this frequency and 4·80 Mc/s. From 5·00 to 5·40 Mc/s the two components are of very nearly equal amplitude and show the same equivalent height.

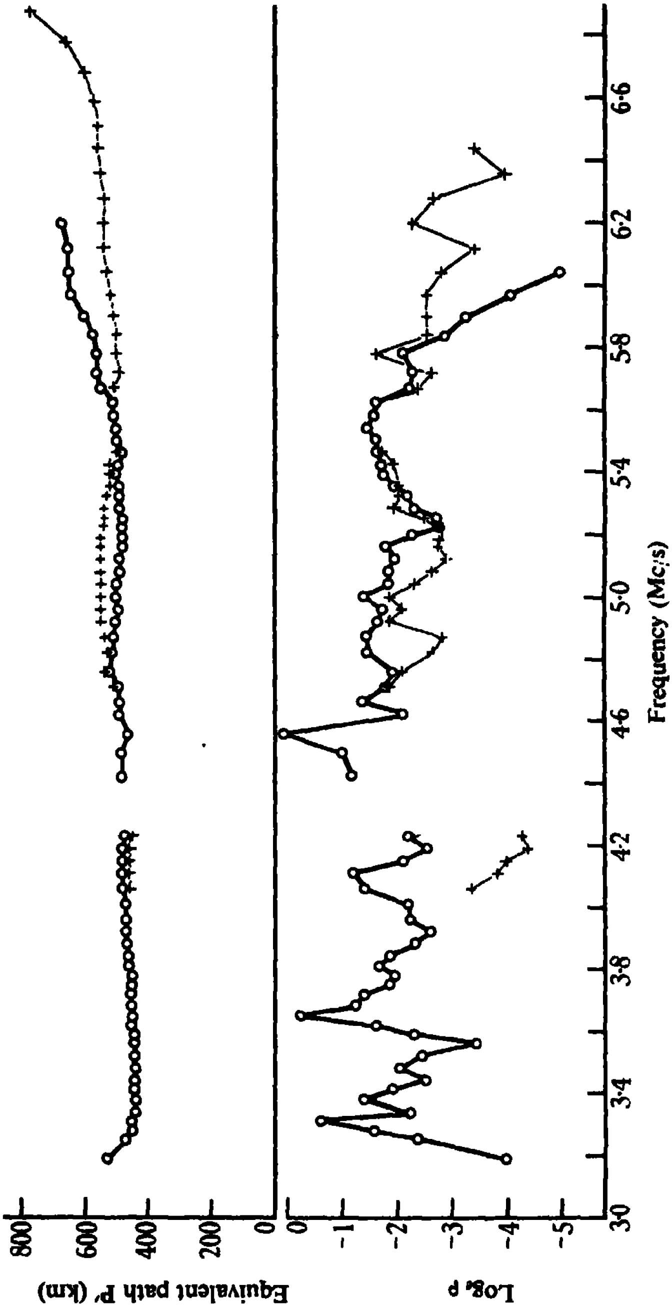

FIG. 3—March 7, 1935, 13.00 G.M.T.

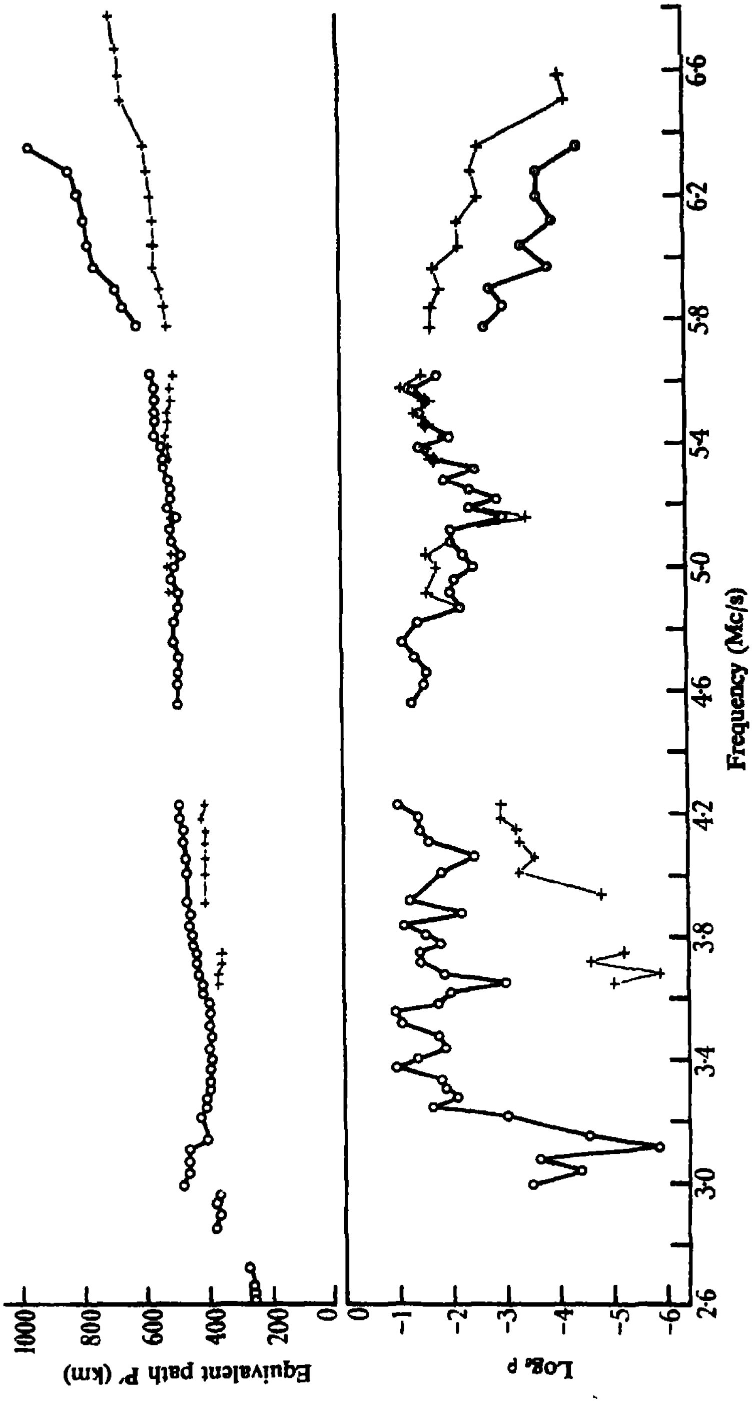

FIG. 4—March 12, 1935, 13.00 G.M.T.

The critical frequency for the extraordinary ray is greater than the maximum calibrated value of 6·6 Mc/s.

Example No. 4, *April* 25, 1935—This curve, fig. 5, shows the transition from E to F region of each component, as well as the existence of F_1 region. The P′-*f* curve for the ordinary ray rises to two maxima, one at 3·59 Mc/s and the other at about 4·30 Mc/s, the latter being the critical frequency of the F_1 region. The maximum at the lower frequency is frequently observed on P′-*f* curves in summer. The curve for the extraordinary ray is very similar to that for the ordinary ray displaced through a range of 0·7 Mc/s. The absorption suffered by the ordinary component decreases considerably after the critical frequency for the E region has been passed, but shows a further increase at 3·59 Mc/s, this increase accompanying the maximum in the P′-*f* curve. Observations over the range 4·22 to 4·68 Mc/s were prevented on this occasion by interference. It is probable that the F_1 maximum for the ordinary component in P′ occurs in this region.

Although at the higher frequencies the value of P′ is constant the absorption suffered by this component increases at 5·20 Mc/s. This may be due to the appearance of " abnormal E " reflexions, the ordinary ray alone being partially reflected.

The extraordinary ray appears at 4·06 Mc/s, and, although the equivalent height of reflexion immediately increases, the frequency being 0·7 Mc/s higher than that of the first maximum for the ordinary ray, the absorption is decreasing. Two factors probably influence the value of log ρ_x; (*a*) the increasing absorption due to increasing P′ in the F region, and (*b*) the decreasing absorption in the E region. Whether log ρ_x increases or decreases will depend upon the relative changes in each of these factors as the frequency is increased. The change in the latter appears to be the greater in this instance. The rate of change of log ρ with frequency for the extraordinary ray near the critical frequency for the F_2 region is, in this example, much lower than that for the ordinary ray.

Example No. 5, *May* 13, 1935—On this occasion, fig. 6, the F_1 maximum for both the ordinary and the extraordinary rays is very pronounced and is accompanied by considerable decrease in amplitude. Observations for the frequency range from 4·22 to 4·52 Mc/s are not recorded on account of the very small amplitude of the downcoming waves. The extraordinary ray over the corresponding range is not so heavily absorbed, but this may be due to a slight temporal change in the F_2 region. Although the critical frequency for the F_1 region is the normal value for this time of the year that for the F_2 region is abnormally low.

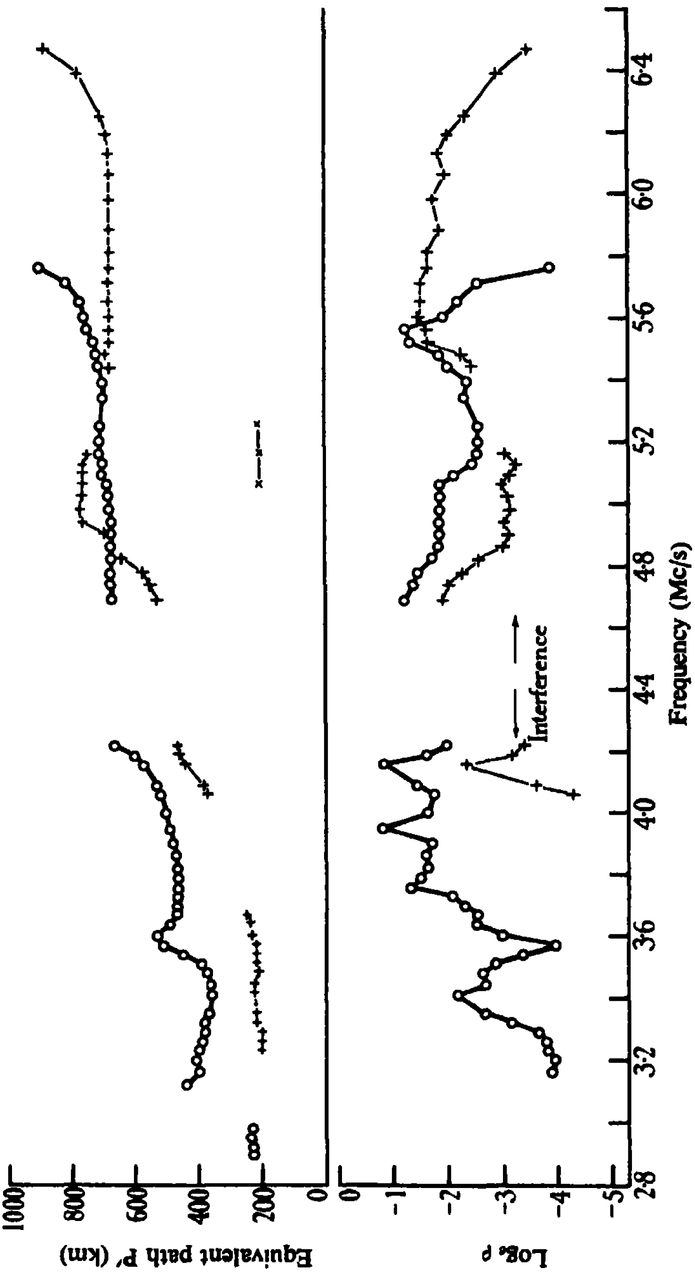

FIG. 5—April 25, 1935, 13.00 G.M.T.

The irregular behaviour of the results for the extraordinary wave near the critical frequency indicates that the conditions in F_2 region were varying considerably during the time of these observations.

5—DISCUSSION OF EXPERIMENTAL DATA

It is convenient to begin the examination of the curves at the high frequency end, for the variation of log ρ with frequency may then be associated, without any doubt, with the penetration phenomenon of F_2 region. In general the decrease in amplitude of either component begins at the same frequency as that at which the corresponding value of P′ begins to increase substantially. This decrease in amplitude may be accounted for on the alternative hypotheses (1) of electron limitation, or (2) absorption. The theory of electron limitation, investigated by Hartree,* describes the diminution in amplitude in terms of the partial

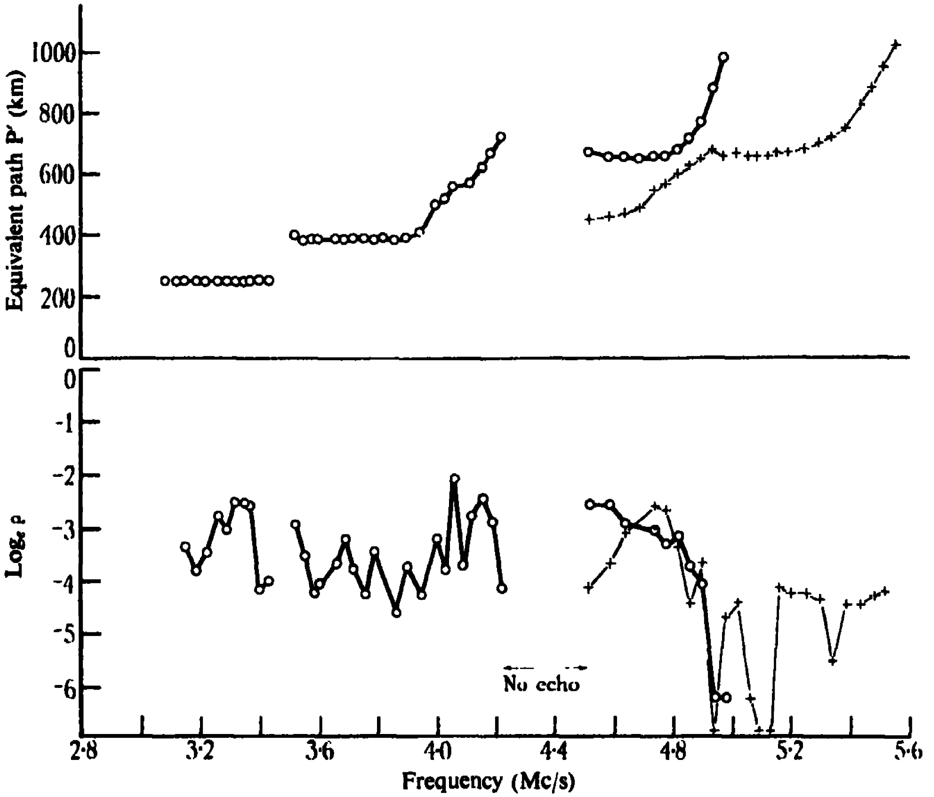

FIG. 6— May 13, 1935, 13.00 G.M.T.

---

* 'Proc. Camb. Phil. Soc.,' vol. 25, p. 97 (1928).

penetration of the reflecting region by the wave due to the small thickness of the former compared with the wave-length in free space. No data from the present experiments which will definitely discriminate between these two hypotheses are available, but it seems fairly certain that if the effect were due to electron limitation alone, the decrease in amplitude as the frequency increases would be very much more rapid than that actually observed.

If it is assumed that an absorption of energy accompanies an increase in P′ near the penetration frequency, the matter may be further elucidated in terms of the magneto-ionic theory by a method due to Appleton.* It has been definitely established that the propagation of either component near the top of the trajectory in the F region is of the quasi-transverse type.† The refractive index μ and the absorption coefficient k, for the ordinary ray, are given by‡

$$\mu^2 - \frac{c^2k^2}{p^2} = 1 - \frac{4\pi Ne^2}{m(p^2+\nu^2)} \tag{6}$$

$$2\mu\frac{ck}{p} = \frac{\nu}{p}\cdot\frac{4\pi^2Ne^2}{m(p^2+\nu^2)}, \tag{7}$$

where

N = number of electrons per cc,
e, m = charge and mass of the electrons,
p = angular frequency of the waves,
ν = collisional frequency of electrons with gas molecules,
c = velocity of light.

The following discussion of the measurement of the collisional frequency of the electrons refers to the ordinary ray only.

Measurements of the Collisional Frequency of the Electrons

Assuming that for a frequency near the critical frequency the absorption takes place in the F_2 region, and that $\nu^2 \ll p^2$ while c^2k^2/p^2 is small compared with μ^2, then

$$k = \frac{\nu}{2c}\frac{1-\mu^2}{\mu}.$$

This relationship can easily be shown to hold for the case of transverse propagation so long as

$$\frac{2p}{\nu} \gg \frac{1-\mu^2}{\mu^2}.$$

---

* 'Nature,' vol. 135, p. 618, April 20 (1935).

† Appleton and Builder, 'Proc. Phys. Soc. Lond.,' vol. 45, p. 208 (1933)

‡ Appleton, 'J. Inst. Elect. Engr.,' vol. 65, p. 640 (1927).

Since p is of the order $6\pi \times 10^6$ radians per second while ν is probably about 10^4 per second the value of μ may be as small as 10^{-3} before the expression becomes invalid. In these experiments the integral $\int k \, . \, ds$ is measured and this is, making use of the above result,

$$-\int k \, . \, ds = \log \rho = -\frac{\bar{\nu}}{2c}(\mathrm{P}' - \mathrm{P}) \tag{8}$$

if the average value of ν over the path is taken. This result will be valid even near the top of the trajectory to a degree of approximation consistent with the ray treatment of the problem which is implied in the above equations.

The result may be expressed conveniently in differential form, for if $\log \rho$ is multiplied by the frequency f and differentiated then

$$\frac{\partial}{\partial f}(f \log \rho) = -\frac{\bar{\nu}}{2c}\left(f\frac{\partial \mathrm{P}'}{\partial f}\right). \tag{9}$$

The measurements given above may, therefore, be used to determine the value of $\bar{\nu}$. This may be done from the curves as plotted using, from (9)

$$\bar{\nu} = -\frac{2c}{\partial \mathrm{P}'/\partial f}\left(\frac{\partial \log \rho}{\partial f} + \frac{\log \rho}{f}\right),$$

or from a curve showing the value of $(f \log \rho)$ plotted against P′ with the expression in the form

$$\nu = -\frac{2c}{f}\frac{\partial\,(f \log \rho)}{\partial \mathrm{P}'}$$

as shown by Appleton.*

In view of the importance of these results, a close experimental examination of this part of the P′-f curve has been made. To eliminate the effects of random fading it is necessary to average carefully the values of $\log \rho$ before a reliable estimate of $\bar{\nu}$ can be made. A set of observations specially taken for this purpose is shown in fig. 7, while the values of $\bar{\nu}$ obtained from this and similar measurements are given in Table I.

The values shown in this table are obtained from the average slope of the curve at a point midway between the greatest and least values of equivalent path taken. Most of the curves show, however, that the average value of ν appears to decrease as P′ increases. Measurements made from the curve of fig. 7 give the values given in Table II.

---

* 'Nature,' vol. 135, p. 618, April 10 (1935).

TABLE I—THE COLLISIONAL FREQUENCY OF ELECTRONS IN F REGION

Date	Collisional frequency per sec	Equivalent path, P′ km	Approximate height km
1935			
January 11	$3 \cdot 4 \times 10^3$	600	230
January 29	$7 \cdot 8 \times 10^3$	510	230
March 7	$4 \cdot 0 \times 10^4$	560	250
March 12	$4 \cdot 6 \times 10^3$	560	230
April 1	$6 \cdot 0 \times 10^3$	750	350
April 25	$2 \cdot 2 \times 10^4$	800	350
May 13....................	$5 \cdot 0 \times 10^4$	800	350

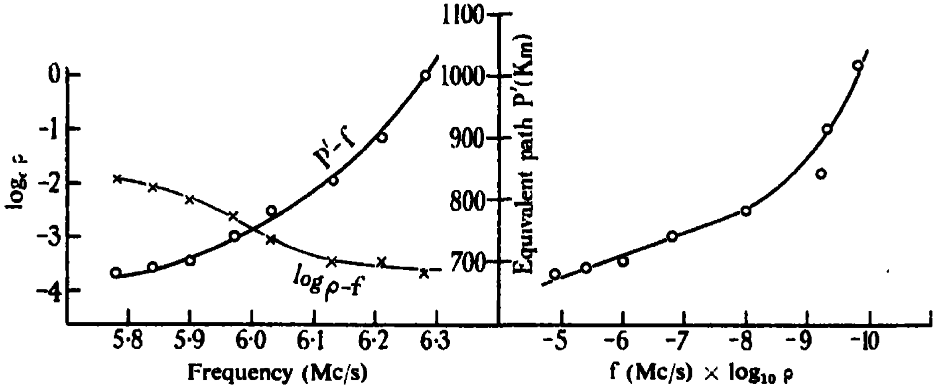

FIG. 7— April 1, 1935, 13.35 G.M.T.

TABLE II

Frequency Mc/s	P′ in km	$\bar{\nu}$ per sec
6·28	1000	$1 \cdot 17 \times 10^3$
6·21	900	$1 \cdot 77 \times 10^3$
6·08	800	$3 \cdot 41 \times 10^3$
5·80	680	$6 \cdot 8 \times 10^3$

The equivalent height of reflexion can increase only if the actual height also increases. If ν decreases with height decreasing values of ν are to be expected for the higher values of P′. The accurate values of the actual height are unknown, but a rough idea may always be obtained from the P′-*f* curve, for it may be assumed that in such a case as that examined above the actual height does not increase by much more than 20 km. If ν decreases exponentially, as is usually assumed, the decrease in ν measured above is of the right order of magnitude.

Absorption in E Region

The transition of reflexion from E to F region cannot be as carefully studied from these curves as is to be desired. This is principally due to the fact that the calibration has not been carried below 2·8 Mc/s. As is to be expected the E_2 region appears frequently at noon. A number of curves taken during the early months of the year are similar to that shown in fig. 2. There appears to be a definite increase in absorption just after the transition from E to F region. This increase is probably connected with the same part of the upper atmosphere as that which causes the small maximum in the P′-*f* curve at a later time of the year, *e.g.*, fig. 5 at about 3·6 Mc/s. For a simple transition from one region to another the amplitude should increase with increasing frequency and be accompanied by a fall in the equivalent height. It seems that, in actual fact, this simple process is often complicated by the presence of a subsidiary maximum of ionization between E_2 and F_1 regions and near to the latter, the critical frequency of this region being nearly the same as that for the E_2 in the early months of the year. If such a region occurs at a level at which the value of ν is great it would have a considerable influence on the absorption without necessarily influencing the equivalent height to an appreciable extent.

If such subsidiary maxima occur we must suppose that the space between E and F region contains a considerable amount of ionization. This might be indirectly deduced from the fact that the extraordinary ray is frequently observed reflected from E region, whereas after the critical frequency has been passed it is very strongly absorbed. The absorption coefficient for this component, for similar conditions of ionization and collisional frequency of the electrons, is greater than that for the ordinary ray since it depends upon the difference between the frequency of the waves and the magneto-ionic gyro frequency. At about 3 Mc/s, however, this fact alone cannot cause such a great difference between the two components unless a large proportion of the trajectory passes through a region where the ionization is appreciably large.

When the P′-*f* curve shows a simple transition from E to F reflexion, *e.g.*, fig. 6, the amplitude of the reflexions from E region before the transition are usually of the same order of magnitude as the reflexions from F region, except over a small frequency range near the critical frequency. Such a result is consistent with the assumption of a fairly sharp maximum in the E region ionization, with little extra ionization between E and F regions.

D Region Absorption

The absorption discussed above is that part of the whole which is associated with the region causing refraction or group retardation after penetration. Such absorption shows a marked variation with frequency since its large value depends principally upon the integral $\int \frac{ds}{\mu}$. It is to be expected that in the middle of the day, ionization may occur in the atmosphere, below E region, at altitudes where ν is large. The magnitude of the ionization density will be small and therefore the refractive index of the order unity. For such a region the propagation is of the quasi-longitudinal type and the absorption coefficient given by

$$k = \frac{\nu}{2c}\frac{p_0^2}{(p \pm p_L)^2}. \tag{10}$$

For the ordinary ray k can be large only for large values of ν. The variation with frequency will depend upon the term $p_0^2/(p \pm p_L)^2$, so that this absorption, for the ordinary ray, will vary much more slowly than that associated with the critical phenomena described above. All the results taken at noon show a minimum absorption which is different from zero. The values of log ρ always decrease, after any of the critical frequencies have been passed, to a minimum value which is determined by this D region, where ν is large and $\mu \doteqdot 1$. On account of the large variations in log ρ due to the critical phenomena the frequency variation of the D region absorption cannot be satisfactorily discussed.

The greater altitude of the sun may be expected to cause more ionization in the D region in summer than in winter. This would be observed as an increase in the absorption. Estimates of this absorption for the ordinary ray, and for frequencies within the range 2·5 to 6·0 Mc/s, during the months November 1934 to June 1935, are given in Table III.

These figures show such an increase, the ratio of the summer to winter values of log ρ_0 being about 2 to 1.

6—GENERAL DISCUSSION

A characteristic feature of the P′-*f* curves is the similarity in behaviour of the two magneto-ionic components. Apart from the fact that the extraordinary ray is often more strongly absorbed, just after the transition of this component from the E to F regions, the log ρ-*f* curves are also very similar for the two components. The greater absorption of the extraordinary compared with the ordinary ray at the lower frequencies verifies the predictions of the magneto-ionic theory. A comparison of their relative amplitudes on a single frequency, in order to test the theory, may be misleading, for it is obvious that the relation of the frequency chosen to any of the critical frequencies must determine to a great extent the relative attenuations.

For instance, the equality of the amplitudes of the right- and left-handed components, at about 5 Mc/s, a fact pointed out by Eckersley,* may certainly be traced to the increased absorption of the ordinary ray as the critical frequency for this component is approached. The extraordinary component is the more strongly absorbed at all lower frequencies. The results given above do not confirm the statement by Eckersley that the attenuation of the extraordinary component is almost stationary over the frequency range from 4 to 6 Mc/s. The values of log ρ obviously depend upon the critical frequencies to a very large extent.

TABLE III—ABSORPTION IN D REGION

Date	$\log \rho_0 = -\int k\,.\,ds$
1934	
November 27	1·15
December 11	−0·92
December 20	−0·46
1935	
January 3	−1·15
January 11	−0·46
January 15	1·15
January 17	−1·15
January 29	−2·06
February 2	−1·15
February 6	−1·38
March 7	1·84
March 12	−1·61
April 8	−1·38
April 25	−1·61
May 13	−3·68
May 17	−2·54
May 30	−3·45
June 21	−2·99

Indeed, it is unsatisfactory to discuss the attenuation of either component at any time of the day unless the associated phenomena revealed by the P′-*f* and log ρ-*f* curves is also known.

---

* 'Proc. Roy. Soc.,' A, vol. 141, p. 697 (1933).

We wish to express our thanks to Professor E. V. Appleton for his encouragement and interest in this work; also to Mr. J. A. Ratcliffe with whom we have had many helpful discussions. The work described in this paper was carried out as part of the programme of the Radio Research Board of the Department of Scientific and Industrial Research.

SUMMARY

In this paper measurements of the reflexion coefficient of the ionosphere for wireless waves are described. The Breit and Tuve technique for ionospheric investigation is employed, the sender-receiver system being calibrated so that the reflexion coefficient may be determined for a wave of any frequency within the range 2·80 to 6·50 Mc/s, from the relative amplitudes of the direct and the singly reflected atmospheric waves. The method of calibrating the system is described in the first part of the paper.

Example measurements, made at noon during the period November 1934 to May 1935, showing the variation of the reflexion coefficient with wave frequency are quoted. They show that the total absorption suffered by the waves is very much dependent upon the critical phenomena at the transition of reflexion from one region to another. The influence of the absorbing regions is estimated from the results.

Estimates, based upon Appleton's theoretical formula, of the collisional frequency of the electrons with gas molecules in the F_2 ionized region of the upper atmosphere, are made. The collisional frequency is of the order 5×10^3 per second at a height of approximately 250 km above the surface of the earth. Some indication of the variation of this quantity with altitude is given.

The Relativistic Theory of the Auger Effect

By H. S. W. **Massey**, Ph.D., Independent Lecturer in Mathematical Physics, Queen's University, Belfast, and E. H. S. **Burhop**, B.A., M.Sc., Exhibition of 1851 Scholar, University of Melbourne, Trinity College, Cambridge

(*Communicated by R. H. Fowler, F.R.S.—Received September* 2, 1935)

In a recent paper by one of us[†] the theory of the Auger Effect has been discussed and calculations carried out of the magnitude of the X-ray K series fluorescence yield for elements of atomic number low enough to justify the neglect of relativistic effects. The comparison of these theoretical results with experiment revealed sufficiently good agreement to justify the extension of the theory to elements of high atomic number by taking account of relativistic effects. As the Auger Effect is capable of direct and accurate experimental investigation any appreciable relativistic modification could be tested quantitatively. Such a test is of special importance owing to the somewhat meagre experimental evidence for the quantitative validity of Dirac's equations of the electron applied to atomic phenomena. Thus the predicted polarization of an electron beam on double scattering by heavy nuclei has received no experimental confirmation, and the theory has not provided exact agreement with the observed values of the internal conversion coefficients for γ-rays. On the other hand, the conspicuous success of the theory in its application to the fine structure of atomic spectra, the scattering of hard γ-radiation, and to pair formation in general makes it difficult to believe it can be markedly incorrect.

Moreover, as the Auger Effect is concerned with the interaction of two electrons it can only be dealt with relativistically by an extension of Dirac's theory to two electrons. No exact method of doing this has as yet been discovered, but Møller,[‡] by a correspondence principle method, has obtained a relativistically invariant formula for the probability of transitions involving two electrons—including retardation effects and spin-spin interaction—which may be expected to hold to a first approximation. Comparison of observed Auger coefficients with those calculated using Møller's formula thus provide a test, not only of Dirac's one-electron theory, but also of its extension in the first approximation to two electrons.

[†] Burhop, 'Proc. Roy. Soc.,' A, vol. 148, p. 272 (1935), referred to as Paper I; also Robinson, 'Nature,' vol. 135, p. 826 (1935).

[‡] 'Ann. Physik,' vol. 14, p. 531 (1932).

We have therefore calculated the probability of the internal conversion of the K series radiation for gold arising from the interaction of the $L_I L_I$, $L_I L_{II}$, and $L_I L_{III}$ shells, using Møller's method. Less accurate calculations have also been carried out for silver. In this calculation we have made two approximations which must be remembered in considering agreement with experiment:

The first approximation consists in treating the problem as one involving two electrons only and so neglecting the perturbation of the wave functions of the other atomic electrons by the transitions concerned. Such effects, which may be appreciable in a heavy atom, cannot be estimated with any accuracy until the Hartree self-consistent field method is applied to the determination of the wave functions of electrons in an atom ionized in an inner shell.

The second approximation is that of using screened hydrogen-like wave-functions for the atomic electrons involved in the calculations. This gave satisfactory results for the non-relativistic theory and probably does not lead to marked error in discussing K and L interactions only. However, the relativistic modifications which we derive are sufficiently great to make it unlikely that any inaccuracy due to these approximations would be sufficient to mask the effect.

THEORY

We consider a transition in which an L electron falls to an unoccupied K level and the surplus energy is given to a second L electron, raising it to a state of the continuous spectrum. In Møller's treatment of such a process the transition of an L electron to a K level produces a radiation field—scalar and vector potentials, Φ, $\mathbf{A}$—which acts upon the second electron and ejects it by a photo-electric effect. The detailed theory of the Auger Effect is given in Mott and Massey, "Theory of Atomic Collisions,"† and we shall merely outline the method here.

If ψ_i, ψ_f are the four-component Dirac wave functions for the initial and final states of the ejected electron, the number of transitions per unit time is given by

$$\left|\frac{2\pi}{h}\int \psi_f^*\{-e\phi - e\rho_1 \mathbf{a} \,.\, \hat{\sigma}\}\, \psi_i \, d\tau\right|^2, \tag{1}$$

ψ_f being normalized to represent one emitted electron per unit time. ρ_1,

---

† P. 264 (1933) (Oxford Univ. Press).

$\hat{\sigma}$ are the usual matrix operators of Dirac's theory of the electron which operate on the suffixes distinguishing the components of ψ_i. The functions ϕ, $\mathbf{a}$ are connected with Φ, $\mathbf{A}$ by the relations

$$\left.\begin{aligned}\Phi &= e^{-2\pi i\nu_{fi}t}\,\phi\,(x\,y\,z) + \text{complex conjugate}\\ \mathbf{A} &= e^{-2\pi i\nu_{fi}t}\,\mathbf{a}\,(x\,y\,z) + \text{complex conjugate}\end{aligned}\right\} \qquad (2)$$

where $h\nu_{fi}$ is the change in energy of the electron in falling from the L to K shell.† In terms of the initial and final wave functions, χ_i, χ_f of this electron, ϕ, $\mathbf{a}$ are now given by the formulae

$$\left.\begin{aligned}\phi &= -\int \frac{e}{|\mathbf{r}-\mathbf{r}'|}\exp\left(\frac{2\pi i\nu_{fi}\,|\mathbf{r}-\mathbf{r}'|}{c}\right)\chi_f^*\chi_i\,d\tau'\\ \mathbf{a} &= \int \frac{e}{|\mathbf{r}-\mathbf{r}'|}\exp\left(\frac{2\pi i\nu_{fi}\,|\mathbf{r}-\mathbf{r}'|}{c}\right)\chi_f^*\rho_1\hat{\sigma}\chi_i\,d\tau'\end{aligned}\right\}. \qquad (3)$$

If we denote by ρ, $\mathbf{j}$ the time-independent part of the charge density and current vector corresponding to the L → K transition, and by ρ', $\mathbf{j}'$ the same quantities corresponding to the L → ∞ ‡ transition

$$\begin{aligned}(\textit{i.e.,}\qquad \rho &= -e\,\chi_f^*\chi_i; & \mathbf{j} &= e\,\chi_f^*\,\rho_1\hat{\sigma}\chi_i;\\ \rho' &= -e\,\psi_f^*\psi_i; & \mathbf{j}' &= e\,\psi_f^*\,\rho_1\hat{\sigma}\psi_i),\end{aligned}$$

then expression (1) may be written

$$\left|\frac{2\pi}{h}\int \frac{e}{|\mathbf{r}-\mathbf{r}'|}\exp\left(\frac{2\pi i\nu_{fi}\,|\mathbf{r}-\mathbf{r}'|}{c}\right)\{\rho\rho' - \mathbf{j}\,.\,\mathbf{j}'\}\,d\tau\,d\tau'\right|^2 \qquad (4)$$

$$= |\,A\,|^2, \text{ say.}$$

This formula takes no account of the possibilities of electron exchange. To include this we introduce the expression $|\,B\,|^2$ analogous to (4) but with the final states of the electrons interchanged. Then the application of the Pauli principle shows that the total probability of occurrence per unit time of the double transition considered is $|\,A - B\,|^2$.

DETAILS OF THE CALCULATION

We now apply the formula (4) to the Auger transitions L_I, $L_I \to K$, ∞ ; L_I, $L_{II} \to K$, ∞ ; L_I, $L_{III} \to K$, ∞ .

---

† $h\nu_{fi}$ is the energy difference of the initial and final states of a single electron. ν_{fi} is therefore not the X-radiation frequency associated with the transition, as this involves energy changes arising from perturbation of the other atomic electrons. In the actual calculation this distinction is not important as the retardation effects are very small.

‡ The symbol ∞ is used to denote a state of the continuous spectrum.

The relativistic wave functions required for these transitions are given below.

K:—Here we have two wave functions corresponding to states of opposite spin and only one of these need be considered, from symmetry. The state we take is represented by the function†

$$\left.\begin{aligned} (\psi_i)_1 &= -iN_K f \cos\theta \\ (\psi_i)_2 &= -iN_K f \sin\theta\, e^{i\phi} \\ (\psi_i)_3 &= N_K g \\ (\psi_i)_4 &= 0 \end{aligned}\right\} \quad (5)$$

where

$$\left.\begin{aligned} f &= \frac{\gamma}{1+\sqrt{1-\gamma^2}}\, e^{-\frac{Zr}{a_0}}\, r^{\sqrt{1-\gamma^2}-1} \\ g &= e^{-\frac{Zr}{a_0}}\, r^{\sqrt{1-\gamma^2}-1} \\ N_K &= \frac{1}{\sqrt{4\pi}}\left[\left(\frac{2Z}{a_0}\right)^{1+2\sqrt{1-\gamma^2}} \cdot \frac{(1+\sqrt{1-\gamma^2})}{2\Gamma(1+2\sqrt{1-\gamma^2})}\right]^{\frac{1}{2}} \end{aligned}\right\}. \quad (6)$$

L_I:—The two L_I wave functions are

(i) L_I^0:

$$\begin{aligned} (\psi_i)_1 &= -iN_{L_I} F_0 \cos\theta \\ (\psi_i)_2 &= -iN_{L_I} F_0 \sin\theta\, e^{i\phi} \\ (\psi_i)_3 &= N_{L_I} G_0 \\ (\psi_i)_4 &= 0 \end{aligned}$$

and

(ii) L_I^{-1}:

$$\begin{aligned} (\psi_i)_1 &= iN_{L_I} F_0 \sin\theta\, e^{-i\phi} \\ (\psi_i)_2 &= -iN_{L_I} F_0 \cos\theta \\ (\psi_i)_3 &= 0 \\ (\psi_i)_4 &= -N_{L_I} G_0 \end{aligned} \quad (7)$$

in which

$$\left.\begin{aligned} F_0 &= \frac{\gamma'}{\sqrt{1-\gamma'^2}+N+1}\, e^{-\frac{Z'r}{a_0 N}} \Big\{ r^{\sqrt{1-\gamma'^2}}(N+1) \\ &\qquad - r^{\sqrt{1-\gamma'^2}-1}\, \frac{a_0}{Z'}\, \frac{N(N+2)(1+2\sqrt{1-\gamma'^2})}{2} \Big\}, \\ G_0 &= e^{-\frac{Z'r}{a_0 N}} \Big\{ r^{\sqrt{1-\gamma'^2}}(N+1) - r^{\sqrt{1-\gamma'^2}-1}\, \frac{a_0}{Z'}\, \frac{N^2(1+2\sqrt{1-\gamma'^2})}{2} \Big\} \end{aligned}\right\} \quad (8)$$

---

† The symbols are defined below.

where

$$\mathrm{N} = \sqrt{2 + 2\sqrt{1 - \gamma'^2}},$$

and

$$\mathrm{N}_{\mathrm{L_I}} = \frac{1}{\sqrt{4\pi}}\left(\frac{2\mathrm{Z}'}{a_0\mathrm{N}}\right)^{\frac{3+2\sqrt{1-\gamma'^2}}{2}}\left[\Gamma(2 + 2\sqrt{1 - \gamma'^2})\{\mathrm{N}(\mathrm{N}+2)\right.$$
$$\left. + 2(1 + \sqrt{1 - \gamma'^2})\}\left\{1 + \frac{\gamma'^2}{1 + \mathrm{N} + \sqrt{1 - \gamma'^2}}\right\}\right]^{\frac{1}{2}}. \quad (9)$$

$\mathrm{L_{II}}$:—The two $\mathrm{L_{II}}$ wave functions are:

$$\left.\begin{array}{lcl}
\text{(i) } \mathrm{L_{II}}^0: & & \text{(ii) } \mathrm{L_{II}}^{-1}: \\
(\psi_i)_1 = -i\mathrm{F}_{-2}\mathrm{N}_{\mathrm{L_{II}}} & & (\psi_i)_1 = 0 \\
(\psi_i)_2 = 0 & \text{and} & (\psi_i)_2 = i\mathrm{F}_{-2}\mathrm{N}_{\mathrm{L_{II}}} \\
(\psi_i)_3 = \mathrm{N}_{\mathrm{L_{II}}}\mathrm{G}_{-2}\cos\theta & & (\psi_i)_3 = -\mathrm{N}_{\mathrm{L_{II}}}\mathrm{G}_{-2}\sin\theta e^{-i\phi} \\
(\psi_i)_4 = \mathrm{N}_{\mathrm{L_{II}}}\mathrm{G}_{-2}\sin\theta e^{i\phi} & & (\psi_i)_4 = \mathrm{N}_{\mathrm{L_{II}}}\mathrm{G}_{-2}\cos\theta
\end{array}\right\}, \quad (10)$$

in which

$$\left.\begin{array}{l}
\mathrm{F}_{-2} = \dfrac{\gamma'}{\sqrt{1 - \gamma'^2} + \mathrm{N} + 1}\, e^{\frac{\mathrm{Z}'r}{a_0\mathrm{N}}}\left\{r^{\sqrt{1-\gamma'^2}}(\mathrm{N} - 1)\right. \\
\qquad\qquad \left. - r^{\sqrt{1-\gamma'^2}-1}\dfrac{a_0\mathrm{N}^2}{\mathrm{Z}'}\dfrac{(1 + 2\sqrt{1 - \gamma'^2})}{2}\right\} \\
\mathrm{G}_{-2} = e^{\frac{\mathrm{Z}'r}{a_0\mathrm{N}}}\left\{r^{\sqrt{1-\gamma'^2}}(\mathrm{N} - 1)\right. \\
\qquad\qquad \left. - r^{\sqrt{1-\gamma'^2}-1}\dfrac{a_0}{\mathrm{Z}}\mathrm{N}(\mathrm{N} - 2)\dfrac{(1 + 2\sqrt{1 - \gamma'^2})}{2}\right\} \\
\text{and} \\
\mathrm{N}_{\mathrm{L_{II}}} = \dfrac{1}{\sqrt{4\pi}}\left(\dfrac{2\mathrm{Z}'}{a_0\mathrm{N}}\right)^{\frac{3+2\sqrt{1-\gamma'^2}}{2}}\left[\Gamma(2 + 2\sqrt{1 - \gamma'^2})\{\mathrm{N}(\mathrm{N} - 2)\right. \\
\qquad\qquad \left. + 2(1 + \sqrt{1 - \gamma'^2})\}\left\{1 + \dfrac{\gamma'^2}{1 + \mathrm{N} + \sqrt{1 - \gamma'^2}}\right\}\right]^{\frac{1}{2}}
\end{array}\right\}. \quad (11)$$

$\mathrm{L_{III}}$:—

$$\left.\begin{array}{l}
(\psi_i)_1 = -i\mathrm{N}_{\mathrm{L_{III}}}\mathrm{F}_1\mathrm{P}_2{}^u(\theta, \phi) \\
(\psi_i)_2 = -i\mathrm{N}_{\mathrm{L_{III}}}\mathrm{F}_1\mathrm{P}_2{}^{u+1}(\theta, \phi) \\
(\psi_i)_3 = \mathrm{N}_{\mathrm{L_{III}}}(u + 2)\mathrm{G}_1\mathrm{P}_1{}^u(\theta, \phi) \\
(\psi_i)_4 = \mathrm{N}_{\mathrm{L_{III}}}(u - 1)\mathrm{G}_1\mathrm{P}_1{}^{u+1}(\theta, \phi)
\end{array}\right\}, \quad (12)$$

with

$$\left.\begin{aligned}
\mathrm{F}_1 &= \frac{\gamma'}{2+\sqrt{4-\gamma'^2}}\, e^{-\frac{Z'r}{2a_0}}\, r^{\sqrt{4-\gamma'^2}-1} \\
\mathrm{G}_1 &= e^{-\frac{Z'r}{2a_0}}\, r^{\sqrt{4-\gamma'^2}-1} \\
\mathrm{N}_{\mathrm{L}_{\mathrm{III}}} &= \frac{1}{\sqrt{4\pi\,(u+2)!\,(1-u)!}}\left(\frac{Z'}{a_0}\right)^{\sqrt{4-\gamma'^2}+\frac{1}{2}} \\
&\qquad \times \left[\Gamma\left(2\sqrt{4-\gamma'^2}+1\right)\left\{1+\frac{\gamma'^2}{(2+\sqrt{4-\gamma'^2})^2}\right\}\right]^{-\frac{1}{2}}
\end{aligned}\right\}. \qquad (13)$$

The $\mathrm{P}_k^u(\theta, \phi)$ are here the Legendre polynomials as defined by Darwin,† and the four $\mathrm{L}_{\mathrm{III}}$ wave functions are represented by putting $u = 1$, 0, -1, -2, in the above equations.

∞ :—We have two types of continuous state.

Type A :—

$$\left.\begin{aligned}
(\psi_f)_1 &= -i\mathrm{N}_{\infty\mathrm{A}}\cdot\mathcal{F}_k\mathrm{P}_{k+1}^{u}(\theta, \phi) \\
(\psi_f)_2 &= -i\mathrm{N}_{\infty\mathrm{A}}\cdot\mathcal{F}_k\mathrm{P}_{k+1}^{u+1}(\theta, \phi) \\
(\psi_f)_3 &= \mathrm{N}_{\infty\mathrm{A}}\,(k+u+1)\,\mathcal{G}_k\mathrm{P}_k^{u}(\theta, \phi) \\
(\psi_f)_4 &= \mathrm{N}_{\infty\mathrm{A}}\,(-k+u)\,\mathcal{G}_k\mathrm{P}_k^{u+1}(\theta, \phi)
\end{aligned}\right\}, \qquad (14)$$

and Type B :—

$$\left.\begin{aligned}
(\psi_f)_1 &= -i\mathrm{N}_{\infty\mathrm{B}}\,(k+u)\cdot\mathcal{F}_{-k-1}\mathrm{P}_{k-1}^{u}(\theta, \phi) \\
(\psi_f)_2 &= -i\mathrm{N}_{\infty\mathrm{B}}\,(-k+u+1)\cdot\mathcal{F}_{-k-1}\mathrm{P}_{k-1}^{u+1}(\theta, \phi) \\
(\psi_f)_3 &= \mathrm{N}_{\infty\mathrm{B}}\cdot\mathcal{G}_{-k-1}\mathrm{P}_k^{u}(\theta, \phi) \\
(\psi_f)_4 &= \mathrm{N}_{\infty\mathrm{B}}\cdot\mathcal{G}_{-k-1}\mathrm{P}_k^{u+1}(\theta, \phi)
\end{aligned}\right\}. \qquad (15)$$

We have

$$\begin{aligned}
\mathcal{F}_k(r) &= \frac{r^s e^{iar}\,(2a)^{2s+2}\,e^{-\pi b}}{2\mathrm{A}\Gamma(2s+3)} \\
&\times \left[\begin{aligned}
&\{(k-s)-i(b+d)\}\,\Gamma(s+2-ib)\,\Gamma(s+1+ib) \\
&\qquad\qquad \times {}_1\mathrm{F}_1(s+1+ib;\ 2s+3;\ 2iar) \\
&+\{(k-s)+i(b+d)\}\,\Gamma(s+1-ib)\,\Gamma(s+2+ib) \\
&\qquad\qquad \times {}_1\mathrm{F}_1(s+2+ib;\ 2s+3;\ 2iar)
\end{aligned}\right] \qquad (16)
\end{aligned}$$

---

† 'Proc. Roy. Soc.,' A., vol. 118, p. 654 (1928).

$$\mathcal{G}_k(r) = -\frac{ir^s e^{-iar}(2a)^{2s+2}e^{-\pi b}}{2\mathrm{B}\Gamma(2s+3)}$$

$$\times\left[\begin{array}{r}\{(k-s)-i(b+d)\}\,\Gamma(s+2-ib)\,\Gamma(s+1+ib)\\ \times\,{}_1\mathrm{F}_1(s+1+ib;\ 2s+3;\ 2iar)\\ -\{(k-s)+i(b+d)\}\,\Gamma(s+2+ib)\,\Gamma(s+1-ib)\\ \times\,{}_1\mathrm{F}_1(s+2+ib;\ 2s+3;\ 2iar)\end{array}\right]. \quad (17)$$

In this calculation the allowed final states were obtained by putting $k = 0$ or 1 in the above.

$$\mathcal{F}_{-k-1}(r) = \frac{r^{s'} e^{-iar}(2a)^{2s'+2}e^{-\pi b}}{2\mathrm{A}\Gamma(2s'+3)}$$

$$\times\left[\begin{array}{l}\{(b-d)-i(k-1-s')\}\\ \qquad\times\,\Gamma(s'+2-ib)\,\Gamma(s'+1+ib)\\ \qquad\quad\times\,{}_1\mathrm{F}_1(s'+1+ib;\ 2s'+3;\ 2iar)\\ +\{(b-d)+i(k-1-s')\}\\ \qquad\times\,\Gamma(s'+1-ib)\,\Gamma(s'+2+ib)\\ \qquad\quad\times\,{}_1\mathrm{F}_1(s'+2+ib;\ 2s'+3;\ 2iar)\end{array}\right] \quad (18)$$

$$\mathcal{G}_{-k-1}(r) = -\frac{ir^{s'} e^{-iar}(2a)^{2s'+2}e^{-\pi b}}{2\mathrm{B}\Gamma(2s'+3)}$$

$$\times\left[\begin{array}{l}\{(b-d)-i(k-1-s')\}\\ \qquad\times\,\Gamma(s'+2-ib)\,\Gamma(s'+1+ib)\\ \qquad\quad\times\,{}_1\mathrm{F}_1(s'+1+ib;\ 2s'+3;\ 2iar)\\ +\{(b-d)+i(k-1-s')\}\\ \qquad\times\,\Gamma(s'+1-ib)\,\Gamma(s'+2+ib)\\ \qquad\quad\times\,{}_1\mathrm{F}_1(s'+2+ib;\ 2s'+3;\ 2iar)\end{array}\right]. \quad (19)$$

The allowed final B states all had $k = 1$.

The above functions have the following asymptotic forms:—

$$\left.\begin{array}{l}\mathcal{F}_k(r) \sim \dfrac{(2a)^{s+1}e^{-\frac{3\pi b}{2}}}{\mathrm{A}r}\sqrt{(k-s)^2+(b+d)^2}\,|\Gamma(s+1+ib)|\\ \qquad\qquad\times\cos\left(ar+b\log 2ar-\dfrac{(s+1)\pi}{2}+\delta+\delta'\right)\\ \mathcal{G}_k(r) \sim -\dfrac{(2a)^{s+1}e^{-\frac{3\pi b}{2}}}{\mathrm{B}r}\sqrt{(k-s)^2+(b+d)^2}\,|\Gamma(s+1+ib)|\\ \qquad\qquad\times\sin\left(ar+b\log 2ar-\dfrac{(s+1)\pi}{2}+\delta+\delta'\right)\end{array}\right\}. \quad (20)$$

where

$$\delta = \arg \Gamma (s + 1 - ib); \quad \delta' = \arg ((k - s) + i (b + d))$$

$$\left.\begin{aligned} \mathcal{F}_{k-1}(r) &\sim \frac{(2a)^{s'+1} e^{-\frac{3\pi b}{2}}}{r\mathrm{A}} \sqrt{(k - 1 - s')^2 + (b - d)^2} \\ &\quad \times |\Gamma (s' + 1 + ib)| \cos \left(ar + b \log 2ar - \frac{(s' + 1)\pi}{2} + \delta_1 + \delta'_1\right) \\ \mathcal{G}_{-k-1}(r) &\sim - \frac{(2a)^{s'+1} e^{-\frac{3\pi b}{2}}}{r\mathrm{B}} \sqrt{(k - 1 - s')^2 + (b - d)^2} \\ &\quad \times |\Gamma (s' + 1 + ib)| \sin \left(ar + b \log 2ar - \frac{(s' + 1)\pi}{2} + \delta_1 + \delta'_1\right) \end{aligned}\right\}, \quad (21)$$

in which

$$\delta_1 = \arg \Gamma (s' + 1 - ib); \quad \delta'_1 = \arg (b - d + i (k - 1 - s')).$$

Further,

$$\mathrm{N}_{\kappa\mathrm{A}}\dagger = \frac{1}{\sqrt{4\pi (k + u + 1)!\,(k - u)!}} \left(\frac{2\pi \mathrm{E}}{hc^2a}\right)^{\frac{1}{2}} \frac{\mathrm{A}\,|\mathrm{B}|}{\{\mathrm{A}^2 + |\mathrm{B}|^2\}^{\frac{1}{2}}} \mathrm{K}^{-1}$$

where

$$\mathrm{K} = \tfrac{1}{2} \sqrt{(k - s)^2 + (b + d)^2}\, |\Gamma (s + ib + 1)|\, e^{-\frac{3\pi b}{2}} (2a)^{s+1} \quad . \quad (22)$$

$\mathrm{N}_{\kappa\mathrm{B}}$ is obtained from $\mathrm{N}_{\kappa\mathrm{A}}$ by replacing s by s', k by $k - 1$, and d by $- d$.

In the above, E = proper energy of the ejected electron,

$$\mathrm{A}^2 = \frac{2\pi}{h}\left(mc + \frac{\mathrm{E}}{c}\right); \quad \mathrm{B}^2 = \frac{2\pi}{h}\left(mc - \frac{\mathrm{E}}{c}\right);$$

$$\gamma = \frac{2\pi e^2 \mathrm{Z}}{ch} \simeq \frac{\mathrm{Z}}{137},$$

$$\gamma' = \frac{2\pi e^2 \mathrm{Z}'}{ch},$$

---

† It is not obvious that this is the correct normalizing factor to take (that for a function representing motion in a Coulomb field of charge Ze) because of phase changes in the wave function which arise from the departure of the effective nuclear charge from the value Z, at nuclear distances greater than the radius of the L-shell. The validity of this normalization has been established by Bethe (Unpublished, *see*, however, Soden, ' Ann. Physik,' vol. 19, p. 409 (1934)) using Jeffreys's method of approximation. An alternative justification will be published shortly in ' Proc. Camb. Phil. Soc.'

Z, Z′ being the effective nuclear charges† for the L and K electrons respectively.

$$s = \sqrt{(k+1)^2 - \gamma'^2} - 1$$

$$s' = \sqrt{k^2 - \gamma'^2} - 1$$

$$a = \frac{2\pi m v}{h\sqrt{1-\beta^2}} \qquad (v = \text{velocity of ejected electron})$$

$$b = \frac{\gamma'}{\beta}; \qquad d = \frac{\gamma'\sqrt{1-\beta^2}}{\beta}; \qquad \beta = \frac{v}{c}.$$

The charge density ρ, ρ' and current density components (j_x j_y j_z, j'_x j'_y j'_z) can now be formed for each particular transition from the relations

$$\left.\begin{aligned} \rho &= (\chi_i)_1 (\chi_f)_1^* + (\chi_i)_2 (\chi_f)_2^* + (\chi_i)_3 (\chi_f)_3^* + (\chi_i)_4 (\chi_f)_4^* \\ j_x &= (\chi_i)_1 (\chi_f)_4^* + (\chi_i)_2 (\chi_f)_3^* + (\chi_i)_3 (\chi_f)_2^* + (\chi_i)_4 (\chi_f)_1^* \\ j_y &= i\,(\chi_i)_1 (\chi_f)_4^* - i\,(\chi_i)_2 (\chi_f)_3^* + i\,(\chi_i)_3 (\chi_f)_2^* - i\,(\chi_i)_4 (\chi_f)_1^* \\ j_z &= (\chi_i)_1 (\chi_f)_3^* - (\chi_i)_2 (\chi_f)_4^* + (\chi_i)_3 (\chi_f)_1^* - (\chi_i)_4 (\chi_f)_2^* \end{aligned}\right\} \quad (23)$$

with similar relations for ρ', j'_x, . ., etc., in terms of the ψ's.

As the complete algebra of the calculation is too long and involved for inclusion in this paper we shall illustrate the methods employed by considering only one typical transition here. The authors would be pleased to supply the algebra for the other transitions to workers in this field to whom it might be useful.

Let us then consider the transition $\mathrm{L_I}\ (u = 0)\ \mathrm{L_{III}}\ (u = 1) \rightarrow \mathrm{K}\ (u = 0)\ \infty_{\mathrm{A}}\ (u = 1)$.

For the direct transition we have

(i) $\mathrm{L_{III}}\ (u = 1) \rightarrow \mathrm{K}\ (u = 0)$

$$\left.\begin{aligned} \rho &= \frac{1}{4\pi}\sqrt{\tfrac{3}{2}}\, e^{i\phi} \sin\theta\, (f^*\mathrm{F}_1 + g^*\mathrm{G}_1)\, \mathrm{N_{L_{III}}N_K} \\ j_x &= \frac{1}{4\pi}\sqrt{\tfrac{3}{2}}\, i \sin^2\theta\, (f^*\mathrm{G}_1 - g^*\mathrm{F}_1 e^{2i\phi})\, \mathrm{N_{L_{III}}N_K} \\ j_y &= \frac{1}{4\pi}\sqrt{\tfrac{3}{2}}\, \sin^2\theta\, (f^*\mathrm{G}_1 + g^*\mathrm{F}_1 e^{2i\phi})\, \mathrm{N_{L_{III}}N_K} \\ j_z &= \frac{1}{4\pi}\sqrt{\tfrac{3}{2}}\, i \sin\theta\cos\theta\, e^{i\phi}\, (f^*\mathrm{G}_1 - g^*\mathrm{F}_1)\, \mathrm{N_{L_{III}}N_K} \end{aligned}\right\} \quad (24)$$

---

† Following Slater's rules the values Z = 78·7, Z′ = 74·7 were taken for gold.

(ii) $\mathrm{L_I}\,(u = 0) \rightarrow \infty_{\mathrm{A}}\,(u = 1)$

$$\left.\begin{aligned}
\rho' &= \frac{1}{4\pi}\sqrt{\tfrac{3}{2}}\,e^{-i\phi'}\sin\theta'\,(\mathrm{G}_0\mathcal{G}_1{}^* + \mathrm{F}_0\mathcal{F}_1{}^*)\,\mathrm{N_{L_I}N_{\infty A}} \\
j'_x &= -\frac{i}{4\pi}\sqrt{\tfrac{3}{2}}\sin^2\theta'\,(\mathrm{F}_0\mathcal{G}_1{}^* - \mathrm{G}_0\mathcal{F}_1{}^*\,e^{-2i\phi'})\,\mathrm{N_{L_I}N_{\infty A}} \\
j'_y &= \frac{1}{4\pi}\sqrt{\tfrac{3}{2}}\sin^2\theta'\,(\mathrm{F}_0\mathcal{G}_1{}^* + \mathrm{G}_0\mathcal{F}_1{}^*\,e^{-2i\phi'})\,\mathrm{N_{L_I}N_{\infty A}} \\
j'_z &= -\frac{i}{4\pi}\sqrt{\tfrac{3}{2}}\,e^{-i\phi'}\sin\theta'\cos\theta'\,(\mathrm{F}_0\mathcal{G}_1{}^* - \mathrm{G}_0\mathcal{F}_1{}^*)\,\mathrm{N_{L_I}N_{\infty A}}
\end{aligned}\right\}\qquad(25)$$

Substituting these expressions in equation (4) and expanding the retarded potential in the form

$$\frac{e^{ik\,|\mathbf{r}-\mathbf{r}'|}}{|\mathbf{r}-\mathbf{r}'|} = \sum_{n=0}^{\infty}(2n+1)\,\frac{\zeta_n(kr')}{r'}\,\frac{\eta_n(kr)}{kr}\,\mathrm{P}_n\,(\cos\widehat{\mathbf{rr}'})\quad(r < r'),\qquad(26)$$

where

$$\left.\begin{aligned}
k &= \frac{2\pi\nu_{fi}}{c} \\
\eta_n\,(kr) &= \sqrt{\tfrac{1}{2}\pi kr}\,\mathrm{J}_{n+\frac{1}{2}}\,(kr) \\
\zeta_n\,(kr') &= \sqrt{\tfrac{1}{2}\pi kr'}\,\{i\,\mathrm{J}_{n+\frac{1}{2}}\,(kr') + (-1)^n\,\mathrm{J}_{-n-\frac{1}{2}}\,(kr')\}
\end{aligned}\right\}\qquad(27)$$

it is seen that it is necessary to evaluate the following integrals over the angles:—

$$\left.\begin{aligned}
&\iiiint\frac{e^{ik\,|\mathbf{r}-\mathbf{r}'|}}{|\mathbf{r}-\mathbf{r}'|}\sin\theta\,e^{-i\phi}\sin\theta'\,e^{i\phi'}\,d\Omega\,d\Omega' = \frac{32\pi^2}{9}\,\gamma_1\,(r, r') \\
&\iiiint\frac{e^{ik\,|\mathbf{r}-\mathbf{r}'|}}{|\mathbf{r}-\mathbf{r}'|}\sin^2\theta\sin^2\theta'\,d\Omega\,d\Omega' = \frac{64\pi^2}{9}\gamma_0\,(r, r') + \frac{64\pi^2}{225}\,\gamma_2\,(r, r') \\
&\iiiint\frac{e^{ik\,|\mathbf{r}-\mathbf{r}'|}}{|\mathbf{r}-\mathbf{r}'|}\sin^2\theta\,e^{2i\phi}\sin^2\theta'\,e^{-2i\phi'}\,d\Omega\,d\Omega' = \frac{128\pi^2}{75}\,\gamma_2\,(r, r') \\
&\iiiint\frac{e^{ik\,|\mathbf{r}-\mathbf{r}'|}}{|\mathbf{r}-\mathbf{r}'|}\sin\theta\cos\theta\,e^{-i\phi}\sin\theta'\cos 0'\,e^{i\phi'}\,d\Omega\,d\Omega' \\
&\qquad\qquad = \frac{32\pi^2}{75}\,\gamma_2\,(r, r')
\end{aligned}\right\}\qquad(28)$$

where

$$\gamma_n\,(r, r') = \frac{(2n+1)\,\zeta_n\,(kr')}{r'}\cdot\frac{\eta_n\,(kr)}{kr}\quad(r < r').\qquad(29)$$

The necessary radial integrals over r, r' are

$$\left.\begin{aligned}
\mathrm{I}_0{}^{\mathrm{A}} &= \mathrm{N}_{\mathrm{K}}\mathrm{N}_{\mathrm{L_I}}\mathrm{N}_{\mathrm{L_{III}}}\mathrm{N}_{\infty\mathrm{A}} \iint \gamma_1 (f^*\mathrm{F}_1 + g^*\mathrm{G}_1)(\mathrm{G}_0\mathscr{G}_1{}^* + \mathrm{F}_0\mathscr{F}_1{}^*) \\
&\qquad\qquad\qquad\qquad\qquad\qquad \times r^2 r'^2\, dr\, dr' \\
\mathrm{I}_1{}^{\mathrm{A}} &= \mathrm{N}_{\mathrm{K}}\mathrm{N}_{\mathrm{L_I}}\mathrm{N}_{\mathrm{L_{III}}}\mathrm{N}_{\infty\mathrm{A}} \iint \gamma_0 \mathrm{F}_0\mathscr{G}_1{}^* f^*\mathrm{G}_1\, r^2\, r'^2\, dr\, dr' \\
\mathrm{I}_5{}^{\mathrm{A}} &= \mathrm{N}_{\mathrm{K}}\mathrm{N}_{\mathrm{L_I}}\mathrm{N}_{\mathrm{L_{III}}}\mathrm{N}_{\infty\mathrm{A}} \iint \gamma_2 \mathrm{F}_0\mathscr{G}_1{}^* f^*\mathrm{G}_1\, r^2\, r'^2\, dr\, dr' \\
\mathrm{I}_6{}^{\mathrm{A}} &= \mathrm{N}_{\mathrm{K}}\mathrm{N}_{\mathrm{L_I}}\mathrm{N}_{\mathrm{L_{III}}}\mathrm{N}_{\infty\mathrm{A}} \iint \gamma_2 \mathrm{F}_0\mathscr{G}_1{}^* g^*\mathrm{F}_1\, r^2\, r'^2\, dr\, dr' \\
\mathrm{I}_7{}^{\mathrm{A}} &= \mathrm{N}_{\mathrm{K}}\mathrm{N}_{\mathrm{L_I}}\mathrm{N}_{\mathrm{L_{III}}}\mathrm{N}_{\infty} \iint \gamma_2 \mathrm{G}_0\mathscr{F}_1{}^* f^*\mathrm{G}_1\, r^2\, r'^2\, dr\, dr' \\
\mathrm{I}_8{}^{\mathrm{A}} &= \mathrm{N}_{\mathrm{K}}\mathrm{N}_{\mathrm{L_I}}\mathrm{N}_{\mathrm{L_{III}}}\mathrm{N}_{\infty\mathrm{A}} \iint \gamma_2 \mathrm{G}_0\mathscr{F}_1{}^* g^*\mathrm{F}_1\, r^2\, r'^2\, dr\, dr'
\end{aligned}\right\} \qquad (30)$$

These integrals were evaluated by double numerical integration in the following way: The first integration over the discrete wave functions involves integrals of the form

$$\int_0^r r^s\, \mathrm{J}_{n+\frac{1}{2}}(\alpha r)\, e^{-\mu r}\, dr, \qquad (31)$$

where s is not integral and the second involves the continuous wave functions (16–19) for Dirac electrons. These were calculated from the series expansions for values of $r' < 4a_0/\mathrm{Z}'$. For greater values of r' the asymptotic expansions (20), (21) were found to be sufficiently accurate. As these functions have not previously been calculated we illustrate them in fig. 1 for gold, with electrons of energy $k^2h^2/8\pi^2$, where $k = 63{\cdot}0$ atomic units (*i.e.*, 51·7 electron kV).

Comparison is also effected in the figure with the non-relativistic function to which $\mathscr{G}_1$, $\mathscr{G}_2$ tend when $c \to \infty$.

Consider now the exchange transition.

We have

$$\left.\begin{aligned}
&\qquad\qquad \mathrm{L_I}{}^0 \to \mathrm{K}^0\dagger \\
\rho &= \frac{1}{4\pi}(f^*\mathrm{F}_0 + g^*\mathrm{G}_0)\,\mathrm{N}_{\mathrm{L_I}}\mathrm{N}_{\mathrm{K}} \\
j_x &= \frac{i}{4\pi}(-\,\mathrm{F}_0 g^* + \mathrm{G}_0 f^*\, e^{-2i\phi}) \sin\theta\, e^{i\phi}\, \mathrm{N}_{\mathrm{L_I}}\mathrm{N}_{\mathrm{K}} \\
j_y &= -\,\frac{1}{4\pi}(\mathrm{F}_0 g^* + f^*\mathrm{G}_0\, e^{-2i\phi}) \sin\theta\, e^{i\phi}\, \mathrm{N}_{\mathrm{L_I}}\mathrm{N}_{\mathrm{K}} \\
j_z &= -\,\frac{i}{4\pi}(\mathrm{F}_0 g^* - f^*\mathrm{G}_0) \cos\theta\, \mathrm{N}_{\mathrm{L_I}}\mathrm{N}_{\mathrm{K}}
\end{aligned}\right\} \qquad (32)$$

---

† The notation K^0 is an abbreviation for K ($u = 0$), etc.

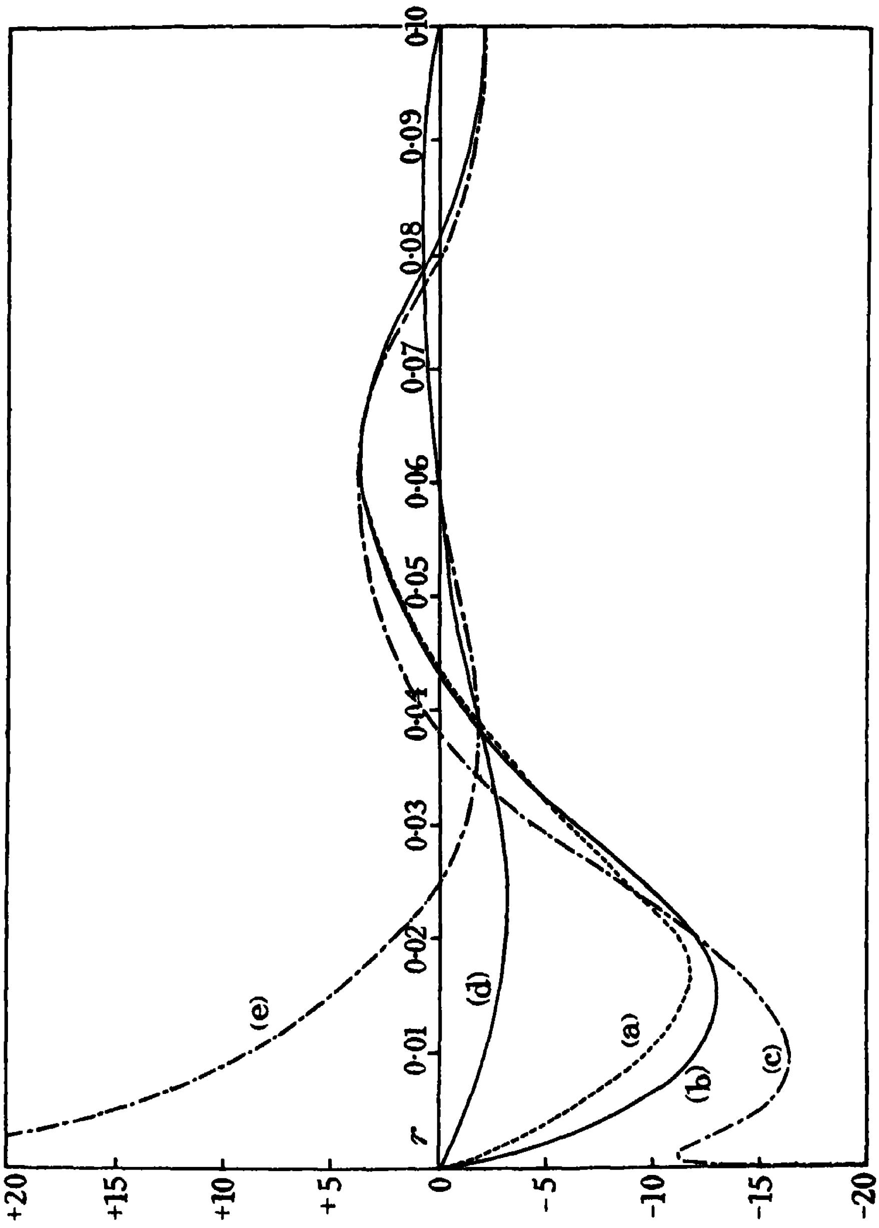

FIG. 1—Radial functions for the continuum for gold (in Hartree units). Energy of ejected electron = 51·7 electron kilovolts. *a*, non-relativistic (normalized) radial function; *b*, relativistic G_1 (normalized) radial function; *c*, relativistic G_{-2} (normalized) radial function; *d*, relativistic F_1 (normalized) radial function; *e* relativistic F_{-2} (normalized) radial function.

and

$$\left.\begin{aligned}
&\qquad\qquad \mathrm{L_{III}}^1 \to \infty_{\mathrm{A}}\,(u=1)\\
\rho' &= \frac{1}{4\pi}\cdot\tfrac{3}{2}\,(\mathcal{X}_1{}^*\mathrm{F}_1+\mathcal{G}_1{}^*\mathrm{G}_1)\sin^2\theta'\,\mathrm{N_{L_{III}}N_{\infty A}}\\
j'_x &= -\frac{i}{4\pi}\cdot\tfrac{3}{2}\,(\mathrm{F}_1\mathcal{G}_1{}^*\,e^{i\phi'}-\mathrm{G}_1\mathcal{X}_1{}^*\,e^{-i\phi'})\sin^3\theta'\,\mathrm{N_{L_{III}}N_{\infty A}}\\
j'_y &= -\frac{1}{4\pi}\cdot\tfrac{3}{2}\,(\mathrm{F}_1\mathcal{G}_1{}^*\,e^{i\phi'}+\mathrm{G}_1\mathcal{X}_1{}^*\,e^{-i\phi'})\sin^3\theta'\,\mathrm{N_{L_{III}}N_{\infty A}}\\
j'_z &= -\frac{i}{4\pi}\cdot\tfrac{3}{2}\sin^2\theta'\cos\theta'\,(\mathrm{F}_1\mathcal{G}_1{}^*-\mathrm{G}_1\mathcal{X}_1{}^*)\,\mathrm{N_{L_{III}}N_{\infty A}}
\end{aligned}\right\}\qquad(33)$$

The angular integrals required are then

$$\left.\begin{aligned}
&\iiiint\frac{e^{ik|\mathbf{r}-\mathbf{r}'|}}{|\mathbf{r}-\mathbf{r}'|}\sin^2\theta'\,d\Omega\,d\Omega'=\frac{32\pi^2}{3}\,\gamma_0(r,r')\\
&\iiiint\frac{e^{ik|\mathbf{r}-\mathbf{r}'|}}{|\mathbf{r}-\mathbf{r}'|}\sin^3\theta'\,e^{i\phi'}\sin\theta\,e^{-i\phi}\,d\Omega\,d\Omega'=\frac{128\pi^2}{45}\,\gamma_1(r,r')\\
&\iiiint\frac{e^{ik|\mathbf{r}-\mathbf{r}'|}}{|\mathbf{r}-\mathbf{r}'|}\sin^2\theta'\cos 0'\cos\theta\,d\Omega\,d\Omega'=\frac{32\pi^2}{45}\,\gamma_1(r,r')
\end{aligned}\right\}\qquad(34)$$

In this case the required radial integrals are

$$\left.\begin{aligned}
\mathcal{J}_0{}^{\mathrm{A}}&=\mathrm{N_{L_I}N_{L_{III}}N_KN_{\infty A}}\iint\gamma_0\,(\mathrm{F}_1\mathcal{X}_1{}^*+\mathrm{G}_1\mathcal{G}_1{}^*)\,(f^*\mathrm{F}_0+g^*\mathrm{G}_0)\\
&\qquad\qquad\qquad\qquad\qquad\qquad r^2r'^2\,dr\,dr'\\
\mathcal{J}_1{}^{\mathrm{A}}&=\mathrm{N_{L_I}N_{L_{III}}N_KN_{\infty A}}\iint\gamma_1\mathrm{F}_0g^*\mathrm{G}_1\mathcal{X}_1{}^*\,r^2\,r'^2\,dr\,dr'\\
\mathcal{J}_2{}^{\mathrm{A}}&=\mathrm{N_{L_I}N_{L_{III}}N_KN_{\infty A}}\iint\gamma_1\mathrm{F}_0g^*\mathrm{F}_1\mathcal{G}_1{}^*\,r^2\,r'^2\,dr\,dr'\\
\mathcal{J}_3{}^{\mathrm{A}}&=\mathrm{N_{L_I}N_{L_{III}}N_KN_{\infty A}}\iint\gamma_1\mathrm{G}_0f^*\mathrm{G}_1\mathcal{X}_1{}^*\,r^2\,r'^2\,dr\,dr'\\
\mathcal{J}_4{}^{\mathrm{A}}&=\mathrm{N_{L_I}N_{L_{III}}N_KN_{\infty A}}\iint\gamma_1\mathrm{G}_0f^*\mathcal{G}_1{}^*\,r^2\,r'^2\,dr\,dr'
\end{aligned}\right\}\qquad(35)$$

Combining the direct and exchange transitions in the manner outlined above to allow for the anti-symmetry property, one finds, for the probability per unit time of this transition, the expression

$$\frac{4\pi^2}{h^2}\left|\begin{aligned}&\tfrac{1}{3}\mathrm{I}_0{}^{\mathrm{A}}-\tfrac{4}{3}\mathrm{I}_1{}^{\mathrm{A}}-\tfrac{7}{75}\mathrm{I}_5{}^{\mathrm{A}}+\tfrac{1}{25}\mathrm{I}_6{}^{\mathrm{A}}+\tfrac{1}{25}\mathrm{I}_7{}^{\mathrm{A}}-\tfrac{9}{25}\mathrm{I}_8{}^{\mathrm{A}}\\ &\quad-\mathcal{J}_0{}^{\mathrm{A}}+\tfrac{3}{5}\mathcal{J}_1{}^{\mathrm{A}}-\tfrac{1}{15}\mathcal{J}_2{}^{\mathrm{A}}-\tfrac{1}{15}\mathcal{J}_3{}^{\mathrm{A}}+\tfrac{3}{5}\mathcal{J}_4{}^{\mathrm{A}}\end{aligned}\right|^2.\qquad(36)$$

For the other allowed transition of the type L_I, $L_{III} \rightarrow K, \infty$, we have $L_{III}{}^1 L_I{}^{-1} \rightarrow K^0 \infty_A \, (u = 0)$:—

$$\frac{4\pi^2}{h^2}\left|\begin{array}{c}\frac{1}{9}I_0{}^A - \frac{4}{9}I_1{}^A + \frac{11}{225}I_5{}^A + \frac{7}{75}I_6{}^A + \frac{7}{75}I_7{}^A - \frac{1}{25}I_8{}^A \\ + \frac{8}{45}(\mathscr{I}_1{}^A + \mathscr{I}_2{}^A + \mathscr{I}_3{}^A + \mathscr{I}_4{}^A)\end{array}\right|^2. \qquad (37)$$

$L_{III}{}^0 L_I{}^0 \rightarrow K^0 \infty_A \, (u = 0)$

$$\frac{4\pi^2}{h^2}\left|\begin{array}{c}\frac{2}{9}I_0{}^A - \frac{4}{9}I_1{}^A - \frac{32}{225}I_5{}^A - \frac{4}{75}I_6{}^A - \frac{4}{75}I_7{}^A - \frac{8}{25}I_8{}^A \\ - \mathscr{I}_0{}^A + \frac{19}{45}\mathscr{I}_1{}^A - \frac{11}{45}\mathscr{I}_2{}^A - \frac{11}{45}\mathscr{I}_3{}^A + \frac{19}{45}\mathscr{I}_4{}^A\end{array}\right|^2. \qquad (38)$$

$L_{III}{}^0 L_I{}^{-1} \rightarrow K^0 \infty_A \, (u = -1)$

$$\frac{4\pi^2}{h^2}\left|\begin{array}{c}\frac{2}{9}I_0{}^A - \frac{8}{9}I_1{}^A + \frac{22}{225}I_5{}^A + \frac{14}{75}I_6{}^A + \frac{14}{75}I_7{}^A - \frac{2}{25}I_8{}^A \\ + \frac{16}{45}(\mathscr{I}_1{}^A + \mathscr{I}_2{}^A + \mathscr{I}_3{}^A + \mathscr{I}_4{}^A)\end{array}\right|^2. \qquad (39)$$

$L_{III}{}^{-1} L_I{}^0 \rightarrow K^0 \infty_A \, (u = -1)$

$$\frac{4\pi^2}{h^2}\left|\begin{array}{c}\frac{1}{9}I_0{}^A - \frac{4}{9}I_1{}^A - \frac{48}{225}I_5{}^A - \frac{11}{75}I_6{}^A - \frac{11}{75}I_7{}^A - \frac{7}{25}I_8{}^A \\ - \mathscr{I}_0{}^A - \frac{11}{45}\mathscr{I}_1{}^A + \frac{19}{45}\mathscr{I}_2{}^A + \frac{19}{45}\mathscr{I}_3{}^A - \frac{11}{45}\mathscr{I}_4{}^A\end{array}\right|^2. \qquad (40)$$

$L_{III}{}^{-1} L_I{}^{-1} \rightarrow K^0 \infty_A \, (u = -2)$

$$\frac{12\pi^2}{h^2}\left|\begin{array}{c}\frac{1}{9}I_0{}^A - \frac{4}{9}I_1{}^A + \frac{11}{225}I_5{}^A + \frac{7}{75}I_6{}^A + \frac{7}{75}I_7{}^A - \frac{1}{25}I_8{}^A \\ + \frac{8}{45}(\mathscr{I}_1{}^A + \mathscr{I}_2{}^A + \mathscr{I}_3{}^A + \mathscr{I}_4{}^A)\end{array}\right|^2. \qquad (41)$$

$L_{III}{}^{-2} L_I{}^0 \rightarrow K^0 \infty_A \, (u = -2)$

$$\frac{4\pi^2}{h^2}\left|\begin{array}{c}- \frac{6}{25}(I_5{}^A + I_6{}^A + I_7{}^A + I_8{}^A) \\ - \mathscr{I}_0{}^A + \frac{1}{15}\mathscr{I}_1{}^A - \frac{3}{5}\mathscr{I}_2{}^A - \frac{3}{5}\mathscr{I}_3{}^A + \frac{1}{15}\mathscr{I}_4{}^A\end{array}\right|^2. \qquad (42)$$

Denoting by $I_0{}^B$, ..., $\mathscr{I}_0{}^B$, ..., etc., the integrals in which $\mathscr{X}_{-2}$, $\mathscr{I}_{-2}$ replace $\mathscr{X}_1$, $\mathscr{I}_1$, we get in the same way the following allowed transitions to continuous B states:—

$L_{III}{}^1 L_I{}^{-1} \rightarrow K^0 \infty_B \, (u = 0)$

$$\frac{6\pi^2}{h^2}\left|\begin{array}{c}- \frac{2}{9}I_0{}^B - \frac{4}{9}I_1{}^B - \frac{4}{3}I_3{}^B + \frac{4}{45}I_5{}^B - \frac{4}{15}I_6{}^B \\ - \frac{2}{9}(\mathscr{I}_1{}^B + \mathscr{I}_2{}^B + \mathscr{I}_3{}^B + \mathscr{I}_4{}^B)\end{array}\right|^2. \qquad (43)$$

$L_{III}{}^0 L_I{}^0 \rightarrow K^0 \infty_B \, (u = 0)$

$$\frac{8\pi^2}{h^2}\left|\begin{array}{c}\frac{1}{9}I_0{}^B + \frac{2}{9}I_1{}^B + \frac{2}{3}I_3{}^B - \frac{2}{45}I_5{}^B + \frac{2}{15}I_6{}^B \\ + \frac{1}{9}(\mathscr{I}_1{}^B + \mathscr{I}_2{}^B + \mathscr{I}_3{}^B + \mathscr{I}_4{}^B)\end{array}\right|^2. \qquad (44)$$

$L_{III}{}^0 L_I{}^{-1} \rightarrow K^0 \infty_B \, (u = -1)$

Same as (44).

$L_{III}^{-1} L_I^0 \rightarrow K \infty_B (u = -1)$

Same as (44).

If now we define $J_0^A \ldots$, $J_0^B \ldots$, $\mathcal{J}_0^A \ldots$, $\mathcal{J}_0^B \ldots$, etc., in a similar way to $I_0^A \ldots$, $I_0^B \ldots$, $\mathcal{I}_0^A \ldots$, $\mathcal{I}_0^B \ldots$, etc., but with F_1, G_1, replaced by F_{-2}, G_{-2}, we get for the possible transitions of the type $L_I L_{II} \rightarrow K, \infty$.

$L_{II}^0 L_I^0 \rightarrow K^0 \infty_A (u = 0)$

$$\frac{8\pi^2}{h^2}\left|\begin{array}{l} \frac{1}{9}J_0^A + \frac{2}{9}J_1^A + \frac{2}{3}J_2^A - \frac{2}{45}J_5^A + \frac{2}{15}J_7^A \\ \quad + \frac{1}{9}(\mathcal{J}_1^A + \mathcal{J}_2^A + \mathcal{J}_3^A + \mathcal{J}_4^A) \end{array}\right|^2. \tag{45}$$

$L_{II}^0 L_I^{-1} \rightarrow K^0 \infty_A (u = -1)$

Same as (45).

$L_{II}^{-1} L_I^0 \rightarrow K^0 \infty_A (u = -1)$

Same as (45).

$L_{II}^{-1} L_I^{-1} \rightarrow K^0 \infty_A (u = -2)$

$$\frac{24\pi^2}{h^2}\left|\begin{array}{l} \frac{1}{9}J_0^A + \frac{2}{9}J_1^A + \frac{2}{3}J_2^A - \frac{2}{45}J_5^A + \frac{2}{15}J_7^A \\ \quad + \frac{1}{9}(\mathcal{J}_1^A + \mathcal{J}_2^A + \mathcal{J}_3^A + \mathcal{J}_4^A) \end{array}\right|^2. \tag{46}$$

$L_{II}^0 L_I^0 \rightarrow K^0 \infty_B (u = 0)$

$$\frac{4\pi^2}{h^2}\left|\begin{array}{l} \frac{1}{9}J_0^B - \frac{1}{9}J_1^B - \frac{1}{3}J_2^B - \frac{1}{3}J_3^B - J_4^B - \frac{8}{45}J_5^B \\ -\mathcal{J}_0^B + \frac{1}{9}\mathcal{J}_1^B - \frac{5}{9}\mathcal{J}_2^B - \frac{5}{9}\mathcal{J}_3^B + \frac{1}{9}\mathcal{J}_4^B \end{array}\right|^2. \tag{47}$$

$L_{II}^0 L_I^{-1} \rightarrow K^0 \infty_B (u = -1)$

$$\frac{4\pi^2}{h^2}\left|\begin{array}{l} \frac{1}{9}J_0^B - \frac{1}{9}J_1^B - \frac{1}{3}J_2^B - \frac{1}{3}J_3^B - J_4^B \\ + \frac{4}{9}(\mathcal{J}_1^B + \mathcal{J}_2^B + \mathcal{J}_3^B + \mathcal{J}_4^B) \end{array}\right|^2. \tag{48}$$

$L_{II}^{-1} L_I^0 \rightarrow K^0 \infty_B (u = -1)$

$$\frac{4\pi^2}{h^2}\left|\begin{array}{l} \frac{2}{9}J_0^B - \frac{2}{9}J_1^B - \frac{2}{3}J_2^B - \frac{2}{3}J_3^B - 2J_4^B - \frac{16}{45}J_5^B \\ - \mathcal{J}_0^B + \frac{5}{9}\mathcal{J}_1^B - \frac{1}{9}\mathcal{J}_2^B - \frac{1}{9}\mathcal{J}_3^B + \frac{5}{9}\mathcal{J}_4^B \end{array}\right|^2. \tag{49}$$

For transitions of the type $L_I L_I \rightarrow K, \infty$, we find only one allowed transition, viz.,

$L_I^0 L_I^{-1} \rightarrow K^0 \infty \quad (k = 0, u = -1)$

$$\frac{4\pi^2}{h^2}\,|K_0^A + \tfrac{1}{3}K_1^A + K_2^A + K_3^A + \tfrac{1}{3}K_4^A|^2. \tag{50}$$

The K's are defined in an analogous way to the $\mathcal{J}$'s with F_1 G_1 replaced by F_0 G_0 and $\mathcal{I}_1$, $\mathcal{G}_1$ replaced by $\mathcal{I}_0$, $\mathcal{G}_0$. Introducing now the integrals $P_{I\,I}$, $P_{I\,II}$, $P_{II\,I}$, $P_{III\,I}$, $P_{I\,III}$ of Paper I, it is not difficult to show that in the non-relativistic limit

$$I_0^A \rightarrow I_0^B \rightarrow 3P_{III\,I}; \qquad J_0^A \rightarrow J_0^B \rightarrow 3P_{II\,I}$$

$$\mathcal{I}_0^A \rightarrow \mathcal{I}_0^B \rightarrow P_{I\,III}; \qquad \mathcal{J}_0^A \rightarrow \mathcal{J}_0^B \rightarrow P_{I\,II},$$

and $K_0^A \rightarrow P_{I\,I}$ whilst all the other integrals occurring in the relativistic theory tend to zero.

Summing all the allowed transitions, in the limit we find for

$$\begin{array}{ll}
L_I\,L_I \rightarrow K, \infty, & |P_{I\,I}|^2 \\
L_I\,L_{II} \rightarrow K, \infty, & |P_{I\,II}|^2 + |P_{II\,I}|^2 + |P_{I\,II} - P_{II\,I}|^2 \\
L_I\,L_{III} \rightarrow K, \infty, & 2|P_{I\,III}|^2 + 2\,|P_{III\,I}|^2 + 2\,|P_{I\,III} - P_{III\,I}|^2,
\end{array}$$

which are the expressions obtained for these transitions in the non-relativistic case.

NUMERICAL RESULTS

Table I gives the values of the various integrals required. In this Table a number of the less important integrals have been calculated neglecting retardation, involving the replacement of the expression (29) for γ_n in (30, 35, etc.), by $r^n\,/r'^{n+1}$ $(r < r')$.

This simplified the numerical work since the first integrals then become incomplete Γ-functions which have been extensively tabulated by Pearson and collaborators. The neglect of retardation was justified since it was found by trial in several cases that its effect on the integrals was negligibly small, as might be anticipated from the relation between the wave-length of the K_α radiation (which has the frequency ν) and the radius of the L shell, from the region inside which the major contribution to the integral arises. Nevertheless, in all the important integrals the retardation term was retained.

In Table I the bracketed values are the non-relativistic limits of the integrals when these differ from zero.

Substitution in (36–50) then gives the probabilities per atomic unit of time for the various transitions shown in Table II.

TABLE I

Integral	Value in Hartree units $\times 10^2$	Integral	Value in Hartree units $\times 10^2$
I_0^A	3·56 (8·32)	J_5^A	0·87
I_1^A	1·81	J_6^A	−0·89
I_5^A	0·75	J_7^A	−0·29
I_6^A	0·31	J_8^A	0·05
I_7^A	−0·26	J_0^B	6·30 (8·32)
I_8^A	−0·12	J_1^B	2·12
I_0^B	6·54 (8·32)	J_2^B	−2·32
I_1^B	1·72	J_3^B	−2·07
I_3^B	1·32	J_4^B	2·28
I_5^B	0·63	J_5^B	0·90
I_6^B	0·27	J_6^B	−1·02
I_7^B	−0·62	J_7^B	−0·73
I_8^B	−0·27	J_8^B	−0·89
$\mathscr{I}_0^A$	4·30 (4·33)	$\mathscr{J}_0^A$	4·18 (4·33)
$\mathscr{I}_1^A$	1·32	$\mathscr{J}_1^A$	0·75
$\mathscr{I}_2^A$	0·42	$\mathscr{J}_2^A$	−0·65
$\mathscr{I}_3^A$	−0·13	$\mathscr{J}_3^A$	−0·07
$\mathscr{I}_4^A$	0·11	$\mathscr{J}_4^A$	−0·31
$\mathscr{I}_0^B$	4·03 (4·33)	$\mathscr{J}_0^B$	6·50 (4·33)
$\mathscr{I}_1^B$	0·08	$\mathscr{J}_1^B$	−0·23
$\mathscr{I}_2^B$	0·41	$\mathscr{J}_2^B$	−0·67
$\mathscr{I}_3^B$	−0·41	$\mathscr{J}_3^B$	−0·61
$\mathscr{I}_4^B$	0·23	$\mathscr{J}_4^B$	−0·41
J_0^A	3·62 (8·32)	K_0^A	−3·46 (−5·04)
J_1^A	2·00	K_1^A	−0·27
J_2^A	−2·21	K_2^A	−0·24
J_3^A	−0·82	K_3^A	−0·04
J_4^A	0·56	K_4^A	−0·97

DISCUSSION

The tabulated results show relativistic effects to be of considerable importance for gold. Many of the charge density integrals (I_0, $\mathscr{I}_0$, J_0, $\mathscr{J}_0$, K_0, etc.) are seen to be greatly altered in value whilst the current density integrals, which vanish in the non-relativistic limit, now have values comparable with the charge integrals. The change in these latter is due to the radial functions $\mathscr{X}_1$, $\mathscr{X}_{-2}$—occurring in the continuous wave functions—which vanish in the non-relativistic case but are as large as the functions $\mathscr{G}_1$, $\mathscr{G}_{-2}$ for small values of r. Most of the apparently peculiar behaviour of the charge integrals (greater than the non-relativistic integrals in some cases, less in others) can be traced to the fact that $\mathscr{F}_1$ and $\mathscr{G}_1$ have the same sign for small values of r whilst $\mathscr{F}_{-2}$ and $\mathscr{G}_{-2}$ have opposite signs.

TABLE II

	Transition type	$\left\{\dfrac{\text{Probability}}{\text{unit time}}\right\} \times 10^9$
	(1) $L_I L_{III} \rightarrow K\infty$	
	$L_{III}^{1} L_I^{0} \rightarrow K^0 \infty_A (u = 1)$	2·20
	$L_{III}^{1} L_I^{-1} \rightarrow K^0 \infty_A (u = 0)$	0·001
	$L_{III}^{0} L_I^{0} \rightarrow K^0 \infty_A (u = 0)$	2·30
	$L_{III}^{0} L_I^{-1} \rightarrow K^0 \infty_A (u = -1)$	0·001
	$L_{III}^{-1} L_I^{0} \rightarrow K^0 \infty_A (u = -1)$	2·53
	$L_{III}^{-1} L_I^{-1} \rightarrow K^0 \infty_A (u = -2)$	0·001
	$L_{III}^{-2} L_I^{0} \rightarrow K^0 \infty_A (u = -2)$	2·07
	$L_{III}^{1} L_I^{-1} \rightarrow K^0 \infty_B (u = 0)$	0·04
	$L_{III}^{0} L_I^{0} \rightarrow K^0 \infty_B (u = 0)$	0·02
	$L_{III}^{0} L_I^{-1} \rightarrow K^0 \infty_B (u = -1)$	0·02
	$L_{III}^{-1} L_I^{0} \rightarrow K^0 \infty_B (u = -1)$	0·02
Total	$L_I L_{III} \rightarrow K\infty$	9·21 (5·77)
	(2) $L_I L_{II} \rightarrow K\infty$	
	$L_{II}^{0} L_I^{0} \rightarrow K^0 \infty_A (u = 0)$	0·10
	$L_{II}^{0} L_I^{-1} \rightarrow K^0 \infty_A (u = -1)$	0·10
	$L_{II}^{-1} L_I^{0} \rightarrow K^0 \infty_A (u = -1)$	0·10
	$L_{II}^{-1} L_I^{-1} \rightarrow K^0 \infty_A (u = -2)$	0·32
	$L_{II}^{0} L_I^{0} \rightarrow K^0 \infty_B (u = 0)$	4·04
	$L_{II}^{0} L_I^{-1} \rightarrow K^0 \infty_B (u = -1)$	0·14
	$L_{II}^{-1} L_I^{0} \rightarrow K^0 \infty_B (u = -1)$	4·73
Total	$L_I L_{II} \rightarrow K\infty$	9·52 (2·88)
	(3) $L_I L_I \rightarrow K_1\infty$	
	$L_I^{0} L_I^{-1} \rightarrow K^0 \infty_A (u = -1)$	1·74
Total	$L_I L_I \rightarrow K\infty$	1·74 (2·54)

We have the following ratios for the relative probability of internal conversion by the interaction of L_I electrons with the L_I, L_{II}, and L_{III} shells.

$$L_I L_I : L_I L_{II} : L_I L_{III} = 1 : 5\cdot5 : 5\cdot3.$$

In the non-relativistic case this was 1 : 1·14 : 2·28. This change of relative transition probability should certainly be capable of experimental test using an arrangement similar to that of Robinson.†

---

† Robinson and Cassie, 'Proc. Roy. Soc.,' A, vol. 113, p. 282 (1926); Robinson and Young, 'Proc. Roy. Soc.,' A, vol. 128, p. 92 (1930).

To obtain the relativistic value of the K series fluorescence yield for gold, it would be necessary to carry out calculations similar to the above for all other possible transitions. The labour involved in such a calculation would, however, be prohibitive. For the transitions we have considered the total relativistic effect is about double the non-relativistic ($20 \cdot 47 \times 10^{-3}$ as compared with $11 \cdot 19 \times 10^{-3}$).

In order to investigate fully the K series fluorescence yield it is also necessary to calculate the optical transition probability for transitions ending on the K shell. The relativistic formula for the probability of emission of dipole radiation has the same form as the non-relativistic expression, viz.,

$$\mathrm{N}_r = \frac{64\pi^4 \nu^3 \, |\mathbf{M}|^2}{3hc^3},\dagger \tag{51}$$

where N_r = number of quanta emitted per unit time, ν the frequency of the emitted radiation, and **M**, the electric moment, is given by the expression

$$e \int \chi^*{}_f \mathbf{r}_i \chi_i \, d\tau. \tag{52}$$

Table III shows the optical transition probability for the various allowed L → K transitions for gold.

Table III

	Transition type	$\left\{\frac{\text{Number of transitions}}{\text{unit of time}}\right\} \times 10^2$
	(1) $\mathrm{L_{III}} \rightarrow \mathrm{K}$	
	$\mathrm{L_{III}}^1 \rightarrow \mathrm{K}^0$	53·0
	$\mathrm{L_{III}}^0 \rightarrow \mathrm{K}^0$	35·4
	$\mathrm{L_{III}}^{-1} \rightarrow \mathrm{K}^0$	17·7
Total	$\mathrm{L_{III}} \rightarrow \mathrm{K}^0$	106·0 (139)
	(2) $\mathrm{L_{II}} \rightarrow \mathrm{K}$	
	$\mathrm{L_{II}}^0 \rightarrow \mathrm{K}^0$	16·5
	$\mathrm{L_{II}}^{-1} \rightarrow \mathrm{K}^0$	33·0
Total	$\mathrm{L_{II}} \rightarrow \mathrm{K}^0$	49·5 (69·4)

The effect of relativity is then to decrease the optical transition probabilities. It is interesting to note that the relativistic effect is nearly twice as great for the $\mathrm{L_{II}} \rightarrow \mathrm{K}$ transition as for the $\mathrm{L_{III}} \rightarrow \mathrm{K}$ transitions. Similar behaviour was found in the Auger transition probabilities. The $\mathrm{L_{II}}$ wave functions are of the B type and it would seem to be a general result that the B type wave functions are much more modified by relativity than are those of the A type. This is illustrated for continuous wave

---

† In Paper I the factor 64 in this formula was wrongly given as 16.

functions, in fig. 1. Thus the type B functions ($\mathscr{F}_{-2}$, $\mathscr{G}_{-2}$) differ more from the non-relativistic functions than do $\mathscr{F}_1$, $\mathscr{G}_1$.

It would appear from the above that the K series internal conversion coefficient (*i.e.*, $1 - \varpi$, where ϖ is the K series fluorescence yield) is about doubled for gold when relativistic effects are considered.

Some calculations of Auger transition probabilities have also been carried out relativistically for silver ($Z = 47$), and the results are shown in Table IV.†

TABLE IV

Transition type	$\left\{\dfrac{\text{Number of transitions}}{\text{unit of time}}\right\} \times 10^3$
$L_{III}{}^1L_I{}^0 \rightarrow K^0\infty_A\ (u = 1)$	0·48
$L_{III}{}^1L_I{}^{-1} \rightarrow K^0\infty_A\ (u = 0)$	0·36
$L_{III}{}^0L_I{}^0 \rightarrow K^0\infty_A\ (u = 0)$	1·08
$L_{III}{}^0L_I{}^{-1} \rightarrow K^0\infty_A\ (u = -1)$	0·48
$L_{III}{}^{-1}L_I{}^0 \rightarrow K^0\infty_A\ (u = -1)$	1·53
$L_{III}{}^{-1}L_I{}^{-1} \rightarrow K^0\infty_A\ (u = -2)$	0·36
$L_{III}{}^{-2}L_I{}^0 \rightarrow K^0\infty_A\ (u = -2)$	1·79

The transitions to the B final state have not been calculated but in analogy with gold, it would be expected that these would be small. The total rate of $L_I\,L_{III} \rightarrow K, \infty$ transitions would thus appear to be about $6 \cdot 5 \times 10^{-3}$ per unit time which has to be compared with the non-relativistic $5 \cdot 77 \times 10^{-3}$.

The values given in Table IV show the same general tendencies as those given in Table II for the corresponding transitions. Relativistic effects are thus of some importance for elements of atomic number as low as 47.

The optical transition probability for silver is the same as the non-relativistic value to within a few per cent. Thus the K series internal conversion coefficient for silver would appear to be increased by about 20% when relativistic effects are taken into account.

COMPARISON WITH EXPERIMENT

Experimental results of the K series internal conversion for elements of high atomic number are practically non-existent. Such experiments would be of great interest since they would throw light on the validity of relativistic quantum theory.

Some measurements of the K series fluorescence yield for elements of medium atomic number have been carried out by Berkey,‡ and these seemed to indicate a decrease of the fluorescence yield with increase of atomic number for elements of atomic number greater than about 45.

---

† The values given in Table IV are probably not so reliable as those of Table II, having been done by an approximate method.

‡ 'Phys. Rev.,' vol. 45, p. 437 (1934); *see also* Stephenson, 'Phys. Rev.,' vol. 46, p. 74 (1934).

Relativistic effects, as calculated here, are seen to be quite incapable of explaining such a phenomenon. No conclusions can be drawn, however, until more experiments in the region of high atomic number are carried out.

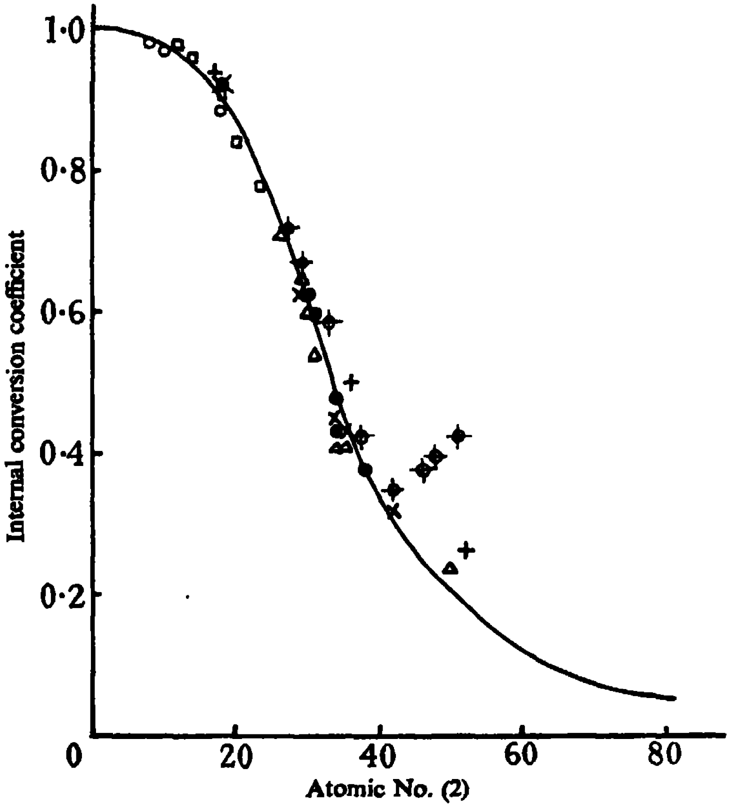

FIG. 2—Comparison of calculated K series internal conversion coefficient with experiment. The full line is the calculated curve. The effect of relativity is to increase the coefficient for gold from 0·03 to 0·06. + Auger, △ Martin, × A. H. Compton, ● Harms, ○ Locher, □ Haas, ⊕ Berkey (Stephenson), ⯐ Martin, Bower, and Laby.

Fig. 2 shows a comparison of the experimental values[†] of the internal conversion coefficient with those to be expected theoretically. To construct this theoretical curve the non-relativistic Auger transition probabilities for the L, L → K, ∞ transitions were obtained from Paper I, and the relative importance of the L, M → K, ∞, L, N → K, ∞, M, M → K, ∞, etc., transitions were obtained from a recent paper by Pincherle.† The values for elements of high atomic number are deduced from the present paper.‡ The agreement between the theoretical curve and the experimental points is very satisfactory.

[†] Auger, 'C.R. Acad. Sci., Paris,' vol. 180, p. 65 (1925); 'J. Phys. Rad.,' vol. 6, p. 205 (1925); 'Ann. Physique,' vol. 6, p. 183 (1926); Martin, 'Proc. Roy. Soc.,' A, vol. 115, p. 420 (1927); Harms, 'Ann. chim. Phys.,' vol. 82, p. 87 (1926); Compton, 'Phil. Mag.,' vol. 8, p. 961 (1929); Haas, 'Ann. Physik,' vol. 16, p. 473 (1933); Locher, 'Phys. Rev.,' vol. 40, p. 484 (1932); Martin, Bower, and Laby, 'Proc. Roy. Soc.,' A, vol. 148, p. 40 (1935).

SUMMARY

The Auger transition probabilities of the type $L_I L_I \rightarrow K, \infty$, $L_I L_{II} \rightarrow K, \infty$, $L_I L_{III} \rightarrow L, \infty$, have been calculated for gold (79), using Dirac wave functions and Møller's method for the relativistic treatment of two-electron problems. The results are compared with those obtained in a non-relativistic calculation. It is found that relativity increases the K series internal conversion coefficient for gold by a factor of two, and gives for the relative importance of the above three transitions the ratio 1 : 5·5 : 5·3 in contrast with the non-relativistic ratio 1 : 1·14 : 2·28.

A few calculations have also been made for silver (47) and it is found that here, too, relativistic effects are appreciable, though much less so than for gold.

The importance of carrying out experiments to test these conclusions, and the light that would thus be thrown on the validity of the Dirac theory of the electron are stressed.

The established features of the Auger Effect are explained quantitatively in a satisfactory way by the wave mechanical theory.

† 'Nuovo Cimento,' vol. 12, p. 81 (1935).

‡ The theoretical curve in fig. 1 of Paper I was incorrect owing to the previously mentioned error in the formula for the optical transition probability. This correction makes the agreement with experiment very much better.

The Absorption Spectrum of Lead Oxide (PbO)

By H. G. HOWELL, B.Sc., Armstrong College, Newcastle-on-Tyne

(*Communicated by W. E. Curtis, F.R.S.—Received September* 10, 1935)

INTRODUCTION

While work on the PbS absorption spectrum was in progress, it was noticed that at the highest temperatures used, 1400° C, a spectrum other than that of PbS was obtained. This was immediately attributed to PbO, formed by the dissociation and subsequent oxidation of PbS, and comparison of the measured wave-lengths with those published by Bloomenthal* confirmed this conclusion. The emission spectrum stretches from 3200 to 6700 A and was first analysed by Mecke,† who recognized three systems which he termed A, B, and C. The spectrum was later remeasured by Bloomenthal,‡ who showed that the existence of the system C was very doubtful as nearly all the bands belonging to it could be fitted into system B. In addition he discovered a rather fragmentary system D in the ultra-violet. It was considered, therefore, that an investigation of the absorption spectrum besides determining the ground state of the molecule might yield additional data with which to test these analyses.

After the present work had been completed, Shawhan and Morgan§ published an account of the absorption spectrum in which they verify Bloomenthal's analysis. They also classify additional bands into two new systems which they designate C and E, the former not to be confused with the original C system of Mecke, which is now included in system B. Using temperatures up to 1200° C, they have extended the spectrum to 3000 A and in the present work higher temperatures than this have been used, the spectrum being extended to yet shorter wave-lengths.

Whilst the analysis proposed here confirms that of Shawhan and Morgan with respect to most of the strong bands, the suggested interpretation of the remaining, usually weaker, bands differs somewhat from theirs.

EXPERIMENTAL

The absorption tube, which was made of vitreosil, was 10 cm long by 1·5 cm in diameter and was open at both ends. It was at first heated in a Silit tube furnace capable of reaching temperatures up to 1400° C. At this temperature the contrast of the bands was not so good as had been obtained with PbS and so it was decided to use higher temperatures with a carbon arc furnace of the type shown in fig. 1. Three carbon arcs in series working off 240 volts were run inside a rectangular cavity cut out of a "New Parex" brick, thermal insulation being provided by a packing of additional bricks. At the working temperature of 1500° C, which was attained by using a current of 25 amp, the PbO was found to be very destructive of the vitreosil and of the alundum liner used for supporting the tube. The spectrum was photographed on the Hilger E1 spectrograph, the dispersion of which varies from 4 to 9 A per mm in the region investigated, and on the Hilger E52 spectrograph having an average dispersion of 5·5 A per mm.

---

* 'Phys. Rev.,' vol. 35, p. 34 (1930).

† 'Naturwiss.,' vol. 17, p. 122 (1929).

‡ *Loc. cit.*

§ 'Phys. Rev.,' vol. 47, p. 377 (1935).

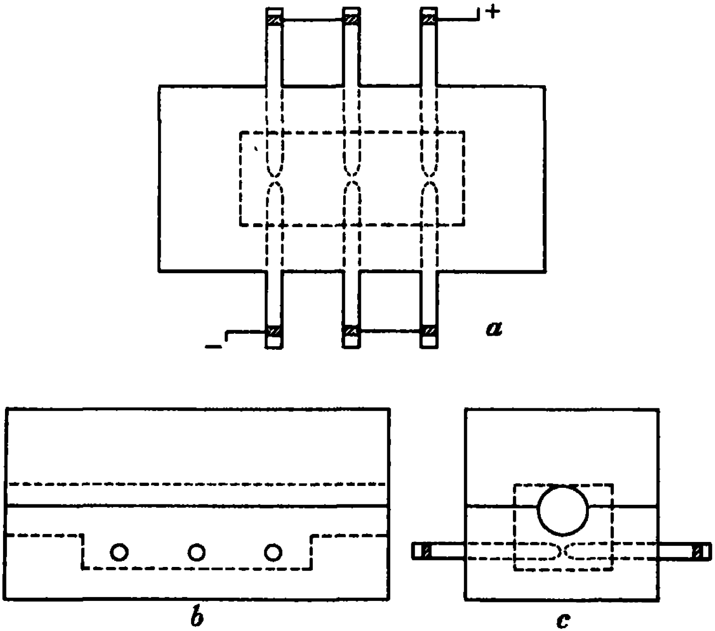

Fig. 1—Carbon arc furnace. *a*, plan; *b*, side elevation; *c*, end elevation.

A 30 volt 900 watt double-spiral filament lamp served as a source in the visible region, whilst a 100 volt ultra-violet lamp was used from 3500–3900 A, and a hydrogen discharge lamp[*] for lower wave-lengths. This worked at 0·1 amp 3000 volts and was of sufficient intensity to give good exposures in 4 minutes. Ilford "Monarch" and Process Panchromatic plates were used in photographing the spectrum, iron arc

[*] For the loan of which I am indebted to O. Darbyshire, M.Sc.

lines serving as wave-length standards, their values being taken from the tables published by the International Astronomical Union (1933).

VIBRATIONAL ANALYSIS

The bands stretch without a break from 2600 to 6000 A and are all degraded to the red. They are so regularly spaced in progressions that

TABLE I—VIBRATIONAL ANALYSIS OF SYSTEM B

v' \ v''	0		1		2		3		4
0	22173·4		21460·1		20750·6		20052·3		19363·0
	(2)	713·3	(5)	709·5	(8)	697·3	(8)	689·3	(3)
	494·7		494·0		490·8		494·7		
1	22667·1		21954·1		21241·4		20547·0		
	(6)	713·0	(5)	712·7	(4)	694·4	(5)		
	489·4		488·5				490·1		
2	23156·5		22442·6				21037·1		
	(10)	713·9	(4)	712·7			(3)		
	484·9		487·9						
3	23641·4		22930·5		22216·0				
	(10)	710·9	(3)	714·5	(2)				
	489·1		483·1		496·7				
4	24130·5		23413·6		22712·7				
	(10)	716·9	(6)	700·9	(0)				
	468·5		476·9						
5	24599·0		23890·5						
	(7)	708·5	(4)						
	469·3		472·1						
6	25068·3		24362·6						
	(4)	707·5	(7)						
			461·8						
7			24824·4						
			(9)						

the analysis presented no difficulty except in the regions where the various systems overlapped and at the ultra-violet extremity where the rotational structure was so open, due to the high dispersion, that it was difficult to identify the band heads with certainty. The three systems A, B, and D were easily recognized, B and D being much more extensive than in emission. The system A, however, is not developed to any greater extent in absorption and so additional data cannot be presented here. The vibrational analyses of the B and D systems are shown in Tables I and II, the assignment of quantum numbers being reliable, as both systems are bounded by strong " zero " progressions, and in agreement with that given by Bloomenthal. Two weaker and smaller systems have

TABLE II—VIBRATIONAL ANALYSIS OF SYSTEM D

v' \ v''	0		1		2		3		4
0	30103·5		29389·0		28681·0		27984·1		27281·0
	(3)	714·4	(6)	708·0	(5)	696·9	(3)	703·1	(2)
	524·0		524·0				523·9		531·0
1	30627·5		29913·1				28508·0		27812·0
	(9)	714·4	(4)	705·7			(4)	696·0	(3)
	520·1		521·0				517·7		
2	31147·6		30434·1		29729·4		29025·7		
	(9)	713·5	(6)	707·8	(5)	703·7	(2)		
	510·4		512·0		508·8				
3	31658·0		30946·0		30238·2				
	(10)	712·0	(6)	707·8	(4)				
	507·7		505·2						
4	32165·7		31451·2						
	(10)	714·4	(4)						
	508·8		493·6						
5	32674·5		31944·8						
	(8)	729·7	(3)						
	491·5		508·1						
6	33166·0		32452·9						
	(5)	713·1	(5)						
	488·0		486·1						
7	33654·0		32939·0						
	(1)	715·0	(5)						
			486·1						
8			33425·1						
			(3)						
			474·8						
9			33899·9						
			(0)						

been discovered, the analyses being presented in Tables III and IV. The first is the same as Shawhan and Morgan's C system, so this title will be retained for it, whilst the other is new and will be called system F. All of the systems have the same lower level which is the ground

TABLE III—VIBRATIONAL ANALYSIS OF SYSTEM C

v' \ v''	0		1
0	24760·0 (6)	706·3	24053·7 (2)
	517·1		
1	25277·1 (7)		
	503·1		
2	25780·2 (8)	710·2	25070·0 (4)
	494·0		496·2
3	26274·2 (6)	708·0	25566·2 (3)
	485·1		478·0
4	26759·3 (4)	715·1	26044·2 (2)
	483·6		
5	27242·9 (3)		
	470·4		
6	27713·3 (1)		

TABLE IV—VIBRATIONAL ANALYSIS OF SYSTEM F

v' \ v''	0		1		2
0	35595·4 (5)	713·0	34882·4 (8)	709·1	34173·3 (2)
	364·9		360·6		363·4
1	35960·3 (8)	717·3	35243·0 (4)	706·3	34536·7 (1)
	354·7				
2	36315·0 (6)				

level of the molecule. The vibrational constants for these systems have been determined by a method of least squares and are given in Table V, the values found by Bloomenthal and Shawhan and Morgan being added wherever possible.

Of the 20 bands listed by Shawhan and Morgan as forming their system E, 15 do not appear on my plates, 2 have been fitted into system D, 2 are very weak, and the remaining one has been associated with five other fairly strong bands to form a single progression as shown

TABLE V—VIBRATIONAL CONSTANTS OF PbO

Level	ν_e	ω_e	$x_e\omega_e$
F	*35769·1	373·1	4·50
	‡30195·0	532·0	3·13
	†30197·0	530·5	1·05
D	*30198·7	530·5	2·92
	‡24871·6	516·0	3·5
C	*24864·0	518·0	3·90
	†22289·8	496·3	2·33
B	*22284·9	498·0	2·20
A	†19723	452·0	3·3
	‡ 0	722·5	3·75
	† 0	722·3	3·73
X	* 0	721·8	3·70

* Data of author. † Data of Bloomenthal. ‡ Data of Shawhan and Morgan.

$$\begin{array}{ccccccccccc} 27213 & & 27671 & & 28123 & & 28569 & & 29009 & & 29444 \\ & \diagdown\;\diagup & & \diagdown\;\diagup & & \diagdown\;\diagup & & \diagdown\;\diagup & & \diagdown\;\diagup & \\ & 458 & & 452 & & 446 & & 440 & & 435 & \end{array}$$

It will be suggested later that this is a $v'' = 0$ progression developed from the ground state of the molecule. It may be that in the present work the use of temperatures higher than those used by Shawhan and Morgan have so extended the rotational structure of the overlapping D system as to mask the weak heads of their E system.

The intensities of the bands have been graded on the usual 0–10 scale, the values being shown in brackets in Tables I to IV.

The Condon parabolas are broad, characteristic of band systems having a large difference in the ω's, and are very similar to those of the related molecules, PbS, SnO, and SnS. By far the strongest bands are those belonging to $v'' = 0$ progressions, this being the only feature of the distributions which differs from those obtained from the emission spectrum.

ENERGY OF DISSOCIATION

Assuming the extrapolation of the vibrational energy to the dissociation limit to be linear, it is possible to calculate the energy of dissociation of PbO in a given electronic state from the relation*

$$D = \frac{\omega_e^2}{4x_e\,\omega_e}.$$

This has been done for the levels given in Table VI.

TABLE VI—DISSOCIATION ENERGIES OF PbO

Level	γ_e	ω_e	$x_e\omega_e$	D cm^{-1}	D volts
X	0	721·8	3·7	34842	4·3
B	22284·9	498·1	2·2	27944	3·4
D	30198·7	530·5	2·9	23188	2·9
A†	19723	452·0	3·3	15490	1·9

† Bloomenthal's data.

The experimental data for the other systems are too meagre to justify similar calculations being made for them. Fig. 2 shows the resulting energy scheme.

It is at once apparent that if any reliance can be placed upon this extrapolation method, the ground level X and the level A dissociate into the same products which can be assumed for the moment to be normal Pb and O atoms in ^3P states, and further, levels B and D also dissociate into identical products which must include at least one excited atom. For X and A dissociate at levels 34842 and 3521 3cm^{-1} respectively above the ground state, whilst the corresponding values for levels B and D are 50229 and 53387 cm^{-1} respectively. Although it is doubtful whether these figures are reliable estimates of the dissociation limits, yet the difference between the mean of each pair is significant and should correspond to an excitation potential E_A of one of the atoms. Now

$$\begin{aligned} E_A &= 51808 - 35028 \text{ cm}^{-1} \\ &= 16780 \text{ cm}^{-1} \text{ or } 1\cdot8 \text{ volts,} \end{aligned}$$

---

* Jevons's "Report on Band Spectra," p. 27.

and the energy difference between the ^3P and ^1D of O is 15641 cm^{-1}, a value so close to the above value of E_A as to suggest that the problem of the dissociation products is settled. However, according to Hund's theory of molecular states, only a triplet state can dissociate into ^3P and ^1D atoms, and Bloomenthal has shown that all the states involved here are $^1\Sigma$. Considering the next atomic pair, which theory allows as possible dissociation products, *i.e.*, ^1D (Pb) and ^1D (O), $E_A = 26600$ cm^{-1}, a value which does not give such a good agreement with the experimental value as that obtained on the assumption that the dissociation products are ^3P (Pb) and ^1D (O).

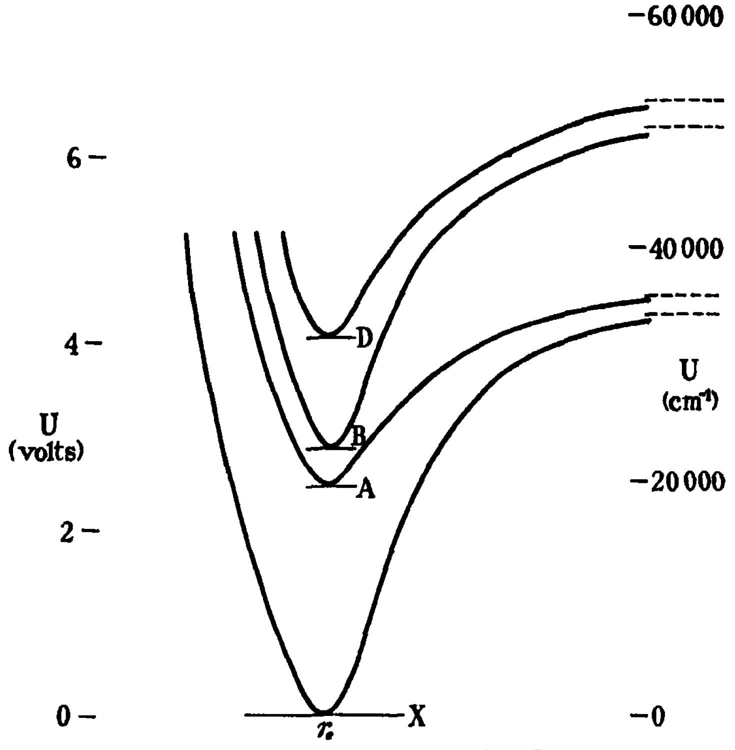

Fig. 2—Dissociation energies of PbO.

A similar discrepancy exists with the CO molecule in which Mulliken has assumed that both the ground $^1\Sigma$ and the $^1\Pi$ states (the latter being the lower level of the Angstrom system) dissociate into normal unexcited ^3P (C) and ^3P (O) atoms. This fixes the dissociation energy D of the $^1\Pi$ state as 2 volts, because the separation of the $^1\Sigma$ and $^1\Pi$ states is known from the analysis of the 4th positive system to be 8 volts and the D value for the $^1\Sigma$ state is definitely known to be 10 volts. That this estimate of 2 volts for D ($^1\Pi$) is too small can be seen from the vibrational scheme of the 4th positive system,* which shows that bands involving the upper level up to $v' = 16$ are known. The vibrational energy at this level is 2·3 volts, *i.e.*, already above the D value previously given, and it is probable that dissociation will take place at a much higher level for at $v' = 0$, $\omega = 1500$ cm^{-1} and is still as high as 970 cm^{-1} for $v' = 15$. The decrease in ω with v' appears to be linear, justifying the use of the extrapolation method of determining D which gives 4 volts. This entails dissociation into a pair of atoms of which one must be excited with an energy of 2 volts, just the energy required to give ^3P (C) and ^1D (O) as the dissociation products. The next lowest pair of excited states allowable by theory are ^1D (C) and ^1D (O), which would mean that D ($^1\Pi$) would have to be 5 volts. The fact that this is higher than the value obtained by the direct extrapolation which usually gives too high a value, renders this possibility unlikely. Now there is the initial assumption in both of these problems that the ground state dissociates into normal unexcited atoms. Past experience has shown that this supposition is reasonable, and it has been absorbed into a general rule advocated by Mulliken† that a molecule dissociates into that pair of atoms allowed by Hund's theory which has the lowest energy. It will be noticed that the value of E_A derived experimentally in both cases is of the order of 2 volts and further, that the O atom occurs in each case, making it appear feasible that E_A corresponds to some excitation potential of O. Professor Curtis has suggested that the ground state may dissociate into pairs of excited atoms ^1D (Pb) and ^1D (O) and ^1D (C) and ^1D (O), in which case it is possible that ^1D (Pb) and ^1S (O) and ^1D (C) and ^1S (O) are the next pairs of dissociation products because $^1D - {}^1S$ for 0 is 17925 cm or 2·2 volts in good agreement with the experimental value of E_A. This hypothesis, therefore, reconciles the evidence with Hund's theory but conflicts with Mulliken's rule.

BAND SPECTRA OF RELATED MOLECULES

It is well known that similarity in the electron configuration of two atoms such as O and S or two homopolar molecules such as O_2 and S_2 is reflected in a similarity of their spectra. It is also to be expected that molecules such as PbO and PbS will have similar electron configurations, and that therefore their band spectra will have certain features in common. Individual differences which will exist will be due primarily to specific differences in the O and S atoms.

---

* Jevons's " Report on Band Spectra," p. 239.

† ' Rev. Mod. Phys.,' vol. 4, No. 1 (1932).

Actually it is found that each spectrum is equally extensive, lying in the same wave-length region and consists of 6 and 5 overlapping systems respectively.* The electron transitions are all alike,† being rather curiously all $^1\Sigma \leftarrow {}^1\Sigma$.

Now the deeper term energies of O are higher than the corresponding values of S and it is therefore reasonable to expect that the molecular term values of PbO will be all deeper than the corresponding ones of PbS.

The actual energy levels and associated vibration frequencies are shown in fig. 3 and, for the reason given, the levels A, B, C, and D of PbO are considered to correspond with A, B, C, and E of PbS.

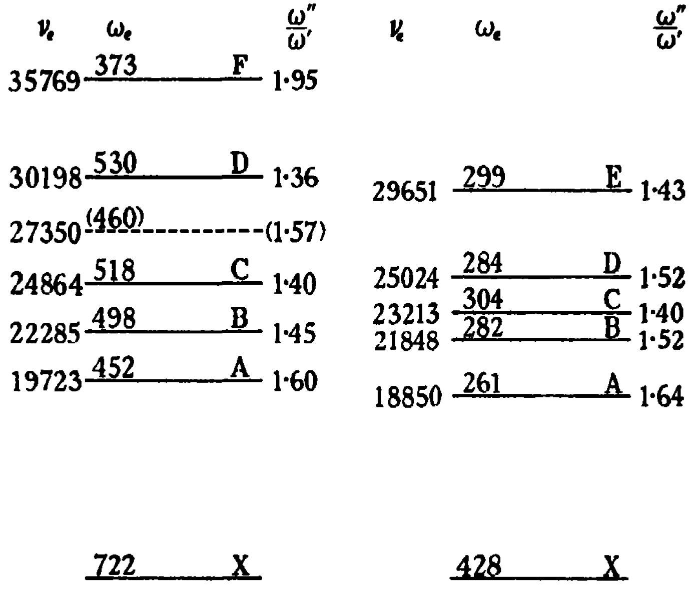

Fig. 3—Energy levels of PbO and PbS.

The following points may be noted in connexion with this figure :—

(1) The ω values of PbO are all higher than those of PbS.

(2) The ω values vary irregularly in the excited states but in the same manner for both molecules. This can best be seen from the ratio of ω''/ω' given at the right of each level in the figure, ω'' being the ground state frequency. This indicates that the same relative loosening takes place in the molecular binding on excitation.

---

* For PbS data, Rochester and Howell, ' Proc. Roy. Soc.,' A, vol. 148, p. 157 (1935).

† Harvey and Bell, *unpublished work*.

(3) There is no level in PbO corresponding to the D level of PbS and no PbS level corresponding to F or Shawhan and Morgan's E system of PbO.

If the correlation between the two molecules were reliable, another PbO level occurring between C and D could be predicted, corresponding to the D level of PbS. It would have a higher value of γ_e than D, and since ω''/ω' for PbS $= 1\cdot 5$ and as the PbO ratio is always a little less it might be expected that the value of ω' for this state would be given by

$$\frac{721\cdot 8}{\omega'} = 1\cdot 45 \quad \text{or} \quad \omega' = 490 \text{ cm.}$$

Now it is significant that the progression of fairly strong bands already reported occurs right in the region expected and furthermore has an ω of 460 cm; it may therefore be tentatively suggested that these bands form part of a v'' progression to this missing level which is represented in fig. 3 as a dotted line.

TIN COMPOUNDS

The recent analysis of the SnS spectrum* enables a similar comparison to be made of the sulphide and oxide systems of this metal. Unfortunately, our knowledge of the SnO spectrum is not so complete as for PbO. Mahanti† found 3 systems A, B, and C, of which the first two have the same lower level which, in his opinion, was not the ground level. Connelly,‡ however, came to the conclusion that only system A existed beyond dispute, and that since it could be obtained in absorption, the lower level was indeed the ground level. Finally Loomis§ and Watson have reported a new ultra-violet system having the same final state as system A. This will be termed system D. Fig. 4 shows the term schemes of SnO and SnS and is drawn up in the same way as with the Pb compounds.

Assuming that a similarity in ω''/ω' value is an indication of some correspondence between an energy level from each molecule, it can be seen that the SnO levels A and D having ω''/ω' values $1\cdot 41$ and $1\cdot 65$ respectively correspond to levels B and C of SnS where the ω''/ω' values are $1\cdot 47$ and $1\cdot 66$. Thus as with Pb the oxide terms are deeper than the corresponding sulphide terms. The agreement between corresponding ω''/ω' values is so good as to rule out the possibility of its being a coincidence and also justifies the prediction of a level for SnO corresponding to A of SnS which has an ω''/ω' value of 1·28. Now Mahanti's disputed B level, which is shown in fig. 4 as a dotted line, has the predicted energy value and, what is more suggestive, has 1·29 as its ω''/ω' value. This appears to be conclusive evidence for the existence of this level. In view of the uncertainty, however, it was considered desirable to examine the absorption spectrum of SnO when produced under the same conditions as that of PbO. It was found that the spectrum could best be developed by using a mixture of metallic Sn and SnO in the absorption tube as the SnO rapidly oxidized to SnO_2. When excess Sn was used a new band spectrum was superposed upon that of SnO. This has been measured and analysed, but as yet the nature of the absorbing molecule has not been determined except that it is definitely known not to be SnO, ω'' being too small. The SnO spectrum itself consisted only, as Connelly found, of the A system, so that definite experimental evidence of the connexion of the B level with the ground state is still lacking.

---

* Rochester, 'Proc. Roy. Soc.,' A, vol. 150, p. 668 (1935).

† 'Z. Physik,' vol. 68, p. 114 (1931).

‡ 'Proc. Phys. Soc.,' vol. 46, p. 222 (1934).

§ 'Phys. Rev.,' vol. 45, p. 805 (1934).

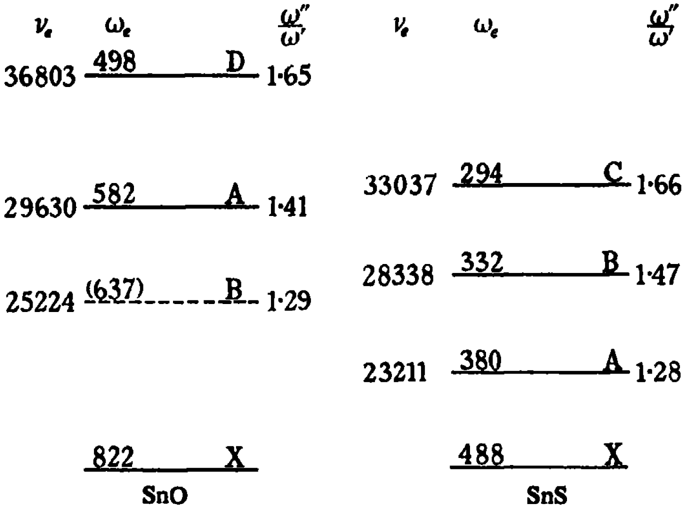

Fig. 4—Energy levels of SnO and SnS.

To complete this comparison, Table VII gives the ω'' values for all the molecules previously considered together with those of GeO and GeS. That the change in passing from oxide to sulphide brings about similar changes in ω'' with similar molecules is shown by the ratio $\frac{\omega_{\text{oxide}}}{\omega_{\text{sulphide}}}$.

This behaviour appears so regular that it is probable that the transition from sulphide to selenide will produce similar changes in ω''.

This constant will, of course, be smaller for the selenides, but the ratio factor will also be smaller than the 1·7 the ratio $\frac{\omega_{\text{oxide}}}{\omega_{\text{sulphide}}}$ because the ratio of the molecular weights decreases from $\frac{\text{oxide}}{\text{sulphide}}$ to $\frac{\text{sulphide}}{\text{selenide}}$.

A rough estimate of the magnitude of this change can be established by examining that which takes place in ω_e'' in passing from $O_2 - S_2 - Se_2$ to Te_2*

$$\frac{\omega_{O_2}}{\omega_{S_2}} = 2\cdot2, \qquad \frac{\omega_{S_2}}{\omega_{Se_2}} = 1\cdot9, \qquad \frac{\omega_{Se_2}}{\omega_{Te_2}} = 1\cdot6,$$

i.e., the ratio changes by 0·3. Assuming that the reduction in the ratio is the same in the present case, $\frac{\omega_{\text{sulphide}}}{\omega_{\text{selenide}}} = 1\cdot4$ and the ω_e'' value for PbSe will be $\frac{428}{1\cdot4} \simeq 300$ cm^{-1}, roughly.

TABLE VII

Metal	ωOxide	ωSulphide	$\frac{\omega_{\text{oxide}}}{\omega_{\text{sulphide}}}$
Pb	722	428	1·69
Sn	822	488	1·68
Ge	984†	576‡	1·71

† Shaw, 'Phys. Rev.,' vol. 43, p. 1043 (1933).
‡ Jevons's "Report," p. 288.

The band systems of PbSe therefore should be displaced towards the red as compared with the corresponding PbS systems and should have a common ground state having a vibration frequency of the order of 300 cm^{-1}.

These bands have been obtained in absorption and await measurement.

CLASSIFICATION OF PbO BANDS

All the PbO bands here classified except those belonging to system A are tabulated in the usual manner in Table VIII.

TABLE VIII—CLASSIFIED BANDS OF PbO (EXCLUDING SYSTEM A)

λ	(Intensity)	ν	O—C	Classification
5163·06	(3)	19363·0	1·2	0, 4 B
4985·58	*(8)	20052·3	−0·7	0, 3 B
4865·60	(8)	20554·7	0·3	1, 3 B
4817·80	(8)	20750·6	−4·6	0, 2 B

---

* Data derived from Jevons's "Report."

TABLE VIII—(continued)

λ	(Intensity)	ν	O−C	Classification
4752·20	(5)	21037·1	1·1	2, 3 B
4706·47	(7)	21241·4	−4·6	1, 2 B
4658·50	(5)	21460·1	0·0	0, 1 B
4553·59	(5)	21954·6	1·4	1, 1 B
4508·64	(2)	22173·4	0·0	0, 0 B
4500·00	(5)	22216·0	−3·9	3, 2 B
4454·56	(5)	22442·6	0·1	2, 1 B
4410·44	(6)	22667·1	0·0	1, 0 B
4401·44	(3)	22712·7	11·0	4, 2 B
4359·78	(7)	22930·0	−3·1	3, 1 B
4317·22	(10)	23156·5	0·1	2, 0 B
4269·82	(8)	23413·6	1·4	4, 1 B
4228·68	(10)	23641·4	0·1	3, 0 B
4185·60	(7)	23890·5	6·5	5, 1 B
4156·20	(3)	24053·7	−5·9	0, 1 C
4103·50	(8)	24362·6	6·9	6, 1 B
4064·06	(5)	24599·0	1·1	5, 0 B
4037·63	(3)	24760·0	−2·0	0, 0 C
4027·16	(9)	24824·4	1·4	7, 1 B
3987·98	(3)	25068·3	1·3	6, 0 B
3987·70	(4)	25070·0	1·2	2, 1 C
3955·04	(7)	25277·1	−1·1	1, 0 C
3910·30	(3)	25566·2	0·4	3, 1 C
3877·85	(8)	25780·2	5·6	2, 0 C
3838·24	(2)	26044·2	−8·4	4, 1 C
3804·94	(6)	26274·2	5·2	3, 0 C
3735·96	(4)	26759·3	2·3	4, 0 C
3669·63	(3)	27242·9	4·0	5, 0 C
3664·50	(2)	27281·0	−9·1	0, 4 D
3607·35	(1)	27713·3	5·3	6, 0 C
3594·56	(3)	27812·0	−2·9	1, 4 D
5372·44	(3)	27984·1	1·1	0, 3 D
3506·80	(4)	28508·0	0·2	1, 3 D
3485·63	(5)	28681·0	−0·9	0, 2 D
3444·24	(2)	29025·7	−1·0	2, 3 D
3401·65	(6)	29389·1	0·2	0, 1 D
3362·71	(5)	29729·4	4·8	2, 2 D
3342·06	(4)	29913·1	−0·6	1, 1 D
3320·92	(3)	30103·5	0·2	0, 0 D
3306·30	(4)	30238·2	−0·2	3, 2 D
3284·84	(6)	30434·1	1·5	2, 1 D
3264·02	(9)	30627·5	−0·6	1, 0 D
3230·50	(8)	30946·0	0·6	3, 1 D
3209·60	(9)	31147·6	0·6	2, 0 D
3178·61	(10)	31451·2	−1·7	4, 1 D
3157·85	(10)	31659·8	−1·8	3, 0 D

TABLE VIII—(continued)

λ	(Intensity)	ν	O—C	Classification
3129·50	(3)	31944·8	−9·7	5, 1 D
3107·93	(10)	32165·7	−0·6	4, 0 D
3080·50	(7)	32452·9	3·0	6, 1 D
3059·60	(8)	32674·5	5·7	5, 0 D
3035·03	(5)	32939·0	0·1	7, 1 D
3014·28	(5)	33166·0	1·7	6, 0 D
2990·89	(3)	33425·1	1·6	8, 1 D
2970·55	(1)	33654·0	0·7	7, 0 D
2949·00	(0)	33899·9	−1·6	9, 1 D
2925·43	(1)	34173·0	0·1	0, 2 F
2894·59	(1)	34537·1	0·0	1, 2 F
2865·46	(8)	34882·0	1·9	0, 1 F
2836·60	(4)	35243·1	−1·0	1, 1 F
2808·60	(5)	35594·5	0·0	0, 0 F
2780·05	(8)	35960·2	1·5	1, 0 F
2752·87	(6)	36315·0	−1·5	2, 0 F

The following bands have not been definitely allocated, those marked with an asterisk forming a single progression. The remainder are very weak having intensities 0 to 2.

TABLE IX—UNCLASSIFIED BANDS

4379·54	(0)	22827·0	3499·34	(6)	28569·0*
4294·05	(0)	23281·5	3446·21	(4)	29009·1*
4212·30	(0)	23733·3	3429·21	(0)	29155·3
3983·68	(2)	25095·3	3395·26	(4)	29444·4*
3854·21	(1)	25938·3	3334·20	(0)	29983·6
3673·62	(3)	27213·3*	3089·75	(0)	32355·7
3612·80	(5)	27671·4*	3039·01	(0)	32896·4
3554·77	(6)	28123·4*	3023·17	(0)	33068·2

* Indicates bands form a progression.

The following lines have also been measured: 2833·0 (10) Pb I, 3099·2 (5) Ag I, 3280·6 (8) Ag I, 3383·8 (5) Ag I, 3683·5 (5) Pb I, 4057·8 (5) Pb I, the Ag being present as an impurity in the PbO.

The author wishes to record here his appreciation of the advice and useful criticism tendered by Professor W. E. Curtis, D.Sc., F.R.S., during the progress of this work.

He is also indebted to the Department of Scientific and Industrial Research for a grant which made possible the completion of this work.

SUMMARY

The band spectrum of PbO has been produced in absorption by using a carbon arc furnace.

The spectrum stretches from 2600 to 6000 A and contains five systems, of which three are found in emission. The vibrational constants of all the levels involved are as shown:—

Level	ν_e	ω_e	$x_e\omega_e$
F	35769·1	373·1	4·50
D	30198·7	530·5	2·92
C	24864·0	518·0	3·90
B	22284·9	498·0	2·20
A	19723	452·0	3·3
X	0	721·8	3·70

No evidence for the E system reported by Shawhan and Morgan has been found.

It is probable that the ground state dissociates into two excited atoms.

The spectra of the related molecules PbS, PbO, SnS, SnO, GeS, and GeO show many similarities and in particular it is found that the vibration frequency varies from state to state in a similar manner with oxide and sulphide molecules. These regularities are used to predict the vibration frequency of the ground state of the molecule PbSe.

The Electrical Conductivity of Transition Metals

By N. F. Mott, H. H. Wills Physical Laboratory, University of Bristol

(*Communicated by R. H. Fowler, F.R.S.—Received September* 23, 1935)

1—In a recent paper* certain properties of the transition metals Ni, Pd, and Pt and of their alloys with Cu, Ag, and Au have been discussed from the point of view of the electron theory of metals based on quantum mechanics. In particular, a qualitative explanation was given of the relatively high electrical resistance of the transition metals. It was shown from an examination of the experimental evidence that the conduction electrons in these metals have wave functions derived mainly from *s* states just as in Cu, Ag, and Au, and that the effective number of conduction electrons is not much less than in the noble metals. On the other hand, the mean free path is much smaller, because under the influence of the lattice vibrations the conduction electrons may make transitions to the unoccupied *d* states, and the probability of these transitions is several times greater than the probability of ordinary scattering. Since the unoccupied *d* states are responsible for the ferromagnetism or high paramagnetism of the transition elements, there is a direct connexion between the magnetic properties and the electrical conductivity.

The purpose of this paper is as follows: in §§ 2, 3, and 4 we develop a formal theory of conductivity for metals, such as the transition metals, where *two* Brillouin zones are of importance for the conductivity; in § 5 we apply the theory to show why, at high temperatures, the temperature coefficient of the paramagnetic metals Pd and Pt falls below the normal value; and in § 6 we discuss the resistance of ferromagnetic metals, and show in § 7 qualitatively why constantan (Cu-Ni) has zero temperature coefficient at room temperature.

2—The element nickel has in the lowest state the electronic configuration $(3d)^8 (4s)^2$, but states with the configurations $(3d)^9 (4s)^1$, $(3d)^{10}$ are separated from it by energies of only a few electron volts. In our theory we shall use essentially a " one-electron " picture, *i.e.*, we treat the electrons, in the first approximation, as moving independently of one another in an electrostatic field. We must therefore suppose that, for a single electron moving in the field of the nickel atom, the $3d$ and $4s$ states have energies near together.

---

* Mott, ' Proc. Phys. Soc.,' vol. 47, p. 571 (1935), referred to as paper A.

In the field of the crystal, instead of quantized energy values for the electron, we have bands or " zones " of allowed energies, a zone (or group of zones) corresponding to each state of an electron in the isolated atom. For nickel the $3d$ and $4s$ zones must overlap (otherwise the $3d$ band would be full, containing all the electrons, and the metal would not be a conductor). Thus, in the language of the electron theory of metals, the surface of the Fermi distribution lies in two zones—as also is the case for divalent metals. As explained in paper A, in nickel there are about $0 \cdot 6$ electrons in the $4s$ and $10 - 0 \cdot 6 = 9 \cdot 4$ in the $3d$ band. Similar results hold for the $5s$ and $4d$ states of palladium and the $6s$, $5d$ states of platinum.*

The theory already put forward in paper A to account for the high resistance of Ni, Pd, Pt is as follows. In the classical theory of Lorentz the conductivity of a metal is

$$\sigma = \frac{ne^2}{\mu} \tau, \tag{1}$$

where n is the number of electrons per unit volume, μ the mass of an electron, τ half the time between collisions or " time of relaxation." In the quantum theory of conduction, as developed for the monovalent alkali and noble metals,† this formula remains true with the following modifications; for μ we must understand the " effective " mass of an electron in the crystal lattice, which will in general be greater than the actual mass μ_0 of a free electron. Secondly, τ must be calculated by the methods of quantum mechanics, so that $1/\tau$ is proportional (for $T > \Theta_D$) to:

(1) The mean square displacement, due to thermal motion, of the atoms from their mean positions. This is proportional to $T/M\Theta_D^2$, where M is the mass of an atom, Θ_D the characteristic temperature.

(2) The density of states N (E) at the surface of the Fermi distribution, *i.e.*, for the occupied states of highest energy.

According to the theory, the electrons in all states belonging to zones which are not fully occupied can contribute to the electric current; therefore the *d* as well as the *s* electrons must be classed as conductivity electrons. The effective masses, however, will be very different; the conductivity electrons of copper and silver have been investigated by Fuchs[*] by the method of Wigner and Seitz[†]; he finds that they behave approximately as free electrons. The same should be true for similar fields of Ni and Pd; we shall thus assume for the *s* electrons

---

* It is possible that in one band there may be wave functions derived from a mixture of s and d wave functions (Jones, Mott, and Skinner, ' Phys. Rev.,' vol. 45, p. 379 (1934)). For our theory it is only necessary that at the top of the lower band the wave functions shall be mostly d, and at the bottom of the upper band mostly s. *Cf.* a paper on the wave functions of copper by Krutter, ' Phys. Rev.,' vol. 48, p. 664 (1935).

† *Cf.* the report by Sommerfeld and Bethe, ' Handb. der Physik,' vol. 24 (2), p. 499

$$\mu_s \simeq \mu_0,$$

where μ_0 is the actual mass of a free electron. For the *d* electrons, on the other hand, owing to the small overlap of one *d* wave function with another, we must assume

$$\mu_d \gg \mu_0.$$

In other words, the *d* electron takes longer to move from atom to atom under the influence of an applied field than does the *s* electron.

The conductivity of a transition metal will therefore be

$$\sigma = \frac{n_s e^2}{\mu_s} \tau_s + \frac{n_d e^2}{\mu_d} \tau_d, \tag{2}$$

where τ_s, τ_d are the times of relaxation for *s* and *d* electrons, μ_s, μ_d the effective masses, and n_s the number of *s* electrons per unit volume. n_d, as we shall see below, should be taken to be the number of *positive holes* in the *d* band rather than the number of electrons.

The low conductivity of the alkaline earths is usually explained as being due to the small overlap from the first Brillouin zone to the second, and thus to small values of n_s and n_d in a formula such as (2). For Ni and Pd we know from a variety of evidence (paper A) that $n_s = n_d \simeq 0 \cdot 6$ N_A, where N_A is the number of atoms per unit volume; thus the high resistance of these metals must be due to a small value of τ_s. As we shall see, τ_s and τ_d are of the same order of magnitude, and hence the conductivity is almost entirely due to *s* electrons.

It is essential to the theory of the high paramagnetism[‡] of Pd, and the ferromagnetism[‡] of Ni that the *d* band should be narrow compared with the *s* band, of the order of magnitude of one electron volt or less. Since, moreover, the number of electronic states in the *d* band is 10 per atom, it follows that the density of states per unit energy range is much larger in the *d* band than for free electrons. The recent determination of the specific heats of nickel by Keesom and Clark† and of silver by Keesom and Kok‡ shows that the density of states at the surface of the Fermi distribution is about 20 times larger in nickel, where the *d* band is not full, than in silver, where it is.§

---

[*] 'Proc. Roy. Soc.,' A, vol. 151, p. 585 (1935).

[†] 'Phys. Rev.,' vol. 43, p. 804 (1933).

[‡] Paper A; *cf.* also Peierls, 'Ergebn. exakt. Naturw.,' vol. 11, p. 264 (1932); Slater, 'Phys. Rev.,' vol. 36, p. 57 (1931).

The large density of states is, of course, connected with the large effective mass; under certain assumptions to be discussed in the next section we may write

$$\mathrm{N}(\mathrm{E})\, d\mathrm{E} = 4\pi \frac{\sqrt{(2\mu^3)}}{h^3} \sqrt{\mathrm{E}}\, d\mathrm{E}. \tag{3}$$

Now the time of relaxation τ_s for *s* electrons is given by

$$1/\tau_s = \mathrm{P},$$

where P is the probability of scattering. An *s* electron can be scattered in two ways: either to another *s* state or to a *d* state. The transition probabilities are proportional to the squares of matrix elements of the type

$$\int \psi^*_2\, \Delta\mathrm{V}\, \psi_1\, d\tau,$$

where $\Delta\mathrm{V}$ is the perturbing potential due to the lattice waves, and ψ_1, ψ_2 the initial and final states of the electron. In the present state of the theory it is exceedingly difficult to evaluate these matrix elements in any way which seems physically significant; there is, however, no reason to believe that they are much smaller when the final state lies in the *d* band than when it lies in the *s* band. On the other hand, the transition probabilities for the two processes, as already stated, are proportional to the densities of states $\mathrm{N}_s(\mathrm{E})$ and $\mathrm{N}_d(\mathrm{E})$ for the two final states considered; N_d is much greater than N_s, and hence we conclude that transitions from the *s* to the *d* band are important for the determination of τ_s, and that τ_s will be much less than for the noble metals, where the *d* band is full, and only *s*—*s* transitions are possible.

In the next two sections we shall investigate in greater detail the scattering probability P, and shall give a proof of (2).

---

† 'Physica,' vol. 2, pp. 230, 513 (1935).

‡ 'Physica,' vol. 1, p. 770 (1934).

§ *Cf.* Mott, contribution to discussion on Supraconductivity, 'Proc. Roy. Soc.,' A, vol. 152, p. 42 (1935).

3—The Scattering Probability

In the quantum theory of metals, each electron has a wave function of the form

$$\psi_k = e^{i(\mathbf{kr})} u_k(x, y, z),$$

where u_k is periodic with the period of the lattice. The corresponding energies will be denoted by E (k).

In the usual quantum theory of conduction, a Debye model for the crystal is used; the electron is considered as interacting with a lattice wave of frequency ν, and gaining or losing a quantum of energy $h\nu$. For our purposes, since we are only interested in temperatures above the characteristic temperature Θ, we may simplify the whole theory by using an Einstein rather than a Debye model for the crystal; we shall consider every atom as vibrating independently of the others with frequency ν, where $h\nu = k\Theta$, and we shall calculate the probability that an electron is scattered by a single atom, and shall then sum for all atoms. Moreover, since the vibrating atom moves slowly compared with the electron, we shall treat it as though it were momentarily at rest, and therefore neglect altogether the change in the energy of the electron during the scattering process. These assumptions are not in the least necessary for our theory, but they simplify its exposition considerably.

Let V (r) be the potential in the neighbourhood of any one ion in the crystal. Then, if that ion is displaced a distance ξ in the x direction, say, the perturbing potential which causes electronic transitions is

$$\Delta V = \xi \frac{\partial V}{\partial x}.$$

By the ordinary methods of quantum mechanics, one finds that if the electron is initially in the state k, the probability that at time t it is in the state k' is

$$\frac{1}{\hbar^2}\left|\int \psi^*_{k'}\, \Delta V\, \psi_k\, d\tau\right|^2 \frac{2(1-\cos\lambda t)}{\lambda^2}, \tag{4}$$

where

$$\lambda = [E(\mathbf{k}') - E(\mathbf{k})]/\hbar.$$

This expression has a strong maximum for E ($\mathbf{k}'$) = E ($\mathbf{k}$), and to obtain a physically significant result one must integrate over it. The transition probability may then best be expressed as follows: we draw in k-space the surface having the same energy as the state $\mathbf{k}$ (*cf.* fig. 1), and take an area dS on this surface, and a cylinder of volume $d\zeta\, d$S as shown.

To obtain the probability that after time t an electron has made a transition to any state in this volume element, we must multiply (4) by the number of states in the volume $d\zeta\, dS$, namely,

$$d\zeta\, dS/(2\pi)^3.$$

We now integrate over ζ; since we may write

$$E(\mathbf{k}') - E(\mathbf{k}) = \zeta \frac{dE(\mathbf{k}')}{dk'_n},$$

the differentiation being normal to the surface, we obtain for the probability $P(\mathbf{kk}')\, dS'$ that after unit time the electron has made a transition to the state k'

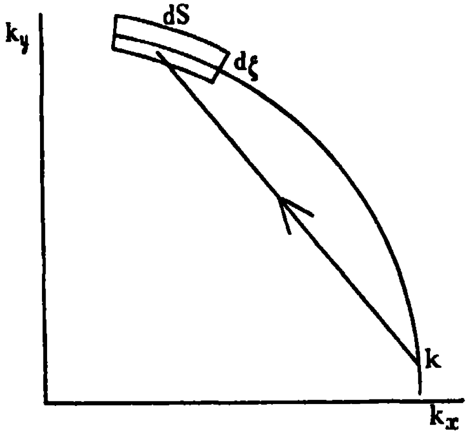

FIG. 1—Part of surface of Fermi distribution in k-space.

$$P(\mathbf{kk}')\, dS' = \frac{dS'}{4\pi^2\hbar}\left|\int \psi^*_{k'}\, \Delta V\, \psi_k\, d\tau\right|^2 \Bigg/ \frac{dE}{dk'_n}. \tag{5}$$

We see, as stated in § 2, that the transition probability is proportional to $1 \Big/ \frac{dE}{dk'_n}$, *i.e.*, to the *density* of states in the neighbourhood of the final state.

The square of the matrix element in (5) is

$$\xi^2 \left|\int \psi^*_{k'} \frac{\partial V}{\partial x}\, \psi_k\, d\tau\right|^2.$$

Since we must sum over all atoms, we must take the mean value of ξ^2, viz.,

$$\overline{\xi^2} = \frac{\hbar^2}{k} \frac{T}{M\Theta^2}.$$

4—We must now prove formula (2), and hence give a more exact definition of τ_s, τ_d in terms of the transition probability (5). This can only be done if we make rather drastic simplifying assumptions. For the *s* electrons we set

$$\mathrm{E}\,(\mathbf{k}) = \hbar^2 k^2/2\mu_s,$$

depending on the modulus k of $\mathbf{k}$ only. μ_s is thus the effective mass of an *s* electron. We shall treat the atomic *d* state as non-degenerate (this can be allowed for afterwards), and shall denote the wave vector of a state in the *d* band by $\mathbf{j}$, $\mathbf{j}$ being so defined that $j = 0$ corresponds to the state of ***highest*** energy. We shall assume also that the energy $\mathrm{E}\,(\mathbf{j})$ of a *d* state depends only on the modulus j of $\mathbf{j}$, and shall write it

$$\mathrm{E}\,(\mathbf{j}) = \mathrm{E}_0 - \hbar^2 j^2/2\mu_d.$$

We must remember that $\mu_d \gg \mu_s$.

For the transition probability between one state and another we write, from (5)

$$\mathrm{P}\,(\mathbf{kk}')\,d\mathrm{S}' = \mu_s\,\mathrm{A}\,(\mathbf{kk}')\,d\mathrm{S}'/k', \tag{6}$$

where

$$\mathrm{A}\,(\mathbf{kk}') = \frac{1}{4\pi^2\hbar^3}\left|\int \psi^*_{k'}\ \Delta\mathrm{V}\ \psi_k\,d\tau\right|^2,$$

and similarly for the transition probability from an *s* to a *d* state of equal energy

$$\mathrm{P}\,(\mathbf{kj})\,d\mathrm{S}_j = \mu_d\,\mathrm{A}\,(\mathbf{kj})\,d\mathrm{S}_j/j. \tag{6.1}$$

We shall assume further that both $\mathrm{A}\,(\mathbf{kj})$ and $\mathrm{A}\,(\mathbf{kk}')$ depend only on the angle θ between $\mathbf{k}$ and $\mathbf{j}$, or $\mathbf{k}$ and $\mathbf{k}'$, so that we may write

$$\mathrm{A}\,(\mathbf{kk}') = \mathrm{A}_{ss}\,(\theta) \qquad \mathrm{A}\,(\mathbf{kj}) = \mathrm{A}_{sd}\,(\theta).$$

Consider now the metal in the absence of a field. The probability that any electronic state is occupied is given by the Fermi function

$$f(\mathbf{k}) = f_0\,(\mathbf{k}) = \frac{1}{e^{(\mathrm{E}-\zeta)/k\mathrm{T}} + 1}\,, \qquad \mathrm{E} = \mathrm{E}\,(\mathbf{k}).$$

If an external field F is applied, say in the x direction, the wave vector of each electron increases according to the equation $\dot{k}_x = -e\mathrm{F}/\hbar$; hence the rate of change of $f\,(\mathbf{k})$ is initially

$$\left(\frac{df}{dt}\right)_{\text{field}} = -\frac{df_0}{d\mathrm{E}}\frac{d\mathrm{E}}{dk}\frac{k_x}{k}\frac{e\mathrm{F}}{\hbar}$$

$$= -\frac{df_0}{d\mathrm{E}}\frac{\hbar^2}{\mu_s}k_x\frac{e\mathrm{F}}{\hbar}, \tag{7}$$

for s electrons, with a similar expression for the d electrons. These two expressions must be equated to the rate of change of f due to collisions.

When a steady current is flowing, the probability that a state is occupied will no longer be given by $f_0(\mathbf{k})$ but by the "perturbed" Fermi functions $f_s(\mathbf{k}), f_d(\mathbf{j})$ for s and d electrons respectively. We shall write

$$f_s(\mathbf{k}) = f_0(\mathbf{k}) + g_s(\mathbf{k}), \qquad f_d(\mathbf{j}) = f_0(\mathbf{j}) + g_d(\mathbf{j}).$$

Now, by the definition of the " time of relaxation " τ_s, we have

$$g_s(\mathbf{k}) = \frac{df}{dt}\tau_s,$$

which may be written

$$g_s(\mathbf{k}) = -\frac{df_0}{dE}\frac{\hbar^2}{\mu_s}k_x\tau_s\frac{eF}{\hbar}, \tag{8}$$

which gives the change of the distribution function due to the field F, in terms of the time of relaxation τ_s.

We now calculate the rate of change of f due to collisions, which has to be equated to (7).

We consider a volume element of k space in the s zone. Let the volume element be situated at the point $\mathbf{k}$, and let its volume be $d\mathbf{k} = dk_x\,dk_y\,dk_z$. Then for unit volume of the metal the number of electrons in states within the element is

$$2f_s(\mathbf{k})\,d\mathbf{k}/(2\pi)^3.$$

Owing to the thermal vibrations of the atoms, electrons make transitions to states of practically equal energy; the number of such transitions in which an electron leaves the volume element $d\mathbf{k}$ is, per unit time,

$$2f_s(\mathbf{k})\frac{d\mathbf{k}}{8\pi^3}\left[\int P(\mathbf{kk}')\{1-f_s(\mathbf{k}')\}\,dS' + \int P(\mathbf{kj})\{1-f_d(\mathbf{j})\}\,dS_j\right]. \tag{9}$$

The integration is over all surface elements dS', dS_j in k, j space which have the same energy as the initial state.

Substituting from (6), (6.1), we have, for (9)

$$2f_s(\mathbf{k})\frac{d\mathbf{k}}{8\pi^3}\left[\frac{\mu_s}{k}\int A(\mathbf{kk}')\{1-f_s(\mathbf{k}')\}\,dS' + \frac{\mu_d}{j}\int A(\mathbf{kj})\{1-f_d(\mathbf{j})\}\,dS_j\right]. \tag{10}$$

Similarly, we obtain for the number of electrons entering the volume element $d\mathbf{k}$ per unit time

$$2\{1-f_s(\mathbf{k})\}\frac{d\mathbf{k}}{8\pi^3}\left[\frac{\mu_s}{k}\int A(\mathbf{kk}')f_s(\mathbf{k}')\,dS' + \frac{\mu_d}{j}\int A(\mathbf{jk})f_d(\mathbf{j})\,dS_j\right]. \tag{11}$$

Subtracting (10) from (11) we obtain for the decrease, due to collisions, in the number of electrons in the volume element $d\mathbf{k}$ per unit time,

$$2\frac{d\mathbf{k}}{8\pi^3}\left[\frac{\mu_s}{k}\int \mathrm{A}\,(\mathbf{kk}')\,\{f_s(\mathbf{k})-f_s(\mathbf{k}')\}\,dS'+\frac{\mu_d}{j}\int \mathrm{A}\,(\mathbf{kj})\,\{f_s(\mathbf{k})-f_d(\mathbf{j})\}\,dS_j\right]. \tag{12}$$

The second term corresponds to the *s–d* transitions, and is large, containing as it does the large factor μ_d (the effective mass of the *d* electrons).

The quantity (12) vanishes if, for f_s and f_d, we substitute the unperturbed Fermi function f_0. Therefore, in formula (12) we may substitute g_s for f_s and g_d for f_d. Using (8) for g_s and g_d, we obtain finally for the decrease in the number of electrons in the volume element $d\mathbf{k}$

$$-2\frac{d\mathbf{k}}{8\pi^3}\frac{df_0}{dE}\frac{eF}{\hbar}\hbar^2\left[\frac{\mu_s}{k}\frac{\tau_s}{\mu_s}\int (k_x-k'_x)\,\mathrm{A}\,(\mathbf{kk}')\,dS'\right.$$
$$\left.+\frac{\mu_d}{j}\int\left(\frac{\tau_s}{\mu_s}k_x-\frac{\tau_d}{\mu_d}j_x\right)\mathrm{A}\,(\mathbf{kj})\,dS_j\right]. \tag{13}$$

This must be equated to the increase in the number of electrons due to the applied field, which is, from (7)

$$2\frac{d\mathbf{k}}{8\pi^3}\left(\frac{df}{dt}\right)_{\text{field}}=-2\frac{d\mathbf{k}}{8\pi^3}\frac{df_0}{dE}\frac{\hbar^2}{\mu_s}\frac{eF}{\hbar}k_x. \tag{14}$$

Equating (13) and (14) and dividing by common factors we obtain

$$\tau_s\int\left(1-\frac{k'_x}{k_x}\right)\mathrm{A}\,(\mathbf{kk}')\,dS'+\tau_s\frac{\mu_d}{\mu_s}\frac{k}{j}\int \mathrm{A}\,(\mathbf{kj})\,dS_j$$
$$-\tau_d\frac{k}{j}\int \mathrm{A}\,(\mathbf{kj})\frac{j_x}{k_x}\,dS_j=\frac{k}{\mu_s}.$$

To simplify the integrals, we denote by θ the angle between $\mathbf{k}$, $\mathbf{k}'$ or $\mathbf{k}$, $\mathbf{j}$, by α the angle between $\mathbf{k}$ and the x axis, and by ϕ the angle between the plane $\mathbf{kk}'$ and the plane containing $\mathbf{k}$ and the x axis. Then,

$$k_x=k\cos\alpha,\qquad k'_x=k\,(\cos\alpha\cos\theta+\sin\alpha\sin\theta\cos\phi)$$
$$dS=k^2\sin\theta\,d\theta\,d\phi.$$

Carrying out the ϕ integration, we have

$$\int\left(1-\frac{k'_x}{k_x}\right)\mathrm{A}\,(\mathbf{kk}')\,dS'=2\pi k^2\int \mathrm{A}_{ss}(\theta)\,(1-\cos\theta)\sin\theta\,d\theta$$
$$=k^2a_{ss}\qquad\text{(say)}$$
$$\int \mathrm{A}\,(\mathbf{kj})\,dS_j=2\pi j^2\int \mathrm{A}_{sd}(\theta)\sin\theta\,d\theta$$
$$=j^2a_{sd}^{(1)}\qquad\text{(say)}$$
$$\int \mathrm{A}\,(\mathbf{kj})\frac{j_x}{k_x}\,dS_j=2\pi\frac{j}{k}j^2\int \mathrm{A}_{sd}(\theta)\cos\theta\sin\theta\,d\theta$$
$$=j^2a_{sd}^{(2)}\,j/k,\qquad\text{(say).}$$

The expressions a_{ss}, a_{sd}, etc., we consider to be all of the same order of magnitude.

Hence finally

$$\tau_s\,[\mu_s k a_{ss} + \mu_d j a_{sd}^{(1)}] - \tau_d \mu_s a_{sd}^{(2)} j^2/k = 1. \tag{15}$$

By considering a volume element of j space, *i.e.*, in the d zone, we may obtain similarly

$$\tau_d\,[\mu_d j a_{dd} + \mu_s k a_{sd}^{(1)}] - \tau_s \mu_d a_{sd}^{(2)} k^2/j = 1. \tag{16}$$

If now, as we assume, $\mu_d \gg \mu_s$, we obtain approximately from (15) and (16)

$$1/\tau_s = \mu_d j a_{sd}^{(1)} \tag{17}$$

$$1/\tau_d = \mu_d j a_{dd}\Big/\left(1 + \frac{k^2}{j^2}\frac{a_{sd}^{(2)}}{a_{sd}^{(1)}}\right). \tag{18}$$

τ_s and τ_d are thus of the same order of magnitude, both depending on the effective mass of a d electron.

Writing out in full the expression for $a_{sd}^{(1)}$ we obtain

$$a_{sd}^{(1)} = 2\pi \int_0^\pi \mathrm{A}_{sd}(\theta) \sin\theta\, d\theta$$

$$\mathrm{A}_{sd}(\theta) = \frac{2\pi}{\hbar^3} \left|\int \psi^*_s \frac{\partial \mathrm{V}}{\partial x}\, \psi_d\, d\tau\right|^2 \frac{\hbar^2}{k} \frac{\mathrm{T}}{\mathrm{M}\Theta^2},$$

where θ is the angle between the vectors $\mathbf{k}$ of the initial s state and $\mathbf{j}$ of the final d state.

With the assumptions made in this section, the density of states in the d zone is (*cf.* (3))

$$\mathrm{N}_d(\mathrm{E}) = 2\mu_d j/\hbar^2;$$

we see, therefore, that

$$1/\tau_s \propto \mathrm{N}_d(\mathrm{E})_{\mathrm{E}=\zeta}, \tag{19}$$

which is the required result.

The current due to the s electrons is

$$i = e \int g_s(\mathbf{k})\, v_x \frac{2\, d\mathbf{k}}{8\pi^3},$$

where $v_x = \hbar k_x/\mu_s$ is the velocity of an s electron. If n_s = number of s electrons $= \frac{8\pi}{3}(k_{\max}/2\pi)^3$, this easily reduces to

$$i = -\frac{n_s e^2}{\mu_s} \mathrm{F} \int \tau_s \frac{df_0}{d\mathrm{E}}\, d\mathrm{E}. \tag{20}$$

Since $df_0/d\mathrm{E}$ is a function which vanishes except in a range $k\mathrm{T}$ in the neighbourhood of $E = \zeta$, i.e., at the surface of the Fermi distribution, and since further $\int (df_0/dE)\, dE = -1$, this reduces to

$$i = n_s e^2 F\, \tau_s / \mu_s,$$

so long as τ_s can be considered constant in the range kT.

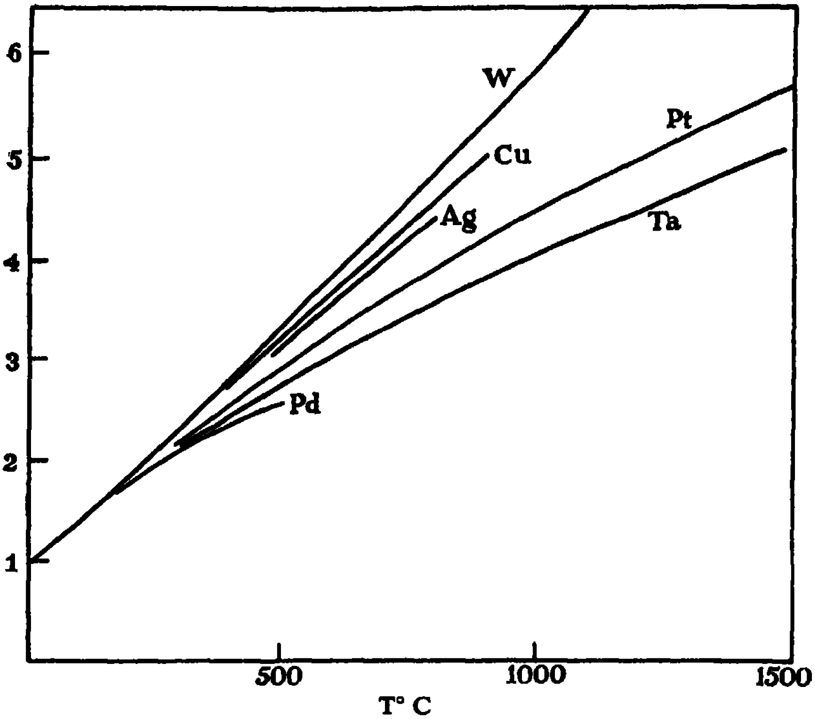

Fig. 2—Experimental values of R/R_0 for various metals; from Grüneisen, 'Handb. d. Phys.,' vol. 10, p. 16 (1928).

5—Resistance of Palladium and Platinum at High Temperatures

At high temperatures the resistance of Cu, Ag, Au, and also of W increases rather more rapidly with the temperature than a linear law implies*; for the paramagnetic elements Pd, Pt, and Ta, on the other hand, the increase is considerably less rapid† (*cf.* fig. 2). This behaviour may easily be explained in terms of the theory of the preceding section.

As we have seen, in order to calculate the resistance, we only need to know the scattering probabilities for electrons in a narrow range of energies kT, in which $-\partial f_0/\partial E$ is finite, at the surface of the Fermi distribution. Now it is quite certain that the velocities, etc., of electrons in the broad *s*-band may be taken as constant throughout this range, but at high temperatures it is possible that $N_d(E)$, the density of states in the *d* band, to which the *s* electrons make transitions, will vary appreciably. Since $N_d(E)$ decreases with increasing energy,[*] we should expect the *s* electrons with most thermal energy to be scattered less often than those with less energy. Thus the resistance of the metal increases less fast than it otherwise would.

---

* Probably because Θ_D decreases as the solid expands.

† The atomic susceptibilities are ($\chi \times 10^6$). Cu, −5·6; Ag, −20; W, +41; Pd, +550; Pt, +160; Ta, +150.

The dependence of resistance on temperature can be discussed quantitatively on the basis of formula (20); we now assume that τ_s is not quite constant over the range of integration. Then by a well-known formula,[†] writing $\tau_s = \tau_s(E)$

$$-\int \tau_s(E) \frac{df_0}{dE} dE \simeq \tau_s(\zeta) + \frac{\pi^2}{6} \left(\frac{d^2\tau_s}{dE^2}\right)_{E=\zeta} (kT)^2.$$

ζ is itself a function of T; we have[†]

$$\zeta = \zeta_0 - \frac{\pi^2}{6} \left(\frac{d \log N}{dE}\right)_{E=\zeta_0} (kT)^2,$$

where ζ_0 is the energy at the surface of the Fermi distribution at $T = 0$. Hence

$$-\int \tau_s(E) \frac{df_0}{dE} dE = \tau_s(\zeta_0) + \frac{\pi^2}{6} (kT)^2 \left[\tau''(\zeta_0) - \frac{\tau'(\zeta_0) N'(\zeta_0)}{N(\zeta_0)}\right]. \quad (21)$$

Now $1/\tau_s$ is proportional, of course, to the amplitude of the atomic vibrations, and hence to T, and also, as we have seen, to $N_d(E)$, the density of states in the *d*-zone. Further, $N(E)$ is approximately equal to $N_d(E)$, so that the factors in (20) and hence in the expression for the conductivity which contain T are

$$\frac{1}{T}\left[1 + \frac{\pi^2}{6}(kT)^2 \left\{\frac{\tau''}{\tau} + \frac{\tau'^2}{\tau^2}\right\}\right].$$

Writing[‡] $N_d(E) = C\sqrt{E_0 - E}$, $\tau \propto 1/N_d$, this becomes

$$\frac{1}{T}\left[1 + \frac{\pi^2}{6}\left(\frac{T}{T_0}\right)^2\right],$$

---

[*] Because the band is nearly full, *cf.* paper A, p. 573.

[†] *Cf.* Sommerfeld and Bethe, *loc. cit.*, pp. 346 and 429.

[‡] The first of these assumptions should not lead to serious error for Pd and Pt, where the *d* band is nearly full, but may be quite incorrect for Ta.

where $kT_0 = E_0 - \zeta_0$; or for the resistance

$$R = \text{const. } T\left[1 - \frac{\pi^2}{6}\left(\frac{T}{T_0}\right)^2\right]. \tag{22}$$

This formula is, of course, only valid if T is small compared with T_0. We may call T_0 the " degeneracy temperature " for the *d* shell.

In deriving this formula, we have neglected the factors which in copper, for instance, make the resistance increase more rapidly than T, and which, presumably, will be operative also in Pd and Pt. To compare our theory with experiment, we shall therefore express the theoretical result in the form:—

$$\left(\frac{R}{R_0}\right)_{Pt} = \left(\frac{R}{R_0}\right)_{Cu}\left[1 - \frac{\pi^2}{6}\left(\frac{T}{T_0}\right)^2\right], \tag{23}$$

which gives

$$\left(\frac{R}{R_0}\right)_{Cu} - \left(\frac{R}{R_0}\right)_{Pt} \simeq \text{const. } T^3. \tag{24}$$

A formula of the type (24) fits the experimental results for Pt well, as is shown in Table I.

TABLE I

I T (° K)	II $\left(\frac{R}{R_0}\right)_{Cu} - \left(\frac{R}{R_0}\right)_{Pt}$	III T^3/column II
571	0·17	1·1
771	0·4	1·2
1071	0·8	1·5
1271	1·4	1·5

From the observed resistances and formula (23) we may deduce T_0; we obtain

	Pd	Pt	Ta
T_0	2100°	3100°	(2800°)

We may compare the value of T_0 for nickel deduced from the atomic heat at liquid helium temperatures, namely* 1950°.

The specific heat due to the *d*-electrons depends on T_0, and is, assuming $N_d(E) \propto \sqrt{(E_0 - E)}$

$$n_d F(T/T_0),$$

where n_d is the number of positive holes in the *d*-shell, and

$$\begin{aligned} F &= \tfrac{1}{2}\pi^2 k\, T/T_0 & T \ll T_0 \\ &= \tfrac{3}{2}k\left[1 - 0{\cdot}0667 \ldots (T_0/T)^{\frac{3}{2}}\right] & T \gg T_0 \end{aligned}$$

---

* Discussion on Supraconductivity, *loc. cit.*

For immediate values F can be calculated numerically.‡ Assuming n_d to be 0·6 per atom,§ the contribution of the *d*-electrons to the atomic heat, with the above values of T_0, is in cal/gm atom

T °C	Pd	Pt
500	1·2	1·1
1000	1·55	1·4
1500	1·65	1·55

The observed values of C_v (the observed atomic heat corrected for dilation) do in fact rise considerably above the value 5·98 for Pd and Pt, as Table II shows, though not quite so much as the theory requires.

TABLE II—OBSERVED ATOMIC HEATS (C_v)

T °C	Pd*	Pt*	Cu†	Ag†	Au†
500	6·594	6·38	6·2	6·0	6·0
900	7·072			6·13	
1000	7·146	6·65	6·5		6·12
1300	7·251				
1500	7·232				
1600		6·8			

* Jaeger and Rosenblum, 'Proc. Acad. Sci. Amst.,' vol. 33, p. 457 (1930).

† The mean of several determinations, *cf.* Euken, 'Handb. exp. Physik,' vol. 8, p. 211 (1928).

The excess specific heat of platinum has been attributed by Born and Brody‖ to anharmonic terms in the potential energy of the lattice waves; such terms may make either a positive or a negative contribution to the specific heat. It is not at present possible to state how large this contribution is.

6—RESISTANCE OF FERROMAGNETICS

The resistance of nickel as a function of temperature and external magnetic field has been extensively investigated by Gerlach¶ and his co-workers and also by Potter.**

Fig. 3 shows the resistance of nickel as a function of temperature. The sharp change in the temperature coefficient near the Curie point should be noted. It is found, moreover, that in the neighbourhood of the Curie temperature, the resistance *decreases* in a magnetic field, the change in the resistance being given by

---

‡ Mott, 'Proc. Camb, Phil. Soc.' (*in the press*).

§ *Cf.* paper A.

‖ 'Z. Physik,' vol. 6, p. 132 (1921); 'Handb. Physik,' vol. 24, p. 675 (1933).

¶ *Cf.* Englert, 'Ann. Physik,' vol. 14, p. 589 (1932), where other references are given.

** 'Proc. Roy. Soc.,' A, vol. 132, p. 559 (1931).

$$\frac{\Delta R}{R} = -\frac{b\Delta(\sigma^2)}{\sigma_\infty^2}, \tag{25}$$

where $\Delta\sigma$ is the increase in the magnetization due to the field.

A qualitative explanation may be given in terms of the above theory. We have seen that the resistance of nickel is mainly due to conduction electrons being scattered by a vibrating atom into the *d* band. The conduction electrons may be considered to have their spins either parallel or antiparallel to an external magnetic field, and the probability that the direction of the spin is changed during the scattering process is negligible. Now at low temperatures, when the spontaneous magnetization of nickel attains its maximum value, all the unoccupied states (" positive holes ") in the *d* shell are those with spin direction antiparallel to the direction of magnetization.* Therefore it is only possible for *half* of the conduction electrons to make transitions to the *d* band, namely those with spin antiparallel to the direction of magnetization. On the other hand, above the Curie temperature, positive holes with both spin directions will be present,

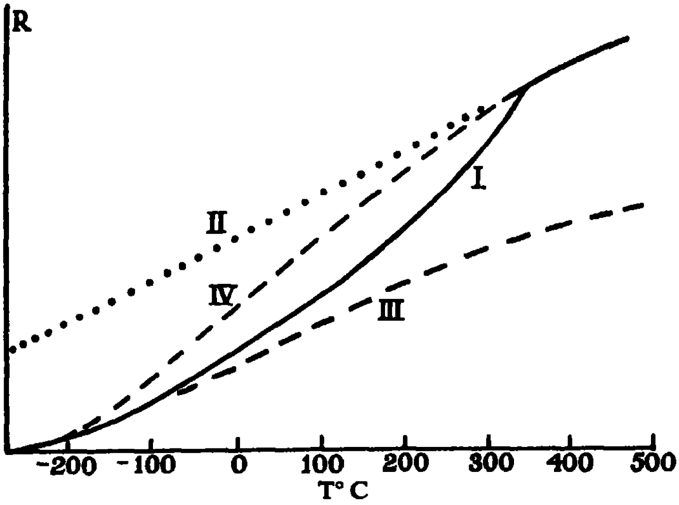

FIG. 3—Resistance of nickel, in arbitrary units. Curve I, experimental values, from Gerlach, 'Leipziger Vortraeger,' p. 21 (1933); Curve II, extrapolation of resistance curve observed above the Curie point; Curves III and IV, types of theoretical curve to be expected for $\sigma = \sigma_\infty$ and $\sigma = 0$ respectively.

---

* Mott, paper A.,

and *all* the conduction electrons can make transitions to the *d* band. We suggest, then, that this is the reason why the destruction of the spontaneous magnetization increases the resistance.

We shall first discuss the dependence of the resistance on σ and hence on H at low temperatures (above the Debye characteristic temperature but well below the Curie point). The probability of scattering is proportional to the density of states $N_d(E)$ in the *d* band at the surface of the Fermi distribution ($E = \zeta_0$). Making the reasonable assumption that $N_d = C\sqrt{E_0 - E}$ (*cf.* § 5) near the head of the *d* band, it follows that $N_d(\zeta_0)$ is proportional to the cube root of the number of positive holes in the band, and hence to

$$\left(1 \mp \frac{\sigma}{\sigma_\infty}\right)^{\frac{1}{3}},$$

for electrons respectively parallel and antiparallel to the direction of magnetization. This for $\sigma = \sigma_\infty$, the scattering probability into the *d* band is proportional to $2^{\frac{1}{3}}$ T for one half of the electrons and zero for the other half, while for $\sigma = 0$ the scattering probability is proportional to T for all the electrons.

The current, then, in the metal, is made up of two parts, contributed by electrons with the two spin directions. We may assume that during a free path an electron changes its spin direction more than once, so that the two currents are equal; it then follows that the resistance is proportional to the mean scattering probability, and hence to

$$R = \text{const.}\, T\left[\left(1 - \frac{\sigma}{\sigma_\infty}\right)^{\frac{1}{3}} + \left(1 + \frac{\sigma}{\sigma_\infty}\right)^{\frac{1}{3}}\right]. \tag{26}$$

For σ/σ_∞ small, this gives

$$R = \text{const.}\, T\left[1 - \tfrac{1}{9}\left(\frac{\sigma}{\sigma_\infty}\right)^2 \ldots\right]. \tag{27}$$

The change of resistance in a magnetic field will thus be for small σ/σ_∞

$$\frac{\Delta R}{R_T} = -\tfrac{1}{9}\,\frac{\Delta(\sigma^2)}{{\sigma_\infty}^2}.$$

Thus we expect that near the Curie point the constant *b* will have the value 0·11.

Actually *b* is not found to be constant near the Curie point*; Stoner, however, has pointed† out that below the Curie point $\Delta(\sigma^2)$ does not correspond to the true magnetization; the work of Potter (*loc. cit.*) shows that $\Delta R/R_T$ is in fact proportional to the change in the internal energy determined from the magneto-caloric effect. Estimating from the latter effect the " true " change in $\Delta(\sigma^2)$, we find

---

* Englert, 'Z. Physik,' vol. 74, p. 748 (1932).

† *In the press.*

$$b \simeq 0 \cdot 5 \quad \text{(experimental)}.$$

The agreement is perhaps as good as we can expect with so simple a model of a ferromagnetic near the Curie point.

The derivation of formulae (25) and (26) is actually valid only for low temperatures, because it neglects the fact discussed in § 4, that $N_d(E)$ cannot be considered constant throughout the range kT at the surface of the Fermi distribution. We shall not attempt to give a quantitative theory of the resistance temperature curve near and above the Curie point. It is, however, clear that the theoretical curve *for constant* σ will be similar to that for Pt and thus concave to the temperature axis. In fig. 3 we show by the dotted lines the sort of curves we should expect to obtain for $\sigma = \sigma_\infty$ and $\sigma = 0$, the ordinates of the two curves being in the ratio $1 : 2^{2/3}$.

7—ALLOYS OF NICKEL

From the theoretical point of view, the resistance of an alloy is made up of two parts:—

$$R = R_0 + R_T,$$

where R_0 is the resistance due to disorder in the alloy, R_T and to the thermal vibration of the atoms. In general R_0 is independent of temperature, while R_T increases linearly with T as for a pure metal. In paper A, however, it was shown from experimental evidence that in certain Pd-Ag alloys, at least part of R_0 (and hence of the resistance at 0° K) is due to transitions from the *s* to the *d* band. This is probably the case for other paramagnetic or ferromagnetic alloys. It follows that R_0 will also be a function of the temperature, that part of R_0 which is due to *s-d* transitions being proportional to

$$\left(1 - \frac{\sigma}{\sigma_\infty}\right)^{\frac{1}{3}} + \left(1 + \frac{\sigma}{\sigma_\infty}\right)^{\frac{1}{3}}. \tag{28}$$

and hence increasing by a factor $2_{\frac{2}{3}} = 1 \cdot 59$ between 0° K and the Curie temperature.

Fig. 4 shows measurements of the resistance of a series of Cu-Ni alloys due to Chevenard.* The sharp rise with T in the resistance of the alloy containing 20% copper below the Curie point, compared with the gradual rise above, suggests that R_0 as well as R_T depends on T below the Curie point, as suggested by formula (28).

---

* 'C.R. Acad. Sci. Paris,' vol. 181, p. 29 (1925). *Cf.* also similar results by Krupkowski and de Haas, 'Comm. Phys. Lab. Leiden,' No. 194*a* (1928).

For paramagnetic and ferromagnetic alloys above the Curie point, that part of R_0 which is due to *s-d* transitions will be given by (*cf.* equation (23))

$$\text{const.}\left[1 - \frac{\pi^2}{6}\left(\frac{T}{T_0}\right)^2\right] \qquad T \ll T_0. \tag{29}$$

Thus if R_T is not too large, the resistance will *decrease* with temperature.

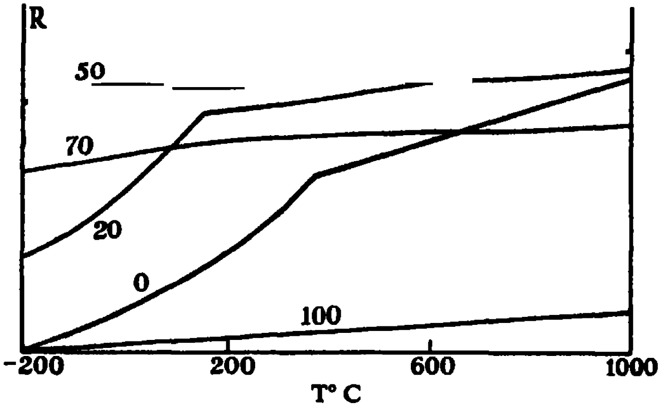

FIG. 4—Resistance of copper-nickel alloys. The figures give the proportion of copper in atomic per cent.

We may thus understand why alloys with about the composition CuNi (constantan) have a maximum in the resistance near room temperature. In these alloys the *d* shell is nearly full up, so that T_0 will have a value considerably less than 1000°–2000°, the values estimated for pure nickel. On the other hand, probably only a small part of R_0 is due to *s-d* transitions and thus dependent on temperature. The parts of the resistance, therefore, which depend on temperature will be a term of the type (29) with T_0, say, 300°, and a term due to thermal vibrations of the same order of magnitude as the resistance of pure copper. Two such terms will account for the observed maximum.

SUMMARY

The quantum theory of electrical conductivity developed by Bloch and others is extended to metals where the conduction electrons occupy more than one Brillouin zone, as is the case for all real metals except the alkalis and noble metals. The theory is applied to the transition metals; certain anomalies in the resistance temperature curves of the paramagnetic metals Pd, Pt, Ta are explained. A theory is given to account for the fact that the resistance of nickel decreases in a magnetic field, and an expression for the decrease obtained, which is of the same order of magnitude as that observed. Finally, a qualitative discussion is given of the resistance temperature curves of copper-nickel alloys such as constantan.

INDEX TO VOLUME CLIII (A)

Adcock (F.) and Bristow (C. A.) Iron of high purity, 172.

Allsopp (C. B.) and Willis (H. F.) Refractive dispersion of organic compounds. VII—The refractive indices of hexane and the refractivities of hydrogen and carbon. Significance of the dispersion constants. VIII—Isomers of the formula $C_4H_8O_2$: dioxan, ethyl acetate, *iso*-butyric acid, and acetoin, 379, 392.

Aluminium, electrical resistance at low temperatures (Boorse and Niewodniczański), 463.

Arnot (F. L.) and Milligan (J. C.) The formation of mercury molecules, 359.

Atomic nuclei, structure (Wilson), 493.

Auger effect, relativistic theory (Massey and Burhop), 661.

Beta-brass and iron crystals, distortion (Elam), 273.

Beta-particles, fast, scattering by nitrogen nuclei (Champion), 353.

Boorse (H. A.) and Niewodniczański (H.) The electrical resistance of aluminium at low temperatures, 463.

Boron, disintegration (Roaf), 568.

Braaten (E. O.) and Clark (G. F.) The diffusion of hydrogen through copper, 504.

Bristow (C. A.) *See* Adcock and Bristow.

Brown (L. W.) *See* White and Brown.

Burgoyne (J. H.) *See* Newitt and Burgoyne.

Burhop (E. H. S.) *See* Massey and Burhop.

Burton (E. F.) and Oliver (W. F.) The crystal structure of ice at low temperatures, 166.

Carbon dioxide, isotherms (Michels and others), 201, 214.

Cassel (J.) Ultra-violet absorption of ice, 534.

Cerebrospinal fluid, method for the determination of lead (Foster and others), 141.

Champion (F. C.) The scattering of fast β-particles by nitrogen nuclei, 353.

Childs (W. H. J.) The structure of the near infra-red bands of methane. I—General survey and a new band at 11,050 A, 555.

Clark (G. F.) *See* Braaten and Clark.

Combustion, hydrocarbon, and pro-knocks (Ubbelohde and others), 103.

Conductivity, electrical, of transition metals (Mott), 699.

Copper and palladium, sorption of hydrogen and deuterium, I and II (Melville and Rideal), 77, 89.

Crystal structure of ice at low temperatures (Burton and Oliver), 166.

Crystal structure of para-dinitrobenzene (James and others), 225.

Deuterium, sorption by copper and palladium, I and II (Melville and Rideal), 77, 89.

Devonshire (A. F.) The rotation of molecules in fields of octahedral symmetry, 601.

Diffraction corrections for the Rayleigh disc (King), 17.

Diphenyl, chlorinated, dielectric loss characteristics (Jackson), 158.

Disc, Rayleigh, theory of the inertia and diffraction corrections (King), 17.

Discs, circular, acoustic radiation pressure (King), 1.

Drinkwater (J. W.) *See* Ubbelohde and others.

Drummond (D. G.) The infra-red absorption spectra of quartz and fused silica from 1 to 7·5 μ. I—Experimental method. II—Experimental results, 318, 328.

Egerton (A.) *See* Ubbelohde and others.
Elam (C. F.) The distortion of β-brass and iron crystals, 273.
Electron pairs, production (Jaeger and Hulme), 443.
Equilibria, gas-solid (Lambert and Heaven), 584.

Foster (J. S.), Langstroth (G. O.), and McRae (D. R.) Quantitative spectrographic analysis of biological material. I—A method for the determination of lead in cerebrospinal fluid, 141.
Frameworks, stress calculation, III (Southwell), 41.
Fuchs (K.) A quantum mechanical calculation of the elastic constants of monovalent metals, 622.

Gee (G.) and Rideal (E. K.) Reactions in monolayers of drying oils. I—The oxidation of the maleic anhydride compound of β-elaeostearin. II—Polymerization of the oxidized forms of the maleic anhydride compound of β-elaeostearin, 116, 129.

Heaven (H. S.) *See* Lambert and Heaven.
Helium, condensed, at absolute zero (London), 576.
Hopkins (Sir F. Gowland) Presidential address, 247.
Horrocks (H.) *See* James and others.
Howell (H. G.) The absorption spectrum of lead oxide (PbO), 683.
Hulme (H. R.) *See* Jaeger and Hulme.
Hydrocarbons, aromatic, oxidation at high pressures (Newitt and Burgoyne), 448.
Hydrogen, diffusion through copper (Braaten and Clark), 504.
Hydrogen and deuterium, sorption by copper and palladium, I and II (Melville and Rideal), 77, 89.

Ice, crystal structure at low temperatures (Burton and Oliver), 166.
Ice, ultra-violet absorption (Cassel), 534.
Inertia and diffraction corrections for the Rayleigh disc (King), 17.
Infra-red bands, *near*, of methane (Childs), 555.
Ionosphere, measurements of reflexion coefficient for wireless waves (White and Brown), 639.
Ions, positive, emission by platinum when heated in oxygen (Rymer), 422.
Iron crystals, distortion (Elam), 273.
Iron of high purity (Adcock and Bristow), 172.
Isotherms of CO_2 between 0° and 150° and pressures from 16 to 250, and 70 to 3000 atmospheres (Michels and others), 201, 214.

Jackson (W.)—The dielectric loss characteristics of a chlorinated diphenyl, 158.
Jaeger (J. C.) and Hulme (H. R.) On the production of electron pairs, 443.
James (R. W.), King (G.), and Horrocks (H.) The crystal structure of para-dinitrobenzene, 225.

King (G.) *See* James and others.
King (L. V.) On the acoustic radiation pressure on circular discs: inertia and diffraction corrections, 1.
King (L. V.) 'On the theory of the inertia and diffraction corrections for the Rayleigh disc, 17.

Lambert (B.) and Heaven (H. S.) Studies on gas-solid equilibria. VI—Adsorption from binary gas mixtures by silica gel, 584.
Langstroth (G. O.) *See* Foster and others.
Lead, method for the determination in cerebrospinal fluid (Foster and others), 141.
Lead halides, band spectra (Rochester), 407.
Lead oxide, absorption spectrum (Howell), 683.
London (F.) On condensed helium at absolute zero, 576.

Massey (H. S. W.) and Burhop (E. H. S.) The relativistic theory of the auger effect, 661.
McRae (D. R.) *See* Foster and others.
Melville (H. W.) and Rideal (E. K.) The sorption of hydrogen and deuterium by copper and palladium. I—The behaviour of copper and copper oxides. II—The sorption of palladium and diffusion through copper, 77, 89.
Mercury molecules, formation (Arnot and Milligan), 359.
Metals, monovalent, quantum mechanical calculation of elastic constants (Fuchs), 622.
Metals, theory of the surface photoelectric effect, II (Mitchell), 513.
Metals, transition, electrical conductivity (Mott), 699.
Methane, structure of the near infra-red bands (Childs), 555.
Michels (A. and C.) Isotherms of CO_2 between 0° and 150° and pressures from 16 to 250 atmospheres (Amagat densities 18–206), 201.
Michels (A. and C.) and Wouters (H.) Isotherms of CO_2 between 70 and 3000 atmospheres (Amagat densities between 200 and 600), 214.
Milligan (J. C.) *See* Arnot and Milligan.
Mitchell (K.) The theory of the surface photoelectric effect in metals, II, 513.
Molecules, rotation in fields of octahedral symmetry (Devonshire), 601.
Monolayers of drying oils, reactions, I and II (Gee and Rideal), 116, 129.
Moon (P. B.) and Tillman (J. R.) Neutrons of thermal energies, 476.
Mott (N. F.) The electrical conductivity of transition metals, 699.

Nakaya (U.) and Yamasaki (F.) Investigations on the preliminary stages of spark formation in various gases by the use of the Wilson chamber, 542.
Neutrons of thermal energies (Moon and Tillman), 476.
Newitt (D. M.) and Burgoyne (J. H.) The oxidation of aromatic hydrocarbons at high pressures. I—Benzene; II—Toluene; III—Ethyl benzene, 448.
Niewodniczański (H.) *See* Boorse and Niewodniczański.
Nitrogen nuclei, scattering of fast β-particles (Champion), 353.
Nuclei, atomic, structure (Wilson), 493.

Oils, drying, reactions in monolayers, I and II (Gee and Rideal), 116, 129.
Oke (B. Y.) On the theory of optical activity. III—A regular tetrahedron twisted through a small angle about a binary axis, 339.
Oliver (W. F.) *See* Burton and Oliver.
Optical activity, theory, III (Oke), 339.
Oxygen afterglow (Stoddart), 152.

Para-dinitrobenzene, crystal structure (James and others), 225.
Photoelectric effect, surface, in metals, II (Mitchell), 513.
Platinum, emission of positive ions when heated in oygen (Rymer), 422.

Polymerization of the oxidized forms of maleic anhydride (Gee and Rideal), 129.
Presidential address (Hopkins), 247.
Pro-knocks and hydrocarbon combustion (Ubbelohde and others), 103.
Quantum mechanical calculation of elastic constants of monovalent metals (Fuchs), 622.
Quartz, infra-red absorption spectra, I and II (Drummond), 318, 328.
Radiation pressure, acoustic, on circular discs (King), 1.
Refractive dispersion of organic compounds, VII and VIII (Allsopp and Willis), 379, 392.
Rideal (E. K.) *See* Gee and Rideal.
Rideal (E. K.) *See* Melville and Rideal.
Roaf (D.) The disintegration of boron, 568.
Rochester (G. D.) The band spectra of the lead halides, PbF and PbCl, 407.
Rymer (T. B.) The emission of positive ions by platinum when heated in oxygen, 422.
Silica, fused, infra-red absorption spectra, I and II (Drummond), 318, 328.
Silica gel, adsorption from binary gas mixtures (Lambert and Heaven), 584.
Southwell (R. V.) Stress-calculation in frameworks by the method of systematic relaxation of constraints, III, 41.
Spark formation, preliminary stages in various gases investigated by use of the Wilson chamber (Nakaya and Yamasaki), 542.
Spectra, band, of the lead halides PbF and PbCl (Rochester), 407.
Spectra, infra-red absorption of quartz and fused silica, I and II (Drummond), 318, 328.
Spectrographic analysis of biological material, I (Foster and others), 141
Spectrum, absorption of lead oxide (PbO) (Howell), 683.
Stoddart (E. M.) The oxygen afterglow, 152.
Stress calculation in frameworks by the method of systematic relaxation of constraints, III (Southwell), 41.
Thermal energies, neutrons (Moon and Tillman), 476.
Tillman (J. R.) *See* Moon and Tillman.
Tomotika (S.) Breaking up of a drop of viscous liquid immersed in another viscous fluid which is extending at a uniform rate, 302.
Ubbelohde (A. R.), Drinkwater (J. W.), and Egerton (A.) Pro-knocks and hydrocarbon combustion, 103.
Ultra-violet absorption of ice (Cassel), 534.
Viscous liquid, breaking up of a drop immersed in another viscous fluid which is extending at a uniform rate (Tomotika), 302.
Waves, wireless, measurements of the reflexion coefficient of the ionosphere (White and Brown), 639.
White (F. W. G.) and Brown (L. W.) Some measurements of the reflexion coefficient of the ionosphere for wireless waves, 639.
Willis (H. F.) *See* Allsopp and Willis.
Wilson (H. A.) The structure of atomic nuclei, 493.
Yamasaki (F.) *See* Nakaya and Yamasaki.

END OF THE ONE HUNDRED AND FIFTY-THIRD VOLUME (SERIES A)